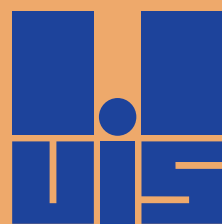




Proceedings of the
17th
International
Congress of
Speleology,
Sydney 2017

Volume Two



Union Internationale
de Spéléologie



**17th INTERNATIONAL
CONGRESS OF SPELEOLOGY**

Sydney, NSW, Australia

July 22–28, 2017

Proceedings

VOLUME 2

Edited by

Kevin Moore

Susan White

2017

17th INTERNATIONAL CONGRESS OF SPELEOLOGY

Sydney, NSW, Australia

July 22–28, 2013

Proceedings

VOLUME 2

Produced by the Organizing Committee of the 167th International Congress of Speleology.

Published by the Australian Speleological Federation Inc and Speleo2017 in the co-operation with the International Union of Speleology.

Design by Kevin Moore

Layout by Kevin Moore

Printed in Victoria Australia

The contributions were assisted with language and edited. Contributions express author(s) opinion.

Recommended form of citation for this volume:

Moore K., White S. (Eds), 2017. Proceedings of the 17th International Congress of Speleology, July 22–28, Sydney, NSW Australia

Volume 1, Australian Speleological Federation Inc. Sydney.

ISBN 978-0-9808060-5-2-07-6

© 2017 Australian Speleological Federation Inc,



This work is licensed under Creative Commons Attribution ShareAlike International License (CC-BY-SA). To view a copy of this license, visit <http://creativecommons.org/licenses/by/4.0/>.

Individual Authors retain copyright over their work, while allowing the conference to place this unpublished work under a Creative Commons Attribution ShareAlike which allows others to freely access, use, and share the work, with an acknowledgement of the work's authorship and its initial presentation at the 17th International Congress of Speleology, Sydney NSW Australia.

Cover photo : Keir Vaughan-Taylor on Lake 2, Koonalda Cave, Nullarbor Plain. (Photo by Kevin Moore)

Back Cover : The Khan and Beagum in Kubla Khan Cave Tasmania (Photo by Garry K. Smith)

Contents

Karst and Caves in Carbonate Rocks, Salt and Gypsum

The Karst in Morocco and the Friouato and Wintimdouine Caves MOROCCO Nadia Aamoum	2
Desert Cave Studies In The Kingdom Of Saudi Arabia Mahmoud Ahmed Alshanti	3
Desert Cave Studies In The Kingdom Of Saudi Arabia Mahmoud Ahmed Al Shanti	4
A Karst Hydrogeologic Investigation to Support Risk Assessment at Patoka Dam, Indiana, USA. Lee Anne Bledsoe, Chris Groves, Kenneth Henn, Jackie Rowe	5
Shallow caves and blowholes on the Nullarbor Plain, Australia – Flank margin caves on a low gradient limestone platform Shannon Burnett, Susan White, John Webb	9
Environmental Vulnerability At The Contact Karst Of Monjolos And The Southern Espinhaço Ridge, Minas Gerais, Brazil Leandro Cosme Oliveira Couto, Luiz Eduardo Panisset Travassos	12
The southernmost authigenic karst plateau of the Levant Amos Frumkin, Daniel Ben-Tov, Vladimir Buslov, Boaz Langford, Eliyahu Valdman, Shemesh Yaaran	13
Hypogenic caves in southern Levant deserts Amos Frumkin, Boaz Langford, Sorin Lisker	17
Hydrogeochemical And Isotopic Characterization Of The Tapalqué Creek Upper Basin And Its Associated Karst, Buenos Aires, Argentina Glok Galli, Melisa; Barredo Codesal, Silvia P.; Martínez, Daniel E.; Trezza, Mónica A.	20
Some new caves under the Dubrovnik city airport in the Dinaric karst of Croatia Mladen Garašić & Davor Garašić	26
The new insights about deep karst springs in the Dinaric karst of Croatia Mladen Garašić & Davor Garašić	30
Cave Sediments In Škocjanske Jame And Unroofed Caves Above Them, Sw Slovenia Nadja Zupan Hajna, Andrej Mihevc, Petr Pruner, & Pavel Bosák	34
Caves of Maratua Island, East Kalimantan-Indonesia Eko Haryono, Haviz Damar Sasongko, Sidiq Harjanta, Mukhammad Awaludin Zaenuri, Juswono Budi Setiawan	37
Morphology of Merabu Karst Mountain, Mangkalihat Peninsula , East Kalimantan-Indonesia Eko Haryono, Ghufrun Zulqisthi, Arief Abdurrahman Hakim, Muhamad Haviz Damar Sasongko, Mohammad Ainul Labib	37
The Jasov Plateau in the Slovak karst as an experimental area for the denudation dynamic research Zdenko Hochmuth, Alena Gessert	38

Tectonic Control of the Permian Gypsum Karst Belt along the Southern Margin of the Harz-Mountains (Germany) Hans-Peter Hubrich and Stephan Kempe	43
Features, exploitation and protection of karst Caves in China Zhongcheng Jiang, Yuanhai Zhang, Weihai Cheng	47
Exploration of the Caves of Isla de Mona, Puerto Rico Patrician N. Kambesis	48
Origin of Enigmatic Caves of the Far Western United States Patrician N. Kambesis, Joel Despain	49
Geomorphology And Hydrogeological Features Of The Rječina Karst Spring - Croatia Mladen Kuhta	50
Peculiar CO ₂ values in the Hungarian cave has a lower and upper entrance Szabolcs Leél-Össy	55
Mechanism Analysis Of Large Scale Sinkhole Formation, Laibin, Guangxi, China Mingtang Lei, Xiaozhen Jiang, Yongli Gao, Weiwan Luo and Jianling Dai	56
Complex Investigations In Novoafonskaya Cave (Western Caucasus) Mavlyudov B.R, Kuderina T.M., Kadebskaya O.I., Grabenko E.A., Tokarev I.V., Ekba Ya.A., Dbar R.S.	60
Use Of The Cave Animal <i>Marifugia cavatica</i> For Reconstruction Of Pliocene To Recent Evolution Of Karst Relief In W Slovenia Andrej Mihevc, Anton Brancelj, Ivan Horáček	65
Speleogenesis by weathering of Upper Cretaceous, Coniacian limestone, Dordogne, France Claude Mouret, Jacques Rolin and Bernard Angeli	69
The Rock Islands of Belau (Palau), Western Pacific: Drowned Polygonal Karst? Joan Mylroie, John Mylroie	73
Some Outstanding Speleological Features Of Lebanon : Typical Semi-Arid Mediterranean Karst Fadi Henri Nader	77
Highlights of Romanian Caves and Karst Gheorghe M. Ponta and Victor Ursu	78
Armenia Karst Project Ruggieri Rosario, Daytyan Smbat, Ugujyan Adranik	82
The Cenote Project: monitoring a high-altitude ice cave in the Dolomites, Italy Tommaso Santagata, Francesco Sauro, Christoph Spötl, Daniela Festi, Klaus Oeggel, Luca Dal Molin, Farouk Kadded, Marco Camorani, Alessio Romeo	86
Karst Hydrology In Sub-Arctic Norway Rannveig Øvrevik Skoglund & Stein-Erik Lauritzen	89
Measurement of the Atmospheric CO ₂ Sink from Carbonate Mineral Weathering for Large River Basins: the Ohio River, USA Autumn Turner and Chris Groves	92
Evolution, Development, And Decay Of The Caves And Karst Of The Greenbrier Valley, West Virginia, USA William B. White* and Elizabeth L. White	97

The Glenelg River Karst Susan White & John Webb	101
The Significance Of The Tiankeng Group Discovery In Hanzhong Of Central China Yuanhai Zhang	104
Karst and Cave Survey, Mapping and Data Processing	
3D cartography: caveGEOmap and ZEB1 LIDAR Angel A Acosta-Colón	106
Application of lidar data for cave entrance identification Miha Čekada, Petra Gostinčar, Borivoj Ladišić,	107
Caveink - a set of Inkscape extensions for drawing cave maps Mateusz Golicz	111
Three-dimensional cave mapping using Structure from Motion John Hellstrom	116
3-D Imaging As A Tool To Understand Speleogenetic Processes Stephan Kempe and Ingo Bauer	117
Surveying Caves using Zebedee and Bentwing Mike Lake and Jill Rowling	122
Comparison Of Shallow Geophysical Cave Detection Methods To 3D Lidar Mapping Evelynn J. Mitchell and Joseph N. Mitchell	126
The Caveatron: An Integrated Cave Survey and LIDAR Scanning Instrument Joe Mitchell and Steve Gutting	130
3D Photogrammetry Modelling Of Ice Moulins On The Grey Glacier, Chilean Patagonia Tommaso Santagata, Alessio Romeo	135
Laser scanning as a powerful tool for speleogenetic studies in quartz-sandstone caves: the example of Imawari Yeuta, Venezuela Francesco Sauro, Tommaso Santagata, Leonardo Piccini, Umberto Del Vecchio, Ada De Matteo, Marco Camorani	136
Inside The Glaciers Project: Laser Scanning Of The Grotta Del Gelo (Mount Etna, Italy) Tommaso Santagata, Marco Vattano, Francesco Sauro, Giuseppe Spitaleri, Gaetano Giudice, Corrado Bongiorno, Alessio Romeo, Marta Lazzaroni	137
Deterministically Defining Chambers in 3D-Scans of Caves Nico Schertler, Manfred Buchroithner, Donald McFarlane, Guy van Rentergem, Joyce Lundberg, Stefan Gumhold	140
The Pilkington-Lewis Squeeze Index; a rating system for cave constrictions. Heather Siebert	143
Lessons learned from a large-scale 3-D mapping project, with Faro laser scanners, of the Gomantong Caves, Borneo Guy Van Rentergem, Donald McFarlane, Joyce Lundberg, Manfred Buchroithner	144
Mathematical modelling of the relationship between terrestrial LIDAR scan point density and volumetric assessment of underground cavities Guy Van Rentergem, Donald McFarlane, Joyce Lundberg, Manfred Buchroithner	147

World's First Geophysical Survey of Bat Guano: Phase 1 and 2 Results George Veni	150
Mapping and Imaging the World's Largest Chambers in 3D Richard Roo Walters	153
Karst, Pseudokarst and Caves in Other Rocks	
An unusual maze cave in sandstone, NE Thailand John Dunkley & Terry Bolger	155
Historical Notes And Research History Of The Non-Karst Caves In Hungary István Eszterhás, George Szentés	156
Origin Of Caves In Glaciers And Glacial Sheets Mavlyudov B.R.	160
Piping Cave Development In A High Gradient Setting: Kutz Canyon, New Mexico, Usa Douglas M. Medville	165
Types of caves present in Kalimantan Barat Province, Borneo, Indonesia Claude Mouret	169
Speleogenesis underneath basaltic lava flows in Niut Mountains, Kalimantan Barat, Borneo, Indonesia Claude Mouret	170
Some fundamental features of speleogenesis in sandstone Claude Mouret	171
Caves and other features in glaciers and icebergs, Graham Land, Antarctica Claude Mouret	177
Scientific Researches And Explorations In Quartzite And Quartz-Sandstone Caves Francesco Sauro, Robert A.L. Wray	181
Lava and Volcanic Caves	
Um Jirsan Lava Tube Cave Mahmoud Ahmed Al Shanti	183
The Complexity Of Pyroduct ("Lava Tubes") Genesis: Bird Park Cave, Hawaii Volcanoes National Park Stephan Kempe, Christhild Ketz-Kempe, Harry Shick	185
Outstanding Universal Values of some lava tube caves in Jeju Island for potential World Heritage nomination Woo, Kyung-Sik, Kim Lyoun, Han Hyung-chul, Ki, Jin-Seok	190
Medicine, Philosophy, Social Aspects	
Human body responses during cave expeditions: a systematic review and potential future implications Loredana Bessone, Lucrezia Zuccarelli, Emily BJ Coffey, Giacomo Strapazzon	193
Caves And Geotourism Greg Brick, Ph.D.	197
Cultural Karst-Landscape: A New Methodology of Social Science Research in Tropical Karst Regions Yayum Kumai	199

Modelling in Karst and Cave Environments

- Small-scale modelling of arenitic caves in South American tepuis: Make your own tepui at home. 201
Roman Aubrecht, Tomáš Lánczos, Ján Schlögl, Marek Audy and Petronela Filipčíková
- Driving pressure of subterranean airflows: an analysis 205
Giovanni Badino
- A theoretical approach to the estimation of local Entropy production in caves 209
Giovanni Badino
- Mapping Carbonate And Evaporite Brackish Aquifers, Texas, USA 214
Andrea Croskrey
- Chemical Analysis Of Underground Waters In Štefanová Cave (Central Slovakia) And Its Use For Finding Connections With Cave Slobody 215
Pavel Herich, David Havlíček, Kateřina Havlíčková
- Geothermal Heat Flow in Caves: Modelling of Geothermal Heat Flow 218
Neville A. Michie, Ph.D.
- Vadose Zone Hydrogeology In The Bossea Cave System (Southern Piedmont, Northern Italy) 222
Bartolomeo Vigna, Adriano Fiorucci, Alessia Nannoni, Jo De Waele
- Effects of photosynthesis and groundwater input on diel variations of electrical conductivity and calcite precipitation in Chaotian River, Guilin, China 226
Cheng Zhang, Jinliang Wang, Qiong Xiao

Speleological Research and Activities in Artificial Caves

- A 100-km-Long subterranean Roman Aqueduct in northern Jordan? 231
Stephan Kempe and Ahmad Al-Malabeh
- Hypogea 2015 and 2017: a short, but very intense, history 236
Mario Parise, Roberto Bixio, Carla Galeazzi, Ali Yamac

Speleogenesis

- Karst morphological processes and evolution of the limestone massif of Georgia from depositional, sedimentary, and structural investigations in Muradi Cave 241
Lasha Asanidze, Zaza Lezhava, Kukuri Tsikarishvili, Nino Chikhradze, Jason S. Polk
- A Third Kind Of Cave In The World: Anthropogenic 248
Greg Brick, Ph.D.
- Evaluation of possible ongoing upwards condensation corrosion in Cueva del Pastor (Iberian Chain), Spain 249
Kelsey Budahn, Ira D. Sasowsky, Francisco Gutiérrez, Mario Gisbert
- Age And Speleogenesis Of Gypsum Caves In Emilia-Romagna (N Italy) 254
Andrea Columbu, Veronica Chiarini, Jo De Waele, Russell Drysdale, Jon Woodhead, John Hellstrom and Paolo Forti
- Why We Should Thank A Proterozoic Meteorite For The Caves At Assynt, NW Scotland, UK 259
Trevor Faulkner
- Are There Any Pre-Quaternary Caves In Scandinavia? 263
Trevor Faulkner

Speleogenesis In Two Highly Contrasting Epigenic Limestone Lithologies Trevor Faulkner And Susan White	269
Carbonate hostrock weathering by sea salt precipitation in El Orón-Arco Cave (Cartagena, SE Spain) Fernando Gázquez, José-María Calaforra, Fernando Rull, Jesús Medina, Andrés Ros, José Luis Llamusí and Juan Sánchez	270
Cave Sediments In Škocjanske Jame And Unroofed Caves Above Them, SW Slovenia Nadja Zupan Hajna, Andrej Mihevc, Petr Pruner, & Pavel Bosák	274
United we divide: Speleogenesis in the vertical vadose zone Philipp Häuselmann	277
Hypogene? Caves Modified By Meteoric Flows - Geomorphology Of Cliefden Caves And The Belubula River Valley Ian Houshold ¹ and Armstrong Osborne ²	280
The oldest meteoric caves in Norway? The Reingardslia Cave Documentation project. Stein-Erik Lauritzen, Rannveig Øvrevik Skoglund, Marie Heggstad, Hege Kilhavn, Severin Lølkes, Einar Taule Øyehaug, Ida Marie Gabrielsen, Alexander Gulbrandsøy Stadheim, Sverre Aksnes	284
Pre-Quaternary, hypogenetic caves in south Norway Stein-Erik Lauritzen, Sven Dahlgren	284
Analysis of scallops in Gomantong Caves, by GIS processing of 3D terrestrial laser scanner data Joyce Lundberg, William Carroll, Warren Roberts, Donald A McFarlane, Manfred Buchroithner, and Guy van Rentergem	285
Flank Margin Caves In Telogenetic Limestones In Italy Arriolabengoa Martin, D'Angeli Ilenia Maria, De Waele Jo, Parise Mario, Ruggieri Rosario, Sanna Laura, Madonia Giuliana, Vattano Marco	289
Geothermal heat flow in caves: Heat Concentration and its Effects on Speleogenesis. Neville A Michie Ph.D.	293
A Chronology of Karstification In Puerto Rico Using Cosmogenic Dating Of Cave Sediments Thomas E. Miller, Gilles Brocard, Jane K. Willenbring	297
Tracing the origin of cave sands: State of the art in the Moravian Karst Jiří Robert Otava	301
Interpretation of Regional Geomorphic Events from Dissolution Caves Arthur N Palmer	305
Variation between lithology, carbonate versus sandstone, as an erosional control on a fluviokarst system Eric Wade Peterson, Toby J Dogwiler, Andrew Francis	306
Exploring The Mechanisms And Consequences Of Cave Roof Collapses Using The National Corvette Museum Sinkhole Case Study Jason S Polk, Leslie North, Pat Kambesis, Brian Ham, Ric Federico	307
Contenda cave genesis (Estremenho karst massif , Portugal) Rodrigues, P., Robalo, P., Amendoeira, V.	308
The Origin Of Jewel Cave And Its Relationship To Landscape-Scale Processes – Part 1 Michael E. Wiles	312
The Origin Of Jewel Cave And Its Relationship To Landscape-Scale Processes – Part 2 Michael E. Wiles	315

Influence factors of Karst Caves Development and Its Response of Quaternary Environment, Jingxi, China Shi Wenqiang, Erin Lynch, Zhang Yuanhai	318
Speleothem Research	
An Hypothesis On The Evolution Of Complex Flowstones Giovanni Badino, José Maria Calaforra, Jo De Waele & Paolo Forti	320
Multiproxy Analysis Of Holocene Stalagmites From Bosnia And Herzegovina Chiarini V., Couchoud I., Drysdale R., Bajo P., Milanolo S., Hellstrom J., Frisia S., De Waele J.	325
Comparison Of South Asian And Tropical Australian Stalagmites Reveals Expansion And Contraction Of The Indo-Pacific Tropical Rain Belt Over The Last 3000 Years Rhawn F. Denniston, Caroline C. Ummenhofer, Alan D. Wanamaker, Jr., Matthew S. Lachniet, Gabriele Villarini, Yemane Asmerom, Victor J. Polyak, John Cugley, David Woods, William F. Humphreys	329
Periods of speleothem growth in northern Eurasian caves: a preliminary overview Yuri V. Dublyansky, Christoph Spötl, Denis Scholz, Gina E. Moseley, Lawrence R. Edwards	333
Stalagmite isotopic record from Mallorca (Western Mediterranean) over the last 120 ka: paleoclimatic implications Oana-Alexandra Dumitru, Bogdan P Onac, Victor J Polyak, Jonathan G Wynn, Yemane Asmerom, Joan J Fornós	334
Geochronology Of Jinfo Cave, The Oldest Cave In China Huang Bao-Jian, Zhang Jing, Zhai Xiu-Min, Luo Shu-Wen, Shi Wen-Qiang	335
Geothermal Heat Flow in Caves: The Physics of the Geothermal Rims in Carlsbad Cavern. Neville A. Michie, Ph.D.	337
The genesis of hollow stalagmites in caves of the Khammouane karst, Laos Claude Mouret	340
Symmetrical Helictites and Geopetal forms from South Eastern Australian Caves Jill Rowling	344
Symmetrical Helictites and Geopetal forms from South Eastern Australian Caves Jill Rowling	349
3D Photogrammetry Of Speleothems With The Astronauts Of The European Space Agency "Caves" Training Course Tommaso Santagata, Jo De Waele, Francesco Sauro, Loredana Bessone	350
Multilevel karst system evolution in relationship to palaeoclimate and palaeogeography: hints from a 500 ky speleothem record from the Piani Eterni Karst System, Belluno Dolomites, Italy Francesco Sauro, Andrea Columbu, Joyce Lundberg, Jo De Waele	352
Recent developments in speleothem research Jon D. Woodhead, John Hellstrom, J.M. Kale Sniderman, Russell N. Drysdale	356
Sustainable Development of Karst	
Support for sustainable eco-tourism in Puerto Princesa Underground River (Palawan, Philippines) – Project 2016-2017 Antonio De Vivo, Paolo Forti, Leonardo Piccini	360
Karst Underground Protection, Education And Rise Of Public Awareness; Examples From Slovenia Nadja Zupan Hajna	365

Educational Film ŽIVO! (“LIFE!”) – Life And Water In The Karst Region Nadja Zupan Hajna, Metka Petrič, Nataša Ravbar	369
Evaluating Human-Environmental Impacts to the Karst Landscape of Phong Nha-Ke Bang National Park, Vietnam using a modified Karst Disturbance Index Methodology: Implications for Sustainable Tourism Leslie North, Jason Polk, Nguyet Vu Thi Minh, Tuan Tong Phuc, Vo Van Tri	373
The Geoheritage Significance Of Cliefden Caves, NSW, Australia Armstrong Osborne	374
Index of the sustainable use of karst environments Philip van Beynen	378
Sanitation And Right To Health: An Analysis Of Urban Solid Waste Disposal In The Karst Of Minas Gerais, Brazil Isabela Dalle Varela, Luiz Eduardo Panisset Travassos	379
 Other Topics	
Finspace Through the Ages Alkantana, Cahyo	381
A Verbal Dispute Between A Bat And A Partridge: A Satiric Allegorical Poem From The Medieval Period Konstantina Aretaki	382
Linked Data, the Semantic Web, and the Karst Information Portal Jason Boczar, George Veni	387
The PSS and the 16th year of the annual Philippine National Cave Congress. Eric Bontuyan	390
Caving Activities As A Support For The Analysis Of Natural And Anthropogenic Disasters Mario Parise	391
Managing WNS-related Increases in Bat-Human Contacts at Mammoth Cave National Park, KY, USA Rickard Stanley Toomey	396
Can the UIS also become a sports body and why should it? Arjan van Waardenburg	397
Restructuring the UIS Arjan van Waardenburg	399
Is in cave competition really unacceptable? Arjan van Waardenburg	401
Author Index	402

Karst and Caves in Carbonate Rocks, Salt and Gypsum

Nadia Aamoum

Abstract

As early as the 1930s, several explorers came to Morocco to explore the karst of the country. Among these explorers is Norbert Casteret, who explored the southern region of Taza. The Moroccan karst contains not only a large number of cavities, but also prehistoric riches and a notable biospeleology. At a time when water management is becoming an economic or even a geopolitical issue of primary importance for most countries of the world, it is time to become aware of the asset of knowledge of karst and their functioning in as major hydrographic reserves. The assessment of the reserves and the resulting water management can't be carried out accurately without an intimate knowledge of these substantial reservoirs constituted in the karst.

The second deepest cave in Morocco and the third longest cave in Africa is Gouffre Friouato, is located 20 km from the town of Taza Morocco. In 1934, Norbert Casteret, a Frenchman, reached the base of the scree at 146 meters depth. It is a circular aven with a depth of 271 m and extends underground for a length of 3500 meters. This length is defined by a siphon that limits the progression in the cave. French cavers tried to cross it in vain in the 1930s. A new attempt to cross this siphon will be of great value to this richness of the karst and possibly discover other links, perhaps to other caves?

In the High Atlas and located a few kilometers from the city of Agadir, Wintimdoine Cave is one of the most important caves in Africa and the largest reservoir of groundwater in the region. Four lakes succeed each other in the first part of the cavity. The water constitutes an exceptional tourist potential. The cave offers an economic interest and its development could constitute an added value for this valley and villages, as it will not only create employment, but also the development of local crafts and the sale of regional products. Moreover, it will contribute to limiting a rural exodus. Partly explored in the 1920s and 1950s by Moroccan, French and Spanish speleologists. The cave is now being investigated by a multidisciplinary expedition involving hydrogeologists, topographers, geologists, mountaineers and biologists with the support of the National Geographic Society.

(Abstract) **Desert Cave Studies In The Kingdom Of Saudi Arabia**

Mahmoud Ahmed Alshanti

Affiliation: Saudi Geological Survey

Abstract

Many of the caves in Saudi Arabia have been known for a long time by the local populations and used as sources of shelter and water. The first exploration started only about 20 years ago, followed by more scientifically planned and organized investigations by geologists from Saudi Geological Survey (SGS). Many explored caves, sinkholes and cavities are found in sedimentary rocks (mainly limestone, and dolomitic limestone areas). In addition to limestone cave exploration and studies in the Kingdom, 89,000 square kilometers of lava fields contain numerous lava tube caves.

Black Scorpion Cave is an example of the dissolving action of water on limestone sediments and has a sinkhole entrance leading to a horizontal tunnels with passages branching in east west direction with a gentle slope. It is formed in a sequence consisting mainly of chalky limestone rock overlain by white indurated limestone. Different shapes of speleothems appear on the cave walls.

Caves are more than a geological resource for the country. Saudi Arabia's caves were found to contain bones, artifacts and living creatures of interest to paleontologists, biologists and archeologists. Cave formations and sediments were found to contain important information for climatologists on the past weather patterns of the Arabian Peninsula and the process of desertification. A study on Show Caves demonstrated that Cave Tourism could be profitably carried out in the kingdom.

(Abstract) Desert Cave Studies In The Kingdom Of Saudi Arabia

Mahmoud Ahmed Al Shanti

Affiliation: Director Caves Explorations Section, Kingdom of Saudi Arabia Geological Survey

Abstract

Many of the caves in Saudi Arabia have been known for a long time by the local populations and used as sources of shelter and water. The first exploration started only about 20 years ago, followed by more scientifically planned and organized investigations by geologists from Saudi Geological Survey (SGS). Many explored caves, sinkholes and cavities are found in sedimentary rocks (mainly limestone, and dolomitic limestone areas). In addition to limestone cave exploration and studies in the Kingdom, 89,000 square kilometers of lava fields contain numerous lava tube caves.

Black Scorpion Cave is an example of the dissolving action of water on limestone sediments and has a sinkhole entrance leading to a horizontal tunnels with passages branching in east west direction with a gentle slope showing a sequence consisting mainly of chalky Limestone rock overlain by white Indurated limestone on the cave walls, Different shapes of speleothems appear on the cave walls.

Caves are more than a geological resource for the country. Saudi Arabia's caves were found to contain bones, artifacts and living creatures of interest to paleontologists, biologists and archeologists. Cave formations and sediments were found to contain important information for climatologists on the past weather patterns of the Arabian Peninsula and the process of desertification. A study on Show Caves demonstrated that Cave Tourism could be profitably carried out in the kingdom.

Keywords: explorations, caves, sinkholes, cavities, limestone, sediments, tunnels, Speleothemes, lava tube, bones, artifacts, tourism.



Figure 1. A selection of views of Saudi Arabian karst

A Karst Hydrogeologic Investigation to Support Risk Assessment at Patoka Dam, Indiana, USA.

Lee Anne Bledsoe¹, Chris Groves¹, Kenneth Henn², Jackie Rowe²

Affiliation: ¹ Department of Geography and Geology, Western Kentucky University, Bowling Green, Kentucky, USA

² United States Army Corps of Engineers, Louisville District, Louisville, Kentucky, USA

Abstract

Several dams throughout the United States have been built on karst terrains, where soluble limestone bedrock has been dissolved to form features such as caves, sinkholes, and underground rivers. In such karst regions, subsurface hydrology can play an integral role in the condition, operation, and safety of dams and should be considered during risk assessment. Patoka Dam, near Jasper, Indiana, is situated on a well-developed karst landscape/aquifer system and faces significant potential challenges. A 2008 risk analysis identified potential failure modes, one of which was abutment seepage and piping failure, identifying the dike as an area of concern. In response, this research focused on describing and quantifying the local subsurface hydrogeology so that potential seepage pathways in the area of the dike, and therefore potential failure modes, could be better understood, ultimately to support the 2015 US Army Corp of Engineers (USACE) dam safety risk assessment.

The groundwater flow investigation utilized multiple fluorescent tracer tests, analysis of water-table elevations, isopach mapping, and spring hydrograph analysis to better understand local groundwater hydrology. Dye-tracing results indicate that groundwater is bypassing the subsurface cut-off wall, adjacent to the dike, at flow rates as rapid as 10 to 15 meters per hour. The recharge area for Robert Hall Cave Spring (RHCS), a significant groundwater discharge point downstream from Patoka Dam, was delineated and the existence of a groundwater divide in the area of the dike confirmed. Spring hydrograph analysis indicates that spring discharge is primarily influenced by precipitation and is only minimally affected by lake pool elevation. In addition, potentiometric and isopach mapping of the Glen Dean Limestone allowed for identification of target areas for additional investigation.

In delineating the RHCS basin, with an important groundwater divide, reviewing potentiometric surface variability, site geology, and spring discharge as it relates to pool elevation, it could be concluded that groundwater flow through the dike embankment is diffuse compared to adjacent areas tested and therefore the likelihood and extent of groundwater pathways in the embankment may be decreased. Patoka Dam is rated 'low risk; marginally safe' following the 2015 risk assessment. While the hydrologic data appears to support the USACE's rating, it should be noted that karst landscapes are dynamic and all results and ratings should be viewed as a 'snapshot in time' rather than a description of a static system.

Keywords: karst hydrology, fluorescent dye tracing, dam risk assessment

1. Introduction

While much is known about the function of karst systems, in some situations aging infrastructure and new development can pose problems in karst areas, creating a need for additional research to address these challenges. Several dams throughout the United States are built on karst terrains (Henn, 2011). These structures face particular challenges with regard to potential failure modes created by the karstic environments within which they operate. Patoka Dam in southern Indiana represents a case where karst processes may impact the integrity and overall safety of the dam.

Patoka Dam was constructed in the Patoka River valley between 1972 and 1978 for flood reduction, water-supply storage, and recreation. The dam impounds the upper reaches of the Patoka River, a tributary of the Wabash River, creating Patoka Lake which covers approximately 3,561 hectares (USACE 2005). Patoka Dam consists of three main areas necessary for impoundment of the lake and continued operation as a flood reduction structure: the main dam, the spillway, and the dike (Figure 1). A concrete cut-off wall and grout curtain were also installed during construction to address groundwater. These structures as well as Robert Hall Cave Spring (RHCS) are shown in Figure 1.

Located in the Southern Hills and Lowlands physiographic region of south-central Indiana and more specifically the



Figure 1. Aerial View of Study Area

Crawford Upland, the study area is characterized by alternating units of limestone, sandstone, and shale of the Chesterian Series of the Mississippian System (Upper Carboniferous). The Glen Dean Limestone, the most probable area of seepage and therefore of greatest concern in this study, is present in the foundations of the dam, spillway, and dike structures. One weak point in particular is the area where the cut-off wall meets a concrete abutment called the 'fillet', constructed to

address a large solution feature, rather than the dike structure proper (Figure 1).

2. Methodology

2.1. Fluorescent Dye Tracing

Three phases of dye tracing that included a total of ten dye injections were conducted. According to USACE, the treatment of rock defects at the dike was not as robust as compared to the dam, creating a greater potential for leakage pathways to form and allow the migration of soils or sediment away from the dike, and therefore dye-injection locations were focused in this area. The injection locations included four excavated soil pits and two existing monitoring wells in the Glen Dean Limestone. Successful dye-injection locations are shown in Figure 2 along with the 1977 and 1996 traces conducted prior to this study.

Charcoal dye receptors were installed at a total of nine monitoring locations. Once a hydrologic connection between the Eosine injection location and RHCS 003 was confirmed in Phase I, duplicate tracer tests in Phase II and III were conducted to establish dye travel time and to better describe flow characteristics. Analysis of charcoal and water samples was conducted using a Shimadzu RF 5301 Scanning Spectrofluorometer and adhere to the Karst Groundwater Investigation Procedures (Crawford Hydrology Lab 2013) of Crawford Hydrology Laboratory (CHL).

2.2. Hydrogeologic Mapping

Potentiometric and isopach maps of the study area were developed based on monthly piezometer data and construction well logs provided by the USACE. Water-level elevation data came from twenty-two piezometers and well points that monitor groundwater levels within the Glen Dean Limestone. Forty of the sixty-six well logs reported vertical thickness of the Glen Dean Limestone or expressed the absence of the Glen Dean. Visual interpolation, guided by previous geologic mapping, was used for contouring.

2.3. Spring Hydrograph Analysis

In order to calculate mean dye travel times and describe potential relationships between lake pool elevation, precipitation, and RHCS discharge, continuous water-level measurements were taken at a fully contracted, 90° v-notch weir installed at RHCS via an Onset Hobo Water Level data logger. Discharge was then calculated based on water-level readings.

3. Results

3.1. Qualitative Dye Tracing

In Phase I, Eosine (EO), injected into a soil pit located between the dike and spillway and upstream of the concrete cut-off, was recovered four days post-injection at RHCS 003 (Figure 2). Fluorescein (FL) injected into a soil pit on the western edge of the dike, was not detected at any monitoring location despite the rapid infiltration of dye and flush water into the soil pit. Subsequent tracing in Phase III revealed that groundwater was traveling from the FL injection location to Patoka Pond Spring 002 and Wagner Spring 009 (Figure 2). It is assumed that the additional flush water and increased

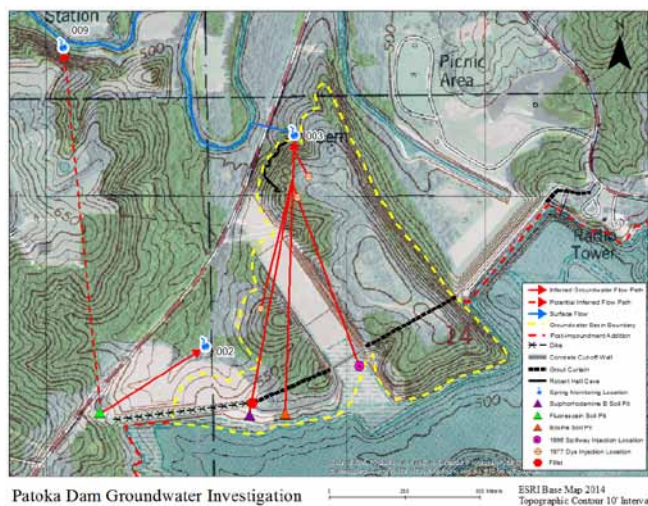


Figure 2. Inferred Groundwater Flow Paths and Basin Boundary

precipitation prior to dye injections created more favorable conditions for dye recovery in the Phase III traces. FL was recovered within 24 hours at Patoka Pond Spring 002 and within seven days at Wagner Spring 009 to the northwest. As background monitoring had not been conducted at this spring, results are shown as a potential flow path. Based on the similar pattern of long-term recovery (July 2014–February 2015) of FL at Wagner Spring 009 as seen in the EO traces at RHCS 003 and the presence of a groundwater divide between the two springs, it is likely that there is a connection to the injection location.

Phase II traces included injections into two wells located on the downstream dike embankment. Both of these wells, although screened in the Glen Dean Limestone, took less than one gallon per minute during capacity testing but were used due to the lack of other injection features on and in the immediate vicinity of the dike. Neither dye was detected during post-injection monitoring which was conducted for twelve months to account for possible laminar flow within the formation. Most likely, the dyes were stranded in the injection wells or were traveling through the diffuse flow portions of the aquifer too slowly to be detected. This could indicate slow, diffuse flow through the dike embankment, making soil and sediment migration from this area less likely.

During Phase III Sulphorhodamine B (SRB) was injected into a soil pit west of the cut-off wall and the 'filet', located on the upstream toe of the dike and a repeat of the Phase I EO trace was conducted. Both dyes were detected at RHCS via charcoal receptor collected seven days post-injection (Figure 2).

From the combined results of all qualitative tracing, inferred groundwater flow paths and the RHCS basin boundary were determined. The flow paths shown in Figure 2 represent connections between the injection locations and monitoring locations and are not meant to represent actual flow paths. The likely pre-dam groundwater-basin boundary for Robert Hall Cave Spring (RHCS) is shown as a yellow dashed line in Figure 2. This boundary was informed by geologic maps of the Glen Dean Limestone and the multiple tracer tests that show a groundwater divide in the area of the dike and represents where the basin boundary was located prior to impoundment of the lake. The boundary roughly follows the 535 foot topographic contour where it is estimated that the

Glen Dean would outcrop on the hillside east of the dike, the original Patoka River valley wall. The boundary then follows the 545 foot contour on the ridge east of the spillway as the Glen Dean is dipping westward and would thus outcrop at a slightly higher elevation to the east. The red dashed line represents the current, post-impoundment addition to the basin boundary (Figure 2). Since lake pool elevation is now at or above the elevation of the Glen Dean Limestone, Patoka Lake is now considered a secondary contributor to the drainage basin for RHCS, although the amount of the contribution of lake water to the groundwater system is unknown.

3.2. Quantitative Dye Tracing

Once a hydrologic connection between the EO injection location and RHCS was confirmed in Phase I, additional tracer tests were conducted to establish dye travel time and to better describe flow characteristics. Based on initial recovery of both EO and SRB, 86 hours and 78.5 hours post-injection respectively, dye travel time from the area of the injection locations to RHCS can be as rapid as 10-15 meters per hour. The breakthrough curve for EO revealed multiple peaks with the highest concentration observed at 238 hours post injection. The SRB breakthrough curve exhibited a more typical dye breakthrough curve with a relatively quick increase to peak concentration within 232 hours and a long recession. Neither EO nor SRB returned to background concentrations before sampling concluded on July 29th, 28 days after dye injection.

While initial recovery of both dyes was within a few days, the center of the dye mass for EO and SRB, which marks the mean travel time of the dye, arrived at RHCS at approximately 358 hours and 264.5 hours post-injection, respectively. Mean velocity based on these time periods is 2.4 meters per hour for the EO trace and 3.3 meters per hour for the SRB trace. These calculations are based on a straight-line distances of 881 meters for the EO trace and 899 meters for the SRB trace and discharge measurements taken at RHCS. Straight-line distances were determined via GIS mapping and represent the shortest possible flow path.

3.3. Hydrogeologic Mapping

The potentiometric surface map indicates that groundwater is generally traveling from south to north from the lake toward the downstream part of the Patoka River, approximately perpendicular to the structural dip of the Glen Dean Limestone. Variation of the potentiometric surface as it is influenced by lake pool elevation was also evaluated by calculating the differences between water-level data at each of the water-level monitoring locations from when the highest pool elevation of the study period was observed and water-level data from when the lowest pool elevation was observed. The piezometers and wells upstream from the grout curtain showed the greatest change in potentiometric surface elevation in regard to increase in pool elevation with all points downstream increasing zero to one meter. Most interesting in the potentiometric surface is the presence of a trough east of the dike, primarily in the area of the spillway, which could be interpreted as area of increased groundwater flow.

The isopach map of the study area shows that the Glen Dean Limestone is thickest, approximately seven to nine meters, in both ridges between the dam and the dike and thins towards

the west until its erosional edge in the valley where the dike is now located. Hazards such as dissolution and collapse features associated with karst development are more likely to occur where the Glen Dean Limestone is the thickest.

3.4. Spring Hydrograph Analysis

The spring hydrograph in general shows higher flow from April through mid-June 2014 compared to the decreased water levels observed from July 2014 to February 2015. Water levels then increased again in early March 2015 and discharge stayed above 0.006 cubic meters per second (cms) for the duration of the monitoring period that ended May 11, 2015. In general, discharge remains above 0.007 cms during the spring months, with occasional decreases to a minimum of 0.004 cms, and then decreases to around 0.001 cms during summer, fall, and winter with increases following rainfall events throughout the year. Low flow from July to September most likely represents baseflow, the groundwater contribution to discharge, for RHCS. Water level measurements recorded at RHCS appear to respond primarily to local precipitation events. However, since pool elevation increases with precipitation it is difficult to distinguish exactly how pool elevation may be influencing flow conditions at RHCS. Spring hydrograph data and potentiometric surface mapping appear to support minimal influence of lake pool elevation on RHCS during this study.

4. Conclusions

Utilizing potentiometric surface mapping and multiple fluorescent tracer tests, groundwater flow directions and velocities within the RHCS drainage basin were identified and confirm that groundwater is generally traveling north, with some amount bypassing subsurface hydraulic control structures to emerge at RHCS 003, Dike Pond Spring 002, and/or Wagner Spring 009. In addition, comparison and analysis of flow rates, dye breakthrough curves, and the RHCS hydrograph, have provided a clearer understanding of the local hydrogeology.

Flow rates determined from quantitative tracing to RHCS appear much slower when compared to the 1996 dye trace (10-15 meters per hour versus 158 meters per hour) that confirmed a connection between a sinkhole in the spillway and RHCS, though all are fast enough to suggest that solutionally enlarged flow paths in the Glen Dean Limestone influence groundwater flow. Dye from all successful traces was injected into soil pits above or into the Mansfield sandstone. This comparison could potentially indicate that the intact Mansfield sandstone over most of the study area, with the exception of the spillway, along with the grout curtain and cut-off wall are inhibiting groundwater movement from the areas where the dye injections were completed at the lake pool elevations observed during the traces. If considering mean flow velocities, 2.4-3.3 meters per hour, the difference between the 1996 spillway trace and traces completed in this study is even greater. Also to be considered is the fact that dye concentrations did not return to background levels during quantitative sampling and therefore mean travel times (based on arrival of the centroid of the dye breakthrough curve) could be even slower. Complicating this conclusion however is the fact that straight-line distances were used in all velocity calculations

as exact flow path lengths are unknown but are almost certainly longer due to the likely circuitous geometry of the flow paths. Based on the comparison of Phase III EO and SRB breakthrough curves, calculated flow rates, and site geology, clearly a combination of diffuse and conduit flow are occurring within the drainage basin.

The dye-trace results also confirmed a groundwater divide in the vicinity of the dike and allowed for an estimated drainage-basin boundary for the recharge area of RHCS. Geologic mapping, which shows the absence of the Glen Dean Limestone downstream of the dike, provided information necessary for a more confident estimation of the RHCS recharge area which includes some amount of leakage from Patoka Lake through the subsurface control structures. However, based on spring hydrograph analysis and potentiometric surface variability with pool elevation, it appears that the lake, though it influences flow direction and hydraulic gradient, is a minor contributor to the amount of flow at RHCS. In this case, the lake should be considered a secondary region of the drainage basin in that it is hydrologically connected to RHCS but drainage appears to be largely constrained by subsurface hydraulic control structures.

Potentiometric and isopach mapping reveal that the central to southern portion of the spillway may be an area for further monitoring and assessment. While significant voids and rock defects were encountered during spillway construction, sinkhole development has continued post-construction as the Mansfield sandstone that originally slowed recharge into the Glen Dean Limestone was removed. This potential for further karst development is also indicated by the presence of a potentiometric trough and vertical thickness of the Glen Dean Limestone of six to nine meters. The 1996 dye trace flow rates, previously discussed, also support this conclusion. However it appears that the greatest potential for development of seepage pathways and sediment/soil migration in this particular area occurs primarily during high pool events when lake pool elevation is above that of the spillway and cut-off wall.

Overall results identify areas where flow paths are most likely and quantify the rates at which this is occurring. In delineating the RHCS basin, with an important groundwater divide, reviewing potentiometric surface variability, and spring discharge as it relates to pool elevation, it could be concluded that groundwater flow through the dike is diffuse and/or minimal compared to adjacent areas, and therefore the likelihood and extent of groundwater pathways may be decreased. However, it should be noted that karst landscapes are dynamic and all results should be viewed as a 'snapshot in time' rather than a description of a static system. The research as presented is intended to assist managers at Patoka Dam in additional intrusive and expensive geologic investigations as well as increase certainty in the risk assessment of potential failure modes related to the karst environment in which the dam operates.

References

Crawford Hydrology Laboratory. 2013. *Karst Groundwater Investigation Procedures*. Accessed April 15, 2014, online at: http://dyetracing.com/?page_id=335

Henn, K. E. 2011. Karst impacts on dam safety risk assessment in the US Army Corps of Engineers. *Proceedings of the 2011 International Conference on Karst Hydrogeology and Ecosystems*. Bowling Green, Kentucky: Western Kentucky University, 94. Accessed August 27, 2015, online at: http://scholarcommons.usf.edu/cgi/viewcontent.cgi?article=1003&context=tles_pub

United States Army Corps of Engineers, Louisville District. 2005. *Patoka Lake: Benefits*. Accessed April 16, 2014, online at: <http://155.80.93.250/patl/article.asp?id=183&MyCategory=1>

Shallow caves and blowholes on the Nullarbor Plain, Australia – Flank margin caves on a low gradient limestone platform

Shannon Burnett, Susan White, John Webb

Affiliation: Environmental Geoscience, Latrobe University Bundoora Victoria 3068

Abstract

The southern Australian Nullarbor Plain is an extensive limestone platform with relatively few large caves for its size. It contains thousands of blowholes, sub-circular vertical shafts up to 1–2 m in diameter, which often connect to similar-sized sub-horizontal passages. These shallow caves are relict phreatic features; their entrances (blowholes) were opened as the land surface was lowered by denudation. Ongoing systematic surveys over the past 16 years have shown that blowholes are concentrated in a 25–30 km-wide band located ~75 km inland from the better-known band of caves closer to the coast. Other such bands may be present further north but exploration and documentation of this area has been hampered by the difficulties of access.

New data on blowhole distribution confirms that the main band formed along the Late Miocene (~6 Ma) shoreline across the Nullarbor, as flank margin caves on a low gradient limestone platform. Cave development ceased when the sea retreated rapidly in the Late Miocene–Early Pliocene due to a period of tilting and uplift. The band of flank margin caves represents a zone of high permeability and substantial porosity within the Nullarbor platform.

Keywords:

1. Introduction

The Nullarbor Plain (Fig. 1) is Australia's largest karst region, famous for its low relief (<10 m over most of the plain), lack of vegetation and lack of surface water. Rainfall, ranging from 400 mm along the coast to <150 mm in the north, is much less than potential evaporation (2000–3000 mm; Fig. 1). Small trees (mallee eucalypts and myalls) grow along the coast, but the vast majority of the Nullarbor Plain is treeless. The Nullarbor Plain has a poorly developed surface karst landscape and contains only ~100 caves with significant passage lengths and depths up to 150m below the surface of the plain, and ~150 collapse dolines, mostly in a coastal strip of limestone 60 km wide. This gives a cave porosity of only ~0.0002% (Webb and James, 2006), very low by world standards (Worthington et al., 2000). The most common karst features are blowholes, thousands of sub-circular smooth-walled vertical tubes typically several metres deep with elliptic to circular openings tens of cm to 1–2 m in diameter; they often connect to shallow caves with small passages which may exhibit cupolas extending to within a few metres of the surface (Lowry and Jennings, 1974; Doerr et al., 2011; Burnett et al., 2013). They generally lack speleothems, but small stalagmites have been dated as predominantly Pliocene in age (2.5–4.0 Ma), although some formed in the Late Miocene (5.5 Ma) (Woodhead et al., 2006, Lipar and Ferk, 2015, Sniderman et al., 2016).

Ongoing systematic surveys of the southern part of the Nullarbor Plain have enabled the distribution of the blowholes and associated shallow caves to be mapped in detail. The aim of this study is to use the newly available distribution data to further investigate the formation of shallow caves and blowholes on the Nullarbor Plain.

2. Geology and geomorphology

Three units of flat-lying Eocene–Miocene limestone were deposited within the Eucla Basin: in stratigraphic order, these are the Middle–Late Eocene Wilson Bluff Limestone, separated by a disconformity from the Late Oligocene to Early Miocene Abrakurrie Limestone, overlain by the Middle Mio-

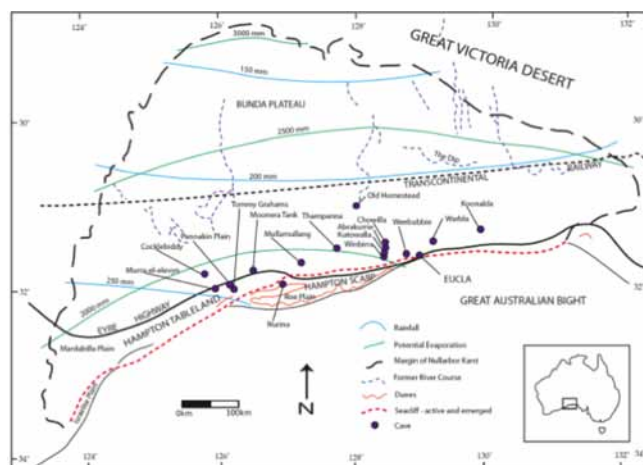


Figure 1. Map of the Nullarbor Plain, showing rainfall and potential evaporation, and major features (after James, 1992, Burnett et al 2013).

cene Nullarbor Limestone (Lowry and Jennings, 1974; James and Bone, 1992; Benbow et al., 1995; O'Connell et al., 2012). Late Miocene–Early Pliocene tilting and uplift, together with a global lowering of sea level, resulted in marine erosion of the southern margin of the Nullarbor Plain, forming the Roe and Israelite Plains (Fig. 1). Subaerial exposure of the surface of the Nullarbor Plain has resulted in very slow denudation of the Nullarbor Limestone.

The relatively flat surface of the Nullarbor slopes gently seaward and is tilted towards the south-east (Davey et al., 1992; Webb and James, 2006). The coastline consists of vertical cliffs unbroken for some hundreds of kilometres, except along the Roe and Israelite Plains (Fig. 1) where the cliffs are inland and have degraded to bluffs. The landscape surface exhibits an undulating pattern of more or less straight bedrock ridges and swales, but has little surface karst development.

3. Methods

Detailed systematic surveys of selected areas of the Nullarbor were carried out between 2000 and 2016 (except 2005) during the annual 3-week expeditions organised by the Victorian Speleological Association Inc. (VSA) and others (White et al 2017, this volume). A small one-seater ultra-light aircraft was used to systematically search a specific area each year, recording the locations of potential features of interest, which were then verified by ground-based parties. Each feature was issued with an official number in accordance with the Australian Speleological Federation Inc. Cave and Karst Numbering Code (2006). The VSA intensive systematic surveys have covered an area of ~20,000 km² and recorded ~over 2000 karst features. This data was combined with another 3000 sites gathered from the Oz-karst database. All site locations were imported into the Global Mapper 18 program using the GDA94 datum and geographic latitude/longitude projection, and overlain onto LandSat 8 images and 3 second topographic DEM images.

4. Results and discussion

4.1. Blowhole and shallow cave distribution

Plotting locations of all known shallow caves and blowholes (Fig. 2) showed that they are scattered over the entire plain, but two high concentration bands are evident, one close to the coast and one running west-southwest to east-northeast (Fig. 2), ~70–100 km inland. The coastal band extends ~60 km inland from the coast (although most features are within 25 km of the coastal scarp), and also contains almost all the deep caves.

Small caves with flank margin characteristics are reported perched about 50m above sea level on the current sea cliffs (Milner, 2017, this volume), and have been exposed by the retreat of the cliffs. They formed when sea-level was relatively higher (i.e. prior to uplift). Interestingly no entrances have been found on the surface above them.

The inland band of caves contains only a few large caves, e.g. Old Homestead Cave (5N83), however a few more have been found since 2012. It mainly contains blowholes and small caves. They have a both a greater cave density and cave porosity than for the coastal band (Burnett et al 2013), considerably greater than indicated by the blowhole density, because strong air draughts that blow from many of the blowholes indicate that they connect to extensive underground systems of inaccessible small passages. The inland band has been extended further east since 2012 and probably extends to the west of its mapped extent, but confirmation awaits detailed surveys in this area. Northwards of the band, there is a rapid decrease in blowhole concentration within the surveyed areas (Fig. 2). However, further exploration is being undertaken just north of the Trans Continental Railway and there is some evidence of another band there (C. Brown, pers comm 2016).

In the searched areas, there is an average density of 0.10 blowholes per km² (1/9.9 km²). Applying this figure to the ~200,000 km² area of the Nullarbor, assuming the same density across the plain, gives an estimated ~20,000 blowholes, but the number is probably less because the density appears to be less in the northern part of the plain.

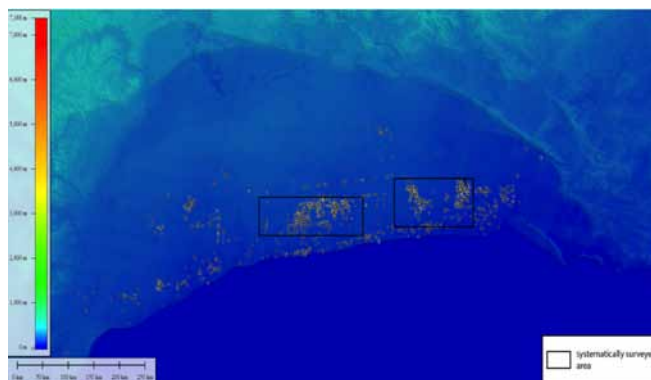


Figure 2. Overall distribution of known shallow caves and blowholes across the entire Nullarbor Plain (after Burnett et al., 2013)

4.2. Blowhole and shallow cave formation

Doerr et al. (2011) postulated that blowholes formed above existing shallow caves where a cupola broke through to the surface as the land surface was lowered by denudation. This accounts for the typical truncated-dome shape of blowhole entrances. Erosion of the surface of the Nullarbor Plain has predominantly occurred as relatively uniform down-wasting over the last ~15 million years (Lowry and Jennings, 1974; Webb and James, 2006).

The cupolas common in the ceilings of the shallow caves are typical phreatic cave features, and most likely formed by vertical convective flow within water-filled passages (Doerr et al., 2011). Therefore, the inland band of shallow caves represents a zone of phreatic caves that formed along the coastline in the Late Miocene (~6 Ma; Hou et al., 2008), when there was a eustatic stillstand (Haq et al., 1987).

The caves concentrated in a band because they developed when sea level was relatively stable, in a zone of enhanced dissolution at the seaward margin of the freshwater lens, i.e., they are flank margin caves that have developed on a low gradient limestone platform (Burnett et al 2013). They lack the larger chambers that characterise some flank margin caves (Mylroie and Carew, 2000), probably because the very low gradient of the water table on the Nullarbor meant that the seaward margin of the freshwater lens was relatively thin.

Flank margin speleogenesis appears to have occurred during sea level still stands and probably occurred at least 3 times, to form the poorly documented band north of the Trans Continental Railway, the main blowhole band and the band on the current coastal cliffs. The main band formed along the Late Miocene shoreline and was drained by 5.5 Ma (the oldest speleothem date from the caves).

References

- Benbow, M.C., Alley, N.F., Callen, R.A., Greenwood, D.R., 1995. Geological history and palaeoclimate. In: Drexel, J.F., Preiss, W.V. (Eds.), *The Geology of South Australia. The Phanerozoic: Geological Survey of South Australia Bulletin* **54**, 2. Geological Survey of South Australia, Adelaide, 208–218.
- Burnett, S., Webb, J.A., White, S., 2013. Shallow caves and blowholes on the Nullarbor Plain, Australia — Flank margin caves on a low gradient limestone platform, *Geomorphology* **201**, 246–253.

- Davey, A.G., Gray, M.R., Grimes, K.G., Hamilton-Smith, E., James, J.M., Spate, A.P., 1992. *World Heritage Significance of Karst and Other Landforms in the Nullarbor Region. Report*. Commonwealth of Australia: Department of the Arts, Sport, the Environment and Territories, Canberra.
- Doerr, S.H., Davies, R.R., Lewis, A., Pilkington, G., Webb, J.A., Ackroyd, P.J., Bodger, O., 2011. Origin and karst geomorphological significance of the enigmatic Australian Nullarbor Plain 'blowholes'. *Earth Surface Processes and Landforms* **37**, 253–261.
- Haq, B.U., Hardenbol, J., Vail, P.R., 1987. The chronology of fluctuating sea level since the Jurassic. *Science* **235**, 1156–1167.
- Hou, B., Frakes, L.A., Sandiford, M., Worrall, L., Keeling, J., Alley, N.F., 2008. Cenozoic Eucla Basin and associated palaeovalleys, southern Australia — climatic and tectonic influences on landscape evolution, sedimentation and heavy mineral accumulation. *Sedimentary Geology* **203**, 112–130.
- James, J.M., 1992. Corrosion par mélange des eaux dans les grottes de la Plaine de Nullarbor. In: Salomon, J.N., Marie, R. (Eds.), *Karst et évolutions climatiques*. Presses Universitaires de Bordeaux, Bordeaux, France, 333–348.
- James, N.P., Bone, Y., 1992. Synsedimentary cemented calcarenite layers in Oligo-Miocene cool-water shelf limestones, Eucla Platform, southern Australia. *Journal of Sedimentary Petrology* **62**, 860–872.
- Lowry, D.C., Jennings, J.N., 1974. The Nullarbor karst Australia. *Zeitschrift für Geomorphologie* **18**, 35–81.
- Mylroie, J.E., Carew, J.L., 2000. Speleogenesis in coastal and oceanic settings. In: Klimchouk, A.B., Ford, D.C., Palmer, A.N., Dreybrodt, W. (Eds.), *Speleogenesis: Evolution of Karst Aquifers*. National Speleological Society, Huntsville, Alabama, pp. 226–233.
- O'Connell, L. G., James, N. P., & Bone, Y. 2012. The Miocene Nullarbor Limestone, southern Australia; deposition on a vast subtropical epeiric platform. *Sedimentary Geology*, **253**, 1-16.
- Sniderman, J. K., Woodhead, J. D., Hellstrom, J., Jordan, G. J., Drysdale, R. N., Tyler, J. J., & Porch, N. (2016). Pliocene reversal of late Neogene aridification. *Proceedings of the National Academy of Sciences*, **113**(8), 1999-2004.
- Webb, J.A., James, J.M., 2006. Karst evolution of the Nullarbor Plain, Australia. In: Harmon, R.S., Wicks, C. (Eds.), *Perspectives on Karst Geomorphology, Hydrology, and Geochemistry — A Tribute Volume to Derek C. Ford and William B. White*. Geological Society of America Special Paper, 404. Geological Society of America, Boulder, Colorado, pp. 65–78.
- Woodhead, J., Hellstrom, J., Maas, R., Drysdale, R., Zanchetta, G., Devine, P., Taylor, E., 2006. U–Pb geochronology of speleothems by MC–ICPMS. *Quaternary Geochronology* **1**, 208–221.
- Worthington, S.R.H., Ford, D.C., Beddows, P.A., 2000. Porosity and permeability enhancement in unconfined carbonate aquifers as a result of solution. In: Klimchouk, A.B., Ford, D.C., Palmer, A.N., Dreybrodt, W. (Eds.), *Speleogenesis: Evolution of karst Aquifers*. National Speleological Society, Huntsville, Alabama, pp. 463–472.

(Abstract) **Environmental Vulnerability At The Contact Karst Of Monjolos And The Southern Espinhaço Ridge, Minas Gerais, Brazil**

Leandro Cosme Oliveira Couto¹, Luiz Eduardo Panisset Travassos²

Affiliation: ¹Geographer, student at the Graduate Program in Geography - Pontifical Catholic University of Minas Gerais (PUC Minas), Brazil. Scholarship provided by CAPES. leandro.cosme@gmail.com

²Doctor in Karstology. Researcher and professor at the Graduate Program in Geography - Pontifical Catholic University of Minas Gerais (PUC Minas), Brazil. luizepanisset@gmail.com

Abstract

With 580,000 square kilometers, the State of Minas Gerais, Brazil, has approximately 29,000 sq. km of carbonate rocks. Many of such areas face environmental problems and this research aims to highlight the geocological dynamics in the contact landscape between the karst of Monjolos and the Southern Espinhaço Ridge, in Minas Gerais, Brazil. Due to its location, the area is an excellent example of a contact karst in southeastern Brazil. By elaborating a geocological profile or transect, three models were applied: 1) *morphodynamics*; 2) *natural vulnerability to soil loss*, and 3) *natural and environmental vulnerability*. Results showed that the Karst of Monjolos, developed in limestone and marble, is a very fragile geosystem regarding environmental impacts being morphodynamically unstable, highly naturally susceptible to soil loss and present noticeable natural and environmental vulnerabilities. In the other hand, the Espinhaço ridge is a more resistant geosystem due to the geological substrate of quartzite, with more stable morphodynamics and an intermediate natural susceptibility to soil loss. However, vegetation cover is decisive regarding environmental fragility. Thus, protective policies should be taken in order to prevent or lower environmental degradation in the region.

Keywords: Environmental vulnerability; Karst; Monjolos; Espinhaço ridge; Minas Gerais; Brazil

The southernmost authigenic karst plateau of the Levant

Amos Frumkin, Daniel Ben-Tov, Vladimir Buslov, Boaz Langford, Eliyahu Valdman, Shemesh Yaaran

Affiliation: Cave Research Center, Institute of Earth Sciences, The Hebrew University of Jerusalem, Israel 91904

Abstract

Karst plateaus with closed depressions, subterranean drainage, vadose shafts and other karst features are common in the north- and north-east Mediterranean regions, but absent in the desert belt of the south Mediterranean. The Ofra karst basin, located in the central ridge of Israel, is the southernmost karst plateau in the Levant. Tens of caves, dolines and karren fields stand in sharp contrast with the nearby Judean Desert. Developed in a plateau of Cenomanian dolomitic limestone, most caves are active vadose shaft systems, up to 93 m deep. Some cut into ancient phreatic systems with 3D development. Water flows in the caves during winter storms. Laminar sub-critical film flow of vadose water is dominant along shaft walls, developing from the epikarst downward. Concentrated flow occurs locally draining small catchments of terra-rossa soil covered karst surfaces. Remains of unroofed shafts indicate karstification over long periods of time. The occurrence of this well-developed authigenic karst close to the desert border suggests using similar relict and paleokarst plateaus as paleoclimatic indicators for delineating the extent of humid conditions in the past.

Keywords: vadose caves, Mediterranean karst, climate constraint, vadose shaft

1. Introduction

One of the most intriguing questions in karst geomorphology is the variation with climate. Climate (particularly precipitation) impact on denudation rates is generally well established, but karst landform variation with climate is complicated due to other effects, such as geology, which obscure the climatic effects (Frumkin 2013a). Daoxian (2013) suggested to overcome this problem, defining each environmental setting by its typical group of landforms, and introducing the karst feature complex concept. He defined this concept as a group of karst features, including surface forms and subsurface forms, as well as dissolutional forms and depositional forms, all of which developed under a similar environmental background. In this way he avoids the confusion of isomorphism (similar features that may result from different processes). By introducing geological modifications into the general concept, the group of features defining a climatic regime is robust enough also to overcome geologic variation.

The East Mediterranean karst plateaus includes features such as dolines and karren fields on the surface, and well-developed vadose caves with shafts and sub-horizontal vadose canyons in the sub-surface. Here we attempt to define the driest conditions which would still support such a karst plateau to develop. For this we discuss the southernmost well-developed authigenic karst plateau of the Levant at Ofra, Israel (Frumkin, 1993).

2. Environmental conditions

The humid northern fringe of the East Mediterranean basin demonstrates well-developed karst plateaus, while the southern East Mediterranean lacks such features, due to the arid climate of the Sahara desert belt. The transition between these climatic regimes occurs in the southern Levant, and is well represented in Ofra. Twenty km to the south of Ofra the climate still sustained karstification during the Holocene, (Frumkin et al. 2000; Frumkin 2013b), but the surface karst morphology is less developed, with hardly any dolines. Within a few km to the SE the semi-arid belt has only slightly active karst features, followed by the desert belt with hardly



Figure 1. Study area on a precipitation map (inches) of the east Mediterranean region.

any active karstification of carbonate rocks during the dry Holocene (Lisker et al. 2010; Vaks et al. 2003, 2006).

The Ofra karst plateau is located on the backbone of the central mountain range of Israel, 20 km north of Jerusalem (Fig. 1). Annual mean precipitation is 500 mm (measured locally from 2000 to 2016), concentrated mainly in the winter, as rainfall and rare snowfall. Bedrock is Cenomanian dolomitic limestone of the 160 m thick Amminadav Formation. The carbonate rock is massive at the upper part of the formation, becoming well-bedded to laminar at the lower part. The overlying and underlying formations are rich in chalk and marls, without karst features.

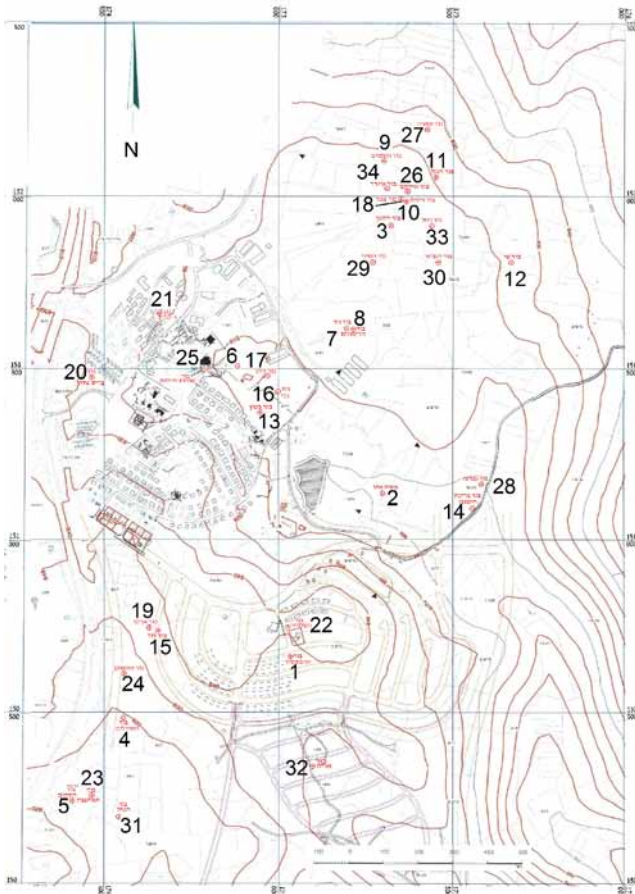


Figure 2. Distribution of caves (numbered) on a topographic map of Ofra karst. Coordinates are given in Israel Grid and contours are in m.

3. The karst system

The studied part of the Ofra karst plateau is 2.3X1.1 km large (Fig. 2), within a larger karst basin whose area is 5 km². (Frumkin 1993). It demonstrates the entire set of features of active epigenetic karstification, including dolines, karren fields, sinking streams, as well as vadose caves with vertical shafts and short sub-horizontal passages (Fig. 3). The deeper dolines are associated with collapse or subsidence of epikarstic decomposed bedrock above vadose shafts (Fig. 4).

This karst plateau is active during the presently dry Holocene, as indicated by aggressive water with increasing solutes along the flow route.

Thirty four vadose caves are known (Figures 2, 5). They consist typically of series of vertical shafts with short sub-horizontal, canyon-like sections (Fig. 6), reaching maximal depth of 93 m. The caves include active dissolutional features, such as scallops, as well as speleothems, indicating various types of water and changes in aggressiveness. In one case (cave 26) the vadose cave clearly dissects a maze cave, probably of hypogenic origin. Other cases of ancient phreatic or hypogenic cavities are less distinctive.

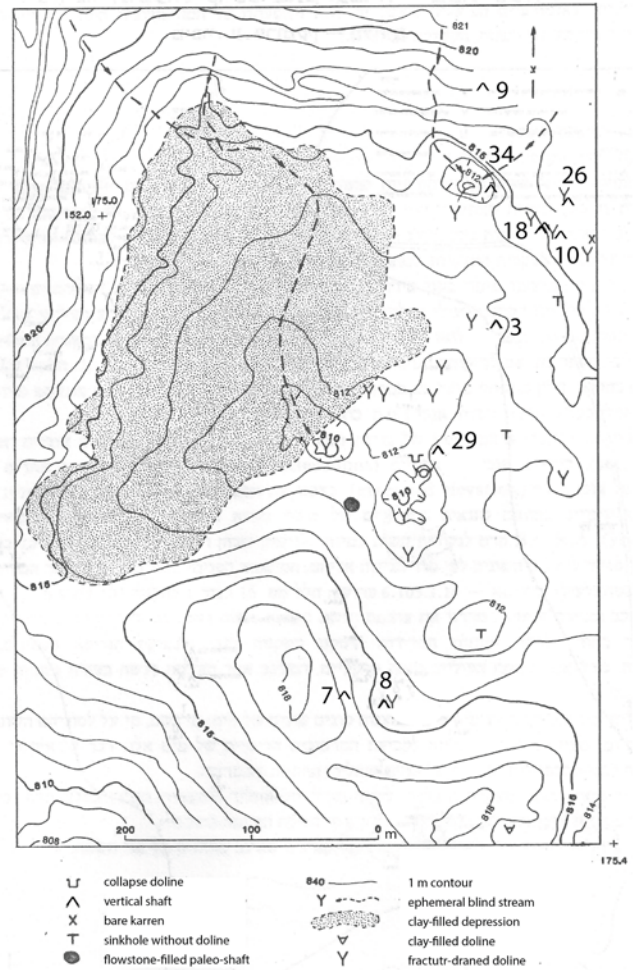


Figure 3. Karst features in the northern part of Ofra plateau.

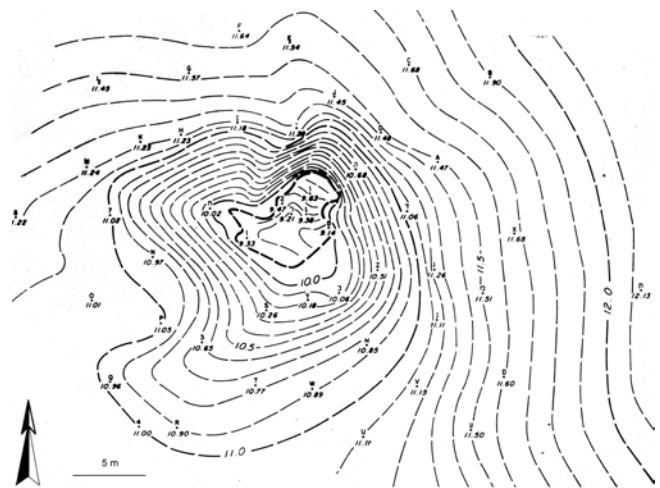


Figure 4. Relief of a sample doline (over cave 29) formed by epikarst subsidence into a vadose shaft. Contour interval is 10 cm.

4. Conclusion

The studied southernmost authigenic karst plateau of the Levant demonstrates a karst feature complex which is basically similar to other Mediterranean karst plateaus. The local environment indicates that such karst plateaus can develop under relatively dry conditions of winter rainfall amounting to 500 mm per year.

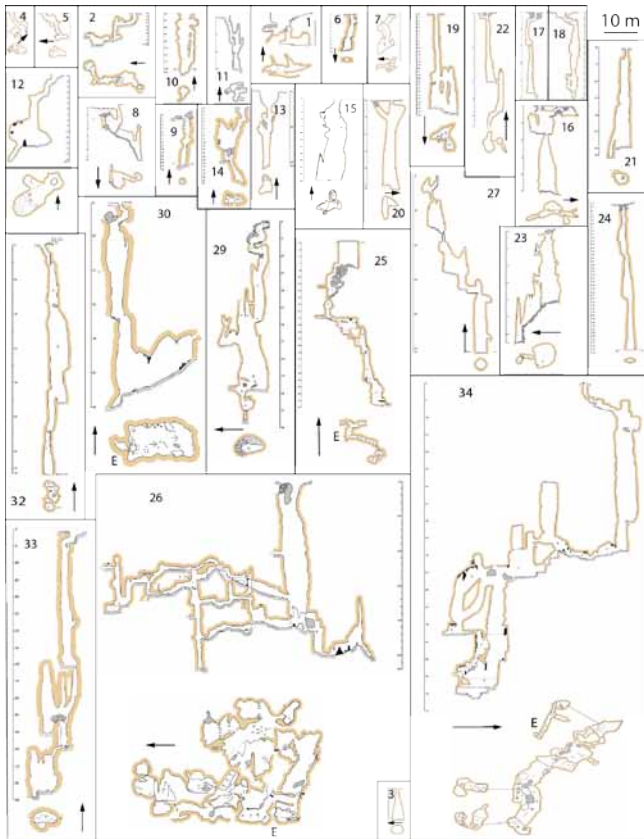


Figure 5. Profiles and horizontal sections of caves at Ofra karst plateau.

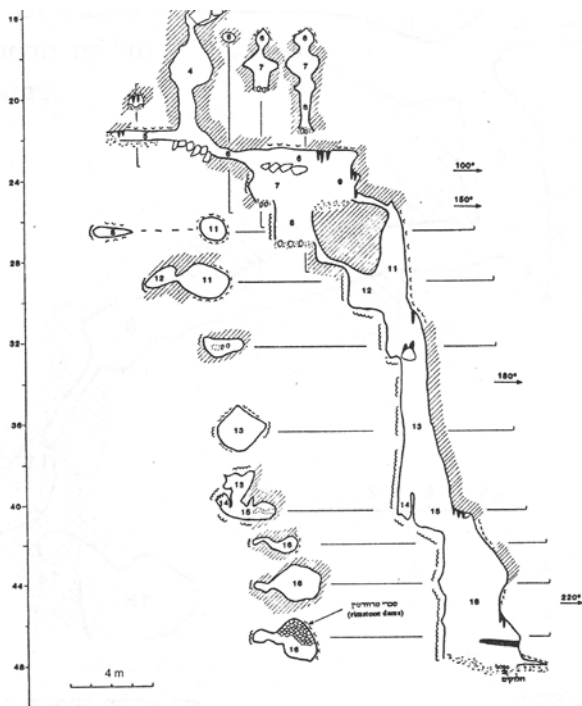


Figure 6. Enlarged profile and horizontal sections showing detailed morphology of cave 25.

Table 1.

Num	Cave name	Depth [m]	Length [m]
1	Haftaot	7	21
2	Achu	9.5	26
3	Katan	9	8
4	Sandalim	~7.5	??
5	Satum	8	15
6	Caravilla	11	11
7	Nir	12.5	28.5
8	Rimonim	15	30
9	Shfanim	16	16
10	Zikit	17	22
11	Naal	18	19
12	Shay	20	26
13	Beton	21	21
14	Brechot Chimtzun	22	23
15	David	24	34
16	Gabi	25	31
17	Biuv	25	27
18	Tzemed	25.3	33
19	Arcko	30	32
20	Beit Sefer Sadeh	26	28
21	Kalab	32	34
22	Shluha	33	36
23	Machtzeva	33	61
24	Meuban	43	43
25	Morot Hayalot	48	76
26	Achikam	50	457
27	Ofra	51	65
28	Nof Amona	~53	??
29	Sinee	59	68
30	Navie	60	104
31	Nachal	~60	??
32	Arieh	66	80
33	Rachel	79	108
34	Uzrar	93	250

References

- Daoxian Y, 2003. Variations of Karst Geomorphology over Geoclimatic Gradients. in: Frumkin A, volume ed., Shroder J, ed. in chief, *Treatise in Geomorphology*, vol. 6, pp. 319-326. San Diego, Elsevier, Academic Press.
- Frumkin A, Ford DC, and Schwarcz HP, 2000. Paleoclimate and vegetation of the last glacial cycles in Jerusalem from a speleothem record: *Global Biogeochemical Cycles*, v. 14, 3, 863-870.
- Frumkin A, 1993. Karst origin of the upper erosion surface in the Northern Judean Mountains, Israel: *Israel Journal of Earth Sciences*, v. 41, 169-176.
- Frumkin A, 2013a. New Developments of Karst Geomorphology Concepts. in: Frumkin A, volume ed., Shroder J, ed. in chief, *Treatise in Geomorphology*, vol. 6, pp. 1-13. San Diego, Elsevier, Academic Press.
- Frumkin A, 2013b. Caves and karst hydrogeology of Jerusalem, Israel. In: Filippi M, and Bosak P, eds.: *Proceedings of the 16th International Congress of Speleology, Brno*: Vol. 3: pp. 60-65
- Lisker S, Vaks A, Bar-Matthews M, Porat R, and Frumkin A, 2010. Late Pleistocene palaeoclimatic and palaeoenvironmental reconstruction of the Dead Sea area (Israel) based on speleothems and cave stromatolites. *Quaternary Science Reviews* 29, 1201–1211.
- Vaks A, Bar-Matthews M, Ayalon A, Schilman B, Gilmour M, Hawkesworth CJ, Frumkin A, Kaufman A, and Matthews A, 2003. Paleoclimate reconstruction based on the timing of speleothem growth, oxygen and carbon isotope composition from a cave located in the rain shadow in Israel: *Quaternary Research*, v. 59, 182-193.
- Vaks A, Bar-Matthews M, Ayalon A, Matthews A, Frumkin A, Dayan, Halicz L, Almogi-Labin A, and Schilman B, 2006. Paleoclimate and location of the border between Mediterranean climate region and the Saharo–Arabian Desert as revealed by speleothems from the northern Negev Desert, Israel: *Earth and Planetary Science Letters*, 249, 384–399.

Hypogenic caves in southern Levant deserts

Amos Frumkin, Boaz Langford, Sorin Lisker

Affiliation: Cave Research Center, Institute of Earth Sciences, The Hebrew University of Jerusalem, Israel 91904

Keywords: rising water, maze caves, desert karst, sulfuric acid, confined speleogenesis

The Judean Desert, and to a lesser degree the northern Negev, are the major provinces of maze caves in the southern Levant. The cave morphology, setting, and sediments all indicate speleogenesis under prolonged confined, hypogenic conditions.

Several lines of evidence indicate speleogenesis by far-field groundwater that arrived at the Negev-Judean Desert from

south-east. Oxygen isotopes in water, vein- and phreatic cave-calcite, as well as Miocene lacustrine calcite are all depleted in ^{18}O , relative to the products of local meteoric water. Today some far-field water from Sinai, south of the Negev, is still upwelling in the Negev, as indicated by groundwater analysis, albeit in a limited amount.

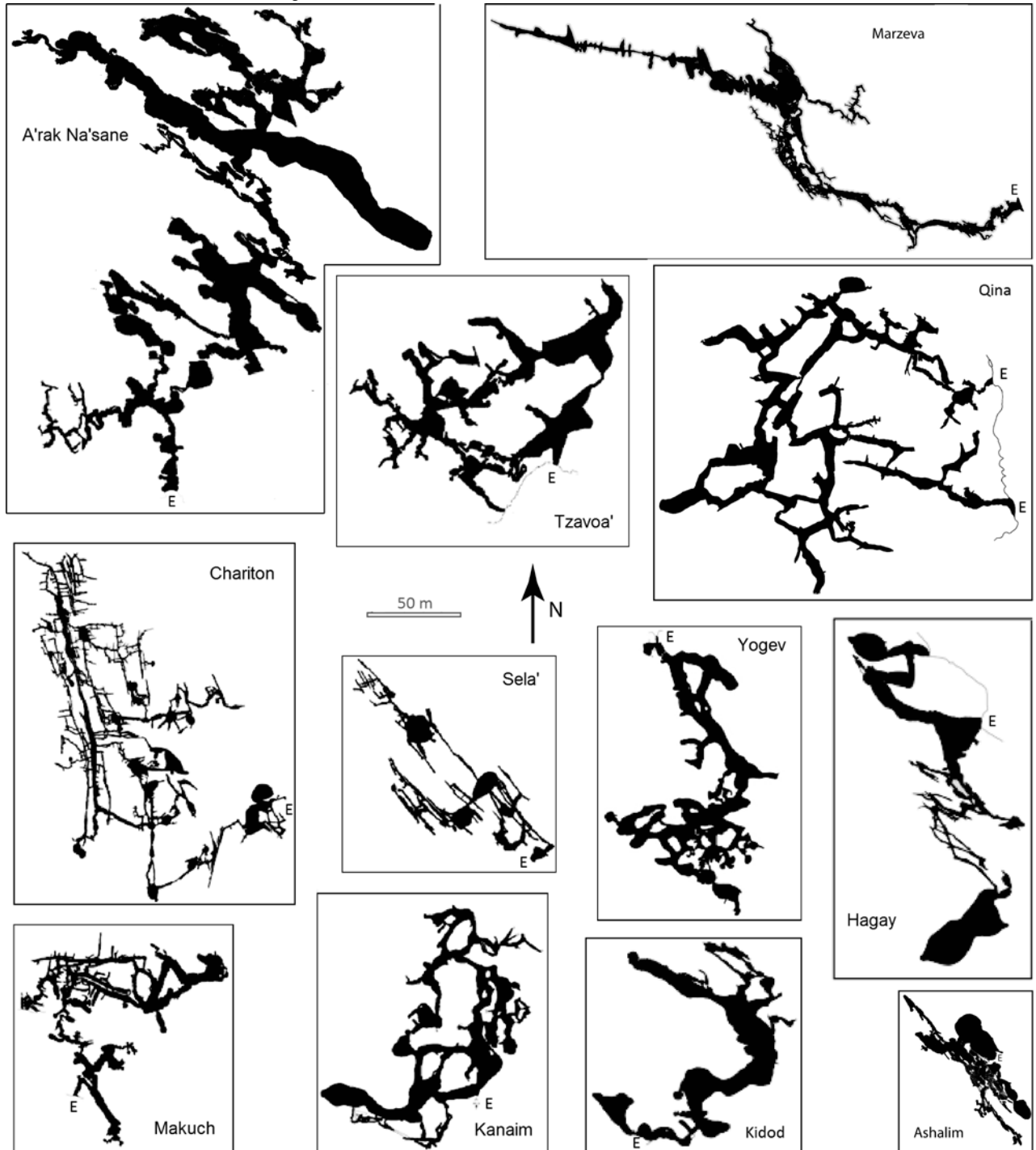


Figure 1. Plans (horizontal projections) of the largest hypogenic caves (length > 500 m) in the Negev and Judean Desert, shown with a common scale. Cave entrances indicated by 'E'

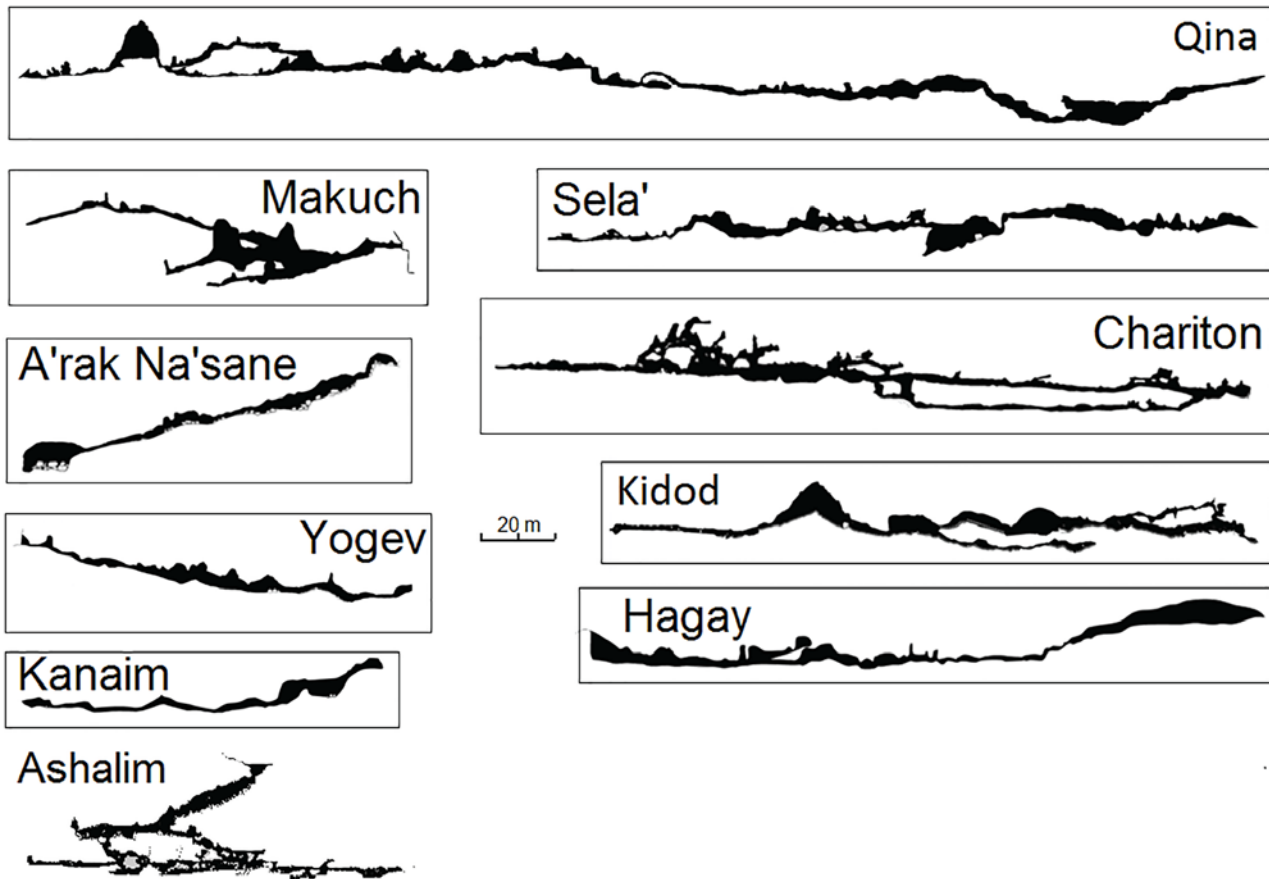


Figure 2. Elevations of the largest hypogenic caves (length > 500 m) in the Negev and Judean Desert, shown with a common scale. Cave entrances indicated by 'E'

The studied caves were predominantly formed by water rising from deep sandstone aquifers, becoming aggressive upon reaching the uppermost karstic beds of the Judea Group, under the confinement of Senonian chinks and marls. The hypogenic water has risen across the formations mainly along deep, re-activated faults. These waters had various hydrochemical properties. In places, the cave-forming water contained hydrogen sulfide that contributed to speleogenesis by sulfuric acid. This is indicated by gypsum crusts, whose relatively low $\delta^{34}\text{S}_{\text{SO}_4}$ indicates dissolution of limestone by sulfuric acid, with co-precipitation of gypsum. The sulfuric acid was derived from oxidized H_2S , probably produced from deep-seated bacterial reduction of Triassic gypsum.

This study suggests that the main speleogenetic period was the Oligocene to early Miocene, prior to the middle to late Miocene development of the Dead Sea rift depression. This corroborates suggestions that major regional uplift (few km) along the Afro-Arabian dome commenced in the Oligocene, earlier than the Red Sea rift divergence between the African Plate and the Arabian Plate.

The middle to late Miocene Dead Sea depression, associated with canyons incision, dewatered the caves, rendering them relict and hanging high above the falling base level. Some caves continued evolving by condensation corrosion following dewatering.

It is suggested that the recharge of the deep-seated aquifers took place at the northern reaches of the Afro-Arabian dome, which was rising and eroding during speleogenesis. The SE



Figure 3. Some features of the studied caves: A. Main passage of Arak Naasane Cave, with convection solution pockets at the ceiling; B. Gypsum crusts covering corrosion grooves, Kanaim Cave; C. Condensation corrosion features and aerosols deposits, Arak Naasane Cave; D. Thick gypsum crust covering vertical fracture and cavity walls, Qina Cave.

side of the Syrian Arc, erosionally truncated during the Oligocene, was a major site for hypogenic speleogenesis by the upwelling deep waters, which mixed with local recharge from the regional truncation surface.

Such hypogenic karst processes can have further implications for understanding migration and reservoirs of petroleum in the major oil-producing flanks of the Arabian Platform. These basinal reservoirs, located at far-field downstream edges of circum-Arabian mountain ranges, may have been affected by long term hypogenic karstification associated with carbonate porosity.

In addition, the study of relict hypogenic karst within desert regions allows better understanding of paleohydrology of such regions, particularly in the presence of large elevated truncated platforms. Such large erosional planes may serve as preferred recharge sites for far-field groundwater flow, which can in turn affect both water and petroleum reservoir development.

The current study indicates that major uplift occurred along the Red Sea shoulders mainly during the Oligocene pre-rifting stage rather than during Miocene times. This was followed by a major erosional event which truncated the entire region, associated with cave formation.

Hydrogeochemical And Isotopic Characterization Of The Tapalqué Creek Upper Basin And Its Associated Karst, Buenos Aires, Argentina

^{1,2}Glok Galli, Melisa; ³Barredo Codesal, Silvia P.; ^{2,4}Martínez, Daniel E.; ¹Trezza, Mónica A.

Affiliation: ¹Facultad de Ingeniería (UNCPBA)/Centro de Investigaciones en Física e Ingeniería del Centro de la Provincia de Buenos Aires (CIFICEN. UNCPBA-CICPBA-CONICET). 5737 del Valle Ave, Olavarría, Buenos Aires, Argentina. melisaglokgalli@gmail.com/glokgalli@mdp.edu.ar/mtrezza@fio.unicen.edu.ar
²Grupo de Hidrogeología (Hydrogeology Group). Instituto de Geología de Costas y del Cuaternario (UNMDP). 3350 Funes St, Mar del Plata, Buenos Aires, Argentina.
³Grupo de Modelado de Cuencas (Basin Modelling), Instituto Tecnológico de Buenos Aires (ITBA)/Grupo Espeleológico Argentino. 399 Eduardo Madero Ave, CABA, Buenos Aires, Argentina. sbarredo@itba.edu.ar
⁴Instituto de Investigaciones Marinas y Costeras (UNMDP-CONICET). 3350 Funes St, Mar del Plata, Buenos Aires, Argentina. demarti@mdp.edu.ar

Abstract

In the center and southern regions of the Argentine Buenos Aires province, South America, isolated karst areas with cave systems exposed. In the central area, these are present in the Sierras Bayas town, located to the NE of the Tapalqué Creek Upper Basin (TCUB) that has a heterogeneous hydrogeological behavior and is mostly situated in the Olavarría district, one of the main mining sites of the country. Karst evolved in the epiclastic depositional sequences of the Sierras Bayas Group: the lowermost, Villa Mónica Formation (~800 Ma), with dolomites and stromatolites present; and the uppermost, Loma Negra Formation (~543-560 Ma), being composed of limestones. These rocks are presently exposed in quarries whose operations led to the discovery of well-developed caves, karstic terraces, collapse dolines and ancient karst features. Four isolated cavities were mapped but recent field work suggest that there are more caves present. The aim of the present work is to carry out speleological interpretation of the karst environment associated with the TCUB, together with a hydrogeological analysis and a hydrogeochemical and isotope ($\delta^2\text{H}$ and $\delta^{18}\text{O}$) characterization of surface water and groundwater of the study site. This will improve the understanding of the TCUB hydrological system, considering that caves are aquifer analogues. The phreatic and topographic morphologies match and groundwater and surface water divides are approximately coincident. The regional flow has a NW-N-NE direction, originating in the S sector and receiving local groundwater contributions from the NW and NE zones (mountain ranges), this latter being where carbonate rocks are outcropping. Discharge occurs through the hydrographic network into the Tapalqué creek (gaining streams). Hydrogeochemical and stable isotopes analyses confirm this, with a groundwater and stream-water general classification mostly as sodium bicarbonate type and also as calcium and/or magnesium bicarbonate waters. Isotopic data show the source of the detritic aquifer (Pampeano aquifer) recharged from rainfall and a groundwater domain into the stream flow. It is proposed that ancient and new caves belong to a same regional system, being semi-active and follow the regional flow of groundwater and stream-water. The existence of tubular passages with elliptical cross sections and large scallops suggest initial phreatic origin although presently they are evolving under vadose conditions. Some unearthed galleries show steep entrances, smaller dissolution features and trickling water confirming the slow evolution in an epiphreatic environment though some inherited features suggest a probable polygenetic origin.

Keywords: hydrogeochemistry, isotope hydrology, karst, carbonate rocks, Argentina

1. Introduction

The Tapalqué Creek Upper Basin (TCUB), in the center of the Argentine Buenos Aires province, South America, occupies approximately 2,093 km² and is mostly located in the Olavarría district, one of the main mining sites of the country. It has a low regional topographic gradient (0.3 %) and covers the northwestern part of the Tandilia Mountain System (TMS) (Nágera 1940), generically named Olavarría mountain ranges, and the northern sector of the inter-mountain plain (Frenaguelli 1950), the hills area being the transition environment. The TMS is characterized by heights up to 310 meters above sea level (m asl) and of limited areal expression. Its structure corresponds to fault bounded and tilted blocks, strata dipping gently to the SW. The Negra and Bayas mountain ranges are outcropping to the E and the Dos Hermanas mountain range toward the W zone of the catchment. A plain is the prevailing geomorphological environment, with elevations up to 120 m asl, which exceptionally reach 250 m asl to the S (Fig.

1A1). The climate of this area is “subhumid-humid, mesothermal, with small or null deficiency of water” according to the Thornthwaite classification (Varela 1992; Auge 1993). The precipitation annual accumulated mean value is 893.1 mm (1949-2015) and the temperature annual average value is 15.3 °C (1988-2015). July was the coldest month, with a minimum monthly mean value of 7.3 °C, and January the warmest, with a maximum monthly average value of 23.4 °C (Glok Galli *et al.* 2016).

From the hydrographic point of view, two sectors can be differentiated in the TCUB: one with an integrated drainage network, scarcely developed, where the Tapalqué Creek is the main collector; and the other, with isolated topographic depressions and ponds. The Tapalqué Creek has a NW-N-NE direction and shows characteristics of a temporary regime conditioned by groundwater storage, with a later permanent basic flow. Smaller courses discharge into its right margin,

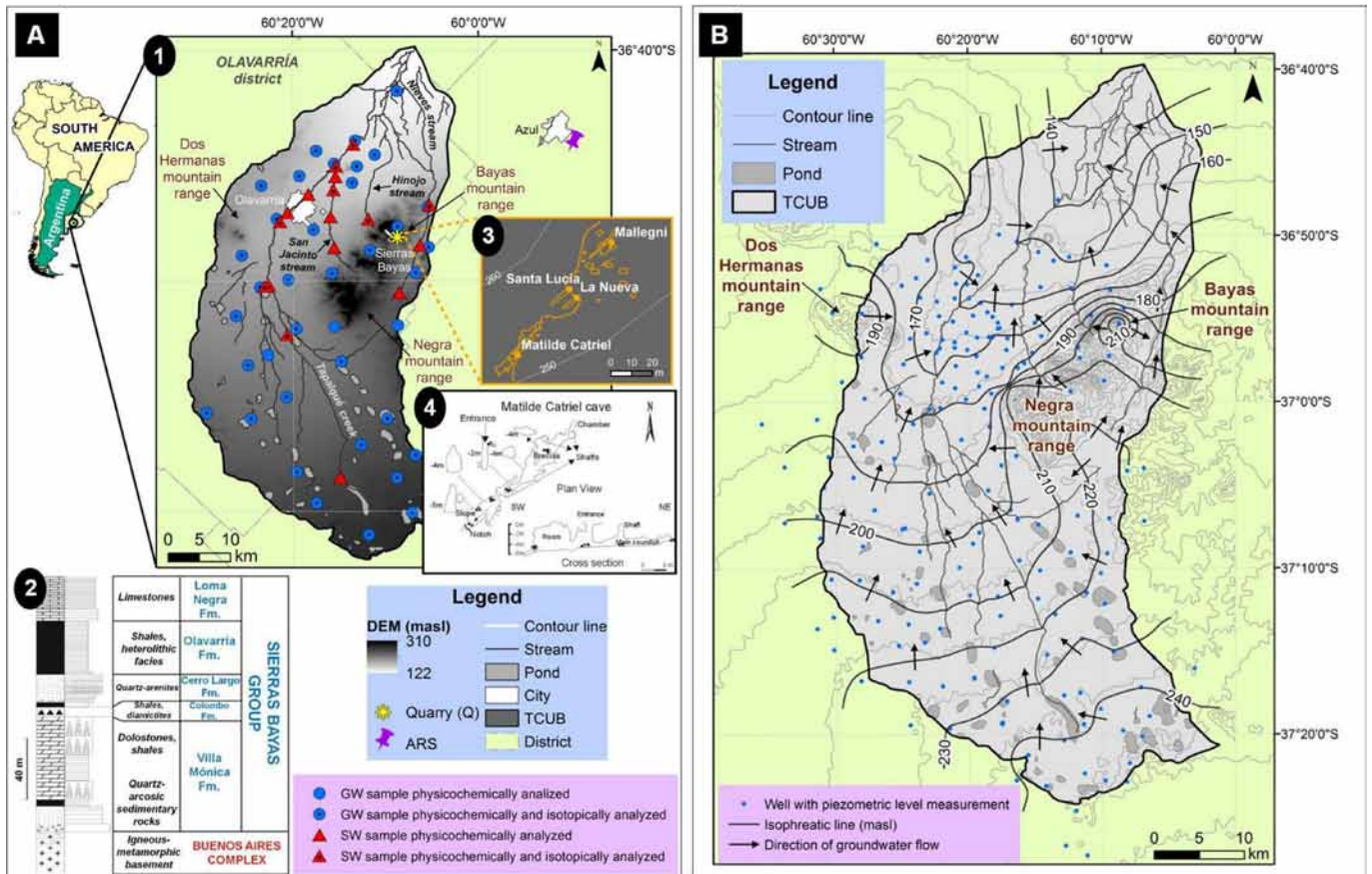


Figure 1. A: 1. Location map [DEM (m asl): Digital Elevation Model (meters above sea level), ARS: Azul rainfall station], 2. Precambrian geological units of the Sierras Bayas area (modified from Poiré and Gaucher 2009), 3. Plant view of the caves studied during 1996-2000, 4. Extended profile of the Matilde Catriel cave (modified from Martínez and Redonte 2000). B: TCUB's updated piezometric map

considered as plain autochthonous, which from W to E are: San Jacinto, Hinojo and Nieves streams (Fig. 1A1). Furthermore, this catchment presents a heterogeneous hydrogeological behavior, with two units that can be recognized: rocks with post-depositional permeability (Proterozoic-Paleozoic crystalline basement and sedimentary rocks), which outcrop in the mountain ranges zone; and sediments with primary permeability, called "Pampeanos" and "Postpampeanos" (Cenozoic) (Frenguelli 1950; Varela 1992). These last are hydraulically linked since they constitute the detritic aquifer of the area, the Pampeano aquifer, the water supply source for urban, agricultural and industrial uses in the Olavarría district. This sequence is composed by silt and sandy silts with clay intercalations. Levels of "tosca" or powdered CaCO_3 and volcanic ash sporadically appear. The conceptual hydrogeological model proposes a Pampeano aquifer's recharge source from rainfall (Varela 1992; Auge 1993).

Within those rocks with post-depositional permeability, the Neoproterozoic Sierras Bayas Group (SBG; Dalla Salda and Iñiguez Rodríguez 1979) is the most important sequence from the speleological viewpoint. This overlies the Paleoproterozoic igneous-metamorphic basement called Buenos Aires Complex (Marchese and Di Paola 1975). The oldest depositional unit of the SBG is the Villa Mónica Formation (~52 m; ~800 Ma, Gómez Peral *et al.* 2014), which shows two facies assemblages. The lower one is quartz-arkosic and comprises shallow marine siliclastics and the upper one corresponds to shelf stromatolitic dolostones and shales. On the other hand, the youngest depositional unit is the Loma Negra Formation

(~40 m; ~543-560 Ma) (Poiré and Gaucher 2009) that comprises red and black micritic limestones (Fig. 1A2).

Previous studies (1996-2000) have demonstrated the existence of a series of caves hosted on the Villa Mónica Formation's dolostones, as well as in the Loma Negra Formation's limestones, which were exposed due to the mining activities carried out to the NE of the TCUB, in the Sierras Bayas town region (250-260 m asl), which in turn destroyed them (Fig. 1A1-3). These resulted from a karst phenomena developed during the Quaternary although a series of dissolution features found in bedding planes suggested that similar processes could have occurred during the lower Paleozoic (Barredo 1997, 1999, 2001). The presence of new tunnels and conduits has been currently proved. In this way, the groundwater dynamic plays a key role within the TCUB, being an important geological agent. It determines the water availability for the external geological processes, such as the chemical and mechanical dissolution of minerals which causes the development of the mentioned karstic environment. In addition, groundwater closely interacts with surface water bodies in this catchment, and a deeper knowledge of these hydrological components and their relationships can be achieved due to the joint application of the hydrogeochemical analysis (Wang *et al.* 2006) and the water environmental isotopes use (deuterium, ^2H , and oxygen eighteen, ^{18}O) (Clark and Fritz 1997; among others). Different types of waters, interaction and mixing between them and recharge-discharge zones determinations are some of the further uses that these tools have. Some background research exist related to groundwater and surface waters hydrogeochemical and isotopic characteriza-

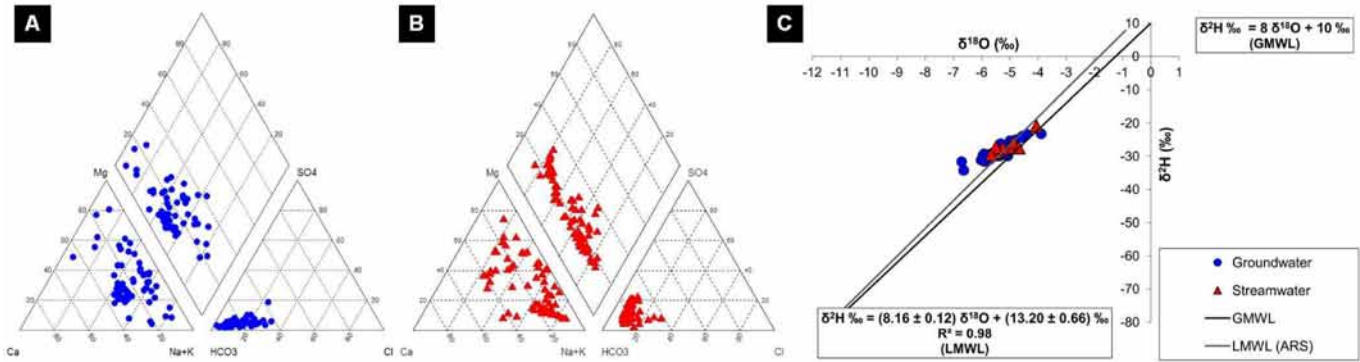


Figure 2. A: groundwater ionic composition. B: streamwater ionic composition. C: isotope composition ($\delta^2\text{H}$ and $\delta^{18}\text{O}$) of groundwater and streamwater (ARS: Azul rainfall station)

tion performed in the TCUB (Varela 1992; Auge 1993; Kruse *et al.* 1993; Glok Galli *et al.* 2016), but there are no references to the link between the karst and cavities and the hydrogeological behavior in this area. The aim of the present paper is to carry out speleological interpretations of the karstic environment associated to this study site, together with a hydrogeological analysis and a hydrogeochemical and $\delta^2\text{H}$ and $\delta^{18}\text{O}$ characterization of surface water and groundwater. This is performed in order to better the understanding of the TCUB hydrological system, considering that caves are aquifer analogues.

2. Materials and methods

Pre-existing data and information related to the study zone (topographical, geological, speleological, hydrogeological, hydrogeochemical) was compiled. Four sampling trips were carried out in June 2015 and February, March and August 2016. New karst features hosted on dolostones of a quarry in the Sierras Bayas area (Q; Fig. 1A1) have been photographed. Piezometric levels were obtained through a bipolar electric probe and a total of 216 measurements were used to update the TCUB's existing piezometric map (Varela 1992; Auge 1993). Electrical conductivity (EC), pH and temperature (T) were determined in situ. Hydrogeochemical and ^2H and ^{18}O analyses were performed at the Hydrogeochemistry and Isotope Hydrology Laboratory at the "Instituto de Geología de Costas y del Cuaternario", Mar del Plata University. Chemical analyses used standard laboratory methods and isotopic determinations by means of laser spectroscopy. 67 groundwater samples and 75 streamwater samples were analysed for the hydrogeochemical interpretation, as well as 37 groundwater samples and 9 streamwater samples for the isotopic characterization. The samples' isotopic compositions were plotted in a conventional diagram of $\delta^2\text{H}$ versus $\delta^{18}\text{O}$, together with the Global (GMWL) (Craig 1961) and Local (LMWL) Meteoric Water Lines. This was obtained by orthogonal regression analysis from precipitation monthly composite samples of the Azul rainfall station (period 1998-2007) (ARS; Fig. 1A1) (Dapeña *et al.* 2010). The isotopic results were expressed as δ values in permil (‰), defined as: $\delta = 1,000 (R_s - R_p) / R_p$ ‰, where δ is the isotopic deviation in ‰; s is the sample; p is the international reference; and R is the isotopic ratio ($^2\text{H}/^1\text{H}$, $^{18}\text{O}/^{16}\text{O}$). The standard is Vienna Standard Mean Ocean Water (V-SMOW) (Gonfiantini 1978). The analytical uncertainties were ± 1 ‰ for $\delta^2\text{H}$ and ± 0.3 ‰ for $\delta^{18}\text{O}$.

3. Results, analysis and discussion

3.1. Hydrogeological, hydrogeochemical and isotopic characterization

For the TCUB, the piezometric level average value is 196.3 m asl (standard deviation, SD: 25.6 m asl), with a minimum value of 139.1 m asl and a maximum of 247.1 m asl. As can be seen in Figure 1B, phreatic and topographic morphologies match (convergent radial type) and groundwater and surface water divides are roughly coincident. Groundwater contributions from neighboring catchments can be discarded (Varela 1992). The regional flow has a NW-N-NE direction, originating in the Southern sector and receiving local groundwater contributions from the NW (Dos Hermanas mountain range) and NE (Negra and Bayas mountain ranges). Natural discharge occurs through the hydrographic network into the Tapalqué creek (gaining streams), while the anthropic outputs are represented by wells exploitation for rural and industrial activities and the urban supply of the Olavarría district.

Groundwater samples present EC, pH and T average values of 838 $\mu\text{S}/\text{cm}$ (SD: 222 $\mu\text{S}/\text{cm}$), 7.5 (SD: 0.3) and 16.3 $^{\circ}\text{C}$ (SD: 1.1 $^{\circ}\text{C}$), respectively. For streamwater samples, the mean value for EC is 839 $\mu\text{S}/\text{cm}$ (SD: 181 $\mu\text{S}/\text{cm}$), for pH, 8.0 (SD: 0.4), and for T, 17.3 $^{\circ}\text{C}$ (SD: 6.7 $^{\circ}\text{C}$). The hydrogeochemical facies analysis conducted by a Piper graphic allows a general classification of groundwater (Fig. 2A) and streamwater (Fig. 2B) as mainly sodium bicarbonate and also as calcium and/or magnesium bicarbonate type; Na^+ and HCO_3^- being the prevailing ions in both cases. These derive from the albite weathering (Logan *et al.* 1999) and the CaCO_3 dissolution of the Pampeano aquifer loessic sediments, this last accompanied by ionic exchange (Bonorino *et al.* 2001). Calcium and/or magnesium bicarbonate type groundwater is present close to the Sierras Bayas town' mountain ranges area (dolostones and limestones' outcrops), from where a local detritic aquifer recharge occurs (Fig. 1B). The similarity between groundwater and streamwater chemical composition is due to the creeks' gaining behavior aforementioned.

With regard to the isotopic characterization, the LMWL is given by the equation $\delta^2\text{H} \text{ ‰} = (8.16 \pm 0.12) \delta^{18}\text{O} + (13.20 \pm 0.66) \text{ ‰}$ ($R^2 = 0.98$) and the precipitation weighted average value is -31 ‰ for $\delta^2\text{H}$ and -5.5 ‰ for $\delta^{18}\text{O}$ (deuterium excess; -13 ‰) (Dapeña *et al.* 2010). Groundwater samples appear grouped in the graph of Figure 2C showing relatively constant isotope composition, which is close to the $\delta^2\text{H}$ and $\delta^{18}\text{O}$ mean contents of rainfall. These have stable isotopes average

values of -29‰ (SD: 3‰) for $\delta^2\text{H}$ and -5.5‰ (SD: 0.6‰) for $\delta^{18}\text{O}$. This fact indicates that this is a well-mixed system from rainwater, supporting the Pampeano aquifer's recharge source from rain infiltration. Streams isotope contents are similar to groundwater, with $\delta^2\text{H}$ and $\delta^{18}\text{O}$ mean values of -27‰ (SD: 2.5‰) and -5.1‰ (SD: 0.5‰), respectively, suggesting an aquifer domain into the creeks' flow, as obtained piezometric contours show (Fig. 1B).

3.2. Speleological setting

During nineties, some caves were explored in the Sierras Bayas town and identified as Mallegni, Matilde Catriel, Santa Lucía and La Nueva (Fig. 1A3) (Barredo 2001). These represent a partial set of a regional system partway unburied by the mineral extraction, which comprised a horizontal development of 83.27 m with a maximum difference in elevation of 7 m. Cavities followed a SW-NE direction almost parallel to the bedding dip, along the contact between the dolostones and the upper geological unit (Fig. 1A2). A system of E-NE trending normal faults, associated with the basement blocks, seems to be the main structural controlling factor and are accompanied by sub-meridional additional faults (N13°W), some of them with a gently sinistral displacement. The explored cavities were dry, internal T showed a mean of 18 °C and moisture was nearly 95 %. Matilde Catriel, the largest and most important, was sub-horizontal and reached 45.37 m in length with a partial difference in elevation of 6 m. Its entrance consisted of vertical pits, with the main gallery showing a rather lenticular profile with elliptical smaller conduits and minor meandering passages (Fig. 1A4) (Barredo 2001). Ancient caves have been destroyed in the last years by mining activities which in turn unearthed new tunnels and conduits (Fig. 3), suggesting that karst and cavities in the TCUB are associated with the groundwater and streamwater regional flow (Fig. 1B), probably constituting a regional system.

Partially, new unburied caves show similar karst features to the ancient caves (Fig. 3). Barely developed stalactites, very few stalagmites and curtains and thick botryoidal like accumulations sometimes can be seen in the remaining walls. Mineralogy consists of rhombohedral, white calcite and orthorhombic aragonite with a clear color banding. Externally, these are mostly white with slight yellowish, dark brownish to reddish tones. Calcite is also present as aggregates of crystals, ranging from 1 to no more than 3 mm in length. In detail, ancient caves developed almost tubular and sub-horizontal galleries and had sub-rounded to sometimes conspicuous elliptical cross section that match with the recently unearthed tunnels (Fig. 3A3, B, C). Some tubular and subhorizontal conduits and shafts associated with major fractures were described for the old caves and directly coincide in morphology and flow direction with those studied here (Fig. 3B, C, D, E), which are interpreted as secondary passages of the main system. Cavity dissolution features also coincide and correspond with well developed ceiling pockets, large scallops indicating slow flows to the NE and solution cups in the ceiling and walls that suggest a similar phreatic origin for all caves (Fig. 3A2-4-5). Some bell shaped ceiling pockets might be associated with water trickling down fissures. A few composite pockets were detected, which form groups up to three in number, laterally connected and no larger than 10 cm. There are also blocks up to 1 m long, and medium to fine debris that build up fan

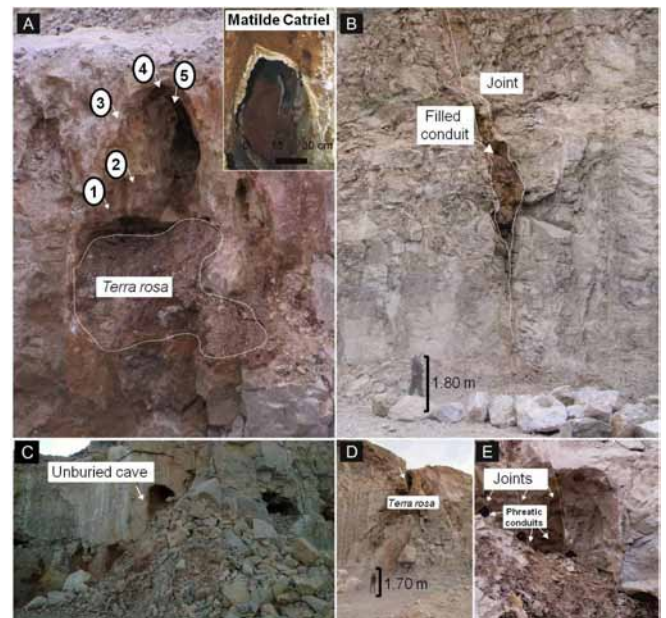


Figure 3. New karst features hosted on dolostones of a quarry (Q) in the Sierras Bayas area. A: 1. Ancient water levels, 2. Solution cups, 3. Elliptical profile of the upper right conduit, the same of the Matilde Catriel cave, presently mined. See the calcite/aragonite crust and barely developed curtain over the walls. A thin, botryoidal and earthy crust coats the walls, 4. Ceiling pocket (independent, simple, semi-circular in cross section), 5. Flute marks (scallop) that point to a NE flow direction. These dissolution features were described for different caves of the region. B: shaft or pit along joint plane, presently filled with terra rosa. C: unburied cave conduit. D: unearthed cave conduit. See the elliptical profile and the development of the passage, almost filled with terra rosa. E: view of a mining hole that shows three joints and their associated phreatic conduits (pits)

shaped piles of angular blocks and clasts related with minor faults and joints. Additionally, previous observations made on the caves showed sporadic water flow in some superficial conduits of the Matilde Catriel and Mallegni cavities (Fig. 1A3) as a response to heavy rains. Intense percolation by dropping and trickling was also seen along the passages. The deeper galleries, on the other hand, were most of the year permanently flooded due to the underlying impermeable facies and groundwater that kept the system overflowing and, at least, seasonally or temporally active. A maximum flooding level line was observed indicating 30 cm depth for the upper levels suggesting that the rising of the phreatic table may have reached shallower levels in the near past (Barredo 2001). Figure 3A1 shows different flooding levels for the conduits of the quarry Q (Fig. 1A1) suggesting variable water table levels and possible flooding of these tunnels.

4. Conclusions

Within the TCUB hydrological system, stream-water and groundwater are closely interacting, this latter playing a vital role as geological agent since it determines the development of the associated karstic environment, where caves are considered as aquifer analogues. Waters are mostly sodium bicarbonate type and also calcium and/or magnesium type. Isotopic data show the Pampeano aquifer's recharge source from rainfall and a groundwater domain into the stream flow. These facts confirm that zonal creeks are gaining streams, which is demonstrated in the updated study zone's piezometric map.

Karst features and caves presently observed match in morphology, groundwater and stream-water's flow direction and origin with those in the Sierras Bayas area. Although these last were demolished, therefore the ancient caves and the conduits and galleries presently unearthed belong to a same regional system. Accordingly to the morphology and disposition of the tunnels, and the described dissolution features, these caves can be considered epiphreatic in their origin but presently are evolving under vadose conditions, at least up to the 10 m that have been explored, as a semi-active karst directly linked with the water table regional variation, suggesting then a probable polygenetic origin.

The TCUB associated karst constitutes an important cultural and natural heritage both for the study zone and Argentina, being of vital interest from different points of view: hydrogeological, speleological, geological, biological, anthropological, paleoclimatic and touristic. The speleological studies integrated with hydrogeochemical and isotopic techniques allow the development of a multidisciplinary research line, new and important in the country.

Acknowledgments

These studies were funded through Projects PICT 2012-0160 and 2014-1529.

References

Auge MP, 1993. *Abastecimiento de agua potable a la ciudad de Olavarría, provincia de Buenos Aires – Informe final*. Consejo Federal de Inversiones, Municipalidad de Olavarría, Obras Sanitarias de la provincia de Buenos Aires. pp 121 + 45 figures, 3 tables y 3 attachments (in Spanish).

Barredo SP, 1997. Estudio espeleológico preliminar en Sierras Bayas, un paleokarst?. *XII International Congress of Speleology*. La Chaux-de-Fonds (Neuchâtel). Switzerland. VI: 1-4 (in Spanish).

Barredo SP, 1999. Una hipótesis sobre el origen de las cuevas de Sierras Bayas, provincia de Buenos Aires. *Revista Salamanca*, **10**:28-31 (in Spanish).

Barredo SP, 2001. The dolomite caves of Sierras Bayas, south-eastern Buenos Aires, Argentina. *XIII International Congress of Speleology*. IV Speleological Congress of Latin America and Caribbean. XXVI Brazilian Congress of Speleology. Brasilia DF, Brasil. 143-149.

Bonorino G, Albouny R, Rossi S, 2001. La influencia del sistema carbonatado sobre el quimismo del agua subterránea (cuenca superior del arroyo Chasicó). *Geoacta*, **26**: 1-11 (in Spanish).

Clark ID, Fritz P, 1997. *Environmental isotopes in hydrogeology*. CRC, Boca Raton, FL, pp 328.

Craig H, 1961. Standard for reporting concentrations of deuterium and oxygen-18 in natural waters. *Science*, **133** (3467): 1833-1834.

Dalla Salda L, Iñiguez Rodríguez AM, 1979. La Tinta, Precámbrico y Paleozoico de Buenos Aires. *Proceedings VII*

Congreso Geológico Argentino, Neuquén, Argentina. **1**: 539-550 (in Spanish).

Dapeña C, Varni M, Panarello HO, Ducós E, Weinzental P, Usunoff E, 2010. Composición isotópica de la precipitación de la Estación Azul, provincia de Buenos Aires. Red Nacional de Colectores Argentina. In: Varni, Entraigas & Vives (ED). *I Congreso Internacional de Hidrología de Llanuras, Proceedings book* 386-393. Azul, Buenos Aires, Argentina. ISBN 978-987-543-393-9 (in Spanish).

Frenguelli J, 1950. *Rasgos generales de la morfología y geología de la Provincia de Buenos Aires*. M.O.P., LEMIT, La Plata, Buenos Aires, Argentina. Series 2: 33 (in Spanish).

Glok Galli M, Martínez DE, Colasurdo V, Grosman F, Sanzani P, Trezza MA, 2016. Caracterización hidrogeoquímica e isotópica de la cuenca alta del arroyo Tapalqué, provincia de Buenos Aires. IX Congreso Argentino de Hidrogeología y VII Seminario Hispano-Latinoamericano Sobre Temas Actuales de la Hidrología Subterránea, San Fernando del Valle de Catamarca, Catamarca, Argentina. *Taller de Calidad del Agua Subterránea*. 272-279. ISBN: 978-987-661-222-7 (in Spanish).

Gómez Peral LE, Kaufman AJ, Poiré DG, 2014. Paleoenvironmental implications of two phosphogenic events in Neoproterozoic sedimentary successions of the Tandilia System, Argentina. *Precambrian Research* **252**:88-106.

Gonfiantini R, 1978. Standards for stable isotope measurements in natural compounds. *Nature* **271**, 534-536.

Kruse EE, Rojo A, Varela L, 1993. Características hidroquímicas subterráneas de la cuenca del arroyo Tapalqué (Buenos Aires). In: *Proceedings XII Congreso Geológico Argentino*, Mendoza, Argentina, VI: 208-215 (in Spanish).

Logan WS, Auge MP, Panarello HO, 1999. Bicarbonate, sulphate and chloride water in a shallow, clastic-dominated coastal flow system, Argentina. *Groundwater*, **37** (2): 287-295 PP.

Marchese H, Di Paola, E, 1975. Reinterpretación estratigráfica de la perforación de Punta Mogotes I, Provincia de Buenos Aires. *Revista de la Asociación Geológica Argentina*, **30**(1), 44-52 (in Spanish).

Martinez O, Redonte G, 2000. *Topografía grado 4D, Sierras Bayas, Buenos Aires, Argentina*. GEA. Unpublished (in Spanish).

Nágera JJ, 1940. Historia Física de la Provincia de Buenos Aires, Tomo I Tandilia. *Biblioteca Humanidades y Ciencias de la Educación*. Universidad Nacional de La Plata, La Plata, Buenos Aires, Argentina. **24**: 1-272 (in Spanish).

Poiré DG, Gaucher C, 2009. Lithostratigraphy. Neoproterozoic-Cambrian evolution of the Río de la Plata Palaeocontinent. In C. Gaucher, A.N. Sial, G.P. Halverson, H.E. Frimmel (Eds.), *Neoproterozoic-Cambrian Tectonics, Global Change and Evolution: a focus on southwestern Gondwana*. *Developments in Precambrian Geology* **16**, Elsevier: 87-101.

Varela LB, 1992. Escurrimiento subterráneo en la cuenca del arroyo Tapalqué. In: *Situación Ambiental de la Provincia de Buenos Aires. A. Recursos y rasgos naturales en la evaluación ambiental*. Coordination: Dr. López, H.L. and Dr. Tonni, E.P. Comisión de Investigaciones Científicas, Buenos Aires, Argentina. Year II, N° 11, pp 15 (in Spanish).

Wang Y, Guo Q, Su C, Ma T, 2006. Strontium isotope characterization and major ion geochemistry of karst water flow, Shentou, northern China. *Journal of Hydrology*, **328**: 592-603.

Some new caves under the Dubrovnik city airport in the Dinaric karst of Croatia

Mladen Garašić^{1,2,3} & Davor Garašić²

Affiliation: ¹ University of Zagreb, Faculty of Civil Engineering, Croatia.

² Society for the Research, Surveying and Photographing of Karst Phenomena (DISKF) Zagreb, Croatia.

³ UIS (Union Internationale de Speleologie) FSE (European Speleological Federation)

Abstract

Eleven caves were explored under the Dubrovnik city Airport in Croatia. This highly weathered area has been in the speleologists' focus of attention ever since the airport was built in 1961/62. Two vertical caves measuring 31 m and 10.5 m in depth were discovered at that time. These two caves are now situated right underneath the new control tower of the Dubrovnik Airport. A tunnel entrance to the cave that has been known to local population for a long time is situated in the immediate vicinity of the control tower. In late 1950s the entrance to the cave was sealed with concrete because of military airport construction. However, a tunnel was built to enable access to the cave. The cave is about 200 m long and it completely occupies the space underneath the concrete runways of the Dubrovnik Airport. Thanks to the efforts made by speleologists in 2010, the cave was adapted to enable tourist visits, and is now the world's only tourist cave underneath an operating airport. During the airport extension activities in May 2012, three additional speleological sites were discovered. They were examined along with the other previously discovered caves, from the standpoint of geophysics, geology and speleology. In 2014 and 2015 five new caves were found. The deepest cave is 58 m deep, and the longest one is about 200 m long. Measurements of Radon gas concentration were taken in all this caves. Results were compared with the ones taken in Biokovo tunnel caverns and Vrata tunnel cavern in Croatian part of Dinaric Karst. All of the mentioned caves didn't have natural entrances on the surface before the first exploration and engineering work on airport and tunnels were done.

Keywords:

1. Detailed speleological investigation (research and exploring)

For the widening purposes of the terminal building "C" of Dubrovnik Airport, a detailed speleological survey was conducted in May and October 2014 and March 2015. Five new caverns were added to the list of six previously known caves under the Dubrovnik airport which sum up to total of eleven caves. One of the caves is open for tourist visitors which is unique example in the world.

The longest cave under Dubrovnik airport measures 197 m, and the deepest one measures 58 m in depth. Researched Caves (K-1a, A-1b, K-2, K-3, K-4, K-5) show signs of gravitational karstification (Garašić 1986; 1989; 1991; 1995) in their upper parts, and K-5, the lower parts of the cave show traces of regressive karstification, i.e. the aggressive progression process of karstification toward the surface (fig.1, fig.2.) The situation is similar in the nearby Djurovic cave. Traces of ground water oscillations were found but the corrosion forms of speleothems were seen. The cave might be larger in size but narrow passages, stone blocks etc. (Garašić 2013; 2014; 2015) prevent cavers from further investigations. According to the main geological map (scale 1:100 000 Dubrovnik (Marković 1966), the location of the planned building "C" structure is made of Cretaceous Danian sediments and the highest parts might be Paleocene (K, Pc?).

The following is a short description of major caves.

Cavern K-2 (fig. 3), which is located on geodetic profiles between 4-H and 5-H, whose descent site at the time of research was located at the altitude of 148.562 m above sea level. After the collapsed rocks at the entrance, it has a vertical continuation. First 3.25 m, then 4.55 m and 14.75 m more

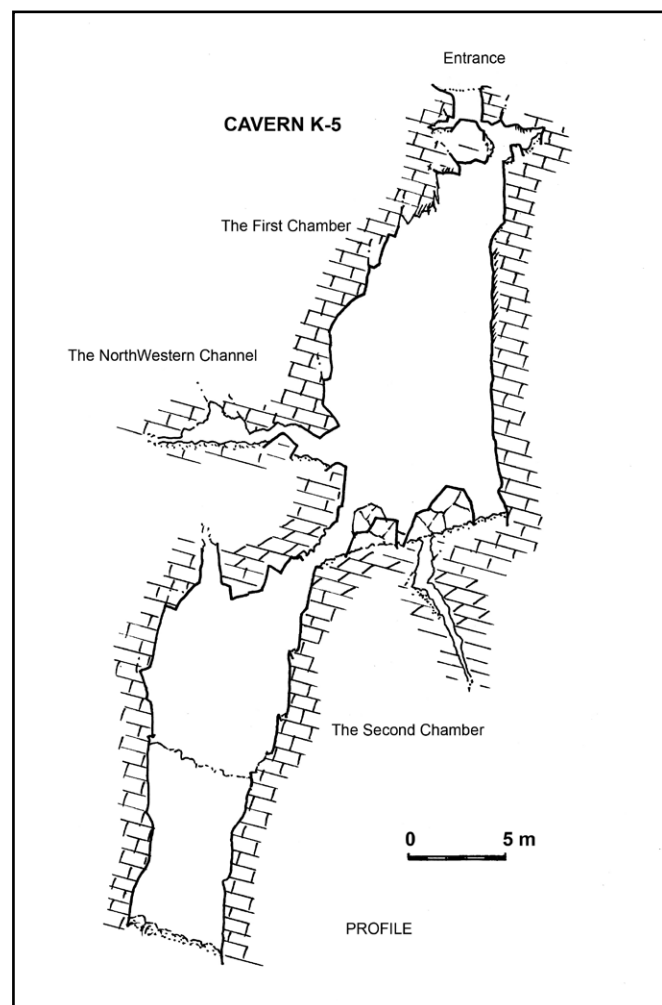


Figure 1. Cavern K-5 - profile

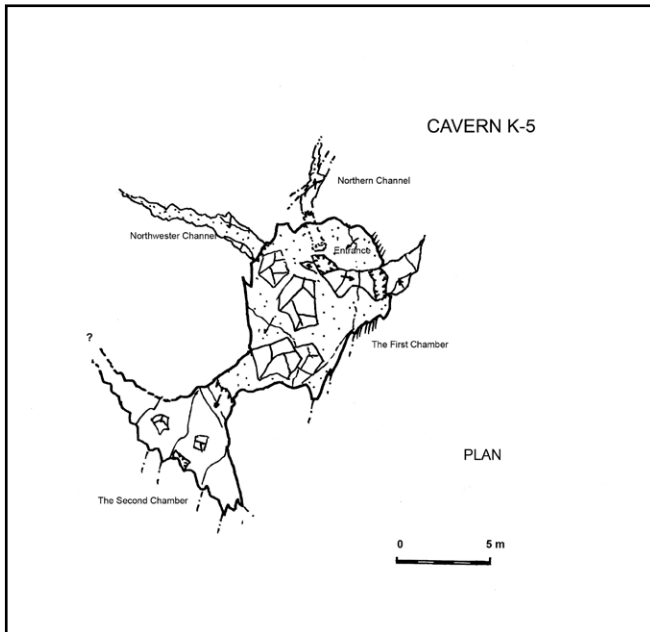


Figure 2. Cavern K-5 - Plan

towards the end. At that depth there is a chamber with the floor of approximately 9.0×12.0 m. The chamber is covered with stone blocks that occupy central and northern parts. Dimensions of the chamber are narrowing down towards the surface at approximately 4.5×6.5 m all the way to the wedged rock at the entrance. Eastern and southeastern part of the chamber is intensively covered with secondary precipitated speleothems (crust and curtains). The cave continues to the southwest of the chamber where the next vertical leads to the next, diagonal chamber of approx 6.0×10.0 m. In this lower, second hall, between the stone blocks there a smaller narrow passage to the lowest point of the cavern K-2 at 58.50 m from the anchor point on the excavator. That is approximately 63.00 m below the vertical alignment of the primary relief before the previous airport building was demolished. A further passage for the speleologists is unavailable. Intensive groundwater activity was not noted even in the deepest parts of the cave but the temperature of the rocks was lower by 0.5°C compared to the first chamber. This can be explained by the periodic air flow that cooled down the rocks during the expedition. Genetically, the cave would continue to extend along the fault plane, direction of approximately $44\text{--}225^\circ$. From the first chamber, at approximately 25 m of depth, below the stone blocks, a steep, narrow passage extends for another 9 m. At that point the channel gets too narrow (sinter formations and boulders) for cavers to continue any exploration.

There's another passage to the northwest of the first chamber. It can be accessed climbing approximately 2 m over the stone blocks. The passage requires crawling for about 15 m before it gets too narrow for cavers. The results of the radon gas concentration measurement in cave K-2: PAEC = 2911 nJ m^{-3} ; EEC = 523 Bq m^{-3} ; PAEE = 497.28 nJh m^{-3} ; dose = $0.744\text{ }\mu\text{Sv}$; Po-218 = 2557 Bq m^{-3} ; can't be linked to the results of the simultaneous radon gas concentration measurement in a nearby cave Djurovic: PAEC = 7792 nJ m^{-3} ; EEC = 1399.8 Bq m^{-3} ; PAEE = $1033.31\text{ nJh m}^{-3}$; dose = $1.447\text{ }\mu\text{Sv}$; Po-218 = 6156 Bq m^{-3} .



Figure 3. Cave exploring of cavern K-2

K-5 cave, which is located on geodetic profiles between 2 and 3-D, whose point of descend was, at the time of the expedition, at an altitude of 147 m above the sea level. The first pit falls to 7.65 m. Then another 2.45 m, followed by the steep slope of 8.15 m. At the beginning of the rock creep, the ceiling height is 5.15 m, at the bottom it's about 2.50 meter with a width of 3.25 m. The bottom of the pit is flat, with the size of 1.55×2.15 m and height of 1.25 m. There's a large number of speleothems. During the construction of the foundations of the building "C" at Dubrovnik airport, a deterioration of the stone material in the underground indicated the existence of caves. A number of such areas was determined (from K-1a to K-5). Those caves were not known or discovered in the earlier researches. Detailed cave explorations determined that all of the caves lie below the future building "C" and therefore must be carefully treated. No live troglobiontic animals have been noticed in the mentioned caves. This is understandable when taking into account that intensive construction works on the Dubrovnik airport are going on for years and all excavations related to building "C" are being performed by "Pick Hammers" rather than explosives. In addition, the airport operates continuously for 40 years so the increased noise is present the whole time. Also there were more buildings on the location of the building "C" that were built 40 years ago and were in the function of Dubrovnik airport which certainly wasn't stimulating for possible habitats of troglobiontic animals.

There is a reduced amount of atmospheric water in the area of future building "C". A similar situation has been found on many previous tunnel construction sites in karst. It's widely known that troglobionts from caverns in tunnels migrate towards the interior of the karst systems due to noise sources, quakes and unnatural frequencies on the very beginning of any construction works (even when it's several kilometers away from its habitat). It has been established that the caverns are not significant in terms of environmental protection. No active groundwater flow has been detected and the dimensions of caves do not indicate the possibility of groundwater level rising. Groundwater level might be at least seventy or more meters below the lowest point of those caverns i.e. a maximum of 40



Figure 4. Entrance in cavern K-4



Figure 5. Inside cavern K-4

to 50 m above the sea level. Caverns are not in any relationship with the nearby Đurović cave. All of the explored caves were formed in layers of carbonate rocks of the upper Cretaceous (Garašić et al. 2013) which are slightly inclined (between 10 °C and 20 °C) to the northeast. But the basic predisposition of their genesis is related to fracture and fault systems that are almost perpendicular to the so-called “Dinaric direction”. The accuracy of these assumptions can be verified by comparing the position of layers with tectonic elements within the nearby Djurovic cave which was done during the last two research expeditions.

Besides the famous Djurovic cave (about 200 m long and over 35 m deep) in the vicinity of the mentioned caverns there are two more caves (“Velika jama” with the depth of 31 meter and “Mala jama” with the depth of 10.5 m). They were documented during the speleological research for the needs of control tower and terminal building of Dubrovnik airport construction back in 1961. These data indicate of the specific intensive vertical karstification in this area. The altitude of this area is about 155 m above the sea level. There are turning axis of tectonic movements. Detailed speleological research of new caves (caverns K-1 to K-5) in the area of Dubrovnik Airport’s buliding “C” next to Čilipi, Konavle, in Dalmatia, contributed to the information about the position, dimensions and morphology of the objects. They are mostly simple pits with the vertical difference of 11 m (K-4) (fig. 4, fig 5.) and 58 m (K-2) which most likely extends even deeper but it hasn’t been proved. The total volumes of the newly researched caverns are estimated to be from 20 to 3000 m³. As mentioned before, no active water flows were detected but the existance of speleothems indicates the presence of dripping water. Speleothems are found in the forms of crust, stalactites, stalagmites and corrosion forms. Caves are formed mainly in the northeast-southwest direction which corresponds to the fault plane system which played a great role in the speleogenesis of this area. It is likely that the future construction works will encounter more caverns with the similar position along the same or the parallel fault planes that are in the same tectonic movement (with a rotating axis) caused by general subduction.

2. Hydrogeology of caves

From the hydrogeological standpoint, it can be stated that a permanently active (but not primary) underground stream has not been found at this speleological site (caves), although

the dripping water is probably present. The water flow in the cavern varies depending on climatic conditions on the ground surface. The water reaches the cavern via joints directly from the ground surface (to a lesser extent) or in deeper parts via joints and paraclases from other parts of Cretaceous carbonate formations (in most cases). Even today, the dripping water exerts an intense mechanical and chemical action on the surrounding rocks (erosion and corrosion), thus creating speleothems (stalagmites, dripstone crusts). The weathering depth in the area of this speleological site, despite the fact that these are practically impermeable rocks, is estimated at 300 to 500 m, and the zone of vertical circulation varies from 50 to 150 m. It is followed by the zone of horizontal circulation in which the ground water is carried via Cretaceous limestones toward submarine springs in the Adriatic Sea. As the Upper Cretaceous Senonian, Danian limestones and dolomites are permeable from the hydrogeological standpoint, and this due to intensive secondary (jointing) porosity, it may be expected that several similar caverns that can not be accessed from the ground surface are situated in the continuation of this joint, or parallel to it in a zone with genetically correspondent joints formed in the area of the same or similar fault due to general subduction. These caves might even be connected with the mentioned hydrogeological system in deeper zones of this part of Konavle. They are probably situated more than 30 m beneath the apron level.

3. Speleogenesis

This speleological site (cavern) has been formed by widening of the fault apron with the strike of 120° - 300°, and with a noticeable rotation of fault apron in intensely weathered Upper Cretaceous Senonian Danian limestones and dolomites. The initial water that is significant in the speleogenesis of the cavern, has penetrated through surface joints, and has widened these joints through its corrosive and erosive action to the present day dimensions. The bottom part of the cavern was formed through regressive palaeo-influence of ground water. These processes occur even today, but only in the parts of the cavern that are at least some fifty m below the apron level. A continuous water stream has not been noticed, i.e. only the speleothems were registered. Cavern dimensions may be even greater, but the narrowness of canals has prevented speleologists from advancing any further. This speleogenesis is related to the weathering processes that occurred after general uplift of the mountainous massif “Cukali Zone”

or “High Karst Zone” starting at the end of Cretaceous and continuing to the present time. The rocks in which the cavern was formed belong to the Upper Cretaceous Senonian limestones and dolomites, K2, 3, and the layer thickness varies from 20 to 50 cm. Limestones alternating with dolomites are quite frequent in this zone (Marković 1966; 1975).

References

- Garašić M, 1986. *Hydrogeology and morphogenesis of Caves in Croatian karst.* – Dissertation, University of Zagreb, 1–161.
- Garašić M, 1989. New conception of the morphogenesis and hydrogeology of the speleological objects in karst area in Croatia (Yugoslavia). – *10. International Congress of Speleology, Proceedings*, vol. 1, 234–236, sl. 8, Budapest, Hungary.
- Garašić M, 1991. Morphological and Hydrogeological Classification of Speleological structures (Caves and Pits) in the Croatian Karst area. – *Geološki vjesnik*, vol. 44, 289–300, fot.3, sl.4, Zagreb.
- Garašić M, 1995. Speleogeneza u okviru hidrogeologije krša i procesa karstifikacije. – *1. Hrvatski geološki kongres, Opatija, Zbornik radova, Proceedings*, 177–182, Zagreb.
- Garašić M, Garašić D, 2013. Some New Caves under Airport in Dubrovnik. *Geophysical research abstracts*, 15 (2013), 1, 4446–4447, Wien.
- Garašić M, 2013. Caves under Dubrovnik airport in Croatia. – *16th International Congress of Speleology, Proceedings, Volume 3.*, UIS, Czech Speleological Society, Praha, Czech Republic, 2013, 66–71.
- Garašić M, 2014. Speleološko istraživanje kaverni u području iskopa temelja zgrade „C“ u Zračnoj luci Dubrovnik. GIZ-110-024/2014, 1–60, Građevinski fakultet Sveučilišta u Zagrebu.
- Garašić M, 2015. Speleološko istraživanje kaverni u području iskopa temelja zgrade „C“ u Zračnoj luci Dubrovnik. GIZ-110-003/2015, 1–40, Građevinski fakultet Sveučilišta u Zagrebu.
- Garašić M, Garašić D, 2015. Some Caves at Dubrovnik airport. 5. *Hrvatski geološki kongres – 5th Croatian Geological Congress – Osijek 2015, Abstracts book*, 92–94, Zagreb.
- Marković B, 1966. *Osnovna geološka karta SFRJ 1: 100.000*, list Dubrovnik, K34–39, Savezni geološki zavod, Beograd.
- Marković B, 1975. *Tumač za OGK SFRJ 1: 100.000*, list Dubrovnik, K34–39, 1–44.

The new insights about deep karst springs in the Dinaric karst of Croatia

Mladen Garašić^{1,2,3} & Davor Garašić²

Affiliation: ¹ University of Zagreb, Faculty of Civil Engineering, Croatia.

² Society for the Research, Surveying and Photographing of Karst Phenomena (DISKF) Zagreb, Croatia.

³ UIS (Union Internationale de Speleologie) FSE (European Speleological Federation)

Abstract

In the recent years, several international cave diving expeditions were organised in the Dinaric karst of Croatia. The objectives were conducting new research of previously known springs and wells and also exploring the new ones. The results are fascinating. They contain documented depth and volume of the cave space filled with water.

The cause of verticality in constantly submerged underground cavities (siphons and springs) in the Dinaric karst can be explained within a wider geological context. The African tectonic plate and the its northern end called Adriatic plate, stresses below the south-west part of Euro-Asian or Dinaric tectonic plate. This is a special tectonic subduction phenomenon very similar to the Nazca plate in Pacific Ocean or the Austral-Indian plate in Indian Ocean, but has lower intensity and depth. The Dinaric plate has neotectonic uplifting, and karstification processes rapidly progress at depth, reaching several hundred m in a carbonate complex. The evidence for this can be found in Mesozoic rocks in the northwestern parts of the Dinaric karst in Slovenia with depths of up to 160 m (Divje Lake near Idrija), in the Croatian part of the Dinaric karst with many deep springs over 200 m, the Bosnian and Herzegovina Dinaric karst (i.e. the karst springs of Buna and Bunica rivers with depths of over 160 m), the Dinaric karst of Montenegro (springs Gurdić, Sopot, Ljuta) with a depth of -133 m to Albania where the deepest spring in Dinaric Karst (spring Viroi) was explored and dived to 267 m. Divje jezero lake is the spring of the Jezernica River, a tributary of the Idrijca and at 55 m long, the shortest river in Slovenia. Water flows from underground and through a steeply inclined tunnel, explored to the depth of 160 m. The discharge occasionally surpasses 60 cubic m per second.

The deepest karst spring in the Croatian Dinaric karst is Spring (Vrelo) of the Una River (with a maximum discharge of about 100 m³/s), where diving shows a depth of -248 m. Spring Sinac in Plaško polje has been dived to the depth of -203 m. Similarly the very popular springs of the river Kupa (-155 m) in Gorski Kotar, the river Gacka (-105 depth, length of 1150m) in Lika), river Cetina (-110 m depth, length of 1300 m) in the Dalmatinska Zagora, the spring Rumin Veliki (depth of -150 m) in the Sinjska Krajina, than rivers Krnjeza and Krupa with diving depths of over 100 m have been dived.

Interestingly, along the Adriatic coast in Croatia there also exists deep and long submarine springs (vrulje), ie. caves under seawater springs. i.e. - vruljas Zecica over 900 m, Vrulja Modrič over 2800 m long and vrulja Dubci, 161 m deep, and all completely flooded. The dominant role of tectonic activity in the creation and functioning of these caves is evident.

Keywords:

1. Una river spring

Cave dives were made to a depth of -248 m (fig 4) by Luigi Cassati (Casati, 2016). This is the deepest cave diving ever made on the Croatian Karst. The first cave dives were made in 2007 to -205 m, also by Luigi Casati (fig 2, fig.3.). This karst spring could be about 400 m deep.

The whole area of the Una River Basin watershed surface is about 9,640 km² (fig.1) and contains the Upper Una River Valley from the spring near Suvaja (Croatia) to Bihać (Bosnia and Herzegovina). From the geological and geomorphological point of view, it belongs to the mega-geomorphic entity of the Middle Dinaric Karst System. This consists of meso-regions similar in a morphostructural and morphogenetic sense in Bosnia and Herzegovina, and going from the SE towards the NW, they are: the regions of the Mountain Chain Jadovnik-Bobare-Sjenica, the region of the Mountain Range Osječenica with the Mountain Group of Ljutoč and Una Basin, and the regions of the Grmeč Mountain Group. In Croatia, there is Lička Plješivica Mountain. The Upper Una Valley with Una river spring is called Vrelo Une and belongs to the Osječenica meso-regions with the Mountain Group of Ljutoč and Una Valley, and the Lička Plješivica Mountain (Garašić 2016).

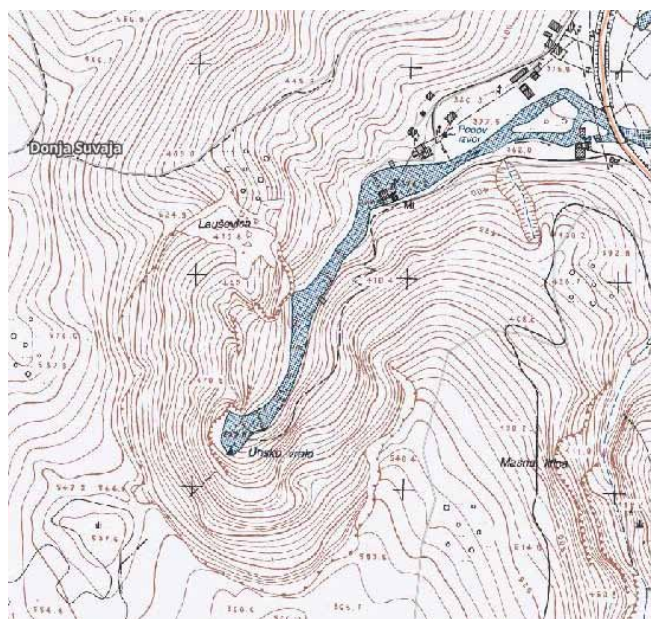


Figure 1. Topographic map of Una river spring in Croatian karst



Figure 2. Cave diving in Una river spring (Luigi Casati and Frederic Swierczynski) the deepest point is -248 m dived by Luigi Casati



Figure 3. At -180 m of depth in Una river spring (Luigi Casati and Frederic Swierczynski)

Faults play a most important role in the structural complex in this area of contact between Triassic dolomites and Jurassic limestones. They are represented by zones of different stretch: the Ličko Petrovo Selo-Bihać-Martin Brod fault (1-reverse, towards the NE and ENE, then southwards of Martin Brod towards the SE; the stretch of the narrower zone by V. Skočaj reaches 1,500 m; the principal faults are followed by branches, also reverse-faults visible near V. Skočaj, Nebljusi and westwards from Kulen Vakuf), then the Grmeč fault (2-reverse, towards the SW), and Drvar fault (3-reverse, towards the WSW, and towards the SW between Martin Brod and Drvar; the zone stretches up to 600 m; steep faults along Osječnica are followed by marked branches). The faults bordering with local uplifted structures are especially prominent. They are prevailingly reverse, bend along their stretching line and often represent branches with opposite wall blocks on the surface. That indicates the space compression and the horizontal movements of the most prominent parts of local structures stand out. Local faults most frequently follow the most important faults of a structural complex. The faults of the NE-SW to E-W system are visible between particular faults of shorter stretch, in areas even traversed by them, especially southwards from Bihać, near Veliki and Mali Ljutoč, westwards from Orašac and in the wider zone parallel with Pištalska Draga near Kulen Vakuf. (Babinka et al 2005, Babinka 2007, Bahun 1970).

Generally, the Una River springs by the village Suvaja in Lika (Croatia) and flows to the settlement of Bihać (length: 75.72 km,) in the direction of SE-NW. The river fall on that sector accounts for 2,351 m on km or 2.35 ‰. However, the Una river flows in direction of SSE-NNW from the confluence with its right tributary Krka to Martin Brod (cca 7.6 km).



Figure 4. Profile of Una river spring after cave diving in the year 2016 by Luigi Casati and Frederic Swierczynski

The watershed of the Una River, belonging to the Bihać region, represents a sensitive and vulnerable karstic environment. Karstic aquifers in this area are hydrologically connected with water flows in the Lika region on the Croatian side from the Korana River catchment area, including the Plitvice Lakes National Park, to the karstic fields (poljes) Koreničko Polje, Lapačko Polje and Krbavsko Polje.

On Mt. Plješevica. (Croatian part), there are about 180 mainly vertical caves, and on Mt. Ozeblin, the Mazin and Bruvno anticline, there are about 270 known caves. Many of these caves are in same Una river watershed (Bognar 2005, Kapelj S 2005).

2. Sinac spring

This is a karst spring in Plaško polje near Plavča Draga village on the edge of a karst polje. There are three karst springs connected together, the deepest being – 203 m dived by Luigi Casati in 2016. The first cave dive was made by Croatian cave divers in 1985 to a depth of -44 m; in 1999 French cave divers went to -103 m, and in 2003 Luigi Casati went to -155 m depth.

3. Kupa river spring

One of the most significant water resources in Croatia is the catchment area of the Kupa River, located in the region bordering the Republic of Slovenia. Cave diving started here in 1982 and continued in 1985 by Slovenian and Croatian cave divers to the depth of -86 m. In 2007, Luigi Casati went to -165 m and in 2017 to deeper than 200 m. About 88% of the total amount of water in this catchment originates in Croatia and just 12% from Slovenia; therefore, the largest part of the catchment area (about 1000 km²) is on the Croatian side of the border. Consequently, the aquifers are highly vulnerable and at risk. Due to the availability of large quantities of high-quality spring water (about 6m³/s), the entire area has a strategic importance within the context of any future development strategy pertaining to the western part of Croatia. The catchment area on the Croatian side was investigated using a wide range of research methods that included a

- Garašić M, 1983. *Hydrogeology and Speleology in region of Karst spring Una river*. Geological Institute Works, 1-86, Zagreb.
- Garašić M, 1987. *Geological mapping near Vrelo Une road Srb – Sucevici*, 1-38, Croatian Civil Engineering Institute, Zagreb.
- Garašić M, 1984. *Report of International Speleological Expedition «Kamensko 1984»*. 1-64, DISKF, Zagreb.
- Horvatinčić N, 2005. Physico-chemical conditions of tufa formation in waters of Una River - comparison with Plitvice Lakes water system, *Third workshop “Building of capacities on local and regional level for water resource management, environment protection and communal infrastructure”*, Bihać.
- Kapelj S, 2005. Hydrogeological working out of the over-boundary aquifer between the river-basins of Plitvice and upper flow of Una River, *ibid.*
- Kapelj J, Kapelj S, 2005. Geological and hydrogeological features of Una River basin. *ibid.*
- Miko S, Peh, Z, Bukovec D, Prohić E, Kastmuller Z, 2000, Geochemical baseline mapping and lead pollution assessment of soils on the karst in Western Croatia. – *Nat. Croat.*, **9/1**, 41–59. Zagreb.
- Obelić B, 2005. Project “*Study of Anthropogenic Pollution after the War and Establishing of Measures for Protection of Plitvice National Park and Bihać Region at the Border Area of Croatia and Bosnia-Herzegovina*”, City hall Bihać, June 6, 2005.
- Surić M, Lončarić R, Lončar N, 2010. Submerged caves of Croatia: distribution, classification and origin. *Environ Earth Sci* (2010) **61**:1473–1480.

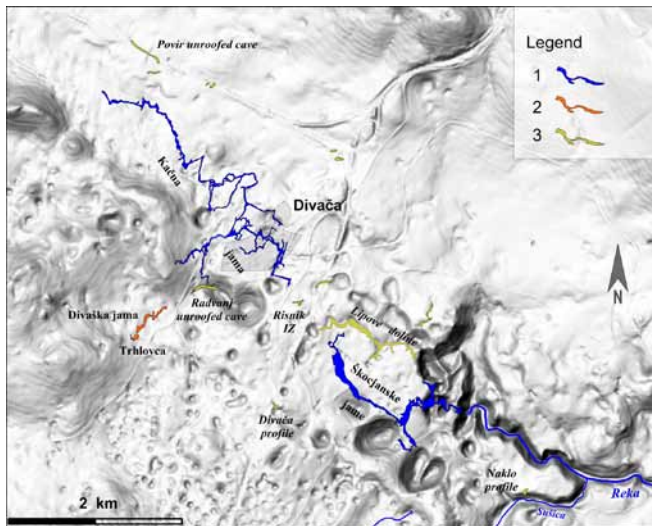


Figure 3. Divaški kras with caves and unroofed caves. Legend: 1- caves with water flow; 2 - relict caves with sampled sediments; 3 - studied unroofed caves.

above Škocjanske jame; also long one is present at Radvanj collapse doline and one at Risnik Industrial Zone (Risnik IZ). The actual underground river bed in Škocjanske jame is 230 m below those unroofed caves. Morphological analysis of several unroofed caves on the Divaški kras (Mihevc 2001) and paleomagnetic dating of sedimentary fills (Zupan Hajna et al. 2008, 2010), have indicated cave origin and an age of a few million years.

2. Methods

During complex research of karst sediments (Bosák et al. 1998; Zupan Hajna et al. 2008, 2010), we have applied number of research methods: paleomagnetism and magnetostratigraphy, stratigraphy (numerical and correlated dating methods including Th/U, paleontology (fauna, pollen), sedimentology and mineralogy (x-ray diffraction). Here are presented the results of x-ray analyses of sediments from caves, roofless caves and recent rivers of Divaški kras. The mineral composition with semi-quantitative amounts of minerals in analysed samples is presented in figure 4.

3. Mineral composition of sediments

Škocjanske jame are caves with active water flow passages; the actual Reka sinks at 317 m a.s.l. and the siphon in Martelova dvorana is at 214 m a.s.l. In sediments from river and from its tributary Sušica quartz prevails, with some clay minerals (illite/muscovite group), plagioclase and chlorite. Recent river sediments dominated by gravel clasts of flysch sandstone, and in the river bed before the siphon limestone pebbles prevail (Kranjc 1989). Recent flood clay from the end of the cave (Martelova dvorana) contains mainly quartz, some plagioclase, illite, kaolinite, chlorite and calcite; with traces of montmorillonite (Zupan Hajna 1995). In an older flood loam from upper part of the caves (Tiha jama at 334 m a.s.l.) quartz also prevails, with some plagioclase, illite and chlorite, and traces of microcline. In Černigojeva dvorana (at 334 m a.s.l.) Gospodarič (1984) described fossil deposits of chert, flysch sandstone and limestone pebbles; also in other parts of the caves are preserved various fluvial sediments. Their charac-

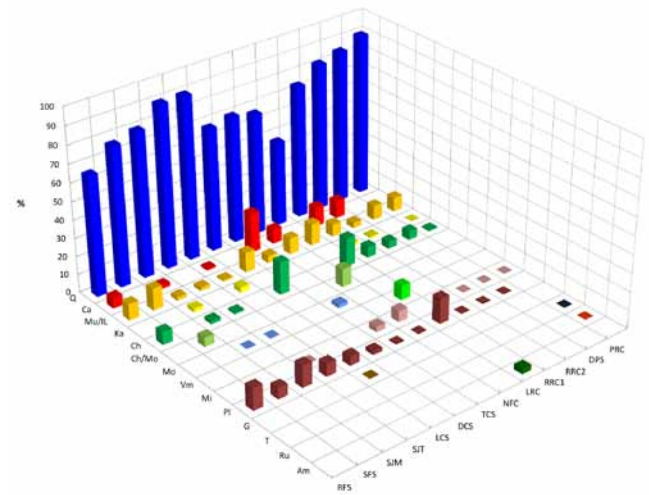


Figure 4. Mineral composition of samples from Reka catchment area, caves and unroofed caves. Legend: RFS - Reka (Zemon), river sediment; SFS - Sušica, river sediment; SJM - Škocjanske jame (Martel. d.), flood loam; SJT - Škocjanske jame (Tiha j.), loam; LCS - Labodnica, flood loam; DCS - Diviška jama, laminated sediments; TCS - Trhlovca, sand; NFC - Naklo, filled cave sand; LRC - Lipove doline roofless cave, soil; RRC1 - Risnik IZ roofless cave, sandy clay from bottom; RRC2 - Risnik IZ roofless cave, yellow sand from upper part; DPS - Divača profile filled cave, sand; PRC - Povir roofless cave, sand; Q - quartz; Ca - calcite; Mu/IL - muscovite/illite minerals; Ka - kaolinite; Ch - chlorite; Ch/Mo - chlorite/ montmorillonite group of minerals; Mo - montmorillonite, Vm - vermiculite, Mi - microcline; Pl - plagioclase; G - goethite; T - tourmaline; Ru - rutile; Am - amphibole.

teristics, color and position indicate the origin of weathered flysch.

Labodnica (Abisso di Trebiciano) is a 329 m deep shaft which reaches the underground river (Reka) channel. The lower part of the cave is occasionally flooded to a height of 92 m. In the bottom of the cave are deposited clays and sands of flysch origin. Samples of a recent flood loam contain quartz, plagioclase, kaolinite, illite and traces of calcite and goethite (Zupan Hajna 1995).

Diviška jama and Trhlovca are inactive caves approximately 200 m above recent water flow. These two caves contain a lot of old fluvial sediments which were dated using paleomagnetic methods and are few million years old (Bosak et al. 1998, 2000; Zupan Hajna et al. 2008, 2010). In Diviška jama and Trhlovca yellow laminated clays alternates with sands; samples contain mostly quartz, chlorite, muscovite/illite group of minerals, plagioclase, and with traces of hematite and goethite.

Close to the highway Ljubljana- Koper on the surface was found a filled-up fossil cave which has a disintegrated roof on one side. The site was named Divača profile (Bosák et al. 1998). Yellow fluvial sediments, laminated clays, silt clays and sands, were strongly cemented in some places. All samples contain relatively high amount of quartz; chlorite and muscovite/illite group of minerals; microcline was detected, in one sample relatively high amount of goethite, and traces of plagioclase (Zupan Hajna 1998). The sediments are older than 1.77 Ma, and may be also about 5.23 Ma old (Bosak et al. 1998; Zupan Hajna et al. 2008, 2010).

Close to the ponor of Reka to Škocjanske Jame at Naklo (slope of Sušica valley), at an elevation of 385 m a.s.l., there were sediments of a completely filled cave. These sediments were mainly flysch sandstone pebbles and sand. The sand consisted of quartz, calcite, muscovite/illite group of minerals, montmorillonite, microcline and traces of plagioclase.

Sediments from unroofed caves (Fig. 3) have very similar mineral composition (Fig 4). From Lipove doline unroofed cave yellow/brown soil consists of quartz, muscovite/illite group of minerals, plagioclase, chlorite, vermiculite and amphibole. Amphibole does not occur in flysch, but indicates an eolian origin (e.g. from some volcanic eruption, desert sand or even loess). In Risnik IZ sandy clay and sand consisting mainly of quartz, calcite, muscovite/illite group of minerals, kaolinite, chlorite and microcline with traces of plagioclase. In the roofless cave at Povir, very similar sediments were found to other caves in the area. Very similar sediments were found in other caves in the area, but there were present also traces of tourmaline and rutile which indicate a slightly different origin than in the Reka catchment area.

4. Conclusions

Nevertheless only detailed mineralogical and paleomagnetic analysis of unroofed cave fill confirm that their nature, origin and their age is older than was initially expected (for summary see Zupan Hajna et al. 2008, 2010 and Knez et al. 2016). Studied paleomagnetic properties of the sediments in the caves Divaška jama, Trhlovca and in Divača profile (Bosák et al. 1998, 2000; Zupan Hajna et al. 2008), gave results that the age of the sediments is most probably up to 5 Ma.

Clastic fills of unroofed caves and still existing caves of Divaški kras consist mainly of weathering products of Eocene flysch rocks eroded from the Reka River catchment. In all cases, relatively equal mineral compositions prevailed, indicating the main source is the flysch sediments which were weathered to different degrees. Mineral composition of Eocene flysch sandstones of Brkini mountain SE of Divača, which is the catchment area of the Reka, varies more in quantity of individual minerals as by the presence of different minerals. On Divaški kras fluvial sediments from unroofed caves are also an important source of superficial soils.

The process of flysch transport into the caves of Divaški kras continues from about 5 Ma ago till now, but the intensity has varied over time.

Acknowledgements

The research was supported by the research Program Karst research No. P6-0119 financed by Slovenian Research Agency and Plan of the Institutional Financing of the Institute of Geology AS CR, v. v. i. No. RVO67985831.

References

Bosák P, Pruner P, Zupan Hajna N, 1998. Paleomagnetic research of cave sediments in SW Slovenia. *Acta carsologica*, **28**, 151-179.

Bosák P, Pruner P, Mihevc A, Zupan Hajna N, 2000. Magnetostratigraphy and unconformities in cave sediments: case study from the Classical Karst, SW Slovenia. *Geologos* **5**, 13-30.

Gospodarič R, 1984. Cave sediments and speleogenesis of Škocjan Caves. *Acta carsologica*, **12** (1983), 27-48.

Gospodarič R, 1985. On the speleogenesis of Divaška Jama and Trhlovca cave. *Acta carsologica*, **13**, 5-36.

Jurkovšek B, Toman M, Ogorelec B, Šribar L, Drobne K, Poljak M, Šribar L, 1996. *Geological map of the southern part of the Trieste – Komen plateau 1-50.000. Cretaceous and Paleogene carbonate rocks*. Inštitut za geologijo, geotehniko in geofiziko, Ljubljana.

Kranjc A, 1989. *Recent fluvial cave sediments, their origin and role in speleogenesis*. Opera 4. razreda, SAZU, ZRC, Karst Research Institute, Ljubljana.

Knez M, Slabe T (Eds.), Gabrovšek F, Kogovšek J, Kranjc A, Mihevc A, Mulec J, Otoničar B, Perne M, Petrič M, Pipan T, Prelovšek M, Ravbar N, Šebela S, Zupan Hajna N, Bosák P, Pruner P, Liu H, 2016. *Cave Exploration in Slovenia. Discovering Over 350 New Caves During Motorway Construction on Classical Karst*. Springer International Publishing, Switzerland.

Mihevc A, 2001. Speleogeneza Divaškega krasa. *Zbirka ZRC*, **27**, Ljubljana.

Mihevc A, Slabe T, Šebela S, 1998. Denuded caves – an inherited element in the karst morphology; the case from Kras. *Acta carsologica*, **27**, 167-174.

Mihevc A, Zupan Hajna N, 1996. Clastic sediments from dolines and caves found during the construction of the motorway near Divača, on the classical Karst. *Acta carsologica*, **25**, 169-191.

Radinja D, 1986. The Karst in the light of fossilized fluvial deposition. *Acta carsologica*, **14-15**, 101-108.

Zupan Hajna N, 1995. A comparison of the mechanical cave sediments from the caves the Škocjanske jame, the Labodnica, the Prevala II and the Mejame. *Annales for Istrian and Mediterranean Studies*, **7**, 117-120.

Zupan Hajna N, 1998. Mineral composition of clastic sediments in some dolines along the new motorway Divača-Kozina. *Acta carsologica*, **27**, 277-296.

Zupan Hajna N, Mihevc A, Pruner P, Bosák P, 2008. Palaeomagnetism and Magnetostratigraphy of Karst Sediments in Slovenia. *Carsologica*, **8**, ZRC Publishing, Ljubljana.

Zupan Hajna N, Mihevc A, Pruner P, Bosák P, 2010. Palaeomagnetic research on karst sediments in Slovenia. *International Journal of Speleology*, **39**(2), 47-60.

(Abstract) **Caves of Maratua Island, East Kalimantan-Indonesia**

Eko Haryono, Haviz Damar Sasongko, Sidiq Harjanta, Mukhammad Awaludin Zaenuri, Juswono Budi Setiawan

*Affiliation: Karst Research Group
Faculty of Geography, Universitas Gadjah Mada, Bulak Sumur, Yogyakarta 55281*

Abstract

Maratua is a small island situated in the easternmost territory of Kalimantan Island. The island is separated from the main island by 60 km of a shallow sea platform. Previous work considered the island as an atoll. This was basically inferred from the V shape plan-form of the island with shallow sea water/lagoon in the inner part. Field surveys conducted in 2012 to 2015 found that the Maratua Island is composed mainly of Oligocene-Miocene Limestone. Only a small portion of the island is covered by Quaternary limestone. The caves of the area are governed by the local geological structure, especially the jointing system. The cave entrances are aligned in the NW-SE orientation parallel to the general pattern or the geologic structure. Caves are found mostly in the western flank of the island. Caves in general have narrow passages formed by enlarged jointing either as a vertical passage or sloping passage. Flank margin caves on the other hand are less prominent in this area. Less developed flank margin caves have likely resulted from the already existed enlarged-fractures and joints when the island was inundated. Fresh water and saline water interface does not obviously exist as proven by the high salinity of the cave water (up to 230 ppm) and the highly fluctuating water level coinciding with the tide oscillation.

(Abstract) **Morphology of Merabu Karst Mountain, Mangkalihat Peninsula , East Kalimantan-Indonesia**

Eko Haryono, Ghufran Zulqisthi, Arief Abdurrahman Hakim, Muhamad Haviz Damar Sasongko, Mohammad Ainul Labib

*Affiliation: Karst Research Group
Faculty of Geography, Universitas Gadjah Mada, Bulak Sumur, Yogyakarta 55281*

Abstract

The Mangkalihat Peninsula in East Kalimantan has been a concern for conservation of nature. The peninsula hosts a Oligocene-Miocene limestone formation where karst develops into a unique pinnacle karst morphology. Morphology investigation was conducted under TFCA-Kalimantan Program to provide geodiversity information in order to promote geoconservation measures of the area. This paper aims to differentiate morphology through morphometry analyses using contour, slope, centroid, and 3D perspective derived from small-format aerial photography. The results show that hundreds of pinnacles and tower karst can be identified using small-format aerial photography. There is differentiation of pinnacle karst density and valley pattern between north part and south part of the mountain which is bordered by very large polje. The direction of pinnacle, valleys, and enclosed depressions development seem to be primarily related to slope aspect and to geological structure. A unique vertical dissolution in the center of tower is found in some localities, forming "Bottle Tower" morphology.

The Jasov Plateau in the Slovak karst as an experimental area for the denudation dynamic research

Zdenko Hochmuth, Alena Gessert

Affiliation: Department of Physical Geography, Institute of Geography, Faculty of Natural Sciences, P.J. Šafárik University, Jesenná 5, Košice, Slovakia.

Abstract

Slovak karst is the largest continuous karst area of Slovakia, which extends into the Hungary as the Aggtelek karst. Together they present the largest plateau karst area of the middle Europe. There is notable mosaic of the dolines, vertical and horizontal caves on these planation surfaces. The area is divided by deep canyons and gorges into individual units (plateaus). The easternmost plateau, Jasov plateau, has the best explored surface and subsurface karst with an area of 60 km². Relative height against the bottom of the Košík kotlina Basin is more than 300 m in the south. From the western Zádiel Plateau is divided by fluvio-karstic valley Hájska dolina. Present researches interlock with speleological research, the result is exploration of the 8 km long karst cave Skalický potok - Rocky Brook Cave. Speleodiving research in the Skalický potok Cave began in 1986 inside the intermittent spring. The long horizontal passage with a lot of siphons was discovered here (more than 30 siphons with length of 2-130 m). The research is not finished; the end of the cave brings the possibility of further progress. In 1989 the vertical passage was discovered continuing almost under the plateau surface, and here we found a connection to the surface. Today the cave is 8123 m long with a denivelation (difference between two levels) of 376 m. This cave with the underground stream we can consider as the main recipient of the karst water circulation of this plateau. In 2008 we began research experiments with limestone tablets to monitor the dissolution rate by measuring the weight loss of tablets on the plateau surface and in the soil. We determined that the weight loss is much smaller in the higher mountain karst of Slovakia. We are monitoring also water chemistry and also discharge of all permanent springs of the plateau to establish the relationship to the rainfall and climate of the area. Three weirs were built in the cave with continuous measuring of the discharge, water chemistry (mineralization, isotopes, tritium and tufa sedimentation) and a meteorological station was installed on the plateau surface.

Keywords: Slovak karst, Jasov Plateau, denudation

1. Introduction

Slovak karst is the largest continuous karst area of Slovakia, which extends into the Hungary as the Aggtelek karst. Together they present the largest plateau karst area of the middle Europe. In Slovakia it occupies an area of about 800 km². It is a mosaic of dolines, karren fields, vertical and horizontal caves on these planation surfaces. The area is divided by deep canyons and gorges into individual units (plateaus). The easternmost plateau, Jasov plateau, has the best explored surface and subsurface karst.

The second largest city of Slovakia, Košice with more than 250,000 inhabitants is located in the Slovak forest. The city is residence of many research institutions and universities. The main university is the University of P.J. Šafárik, where at the Institute of Geography both of the authors work. The branch office of the Slovak Museum of Nature Protection and Caving, that focuses on the karst problems and the Slovak Hydro-Meteorological Institute resides here also. The Institute of Biological and Ecological Sciences of the same university deals with karst topics and BERG faculty of Technical University in Košice. The activity of 3 speleological groups (Drienka, Cassovia, Speleoklub P.J.Šafárika) is also not negligible. This is why the Jasov Plateau is an appropriate model area for research into the karst processes, tectonic, hydroclimatic, denudation, biogeographical and present landscape change.

The authors have worked for a long time on the survey and study of speleological matters of this plateau. Also students are involved in this research via bachelor and diploma theses. Finances for the research has been continuously provided from Slovakian and foreign grant projects, from 1998 from

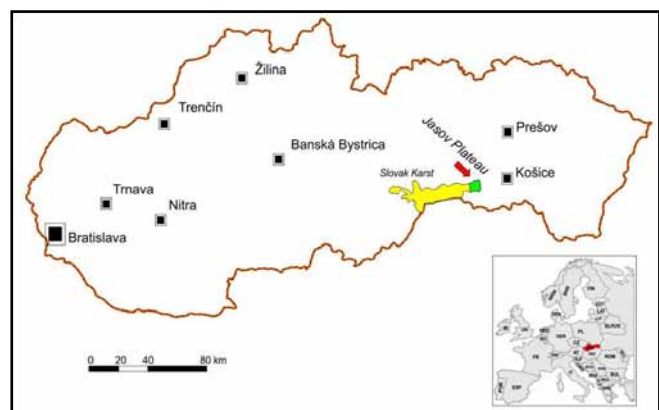


Figure 1. Position of Slovakia and Slovak karst with research area

VEGA agency, later APVV. From all projects the APVV project of Slovak-Chinese co-operation “Comparative study on the karst carbon cycle and carbon sink coupling with the ecological rehabilitation under China subtropic and Slovakia temperate zones (2016-2017)” and other APVV project “New methods of spatial modeling with laser scanning data and 3-D GIS (SPATIAL3D), 2013-2017” dealing with the 3D modelling of processes and events in the Domica cave system. We were also investigators of some VEGA national projects, e.g. “Geomorphological evolution peculiarities of the Slovak karst east part, 2012-2014), “The morphology and genesis of Pre-Cenozoic cave systems in the Western Carpathians, 2009-2011); “Regionalization and geographic information database of karst areas in Slovakia, 2006-2008); “Natural landscape

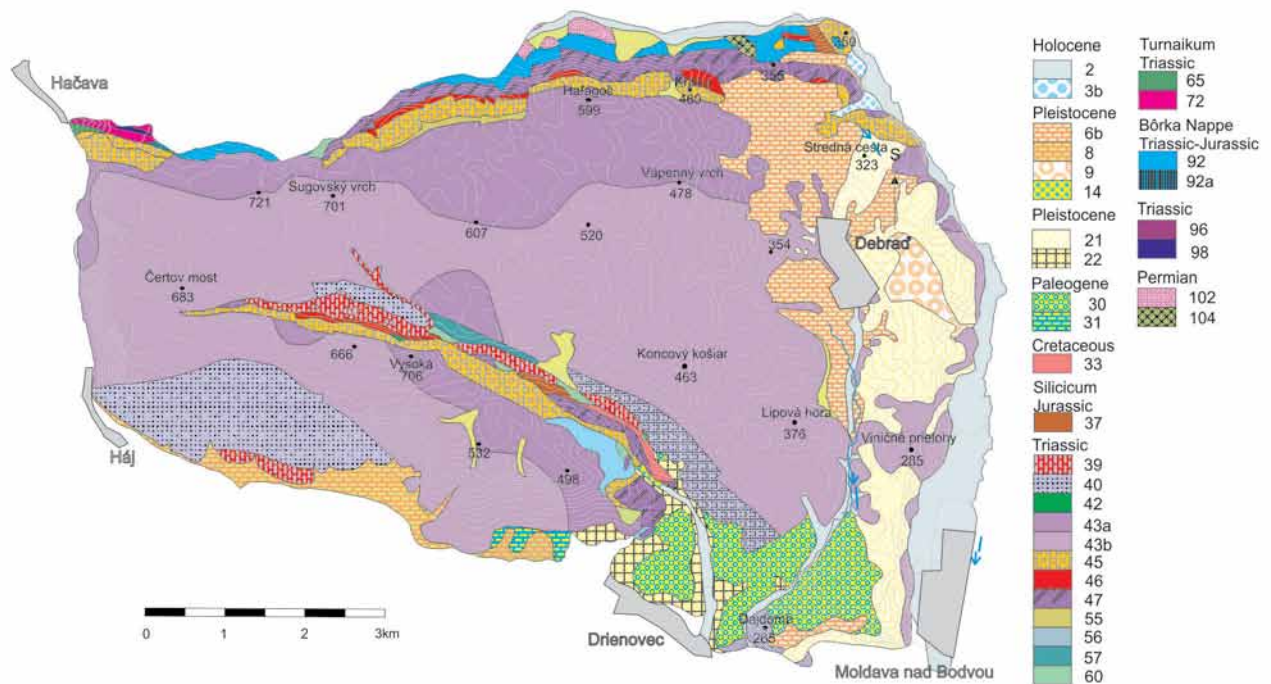


Figure 2. Geological situation of the Jasov Plateau (based on Mello et al., 1996).

Legend:

2) fluvial sediments 3b) proluvial sediments 6b) deluvial sediments 8) deluvial-proluvial sediments 9) deluvial sediments 14) gravel sediments 21) Poltar formation (clays, gravels, sands), 22) Pannonian clays, silts, sands 30) Drienovec carbonatic conglomerates 31) Šomodý formation gray fresh water limestones 33) Miglic white massive limestones 37) Adnet and Hierlatz limestones 39) Dachstein limestones 40) Waxeneck limestones 42) Wetterstein dolomites 43a) Wetterstein riff limestones 43b) Wetterstein lagoonal limestones 45) Steinalm limestones 46) Gutenstein dolomites 47) Gutenstein limestones 55) Nádaska limestones 56) Schreyeralm limestones 57) Szin Beds (shales, marlstones, limestones) 60) Bodvaszilás Beds (sandstones and shales) 65) Dvorníky Beds 72) Gutenstein dolomites 92, 92a) Dark and black phyllites 96) Serpentinities 98) light crystalline limestones 102) Sericite and chlorite sericite phyllites 104) Metamorphosed rhyolites

of the Slovenský kras and its anthropogenic transformation, 2003-2005”, “The relief evolution of the Slovak Karst and surrounding parts of Veporské vrchy Mts. and Košice Basin, 2000-2002).

2. Physic-geographical characteristic of the plateau

Jasov plateau is a separate geomorphological subunit (ca. 60 km²), but geologically and hydrologically it is also necessary to take into consideration adjacent parts of the Košická kotlina Basin ca. 20 km²). The Plateau is a very well delineated geomorphologic area. The area is connected to the non-karstic areas of the Slovenské Rudohorie Mts. to the north, to the south and east is connected to Košická kotlina Basin, to the west it is separated from the Zádiel Plateau by the deep canyon of Hájský potok Brook. The gently sloping plateau surface is situated in the height of 650-500 m ASL (against depressions on the south and east at 210-220m ASL).

2.1. Geological settings

The main part of the area, similar to the whole Slovak karst, consists of the Middle Triassic limestones called “Wetterstein”. These limestones originated in the coral reef conditions of the shallow sea and contain fossil algae *Dasycladacea* and coral. The lower part of the plateau is built up by Steinalm and Waxeneck limestones (Triassic) containing well-preserved clam fossils (*Megalodont*). Tectonic lines are predominantly in the W-E direction. On the north edge of the plateau the

ascending Gutenstein limestones and dolomites are visible as the result of the Silický príkrov Nappe overthrust. The plateau is divided lengthwise by the deep tectonic depression of the Miglic valley which relates to the lamellar structure of the area, it is a part of the Rožňavská línia Fault. Its slopes ascend different non-karstic rock of Jurassic age. This valley is very clear delineation of the sort of independent hydrological units. Very steep subvertical tectonic faults are situated on the south edge of the plateau against the depression of the Košická and Turnianska kotlina Basin. These have had an important role in the hydrological drainage formation that represents Skalístý potok Cave (Fig. 2).

2.2. Climate

The plateau surface at 500-650 m ASL has similar climate conditions as other areas of the Slovak karst. A representative meteorological station for is Silica. It is the only station situated on the karst plateau and is at a height of 538 m ASL. We positioned our own station on the Jasov plateau, at an altitude of 465 m ASL and a rainfall station with short monitoring intervals at an altitude of 570 m ASL. Correlations made by Dobrovič (2015) shown good correspondence of short-term rainfall events that have impact on the underground flow regime. Rainfall stations situated at the foothill of plateau (Turňa nad Bodvou, Moldava nad Bodvou, Jasov) are not useful for our research because they do not offer us useful data due to a rain shadow effect.

2.3. Hydrology

Allogenic surface streams surround the research area on all sides. The most important is the Bodva River flowing from the non-karstic area of Slovenské rudohorie mountains. On the east edge are visible sinking points with connections to shorter caves on the east (Barabas, Haviarová, 2003). On the west runs Hájský potok Brook in the canyon-like valley. There are also some indication of partial sink and river bed infiltration.

On the plateau foothills a few important springs exist that have been a long monitoring record by state organization – Slovak Hydrometeorological Institute. These are Travertínový prameň (Travertine Spring) in the Háj valley (tufa sedimentation); the intermittent spring of Skalistý potok (subsurface cave stream); the permanent concentrate outlet Vinica (with annual average discharge 60 l.s^{-1}); Bereg Spring, Prameň v Slivkovom sade (Spring in the plum garden); Drienovecká Cave Spring; Helena Spring and a few smaller springs along the Bodva valley and on the north foothills is situated an important permanent spring, Teplica. Relatively long subsurface cave stream passages are known from this area. In the Skalistý potok Cave the permanent subsurface stream flows for more than 2.3 km, and another 2,5 km as an intermittent stream. Drienovecká Cave is well-known 0.8 km long stream and 150 m long siphonal segment from Teplica Cave.

2.4. Surface karst

Based on the geomorphological mapping of the Jasov Plateau there are 206 dolines with a density of 6 dolines per km^2 (Petrvalská – Gessert, 2014). The depth of dolines ranges between 3 and 20 m and are up to 100 m in diameter. Compared to other plateaus of the Slovak karst these parameters are lower, but this doesn't mean little karstification. Dolines and other depressions were filled by locals in the past because of better agricultural possibilities. Older scientific work considered poor limestone quality or dolomitisation (impurity presence). But from the chemical analyses of Sládek (2012) and Petrvalská – Gessert (2014) these limestones are pure and appropriate for karstification. We are explaining dolines dimensions by strong sediment cover what can suggest higher age of these forms. The sedimentation can indicate also karren absence inside dolines.

Depressions are mainly of corrosion and alluvial origin (on the longitudinal valleys), and it is likely that buried and suffosion types are also present. They group on the plateau margin in the general inclination direction. Two bigger depressions were mapped – uvalas of irregular shape (depth max. 30 m and length max. 300 m) with small depressions situated on the bottom. These are probably anthropogenic lime pits and sinks.

Close to the north plateau slope along the edge were a series of the cone-like peaks at 670-707 m ASL. We consider these peaks as the remnants of the higher and later denuded surface of the Baden age.

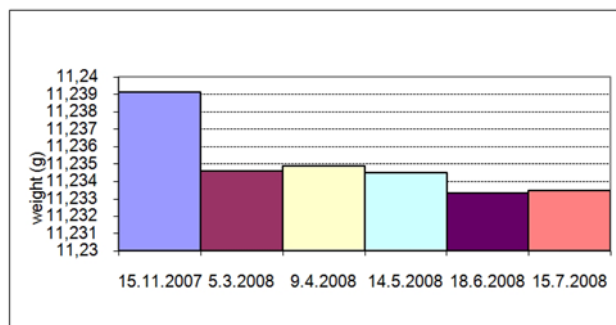


Figure 3. Weight changes during study period on two the limestone tablet sample

3. Selected research results in the study area

3.1. Geochemical research and relief denudation

Since 2007 some experiments with limestone tablets and monitoring the dissolution rate by measuring of the weight loss on the plateau surface and in the soil. This research built on the Slovakian research of A. Droppa (1976) and was in collaboration with newer foreign research. The weight loss is much less in the higher mountain karst of Slovakia than at lower elevations. Regular and relatively representative limestone tablet samples were created from original rocks that were exposed in situ – on the top of the karst surface, buried in the soil and immersed. (also 4 tablets were put in Slovak Paradise geomorphological unit). We focused on detecting of the total and the seasonal changes in tablet weight loss (Fig. 3). This data hopefully can help understand how quickly is the karst surface denudation occurring and surface karst forming (karren, dolines e.g.).

Measurement showed the applicability of the approach for the weight loss estimation. Hydrosopicity of the samples proved to be one restriction of obtaining accurate measurements. The relatively low values of the weight loss are surprising. They suggest a low rate of superficial corrosion with respect to the total chemical denudation. In some intervals of observation, the mass of samples increased, although the trend of material loss was unmistakable. The values are 25-50 times lower than the value of total erosion. We conclude that the proportion of surface dissolution in less than 10% of the total loss. The total loss arises more in the zone of vertical circulation thus it is due to precipitation and water infiltrating into the karst massif. This is confirmed by the fact that the karst rock surface changes only slightly. For that reason the landforms are well conserved in the recent climate as, for example, planation surfaces. Therefore, the substantial part of dissolution occurs beneath the surface corroding primarily cracks, walls and bottom of caves and chasm in the vadose zone.

3.2. Speleology

Skalistý potok Cave (Rocky Brook, Fig. 4)). Speleo-diving research began in 1986 in the area of the intermittent spring. A long horizontal passage was discovered with a lot of siphons (more than 30 with length of 2-130 m) and exploration is still continuing In 1989 the ascending passage was discovered that almost reaches the plateau surface. Here a connection with the surface was discovered. At present the cave is 8,123 m long with 376 m between the bottom and top of the cave. This cave

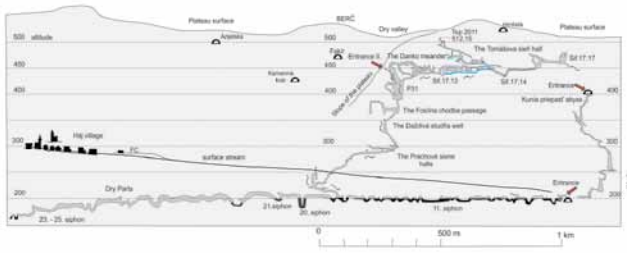


Figure 4. The schematic profile of the Jasov Plateau (under the angle 45-225°)

with its subsurface stream is considered as the plateau main recipient of the karst water circulation (Hochmuth, 2013).

On the basis of these findings, we identify several paleolevels 250 metres above the bottom of the valley over a length of 2 kilometres. They are drained by a stream of unknown origin and source location. The Pre-Quaternary Age is indicated by old, corroded speleothems, large calcite crystals and manganese crusts. There is no apparent relationship with the superficial landforms, dolines, even though these were ground surveyed and mapped in detail. Only a few corridors of the W-E directions can be related with the fault directions in the marginal parts of the karst plateau.

3.3. Karst hydrology

Jasov Plateau has very clear hydrological boundary. Rainfall from its surface infiltrates into underground and streams via many springs on the plateau perimeter. Karst springs have variable water yield, many are only seasonal. But the strongest 4-5 springs (with yearly average discharge 20-50 l. s⁻¹) are outlets from underground passages. The most important is the double spring of Skalický potok cave (permanent and intermittent), that drains more than 8 km of cave. Similarly the Drienovecká Cave where more than 1 km of the underground stream is known and short sections in Teplica Cave – Spring. The underground flow and surface stream infiltration rate were previously studied by dye tracing methods (Hochmuth, 2013, Orvan, 1977, Barabas, Haviarová, 2003).

3.4. Catchment areas

Based on subsurface stream fragments in caves, geological structural boundaries, specific run off and karst spring distribution we have delineated 10 catchment areas on the plateau surface (Fig. 5). We are working to increase the precision of their boundaries. We will use dye tracing in the dolines to further interpret the chemical analyses of the hydrological regime.

The building of three underground hydrological profiles for continuous measurement has been significant for our research. Other important measurements are from Teplica Cave. Spring discharge is monitored by Slovak hydrometeorological institute (SHMÚ) and these are measurements are important to understanding the hydrological regime. We built three rainfall stations on the plateau surface, but we use also data from other meteorological stations in the neighborhood. The station in Silica (on the Silická planina Plateau) is situated in the similar nature conditions. We obtained interesting correlation between rainfalls, temperature, and underground

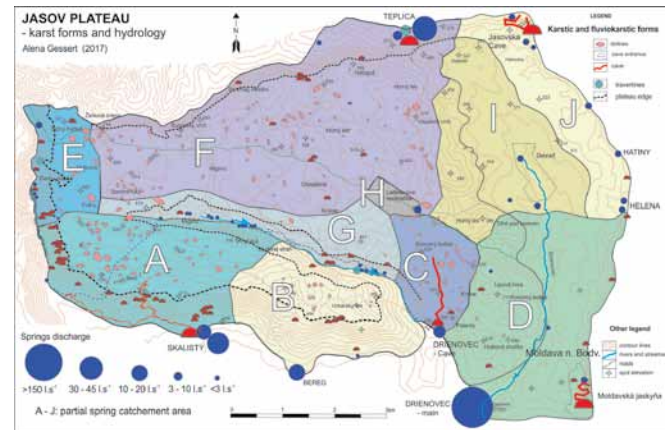


Figure 5. Karst forms and simple hydrology of the Jasov Plateau

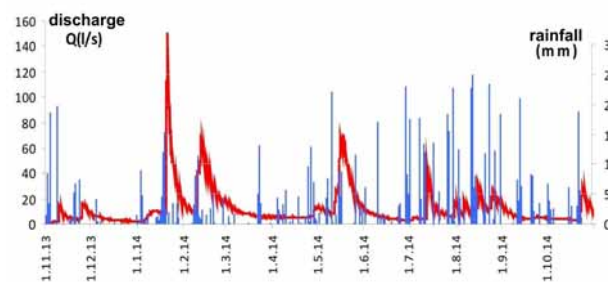


Figure 6. Rainfall impact on the stream discharge in the Skalický potok Cave in 2013 hydrological year

Source: Slovak Hydrometeorological Institute and own measurements

stream discharge and underground water level (Kandričák, 2014, Dobrovič, 2014, Fig. 6).

4. Conclusions

Jasov plateau has very well developed subsurface karst and dynamic processes being monitored in different natural environment. Research potential on the University in Košice has brought interesting results that are applicable on the karst of neighboring similar areas. Individualities of the plateau surface karst processes in the middle Europe is possible to compare with other areas in different climate zones. We hope that our results can help to better understand these speleological localities.

Acknowledgement

This work was supported by Slovak Research and Development Agency within the project [APVV-0176-12] and [SK-CN-2015-0030].

References

- Barabas, D., Haviarová, D., 2003. Evaluation of reciprocal relation of several hydrological factors in connection with the distribution of waters circulation in the Jasov region during 1999 – 2002. *Výskum, využívanie a ochrana jaskýň*, Zborník referátov 5-8. októbra 2003, Tále, st 104-108. In Slovak
- Dobrovič, R., 2014. *Microtectonic impact on Skalický potok and Drienovecká Cave passages forming*. Bachelor thesis, Institute of Geography, PF UPJŠ Košice, 55 s. In Slovak

Droppa, A., 1976. Corosion intensity of karst streams in Demenovská Valley. *Slovenský kras*, **14**, Martin, s. 3-30. In Slovak

Hochmuth, Z., 2013. *Skalistý potok Cave atlas*. Liptovský Mikuláš (Slovak Speleological Society). 80 s. In Slovak.

Hochmuth, Z., Petrvalská, A. 2010. Surface and subsurface karst forms of the Jasov plateau. In: *Geografie pro životve 21. Století*, Ostrava 2010. s.15-19. In Slovak

Hochmuth, Z., Vadelová, I. 2010. Quantitative surface corrosion research of the karst rocks in the Slovak Paradise and Slovak Karst. *Slovenský kras*, **48**, 2, s. 239-250. In Slovak

Kandričák, P., 2014. *Water regime of Skalistý potok Cave in the connection to climate and other physical geographical conditions of the Jasov plateau*. Master thesis, Institute of Geography, PF UPJŠ Košice, 103 s. In Slovak.

Mello, J. et. al., 1996. *Geological map of the Slovak karst*. Geological institute of Dionýz Štúr. In Slovak

Orvan, J., 1977. Contribution to the hydrological conditions of the Jasovská Cave. *Slovenský kras*, **15**, 53-61. In Slovak

Petrvalská, A. 2014. *Relief of the Jasov Plateau in the Slovak karst*. Univerzity of P.J. Šafárik, Košice. 112 s. In Slovak.

Sládek, I. 2014. Pre-research results of the dolomite component impact on the limestones of the Slovak karst east part in the process of karst corosion. *Geographia Cassoviensis*, VIII, **2**. 173-180. In Slovak

Zacharov, M., 2008. Geological and tectonical conditions of the Drienovecká Cave in the Slovak karst. *Slovenský Kras*, **1**, 41-52. In Slovak

Tectonic Control of the Permian Gypsum Karst Belt along the Southern Margin of the Harz-Mountains (Germany)

Hans-Peter Hubrich and Stephan Kempe

Affiliation: Institute of Applied Geosciences, Technische Universität Darmstadt, Schnit spahnstr. 9, D-64287 Darmstadt, Germany. hphubrich@tonline.de kempe@geo.tu-darmstadt.de

Abstract

The Harz Mountains in Germany are an uplifted block of variscan-folded Devonian and Carboniferous rocks with a kilometer-high northward thrust. The overlying, unfolded upper-most Carboniferous, Permian and Buntsandstein (lower Triassic) series are exposed in a wide belt along the South Harz, including a thick series of evaporitic rocks from the upper Permian (Zechstein), dipping with about 10° S to SE. The Zechstein forms an almost continuous karst area nearly 100 km long. The first author, in his dissertation, compiled a geological map for the Zechstein at a scale of 1:10.000, covering an area of 338 km², thus revealing the tectonic structure in order to advance our understanding of the karstic features.

Karstification determines the morphology of the area including 184 registered caves, sinkholes, uvalas, sinking creeks and large karstic springs. Specifically, lines of sinkholes appear to follow faults. By detailed mapping of the three lowermost Zechstein cycles, a dense matrix of faults is revealed. 85° to 125° striking faults reoccur every few 100 m, many of them reverse faults with a N-ward thrust. This leads to repetitive exposure of the strata, causing the broadening of the Zechstein outcrop much beyond of what is expected from the local dip of the series. In other areas horst- and graben-structures are apparent, resulting in kilometer-long Lower Buntsandstein ridges that sink into the surrounding Zechstein. Below ground, the groundwater flowing southward along the dip is diverted into the direction of the strike, thus causing strike-parallel depressions, valleys and sinkhole rows. In the final extension phase, faults striking 150° to 180° have caused graben-structures, allowing groundwater and surface rivers to flow southward, breaking through the escarpment of the overlying Lower Buntsandstein. The tectonic structure therefore of the South Harz determines its hydrology and the karst features apparent at the surface.

Keywords:

1. Introduction

Karstification and speleogenesis depend not only on the solubility of rocks and the chemical reactions involved in their dissolution processes, but also on the tectonic structure of the karst-bearing strata. Here we present results of the first author's doctoral thesis that investigates a 338 km² large area along the South Harz. The hypothesis is that the tectonic structure is largely determining the hydrogeology and the morphology of this area.

1.1. Geological Situation

Central Europe is characterized by "inversion tectonism", the result of temporal change between (i) extension, (ii) compression, and (iii) extension, locally called "Saxonic Tectonism" (e.g. Kley 2013). After the variscan orogeny in the Upper Carboniferous, that folded much of Central Europe along NE-SW striking axes, the continent extended and sank (i), allowing the deposition kilometers-thick deposits of terrestrial and marine epicontinental series from the uppermost Carboniferous to the Upper Cretaceous. These series came under compression (ii) exerted by the northward thrust of the African Plate underthrusting the Adriatic below the European Plate. This caused the uplift of the Alps and its overthrust tectonics while Central Europe reacted with uplift and dextral tectonics, compensating the thrust. Finally, the expanding Atlantic (iii) dilated the continent E-W that reacted with graben formation.

The compression (ii) led to the uplift of southward dipping blocks of variscan folded series along steeply northward inclined thrust faults striking NW-SE. One of these blocks is the Harz, a mountain range of roughly 90 km NW-SE length



Figure 1. The Harz Mountains, a 80 km long block of raised Devonian and Carboniferous rock. Along the southern border the Zechstein is exposed with varying outcrop width (shaded light blue area). The blue lines represent state-borders. The eastern border of Lower Saxony to the west was the former border between West- and East-Germany that dissected Harz and South Harz for 40 years, hampering the geological research. The heavy yellow line marks the Eichsfeld High, a paleogeographic rise within the Zechstein Basin

and 30 km width dominated by Devonian and Carboniferous rocks (Fig 1). It was thrust over the Upper Cretaceous series in several pulses along its northern, kilometer-high fault, striking NW-SE (e.g., "wrench-faulting", Wrede 1979, 1988). The direction of this fault system is therefore called "hercynian" (i.e. lat. "Hercynia" for "Harz") and is the dominating direction of faults and joint systems in Central Europe. The dilatation of the continent on the other hand (iii) led to prominent graben systems. The largest of those is the NNE-SSW striking Upper-Rhine-Graben. Its direction is therefore called

SU	Lower Buntsandstein	Trias
z4A	Aller Anhydrite	4. Cycle Aller
z4T	Aller Clay 0 - 10 m	
z3A	Leine Anhydrite 50 m	
z3K	Leine Limestone 0 - 35 m	3. Cycle Leine
z3T	Leine Clay 0 - 10 m	
z2A	Stassfurt Anhydrite 20 - 100 m	
z2K	Stassfurt Limestone 10 - 50 m	2. Cycle Stassfurt
z2T	Stassfurt Clay 0 - 10 m	
z1A	Werra Anhydrite 30 - 250 m	
z1K	Werra Limestone 5 - 25 m	1. Cycle Werra
z1T	Kupferschiefer - Copper Clay <1 m	
r	<div style="display: flex; justify-content: space-between;"> <div style="background-color: red; color: white; padding: 5px; text-align: center;"> Unconformity Rotliegend </div> <div style="background-color: orange; padding: 5px; text-align: center;"> Unconformity Upper Carboniferous </div> </div>	

Figure 2. Stratigraphic column of the South-Harz Zechstein.

“rhenish”, representing the second most important direction of faults and joints in Central Europe.

In contrast to the prominent thrust-faults on its northern side, the Harz block dips below the unfolded uppermost Carboniferous and Permian series on its southern rim. This area, geographically called South Harz, is by area, the largest outcrop of the upper Permian, marine Zechstein in Germany. The Zechstein, one of the oldest formation names in geological history, is today considered a lithostratigraphic group correlating to the chronostratigraphic stages of Wuchiapingium and Changhsingium comprising the series of the Lopingium (257.3 to 251 Ma). The Zechstein contains up to seven cycles of evaporitic rocks including kilometer-thick salt layers

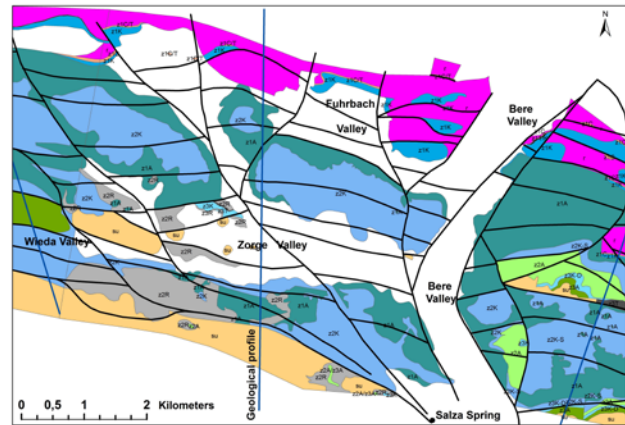


Figure 3. Geological and tectonic map of the Zechstein area on both sides of the Bere-Graben north of Nordhausen. The area is structured into blocks defined by ca. E-W striking faults and by later NW-SE faults converging at the site of the Salza Spring, one of the large karstic springs of the area. The general dip of all blocks is to the S. Color coding see Fig. 2. White areas are covered by Quaternary deposits.

that underlie much of Germany. They formed in a sinking intracontinental basin with restricted access from the world ocean at a tropical latitude. Along the South Harz the lower four Zechstein-cycles are exposed (Werra-, Stassfurt-, Leine, Aller-Cycles), typically starting with a clay-layer, followed by limestone and/or dolomite and superseded by anhydrite, surficially altered to gypsum. These series can be up to 300 m thick (Fig 2). The originally intercalated Na- and K-salts are dissolved at depth and are not exposed due to the humid climate of Europe. To the south, the Zechstein is overlain by thick Lower Triassic continental series, the “Buntsandstein”, forming an impervious cap over the Zechstein.

2. Methods

In Germany, systematic geological mapping at a scale of 1:25 000 started in the late 19th century. Some of the quadrants have never been remapped and still show the old Zechstein bipartition into older and younger series instead of the tripartition (neglecting the Aller-series that is mostly buried below solifluction blankets of the clayey Lower Buntsandstein). Furthermore, the Zechstein was considered as being disturbed by karstification, preventing its thorough tectonic analysis. The latest edition of a South Harz map is sheet Osterode (Jordan 1976) which is still lacking adequate tectonic treatment.

The division of Germany prohibited a comprehensive and unified approach to the South Harz, its stratigraphy and tectonics. The second author therefore started in the 1980s to conduct advanced mapping courses within the curriculum of the geosciences at the University of Hamburg and later at the University of Technology, Darmstadt. Additionally, about 40 diploma theses (equivalent to MSc) were supervised that mapped Zechstein areas. After the reunification in 1989, courses and thesis works were extended to the area east of the former border. This material, plus the published geological maps plus additional field work, lists of wells and of sinkholes are summarized in the current PhD thesis. All data were georeferenced and entered into ARCGIS, enabling us to deduce areas and lengths and undertake statistical analyses. Layers containing the different geological and morphological maps,

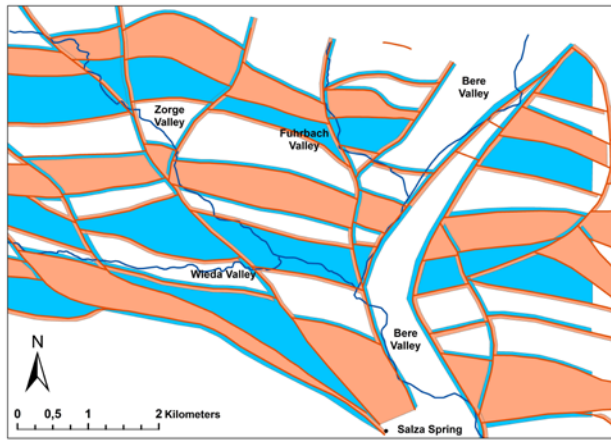


Figure 4. Tectonic model of the area in Figure 3 showing Hercynian reverse faulting and resulting horst (red) and graben (blue) blocks as well as dilatational “rhenish” faults offsetting the older compressional faulting, the downthrow blocks are blue and the upthrow blocks are red marked.

geological units and other features allow to compare results and to find the best overall interpretation of tectonics.

In the field, the three series are best differentiated by the z2K, a brittle limestone formation with a characteristic smell called “Stinkschiefer” and the z3T, a typical gray clay (“Grauer Salztön”). By mapping these, a unified geological map showing all three series of the entire South Harz was derived for the first time. Wide-spread Harz river terraces, Elsterian moraines as well as glacial solifluction blankets cover about 43% of the Zechstein outcrops.

Our tectonic analysis assumes that the Zechstein basin is dipping with about 10 to 15° S-ward. This is measurable at the lower border of the series where the – undisturbed by karstification and salt-leaching – z1K (“Zechsteinkalk”) overlies clastics of either the lower Permian or uppermost Carboniferous or peneplained folded Variscan series (all of these constituting the basement of the Zechstein). Because of this relatively large inclination, the surface outcrop of the undisturbed series is generally only a narrow belt. However, the outcrop width reaches several kilometers in places. This can be explained by repeated reverse faulting. In contrast to this model most earlier authors assumed that the basement dip is diminishing or even reversing southward, avoiding thereby the necessity

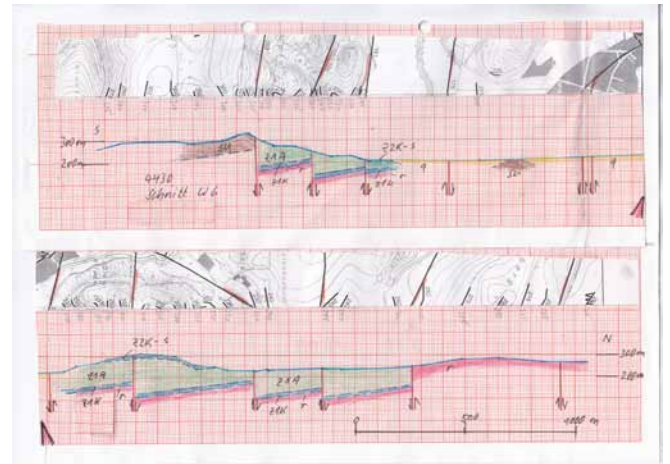


Figure 5. N-S Geological profile showing the tectonic structure of a section from the area in Fig. 3. Lower section fits to the right (N) of upper section.

to assume faulting. One more geological feature complicates the analysis, and this is the “Eichsfeld Schwelle” (ES, Fig 1), a paleogeographic high within the Zechstein basin.

On top of the ES, the z1A and z2A are missing. Along the sides of the ES their thickness first increases to a few hundred meters and then reduces towards the W and E, i.e. towards the centers of the marine basin (Herrmann 1956).

3. Results

Figure 4 shows a central area of the South Harz, north of the city of Nordhausen. It features repeating E-W striking ridges of Werra Anhydrite (z1A) overlain by the Stinkschiefer (z2K) and a graben with lower Buntsandstein. In the S the Lower Buntsandstein is downfaulted against the Zechstein. The E-W ridges are transected by a N-S striking graben, the Bere valley. It could be a small pull-apart basin with the associated dextral strike-slip faults being located north of Ilfeld in the lower Permian volcanics and south of Nordhausen in the Buntsandstein. The presence of pull-apart structures is consistent with transpressional ridges that are also present within the Zechstein in a few sites near Osterode (even though these may be more associated with the Gittelde Graben terminating the Zechstein outcrop in the West). Further NW-SE striking fault lines, along which valleys developed, are offsetting the

Table 1. Areal distribution of important formations and units within the South Harz Zechstein outcrop.

Toposheet Quadrants	Area [km ²]	Quaternary [km ²]	Soli-fluction area [km ²]	z1A [km ²]	z2A [km ²]	z3A [km ²]	z1K [km ²]	z2K [km ²]	z3K [km ²]
4227	39	24	2	3	3	3	-	21	0
4327	43	31	0	3	0	1	1	2	0
4328	39	11	1	-	-	0	7	14	3
4428	11	1	0	-	-	-	1	5	0
4429	67	27	2	7	0	2	2	24	1
4430	47	24	2	10	1	0	1	9	0
4431	50	16	2	5	3	1	3	6	1
4532	18	6	1	3	2	1	2	1	-
4433	24	6	3	1	2	2	2	2	0
Summen	338	146	12	31	11	12	20	83	5

hercynian ridges as well. The vertical thrust of all these faults is varying between a few to a few hundred meters. In Figure 4 the pattern of relative horsts (red) and grabens (blue), as well as series of N-up-thrusted blocks (white) are highlighted, showing the overall structure of the area more clearly.

Figure 5 shows one of the 150 geological profiles that have been constructed every 500 m throughout the entire stretch of the Zechstein outcrop. Constructing these profiles add additional constrains on the tectonic interpretation. The profile illustrates that where the basement is thrust upward by the revers faulting impervious (or less pervious) shoulders are created representing underground barriers against the southward flowing karst waters. The Zechsteinkalk (z1K) is, because of its bedding planes and jointing, a good aquifer even without considering its potential karstification. Water can thus sink underneath the Werra Anhydrite (z1A), dissolving it from below, a typical hypogene karstification (e.g., Kempe, 1996). Therefore, the valleys develop faster along the reverse faults than along normal faults. In turning around the argument one can assume that the larger dissolutional valleys are developed above reverse fault lines. Figure 4 also shows that several of the NW-SE striking faults converge at a point. At this junction, a large karstic spring exists, the Salza-Quelle. Its discharge amounts to ca. 440 l/sec on average (Völker and Völker 2016). The tectonic pattern shows that the faults can in fact guide water underground from a large tributary area to this point of emergence.

4. Conclusions

In summary, we have to solve an equation with three unknowns when trying to understand the tectonic structure

of the Zechstein plateau along the South Harz: Thicknesses of the series, faulting, and inclination, knowing only one factor: Surface geology. However, the reconstruction not only shows internal consistency, it also is embedded into the larger tectonic history of Central Europe and it can explain prominent features of the karst hydrology and morphology.

References

- Herrmann A, 1956. Der Zechstein am südlichen Harzrand. *Geol. Jahrbuch*, **72**, 1-72 pp.
- Jordan H, 1976. *Erläuterungen zu Blatt Osterode, Nr. 4227, der Geologischen Karte von Niedersachsen 1:25 000*. Hannover, 148 pp., 14 Fig., 12 Tab., 5 Maps
- Kempe S, 1996. Gypsum karst of Germany. In: A Klimchouk, D Lowe, A Cooper, U Sauro (Eds.). Gypsum Karst of the World. *Intern. J. Speleol. Spec. Issue*, **25**(3-4), 209-224.
- Kley J, 2013. Saxonische Tektonik im 21. Jahrhundert. *Zeitschrift Deutsche Gesellschaft für Geowissenschaften*, **164**(2), 295-311.
- Völker C, Völker R, 2016. *Der Salzaspring*. Private printing, Ufrungen, 18 pp.
- Wrede V, 1979. Beobachtungen zum tektonischen Bau des N-Harzrandes bei Goslar. *Der Aufschluss*, **30**, 253-265.
- Wrede V, 1988. Der nördliche Harzrand – flache Abscherbahn oder wrench-fault-system? *Geologische Rundschau*, **77**(1), 101-114.

(Abstract) **Features, exploitation and protection of karst Caves in China**

Zhongcheng Jiang, Yuanhai Zhang, Weihai Cheng

*Affiliation: Institute of Karst Geology CAGS. Guilin Guangxi 541004 China;
Cave Research Committee of China. Guilin Guangxi 541004 China*

Abstract

There are millions of karst caves in China. However, most caves are not so long as Mammoth Cave in North America. The longest cave in China is the Shuanghe Dong cave system, 182 km long and which currently ranks 10th in the world. The deepest cave in China is the Tianxing cave system in Chongqing region, about 1000 m deep. Most of the world's known large cave chambers are in China, half of the largest chambers are in China. The largest chamber in the world by volume is China's Miao Chamber, and Cloud Ladder Hall in China is the tallest big chamber, with a vertical range of 365 meters.

Caves in China are most commonly formed in limestone and dolomite rock. The karst caves are "epigenic", formed through dissolution by rain, water flow and underground rivers; almost no "hypogenic" caves are found. Large caves are common in south China where there is abundant rainfall and warm temperatures, but the large caves in north China need allogenic water flow for the karst dynamics.

As a resource, caves in China have been widely used in agricultural production, material storage, water reservoirs and cave expedition activities. The high-resolution reconstruction of paleo-environmental studies of karst caves using stalagmite dating, have achieved widespread attention. A lot of research results have been published in top international journals.

However currently, cave tourism is the most important use cave resources, because there are wonderful and colorful formations and secret environment in karst caves. More than 400 karst caves in China have been open to tourists. Many show caves are in World Heritage Sites and World Geoparks, such as South China Karst's Furong Dong near Chongqing and Jijin cave in Guizhou. Cave tourism creates good jobs for the locals, stimulating the local economy, and encouraging them to be active in protecting the cave.

Keywords: Karst cave; Cave resources; Cave tourism; China

(Abstract) **Exploration of the Caves of Isla de Mona, Puerto Rico**

^{1 2}Patrician N. Kambesis

Affiliation: ¹ Center for Human Geo-Environmental Studies, Department of Geography and Geology, Western Kentucky University, Bowling Green, Kentucky, "United States"
² Cave Research Foundation

Abstract

Isla de Mona displays a spectacular series of large cave entrances ringing its entire perimeter. Located east of Hispaniola and west of Puerto Rico in the Caribbean Sea, the island is a tectonically uplifted carbonate platform with a flat-topped topography. The island contains the largest flank margin cave in the world and has one of the highest concentration of caves amongst the Caribbean islands. The caves hold significant cultural, historical, and archeological materials. Their speleothems, sediments and mineralogy contain geologic and paleoclimate information about the caves, the island, and region.

Geologically, the island is composed of Miocene-age carbonate units: Isla de Mona Dolomite and the overlying Lirio Limestone. There is no surface drainage or associated features and recharge into the island is entirely autogenic and diffuse. Meteoric water sinks into the fissures and small pits atop the island and slowly migrates downward to join a freshwater lens. The lens floats on a denser layer of saltwater. The salt-freshwater interface is dissolutionally aggressive and forms a mixing zone resulting in the formation of the flank margin caves. Most of the flank margin caves occur at the contact between the Lirio limestone and the Mona dolomite though some cave development extends into the dolomite. Large cave entrances have also developed within the lower sections of the Mona dolomite. These caves appear to be strongly influenced by littoral processes though they may have originated as small flank margin caves. Cave location is a function of tectonic uplift and sea level changes.

The flank margin caves of Mona are characterized by multiple cliff-side entrances and skylights, and large ramiform passages. Cave development extends up to 270m inland from the cliff line. The caves formed without entrances and are exposed with erosion of the cliff line. The littoral caves tend to have more linear passage morphology and extend up to 150m inland. Entrance dimensions are up to 100m wide and 40m in height, and many are 20-30m above current sea level. All of the caves contain evidence of pre-historic Taino activity and of historic saltpeter mining.

Proyecto Isla de Mona has fielded annual expeditions since 1998 and so far, 210 caves (75 km) are mapped with more that have not yet been accessed. The Project works in partnership with Natural Reserves and Wildlife Refuges Division of Puerto Rico and with researchers conducting archeological, geological, and biological fieldwork.

(Abstract) **Origin of Enigmatic Caves of the Far Western United States**

^{1,2}Patrician N. Kambesis, ²Joel Despain

Affiliation: ¹Center for Human Geo-Environmental Studies, Department of Geography and Geology, Western Kentucky University, Bowling Green, Kentucky, United States”
²Cave Research Foundation

Abstract

The far western United States contain a variety of karstic landscapes some of which display characteristics suggesting hypogenic origin. This study focused on karstic caves within three Western US physiographic provinces – the Motherlode and southern Sierra of the Sierra Nevada Mountains (CA), Klamath Mountains of northern California, and the eastern Great Basin of Nevada. Most of the caves of California formed by epigenic processes though there appear to be exceptions which are included in this study. Many of the karstic caves of the eastern Great Basin are characterized by features that indicate hypogenic origin.

Parameters that definitively constitute hypogenic speleogenesis are currently equivocal within the field of karst science. Two different approaches are utilized to identify speleogenetic processes that determine karstic cave origin. The hydrogeological approach defines hypogenic caves by their overall and passage morphology and through their place and position in a hydrogeological system, specifically via upwelling flow of deep phreatic water. Recharge of a soluble formation is from below, independent of recharge from the overlying or immediately adjacent surface.

The geochemical approach emphasizes processes of dissolution, and the source of aggressiveness of cave-forming waters. This approach considers that epigenic processes are controlled through kinetics where chemical exchange occurs via movement and mixture of water, and dissolutional capacity is enhanced by direction of flow. Hypogenic processes are a function of mass balance, and chemical exchange that only occurs in distal areas that are connected to a phreatic aquifer where dissolution capacity is independent of lateral flow.

In this study a combination of hydrogeological and geochemical parameters was considered to determine speleogenetic origin of the enigmatic caves of this study. Parameters analyzed were morphological footprint, occurrence and morphology of speleogens, identification of secondary mineralization such as speleothems, crystalline coatings, exotic minerals and clay occurrence and distribution, hydrogeological function, and geochemical regime.

Our analysis indicate that the study caves are relict features formed when groundwater levels were higher. Eastern Great Basin caves are hypothesized to have formed by mixing zone dissolution within the carbonate-rock aquifer characteristic of the region. The Mother Lode and Klamath Mountain caves may also have mixing zone origin, due to lack of relationship to surface topography, and 3-dimensional maze configurations. Caves of the southern Sierra Nevada are unusual exceptions in an area of extensive epigenic karst. Genesis of these caves is tied to local conditions including ore deposition by hot fluids and sulphate dissolution chemistry.

Geomorphology And Hydrogeological Features Of The Rječina Karst Spring - Croatia

Mladen Kuhta

Affiliation: Croatian Geological Survey, Sachsova 2, 10000 Zagreb, Croatia

Abstract

The Rječina spring is one of the major springs in the Dinaric Karst. The spring occurs approximately 10 km in the north from the town of Rijeka, 325 m above sea level and offers an outstanding opportunity to cover gravitationally the public water demand of a town of about 200,000 inhabitants, and the tourist needs of the whole region, with a groundwater of excellent quality. The spring appears at the tectonic contact between permeable Cretaceous carbonates and impermeable Paleogene clastic rocks, with a maximal discharge of 120 m³/s, but it is inactive during the summer dry seasons for up to three months a year. Over the past few decades, the spring and its catchment areas were the subject of comprehensive hydrogeological investigations. Part of these studies have been caving and cave-diving investigations that contributed to a better knowledge of spring cave geomorphology, and ultimately a better understanding of its hydrogeological features.

Groundwater at the Rječina spring discharges from the approximately 300 m long cave, which consists of two main branches. The Upper channel morphology has characteristics of epiphreatic development while the Lower channel is more of artesian (Vauclusian) structure. The research results show that Upper and Lower inlet channels of the spring are hydraulically separated and probably connected to the different drainage systems, i.e. different retention areas. In the dry period both underground canals have no direct connection with the retention areas and the water present in the spring is only the rest of the last outflow detained in the cave channels. The recession coefficient obtained from hydrograph analysis indicates the lack of the base-flow spring component, and only fast-flow component was determined. Flow model calculations were conducted for ¹⁸O with the exponential (EM) and dispersion model (DM). The obtained mean residence time (MRT) of 3.6 months confirms dominant recent groundwater recharge.

Keywords: Karst spring, geomorphology, hydrogeology, Rječina, Croatia

1. Introduction

The Rječina spring is one of the largest springs in the Dinaric Karst (Fig. 1). It is located about 10 km north from the city of Rijeka, about 2 km upstream from the village Kukuljani. Regarding to the high spring altitude (325 m a.s.l.), which allows the development of gravity-fed water system, and significant quantities of very high quality groundwater, the Rječina spring has been used for the public water supply of the coastal town Rijeka and surrounding settlements (about 200.000 inhabitants) since 1915. The main disadvantage is that during the dry summer period, when the water needs are the largest (tourism), the spring regularly dries up. Depending on the hydrological conditions the outflow interruption takes from 0 to 157 days. In order to enable permanent water supply during dry season, over the past few decades, the spring and its catchment area were the subject of the comprehensive hydrogeological investigations. Several possible solutions were considered, from construction of the dam, which would be, in addition to the surface accumulation, raise the overflow level of the spring and consequently increase underground reserves, to a completely different solution related to spring over-pumping. In recent years, research has focused on the study of geometry and dynamics of the underground aquifer in the wider spring hinterland, and possibly the groundwater abstraction by deep wells.

Part of these studies occasionally have been caving and cave-diving investigations that contributed to a better knowledge of spring cave geomorphology, and ultimately a better understanding of its hydrogeological features.

2. Reserch Review

The first data on the Rječina spring morphology originate from Italian cavers. The source is registered in the cave cadastre of Alpine Club of Rijeka (Club Alpino Italiano, 1928) under the number 33 as "Sorgente della Recina". With the record is enclosed a sketch of the water submerged parts. Boegan (1930) mentions this phenomenon with the depth of 15 m.

The first known results of diving research dating back to 1971 (Pilipić, 1971), when autonomous diver reached a depth of 34 m in the Lower channel. During the dry season of the same year, the first pumping test of the spring was conducted. Pumping was carried out in several stages with different stations and capacity. Due to water level drawdown, the pumps were gradually lowered deeper into the Lower channel. At the end of the pumping the bottom of the channel was reached at the depth of 34 m (Hraba, 1973a). Since the pumps were turned off there was no return of the water level for two days, and the open underground space was topographically recorded (Božičević, 1973). During the whole time of the pumping test the water level in Upper channel was stagnant at about 3 m above the spring spillway level, i.e. 37 m above the water level in the Lower channel on the end of test. Source was abruptly activated after a few hours of the heavy rain during the night.

The next pumping test was conducted after the termination of discharge, in September 1973. In the meantime 22 m long access tunnel was excavated from the surface to the underground chamber in front of the Upper channel, which allowed direct access and pumping of the upper siphon. After nine days of pumping, the water level in the Upper channel was lowered by about 19 meters, up to the level 307.5 m a.s.l.



Figure 1. The Rječina spring during average hydrological conditions – discharge $5.6 \text{ m}^3/\text{s}$. Photo: M. Kuhta

(Hraba, 1973b), which allowed the caving team to enter and the recorded upper channel topographic length of discovered underground system increased to about 250 m.

Spring research has continued ten years later, in 1984 respectively. As part of these studies, diving in the Lower channel was repeated. The spring was active with a discharge of about $2 \text{ m}^3/\text{s}$. Divers have reached a depth of 36 m, and observed that a steep channel continued further in depth. It is important to recall that this channel in 1971 was completely closed at a depth of 34 m, and the results of the dive need to be taken with reservations.

In order to solve doubts regarding the Lower channel morphology the cave diving investigations at the entrance area of the spring were conducted in 1997 (Kuhta, 1999). The Lower channel was explored to a depth of 50.5 m and 100 meters in length. It was seen that channel continues to a depth of at least 60 m and the underground space expands. The newly investigated sections were added to the existing topographical cave map (Fig. 4). During the explorations it was determined that there was no flow from the Upper channel and the whole spring discharge (about 400 L/s) was related to flow from Lower channel.

Hydrogeological characteristics of the Rječina spring were investigated as part of several projects carried out since the mid-sixties of the last century. During these studies, numerous detailed mapping and groundwater tracings were made in the carbonate hinterland of the spring, which helped to define the catchment area. The main objectives of the recent research of the area was to determine the hydrodynamic relations in the hinterland of the Rječina spring and periodic springs of Grobnik Polje (karst field), using the findings of the groundwater level and spring discharge monitoring as well as data of chemical and isotopic analyzes of groundwater and precipitation (Kuhta *et al.*, 2014). The research results contribute to a better knowledge of the recharge conditions and the assessment of groundwater resources of the studied area.

3. Geology

The base for the hydrogeological exploration of karst areas is a good knowledge of the geological structure and composition of the deposits. It is of a special importance for the Rječina spring where all the complexity of the structural composition of the Dinarides is fully displayed. Litostratigraphy and tectonics define the geometry of karst aquifer and recharge area.

The Dinaric karst is characterized by a succession of more than 8000 m of predominantly carbonate sediments (Vlahović *et al.* 2005) that was deposited and exposed to intense tectonic disturbances in several phases from the Triassic period until the present. The main deformation episode began in the Late Cretaceous, when synsedimentary tectonics became stronger, and reached a maximum in the Oligocene/Miocene. This led to tangential movements and the uplift of the Dinarides, including the wider area of the Rječina spring. Due to the strong NE-SW-oriented regional tectonic stress, the main resulting structures, including folds, faults, thrusts and imbricate structures, are of the NW-SE strike (i.e., the Dinaric strike). Later orogenic movements shifted the regional tectonic stress to the N-S direction and caused wrenched tectonic deformations.

The catchment basin of the Rječina spring is located in the mountainous area of the Gorski Kotar in Croatia but comprises parts of the Mt. Veliki Snežnik (1796 m a.s.l.) in neighboring Slovenia. The main part of the catchment consists of shallow-water carbonates, mostly limestones and dolomites with subordinate carbonate breccias, deposited in the period from the Lower Jurassic to the Eocene. The Rječina river spring is formed at the tectonic contact of the highly permeable Lower Eocene and Cretaceous limestones and impermeable clastic sediments, Middle to Upper Eocene flysch respectively. Contact between carbonate sediments and flysch is clearly morphologically indicated by steep, often vertical sections of the terrain. Due to increased erosion in the area of the spring, here it is especially pronounced. Carbonate deposits steeply rising about 250 m above the spring, forming an impressive amphitheater. Downstream, the Rječina river

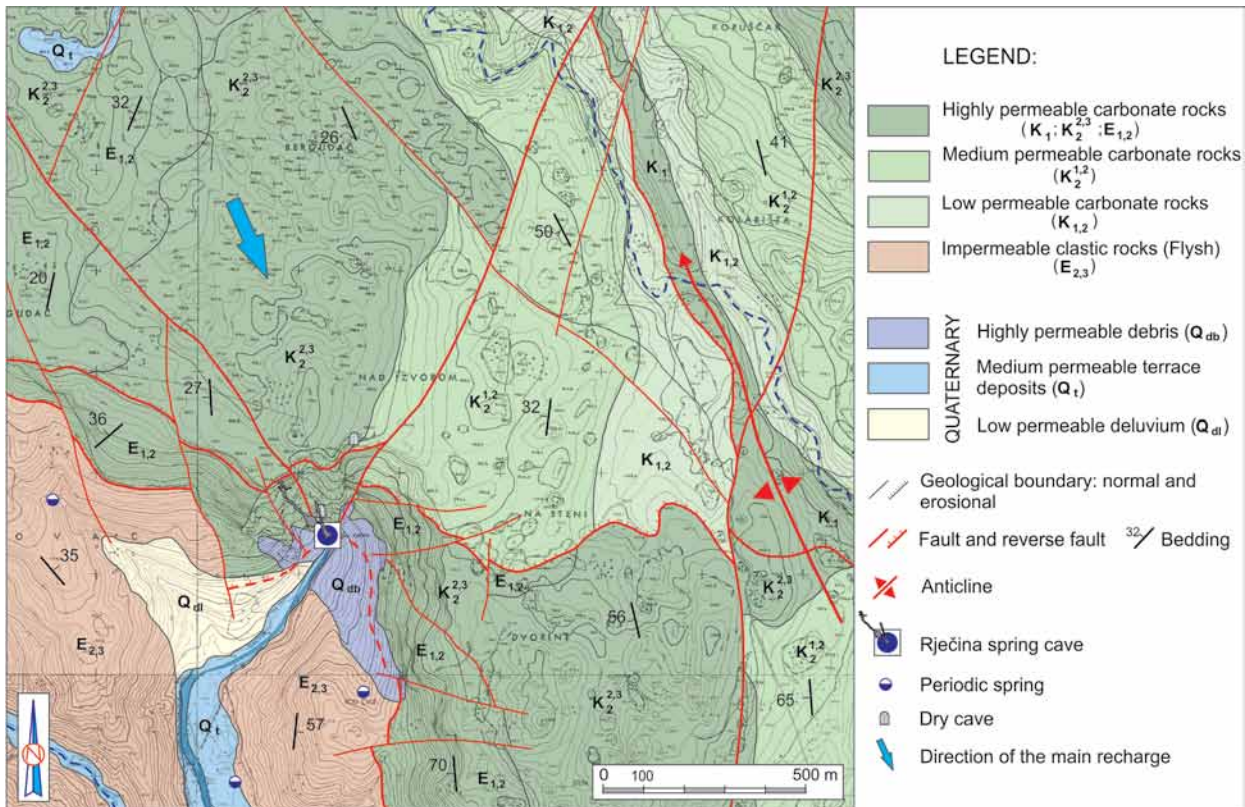


Figure 2. Hydrogeological map of the Rječina spring area

valley is deeply cut into the flysch sediments and represents the erosion base of the wider area.

4. Hydrogeology

Within the carbonate complex, in the catchment area of the Rječina spring, three groups of rocks of different hydrogeological characteristics may be distinguished (Fig. 2). The litho-stratigraphic units consist mainly of limestones represent a medium of good permeability and generally the main groundwater collectors, while the units characterized by roughly equal content of dolomites and limestones are considered as medium permeable carbonate rocks. The units that mainly consist of dolomites and dolomite breccia represent low permeable medium, and very often form barriers to groundwater flow or they direct this flows along the bounding structures.

The flysch deposits are lithologically heterogeneous; however, due to the dominance of marls, this sediment series, when considered in its entirety, is impermeable to water. Considering their structural position and their nearly uninterrupted stretch from Slovenia to the coastline, the flysch deposits form a complete hydrogeological barrier to groundwater movement from the carbonate hinterland toward the sea. Flysch deposits had a crucial role in the formation and development of the Rječina spring, but also they have a significant impact on the regional hydrogeology.

The Rječina spring and its catchment area are just a part of the wider and complex catchment area of permanent karst springs located along the coast in the town of Rijeka. This is the most productive catchment area in the north Adriatic

region and the main potable water supply for the Kvarner Bay area (approximately 3 m³/s during the dry summer seasons).

The Rječina spring occurs high in the catchment area (325 m a.s.l.) and has the function of an overflow for medium and high groundwater. During summer dry season, the Rječina spring is without runoff (although its cavernous conduits are filled with retained groundwater), but the water flows through the deep karst underground, first towards the Grobničko Polje on the southeast, and after that through the tectonically reduced flysch barrier toward permanent coastal springs on the south (Biondić *et al.*, 1997).

The Rječina spring is an periodic karst spring. During the analyzed period 1948-2002 the average annual dry up period lasted 42 days, and varying between years without drying up and a maximum of 157 days. It is considered that a maximum discharge rate of 120 m³/s can be expected, but during the mentioned period of observations the measured maximum was 60.1 m³/s, while the average annual discharge was 7.21 m³/s. Hydrograph of the spring (Fig. 3) for the hydrological year 2012/13 shows its karst features and high correlation with rainfall.

The recession coefficient obtained from hydrograph analysis indicates the lack of the base-flow spring component, and only fast-flow component was determined. Flow model calculations were conducted for ¹⁸O stabile isotope with the exponential (EM) and dispersion model (DM). The obtained mean residence time (MRT) of 3.6 months confirms dominant recent groundwater recharge (Kuhta *et al.*, 2014).

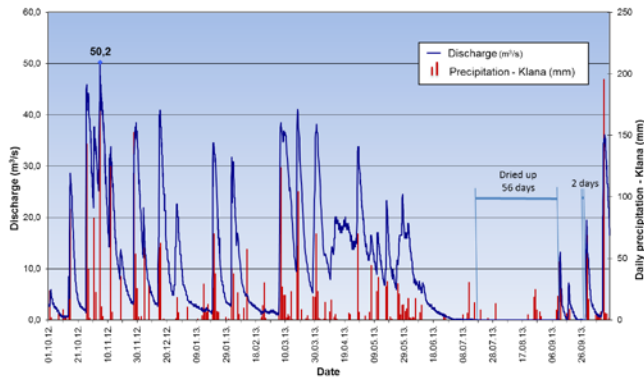


Figure 3. Hydrograph of the Rječina spring for the period from 1/10/2012 to 15/10/2013 in comparison with daily precipitation on the rain gauge station Klana

5. Geomorphology Of The Rječina Spring Cave

Geomorphological phenomena, as in all karst areas of Dinarides, are a direct result of the lithological characteristics, geological structure, hydrogeological properties of rocks and the changes in hydrological and meteorological conditions, particularly during the Quaternary epoch. The relief forming processes must be considered dynamically, through time, because the present state is only a momentary reflex of interaction of endogenous and exogenous processes. The material traces in the shape of morphological phenomena and younger sediments (river valleys, river terraces, underground phenomena etc.) enable, at least, a particular reconstruction of geomorphological development of a terrain and, importantly provide insight into the genesis of the actual hydrogeological relationships and groundwater dynamics.

In the wider area of the Rječina spring terrain surface is exposed to endogenous processes from Neogene, as well as in the whole area of the Karst Dinarides, the most significant changes and the formation of today's relief, took place in the Pleistocene period that began 2 million years ago. This period characterized significant climatic variations related on the alternation of glacial and interglacial stages. During interglacial, as a result of intensive rainfall and ice cover melting, the terrain surface was exposed to strong endogenous processes, and particularly intense erosion. Through the development of karst processes, water from the surface progressively was descending into the carbonate underground where the drainage systems were being developed. The discoveries of smaller dry caves, fossil springs respectively, highly in the cliff above the present spring confirm the gradual canyon opening and the water removal into a deeper karst underground. The Rječina spring cave is the part of recently active underground hydrographic network.

Groundwater at the Rječina spring discharges from the approximately 300 m long cave, which consists of two main branches (Fig. 4). The entrance siphon is 15 m deep and about 30 m long, and ends in an enlarged underground chamber (25 x 20 m). The entrance to the upper channel is about 4 meters above the level of the spring spillway (329.45 m a.s.l.). During the pumping in September 1973 the channel was investigated in a total length of 150 m (Božičević, 1974). For the most part, the channel runs northwest with an average width of 4 and a

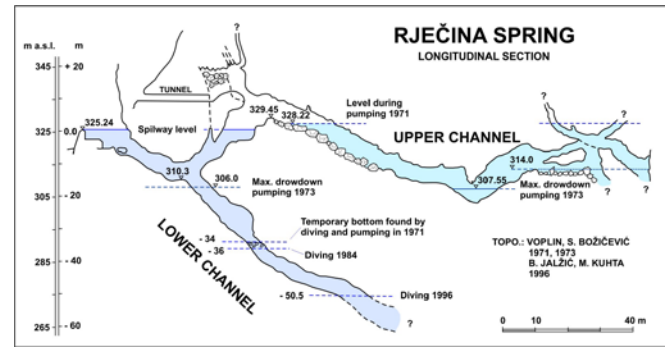


Figure 4. Longitudinal section of the Rječina spring cave

height of 5 m. The channel ends with several somewhat narrower branches and a few unexplored siphons. The Upper channel morphology has characteristics of epiphreatic development. The Lower channel is of simple morphology and a more artesian (Vauclusian) structure. Generally it is directed toward north in length of 100 m (from the entrance), and so far, divers have explored it to a depth of 50.5 m (274.7 m a.s.l.). Explored parts of the channel are very spacious with average size 3x4 m, and to a depth of 40 meters slope at an angle of approximately 40°. In the deeper parts the slope is reduced to 20° – 25°.

The research results show that Upper and Lower inlet channels of the spring are hydraulically separated (independent) and according to preliminary results of recent research (in progress), the larger part of the spring discharge flows through the Lower channel. Recharge through the Upper channel significantly increasing after heavy rainfall but lasts a relatively short. During low discharge conditions the flow from the Upper channel almost stops and source is fed by inflows from the Lower channel. Furthermore, preliminary results of continuous monitoring of temperature and electrical conductivity in channels show different values suggesting ability of their connection to different retention areas or different drainage pattern (fast flow - base flow). In the dry period both underground channels have no direct connection with the retention areas and the water present in the spring is only the rest of the last outflow detained in the cave channels.

6. Conclusion

The Rječina spring is one of the largest springs in the Dinaric Karst. Spring occurs high (325 m a.s.l.) in the complex catchment area of permanent karst springs located along the coast in the town of Rijeka, and it has the function of an overflow for medium and high groundwater. During summer dry season, the Rječina spring is without runoff.

Speleological and cave-diving investigations of the Rječina spring conducted over several decades contributed to a better knowledge of spring cave geomorphology, and ultimately a better understanding of its hydrogeological features. Studies have shown that the spring recharges by a well-developed system of spacious underground channels. The Upper channel morphology has characteristics of epiphreatic development while the Lower channel is more of artesian (Vauclusian) structure. The research results show that Upper and Lower inlet channels of the spring are hydraulically separated and probably connected to the different drainage systems, i.e. dif-

ferent retention areas. In the dry period both underground canals have no direct connection with the retention areas and the water present in the spring is only the remainder of the last outflow in the cave channels.

The recession coefficient obtained from hydrograph analysis confirms the lack of the base-flow spring component, and only fast-flow component was determined. Furthermore, flow model calculations were conducted for ^{18}O stable isotope with the exponential (EM) and dispersion model (DM). The obtained mean residence time (MRT) of 3.6 months confirms dominant recent groundwater recharge.

References

Biondić, B., Dukarić, F., Kuhta, M. & Biondić, R. 1997. Hydrogeological Exploration of the Rječina River Spring in the Dinaric Karst. *Geologia Croatica*, **50**(2), 279-288.

Boegan, E. 1930. *Catasto delle grotte Italiane. Fascicolo I. Grotte della Venezia Giulia*. Istituto Italiano di Speleologia, Trieste. (in Italian)

Club Alpino Italiano, Sezione di Fiume, 1928. *Catasto delle grotte, Rijeka*.

Božičević, S. 1973. Prilog hidrogeologiji izvora Rječine. *Geološki vjesnik*, **25**, 277-283. (in Croatian)

Božičević, S. 1974. Morfologija vodenih kanala izvora Rječine. *Geološki vjesnik*, **27**, 273-281. (in Croatian)

Hraba, B. 1973a. *Izvještaj s ispumpavanja izvora Rječine 1971. godine*. Professional report. Voplin waterworks company, Rijeka. (in Croatian)

Hraba, B. 1973b. Izvor Rječine 1973. Professional report. Voplin waterworks company, Rijeka. (in Croatian)

Kuhta, M. 1999. Speleoronilačka istraživanja izvora Rječine. *Speleolog*, **44/45**, 13-17. (in Croatian)

Kuhta, M., Brkić, Ž. & Kuhta, L. 2014. Izvor Rječine i sjeverozapadni rub Grobničkog polja, *Hidrogeološki radovi – hidrokemijska i izotopna istraživanja*. Professional report. Croatian Geological Survey, Zagreb. (in Croatian)

Pilipić, M. 1971. *Speleoronilačka istraživanja izvora Rječine*. Professional report. Voplin waterworks company, Rijeka. (in Croatian)

Vlahović, I., Tišljarić, J., Velić, I. & Matičec, D. 2005. Evaluation of the Adriatic Carbonate Platform: paleogeography, main events and depositional dynamics. *Paleogeography, Paleoclimatology, Paleoecology*, **220**(3-4), 333-360.

(Abstract) **Peculiar CO₂ values in the Hungarian cave has a lower and upper entrance**

Szabolcs Leél-Össy

Affiliation: Hungarian Cave Research Society, Budapest, Hungary

Abstract

Between January of 2013 and April of 2016 we measured the CO₂ level in the Béke Cave in every month. The Béke Cave (it is on the list of UNESCO World Heritage) was discovered by Prof. László Jakucs in 1952 based on successful water tracing.

The very spectacular stream cave is very rich in dripstones, standing of a main corridor and one accessory passage which was the discovery passage. Above the cave there is a 40-70 m thick Triassic limestone. In 1953 opened an artificial entrance in the upper part of main passage. In 1966 opened another, also artificial exit near to the end point of the cave 68 m under the entrance. From 1968 in winter the air went into the cave across the lower exit, and went out across the upper entrance, and in summer inversely. After the discovery until 2013 we never measured high CO₂ level, it was always under 1%.

In the March of 2013 this value started to rise, and in summer of 2013 it was above 3 % in the middle of the cave. From the upper entrance we found higher and higher values, therefore we don't go to the lower part of the cave: we supposed there 5-6 % CO₂. At the end of 2013 the CO₂ value was under 1% again (in the middle of the cave). But in the spring of 2014 again started to rise, and in July was again above 3 %! We were at the lower exit (it is out of using), but we can't go into the cave, because the artificial tunnel was under water. In January of 2015 the CO₂ value was again under 1%, and we tried to take a full crossing tour But we can't reach the Giant Hall at the end of the cave, because in the stream we found a new syphon, the water reached the ceiling. In the summer of 2016 we measured more than 3% CO₂ again, and in January of 2016 it was again under 1%.

We suppose, that in the spring of 2013 after a big cave-flood the Margitics syphon at the end of the cave filled up with sediment. Behind the syphon the water closed the exit, and created a new syphon in the main passage. Therefore no chance the movement of the air across the exit. In the summer vegetation age the water of the stream, and the seeping water across the roof bring many CO₂ which accumulates in the lower part of the cave. In winter the air, which is coming across the invisible cracks into the lower part of the cave transports the CO₂ from the cave across the upper entrance. In next spring everything start from the beginning/afresh.

Mechanism Analysis Of Large Scale Sinkhole Formation, Laibin, Guangxi, China

Mingtang Lei¹, Xiaozhen Jiang^{1,2}, Yongli Gao², Weiwan Luo¹ and Jianling Dai¹

Affiliation: ¹Institute of Karst Geology, CAGS, Guilin, China, mingtanglei@hotmail.com

²Department of Geological Sciences, University of Texas at San Antonio, TX 78249, USA.

Abstract

On 3 June 2010, during and after a heavy rainfall event, a series of sinkholes collapsed at Jili village and Shanbei village, Laibin Guangxi, China. The incidents resulted in 19 cover collapse sinkholes and 3 ground curved fissures, the diameter and depth of the largest sinkhole is 85 m and 38 m. Four sinkholes expanded and merged to form a 200 m long collapse zone. Many ground failures and fractures occurred and an area of 0.4 km² was impacted by the collapsing event. Because the events occurred within two villages, with a high population density, there are 130 houses, a dam and a highway impacted. After sinkhole formation, extensive investigations including sinkhole measurement by drone and 3D Laser Scanner, cave measurement, advancement of exploratory boreholes, geophysical detection, real-time monitoring of karst water pressure and rainfall, and geotechnical testing of soil samples were conducted to determine the contributing factors to these sinkhole formations. It is showed that the precipitation as high as 469.8 mm within one day was a record, and was probably the key factor triggering the sinkhole. In this paper, the result of sinkhole investigation will be discussed.

Keywords: sinkhole, karst collapse, geological hazard, karst

1. Introduction

On 3 June 2010, a series of sinkholes collapsed at Jili village and Shanbei village, Laibin Guangxi, China. The collapsing event formed 22 sinkholes and 4 extremely large sinkholes merged to form a 200 m long collapsing zone. Many ground failures and fractures occurred and an area of 0.4 km² was impacted by the collapsing event. Because the collapsing events occurred in areas of high population density, initial investigation revealed severe damage to residential houses and 130 families, more than 600 people, a dam and a highway were affected by the collapsing event. This paper discusses the geological background of the study area, the mechanism of the sinkhole collapses, and prevention and treatment of sinkhole hazards in the study area.

2. Geologic Settings

Jili village is located in central Guangxi province, a highly active karst area with many karst features such as sinkholes, springs, karst windows, caves, and conduit systems widely distributed in this area (Figs. 1 & 2).

This is a typical fengcong and fenglin karst area with isolated karst hills and valleys. The geology includes the Quaternary surficial material, Middle Carboniferous limestone, Lower Carboniferous siliceous rocks, and Middle Cretaceous conglomerates. The unconsolidated sediments above bedrock are Quaternary alluvium and colluvium of silty clay, clay containing gravels, and clay, to a thickness of 5-15m.

Surface water and Quaternary groundwater are scarce in the study area. The groundwater resources include karst water within bedrock matrix, fractures, and conduits and limited amount of Quaternary water in porous sediments. Fairly large springs exist in the area recharged through sinkholes, active karst fractures and conduits. Three large springs with discharge rate of 100 – 1336.5 l/s are located near Liangxian and 100 – 400 ton/day of water flows out of drilled holes. The Hongshui River, located 16 km north of the study area, marks the regional base flow level, and receives water from most base flow in the study area. Preliminary investigations of



Figure 1. Geographic location of Laibin.

sinkholes, springs, and large springs reveal a large cave stream existing in the study area with an approximate N - S orientation. The three large springs may serve as discharge outlets of this cave stream. The cave stream passes through the sinkhole plain and discharges to Chenglong Creek, a tributary of Hongshui River.

3. Weather condition

Laibin is located in the subtropical monsoon climate zone close to the Tropic of Cancer with a typical subtropical monsoon climate characteristics, mild climate, adequate sunshine, abundant rainfall, but droughts and flood disasters are relatively frequent. From 1957 to 2009, the average annual rain-

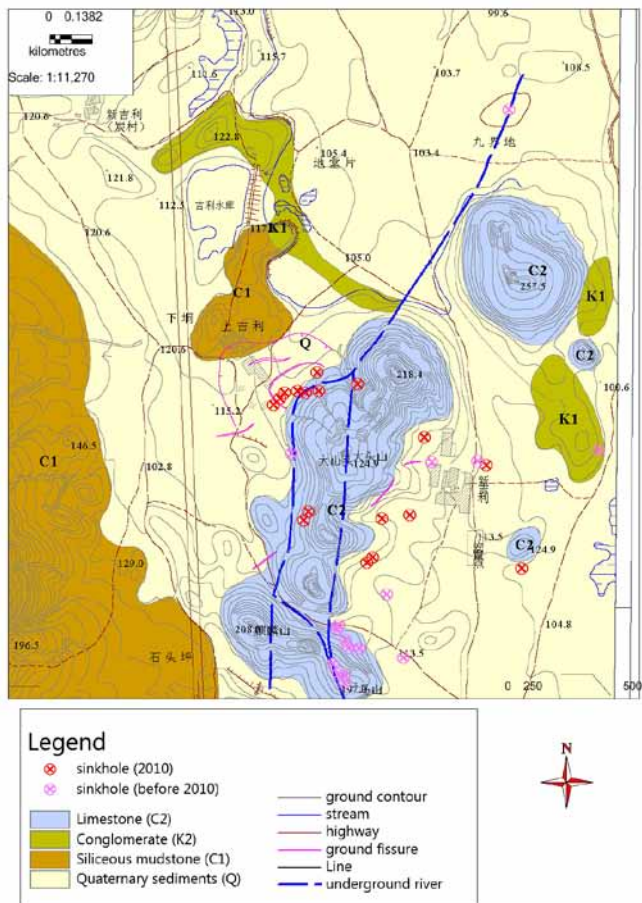


Figure 2. Sinkhole distribution in the study area.

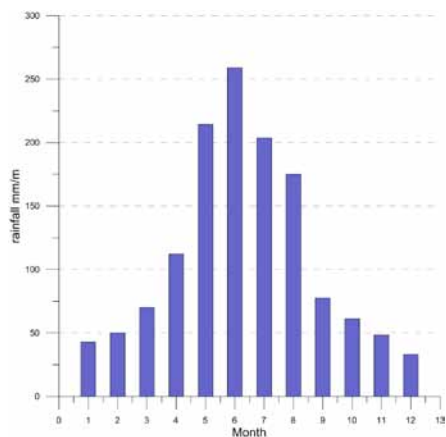


Figure 3. Annual average monthly rainfall distribution (1957-2014)

fall of was 1347 mm, the rainy season is from May to August. (Figs. 3 & 4)

In 2009, China's southwestern region suffered a rare drought; rainfall in 2009 was only 991.7mm, well below the average annual rainfall of 1347mm. Between May 31 to June 1, 2010, Laibin suffered heavy rainstorms, including the June 1 rainfall of 441.2mm, and a large number of villages and towns flooded (Fig. 5a, b).

4. Karst collapse formation process

Before the sinkhole collapse occurred on June 1, 2010, there were two minor earthquakes in this area. The first at 11:35:01 am, at latitude 23 ° 41'7 " , longitude 109 ° 13'4", and the mag-

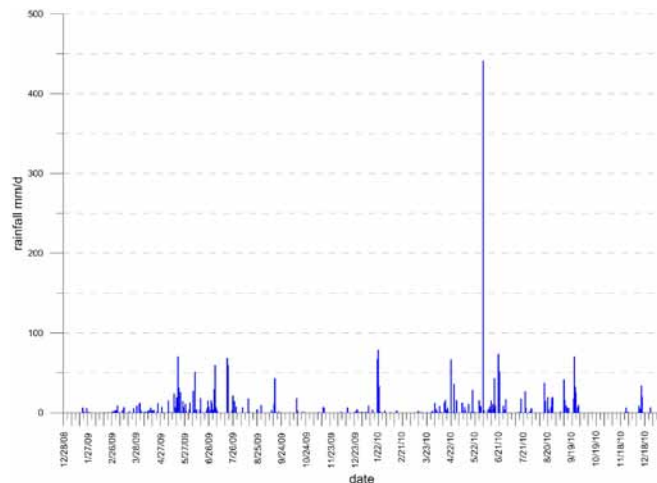


Figure 4. Distribution of daily rainfall (2009-2010)



Figure 5. Floods after the 1 June storm

nitude was 1.7. The second time was at 15:29: 01, at latitude 23 ° 38'24 " , longitude 109 ° 13'18", with a magnitude of 1.6.

The first sinkhole collapsed at 9:00 am on June 3, 2010. Four sinkhole pits formed within 3 hours. These sinkholes expanded and merged to form a 200 m long collapsing zone. By 27 September, 2010, a total of 19 sinkholes and 3 arcuate fractures were formed. Figures 2, 6, 7, & 8.

5. Mechanism analysis of sinkhole formation

The investigations revealed that the extremely heavy rainfall between May 31 and June 1 2010 probably triggered this collapsing event. The biggest sinkhole is a bedrock sinkhole and is the result of cave roof collapse. The other sinkholes are soil sinkholes in the overburden soil.



Figure 6. The biggest sinkhole of 80m diameter and 32m in depth and the destroyed building



Figure 7. Aerial photo by eBee Drone

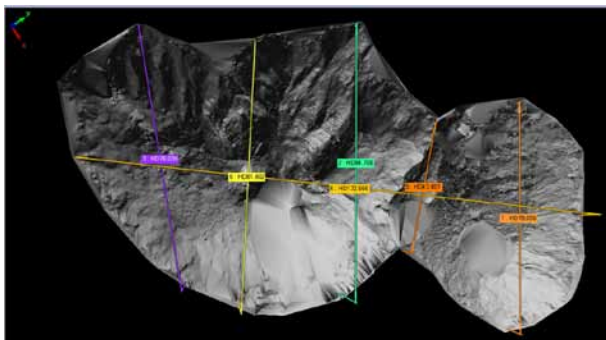


Figure 8. Dimensions of the sinkholes measured by Leica Scanstation

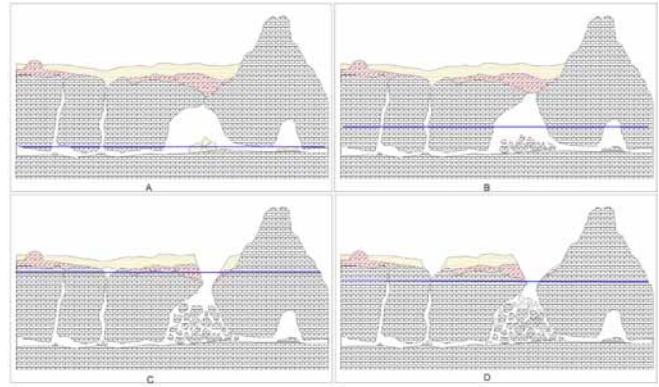


Figure 9. Reconstruction of sinkhole formation

The sinkhole formation process can be reconstructed:

- First, after the storm event, the groundwater level rose rapidly, the groundwater velocity increased, and the water laden overburden increased weight caused a series of cave roof collapse. Figure 9 A.
- The two earthquakes occurring on June 1 are “collapsing earthquakes”, caused by the roof collapse of big a karst cave hall (bedrock sinkhole).
- This collapsing earthquake may have created a “water hammer” effect within underground stream system, which may have also causes fractures in many houses. Figure 9 B
- The “water hammer” effect causes the water and gas pressure in the karst conduits to rise abruptly, but then quickly dissipates. The overburden of the cave opening is destroyed as a result and the soil cave is formed, finally leading to the occurrence of soil collapses. Figure 9 C and D

6. Conclusions

The rapid water level rise after the storm event caused a series of collapses in the study area. These were caused by the extreme weather conditions (Lei et al. 2012).

The on-site investigations revealed that the initial collapses occurred during heavy rainfall. The 469.8 mm precipitation within one day was a record high in the study area. The long period of drought in 2009 followed by extremely heavy rainfall along with cave roof collapse may have caused the collapsing event on June 3, 2010. The cave roof collapse may have triggered a “water hammer” effect in the karst conduits. This “water hammer” effect can cause severe soil damage and trigger subsequent collapses (Lei et al. 2010, 2012). Soil disturbance would change the hydraulic gradient, water level fluctuations, and eventually result in new sinkholes.

Monitoring pressure changes of karst water, sinkhole survey and potentiometric mapping, tracer test of surface water and groundwater interaction, locating soil voids and soil disturbances using ground penetrating radar (GPR) are suggested to assess sinkhole hazards in the study area.

The karst water level is recovering to normal conditions after this event, but it may take several years to stabilize the soil to normal conditions. A 10 m x 10m soil collapse area was recently discovered in the south of the study area. A donut shaped subsidence area formed around the new collapse site.

The diameter of the subsidence area is 100 m with ground failures and fractures formed inside of the study area. This area is located directly above the subterranean stream.

Large scale sinkhole collapses may occur again during monsoon seasons. Residents in Jili village and Shanbei village may need to be relocated to a safer place. Jili Dam and Guibei highway need to be evaluated for further damage. Further studies of the relationship between extreme weather event and sinkhole collapses need to be studied to prevent such large scale collapsing event in the future.

7. References

Lei M, Jiang X, Li Y, Meng Y, Dai J, Gao Y. 2010, Predicting sinkhole collapse by long-term monitoring of karst water pressure in Zhemu, China. *Geologically Active: Proceedings of the 11th IAEG Congress*, Auckland, New Zealand. 355-362.

Lei M, Gao Y, Jiang X, Guan Z. 2012 *Emergency Investigation of Extremely Large Sinkholes*, Maohe, Guangxi, China (this volume).

Complex Investigations In Novoafonskaya Cave (Western Caucasus)

Mavlyudov B.R.¹, Kuderina T.M.¹, Kadebskaya O.I.², Grabenko E.A.³, Tokarev I.V.⁴, Ekba Ya.A.⁵,
Dbar R.S.⁵

Affiliation: ¹ Institute of geography RAS, Moscow, Russia, bulatrm@bk.ru

² Mine Institute of Ural Division of RAS, Perm, Russia

³ Caucasus state natural biosphere reservation, Maikop, Russia

⁴ Resource centre «Geomodel» of Scientific Park of St.-Petersburg University, St.-Petersburg, Russia

⁵ Institute of ecology ASA, Sukhum, Abkhaziya

Abstract

Scientific research in Novoafonskaya Cave (one of the famous show caves of the former USSR) occurred previously spent the 1970s. In 2014–2016 complex research in a cave were undertaken that included geomorphological, geological, hydrological, hydrochemical, radiological, climatic, hydrogeochemical and isotope work. Geological and geomorphological research shows that: 1) cave chambers were generated in anticline fold in the Barrem limestone; 2) there is large quantity of gypsum in the limestone (inclusions up to 20 cm) that could promote rock destruction and formation of large volume cavities; 3) there is extensive secondary gypsum mineralization on cave walls that is not typical for region's caves; 4) there is flint destruction containing gypsum and transformation of it, presumably into mineral marshalite. Hydrochemical research shows that all three permanent lakes of a cave (Anatoliya, Goluboe and Nartaa) at low water are isolated and have no connection with Psyrtskha Spring which is noted at high water. Water research in the lakes show that there is no chemical similarity of lake water at high water. Chemical elements of regional and local distribution also were collected in the summer from lake water. The climate of the Novoafonskaya Cave after the construction of drainage tunnels in 1980s has changed. The cave has a natural upper shaft entrance and now has a lower entrance (elevation difference 180 m) that produces winds in the cave and seasonal switching of air draught direction. A cold temperature anomaly also appears in the drainage tunnel system. A warm temperature anomaly in the cave connected to the entrance shaft and with part of Anakopiya Chamber. Study of the radiation background in the cave has shown that it is low everywhere in the caves except for Khram Chamber (0.51–0.65 mSv in hour). In winter water-drop mineralization decreases and fluctuates about 116–120 mg/l, and the oxygen isotope varies from -8.5 to -8.6‰ SMOW. In the summer dripping water mineralization rate increases to 160–180 mg/l and the oxygen isotope ratio fluctuates from -8.3 to -9.0‰ SMOW. For deuterium the greatest variations in values are noted in the winter and more stable values are in summer. During our investigations we used a pilotless vehicle for reception of a digital model of the area over a cave and for exact locating of cave entrances on the map.

Keywords: limestone cave, gypsum mineralization, cave climate, geochemistry, isotopic investigations

1. Introduction

Novoafonskaya Cave is situated in the front ridges of the Caucasus foothills on the coast of the Black Sea near the Novyj Athon settlement (Republic Abkhazia). Originally the cave existed as a vertical shaft with depth of about 140 m which penetrates into a system of large chambers. Cave was opened in 1961 by local resident Givi Smyr. Cave research have occurred since 1963. The shaft entrance is located at about 230 m asl. In the 1970s a transport tunnel has been constructed from about 50m asl for about 2km and which has become the new cave entrance. Now the train delivers tourists to the station at the excursion start and then collects them at another station at the end of the trip. The underground route in a cave about 1,5 km long (Fig. 1). There are three permanent lakes in the cave: Anatoliya, Goluboye and Nartaa, the water level of which rises during floods (up to 45 m) covering the tourist track. To avoid such high floods in the cave in the 1980s a system of drainage tunnels having connection with Goluboye Lake, Nartaa Lake and Makhadzhirov Chamber were built. Therefore during floods, the water level in the lakes does not rise above mouths of the drainage tunnels. During Soviet times the cave accepted up to 1000000 visitors per year, and now, about 300000 visitors per year.

The basic scientific research in the cave were mainly undertaken before the opening of the cave as a show cave from 1965 to 1975 (Tintilozov, 1968, 1975, 1976, 1983, Tsikarishvili,

1978). Some research have revived in the 2000s (Ekba, Dbar, 2007).

In 2014 we have undertook reconnaissance work, and in 2015–2016 work continued (Grabenko et al., 2016). Here we present some results of this work.

2. Methodology

In the cave geological, geomorphological, hydrological, geochemical, climatic, radiological, isotopic research by standard methodologies have been undertaken. Analyses of samples were undertaken in laboratories in Moscow, St.-Petersburg, Perm and Irkutsk. For the creation of a digital relief model over the cave, a pilotless vehicle (drone) was used. For taking photos of inaccessible places in the cave and for water sampling from Goluboye Lake the drone was also used. The area over the cave and within its possible catchment has been observed.

3. Results of research and discussion

3.1. Geology and geomorphology.

The cave is located in core of the western part of the Ahz-Amgvskaya anticline which aligns almost parallel to Black Sea shore. Novoafonskaya Cave is located in the massive about 300 m thick Lower Cretaceous limestone (Barrem stage).

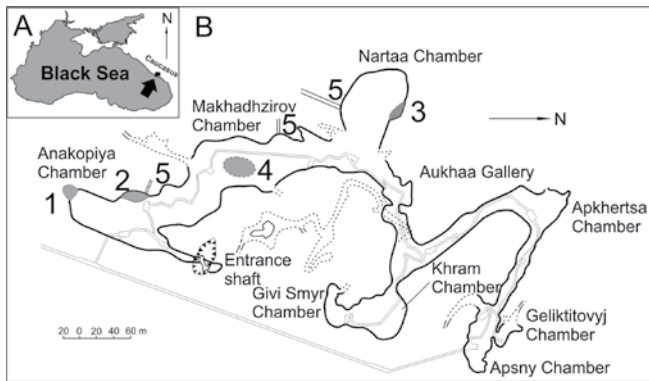


Figure 1. A - position of the Novoafonskaya Cave, B - the plan of the Novoafonskaya Cave with the transport tunnel and tourist track. 1 - Anatoliya Lake, 2 - Goluboye Lake, 3 - Nartaa Lake, 4 - temporary lake in Makhadzhirov Chamber, 5 - entrances into drainage tunnels.

The limestone is relatively pure (83 % carbonate) with an insignificant amount of insoluble (Tintilozov, 1983). Barrem sediments are subdivided into three parts. The lower part is a thick layer of massive, granular grey limestone; the middle part limestone sometimes is yellow-grey colour and becomes brecciated and there is a dolomitic limestone. In the upper part of Barrem sediments are again presented thick layered, massive, grey limestone with small concretions of black flint and pyrite (Tintilozov, 1983).

Our researches have shown that average part of Barrem contains layers of limestones with large amounts of gypsum in the form of numerous roundish concretions up to 20 cm in diameter. Concretions are composed of crystals of pure fine-grained gypsum with separate grains of barite and selenite. Concretions are partially replaced by chalcedony on the edges. There are gypsum crystals in the limestone. We consider that the presence of readily soluble gypsum in limestones with a lower solubility promoted easier destruction of such mixed rocks in comparison to pure limestone resulting in the formation of large volume cavities which are characteristic for Novoafonskaya Cave and other caves of this area (Tintilozov, 1983). Gypsum dissolution in cave walls and in chamber arches from infiltration, condensation and flood water could promote collapse of the arches and partial dissolution of country rocks and their fragments. Presence of gypsum in limestones promoted the formation of an extensive secondary gypsum mineralization in the cave that is not typical for the majority of regional caves. At the base of the walls in Anakopiya Chamber secondary gypsum stratifications with thickness of about 30 cm have been found. Secondary gypsum mineralization is probably connected with the cave being a show cave due to the occurrence of light sources in the cave resulting in evaporation.

An interesting feature of Novoafonskaya Cave is the destruction of flint concretions present in a middle limestone layer containing some gypsum. Under the influence of infiltration and condensation waters, gypsum is washed away and flint turns presumably into the mineral Marshallit. The flint became friable and is easily crumbled out and falls from the arches.

In the cave there are following types of secondary sediments: collapse, lake, residual, secondary gypsum, flowstone and

organic. The largest volumes are collapse sediments (arch collapse) and lake sediments which are mainly in the chambers: Anakopiya, Makhadzhirov and Nartaa. Lake sediments have been brought in by flood water and are represented by clay and aleurite. Research of aleurite-clay sediments from different points of Novoafonskaya Cave shows the following mineral content: quartz – 8-50%, calcite – 5-25%, feldspars – 10-15%, dolomite – 5-9%, smectite and mixed layered minerals to 58%, kaolin (trace and an amorphous phase (presumably, organic)) have been found. The main components of the residual sediments are quartz, gypsum, calcite, barite, muscovite (hydromica) and other layered minerals. Also present are Na^{+} smectite, feldspar, jarosite, traces of kaolin, chlorite, vermiculite, hydrobiotite and radioamorphous phase. In comparison with country rocks for sediments of quartz-gypsum composition TiO_2 , SO_3 , Al_2O_3 , Fe_2O_3 are more common. In sediments of quartz-hydro-micaceous composition SiO_2 , TiO_2 , Al_2O_3 , Na_2O , K_2O , Sc , V , Pb , Sn , Ba are present, in sediments with jarosite, Cr and Zn are present. In calcite-quartz-hydro-micaceous sediments almost all petrogenic elements except MnO , CaO , CO_2 and rare elements are higher, except Ba , although the Sr quantity remains at the level of country rocks.

Flowstones are widely developed in the cave and represented by most of the well-known forms of stalactite-stalagmite crust: stalactites, stalagmites, columns, coralloids, helictites, draperies, flowstone dams, complex flowstone forms (ensembles), sinter crusts and also mondmilch (moonmilk). The mineral structure of flowstones is typical for caves of carbonate karst and is calcite, and occasionally aragonite, gypsum and hydrohematite.

Organic sediments in Novoafonskaya Cave are connected with: 1) bats or penetration of organic from superficial soils, 2) with human activity.

3.2. Hydrology.

As the catchment of the Novoafonskaya Cave has not been known until now, we undertook hydro-chemical water research in streams not only in the vicinity of the cave, but also the neighbouring rivers. The Aapsta and Hipsta Rivers and the Mchishta spring were included in the sampling area. The Hipsta River and Mchishta spring were included in the sampling program as they relate to the of Illusiya-Mezhennogo-Snezhnaya cave system catchment. This probably is overlaps with the Novoafonskaya Cave catchment (Mavlyudov, 2016). Besides it was important to have some background hydro-chemical indicators of water of research area. Water sampling also occurred from bore holes and from Bzyb River.

On the basis of our measurements of water conductivity it can be concluded that Hipsta River and Mchishta spring have similar chemical composition and condition (mineralization is about 125-127 mg/l) and confirms their close connection. The Aapsta River has more water mineralization (about 150 mg/l), and Bzyb River less (about 73 mg/l). There fore the spring supplying the Aapsta and Bzyb rivers are different from those supplying the Mchishta Spring and Hipsta River.

As the Snezhnaya-Mezhennogo-Illusiya cave system water influences water chemistry of the Hipsta River and in particular on Mchishta spring (as reflected in their isotope chemistry),

the influence of water of Snezhnaya-Mezhennogo-Illusiya cave system on water of Aapsta River is only slight or occurs only during strong rain. On the other hand the similar isotopic content of the water of the Hipsta and Aapsta rivers and Mchishta spring are different from the water of lakes in Novoafonskaya Cave. Therefore to what degree does the water of caves of a high-mountainous karst (from such as Snezhnaya-Mezhennogo-Illusiya cave system) influence the water of low mountain caves (such as Novoafonskaya Cave) and what influence do they have on the cave sediments present. This helps in understanding the sediment composition of low mountain caves, and the origin of Novoafonskaya Cave.

Studying of small hydrological objects in the cave (drops, flowstone dam pools) has shown seasonal water influx on flowstones. It has appeared that during low water many pools dry up, thus in many places drops on stalagmites (including, on Belaya Gora) also stop and stalactites and sinter crust dry up. At the same time there are areas in the same cave which do not dry up, for example, in Apsny Chamber.

Hydrogeochemical research of lake water of Novoafonskaya Cave occurred in the summer and winter over three years. Hydrochemical research (pH, ppm, t) in low water of 2014 and 2015 showed that all three permanent lakes (Anatoliya, Goluboye and Nartaa) are isolated from each other during this period and have no connection with spring Psyrtskha which has been noted earlier in flood periods (Tintilozov, 1983, Ekba, Dbar, 2007, Ekba et al., 2014). The lake in Makhadzhirov Chamber is temporal. Lake water pH values were typically 7,4-7,6, common mineralization changed from 105 to 122 mg/l. Thus in low water the water temperature in all lakes has appeared variable. The water level in the cave lakes depends on the precipitation in the catchment area. Water sampling from Goluboye Lake located at the bottom of pit used a pilotless vehicle (drone).

As water mineralization and temperature in the Psyrtskha spring and in the Novoafonskaya Cave lakes mismatch each other (higher in spring) it is concluded that there is no connection of lake water with spring water at low water (Mavlyudov et al., 2014) and this is confirmed by the difference of elevation between the two. During high water this connection is present (Tintilozov, 1983).

Connection is observed not with main stream from the left-hand valley side but with the temporal stream from the right valley side. Our observations of spring Psyrtskha in 2014 and 2015 during low water when there was no spring from the right-hand side do not show any connection between the spring water and cave lakes. In the wet autumn of 2016 when the water level in lakes rose and the spring on the right valley side appeared. This was confirmed by the water temperature and mineralization corresponding to the water in Nartaa Lake. Also the left hand spring water mineralization lower than that of the water from right hand though their temperature was almost identical. However it does not mean that water from a cave has direct connection with a river Psyrtskha valley always but. this connection is unlikely to exist as. the water level in the spring is about 50 m asl but water level in cave lakes did not reach 45 m asl. From this follows that water in Psyrtskha Valley and into cave penetrates from one source along channels which branch both towards the cave and to

a valley. This branching is located a little above spring level. However when the water level in cave lakes exceeds the level of the water in right hand spring Psyrtskha, such a connection appears.

3.3. Geochemistry.

During wet winter times accumulation of elements of global distribution (*B, Na, Mg*) and a number of heavy metals *Fe, Co, Ni, Cu, Zn* accumulate in lakes (Kuderina et al., 2015, 2016). In summertime the differentiation of elements is more variable and depends from mode of humidifying of a cave and surrounding landscapes. From elements of global distribution are allocated elements *C, K, Ca, Sr*. Elements of regional and local distribution *Ti, V, Cr* also accumulate in the summer in the cave lakes.

There is no full convergence of a chemical compound of lakes waters and at flood mode which relates to their isolation. As many elements show the same fluctuations (but sometimes with different amplitude) during time a connection between lakes exists. This connection becomes larger during high water and the least during low water. Different elements show multidirectional fluctuations during rising water levels in the lakes. For example, the quantity of *B, C* and *Mg* decreases with the rise of water level in the lakes, but the quantity of all other elements with rise of water level in lakes increases. The exception is *Ti* which changes differently in different lakes.

3.4. Cave climate.

Research on the climatic system of Novoafonskaya Cave has shown that after a construction of transport tunnel in 1970th and drainage tunnels in the 1980s the system of air circulation in the cave changed. Originally the cave represented a descending bag almost without air ventilation. Because of depth of the cave chambers (about 140 m from a surface) the influence of an external climate on the cave climate was minimal. Water penetration from the surface can influence cave temperature (specifically on Anakopiya Chamber). Depending on the season water could have warming or cooling influence on the cave climate. Rotting of organic material brought into the cave by water was a second influence on the cave climate. Additional heat and CO₂ was thus isolated. Flood water which resulting in water level rise in the cave lakes was probably the biggest agent of influence on a cave climate. The lakes occupy half of the cave chambers area (especially, in the lower chambers). Therefore if the flood water has a lower temperature than the cave there is a significant influence on the temperature and humidity of the cave.

The construction of the transport tunnel has transformed the cave into limited dynamic system as train movement resulted in air movement (despite the available doors separating the tunnel from a cave). After the construction of drainage tunnels the cave was also ventilated by stove draught. The chambers Anakopiya, Makhadzhirov and Nartaa are ventilated directly as drainage tunnel exits are located in them and other chambers and galleries are ventilated indirectly. The cave has a natural upper entrance and a lower entrance (height difference between entrances is about 180 m) and air circulates and there is also a seasonal switching of the draught direction characteristic for caves with entrances located at different elevation levels. The air in the cave is strongly stratified: the

lowest air temperatures are typical for lake depressions and at rising up-slope on 2-3°C to a tourist track air temperature. The warming of cave arches is from: 1) warm air from a surface penetrating through entrance shaft, 2) warm air from lighting and power plants, 3) warmth from tourists and transport. In the winter the cold air does not penetrate into the cave as it warms the drainage tunnel (1500 m long). There is therefore a cold temperature anomaly, where (mean annual temperature (MAT) in the cavity is below the MAT of the rocks in a karst massif in the drainage tunnel system (Mavlyudov, 1997). Measurements of air temperatures in September, 2015 in the drainage tunnel shows 12.6°C i.e. below usual air temperature in the cave but this tunnel was warmed by cave air during all summer. A warm temperature anomaly exists in the cave where the MAT in the cavity is above the MAT of the rocks of a karst massif and affects not only the entrance shaft but also a part of Anakopiya Chamber. For example, in September, 2015 at the exit from entrance shaft in Anakopiya Chamber air temperature was 18.2°C but usual air temperature in a cave at the level of tourist track was 13-14°C. Such big fluctuations of air temperature as in Anakopiya Chamber (up to 5°C during year) are not observed in other chambers of Novoafonskaya Cave a neutral climate zone of the cave.

Drier winter air does not arrive through the drainage tunnels from the surface dry areas in neighbourhood in the cave tunnel exits. However the summer damp air penetrates from a surface through an entrance shaft and increases air humidity in the Anakopiya Chamber resulting in moisture condensation on the arches that in turn promotes gypsum dissolution of and re-sedimentation on the lower chamber walls.

There are two main moisture streams in the cave: 1) from Apsny Chamber through Ayuhaa Gallery into Nartaa Chamber and further branches in the drainage tunnel and to Nartaa Lake; 2) from the natural entrance of Anakopiya Chamber and to Anatoliya and Goluboye Lakes and also in the drainage tunnel. Despite the switching of draught air direction in the cave between summer and winter seasons, the direction of moisture streams in the cave remains constant.

3.5. Radiation.

Studies of the radiation background in the cave show that practically everywhere in the cave radiation is low except for Khram Chamber (0.51-0.65 mcSv/hour). According to the Abkhazian researchers measurements of mass activity of radioactive sources of radiation in Novoafonskaya Cave in Makhadzhirov Chamber around Belaya Gora are on the verge of maximum concentration limit - about 200 Bq/l. Radiation increase is presumably connected with organic accumulation in the cave (bat guano and soil humus brought from a surface into a cave through cracks in limestones) (Kuderina et al., 2015b).

3.6. Isotopes.

Studies of isotope water drops in the cave has shown that during the winter when the air draught is directed from lower entrance of cave to the upper one, water mineralization in the drops decreases and fluctuates between 116-120 mg/l. During the same period oxygen isotopes fluctuates between -8.5 - -8.6 ‰ SMOW. In summer the air draught dripping water mineralization increases to 160-180 mg/l, and in September, 2015

to 203 mg/l. The oxygen isotope fluctuates from -8.3 to -9.0 ‰ SMOW. On the contrary, for deuterium the greatest variability is in winter and more stable in summer.

Comparing results of isotope measurements of surface and underground waters around Novyj Afon with the precipitation mean annual isotopes values for the area there is similarity for the monthly average precipitation at heights about 1000 m asl. It is therefore feasible to assume that the main catchment area of waters of area of Novyj Afon most likely is situated at heights from 500 to 1500 m asl. Based on these results we do not believe in a hydrothermal origin of cavities of the Novoafonskaya Cave. However large volume cavities apparently are connected with presence of gypsum in limestone layers.

During works in September, 2015 and February, 2016 we undertook a landscape survey with use of a pilotless vehicle to develop digital elevation model (DEM) of the district above the cave and locate cave entrances on the map.

4. Conclusions

The research undertaken in 2014-2016 in Novoafonskaya Cave have allowed: 1) to more accurately characterize the geological structure of the rocks containing the cave, 2) to reveal for the first time the gypsum mineralization of limestones in which the largest cave chambers are located, 3) to characterize the secondary sediments of the cave, including the unrecorded earlier secondary gypsum mineralization of the cave; This connected the deposition of secondary gypsum during the changed cave climate after beginning to use it as show cave, 4) to characterize the water hydrochemistry for Novoafonskaya cave and the nearby and more distant rivers, 5) to show the isolation of the cave lakes during low water and incomplete connection of lakes during flood mode, 6) the absence of a connection between the cave water and the permanent Psyrtskha spring, 7) identification of a good but incomplete connection between the cave lakes with the Psyrtskha spring during high water, 8) to show to the migration of elements within the Novoafonskaya Cave, 9) using isotope data to estimate the height interval of the Novoafonskaya Cave lakes catchment area of at 500-1500 m asl, 10) to discount the hydrothermal origin of cavities of Novoafonskaya Cave, 11) using a drone to develop a digital terrain model above the cave, to photograph inaccessible places in a cave and to take water samples from inaccessible Goluboye Lake.

Acknowledgements

Article is devoted to memory of Givi Smyr, the first researcher and the long-term director of Novoafonskaya Cave. This work was supported by the Russian Foundation for Basic Research, projects no.15-55-40014 and 17-55-40003.

References

Grabenko E.A., Kadebskaya O.I, Kuderina T.M., Mavlyudov B.R., Ekba Ya.A., 2016. Novoafonskaya Cave, results of researches in 2015-2016. *Theory and methods of modern geomorphology: Materials of XXXV Plenum of the Geomorphological commission of the Russian Academy of Sciences, Simferopol, October, 3-8rd, 2016*. Eds.:

- Kladovshchikova M.E., Tokarev S.V. Simferopol. V. 2. PP. 180-184 (in Russian).
- Kuderina T.M., Mavlyudov B.R., Grabenko E.A., Ekba Ya.A., Marholiya V.V., 2015. Measurement of a radiating background in caves of the Western Caucasus. *Peshery (Caves)*. Perm. V. 38. PP. 89-95 (In Russian).
- Kuderina T.M., Mavlyudov B.R., Grabenko E.A., 2015. Hydrogeochemistry of caves of the Western Caucasus. *Materials of VI International scientific conference «Problems of wildlife management and an ecological situation in the European Russia and the adjacent countries»*. Belgorod: Publishing house "POLYTERRA". PP. 244-248 (In Russian).
- Kuderina T.M., Mavlyudov B.R., Grabenko E.A., 2016. Geochemical structure of superficial waters of natural and anthropogenous landscapes of Abkhazia. Nature, science, tourism in protected objects of nature areas. *Materials of the international anniversary scientific conference devoted to the 20 anniversary of Ritsinskij relic national park* (October, 15-19th, 2016, Gudauta). Gudauta: Ritsinskij relic national park. PP. 24-27 (In Russian).
- Mavlyudov B.R. Cave climatic systems. *Proceedings of 12th International Congress of Speleology, La-Shau-de-Font, 1997* V. 1, p. 191-194.
- Mavlyudov B.R., Ekba Ya.A., Dbar R.S., 2014. Some features of a hydrology of the Novoafonskaya Cave. *Collection of materials of V Regional scientific-practical conference «Karst and caves of Caucasus: results, problems and prospects of researches»*. Sochi, 2014. PP. 18-26. (In Russian).
- and caves of Caucasus: results, problems and prospects of researches». Sochi. PP. 27-30 (In Russian).
- Mavlyudov B.R., 2016. Cave system Snezhnaya-Mezhennogo-Ilyuziya, the Western Caucasus. *Boletín Geológico y Minero*. V. 273 (1). PP. 219-235.
- Tintilozov Z.K. *Anakopijskaya propast*. Tbilisi: Metsniereba. 1968. 112 p. (In Russian).
- Tintilozov Z.K. *Novjafonskaya Cave*. Tbilisi: Sabchota Sakartvelo. 1975. 40 p. (In Russian).
- Tintilozov Z.K. *Karst caves of Georgia*. Tbilisi: Metsniereba. 1976. 276 p. (In Russian).
- Tintilozov Z.K. *Novoafonskaya cave system*. 1983. Tbilisi: Metsniereba. 149 p. (In Russian).
- Tsikarishvili K.D. Studying of a microclimate of Novoafonskaya Cave. *Peshery Gruzii (Caves of Georgia)*. № 7. 1978. PP. 17-25. (In Russian).
- Ekba Ya.A., Dbar R.S. *Ecological climatology and natural landscapes of Abkhazia*. Sochi: Papyrus-M-Design. 2007. 324 p. (In Russian).
- Ekba Ya.A., Dbar R.S., Ahsalba A.K., Kuderina T.M. Hydrology and hydrochemistry of karst underground water of Novoafonskaya Cave. *Collection of materials of V Regional scientific-practical conference «Karst and caves of Caucasus: results, problems and prospects of researches»*. Sochi, 2014. PP. 18-26. (In Russian).

Use Of The Cave Animal *Marifugia cavatica* For Reconstruction Of Pliocene To Recent Evolution Of Karst Relief In W Slovenia

Andrej Mihevc¹, Anton Brancelj², Ivan Horáček³

Affiliation: ¹Karst Research Institute ZRC SAZU, Titov trg 2, SI-6230 Postojna, Slovenia, Andrej.Mihevc@zrc-sazu.si

²National Institute of Biology, Večna pot 111, SI-1000 Ljubljana, Slovenia, Anton.Brancelj@nib.si

³Department of Zoology, Faculty of Science, Charles University, Viničná 7, 128 44 Praha, Czech Republic, horacek@natur.cuni.cz

Abstract

Marifugia cavatica is a freshwater cave animal of the family *Serpulidae*. The first few cm of the calcareous tube of *Marifugia* are attached to the cave wall. Later the tube remains more or less perpendicular to the wall as the worm grows. *Marifugia* is an endemic animal and is widely though patchily distributed throughout the whole Dinaric Karst. Finds of attached or broken-off parts of *Marifugia* tubes in old relict caves can give important information about former hydrological and geomorphological conditions in the karst.

Tubes have been found to date in two relict caves in Slovenia. In the Črnotiče quarry, on the edge of the Podgorski kras plateau, *Marifugia cavatica* was found in a sediment-filled relict cave. The tubes were attached to the wall or found loose in fine sediments. For this reason we can be sure they were true cave animals. The locality is about 400 m above recent water caves containing living *Marifugia* fauna. The tubes were dated using different methods to 1.7 Ma – 5.2 Ma, which makes the worms the oldest known cave animals. In Velika Pasica, a relict cave located E of Krim (1,107m ASL), 300 m above the recent valley of the river Iška, tubes were found in sediment only. Preliminary dating puts them at the age about 2 Ma. There are no known *Marifugia* living in that part of the karst now.

The present position of the caves with preserved remains of fossil *Marifugia* indicates that several hundred metres of tectonic uplift have occurred, with a lowering of the water level and active water caves. Disintegration of the originally more level surface to separate blocks of different heights has drastically changed conditions for some aquatic animals. It also shows that some species of cave animals are older than the caves they are living in and also predate the present karst relief.

Keywords: cave animal, *Marifugia cavatica*, karst, geomorphology, Pliocene.

1. Introduction

The Dinaric Karst is a major karst area of Slovenia and is the main relief type of the Dinaric Mountains. The mountain range extends in the NW–SE direction. The central part of the range consists of a row of high karst plateaus between 1,000 and 1,700 m high. From them, step-like low karst plateaus and planation surfaces descend on both sides. The tectonic evolution of the area has been characterised since the late Tertiary by the motion of the Adria micro-plate, which caused contraction deformations. About 6 Ma ago it was followed by rotation accompanied by uplift, folding and strike-slip basin formation. These took place in two distinct tectonic phases (Vrabec *et al.* 2006).

The main characteristics of the relief are planation surfaces and plateaus intersected with closed karst depressions caves and collapse dolines. Their correspondence with tectonic units indicates the great importance of geological structures for the present shape of the relief, although the following are not entirely clear: a. the time frame of this development; b. whether planation surfaces were formed by the gradual disintegration of one big quasi-planation surface or instead formed at different heights under the influence of local hydrological conditions.

The dating of karst sediments, particularly cave sediments, using palaeontological, palaeomagnetic methods and cosmic nuclides (Bosak 2004, Zupan Hajna *et al.* 2010, Häuselmann

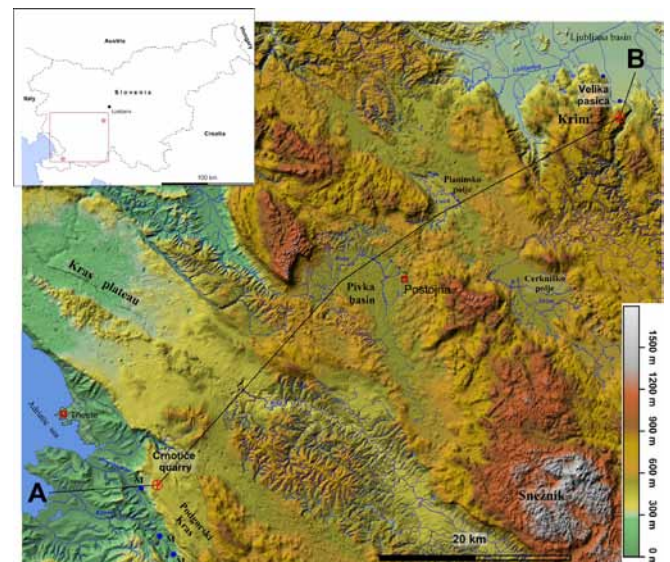


Figure 1. Map of the study area with locations of the caves containing fossil remains of calcareous tubes of *Marifugia cavatica*. Karst areas are without surface rivers, except for Cerkljansko polje, Planinsko polje and Pivka basin. Fluvial system developed on dolomite and siliciclastic rocks. Blue dots are marking karst springs. Letter M marks the springs where recent *Marifugia* tubes were found. Black line marks the profile across the area.

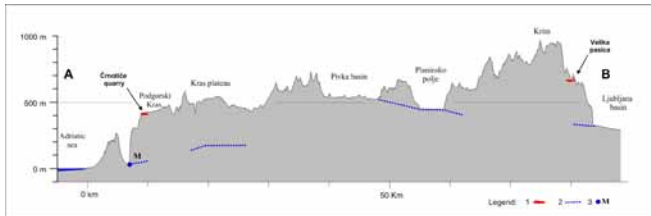


Figure 2. Profile across the Dinaric Mountains from the Adriatic coast to Ljubljana basin. Legend: 1 relict caves where *Marifugia* tubes were found, 2 karst water level observed in caves, 3 letter M indicates springs where recent *Marifugia* tubes were found.

et al. 2015, Mihevc et al. 2015) corresponds to the principal tectonic events. Sediments were deposited in three distinct phases of massive deposition in caves and have been dated to about 5.4–4.1 Ma (Miocene–Pliocene), 3.6–1.8 Ma (Pliocene) and Quaternary. Older sediments, karstification has been continuous since the late Oligocene, were presumably removed by denudation processes.

Morphological analysis of the relief points to the gradual fragmentation of a single planation surface into the smaller units because of the uplift of the central part of the Dinaric Mountains. Planation surfaces were raised to different heights, tilted or even arched. At the same time karstification processes have resulted in the formation of various karst depressions. Allo-genic rivers have formed blind valleys, canyons and dry valleys (Mihevc 2007).

Recently we found fossil remains of the freshwater cave-dwelling tube worm *Marifugia cavatica* (Mihevc et al. 2001). This is an aquatic animal adapted to the cave environment, and since it lives in water caves in specific conditions it can be a good environmental marker. Below we describe the two locations where the tube worm was found and discuss their speleological and geomorphological importance.

2. *Marifugia cavatica*

Marifugia cavatica is the only truly freshwater member of the family *Serpulidae* and the only known tube worm inhabiting continental caves. It is widely though patchily distributed throughout the whole of the Dinaric Karst. The calcareous tube of *Marifugia cavatica* is attached to cave rock walls or ceiling for its initial centimetres, becoming more or less perpendicularly erect and straight as the worm grows up. The outer diameter of the erect parts of the tubes is 0.65–0.85 mm. Broken-off erect parts of tubes are very often found in the sand of karst springs close to their original locations.

Marifugia is a filter feeder with a free-swimming larva (Matjašič and Sket 1966). It can be very sparsely settled in clear cave streams and aggregate to very dense colonies in waters where larvae are not swept away by the currents and where particulate organic matter is richer. In Slovenia it lives in several caves on the W (coastal) side of the Dinaric Mountains and in low karst on the E side. No living animals have been found in the central part of the Dinaric Mountains.

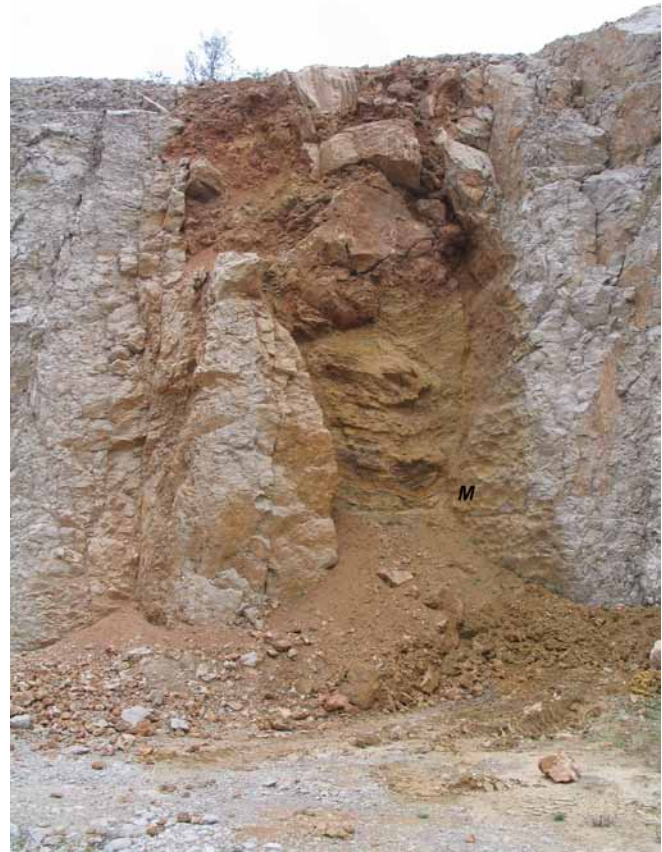


Figure 3. Črnotiče Quarry relict filled cave is exposed in quarry face. *Marifugia* tubes are attached to the preserved cave wall.

3. Locations where fossil remains of *Marifugia cavatica* were found.

3.1. Črnotiče Quarry

We found calcareous tubes of the *Marifugia cavatica* in a sediment-filled cave in Črnotiče quarry. The quarry is situated on the W edge of the Podgorški kras plateau, W Slovenia (45°33'57" N, 13°52'48" E). The surface of the plateau is levelled at about 450 m a.s.l. and dismembered only by numerous dolines. The deepest cave is 150 m deep but no active flow can be reached through it. Karst springs with a maximum discharge of several m³s⁻¹ are 3 km away, at the foot of the plateau, at an elevation of below 50 m a.s.l.

Quarrying operations worked through a relict cave up to 20 m wide, 20 m high and more than 300 m long that was completely filled with sediments. Part of a passage has survived in the quarry wall and within it a profile of sediments. The profile is 17 m high and consists of strata of clays, quartz sands and pebbles and, at the top, a 7 m thick layer of flowstone. Sand and pebbles are allo-genic and were brought into the cave by a sinking stream flowing across Eocene flysch rocks.

Marifugia tubes were found on the walls covered by sediments. Hundreds of tubes were attached to the wall of the passage, while sieving the sediment revealed several hundred broken-off tubes. Clay and sand sediments also revealed the remains of small mammals carried into the cave by a sinking stream. They were deposited simultaneously with the clays that covered the living *Marifugia* and protected their fragile tubes (Mihevc 2000).



Figure 4. Attached tubes of fossil *Marifugia cavatica* in Črnotiče quarry

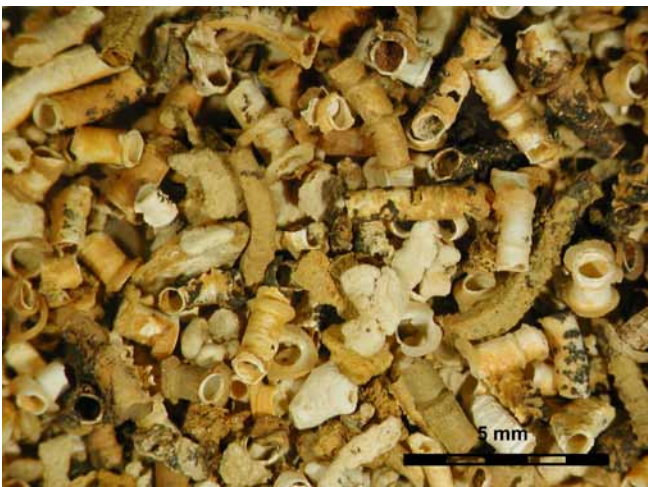


Figure 5. Broken off tubes of fossil *Marifugia cavatica* in Črnotiče quarry.

Dating of sediments based on analyses of the fossil remains of small mammals (Horáček *et al.* 2007) and paleomagnetic properties of fine sediments. Paleontological remains suggested mammalian biozone MN 15–16 as the most probable date (about 3.0–4.1 Ma). The arrangements of obtained magneto-zones were interpreted as older than 1,770 Ma, most probably belonging to the Gauss Chron (2.5–3.6 Ma). The combination of paleontological and paleomagnetic data indicates that the fauna cannot be older than about 3.6 Ma (Zupan Hajna *et al.* 2008).

3.2. Velika Pasica

The Velika Pasica cave, where we recently found remains of *Marifugia cavatica*, lies in central Slovenia on the NE edge of the Dinaric Karst (45°55'7.87"N, 14°29'34.97"E). The cave lies on a karst plateau at an elevation of 665 m a.s.l. West of the cave the plateau rises up to mountain Krim (1,107 m), while to the north it descends in a steep slope into the Ljubljana tectonic basin, which lies at around 300 m a.s.l. The allogenic river Iška has cut a 300 m deep canyon into the karst plateau. The cave is nearby, just 270 m from the edge of the canyon, the bottom of which is below the cave at an elevation of 345 m.



Figure 6. Sediment profile in Velika Pasica cave where fossil tubes were found.



Figure 7. Tubes of *Marifugia* from Velika Pasica cave.

The horizontal cave is 105 m long and lies at a shallow depth (a maximum of 12 m below the surface). Its passages are 5 m wide and high, with some wider sections, and end in sediment fills (Brancelj 2015). The cave is a remnant of an old epiphreatic cave which karst erosion has brought closer to the surface. Karst erosion also caused the formation of the present entrance.

We can conclude from the shape of the passage that the cave was formed by a small sinking stream. The water flowed from dolomite with inclusions of bauxite. At the end of fluvial development, in paragenetic conditions, strata of red clay several metres thick were deposited in the cave, in some cases up to the ceiling. It was only in this period that *Marifugia* could have lived in the cave. Later on, conditions in the cave were no longer suitable. The majority of the clay was subsequently eroded and mixed with large, poorly rounded dolomite pebbles and sand, before being re-deposited in the cave. Strata of calcium carbonate up to 1 m thick were then deposited over this sediment, which in places is also cemented. In some places water percolating underground has also washed sediment away, with the result that there are exposed sediment profiles in the cave.

Some scant remains of *Marifugia* tubes were found in cemented sediment in the cave mixed with fine gravel and red clay. We also found a relatively rich fauna of small mammals, which according to a preliminary estimate are 1.8–2.2 Ma old (Horaček, personal communication).

4. Conclusion

Marifugia cavatica is a good environmental indicator since it only lives in slow-flowing, nutrient-rich waters. The animal is sensitive to long periods of drought and, given its small free-swimming larva, its diffusion against the current is presumably not possible (Kupriyanova *et al.* 2009). We can therefore assume that the species has better conditions for survival in large karst areas in low elevation, close to karst water level.

In such conditions only adaptation of the animal from sweet water lakes and rivers to cave rivers could occur. These conditions were met in Dinaric Mountains in upper Miocene before and during the formation of fresh water lake system in (Mandić *et al.* 2012) that exist in much lower relief that they are today.

It is in this sense that we may also interpret the finds of fossil tubes of *Marifugia cavatica* in the two caves. The fossil remains preserved in two different karst plateaus indicate that the areal where *Marifugia* lives was larger in the past and that the suitable conditions there were still present in Pliocene at least 3.6 Ma ago. Both caves were in epiphreatic conditions not far the ground water level. Tectonic uplift of more than 300 m that followed caused the disintegration of the original karst into separate blocks of different heights. Level of the ground water drop and epiphreatic cave systems were disintegrated.

Such conditions in the highest part of Dinaric karst were not suitable for *Marifugia* as they shrink the optimal habitat. In W Slovenia at Črnotiče Quarry the animals were able to follow the lowering of the karst water level and we can still find them in actual karst springs or in caves about 300 m below the present surface of the karst plateaus.

In area where Velika Pasica is located the animals were not able to follow the evolution of relief and changes in karst hydrology in caves and they get extinct.

References

Brancelj A 2015. *Jama Velika Pasica/The Velika Pasica Cave*. Založba ZRC, Ljubljana.

Bosák P, Mihevc A, Pruner P, 2004. Geomorphological evolution of the Podgora Karst, SW Slovenia: Contribution of magnetostratigraphic research of the Črnotiče II site with *Marifugia* sp. *Acta Carsologica*, **33**, 1, 12, 175-204. Ljubljana.

Häuselmann P, Mihevc A, Pruner P, Horaček I, Čermak S, Hercman H, Sahy D, Fiebig M, Zupan Hajna N, Bosak P

2015. Snežna jama (Slovenia): interdisciplinary dating of cave sediments and implication for landscape evolution. *Geomorphology*, **247**, 10-24.

Horaček I, Mihevc A, Zupan Hajna N, Pruner P, Bosak P 2007. Fossil vertebrates and paleomagnetism update of one of the earlier stages of cave evolution in the Classical karst, Slovenia: Pliocene of Črnotiče II site and Račiška pečina cave. *Acta Carsologica*, **36**(3), 453-468.

Kupriyanova E K, Hove H A, Sket B, Zakšek V, Trontelj P, Rouse GW 2009. Evolution of the unique freshwater cave-dwelling tube worm *Marifugia cavatica* (Annelida: Serpulidae). *Systematics and Biodiversity*, **7**(4), 389–40.

Mandić O, De Leeuw A, Bulić J, Kuiper K, Krijgsman W, Jurišić-Polšak Z 2012. Paleogeographic evolution of the Southern Pannonian Basin: 40Ar/39Ar age constraints on the Miocene continental series of northern Croatia. *International Journal of Earth Sciences*, **101**, 1033–1046.

Matjašič J, Sket B 1966. Developpement larvaire du Serpulien cavernicole *Marifugia cavatica* Absolon et Hrabec. *Int. J. Speleol.*, **2**(1), 9-16.

Mihevc A 2000. The fossilized tubes from the roofless cave – probably the oldest known remains of the cave worm *Marifugia* (Annelida: Polychaeta). *Acta Carsologica*, **29**, 2, 261-270.

Mihevc A, Sket B, Pruner P, Bosak P 2001. Fossil remains of a cave tube worm (Polychaeta: Serpulidae) in an ancient cave in Slovenia. In: *Speleology in the third millenium: sustainable development of karst environments : proceedings*. Campinas: Sociedade Brasileira de Espeleologia, 349-354.

Mihevc A 2007. The age of Karst relief in West Slovenia. *Time in karst*, Postojna 2007, 35–44.

Mihevc A, Bavec M, Häuselmann P, Fiebig M 2015. Dating of the Udin Boršt conglomerate terrace and implication for tectonic uplift in the northwestern part of the Ljubljana Basin (Slovenia). *Acta Carsologica*, **44**(2), pp. 169-176.

Vrabec M and Fodor L 2006: Late Cenozoic tectonics of Slovenia: structural styles at the Northeastern corner of the Adriatic microplate. The Adria microplate: GPS geodesy, tectonics and hazards, *NATO Science Series, IV, Earth and Environmental Sciences*, **61**. Dordrecht: Springer, 151-168.

Zupan Hajna, N, Mihevc A, Pruner P, Bosák P 2010. Palaeomagnetic research on karst sediments in Slovenia. *International journal of speleology*, **39**(2), 47-60.

Zupan Hajna N, Mihevc A, Pruner P, Bosák P 2008. Palaeomagnetism and magnetostratigraphy of Karst sediments in Slovenia, *Carsologica*, **8**, Založba ZRC, Ljubljana.

Speleogenesis by weathering of Upper Cretaceous, Coniacian limestone, Dordogne, France

Claude Mouret, Jacques Rolin and Bernard Angeli

Affiliation: Freelance geologist
claude.mouret.geospel@orange.fr
Km1 La Tamanie, 87 380 MAGNAC-BOURG, France

Abstract

Pantaléon Cave in Bourdeilles, Dordogne, France, was first discovered by one of us (BA). It was initially a rather narrow and short hole in a cliff on the side of a dry valley. Cave digging and removal of loosened formations over a length around 30 m were performed by two of us (BA and JR), together with a few other cavers. Then, the first author was asked to give a diagnosis of cave formation processes, and, a detailed survey of the cave fill was conducted along both cave walls.

Two subhorizontal detailed sedimentological long sections show that the cave limestone basement is irregular in elevation and in lateral distribution. It is surrounded by loosened to weathered limestone displaying a marble-like aspect, then by grey or brown clay, bearing limestone fragments. In some locations, loose very-fine-grained, whitish sand seems to be interbedded with the limestone. Above this, there is a vertical succession of bodies of brown clay and on the top, an unconformable layer of dark grey clay, which was bioturbated by badgers.

The previous lithological succession is around 1.2 m thick and develops all along the 30 m long cave. The cave shows a horizontal succession of enlargements along the walls together with higher though moderate roof elevations. Some empty space exists between the top of sediments and the cave roof, i.e. some 10 to 20 cm in many places and up to 40-50 cm in enlargements. The roof is carved by many small cupolas which are interpreted as condensation-related.

An extensive layer of probable manganese is impregnating sediments in a broadly parallel distribution to the cave walls. It is also present along the cave wall proper and locally around remaining limestone boulders. It is partly unconformable within the sediments.

The paper is aimed at documenting the geometry of the formations, with detailed sections, and proposing a formation process. *In-situ* limestone weathering better explains the cave processes and characteristics.

Keywords:

1. Natural setting

Pantaléon Cave is located on the edge cliff of a small dry valley (Fig. 1), which descends towards the Dronne River. The dry valley is connected to Würmian terraces of Dronne valley.

The cave opens in the variably sandy Middle Coniacian limestone, below alluvium deposited during Riss glaciation (added on BRGM map, Fig. 2).

2. Pantaléon Cave characteristics

Pantaléon Cave consists of a main dug out passage (Fig 5) and several lateral passages which are still to be investigated. Despite no fracture being visible in the roof, several rectilinear orientation trends clearly appear on cave map, which suggests that microfractures were probably present in the cave-bearing horizontal strata. The initial cave floor (Fig 5, arrow), prior to digging, was originally subhorizontal and above a continuous interval of loose material largely bioturbated by badgers (strata 12 on Fig 6). Below it, the rock was loose though still showing some degree of hardness. The loose rock shows a transition zone with embedding limestone. The roof is of limestone and was initially separated from the floor (which has been dug out) by an aerial open space (Fig 5, Photo 1). The roof shows a succession of larger cupolas (Fig 5, Photo 2), some of which are connected, or prolonged, by a broad channel-like groove of various size and length. Larger cupolas are

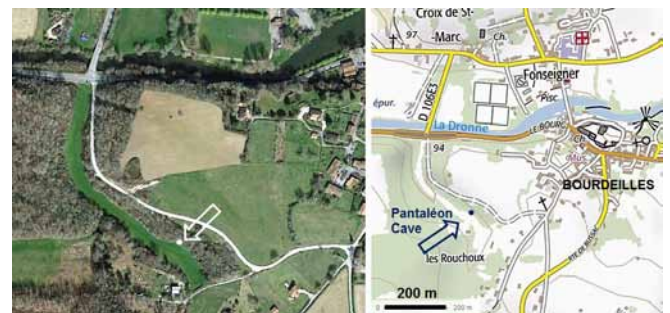


Figure 1. Cave location (arrows). Left image is based on a Google Earth background). Right image is extracted from Geoportail website Dronne River flows from East to West. North is upward.

pocketed with much smaller cupolas of irregular shape and variable depth (Fig 5, Photo 3). Larger cupolas correspond to cave enlargements between the walls (Fig. 4), which alternate with constrictions.

3. Stratigraphy of cave fill

Two long litho-stratigraphic sections have been made along both cave walls (Fig. 4, 6 and 7). Each of them is divided into several rectilinear parts. The slightly sinuous cave walls are projected on the vertical plane of the nearest rectilinear parts. No axial longitudinal section was possible because the cave

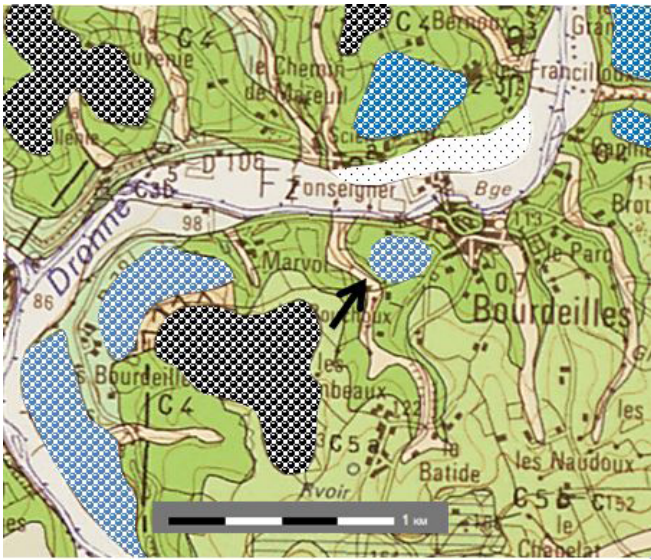


Figure 2. Geological map of Pantaléon Cave area. Background is from BRGM map at 1:50 000. The cave location is indicated by the arrow. Small black dots, large blue dots and large black dots respectively represent Würm, Riss and probable Mindel or older fluvial sediments, partly removed by subsequent erosion. Dry valleys toward Dronne River are filled up with colluvium. C4 is Coniacian limestone and C5 (a, b) overlying Santonian. Overall dip is toward the South

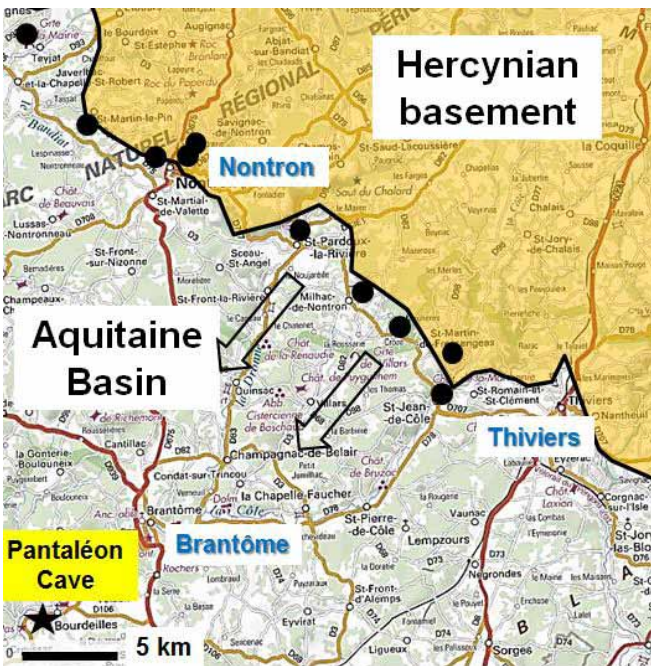


Figure 3. Sedimentary manganese deposits (black dots, after Lougnon, 1984) were exploited during the nineteenth century near the edge of Hercynian basement. Fluvial paleocurrents during Cenozoic times were regionally directed toward SW (white arrows). Pantaléon Cave shows a black deposit across its loose fill which is likely manganese.

was already dug out when we the survey was done. Described formations do not show a constant dip. In many places, part of the formations, near the cave wall, dip towards the longitudinal axis of the cave. Only some parts show low dip.

The lithological succession is relatively constant from bottom to top, despite some secondary variations. The hosting lime-

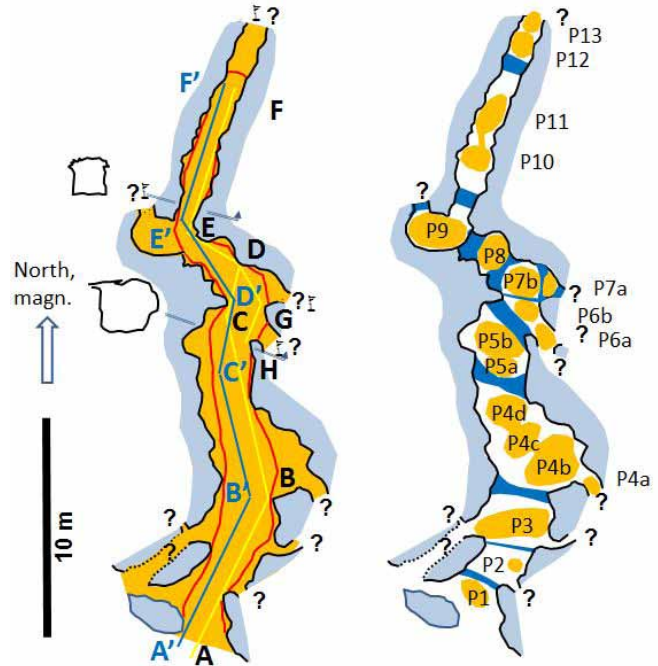


Figure 4. Pantaléon Cave.

Left: floor map. Plain orange: cave after being dug out. Plain blue: surrounding limestone. Black lines: cave walls. Red lines: external edge of dug out axial part, and transverse limit of digging near the northern end. Blue line: projection plane of western cave wall, long section. Yellow line: idem eastern wall. Flags: places under desobstruction. Map by B. Angéli, J. Billant, C. Mouret, J. Rolin.

Right: Features of the cave roof. Orange: cupolas and intermediate roof channel-like grooves. Blue: lows of the roof (see long sections here below). White: intermediate levels and side passages (CM).

stone is present at the bottom and surrounded by weathered, clayey parts which are covered with even more weathered intervals. These formations are crossed through by a black, irregular, impregnation interval rich in likely manganese. The top of the section is the bioturbated interval already mentioned.

The black interval is almost continuous all along the cave. It has a sinuous, contorted, top surface and it shows different facies. It is secant on loose formations and it can also be present as a film on limestone surface. Its base is often "fuzzy".

4. The bottom part of the section

The description follows the upward vertical succession of lithologies and facies (Fig. 6 & 7).

Limestone (1) is the bottommost layer. It shows a rundkarrren-like bottom morphology protruding from the ground or along the excavated wall. It also displays wall pillars protruding in the passage constrictions. The limestone is hard in its core areas and loose, even powdery, near the edges. It is encountered as small fragments in overlying formations.

Fine- to very-fine-grained quartz sand (2), porous and shaly, variably, light-coloured, mainly whitish to cream-coloured, is present at several locations in the cave, mainly in the lower part of the section. It forms massive strata clearly imbricated in the limestone and associated weathering products (Fig 10. Photo 16). Zebra shale is crossing through sand laminae (Fig 10. Photo 17). The sand was likely interbedded with the limestone during marine sedimentation. Sand laminae locally



Figure 5. Photos 1, 2 and 3. Left: View of the dug out passage, with apparent base of empty space (arrows) at the contact of limestone roof and loose part. Centre: one of the larger ceiling cupolas and a lower roof part at the rear; view width is around 1.5 m. Right: small cupolas in a larger one.

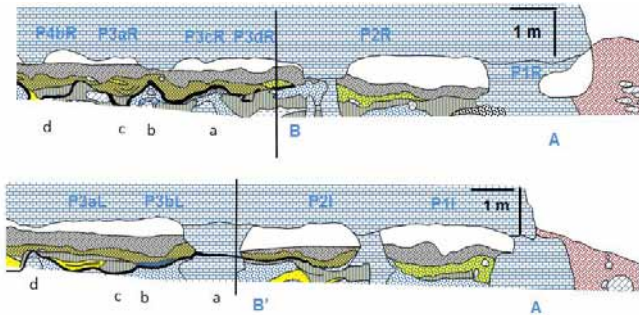


Figure 6. Long sections of cave fill: Proximal part

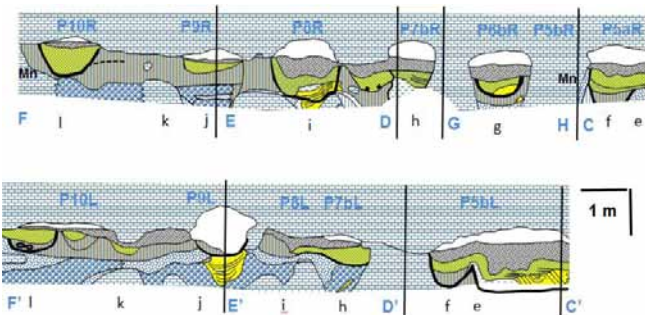
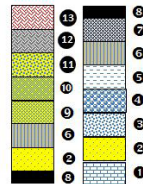


Figure 7. Long sections of cave fill: Distal part

"P" indicates the successive roof cupolas. Small letters are for wall correlations. Capital letters refer to angles of section.



look truncated by overlying products, but this is only a bias due to weathering (Fig 10. Photo 18). Ochre or yellow-brown coloured stains are due to oxidation. The original dip has probably been exaggerated during limestone weathering.

Weathering shaly products surround the limestone and a lithological transition is clearly seen. The limestone is replaced to a variable extent by neof ormation or replacement clay with various facies.

- **Gravelly brown shale (3)** with loose, gravel-sized, matrix-supported remnants of limestone, which is mostly medium to dark brown, occasional showing ochre colour and sometimes a grey colour. It is more common in the proximal part of the cave.
- **Zebra shale (4)** is present along the gravelly brown shale, or directly in contact with the loosened host limestone. It shows linear thin seams floating within a dominantly grey matrix. This zebra shale may display other colours, such as brownish, ochre or yellow-brown. It is present mainly in the distal part of the cave.



Figure 8. Photos 4, 5 and 6. Arrows show the black interval. Left: above the limestone (left) and in the loose formations (right). Centre: in the loose formations at P6bR, at some distance of the cave walls, with a boat shape; also on the limestone wall to the left. Right: on both sides of a prominent limestone wall angle (P6br to the right of the view and P7bR to the left).



Figure 9. Photos 7 to 10. Several facies of the black interval (camera cap for scale is 45 mm large) in the loose formations and around limestone fragments. Photo 11. Gastropod discovered in the black interval, 3.5 cm long. Photo 12. Black interval is perfectly secant on this laminated sand formation.

- **Grey shale (5)** is often surrounding zebra shale, though it may also cover gravelly brown shale and even be inside. In some places, it is located along the limestone.
- **Brown shale (6)** rich in slickensides is present near the cave walls and has suffered microsliding towards the passage axis. Locally, a **silty to sandy shale (7)** is present near the black interval (Fig 9. Photo 8, at P3cR), similar, but differently coloured, to layer 9.

Despite it is secant on loose formations, the **black interval (8)** is often encountered at the top of brown shale.

5. The upper part of the section

Fine- to very-fine-grained quartz sand (2), laminated or not, is also present above the black interval. It is also seen passing laterally to shaly products related to weathering.

Brown shale (6) rich in slickensides is also present. Gravity motion towards the passage axis is indicated by dominant dip-slip slickensides.

Yellow-brown shale (9), silty (9) to sandy (10) to a variable amount, largely overlies the two previous formations. It is shalier in the distal part (8), much sandier with medium to coarse sand (9) at P7bR (Fig. 7), and coarser at the bottom of P4bR, overlain by a lighter-coloured interval with fine to medium sand (8). **More weathered facies (11)** are present near the cave entrance.

Bioturbated, organic-rich silty clay (12) is the uppermost layer and the result of intense activity of badgers. It is dark brownish grey and it shows quartz pebbles which have been brought in by badgers from surface colluvium. It also contains some bones of chicken.



Figure 10. Photos 13, 14 and 15. Lower part of section. Left: a dug hole in the floor shows limestone (bottom left and below pencil) overlain by grey clay, then ochre-coloured clay, then by ochre sand and light grey sand. Centre: zebra brown shale. Right: zebra grey shale, besides gravelly brown shale.



Figure 11. Photos 19, 20 and 21. Upper part of the section. Left: yellow brown silty shale (9) (left) above black interval (8) and brown shale (6) with slickensides. Centre: on both sides of a wall pillar, yellow brown shale, sandy to silty (9). Right: the formations below and above the black interval are both yellow brown shale, but their colour is not exactly the same (layers 7, 8 and 9). The upper layer is the bioturbated, organic-rich silty clay (12).

Photos 16-17-18. Laminated sand. Left: forming a low and, on the sides, passing to shaly parts; partly stained in ochre-colour. Centre: grey clay (zebra shale) crossing through sand laminations. Right: curved sand laminations continuing in brown shaly part above it.

6. Interpretation and conclusion

The loose formations which have been excavated along what is now a human-size cave show transition from limestone and interbedded sands to a variety of weathering products. Except the sand laminations which likely date back to the marine sedimentation during Coniacian, no sedimentary figure is present in the cave fill, which might have indicated deposition related to water motion. Instead, there is plenty of features indicating *in-situ* weathering, with variegated colours showing variable redox conditions, with imbricate products (e.g. the weathering shale crossing sand laminations), with a fossil gastropod (Fig 9. Photo 11) encountered *in-situ* in the cave fill.

The weathering process seems to develop downward, because limestone weathering is better developed upward. However, there is an axial longitudinal depression, indicated by the slickensides in layer (6) present near and along the cave walls and perhaps by highly dipping sand laminations. The cave floor has so far shown only a rundkarren like morphology, observed on a small surface only. It is important to mention that the apparent cave litho-stratigraphy is the result of imbrication of depositional and diagenetic (weathering) products. Transitions between both features are clearly seen. The cave roof morphology, i.e. channel-like grooves and cupolas, is interpreted as related to corrosion by (observed) condensation water and wet air circulation.

The origin of the cave is therefore interpreted as being due to limestone weathering starting along pre-existing fractures and possibly along porous sands, with clay neof ormation and other chemical and mineralogical transformations. We

interpret the weathering as younger than the Upper Eocene Pyrenean compression, which likely created the N30 trending fissures, and possibly as younger than the N 110 fissures which might be alpine (Mio-Pliocene). It likely occurred under phreatic conditions, hence before the post-Riss pre-Würm lowering of base level. Was it during Cenozoic warm climate conditions? Possibly, but perhaps not. Further work in the laboratory is necessary to answer this question. The cave entrance is at a 104 m a.s.l. elevation and the base of coarse siliciclastic Riss sediments are only at 115 m a.s.l., just above the cave.

We consider that the change of phreatic to vadose conditions after the Riss resulted in the compaction of weathered rock, due to Archimedes' buoyancy removal and so created the aerial space between the cave fill and the roof. Water condensation took place afterwards.

The nature of black deposit, likely manganese, still needs to be confirmed but it would be fully consistent with regional data (Fig. 3).

We have presented here conclusions based upon field observations only. This is a first step. Certainly, chemostratigraphic correlations, mineralogical studies of grains and clay fraction and petrographic studies would allow refining conclusions. However, Pantaléon Cave is clearly not a classical karst cave but, instead, the result of limestone weathering.

Reference

LOUGNON, J. 1984?- Ressources minières françaises. Tome 10. Les gisements de manganèse (Situation en 1981). Orléans, BRGM, 131 p.

Acknowledgements

We wish to address our warm thanks to Mr Joseph Billant, the owner of Pantaléon Cave entrance, who very kindly encouraged our work.

The Rock Islands of Belau (Palau), Western Pacific: Drowned Polygonal Karst?

Joan Mylroie¹, John Mylroie¹,

Affiliation: ¹Department of Geosciences, Mississippi State University, Mississippi State, MS 39762 USA mylroie@geosci.msstate.edu

Abstract

The Belau (Palau) Archipelago is a group of islands located in the western Pacific at 6° 53' to 8° 12' North and 134° 6' to 134° 44' East; about equidistant between Guam, the Philippine Islands, and New Guinea (Fig 1a). The archipelago is an independent country in the previously named western Caroline Islands. The archipelago extends for 160 km in a north-south arc, with 414 km² of land area (Fig 1b). The northern islands are mostly Cenozoic volcanic rocks, but the southern islands are Miocene to Pleistocene limestones (Fig 1c) which display significant karstification (USGS, 1956). The signature feature of the southern archipelago are the Rock Islands (Fig. 2), which rise from shallow lagoons as steep-sided hills, some free-standing, others grouped so as to create internal depressions, many which have become inland water bodies (Figure 2d). The overall appearance is of a cockpit or polygonal karst that has been drowned as a result of Holocene sea-level rise. In the open lagoon that separates the groups of Rock Islands, carbonate sedimentation and transport has commonly masked any pre-existing karst depressions (Fig 2b). Within the interior water bodies of the Rock Island groups, lower carbonate sedimentation rates have preserved, with coral overgrowth modification, the karst depressions or cockpits.

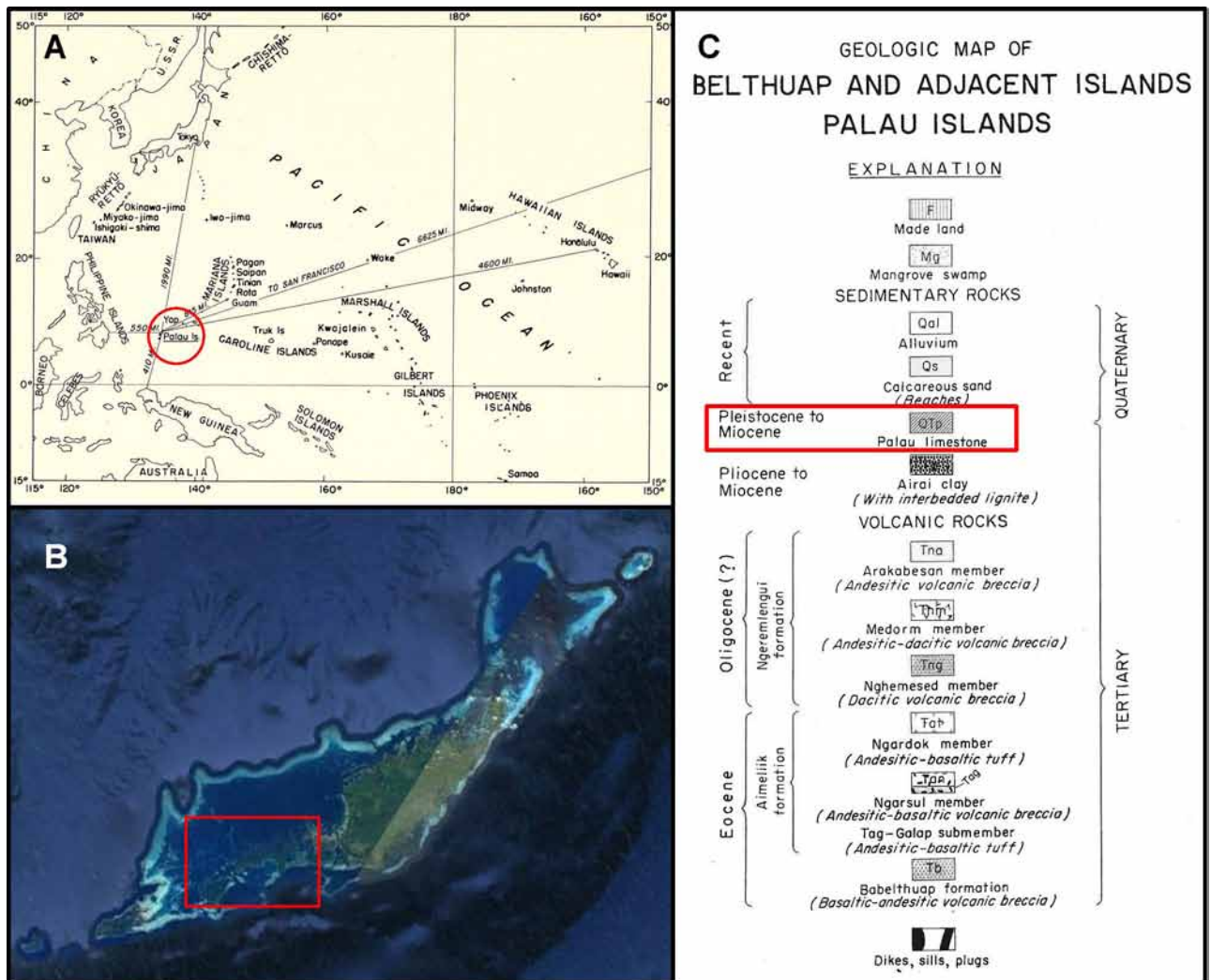


Figure 1. A) Map of the western Pacific Ocean, showing the location of Belau (USGS, 1956). B) Google Earth image of the Belau Archipelago, box delineates the location of the Rock Islands. C) Geologic column for Belau; the islands north of the Rock Islands are primarily volcanic, the Rock Islands and islands to the south are primarily the Palau Limestone (boxed unit); from USGS, 1956.

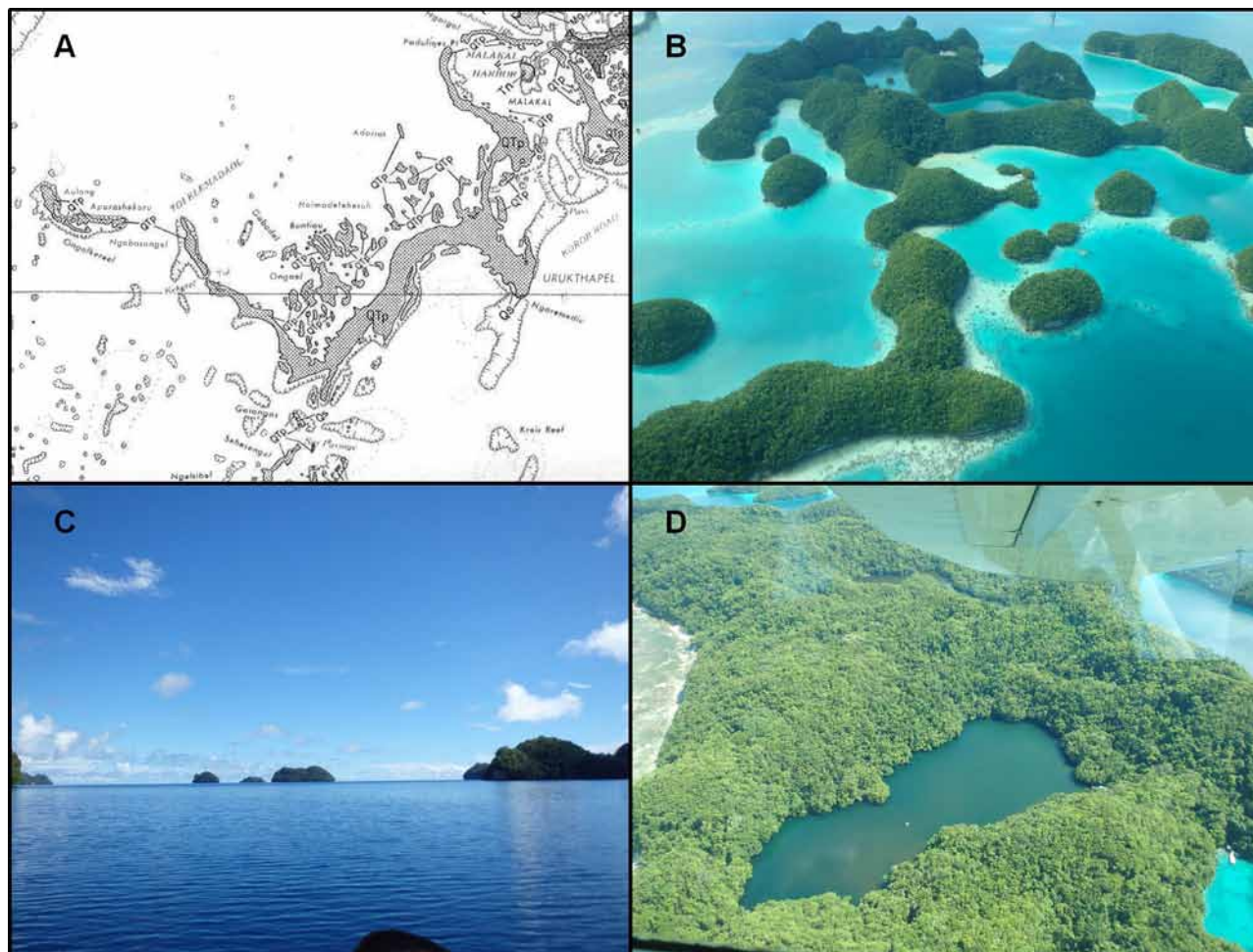


Figure 2. Map of the Rock Islands area (Box of Fig 1b). What appear to be closed contour depressions in the lagoon areas are actually symbols for reefs, which may be preferentially formed on submerged hills (USGS, 1956). B) Aerial view of the Rock Islands, showing the steep-sided nature of the islands, and the fringing reefs that extend from them. C) the Rock Islands as seen from the lagoon surface. D) Rock Island with an interior basin flooded at current sea level.

The Rock Islands display remnant flank margin caves (Myroie and Myroie, 2007), most likely from the last interglacial, MIS 5e, ~120 ka (Fig 3). Deep bioerosion notches surround most Rock Islands (Fig 3c). Given that for over 90% of the Quaternary, sea level has been lower than the lagoon, the Rock Islands evolved primarily in a subaerial condition. In their current environment, bioerosional notching over a 3 meter tidal range, and failure of the flank margin caves, has over-steepened the hills, initiating collapse that has amplified the verticality of the hills from cones into towers (Fig 3). Flank margin caves in various stages of erosional removal are found at 1 to 6 m above sea level, consistent with the last interglacial sea-level highstand (MIS 5e), and minimal tectonic activity or isostatic subsidence since that time. In this case, the karst features have helped resolve a debate regarding tectonic motion in the archipelago in the last ~100 ka. This denudation has removed older surficial features such as pre-Holocene bioerosion notches and fossil reefs from the hillsides.

Deep bioerosion notches in some cases have tubular passages that penetrate into the interior water bodies (Fig 4). These caves must be Holocene in age, and may have begun by mixing dissolution between the interior lakes, which were initially fresh-water in chemistry, with the marine water of the lagoons. Perhaps the caves are also the result of the high heads generated by the 3 m tides that produce locally steep flow gradients (note the short transit distance seen in Fig 4c). The Rock Island caves display significant archeological and historical features, especially from WWII (e.g. Fig 3d).

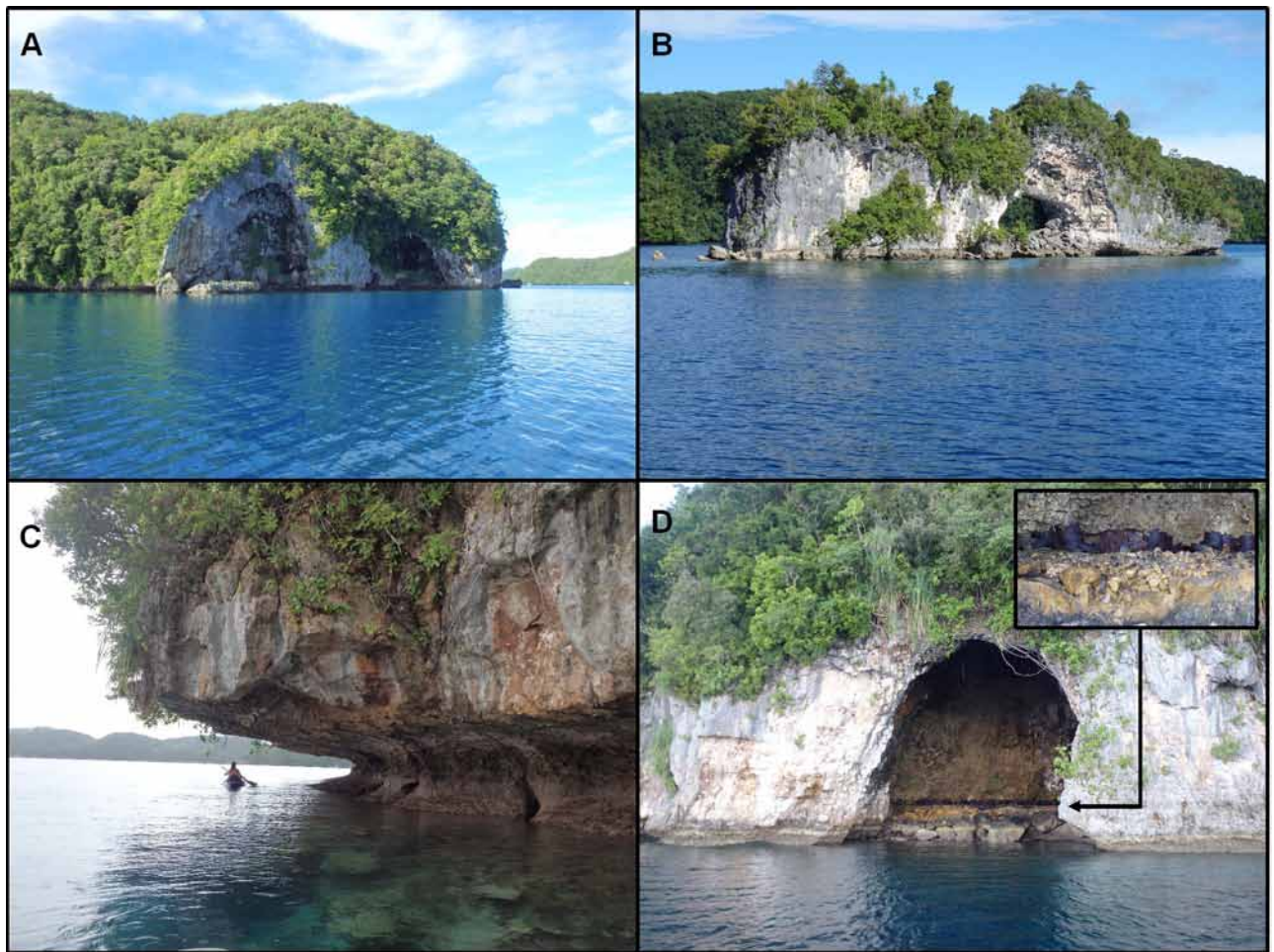


Figure 3. Steep-sided nature of the Rock Islands. A) Cliff formed by collapse of a flank margin cave. B) Isolated small island with a remnant flank margin cave. C) Bioerosion notch common to most Rock Islands. D) Flank margin cave breached by cliff retreat. The inset photo shows that the dark line within the cave (arrow) are oil drums placed there by the Japanese in 1944 to be protected from WWII bombing.

Acknowledgements

The authors thank Destin Penland for his important assistance in handling logistics for the field work on Belau, and for his scientific expertise. Ron Leidich provided boat transport for the Rock Island work. Smile Air provided overflight access, and Tiffany Kasiano arranged logistics on Angaur. The Koror State Government Department of Conservation and Law Enforcement is thanked for permits and permission to visit the Rock Islands.

References

Myroie, J. E. and Myroie J. R., 2007, Development of the Carbonate Island Karst Model: *Journal of Cave and Karst Studies*, v. 69, p. 59-75.

United States Geological Survey, 1956, *Military Geology of Palau Islands, Caroline Islands*. Intelligence Division, Office of the Engineer, Headquarters of the United States Army Far East, 209 p.

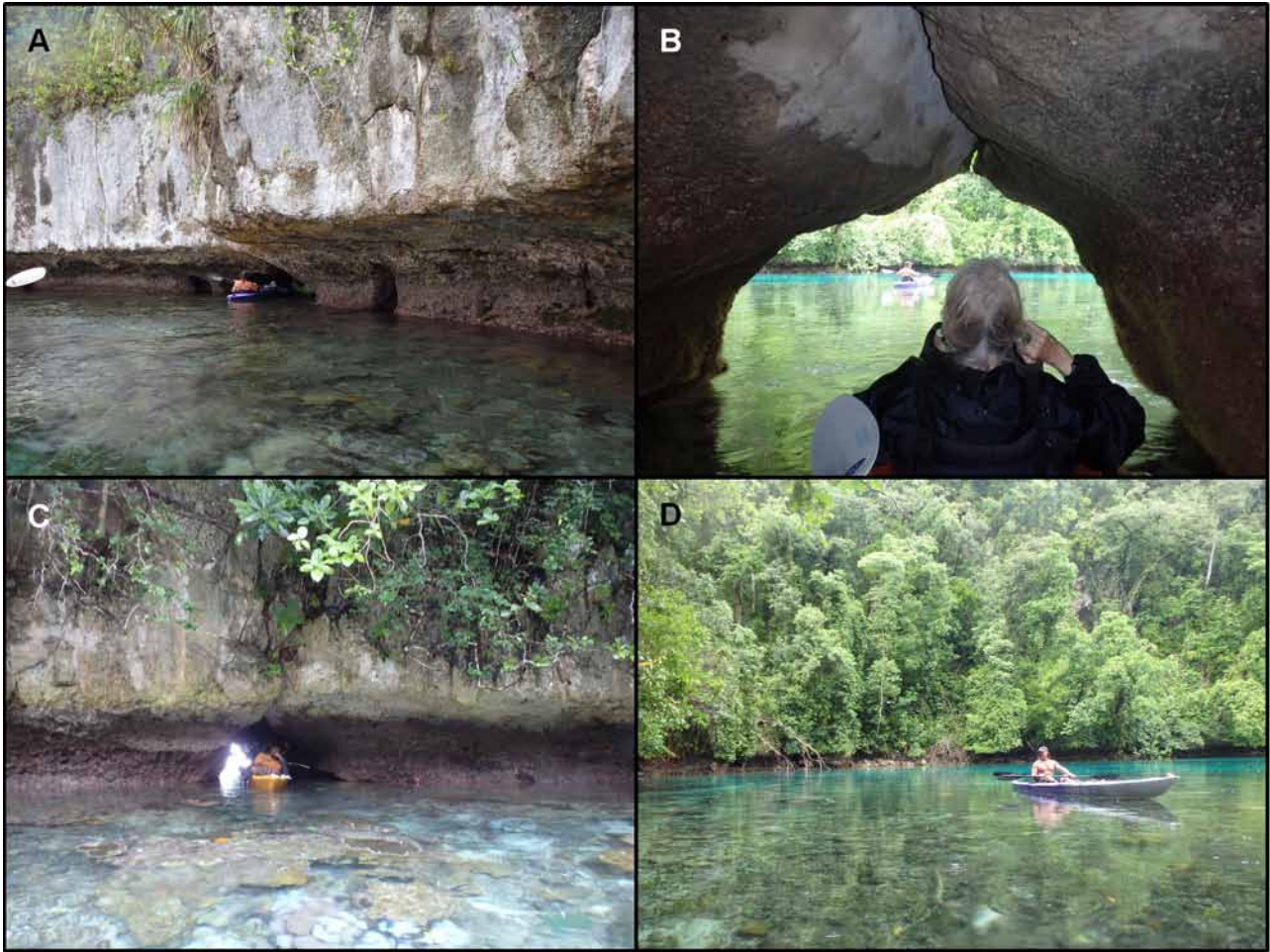


Figure 4. A) Bioerosion notch with a cave opening at the back wall (position of kayak entering the cave). B) In the short dissolution passage connecting the lagoon to an interior lake. C) The cave passage as seen from the lake side; note the corals on the lake floor, and the short length of the cave. D. The lake, entirely surrounded by steep-sided hills.

(Abstract) **Some Outstanding Speleological Features Of Lebanon : Typical Semi-Arid Mediterranean Karst**

Fadi Henri Nader

Affiliation: Speleo-Club du Liban, Lebanon

Abstract

Lebanon is located along the central-eastern coast of the Mediterranean Sea (between latitudes 32°34'N and 34°41'N). The total Lebanese land surface is about 10,452 km², out of which about 7,000 km² consist of karstified Mesozoic and Cenozoic carbonate rocks. Mount Lebanon, stretches along the coastline with a SSW-NNE orientation, and rapidly rises to altitudes higher than 1500m (with the highest point at 3083m above sea-level, at Qornet el Saouda). This mountain has a continuous summit line around 170km long with altitudes above 2200m, forming an efficient obstacle for the westerly winds blowing from the eastern Mediterranean region. Hence, precipitation (rain and snow) falls in abundance on the Lebanese mountains, while the Levantine hinterland remains sub-arid to arid. The position of Lebanon between the wet Anatolian highs and the dry north African and Arabian areas relates to that of a climatic belt very efficient in recording past and present climatic variations. Wet winters and dry summers (80% of precipitation falls from November through February; the highlands receive yearly overall precipitation rates exceeding 1500mm) characterize Lebanon, allowing the development of major karst networks. Deep vertical caves (>500m in depth) are found on the highlands (>1500m asl), reaching the water-table.

Lateral caves are found near the coastline or at hydro-stratigraphic boundaries, where the aquifers discharge groundwater (e.g. the famous Jeita Grotto, >10km long). Typical karst springs are common, with their highest discharge taking place at the snow-melt period (March-April). Mount Lebanon is rich in a variety of caves influenced by the variety of the carbonate rocks, lithologies and textures (e.g. limestone, chalk, bioclastic limestone, dolostones). Karst landforms are also diverse with amazing natural bridges, karst plateaus, dolinas and sinkholes, etc. Owing to its position on the Levant climatic belt, Lebanon has provided valuable speleothems which has recorded the paleoclimatic variations since more than a hundred thousand years. Recent studies confirmed a gradual climatic degradation since 6,000 years ago. Hundreds of caves have also been used by humans for at least 10,000 years, such as the caves of the Ouadi Qadisha (in northern Lebanon). They have been at the center of many legends and witnessed historical moments. Mount Lebanon is geographically small, yet it has a lot to offer and I hope that this contribution will take you on a pleasant journey to discover yet another beautiful and interesting spot of our planet that needs to be protected.

Highlights of Romanian Caves and Karst

Gheorghe M. Ponta¹ and Victor Ursu²

Affiliation: ¹Geological Survey of Alabama, 420 Hackberry Lane, Tuscaloosa, Alabama, 35401, U.S.A., gponta@yahoo.com
²Co-editor, www.speologie.org, 375 Middlewood Rd, Middletown, New Jersey, 07748, U.S.A., victor@ursu.net

Abstract

Romania with an area of 238,391 km², located in Southeastern Europe, has a karstifiable area of about 5,500 km² (approx. 2.3%). A website, www.speologie.org, was set up to collect and centralize all cave related data within the Romanian karst. It is an online searchable database of 8,166 identified caves with 964.50 km of surveyed passages. The web page was started by cavers and is open for community contributions. The data structure extends the systematic catalogue started by Cristian Goran in 1981. The diverse spectrum of Romanian caves is briefly presented in this paper.

Keywords: karst, caves, catalogue, recreational caving

1. Introduction

Romania with an area of 238,391 km² is located in Southeastern Europe and is surrounded by the Black Sea and Moldova in the east, Serbia and Hungary in the west, and Ukraine in the North. The Danube (Dunărea) River forms most of the southern border with Serbia and Bulgaria.

The karstifiable rocks (limestones, dolomite, salt, gypsum) occupy about 5,500 km² (Onac and Cocean, 1996; Onac, 2000) of the Romanian territory (approx. 2.3%), and are Paleozoic, Mesozoic and Neogene deposits (Figure 1).

Romania has a temperate-continental climate, with four seasons, with average annual temperature ranging between 8 °C to 11 °C and precipitation between 600 mm to 1,010 mm per year. The temperature ranges from -25°C in January to 31°C in July.

Beginning in 1920, when the Institute of Speleology "Emil Racoviță" (ISER) was established in Cluj-Napoca, collection of documents and maps related to the caves of Romania started, and a depository established. Between 1920 and 1956, over 300 caves were recorded, the majority of them being documented in the ISER's publications.

Shortly after 1956, when the ISER was reorganized, with offices in Bucharest (București) and Cluj-Napoca, the recreational caving movement began, the first grottos/caving clubs began their activities in late fifties and sixties in several major cities in Romania: Cluj-Napoca, Reșița, București, Arad, etc. In 1965, the map of Romanian Karst Areas was published by ISER, which included about 1,000 caves (Goran 1981).

The first Catalogue of Romanian Caves was compiled by Marcian Bleahu and Ioan Povară in 1976, and recorded about 2,000 caves, including the early discoveries of the recreational cavers. In the same year, The Central Committee of Sportive Speleology (CCSS) was formed as a subsidiary of Romanian Federation for Tourism and Alpinism, which up to 1989 was the largest organization in Romania with about 500 members and 40 to 50 grottos/caving clubs. For almost 15 years, CCSS with ISER promoted speleology, organizing short courses/camps for caving/climbing technique (SRT), cave survey, biology, and cave photography, through the National School of Speleology.

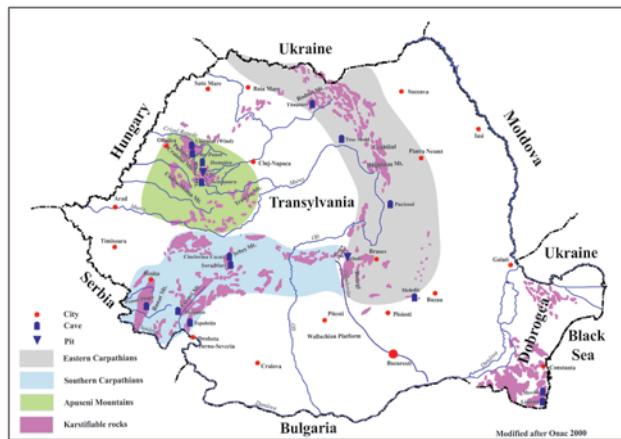


Figure 1. Karstifiable rocks of Romania

CCSS had its own publication (Buletin F.R.T.A; later becoming Buletin Speologic) and several caving clubs published new discoveries and trip reports in their bulletins and newsletters. Between 1972 and 2000, CCSS (after 1994 Romanian Federation of Speleology) organized annual conventions (Speosport), and sponsored survey camps to validate the maps of the main Romanian caves. In 2000 Speosport became the National Congress of Speleology.

As a result of these activities, in 1981, The Systematic Catalogue of Romanian Caves/Catalogul Sistematic al Peșterilor din Romania (Goran, 1981) was published and included data about 6,816 caves. By 1989, the number of caves discovered and surveyed reached 12,000. Based on the Romanian Federation of Speleology's (FRS) web page (www.frspeo.ro), the number of known caves today in Romania is 12,600. The database related to these caves is hosted by ISER (official depository); a copy was at CCSS/after 1994 FRS, and the grotto/caving club who made the discovery and survey held a third one.

After 1989, the caving activity decreased due to better opportunities to travel outside Romania, and most of the old generation of cavers abandoning the activity. Permission to access the cave database was allowed to the author/s of the discovery, or by others with his/their permission. The new generation of cavers, found it difficult to get permission to view the cave

related maps and documents, and the database became obsolete and restricted.

In these circumstances, the webpage *www.speologie.org*, was started, where with cavers contributions, a new database was generated and made available on the web. The web page follows the same structure as the catalogue designed by Cristian Goran in 1981. The difference was between approx. 8,166 entries to 12,600 indicating that either the webpage missed some information, or that some hundreds of caves were duplicates.

2. Geology

Romania consists of four major geological areas: The Eastern Carpathians (Carpații Orientali), The Southern Carpathians (Carpații Meridionali), Apuseni Mountains, and Dobrogea. The Carpathians Mountains arcs have been shaped around an old rigid central structure in the alpine cycle.

The Eastern Carpathians with 611 caves are located between the Tisa River in the North and Dâmbovița River in the South, and consist of numerous karstifiable rocks (limestones and dolomites of Triassic through Miocene age) scatters across this mountain range, overlaying a crystalline zone of Paleozoic and Precambrian age, and a flysch zone (Mesozoic rocks). The longest caves (e.g. Tăușoare) in Eastern Carpathians are located in the Rodnei Mountains, and are developed in Eocene (Priabonian) limestones.

Miocene salt deposits located at the south end, host a unique karst landscape, with sinkholes and closed depressions (Ponta, 1984-85). Neogene volcanoes exist in the central part of the Eastern Carpathians, host tree mold type caves, lava caverns with opal, and others formed by the underground erosion of tufa layers of cemented agglomerates (Naum and Butnariu, 1967).

Dâmbovița River in the East, the Danube River in the West, and Mureș River and Transylvania in the North, defines the Southern Carpathians with 4,131 caves. The Southern Carpathians consists of three structural units: the Danubian terrane, the Severin nape, and the Getic terrane. The Danubian and Getic terranes consist of Mesozoic rocks that overlie Paleozoic and Precambrian sedimentary and crystalline rocks (Burchfiel et al., 1974). The majority of these caves are located in Jurassic-Cretaceous limestones. One of the longest underground streams in the country (Șura Mare) (Ponta, 1991) with a large bat colony, and a cave rich in minerals (Cioclovina Uscată) (Onac, 2000) was identified in this area. Ardealite (name comes from Ardeal, another name used for Transylvania) is a phosphate mineral found in Cioclovina Uscată and described for the first time by Halle in 1931.

In the Jurassic and Cretaceous limestones of Banat, karst platforms developed, with numerous caves and potholes. In one of the cave, Peștera cu Oase/Bones Cave, one of the oldest remains of a modern human (c. 40 ka) that shows evidence of admixture with Neandertalians was found (Trinkaus et al., 2013).

Hydrothermal karst is present within the Cerna Valley in southwestern Romania (e.g. Hercules Cave) in the Jurassic and Cretaceous limestone with air temperatures as high as

40°C, due to the presence of thermal water flowing through the caves (Povară, 2012).

The Apuseni Mountains with 3,234 caves are located between Mureș River in the south and Crișul Repede River in the North. The majority of the limestones are in the northern Apuseni Mountains, which consist of Mesozoic sedimentary rocks overlying Paleozoic and Precambrian sedimentary and metamorphic rocks. The longest caves in the country (Wind/Vântului, Humpleu caves, and Ciur Ponor) (Ponta et al., 1991), the deepest pothole (V5 Pit), and biggest perennial ice cave in Romania (Scărișoara) are located in these mountains. In Humpleu Cave 80 cm long single crystals were found, and in Valea Rea Cave 37 minerals were identified. In Ciur Izbuca Cave, about 400 footprints in mud, several thousand years old, and in Vârtop Cave three footprints preserved in a calcite crust were found. Also the Bears Cave (Pestera Urșilor) is known for several cave bear skeletons.

The Dobrogea area comprises a group of low mountains, where 99 caves were identified. Upper Jurassic and Barremian limestones and dolomites, Senonian chalk and Sarmatian limestones occur in this area. Here is the location of Movile cave with its groundwater ecosystem rich in hydrogen sulfide and carbon dioxide, and Limanu cave with 4,000 meters of passages formed by solutioning with several man made enlarged passages.

3. Karst

The Romanian karst landscape was generated in the Quaternary and can be classified into three categories, characterized by the hydrodynamic conditions of the karst aquifers and the relationship between karst aquifer and land surface (Ponta 1998):

1. **Deep Karst type features** (paleokarst) occur in the sedimentary rocks underlying non-soluble bedrock and overlain by aquicludes or aquitard deposits. These confined aquifers are typical to the Wallachian Platform. The Carbonate Deposits of Malm-Barremian Ages are 1,500 m thick, and can be found at a depth ranging between 1,800 m to 2,000 m in the Wallachian Platform (Ponta 1998).

2. **Shallow Karst type features** are in sedimentary rocks overlain by unconsolidated sediments. The thickness of the overburden range between 10 m to 50 m. This type of karst has the greatest extension in Dobrogea, where the overburden is formed mainly by loess (Ponta, 1998).

3. **Bare/exposed karst** occupies about 5,500 km² (Onac, 2000) on the Romanian territory (approx. 2.3% of the Romania's surface). The most karstified deposits belong to the Jurassic-Cretaceous sedimentary cycle. In the Southern Carpathians, the largest exposed carbonates region is Banat (800 km²) and the most karstified area is in the Bihor Mountains (Apuseni Mountains) (Bleahu and Rusu, 1965).

Recrystallized Paleozoic carbonate deposits represent about 16% of the total bare karst. The Mesozoic deposits belong to two sedimentary cycles (Triassic 17.8% and Jurassic-Cretaceous 47.3%), and the Neogene deposits to a third cycle (Eocene, Tortonian and Sarmatian 16.8%) (Bleahu and Rusu, 1965).

Based on the geomorphological and structural aspects, there are three types of karst landscape specific to the Romania's territory:

1. Plateau type karst is characterized by large dolomite or limestone plateaus with surface karstic features like karrens (lapies), dolines (sinkholes), closed depressions, dry valley and streams with elevation range between 600 m to 2000 m, and covers areas between 20 km² and 120 km². The thickness of the carbonate deposits ranges between 200 m and 600 m and alternates with non-carbonate rocks. The most important plateaus are in the Bihor, Pădurea Craiului, Codru Moma, Sebeș or Banat Mountains (Bleahu, 1972).

2. Bar/Ridge type karst is ridges derived from carbonate deposits approx. 200 m thick, which dip at over 45°. As in the previous case, generally the carbonate rocks alternate with non-soluble rocks. Due to the differentiated erosion processes very prominent limestones-dolomite ridges appear. The strike or these is controlled by longitudinal faults with regional extension and are cut by transverse faults, on which the karst aquifer is opened and emerges to the surface through springs. The most representatives' ridges are in the Hăghimaș, Piatra Craiului, Vânturarița, and Trascău massifs (Bleahu and Rusu, 1965).

3. Isolated massifs are an intermediate type between the previous two, being less extended plateaus such as the Ceahlău or the Dâmbău in the Metaliferi Mountains or olistoliths on the limestones in the Piatra Mare and Bucegi Mountains (Bleahu and Rusu, 1965).

4. CONCLUSIONS

While the extension of karstifiable rocks represents only 5,500 km² scattered across Romania, a diverse range of caves are present:

- **Limestones and dolomite caves.** From the total of 8,166 caves, 97% are developed in limestones and dolomites rocks, only 3% being hosted in other rocks. The largest numbers of caves are located in Bihor Mountains (1082), which represents 13%, followed by Pădurea Craiului with 921 (11%) and Vâlcan Mountains 803 (10%). The total length of surveyed passages is 964.50 km. There are 144 caves over 1 km long, 91 caves with vertical development higher than 100 m, 22 caves in salt, and 102 caves protected by law. The longest cave is Peștera Vântului (42,165 m) and the deepest one is Vărășoia (V5 Pit) with -653 m. 80 caves are totally submerged being accessible only by divers. The deepest sump is in Coiba Mare-Coiba Mica Cave (-93 m), and the longest one is Sifonul Negru (Black Sump) in Ișverna cave, almost 700 m long. In the database, elevation of the entrances is known for 4,244 caves, of which 3,475 ranges between 300 to 1200 m. The intervals with the highest number of caves (at 100 m increments) are 400-500 with 625 caves, followed by 500-600 interval, with 532 caves, and 1,100-1,200 m interval with 401 caves.
- **Evaporates/salt karst.** The karst formed on evaporite rocks represents 5% of the Romania's bare type karst and is in the lowland hills of Eastern Carpathians. The largest zone is Săreni-Trestioara situated between Slănic Valley,

Sări Valley and Meledic Valley, known under the name of Meledic plateau. The average altitude of the area is 600 m, and presents caves, deep valleys, karren and sinkholes (50 m in diameters) (Ponta, 1998).

- **Volcanic caves.** Puciosul cave (Pestera din Muntele Puturosul) located in the central part of the Eastern Carpathians is 14 m long, with sulfur deposits on the walls as a result of hydrogen sulfide and carbon dioxide released by volcanic activity. Carbon dioxide (CO₂) is heavier than air, so operating below the CO₂/air interface is fatal. Tree Mold caves are located on the upstream section of Mureș River, in the Toplița-Deda gorges. The caves were formed when the Călimani-Gurghiu volcano was active, and its lava flew out and covered the forest, trapping trees. In time, the trees were washed away, leaving behind the tree mold/shape caves (Moreh, 2010).
- **Thermal Caves.** Thermo-mineral karst (thermal waters) is present in the Băile Herculane, Mangalia and Geoagiu areas (Bleahu and Rusu, 1965). The largest hydrothermal karst reservoir is in Băile Herculane within the Cerna Valley, in southwestern Romania, where the longest thermal water cave, Hercules (82 m long) is traversed by a stream with temperatures as high as 28°C to 30°C.
- **Ice Caves.** Several ice caves are known in Romania as: Focul Viu, Avenul cu Zăpadă, and Scărișoara. Scărișoara cave host a 3,000 to 5,000 years old deposit of perennial ice with a volume estimated at 100,000 cubic meters (Onac et al., 2010).
- **Mineralogy.** Minerals were identified in several caves in Romania. Cioclovina Uscată and Peștera din Valea Rea Cave are rich in minerals. Ardealite (name comes from Ardeal, which is another name for Transylvania) is a phosphate mineral found in Cioclovina Uscată and described for the first time by Halle in 1931.
- **Sulfuric Acid/Hypogene Speleogenesis Caves.** Movile Cave (Romanian: Peștera Movile) is known for its groundwater ecosystem rich in hydrogen sulfide and carbon dioxide. Life in the cave is in the forms of microbial mats (bacteria) on the cave walls and the surface of pools, based on chemosynthesis (Sârbu et al., 1996).
- **Historical and Anthropological Caves.** Paintings were found in Cuciulat and Coliboaia Caves. Marin Cărciumaru estimated that the Cuciulat cave paintings were completed in the Upper Paleolithic, about 12,000 years ago (Cărciumaru and Bitiri, 1988). The oldest cave paintings in Central Europe, estimated at between 23 000 and 35 000 BP (Gravettian or Aurignacian) have been discovered by a team of Romanian speleologists in the Coliboaia Cave, Bihor Mountains (Clottes et al., 2012). In Peștera cu Oase/Bones Cave, one of the oldest remains of a modern human (c. 40 ka) that has shown proof of admixture with Neandertalians was found (Trinkaus et al., 2013). In Ciur Izbuca cave about 400 footprints in mud several thousand years old, and in Vârtope Cave three footprints preserved in a calcite crust were found.

- **Biospeleology.** Romania is one of the best-investigated European countries for biospeleology. In 1920 Emil Racoviță founded world's first Institute of Speleology in Cluj-Napoca. Romania has a rich cave fauna with many endemic elements. There are 31 bat species located in 7 caves that are considered shelters of major importance (Coroiu, 2017). Bone remains belonging to the Upper Pleistocene cave bear (*Ursus spelaeus*) were found in numerous caves, as Pestera de la Vadul Crișului or The Bears Cave (Pestera Urșilor).

The longest caves in Romania

1. Peștera Vântului	42,165 m
2. Peștera Mare din Valea Firii (Sistemul Humpleu)	36,600 m
3. Peștera din Pârâul Hodobanei	22,142 m
4. Peștera Topolnița	20,500 m
5. Sistemul Ciur Ponor-Toplița de Roșia	20,150 m
6. Sistemul Vărășoaia (V5-V24)	19,250 m
7. Peștera de la Izvorul Tăușoarelor	18,107 m
8. Peștera din Valea Rea	16,357 m
9. Sistemul Zăpodie-Peștera Neagră	12,048 m
10. Peștera Șura Mare	11,694 m

The deepest caves in Romania

1. Sistemul Vărășoaia (V5-V24)	653 m
2. Avenul de sub Colții Grindului	561 m
3. Peștera de la Izvorul Tăușoarelor	461 m
4. Peștera Șura Mare	425 m
5. Peștera din Valea Rea	372 m
6. Avenul din Dealul Secăturii	366 m
6. Avenul din Stanul Foncii	339 m
7. Peștera Mare din Valea Firii (Sistemul Humpleu)	314 m
9. Peștera Jgheabul lui Zalion	303 m
10. Peștera din Sâncuta	295 m

References

Bleahu M, Rusu T, 1965. Carstul din Romania. O scurtă privire de ansamblu - *Lucrările Institutului de Speologie Emil Racoviță Tom IV*.

Bleahu M, 1972. Karst of Rumania. In: *Karst: Important Karst Regions of the Northern Hemisphere*. (Herak M, Stringfield VT (Eds.) Elsevier, Amsterdam, pp. 341-353.

Burchfiel BC, Bleahu M, Borcoș M, Patrulius D, Săndulescu M, 1974. Geology of Romania. In: *GSA Special Papers Geology* 2 (8).

Cârciumaru M, Bitiri M, 1983. Peintures rupestres de la grotte Cuciulat (Roumanie) - *Bulletin de la Société préhistorique française*, 80, fasc. 3, pp. 94-96.

Clottes J, Besesek M, Gely B, Ghemiș C, Keneszi M, Lascu VT, Meyssonier M, Philippe M, Plichon V, Prud'homme F,

Radu VA, Rus T, 2012. Découverte d'une nouvelle grotte ornée paléolithique en Roumanie, dans le département du Bihor. In: *Clottes J. L'art pléistocène dans le monde, Actes du Congrès IFRAO, Tarascon-sur-Ariège, septembre 2010 – Symposium "Art pléistocène en Europe"*, pp.513-528.

Coroiu, 2017. Chiropteran fauna in the caves of Romania (un published).

Goran C, 1981. *The Systematic catalogue of Romanian Caves* (Catalogul Sistematic al Peșterilor din Romania, Institutul de Speologie Emil Racoviță, Federația Română de Turism-Alpinism, Comisia Centrala de Speologie Sportivă), p.496.

Halla F, 1931. Isomorphe Beziehungen und Doppelsalzbildung zwischen Gips und Brushit. *Z. Krist.* 80: pp. 349-352

Moreh K, 2009. Peșteri de mulaj. *Speomond No. 9, Federația Română de Speologie*, pp. 44-48.

Naum T, Butnariu E, 1967. Le vulkano-karst de Călimani (Carpathes roumaines). *Ann. Speol.* 22: pp.727-755.

Onac BP, Cocean P, 1996. Une vue global sur le karst roumain. *Kras i Speologia*, 8(17): pp. 105-112.

Onac BP, 2000. *Geologia regiunilor carstice*, Editura Didactică și Pedagogică R.A., București, Romania, p.399.

Onac BP, Racoviță G., Brad T, 2010. Atlasul Peșterilor din Munții Apuseni, Bazinul Arieșul Mare, University of South Florida Libraries, p.91.

Ponta G, 1984-1985. The Evaporate Karst of Rumania. In: *Atti Simposio Internazionale sul Carsismo helle Evaporiti: La Grotte d'Italia*, (4) XII, Editat de Instituto Italiano di Speologia, Bologna, Italia: pp. 407- 415.

Ponta G, 1998. Karst of Romania. In: *Global Karst Correlation IGCP 299*, pp. 193 – 207.

Ponta G, 1991. New tracing experiences in the Sebeș Mountains - Rumania, *Proceedings of the International Conference on Environmental Changes in Karst Areas*, Universita di Padova, pp.195-204.

Ponta G, Terteleac N, Gaspar E, 1991. Three karstic systems (Roșia, Toplița de Roșia and Vadul Crișului) in the Pădurea Craiului Mountains, Rumania, *Theoretical and Applied Karstology*, volume IV, pp. 129 –142.

Povara I, 2012. Valea Cernei- Morfologie, hidrologie, ape termominerale, Academia de Științe Tehnice din Romania, Editura AGIR București, p. 304. (In Romanian)

Sârbu SM, Kane TC, Kinkle BK, 1996. A chemoautotrophically Based Cave Ecosystem. *Science*, Washington.

Trinkaus E, Constantin S, Zilhão J. (Eds.), 2013. *Life and Death at the Pestera cu Oase. A Setting for Modern Human Emergence in Europe*. Oxford University Press USA, p. 438.

Armenia Karst Project

Ruggieri Rosario¹, Daytyan Smbat², Ugujyan Adranik³

Affiliation: ¹Hyblean Center of Speleo-Hydrogeological Research, Ragusa, Italy, info@cir-s-ragusa.org
²Faculty of Geography and Geology, Yerevan State University, Armenia, srdaytjan@mail.ru
³Faculty of Biology, Department of Bioinformatics, Yerevan State University, Armenia
ugujyanandranik@gmail.com

Abstract

This paper reports the results of the first phase of the expedition *Armenia Karst Project*, carried out by the Faculty of Geography and Geology of Yerevan State University, Armenia and the Hyblean Center of Speleo-Hydrogeological Research Ragusa, Italy. The expedition aimed at the exploration, study and documentation of the karst morphologies and hydrokarst systems present in some areas of the Armenian southern Caucasus. The first phase of researches conducted in September 2016, was concentrated in the karst area of *Yeghegnadzor*, located in southern Armenia. This area is composed of geological units of different ages ranging from the Late Paleozoic to the Anthropocene. The limestone relief is dissected by deep valleys up to 20 km long and up to 200 m deep and is characterized by surface and deep features including spectacular fluviokarst gorges, dolines, a wide type of karren and many caves. The last are located both on the valley floors and to specially on the vertical sides of the gorges. The area for this preliminary research was the *Vayk Ridge* where the lowest point corresponds to 975 m (the *Arpa River* valley), and the highest one is *Mount Harsnaqar* (2773 m). In this sector twelve karst morphologies were observed, in the basins of the *Arpa River* and the *Grav River*. The collected data are used for the first speleogenetic model of the area. In a more general context, the surveyed karst features, such as surface relict karst relief, relict karst caves, active and inactive karst systems and palaeokarst fillings, highlight the great importance of the karst studies as further contribution to the knowledge of the geological history of this area. The continuation of the research is planned in 2017 in some karst areas in northern Armenia.

Keywords: Armenia, Yeghegnadzor, karst, hypogene cave, doline, sinkhole.

1. Introduction

In September 2016, the first phase of the investigation “Armenia Karst Project” was carried out by a team of researchers from the Faculties of Geography and Geology and Biology, of the State University of Yerevan, Armenia and the Hyblean Center of Speleo-Hydrogeological Research, Italy. The aim of the research was the survey and study of the karst morphologies present in some areas of Armenia. The investigation concerned the karst area of Yeghegnadzor Vaoz Dzor, Marz Province where Permian limestone and Cretaceous-Eocene conglomerates outcrop. The relief is characterized by a deeply etched highland which shows spectacular fluviokarst gorges with several cave entrances on the vertical high cliffs. The team has both explored and documented a number of caves and done some preliminary reconnaissance for the further research planned for 2017. This paper reports on the main physical and geological features of the karst area and the preliminary surveyed karst data obtained both on the surface and underground inside the explored caves.

2. Geographic aspects

The karst complex of Yeghegnadzor is located in the South-Eastern part of Armenia (Fig. 1). It includes the downstream basin of the *Arpa River* (within the limits of the Republic of Armenia), extending mainly to its southern part. The main orogenic unit of the area is represented by the *Vayk Ridge* accommodating the *Yeghegnadzor* karst complex on the northern slopes of its western part. The northern and the eastern boundaries of the karst complex follow the valleys of the *Arpa River* and the *Grav River*, respectively, and the southern and western boundaries follow the contour of the RA state



Figure 1. Map of Armenia with area of research in the enclosed black box

border. The elevation of the lowest point corresponds to 975 m (the *Arpa River* valley), and the highest is *Mount Harsnaqar* (2773 m). The northern slopes of the western part of the *Vayk Ridge* are dissected by deep valleys of the left-hand tributaries of the *Arpa River* such as the *Grav River*, the *Erdichi River*, and the *Gnishkadzor River*. They are up to 20 km long, and their valleys are up to 200 m deep. Several mountain spurs with steep slopes; among them are *Gandzak*, *Harsnaqar* and others. The climate is dry and strongly continental. The precipitation does not exceed 400 mm and is mostly realized during spring rains.

3. Geological structures, stratigraphy and tectonics

The karst complex of *Yeghegnadzor* is composed of geological units of different ages ranging from the Late Paleozoic to the Anthropocene. The 500 m thick Paleozoic marine sedimentary formations are rich in fossils (petrified corals, brachiopods) and include Middle and Late Devonian limestone, marls, sandy limestone, and quartzites exposed in anticlinal structures. Permian rocks, 400 m thick, cover significant areas in the central part of the study area and are represented mainly by bituminized limestone. The presence of bitumen determines black and dark-brown colors of the rocks. Late Cretaceous units are represented by terrigenous, volcanogenic-sedimentary and carbonate rocks and correspond to the anticlinal structures. The Turonian-Early Coniacian stage is represented by a 250-300 m-thick suite of conglomerates, sandstone and clay. The Campanian-Maastrichtian stage consists of up to 400 m of limestone and marls. The Cenozoic era is mainly represented by the Paleogene, especially Eocene sediments. Part of the large karst caves are developed within the Early Eocene 100 m thick limestone and limestone conglomerates. Volcanic-sedimentary rocks such as tuff, tuffite, and tuff sandstone are predominant in the Middle Eocene rocks. The Quaternary is represented primarily by alluvial sediments which do not to exceed 100 m in thickness.

The area of the *Yeghegnadzor* karst complex is accommodated within 2 tectonic structures – the *Yeghegnadzor* synclinorium and the *Vaik* anticlinorium. The *Yeghegnadzor* synclinorium involves the mid-stream and upstream basins of the Arpa River. It is composed of the Late Cretaceous, Paleogene and Neogene sedimentary and volcanogenic-sedimentary units, bedded on the base of the Late Paleozoic terrigenous-carbonate complex. All pre-Pliocene rocks are strongly folded, forming many folds striking primarily to the northwest. In the limits of the synclinorium, faulting discontinuities are common. The *Vaik* anticlinorium is located south of the *Yeghegnadzor* synclinorium. It includes the *Vaik Ridge* and strikes to the northwest. The core of the anticlinorium is composed of the Late Paleozoic and Triassic terrigenous-carbonate and terrigenous sediments that are discordantly overlain on the flanks with the Late Cretaceous, and partly Paleogene rocks. The *Vaik* anticlinorium consist of a series of brachy-anticlinal folds with brachy-synclinal folds in between. The folded structures are broken by several fault discontinuities of varying directions.

4. Background of the Study

The first studies in the karst complex of *Yeghegnadzor* are related to the 1920-30s. In his “Review of the Geology of the Western Part of Daralagyaz Province of the Armenian SSR”, A. Krzhechkovsky wrote about several caves in the valley of *Jaghchi* (which is one of the *Grav River* tributaries). Aragonite crust is encountered in some caves and a high-flow spring was found in one cave (Krzhechkovsky 1930). In 1980-1990s, complex speleological surveys were undertaken in this area by the speleological party of the Armenian Geography Association and by other scientists. The *Arjeri*, *Magellan* and *Mozrovi*, as well as tens of other caves were discovered and investigated during that study (Balyan and Vanyan 1986). Caves development in Armenia (and also within the *Yeghegnadzor* karst complex) was suggested to be determined by tectonic pro-

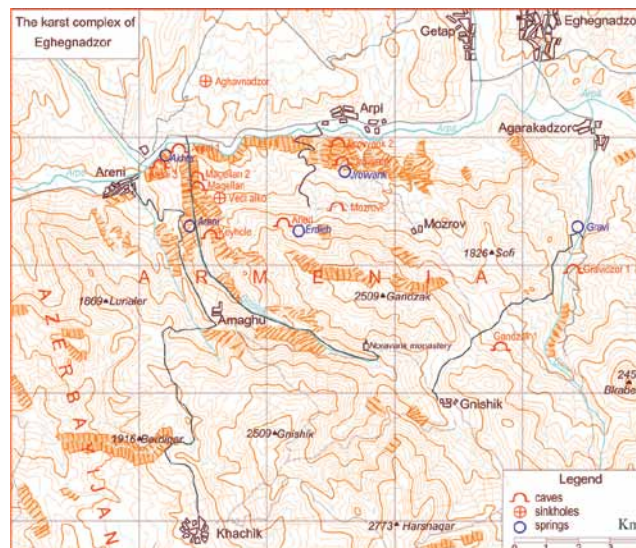


Figure 2. Locations of the main karst features

cesses and volcanic phenomena (Movsesyan *et al.* 1983). In 1983-1985, the staff of the Geological Sciences Institute of the Ukrainian Academy of Sciences studied the *Arjeri* and the *Mozrovi* Caves with the purpose of designing underground routes for tourism and making the caves suitable for excursions. According to those studies, the *Arjeri* and the *Mozrovi* Caves formed under the impact of thermal waters (Doublyansky 2010).

5. The caves surveyed and studied in the karst complex of Yeghegnadzor

The karst complex of *Yeghegnadzor* is characterized by surface and deep forms of karst relief including karst, craters, grottos and caves. Ten of the identified caves are more than 100 m long, and two of them (*Magellan* and *Arjeri*) are more than 1 km long, 1720 m and 3500 m for *Magellan* and *Arjeri*, respectively (Fig. 2). The surveyed caves are mainly developed within the Devonian limestone, Cretaceous and Eocene limestone and conglomerates and are described as follows.

Jrovvank 2 cave (Fig.3A), located in the left slope of the Erdich river canyon at an elevation of 1,203 m a.s.l., is a structural cave developed in Devonian limestone along an angular unconformity between two formations. In this regard, the upper formation is comprised of limestone alternating with sandstone layers and has a dip direction of N 150 at 20°, while the lower formation, comprising massive limestone, has a dip direction of N 320 at 25°. The cave is a single large chamber with a length of 14.1 m and a positive depth of 2.2 m.

Gandzak 1 cave (Fig. 3B-C), located in a tributary valley of the Gravi at an elevation of 1,948 m a.s.l., is a relict karst cave developed in a Eocene limestone with a dip direction of N 210 at 25°. It consists of a large room with a surface length of 19.6 m, a surface width of 24 m and a total positive depth of 4.7 m. During the survey some paintings of animals in red ochre were discovered. Outside the cave some relict karst morphologies were observed such as large mushroom-like monolithic stones, a stone bridge, an arch and micro/elementary karren such as rillenkarren, rinnenkarren, rainpits and solution pans.

Keyhole cave (Fig. 3D), located on the right slope of the gorge of the river Gnishik at an elevation of 1,450 m a.s.l., consists

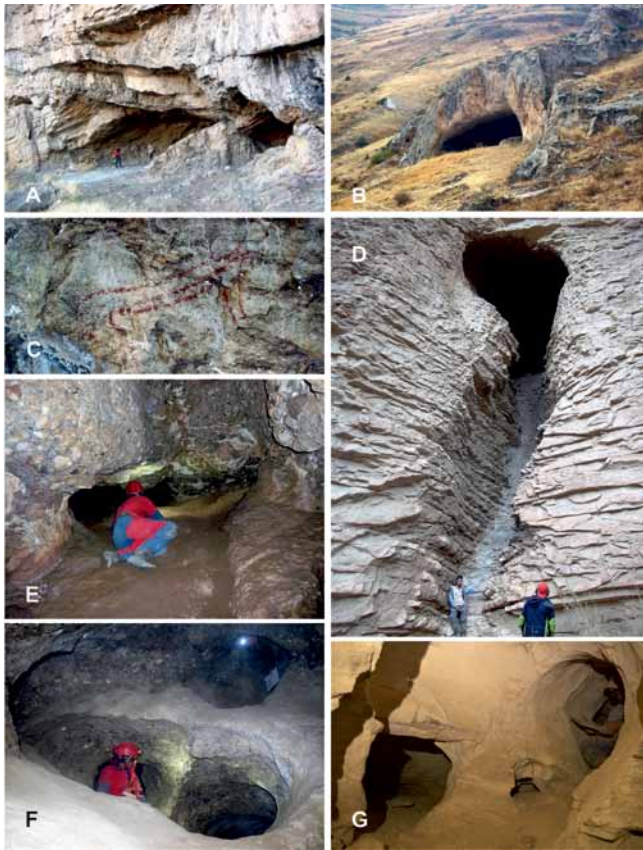


Figure 3. Typical cave morphologies in the Karst complex of Yeghegnadzor. A. Irovvank 2 cave developed along an angular unconformity in the Devonian limestone. B-C. Relict karst Gandzak 1 cave and painting of animal. D. Half shaft (probabl hypogene feeder) of the Keyhole cave. E. Phreatic sub-elliptic conduit in the Eocene conglomerate of the Magellan 1 cave. F. System of phreatic conduits along bedding planes in the Eocene conglomerate of the Magellan 2 cave. G. Sub-circular phreatic conduits in the Cretaceous limestone of the Areni 3 cave.

of a half vertical shaft about 20 m long, culminating in a large chamber with an sub-elliptic shape developed in Eocene limestone. This morphology appears to be a relict karst form probably due to hypogene processes cut by the erosion during the deepening of the valley.

Magellan 1 cave (Fig. 3E), located on the right slope of the Gnishik canyon river at an elevation of 1,060 m a.s.l., is developed in the Cretaceous polygenic conglomerate formation, along a series of sub-parallel faults jointed by some phreatic conduits with a sub-elliptic shape, originating on bedding planes. Secondary conglomerate deposits due to the solution of the conglomerate's calcite cement are present in some parts of the cave. Some speleothems show corrosion probably due to an acid environment condition, while others present yellow drip coatings probably due to uric or humic and/or fulvic acids. In the cave a colony of bats is present and the associated guano deposit has with white filamentous mushrooms. In one room of the cave, osteological and archeological deposits are present on the floor.

Magellan 2 cave (Fig. 3F), located on the right slope of the Gnishik canyon river at an elevation of 1,041 m a.s.l., develops in the Cretaceous conglomerate formation. It has a maze pattern with a series of elliptic and sub-circular phreatic conduits



Figure 4. A-B. Hypogene morphologies and speleothems in the Mozrovi cave. C-D. Phreatic conduit and remain of fillings in the relict karst Gravidzor 1 cave. E. Vedi-alko doline in the territory of Arpi Village. F. Aghavnadzor sinkhole in the Quaternary moraine sediments overlying the limestone formation.

at different levels developed along bedding planes with a dip direction N 100 at 15°. In the cave, which extends for 122.3 m with a positive depth of 7.2 m, a structural discontinuity was surveyed with a direction N 330.

Areni 3 cave (Fig. 3G), located on the left vertical slope of the Arpa river at an elevation of 1,026 m a.s.l., extends for 65 m with a positive depth of 3.3 m in the Cretaceous limestone. It has phreatic conduits of a sub-circular shape with dip direction N 100 at 20°. The general pattern of the cave is maze-like with conduits, which develop along a number of levels, both on the same tilted bedding plane and on different ones. The cave is fossil and in some parts a thick sandy-silt relict deposit is present; evidence of a past phase of filling of the karst system. On the vertical limestone cliff, which is particularly disjointed, two fracture systems, N 50 and N 80, have been surveyed.

Mozrovi cave (Fig. 4A-B), located in the Gnishik Municipality area at an elevation of 1,535 m a.s.l., has a large sinkhole type entrance due to the collapse of the vault during the adjacent road works. The cavity, after a steep descent among boulders of the collapse, develops on two levels, the upper has large rooms characterized by typical morphologies from the hypogenic genesis such as tubes, ceiling pockets, domes, and a rich variety of multi-coloured mineralogical deposits. The lower level, joined to the upper cave level through some short narrow pits (feeders?), develops along a main structural discontinuity, which is completely covered by a widespread series of astonishing mineral deposits of different genesis, shapes and colours. The cave develops in Eocene limestone.

Gravidzor 1 cave (Fig. 4C-D), located in the right slope of the Grav river gorge at an elevation of 1,473 m a.s.l., is a relict karst cave in Eocene limestone. It is developed along a N 90/75 fault, which extends for about 40 m with a depth of 8.2 m. In the ceiling some small, chimney-like phreatic conduits

are present, while in the wall at the cave end, a relict crust of cemented material is present comprised of black stones (2-10 cm in size) embedded in a detrital sand-silt with a cemented matrix. Next to the cave entrance a small elliptic conduit of about 5 m long is present, bounded by two karstified narrow fractures.

Vedi-alko doline (Fig. 4E), located in the territory of the Arpi village at an elevation of 1,222 m a.s.l., is a sub-circular depression, about 50 m in diameter and 3-5 m in depth, which develops along a slope, in the collapse of a karst void in Eocene limestone.

Aghavnadzor sinkhole (Fig. 4F) is a collapsed doline located in the area of Aghavnadzor village, at an elevation of 1,195 m a.s.l.. This morphology has a diameter of 13 -14 meters and a depth of 9 m. and has developed in a Quaternary moraine; polygenic sediments made up of large boulders of basalt and limestone/sandstone pebbles incorporated in a sandy-silt matrix.

6. Conclusions

The described surveyed karst morphologies have been classified as eight epigene features (caves, spring and dolines), two hypogene caves, one cave with both epigenic and hypogenic morphologies and one structural cave. Furthermore, an interesting new archeological discovery was made in the cave for the presence of red ochre drawings of animals on the walls, which will have to be studied by specialists. The hydrokarst research was carried out on the survey of five karst springs, for two of them, such as Akhta spring in the Arpa river and the temporary/vaucluse Erdhich spring, future geochemical sampling and tracer tests are planned. The collected data will

be analysed for the development of an initial speleogenetic model of the area.

In a more general context, the surveyed karst features, such as surface relict karst relief, relict karst caves, active and inactive karst systems and palaeokarst fillings, highlight the great importance of the karst studies as a further contribution to the knowledge of the geological history of this area. The continuation of the research is planned in 2017 in a number of karst areas in northern Armenia.

Acknowledgments

We would like to thank prof. Samvel Shanhian Chair of Geology and Biosafety of the National University of Architecture and Construction of Armenia in Erevan who created the conditions, enabling us to carry out this initial phase of research.

References

- Balyan, S. P., and Vanyan, R. A., 1986. Caves in Armenia and Ways to Use Them in Economy. *The Caves: Volume of Scientific Transactions of the Higher Education Institutes*, Perm, pp. 6-12 (in Russian).
- Doublyansky, V. N., 2010. *Caves and My Life*, UISK, 268 pp. (in Russian). University, Natural Sciences, 1983-1, pp. 153-158 (in Russian).
- Krzhechkovsky, A., 1930. Review of the Geology of the Western Part of Daralagyaz Province of the Armenian SSR. *General and Applied Geology Materials*, Issue 136, Leningrad, pp. 45-81 (in Russian). Movsesyan, M. A., Asratyan, V. P., Ananyan, A. L., and Vartanyan, G. O., 1983. Some Issues of Quaternary Karst Formation in the Territory of the Armenian SSR, *Scientific Proceedings of the Yerevan State*.

The Cenote Project: monitoring a high-altitude ice cave in the Dolomites, Italy

Tommaso Santagata¹, Francesco Sauro^{1,2}, Christoph Spötl³, Daniela Festi⁴, Klaus Oegg⁴, Luca Dal Molin⁵, Farouk Kadded⁶, Marco Camorani⁷, Alessio Romeo¹

Affiliation: ¹La Venta Esplorazioni Geografiche, Via Priamo Tron 35/F -31100 Treviso

²Dipartimento di Scienze Biologiche, Geologiche e Ambientali, Università di Bologna, Istituto Italiano di Speleologia, Via Zamboni 67 – 40126 Bologna (Italia);

³Institute of Geology, University of Innsbruck, Innrain 52, 6020 Innsbruck, Austria.

⁴Institute of Botany, University of Innsbruck, Sternwartestraße 15, 6020 Innsbruck, Austria

⁵Club Speleologico Proteo, Vicenza

⁶Leica Geosystems France, Paris.

Abstract

The Conturines Abyss, known also as “Cenote Abyss”, represents one of the deepest and most voluminous caves of the Dolomites. This 280 m deep cave is characterised by a huge ice deposit, which makes it of primary interest for the study of palaeoclimate and modern climate change in this region of the Alps. The cave was discovered in 1994 after the abrupt emptying of a lake at 2940 m a.s.l. in the Natural Park of Fanes, Sennes and Braies.

In 2015, a research project started to monitor long-term movements and volume changes of this ice deposit as well as to understand the cave microclimate and the potential for future palaeoclimate research. With two expeditions organised in October 2015 and September 2016, a complete survey of the cave was performed using laser scanning equipment (a Leica HDS7000 in 2015 and a Leica P40 in 2016). The installation of barometric, temperature and humidity dataloggers in different areas of the cave have provided a one-year record of the microclimate. In addition, pollen traps have been installed to study the present flux of pollen at the surface and inside the cave, while preliminary analyses on pollen grains preserved in the ice are being carried out.

The Cenote ice cave research project aims to shed light on the climate evolution of the Dolomites during the last hundreds or possibly thousands of years, as well as on the more recent environmental changes that led to the upward melting of the cave glacier.

Keywords:

1. Introduction

The Cenote Abyss represents one of the deepest and most voluminous caves of the Dolomites. The cave is characterised by a huge ice deposit for the first 150 metres, which makes this cavity of primary interest for the study of palaeoclimate and modern climate change in this region of the Alps.

Speleological exploration started in 1994 with the abrupt emptying of a small lake (labelled on the maps as “Lago delle due Forcelle”) at 2940 m a.s.l. in the Natural Park of Fanes, Sennes and Braies (Fig. 1a-b). Italian speleologists from the caving club “Proteo” (Vicenza) noticed the presence of a cavity in the ice at the bottom of the emptied doline and started the exploration during the summer season. However, after several expeditions it was impossible to proceed beyond a depth 70 m inside the ice due to the difficult hydrological conditions caused by the ice meltwater feeding an underground stream. In the following years the cave passage inside the ice deposit was again closed by winter snow accumulation, or the stream entering the shafts in summer was too dangerous to permit new explorations. Only in 2010, a new expedition took advantage of the low autumn temperature (below zero during the night) to descend into the cave in dry conditions and to explore a huge 160 m deep shaft present below the main ice mass. The exploration ended in a wide chamber (Baratro Paolo Verico) whose floor is characterised by an impressive rock glacier with signs of recent movement due to ice recharge from above (Fig. 1c). The cave was surveyed down to a depth of 285 m.



Figure 1. Fig. 1. A) The Lake of two Fork in the year 1994 few months before its sudden emptying; person on the top centre for scale (photo C.S. Proteo). B) The entrance depression after draining of the lake in late August 1994 (photo C.S. Proteo). C) The giant chamber Paolo Verico at the bottom of the 160 m deep shaft during the laser scanning operations in 2015. The floor is composed of a mixture of ice and rock fragments, while a glacier tongue is hanging 130 m above this huge chamber .

After this expedition the cave was again inaccessible due to snow accumulation during the following four years, until the passage was found open in the summer of 2015. The dimension and peculiar morphology of the cave ice deposits and their position and altitude led to the idea of a long-term research project to monitor movements and volume changes of the ice as well as to understand the cave microclimate and to explore the potential for future palaeoclimate studies. Two expeditions, in 2015 and 2016, were organised mainly to acquire scientific data, installing pollen traps, microclimate loggers (humidity and temperature) in different points of the cave and to perform a 3D scan of the whole cave. The data



Figure 2. The wind tunnel at 70 m of depth is completely carved into the ice and is characterized by strong airflow during summer (Photo A. Romeo/Inside the Glaciers).

acquired until now are the base for a long-term monitoring of the cave in order to understand the evolution of cave ice deposits in this region of the Alps.

2. Geological settings and cave description

Located in the South Tirol region about 3 km east of the village of San Cassiano in Badia, Piz of les Conturines (also known as Piz of Two Forks), with its summit at 3064 m a.s.l., is the highest peak of the Conturines group.

The area of the Cenote cave is characterised by a wide syncline structure comprising sedimentary rocks ranging from the Upper Triassic to the Lower Miocene and mainly composed of a succession of dolomite layers, with a total thickness of 1 km (Sauro et al., 1995). These sediments are overlain by other formations such as the Dachstein Limestones (Uppermost Triassic) of about 300 m thickness and the Grey Limestone (Early Jurassic, Liassic), which is the most interesting Formation from a speleological point of view (Marchetto, 2007).

The cave starts with a karst depression (the original lake “delle due forcelle”), about 20 m deep and 50x30 m wide. The bottom of this doline is occupied by an ice and snow cone, characterised by elongated fractures parallel to the depression’s major axis. Depending on the height of the snow cone, it is sometimes possible to enter a chamber on its SW side in late summer with a floor of transparent ice. On one side of this room it is possible to descend down a channel carved between the ice deposit and the rock wall. This conduit is characterised by strong air current (breathing in summer and blowing in winter), with the ice walls sculptured with 1 m wide melting niches. From there it is possible to descend down a series of shafts developed at both the rock wall-ice contact and completely inside the ice mass. At a depth of 70 m the cave extends completely within the ice inside a tunnel carved by the airflow (the wind tunnel, Fig. 2). The cave then descends 30 m via another shaft opening in a long NW-SE-oriented passage that progressively opens into a large underground room. From this point onward the descent is along the ice deposit and the rock wall with the first ending after about 60 m with a huge ice tongue suspended above the final chamber. The free-hanging depth of this deep chasm is 165 m (Baratro Paolo Verico). The chamber at the bottom is 130 m long and about 40 m wide,

progressively descending to the lowest point of the cave with a cone composed of a mixture of ice, sands and boulders.

Since the first exploration in 1994, although the ice deposit has slowly evolved, but the airflow paths do not appear to have changed substantially. Air currents opened tunnels in the ice mass, with cupolas and melting niches, suggesting a potential connection with cavities and fractures at the base of the external ridge walls of San Cassiano.

3. Scientific objectives

3.1. Monitoring ice evolution through laser scanning

One of the main objectives of the two expeditions was to realise a complete 3-dimensional survey of the final chamber and the ice deposit in order to acquire detailed data about volume and sizes of this important underground palaeoclimate resource of the Dolomites, and to obtain a quantitative record of the cave glacier. Using a laser scanner to survey large and complex subsurface environments such as the Cenote Abyss allows rapid acquisition of high-precision data.

Because of its high altitude and the difficult access, a helicopter was used to transport most of the gear and participants to the site. Inside the cave, laser scanners and other necessary tools were transported attached to the cavers’ harnesses to the depth of -285 m.

The instrument used in 2015 was a Leica HDS 7000, a phase difference laser scanner equipped with a dual axis compensator, on board control, a wavelength of 1.5 microns, laser “CLASS 1” with a flow rate of 187 m and a resolution of 0.3 mm.

During the operations inside the cave, circular targets with a magnetised support base rotating over 360° were used to have easily identifiable connection points between the scans. The giant chamber at the bottom of the shaft was surveyed using 11 scans at resolution of 12 mm. One scanning station was located on an artificial platform installed on the wall of the shaft at 110 m above the floor. This station enabled to map in detail the lower side of the hanging ice glacier. In 2016, the scan continued in the upper part of the shaft (over the ice tongue, and through the series of short shafts and tunnels carved between rock and ice up to the doline entrance).

This survey provides the detailed volume of the chamber (420,000 m³), the first record of a rock glacier at the base, as well as the presence of an over 100 m thick ice deposit in the upper part of the cave.

In 2016 we used a Leica P40 model, a time-of-flight laser scanner enhanced by Waveform Digitising (WFD) technology with a scan rate of up to 1 million points per second and a flow range from 0.4 m to 270 m.

The aim of the 2016 expedition was to detect the upper part of the cave to a depth of about -140 m in order to connect with the survey executed in 2015 and obtain a three-dimensional model of the cave (Fig. 3a). Scanning operations with this instrument have been also used inside the ice tunnel, providing the detailed shape of this important part of the cave with a resolution of less than one centimeter.

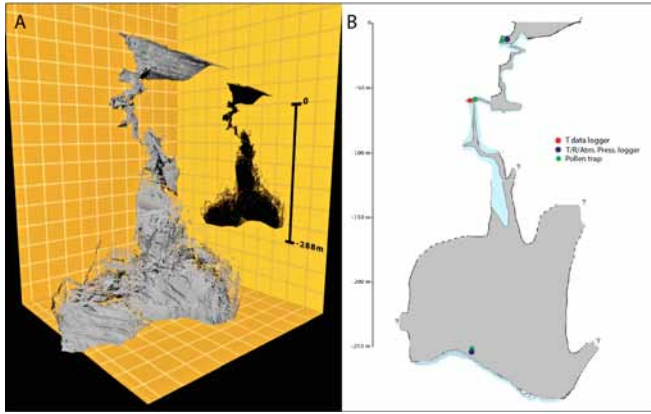


Figure 3. A) Projection of the laser scan 3D model of the Cenote Abyss. B) Vertical section of the Cenote Abyss showing the location of the data loggers and pollen traps.

This high-precision 3D model will be the base for future monitoring of the long-term evolution of the ice masses inside this cave.

3.2. Microclimate monitoring

During the first expedition in 2015, temperature and humidity dataloggers were installed in three points of the cave in order to study the microclimate during the year and to correlate them with ice-volume variations in the cave (Fig. 3b). The dataloggers were positioned at the following sites:

1. At the bottom of the entrance depression close to the first conduits carved in the ice by air flow (barometric, temperature, humidity logger)
2. At the end of the wind tunnel, hanging over the following 30 m deep shaft (temperature)
3. At the beginning of the rock glacier tongue on the floor of Baratro Paolo Verico (temperature, humidity logger)

In 2016 the data were downloaded from the loggers. These preliminary data obtained in this first year were compared to temperature variations at the Rossalm weather station (15 km from the cave entrance, 2340 m a.s.l.) (Fig. 4). Seasonal temperature fluctuations at the bottom of the final chamber are between 0 to 0.05 °C in the winter season (from November to May) and rise to 0.2 °C in summer. This delicate equilibrium is controlled mainly by air currents: from March to December at the wind tunnel temperature changes are triggered by external fluctuations (between -1.4 and 0.4 °C) while during the winter season from January to March the temperature is stable around 0 °C. This stabilization is probably related to periods of closure of the main cave entrance or of other unknown lower entrances by snow, blocking the air currents. It is therefore clear that climatic conditions at the surface (seasonal mean temperatures and winter snow accumulation) have a direct impact on the melting rate of the cave glacier up to considerable depths. It is probable that the opening of the passage through the ice with the emptying of the lake in 1994 has started an irreversible process of warming of the cave environment resulting in considerable volumes of ice melting year by year. The preliminary data show that microclimate monitoring of the cave provides robust information that can be compared to quantitative loss of ice in the future due to the volumetric record obtained with the laser scan high-precision 3D model.

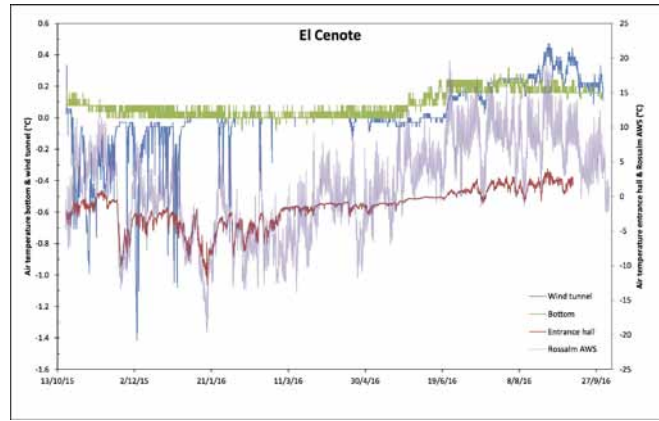


Figure 4. Temperature curves of different stations in the cave and the Rossalm weather station, from early October 2015 to the end of September 2016.

3.3. Pollen traps and pollen analysis of ice samples

During the two expeditions pollen traps were installed at different locations to assess the flux of pollen into the cave. These traps are composed of a container with a micrometric mesh collecting microparticles from the air. The traps were positioned in the same place as the sensors, and the entrance tunnel and the wind tunnel are strategical for this study test, because of the strong winds blowing from the outside during the summer season. The ongoing study will provide an average of total pollen amount trapped by the cave and potentially recorded in the ice deposits. A few ice samples were also collected inside the wind tunnel in order to obtain preliminary data on the pollen content of the ice.

4. Conclusions

The expeditions of 2015 and 2016 are the first steps of a long-term monitoring project that could provide interesting data about the past conditions of the cave ice masses and of their evolution in response to climate change. In this first phase of the project the main objective to record a high-definition 3D model of the volumetric and morphologic conditions of the ice deposits inside the cave, coupled with an ongoing monitoring of cave microclimate was achieved. In addition, preliminary pollen data could open the prospective for the study of the ice layers as palaeoclimate archive.

However, the research activities in this cave hinge on the ability of being able to enter the cave in late summer/early autumn, and to the weather conditions, requiring complex and expensive logistics. Nonetheless, a new expedition is planned for 2018 or 2019 in order to repeat the laser scans and compare ice volume losses, in correlation with the climatic conditions recorded at the surface.

References

- Marchetto GC. (2007): "Speleologic researches in the Natural Parks of Fanes-Sennes-Braies and Dolomiti d'Ampezzo (Italy)". In: *Untertage Alpine 2007*, Ramsau bei Berchtesgaden, 9-11 November 2007, 64-66.
- Sauro U., Meneghel M., Bini A., Mietto P., Siorpaes C. (1995): Altopiani Ampezzani. *Geologia geomorfologia speleologia*. La Grafica Editrice, 156 pp.

Karst Hydrology In Sub-Arctic Norway

Rannveig Øvrevik Skoglund¹ & Stein-Erik Lauritzen²

Affiliation: ¹ Department of Geography, University of Bergen, Norway

² Department of Earth Science, University of Bergen, Norway

Abstract

The karst areas in northern Norway are mainly characterized as stripe karst, an extreme end-member of contact karst. The karstic rock is marble, and it appears in a sandwich-like situation interbedded with mica schist in the Caledonian thrust nappes. Accordingly, predominantly autogenic karst aquifers larger than 1 km² are exceptional in Norway, and the objective here is to study some of the largest autogenic karst catchments in the country.

Two karst springs draining two separate, unconfined karst aquifers in Rana have been monitored for water temperature, specific conductivity and water stage since October 2015. These springs are situated at similar altitude, about 60 m a.s.l., and less than 10 km apart. *Mosabekken spring* is an exsurgence (fed by autogenic seepage water) that drains the 2 km² large karst plateau above Hammarnesgrotta and associated caves of a total known length of >8 km. The calcite marble is about 100 m thick. Water is only seen at the most downstream end of the cave system. *Nyrud spring* drains a 1 km² large area where the marble layer is folded and interbedded with schist, which makes the water partly allogenic. However, there are no proper surface streams, nor stream sinks in the catchment area. Underground, in the extensive Reingardslia cave system (9 km total length) there is an underground stream with several sumps.

Preliminary results show that the mean water temperatures in the springs (3.8 °C and 4.1 °C) are quite close to the mean annual air temperature in the area (3.4 °C). However, while the range in air temperature was 49°C, the range in water temperature was less than 2°C in the springs. The average specific conductance is about 200 µS/cm, with a range of about 120 µS/cm related to changes in flow rate. During dry periods the flow rate is only a few liters per second, while during flood it is several hundred, possibly as much as thousand, liters per second. The presentation will discuss the similarities and differences in response time and behavior of the two springs in light of the settings in their catchment areas.

Keywords: karst hydrology, hydrographs, Norway

1. Introduction

There are relatively few papers about karst hydrology in Norway, and it is quite a long time since new data have been published (e.g. Lauritzen 1981, 1986; Bakalowicz 1984; Lauritzen et al. 1985; Øvstedal & Lauritzen 1989; Skoglund & Lauritzen 2013). During the on-going Reingardslia-project (Lauritzen et al. 2017, this volume), a re-mapping of the caves and new investigations on several aspects of speleogenesis have been addressed. This made it appropriate to also investigate the active karst hydrology of the system. At the same time we also monitor another spring in the area, where the underground aquifer is totally unavailable. Autogenic karst system used for drinking water, gives some restriction to possible ways to investigate them. The catchments are of similar size (1-2 km²) and altitude (less than 400 m), and more or less autogenic. This means that they are exposed to similar hydrological input (rainstorms and snowmelt) and thus by comparing their behavior, we can learn more about the underground system of both. Moreover, these catchment areas hold some of the oldest caves in the country, and previous dating of speleothems has put speleogenesis back beyond half a million years (Lauritzen et al. 1990, 1994). It is interesting to better understand the present karst aquifers, because they serve as an analog to former interglacial karst systems that later were overrun by glaciers with frequent and strong shifts of the hydrologic regime.

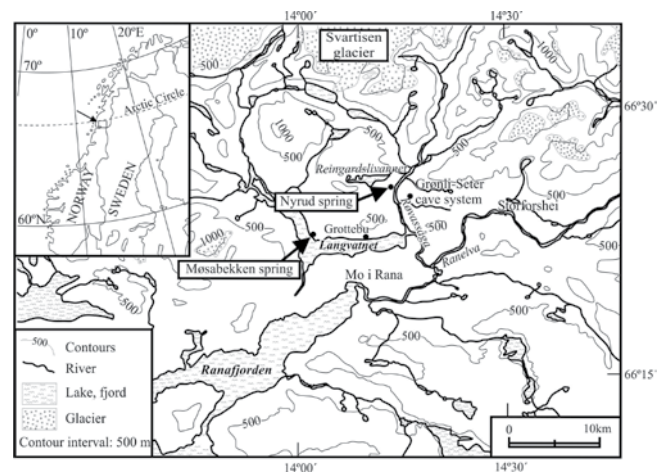


Figure 1. Key map and location of the field area.

2. Geographical, geological and climatic setting

The field area is located north of Ranafjorden and south of Svartisen ice cap in Rana county, just south of the Arctic circle at about 66°N 14°E (Fig. 1). The landscape is glacially sculptured through iterate glaciations during the Quaternary. The karstic rock is a metamorphic calcite marble of late Precambrian to Cambro-Silurian age, thrust, folded and displaced during the Caledonian orogeny (Gustavson & Gjelle 1991). In total, this gives the terrain a rugged topography where the marble outcrops essentially appear as narrow stripes interbedded with non-karstic rocks, making the individual marble

layers into isolated aquifers constricted by schist aquitards. Consequently, few karst plateaus and autogenic karst drainage areas exist in Norway.

Through metamorphism, the marble lost its primary porosity, but secondary porosity developed through a long history of tectonism during the Caledonian orogeny, the following detachment, opening of the North-Atlantic ocean and development of the passive continental margin. Pressure release due to erosional unloading, glacial erosion and glacial rebound has provided the marble with sets of wider fractures, faults and thrust rock interfaces near the terrain surface.

Rainstorms and snowmelt are the main hydrological components in the coastal area of northern Norway. The sub-arctic oceanic climate is strongly influenced by the dominating westerlies, which frequently bring mild, humid air onshore. The drainage area of the springs at altitudes less than 400 m, are expected to get an annual precipitation of about 1500 to 2000 mm. In contrast, the coastal mountains with ice caps get more than 4000 mm of precipitation annually, most of it as snow. The annual snow depth in the field area is normally between 1 and 1.5 m.

Mosabekken spring is situated at Hammarneset, along the northern shore of Langvatnet lake, at an altitude of 54 m, well below the post-glacial marine limit (approximately 115 m above the present sea level). *Mosabekken* spring drains a karst plateau of about 2 km² with several shallow dolines. The marble layer is about 100 m thick dipping about 20° towards northeast, overlying layers of amphibolite and mica schist. The caves along the Hammarneset escarpment comprise more than 8 km of surveyed passages, and water is only seen in the lower part of the system.

Nyrud spring is situated 10 km further northeast, in Rødvasdalen valley. Both Langvatnet lake and the valley basin in Rødvasdalen are overdeepened glacial troughs. *Nyrud* spring is situated at 63 m above sea level, also far below the local post-glacial marine limit. *Nyrud* spring drains an area of about 1 km² south of lake Reingardslivatnet. In this catchment area the rock layers are more tightly folded with an overall strike direction trending east-west and a hinge line dipping towards east. Underground, in the extensive Reingardslia cave system (Lauritzen et al. 2017) there is a cave stream, which flows through shorter sections of Lapphullet cave, and through longer sections of Larshullet cave. In the upper part of the cave system there are three sumps in three adjacent caves at approximately the same altitude (about 328 m). In the lower most part of Larshullet (approximately 500 m north-west of the spring), in a low vadose passage at almost the same altitude as the spring, the cave stream flows beyond reach.

The objective here is to present the first results from new time series on water stage, temperature and specific conductance in the two springs. *Mosabekken* represents a black-box system where there is almost no available information about the underground hydrology upstream of the spring. The *Nyrud* system, on the other hand, is considered a grey-box system because an underground stream can be followed through long cave sections, more extensive seepage zones are observed along extensive N-S trending fracture zones, and a hanging sump level is known in the upper part of the catchment. Another karst aquifer nearby, was monitored some years ago

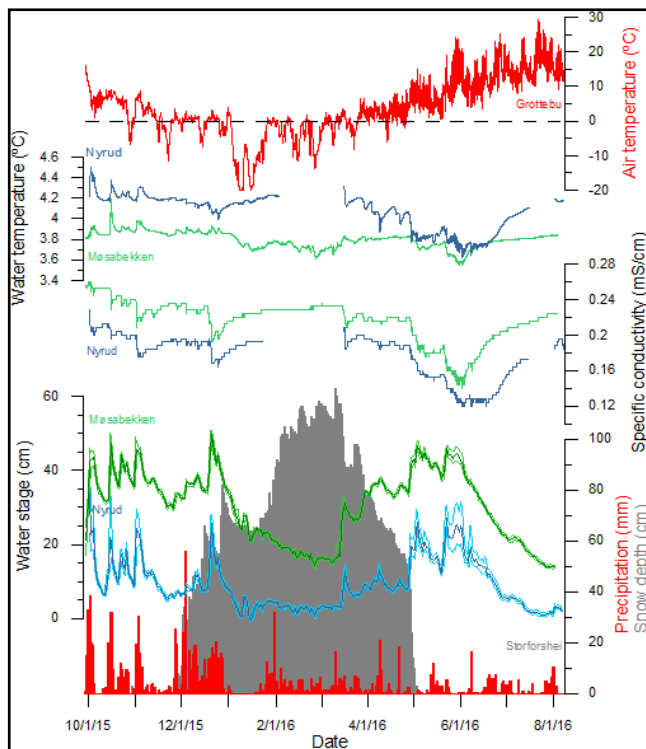


Figure 2. Data from the two logging stations at *Mosabekken* (green) and *Nyrud* (blue), air temperature from *Grottebu*, and precipitation and snow depth from *Storforsthei* (110 m a.s.l.) about 15 km east of *Nyrud*. The water data from the springs are shown as daily average values, as well as daily maximum and minimum values (lighter colour). Note that water and air temperature are shown on different scales. Gaps in the graphs occurred because the datalogger at *Nyrud* spring was dry during low flow.

and shows how a well-developed conduit aquifer respond to similar rainstorm and snowmelt events (Skoglund & Lauritzen 2013).

Results

The hydrographs and chemographs show that both systems respond quickly to storm events and snowmelt events (Fig. 2). Rain and meltwater have a lower specific conductance than the base flow. Higher flow rates and shorter residence time give shorter contact time between water and rock and consequently lower concentration of dissolved carbonates in the event water, as is typical for karst springs (e.g. Dreiss 1989). There is a strong correlation between the water stage in the two springs, and also between the specific conductances in the two springs. The specific conductance in *Nyrud* spring approach 200 µS/cm during low flow, while the water in *Mosabekken* is a bit higher and approach 240 µS/cm, though there seem to be a seasonal change due to the growth season. The specific conductance observed in the resurgence of Grønli-Seter karst aquifer was much lower, typically less than 50 µS/cm (Skoglund & Lauritzen 2013). Grønli-Seter karst aquifer is situated just at the opposite side of the valley from *Nyrud spring*, but is an invasion aquifer where water from a surface stream is diverted mainly through large conduits, with large hydraulic radius and shorter residence time. As expected, this gives much lower concentrations of calcium carbonate in the water though much higher flow rates through the rock which means that the total amount of dissolution probably is quite high. In Grønli hillside, a schist layer covers the marble, and

efficiently prevents diffuse recharge of rainwater and snow-melt. Water chemistry data from the Grønli-Seter aquifer showed that, even though storm water had a slightly higher concentrations of Cl^- and Na^+ , these components only gave a minor contribution to the total ion concentration and specific conductance, which was totally dominated by Ca^{2+} and HCO_3^- (Skoglund & Lauritzen 2013).

There seem to be no pronounced delay in specific conductance or water temperature fluctuations compared to shifts in flow rate. Based on this first batch of data the response seems to be more or less synchronous, which suggest that the actual event water reaches the spring as the discharge increase during a flood event. According to White (2015) this may indicate that storm water transverse the aquifer through karst voids (well-connected open fractures and conduits) and mainly through the vadose zone. Longer phreatic sections are expected to give a water level rise before the floodwater with low specific conductance reaches the spring (White 2015).

During late spring and early summer, a period with diurnal fluctuations in flow rate, specific conductivity and water temperature indicates a discharge pattern dictated by fluctuations in air temperature. This implies that snow patches persists longer in the field area than at the weather station at Storforshei. Diurnal air temperature fluctuations are followed by fluctuations in water stage, with a peak delay between 4 and 5 hours most days. The fluctuations in specific conductance and water temperature are even more delayed, but the delays seem to be more variable.

During autumn storms there is a distinct response in water temperature when the flood water reaches the spring, and the storm water is warmer than base flow in both springs. During winter there is less pronounced response in temperature to changes in flow rate and at some point the temperature shifts during flood events are opposite in the two springs. During melt season, water temperature drops quite low, especially in *Nyrud spring*, which normally has a temperature a bit higher than in *Mosabekken*.

3. Concluding remarks

These preliminary results show that efficient karst dissolution is going on in both aquifers at both high and low flow rates. These relatively small catchments have a quick response in stage, temperature and specific conductance and very low flow rates during periods of low recharge. This means that both systems have a low storage component and short phreatic sections. There is a strong correlation between the water stage in the two springs, and also between the specific conductivity of them. The synchronous response in the two springs suggests that the systems are quite similar. This has implications for the interpretation of *Mosabekken* aquifer. It implies that also this aquifer is probably dominated by well-connected (possibly dissolved) fractures and conduits which give low residence time and low storage. In addition, a slightly

lower temperature (closer to mean annual air temperature) and higher specific conductance in *Mosabekken* are probably caused by a larger contact surface and/or longer contact time between water and rock.

Acknowledgement

Sverre Aksnes is thanked for his assistance during fieldwork.

References

- Bakalowicz M, 1984. Water chemistry of some karst environments in Norway. *Norsk Geografisk Tidsskrift* **38**, 209–214.
- Dreiss SJ, 1989. Regional scale transport in a karst aquifer 1. Component separation of spring flow hydrographs. *Water Resources Research*, **25**, 117–125.
- Gustavson M, Gjelle ST, 1991. *Geologisk kart over Norge. Berggrunnskart Mo I RANA 1:250 000*. Norges Geologiske Undersøkelse.
- Lauritzen SE, 1981. A study of some karst waters in Norway. Spatial variation in solute concentrations and equilibrium parameters in limestone dissolution. *Norsk Geografisk Tidsskrift* **35**, 1–19.
- Lauritzen SE, 1986. Hydraulics and dissolution kinetics of a phreatic conduit. *Proc. 9th Int. Speleological Cong.*, Barcelona, pp. 20–22.
- Lauritzen SE, Abbott J, Arnesen R, Crossley G, Grepperud D, Ive A, Johnson S; 1985. Morphology and hydraulics of an active phreatic conduit. *Cave Science* **12**, 139–146.
- Lauritzen SE, Haugen JE, Gilje-Nilsen H, Løvlie R, 1994. Geochronological potential of isoleucine epimerization in calcite speleothem. *Quaternary Research* **41**, 52–58.
- Lauritzen SE, Lovlie R, Moe D, Ostbye E, 1990. Paleoclimate deduced from a multidisciplinary study of a half-million-year-old stalagmite from Rana, northern Norway. *Quaternary Research*, **34**, 306–316.
- Skoglund RØ, Lauritzen SE, 2013. Characterization of a post-glacial invasion aquifer: the Grønli-Seter karst system, northern Norway. *Norwegian Journal of Geology*, **93**, 61–73.
- Lauritzen SE, Skoglund RØ, Heggstad M, Kilhavn H, Lølkes S, Øyehaug ET, Gabrielsen IM, Stadheim AG, 2017: The oldest meteoric caves in Norway? The Reingardslia Cave Documentation project. *Proc. 17th Int. Speleological Cong.*, Sydney, Australia.
- White WB, 2015. *Chemistry and karst. Acta Carsologica* **44** (3), 349–362.
- Øvstedal J, Lauritzen SE, 1989. The Sirijorda karst aquifer, Nordland, Northern Norway. *Proc. 10th Int. Speleological Cong.*, Budapest, pp. 121–122.

Measurement of the Atmospheric CO₂ Sink from Carbonate Mineral Weathering for Large River Basins: the Ohio River, USA

Autumn Turner and Chris Groves

Affiliation: Crawford Hydrology Laboratory Western Kentucky University
Bowling Green, Kentucky 42101 USA

Abstract

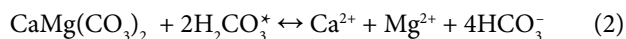
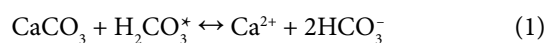
Changing climate and increasing atmospheric CO₂ concentrations have motivated efforts to better quantify reservoirs and fluxes of earth's carbon. Numerous studies have set out to develop a carbon budget and quantify fluxes among the atmospheric, ocean, terrestrial and biosphere sources and sinks, yielding inconsistent results. A flux that has received relatively little attention is the atmospheric carbon sink associated with carbonate mineral weathering on the continents that transfers atmospheric CO₂ to dissolved inorganic carbon in rivers and eventually the oceans. Recent work has explored new techniques to improve and standardize a process for measuring this flux over larger river basins within the upper Green and Barren River drainage basins in south central Kentucky, USA yielding normalized flux values in relatively close agreement. We are currently investigating the 490,600 km² Ohio River to determine if these normalization parameters are applicable over even larger basins. The magnitude of the carbon flux leaving the basin and a selection of nested sub-basins of various sizes for Water Year (WY) 2014 is being estimated based on secondary hydrogeochemical, geologic, and climate data. Resulting DIC flux values are being normalized by duration, carbonate rock area, and precipitation minus evapotranspiration. If the normalized flux value for the Ohio River Basin and its sub-basins over one year agrees with earlier measurements over a range of smaller basins and sampling periods, then these flux calculations may be possible for other, larger areas by statistical correlation with existing climatic and geologic data. This could potentially eliminate the need for field hydrochemical data collection. Accordingly, principles and techniques applied herein could be directly applicable to an array of basin sizes, locations, climatic and geologic conditions across the globe. Ultimately this may significantly enhance the ease and efficiency of making global carbon flux estimates by improving estimates for the portion of the atmospheric carbon sink caused by carbonate rock weathering. The normalized DIC flux for the Ohio River was estimated at 3.5×10^8 g C day⁻¹ km⁻³ relative to previous estimates of 5.6×10^7 g C day⁻¹ km⁻³ and 7.4×10^7 g C day⁻¹ km⁻³ for the Barren and Green River, respectively.

Keywords: carbon cycle, carbonate geochemistry, karst, carbon sequestration, climate change, atmospheric carbon storage

1. Introduction

Atmospheric carbon dioxide has steadily increased in association with human activities since the mid-seventeenth century. Concentrations currently exceed 400 ppm (Keeling, 2016) and are expected to continue rising (Cox *et al.*, 2000). Carbon dioxide is a known greenhouse gas (GHG) which has been shown to trap heat within the atmosphere leading to increasing global temperatures (Solomon *et al.*, 2009). The Intergovernmental Panel on Climate Change acknowledges that anthropogenic GHG emissions are “*extremely likely to be the dominant cause of the observed warming since the mid-20th century*” (2014). Concerns over the mitigation and prediction of climate change have resulted in much investigation into the factors which control atmospheric concentrations of CO₂ (Cox *et al.*, 2000; Falkowski *et al.*, 2000). Carbon budgeting is an appropriate method for tracking fluctuations of carbon as it cycles through the major reservoirs. Recent studies estimate that of the billions of tons of carbon produced annually, approximately half remains in the atmosphere while the remaining carbon is unaccounted for, leading to the so-called “*missing sink*” (Sabine, 2004). The remaining carbon is assumed to be stored in the ocean and terrestrial reservoirs. However, the comparative roles of ocean and terrestrial carbon storage are not fully understood and conflicting reports of the magnitude of carbon uptake by the oceans present a challenge to the goal of understanding where and how carbon is exchanged among Earth's carbon reservoirs (Siegenthaler and Sarmiento, 1993).

Among the terrestrial reservoirs, the lithosphere is thought to have substantial sink capacity. Carbonate rocks are considered an atmospheric sink because they contribute alkalinity and consume CO₂ from the atmosphere via dissolution and precipitation processes. Here, waters that have been acidified through interactions with carbon dioxide in the air and soil react with calcium carbonate (CaCO₃) found in carbonate rocks. Carbonate rock weathering in natural waters can be described by the following set of chemical equations for limestone and dolomite respectively:



This process of chemical weathering can result in the burial of carbon-bearing sediments among inland waters, or the transport of dissolved aqueous species to the oceans where they are eventually precipitated. It is thought that the North American continent is particularly well-suited to act as a terrestrial sink with relatively widespread carbonate rock development, but uncertainty exists as to the actual magnitude of the potential sink. A standard method for measurement is recommended to assess the capacity of carbonate rock more accurately to sequester atmospheric carbon.

In this study, we investigate the validity of a proposed calibration for dissolved inorganic carbon (DIC) flux (Osterhoudt, 2014; Salley, 2016) to test its applicability over a broad range of basin areas, geologic conditions, study periods and climate types. Previous work has suggested that by normalizing

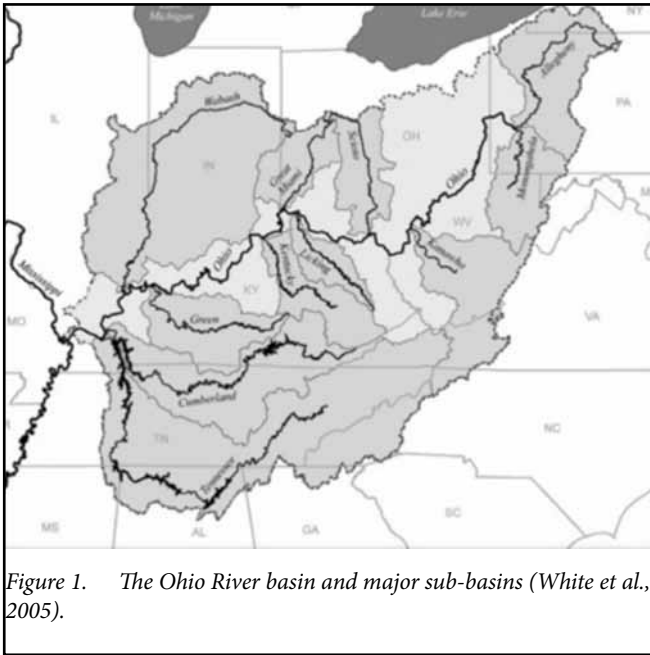


Figure 1. The Ohio River basin and major sub-basins (White *et al.*, 2005).

calculations of DIC flux by area of carbonate rock outcrop, duration of exposure and the amount of water available for dissolution, the major variables affecting carbon flux are accounted for. If so, it would indicate that other factors (e.g. land use practices and carbon-soil interactions) are negligible in terms of estimating DIC flux at the basin scale. Prior investigations suggest that a calibration exists that would enable researchers to estimate the mass of inorganic carbon leaving a basin using only the area of the carbonate rock exposed and the total amount of water available (rainfall- evapotranspiration) over a given time interval. Studies employing this technique over smaller regional basins have yielded results in very close agreement and regression analysis of these data points reveals a linear correlation ($r^2 = 0.97$) (see Osterhoudt, 2014; Salley, 2016) for the inorganic carbon flux (grams of carbon) as a function of water landing on carbonate rock areas in each basin ($\text{km}^3 \text{H}_2\text{O day}^{-1}$). However, this approach has not been tested on larger scales.

2. Study Area

The Ohio River basin (Figure 1) has the third largest discharge (average $8,733 \text{ m}^3/\text{s}$) in the United States. The basin spans an area draining major portions of eight states, totaling $490,601 \text{ km}^2$. Eleven major sub-basins are nested within the Ohio River basin including the Tennessee, Cumberland, Green, Kentucky, Licking, Kanawha, Monongahela, Allegheny, Scioto, Great Miami and Wabash basins. Numerous geologic formations are present among the provinces encompassed within the Ohio River basin. The western region of the Appalachian Plateau covers eastern Tennessee, Kentucky and Ohio and exhibits Mississippian and Pennsylvanian limestones.

Extensive karst development is characteristic of the Mississippian rocks in this province, with karst topography stretching from central Indiana through northern Alabama. Relatively few surface streams are found in this area, with most water flowing in subsurface conduits (White *et al.*, 2005). Mean monthly temperatures in the region range from -7°C to 10°C in winter and 24°C to 28°C in the summer. Mean monthly precipitation is relatively consistent over the basin area, experiencing significant snow accumulations in the north

and Appalachian regions. Annual precipitation for the basin ranges from 94 cm in northern parts of the basin to about 135 cm in lower parts of the basin with slightly increased measurements among high elevations (White *et al.*, 2005).

3. Methods

The Ohio River Basin and the eleven major sub-basins were delineated using Hydrologic Unit Code (HUC) shapefiles in ArcGIS 10.2. Sub-basins were adjusted to reflect the area of the drainage upstream from the point where hydrochemical measurements were taken. Area of exposed carbonate rock was calculated using ArcGIS 10.2 from the Karst Atlas of the United States (Doctor and Weary, 2014) shapefile. Carbonate distribution was then clipped to the extent of the Ohio River Basin and the major sub-basins using geoprocessing tools.

Average monthly temperature ($^\circ\text{C}$), monthly precipitation totals (cm) and station coordinates were collected from 37 Cooperative Observed Network (COOP) weather stations distributed approximately evenly throughout the basin area. Potential evapotranspiration (ET) was calculated per Thornthwaite and Mather (1957) using the following equation:

$$PET = 1.6 \times \left(\frac{10T_a}{i} \right)^\alpha \quad (3)$$

Where T_a is the mean monthly air temperature ($^\circ\text{C}$), i is the heat index summed over a 12-month period and α is an empirically-derived exponent that is a function of i . Depth of water available for carbonate dissolution was determined by subtracting water lost to ET from the total precipitation and resulting values were then interpolated with user-defined Kriging in ArcGIS 10.1 to create lines of equal water availability throughout the basin. Isohyets were clipped to the area of exposed carbonate rocks using geoprocessing tools and then converted to raster data points. Per basin, the total volume of water available for dissolution was calculated as the depth of precipitation minus ET (km) multiplied by the area of the exposed carbonate rock (km^2) on which the precipitation accumulated.

Relative concentrations of carbonate species in solution were calculated from pH, temperature, and alkalinity (mg/l HCO_3^-) measurements of surface waters from routine monitoring programs at water treatment facilities located near basin outlets. The frequency of sampling varied considerably among hydrochemical data set. To account for these differences, hydrochemical data was aggregated using the highest resolution available to represent daily values that would be directly comparable to daily resolution discharge measurements.

Bicarbonate (HCO_3^-) species activity (a_i) was calculated using Debye-Hückle (1923) equation:

$$-\log \gamma_i = \frac{Az_i^2 \sqrt{I}}{1 + \alpha_i B \sqrt{I}} \quad (4)$$

$$a_i = m_i \gamma_i \quad (5)$$

Where A and B are constants for a given temperature and solvent, α° is the effective diameter of the HCO_3^- ion complex, z_i is the formal charge of HCO_3^- , and I is the ionic strength of the solution, given by:

$$I = \frac{1}{2} \sum_i m_i z_i^2 \quad (6)$$

Activities of carbonic acid (H_2CO_3) and carbonate (CO_3^{2-}) were calculated using acid-base equilibria as follows:

$$[\text{H}_2\text{CO}_3] = \frac{[\text{H}^+][\text{HCO}_3^-]}{K_1} \quad (7)$$

$$[\text{CO}_3^{2-}] = \frac{K_2[\text{HCO}_3^-]}{[\text{H}^+]} \quad (8)$$

Where K_1 and K_2 are temperature dependent solubility product constants. Total dissolved inorganic carbon (TDIC) is given by the sum of carbonate species in solution.

Daily resolution discharge (Q) measurements were obtained from US Geological Survey stations located at or very near locations where hydrochemical measurements were taken. Hydrochemical data was aggregated to match discharge sampling frequency. This approach was chosen over averaging of high resolution discharge data to match lower resolution chemistry measurements since the range of discharge measurements varied more greatly than hydrochemical data over the year.

Dissolved inorganic carbon (DIC) export was calculated as the product of the sum inorganic carbon species in solution and discharge. The total annual DIC mass exported from each basin was divided by the product of days in the sample period, area of exposed carbonate rock and depth of precipitation minus ET to achieve normalized DIC flux per time-volume unit. The competence of the calibration in direct estimation of DIC flux as a function of time-volume normalization parameters was tested by statistical correlation. DIC flux values were plotted for each basin and compared using linear regression analysis. Inorganic carbon flux from the atmosphere to the terrestrial reservoir is one-half of the total DIC export from a basin. This is because for every 2 moles of carbon produced in equation (1), one mole of carbon originated as CO_2 in the atmosphere and the other mole was derived from the carbonate rock itself.

4. Results

Discharge of the Ohio River varied considerably, ranging from 1.79×10^6 L/s to 2.14×10^7 L/s with a mean discharge of 8.64×10^6 L/s. Discharge measurements for sub-basins ranged from 2,888 L/s to 4,847,759 L/s. The total DIC export from the Ohio River basin for WY 2014 prior to normalization was estimated at 7.54×10^{12} g C. TDIC export without normalization among the major sub-basins ranged from 1.83×10^{10} g C to 1.15×10^{12} g C. The main objective of the study was to evaluate the efficacy of the normalization technique involving time and volume of water available for carbonate dissolution to predict DIC flux with suitable precision to be applied on larger scales. TDIC flux, normalization parameters and normalized flux values are summarized in Table 1. The normalized DIC flux for the Ohio River was estimated at 3.5×10^8 g C $\text{day}^{-1} \text{km}^{-3}$ relative to previous estimates of 5.6×10^7 g C $\text{day}^{-1} \text{km}^{-3}$ and 7.4×10^7 g C $\text{day}^{-1} \text{km}^{-3}$ for the Barren (Salley, 2016) and Green River (Osterhoudt, 2014), respectively. DIC flux values for sub-basins are listed. The Ohio River exports 2.95×10^8 g C $\text{day}^{-1} \text{km}^{-3}$ more DIC than the Barren River and an additional 2.77×10^8 g C $\text{day}^{-1} \text{km}^{-3}$ more DIC than the Green River. The magnitude of the atmospheric sink from carbonate rock dissolution for the Ohio River Basin was 1.75×10^8 g C $\text{day}^{-1} \text{km}^{-3}$, or one-half the total DIC flux. Regression analysis yielded positive statistical correlation ($R^2 = 0.86$) between DIC flux and time-volume normalization parameters for Ohio River basin and nested sub-basins (WY 2014) along with the Barren and Green River basins from previous inquiry (WY 2013) (Figure 2A). The same analysis applied to Ohio River basin and the nested sub-basins for only WY 2014 yielded very similar results and a positive correlation ($R^2 = 0.85$) (Figure 2B). The Wabash, Great Miami and Scioto sub-basins exhibit elevated normalized flux values relative to other basins evaluated. Here the distribution of carbonate rocks is diffuse and geology characterized by quaternary deposits. The Kanawha River basin was found to be entirely devoid of exposed carbonates, such that zero DIC flux is contributed by carbonate rock dissolution. To evaluate the influence of these basins in skewing the strength of statistical correlation testing the calibration technique, additional regression analysis was conducted on a data subset which excluded said basins. The results yielded a strong statistical correlation ($R^2 = 0.91$) (Figure 2C). When applied

Table 1. Summary of DIC Flux and Normalization Parameters by Basin Water Year 2014

Drainage Basin	Annual TDIC Flux (g C)	Carbonate Rock Area (km ²)	P-ET Depth on Carbonate Rock (km)	Normalized DIC Flux (g C $\text{day}^{-1} \text{km}^{-3}$)
Kanawha	2.31×10^{11}	0.00	0.00	NA
Tennessee	7.49×10^{11}	44308.56	5.27×10^{-4}	8.79×10^7
Cumberland	5.55×10^{11}	25181.00	5.33×10^{-4}	1.13×10^8
Kentucky	1.92×10^{11}	4415.45	5.10×10^{-3}	2.34×10^8
Monongahela	8.94×10^{10}	2173.27	4.84×10^{-4}	2.50×10^8
Green	3.00×10^{11}	11506.13	5.00×10^{-4}	2.88×10^8
Licking	1.19×10^{11}	3352.97	5.06×10^{-4}	3.28×10^8
Ohio	7.54×10^{12}	120401.80	4.90×10^{-4}	3.51×10^8
Allegheny	1.92×10^{11}	2374.25	5.29×10^{-4}	4.18×10^8
Wabash	1.15×10^{12}	56.76	4.55×10^{-4}	1.22×10^{10}
Great Miami	3.19×10^{11}	52.94	4.79×10^{-4}	3.44×10^{10}
Scioto	3.78×10^{11}	55.65	4.56×10^{-4}	4.08×10^{10}

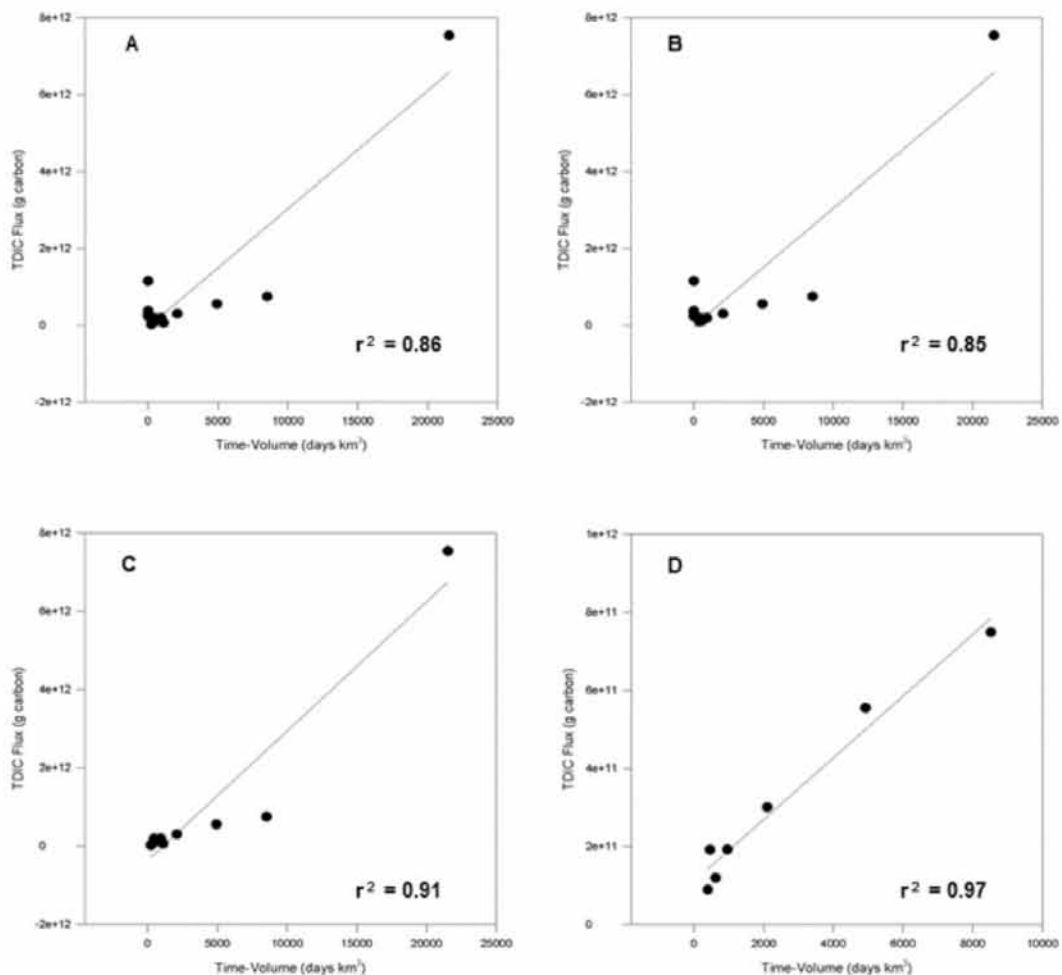


Figure 2. (A) The Ohio basin and nested sub-basins WY 2014 with Barren and Green basins WY 2013. (B) The Ohio basin and nested sub-basins WY 2014 only. (C) Carbonate dominant basins WYs 2013 & 2014. (D) Carbonate dominant sub-basins WY 2014 only.

to carbonate dominated sub-basins, a strong statistical correlation ($R^2 = 0.96$) (Figure 2D) was revealed.

5. Conclusions

DIC flux values were calculated for multiple basins, the normalized results compared, and a positive statistical relationship discovered between DIC flux, time and the volume of water available for carbonate rock dissolution. The strength of statistical correlation demonstrated in scaling the normalization technique to larger basin sizes suggests the parameters of time and volume may adequately capture the variables associated with the phenomena among basins of assorted water availability and carbonate rock distribution. The normalization appears effective on various time scales, as evidenced by the positive statistical relationship observed over 14 datasets spanning 2 hydrologic years. These findings support the idea that this technique can be used to effectively estimate DIC flux and atmospheric CO₂ sink from carbonate rock dissolution without the direct use of hydrochemical or discharge data in future studies attempting to quantify this flux. Furthermore, the success of this technique using secondary water chemistry and discharge measurements negates the need for data logging equipment. Together, these capabilities may drastically decrease the time, labor and cost associated with direct measurement of water chemistry and discharge. Increasing the

ease and efficiency of these calculations could greatly enhance the practicality in making flux estimates on the global scale.

The limitations of this method are revealed in other processes that may influence carbonate rock dissolution aside from time and volume of water available. The technique assumes that alkalinity of water is dominated by bicarbonate, when other sources of basic ions may exist within the sampled waters. Water availability per basin may also be limiting as it depends on the accuracy of the precipitation data, the estimation of evapotranspiration, and the interpolation of water availability over the basin area. Other variables such as land use practices and related soil CO₂ concentrations (Zhang, 2011) and weathering of calcite found in igneous and/or sedimentary rocks (Amiotte Suchet *et al.*, 2003) and various minor processes may also influence DIC flux in a basin. Yet it remains impractical to account for all the variables influencing DIC flux in a basin and therefore this method is offered as an alternative to estimating DIC flux using minimal inputs. Interpretation of the strength of statistical correlations must be approached with caution. The existence of a large data point (i.e., Ohio River basin) compared against a collection of smaller sub-basin data points can generate a relationship that appears to be strongly positive by default. Testing of this method over other moderately-sized basins and basins larger than the Ohio is recommended to determine the ability of

the procedure to accurately estimate DIC flux as spatial scale increases. If the strength of the correlation is maintained over additional basin scales, it would add confidence that this normalization technique is practical for global application. The results of this study suggest that there is cause to continue inquiry along these lines.

References

- Amiotte Suchet, P., Probst, J.-L., & Ludwig, W. 2003. World-wide distribution of continental rock lithology: Implications for the atmospheric/soil CO₂ uptake by continental weathering & alkalinity river transport to the oceans. *Global Biogeochemical Cycles*, **17**(2).
- Cox, P.M., Betts, R.A., Jones, C.D. & Spall, S.A. 2000. Acceleration of global warming due to carbon-cycle feedbacks in a coupled climate model. *Nature* **408**(9 November): 184-187.
- Debye, P. & Hückel, E. 1923. The theory of electrolytes. Lowering of freezing point & related phenomena. *Physikalische Zeitschrift*. **24**: 185–206.
- Falkowski, P, Scholes, R.J., Boyle, E., Canadell, J., Canfield, D., Elser, J., Gruber, N., Hibbard, K., Hogberg, P., Linder, S., Mackenzie, F.T., Moore III, B., Pederson, T., Rosenthal, Y., Seitzinger, S., Smetacek, V., & Steffen, W. 2000. The global carbon cycle: A test of our knowledge of Earth as a system. *Science* **290**(5490): 291-296.
- Keeling, C.D., Piper, S.C., Bacastow, R.B., Wahlen, M., Whorf, T.P., Heimann, M. & Meijer, H.A. 2016. Exchanges of atmospheric CO₂- & ¹³CO₂- with the terrestrial biosphere & oceans from 1978 to 2000. *Global aspects, SIO Reference Series*, No. 01-06, Scripps Institution of Oceanography, San Diego.
- Intergovernmental Panel on Climate Change. 2014. Climate Change 2014. Synthesis Report Summary for Policymakers. Report of the Intergovernmental Panel on Climate Change. Geneva: Switzerland, pp. 151.
- Osterhoudt, L.L. 2014. *Impacts of carbonate mineral weathering on the hydrochemistry of the Upper Green River Basin, Kentucky*. Western Kentucky University Masters Theses & Specialist Projects. Paper 1337.
- Salley, D.C. 2016. *Advancing methods to measure the atmospheric CO₂ sink from carbonate rock weathering*. Western Kentucky University Masters Theses & Specialist Projects. Paper 1603.
- Sabine, C.L, Feely, R.A., Gruber, N., Key, R.M. Lee, K., Bullister, J.L., Wanninkhof, R., Wong, C.S., Wallace, D.W.R., Tilbrook, B., Millero, F.J., Peng, T., Kozyr, A., Ono, T. & Rios, A.F. 2004. The oceanic sink for atmospheric carbon. *Science* **305**(5682): 367-371.
- Solomon, S., Plattner, G.K., Knutti, R. & Friedlingstein, P. 2009. Irreversible climate change to due carbon dioxide emissions. In *Proceedings of the National Academy for Sciences Journal* **106**(6): 1704-1709.
- Siegenthaler, U. & Sarmiento, J.L. 1993. Atmospheric carbon dioxide & the ocean. *Nature* **365** (9): 119-125.
- Thorntwaite, C.W., & Mather, J.R. 1957. Instruction & tables for computing potential evapotranspiration & the water balance. Drexel Institute of Technology, Laboratory of Climatology, *Publications in Climatology* **10** (3): 311.
- Weary, D.J., & Doctor, D.H. 2014. *Karst in the United States: A digital map compilation & database*: U.S. Geological Survey Open-File Report 2014–1156, 23 p.
- White, D., Johnstron, K, & Miller, M. 2005. “The Ohio River Basin.” *Rivers of North America*. Elsevier: Amsterdam. pp. 375-409.
- Zhang, C. 2011. Carbonate rock dissolution rates in different landuses & their carbon sink effect. *Chinese Science Bulletin*, **56**(35), 3759–3765.

Evolution, Development, And Decay Of The Caves And Karst Of The Greenbrier Valley, West Virginia, USA

William B. White^{1*} and Elizabeth L. White²

Affiliation: ¹Department of Geosciences, Deike Building, The Pennsylvania State University, University Park, PA 16802, USA

²Hydrologic Investigations, 4538 Miller Road, Petersburg, PA 16669, USA

* Corresponding author: Tel: +1 814 667 2709. E-mail address: wbw2@psu.edu

Abstract

The Greenbrier karst is formed on a roughly triangular exposure of Mississippian age Greenbrier Limestone that extends 90 km NNE to SSW in Pocahontas, Greenbrier, and Monroe Counties, West Virginia. The Greenbrier Limestone thickens from 100 m at the northern boundary to 365 m at the southern boundary. The lithology of the Greenbrier is highly variable ranging from thick massive limestone to interbedded shales. The limestone section is bounded top and bottom by impermeable shales and sandstones. The geologic setting is conducive to the development of long caves but not deep caves. Within the Greenbrier karst are 24 caves with surveyed lengths greater than 5 km of which 9 have lengths greater than 20 km for a total of 500 km of cave passage plus many smaller caves. The surface karst consists primarily of dolines and blind valleys. Analysis of the profiles of active surface streams and abandoned stream beds gives some insight into the developmental history of the karst. The Greenbrier karst appears to be the remnant of an older erosion surface, assumed to be the Harrisburg surface that apparently developed throughout the Appalachians in the mid- to late Miocene. Based on cosmogenic isotope dates elsewhere in the Appalachians, dissection of the Harrisburg surface began about 5 to 3.5 Ma ago. At the measured denudation rates of 21 m/Ma, 75 m of the original karst surface has been removed. The result has been fragmentation of the cave systems, deep doline development, and return of some drainage to the surface. Synclinal structures that preserved the overlying sandstone remain as synclinal ridges with 100 m scarps facing into the karst plain.

Keywords: Greenbrier karst, erosion surfaces, sinkholes, large caves

1. Introduction

The Greenbrier Valley in southeastern West Virginia contains some of the longest caves in the United States. The Greenbrier karst is part of the extensive Appalachian Karst and is located in Pocahontas, Greenbrier, and Monroe Counties, West Virginia (Fig. 1). For the relationship of this karst area to other karst regions in the Appalachians and in the United States overall, see Palmer and Palmer (2009). A State-wide description of the karst of West Virginia is given by Dasher (2012). Details of the topography and stream profiles were extracted from the U.S. Geological Survey 7.5 minute (1:24,000) quadrangles.

2. Geologic, Hydrologic, And Topographic Setting

The Greenbrier River has its headwaters in the Allegheny Mountains near Spruce Knob, West Virginia and flows southwest following the regional strike for 278 km to its confluence with the New River. The total basin area is 4290 km². Portions of the Greenbrier Valley are underlain by the Mississippian Greenbrier Limestone which forms a karstic zone between the Allegheny Mountains to the east and the main Appalachian high plateau to the west. The controlling structural feature is the Browns Mountain Anticline, a major fold west of the Allegheny Escarpment. The Greenbrier Limestone is exposed along the western flank of the anticline. To the west the limestone dips beneath the younger rocks of the Plateau.

In the northern and central part of the region, the river flows along the eastern margin of the karst where it has incised a secondary valley into the clastic rocks that underlie the limestone. Because of the westerly dip, these clastics form a

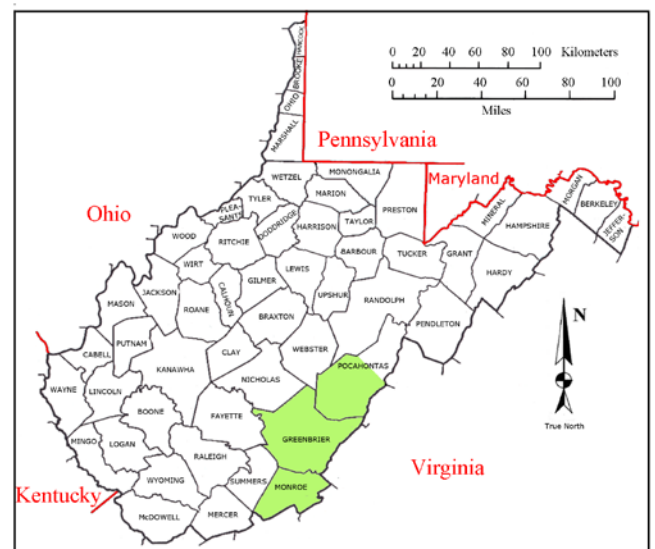


Figure 1. Location map for the Greenbrier Karst

ground water dam that prevents the development of underground routes directly to the river.

Thus, tributary streams entering the river from the east flow entirely on clastic rocks, whereas the tributaries entering from the west have a pronounced fluviokarstic component. It is these western sub-basins that are the subject of the present paper.

The thickness of the Greenbrier Limestone varies from about 100 m at the northern border to 365 m at the southern limit of the karst (Fig. 2). There are massive, cave-forming limestones such as the Union, Pickaway, and Patton units and there are interbedded shales such as the Greenville Shale, the Taggard

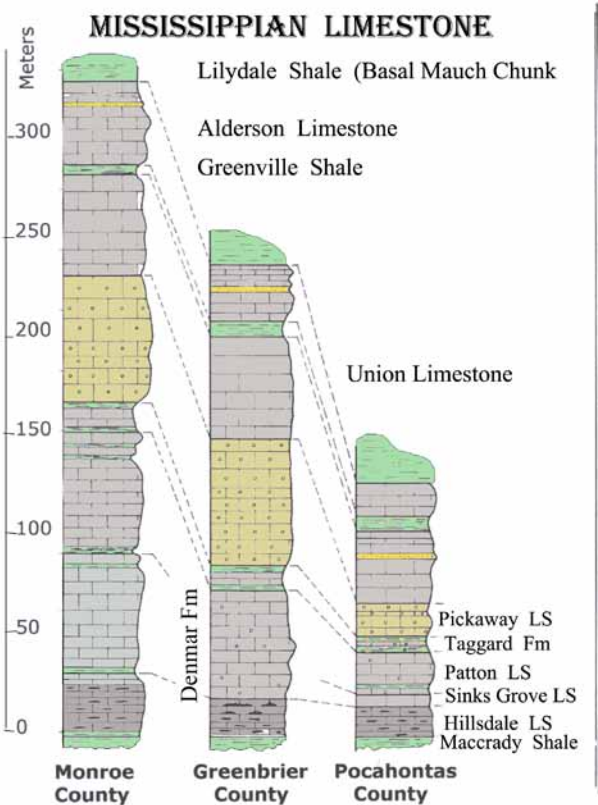


Figure 2. Stratigraphic columns for the Mississippian Greenbrier Limestone in three counties.

Formation of mixed shales and shaly limestones, and some other thin unnamed shales. The shales act as confining layers that guide the initiation paths of cave passages. At the bottom of the section is the Maccrady Shale which serves as an aquiclude for the karst aquifer.

The most important structural feature is a regional westward dip created by major fold structures in the clastic rocks to the east. Superimposed on the regional dip are a sequence of low-amplitude anticlines and synclines with a general north-south trend. One synclinal structure exposes the overlying sandstones and shales to produce Muddy Creek Mountain, a north-south ridge with steep out-facing escarpments that bisects the karst.

3. The Greenbrier Karst

3.1. Surface Karst: Closed Depressions

Long exposure to weathering has lowered the limestone surface and created closed depressions of many shapes on many size scales. There are near-circular sinkholes (dolines), there are the blind valleys formed by small sinking streams, and there are wide regional scale closed depressions. The latter are the result of exclusively internal drainage over large areas of which a sample is shown in Figure 3.

Earlier studies of sinkhole depths in the Appalachians (White and White, 1979; Troester et al., 1984) show that sinkhole depths follow an exponential distribution of the form

$$N = N_0 e^{-Kd}$$

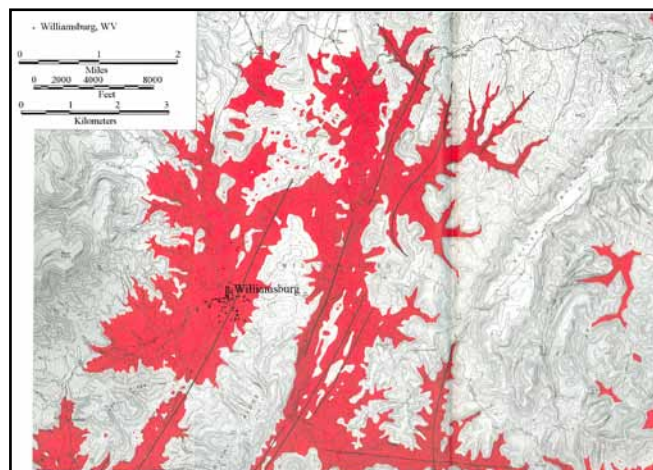


Figure 3. Closed depressions (red areas) near the village of Williamsburg, Greenbrier County. Extracted from a regional scale map by Lessing (1979). Black lines are lineaments marking lines of sinkhole development.

N = number of sinkholes of a given depth, d = depth of sinkholes, and N_0 and K are fitting parameters. The parameter K is representative of the sinkhole population and has a value for the Appalachians of $K = 0.22 \text{ m}^{-1}$ independent of rock type (limestone vs. dolomite), structure (flat-lying rocks vs. strongly folded rocks), and age of rocks (Mississippian vs. Devonian vs. Ordovician) based on measurements of more than 5000 sinkholes. A detailed study of the Greenbrier karst (Soriano and White, unpublished data) gave essentially the same result. The exponential distribution of sinkhole depths has the same form as the depth distribution of corrosion pits on boilers and nuclear reactor vessels (on a vastly different size scale). Corrosion engineers (e.g. Macdonald and Urquidí-Macdonald, 1992) have been able to model the corrosion process to reproduce the observed exponential pit distribution. If karst, also, is regarded as a corrosion surface, a more mechanistic model of its development might be possible.

A somewhat different type of closed depression is formed by unroofed cave passage of which Sinking Creek provides a possible example. Sinking Creek rises in the mountains north of the karst area and flows into an alluviated blind valley. The stream meanders over the floor of the depression for 7 km to the downstream end of the blind valley at the entrance of a cave known as the "Sinks of Sinking Creek". The cave is a 230 m-long fragment of 10 to 20 m diameter master trunk. The stream emerges at the upstream end of a narrow, nearly linear, closed valley that extends nearly 10 km to a blind footwall where the stream again goes underground. It reappears as a large spring at Piercys Mill Cave 5 km to the southwest where it forms the headwaters of Muddy Creek. The linear course of the closed valley is dictated by the contact between the limestone and the underlying shale brought up by the Brushy Ridge Anticline to the east. Topographic evidence suggests that this 10-km long closed valley is an unroofed cave passage with a small fragment of cave surviving at the upstream end and a much larger cave segment at the downstream end.

3.2. Fluviokarst and Stream Profiles

The fluvio-karst basins are generally small but have the characteristic that a portion of the drainage is underground through karstic conduit systems. In some basins, a portion of the dis-

charge remains in surface channels during high flows. In other basins, the drainage is entirely underground and the surface profile of the channel may become irregular or ragged. An earlier comparison of channel profiles in a set of small basins in the western margin of the Cumberland Plateau suggested that the underground flow routes maintain grade with the active surface channels and that dry channels can be related to old base levels (White and White, 1983).

Profiles, breaks in profiles, and extrapolations of profiles of sinking stream in the Greenbrier karst give similar results and provide clues to the evolution of the karst.

3.3. Caves

The geologic setting of the Greenbrier karst is optimum for the development of long caves but not deep caves. Table 1 lists the caves with surveyed lengths exceeding 5 km. The rank on the U.S. long cave list is given for those with lengths greater than 20 km and the world rank for those with lengths greater than 30 km. Adding up the lengths yields a total of 498.2 km of mapped cave passage, making the Greenbrier Valley one of the most cavernous regions on the planet. A complete tally would require adding in the accumulated length of more than 2000 smaller caves, many of which are of substantial length.

Table 1. The long caves of the Greenbrier Valley

CAVE	LENGTH (km)	US RANK	WORLD RANK
Friars Hole System	73.4	6	31
Organ Cave	61.9	10	42
Scott Hollow Cave	47.5	17	68
The Hole	37.0	24	104
Culverson Creeks System	33.7	30	134
McClung Cave System	29.1	36	
Windy Mouth Cave	29.0	37	
Benedict's Cave	23.9	52	
Bone-Norman System	22.7	55	
Maxwellton Cave	18.8	64	
Portal-Boar Hole System	16.8	71	
Ludington's Cave	14.7	81	
Acme Quarry Cave System	13.6	87	
Overholt Blowing Cave	12.6	98	
Dry Cave	9.2		
Destitute Cave	8.0		
Union Cave	7.4		
Buckeye Creek Cave	7.2		
Carpenter's - Swago System	7.0		
Greenville Saltpetre Cave	6.7		
Wades Cave	6.4		
Laurel Creek Cave System	5.8		
Zicafoose Blowhole	5.8		
Plastic Bag Cave	5.5		

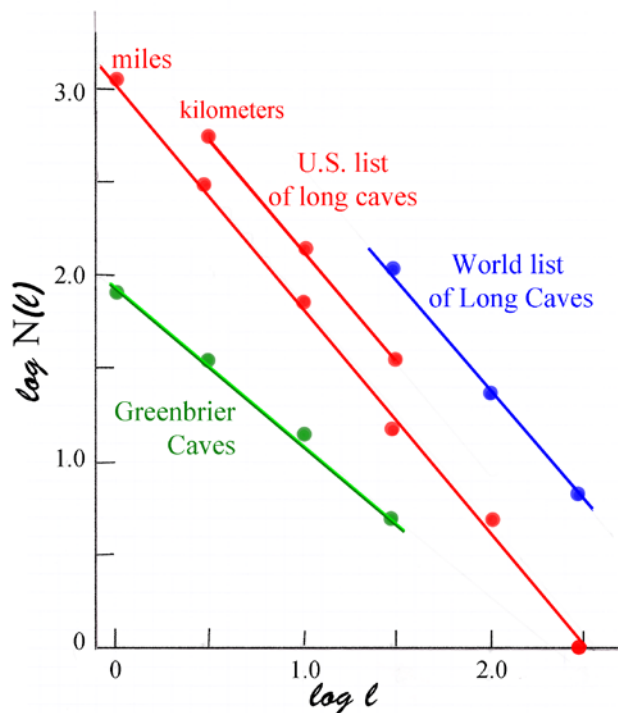


Figure 4. Distribution of cave lengths for World, US, and Greenbrier cave populations.

Most caves are fragments of conduit systems, truncated by surface erosion, breakdown, flowstone barriers, or sediment plugs. The population of cave lengths in a given region is a natural fractal (Curl, 1986). According to Curl, the cave lengths should follow a power law of the form

$$N(\ell) = N(\ell_0) \left(\frac{\ell}{\ell_0} \right)^{-\nu}$$

where $N(\ell)$ is the number of caves longer than ℓ , ℓ_0 is the reference length (m, km, or miles), and ν is the fractal dimension. Figure 4 shows length distribution plots for long caves drawn from Robert Gulden's Long Cave Lists (<http://www.caverbob.com>). The fractal dimension of the U.S. list of long caves is 1.25 and for the world list 1.21, both in the range of 1.2 to 1.6 reported by Curl for other cave populations. The Greenbrier Valley caves with lengths greater than one kilometer, however, have a fractal dimension of 0.86. The population is skewed toward larger caves.

3.4. Age And Evolution Of The Greenbrier Karst

The Greenbrier karst appears to be related to the Harrisburg erosion surface as also identified in other parts of the Appalachian karst (White, 2009). The Greenbrier karst consists of limestone uplands now dissected by the Greenbrier River and its tributary streams. From northeast to southwest, the components are the Swago Creek basin with the uplands represented by hill summits at 760 m, the Little Levels, an undulating doline plain at 730 m, and the main Greenbrier karst (sometimes called the Big Levels) at 670 m. The question is: How did the karst and its caves evolve?

According to cosmogenic isotope dates on cave sediments in the Cumberland Plateau (Anthony and Granger, 2007), the eastern Highland Rim, a Tennessee equivalent to the Harrisburg Surface, received a deposition of gravel from 5 to

3.5 Ma ago with active dissection beginning about 3.5 Ma. Cosmogenic isotope dating of cave sediments on the New River upstream from its confluence with the Greenbrier River produced a rate of downcutting of 27 m/Ma (Granger et al., 1997). As a karst surface, the Greenbrier karst is lowered by chemical denudation at a rate of 21 m/Ma based on measurements by Ogden (1982) on three spring basins.

Using these rates, over the past 3.5 million years, the limestone surface would have lowered by 75 m, bringing the karst surface close to the top of sandstone-protected Muddy Creek Mountain at 800 m, removing much of the relief in the topography. During this time the river would have deepened its channel by almost 100 m. The large master conduits appear to have developed since the Pliocene with the deepening of the Greenbrier River channel and the concurrent lowering of the karst surface.

4. Conclusions

The Greenbrier karst in southeastern West Virginia has a geological setting optimum for the development of exceptionally large cave systems. These developed with the dissection of the Harrisburg erosion surface beginning about 3.5 million years ago. The caves are past their maximum development and at present are being fragmented and some of the surface drainage restored.

Acknowledgements

This paper is a synopsis of a forthcoming volume on the Greenbrier karst which itself is a synopsis of more than 50 years of exploration by members of the West Virginia Association for Cave Studies (WVACS), the West Virginia Speleological Survey (WVASS), and many individual scientists and explorers.

References

Anthony DM, Granger DE, 2007, A new chronology for the age of Appalachian erosional surfaces determined by cosmogenic nuclides in cave sediments. *Earth Surface Processes and Landforms*, **32**, 874-887.

Curl RL, 1986. Fractal dimensions and geometries of caves. *Mathematical Geology*, **18**, 765-783.

Dasher GR, 2012. The caves and karst of West Virginia. *West Virginia Speleological Survey*, Bulletin 19, Barrackville, WV.

Granger DE, Kirchner JW, Finkel RC, 1997, Quaternary downcutting rate of the New River, Virginia, measured from differential decay of cosmogenic ²⁶Al and ¹⁰Be in cave-deposited alluvium. *Geology*, **25**, 107-110.

Lessing P, 1979. Karst subsidence and linear features, Greenbrier and Monroe Counties, West Virginia. *West Virginia Geological and Economic Survey Environmental Geology Bulletin* EGB-17.

Macdonald DD, Urquidi-Macdonald M, 1992. Corrosion damage function - Interface between corrosion science and engineering. *Corrosion*, **48**(5), 354-367.

Ogden AE, 1982, Karst denudation rate for selected spring basins in West Virginia. *National Speleological Society Bulletin*, **44**(1), 6-10.

Palmer AN, Palmer MV, 2009. *Caves and karst of the USA*. National Speleological Society, Huntsville, AL

Troester JW, White EL, White WB, 1984. A comparison of sinkhole depth frequency distributions in temperate and tropic karst regions. *Proceedings of the First Multidisciplinary Conference on Sinkholes*. Orlando, FL, 65-73.

White EL, White WB, 1979. Quantitative morphology of landforms in carbonate rock basins in the Appalachian highlands. *Geological Society of America Bulletin*, **90**, 385-396.

White EL, White WB, 1983. Karst landforms and drainage basin evolution in the Obey River basin, north-central Tennessee, USA. *Journal of Hydrology*, **61**, 69-82.

White WB, 2009, The evolution of Appalachian fluviokarst: Competition between stream erosion, cave development, surface denudation, and tectonic uplift. *Journal of Cave and Karst Studies*, **71**(3), 159-167.

The Glenelg River Karst

Susan White^{1,2} & John Webb¹

Affiliation: ¹ Environmental Geoscience, Latrobe University Bundoora, Victoria 3058
² Victorian Speleological Association, Inc.

Abstract

The Glenelg River karst area forms part of a composite karst area on the coastal plains of the Gambier Karst Province. It is concentrated along the Glenelg River and its immediate environs. It has been known as a caving area for many years but its known caves are restricted. The influence of the incised Glenelg River on surface and underground water flows and the tectonic activity of the faults along the escarpment to the east of the river, has resulted in a significantly different karst landscape to the drowned cenote karst to the west or the Naracoorte. Within the Glenelg River karst there are known two sub-areas: the escarpment and the immediately adjacent incised Glenelg River karst area which, include several poorly defined cave documentation areas used by the VSA and CEGSA; a small part of the lower southeast of South Australia (L) just to the west of S.A./Victoria border, known as Dry Creek, including areas of pine forest and farmland nearby, and in Victoria, the Glenelg (G), Drik Drik (DD) and poorly documented areas between the fault escarpment and the Glenelg River. Although formed in the Tertiary limestones, like Naracoorte, the karst landscape evolution is very different. This paper will look at the landscape development of the karst through the Pleistocene, compare it to what happened in Naracoorte and discuss potential for further discoveries.

Keywords:

1. Introduction

The Glenelg River karst area lies within the Gambier Karst Province (White, 2005), along the Glenelg River and its immediate environs (Fig. 1). The karst forms part of the composite karst area on the coastal plains of the Gambier Karst Province (Grimes et al., 1995; Marker, 1975) and is significantly different to the drowned cenote karst to the west and the Naracoorte karst to the north. Within the Glenelg River karst there are two sub-areas: the escarpment and the incised Glenelg River karst area. It includes several poorly defined cave documentation areas used by the VSA and CEGSA (Matthews, 1985): the Dry Creek part of the lower southeast of South Australia (L), and the Glenelg (G), Drik Drik (DD) and poorly documented areas between the fault escarpment and the Glenelg River (Fig. 1).

2. Geology

The karst has developed in both gently folded Gambier Limestone and overlying Pleistocene Bridgewater aeolianite dunes west of the Kanawinka and associated escarpments. The main karst host rock in this area is the marine Oligo-Miocene Gambier Limestone. Extensively weathered Pliocene basalts (2.2 and 2.4 Ma) (Aziz-Ur-Rahman and McDougall, 1972) blanket the uplifted erosional surface developed on the Tertiary limestone plateau to the east of the Kanawinka Escarpment. The limestone is well jointed which have influenced the cave passage orientations.

3. Surface Landforms and Processes

The dominant surface landforms of the area are the incised Glenelg River and the fault escarpments. Otherwise it has a subdued relief with dunes on the coastal plains. Much of the drainage of the area is underground, some of which has been disrupted by underground capture to form dry valleys, which carry water only during irregular periods of high flow, e.g. Dry Creek.

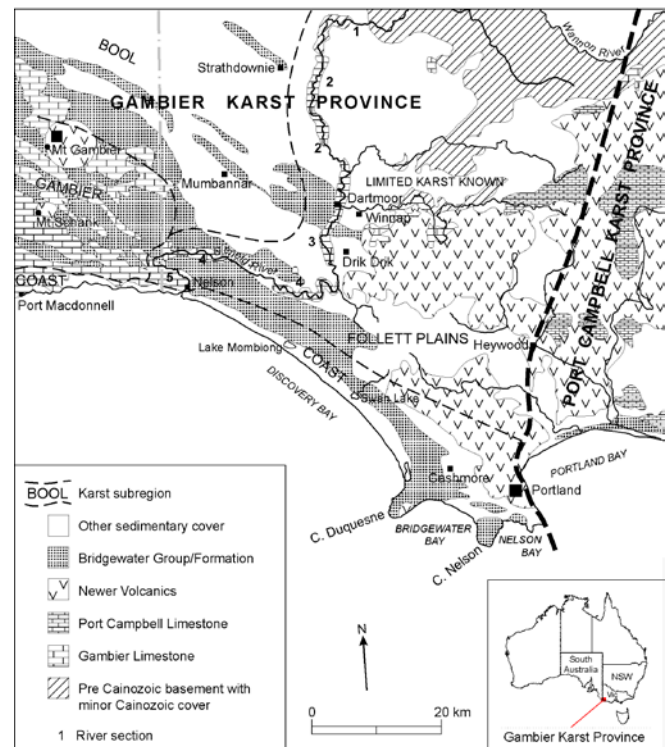


Figure 1. Glenelg River karst area: location map (White, 2005)

The Glenelg River, the largest perennial river in the region has a complex drainage pattern, which has been modified since the Late Tertiary (Boutakoff, 1963) and is further complicated by the influence of karst ground water flow. The westerly flowing stretch of the Glenelg River downstream from Keegan's Bend is parallel to the dunes of the Bulley Range, indicating that these dunes were present when this section of the gorge was incised.

The relatively soft limestone does not develop extensive surface solutional microfeatures. Very little karren is present and sub-soil karren is poorly developed. Enigmatic solutional pans, hollows and dolines are similar to those found further

north. Solutional conical dolines are widespread, particularly along the escarpment. Large elongated basin-shaped enclosed depressions, up to 500 m across and up to 10 m deep, occur in the dune ranges south of the Glenelg River and west of Moleside Creek. These are solution-modified dune swales and usually have soil floors. A few contain “runaway holes”, which funnel surface water underground during periods of high runoff. Concentrated along the escarpment at Drik Drik are nested solutional dolines and large collapse dolines, some of which are formed in Bridgewater Group climbing dunes and have collapsed into the underlying Gambier Limestone.

4. Underground Features

Although over 100 features, including 67 caves, are known from the Glenelg River karst area, this reflects an incomplete knowledge of the area. Caves are concentrated in two areas, along the Glenelg River and along the escarpment at Drik Drik, and there is a paucity of known caves elsewhere.

Whether the distribution and numbers of caves is an artifact of exploration or not is unclear, but current exploration indicates that more caves exist.

Most caves, including all of the larger ones, have the majority of passages developed within the Gambier Limestone. Entrances, especially solution pipes and passages connected to the surface, often pass through the overlying Bridgewater Group.

The caves occupy five general positions in the landscape:

1. Caves with entrances close to river level, i.e. within 1 m of the level of the present river or a tributary such as Curran's Creek, e.g. Curran's Creek Cave (G 4). These sometimes contain perennial streams.
2. High level caves close to the river, at 10 to 15 m above present river level with entrances in the cliffs, e.g. Amphitheatre Cave (G 2).
3. High level caves which are not close to the river, e.g. McEachern's Death Trap (G 49). These are positioned at the same altitude as the other high level caves, but are over 1 km from the river and are more modified by collapse and sediment infill.
4. DD 4, a complex two-level branchwork cave that contains an underground tributary of the Glenelg River flowing towards the Glenelg River from the higher elevation area of the Jones Ridge escarpment. This cave is atypical for the area.
5. Small syngenetic caves developed in Bridgewater Group aeolianites that have solution pipe entrances, e.g. G 10 or “Runaway” holes and dolines on the flatter plains away from the river, e.g. G 48D.

The caves are predominantly simple, short single passages, i.e. single conduit caves. There are few multilevel or branchwork caves and no cave of the complexity of the maze caves observed at Naracoorte. Caves vary in length from a few metres, e.g. Hand Cave (L 3), to over 2 km (DD 4). Most cave passages are narrow, high rifts with near vertical walls, e.g. Princess Margaret Rose Tourist Cave (PMR) (G 6). Both phreatic and

vadose passage shape are evident and many show evidence of phreatic initiation as either a sub-circular or elliptical tube in the ceiling, e.g. PMR (G 6). Surface weathering on the cave walls commonly obscures distinctive and diagnostic phreatic or vadose wall features. The influence of the predominant regional joint patterns on cave passage orientation is marked. Some passages have been modified by collapse, but the rubble piles found in many caves are generally small and collapse is not as important in cave modification as at Naracoorte. Although a number of caves in the Glenelg River karst area contain water, this represents flowing streams and not groundwater pools. The two branchwork caves, Amphitheatre Cave (G 2) and Curran's Creek Cave (G 4) are not distinctively different from the single conduit caves. Although collapse has modified passages in the Glenelg River karst area, the uniformity in passage dimensions is at least partly because there is no large collapse chambers.

Extensive unconsolidated clastic sediments containing Pleistocene bone material are found in very few caves in the Glenelg River karst area: Amphitheatre Cave (G 2), McEachern's Cave (G 5), McEachern's Death Trap (G 49) (Baird, 1986; Hope and Wilkinson, 1982; Kos, 2001; Link, 1967; Wakefield, 1967). Speleothem development is limited, with a few exceptions, e.g. Princess Margaret Rose Tourist Cave (G 6)

5. Cavern development and speleogenesis

The caves were initially developed as phreatic conduits and later modification occurred as the river incised into the landscape in response to the lowering sea levels, the subsequent water table lowering and the draining of phreatic conduits. These passages may have been flooded again at times of high sea levels. As they drained, the caves modified by entrenchment rather than collapse, so rift-shaped passages are common rather than collapse domes. As the river has very few surface tributaries, these vadose fissure caves are significant contributing tributaries down stream from Moleside Creek.

Collapse features are less common and not as large as at Naracoorte and no large collapse chambers of the dimensions found at Naracoorte occur.

The two main karst areas at Glenelg River formed at different times. At Drik Drik karstification occurred at similar times to the formation of karst at Naracoorte (between 1.1 Ma and 400 ka), whereas the caves along the Glenelg River lower reaches and the Bulley Ranges developed no earlier than the 400 ka (MIS stage 11) still-stand. The caves do not appear to be formed as flank margin caves, unlike those at Naracoorte.

References

Aziz-Ur-Rahman and McDougall, I., 1972. Potassium-argon ages on the Newer Volcanics of Victoria. *Proceedings of the Royal Society of Victoria*, **85**: 61-69.

Baird, R.F., 1986. *The Avian Portions of the Quaternary Cave Deposits of Southern Australia and their biogeographical and Palaeoenvironmental Interpretations*. PhD Thesis, Monash University, Melbourne.

- Boutakoff, N., 1963. *The geology and geomorphology of the Portland area*. Memoir 22, Geological Survey of Victoria, Melbourne.
- Grimes, K.G., Hamilton-Smith, E. and Spate, A.P., 1995. *South East Karst province of South Australia*, Australian Caves and Karst Management Association.
- Hope, J. and Wilkinson, H.E., 1982. Warendja wakefieldi, a new genus of wombat (Marsupialia, Vombatidae) from Pleistocene sediments in McEachern's Cave, western Victoria. *Memoirs of the National Museum of Victoria, Australia*, **43**(1 & 2): 109-120.
- Kos, A.M., 2001. Stratigraphy, sedimentary development and palaeoenvironmental context of a naturally accumulated pitfall cave deposit from southeastern Australia. *Australian Journal of Earth Sciences*, **48**(5): 621-630.
- Link, A.B., 1967. Late Pleistocene-Holocene climatic fluctuations: Possible solution pipe - foibe relationships; and the evolution of limestone cave morphology. *Zeitschrift für Geomorphologie*, **11**(2): 117-145.
- Marker, M.E., 1975. *The Lower Southeast of South Australia: A Karst Province*. Department of Geography and Environmental Studies, University of Witwatersrand, Johannesburg, Occasional Paper No. 13, 68 pp.
- Matthews, P.G. (Editor), 1985. *Australian Karst Index 1985*, Australian Speleological Federation Inc., Melbourne.
- Wakefield, N.A., 1967. Preliminary Report of McEacherns Cave, SW Victoria. *The Victorian Naturalist*, **84**: 363-383.
- White, S.Q., 2005. *Karst and Landscape Evolution in parts of the Gambier Karst Province, Southeast South Australia and Western Victoria, Australia*, PhD Thesis, La Trobe University Bundoora, Victoria

(Abstract) **The Significance Of The Tiankeng Group Discovery In Hanzhong Of Central China**

Yuanhai Zhang

Affiliation: Institute of Karst Geology, Guilin, Guangxi China

Abstract

Hanzhong, located by the Sichuan border in the south of the Qinling Mountains in Shannxi Province of central China, the headstream of the Han River and in the transitional zone between Yangtze plate and Qinling orogeny, has a contiguous carbonate rocks area of 5000 square kilometers from west to east, where the landform features karst table mountains and cone karst with an elevation of 1500-1900m.

According to the drone image and on-site investigation, 49 tiankengs are discovered. The largest one has a 520 by 310m diameter entrance, 320m in depth. These tiankengs are intact, beautiful in shape, unique and original at the bottom. They developed in at least four underground rivers, including Didonghe River in Ningqiang County, Xiaonanhai River in Nanzheng County, Bailongdong River in Xixiang County and Jinzhudong River in Zhenba County. These underground rivers are closely related to many caves.

These tiankeng and caves were first discovered in central China. They are very similar to those in southern China, but they are mostly smaller than those in southern China, mainly because of the difference of rainfall. There is 1700-1900mm rainfall in southern China, however it has only 700-1100mm in central China. Additionally the carbonate rocks are little bit different even though they are Permian limestone. The limestone formations are Qixia and Maokou in Southern China, pure and very thick, it is the Permian Wujiaping Formation in central China, characterized by interbedded chert and muddy limestone, so that it forms waterfalls in the tiankeng wall or at the bottom, as well as levels of cave passages in the same cave system.

The tiankeng group discovered in central China is of great significance to the comparative study of the geological evolution and bio-ecological processes of the important karst landform in north and south of China, and the utilization of its aesthetic value in tourism development and economic sustainable development.

Keywords: tiankeng group, karst, Hanzhong, central China

Karst and Cave Survey, Mapping and Data Processing

(Abstract) **3D cartography: caveGEOmap and ZEB1 LIDAR**

Angel A Acosta-Colón

Affiliation: University of Puerto Rico at Arecibo

Abstract

Different tools and software are used these days to create 3D digital cave cartography maps. Our research group are developing and using two modern techniques to create 3D digital cartography of caves; these are: i) ZEB1 LiDAR and ii) caveGEOmap. The Geoslam ZEB1 hand held mobile LiDAR was used to obtain the measurements. This system provides us with more than 40,000 data points per second in a totally random three-dimensional pattern with a 270° angular field of view. After the data collection, which provides us with millions of data points, and decrypt the data, a powerful computer and advance software are needed to create the 3-D high-resolution cave maps. Secondly, CaveGEOmap is a Matlab® code developed that uses basic surveyor cartography measurements to create 2-D and 3-D maps of the cave with minimal user interaction. A cave cartographer will use a digital laser distance measurer, clinometer and a compass to obtain the measurements of the cave, however this method is time consuming and as a result few measurements are usually obtained. Our method consisted in measuring distances as a function of the azimuth and inclination for a total of 54 data points per station. Then, caveGEOmap evaluates the given measurements using Spatial Analysis and uses the data itself to estimate the necessary variables to produce the 2-D and 3-D cave maps. The cartography was performed in different caves in the north coast karst belt region in Puerto Rico. In conclusion, comparisons between two modern cave cartography methods were used for this study and the main objective was to verify if caveGEOmap (uses basic surveyor measurements, is time consuming and inexpensive) method is comparable to the ZEB1 LiDAR (high quantity data collection, expensive and less time consuming) method.

Application of lidar data for cave entrance identification

Miha Čekada¹, Petra Gostinčar², Borivoj Ladišič³,

Affiliation: ¹Speleo club Železničar, Speleological Association of Slovenia

²Karst Research Institute, Research Centre of the Slovenian Academy of Sciences and Arts

³Speleo club Novo mesto, Speleological Association of Slovenia

Abstract

The data about caves in Slovenia are collected in the Cave Registry. In the past, the cave locations were determined either descriptively, with the use of various large-scale maps, or with a GPS. Recently the lidar data for the entire country has been released; the data are entirely freely available online, including the classified point cloud. There are obvious benefits of a lidar-data based digital elevation model or even a simple raster shaded relief. However, most cave entries are pits, and isolated lidar reflections from well below the terrain are typically filtered out as »low points«, and therefore not visible in the digital terrain model. Hence, the classified point cloud, where all classification classes are included (including the »low points«), needs to be used for caving purposes. A case study is presented, where a single »low point« guided us to the discovery of a new pit. Using lidar data, promising cave entrances can be pinpointed in advance. In contrast to traditional browsing across a terrain, the field survey is reduced to hopping from one potential entrance to another. In this way, the discovery rate of finding new caves is greatly enhanced. In addition, lidar data can also be used to enhance the precision of cave coordinates. Though GPS has been taken for granted as the most precise tool, in reality its precision is compromised by terrain and vegetation cover. Analysing a large set of cave coordinates, determined in the previous years by one single caver using GPS, we made a re-evaluation of these coordinates using lidar. In this way we were able to determine the real precision of a GPS for caving use.

Keywords: lidar, cave, karst, entrance pit, caving

1. Introduction

For any successful speleological analysis at a given area, a trustworthy database of cave entrance locations is needed. In essence, the applicability of these data becomes meaningful only if the cave entrance coordinates are accurate enough to locate the cave in the field. As caving is primarily an amateur activity, cave coordinates have generally been determined using large-scale topographical maps or (since around 2000) a handheld GPS. The precision of these coordinates is often questionable, especially the ones from several decades ago.

In Slovenia, upon which territory this paper is limited, there are several advantages regarding the study of coordinate precision. The country is small (20,000 km²), easily accessible, with a high caver population and strong caving tradition. The cave data are organized in the Cave Registry, which is jointly operated by the Speleological Association of Slovenia and the Karst Research Institute of the Slovenian Academy of Sciences and Arts. The Cave Registry has been in operation since early 1920's thus it is one of the earliest cave databases in the world. However, during the communist regime, precise maps were off-limits for general public thus locations of caves discovered before 1990's typically have a poor precision; an error of 100 m is not uncommon. A recent study based on coordinate improvements showed that the average precision equals about 4 mm on the map, upon which the location was determined (Čekada 2013). On the most precise national topographic map (1 : 5,000) this translates to 20 m in the field.

The introduction of the GPS generally substantially improved the location precision, but there are several drawbacks, often not taken into account: (i) the precision as specified by the manufacturer applies for ideal cases, while in real terrain it is often less accurate, especially in adverse conditions (forest,

valleys, rock walls); (ii) amateurs tend to make beginner's mistakes, like using the wrong datum, wrong coordinate transformations, using the first reading rather than the average, etc.; (iii) eventual mistakes are difficult to trace.

Laser scanning, also known as lidar, is a remote sensing technique where the terrain data are obtained from laser pulse reflections. The result is a georeferenced point cloud, which can further be classified based on the reflection type. The discussion in this paper is limited to aerial laser scanning, where a high-precision digital terrain model can be obtained with an important advantage of obtaining the terrain below the vegetation cover (Triglav Čekada 2011). In contrast, terrestrial laser scanning has been successfully implemented in cave survey, but this is beyond the scope of this paper. The lidar data thus greatly improves the available cartographic background (Plan and Dečkar 2006) upon which the cave locations can be determined. In Slovenia, the nation-wide lidar data acquisition was completed in 2015 (Triglav Čekada and Bric 2015). In contrast to some other countries, the complete data is freely available online, which is of great benefit for the mostly non-professional caving community (Čekada and Gostinčar 2016).

2. Methods

The national lidar scanning of Slovenia was mainly conducted with a density of 5 pt/m². Only a minor part of the territory was scanned with a lower density of 2 pt/m², primarily the scarcely inhabited forested areas; unfortunately this terrain is often of major interest for caving. Three sets of data are available: georeferenced classified point cloud (.las file), digital terrain model (.ASCII file, 1×1 m grid) and raster shaded relief (.tif file). In our work only the classified point cloud data were used, as the other two are simplified derivatives of the former (Triglav Čekada and Bric 2015).

The georeferenced point cloud data is classified in six classes: ground, low vegetation (<1 m height), medium vegetation (1–3 m), high vegetation (>3 m), buildings, and unclassified points (Triglav Čekada *et al.* 2015). In addition, there are several other classes which are primarily not dedicated to the end-user as they include points predominantly identified as mistakes (Mongus *et al.* 2013). One of these classes is the »low point« (»low noise«, i.e. class 7 of the ASPRS (LAS specification 2013). It includes outliers below the terrain. An isolated point of, say, 5 m below the neighbouring terrain is indeed probably an artefact (e.g. due to multiple reflections), however, in karst it may be a real reflection from a 5 m deep pit.

The analyses and visualisations were made using the software Fugroviewer, ArcGIS and Surfer. Existing cave data was taken from the Cave Registry (2016). Lidar data of Slovenia are available at the e-Vode online viewer (e-Vode 2016).

Regarding the precision of previous GPS-derived locations, any analysis is compromised by the question of trustworthiness of individual cavers who contributed the data. To avoid the selective bias we checked the locations obtained by one single caver (third co-author of this paper). So far he has discovered more than 600 new caves. Among these we selected 112 caves which have a well-recognizable entrance from the lidar data. For each cave a map of the immediate neighbourhood was made and the author pinpointed the standpoint he had used during the GPS survey. The coordinates of this point determined from lidar data were then compared to the coordinates obtained by GPS during the discovery. All the measurements were taken by the same handheld Garmin Colorado 300 unit, in the timespan 2008–2016. At least three consecutive measurements were made for each cave over a period of 10 minutes.

3. Results and discussion

3.1. Large and medium-sized cave entrances

Large cave entrances, such as collapse dolines (lateral dimensions in the 100 m range), are sometimes shown in the most precise topographic maps in real contours rather than point symbols. Due to a substantially better density of lidar data, entrances of much smaller caves can be easily visualised and studied (Andrić and Bonacci 2014, Kobal *et al.* 2014, Zini *et al.* 2015, Zho and Pierskalla 2016). The most straight-forward case is a pit, where the laser points from inside the pit are typically classified as »low points«.

Fig. 1 shows the pit Gradišnica (20 m wide and 65 m deep), which was first explored in late 19th century. On the most precise national topographic map (1 : 5,000, Fig. 1a) it is marked by a circular symbol only, despite its relatively large diameter. A lidar-derived map (Fig. 1b) on the other hand shows the precise shape of the pit rim, morphology of the walls (provided there are no overhangs) and the topography of the bottom. Other geometrical data can be extracted: cross-section area (at several levels), volume, maximum depth, etc. The altitude above sea level is routinely extracted, which can be a problem even in the most precise maps where contour lines are often omitted in too steep sections. In addition to the pit plan, cross-sections in different bearings can be made (Fig.

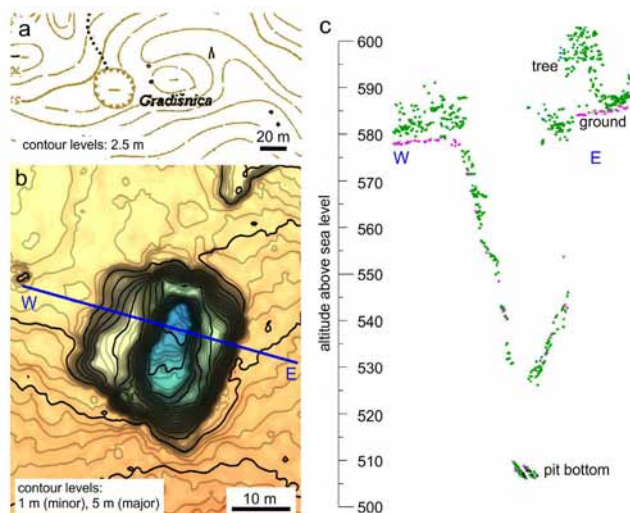


Figure 1. Large pit Gradišnica, shown in a plan at the 1 : 5,000 topographic map (a) and a lidar-derived map using »ground« and »low point« classes (b); elevation along the W–E line using all classification classes (c).

1c). In this way, there is a gradual transition from a large-scale topographic map to a cave survey.

By decreasing cave entrance dimensions, there is a decreasing amount of information one can extract from the lidar data, and it tends to be less reliable. For instance, a two-metre wide entrance of pit will yield only a rough estimate of the entrance size and shape. If the pit is precisely vertical, the laser point reflection can in theory be obtained from the pit bottom. In reality, however, the pit may be oblique, and the laser scanner oscillates in a range of angles; therefore the maximum pit »depth« is typically underestimated. Nevertheless, even these relatively scarce data on entrance morphology enables us to identify the cave and ensure easy determination of its coordinates.

3.2. Small cave entrances

Often the smaller cave entrances may not be as easily recognizable from the lidar data. The pit may be very narrow, with no surrounding depression as a hint of its existence. Other obstacles include dense vegetation above the entrance, oblique direction of the pit, or plainly low lidar scanning density. If there is not a single reflection from within the pit, the method cannot be applied. One can only indirectly suspect the cave entrance based on neighbouring terrain configuration, which is indeed the case for all horizontal cave entrances. Nevertheless, as shown below, a single reflection from within the pit can enable positive cave identification, however, the interpretation is no longer straight-forward.

Let us discuss a case of such a cave. A typical map of the immediate neighbourhood of this cave is shown in Fig. 2a; it was generated with a standard 1 m grid size, using the »ground« class only. This is roughly what a common digital terrain model would give; a raster shaded relief would look similar too. On this map, there is no hint of a cave whatsoever. We may opt to decrease the grid size, in this case down to a rather unrealistic 0.25 m, but keeping the »ground« class only (Fig. 2b). There are several signs of oversampling, but beside a faint depression in the middle, nothing really hints

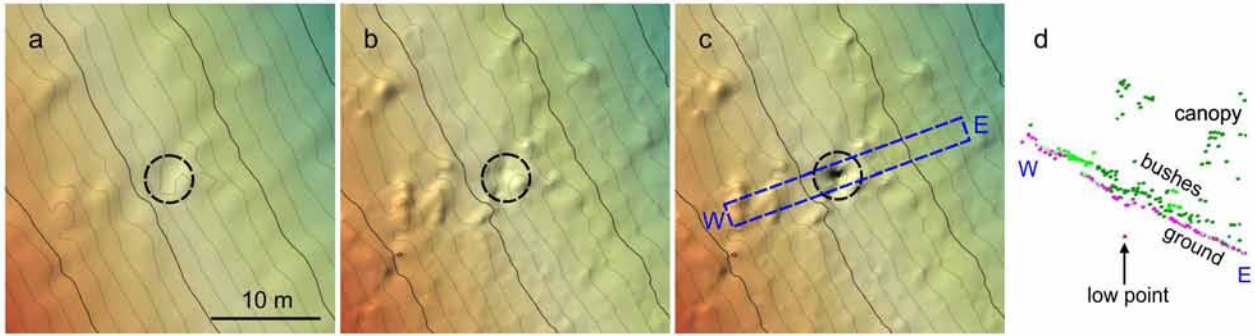


Figure 2. Example of a narrow pit with a single laser reflection from within: digital terrain model 1×1 m, class “ground” (a), same but grid reduced to 0.25×0.25 m (b), additional class “low point” included (c), point cloud in a narrow band across the cave (d).

at the cave entrance location, either. The inclusion of the class “low points” (Fig. 2c), though actually including one single point, convincingly changes the map outline, where a cave-like object is clearly visible. Whether this is really a pit or just a crevasse or the like, needs to be verified in the field.

Though more time-consuming, most information can be gained by looking the point cloud directly. A cross-section was extracted across the terrain as indicated in Fig. 2c (blue dashed line). The relevant point cloud section is shown in Fig. 2d with the single low point indicated by an arrow. The case presented proves that for cave searching standard digital terrain models, based on the “ground” class only, are not sufficient. Proper inclusion of relevant classes is crucial.

3.3. Advance planning of discoveries

As any caver knows, there are not many shortcuts if one wishes to discover new caves. The standard method is to browse across an area, hoping to find a new entrance. An experienced caver will indeed concentrate his search in more promising directions, but essentially the movement in the field is in most cases no more than blind search with sheer luck more contributing to a discovery than any planning.

In the previous cases we discussed about known cave entrance locations – how much information about the cave can be obtained using the lidar data. This technique can be used the other way around. In contrast to classic browsing the terrain, a lot of work can be done in advance at home, using the lidar data. In our experience, optimal stages for a fruitful discovery mission are the following:

1. Setup of the desired area. A 1×1 km area is a suitable size.
2. Extensive screening of the lidar point cloud data. Each potentially interesting object is recorded and evaluated (coordinates, pit depth). We do this manually, taking consecutive sections 100 m square, while in the future the task may be automated.
3. Construction of a standard topographic map with added symbols showing objects – possible cave entrances. This map is uploaded to each participant's GPS.
4. Terrain work. In contrast to classical browsing the cavers move from one object to another.

Using such a targeted approach the discovery rate is greatly enhanced. The team of cavers checks each object whether it

is an entrance into a cave. If unsuccessful at one object, they simply move to another. The cave presented in Fig. 2 was found using such a method. At the end we have to stress, that GPS is no longer a tool for cave coordinates determination with approach described above. The coordinates are evaluated for each object in advance, while GPS is only a guiding tool for orientation while conducting fieldwork. As an example, a field trip was organized according to the above mentioned stages. In only five hours of field work we were able to visit 18 previously designated objects. In eight cases there was nothing reminiscent of a cave entrance, so the origin of “low points” in the lidar data must have been an error, such as a double reflection. In six cases there was indeed a pit, but not meeting the national threshold of 10 m to be considered as a cave. Nevertheless four cases reflected true cave entrances.

3.4. Lidar evaluation of cave entrance locations, originally determined by GPS

In the final section we would like to focus on the cave entrance coordinates, determined by a hand-held GPS. The precision of these coordinates was evaluated looking at lidar data of these cave entrances. Fig. 3a shows an overview of all evaluations of the 112 cave locations (see section 2). Each point presents the degree of misplacement by GPS in comparison to the lidar data. The 112 caves were chosen in such a way that they were easily recognizable in the terrain: mostly pits, entrance diameter 1–5 m. Therefore the error of identification in lidar data does not exceed 2 m. The positional precision of the lidar point cloud as specified by the data supplier is 0.2 m. Thus by far the largest contribution to the misplacement comes from the imprecise GPS measurements.

The first observation is a net shift of measurements towards north. This is probably due to imprecise conversion from WGS84 to the local Gauss-Krüger coordinate system. The conversion parameters would be interesting to verify had the particular GPS unit been still in use, but this is anyway not the topic of this paper. Another feature worth pointing out are two faraway outliers (50 m each), followed by three moderate misses (around 30 m). To study the magnitude of misplacements it is better to present a distribution (Fig. 3b). A Poisson curve gives a reasonable fit with the most probable misplacement of 5 m and the average misplacement of 9.5 m (due to the long tail towards larger misplacements).

For years, GPS has been considered as “the ultimate” method of coordinate determination, achieving precision in the metre range. On the other hand, the negative influences of

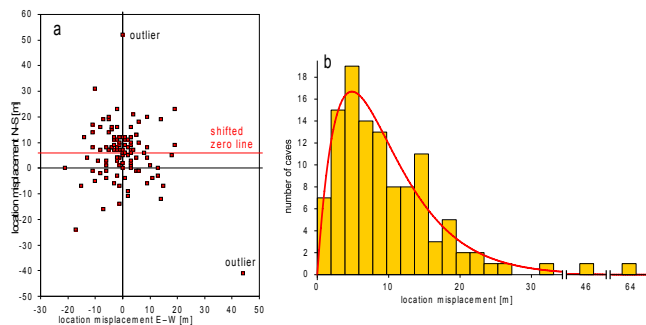


Figure 3. Location misplacement by GPS compared to lidar data: lateral (a) and distribution of magnitude (b).

shadowing by terrain and canopies, or poor satellite constellations, have been well known but not taken very seriously into account by amateur cavers. Metre digits in coordinates have become a norm. This study shows that an experienced caver has been reporting cave entrance coordinates with a 10 m error of measurement; one can only guess how large this error can be for a novice. In this respect, metre digits in coordinates may easily be rounded to zero. The only step further in determination of cave entrance coordinates is to use a GPS as a guideline only, while the precise coordinates are extracted from lidar data, as described above.

4. Conclusions

The lidar data enable an immense step forward in cave entrance evaluation. In metre-size entrances precise coordinates and altitude can be obtained routinely, while in large entrances (10 m pit diameter or above) we can also acquire quantitative data on basic morphology of the entrance.

If the original point cloud data are available, they should preferably be used because reflections from pits are often classified as “low points”, i.e. a class typically assigned to errors within the data. In lidar data for Slovenia, for instance, optimum combination of classification classes is “ground” and “low points”. Particularly for narrow pits, such a combination gives much better results than the standard lidar-derived data (digital elevation model, shaded relief). Nevertheless, even the lidar-derived data have a far better resolution than any topographic map.

Discovery of new caves can be planned in advance from home by a systematic analysis of the point cloud data for possible cave entrances. Afterwards, these objects are visited in the field by a point-by-point check, which greatly accelerates the cave discovery rate.

We also made a re-evaluation of cave entrance coordinates, which had been determined by a handheld GPS in the last few years. Taking more than 100 caves in consideration and applying the Poisson statistics, the average location misplacement was found to be 10 m, even though the measurements had been acquired by an experienced caver.

References

- Andrić I, Bonacci O, 2014. Morphological study of Red lake in Dinaric karst based on terrestrial laser scanning and sonar system. *Acta Carsologica*, **43**(2-3), 229.
- Čekada M, 2013. Statistical evaluation of cave location precision based on cartographic sources. *16th International Congress of Speleology*. Brno, Czech Republic, pp. 285-289.
- Čekada M, 2015. Contemporary cave exploration in Slovenia. *23rd Karstological School »Classical Karst«, Caves – Exploration and Studies*. Postojna, Slovenia, pp. 108.
- Čekada M, Gostinčar P, 2016. *Uporaba lidarja v jamarstvu (Application of lidar in caving)*. Založba ZRC, Ljubljana.
- eVode, 2016, <http://evode.arso.gov.si/indexd022.html?q=node/12> (access 28. Jan 2016).
- Kataster jam. *Jamarska zveza Slovenije*, Inštitut za raziskovanje krasa ZRC SAZU. Ljubljana, Postojna, Slovenia, 2016.
- Kobal M, Bertonec I, Pirotti F, Kutnar L, 2014. Lidar processing for defining sinkhole characteristics under dense forest cover: a case in the Dinaric mountains. *ISPRS Technical Commission VII Symposium*. Istanbul, Turkey, pp. 113-118.
- LAS specification, 2013. *The American Society for Photogrammetry & Remote Sensing*, http://www.asprs.org/a/society/committees/standards/LAS_1_4_r13.pdf (access 1. April 2016).
- Mongus D, Triglav Čekada M, Žalik B, 2013. Analiza samodejne metode za generiranje digitalnih modelov reliefa iz podatkov lidar na območju Slovenije. *Geodetski vestnik*, **57**(2), 245-258.
- Plan L, Decker K, 2006. Quantitative karst morphology of the Hochschwab plateau, Eastern Alps, Austria. *Zeitschrift für Geomorphologie*, **147**, 29-54.
- Triglav Čekada M, 2011. Možnosti uporabe zračnega laserskega skeniranja (LIDAR) za geomorfološke študije. *Geografski vestnik*, **83**(2), 81-93.
- Triglav Čekada M, Bric V, 2015. Končan je projekt laserskega skeniranja Slovenije. *Geodetski vestnik*, **59**(3), 589-592.
- Triglav Čekada M, Bric V, Mongus D, 2015. Napredne analize površja s podatki laserskega skeniranja Slovenije. *Zbornik posveta 43. geodetskega dne*. Ljubljana, Slovenia, pp. 59-66.
- Zhu J, Pierskalla W, 2016. Applying a weighted random forests method to extract karst sinkholes from LiDAR data. *Journal of Hydrology*, **533**, 343-352.
- Zini L, Calligaris C, Forte E, Petronio L, Zavagno E, Boccali C, Cucchi F, 2015. A multidisciplinary approach in sinkhole analysis: The Quinis village case study (NE-Italy). *Engineering Geology* **197**, 132-144.

Caveink - a set of Inkscape extensions for drawing cave maps

Mateusz Golicz

Affiliation: Polski Związek Alpinizmu / Polish Mountaineering Association, ul. Corraziego 5/24, 00-087 Warszawa, Poland, caves@pza.org.pl

Abstract

Caveink, developed between 2012 and 2016, is a set of extensions facilitating laying out cave maps in generic drawing software. Itself free and open source, *caveink* is specifically designed for Inkscape, an open source vector drawing program, available for free download even for commercial use. Building up on previous work by Thomas Holder, it extends Inkscape with Survex and PocketTopo import capability, basic cave map symbols and line styles, as well as tools for generating grids, depicting intersecting passages and - in simple cases - adjusting maps for loop closures. Although inherently lacking the flexibility of Therion, *caveink*-extended Inkscape is very easy to learn for beginners and as such since 2013 is taught on annual introductory surveying courses in Poland.

Keywords: cave maps, symbol library

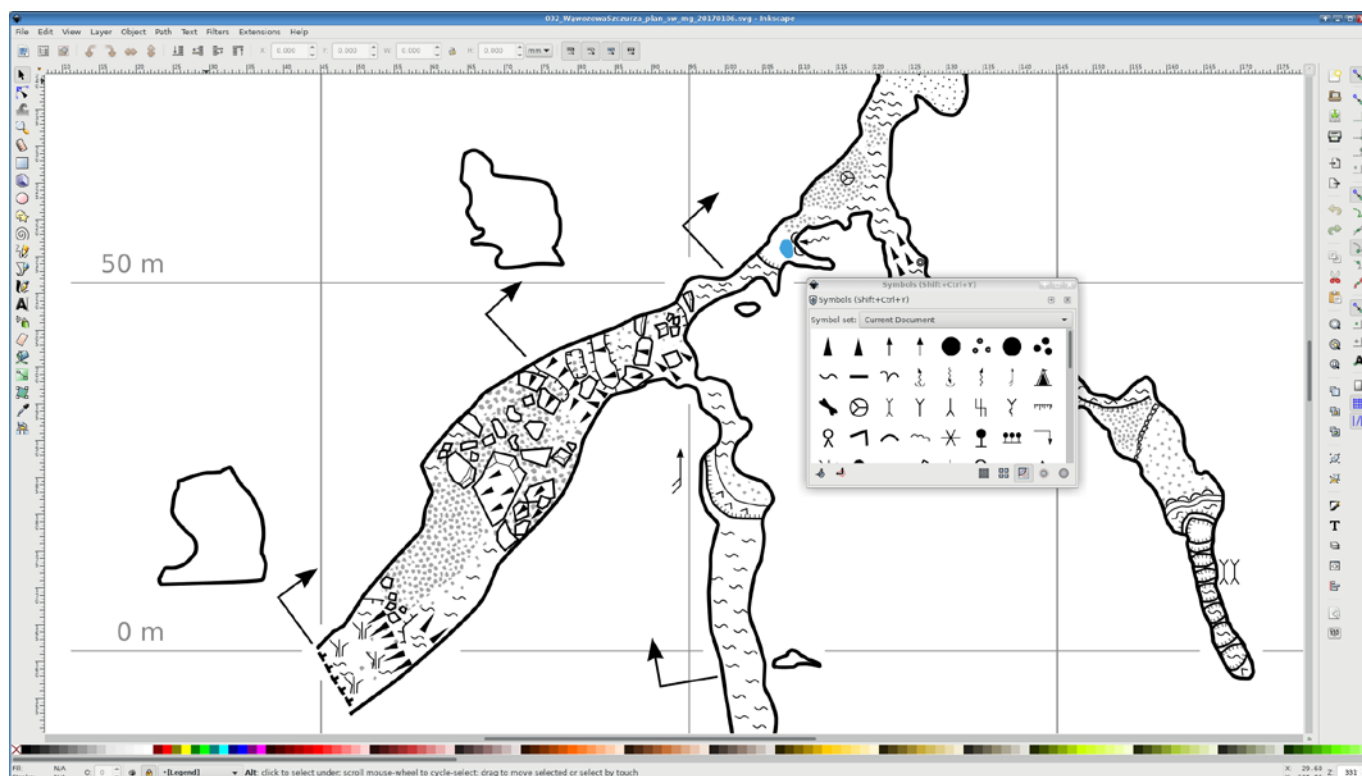


Figure 1. A fragment of a real life cave map created with *caveink*-extended Inkscape. The symbol library window is visible open in the foreground.

1. Introduction

Compared with a variety of survey data processing software - such as Survex, Walls, Therion, PocketTopo, TopoDroid, Compass etc. - the choice of computer software designed specifically for drawing finished cave maps is currently very limited. Cartographers all around the world either use Therion (Mudr'ak and Budaj 2016) - up to date the only widely known comprehensive cave surveying software package - or resort to generic drawing, publishing or engineering software, such as Adobe Illustrator, Corel Draw or AutoCAD. Both solutions have significant drawbacks, Therion being complex to learn and use for surveying novices and generic software requiring much manual work from the cartographer when it comes to laying out complex cave systems, closing survey loops or assuring

that a consistent set of conventional symbols is used on a collaboratively created cave map.

Some of the latter issues can be mitigated by using specialized extensions or symbol libraries. This paper presents an author's overview of a relatively new solution called *caveink*. It is essentially a collection of extension scripts for Inkscape (Bah 2011), a free and open source vector graphics editor conforming to Scalable Vector Graphics (SVG) specification. *Caveink* adds a few caving oriented features through drop-down menus and hotkeys. In order to use *caveink*, the cartographer either installs Inkscape on their computer using a special installer or manually copies files into an already existing Inkscape installation directory. Besides the scripts, *caveink* comes with SVG files replacing the default pattern fills and enriching Inkscape's symbol library.

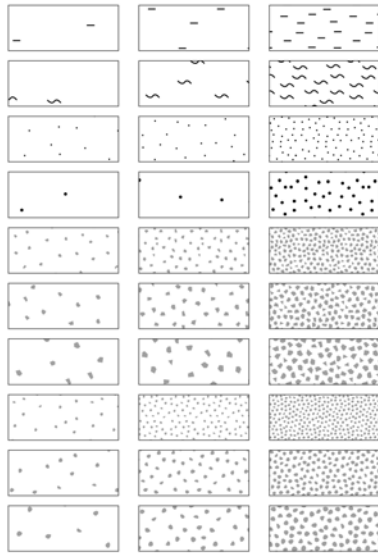


Figure 2. Predefined fill patterns included in caveink.

2. Covered issues

2.1. SurveX and paperless data import

Drawing a cave map in Inkscape begins with loading a sketch into canvas and aligning it with survey centerline, which in absence of a well-defined surveying coordinate system serves as the main reference for all other elements of the map. Therefore, *caveink* extends Inkscape to support two extra input file formats, namely SurveX processed survey data (.3d) and Pocket Topo drawings in the Therion Export format (.the). The input filters are configurable, allowing for scale adjustment, different projections and suppression of splay measurements. Obviously, a paper scan can also be used as a background through a raster file import feature, which is available in Inkscape by default.

2.2. Symbols and carpeting

Starting from version 0.91, Inkscape features a convenient symbol palette feature. Upon selecting Object / Symbols, a docking window with pre-defined symbols appears outside of the canvas. Symbols are placed onto the drawing by simply dragging them from the palette to the drawing area.

This function is perfect for cave map symbols depicting formations or hydrology, as well as for arrows indicating gradient and cross-section planes. *Caveink* adds a basic symbol library (Figure 1) conforming to guidelines of International Union of Speleology (UIS) working group on cave survey and mapping (Neumann 2016). Another set of symbols, featuring a few rocks and pebbles in various shapes and dimensions is also provided. With a small script invoked via a hotkey (Alt+3) one or more rock symbols can be “stirred”, that is randomly rotated and randomly exchanged into another rock shape without scaling.

The symbols are in fact inserted by reference rather than by duplicating. Thus, in future it is theoretically viable to implement switching to another symbol set without editing the drawing.

Although it is possible to duplicate a symbol many times to indicate a whole area covered by sediments or debris, it is not

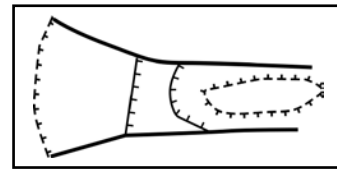


Figure 3. Dripline and step lines as rendered by caveink.

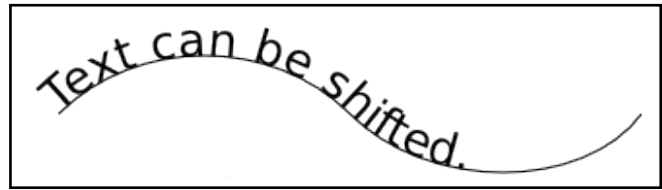


Figure 4. Typical usage of text-on-path (source: Bah 2011)

recommended, since in the end thousands of individual entities to re-draw make Inkscape perform slow when navigating the canvas (panning or zooming). Instead, it is better to draw a polygon defining the actual area and fill it with a repeating pattern, which is much faster to render on screen. *Caveink* replaces default Inkscape patterns with a set of more cave oriented designs, such as gravel or silt (Figure 2). Even though the patterns have to be repeating by design, they are prepared seamlessly and with a touch of randomness, so that the repetition is evident only on very large areas.

2.3. Line styles

Cave map line styles such as ceiling feature/dripline or step/pit symbols (Figure 3) are by their nature nonsymmetrical, which makes them impossible to describe using standard SVG provisions for line styles. It is therefore difficult to draw these lines conveniently with stock Inkscape. Drawing the perpendicular ticks manually, as individual objects, is tedious. A slightly faster option is to turn a single tick into a so-called mid marker, which is rendered by Inkscape at every control point of a line. Yet, this requires creating a lot of artificial control points wherever a tick should appear, which in turn obstructs editing the line should it be necessary.

Another way around is to use the text-on-path function, which was originally designed for creative text artwork (Figure 4). Instead of a meaningful text, a repeating string of punctuation characters is placed along the line representing a step or a ceiling feature. The original line either stays on the drawing (in case of steps) or is made invisible through suitable application of object transparency (in case of dripline or ceiling feature).

This method is available in standard Inkscape, although it requires a couple of steps to complete. *Caveink* adds a script that automates this process and binds it to a hotkey, so that the cartographer may just draw a line and press Alt+1 or Alt+2 to turn it into a step or dripline respectively.

Albeit theoretically standard ASCII characters (such as “T” or the vertical bar “|”) could be used for this technique, for better effects and for historical reasons, *caveink* provides a special font.

2.4. Overlying passages

Making a readable map of a cave featuring multiple levels often requires a lot of creativity and effort on the part of car-

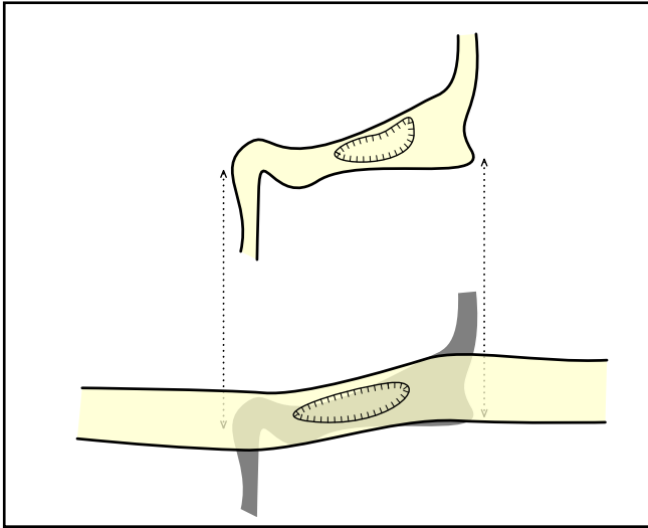


Figure 5. An offset copy that clarifies overlapping passages (source: Mudr'ak and Budaj 2016).

```
map m12
  m1
  break
  m2 [0 8 m] below
endmap
```

Figure 6. Therion code for automatically generating an offset copy (source: Mudr'ak and Budaj 2016).

topographer. Layered drawing composition, now a standard tool in vector or raster drawing software, makes it easy to work on overlying passages by simply making all cave levels but the currently edited invisible. The final drawing however has to somehow include information about all the levels, which often means the detail of lower levels will be obscured by overlying passages, even if the latter are made semi-transparent on the drawing.

A standard approach to this problem is to draw an offset copy of the ambiguous fragment that emphasises detail on the passages obscured on the original drawing (Figure 5). With Therion, an adequate code (Figure 6, see also Mudr'ak and Budaj 2016) can generate such an offset copy automatically. However, when using any generic drawing software, following this approach usually means additional tedious work involving cutting fragments from original drawing and arranging them differently. What is even worse, if the drawing has to be updated, obviously both the original and the offset copy require cartographer's attention.

Caveink makes a novel use of SVG cloning to slightly reduce the burden normally associated with offset drawing copies. By drawing a defining shape (typically a rectangle) and invoking a script through a suitable menu option, a fragment of drawing is copied by reference and can then be shifted to an offset position. Although this fragment is automatically updated every time the main drawing is edited, it retains its own layer order. This means the cartographer can position the drawing layers so that the normally hidden passages are on top, create a snapshot of this picture, return the layers to their proper order and then position the snapshot close to the obscured

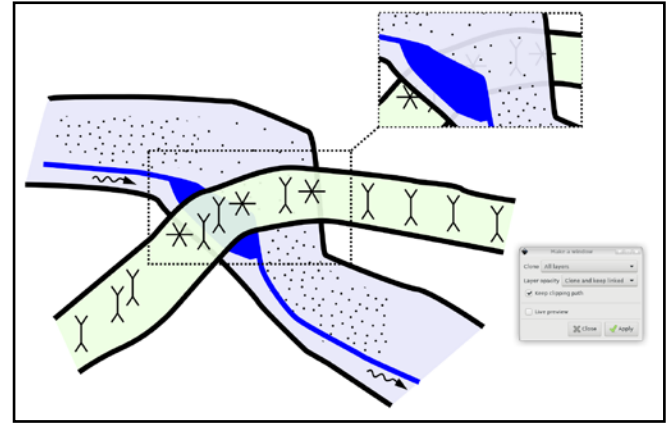


Figure 7. An offset copy created in Inkscape using *caveink*.

fragment (Figure 7). Since the snapshot is a linked copy rather than a simple duplicate, any changes in the main drawing are immediately propagated to the snapshot.

2.5. Merging drawings

When drawing cave maps, it is sometimes desirable to divide the tracing to be done among a couple of members of an expedition team. After everyone finishes their drawing, the final map has to be assembled from a few files.

Unfortunately, Inkscape features only basic merging capability, that can be used by importing a whole document as an object embedded in another document. The layer structure of the imported document is hidden and there are no provisions to easily merge layers.

It is possible to manually split the imported document into groups containing the original layers and move them one by one into the corresponding layers of the target document. However, with many layers and many files to merge this is again tedious.

Caveink installs three scripts that can be invoked through Inkscape menu to aid in this process. With the first one, a whole document is packed into a single object that preserves layer structure. This object is then easily copied between Inkscape windows into a new layer in the target document. Upon selecting the second script, the object is unpacked back into its original layers, that now become sublayers of the newly created layer. The third script merges all layers that have identical names. This way, efficient collaboration only requires coordinating layer names - or simply starting work from a common template file with all the required layers already defined and named.

2.6. Final touch: grids and scalebars

Caveink provides minor utilities to quickly draw grids and scalebars, so that the cartographer's time is not wasted on these trivia. Contrary to default Inkscape grid generators, *Caveink* automatically generates a grid matching a selected scale and density. The grid may also be automatically annotated with coordinates placed next to every lattice line. The grid's extent and origin can also be easily specified by drawing two rectangles that are selected before invoking the suitable menu item.

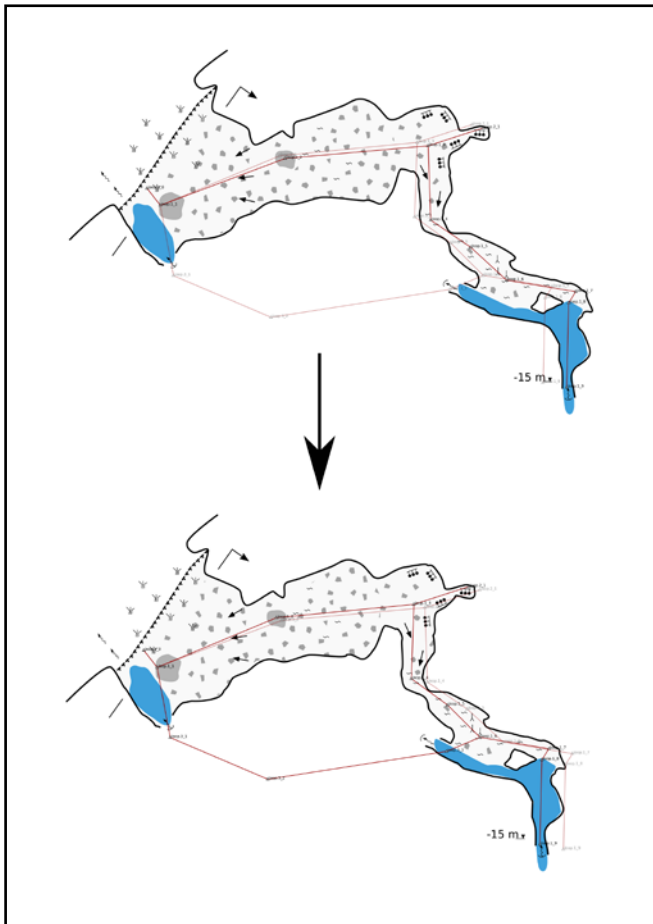


Figure 8. Adjusting drawing for loop closures with *caveink*.

2.7. Splitting into pages

The SVG format – and in turn, Inkscape – does not support multiple pages within a single document. Thus, it is difficult to split a cave map into a few paper sheets should the chosen scale demand it. While it is obviously possible to edit each page as a separate document, it is not practical. Usually some overlap between pages is required near the page edges and having every page in a separate document implies a lot of copying between the documents and even more redundant work when a fragment of the cave map near a page boundary requires updating.

Fortunately, the cloning technique, as outlined in the section about overlying passages, can also be used on a larger scale. With *caveink* it is possible to draw the map as a whole and then define each paper sheet as an offset copy, sized adequately to the paper size. The copies may overlap and it is also viable to have a few sets of copies for printing on different paper sizes. The copies are made by reference and not by duplication, which means that any changes to the map itself only have to be done once, on the main drawing.

One problem with this method is that the pages have to be extracted one at a time as PDF files, using an Inkscape option to limit the PDF export area to a particular drawing fragment (where the offset copy defining the page has been placed). Every page is saved as a separate file and combining them into a multi-page cave atlas requires using external tools.

2.8. Closing loops

One important and frequently worked around (eg. Fish 2015) drawbacks of laying out cave maps in any generic drawing software is lack of provisions for adjusting the drawing in case the centerline changes. It is indeed a serious problem in case of maps of caves that are still being explored. Whenever the survey stations are moved, for example due to resurveying, distributing an error of a loop closure or simply locating a blunder, the drawing has to be manually edited to match the new station positions. This is especially tedious in case of loop closures in large caves, since the relative movement of stations is then minute, yet it adds up to a noticeable error vector. Thus, it is neither viable to simply move a whole section of a drawing nor leave the drawing as it is. Every object on the drawing has to be slightly moved and some (such as gradient arrows) even have to be rotated.

Caveink includes an experimental script to facilitate this process. The feature is invoked with two sets of survey stations on the drawing, each on a separate layer. One of them is considered the original survey to which the rest of the drawing is referred. The other one is supposed to be the new survey. The stations have to be labelled, with every station symbol grouped together with its label. All station labels from the original survey should be present in the new survey.

Upon selecting the suitable menu item, all visible objects on the drawing are referred to their nearest stations from the original survey and then moved by the same vector the closest station is displaced between the two surveys (Figure 8). In case of linear objects (SVG paths), this process is actually performed for every control point of the line.

Optionally, the second closest station can be identified. By analysing changes in relative placement of the two closest stations between original and new centerline, *caveink* is able to appropriately rotate objects on the map or even adjust their distances to their closest stations.

It is worth noting that by using this feature creatively, it is also possible to morph traces of paper sketches to match real centerlines. Its most important limitation is the assumption that every object on the canvas is referred to the geometrically nearest survey station, which could not necessarily be the case in complex caves.

3. Limitations and known issues

With Inkscape, the whole cave map is edited as a single file, with all of its contents being rendered even when the cartographer is working just on a section of the map. Rendering time increases with drawing complexity, especially with the number of individual objects present on the canvas. As such, even most powerful computers running Inkscape for drawing cave maps have a practical limitation on the size of the cave being mapped. If too many lines and symbols are present, Inkscape becomes unresponsive. For a typical modern ultrabook computer w/double core Intel i7 CPU and 8 GB of RAM, this limit is on the order of 10 kilometers at 1:1000, although it could be much more or much less, depending on average passage width, amount of detail and patience of the cartographer.

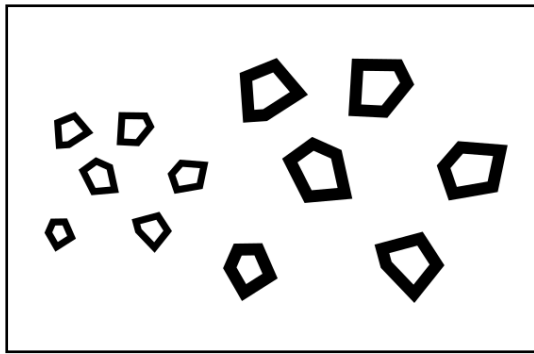


Figure 9. According to SVG specification, contour lines should be scaled along with the objects. This is not always what is desired on cave maps – bigger rocks should not necessarily have thicker edges.

Currently *caveink* requires a special font in order to render dripline/ceiling feature and step/pit line styles. Although it does not matter when publishing the map in PDF or any raster format, it results in these line styles wrongly rendered when opening the original SVG map file on a computer that does not have *caveink* installed. Most probably, in future releases *caveink* will switch to so-called path effects for rendering line styles. This way, until recently not viable due to frequent crashes of Inkscape when using path effects, SVG files created with *caveink*-extended Inkscape will become compatible with default Inkscape installations and possibly other software supporting the SVG specification.

Another two minor annoyances are related to carpeting patterns. As of version 0.92, Inkscape duplicates patterns for every object that is assigned a specific pattern fill (eg. silt, sand, debris). This results in unnecessarily large files. Also, although patterns can be readily scaled when applied to a particular shape (area), in accordance with SVG specification, the contour lines of objects forming the pattern are scaled as well. It is particularly an issue when filling areas with symbolic debris. If the cartographer wishes to indicate an area with larger debris fragments, scaling the pattern results not only in larger rock symbols, but also in thicker outlines of these symbols, which appears inconsistent. As a workaround, *caveink* provides gray, solid-filled debris, without any outlines (Figure 9). If this is not in line with the desired map style, the cartographer has to resort to placing multiple individual rocks instead of pattern fills.

Filling of a cave outline with a solid background, if desired, still has to be done in a manual way. A semi-automatic script for facilitating this task is viable and likely to be included in future releases of *caveink*.

Even in the digital age, cave maps are still drawn to scale. Like on any other map, the amount of detail on a cave map obviously should vary according to scale or, nowadays, zoom level. If a cave is to be presented in radically different zoom levels, for example in an atlas consisting of an overview map and detailed sheets, Therion is able to automatically adjust the level of detail to the requested map dimensions. On the contrary, with a generic drawing program such as Inkscape, the map has to be drawn from scratch every time a radical

change of scale is required. This problem is unlikely to be solved, since it is deeply linked to limited awareness of drawing software about the actual canvas contents.

4. Summary

Caveink-extended Inkscape is a practical software package for drawing small and medium sized cave maps. Whereas in terms of flexibility and task automation it is far outperformed by Therion, it is very easy to learn due to its inherent what-you-see-is-what-you-get nature and a good generic drawing interface, resulting from much more people working on the software. Between 2013 and 2016 six basic surveying courses in Poland were conducted, with Inkscape introduced as the software to trace the student's first cave map with. Of the more than 120 attendees, most were able to grasp the basics and trace a scan of their debut A4 or A5 sized map within two hours.

Caveink-extended Inkscape has also been the exclusive software technology in use for drawing finished cave maps on five Polish expeditions to China between 2012 and 2016. Due to limited human resources, the management of these expeditions asserted that every member of the team has to be capable of surveying and drawing a clean copy of what they discover, preferably within a few days after field work. With modern paperless surveying technology in place underground and *caveink*-extended Inkscape on the surface, this assumption proved viable (Figure 1), with over 43 km of cave passages mapped using *caveink* (Ciszewski *et al.* 2014).

Despite these successes, *caveink* has to be still considered work in progress, although public releases are available from the author's web page (<http://jaskinie.jaszczur.org/>) since 2013.

Acknowledgements

Thomas Holder authored the original Survex import filter and scalebar generator that are now part of *caveink*.

References

- Mudr'ak S., Budaj M., 2016. *The Therion book*. Therion home page, <https://therion.speleo.sk/downloads/thbook.pdf> (access 30 Jan 2017).
- Bah T., 2011, *Inkscape: Guide to a Vector Drawing Program, Rough Cuts*, 4th Edition, Prentice Hall, London
- Neumann A., 2016, *Cave symbols: The official UIS List*. <http://www.carto.net/neumann/caving/cave-symbols/> (access 30 Jan 2017)
- Fish L., 2015, *Merging and Morphing (Round tripping)*. Compass cave survey software tutorials. <http://www.fountainware.com/compass/Cartography/MergeMorph/MorphMerge.htm> (access 30 Jan 2017)
- Ciszewski A., Ciszewski M., Golicz M., Ramatowski P., 2014, *Caves of shizilu area*. Pracownia Kreatywna Bezliku, Kraków.

(Abstract) **Three-dimensional cave mapping using Structure from Motion**

John Hellstrom

Affiliation: School of Earth Sciences, University of Melbourne, Parkville, Victoria

Abstract

Structure from Motion (SfM) is a photogrammetric technique in which surfaces can be characterised in three dimensions using redundantly overlapping photographs. It is commonly used in high-resolution mapping of the earth's surface using unmanned aerial vehicles, and for producing models of discrete objects. In archaeology it is used for documenting sites, including rock shelters and short sections of cave, and artefacts. It is a rapidly expanding field in the geosciences where it is being used as an accessible alternative to more expensive imaging techniques such as airborne lidar.

SfM is a highly effective technique for imaging caves, incorporating all surfaces which can be seen from at least two different positions. The only input data required to produce an accurate colour three-dimensional model are overlapping photos. To scale and orient the model requires either three or more independently surveyed ground points, or the inclusion of objects of known scale and orientation within the source photos. The models can be stored and viewed using common 3D object file formats, and plans and elevations produced from them. These plans have been found to be surprisingly accurate when compared to traditional cave survey techniques, for caves of up to at least 1000 m in length.

Cave imaging by SfM requires good lighting and a sensitive, wide angle camera. Constricted passages require several photos per metre of centreline to successfully map, whereas large chambers require only one photo every several metres. It is possible to map at a rate of between 100 and 1000 metres of passage per hour. The cave needs to be lit either by multiple fixed light sources placed in the cave or by a single light source close to the camera. An alternative is to use a helmet-mounted camera set to record high-resolution video from which individual frames can be extracted at a later time. Construction of models from the photographs can be achieved using commercially available software.

SfM cave models are an aid to research conducted within caves, allowing insight into cave structure and calculation of accurate chamber volume. They allow three-dimensional location of objects investigated or collected, and the in-context visualisation of resulting data such as speleothem ages and geochemical properties. With increasingly powerful computers and some customisation of data processing workflows it is likely that large and complex cave systems will be able to be mapped in this way.

3-D Imaging As A Tool To Understand Speleogenetic Processes

Stephan Kempe and Ingo Bauer

Affiliation: Institute of Applied Geosciences, Technische Universität Darmstadt, Schnittspahnstr. 9, D-64287 Darmstadt, Germany, email: kempe@geo.tu-darmstadt.de

Abstract

Cave morphology is the sum of past speleogenetic processes. So far, morphology was mostly dealt with descriptively. With the advance of light-weight, battery-powered 3D-laser-imagers, it is now possible to scan entire caves in high resolution, making it possible to do morphometrics in unprecedented detail, including features along high ceilings. Details such as joints, bedding planes, faults, speleothems, breakdown, fossils, scallops, karren, cupolas, water levels, sediment profiles and other features become accessible to quantitative analysis and scientific evaluation. Here we present examples from several caves in Germany that were scanned with a Faro 3D-S 120 Scanner operating with an IR laser of the wave length of 905 nm at 20 mW.

Keywords: Cave surveys; laser scanning; 3D survey; morphology; speleogenesis; applied karstology

1. Introduction

Cave surveying has seen a long history. From the first sketches of cave outlines to maps having scale and direction we have seen steady improvements. These improvements are not so much a question of grid accuracy because cave surveys were often done by mining surveyors, who already used high-accuracy methods. An example of such a high-grade survey is the first comprehensive map of Postojnska jama of 1833 conducted by the surveyor Johann Fercher and his team from the mercury mine at Idria (Kempe 2005). Scientific mapping on the other hand, is not so much depending on a high accuracy grid, but on the observation, documentation and survey of specific details in a cave. The difficulty is to do this quantitatively because 3D documentation with standard survey techniques, i.e. compass, inclinometer and tape, is almost impossible. 3D laser imaging has solved this problem.

2. Methods

We used a Faro 3D-S 120 Laser scanner (Fig. 1) to survey and document a variety of caves in Germany. The scanner uses an IR wave length of 905 nm at 20 mW and has a range of up to 120 m. It rotates horizontally from -60° to 60° and horizontally 180° , thereby covering almost an entire sphere, except for a narrow cone below the scanner. Therefore, even high ceilings can be scanned in detail. The scanner has a built-in compass and level. Therefore, it can be mounted on a standard tripod and leveled by eye-sight. Thus, the instrument can be relocated within minutes. Up to 900 points can be scanned per second. The instrument stores direction, azimuth and distance and a reflectance value that gives the scan cloud the appearance of a black-and-white picture. If ambient light is available, color can be recorded as well. At a distance of about 10 m, accuracy is about 1 mm. A typical station with 40 million points takes a few minutes. If higher resolution is intended, a scan can take up to 10 min. In order to link stations with one another, white reference balls, 14 cm in diameter, are used (Fig. 1). At least three of them should be placed within a range of 4 to 10 m visible from consecutive stations. One battery charge allows up to 30 stations, a normal day's survey work. Extra battery packs can easily extend this. Point clouds are processed by the Program SCENE by Faro.



Figure 1. The Faro Scanner in the Binghöhle/Franconia. The instrument is programmed by a touchscreen. A standard tripod can be used and the instrument is self-levelling. Note the three 14cm-reference balls on the floor that are used to link one station to the next by the SCENE program. The cave has seen turbulent flow as witnessed by scallops on walls and ceilings

3. Caves scanned

These caves were scanned representing a range of different genetics, morphologies and applied questions:

- Himmelreichhöhle, South Harz, a cave in anhydrite, representing a large (110 * 80 m) hall vaulted by breakdown through which a railroad tunnel was built.
- Barbarossahöhle, Kyffhäuser, also an anhydrite cave, developed by epigene and hypogene waters and enlarged by shedding wall-slices due to gypsification.
- Jettenhöhle, South Harz, a cave in gypsum, developed at the water table by upwelling (hypogene) groundwater and expanded upward by breakdown.
- Iberger Tropfsteinhöhle, Upper Harz, a cave in Devonian reef-carbonates, developed by hypogene siderite weathering (as a source of acidity).

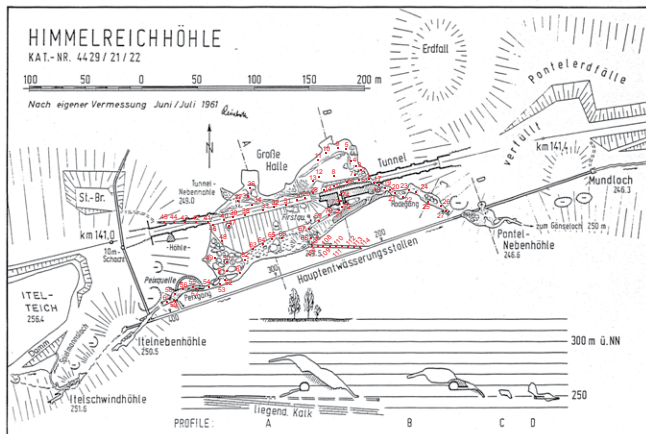


Figure 2. Map and cross-sections of the Himmelreichhöhle (Reinboth 1970) including scan stations (Legner 2014).

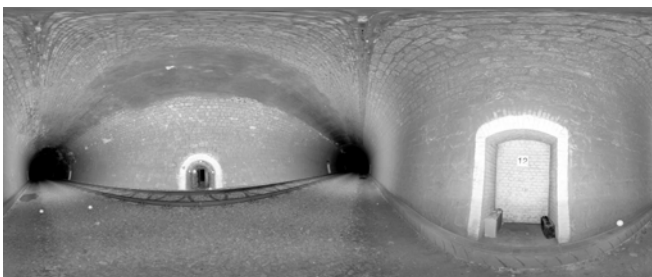


Figure 3. The railway tunnel in scanned panorama view, note that only one track is left because of safety concerns. Across the track on the left the entrance to the cave is seen. On the right a waiting-niche to be used when a train comes through.

- Geisloch, Franconian Alb in upper Jurassic limestone, a large hypogene hall with rich speleothems damaged presumably by glacial cave ice.
- Binghöhle, near the same location, an epigene cave scanned for scallops and other flow features.
- Grotta del Paranco, Italy, scanned for speleothem damage and tectonic situation.

3.1. Himmelreichhöhle

This 580 m-long cave (Fig. 2) is developed in anhydrite of the southern Harz Mountains (Werra Series of Upper Permian Zechstein; Reinboth 1970) (gypsum and anhydrite cave lengths see Kempe and Helbling 2000). It was formed by a creek creating one of the largest cavities in Germany. Not knowing that the Himmelreich-Ridge contained a cave, a railroad tunnel was planned through it as one of the early German E-W routes. When the cave was encountered, the tunnel had to be constructed inside the cave (Fig. 3). Because of the ever-present danger of breakdown, the tunnel was covered with a thick cushion of earth. Today one can walk on top of the tunnel among the breakdown blocks that fell in the last 150 years (Fig. 4). Scanning tunnel and cave therefore served to document ongoing breakdown and to monitor the state of the tunnel that may be subject to damage both by heavy rock fall from above as well as by further leaching of the anhydrite below it.



Figure 4. Standing on top of the railroad tunnel. Note breakdown blocks in foreground.



Figure 5. Anhydrite slab detaching from ceiling due to gypsification. Note that the detachment is across the lamination not along it.

3.2. Barbarossahöhle

This large, 670 m-long anhydrite cave formed along the water table is in a similar stratigraphic position as the Himmelreichhöhle, but situated at the Kyffhäuser. It was discovered by miners prospecting for the copper shale below the Werra anhydrite. Today a show cave, it features the processes of gypsification: Along ceiling and walls the finely laminated anhydrite detaches in thin slaps curving away from the wall (Fig. 5). Scanning serves to document “growth” of these unusual “speleothems”. It is known that they form within years, but exact time estimates on curving and detaching are missing. Specific areas were marked for repeated scanning in a few years to measure alterations.

3.3. Jettenhöhle

The 750 m-long Jettenhöhle, a voluminous gypsum cave developed within the shallow groundwater that has grown upward by breakdown, is situated in the South Harz in the Leine Series of the Zechstein. Since its last survey (Kempe *et al.* 1972), large blocks have fallen from the ceiling. We scanned the cave to resurvey it and to have a documentation of the state of all breakdown, which could not be done by conventional surveying (Fig. 6).

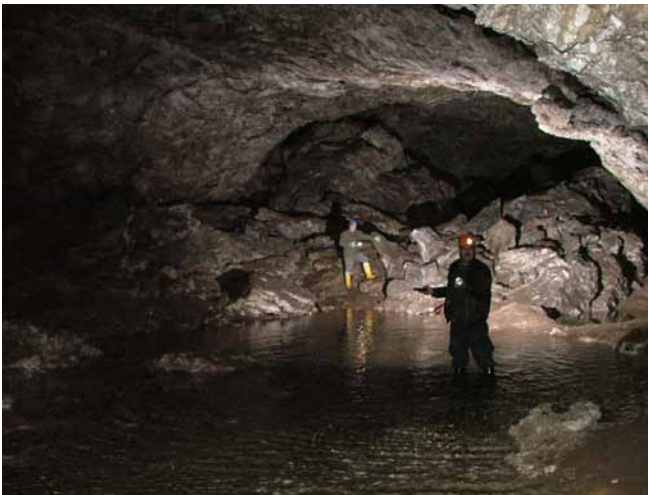


Figure 6. The Jettenhöhle, a large gypsum cave growing upward by breakdown.

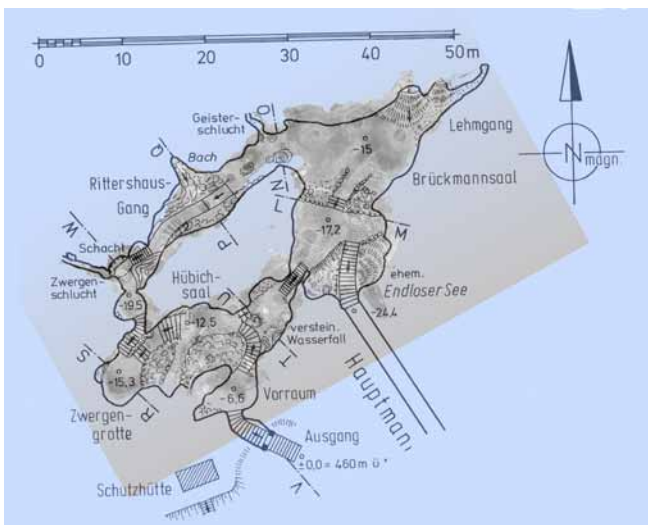


Figure 7. Scan (grey) underlying the conventional survey of the main part of the Iberger Höhle showing a very good agreement.



Figure 8. Lateral, horizontal W-ward view of the entire Iberger Cave. Main section as in Fig. 7 is on the right. Access-tunnel intersected three more isolated chambers.

3.4. Iberger Tropfsteinhöhle

This cave is developed in the Iberg, Harz Mountains, a Devonian isolated reef-block (Kempe *et al.* 1985). It was discovered by iron ore miners and employed in the 18th century as a show cave. It is morphologically a typical hypogene cave, featuring cupolas and side-wall facets (Kempe *et al.* 2016). It is probably the only show cave formed by CO₂-released by siderite weathering (Kempe 1975). An access passage drilled in 1910 discovered more cavities, unknown before. The scanned cave, viewed from above, is very close to the existing cave survey (Fig. 7) but also allows the view in slanted or horizontal view (Fig. 8). Using cuts from the point cloud one can study the morphology of phreatic, hypogene cupolas (Fig. 9).

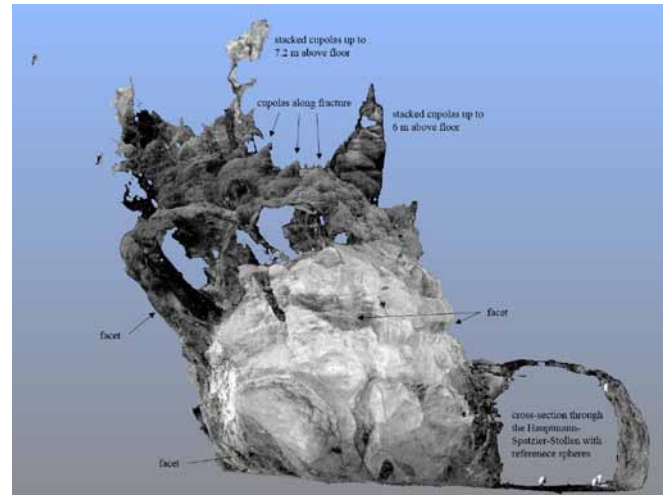


Figure 9. An isolated room (O. Klingebiel Grotto) intercepted by the artificial passage (to the right). This view shows the upward directed stacks of cupolas indicative of slow phreatic convective cave genesis due to internal CO₂-generation by siderite weathering (Kempe *et al.* 2016).

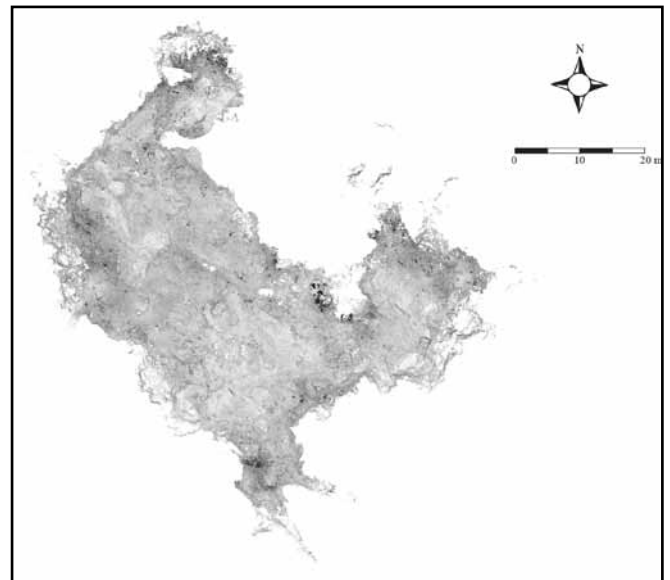


Figure 10. Top-view of the scanned main hall of the Geisloch (Fenzlein 2015).

3.5. Geisloch

The cave is situated in a dolomite knoll of the upper Jurassic (Malm) in the Franconian Alb, Northern Bavaria. The cave is famous for its pristine speleothems. Pristine in the sense that it has been protected from anthropogenic impact. Nevertheless, the speleothems show massive damage, albeit by natural causes. Scanning the cave (Fig. 10) and its speleothems (Fig. 11) has substantiated the hypothesis that this damage is caused by glacial cave ice and not by earthquakes, an otherwise popular but largely unfounded hypothesis in the literature. Similar damage patterns are reported from many other speleothem-rich caves as far south as Slovenia (e.g., Kempe 2004; Will 2013). One of the most striking damages observed are stalagmites broken off the base, moved by a few centimeters but not toppled (Fig. 12). Scanning allows to quantify numbers, sizes and directions of deposited fragments (e.g. Fenzlein 2015; Soares de Araujo 2016).

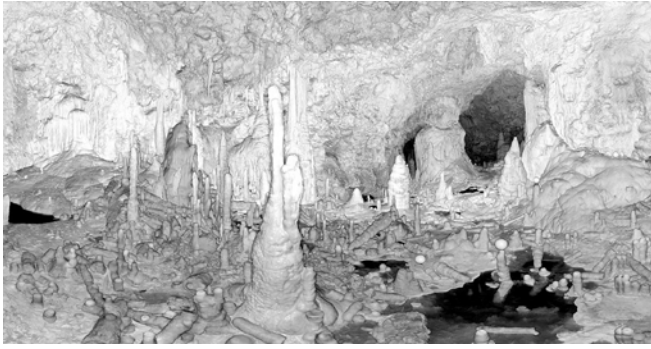


Figure 11. Scanned view of the interior of the Geisloch. Note the large number of naturally broken speleothems, specifically toppled stalagmites, traces of a glacial ice fill. Note the two reference balls on the lower right with 14 cm diameter for scale (Fenzlein 2015).



Figure 12. Broken and shifted but not toppled stalagmite from the Geisloch.

3.6. Binghöhle

The ca. 300 m-long cave (Brand *et al.* 2006), located not far from the Geisloch, is also developed in Malm deposits, although in the lagunal facies comprised of thick limestone strata. The cave, today a show cave, is one of the few caves in Franconia with the morphological evidence (scallops) of turbulently, laterally flowing water (Fig. 1). The cave essentially is one continuous passage plugged upstream by glacial mudflows and decorated with speleothems, many of them also broken by cave ice. The cave was scanned to illustrate its tectonic situation (Wiesler 2016). The cave is rather horizontal while the bedding is sloping steeper into the same direction. Therefore the water had to shift upward to higher bedding planes along vertical joints. In addition to the tectonically interesting results, U/Th dates were obtained. One of those showed that the current set of scallops was formed also on a speleothem aged 225.2 ± 8.62 kaBP (U/Th date, Dr. P. Fohlmeister, Heidelberg, Lab 6843 Bing 2) (Fig. 13). This corresponds to the end of the warm phase Marine Isotope Stage (MIS) 7e. The next speleothem generation rest on the mudflow and is dated to 189.9 ± 8.26 ka BP (Lab 6844, Bing 3), i.e. to the warm stage MIS 7a. Thus, the last scallop-forming



Figure 13. Scallops developed on a wall-speleothem dated by U/Th to 225 ka BP (MIS 7e).

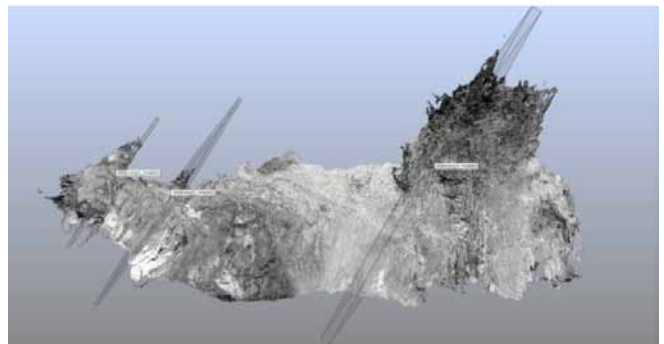


Figure 14. The faults in the large hall of the Grotta del Paranco (view to $130^\circ/-30^\circ$) (Both 2016).

event and the consecutive mudflow clogging the upstream section of cave must have occurred in the cold phases within MIS 7, a very interesting and controversial date that has far reaching consequences on the history of the valley incision of the Franconian Alb.

3.7. Grotta del Paranco

The 157 m-long cave is situated near the Grotta Gigante, a famous show cave in in the classical Karst near Trieste in Upper Cretaceous limestone. Its two large halls were scanned to analyze the cave's speleogenesis and tectonic situation (Both 2016) (Fig. 14) and its natural speleothem damage; (Soares de Araujo 2016) (Fig. 15).

4. Outlook

3D-scanning of caves has opened an entirely new dimension of documentation and scientific interpretation of caves. The most obvious is that the scans, viewed from above or laterally, allow to draw much more accurate cave maps and projected longitudinal sections. This is because the internal compass and level, as well as the concatenation technique among the various stations is less prone to surveying mistakes made by the human cave surveyor. Furthermore, scans will allow exact calculation of cave volumes and sizes of specific details can be measured in three dimensions and directions (Fig. 15). Morphologically, the essence of different cave types and their

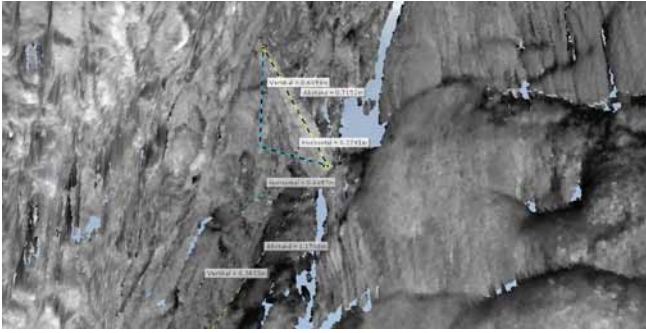


Figure 15. Scan of a broken and leaning stalagmite at the ceiling of the Grotta del Paranco with direct measurements in the point cloud (Soares 2016).

detailed morphology can be illustrated. In anhydrite and gypsum caves that show alterations within decades these can now be documented and quantified. This has also practical implications because cave stability can now be judged much better. One more project is apparent, that is documentation of fresh sinkholes and their gradual collapse and widening.

Acknowledgements

This study was made possible by special grants of the Technische Universität Darmstadt to acquire the Faro Scanner. Several students helped in field work. Access to caves was granted or organized by O. Krause, H. Daum, K. Huhn, among others.

References

Both S, 2016. *Speläogenese und Geologie der "Grotta del Paranco", Triest*. Bachelor thesis, Inst. for Appl. Geosciences, Techn. Univ. Darmstadt, 87 pp., unpublished.

Brand F, Illmann R, Leja F, Preu D, Schabdach H, 2006. *Die Binghöhle bei Streitberg - Auf den Spuren eines unterirdischen Flusses*. Marktgemeinde Wiesenthal, 60pp.

Fenzlein R, 2015. *Statistische Auswertung der Sinterschäden im Geisloch bei Oberfellendorf (Oberfranken, Bayern)*. Bachelor thesis, Inst. for Appl. Geosciences, Techn. Univ. Darmstadt, 55 pp. plus appendix, unpublished.

Kempe S, 1975. Siderite weathering, a non-biogenetic source of CO₂ (illustrated by the Iberg/Harz/Fed. Rep. of Germany). *Ann. de Spéléologie* **30**(4), 703-704.

Kempe S, 2005. The inscriptions of the Tartarus panel and the 1833 Fercher-Survey, Postojnska jama. *Acta Carsologica*, **34**(1), 221-235.

Kempe S, 2004. Natural speleothem damage in Postojnska jama, Slovenia, caused by glacial cave ice? A first assessment. *Acta Carsologica*, **33**(1), 265-289.

Kempe S, Helbing A, 2000. Die „Größe“ deutscher Gipshöhlen. *Die Höhle* **51**(1), 13-20.

Kempe S, Mattern E, Reinboth F, Seeger M, Vladi F, 1972. *Die Jettenhöhle bei Düna und ihre Umgebung*. Abh. Karst- u. Höhlenkunde A6, 63 pp.

Kempe S, Reinboth F, Knolle F. (Eds.) 1985. *Die Iberger Tropfsteinhöhle bei Bad Grund (Harz)*. Bad Grund: 58 pp.

Kempe S, Bauer I, Krause O, 2016. Iberger Tropfsteinhöhle, Iberg, Harz Mountains, Germany: Hypogene Morphology and Origin by Siderite Weathering. In: T Chavez and P Reehling (Eds.). NCKRI Symp. 6; *Proc. of "Deep Karst, 2016: Origins, Resources, and Management of Hypogene Karst"*, Carlsbad, New Mexico, 11.-14. April, 35-44.

Legner J, 2014. *Himmelreichhöhle*. Field report, unpublished.

Reinboth F, 1970. Die Himmelreichhöhle bei Walkenried und ihre Geschichte. *Mitt. Verb. dt. Höhlen- u. Karstforscher* **16**(3/4), 29-44.

Soares de Araujo JA, 2016. *Sinterschäden in der Grotta del Paranco, Zeugen glazialer Vereisungen*. Bachelor thesis, Inst. for Appl. Geosciences, Techn. Univ. Darmstadt, 52 pp. unpublished.

Wiesler S, 2016 *Speläogenese der Binghöhle, Oberfranken, Bayern*. Bachelor thesis, Inst. for Appl. Geosciences, Techn. Univ. Darmstadt, 83 pp. plus appendix, unpublished.

Will J, 2013. *Quantifizierung der Sinterschäden der Postojnska jama, Slowenien*. Bachelor thesis, Inst. for Appl. Geosciences, Techn. Univ. Darmstadt, 31+XV pp. unpublished.

Surveying Caves using Zebedee and Bentwing

Mike Lake and Jill Rowling

Affiliation: Sydney University Speleological Society.

Abstract

Several caves and a quarry in the Cliefden Caves and Wombeyan Caves areas of New South Wales were surveyed with “Zebedee” and “bentwing” during January 2014.

Zebedee is a hand-held 3D mapping system developed by Australia’s scientific research organisation CSIRO (Commonwealth Scientific and Research organisation) that utilises a scanning laser beam and a industrial-grade inertial measurement unit mounted on a simple spring. As the scanner oscillates about the spring the laser’s inherent 2D scanning plane maps into a 3D field of view. The Zebedee trajectory is accurately and continuously calculated from the laser and inertial measurements in real-time and this enables the device to perform simultaneous localization and mapping (SLAM). A three dimensional “point cloud” representation of its environment is thereby created. A caver can just walk through a cave to map the system.

Bentwing is a Zebedee-like system mounted on a drone which can be flown through a cave of sufficient size.

3D point cloud data is more detailed, can be more accurate, and can show us clues to the geomorphology of a cave which are often omitted in conventional two dimensional maps.

Devices that perform SLAM and generate 3D point cloud data are the future of surveying methods in speleology and in archeology, mining, forensics and many other fields but there are still challenges in processing and visualising the large amounts of data and in integrating this data with conventional surveying methods.

This project was commenced by the Sydney University Speleological Society (SUSS) to produce a report to the Department of Environment on the potential of the abandoned Melocco quarry for an educational site. The project is funded by an ASF Conservation Fund Grant.

Keywords:

1. Introducing Zebedee and Bentwing

Zebedee is a hand held device that scans its surroundings using a rotating laser attached to a spring on a handle. As one walks the spring wobbles back and forward so the laser ends up scanning in just about every direction. Each laser reflection off an object, whether a quarry wall or a rock, person or tree, means a distance is measured. All of these distance measurements in all directions creates a “point cloud” of data that can be visualised using suitable software.

Zebedee was developed by Robert Zlot and Michael Bosse, both Research Scientists in the CSIRO Autonomous Systems Laboratory, Brisbane. Lukas Kaul, an Industrial Trainee from CSIRO, modified an off-the-shelf quadcopter platform (an “Eagle” from SkyBit Systems) to carry the same sensors used in Zebedee as a 3D mapping payload. This quadcopter mapping system has been named “bentwing”, after the wing-like structures that make use of the vehicle’s downdraft to rotate the laser scanner. The first use of bentwing in the field was at Jenolan Caves just a few days before this Wombeyan trip.

There have been laser based surveying systems that generate point cloud data sets for a few decades. They consist of a laser beam that is mounted on a fixed tripod and the laser usually scans up-and-down whilst being rotated. The up and down motion and rotation is controlled by a stepper motor that ensures that elevation and bearing are accurately known. Knowing those angles and the distance from the laser measurement results in the location of one point being known precisely - just like we do with Suuntos and fibreglass tape or with a DistoX. The laser scanner though does this for mil-



Figure 1. This is a Zebedee. At the top of the unit is the laser scanner behind a round reddish plastic cover. The laser is an infra-red laser with wavelength of 905 nm and scans at 40,000 times a second. Below that is a black box which is the inertial measurement unit (IMU) and which contains a 3-axis accelerometer and a 3-axis gyroscope. These perform a rough estimation of the motion of the device over short time intervals. This forms a prior estimate of the position that is later corrected by the software using the laser data and other constraints. A spring then attaches these to the blue handle at the bottom. When you hold the blue handle you can “wobble” the unit at about once per second whilst you walk, climb or crawl around the cave. Because the laser is in the infra-red and low power you cannot see the laser and it is quite safe. Photo by Mike Lake.

lions of points. Most of these tripod based laser scanners cost \$100,000 or more and take an hour to do a scan per site. They are mainly used by land surveyors but are extensively used by archaeologists and mining companies.

Zebedee is a fundamentally new method and technology. It is though made using off-the-shelf hardware with a few modifications. One could purchase it all for less than several thousand dollars. The software though is proprietary to CSIRO. It implements a SLAM technique (Simultaneous Localization and Mapping). SLAM is a software method used in robotics to construct a map of an unknown environment while simultaneously keeping track of the location in that environment. In this way a complete map of the cave as a point cloud is constructed. The track of Zebedee's laser scanner origin is also recorded during a survey session.

The unique aspects to this device are the use of a wobbling spring instead of a steady scanning motor on a tripod, and its advanced software. This software fine tunes "where you are" by recognising prior locations from the point cloud and closes any loops like in normal surveying. The software also uses the motion estimation data from the inertial measurement unit (IMU) data to further enhance the accuracy of the point cloud data.

2. Operation in The Field or Cave

One does not have to position the device in known surveyed positions like conventional laser scanning survey devices, one just walks around with it in your hand. However if you are surveying in tight places like crawlways you have to be careful not to bump the device on the walls which can cause a data error.

To avoid confusing the instrument only the operator should be present within the devices "field of view". However as the devices field of view is 270 degrees there is a blind spot towards the rear where a second person can stand safely without getting in the picture.

It takes a bit of practice to use the device, you need to walk (or crawl) at a slow pace and the wobble has to be about one wobble a second. If you walk too quick or wobble it too fast you will get a sparser 3D point cloud. Walk too slow and the amplitude of the wobble will probably be too small and the device will then have too small a field of view.

Once data is obtained from a survey, it has to be further processed in order to merge overlapping data sets, correlate features and generate a final corrected point cloud. This can take several hours.

There is free software available for viewing and editing the final point cloud data (CloudCompare and Meshlab). However you really do need a dedicated high-end graphics device in your computer or laptop to handle the large data sets.

3. Results

Some results of this project are shown in the figures below. One of the main reasons for using a Zebedee or bentwing was to obtain a more accurate survey of the Wombeyan quarry in a quicker time than a conventional compass and laser tape survey. The latter would have required several months of work

to map the levels in the quarry. The work done in surveying two tourist caves and the Victoria Arch at Wombeyan Caves were incidental to the project. The surveying of the caves at Cliefden was for another project.

3.1. The Melocco Quarry at Wombeyan Caves, NSW



Figure 2. A view from one of the quarry benches looking down at the cut marble blocks. Photo by Jill Rowling.



Figure 3. The quarry is of educational value; cave development is clearly seen and it's easily accessible. Photo by Jill Rowling.



Figure 4. A 3D point cloud image of the quarry. The width of this quarry from wall to wall is about 20 m. The rectangular blocks visible in the bottom of the quarry are about 3 m across. The round fuzzy objects are trees. The accuracy of the data is better than several centimetres.

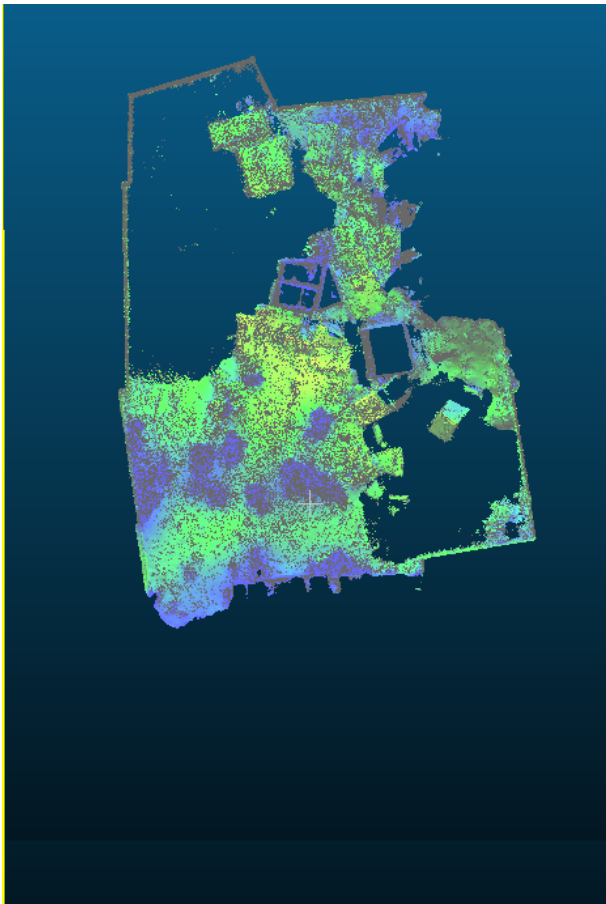


Figure 5. This is a horizontal slice through the 3D point cloud image of the quarry at a height of a metre above ground level.

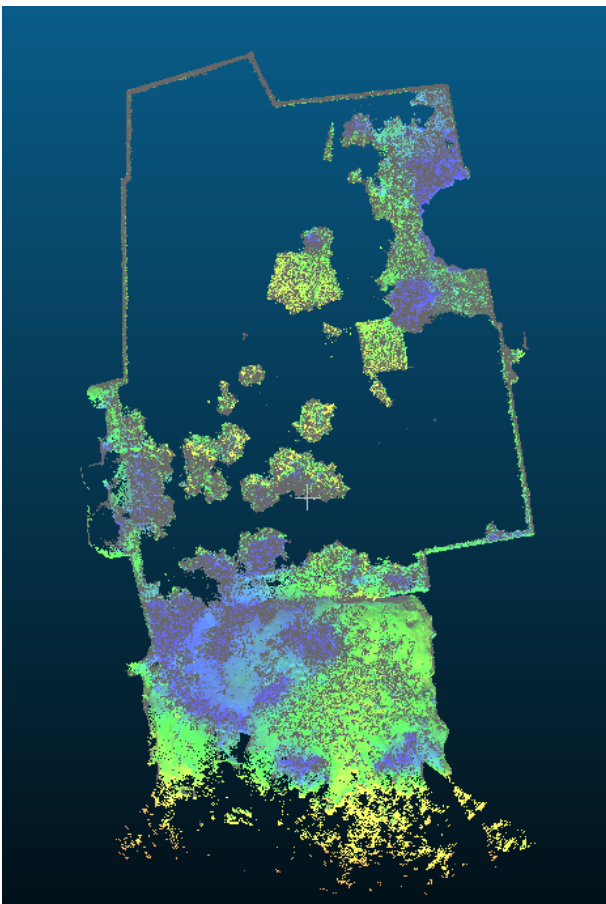


Figure 6. This is a slightly higher horizontal slice through the 3D point cloud image of the quarry at a few metres above ground level.

3.2. Swansong Cave at Cliefden Caves, NSW



Figure 7. This is an overhead view of Swansong Cave at Cliefden generated from the Zebedee point cloud data. Note the clearly visible fault or joint influence on the cave morphology.

3.3. Cliefden Main Cave at Cliefden Caves, NSW



Figure 8. This is a side elevation view of Main Cave at Cliefden generated from the Zebedee point cloud data. At least two, clearly delineated, older water table levels are clearly visible.

3.4. Operations in the Field

The remaining figures show aspects of the operation of Zebedee and bentwing in the field.



Figure 9. Mike Lake and Robert Zlot setting up Zebedee in the Wombeyan Quarry. Photo by Jill Rowling.



Figure 10. Scanning with Zebedee in the Wombeyan Quarry. Photo by Jill Rowling.



Figure 11. The quadcopter surveying in the quarry. Photo by Mike Lake.

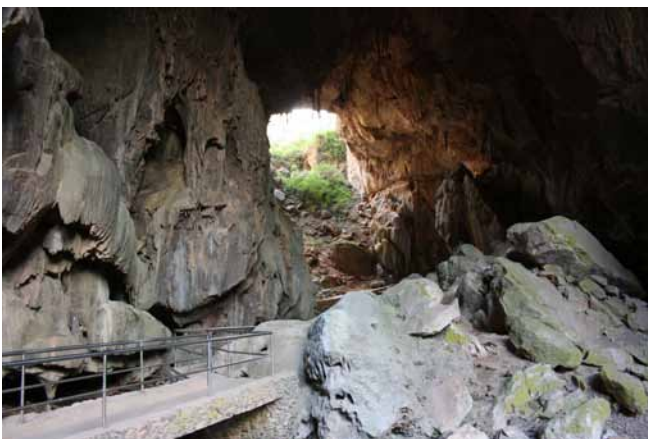


Figure 12. The Victoria Arch, Wombeyan Caves. Photo by Jill Rowling.

Acknowledgments

The authors would like to thank the following persons and organisations. Robert Zlot and Lukas Kaul from the CSIRO Autonomous Systems Laboratory who provided their time, expertise, Zebedee and Bentwing. Dave Smith and Geoff Lang, Wombeyan Guides for permission to do this work at Wombeyan, Orange Speleological Society and Denis Marsh for their assistance to Robert Zlot and ourselves at Cliefden



Figure 13. Lukas Kaul setting up “bentwing”, the quadcopter with the same sensors as Zebedee, in the Victoria Arch, Wombeyan Caves. Photo by Mike Lake.



Figure 14. The quadcopter surveying in Victoria Arch, Wombeyan Caves. Photo by Jill Rowling.

Caves and the Australian Speleological Federation for the Conservation grant to cover costs associated with this project.

References

ASF, Australian Speleological Federation <http://www.caves.org.au>

SUSS, Sydney University Speleological Society <https://suss.caves.org.au>

Zebedee information is available at <https://wiki.csiro.au/display/ASL/Zebedee>

SLAM, *Simultaneous Localization and Mapping*, reference at Wikipedia. http://en.wikipedia.org/wiki/Simultaneous_localization_and_mapping

Meshlab is open-source point cloud viewing and editing software. <http://meshlab.sourceforge.net/>

CloudCompare is open-source point cloud editing software. At this site is also ccViewer which just views point clouds and is much easier to use. <http://www.danielgm.net/cc/>

Comparison Of Shallow Geophysical Cave Detection Methods To 3D Lidar Mapping

Evelynn J. Mitchell¹ and Joseph N. Mitchell²

Affiliation: ¹ St. Mary's University, Department of Physics and Environmental Sciences, One Camino Santa Maria, San Antonio, TX, 78228

² Texas Speleological Survey and Bexar Grotto, 11463 Enchanted Sunset St., San Antonio, TX 78253

Abstract

Shallow subsurface geophysical techniques have become popular for locating voids as the technology advances, but just how accurate are these methods at determining passage dimension? Cricket Cave, a shallow cave was chosen outside of Boerne, Texas, USA, to study 3 different systems and compare the dimensions measured. The Caveatron 3D LIDAR caving mapping device was utilized to map all the human accessible portions of the cave and generate a meshed model of the passage walls. A GSSI 270 MHz ground penetrating radar system was utilized to detect the upper passage of the cave, but was unable to penetrate far enough into the ground to detect the lower passages. A final survey was run using an AGI R8 resistivity system in a 3D grid over portions of the cave containing both the upper passage and the lower passage. Comparisons of both geophysical systems to the LIDAR-generated model show the strengths and weaknesses of cave passage detection for each instrument.

Keywords: Ground Penetrating Radar, Resistivity, LIDAR

1. Introduction

Because karst areas are often links to local groundwater supplies, in karst terrains undergoing development it often becomes important to locate karst features prior to construction so that development can be designed to avoid such features. Shallow surface geophysical techniques have become a significant tool in locating previously unknown features, with resistivity (Marinez-Moreno *et al.* 2013; Yeboah-Forsen *et al.* 2014; Zajc *et al.* 2014; Kaufmann *et al.* 2015) and Ground Penetrating Radar (GPR) (Chamberlain 2000; Beres *et al.* 2001; Al-fares *et al.* 2002; Zajc *et al.* 2014) often utilized in void detection with variable success.

In recent decades, 3D LIDAR technology has advanced such that many devices have been developed to be utilized in cave survey (Zlot and Bosse 2014; Gallay *et al.* 2015). This newly portable technology has started to revolutionize the way that cave explorers and scientists document cave passages at a high level of detail, allowing them to produce 3D point clouds, simulations, and even games (Fort Stanton Cave Study Project 2017) based on the caves mapped.

This paper will utilize 3D LIDAR technology to examine the accuracy of the ability of two geophysical techniques to detect passages of a known size and dimension. Ground resistivity and GPR results for Cricket Cave will be compared with a LIDAR-produced model to measure passage detection abilities.

2. Geologic Description

Cricket Cave is located within the lower portion of the Glen Rose Formation, which is one of the most cavernous units in Texas (Veni 1994), and is part of a larger block of karst features within the Cave Without a Name group. Many of the caves in this area are still undergoing highly active dissolution processes, as there are also active stream channels in the deeper features. Cricket Cave has a clearly defined entrance sinkhole, with an upper passage that extends horizontally approximately 5.7 m at a depth of 3.1 m before a vertical shaft approximately six m tall drops down to the main portions of the cave, which continues horizontally at a depth of 12 m. The

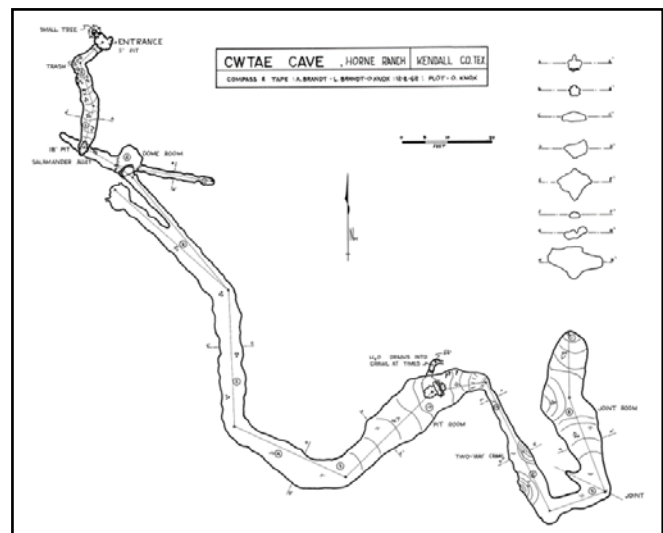


Figure 1. Map of Cricket Cave. At the time this map was made the cave was called CWTAE Cave.



Figure 2. Mesh rendering of the LIDAR data for Cricket Cave. The entrance sinkhole can be seen on the upper left portion of the image. The majority of the cave passage is at approximately 12 m below the surface.

total surveyed length of the cave is 98.2 m. Although the cave is shallow in comparison to nearby Cave Without a Name, and does not have a known stream passage, there is a mud floor at the end of the cave that has been noted to hold water when there have been significant rains in the area. A map of

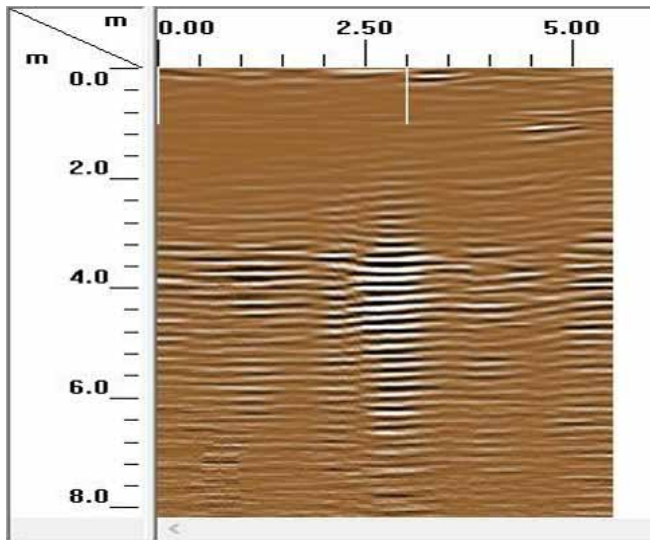


Figure 3. GPR scan over upper level passage of Cricket Cave

the cave is shown in Figure 1 and the full extent of the cave as rendered from the LIDAR data can be seen in Figure 2.

3. Methods

A 3D LIDAR scan was taken of Cricket Cave using the Caveatron hand-held survey device. It is designed to provide a complete, low cost, cave mapping solution that is easy to use with its graphical touchscreen interface and is housed in a compact enclosure that is durable for cave use. The Caveatron is used to acquire conventional station-to-station distance, azimuth, and inclination measurements between stations set in the cave using its built-in laser rangefinder and inertial measurement unit. The LIDAR scan data is then collected by traversing the cave in lines toward each station or gathering additional rotational scans to cover alcoves and other occluded areas. All scans are referenced to a retroreflective card that is held on each survey station from which the Caveatron gathers positional information while scanning in motion or uses as a positional reference prior to a rotational scan. From the survey data file, a line plot is generated from which the absolute X, Y, and Z coordinates of each station are computed. These, along with the LIDAR scan data, are input into a custom-written post-processing program that filters and smooths the data, removes noise and poor quality readings, and produces a point cloud. The vector normals for each point are also computed by the post-processing software, which allows the data to be meshed into a rendered 3D model of the cave using a program such as Meshlab.

The GSSI 270 MHz GPR was utilized to take single line scans over known locations of the cave. Several ranges were tried to determine what would need to be utilized to “see” the upper passage of the cave. Although ranges of 75 ns and 175 ns are typically utilized to perform surveys in other area lithologies, such as the Edwards limestone, the range needed to detect the upper level passage of Cricket Cave was 250 ns. Once the proper range for detection was determined, a scan of five-meter length was performed otop of the upper level passage. Images were processed using the GSSI Radan 7 software.

For the resistivity survey, an AGI R8 Supersting system was utilized. A 56-electrode 3D array was arranged as a 4 x 14 array with a five-meter spacing. The array was positioned to

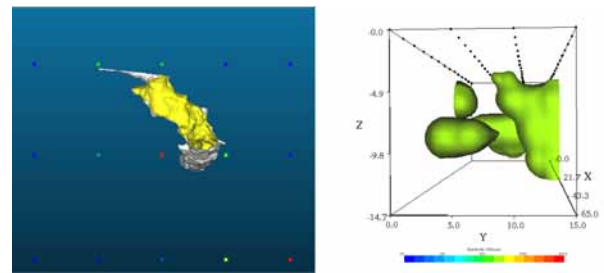


Figure 4. Comparison of 3D LIDAR model of passage (left) to Earth Imager 3D Resistivity Contour Plot (right). The feature on the right of the resistivity model is the cave passage that connects the upper level to the lower level of Cricket Cave.

be centered over the cave entrance, and was designed to penetrate to a depth of 14.67 m, as the main passage of the cave was surveyed to be at a depth of 12 meters.

To compare the results of the 3D resistivity survey with the LIDAR survey, the electrodes from the corners of the resistivity survey and the ones nearest the entrance of the cave were surveyed from the point at the entrance that starts the LIDAR survey. The apparent resistivity points were then imported into CloudCompare and the resistivity data was aligned with the 3D cave mesh. The positioning of the data sets allowed for thin sections of the LIDAR plot. EarthImager 3D software was used to create an inversion model of the data, and then iso-surfaces and cross sections of the 3D Resistivity Contour Plot were compared to the LIDAR model thin sections.

4. Results

As seen in Figure 2, the LIDAR data shows Cricket Cave to have small upper passages and larger passages in the lower level, with a tight drop connecting the upper passage to a domed room that starts the lower level passages. The GPR analysis was only able to penetrate to a depth of eight meters, and was thus unable to detect the lower portions of the cave. However, when analyzing the scan of the upper passage, it was found that the image (Figure 3) shows a feature 1.025 m wide. The height of the passage is difficult to measure due to reverberation effects that can occur when sound waves encounter a void, but the width of the passage is easily defined using the Radan 7 processing tools. Figure 3 also shows the top of the cave passage to be approximately three meters below the surface.

The resistivity survey is more complex to interpret, but utilizing the 3D Resistivity Contour Plot feature in the EarthImager 3D software shows that at 799.03 ohm-m contour, the outer surface of the passage appears to be detectable in a similar shape seen in the LIDAR model, as shown in Figure 4.

The Dynamic Slices feature in the EarthImager software allowed a look at the cross sections of the area where the cave passages were detected by the resistivity survey (Figure 5) and shows how the model compares with the LIDAR mesh. By moving the x, y, and z planes in the model, measurements were taken of resistivity values higher than 799.03 ohm-m to estimate the size of the passage. The main chamber of the passage in the resistivity model was thus measured to be 7.80 m high x 6.75 m x 4.76 m, or a volume of 250 m³. The measurements of the LIDAR point cloud show the same chamber to

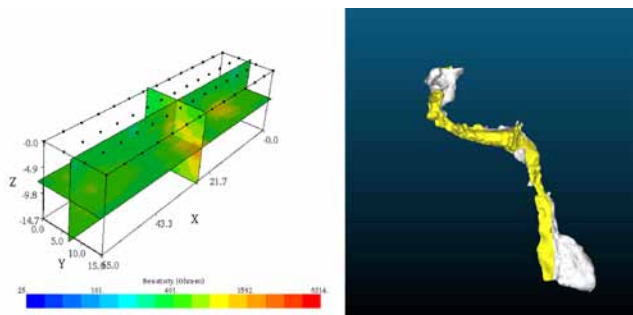


Figure 5. Resistivity displayed on x, y, z slices of the model as compared to the LIDAR model. In the resistivity rendering the main crawlway and dropdown passage are shown where the slices meet.

be 6.10 m high x 1.90 m x 1.00 m, or a volume of 11.6 m³. The resistivity model shows the crawlway into the drop down passage to be 5.57 m long x 4.67m wide x 2.08 m high, or a volume of 54.1 m³, while the LIDAR measurements showed the crawlway to be 5.70 m long x 1.00 m wide x 0.80 m high, or a volume of 4.56 m³.

The 3D Resistivity Contour Plot shows the data set penetrating to a depth of 14.7 m, but there is no detection of the lower level passage, the ceiling of which is shown with the LIDAR survey to be at a depth of approximately 12.0 m from the surface.

In addition to detecting a significant pocket of higher resistivity in the location of the crawlway and dropdown, additional pockets of higher resistivity are detected at a depth of 5 to 10 meters where $x = 10$ to 20 m and $y = 0$ to 12 m, and at a depth of 10 m where $x = 55$ to 60 m and $y = 4$ to 8 m. These features are not part of the known cave.

5. Discussion

The GPR data showed that the width measurement for the upper level passage was consistent with the measurements taken from the LIDAR data, and the depth of the passage is also in agreement with the LIDAR survey. A 3D grid with the GPR would likely reveal good detail of the upper passage, but would not detect the majority of the cave passages. (A 3D grid was not performed in this area due to the fact that it is located in an ashe juniper forest, and would have required significant clearing of the vegetation, which the land owner did not want to happen.) However, in an area where one is worried about groundwater recharge, locating near-surface features in important in determining the pathways through which recharge takes place, and the GPR would likely find most near surface features.

With the resistivity survey, the dropdown portion of the cave is detected in addition to the crawlway, but the passages present at 12 m deep are not detectable. The inversion model indicates that the resistivity survey penetrated to 14.7 m, but since the LIDAR survey has shown the lower passages to be at approximately 12 meters, the depth scale for the resistivity survey seems to be rather inaccurate. When comparing the dimensions of the measured passages, the volumes calculated for the for the passages in the resistivity model were at least 10 times greater than the volumes calculated using the LIDAR survey data. According to work done by Abu-Shariah (2009) however, there may be a need to change the inversion pro-

gram to deal with the shape of the cave, as shown in his paper on the Batu Caves, and this may account for the difference in volume measurements.

The resistivity model also shows additional potential features at a depth of 5 to 10 meters that do not connect to the LIDAR survey. These could be isolated void pockets that are connected to the system through cracks or fractures. The LIDAR survey covers the extent of the humanly passable portion of the cave, and would miss any voids that are connected through small conduits.

6. Conclusions

Although both the GPR and resistivity systems have their drawbacks, both systems were able to detect a portion of Cricket Cave. The GPR data showed the most accurate dimensions when compared with the LIDAR model, but was unable to detect anything lower than the upper crawlway. The resistivity system detected more of the cave passage, and the 3D model showed similar passage shapes to the LIDAR rendered model, but the measurements of the passageways were much less accurate. However, the resistivity system was able to detect more potential passage that could not be accessed by exploring the cave. Thus, both systems can be utilized in identifying near surface features, but for estimating size, the GPR appears to be a better tool.

The depth of the GPR scan could be potentially increased with a lower frequency antenna, and future work could determine the frequency that would be necessary to penetrate the Glen Rose Limestone to a depth of 12 meters. To increase the depth of the resistivity survey, the spacing between the electrodes could be increased, and the number of electrodes could be increased. While changes to both of these surveys may increase the depth of void detection, the resolution of the passage size would have to be analyzed to determine if there is an improvement in detecting void size.

Acknowledgements

Thanks to Mike Burrell at the Cave Without a Name property for access to Cricket Cave and for assistance with the GPR and Resistivity surveys, to Michael Cunningham for grounds preparation and to Gregg Williams, Joe Schaertl and Wade McDaniel who assisted with the LIDAR survey of Cricket Cave. Additional thanks to Harold Campbell for assistance with both geophysical surveys to James Ford, Liz Hoffman, John Lopez and Jen Espinosa for support for the resistivity survey, and to Ben Schwartz for use of his R8 Supersting system.

References

- Abu-Shariah M, 2009. Determination of cave geometry by using a geoelectrical resistivity inverse model. *Eng. Geol.* **105**, 239–244.
- Al-fares W, Bakalowicz M, Guerin R, Dukhan M, 2002. Analysis of the karst aquifer structure of the Lamalou area (Herauld, France) with ground penetrating radar. *J. Appl. Geophys.* **52**, 97–106.

- Beres M, Luetscher M, Olivier R, 2001. Integration of ground-penetrating radar and microgravimetric methods to map shallow caves. *J. Appl. Geophys.* **46**, 249–262.
- Chamberlain A, 2000. Cave Detection in Limestone using Ground Penetrating Radar. *J. Archaeol. Sci.* **27**, 957–964.
- Fort Stanton Cave Study Project - Caver Quest Simulation. (accessed 25 Jan. 2017). <http://www.fscsp.org/CQ6/>
- Gallay M, Kanuk J, Hochmuth Z, Meneely JD, Hofierka J, Sedlak V, 2015. Large-scale and high-resolution 3-D cave mapping by terrestrial laser scanning: a case study of the Domica Cave, Slovakia. *Int. J. Speleol.* **44**, 277–291.
- Kaufmann G, Nielbock R, Romanoz D, 2015. The Unicorn Cave, Southern Harz Mountains, Germany: From known passages to unknown extensions with the help of geophysical surveys. *J. Appl. Geophys.* **123**, 123–140.
- Marinez-Moreno FJ, Pedrera A, Ruano P, Galindo-Zaldivar J, Martos-Rosillo S, Gonzalez-Castillo L, Sanchez-Ubeda JP, Marin-Lechado C, 2013. Combined microgravity, electrical resistivity tomography and induced polarization to detect deeply buried caves: Algaidilla cave (Southern Spain). *Eng. Geol.* **162**, 67–78.
- Veni G, 1994. *Geomorphology, Hydrogeology, Geochemistry, and Evolution of the Karstic Lower Glen Rose Aquifer, South-Central Texas*. (Texas Speleological Survey Monographs).
- Yeboah-Forson A, Comas X, Whitman D, 2014. Integration of electrical resistivity imaging and ground penetrating radar to investigate solution features in the Biscayne Aquifer. *J. Hydrol.* **515**, 129–138.
- Zajc M, Pogacnik Z, Gosar A, 2014. Ground penetrating radar and structural geological mapping investigation of karst and tectonic features in flyschoid rocks as geological hazard for exploitation. *Int. J. Rock Mech. Min. Sci.* **62**, 78–87.
- Zlot R, Bosse M, 2014. Three-dimensional mobile mapping of caves. *J. Cave Karst Stud.* **76**, 191–206.

The Caveatron: An Integrated Cave Survey and LIDAR Scanning Instrument

Joe Mitchell¹ and Steve Gutting²

Affiliation: ¹Texas Speleological Survey, Bexar Grotto, Southwest Research Institute
11463 Enchanted Sunset St., San Antonio, TX 78253, USA
²Bexar Grotto, Southwest Research Institute
11530 High Meadow, San Antonio, TX 78253, USA

Abstract

The Caveatron is a unique handheld electronic device specifically designed as a complete survey and 3D mapping tool for caves or other underground environments. It provides a caver-friendly, self-contained system for recording all station-to-station measurements, “sketching” the passage with walk-through 3D point-cloud scanning using its integrated LIDAR, and entering data, such as station names, and reviewing line plots. Using its graphical touchscreen interface, various survey functions are quickly performed. In “Shot Mode”, distance, azimuth, and inclination measurements between survey stations are recorded by simply aligning the integrated red laser to a station and activating the 4-second measurement process. 3D LIDAR scan can be quickly recorded either in “Passage Mode”, by traversing (i.e. walking or crawling) toward a survey station, or in “Room Mode”, where the device is manually rotating over a fixed point. The LIDAR scans 360 degrees making continuous cross-sections with a few centimeter resolution at a typical slow walking pace, allowing most scans to be completed in about 1 minute. The absolute position is continuously referenced to a special card held on a nearby survey station, avoiding inertial drift or the need for separate fiducial markers. The Caveatron is designed to be lightweight and compact with an environmentally sealed enclosure that contains a rechargeable battery, data storage, and a standard USB port for charging and data download. The LIDAR scanner is housed in a separate small enclosure that detaches so that the system can be used as a more compact survey-only tool. A spin-off design on a telescoping pole with a more advanced LIDAR was also developed to scan areas that may not be accessible to personnel. Scans from the system are easily reviewed and post-processed with custom-written PC software into 3D point clouds which can be rendered into meshed solid models for visualization or 3D printing.

Keywords: Electronic cave survey, LIDAR, mapping, 3D models

1. Introduction

Cave survey and mapping is still largely done in a traditional manner – with mechanical instruments and paper sketchbooks. While these techniques are trusted and for the most part reliable, the process is time consuming, limited in the level of detail possible, and prone to error and estimates (especially in the sketches). In recent years, cavers with electronics knowledge have begun developing devices to address some of these challenges, most notably, the DistoX (DistoX 2017), which can rapidly and accurately acquire all station-to-station shot measurements electronically, though the station names and sketch must still be recorded separately.

Other cavers have been looking at how to replace sketching with a three-dimensional electronic scan of the interior of the cave using LIDAR (Light Imaging, Detection And Ranging). Early LIDAR systems were bulky, extremely expensive and not suited to cave environments. Newer LIDAR units, while still expensive, are substantially smaller and have been successfully employed in caves, producing impressive results (Gallay et al. 2014). An even more compact system, which eliminates the tripod for in-motion scanning in caves, has also been developed (Zlot and Bosse 2014). However, these systems typically require additional support equipment, special markers to localize the system, and require technical expertise to operate. The DIY electronics hobby community has driven demand for smaller and lower cost rangefinder modules, and cavers have begun to build their own tripod-mount LIDAR systems suited for cave use (Buecher 2016). These systems must be spatially oriented and tied into the survey, requiring additional measurements or markers.

The Caveatron takes a novel approach, combining the survey instruments with a LIDAR scanner into one complete system that can replace the instruments and in some cases even the sketchbook. A major advantage of the Caveatron is that it scans while in motion, avoiding the need for tripods, special setup, or and additional equipment. The design is focused on low cost, user friendliness, and a reasonably compact and integrated package that can stand up to the cave environment.

2. Design

The design of the Caveatron initially started in 2012 as a simple tool to assist sketching plan and profile views, relying on inexpensive ultrasonic sensors for both wall and station measurements. Although this approach produced good data, the ultrasonic sensors had a wide beam and were affected by the high humidity in caves, rendering them unreliable after a couple hours of exposure. Four major design iterations gradually shifted from ultrasonic to laser based sensors, when new components were found with acceptable cost and performance. The laser sensors have much higher resolution allowing the system to be sealed against moisture and dust ingress. As the potential of the system to be a complete cave survey tool became apparent, the design and user interface evolved from an alphanumeric LCD and keypad to a more sophisticated, self-contained, sealed enclosure with a full-fledged touchscreen graphical user interface (GUI).

The Caveatron employs a modular design, consisting of a base unit and LIDAR module (Figure 1). The base unit contains the main processor, sensors, and battery. On the top is a cutout for the recessed 3.5”, 480x320 pixel color touchscreen. The top also has a rail for mounting the LIDAR module and a con-



Figure 1. The Caveatron with the LIDAR module attached.

connector for the LIDAR module cable. On the right hand side is a recessed power switch, while on the left side is a capped mini-USB port used to charge the battery, download data, and update the firmware. On the front is a small window for the laser rangefinder, and on the rear are rings for the neckstrap.

The system uses an Arduino Due as the main processor. It has an 84 MHz, 32-bit Atmel ARM processor and 512 kB of flash storage, giving it the speed and capacity to handle the LIDAR data and GUI. The system is powered by a Li-ion battery pack capable of operating the Caveatron for more than seven hours. Additional electronics include power supply boards and a real-time clock/EEPROM board with separate battery backup. Azimuth and inclination measurements are obtained using an ST Microelectronics three-axis magnetometer and accelerometer with 12-bit resolution. A modified laser rangefinder provides distance readings at a 0.9 Hz sampling rate at distances up to 40 meters.

The Caveatron LIDAR module contains the LIDAR scanner, which obtains one point per degree over a 360° scan at a rate of 4.5 rotations per second. It is compact and very low cost, but has the trade-off of a limited range of four meters. The module has sealed acrylic windows for the LIDAR on all four sides and attaches to the base unit rail by thumbscrews. Separating the LIDAR from the main unit allows the system to be more compact for transport or for use without the LIDAR, if only station-to-station shot measurements are required.

It also provides design flexibility to permit more advanced LIDAR modules in the future that will have greater range.

The enclosure is made from heavy-duty ABS plastic. The windows and display are recessed to reduce the risk of scratches or impact damage and each penetration has an O-ring or sealing gasket to protect against dust and moisture ingress. Although the Caveatron has not been tested for total water immersion, it does operate normally in moderately wet and muddy environments. Detailed specifications for the Caveatron are provided in Table 1.

3. Operation

A major challenge for the Caveatron design effort was to develop a simple, user-friendly method of operation based as much as possible on conventional cave survey techniques, and using normal survey stations. Measurement shots of the distance, azimuth, and inclination between stations are obtained with the Caveatron followed by a LIDAR scan of the region between stations to “sketch” the cave. One key aspect of the system is the use of a retroreflective card held on the station to which the shot is being taken. A neutral density filter is applied to the rangefinder so that valid distance measurements are obtained only when aligned with the card. Since it is nearly impossible to reliably hold the Caveatron on station while traversing (walking or crawling) without heroic effort, this approach guarantees that only correctly oriented measurements are used as absolute position references. Random hits on the card while moving provide sufficient fixed position references with interpolation providing the intermediate positions. Although the system has been designed to allow an inexperienced operator to obtain acceptable data, greater precision and denser scan coverage can be obtained through practice.

The Caveatron’s custom designed GUI steps the user through three main operating modes (Figure 2). SHOT mode is used to obtain the station-to-station measurements. The operator enters the “From” and “To” station names, then places one

Table 1. Specifications of the Caveatron.

Parameter	Specification
Compass accuracy	< +/- 2°
Inclination accuracy	< +/- 1°
Distance range	> 40 m
Distance accuracy	+/- 2 mm
LiDAR range	< 4 m
LiDAR spatial resolution†	~ 3-5 cm in a 5 m wide passage
LiDAR range accuracy	< 1% of range
Approximate run time‡	7.2 hours
Enclosure dimensions (with LIDAR)	20.5 cm x 14.1 cm x 19.0 cm
Weight (with LIDAR)	1.1 kg

† Depends on wall distance and operator speed.

‡ Assumes unit is continuously on and taking one shot and LIDAR scan every five minutes.



Figure 2. Sample screenshots of the Caveatron GUI including the Main Menu (left) and Shot Result screen (right).

of the rear corners on the “From” station. A red alignment laser activates to align the Caveatron with the “To” station. The operator activates the shot, which takes about 3 seconds to complete, with audible tones indicating the start and finish. The measurement results are displayed and the shot can be accepted or retaken. If a problem occurred, such as the Caveatron detected significant motion or too much variability in the measured values, the shot will fail with a low-pitched tone and displayed message.

The other two operating modes are used for LIDAR scanning. In PASSAGE Mode, the operator traverses down a passage toward a station, attempting to keep the visible laser pointed toward the retroreflective card held on the station (Figure 3). The LIDAR continually spins perpendicular to the direction of motion, producing passage cross-sections every few centimeters. For each LIDAR rotation, the Caveatron measures the azimuth and inclination, with the distance measured as frequently as a valid reading can be obtained from the card. Since the position is being continually determined, there is no need for the operator to maintain a perfectly straight line of motion toward the station but can move around obstacles and take whatever path optimizes scan coverage. Periodic acoustic tones provide feedback for valid distance readings. If the operator does not hit the card frequently enough, warning tones sound and eventually the scan will abort. Errors that would yield poor data are also detected, such as excessive velocity or large angular excursions. Many traverses may be made to any given station to cover a larger area than the LIDAR can reach or to obtain additional coverage for occluded areas.

In ROOM Mode the Caveatron is held at a fixed location and is rotated in place to build up a scan of the area around it. This is useful when there is an alcove, corner, or room that may not be suited to a traverse-type measurement. The position relative to a survey station is determined by an initial reading and the unit is then rotated to the scan’s starting orientation. During the scan, only azimuth and inclination readings are acquired to track the angle of each LIDAR rotation. This is the preferred mode for safely scanning pits by taking scans at periodic locations while descending.

The Caveatron GUI provides other useful functions. MANUAL Mode is used to obtain quick, readings of distance, azimuth or inclination. The SURVEY menu provides



Figure 3. The Caveatron performing a PASSAGE Mode LIDAR scan in Fort Stanton Cave. The operator (right) moves gradually toward the retroreflective card (center) held on a survey station. Photo by Pete Lindsley, courtesy BLM.

functions for initial setup, viewing survey data, statistics, and displaying a graphical line plot in plan and profile views. The SETTINGS menu provides utilities such as adjusting system parameters and displaying a live view of the LIDAR data to assist in determining the amount of coverage.

Proper calibration of electronic accelerometers and magnetometers is important to obtain accurate readings. Although the design of the Caveatron is not oriented toward very high precision, accuracy at least comparable to that obtained by an average cave survey team is a goal. Calibration can be a complex process, but effort has been made to make it as simple as possible. Most of the calibration is done only at the time of assembly. This is the case for the 12 accelerometer coefficients which are computed by carefully leveling the Caveatron and taking readings in all six orientations. The magnetometer misalignment vector and rotation offset are also determined during assembly using an outdoor calibration range. However, the other 15 magnetometer calibration values, representing the hard and soft iron corrections, have been found to drift over time (typically a few weeks), requiring user recalibration. An automatic point collection and least-squares fit routine was written to perform this computation onboard the Caveatron, only requiring the operator to continuously rotate the unit in all directions of an imaginary sphere for about 1 minute. Example residual error data after calibration is shown in Figure 4.

It was found that the presence of the LIDAR module motor impacts the magnetometer calibration. As such, two separate magnetometer calibration sets are stored with the correct one loaded at startup depending on whether the LIDAR is attached. No significant additional effect on the magnetometer was observed when the LIDAR motor was actively spinning. To easily facilitate updates, all calibration and hardware parameters are stored on an independent EEPROM chip separate from the firmware.

4. Post-Processing

Data is stored on a built-in SD card in two plain-text files for each survey trip. The survey file contains the station shot

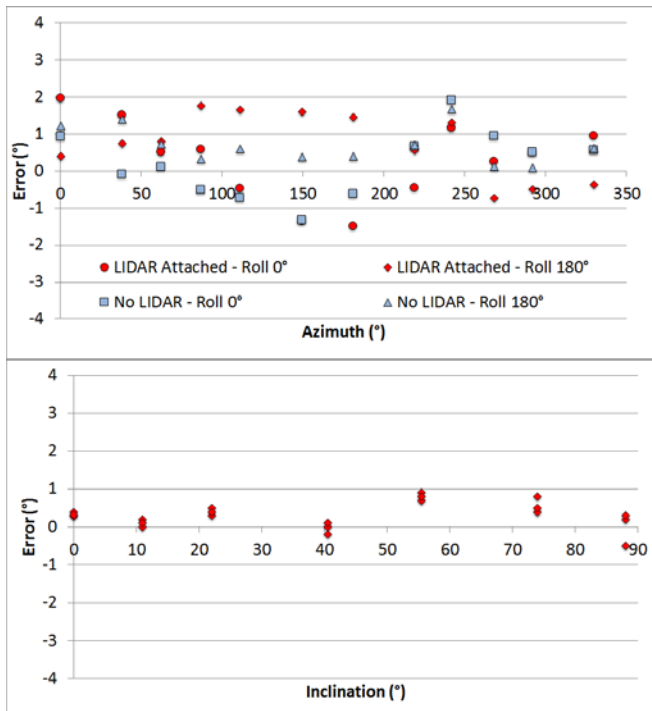


Figure 4. Residual measurement error of one unit after calibration. The azimuth error (top) is shown for different configurations and orientations. The inclination error (bottom) shows three sets of measurements taken at different times.

data and is formatted for Walls – a freely available cave survey processing program (Walls 2017). A separate LIDAR file contains only minimally processed scan data, since the Caveatron processor is limited in its capabilities. Noise filtering, data smoothing, and conversion into an x, y, z point cloud is performed in post-processing using a program for Windows or Mac platforms called “Caveatron Process”.

The first step is to generate a station coordinate file to link together the LIDAR scans. This is created from the stored survey file either in Walls or directly in the Caveatron Process application. Using Walls has the advantage of utilizing its powerful tools to optimize the line plot when loop closures are present as well as geo-referencing the survey. In the Caveatron Process software, the line plot can be viewed, global references set, and a magnetic declination applied.

The second step is to load the LIDAR file to review and process each scan. The software automatically removes bad data and noise, interpolates the Caveatron location between fixed position measurements, and filters excessive motion. The GUI allows the user to step through each rotation of the scan, showing cross-section, plan and profile views. The occasional bad data that slips through the filters can also be selected for removal. A normal vector is computed for each point based on the vector toward the LIDAR and the position of neighboring points. This vector is important if the point cloud is to be meshed and defines the direction straight in from the cave wall. The point cloud is stored as a delimited text file, which can be viewed in a program such as CloudCompare (CloudCompare 2017). Another program, Meshlab (Meshlab 2017) has the capability to render a meshed model of the cave, allowing it to be explored virtually – both inside and out. An accurate-scale 3D-printed physical model of the cave can also be generated.

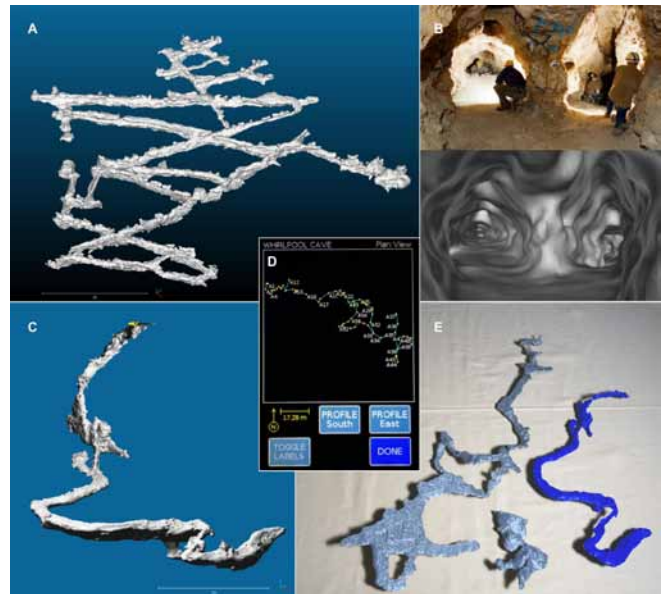


Figure 5. Example data from the Caveatron: A – Rendering of about 550 m of Robber Baron Cave in San Antonio, TX; B – Interior of Robber Baron Cave showing a comparison of a photo and the rendered data; C – Rendering of the entire 98 m-long Cricket Cave near Boerne, TX; D – Screenshot of the line plot displayed on the Caveatron from a survey of 229 m of Whirlpool Cave in Austin, TX; E – 3D printed cave models of Whirlpool Cave, Canyon Wren Cave, and Cricket Cave (left to right).

5. Testing

Four complete systems have been built and the Caveatron has been evaluated in several caves in south Texas, for which some sample data is shown in Figure 5. It was found that in a typical mix of walking and hands-and-knees crawling passage, with effort taken to ensure good scan coverage, the survey rate is generally about 40 meters per hour. A variety of caves have been scanned including those with solutional and breakdown mazes, small and tight crawls, large rooms, wet and muddy areas with dripping water, pits, and shelter caves. For some of these trips, the Caveatron was used for a full day of survey and did not exhaust its battery. The Caveatron performed well in all of these tests without significant problems. Rendered and 3D printed models have revealed previously unseen morphology such as bedding planes, passage meanders, and other relationships that were not obvious on the traditional maps.

A major test of the Caveatron was at the Fort Stanton Cave Study Project in New Mexico in October 2016. Part of this project includes an ambitious goal of producing a 3D model of as much of the 50 km long cave as possible. During this trip, both the Caveatron and a different LIDAR system that is stationary but has a longer range (Buecher, 2016) were employed. It was found that the two systems were complimentary, with the Caveatron being best suited for small to medium sized passageways and the other system most effective in larger rooms. Data from the two systems combined well in overlap areas, giving confidence in the accuracy of both designs.

6. Telescoping-Pole Cave Mapper System

A spin-off design of the Caveatron has been developed for the City of Austin, Texas that allows for mapping the near-entrance interior of caves without requiring human access. The system is intended for use when there is concern about



Figure 6. Telescoping pole cave mapper system.

sending personnel into caves that have been newly uncovered through construction operations, where the entrance area may be unstable. This design places the scan head on the end of a 7.5-meter telescoping pole, which is inserted into the cave (Figure 6). The head contains a professional-grade LIDAR with a 30-meter range and a 25 Hz scan rate. Unlike the Caveatron, this LIDAR is oriented along the axis of the pole and rotation of the pole is used to build up the 3D scan. The head contains an inertial measurement unit to determine the head's orientation, illumination LEDs, and a high-definition video camera to remotely visualize the cave and guide the head into position. Since portability was less of a constraint with this design and the LIDAR data rates are high, a Windows laptop PC is used to control the system and record data. Custom software was written to allow the operator to preview the scan, record data, and post-process the results into a point cloud.

In operation, the head is inserted into the cave and the pole extended to guide it to the scan location. To assist in moving the head around obstacles, a spring-tensioned pull-cord provides one axis of articulation. Once in place, the operator uses a separate laser rangefinder to measure the distance from a reference point at the cave entrance to a spot on the rear of the scan head. The distance value is entered into the software to start the scan and then the operator slowly rotates the pole at least 180° to complete the scan. Additional scans to obtain

greater coverage can be conducted from the same reference point by moving the head to a new location and repeating the process.

7. Planned Developments

We continue to evaluate potential new components for the Caveatron to enhance its capabilities. A new, relatively low cost LIDAR scanner became available at the beginning of 2017, which can address the scan range limitation of the current LIDAR. The new scanner should increase the range to more than 25 meters with only a slight reduction in scan rate versus our current module. Its similar interface and form factor will allow it to be interchangeable with the existing LIDAR. Another planned improvement is to fabricate a custom printed circuit board to eliminate much of the wiring and provide an integrated baseplate with plug-ins for the each sub-assembly. Software revisions continue to be developed to add features, improve processing, and eliminate bugs. We hope to eventually provide the Caveatron for sale on a limited basis and to open-source the code and documentation online so that anyone can build their own.

Acknowledgements

The authors would like to acknowledge Gregg Williams for machining the enclosure and 3D printing cave models, Matt Capps for the design of the LIDAR head cover, Alan Craig for mechanical design of the pole-based system, Jill Orr for the GUI icons, and Ellie Watson for the Caveatron logo. We would also like to thank the many people have helped test the system and provide ideas for improvements.

References

- Buecher, Bob, 2016. *Do It Yourself LIDAR for Caves*, Presented at 2016 NSS Convention, Ely, NV.
- CloudCompare 2017. <http://cloudcompare.org> (access Jan 2017)
- DistoX 2017. <http://paperless.bheeb.ch> (access Jan 2017)
- Gallay M, Kanuk J, Hochmuth Z, Meneely JD, Hofierka J, Sedlak V. 2015. Large-scale and high-resolution 3-D cave mapping by terrestrial laser scanning: a case study of the Domica Cave, Slovakia. *Int. J. Speleol.* **44**:277–291.
- Meshlab 2017. <http://www.meshlab.net> (access Jan 2017)
- Walls 2017. <https://www.texasspeleologicalsurvey.org/software/walls/tsswalls.php> (access Jan 2017)
- Zlot R, Bosse M. 2014. Three-dimensional mobile mapping of caves. *J. Cave Karst Stud.* **76**:191–206.

(Abstract) **3D Photogrammetry Modelling Of Ice Moulins On The Grey Glacier,
Chilean Patagonia**

Tommaso Santagata, Alessio Romeo

*Affiliation: La Venta Esplorazioni Geografiche, Via Priamo Tron 35/F - 31100, Treviso (Italy), www.laventa.it
tommaso.santagata@laventa.it*

Abstract

The Chilean Patagonia icefield hosts some of the most spectacular glaciers of the world, including the Grey Glacier located in the Torres del Paine National Park.

Most of the moulins located on the crio-karstic area of this glacier were explored and mapped in 2004 during a speleological expedition organized by the Italian association La Venta Esplorazioni Geografiche. Twelve years after these first explorations a new survey was carried out to verify the evolution and conditions of the caves of this glacier. Thanks to the use of photogrammetric techniques, two of the main moulins explored during the 2016 expedition were mapped in 3D using a common camera in order to acquire detailed data on their shapes. Thanks to the realized 3D models it was possible to reconstruct the surface of the detected areas, which were analyzed using photogrammetric software and digitization and contour extractions tools. The information obtained has proven to be very accurate to study moulin morphologies and this method could be applied in future to obtain new data for comparisons.

This article is focused on the 3D mapping techniques and analyses performed.

Laser scanning as a powerful tool for speleogenetic studies in quartz-sandstone caves: the example of Imawari Yeuta, Venezuela

Francesco Sauro, Tommaso Santagata, Leonardo Piccini, Umberto Del Vecchio, Ada De Matteo,
Marco Camorani

Affiliation: La Venta Geographical Exploration, University of Bologna

Abstract

Laser scanning has been recognized as a useful tool for speleogenetic studies and morphometric analysis applied to epigenic and hypogenic cave morphologies. In March 2016 an expedition to Venezuelan tepuis was able to perform laser scanning (using a Leica HDS7000) in the cave Imawari Yeuta, one of the longest quartzite caves in the world with 23 km of development. The scanning has been focused in two main areas of the cave, the Thousand Columns Gallery (58 scans) and the Paolino Cometti Room (34 scans). The first section is characterized by hundreds of funnel shaped columns whose origin has been discussed previously by several authors. The second section instead represents the biggest known underground chamber in quartzite rocks.

The 3D modelling has shown the potential to easily obtain statistical analysis of column shape and orientation, their self-distribution along the cave, providing new hints to solve the debate on their formation. The 3D model of the giant chamber provides new information on how these collapse environments develop in quartzite settings due to lateral stream erosion along gently dipping stratification.

Keywords:

Inside The Glaciers Project: Laser Scanning Of The Grotta Del Gelo (Mount Etna, Italy)

Tommaso Santagata¹, Marco Vattano², Francesco Sauro¹, Giuseppe Spitaleri^{1,2}, Gaetano Giudice³, Corrado Bongiorno², Alessio Romeo¹, Marta Lazzaroni⁴

Affiliation: ¹Associazione di Esplorazioni Geografiche la Venta, Via Priamo Tron 35/E, 31030, Treviso, tommy.san84@gmail.com, cescosauro@gmail.com

²Federazione Speleologica Regionale Siciliana, via Terrasanta 7, 90141, Palermo, Italy. fsrs@federazioneSpeleologicaSiciliana.it

³Centro Speleologico Etneo, via Valdisavoia 3, 95100, Catania, Italy

⁴Gruppo Speleologico Archeologico Livornese

Abstract

As part of activities of the “Inside the Glaciers” project, managed by an Italian team of speleologists and geologists with the purpose of studying several ice-caves in Europe and South America, a research campaign was recently carried out in Mount Etna (Sicily, Italy). This volcano is the highest active in Europe and hosts more than 200 caves including Grotta del Gelo (Ice Cave) which is located on the Northern flank of Mount Etna at an altitude of about 2040 m a.s.l. This cave was formed during the Etna’s long and most destructive eruption dated from 1614 to 1624 and is one of the most famous because it hosts a small glacier, maybe the southernmost of the Northern hemisphere.

Aim of this project was to realize a detailed survey of Grotta del Gelo using a Leica HDS 7000 terrestrial laser scanner in order to acquire precise data measurements of the ice deposits. This survey was the first step of a monitoring project that will be developed in the next years in collaboration with the Etna Regional Park, the Sicilian Regional Speleological Federation and the Centro Speleologico Etneo of Catania which by many years are involved in the topographic monitoring of this particular cave.

The proposed article introduces the methods used for this first laser scanning survey campaign of Grotta del Gelo and the results obtained.

Keywords: Laser scanning; 3D modelling; ice caves; geomorphology; documentation

1. Introduction

Starting in October 2014 with the 1° International Glacier-Caving Camp on the Gorner Glacier (Zermatt, CH), the main objectives of the “Inside the Glaciers” (ITG) Project are to organize scientific expeditions and research campaigns related to the exploration and study of glacier-caves and ice-caves all over the world.

New technologies are widely used during these projects, especially in the field of 3D mapping.

In the last decennia Terrestrial Laser Scanning (TLS) has been increasingly applied for the survey of underground environments including natural caves. One of the most interesting application of TLS in caves is the possibility to monitor underground ice deposits.

For this reasons, in this study we applied TLS surveying to the Grotta del Gelo (Mount Etna, Southern Italy) to measure the glacial mass present inside this particular cave.

The Etna area has been protected since 1987 by the Sicilian Regional Government as a Regional Park which covers an area of 59,000 hectares divided into an “A” zone of total reserve area (19,000 hectares), a “B” zone of general reserves (26,000 hectares) and a pre park area of about 14,000 hectares.

The Grotta del Gelo opens in the “A” zone of the Etna Park and the authority’s permission was therefore necessary for these research activities. These, entirely non-invasive, were carried



Figure 1. Scanning operations with the laser scanner inside the cave. The tripod was fixed with ice screws to scan on the ice floor (Photo: Alessio Romeo).

out minimizing the number of speleologists and hours of permanence inside the cave.

2. Geology Of The Area And Cave Description

Mount Etna lies in a complex geodynamic zone due to the convergent margin between European and African plates, the subduction of the Ionian slab under the Aeolian arc and to the Hyblean-Maltese escarpment, which represents the boundary between the subducting Ionian plate (oceanic crust) and Sicily (continental crust). Located at an altitude of about 2.040 m a.s.l., Grotta del Gelo is well known among Mt. Etna volcanic

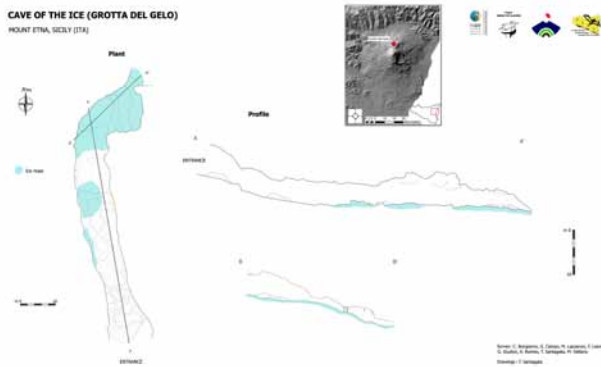


Figure 2. Topographic plant and section of the cave derived from point cloud digitizing. The ice part are highlighted in cyan (Photo Tommaso Santagata).

caves due to the presence of a stack of ice on its walls and floor which occupies about the 30% of the cave's volume. This small lava tube of less than 125 m long shows only one entrance of big dimensions (roughly 10 m wide and 5 m high). The cave is SW oriented and was formed by the lava flows called the "Lave dei Dammusi" during the Etna's longest eruption that affected its northern flank from 1614 to 1624 A.D. Lava from this eruption has flowed in different channels, often overlapped, that have formed several lava tubes.

The cave seems to work as a cold trap where the snow coming from the outside is able to preserve and feed the glacier. Grotta del Gelo plays a primary scientific and climatological role due to the evolution of the ice mass. The first important monitoring project was carried out from 1996 to 1999 performing a series of studies managed by the Etna Park in collaboration with speleologists of the Centro Speleologico Etneo and volcanologists from the Italian National Institute of Geophysics and Volcanology to monitor temperature and humidity by means of automatic micro data loggers and measuring the variations in height of the ice deposits by measuring some fix points marked on the ceiling and on the walls of the cave.

3. Laser Scanning Survey

Laser scanners are measuring instruments able to automatically acquire spatial coordinates of a region or a surface of an object. This technology is based on the emission and reception of a light beam that emits their own electromagnetic radiation and collects and measures the reflected emissions with high accuracy. For this work a Leica HDS7000 laser scanner was used. This device is equipped with a CLASS 1 laser with a flow range of 187 m and a wavelength of 1.5 micron. The survey phase was completed with the acquisition of 17 scans of which 11 in the area of the cave with the floor covered by ice. Scanning operations were performed in less than 5 hours starting the survey from the inner parts of the cave. To put the instrument in the areas of the cave with the floor covered by ice, it was necessary to fix the tips of the tripod with the head of ice screws that were positioned inside the ice trying to maintain the correct angle in order to put the scanner at the right level.

The data was processed to give a three-dimensional model of the entire cavity in the form of point cloud from which it was possible to derive a triangulated mesh model and perform morphological analysis in particular on the glacial deposit.

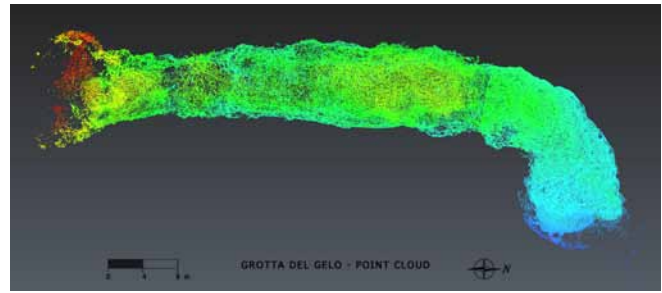


Figure 3. Point cloud 3D model of the Grotta del Gelo obtained by the union of the 17 scans realized (Photo Tommaso Santagata).

4. Data Analysis And Results

Through digitization of the point clouds, 2D and 3D polylines were extracted to produce different types of topographical works (plant, sections, contour lines), that will serve as a fundamental basis for all future monitoring of the ice mass present into the cave. The overall length of the entire cave calculated is of about 120 m with a vertical drop of 12 meters with the height of the ceilings vary from a few cm to 7 m. The width of the cave walls is substantially constant on all the 7 m along all the lava tube, except in the area near the entrance where the width is more than 12 m. The total volume of the cave, calculated on the basis of the mathematical model given by the triangulation of individual points from which it was possible to reconstruct the surface of the cavity, is reported to be 4,107 m³. As regards the glacial deposit present in the terminal part of the cave, the development calculated is higher than 30 m in length with a few cm from the end part to the heights of the cavity ceiling variables up to 6.30 m in the central part of the cavity and a volume of approximately 1,500 m³.

5. Conclusions And Future Perspectives

Laser scanners offer many advantages in comparison to more traditional surveying techniques, in fact these devices are able to deliver a very high amount of precise measured points quickly, and making it possible to realize 3D models.

The TLS survey of Grotta del Gelo have allowed us to calculate the precise volume of the ice mass present in this cave and obtain a high amount of information that will be used in the next years to study the ice mass.

Further analysis on the data have allowed us to evaluate the presence of the ice inside the cave by the possibility of digitizing the surrounding environment in a very short time.

This first survey campaign represents just the first step of a monitoring project that will be developed in the next years with the aim to study the evolution of the ice deposit inside this cave.

References

- Buchroithner M, Gaisecker T, 2009. Terrestrial laser scanning of a complex dome in an extreme Alpine cave system. *Photogrammetrie – Fernerkundung – Geoinformation* (PFG) 4, 329-339.
- Buchroithner M, Milius J, Petters C, 2011. 3D Surveying and visualisation of the biggest ice Cave on Earth. *Proceedings of*

the 25th International Cartographic Conference, Paris, France, 3-8 July, CD-ROM: 6p

Fabbri S, Sauro F, Santagata T, Rossi G, De Waele J, 2017. High-resolution 3-D mapping using terrestrial laser scanning as a tool for geomorphological and speleogenetical studies in caves: An example from the Lessini mountains (North Italy). *Geomorphology*, **280**, 16-29.

Marino A, The Ice Cave and its glaciological phenomenon, 1991. *Proceeding of the 1xth International Simposioum of Volcanospeleology*.

Gallay M, Kanuk J, Hochmuth Z, Meneely J D, Hofierka J, Sedlák V, 2015, Large-scale and high-resolution 3-D cave mapping by terrestrial laser scanning: a case study of the Domic Cave, Slovakia. *International Journal of Speleology* **44**(3), 277-291.

Santagata T, Lugli S, Camorani M E, Ercolani M, 2015, Laser scanner survey and TruView application of the Grotta della Lucerna, a roman mine for lapis specularis. *Proceedings of the International Congress of Speleology in Artificial Cavities*, Rome, March 11-17, 2015, 143-147.

Deterministically Defining Chambers in 3D-Scans of Caves

Nico Schertler¹, Manfred Buchroithner¹, Donald McFarlane², Guy van Rentergem³, Joyce Lundberg⁴, Stefan Gumhold¹

Affiliation: ¹ TU Dresden, Germany

² Keck Science Center, The Claremont Colleges, California, USA

³ Koningin Astridstraat, Deinze, Belgium

⁴ Carleton University, Ottawa, Canada

Abstract

Increasingly, speleologists are employing terrestrial laser scanners to generate highly detailed 3D maps of caves, which can be used for quantitative analysis and comparison. Although their high precision allows very accurate volume computations, one of the key aspects of cave mapping – the identification of chambers for volumetric comparisons – still remains a manual post-processing step. Naturally, such manual steps are heavily influenced by subjective preferences and not suited for objective comparisons. In this paper, we present a novel algorithm that bridges this gap. Given an appropriate 3D model of a cave, our algorithm produces a unique and unambiguous segmentation of the cave into distinct chambers and passages. It is free of human bias and insensitive to scanning noise, scaling, and orientation of the model. The foundation of our work is a thorough analysis of cave geometry. We transfer the results of this analysis into a mathematical model and use state-of-the-art methods from computer graphics to derive the segmentation. We initially tested our approach with various cave models and a group of speleologists, which confirmed that our algorithm's results conform closely to manual segmentations. Therefore, it seems to be well-suited as a substitute for “classical” but ambiguous existing approaches to comparing chamber volumes, and can provide objective comparability to the process.

Keywords:

1. Introduction

In recent years, digital surveying of caves has become increasingly popular. Highly accurate laser scanners in combination with reference markers that help to assemble multiple partial scans to a single model have been used successfully to generate detailed three-dimensional maps of caves (McFarlane, *et al.*, 2013) (Canevese, *et al.*, 2013). For the first time, the availability of these maps allows precise measurement of cave sizes in terms of length, volume, or surface area up to an accuracy that is superior to any manual method.

However, an important piece of information is still missing that is required to measure chamber sizes: the actual borders of the chambers within a cave system. A scanning solution that acquires a cave's geometry is obviously not able to capture this semantic information since it is mainly dictated by convention and experience of professionals. Furthermore, the opinions of different professionals may vary slightly when asked to outline the chambers in the same cave. Thus, any advantage of the high-accuracy geometry would be lost immediately as soon as human interaction is involved in the process of defining chamber extents.

Instead, we present a fully automatic algorithm to solve the aforementioned problem: Given the result of a scanning expedition in form of a 3D model of a cave, our algorithm deterministically calculates the locations and extents of all chambers in the cave system, which allows objective size calculation without human bias. We developed our algorithm in conformance with the common sense in speleology, such that the results match manual segmentations from professionals closely. Yet, our algorithm provides enough degrees of freedom to alter the underlying definitions.

The basis of our algorithm is a so-called curve skeleton (Cornea, *et al.*, 2007), which is a network of paths through the cave. At every point of the skeleton, we then compute the per-

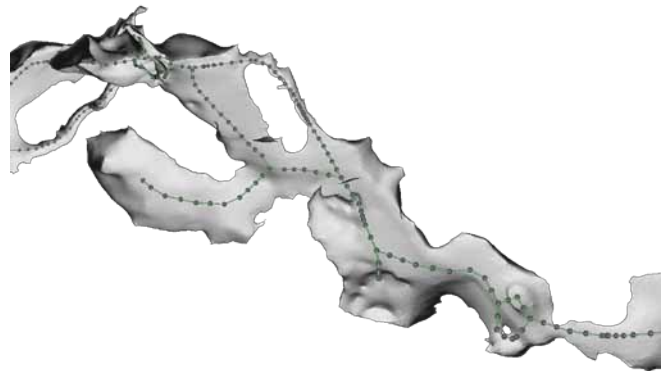


Figure 1. Curve skeleton represented as connected dots inside the Eisriesenwelt caves, Austria

ceptible size of the cave surrounding the skeleton point. This size measure is a generalized radius and captures the local extents of the cave. The change of the perceptible size along the skeleton gives important hints about entrances of chambers. More specifically, a sudden increase in size, which we determine from the first two derivatives, is a strong indicator that the corresponding skeleton path leads into a chamber. We gather all those indicators from the skeleton and generate a probabilistic model that describes the likelihood of entrances at every position of the skeleton. We then find the maximum-likelihood segmentation of the skeleton with respect to the probabilistic model, which allows us to uniquely classify each part of the cave model as either a passage or a chamber.

In this paper, we give a high-level overview of our algorithm. For a thorough explanation, we refer the reader to the according technical paper (Schertler, *et al.*, 2017).

2. Input Data and Preparation

Our algorithm takes as input the watertight reconstructed surface from a series of scans, i.e. any holes are closed in the resulting 3D model. Such models can be generated easily from the raw point cloud data that virtually all scanning solutions expose, e.g. with Poisson Surface Reconstruction (Kazhdan & Hoppe, 2013).

Fine details in the cave's geometry are irrelevant for chamber recognition. Therefore, we reconstruct the surface with a low resolution and identify chambers in this coarse representation. Once the chambers are found, they can be mapped back onto a highly-detailed model, allowing accurate size calculation.

3. Curve Skeleton

The first step of our algorithm calculates the cave's curve skeleton by successively contracting the 3D model until a thin path network remains (Tagliasacchi, *et al.*, 2012). Figure 1 shows the result of this procedure. As can be seen, the skeleton is a smooth path that is centered inside the cave and reflects the cave's overall topology, i.e. branching in the cave results in a corresponding branching in the curve skeleton.

Due to the contraction procedure, every point on the skeleton is also equipped with a set of corresponding points on the surface (i.e. those points that have been contracted to the according skeleton point). This correspondence allows to project the final segmentation from the curve skeleton back onto the cave surface. In perfectly cylindrical regions of the cave, these correspondences form a circle around the skeleton vertex, whereas more general cave shapes lead to irregular correspondence distributions.

We represent the curve skeleton in its discretized form, i.e. as a graph, consisting of vertices and edges. In the following step, we will calculate the perceptible size for every skeleton vertex and derive the first two derivatives on the edges. Intuitively, the first derivative corresponds to the direction of size changes and the second derivative represents how rapidly the change happens (cf. curvature).

4. Perceptible Size

The perceptible size at any skeleton position is the essential measure on which we base our segmentation algorithm. We define it in a way such that it corresponds to the perceived size of the cave for an observer located at the according skeleton vertex.

Our perceptible size measure is a generalized radius of the cave. E.g., for a cylindrical cave part, the size is equal to the cylinder's radius. Similarly, for elliptical cylinders, we use the average radius. In the following section, we extend this idea and explain how we calculate the perceptible size for arbitrary cave shapes, especially in the presence of branching.

The examples of the cylindrical caves have in common that the resulting perceptible size is the average radius over a circular line around the according cave part, where the radius is defined as the distance of the skeleton vertex and the cave surface in a given direction. We generalize this approach for arbitrary cave shapes as follows:

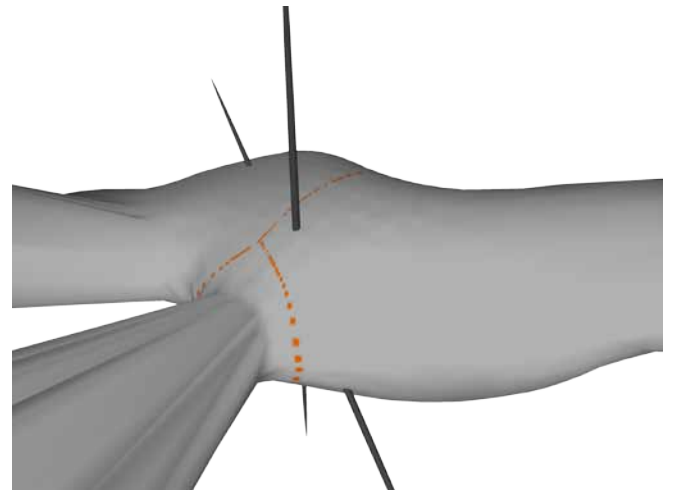


Figure 2. Visualization of the cave part that is visible from the skeleton vertex at the intersection of the dark axes along with the corresponding valley line network on the surface used for perceptible size calculation visualized as orange dots. Gomantong caves, Borneo

The cave part surrounding a skeleton vertex can be expressed as a spherical radius field. In this radius field, we find a closed network of valley lines that encompasses the vertex completely, i.e. the connected area on the unit sphere between the valley lines is smaller than a prescribed threshold. As a consequence, these lines are most compact in the sense that they would not contract further if they were rubber bands around the physical cave. As such, they naturally avoid incident passages and tend to align with the areas of smallest radius. Please note that the rubber band analogy was only chosen for demonstration purposes and is not completely accurate as there is no actual physical model in our calculation. Please refer to the technical paper (Schertler, *et al.*, 2017) for a rigorous definition of this line network. An example network can be found in Figure 2.

Once this line network is found, we average the radius over the network to find the perceptible size. By construction, cylindrical caves produce networks that consist of a single circle with constant radius, resulting in the same perceptible size as in the introductory examples.

The steps to calculate the perceptible size over the entire data set are therefore as follows: For every skeleton vertex, we generate a spherical radius field. In this field, we find a network of valley lines and calculate its average radius. The result is then used as the skeleton vertex' perceptible size.

After calculating the perceptible size, we evaluate the first and second derivative numerically. These values are then used to guide the actual segmentation of the skeleton.

Segmentation

The goal of the segmentation step is to assign one of two possible labels (chamber or passage) to every skeleton vertex that describes if the vertex belongs to a chamber or a passage. If this segmentation is known, distinct chambers can be separated easily by analyzing connected components.

To find the segmentation, we generate a Markov Random Field from the curve skeleton that describes the likelihood

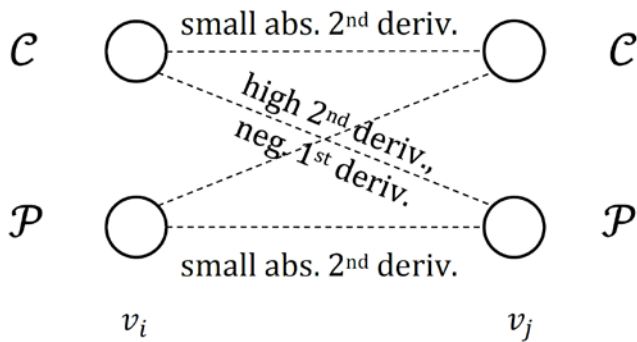


Figure 3. All possible label transitions for an edge between skeleton vertices. The geometric characteristics that lead to high probabilities for the respective transitions have been annotated for three of the four transitions.



Figure 4. Segmentation result for the Eisriesenwelt caves, Austria. Chambers are visualized with distinct colors, passages are grey.

of every possible label transition for every skeleton edge in a probabilistic framework. Figure 3 shows the four possible transitions for a single edge. The underlying geometric properties on the edge (i.e. the first and second derivatives of the perceptible size) allow us to define the probabilities for every transition. E.g., a high absolute second derivative is characteristic for an area where the cave size changes rapidly and thus indicates a chamber entrance. Therefore, the two transitions $C \rightarrow P$ and $P \rightarrow C$ are very unlikely because they do not introduce an entrance on this edge. And depending on the sign of the first derivative, one of the two remaining transitions should have a higher probability than the other.

In this manner, we calculate all four transition probabilities for all edges of the curve skeleton. These partial probabilities then allow us to calculate a final objective function in form of the total probability: Given a specific labeling of the skeleton vertices, every edge is fixed to the according probability value defined by the labels of its two incident vertices. The product of all transition probabilities is then the total probability of the labeling given the underlying geometric properties. We finally maximize this objective function to find the most probable labeling with QPBO (Rother, *et al.*, 2007).

Once the labeling is found on the curve skeleton, we find distinct chambers via connected component analysis. The result is then projected back onto the cave surface, such that every point of the 3D model is uniquely associated to a specific chamber or a passage.

5. Results and Conclusions

The chamber recognition algorithm presented in this paper leads to expressive segmentations of arbitrary cave data sets (cf. Figure 4). In a formal evaluation, we found that a reasonable parameterization achieves a similarity between automatic and manual segmentations from experts of over 95 %.

The high similarity with professional opinions makes our algorithm a perfect candidate to substitute the manual and potentially error-prone segmentation step in existing chamber size calculation pipelines. Furthermore, our algorithm is deterministic, i.e. running it multiple times on the same data yields exactly the same result, which is an obvious prerequisite for objective comparability.

Although finding a good parameterization is not trivial, a rich data base of cave scans and manual annotations can help significantly in both improving the core algorithm and determining a global parameter set that is applicable to a variety of cave types.

References

- Canevese, E. P., Forti, P. & Tedeschi, R., 2013. New Acquisition, 3D Modelling, and Data Use Methods: The Laser Scanning Survey of Re Tiberio Cave. *ICS Proceedings*.
- Cornea, N. D., Silver, D. & Min, P., 2007. Curve-skeleton properties, applications, and algorithms. *TVCG*.
- Kazhdan, M. & Hoppe, H., 2013. Screened Poisson Surface Reconstruction. *ACM TOG*.
- McFarlane, D. *et al.*, 2013. Integrated Three-Dimensional Laser Scanning And Autonomous Drone Surface-Photogrammetry at Gomantong Caves, Sabah, Malaysia. *ICS Proceedings*.
- Rother, C., Kolmogorov, V., Lempitsky, V. & Szummer, M., 2007. Optimizing binary MRFs via extended roof duality. *CVPR*.
- Schertler, N., Buchroithner, M. & Gumhold, S., 2017. Chamber Recognition in Cave Data Sets. *Eurographics* (to appear).
- Tagliasacchi, A., Alhashim, I., Olson, M. & Zhang, H., 2012. Mean curvature skeletons. *Computer Graphics Forum*. Vol. 36. No. 2 (Proceedings of Eurographics 2017)

The Pilkington-Lewis Squeeze Index; a rating system for cave constrictions.

Heather Siebert

Affiliation: Scout Caving Group South Australia

Abstract

Squeezes in caves may be a necessary evil to push the boundaries of cave exploration, a painful passage to a beautifully decorated room or simply a fun physical challenge. As all cavers know, a squeeze is a passage or element of a cave that requires careful consideration or planning of body positioning and movement to pass through. With the Pilkington-Lewis Squeeze Index (PiLSI) cave constrictions can be rated in a similar way to the climbing grades used by rock climbers. Information can be communicated on cave maps about the shape, incline, surface type, hazards and degree of difficulty in a concise manner. In the PiLSI, difficulty pertains to the degree of technique required to get through which may relate to skills needed, such as twisting through a corkscrew, or the average caver's body habitus as no matter how willing the mind may be, some bodies will never fit through the 8 1/4 inch squeeze! The PiLSI is easy to add to any cave map with ratings such as '10C-' which is a downwards sloping corkscrew shaped restriction with a difficulty rating of 10- tight enough to require helmet removal to pass through. With difficulty ratings of 1 (easy) to 15 (practically impossible) and many different shapes, the PiLSI is easy to understand and implement to any cave setting and corresponding cave map.

Keywords:

Lessons learned from a large-scale 3-D mapping project, with Faro laser scanners, of the Gomantong Caves, Borneo

Guy Van Rentergem¹, Donald McFarlane², Joyce Lundberg³, Manfred Buchroithner⁴

Affiliation: ¹K. Astridstraat 57, Deinze, Belgium. guy.van.rentergem@skynet.be

²Keck Science Department, The Claremont Colleges, California, USA

³Department of Geography and Environmental Studies, Carleton University, Ottawa, Canada

⁴Institut für Kartographie, Technische Universität, Dresden, Germany

Abstract

During a 24-day T-Lidar scanning project of the Gomantong Caves in Sabah, Malaysia (some 4 km of often very physically-demanding passage), we collected 271 scans, resulting in a massive data set of 12.6 billion scan points. In hindsight, we can now offer some new protocols that should enhance future field work and subsequent data processing. The main lesson we learned is that using reference spheres is not really necessary: instead, we can use features of the complex natural surfaces of the cave as reference. This accelerates the pace of scanning greatly, and eliminates the dangers associated with placements of spheres in hazardous situations. This increase in scanning efficiency does come at a price because subsequent scan registration becomes more complex. However, the extended time required for a more complex cloud-to-cloud registration in an office environment is more-than-compensated for by the increased efficiency and reduced risk of the fieldwork. In this paper, we also review some other lessons learned during this project.

Keywords:

1. Introduction

The Gomantong Caves, Sabah, Malaysia consist of more than 4 km of large passages that are of notable geomorphological, biological and cultural significance. Beginning in July 2012, an ambitious project was undertaken to map the caves using Faro terrestrial LIDAR scanning with the goal of providing 3D point cloud data to address specific biological and geomorphological questions (Lundberg *et al.* 2012, McFarlane *et al.* 2013). The project continued in July 2014, requiring approximately 24 field days to complete the job in this very demanding environment. A total of 271 scans was collected, resulting in a dataset of 12.6 billion scan points. The size of the dataset creates significant difficulties in data processing and analysis. Addison (2011), faced with 18 million data points from a scanning in Mammoth Cave, summarizes very well the difficulties: “The ability to collect massive point data sets appears to be well beyond the ability to do anything meaningful with the data back at the office”. The Gomantong Caves project engendered 700 times more data than this, considerably exacerbating the difficulties that Addison encountered. Valuable lessons were learned in the course of both field work and data processing, which provide the basis for planning future projects of this nature.

2. Planning the project

Scanning a cave is a costly affair. So, before doing the field work, time should be spent defining the goal of the final product: for example, are the data to be used to create a virtual cave, or for volume calculations, or for map making, for bat counting, for printing a 3D model, etc.? The goal of the project will determine the resolution needed for the scans. For example, a 3D print of the cave requires only low resolution scans and it makes no sense to spend additional resources scanning in full resolution, whereas the highest possible resolution should be used if, for example, a bat roost is to be scanned for determination of species (Azmy *et al.*, 2012).

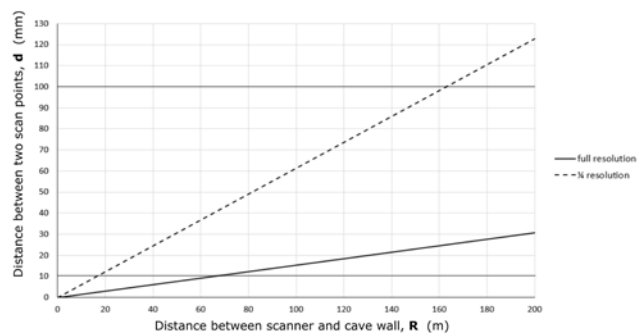


Figure 1. Influence of the resolution angle and distance from the scanner, R , on the distance between two adjacent scan points, d

Modern scanners have the capacity for very high resolution, but a basic knowledge of the limitations is necessary. As an example, the Faro Focus 3D X 330 has a resolution of 40960 points over 360°, which can be translated to a resolution angle of 0.009°. A full scan like this takes almost an hour and produces a massive point cloud of 711 million points. So, in most cases, scanning at 1/4 resolution, with 10240 points on 360° or 0.036°, which results in clouds with 44 million points, will suffice.

The main factor to consider, in order to achieve the requisite resolution, is the distance between the instrument and the scanned surfaces (Figure 1). For example, the distance between the Lidar and the cave walls should be closer than 20 metres when centimetre resolution is needed and the scanning is at 1/4 resolution. If the project involves detailed scans of high cave ceilings it might be impossible to get the wanted resolution even when working with full resolution. As figure 1 illustrates, it is not possible to get centimetre-scale detail if the ceilings are higher than 70 m.

3. Fieldwork

3.1. Reference spheres

Scanning caves is often a risky business. So the shorter the time spent in the cave the better. A time-management analysis of the scanning process underground reveals that most of the time is used for transportation of the equipment and setting up the reference spheres. Placing these spheres can be tedious, and optimal placement often involves significant risk to personnel. Another difficulty with the spheres is trying to keep them clean in muddy environments. Furthermore, complex caves may require many spheres, adding a layer of complexity to transportation arrangements and required workforce.

The lesson we learned from field experience is that reference spheres are really not needed. They are used for semi-automatic registration of the point clouds, with specialized software. However, alternative registering processes are available that do not require reference spheres (see section 4.1 below). We conclude that not using the reference spheres will significantly speed up the scanning process, thus minimizing the dwell time underground and also reducing the risk of accidents.

3.2. File names for scans

The second lesson we learned is to use logical file names for the scans (rather than something without much geographic meaning such as numbers). One should define a logical pattern for naming the individual scans and stay with this definition during the entire project. This is certainly important for big projects where different people will work with the scanner or where the project is stretched over different scanning periods. It would be helpful to integrate the date, name of the cave and a section number into the name. Well-chosen filenames during field work will greatly facilitate the subsequent registration, management and archiving of scanner files.

3.3. Additional graphical documentation

The third lesson we learned is that it is important to take many photographs in the field. Scans may not be enough for registering the cave after the field work. Point clouds taken in the dark have only reflection data and no colour information. A photograph can be used for reference to solve difficulties while registering or analysing the cave. The photographs do not have to be of good quality; they simply need to be taken often and consistently, in logical relation to the scanning. Pictures are also useful reminders while analysing the data when the fieldwork has long been finished.

3.4. Backup

Unfortunately, data files can become lost or corrupted over time. Therefore, the fourth lesson we learned is that scan files should be backed up during field work, labelled clearly, and archived in several different and trustworthy locations (preferably after each day of data collection).



Figure 2. A mesh generated from the Gomantong dataset rendered with Blender.

4. Post-field data processing

4.1. Registering the scans

The process of joining all the point clouds scanned with reference spheres into one big point cloud is called *target-base registering*. Specialized software uses these spheres to semi-automatically find matches between the different scans, speeding up the process of registering. This is not so demanding on CPU resources (match the spheres and the rest will follow) and can be done with a powerful laptop, and possibly even during the fieldwork.

When no reference spheres are used, the scans are processed instead with **cloud-to-cloud registering**. This works by manually positioning the scans as well as possible. This has to be checked in the horizontal and vertical planes. The computer will try to do the final match. This is very demanding on CPU resources and needs long processing times, but the results are very good, with low mean target tensions. To use cloud-to-cloud registering a powerful computer is needed with many and fast cores, a lot of RAM (64 GB is a good start) and fast SSD disks. A laptop would not normally meet these requirements. So registering will not be possible during the fieldwork and can only be done afterwards. This also means that registering is best done by a person who knows the cave well. This insight into the cave will make solving the 3D jigsaw-puzzle during registration a lot easier.

4.2. Final product

Further data manipulation can only proceed after registering the point clouds. The complexity and time needed to create the final product depends on the predetermined goals of the project.

Illustrations or animation

3D point clouds of caves result in wonderful X-ray-like pictures. This output is easy to produce using an image editor to process the pictures. Animations of point clouds are normally used for fly-throughs. Most registering software has a built-in function for making these amazing videos.

Making a mesh

Making a mesh (Figure 2) from a point cloud is not an easy task and can take a lot of time. A mesh is used for, e.g., 3D rendering, printing a 3D model (STL file) or analysis for a science

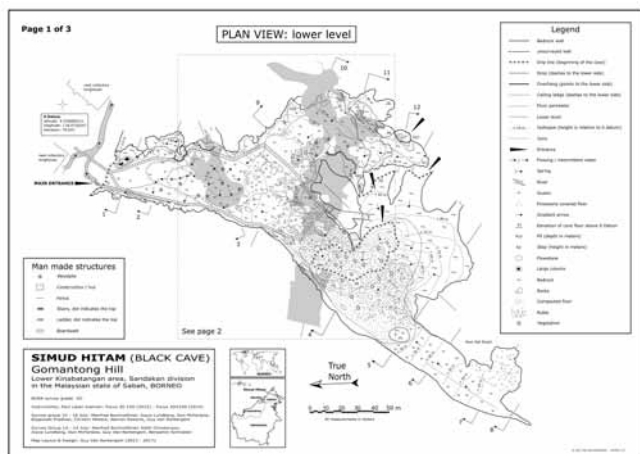


Figure 3. Cave map of Simud Hitam, one of the Gomantong caves, made solely based on T-Lidar-obtained data (still a work in progress).

project with, e.g., GIS applications. There is a learning curve involved in getting the mesh ready. Here are some useful tips:

- Delete the foliage around entrances. Meshing software cannot easily process foliage and will give poor results.
- Filter the point cloud to remove stray points.
- Reduce the number of points by Poisson disk sampling (in accordance with the requirements of the goal of the mesh, such as 3D printing or rendering).
- To print a 3D model a closed mesh is needed. This can involve closing entrances by hand with specialized mesh-editing software.
- Specialized software can be expensive. A lot of work can be done with open source software, e.g. :

MeshLab (<http://www.meshlab.net/>) the swiss knife application for meshing, filtering and a lot more.

CloudCompare (<http://www.danielgm.net/cc/>) can be used for registering.

Blender (<https://www.blender.org/>) for rendering the point cloud.

Polymender tool (<http://www1.cse.wustl.edu/~taoju/code/polymender.htm>) for repairing the mesh.

Making a map

Classic cave maps incorporating plans, profiles and sections are universally used by cavers for navigation and exploration. These maps are made with great determination and effort by cave surveyors and are, to some extent, personal interpretations of the underground landscape. Cave maps can be considered as pieces of art and the introduction of T-Lidar will

not make them obsolete. A printed point cloud or mesh is not very effective to find your way in a cave, and the fragility of a tablet with a 3D model of the cave precludes its use underground. Therefore, cave maps are still required.

However, creating a classic cave map (e.g., Figure 3) from a point cloud is very tedious. One of the reasons is simply because there is just too much detail available. It needs experience to filter through the overwhelming amount of data. But using a point cloud for making sections of the cave is incomparably superior to the classic way of guesstimating the dimensions and features of the passages. Working with point clouds opens the door to new insights into the cave genesis because of all the details available in the scans of the ceilings, the birth ground of many caves. In classic caving the ceilings are, most of the time, hidden in the dark. Darkness is no obstacle for the laser of the scanner and will register the ceilings in full detail.

5. Conclusion

T- Lidar is opening fantastic new ways to analyse caves and has much more to offer than classic cave surveys. But the cave surveyor will not be a dying breed. Point clouds won't replace a classic cave map any time soon because of costs and the amount of work involved.

Before starting a scanning project it is good to know the limitations of your scanner. It is quite possible that the unit cannot achieve the desired goals. Cave scanning needs a different approach than architectural or industrial scanning. The usual scanning routines used at the surface may be cumbersome and even dangerous in a cave environment. Time can be saved by not using reference spheres and by using cloud to cloud registration.

References

- Addison A, 2011. LiDAR at Mammoth Cave. *Civil Engineering Surveyor*, April 2011, 22-25.
- Azmy SN, Sar SAM, Shafie NJ, Ariffin A, Majid Z, Ismail MNA, Shamsir MS. 2012. Counting in the dark: Non-intrusive laser scanning for population counting and identifying roosting bats. *Scientific Reports*, 2(524),1-4.
- Lundberg J, McFarlane DA, 2012. Post-speleogenetic biogenic modification of Gomantong Caves, Sabah, Borneo. *Geomorphology*, 157/158, 153-168.
- McFarlane DA, Buchroithner M, Lundberg J, Petters C, Roberts W, Van Rentergem G, 2013. Integrated three-dimensional laser scanning and autonomous drone surface-photogrammetry at Gomantong caves, Sabah, Malaysia. In: Filippi M. & Bosák P. (Eds.), *Proceedings of the 16th International Congress of Speleology, Brno, Czech Republic*, 2, 317-319.

Mathematical modelling of the relationship between terrestrial LIDAR scan point density and volumetric assessment of underground cavities

Guy Van Rentergem¹, Donald McFarlane², Joyce Lundberg³, Manfred Buchroithner⁴

Affiliation: ¹K. Astridstraat 57, Deinze, Belgium. Corresponding author: guy.van.rentergem@skynet.be

²Keck Science Department, The Claremont Colleges, California, USA

³Department of Geography and Environmental Studies, Carleton University, Ottawa, Canada

⁴Institut für Kartographie, Technische Universität, Dresden, Germany

Abstract

Terrestrial LIDAR (T-Lidar, or 3-D) scanning gives outstanding detail in cave surveying, generating extremely large datasets of dense point clouds, resulting in very detailed and precise 3D models of the scanned caves. These models are commonly used to determine the volume of chambers.

Intuition tells us that the denser the point cloud, the better it will fit the real dimensions of the cave. Here we prove that this is not the case. We show that with a low number of measured points it is possible to calculate volumes which will match the true volumes of a cavity with high precision.

Scanning at extremely coarse resolution with angles as high as 4.3° (approximately 1/400 of full resolution) gives a good estimate of volume, although detail is not rendered. The linear relationship between the distance of the scanner and the scanned resolution of the cave wall indicates that < 1 cm-scale detail can be rendered by scanning at ¼ resolution up to ~20 m distance. For the same detail, at distances between ~20 and ~70 m, scanning at higher resolution will be required. It is not possible, even with full resolution, to get centimetre-scale detail at distances greater than ~70 m. Therefore, it is apparent that scanning caves at only ¼ resolution is generally quite sufficient to represent the real volume of the cave and most of the detail.

Keywords:

1. Introduction

Terrestrial LIDAR (T-Lidar, or 3-D) scanning is increasingly being used for surveying caves, with remarkable results (Buchroithner 2015; Gallay *et al.* 2015; McFarlane 2013; McFarlane *et al.* 2013). The laser measurements generate immensely dense point clouds that can be used to generate very detailed and precise 3D models of the scanned caves. A common goal of 3D modelling of caves is the determination of cavity volume (including those recognised as, or claimed as, the largest natural underground cavities on Earth). Intuition tells us that the denser the point cloud, the better it will fit the real dimensions of the cave, and thus the better the estimate of volume will be. This concept is used in many discussions about the precision of volume determination by terrestrial LIDAR. Here, we test this assumption by considering how well the generated 3D model is likely to match the real scanned volume of the cave, represented here by a theoretical structure whose volume can be calculated precisely.

2. Determining the fit of a triangulated sphere in the circumscribing sphere

Imagine a perfect sphere with a given radius that precisely contains a Platonic solid with the same centre as the sphere. Each vertex of this regular polyhedron must be on the surface of the sphere. To keep it simple, we only consider polyhedrons that solely contain identical equilateral triangular faces (Figure 1). This is acceptable because triangles are one of the basic building elements of a polygonal mesh. From the five Platonic solids only three fit this requirement: the tetrahedron, the octahedron and the icosahedron.

The volume with the lowest face count possible is a tetrahedron made from only 4 triangles and 4 vertices, but it does

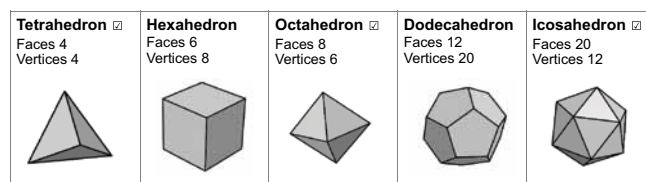


Figure 1. The five Platonic solids. Tick marks indicate polyhedrons with identical equilateral triangular faces.

not resemble a sphere. If we add more triangles we get an octahedron with 8 faces and 6 vertices. The next step is an icosahedron with 20 faces and 12 vertices. The icosahedron resembles a sphere already, but still more triangles are needed. However, it is mathematically not possible to add more equilateral triangles. We cannot create a new volume by adding a sixth triangle around one of the vertices of an icosahedron. This operation will only result in a flat face. The trick is to divide the faces of the icosahedron into 4 new triangles and make sure that the new vertices are contained on the circumscribed sphere. This can only work with isosceles triangles instead of equilateral ones.

This can easily be demonstrated with 3D computer graphics software, such as, for example, the open-source software *Blender* (<https://www.blender.org/>). With *Blender* it is possible to create so called “icospheres” – the name for a polyhedral sphere made up of triangles. During the creation of an icosphere the user can specify a number of subdivisions. Each increase of subdivision splits each triangle face into four triangles. A subdivision with $n = 1$ generates the already-mentioned icosahedron. A subdivision with $n = 5$ creates an icosphere with 6820 faces, which results in a nearly perfect sphere (Figure 2).

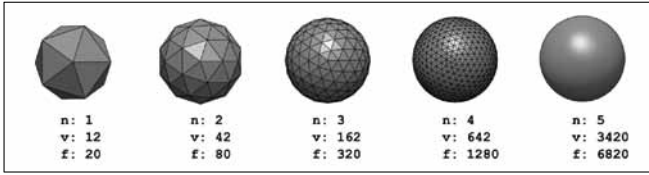


Figure 2. Consecutive subdivided icospheres created in Blender; “n” is the number of subdivisions, “v” the number of vertices, and “f” the number of faces.

We now compare the surface area (S_{sphere}) and volume (V_{sphere}) of a real sphere with the surface area (S_{ico}) and volume (V_{ico}) of the generated icospheres. Blender has specific functions to calculate these values.

In the calculations, the following symbols and equations are used:

S_{ico} Surface area of icosphere (m^2) calculated by Blender

V_{ico} Volume of icosphere (m^3) calculated by Blender

d average length of the sides of the triangles of the icosphere (m) calculated by Blender

ΔS difference between surface areas S_{sphere} and S_{ico} (m^2)

ΔV difference between volumes V_{sphere} and V_{ico} (m^3)

$\Delta S\%$ percent difference between surface areas S_{sphere} and S_{ico}

$$\Delta S\% = \frac{\Delta S}{S_{sphere}} \cdot 100 \quad (1)$$

$\Delta V\%$ percent difference between volumes V_{sphere} and V_{ico}

$$\Delta V\% = \frac{\Delta V}{V_{sphere}} \cdot 100 \quad (2)$$

Res calculated resolution angle in degrees ($^\circ$) based on R and d (Figure 3)

$$Res = 2 \sin^{-1} \left(\frac{d}{2R} \right) \quad (3)$$

Assume we are in a perfectly spherical cave chamber with a radius, R . In the centre of this void the T-Lidar scanner is positioned. From the distance, d , between two adjacent scan points of the resulting point cloud and the radius, R , of the sphere, the resolution angle of the scanner can be calculated using equation 3.

The test case (Table 1) is a sphere with radius, R , of 1.00 m. This sphere has a surface area, S_{sphere} , of 12.566 m^2 and a

Table 1. Relation between different icospheres and the real sphere with R of 1 m, surface area, S_{sphere} , of 12.566 m^2 , and volume, V_{sphere} , of 4.189 m^3 .

Subdiv.	verts	faces	Sico	Vico	d	ΔS	ΔV	$\Delta S\%$	$\Delta V\%$	Res ($^\circ$)
1	12	20	9.574	2.536	1.051	2.992	1.653	23.81	39.46	63.40
2	42	80	11.66	3.658	0.582	0.906	0.531	7.21	12.68	33.84
3	162	320	12.32	4.047	0.298	0.246	0.142	1.96	3.39	17.14
4	642	1280	12.50	4.152	0.150	0.066	0.037	0.53	0.88	8.60
5	3420	6820	12.55	4.179	0.075	0.016	0.010	0.13	0.23	4.30

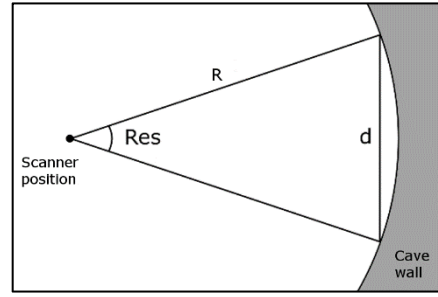


Figure 3. Relation between resolution angle “Res”, radius “R”, and side of triangle “d”.

volume, V_{sphere} , of 4.189 m^3 . The results can be applied to a sphere of any radius. Suppose we have a spherical cave room with a radius, R , of 100 m and this room is scanned with a device using a resolution angle of 4.30° (last line of Table 1). The distance between two neighbouring scan points on the cave wall will be $d = 7.5$ m.

It is remarkable to see that this coarse resolution results in an extremely low difference between the real volume and the scanned volume: $\Delta V\% = 0.23\%$. Of course, commercial T-Lidar scanners have a much smaller resolution angle, at least two orders of magnitude better than 4.30°. For example, the Faro Focus 3D X 330 has a resolution of 0.009° or 15 mm at 100 meters distance, or 478 times better than the 4.30° in our example. We can conclude that volume determinations based on the results from a commercial scanner are more than adequate to represent the real volume of the cavity.

Although scanning with a resolution angle as big as 4.30° might result in good volume estimations, the resulting scans will lose all the detail of real world caves. In the next section we look more closely into the relation between scan resolution and the detail obtained.

3. Relation between scan resolution and detail

The Faro Focus 3D X 330 has a resolution of 40960 points over 360°, which can be translated to a resolution angle of 0.009°. A full scan like this takes rather a long time and produces a point cloud of 711 million points. So, in most cases, while scanning in the field, a ¼ resolution is used, with 10240 points over 360° or 0.036°, which results in clouds of 44 million points.

Using these two resolutions (0.009° and 0.036°) we can calculate the distance (in m) between two adjacent scan points, d , as a function of the distance between the scanner and the cave wall, R . We can rewrite equation 3 to get the value d .

$$d = 2R \sin^{-1} \left(\frac{Res}{2} \right) \quad (4)$$

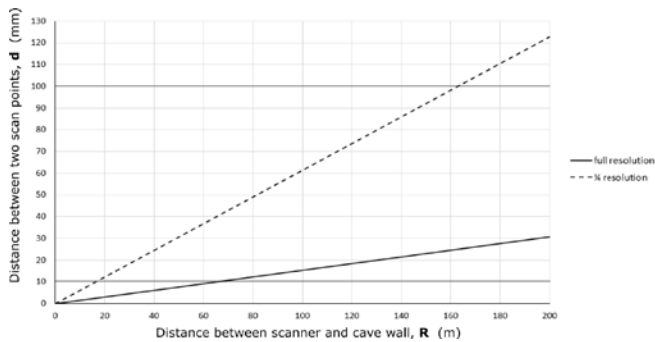


Figure 4. Influence of the resolution angle and distance from the scanner, R on the distance between two adjacent scan points.

There is a linear relation between the distance of the scanner and the scanned resolution of the cave wall. This relationship must be taken into consideration before starting an underground scanning campaign. For example, if centimetre-scale resolution is required (as, for example, might be the case when scanning bat roosts; cf. Azmy *et al.*, 2012) and the scanner is set at $\frac{1}{4}$ resolution, then the instrument should not be placed more than 20 metres from the walls. If centimetre-scale resolution is required for high cave ceilings, it might be important to work at full resolution. However, as figure 4 shows, it is not possible, even with full resolution, to get centimetre details for ceilings that are higher than 70 m.

4. Conclusion

Here, we have shown the falseness of the intuitive concept that higher resolution should yield more accurate estimates of cave volume. Scanning caves with commercial T-Lidar scanners, even at only $\frac{1}{4}$ resolution (i.e., a resolution angle of 0.036°), is generally quite sufficient to represent the real volume of the cave and most of the detail. At $\frac{1}{4}$ resolution, detail at <1 cm scale can be achieved up to a distance of ~ 20 m from the cave wall. Scanning at full resolution (i.e., a resolution angle of 0.009°) would render detail at <1 cm scale up to a distance of ~ 70 m. If volume were the only consideration, then scanning

at a resolution an order of magnitude lower would suffice, but much of the detail would be lost.

Therefore, it is clear that before starting a scan project in the field it is important to consider the required resolution of the final cave model. The maximum distance between the scanner and the cave walls depends on this resolution. High resolution cannot always be obtained in caves with high ceilings or over long distances. Scanning at $\frac{1}{4}$ resolution at distances over 150 m becomes increasingly inaccurate. Therefore, for most caves, it is advisable to delete all scan points which are farther away than ~ 100 m from the scanner before registering the scans.

References

- Azmy SN, Sar SAM, Shafie NJ, Ariffin A, Majid Z, Ismail MN.A, Shamsir M, 2012. Counting in the dark: Non-intrusive laser scanning for population counting and identifying roosting bats. *Scientific Reports*, 2 (524):1-4.
- Buchroithner, MF, 2015. High up and Deep below - Dynamic 3D Cartography at the Roof of the World and in Sea-Level Caves. *Photogrammetric Week '15*, Wichmann, Stuttgart, pp.235-245.
- Gallay M, Kaňuk J, Hochmuth Z, Meneely JD, Hofierka J, Sedlák V, 2015. Large-scale and high-resolution 3-D cave mapping by terrestrial laser scanning: a case study of the Domica Cave, Slovakia. *International Journal of Speleology*, 44 (3): pp. 277-291.
- McFarlane DA, 2013. The hollow hill of Gomantong. *Descent*, 230, February/March 2013: pp. 35-36.
- McFarlane DA, Buchroithner M, Lundberg J, Petters C, Roberts W, Van Rentergem G. 2013. Integrated three-dimensional laser scanning and autonomous drone surface-photogrammetry at Gomantong Caves, Sabah, Malaysia. In: Filippi M. & Bosák P. (Eds.), *Proceedings of the 16th International Congress of Speleology*. Brno, Czech Republic, 2: 317-319.

World's First Geophysical Survey of Bat Guano: Phase 1 and 2 Results

George Veni

Affiliation: National Cave and Karst Research Institute
400-1 Cascades Avenue, Carlsbad, NM 88220 USA
gveni@nckri.org

Abstract

Bracken Bat Cave, Texas, USA, holds the world's largest bat colony with an estimated population of about 15 million. Deep deposits of guano cover most of the cave's floor and may contain a well-stratified paleoecological and paleoenvironmental record of the cave and its karst area. A series of electrical resistivity surveys, the first ever of bat guano, indicate the guano has a total depth of about 35 m. Preliminary attempts to core the guano for study have failed. The 1-m spacing of the resistivity electrodes has not been sufficient to reveal buried rocks, which coring attempts discovered in areas seemingly free of rocks. A three-dimensional survey at 0.5 m intervals is tentatively planned for Spring 2017; those results will be presented if completed. The primary challenges in conducting the surveys include a limited time-frame to work in the cave while the bats are away for the winter, and the dry, dusty nature of the upper meter of the guano which increases electrical contact resistance, damages electrical connections, and requires protective equipment for human health and safety. Rainfall in the days prior to some extended resistivity surveys lessened the resistivity contrasts in the data. This made interpretation of the survey, which was looking for a continuation of the cave beyond its collapsed entrance, more difficult.

Keywords:

1. Introduction

Bracken Bat Cave, located in south-central Texas, USA, holds the world's largest colony of bats. Each spring, millions of pregnant Mexican freetail bats (also called Brazilian freetail bats), *Tadarida brasiliensis mexicana*, return from their winter migration to Mexico and give birth to an average one pup each, doubling the population by early summer. Population counts vary. Bat Conservation International (BCI), which owns the cave, estimates the maximum summer population at about 15 million (Mylea Bayless, BCI, personal communication June 2016). The bats' nightly exit from the cave appears on the radar of the San Antonio International Airport and on Doppler weather radar.

The cave's entrance is about 20 m wide by 7 m high at the base of a 30-m diameter by 13-m deep collapse sinkhole. The cave's dimensions are less impressive. Although it maintains a large average size of 15-20 m wide by 10-15 m high, the cave descends steeply another 12 m down a bat guano-covered rubble slope, then continues south along a roughly level guano floor to where the ceiling abruptly lowers at a horizontal distance of about 130 m from the entrance, and the passage beyond is filled with guano at a depth of 31 m (Figure 1 indicates 36 m, but that has since been revised by a high-precision survey for the in-cave geophysical surveys described below, although 36 m may have been accurate at the time and the 5 m difference may reflect the accumulation of guano). The cave is undoubtedly much longer and deeper, if only we could see north past the collapse of its entrance and the guano at its opposite end.

It is not known when the cave was discovered, but it was almost certainly located due to its impressive evening bat flights, as large clouds of bats emerge nightly during the spring through fall months. The cave was named for the nearby town of Bracken. Guano mining began in 1856, with most of the guano used as fertilizer. The cave yielded up to 70 metric tons of guano annually. Mining was usually done in the winter when the bats were absent. During the US Civil War (1861-1865) the guano was leached for saltpeter used in Confed-

erate gunpowder. Mining has continued sporadically to the present. Elliott (1994) provides more general information. For the most recent news, plus a web cam to watch the evening flights live, visit BCI's website, <http://www.batcon.org/>

Working in Bracken Bat Cave poses special challenges. During the months when large numbers of bats are present, their body heat raises the cave temperature to over 40°C and the guano and urine create hazardous atmospheric ammonia levels measured as high 55 ppm. Meanwhile, the floor literally moves due to the probably millions of dermestid beetles feeding on guano and dead bats. The cave is rarely entered and usually only in the winter to not disturb the bats, but also when temperature and ammonia levels are at their lowest. Masks with filters are a necessity at all times, if only to prevent inhalation of the cave's fine guano dust that pervades its air.

2. Geology

Bracken Bat Cave is formed in the Cretaceous-age Kainer Formation of the Edwards Limestone Group and the underlying upper member of the Glen Rose Limestone. The Dolomitic Member of the Kainer extends from the surface down 9 m to the dripline of the cave's entrance (Figure 1, profile). This thick-bedded, structurally competent unit forms the roof of many large cave chambers in the area, as well as the namesake bridge of the show cave Natural Bridge Caverns located 1.1 km to the northeast.

The humanly accessible portion of the Bracken Bat Cave is mostly within the 15-m thick Basal Nodular Member of the Kainer, previously designated as the Walnut Formation when Figure 1 was drafted. Large solutionally-formed chambers and passages often form in the Basal Nodular in the local area, but the large passage of Bracken Bat Cave is not formed by solution; see Veni (2005) for a review of lithology as it affects cave morphologies in this area.

The deepest 7 m of Bracken Bat Cave are formed in the Cavernous Hydrostratigraphic Unit of the upper member of the

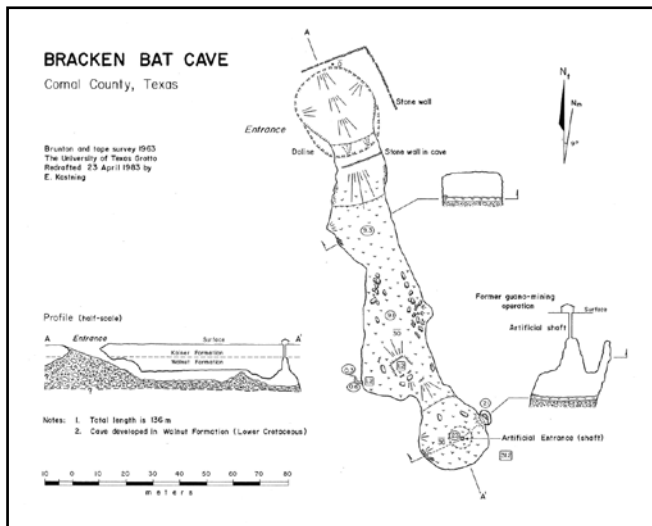


Figure 1. Map of Bracken Bat Cave (Kastning, 1983).

Glen Rose Limestone (Clark *et al.*, 2013). This 37-m thick unit contains most of the largest solutionally-formed cave chambers and passages in the area. Like the Basal Nodular's exposure in the cave, its humanly-accessible section in the upper Glen Rose is not formed by solution. The entire known cave is formed by collapse. Natural Bridge Caverns extends at least 18 m below the Cavernous Unit into the upper Glen Rose's Camp Bullis unit (Clark *et al.*, 2013), which is otherwise a poor to minor cave-forming unit. Given the similarity in origin between the caves, it is suspected that Bracken Bat Cave may also reach into the Camp Bullis unit.

Cave Geophysics

In 2013, a drilling company offered its services to BCI. Upon consideration, BCI contacted the National Cave and Karst Research Institute (NCKRI) to use the drilling services to core the guano in Bracken Bat Cave and analyze it for paleoenvironmental and paleoecological data. NCKRI organized a team of specialists to work on the study. Staff at Southwest Research Institute in San Antonio had previously worked at the cave conducting surface geophysics and possesses extensive analytical abilities. Dr. Bogdan Onac, of the University of South Florida, USA, brought practical experience from his published research on coring guano in other caves and also has access to his university's lab facilities for additional analyses. Dr. Rick Toomey, of the Mammoth Cave National Park, Kentucky, USA, is a vertebrate paleontologist who is highly knowledgeable about both bat and Texas cave faunal remains. He would identify the bones recovered to determine what changes in species, if any, occurred over time. But the first step was to determine where to drill inside the cave.

NCKRI's primary role was to conduct an electrical resistivity survey, the first known in bat guano. The resistivity work has been conducted in two phases. The first occurred in January 2014 when BCI organized a team of volunteers to assist NCKRI in conducting four electrical resistivity surveys in the cave. The wintertime study period coincided with the time when most of the bats would be in Mexico, resulting in minimal disturbance but also better working conditions. NCKRI used its SuperSting R8/IP electrical resistivity equipment, manufactured by Advanced Geosciences, Inc., to collect the resistivity data. The data were later processed using EarthImager™ software.

Three 2-dimensional surveys were conducted. Resistivity Line 1 began in the cave about 40 m from the entrance and ran south, close to the cave's west wall, 56 m to a corner at the widest part of the cave. Line 2 began in the cave approximately 25 m south of the entrance and ran south down the middle of the passage 56 m to a large breakdown pile. Lines 1 and 2 used 56 electrodes spaced at 1-m intervals. Line 3 followed the cave's east wall, beginning 45 m from the entrance and extending 80 m southeast to the end of the cave. Its 84 electrodes were placed at 0.95-m intervals.

One 3-dimensional survey was conducted at the back of the cave below the mine shaft. The electrodes were placed at 2-m intervals in a 14- by 12-m grid; a larger grid with 1-m spacings was initially planned but abandoned due to damage to some of the resistivity cables.

The powdery nature of the guano cast some concern on the feasibility of conducting an effective resistivity survey. The contact resistance could have been too high to yield meaningful results. To maximize electrical transmission into the guano, the 46-cm long electrodes were pushed as deep into the guano as possible. Saline was poured onto electrodes showing high contact resistance during testing prior to starting the survey, which reduced contact resistance for most but not all such electrodes. In the end, the results proved acceptable and better than expected.

The purpose of the close electrode spacing was to maximize the resolution of the survey to detect breakdown hidden in the guano that could interfere with coring. The expected stratigraphic sequence was guano, interlaced with breakdown, underlain by a thick section of breakdown. While the thickness of the breakdown could be estimated, using Natural Bridge Caverns as an analogue, there was no model to estimate the depth of the guano.

Line 2 was imaged to a depth of about 15 m and interpreted to show a considerable mix of breakdown and guano. Lines 1 and 3 image to depths of about 18 m and showed areas with less breakdown, more conducive to coring. Figure 2 shows the results of the Line 3 survey. The warmer colors likely correlate to buried breakdown. The cooler colors indicate guano. As guano decomposes, it develops a clay-like composition with lower resistivity. The lowest resistivity values occur under the mine shaft where water drips regularly, lowering the resistivity even further. While this location seems optimal for coring, it is also the area excavated by guano miners to an estimated depth of 9-18 m, so most or all of the guano in that area is recent and probably of little paleoenvironmental value. The abrupt transitions in resistivity in that location likely reflect the excavated pit. The area 48 m from the start of the Line 3 was identified as a better coring location.

The Phase 1 results that the guano was at least 18 m deep left the main question unanswered, how deep is the guano? NCKRI returned to the cave two years later, in January 2016 and conducted Phase 2 with two additional surveys. The 2014 surveys were focused on trying to find buried breakdown to avoid, as well as establishing the guano's depth. The 2016 survey focused on depth. The goal was to see through the guano and breakdown, and continue deeper through the sediment that probably underlays the breakdown to the floor of the original solutionally-formed cave passage. Natural Bridge Caverns again served as a model to estimate target depths, except that the elevation and stratigraphic position of its solu-

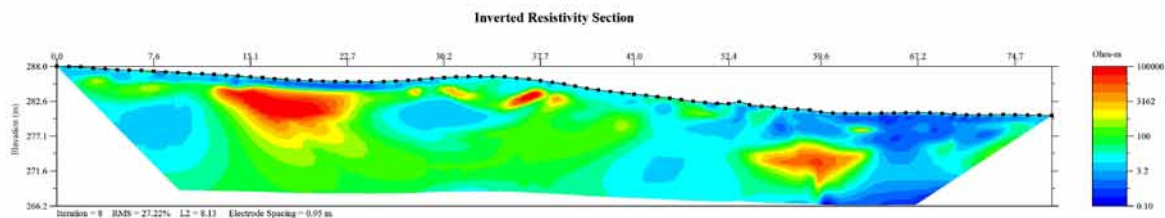


Figure 2. Resistivity profile of Line 3 along the east side of Bracken Bat Cave.

tional-formed bedrock floor are unknown. The deepest levels of that cave are covered in thick mud of unmeasured depth.

The Phase 2 surveys consisted of two lines. Both used 112 electrodes at 2-m spacings. Both lines were surveyed twice, once in a dipole-dipole configuration and then again in a pole-dipole configuration with an infinity electrode placed about 700 m to the north along BCI's property line to increase the depth of penetration. The results were merged for a more complete and detailed image and interpretation. The first 56 m of Line 5 used the even-number electrode positions of Line 1 and then continued out of the east side of the cave's entrance and onto the surface. Line 6 could not overlap Line 3, due to the curvature of the cave wall, but ran subparallel to that line from the back of the cave and out of the west side of the entrance.

These surveys suggest the guano reaches a maximum depth of about 35 m to breakdown, which continues at least 20 m deeper. The original cave floor was not apparent based on a morphologic interpretation of the resistivity values. Presumably due to rainfall only a few days before the 2016 surveys, the resistivity values were similar for areas of known bedrock and breakdown and the two could not be distinguished. A return is planned when conditions are drier to provide more contrasts in the data, and with the resistivity array deployed to see deeper still into the cave floor.

3. Summary

Bracken Bat Cave is one of the longest and best known caves in Texas, yet knowledge of its hydrogeology and paleoclimatic record are just now being revealed. Collapse of the original large solutionally-formed passage within the Glen Rose stopped upward to breach the surface, creating the cave's entrance. The humanly accessible portion of the cave is only about 130 m long and at the top of the collapse pile. Bat guano covers the entire floor of the cave and buries most of the breakdown. The stratigraphic position of the original solutionally formed passage is assumed to coincide with the lower levels of nearby Natural Bridge Caverns. While the level of the ceiling is known in Natural Bridge Caverns, the bedrock floors in both caves are covered and their stratigraphic position is currently unknown.

Two phases of electrical resistivity investigations have occurred inside the cave. They were the first to evaluate bat guano, which is geophysically-interpreted as up to 35 m deep. The solutionally formed bedrock floor of the cave, buried below the guano and breakdown, could not be reliably identified. It is likely more than 55 m below the modern cave floor

but requires verification by deeper-penetrating surveys. The third phase of this study is tentatively planned as a detailed 3-dimensional survey of one area of guano for possible coring. If it is conducted before the 17th International Congress of Speleology, its results will be included in the presentation of this paper.

Acknowledgements

None of this research would have been possible without the encouragement, support, and access to Bracken Bat Cave provided by Bat Conservation International, with special thanks to staff members Mylea Bayless and Fran Hutchins. The geophysical surveys were also made possible due to the assistance of the following excellent volunteers: BCI volunteer Lee McKenzie; the National Speleological Society's Bexar Grotto members Jennifer Adkins, Tom Brown, Allan Cobb, Gayle Corbell, Rick Corbell, Steve Damon, Leia Hill, Joel King, Kurt Menking, Jill Orr, Linda Palit, and Zach Schudrowitz; ResearchWild.com's staff members Michal Birt, Brian Bower, Robert Garner, Peter Hayes, and Monika Libson; and St. Mary's University geology students Harold Campbell, Olivia Jimenez, Obed Rodriguez, and Anvy Vu, led by professor Dr. Evelyn Mitchell.

References

- Clark, A.K, Pedraza, D.E., Morris, R.R., and Garcia, T.J., 2013, Geodatabase and characteristics of springs within and surrounding the Trinity Aquifer outcrops in northern Bexar County, Texas, 2010–11: U.S. Geological Survey, Data Series 750, 20 pp.
- Elliott, W.R, 1994, Bracken Bat Cave, in *The Caves and Karst of Texas*: National Speleological Society, p. 173-175.
- Fieseler, R.G., Jasek, J., and Jasek, M., 1978. *An introduction to the caves of Texas*: Texas Speleological Survey, NSS Convention Guidebook 19, 116 pp.
- Kastning, E.H., Jr., 1983, *Geomorphology and hydrogeology of the Edwards Plateau karst, central Texas*: Ph.D. Dissertation, The University of Texas, Austin, 656 pp.
- Veni, G., 2005, Lithology as a predictive tool of conduit morphology and hydrology in environmental impact assessments, in *Sinkholes and the Engineering and Environmental Impacts of Karst*, Geotechnical Special Publication No. 144: American Society of Civil Engineers, p. 46–56.

(Abstract) **Mapping and Imaging the World's Largest Chambers in 3D**

Richard Roo Walters

Affiliation: British Cave Research Association

Abstract

For the last two years a team consisting of Roo Walters, Andy Eavis, Tim Allen, Prof. Pete Smart, supported by many others have been visiting the largest cave chambers in the world to map them using modern Laser 3D Imaging methods. Highly accurate models of all the caves have been built with a view to calculating their volume and ranking them in order. The scans also reveal features of these vast caverns never seen before and provide a data set that can be used for further research. This paper discusses methods, choice of equipment, practicalities of scanning in the caves, gathering data, post processing and analysing the results. Withheld is the final table of results which will be revealed during the conference. The paper will be presented over two lectures. Firstly to introduce the project and to invite discussion during the week about the findings with a view to presenting the results in a final session at the end of the conference.

Karst, Pseudokarst and Caves in Other Rocks

(Abstract) **An unusual maze cave in sandstone, NE Thailand**

John Dunkley¹ & Terry Bolger²

Affiliation: ¹ Highland Caving Group (HCG)
² Cave & Karst Specialist, PO Box 4226, Vientiane, Laos

Abstract

Trending NW-SE across Northeast Thailand, the Phu Phan Mountains hosts sandstone caves, karst-like features & cultural sites of archaeological, religious and historical significance, most being on Buddhist community property and some attracting huge crowds of people for Buddhist events. The sites are significant more for their culture than their morphology, but some are noteworthy. About 300 such sites are known; many have only a small cave-like structure occupied by a Buddhist monk, or even just an undercut rock converted to a shelter. Some have extensive longitudinal overhangs, often levelled and sometimes elaborately cemented and tiled for habitation or ceremony. Some, the so-called forest wats are essentially retreats and may dissuade visitors, others welcome them readily and a small donation is appropriate (wat = temple; tham = cave). At least 6 longer and mostly dark caves show evidence of underground running water.

Our recent research in north-east Thailand identifies at least 300 known sites of sandstone caves, mostly in the Phu Phan Formation stretching for 500km NW/SE west of the Mekong River. Most are quite small, some of little consequence but with associated pseudokarst morphology. The longest is about 550m, & another one 450m. A few have small streams. Most have religious significance for long-established historical reasons associated with Buddhist beliefs related to caves and unusual rocks. There is a close relationship between pseudokarst features & sandstone cultural sites of archaeological, religious and historical significance. Many of these sandstone sites attract huge crowds of people for Buddhist events & most are on Buddhist community property.

Historical Notes And Research History Of The Non-Karst Caves In Hungary

István Eszterhás¹, George Szentes²

Affiliation: ¹Köztársaság-út 157, 8045 Isztimér, Hungary, eszterhas.istvan@gmail.com

²125 Seabrook Avenue, New Lynn, 0600 Auckland, New Zealand, szentesg@yahoo.de

Abstract

From historic times until the year 1983 only a few references, occasional observations and scientific studies characterised the non-karst caves related knowledge. Organised research began in 1983 with the launch of the Vulcanspeleological Collective. Their comprehensive activity controlled the exploration and research of non-karst caves in Hungary. Currently 996 non-karst caves have been listed, described and surveyed by the members of the Collective. Up to now they have organised 30 successful research camps and 26 expeditions to foreign countries. They have expounded the genetic types of non-karst caves. They engaged in the systematisation of speleothems occurring in the non-karst caves and they have solved the problem of ice development in low elevation basalt caves. They have carried out biological investigations in non-karst caves and investigated the historical data on the utilisation of non-karst caves and cave dwellings. The results have been published mainly in Hungarian, but occasionally in German or in English.

Keywords:

1. Introduction

In Hungary up to 2015, 4144 caves have been listed. Nearly a quarter of them, namely 996 are non-karst caves. The non-karst caves occur in almost every type of rock formations, however the majority of them are to be found in volcanic rocks and in sandstone. In Hungary about 3100 km² of mountainous area is composed of volcanic rocks (basalt, andesite, rhyolite etc.). Most notable are the Tokaji, Mátra and Börzsöny Mountains (Fig. 1). Sandstone covers about 1200 km². The non-karstic caves were formed by three major developing factors in the mass movement, fragmentation chemical and physical weathering. The non-karst caves are generally small, 2 – 10 m long. The longest non-karst cave in Hungary is the 428 m long Csörgő Hole in the Mátra Mountains.

2. Historical overview

Archaeological finds have been discovered in some of the non-karst caves. The oldest artifacts are Neolithic potsherds which were excavated in Big Cave on Mount Fuló. In Pokol Hole near the village of Kapolcs, in Gyula Cave in the Mátra Mountains, in Bărăcházi and Cserepes Caves in the Velenicei Mountains potsherds have been found dating from the Bronze Age, proving that contemporary humans knew of and utilised the caves.

In the past no distinction was made between karst, non-karst caves or artificial cavities. All underground holes were considered as caves. The earliest mention of a non-karst cave was in the year 1295 AD in the quartzite of Likas-kő in the Velenicei Mountains (Fig. 2). The quartzite cliff and the cave are a reference point on an administrative boundary.

Up to the 16th century non-karst caves had only some brief mention and notes. These are not scientific works but historically valued records. In 1549 György Werhner describes briefly Füleki Cave in his voluminous hydrological handbook. The Palatine György Thurzó, a highly educated person in the field of natural sciences, has also been recorded as visiting Pokol Hole near the village of Kapolcs in 1610 (Pátyi 1870).

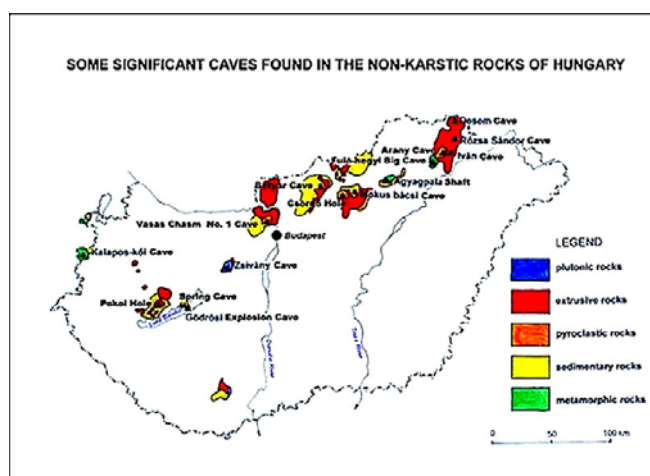


Figure 1. The non-karstic rocks in Hungary and some significant non-karst caves



Figure 2. The Likas-kő in the Velenicei Mountains



Figure 3. Entrance to the Szentkúti Monastery

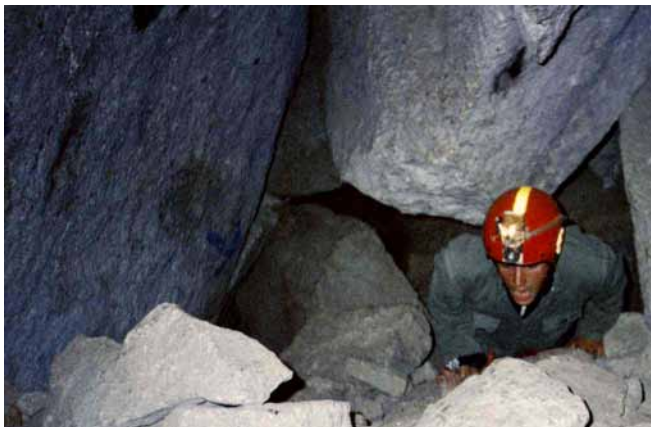


Figure 4. Csörgő Hole, The layers are broken apart and boulders are piling up on one another.

Mátyas Bél (1742) in his “Notitia Hungariae novae historico-geographica” study mentions some non-karst caves, however he never visited these caves only hearing about them from his contributors. Antal Mocsáry in the 1826 Nógrád County monograph describes three non-karst cave related legends. Frigyes Pesty (1846) in the Gazetteer of Hungary reports several non-karst caves. In Hungary the remains of three cave monasteries are known including the cave dwellings on the Tihanyi Peninsula, and the Hermit Caves near the settlements of Nagymaros and Szentkút (Eszterhás 2012) (Fig. 3). The monasteries are composed of 4 – 5 artificial cavities which have been carved in non-karstic rocks. More hermit caves are to be found in non-karst rocks in which hermits dwelt for varying amounts of time. Many artificial holes have been dug in either loess or sandstone for various purposes such as the Tatar Holes near the village of Balatonkenese and Outlaw Cave in Somogy County. Finally there are several thousands of cave dwellings widespread in the sandstone, loess and rhyolite tuff regions.

3. Beginnings of scientific research

Interest was awakened in cave sciences in the second half of the 19th century. Jenő Nyáry performed archaeological excavations not only in the karst caves, but also in the basalt caves in Pogányvár (Nyáry 1868–69). He discovered that Lakó (Resident) Cave (today located in Slovakia Jaskyňa nad komenným more) was an occasional dwelling site of late Bronze Age people. The nearby cold Labyrinth Cave (Labirintová jaskyňa) had been utilized as a “cold store” and many long bones of large mammals were found in this cave. Archaeological exploration in Pogányvár was continued by Václav Furmanek in 1994. He discovered an urn cemetery of the kyjatice culture in the small caves of nearby Mount Béla (Beleinská hora) (Furmanek 1996).

In 1869 the geologist József Szabó organised an expedition to explore Csörgő Hole in the Mátra Mountains (Fig. 4). One hundred and forty metres was surveyed and he identified how the landslide had formed the development of the cave: “*The position of the surroundings and the direction of the passages indicates that the layers, obeying to the pull of gravity are sliding slowly and continuously toward the bottom of the valley. As a result of this mass movement the layers are broken apart and boulders moving at different rates are piling up on one another....*” (Szabó 1871, 9-10).

Lajos Lóczy asked renowned professionals to describe different subjects in his 33 volume Balaton Monograph (Lóczy 1891–1918). At this time no caves were known in the Balaton region, therefore a gas bubble cavity in the basalt of the Castle Mount near the village of Szigliget described by István Vitális (1911) was treated as a curiosity. János Jankó (1901) looked at 18 Tatar Holes near Balatonakarattya settlement.

In the first half of the 20th century there does not appear to be any investigations of the non-karst caves, and only in the 1950s did speleologists begin to deal with the non-karst caves. In 1952 Sándor Leél-Össy published a study on the Csörgő Hole and in 1959 investigated some basalt caves and basalt gnammas in the Bakony Mountains. András Székely wrote a monograph on Csörgő Hole in 1953. From in the Bakony Mountains. András Székely wrote a monograph on Csörgő Hole in 1953. From 1957 on twenty non-karst caves have been investigated and described by György Ozoray. He studied the caves over seven years and explained their development (Ozoray 1962). In 1958 Károly Bertalan listed 51 non-karst caves including short descriptions and a bibliography. George Szentes in his study, elaborated the genetic types of 27 non-karst caves. (Szentes 1971). Furthermore, we would like to mention the activities of Ervin Göbel, András Hoffer, and Lajos Jugovics (Eszterhás 1994-b).

4. How the Vulcanspeleological Collective was formed.

The Vulcanspeleological Collective was inaugurated by István Eszterhás in Sangerhausen, Germany in December 1982. He was a delegate to a speleology meeting where he delivered a lecture on the basalt and geyserite caves of the Bakony Mountains. The German cavers showed keen interest and decided to organise an expedition to the area. As knowledge of these non-karst caves was imperfect, in the summer of 1983, István Eszterhás and his colleagues decided to study the existing lit-



Figure 5. Exploration camp in Szilváskő Region

erature and to visit and describe the caves in order to be able to better guide the German cavers. They visited the described caves and found some new ones. After a successful expedition the group continued the exploration of the non-karst caves in the Bakony Mountains and on the Tihanyi Peninsula.

This successful study encouraged the team to extend their investigation to all the non-karstic regions in Hungary. The Hungarian Speleological Society (MKBT) had launched a scientific program in 1985 and the Collective was invited to take part in the project with the theme of "Investigation of non-karst caves". Consequently the MKBT adopted the Vulcanspeleological Collective as an official committee of the Society on 17th March 1992 (Eszterhás 1994-A, 2011).

5. Activity of the Vulcanspeleological Collective

The pivotal activity of the Collective is to list non-karst caves. In order to carry out this aim annual research camps have been organised. (Fig. 5). The Collective has a core research group of 15 persons. but over 30 years of activity, 240 people have intermittently joined to undertake certain tasks. Altogether 996 non-karst caves have been listed.

As the excavation of caves has not been the main task of the Collective it is a secondary activity, and has result in 1153 m of cave passage in 53 caves (e.g. Csörgő Hole 428 m, Paulai Basalt Cave 151 m, Halász Árpád Cave 64 m Betyár Cave 87 m etc.) being excavated.

The genetic system of the non-karst caves has been worked out and new genotypes have been defined. The new genotypes are the consequence caves (30 caves in Szilváskő), the fumarole caves (Kámori Foxhole), alkaline solution caves (10 caves on Mount Fuló and the caves of Kőszörű Valley).

Tree mould caves have been identified by the members of the collective near the Ipoly River.

They have identified 52 examples of speleothems which are most characteristic in the non-karst caves of the world (Eszterhás 2015). Silicate stalactites have been found in Arany Cave (Fig. 6). Hisingerite disks (an iron phyllosilicate mineral) have been described from Pulai Basalt Cave. The Nyári



Figure 6. Silicate stalagmites in the Arany Cave



Figure 7. Ice formations in the Nagy Sárkány Ice Cave

Cave (Slovakia) is the only non-karst cave where living speleothems, root stalagmites have been observed.

There are ice formations in the low elevation basalt caves. The condition of the ice development in these caves is different from that which occurs in the caves of alpine or polar regions. The ice development depends on the porosity of the surrounding basalt. The porosity expands the rock surface and induces an increased evaporate cooling, therefore the cave wall can be cooled below 0 °C and the seeping and dripping water will freeze. In Hungary five smaller natural ice caves occur solely in volcanic rocks: (Nagy Sárkány Ice Cave (Fig. 7), Kis Sárkány Ice Cave, Sárkánytorok Cave, Kis Szilváskői Chasm and the Ice Pit in the Damsa Chasm). Ice development in an artificial tunnel near the village of Telkibánya can be observed throughout the year.

One hundred and ninety-eight animal species have been listed in the non-karst caves in Hungary. Some species are unusual such as the blind flea cancer (*Niphargus hungaricus*), the mouse yellow beetle (*Leptinus testaceus*), and a species of

the harvestman (*Phalangidae*) part of the family of the cave daddy-long-legs (*Holoscotoleman jaqueti*).

Palaeontological findings have been found only in those non-karst caves which have developed in calcareous sandstone due to the preservation properties of the lime. Significant finds include cave bear (*Ursus spelaeus*) from Betyár Cave and the giant hamster (*Cricetus cricetus major*) from Seybold Cave.

The elaboration of the flora around the non-karst cave entrances began in 2014. Recently 37 species of mosses, lichens ferns and woody plants have been studied at 22 cave entrances. Archaeological finds have been made in 17 non-karst caves, and have been described in the chapter on “*Historical Overview*”. We now know that the caves of Asztag-kő and Lélek Hole had defensive fortifications and 29 non-karst caves-related legends have been recorded.

A digital list of the non-karst caves was compiled. Digital maps on different scales have been created for 20 specific regions of non-karst caves with additional data of cave surveys, cave photographs and descriptions. The digital list can be found through the following link <<http://nonkarstic.geo.info.hu>>. The List is continually upgraded and includes 1255 caves (some of them reach beyond the national boundary of Hungary and are in Austria and in Slovakia).

As well as publications, the members of the Collective have delivered many presentations both in Hungary and overseas. The Collective is connected to several foreign speleological institutions and with their cooperation has organised expeditions and study trips to some important regions of volcanic caves e.g. Canary Islands, Sicily, Iceland and Hawai'i. Members of the Collective frequently attend international symposiums and conferences on non-karst and volcanic caves and give lectures at these.

The activities of the Collective have been recognised and members have been awarded with the Cholnoky Prize, Kadic Prize, Vass Imre Medal and Honorary Membership of the Hungarian Speleological Society. One person is a member of the “Explorer Club” in New York and has been awarded the “Outstanding Nature Research Scientist of the 21st Century” title from Cambridge University, Great Britain.

Literature

Bertalan K., 1958. Magyarország nem karsztos eredetű barlangjai – *Karszt- és Barlangkutató Tájékoztató* (jan-jún.), Budapest p. 13-21.

Eszterhás I., 1994-a. Lett egyszer egy kollektíva – *Lychnis, a Vulkánspeleológiai Kollektíva kiadványa, Kapolcs* p. 4-6.

Eszterhás I., 1994-b. A magyar vulkánbarlangok keletkezése és ismertetése a 16. századtól – *Lychnis, a Vulkánspeleológiai Kollektíva kiadványa, Kapolcs* p. 16-20.

Eszterhás I., 2011. A Vulkánspeleológiai Kollektíva két évtizede – *100 éves a szervezett magyar barlangkutatás*

(Konferenciai előadások), kiadta a Magyar Karszt- és Barlangkutató Társulat, Budapest p. 28-31 .

Eszterhás I., 2012. Őzéporkori barlangmonostorok Magyarországon – *Karsztfejlődés XVII. kötet – kiadta a Nyugat-magyarországi Egyetem Savaria Egyetemi Központ Természetföldrajzi Tanszéke, Szombathely* p. 235-243.

Eszterhás I., 2015. Speleothems of the non-karstic caves – *Proceeding of the 13th International Symposium on Pseudokarst, Kunčice pod Ondřejníkem*, p. 8-11 & “*Lap Lambert*” Academic Publishing, Saarbrücken p. 18-42.

Furmanek, V., 1996. Weitere Belege über die Benützung von Pseudokarsthöhlen in der Urzeit – *Proceedings of the 6th International Symposium on Pseudokarst, Galyatető*, p. 105-109.

Jankó J., 1902. A Balaton-mellék lakosságának néprajza – *A Balaton Tudományos Tanulmányozásának Eredményei*, III. kötet, Budapest p. 42-79 és 168-175.

Leél-Össy S., 1952. Adatok az ágasvári Csörgőlyuk-barlang eredetéhez – *Földrajzi Értesítő I. évf. 4. füzet* Budapest p. 710-711.

Lóczy L. Szerkesztő, 1891–1918. *A Balaton Tudományos Tanulmányozásának Eredményei* I-XXXIII. kötet, Budapest.

Mocsáry A., 1820. *Nemes Nógrád vármegyének Historiái, Geographiai és Statistikai Esmertetése*, Pest I-III. kötet p. I-226-227, III/19.

Nyáry J., 1868–69. Ó-básti barlangok – *Archeológiai Értesítő* I. kötet, Pest.

Ozoray Gy., 1962. The genesis of non-karstic natural cavities as elucidated by Hungarian examples – *Karszt- és Barlangkutatás*, Budapest p. 127-136

Patyi L., 1870. Kapolcs és vidéke Zala megyében – *Hazánk és a Külföld* VI. évf. 15. szám, Pest p. 226

Pesty F., 1846. Magyarország helynevei – *kézirat az Országos Széchényi Könyvtár kéziratárában*, Budapest

Szabó J., 1871. Az ágasvári barlang a Mátrában – *Földtani Közöny I. évfolyam*, Pest p.11-12.

Székely A., 1953. Az ágasvári Csörgőlyuk-barlang – *Földrajzi Értesítő I. sz.* Budapest p. 114-124.

Szentes Gy., 1971. Caves formed in the volcanic rocks of Hungary – *Karszt- és Barlangkutatás* VI. évf. Budapest p. 117-129.

Vitális I., 1911. A balatonvidéki bazaltok – *A Balaton Tudományos Tanulmányozásának Eredményei*, I. kötet, Budapest, p. 105-106.

Wernher Gy., 1549. *De admiralis Hungarie aquis hypxomniation* – Basel.

Origin Of Caves In Glaciers And Glacial Sheets

Mavlyudov B.R.

Affiliation: Institute of geography RAS, Moscow, Russia, bulatrm@bk.ru

Abstract

Water from a glacier's surface can penetrate into the ice through crevasses and forms channels similar to karst channels (karst of glaciers). Places of water input into ice (crevasses and moulins) and exit places (glacial caves, upwellings and springs) are known, but it is not known how water moves inside glaciers. The majority of researchers tend to have thought that water from glacier and glacial sheets' surface penetrates to their base and further moves along it. However researches of glacial caves in different regions have shown that in many cases water on the glacier base does not penetrate. It is especially difficult for water to move to the base of glacial sheets if the ice is thick (about 1 km) and has significant negative temperature. Research in Antarctica has shown that in thick ice there are sliding planes which can divide the total thickness of ice not only with different velocities of movement, but also can involve different directions of ice movement. These sliding planes have been tracked on distance to 1400 km. If such ice sliding planes exist in Antarctica, they should be on other glacial sheets and glaciers. In this case water penetrating into vertical crevasses in ice conducts, not only to form moulins but also delivers water to sliding planes inside glaciers. This results not only in wetting of the sliding plane and an increase in velocity of ice movement, but also to formation of internal glacial drainage systems for such sliding planes. These sliding planes are present in Antarctic at a depth of about 100 m from an ice surface. In Greenland (by indirect data) sliding planes are located at a depth of about 50-200 m from the ice surface. Apparently on mountain-valley glaciers, sliding planes are located at a depth of about 100-150 m from the ice surface. Where the ice thickness is less than this, sliding planes start to contact with glacier base on rocky ledges. Therefore glacial caves in glacier tongues are subglacial when they are in area of a rocky ledges, and englacial when sliding planes pass over base deepening. The proposed scheme explains the formation of the internal drainage systems of glaciers and glacial sheets of any extent from tens meters to hundreds kilometers. Water drainage through sliding planes explains not only the internal glacier drainage but also spring increasing of ice velocity and outbursts of glacial lakes and surges.

Keywords: glacier caves, glacier hydrology, glacial drainage systems, sliding plains

1. Introduction

For many glaciers presence of an internal drainage is characteristic. Melt water moves on a surface of glaciers and penetrates inside ice through crevasses forming internal drainage systems of glaciers which by structure and morphology are in many respects similar to karst drainage systems. The main distinction consists that in glaciers there is an ice melting instead of rock dissolution (Mavlyudov, 2007). Besides ice more plastic substance than rocks that leads to fast closure of cave channels in the heart of glaciers. Thus cavities in glaciers are formed very quickly (during months) but they also quickly disappear. Formation of cavities in glaciers carries the name "glacial karst". In connection with fast formation of cavities in ice they can serve as physical models of karst cavities formation which are formed for many tens and hundreds thousand years (Mavlyudov, 2006b).

Now there is a paradoxical situation. Glacial caves were studied many years mainly by cave explorers and only last years glaciologists began to study glacial caves (Gulley *et al.*, 2009). Nevertheless, the majority of glaciologists prefer to receive data about structure of an internal drainage of glaciers by using of indirect methods: geophysical, hydrological (dye tracing), modeling (Hewitt, 2013). But the trouble consists in that in a basis of the majority of mathematical models lay not facts but only assumptions which in most cases have no any base. For example, among glaciologists the theory is very popular that water from a surface of glaciers penetrates directly to the base, moistens it that promotes acceleration of glaciers movement at the beginning of summer (Zwally *et al.*, 2002, Das *et al.*, 2008). However the numerous facts received by speleological methods say that in many cases water on glaciers base is not

penetrate. Especially strange statements look that water penetrate to glacier base in Greenland at ice thickness about 1 km and its temperature up to -29°C (Das *et al.*, 2008).

In this article we will try to understand as water moves inside glaciers and glacial sheets.

2. Methodology

The author has been undertaking his own speleological research on channels in glaciers (since 1982) in different regions: Spitsbergen, Caucasus, Alpes, Tien-Shan, Pamir, Himalayas, Eastern Siberia, Cordilleras, Antarctic, and also on existing speleological and glaciological publications.

3. Results and discussion

This paper does not consider the formation of separate elements of an internal drainage of glaciers such as moulins, pits, cascades, galleries, cave channels, as they are well studied (for example, Fountain, Walder, 1998, Mavlyudov, 2006a, 2007, Eraso, Pulina, 2010, Benn, Evans, 2010, etc.).

We have analyzed possibility of any of glacial channels to generate uniform system of an internal drainage of glaciers. It has appears that no known channels are capable of creating such a system but even the complex of all known channels is not capable of creating a uniform system of an internal drainage. Therefore there is a question: how do systems of an internal drainage in glaciers form? There are some theories on the formation of internal drainage systems in glaciers: 1) water penetration along crevasses to glacier base and the further water movement along a base (Zwally *et al.*, 2002, Das *et al.*, 2008.), 2) incision of channels from the glacier surface or from the

bottom of crevasses (Fountain, Walder, 1998, Gulley *et al.*, 2009a), 3) formation of channels on systems of transverse crevasses with the subsequent displacement of channels downwards during glacier movement and evolutionary expansion of channel systems by the formation of new crevasses above on an ice current (Mavlyudov, 1995), 4) formation of a central drainage systems of glaciers at the merging of buried marginal drainage systems (Mavlyudov, 1995).

It would seem that the first mechanism gives an explanation for the formation of an internal drainage on glaciers and glacial sheets. However ice has fissure and crevasse permeability only to temperatures about -8°C (Shumskij, 1955, Mavlyudov, 1998). Crevasses physically cannot penetrate through kilometer ice thicknesses. Hydrofractures also cannot penetrate through such ice thickness as ice movement will interfere with it. However water can reach a glaciers' base if the ice thickness is insignificant, However along glacier base, water does not move, even in a thin ice sheet (see below). Therefore this mechanism of formation of systems of an internal drainage which is currently the most popular among glaciologists simply does not work.

The second mechanism can work in a very limited number of cases. For formation of channels along crevasses, the presence of crevasses everywhere on glaciers is necessary which is not always the case (for example, often crevasses are not present at glacier tongues or on cold glaciers). The second part of the mechanism, is suitable for the formation of a shallow internal drainage network in mainly cold glaciers and glaciers which do not have crevasses. In this case, the depth of a channel's position should not exceed 30 m from a surface. At a greater depth, these channels will be simply closed by plastic deformation or filled by reformed ice. In some cases channels can form in such way in warm glaciers (in the top few meters) and are named «epidermal» channels (Badino, 2002).

The third mechanism is possible but difficult to realize, as rising crevasse channels are less likely to remain after the winter periods when the compression of channels continues but the melting of channel walls has already stopped as there is no moving water. This is especially important where the drainage system could be generated along transverse crevasses. Besides the formation of such an internal drainage needs a very long time and previous crevasses will move to glacier tongues. This would need hundreds or thousands years, which is not typical for a glacial karst which quickly form and quickly disappear.

The fourth mechanism recognizes that at the base along the edges of glaciers, shear cracks form marginal drainage systems (Mavlyudov, 1995). Usually these are at superficial locations which can be partially englacial and supraglacial (ice canyons). Where two glacier branches merge, two marginal channels should unite in one central channel. In some cases this works but, unfortunately, locations of channels of an internal drainage to median moraines has not been proven.

Thus all offered mechanisms of formation of internal drainage systems in glaciers can work only in some cases but, unfortunately, are not universal. Differently, and on separate parts of glaciers or sometimes on the whole glaciers we can use one of these mechanisms, but on the majority of glaciers they do not work. It is especially difficult to use these mechanisms of for-

mation of a glacial internal drainage on glacial sheets where length of internal drainage systems can be estimated in tens of kilometers.

Why do we speak about the impossibility of water movement along the base of glaciers? Speleological research spent in cave channels glacier tongues has shown that in variety of cases, cave channels represent alternation of subglacial and englacial parts (Mavlyudov, 2014). Englacial parts of cave channels are typical for base overdeepenings and subglacial sites – for base ledges (riegels). Our results were confirmed by observations on other glaciers, for example, on Stor Glacier in Sweden above base overdeepening of the the drainage channel also is englacial (Hooke, Pohjola, 1994). The absence of water at base overdeepening was revealed at hydraulic engineering works under d'Argentière Glacier (France) (Hantz, Lliboutry, 1983). In many cases the primary channel for a cave's origin in glacier tongues is subhorizontal slots. We observed such channels on glaciers of Spitsbergen. We consider such type of channels as universal which can be formed inside glaciers and can be modified in all other well-known glacier cave channels as englacial and subglacial (Mavlyudov, 2005). From this, the assumption has grown that channels at glacier tongues are formed on the base of subhorizontal cracks (Mavlyudov, 2006a, 2007). We observed traces of similar cracks in cave channels in the tongue of Aldegonda Glacier (Spitsbergen). despite these initially slot-hole channels being used for outflow of water from the central warm part of polythermal glaciers through freezing to a base cold ice of glacier tongues. However the mechanism of the formation of such cracks or crevasses at the base of glaciers was not clear. We have assumed that it can be sliding planes as only these have a possibility to “flow round” base over-deepenings at the glacier base. In that case there was an explanation of formation of drainage systems in mountain glaciers (Mavlyudov, 2014). This does not exclude that some thrust-faults at glacier tongues (Phillips *et al.*, 2014) are connected or have continuation with sliding planes. In this case water from a glacier surface penetrates through a crack or system of cracks in ice, and along them water reaches sliding planes, along which water starts to move towards glacier tongue. Such sliding planes are situated on depth about 100-150 m or less from glacier surface (Fig. 1). At the deeper depths, the existence of sliding planes is more problematic because of the high pressure of the ice. Therefore in thicker glaciers sliding planes are also situated at depths of about 100-150 m. Sliding planes start to contact to a glacier base only in areas where the ice thickness decreases to 100-150 m. Probably in the large ice thickness some sliding planes can exist at different depths but water always uses the upper sliding plane.

A similar mechanism of water movement in glaciers can explain both evolutionary changes of internal drainage systems and some features of glacier's behavior. In the spring when snow melting on glaciers surfaces begins, water starts to move along cracks, crevasses and moulins, formed on the base of crevasses up to the sliding plane. At first when the sliding plane is not yet cut by channels, water is distributed uniformly along it under pressure, which it creates by a water column in crevasses or moulins. Wetting by water of the big area of sliding plane leads to acceleration of glacier movement known as spring acceleration. At this time water moves along sliding plane very slowly that finds reflection in dye tracing experi-

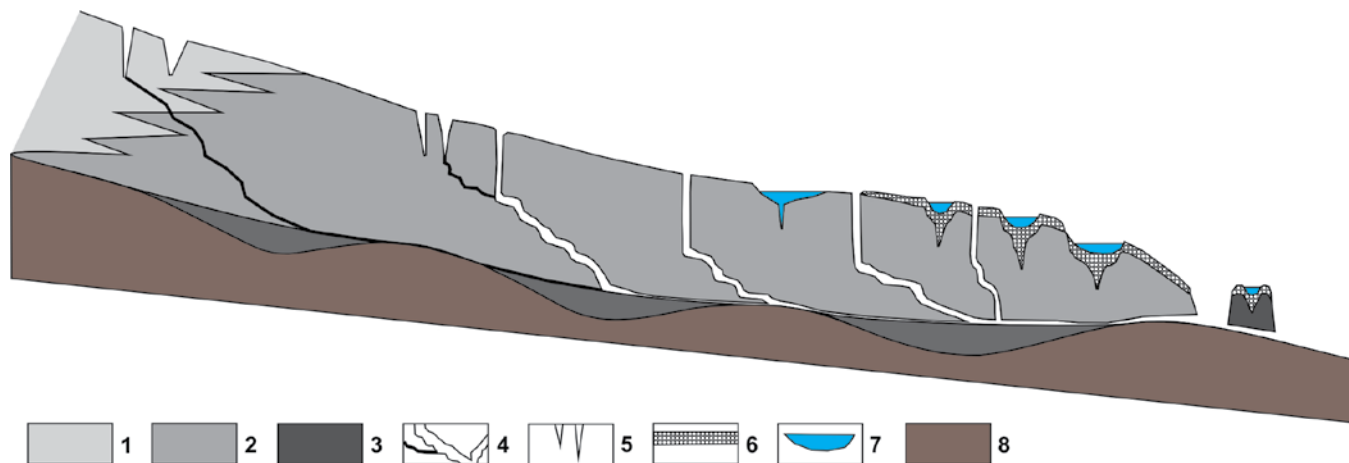


Figure 1. Longitudinal cross section through mountain valley glacier with internal drainage system; sliding plain located at the bottom of glacier. 1 – firn, 2 – ice, 3 – dead ice, 4 – channels of internal drainage system, 5 – crevasses, 6 – moraine deposits, 7 – lakes, 8 – glacier base.

ments with glacial waters at the beginning of ablation season (Hooke *et al.*, 1988). After some time channels begin to grow along the sliding plane and these conduct water, to increasing in speed inside glacier and reducing the water pressure on the sliding planes. This in turn, leads to some reduction of glacier movement speed. At the end of the ablation season large enough channels are developed along sliding plane according to its surface relief. The central channels on a glacier can be few or one depending on the surface relief. Channels will coincide with thalwegs on sliding plane that may or may not coincide with thalwegs of subglacial relief. Therefore when modeling of channels position inside glaciers, it is necessary to be guided not by the subglacial relief but by the relief of the sliding plane. The relief of the sliding plane in the most simple case, corresponds to a surface which touches to upper parts of base ledges. More difficult cases require additional research.

When water ceases to penetrate on a sliding plane, plastic deformation starts to compress channels which have developed along it during summer. Because of the considerable ice pressure which is not compensated for by water pressure in channels, the closing of channels occurs quickly. Observations on glaciers show that for this purpose several days of cold weather is all that is needed. If, after a short-term cold snap, warming occurs and the drainage system along the sliding plane can be opened again. If warming does not occur the drainage system along sliding plane remains closed until spring. It all repeats with approach of a new season of melting.

However it is less clear as regards the position of sliding planes. For polythermal glaciers clearly the sliding plane will be located at the boundary between cold and temperate ice. In these glaciers the upper more rigid layer of cold ice moves above lower softer layer of temperate ice. However such explanation is not good for cold and temperate glaciers. For cold glaciers movement of all ice thickness will occur, i.e. sliding plane on such glaciers locates at the base of glaciers. This is also most likely for temperate glaciers.

This is good for valley glaciers, but what occurs on glacial sheets? This question has remained open for considerable time. It is clear that water does not penetrate to glacier base but how it moves in glaciers is not clear. There are however places in thick ice on glacial sheets that there are sliding planes. Research in the bore holes drilled on different distances from edge of the continent on a route ~ 1400 km long

traverse from Mirnyj Station to Vostok Station has shown presence of a uniform sliding plane at about 100 m depth from the glacial surface (Markov, 2007a, b). It also appeared that the ice movement in the lower and in the upper parts of ice thickness occurs not only at different speeds but also in different directions. The origin of such a sliding plane is not quite clear. It is possible to assume that as a sustained sliding plane exists in Antarctic glacial sheet, it should be possible on other glacial sheets. In this case water from the glacial surface can reach sliding plane and move along it. In that case the formation of a system of an internal drainage on glacial sheet also will be connected with sliding planes in ice (Fig. 2). Thus an annual evolution of an internal drainage system of glaciers and glacial sheets will be similar and they will differ only by scale.

However to confirm the presence of sliding planes on other glacial sheets it is necessary to have any proofs. The most studied among glacial sheets now is the Greenland glacial sheet, especially its western part where a lot of glaciological research has occurred. Speleological research also occurred here. In particular speleological research has shown that the depth of moulines in Greenland can reach 174 m from surface (Reynaud, Moreau, 1995) or by other data to 205 m (Gulley *et al.*, 2009b). Deeper moulines in Greenland were not found. It may be the evidence that the sliding plane can located at a depth of about 200 m on the western slope of the Greenland glacial sheet.

However if such sliding plane is present in this thickness of cold ice, the layer of warmer ice should be close to it. Most likely this layer is not very thick and may be estimated measured with the more often located measurement of ice temperatures in bore holes where the measurement usually stops at about 50 m. However in the work (Ryser *et al.*, 2014) such a layer with temperatures close to the freezing point of water in Greenland was found at the depth of about 50-70 m from ice surface in several bore holes. This depth of the sliding plane position is different from previous estimated depths. Probably in the conditions of ice melting on a glacier surface, as shown on the western slope of Greenland, the thickness of ice above sliding plane will not be as sustained as in Antarctica where ice melting is absent. Other indirect confirmation of the presence of sliding planes in the Greenland glacial sheet is seismic data (Röösli *et al.*, 2014). In summertime seismic signals

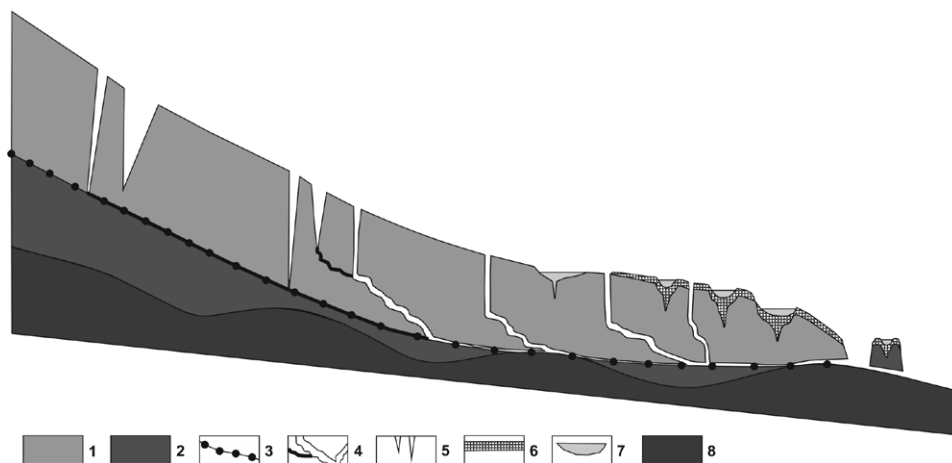


Figure 2. Longitudinal cross section through tongue part of mountain-valley glacier or margin of glacial sheet with internal drainage system. 1 – active moving ice, 2 – inactive moving or dead ice, 3 – sliding plane, 4 – channels of internal drainage system, 5 – crevasses, 6 – moraine deposits, 7 – lakes, 8 – glacier base.

occurred from depths near to ice surface and at depths about 100-150 m from ice surface. Thus signals from base of the glacial sheet are absent. Superficial signals were connected with crevasse formation, but signals from depth at about 100-160 m can be connected with a sliding plane. Absence of seismic signals at the glacier base also confirms the absence of obvious movement in the base of glacial sheet.

Certainly for the present this is not proof of the presence of sliding planes in the Greenland glacial sheet, but this is most likely due to the absence research to find sliding planes in thick glacial ice. For example, more detailed measurements of ice temperature in the upper 200-300 m of ice thickness may give the proof of the presence or absence of sliding planes in the thick ice of the Greenland glacial sheet. And if this proof of existence of sliding planes can be found, then, as well as on mountain valley glaciers formation of systems of an internal drainage on glacial sheets will receive a clear and logical explanation. The presence of sliding planes in the thick ice of glaciers and glacial sheets may additionally explain some events: drainage of supraglacial, glacier-dammed and glacial lakes, surges, and esker formation.

4. Conclusions

This article discusses the origins of the systems of internal drainage of glaciers and glacial sheets. Not one of channels now known is capable of forming a system of internal drainage of glaciers and glacial sheets by itself. Nor is it possible to form a system of internal drainage of glaciers and glacial sheets for them in a complex way. Discussion of all existing theories for these systems of internal drainage of glaciers and glacial sheets origin finds that all of them can be used only for small number of specific cases and are not universal. We used the hypothesis of formation of internal drainage systems on the base of sliding planes which are located inside glacial ice. This hypothesis can explain formation and evolution of internal drainage systems of glaciers and glacial sheets of any dimension. Except for the formation and evolution of internal drainage systems of glaciers, the hypothesis can explain many phenomena connected with glacier hydrology: spring acceleration of glaciers movement including glacial sheets, surface change of glacial sheets after drainage of superficial lakes, outbursts of glacier-dammed lakes, glacial surges and eskers formation.

Acknowledgements

This work was supported by State Program No. 0148-2014-0004.

References

- Badino G, 2001. Glacial karst phenomenology. *Proc. 13th International Congress of Speleology*. Brasilia, pp. 211-216.
- Benn DI, Evans DJA, 2010. *Glaciers and glaciation*. 2nd ed. Hodder Education, London. 802 p.
- Das SB, Joughin I, Behn MD, Howat IM, King MA, Lizarralde D, Bhatia MP, 2008. Fracture propagation to the base of the Greenland ice sheet during supraglacial lake drainage. *Science*, **320**(778), 778-781.
- Eraso A, Pulina M, 2010. *Cuevas en hielo y ríos bajo los glaciares*. 3rd ed. McGraw-Hill, Madrid. 300 p. (In Spanish).
- Fountain AG, Walder JS, 1998. Water flow through temperate glaciers. *Reviews of Geophysics*, **36** (3), 299-328.
- Gulley JD, Benn DI, Muëller D, Luckman A. 2009a. A cut-and-closure origin for englacial conduits in uncrevassed regions of polythermal glaciers. *Journal of Glaciology*, **55** (189), 66-80.
- Gulley JD, Benn DI, Screatton E, Martin J, 2009b. Mechanisms of englacial conduit formation and their implications for subglacial recharge. *Quaternary Science Reviews*, **28**, 1984-1999.
- Hooke RLeB, Miller SB, Kohler J, 1988. Character of the englacial and subglacial drainage system in the upper part of ablation area of Storglaciaren, Sweden. *Journal of Glaciology*, **34** (117), 228-231.
- Hooke RLeB, Pohjola VA, 1994. Hydrology of a segment of a glacier situated overdeepening, Storglaciaren, Sweden. *Journal of Glaciology*, **40**(134), 140-148.
- Hantz D, Lliboutry L, 1983. Waterways, ice permeability at depth, and water pressures at Glacier d'Argentière, French Alps. *Journal of Glaciology*, **29**(102), 227-239.

- Hewitt IJ, 2013. Seasonal Changes in Ice Sheet Motion due to Melt Water Lubrication. *Earth and Planetary Science Letters*, **371–372**, 16–25.
- Markov AN, 2007a. Difference of dynamic of surface of Eastern Antarctica glacial sheet in depth interval 0-200 m. *Materialy glatsiologicheskikh issledovaniy* (Data of glaciological studies), **102**, 12-22 (In Russian).
- Markov AN, 2007b. Correlation specific by depth and spread of dynamic properties of glacial sheet of Eastern Antarctica in depth intervals 0-450 m. *Materialy glatsiologicheskikh issledovaniy* (Data of glaciological studies), **103**, 11-24 (In Russian).
- Mavlyudov BR, 1995. Problems of En- and Subglacial Drainage Origin. M Griselin (ed.). Actes du 3e Symposium International Cavites Glaciaires et Cryokarst en Regions Polaires et de Haute Montagne, Chamonix-France, 1er-6. XI.1994. *Annales Litteraires de l'universite de Besancon 561, serie Geographie*, **34**, 77-82.
- Mavlyudov BR, 1998. Glacier cave origin. 4th International Symposium of Glacier Caves and Cryokarst in Polar and High Mountain Regions. *Zalzbürger geographische materialen*, heft **28**, Salzburg, 123-130.
- Mavlyudov BR, 2005. About new type of subglacial channels, Spitsbergen. *Glacier Caves and Glacial Karst in High Mountains and Polar Regions*. BR Mavlyudov (ed.) Moscow, Institute of geography of the Russian Academy of Sciences, 54-60.
- Mavlyudov BR, 2006a. *Internal drainage systems of glaciers*. Institute of geography RAS, Moscow. 396 p. (in Russian).
- Mavlyudov BR, 2006b. Glacial karst, why it is important to research. *Acta Carstologica*, **35**(1), 55-67.
- Mavlyudov BR, 2007. Internal drainage systems of glaciers. *Karst and Cryokarst*. A Tyc and K Stefaniak (eds.), Proceedings of 8th GLACKIPR Symposium. Univ. of Silesia Faculty of Earth Sciences, Univ. of Wroclaw Zoological Institute, Sosnowiec-Wroclaw, 49-64.
- Mavlyudov BR, 2014. Internal drainage of glaciers and its origin. L Land, Z Kern, V Maggi, S Turri (eds.). *Proceedings of the Sixth International Workshop on Ice Caves, August 17-22, Idaho Falls, Idaho, USA*. NCKRI Symposium 4. National Cave and Karst Research Institute, Carlsbad (NM), 50-58.
- Phillips E, Finlayson A, Bradwell T, Everest J, Jones L, 2014. Structural evolution triggers a dynamic reduction in active glacier length during rapid retreat: evidence from Falljökull, SE Iceland. *J. Geophys. Res. Earth Surf.*, **119**, doi:10.1002/2014JF003165.
- Reynaud L, Moreau L, 1995. Moulins Glaciaires des Temperes et Froids de 1986 a 1994 (Mer de Glace et Groenland). M Griselin (ed.). Actes du 3e Symposium International Cavites Glaciaires et Cryokarst en Regions Polaires et de Haute Montagne, Chamonix-France, 1er-6. XI.1994. *Annales Litteraires de l'universite de Besancon 561, serie Geographie*, **34**, 109-113 (in French).
- Röösli C, Walter F, Husen S, Andrews LC, Lüthi MP, Catania GA, Kissling E, 2014. Sustained seismic tremors and icequakes detected in the ablation zone of the Greenland ice sheet. *Journal of Glaciology*, **60**(221). doi: 10.3189/2014JoG13J210
- Ryser C, Lüthi MP, Andrews LC, Hoffman MJ, Catania GA, Hawley RL, Neumann TA, Kristensen SS, 2014. Sustained high basal motion of the Greenland ice sheet revealed by borehole deformation. *Journal of Glaciology*, **60**(222). doi: 10.3189/2014JoG13J196
- Shumskij PA, 1955. *Theory of structural glaciology*. Publishing House of Academy of sciences of the USSR, Moscow. 492 p. (in Russian).
- Zwally HJ, Abdalati W, Herring T, Larson K, Saba J, Steffen K, 2002. Surface melt-induced acceleration of Greenland ice-sheet flow. *Science*, **297** (5579), 218-222.

Piping Cave Development In A High Gradient Setting: Kutz Canyon, New Mexico, Usa

Douglas M. Medville

Affiliation: Hawai'i Speleological Survey medville@centurylink.net

Abstract

Kutz Canyon in NW New Mexico consists of over 14,000 hectares of smaller canyons and gullies developed in the 525 meter thick Paleocene Nacimiento Formation, a mix of bentonitic mudstones and claystones with interbedded sandstones. Local relief from canyon rim to floor varies from 120 to 150 meters with gully gradients ranging from 10 to 30 degrees. A mature pseudokarst is developed on these beds with numerous dolines in the upper member of the Nacimiento Fm capturing storm runoff and channeling this water into a complex of caves below. A majority of the caves are developed in debris flows beneath gullies and side canyons and have the same gradients as the gullies above. The high gradient piping caves found in Kutz Canyon are among the longest and deepest such caves in the United States. To date, over 160 caves having a cumulative surveyed length of over 5.0 km have been located. Although lengths generally range from 100–250 meters, the largest cave has a length of over 600 meters and a vertical extent of 90 meters.

The caves are developed as a result of swelling/shrinking of high sodium content swelling soils, primarily montmorillonite, with water infiltrating to depth by following the cracks resulting from swell/shrink cycles. Over time, small sinks and vadose pits are formed, carrying water downward to less permeable surfaces such as sandstone beds or the original valley floor. Subsequent corrasional passage enlargement via grain by grain removal of material takes place with material transported to a discharge point, usually at the base of the canyon. Cave passage morphologies vary but commonly have canyon-like cross sections with typical widths of a 1–3 meters and heights of up to 10 meters. Numerous skylights and pits resulting from ceiling collapse and ceiling stoping connect these passages to the valley floors above. In the more vertically extensive caves, sandstone beds in the Nacimiento Fm. are encountered. These act as aquitards and when breached, internal pour offs with abrupt drops in floor levels of up to 7 meters are encountered in the caves.

Keywords:

1. Introduction and background

Kutz Canyon in San Juan County, NM is a 14,240 hectare (54.9 mi²) complex of canyons and badlands administered by the U.S. Bureau of Land Management (BLM). The canyon, drained by a north flowing seasonally dry stream called Kutz Wash, contains numerous small infeasible canyons and gullies (Figure 1).

A pseudokarst containing dolines, swallets, pits, piping caves, and resurgences is found in Kutz Canyon. The vertical relief from the canyon rim to its floor ranges from 120 to 150 meters. Mean annual precipitation is 23.6 cm per year and the annual average temperature is 12.2 °C.

All but the upper 10-20 meters of Kutz Canyon is developed in the 65-61 Ma Paleocene Nacimiento Formation, consisting of nonmarine fluvial and lacustrine strata composed of red, green, and black bentonitic mudstones and claystones with interbedded sandstones. In ascending order, the Nacimiento contains three members: the Arroyo Chijuillita Member, the Ojo Encino Member, and the Escavada Member. In Kutz Canyon, the lower two members cannot be distinguished and they are referred to as the main body of the Nacimiento Formation (Williamson, 1992). The Cuba Mesa sandstone member of the San Jose Formation overlies the Escavada Member and comprises the upper 15–20 meters of the canyon and the canyon rim. Piping caves and related pseudokarst features are found in all three members of the Nacimiento Formation.

A brief description of the badland topography in Kutz Canyon, focusing on vertical soil pipes developed in the



Figure 1. View of Kutz Canyon

Nacimiento Formation, is provided in Parker, *et. al.*, 1990. That paper described “...two of the largest known pipes in the United States, about 17 meters deep and with greatest diameters 6 to 8 meters. They are developed on the north wall of Kutz Canyon, about 22.5 km south of Bloomfield, New Mexico. These pipes occur on hard gray sandstone and claystone of the Paleocene Nacimiento Formation, which is cemented with coatings and inter-grain fillings of a smectite clay.” Although the paper made no mention of horizontal piping caves, as of late 2016 over 160 such features had been located and documented in many of the side canyons and gullies in Kutz Canyon. To date, 71 of these caves have been surveyed with a combined length of over 5.0 km. Although the longest of these caves is over 400 meters in length, the median length of the caves is 47 meters.



Figure 2. Dolines in Escavada member of Nacimiento Formation



Figure 3. Sampling site (left wall) from large passage in a Kutz Canyon cave



Figure 4. Sandstone ceiling at cave entrance

Several of the caves extend over a vertical range of up to 90 meters; perhaps the most vertically extensive piping caves known.

2. Clay mineralogy in Kutz Canyon

Four samples of the material in which caves are developed in Kutz Canyon were analyzed for their clay mineralogy using powder X Ray diffraction. One was taken on a sandy bed in the upper (Escavada) member within which numerous small dolines are developed (Figure 2).

A second was taken from a claystone slope next to a cave entrance at the base of the canyon and in the main body of the Nacimiento Fm. The third was taken from the wall of a voluminous cave also at canyon bottom level and 5 km east of the second sample (Figure 3).

The fourth sample was taken from a hard sandy bed that forms the ceiling of this cave (Figure 4).

As expected, all of the samples have quartz contents of 40%-75%, reflecting the sandy nature of the Nacimiento Fm. For all samples, the principal clay components were montmorillonite and kaolinite.

Hobbs (2016) also analyzed the clay composition of members of the Nacimiento Fm in Kutz Canyon and obtained results for samples taken in the same general area; i.e., at the western and eastern sides of the south end of Kutz Canyon that differed somewhat from the samples analyzed for this paper but which confirm the propensity of the clays to swell. These samples contained 57-71% montmorillonite, 18-35% illite, and 8-10% kaolinite.

When wetted, montmorillonite can swell, break down into smaller particles (deflocculate) and disperse. Previous studies (Charman, 1969, Heede, 1971, Parker, 1983) have demonstrated a strong relationship between the propensity for soil piping to take place and measures such as the exchangeable sodium percentage (ESP) in the soil where $ESP = [Na / (Na + Ca + Mg + K)] * 100$, the sodium adsorption ratio (SAR) where $SAR = Na / [0.5 (Ca + Mg)]^{0.5}$, and the cation exchange capacity (CEC) of the soil; a measure of the capacity of the soil to hold exchangeable cations. Heede (1971) stated that "piping soils had a significantly higher sodium percentage (ESP) and sodium adsorption ratio (SAR) than non-piping soils".

For this study, the samples taken from the upper doline-pocked surface and the caves on opposite sides of the canyon were similar. The sodium content varied between 41.8 and 98.7 meq/L, SARs ranged from 30.4 to 40.0, ESPs ranged from 31.4 to 36.7, and CECs varied from 22.0 to 25.5; all measured in meq/100g. The SAR values reflect a high soil sodicity while the CEC values are indicative of the ability of the clay samples to exchange cations and, as a result, to swell in the high sodium content soils sampled.

The fourth sample, taken from the flat massive ceiling of the eastern cave, differed from the others. For this sample, the sodium content was only 4.0%, the clay content was only 9%, and the measures of the propensity to swell were also low: sodicity was 8.4 meq/100g, the ESP was 9.2 meq/100g, and CEC was 9.3 meq/100g. Sandy beds similar in appearance and

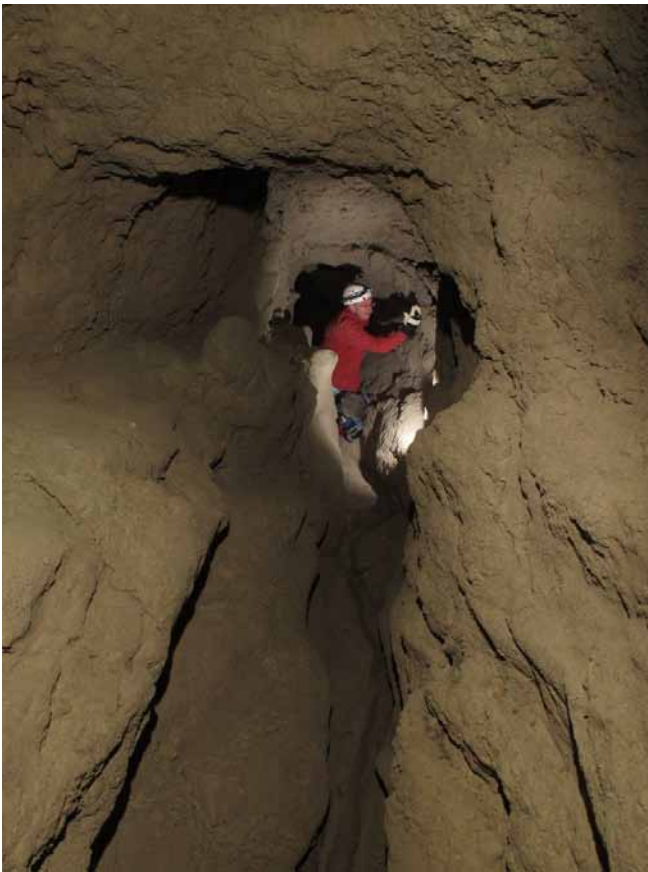


Figure 5. Rounded passage with vadose trench in floor

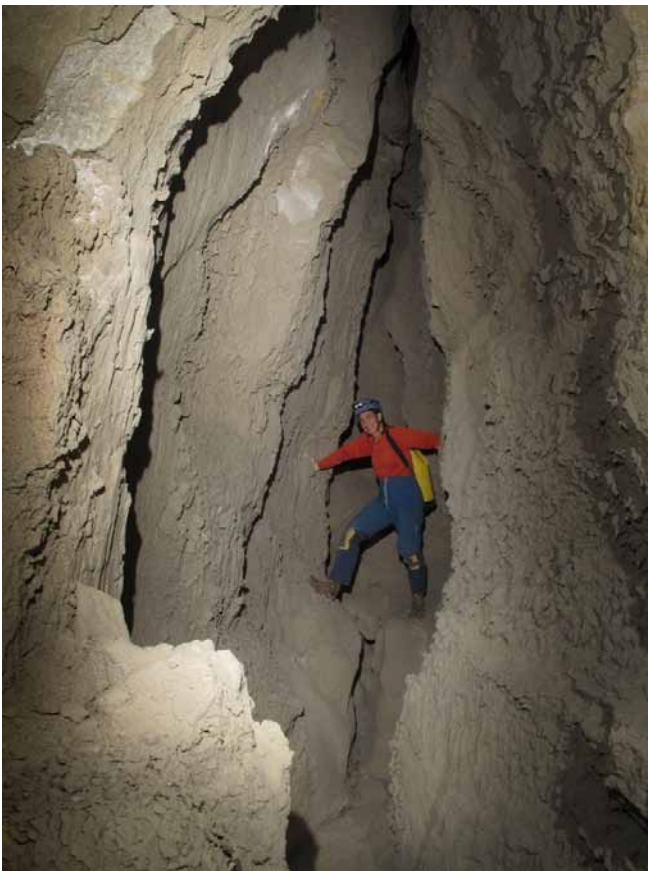


Figure 6. Flared canyon passage

probably composition to this are seen in several caves in Kutz Canyon and provide structural stability, preserving the passages in the higher clay content soils beneath.

3. Speleogenesis

Following a precipitation event, the clays will shrink upon drying, resulting in desiccation cracks. With repeated swell/shrink cycles, the cracks deepen with most of the wetting and consequent swelling and shrinking taking place at the bottom of the cracks. As a result, they grow deeper until either base level or a less permeable surface is reached, e.g. a harder sandstone bed. Water then moves down gradient/down valley to an outlet on the valley floor. In some cases, continued wetting and swelling of the walls of the crack as well as debris flows from above can result in closing of the upper parts of the crack and the formation of a closed conduit at depth. In other cases, water pouring off of a higher sandstone bed or reaching the top of a crack falls vertically, resulting in a vadose shaft being developed. If an outlet exists at the base of the shaft, water will move sub-horizontally down-valley to a proto-outlet. Some of these shafts or vertical pipes can be sizeable. Parker notes that "Sandstones, if clean and well cemented, rarely become piped, but where they are poorly cemented or contain silt or silty clay, they may develop pipes, some of spectacular size". This is the case in Kutz Canyon where corrosion of a sandy matrix cemented by swelling (smectite) clays has resulted in the development of passages up to 10 meters across and 7 meters high. Following repeated clay swell/shrink cycles, the sand grains wash away, leaving large voids.

In either case, the moving water transports grains of the matrix (sand, clay), gradually enlarging the initial conduit through mechanical means (corrosion) until passages are large enough for human entry. The concentrated flow of water in the conduit enlarges it as a result of scour and the removal of loose, detachable particles on the conduit walls. Where the hydraulic gradient of the stream in the conduit is high as is the case in Kutz Canyon, particles are transported in suspension to an outlet, usually at the valley floor or gully wall. The removal of particles takes place primarily on the passage floor as the moving water down cuts into the floor, resulting in a vadose trench. A common passage morphology observed is one in which the upper part of the passage is rounded (the original conduit) and the lower part consists of a deep, narrow floor trench, usually less than a meter in width but up to 5 meters in depth (Figure 5).

Another passage configuration consists of a high narrow ceiling crack (the initial passage) with the passage becoming more rounded and wider at the base (Figure 6), especially where the passage floor is on a more impermeable bed.

If these beds are breached, the passage abruptly migrates downward in a stair step pattern with drops of 3–7 meters observed.

As the process continues and passages are widened, sections of the ceiling may slope upward to the surface and collapse, resulting in skylights when viewed from below (Figure 7) and pits when viewed from above that can funnel additional material as well as runoff into the cave below.

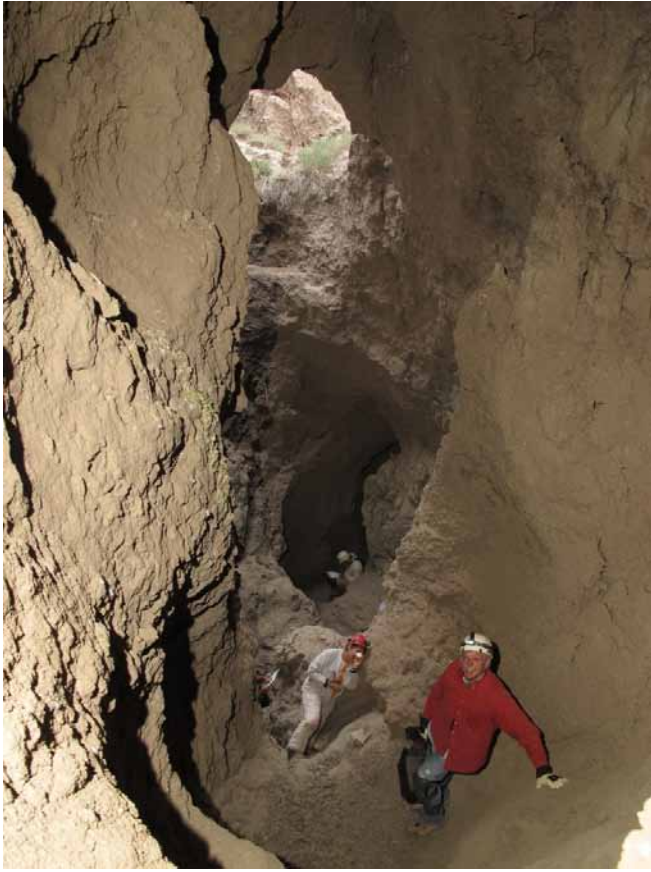


Figure 7. Skylight above a steeply ascending passage

Over time, the pits coalesce and further ceiling slumping and collapse takes place, resulting in a series of remnant natural bridges rather than a continuous subsurface conduit. The resulting topography containing dolines, pits, sinking streams hanging valleys, and resurgence entrances resembles a karst topography, although solutional process are not a factor. Rather, this piped landscape is a form of pseudokarst.

To sum, the piping caves and the pseudokarst landforms above them result from the removal on a grain-by-grain basis of clastic rocks by flowing water. Minimum requirements for their development are (1) intermittent rainfall sufficient to wet the soil and fill incipient cracks, (2) the presence of swelling/shrinking clays, (3) desiccation of the clays between wetting cycles, (4) a hydraulic gradient sufficient for water to flow at the base of the cracks, and (5) an outlet for the drainage.

Photographic credits

Figures 1 and 2: Douglas Medville

Figures 3-7: Edward Lappin

References

Charman, P.E.V., 1969. The influence of sodium salts on soils with reference to tunnel erosion in coastal areas. *Soil Conservation Service of New South Wales Journal*, v. 25, 331-347.

Heede, B.H., 1971. Characteristics and processes of soil piping in gullies, U.S. Department of Agriculture Forest Service, *Rocky Mountain Forest and Range Experiment Station Research Paper RM-68*.

Hobbs, K.M., 2016. *Sedimentation, Pedogenesis, and Paleoclimate Conditions in the Paleocene San Juan Basin, New Mexico, U.S.A.* PhD Dissertation, Earth and Planetary Sciences, The University of New Mexico. Albuquerque, NM.

Parker, G. G. and C. G. Higgins. 1990. Piping and Pseudokarst in Drylands, in: *Geological Society of America Special Paper 252: Groundwater Geomorphology: the Role of Subsurface Water in Earth-Surface Processes and Landforms*.

Williamson, T.E. and S. G. Lucas. 1992. Stratigraphy and mammalian biostratigraphy of the Paleocene Nacimiento Formation, southern San Juan Basin, in: *San Juan Basin IV, New Mexico Geological Society Guidebook*, 43rd Field conference, 265-296.

(Abstract) Types of caves present in Kalimantan Barat Province, Borneo, Indonesia

Claude Mouret

Affiliation: *Freelance geologist*
claude.mouret.geospel@orange.fr
Km1 La Tamanie, 87 380 MAGNAC-BOURG, France

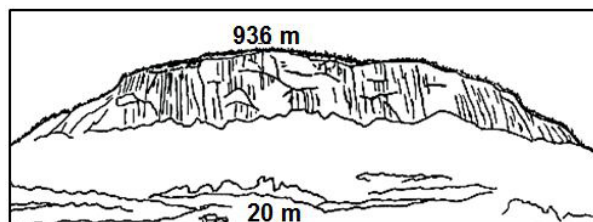
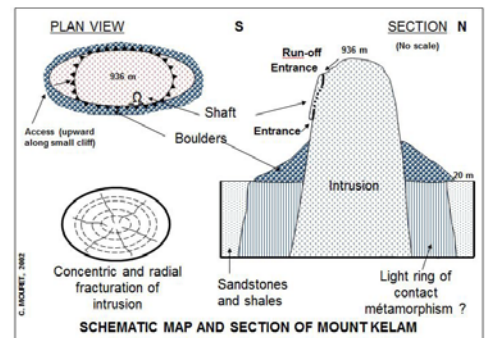
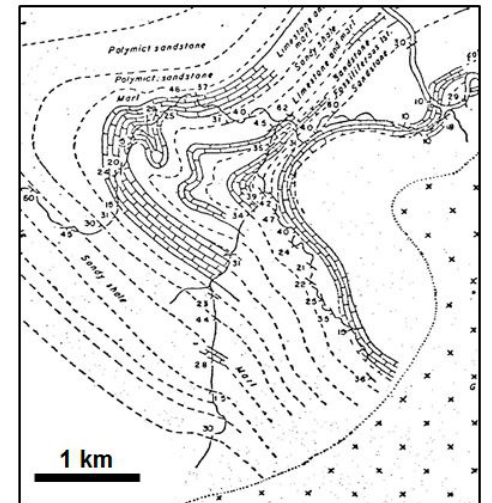
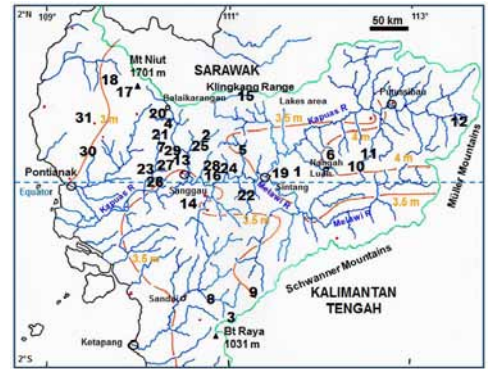
Abstract

Kalimantan Barat displays a few small limestone areas which exhibit some caves.

Besides this, many caves or voids have formed in other kinds of rock formations:

- In Cenozoic sandstones, caves have formed underneath massive layers which are bearing surface streams. Stream water penetrates the rock and generates an underlying cave along the contact between the sandstone and less permeable rocks such as siltstone or shale. Such caves may reach a hundred metres long. They are created by grain disintegration and export by flowing water.
- Caves also form in thin limestone bodies of limited extension, which are interbedded with sandstone. These bodies may be former caliches which were eroded, then redeposited.
- In sandstones or other siliciclastic formations underneath basalt lava flows, particle export at the interface does result into large caves.
- In the basalts themselves, passages do exist.
- In medium-depth intrusive rocks which have been brought to ground surface by erosion and now exist as necks, deep shafts have formed. One of them is 330 m deep approximately. Such shafts are related to rock weathering much more than to gravity-related lateral opening of the neck.
- In recent alluvial formations along rivers, meandering results into the lateral erosion of alluvium. In such places, buried tree trunks may carry water in their inside and behave as springs at their end to the open sky, sometimes with a significant flow rate.
- Gravity-related shafts are present behind high cliffs around massive sandstone bodies.
- Passages large enough for penetration by man are dug out by turtles in river banks.

Other kinds of voids are also present.



(Abstract) **Speleogenesis underneath basaltic lava flows in Niut Mountains, Kalimantan Barat, Borneo, Indonesia**

Claude Mouret

Affiliation: *Freelance geologist
claude.mouret.geospel@orange.fr
Km1 La Tamanie, 87 380 MAGNAC-BOURG, France*

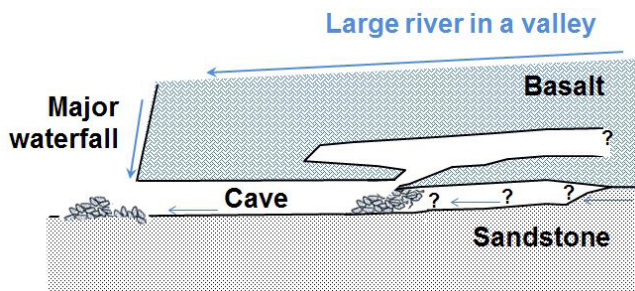
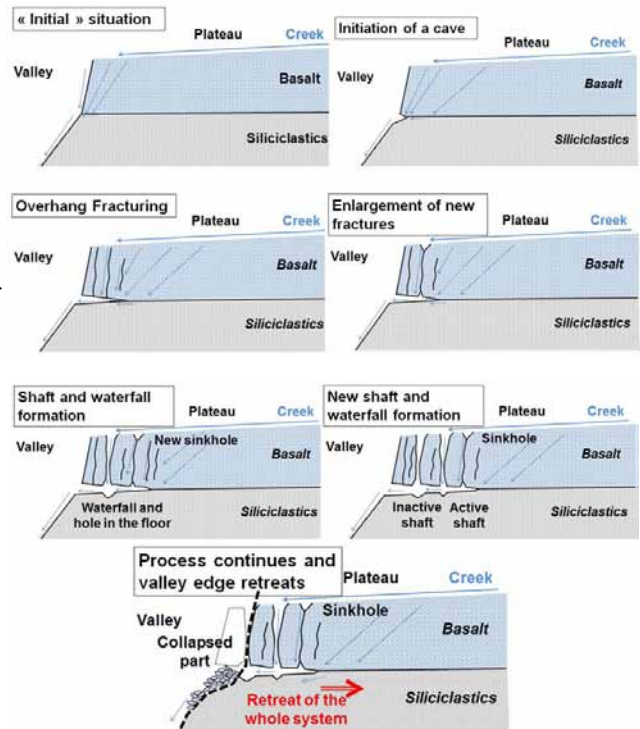
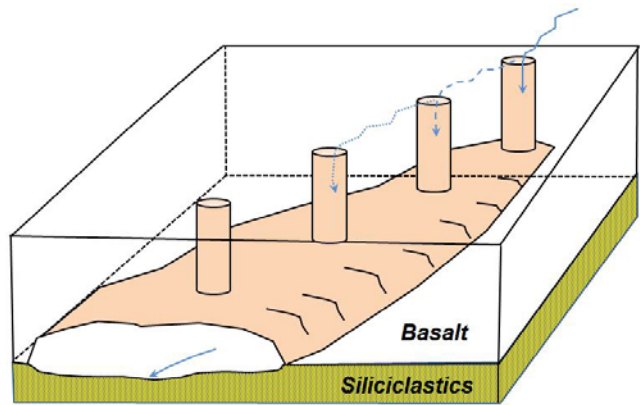
Abstract

Large and low-roofed caves exist in a variety of siliciclastic sediments underlying extensive Cenozoic lava flows in Borneo.

Field research and speleological investigation has shown that such caves are rather large, up to 45 m, a few metres high and that they usually do not exceed 100 m in length. They are present in massive sandstone bodies or even in sandstone-siltstone-shale alternations, always along and below the contact surface with overlying basalt. One of the caves displays a maze in sandstone, which is crossed through by a stream. A boulder choke closes the way upstream, but continuation exists within overlying basalt.

This speleogenesis is by a self-accelerating process. It is most often encountered near valley flanks. Initially, water percolates vertically within the basalt and reaches the interface with underlying, less permeable, siliciclastics, along which it flows down to the nearest valley margin. Rock grains are carried away with water. This creates a thin, large void that progressively enlarges and gets higher. The void destabilises the basaltic mass from below, which generates cracks enlargement.

More surface water can therefore infiltrate the cracks and at some stage the capture of a surface streamlet may occur. This leads to shaft formation through the basalt and these are seen at the roof of the caves. Shafts are active during rainy episodes only, and behave as waterfalls bringing much water into the cave. Void enlargement develops accordingly. Progressively, new shafts form more upstream and previous ones are progressively abandoned by water. Due to this migration, the cave gets longer and longer, as the water injection point is further and further away from the valley margin.



Some fundamental features of speleogenesis in sandstone

Claude Mouret

Affiliation: Freelance geologist, Km1 La Tamanie, 87 380 Magnac-Bourg, France claudemouret.geospel@orange.fr

Keywords:

As more and more caves in sandstone are discovered and studied, with fascinating results, the consequences on speleogenesis of the geological history of the sandstones have seldom been taken into account. We wish to stress some facts.

The geohistory of the sandstone is a major key to help understanding speleogenesis. After sand deposition, whatever the depositional environment, the sediment follows a long evolution from loose medium to consolidated rock. Burial depth varies versus time, depending on the rate of subsidence and types of tectonics. The sand sediment follows a progressive compositional and mechanical evolution from ground surface or sea bed down to depth. Some burial depth vs time pathways bring the sediment at great depths, some others not.

Because we now observe sandstone caves from ground surface, the rock has necessarily been subject to uplift and erosion after burial. Therefore, we see at ground surface rocks that owe a significant part of their physical properties to pressure, temperature and chemical conditions at depth.

Sandstones in the Paris Basin, France, have been poorly buried. They are often harder near the edges of the plateaus, due to specific diagenesis, meanwhile some relatively loose parts occur in places. Caves in these sandstones are commonly maze-like and show siliceous concretions aggregating volumes of grains and plugging rock porosity.

In contrast, sandstones of the Khorat Plateau in Thailand have undergone deep burial followed by major uplift and erosion. Such sandstones are prone to large cave systems provided hydraulic potential is applied to the formations. Comparable conditions apply to the world-famous sandstone plateaus in Venezuela.

In these different cases, the petrographic rock evolution is of paramount importance, together with the initial depositional environment, because the latter has also an influence on rock composition. The paper shall explain all this with documented examples, and petrographic data.

Sandstone caves are encountered all over the world, in a great diversity of natural environments, climate conditions and geological origins. They are as diverse as limestone caves can be. Past authors have extensively discussed cave formation in sandstone, but petrographic factors have not yet been considered globally.

Firstly, one has to consider initial grain composition, shape and sorting, then successive diagenetic phases, which are closely related to the geological history. Speleogenesis occurs in such sandstones with different histories. Secondly, geohistory plots make up a convenient and powerful tool how to integrate most, if not all, factors of the succession of geological events, because they cannot be built efficiently without a previous review of all what is known on regional and local

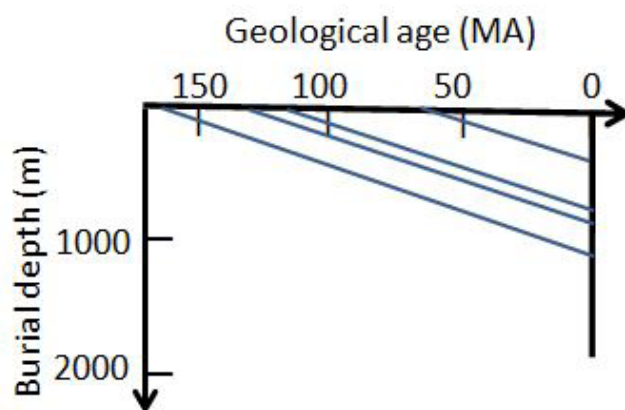


Figure 1. Building the geohistory plot.

geology and without a thorough understanding of it. Thirdly, sandstone fabric and related petrophysical properties are greatly dependent on the geohistory and the types of caves may differ accordingly. Therefore, caves in sandstones should be analysed in the light of the degree of mechanical and chemical compaction suffered by the rock (and, of course, at the light of all other classically considered factors).

1. Geohistory plots: sediment burial and uplift through time

Building geohistory plots consists of representing the burial depth versus time of all sediments present in the studied area, therefore also of the sandstone. Because formation thicknesses are involved and because they may greatly vary from a place to another one, the plot is valid only over a small area of land. Depths are the sums of the thicknesses of successive formations.

The plot is conveniently constructed by starting it at the present. The present stratigraphic column is placed vs depth at time 0 on the plot. Then, for each top of stratigraphic interval, one curve will describe the successive states of burial, based on available data. The curve starts at surface (the deposition depth) at the deposition time, then burial vs time is obtained by adding successive strata thicknesses (Fig. 1). In the most common approach, formation thickness reduction by overburden is not integrated in the plot (it can be done in a second step if more precise results are required). If necessary, one can superimpose other curves to burial curves on the plot, e.g. temperature or pressure vs time curves.

Despite geohistory plots being based on rather simple principles, constructing them may be rather difficult. For instance, long periods of erosion before subsequent burial may have erased a substantial part of the geological record, which makes reconstructions difficult. The task is even more diffi-

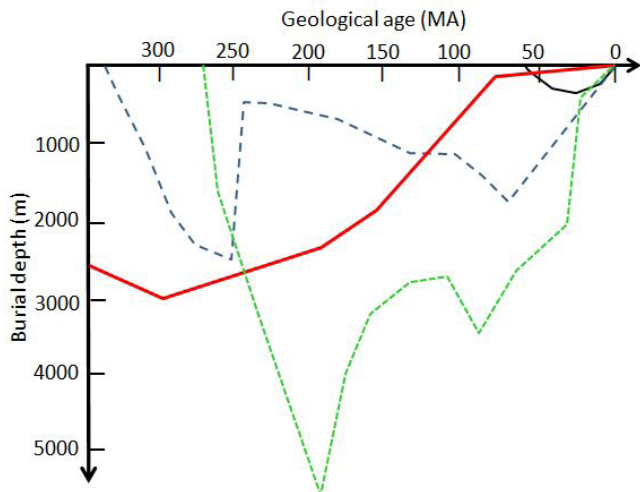


Figure 2. Geohistory plot. Four examples (purely imaginative) of burial vs time pathways which might have been followed by a sandstone bed now at surface conditions. Some sandstones have not been deeply buried. Others may have suffered great burial depths and successive periods of burial and uplift.

cult when two long stratigraphic gaps are present. In this case, specific methods have to be used in order to quantify eroded thicknesses and reconstruct missing series.

2. What sediment thickness was eroded?

For instance, on the Khorat Plateau of Thailand, post-Permian erosion and non-deposition resulted in a stratigraphic gap up to 20 MA and even up to 45 to 60 MA elsewhere in SE Asia (Mouret, 1994a). In addition, an erosion period which started around 65 MA has removed up to around 3000 m of sediments. No sediment younger than the base of Upper Cretaceous strata (Mouret *et al.*, 1993) is known on the Khorat, except Quaternary alluvium. We give here below a sampling of the combined methods and data which were used to evaluate the post-65 MA erosion thickness (Mouret *et al.*, 1993):

- Physical data: sonic transit time of 75 microseconds/foot; seismic velocities of 3560 m/s at sea level and 4035 m/s at 0.5 s TWT (two-way time), which are close to those observed at the base of the Paris Basin.
- Petrophysical data: vitrinite reflectance up to 1.2%; apatite fission tracks which indicate around 2950 m of erosion.
- Petrographic data: quartz grains suturing in the Phra Wihan sandstone and in sediments below it, indicating around 3000 m of erosion (by comparison with data from oil wells in different parts of the world)
- Sedimentological data, based on the study of sedimentation rates and comparison with the thickness of eroded section.

Altogether, a likely (but not a maximum) 3000 m erosion thickness was estimated in 1993 and 3250 m were subsequently measured on a seismic line (Mouret, 1994b). The quartz grain suturing was itself a strong indicator for the final conclusion. A difficulty in this kind of approach consists of bringing to the same datum facts which may concern different stratigraphic units.

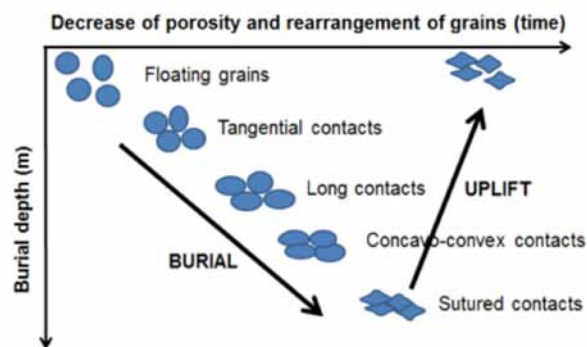


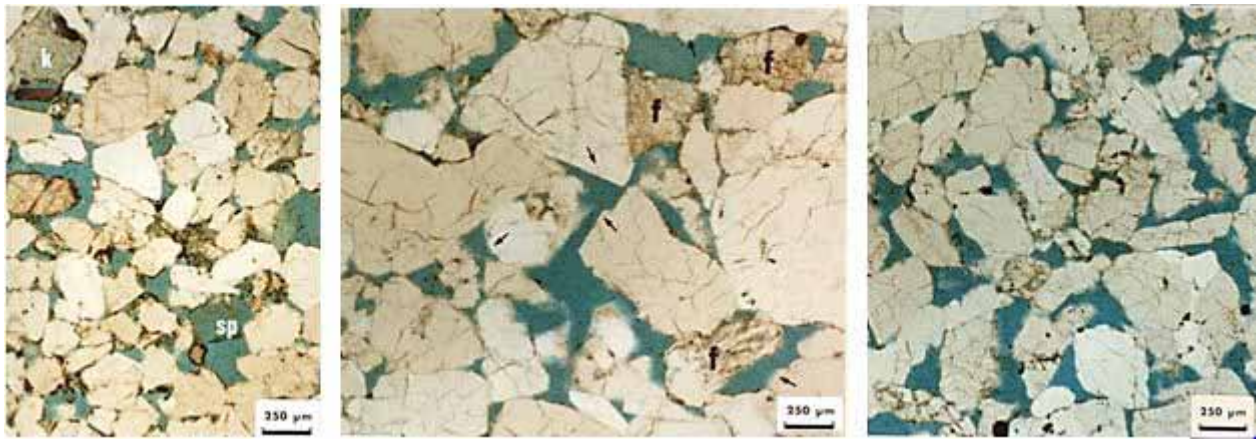
Figure 3. Mechanical evolution of grains during burial and uplift. Deliberately, no scale is shown because the depth at which grain contacts have a characteristic shape is not a unique, linear function. It depends also on basin evolution. However, the evolutionary order remains the same.

Another example comes from the Eocene/Oligocene siliciclastic formations in the Melawi Basin in Kalimantan Barat, Borneo, Indonesia. After his detailed field studies, the author constructed a regional map of vitrinite reflectance values at ground surface which proved an erosion of 2000 m at least. Detailed petrographic and petrophysical studies were conducted in order to cross-check this result. Some field samples of quartzose sandstones were displaying good values of measured porosity and permeability, despite their loose though imbricate-like quartz grains. The 5 samples with the highest values came from locations several tens of kilometres apart. Each of the strata from which these samples were collected was drilled in such a way that new samples could be collected at a nearly 30 m depth. Then surface and depth samples were oriented in the 3D space in order to be comparable. New measurements on oriented plugs from all samples proved that porosity at the 30 m depth is around ten times less than at surface and permeability around 1000 times less. In other words, the sandstones were heavily compacted at depth and it was even worse than what vitrinite reflectance had indicated. It was hypothetically concluded that tectonic stress due to plate collision might have been the cause for the overcompaction of the sandstones.

This second example shows that the decompaction of compact sandstone near ground surface tremendously increases porosity and permeability. The decompacted zone is thinner where the initial rock compaction was higher, as the author could also observe.

3. Shape evolution of quartz grains vs depth

In siliciclastic sandstones (we exclude calcarenites which are entirely calcareous rocks), grain nature determines specific names, depending on what kind of grain is dominant: quartz is dominant in quartzoses, (not to be confused with quartzite which is a metamorphic rock), feldspars in arkoses and rock debris in greywackes. Most common cements are either silica or calcite, both being often organized as successive phases. Additionally hematite cement is present in some sandstone

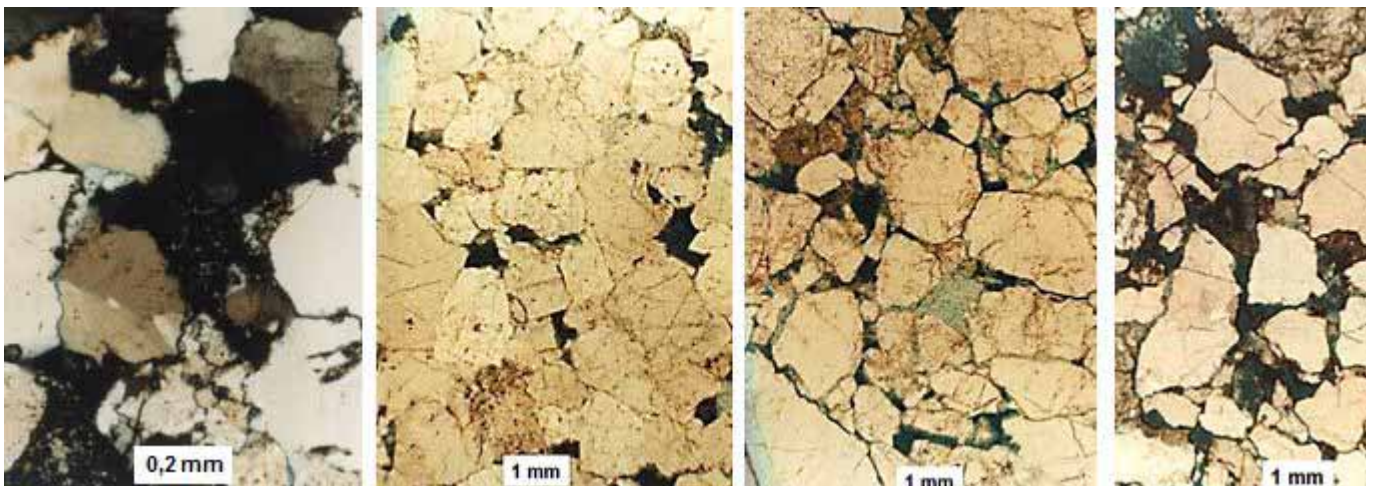


Photos 1, 2 and 3, from left to right. Each scale bar represents 250 µm. Natural light. Moderately compact sandstones with some grain dissolution (feldspars, rock fragments). All near a 3500 m depth in North Sea.

Photo 1 Medium grain size; poor sorting; contacts are long to tangential; k= authigenic kaolinite; sp= large secondary pores from dissolved grains, probably feldspars.

Photo 2 Medium to coarse grain size, poor sorting, no clay; f=remaining feldspars; silica cement (arrows); contacts are tangential to long.

Photo 3 Medium grain size; poor sorting; no clay; mainly tangential to long contacts.



Photos 4 to 7, from left to right. Surface samples of sandstones from the Melawi Basin, Indonesia. 4 and 7: polarized light; 5 and 6: natural light. Heavy compaction before weathering:

Photo 4 Sutured to concavo-convex grains. Probable feldspar grains have been dissolved and generated pore filling kaolinite (in black-coloured pores).

Photo 5 Almost unweathered quartzose with a few small dissolved grains. Concavo-convex to sutured contacts.

Photo 6 Similar rock in composition and fabric, but decompacted (see close-up on Figure 8).

Photo 7 Quartz grains and leached feldspars and rock fragments. Concavo-convex to sutured grain contacts. Decompaction present.

formations, e.g. on the Khorat Plateau. A variable amount of clay is possible and sandstones are characterised as shaly or argillaceous, or to the contrary “clean”. A variety of names is available for sandstones of intermediate composition.

During burial and uplift phases, grains composition may evolve to a variable amount according to changing pressure and temperature conditions and depending on initial grain nature. Rock debris grains are altered, possibly dissolved, and often generate clay minerals. Feldspars become loose, corroded and generate silica and clay minerals. Quartz grains themselves suffer pressure dissolution and peripheral silica deposition, depending on the conditions. Clay neoformation occurs mainly in porosity, for instance kaolinite, illite, chlorite... Mineral dissolution makes grains less resistant to

mechanical compaction and, to the opposite, cements consolidate the rock. Deposition of cements is chemical compaction. Besides, strong mechanical compaction does occur during burial. Quartz grains are first rearranged in a tighter way, then some dissolution occurs at their contacts with other quartz grains. Packing becomes tighter and tighter with depth (Fig. 3).

As the burial rate is not constant throughout time and throughout space, the time spent by grains at a given range of depth may vary a lot from a place to another. There are slow burials and fast burials. Uplifts do not significantly change the already acquired grain pattern, but they create retrogressive chemical conditions in the rock if all other conditions

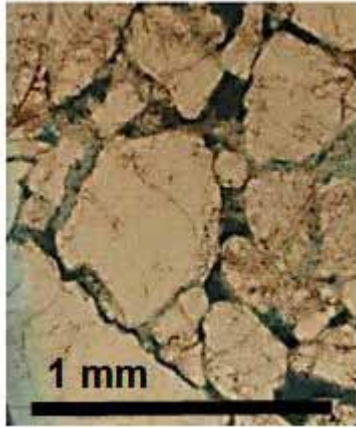


Photo 8 Close-up view on the decompact sandstone of Photo 6. Formerly sutured or adjacent grains are not in close contact anymore. The rock fabric is looser than before. Porosity and permeability are greatly enhanced in this way (see text).

are favourable. Unstable minerals will be affected. Only near surface, decompaction significantly loosens the rock grains.

We have seen with the Melawi Basin example that the interpretation of the depth of occurrence of grain-suturing is not a straight forward process. Integration of other regional data is necessary as much as possible.

Contacts' loosening facilitates grain removal by infiltration water and is therefore prone to voids formation and subsequent caves of various sizes.

4. Examples of cave settings in differently compacted sandstones

4.1. Low compaction: Fontainebleau sandstones, France

Fontainebleau sandstones were deposited as sands during the Oligocene (Lower and Middle Stampian) in the central part of the Paris Basin, France. They have never been buried more than several tens of metres. They are very clean and have been subject to diagenesis, mainly deposition of secondary silica cement and less frequently of calcite cement. Lithification did occur especially in the top part of the formation, where a massive sandstone interval developed. It also occurred at various elevations underneath, where elongated sandstone bodies are oriented towards late valleys. They are related to successive levels of the phreatic table. Lithification also occurs near valley edges.

Besides caves which developed in the upper sandstone, some others are encountered in loose sand located near lithified parts, with often some imbrications between the two facies. Concretions made of sand grains inserted in much bigger cemented volumes of rock may be encountered in these caves and even speleothems in various quantities (Combredet, 2004). These caves are commonly a few tens of metres long.

4.2. Sutured quartz grains: Khorat Plateau, Thailand

So far known caves on Khorat Plateau correspond with the smaller petrographic domain on Fig. 4 and are located mostly in braided stream deposits. These have a more mature grain

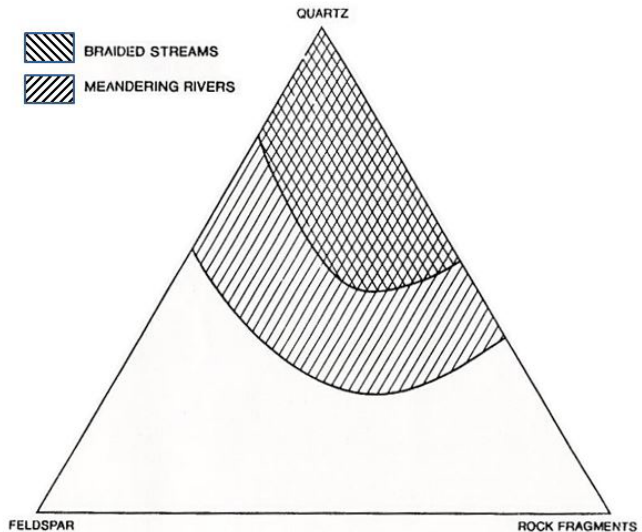


Figure 4. Petrographic present-day grain compositions of sandstones of the Mesozoic Khorat Group of Thailand, Mouret *et al*, 1993. Braided stream deposits have a more restricted, mainly quartzic, grain composition with rock fragments and a moderate proportion of feldspars. Meandering rivers deposits cover a larger domain, also with up to 100 % quartz, though less frequently.

composition, are coarser-grained and better sorted. They probably have a different source area and may rework older less mature sandstones from meandering rivers (Mouret *et al*, 1993). Feldspars are mainly plagioclases; at depth, they are almost unleached; at present day surface, they are leached and bear correlative higher kaolinite content. Primary, detrital, clay minerals are usually around 5% and do not exceed 15%. Early calcite cements are abundant. Secondary silica cements are rarer and usually amount less than 15%. Hematite cement is present. Grain suturing is well developed in favourable facies.

Sandstone caves on the Khorat Plateau are numerous, but usually not very long. Tham Patiharn (located 55 km to the North of Khong Chiam, near the Mekong River) is a two-level cave (776 m of total length), with a lower, temporarily active stream and an upper one, usually not active, as it is occupied by Buddhist temples. The stream originates from a surface creek which is sinking at the cave entrance and flows directly down to the lower passage. This lower passage shows potholes, boulders and clay on the floor, and cupolas at the roof. The upper passage displays a more classical clastic morphology, and sandstone boulders and clay on the floor. Ferruginous deposits are present in both passages and silica is encountered, especially in the lower one: both locally bind boulders. Some small speleothems of silica and (?) limonite are present. The host rock is a sandstone which was deposited by the braided streams of the Phu Phan Formation.

Tham Cham Pha Tong (located 20 km to the West of Waritchaphum, Sakon Nakhon Province) is a 120 m long branching cave which follows sedimentary and tectonic discontinuities. Grain disaggregation and export is the main cause to the cave formation. It is facilitated by decompaction (in a cliff high in the landscape) and some cement leaching.



Photos 9, 10 and 11 Sandstone caves of the Khorat Plateau.

Top: Tham Cham Pha Tong; Dev. 120 m; Depth 8 m; average width: 6 m; av. height 4 m; maxi height: 7 m. Branching cave in Phra Wihan Fm (braided stream deposit). Passages follow sedimentary discontinuities and fractures. Strong dripping during rainy episodes.

Bottom: Tham Patiharn. Total length of 776 m, 746 m projected on plan. Sinuosity ratio: 1.12; Depth: -26.5 m. Upper passage is 471 m long. End on tight boulder choke. Av. width 12 m; maxi width 20 m. Av. height 2 to 5 m, maxi 8 m. Entrance is 35 x 14 m wide. Lower passage width: 8 m av., 19 m maxi. Height 1.5 and 4 m. 149 m long to a choke.

4.3. Sutured grains: caves in sandstones of Roraima Group, Venezuela

Giant cave systems are reported in the high plateaux which lie in the South of Venezuela and North of Brazil and which are known as tepuis. These cave systems have been the matter of many published papers, among which we extract one from the previous International Congress of Speleology, by Aubret *et al* (2013) and one from "Sedimentology" Magazine by Sauro *et al* (2014). The quartzite nature of the rock is mentioned by these authors. The rock microphotograph in Sauro *et al* (2014) shows concavo-convex to sutured grain contacts.

The quartzite name and the types of grain contacts observed suggest that the rock suffered heavy compaction down to a depth of around 4000 m at least. This indicates that a huge thickness of sediments has been eroded, which was forming in the past a thick coverage above the Roraima Group. This is consistent with the fact that the area is located on the Guyana Shield, a core area which delivered sediments to peripheral

depocenters. Heavy speleogenesis is consistent with the large decompaction of the tepuis (isolated plateaus).

5. Brief conclusion

The principles and the examples presented in this paper show that there is a wide field for research on the influence of geohistory and rock compaction regarding the formation of caves. It is important to highlight that compaction is not a vertically linear process. It shows variations which depend upon rock composition and characteristics. Trends must be considered, rather than punctual data. In deep wells, wireline logging (e.g. sonic and density logs) helps in sorting this out. In the field, in caves, sufficient rock sampling must be implemented for petrographic analysis and other analyses. Only upon these conditions, can the interpretations be improved.

References

- Aubret R, Lanczos T, Schlogl J, Vlcek L, Smida B, 2013. Arenitic caves in Venezuelan tepuis: what do they say about tepuis themselves? *Proc. 16th Inter. Congr. Speleo*, Brno, Vol. 3, pp 221-226.
- Combredet J-P, 2004. Quelques photos présentées [sur les grottes des grès de Fontainebleau]. *Proc. 14ème Rencontre d'Octobre*, Florac, Spéléo-club de Paris, p. 57.
- Mouret C, 1987. Geological study of the Melawi Basin, Kalimantan Barat, Borneo, Indonesia. Unpubl. Study, 1984-1987. 4 Vol.
- Mouret C, 1994a. Paleokarsts at the Permian-Triassic boundary in Southeast Asia. An introduction. Beijing, Academia Sinica, *Proceed. XIth Internat. Congr. Speleology*, Beijing Août 1993, Supplement, pp 9-31.
- Mouret C, 1994b. Geological evolution of Northeastern Thailand since the Carboniferous. Relations with Indochina and Carboniferous to Cenozoic evolution model. Bangkok, 15-20 Nov. 1994, *Proc. Intern. Symp. Congr. IGCP 306, Stratigr. Correl. of SE Asia*, pp 132-158.
- Mouret C, -2004- La spéléogenèse des grès : quelques principes fondamentaux. *Actes 14ème Rencontre d'Octobre*, Florac, Spéléo-club de Paris, pp 55-56.
- Mouret C, Heggemann H, Gouadain J, Krisadasima S, 1993. Geological history of the siliciclastic Mesozoic strata of the Khorat Group in the Phu Phan Range area, Northeastern Thailand. *Chiang Mai, Internat. Symp. on Biostratigraphy of Mainland Southeast Asia: Facies & Palaeontology*, 31 Jan. - 5 Feb. 1993, Proc., Vol. 1, pp 23-49.
- Mouret C, Mouret L, 1994. Thaïlande. Prospection des karsts gréseux du nord-est de la Thaïlande (Esarn). *Spelunca Bull.*, n° 55, pp 6-9.
- Sauro F, Tisato N, De Waele J, Bernasconi S M, Bontognali T R, Galli E, 2014. Source and genesis of sulphate and phosphate-sulphate minerals in a quartz-sandstone cave environment. *Sedimentology*, **61**, pp 1433-1451.

Caves and other features in glaciers and icebergs, Graham Land, Antarctica

Claude Mouret

*Affiliation: Freelance geologist
claude.mouret.geospel@orange.fr
Km1 La Tamanie, 87 380 MAGNAC-BOURG, France*

Abstract

Graham Land is the northwesternmost tip of Antarctic Continent. It greatly represents polar conditions with a very thick snow and ice cover on both high mountains and coastal regions. Many radial glaciers reach the sea shore and lead to calving and formation of icebergs. Besides this, tremendous quantities of large flat-topped icebergs float on the sea over long journeys. A lot of them originate from the Weddell Sea, which is largely covered with a thick ice sheet.

All these environments display underground holes, which encompass mechanical crevasses, melting holes in the ice, sea surface processes (tide, waves), large cave-like voids in icebergs, and residual arches. Other features include marine notches, karren-like features, scallops and ice speleothems. Processes are not always comparable to what exists in karst and require original explanations.

The paper documents all types of voids which were observed by the author, as well as notches and other features. It proposes an explanation of the formation of large caves and arches in icebergs.

Graham Land is located in the western tip of Antarctic Continent (Fig. 1), to the West of Weddell Sea. Polar environment is confined within the Antarctic Convergence Zone (ACZ) and isolated from the rest of the world, in the sense that no current from the North can enter it. To the contrary, it does expel icebergs and sea currents towards the North. Icebergs are sometimes encountered as far away as is Namibia. Internal gyres in the Weddell and Ross Seas move fluids and floating objects such as icebergs, as does the ACZ around Antarctica. The Ronne Ice Shelf in the Weddell Sea and the Ross Sea Ice Shelf (Fig. 1, darker blue), the Larsen Ice Shelf (Fig. 2) are the largest floating freshwater ice shelves in Antarctica. They are found in deep gulfs, but other smaller gulfs around the continent bear smaller ice sheets.

In winter, extensive sea ice develops all around the continent up to almost the 50° latitude (Fig. 1), though it largely melts in summer. Freshwater ice partly melts as well and it liberates large tabular icebergs, which may be hundreds of metres long, sometimes kilometres long and occasionally hundreds of kilometres.

Antarctica is an overall mountainous continent, with an average elevation of 2300 m. However, the main, eastern, part is much higher than the western part. High elevation ranges which are located immediately to the East of the Weddell and Ross Seas make up the boundary with the Western part. Nevertheless, the latter part is mountainous as well and shows continuous ranges which culminate above 1000 m and even up to more than 2500 m. Graham Land proper and parallel

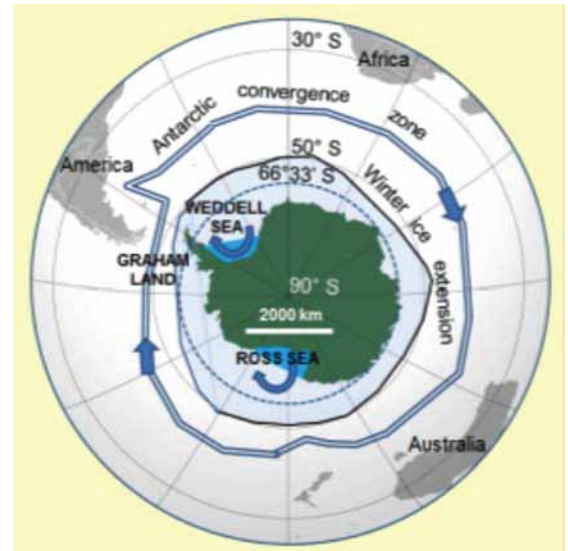


Figure 1. Antarctica and the location of Graham Land. Winter ice is shown in blue: it reaches near the 50° parallel.

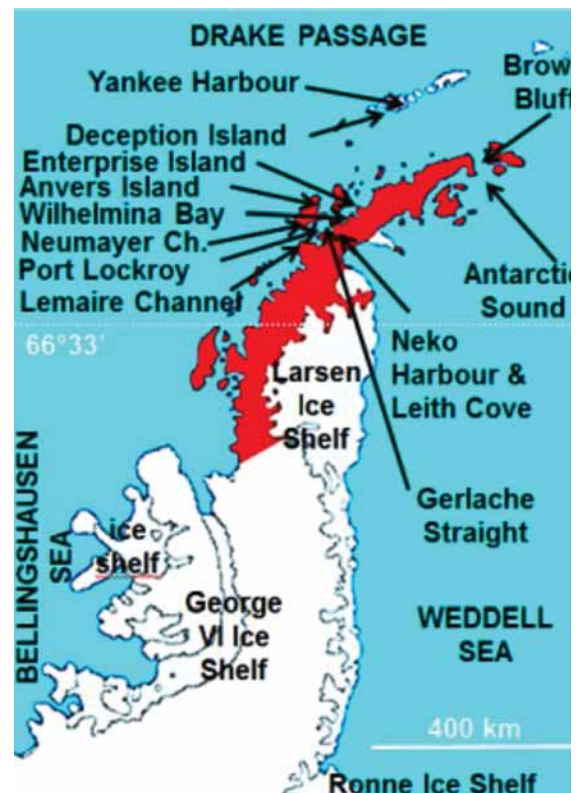


Figure 2. Graham Land, as the NW tip of Antarctica. To the North of it: the South Shetland Islands. Main visited places are indicated (extreme point reached: 64°58.21' S; 63°44.14' W). Antarctic Circle is at 66°33' S. Nevertheless, ground conditions are fully polar in the whole of Graham Land.

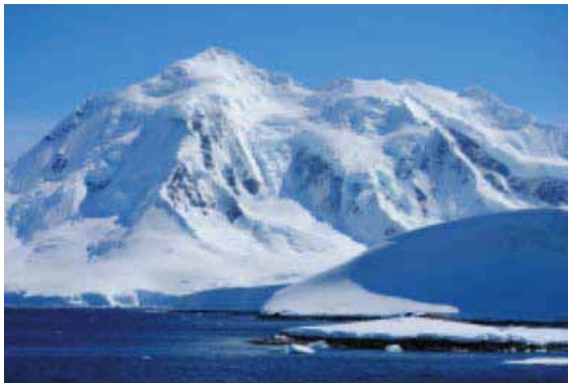


Photo 1: Mountains to the West of Port Lockroy, higher than 1000 m in elevation. Glaciers are here located in cirques at the bottom of steep slopes, but the top of the mountains is covered with a ca 40 m thick cap of ice and snow (to the right, on top of cliffs)



Photo 2: Wilhelmina Bay. In the front: flat-topped sea ice, a few metres thick (seawater is to the right). At the back, a second, thicker, blanket of sea ice (beyond the darker line). At the very back: a very high wall of freshwater ice originating from surrounding mountains

islands geologically represent a continuation of the Andes Mountains and still show some active volcanism (Deception Island).

During the author's trip (1st -10th of December 2016), temperature did not decrease below -6°C at sea level and was currently around 6 to 8°C in the middle of the day. Air humidity was around 45%. Indeed, precipitation in Antarctica are low, around 300 mm per year (as snow). However, owing to the size of the area (1.3 times Europe size), many glaciers move from inland towards the sea, where, by calving, they give birth to large icebergs. Iceberg B15 was the size of Jamaica (11000 km²). Glacier motion velocity may reach 1 m per day.

Ice on the sea is of two main types: freshwater ice is related to continuous feeding from inland and it covers large sea areas (Ronne, Larsen and Ross Ice shelves...). Sea ice forms during winter and the sea can start freezing within a quarter of an hour after a temperature drop of strong wind blow. Freshwater ice may be hundreds of metres thick; sea ice is commonly a few metres thick only.

We now present what voids were observed in the different ice environments, from tops of mountains down to the sea.

1. Voids in ice coverage of protruding relief

Protruding relief separates successive, adjacent, radial valleys which are sloping towards the seashore. Those reliefs are capped by very thick ice which originates from successive snowfalls. Gradually with time, the coverage moves down-



Photo 3: (t) Neko Harbour in Antvorde Bay. In the centre, a protruding hill is capped by thick ice (ca 50 m) pierced with many voids. The ice collapsed on the steeper, front side of the hill. To the left, a valley glacier is cracked by gravity-related extension following ice breaking on a rocky bump of the valley floor. In the front, the glacier front, where calving occurs. Note rotated ice blocks.

Photo 4: (m) close up view. Tensional cracks to the left and to the right, and larger voids related to ice blocks rotation. Some cracks are "en échelon" and some others are sigmoidal, which indicates shear stress and rotation.

Photo 5: (b) Neko Harbour, other location. Left to right: open cracks at the top of the ice cap, crack and void (poorly visible) associated with the right side of an extensional graben, large void partly filled with snow in apparently undeformed ice, collapse cracks.

ward. Some parts move towards valleys. Some other parts reach steep slopes where they collapse and disclose the bare rock.

Observed voids are mainly related to internal deformation in the ice, due to tensional shear, rotated blocks, extrados cracks, ice cap deformation by sliding above rocky basement and internal extension. Some larger voids (Photo 5) do not show obvious associated deformational feature (which however cannot be fully excluded) and may be partly filled with snow. Some might find their origin in water flows related to summer ice melting.



Photo 6: Neko Harbour. Ice rubble and voids associated with gravity-related sliding. Ice thickness is around 50 m.



Photo 7: Neko Harbour. Ice sliding here induces the formation of a sole of rubble and voids, including larger ones

2. Voids in glacier tongues

Voids in mountain glacier tongues have been described in literature for years. The main additional feature in Graham Land glaciers is that they are coalescent and behave in places more as glacier (thick) blankets than as separate glaciers (Photo 9). Deformation in one glacier tongue may occur in competition with deformation in adjacent ones.

Longitudinal cracks (crevasses) are parallel to the glacier edge, due to differential flow velocity which is related to friction of ice against the bounding rock. Transverse cracks are mainly due to extension at the extrados of ice sheet folded above underlying rocky bumps; owing to the faster velocity along the glacier axis, they get convex towards the downstream glacier end (Photo 11). More complex patterns exist, which are the result of coexisting processes, such as longitudinal friction, extrados effect, gravity sliding, formation of a sole at the base of the glacier (detachment surface or interval), above which tilted rocks may develop, leading to additional voids in between the blocks.

Ice melting does occur significantly during the austral summer, as proved by the annual retreat of frozen seawater. Melting at glacier surface occurs in a variety of forms. We could observe melting at Brow Bluff, near a glacier edge. Obviously, where ice is thin, warming of underlying basalt pebbles by sunrays gives birth to narrow chimneys above them, where air replaces water. Similar morphologies are well known in limestone caves, where they originate from different processes, i.e. water dripping from passage ceiling. Narrow chimneys on the glacier can become coalescent and leave place to scattered, remaining narrow pillars, which eventually melt and disappear.

Human penetration on the glaciers surface is extremely risky, due to cracks and crevasses, many of them being covered with younger snow cap. However, bédrières and moulins have been mentioned in Antarctica, though perhaps not in Graham Land (where nevertheless they are likely to exist).



Photo 8: (l) Anvers Island (NW of Neumayer Channel). Two distinct spectacular glacier tongues are separated by an interfluve, in an area where relief is steep close to the sea.

Photo 9: (r) Near Photo 8. Coalescent glacier tongues, to the left of the view. Ice shows near the sea a succession of steps, which are due to normal faults. Elsewhere, some deformation occurs on rocky bumps of the substratum.



Photos 10 and 10b: (l) Neko harbour. Cracks in a glacier tongue. At the rear (right): longitudinal cracks. In the front: extensional cracks and longitudinal cracks within the ice blocks.

Photo 11: (r) Brown Bluff glacier. Transverse cracks are convex towards the bottom end of the ice tongue (here 15 m thick). A few persons stand at the bottom right of the view.



Photo 12: Brown Bluff glacier. Length of the view: 1 m. Melting at the edge of the tongue occurs at first above dark-coloured basalt pebbles and it gives way to narrow corridors in which flowing water is collected and evacuated. Such water streamlets join together further downstream and flow down to the sea.

3. Voids at glacier front

In many places, as we could see in December 2016, the glacier front follows the contact of the seawater surface and the rock formation below the glacier. In other places, the front is either onshore (rare in this season) or in the sea, where calving gives birth to icebergs of moderate size, because ice thickness is around 50 m “only”.

Due to lack of space, we will simply write here that voids observed in the ice cap at the sea shore show wide and rich variety but are broadly similar to those already presented above.



Photo 13: Esperance Bay. The glacier front is located at the contact of the rocky substratum and the sea level. A well visible listric crack opens both on the side and on the top of glacier (25 m high).



Photo 14: Esperance Bay. Marine caves at the bottom of a 20 m high ice cliff. To the left, behind the canoe, ice removal by sea is associated with the mechanical formation of scales, which form the vault. To the right, a more complex cracks system ensures the (very temporarily) cave stability. Such places are extremely dangerous and may suddenly collapse at any time.

4. Freshwater icebergs

Besides icebergs of limited size which originate from local glaciers, gigantic, tabular, icebergs much wider originate from the hundreds of metres thick ice shelves in the Weddell and Ross Seas and elsewhere. Transported by sea currents (gyres and others), they may travel during years and also get stranded by tide oscillations. They present notches, which are due to freshwater ice melting along the surface of salty sea-water. There is often more than one notch and these notches may display different slopes with regard to sea level. This indicates successive steps of iceberg flotation, due to successive episodes of floating and possible stranding. In addition, initial notches become higher above sea level due to iceberg erosion at the top. Full upside down movements of icebergs also exist.

The notch development is often, though not always, associated with crack enlargement at sea level. Some of the cracks may enlarge as cave-like voids which partly penetrate the bulk of the iceberg. Roof collapse commonly occurs. If not, the cave gets longer, and higher as the iceberg is progressively pushed up, due to the erosion of its emerged part.

Large caves/ arches in large tabular icebergs are commonly bounded by two pillars only. Following J. Bruthans et al. theory on arches (2014, <http://dx.doi.org/10.1038/ngeo2209>, Nature Geoscience), we consider likely that a reorganisation of ice crystals forms in the areas under pressure from the top of the arch. In this way, pillars are stronger and so better resist melting and erosion. This is why big arches are encountered in narrow, high icebergs.



Photos 15a to c, left to right: progressive initiation of voids at sea level, along minor cracks at notch level.

Below, d and e: formation of void in the notch (d) and through void at notch level, with roof collapse (e).

a: Leith Cove; b: Chilean base near Enterprise Island; c: Leith Cove; d: Antarctic Sound; e: Enterprise Island.

Stalactites are commonly encountered under icebergs overhangs.



Photos 16a and b: Antarctic Sound. Gigantic arch, around 30 m high, between two side pillars, which are wall remnants. Around 40% of the height corresponds to notches and the rest to vault collapse.



Photo 17: Gerlache Straight. Large cave in an undisturbed tabular iceberg, which might originate from Ross Sea. Cave height is around 6 to 8 m.



Photo 18: Lemaire Channel area. Upside down iceberg showing karren-like features interpreted as air degassing from the ice. Scallops may be current-related.

During aging, ice progressively degasses, which might be the reason for karren-like features exist. Degassing ice becomes more compact and progressively becomes blue-coloured. Older icebergs show arches, pools of blue to emerald colour.

(Abstract) **Scientific Researches And Explorations In Quartzite And
Quartz-Sandstone Caves**

Francesco Sauro¹, Robert A.L. Wray²

Affiliation: ¹ *Associazione di Esplorazioni Geografiche la Venta, Via Priamo Tron 35/E, 31030, Treviso, cescosauro@gmail.com*
² *School of Earth and Environmental Sciences, University of Wollongong,*

Abstract

Quartz is considered one of the less soluble minerals of the Earth's crust, and thus hardly affected by chemical weathering. Despite this, since more than forty years, it's clear that the formation of caves and peculiar surface weathering morphologies in quartz-rich lithologies is common and very similar to the well-known karstic ones in carbonate rocks.

The first attempt to explain the processes responsible for these formations was given in the late seventies with the Arenisation theory by J.J. Martini. Later an ever increasing number of evidences of these weathering mechanisms were reported from several areas of the world. Arenization implies a slow but pervasive dissolution of the quartz grain/mineral boundaries increasing the general porosity until the rock becomes incohesive and can be easily eroded by running waters. The loose sands produced by the weathering processes are then evacuated to the surface through processes of piping due to the infiltration of waters from the fracture network or the bedding planes.

The range, volume, and availability of information to geomorphologists on this topic are now much greater than twenty years ago. Thus, our understanding of the distribution, morphology, chemistry and evolution of karstified quartz-sandstones and quartzites has improved substantially in the past few decades. The exploration of some giant maze cave systems in the quartz-sandstones in the tepuis of the Guyana Shield in Venezuela, as well as peculiar caves and landforms in Australia, Brazil and Europe has led to an urging need of new studies and theories on these processes.

Quartz-sandstone and quartzite landforms have begun to be recognised as more than just a curiosity, and accepted as being important in their own right. This has even developed to the extent of several geomorphologists reassessing the definition of the term 'karst', and its application to these peculiar lithologies.

Since 2000, more than fifty research papers were published on this topic, supporting new ideas or presenting new quantitative data about the arenization process. Substantial progresses were obtained in the fields of silica chemistry, modelling, petrography, geomicrobiology and secondary caves minerals in these environments. In addition, the study of hypogenic speleogenesis in quartzites has made an important breakthrough which will have several implications not only in the field of karstology.

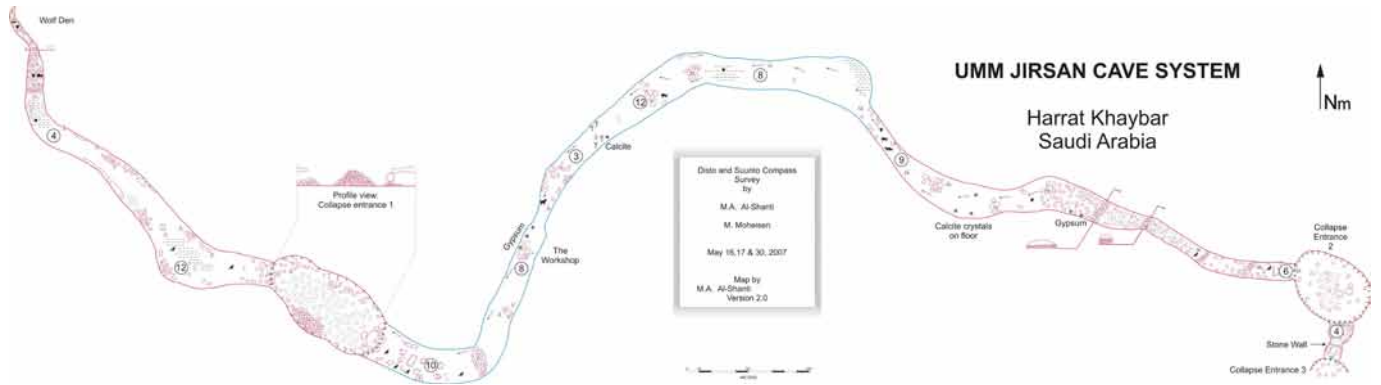
Lava and Volcanic Caves

(Abstract) **Um Jirsan Lava Tube Cave**

Mahmoud Ahmed Al Shanti

Affiliation: Director Caves Explorations Section, Kingdom of Saudi Arabia Geological Survey

Abstract



Map 1. *Um Jirsan Cave Map*



Figure 1. *Cave Entrance; plane for scale*



Figure 2. *Eastern Passage*



Figure 3. *Surface view*

Umm Jirsan lava tube tunnel is located in the center of Harrat Khyber, part of an area comprising 20,560km² of lava flows. The lavas and volcanoes in Harrat Khyber are mildly alkaline with low Na and K content and include alkali olivine basalt. The age of the Khyber lavas ranges from ~5 million years old to post-Neolithic to historic. Umm Jirsan lava tube cave, is may be a 3 million years old (Roobol, camp).

The total length of the cave is 1.4 km with a vertical depth of 6m. The main entrance of the cave is an east-west trending collapse, 89m long, north-south trending 45m wide, with a depth of 14m. (Fig.1). The main passages of the system extend east-west (Fig.3).

Loose sediment covers the floor near both entrances of the cave, with dome structures showing mud cracks 15-30 cm in diameter. (Fig.4).

Bones at the end of the western passage, were presumably carried in by several periods of water flooding. (Map.1).

Eastern passage:

The eastern passage or tunnel is 948.6 m long, with a maximum height of 12 m, and a maximum width of 45 m (Fig.2). There are three collapse entrances along this passage; the first entrance which is the largest is blocked by a giant desert fig tree which measures about 10 m high and 35 m wide (Fig 5).

Loose sediment covers the floor near the entrance of the cave indicating the water flow into the cave and inside the passage



Figure 4. Mud cracks

the floor takes the form of domed structures showing mud cracks 15-30 cm in diameter (Fig 6). (XRD analysis of samples taken from the domed structure mud cracks show that they are composed mainly of the minerals, quartz, albite (feldspar) and kaolinite, with less abundant montronite, biotite, microcline and augite and traces of sparite, montmorillonite and hematite. This indicates their derivation from variable rock sources near the entrance, probably felsic in nature.

At about 914m along this eastern passage, a second collapse occurs trending and curving south east. It is 34 m long with a maximum of 20 m wide, and 4 m high. A second 14m long passage, showing remains of a stone wall built by humans, is observed here. A third collapse 33m long and 21m wide, blocks the end of the eastern passage.

Western passage:

The Western passage or tunnel is 341 m long, with a maximum width of 45 m and maximum height of 12 m and curves in a north-west direction. It has one entrance (Fig. 7). A pile of loose sand and dirt of dried leaves, birds and bat guano is on the floor of the entrance, After passing a pile, 34 m inside, it slopes down to a sandy floor, with a muddy water channel running on the right side of the passage. Lava levees are common in this section, on both sides and on different parts of the passage. Bones and remains of a fox den were observed at about 200m inside. Huge breakdown blocks of basalt occur at 315m, blocking the passage. Crawling between the breakdown blocks, there is a pile of bones which extends for 22m to the end of the passage. These bones were presumably carried in by different flood-water events, particularly concentrated at the extreme end of the passage. There is a strong bat guano smell near the bones.

A human skull and two human skull-cap fragments (Fig. 8), large animal bone and one curved wooden stick were collected.

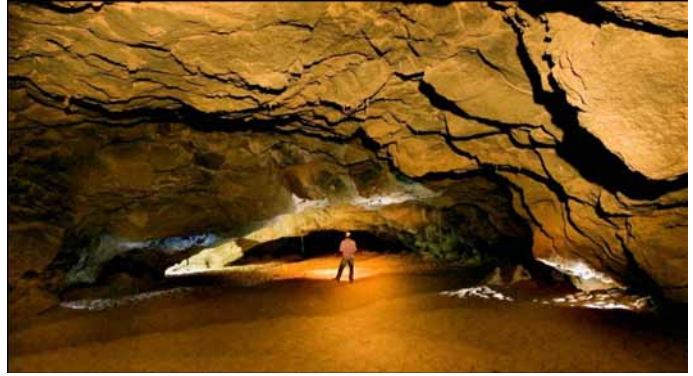


Figure 5. Eastern Passage



Figure 6. Domed mud cracks



Figure 7. Western Passage

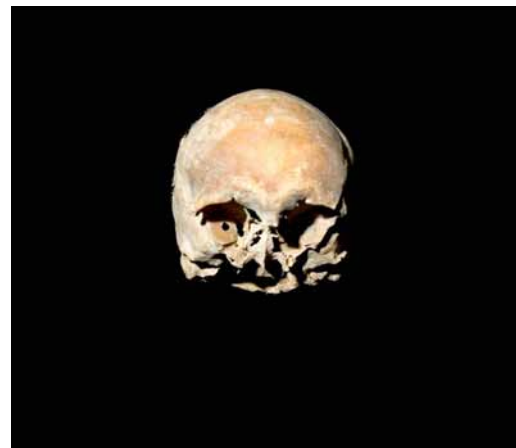


Figure 8. Human skull

The Complexity Of Pyroduct (“Lava Tubes”) Genesis: Bird Park Cave, Hawaii Volcanoes National Park

Stephan Kempe¹, Christhild Ketz-Kempe¹, Harry Shick²

Affiliation: ¹Institute of Applied Geosciences, Technische Universität Darmstadt, Schnittspahnstr. 9, D-64287 Darmstadt, Germany, email: kempe@geo.tu-darmstadt.de
²General Delivery Kea’au 96749, Hawaii, USA, email: hashick@hotmail.com

Abstract

Erupted basaltic lava flows downhill either in channels or conduits. The latter, termed “pyroducts” or colloquially “lava tubes”, can form by different processes. Pyroducts function as self-insulating conduits allowing lava to flow for long distances across low-slope terrain, thereby building shield volcanoes. Studies of roof structure serve to understand the initial roofing of the flow and studies of internal features can unravel processes that reshape the original conduit during prolonged activity. Therefore, even a “mono-trunked”, “simple tube” may be of complex development.

In spring 2016 we surveyed and studied Bird Park Cave, a 200-m-long, unbranched pyroduct section underlying the Kipuka Puau (kipuka = land surrounded by later lava flows) in Hawaii Volcanoes National Park (HVNP). The kipuka is an outcrop of the Pāhala ash. The underlying cave in Mauna Loa lava is therefore stratigraphically one of the oldest in the HVNP. Geologically, the cave is interesting because of its overall good preservation, its many features and the fact, that it cut through an underlying ash layer. Access is through a cold puka (i.e. sinkhole), filled with ash and the cave ends at another cold puka, also filled with ash. A third puka opened during activity (hot puka) and, by allowing air flow, not only caused the freezing out of a secondary ceiling, but also caused other interesting features such as ripple-marks on the walls. The primary roof of the cave is composed of pāhoehoe lava sheets either emplaced by inflation or by surface flows. In the upper part the underlying ash-layer, hematized to a bright red by the heat of the transgressing lava, is situated near the ceiling, suggesting immediate downcutting after the first emplacement of the conduit. In the lower section tree casts mark the initial lava sheet while the underlying ash layer is found lower down in the passage, suggesting less down-ward erosion but more upward and side-ward enlargement by breakdown. These differences may be due to a change in slope that is overall 5°. The upper section of the cave shows a series of lining (and glazing) events, possibly associated with an oscillating process of down-cutting and ceiling accretion in the sections of lower slope. Two lavafalls are present, providing a mechanism of rapid down-cutting.

Keywords: Lava caves, pyroducts (lava tubes), speleogenesis, Hawai’i, volcanology, erosion

1. Introduction

Caves in volcanic rocks (for review see Kempe 2012, 2013) are formed by many different processes either during the deposition of the rock itself (primary caves) or at some time after rock deposition (secondary caves). Primary caves include those associated with the eruption itself such as vent conduits or hollow dikes, with the post-eruptive flow of lava, such as pyroducts (lava tubes; for terminology see Lockwood and Hazlett 2010), pressure ridge caves, empty flow lobes, of lava sheets splitting along the maximum of vesicle distribution, gas blisters, casts of animals and trees, and a score of other ill-defined cavities. The class with the longest caves are pyroducts that form by the subterranean, gravitational, lateral transport of lava (Lockwood and Hazlett 2010). With a few exceptions, pyroducts form within the petrographic basalt window. They are responsible for the formation of shield volcanoes.

The genesis of a pyroduct, i.e. the formation of its primary roof, and its further evolution during and also after activity involves complicated processes that are poorly understood and documented. Fig. 1 summarizes four different modes that appear operative in forming pyroduct roofs. Those conduits that operate for longer periods are eroding into underlying strata. That this process is truly occurring was first illustrated beyond doubt for Earthquake Cave (Kempe and Ketz-Kempe 1993a,b). This cave (Hilina Pali area, HVNP) eroded through

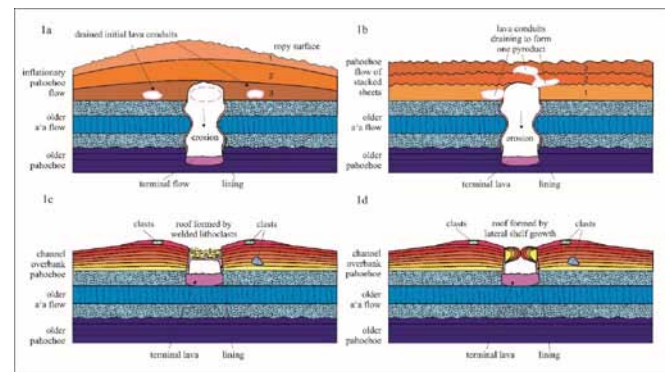


Figure 1. Within the pyroduct type at least four different formation modes exist: Caves formed by inflation of the lava flow front and later downward erosion (1a), caves formed by coalescence of small ducts and consecutive downward erosion (1b), caves formed by the crusting-over of channels by floating lithoclasts, welded together (1c), and by channels crusted-over by lateral shelf accretion and consecutive closure (1d) (Kempe 2012).

the Pāhala ash, and served as an initial incentive to look at other caves and the evidence for downcutting (Greeley *et al.* 1998). Down-cutting was also observed in active flows by measuring lava levels through skylights in conduits of the current Kilauea eruption (Kauahikaua *et al.* 1998), where it amounted to 10 cm/day. These processes ensure that a gas-

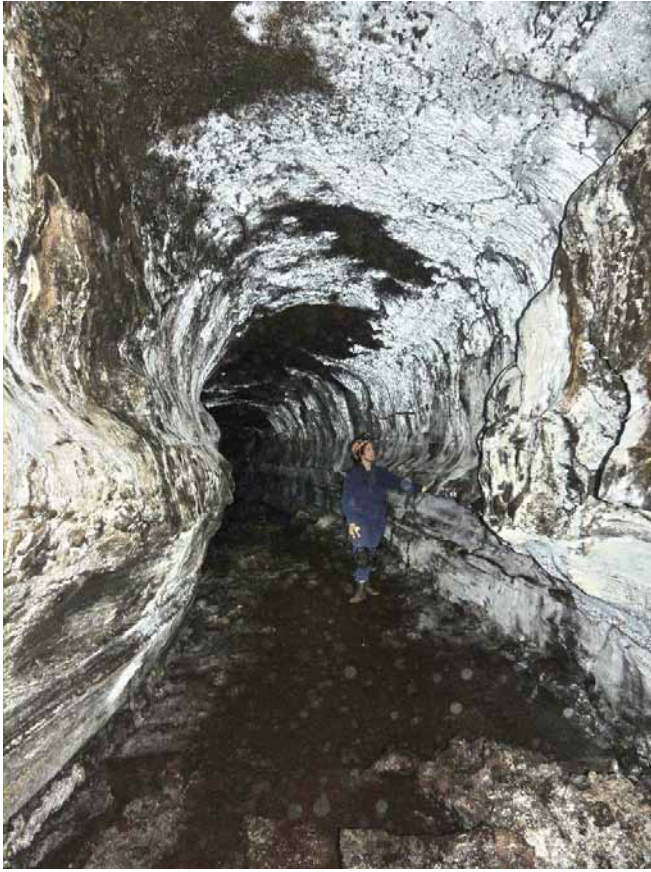


Figure 2. Downhill view into Bird Park Cave. Note washed-in ash on floor and bright biomats on walls.



Figure 3. Uphill view onto the lower end of the Bird Park Cave "Bear Walk" crawl.

filled space, and therefore a cavity, can already form during activity, regardless whether the lava empties the conduit or not.

2. Geographical and geological situation of Bird Park Cave

Bird Park Cave (BPC), or more precisely Upper BPC, is situated in Kipuka Puauulu in the Hawaii Volcano National Park north of Kilauea Caldera. Its entrance is at Marker 6 of the Bird Park Loop at 1249 m a.s.l. It is one section of a pyroduct,



Figure 4. Uphill view onto the second lava fall.

including Central BPC (#2) and Lower BPC (#3 with skylight #4) (Halliday and Martin 1990). Geologically, the Kipuka Puauulu is forming an isolated outcrop of volcanic ash on the Mauna Loa lavas, broadly classified as Pāhala Ash. On the Kilauea summit geological map (Neal and Lockwood, 2003) the Kipuka is overprinted by signatures of both the Uwēkahuna and the Pāhala Ashes. Because BPC is below these ash layers, it is situated in relatively old Mauna Loa lavas, i.e. in a similar geological situation as Whitney Cave (Kempe *et al.* 2010). It may be one of the oldest caves in HNP and one of the oldest in Mauna Loa lavas, possibly older than 10 000 years. Bird Park Cave is also a biospeleological landmark because here the first Hawai'ian true troglobionts were discovered by F. Howarth (pers. com. F. Stone).

3. Short description of the cave

The cave entrance is a small puka surrounded by ash. The roof of the cave is not very thick and of inflationary origin. A steep ash cone leads into a spacious, walking-size passage with well-preserved walls and ceiling (Fig. 2). White, reflective biomats make the cave bright. The cave curves slightly E for about 50 m where the ceiling lowers before the first lava fall, 1.5 m high, is encountered. A lava cataract follows and fallen lining plates cover the floor for some time. The cave leads E for another 50 m when the ceiling lowers to crawling height. The crawl is rather flat on relatively smooth lava and opens up abruptly to a walking-size (Fig. 3) passage wider than high. After a turn to the SE and a further 25 m a second lava fall is reached, again over 1 m high (Fig. 4). Beyond, the passage turns E again and breakdown covers the floor. Above, an initially very thin secondary ceiling begins, separating the passage into two levels (Fig. 5). Shortly beyond this feature, an up to 7 m wide hall - filled with blocks of the collapsed secondary ceiling and the primary ceiling - is entered. The secondary ceiling is once more stable carrying the foot of an ash cone. The secondary ceiling ends after 10 m and sediment has been washed down through a small passage from above the secondary ceiling.

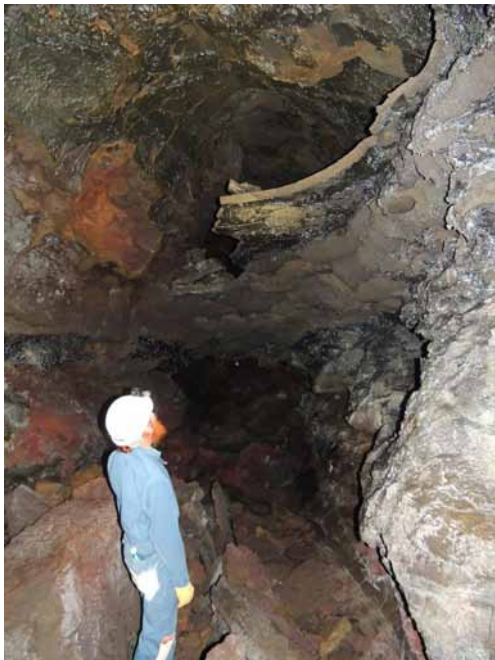


Figure 5. Downhill view of begin of secondary ceiling.



Figure 6. The ash cone at the end of the cave. Note irregular glazing and ceiling with post-activity breakdown trace.

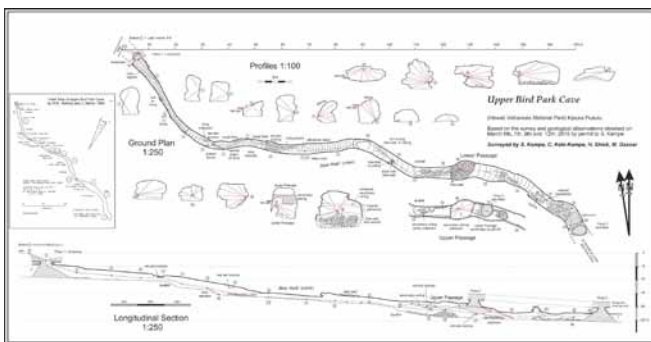


Figure 7. Map, longitudinal section, and cross-sections of Upper Bird Park Cave

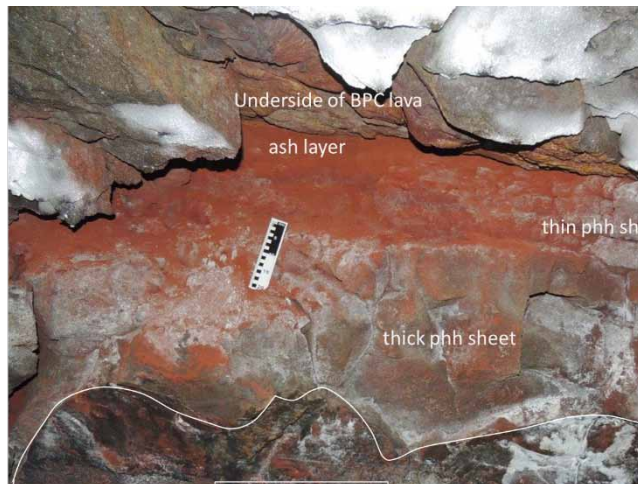


Figure 8. Outcrop of hematized ash at St. #6.

Bird Park Cave Outcrop Station #6 Stratigraphy

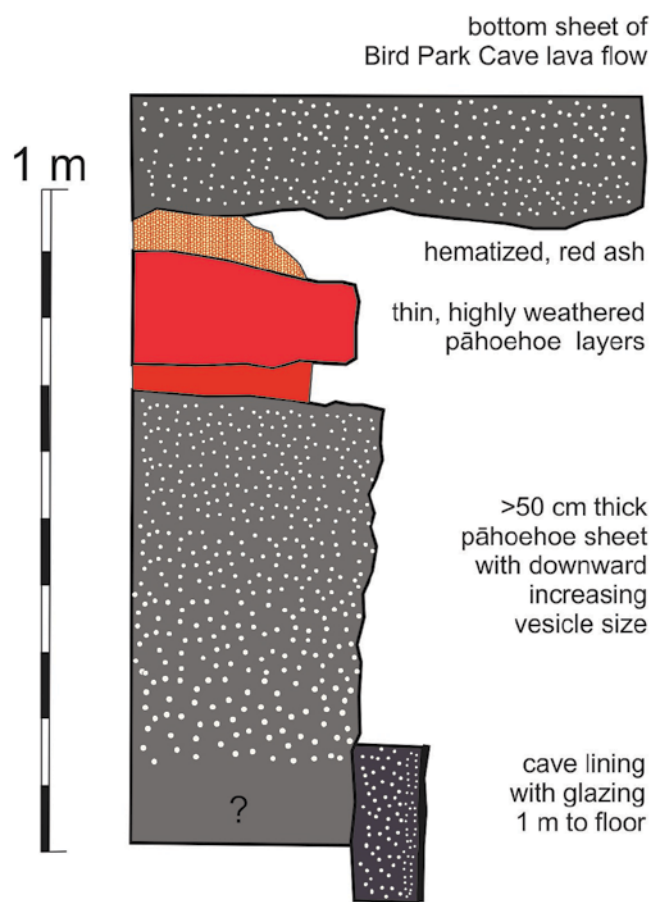


Figure 9. Stratigraphy St. #6



Figure 10. interior of tree cast in ceiling near St. #12.



Figure 11. Asymmetrical, vertical grooves that are most likely ripple marks

The passage turns SE, again altering its character, the walls are rough and not entirely glazed but covered with runners. A breakdown pile is found below a cupola providing a view onto the underside of an lithoclast layer stabilized by squeeze balls. 200 m from the entrance the final hall is reached, covered by blocks and ending in a 6 m-wide ash cone (Fig. 6).

4. Survey of the cave

The re-survey (first survey Halliday and Martin, 1990; inset Fig. 7) was carried out with a compass and a Leica Disto and inclination instrument. Local declination was 9.5° in February 2016. Total length amounts to 200 m, horizontal 196.64

m, vertical 18.16 m, slope 5.3°, sinuosity 1.1 (a value comparable to other pyroducts). There is a strong correlation between the length of the cave and its width, but not with its height. Plan and longitudinal section were drawn at a scale 1:250 and cross-sections at a scale of 1:100 (Fig. 7).

5. Geological observations and interpretation

The cave can be classified as medium-sized, unbraided and mono-trunked, i.e. it forms a single conduit, not interacting with any other in parallel or being overlain by others. The cave has three pukas (ceiling collapses) (Fig. 7). Puka 1 is the current entrance. The second puka is found above St.# 17. It also features an ash cone, but it rests on the secondary ceiling suggesting that this puka is a “hot puka”, i.e. a puka that opened during activity, allowing air to enter and thus “freezing out” the secondary ceiling above the flowing lava. Puka #3 at the cave’s end is a “cold puka”, i.e. it opened after the activity terminated (e.g., Kempe 2012), and therefore did not influence the structure of the pyroduct.

BPC is of major geological interest because it shows clear signs of downcutting, evident at four prominent outcrops (St. 6, 9, 15 and 17) of a bright red ash (Figs. 8, 9). When the BPC flow transgressed the underlying glassy ash, the ash’s Fe²⁺ was oxidized to Fe³⁺ (hematized) by the heat. The three ash outcrops show that the flowing lava has cut down up to 2 m into older ash and lava. The underside of the BPC lava flow shows bulbous surface with imprints of plant fibers. When the BPC lava transgressed the ash layer, it was wooded. This is evident by three tree casts in the transgressing lava immediately above the ash outcrops. The longest is seen in the ceiling of the cave at St. #12 and is at least 6 m long and 30 cm thick (Fig. 10).

The downcutting exposed older, cold layers that were eventually coated with often multiple linings. Because of the downcutting, the lava flowed in a canyon, i.e. there was ample gas space above its surface. The gas must have been extremely hot, because it seemingly was able to sculpture the glazing on the walls. Fig. 11 shows vertical, asymmetrical grooves and ridges with the less steep side pointing uphill, reminding of ripple marks. Apparently, the air flowing uphill was structured in regularly-spaced vortices with vertical axes.

Secondary speleothems are missing except for some opaline, inconspicuous forms.

6. Outlook

Even though the cave seems to be at first view just a “simple tube”, the close inspection shows very interesting details. The lava falls for example are important features, acting as erosive focal points, explaining how the observed downcutting was mechanically achieved (Kempe 1997; Allred and Allred 1997). In essence the pyroduct displays the morphology of a stepped canyon.

The cave is only one section of a longer pyroduct (Fig. 12). It will be interesting to explore and survey the Lower Bird Park Cave as well and compare its features with those discussed in the UBPC.

Overall, not all of the problems posed by the cave, its morphology and stratigraphy could be solved, making it an inter-



Figure 12. Situation of the HVNO Bird Park Loop, the Upper Bird Park Cave survey line and the general extent of the Lower Bird Park Cave (straight line extending 125°; according to map of Halliday and Martin 1990).

esting area, not only for further geological research but also for the development of interpretive, guided tours for visitors interested in learning more about pyroducts and the processes governing them.

Acknowledgements

The study was made possible by permit of the Hawaii Volcanoes National Park (Study HAVO-00553; permit HAVO-2016—SCI-0020; 26 February - 15 March 2016; “Geology of Pyroducts”) and was supported by staff members Jadelyn Moniz-Nakamura and Dr. Rhonda Loh. Prof. Dr. Diana Northup invited me to participate in her visit to the cave on 15 Febr. Prof. Dr. P. Boston, K. Ingham, Prof. Dr. D. Northup, W. Olenick, Dr. M. Spilde (15 Febr. 2016) as well as C. Ketz-Kempe, Dr. M. Gasser and H. Shick helped in discussions and with the survey or served as scale for pictures. I. Hirmüller drew the cave map in Corel Draw.

References:

Allred K, Allred C, 1997. Development and morphology of Kazumura Cave, Hawaii. *J. Cave Karst Stud.*, **59**(2), 67-80.

Greeley R, Fagents SA, Harris RS, Kadel SD, Williams DA, 1998. Erosion by flowing lava: Field evidence. *J. Geophys. Res.* **103** (B11), 27, 325-27, 345.

Halliday WR, Martin J, 1990. *Main Bird Park Cave; Bird Park Cave #3*. HSS reports, maps and 3 pp of descriptions.

Lockwood JP, Hazlett RW, 2010. *Volcanoes, a Global Perspective*. John Wiley, 624 pp.

Kauahikaua J, Cashman KV, Mattox TN, Heliker CC, Hon KA, Mangan MT, Thornber CR, 1998. Observations on basaltic lava streams in tubes from Kilauea-Volcano, Island of Hawai'i. *J. Geophys. Res.* **103** (B1110) 27,303–27,323.

Kempe S, 1997. Lava falls: a major factor for the enlargement of lava tubes of the Ai-la'au shield phase, Kilauea, Hawaii. *Proc. 12. Intern. Congr. Speleol.* 10-17, Aug. 1997, La Chaux-de-Fonds, Switzerland, **1**, 445-448.

Kempe S, 2012. Volcanic rock caves. In: W White, DC Culver (Eds.). *Encyclopaedia of Caves, 2nd ed.* Academic Press / Elsevier, Amsterdam, 865-873.

Kempe S, 2013. Morphology of speleothems in primary (lava-) and secondary caves. In: J Shroder (Editor in Chief), A Frumkin (Ed.), *Treatise on Geomorphology*. Academic Press, San Diego, CA, vol. 6, Karst Geomorphology, 267–285.

Kempe S, Ketz-Kempe C, 1993a. Lava tube systems of the Hilina Pali area, Ka'u District, Hawaii. *Proc. 6th Intern. Symp. Vulcanospeleology.*, Hilo, 1991, 15-25.

Kempe S, Ketz-Kempe C, 1993b. Underground observations during the Pu'u O'o earthquake, 4.06 p.m., Aug. 8, 1990. *Proc. 6th Intern. Symp. Vulcanospeleology.*, Hilo, 1991, 29-34.

Kempe S, Bauer I, Bosted P, Smith S, 2010. Whitney's Cave, an old Mauna Loa/Hawaiian pyroduct below Pahala ash: an example of upward-enlargement by hot breakdown. *Proc. 14th Intern. Symp. on Vulcanospeleology*, 12.-17., August, 2010, Undara Australia, 103-113.

Neal CA, Lockwood JP, 2003. *Geologic Map of the Summit Region of Kilauea Volcano, Hawaii*. USGS Geol. Investig. Ser. 2759.

Outstanding Universal Values of some lava tube caves in Jeju Island for potential World Heritage nomination

Woo, Kyung-Sik, Kim Lyoun, Han Hyung-chul, Ki, Jin-Seok

*Affiliation: Department of Geology, Kangwon National University, Chuncheon, Gangwondo, Korea
Cave Research Institute of Korea
World Heritage Office, Jeju Special Self-governing Province*

Abstract

The "Jeju Volcanic Island and Lava Tubes" was inscribed as a UNESCO World Natural Heritage site in 2007 and the property includes the three sites as a serial nomination (Mt. Hallasan, Seongsan Ilchulbong Tuff Cone and Geomunoreum Lava Tube System). In 2007 UNESCO (and IUCN) recommend future extension of the property to include other significant volcanic landforms including lava tube caves. Extension of the Jeju World Natural Heritage property has great significance to facilitate maximization of the integrity and diversity of Jeju geoh heritage sites. To select the potential candidates, 171 natural caves were evaluated based on previous reports. Among them, 6 caves with significant geoh heritage values were chosen based on; 1) representativeness, rarity, uniqueness, 2) cave speleothems and microtopographic features, and 3) integrity. Among them, the potential nominated caves are Socheongul Cave with carbonate speleothems and the recently discovered Upper Geomunoreum Lava Tube System (Utsanjeon, Buloreum and Daerim lava tube caves). The ages of carbonate sand dunes and carbonate speleothems above and in already WH-inscribed Dangcheomuldonggul and Yongchoendonggul caves are about 5,000 and 2,000 yr BP, however those of the Socheongul Lava Tube are estimated to be less than 1,000 yr BP. This indicates that carbonate speleothems in Socheongul Lava Tube denotes the initial growth stage, providing geological integrity of the growth history of carbonate speleothems. Also, the recent discovery of the Upper Geomunoreum Lava Tube System complete the geological history of the Outstanding Universal Values of the Geomunoreum Lava Tube System. However, Bilemotdonggul and Susangul lava tube caves needs more information on geological history of formation and better management plans for conservation.

Keywords:

1. Introduction

"Jeju Volcanic Island and Lava Tubes" has received a recommendation to "consider the potential for extension of the nominated property to include other significant lava tube systems and volcanic features on Jeju" when the island was inscribed in the list of World Heritages in 2007. Extension of the Jeju World Natural Heritage properties has great significance in that it can facilitate 1) areal enlargement of the World Heritage properties and balanced development of the whole area of Jeju Island and 2) maximization of the wholeness, integrity and diversity of Jeju World Natural Heritage. There is no known case of extension of World Heritages in Korea. Internationally, however, there are continual cases of minor and major modification of World Heritage properties and renomination. Thirty six World Heritages have been approved for minor modification or major extension of World Heritage properties between 1982 and 2016. In order to assess the level of recognition and knowledge about the extension of the World Heritage by the residents of Jeju Island and local people, public opinion was surveyed through public hearing and opinion survey. The opinion was generally affirmative, but there were serious concerns about the limitations of private property rights.

2. Procedure and methods

A minor modification is one which has neither a significant impact on the extent of the property nor affects its Outstanding Universal Value (OUV). A minor modification can be approved after evaluation of the application document. If a state party wishes to significantly modify the boundary of a property already on the World Heritage List, the state party should submit this proposal as if it were a new nomination.

A state party can submit only two proposals at the same time, including applications for extensions and new nominations. The document must be submitted by 1 February, and it will take about one and a half years to finish the evaluation. In the case of extensions to properties, the attributes of the original nomination are examined and consideration is given to how these might be exemplified, extended, complemented or amplified by the attributes of the proposed extension, while bearing the same Outstanding Universal Value. The volcanic features on Jeju Island were classified according to volcano types, e.g., scoria cones, hydromagmatic volcanoes, lava domes, and etc. They were then evaluated according to their geological characteristics, academic values (publications in domestic and international journals, recognition in the international scientific communities), conservation status (e.g., whether they are designated as natural monuments), rarity, aesthetic value, and easiness of management.

To select the potential lava tube caves, 171 caves were evaluated based on previous cave expedition reports. Among them, 27 caves with national and provincial heritage values were selected, and 15 caves with only geoh heritage values were chosen. For 15 caves, evaluation took place based on; 1) representativeness, rarity, uniqueness, 2) cave speleothems and microtopographic features, 3) cave sediments and special setting, and 4) integrity.

3. Results

Among 5 evaluation standards (A to E), only 25 A and B caves were chosen. A and B ranks are the caves with the national monument and provincial monument values, respectively. Among them, 6 caves in the Geomunoreum Lava Tube System were excluded. Also, two lava tube caves in Mt. Hal-

lasan (Pyeonggul Cave and Guringul Cave), one cave that cannot be entered by people (Samseonghyeol), one sea cave (Dongangyeonggul Cave) were excluded, thus 15 lava tube caves were finally selected (Table 1)

Among the 15 candidates, the final caves were chosen based on; 1) representativeness, rarity, uniqueness, 2) cave speleothems and microtopographic features, 3) cave sediments and special setting, and 4) integrity. However, Bilemotdonggul and Susangul lava tube caves were excluded because the geological characteristics of both caves need to be further investigated, and Bilemotdonggul Cave has integrity problem.

4. Outstanding Universal Values (OUVs) of nominated properties

4.1. Socheongul Lava Tube

Around Jeju Island, shallow seas have provided accommodation space for temperate carbonate sediments. Due to a possible sea-level drop during the Holocene, carbonate sands were transported by wind onto the area where Yongcheondonggul, Dangcheomuldonggul and Socheongul lava tube caves are located. Meteoric water dissolved calcium carbonate and transported into the caves and carbonate speleothems developed. The ages of carbonate sand dunes and carbonate speleothems above and in Dangcheomuldonggul and Yongcheondonggul are about 5,000 and 2,000 yr BP, however those of the Socheongul Lava Tube are estimated to be less than 1,000 yr BP. This indicates that carbonate speleothems in Socheongul Lava Tube denotes the initial growth stage, providing geological integrity of the growth history of carbonate speleothems in the nominated lava tube caves in Jeju Island.

4.2. The Upper Geomunoreum Lava Tube System

One of parasitic volcanoes, the Geomunoreum scoria cone on the northeastern flank of the Hallasan Volcano, produced a large number of basaltic lava flows. Some of these lava flows constructed a series of lava tubes including *Bengdwi*, *Manjang*, *Gimnyeong*, *Yongcheon* and *Dangcheomul Caves*, and the Upper Geomunoreum Lava Tube System (Utsanjeongul, Bukoreumgu. and Darimgul lava tube caves). Thus, the recent discovery of the Upper Geomunoreum Lava Tube System complete the geological story of the Outstanding Universal Values of the Geomunoreum Lava Tube System.

Table 1. Fifteen selected caves which were selected for Class A and B. Class A and B denotes the caves with national and provincial monument values, respectively.

No	name	length (m)	rank	remarks
1	Hyeopjaegul Cave	99	A	-
2	Ssangnyonggul Cave	393	A	-
3	Hwanggeumgul Cave	180	A	-
4	Socheongul Cave	3,799	A	-
5	Bilemotdonggul Cave	9,020	A	-
6	Utsanjeongul Cave	2,385	A	can be treated as one system (the Upper Geomunoreum Lava Tube System)
	Bukoreumgul Cave	221	A	
	Darimdonggul Cave	173	A	
7	Susangul Cave	4,520	A	-
8	Gosanrigul Cave	150	B	-
9	Handeulgul Cave	1,500	B	-
10	Gamnamdapgul Cave	450	B	-
11	Waheulgul Cave	1,610	B	-
12	Bukchondonggul Cave	120	B	-
13	Doteulgul Cave	331	B	-
14	Pyoseongul Cave	38	B	-
15	Micheongul Cave	1,700	B	-

Table 2. Final grade of the lava tube caves for potential World Heritage extension in Jeju Island.

no.	Cave	Evaluation standards				Total grade
		representativeness & rarity	Speleothems & microtopography	Carbonate Speleo-thems	Integrity	
1	Upper Geomunoreum Lava Tube System	A ⁺	A ⁺	-	A ⁺	A ⁺⁺
2	Socheongul Cave	A ⁺	A ⁺	A ⁺	A ⁰	A ⁺
3	Bilemotdonggul Cave	A ⁺	A ⁰	-	A ⁰	A ⁰
	Susangul Cave	A ⁰	A ⁰	-	A ⁰	A ⁰

Medicine, Philosophy, Social Aspects

Human body responses during cave expeditions: a systematic review and potential future implications

Loredana Bessone¹, Lucrezia Zuccarelli^{1,2}, Emily BJ Coffey³, Giacomo Strapazzon⁴

Affiliation: ¹Directorate of Human and Robotics Exploration, European Space Agency, Linder Höhe, 51147 Köln, Germany, loredana.bessone@esa.int

²Institute of Molecular Bioimaging and Physiology, National Research Council, Via Fratelli Cervi 93, 20090 Segrate, ITALY, lucrezia.zuccarelli@unimi.it

³Montreal Neurological Institute (MNI), McGill University, 3801 Rue University, H3A 2B4, Montreal, Quebec, Canada, emily@flighteducation.net

⁴Institute of Mountain Emergency Medicine, EURAC research, Viale Druso 1, 39100 Bolzano, Italy, giacomo.strapazzon@eurac.edu

Abstract

Speleology is a rather recent scientific discipline that investigates topics such as the geomorphology, hydrology, meteorology, biology and microbiology of underground environments. Since 1938, studies have also been conducted on human behavior and physiology. Despite the potential implications for preventing accidents during cave exploration and training courses, little is still known about human physical and mental responses during a stay/exploration in a cave; many areas of research on human body responses in cave environments still rely on very early work that was primarily composed of case

studies. The aim of our review was to conduct a systematic bibliographic research of human studies associated with long permanence, expeditions, and cave rescues, with a view to establishing open questions and enumerating opportunities for scientific investigation of human behavior and physiology in the cave environment. We also aim to extend the application of previous results for application to future human planetary exploration missions, taking advantage of the many analogies between caving expeditions and human spaceflight.

Keywords: speleonautics, human research, bibliography, isolation studies, caves

1. Introduction

Speleology is an established scientific discipline, covering topics spanning from geomorphology to hydrology, meteorology, biology and microbiology. Cave environments have become one of the last frontiers of exploration on earth, bringing humans to vastly un-explored and highly inaccessible areas of the world. In addition to their value for environmental sciences, caves have been recognised as earth analogues to space exploration missions, offering an ideal platform to prepare astronauts to long duration spaceflight (Bessone, 2014; Pagel *et al.* 2016). However, little is known of the impact of multiple days cave expeditions on the human body and mind, or on team processes; this represents a relatively untapped opportunity to study these topics to the mutual benefit of cave and spaceflight operations.

Despite the potential implications for prevention of accidents during cave exploration or training courses, little is still known about human physical and mental responses during a stay/exploration in a cave; many areas of research on human body responses during a stay/exploration in a cave still rely on unique case series from very early work, or from other environments. For example, tips on nutrition and suggestions on energetic consumption during cave exploration activities mostly refer to comparable activities like mountaineering (Antoni *et al.*, 2016). Some studies associated with longer permanence in caves have been conducted as early as 1938 by Kleitman, who spent 32 days in the Kentucky's Mammoth Cave with an assistant, attempting to research the effects of

darkness on circadian rhythms (Kleitman N. 1963). In the 70's Siffre and Montalbini's isolation studies have attracted public attention, and for a while space agencies were interested in the results (Siffre 1987; Siffre 1988; Siffre 1990, Sonnenfeld 1992). However, many of those studies studied individuals or two too few individuals for statistical evaluation, few have been published in peer review journals, and most have been conducted in unrealistic speleological settings, and many are difficult to access. In order to provide a solid basis for future scientific work, a comprehensive review of existing studies and an analysis of their scientific merit are necessary.

The aim of our review was to conduct a systematic bibliographic research of human studies associated with long permanence, expeditions, and cave rescues, with a view to establishing open questions and enumerating opportunities for scientific investigation of human behavior, physiology and neurosciences in the cave environment. We further aim to seek ways in which the results of those studies may further knowledge of human behavior and physiological/neurological and psychological responses during future human planetary exploration, taking advantage of the many analogies between caving expeditions and human spaceflight (Strapazzon, 2013; Bessone, 2014).

2. Methods

We first compiled a summary of long permanence studies performed in cave environments, to collect a database of confinement/isolation experiments, and events involving

prolonged permanence of individuals and groups in underground environments, recorded mainly by news and speleological bulletins. The only existing summary of such form, albeit incomplete, was published in 2005 (Mohr). This initial search attempted to validate or update the previous summary by cross-referencing multiple sources. From the updated database, a few references to scientific studies were identified, in various languages, as well as contacts for individuals involved in the studies. Specific bulletins and reference material were retrieved from speleological and private libraries (i.e., biblioteca Anelli, biblioteca commissione grotte "E. Boegan", bibliothèque du speleoclub de Paris, Croatian Cave Rescue, Speleo Secours Française). Fifty-one European and non-European experts (i.e., from Austria, Croatia, France, Germany, Italy, New Zealand, Poland, Russia, US) including authors of scientific publications, speleologists of national and international speleological societies, and emergency medical doctors of cave rescue organizations were contacted. For a number of the studies, only a bibliographic reference could be retrieved. Forty-two people answered, and three provided additional materials that were included in the review. From this initial database, a systematic search was conducted, following the structured guideline PRISMA (Preferred Reporting Items for Systematic Reviews and Meta-Analyses) (Moher et al., 2009) of electronic databases (Google Scholar, MEDLINE, NASA Technical Reports Server, OPAC, WorldCat) and manually searching reference lists of the articles investigating human body responses during a stay/exploration in a cave.

3. Results

The initial search allowed the compilation of a summary (Table 1), which updated the original list in (Mohr 2005), and provided a base from which to identify materials not published in English or in standard journals.

The systematic search retrieved 2097 articles. There were 156 articles selected for further revision. Articles were classified into seven categories: atmospheric science (24), emergency medicine (61), human factors (0), human physiology (23), neuroscience (29), psychological aspects (4) and radiation (15) (Table 2).

An analysis of the methods of each study revealed that the majority of studies were conducted heterogeneously, with widely varying degrees systematization with respect to selection and number of participants, and experimental protocols. Furthermore, the majority of studies took place in conditions that are unrepresentative of speleological exploration activities. A quantitative meta-analysis was therefore not possible. Nevertheless, a descriptive analysis of the studies was conducted. We decided to focus on physiological studies first, then neurosciences, and finally emergency medicine. At the time of the compilation of this article, the physiological analysis has been completed (results from the neuroscience analysis will be available shortly).

The studies evaluated in this review were categorized based on the duration of time spent in the cave: acute effect studies were defined as permanence in the cave up to 72 hours and chronic effect studies for more than 72 hours (Tables 1, 2). The responses of endocrine, metabolic, muscular, bone, visual system and the hematological parameters were the primary outcomes measured.

4. Discussion and further work

Our study provides a comprehensive list of existing human studies related to the underground environment. This review will allow for comparison with knowledge in related disciplines and facilitate research on human behavior and physiology/neurology in controlled yet realistic underground expeditions, with the ultimate goals of improved safety and performance of teams working in cave environments, and for a basis for the design of human space analogue research in underground environments. Further work is being conducted to review research in neurosciences and in emergency medicine.

A direct follow-up to these topics is planned: we will study physiological, psychological, neurological and behavioral effects of prolonged permanence in caves during realistic exploration activities with the use of a questionnaire, to obtain a compendium of important physiological/neurological/psychological/behavioral effects of prolonged stay/exploration in a cave, or in extreme conditions (remote exploration areas, deep exploration, multiple obstacles/sumps, long progression to/from exploration area). The result of this research, including all retrieved references, will be made available as a public database, allowing the submission of further references, to serve the speleological and scientific community, and to serve as a basis for future studies to be conducted in caves as space analogues, in preparation for future planetary exploration missions.

References

- Bessone L, Sauro F, Stevenin H, 2014. Training Safe and Effective Spaceflight Operations Using Terrestrial Analogues, *Proc. 7th IAASS Conference – Safety is no accident*
- Antoni G, Rinaldi A, Tuveri V, 2016. Progetto di rilevamento e monitoraggio del dispendio energetico durante l'attività speleologica. *Speleologia* 74.
- Moher D, Liberati A, Tetzlaff J, Altman DG, & Prisma Group, 2009. Preferred reporting items for systematic reviews and meta-analyses: the PRISMA statement. *PLoS med*, 6(7), e1000097.
- Mohr P, Mohr J, 2005. Rhythms of the Dark – a short history of the endurance caver. *British Caver* 128
- Kleitman N, 1963. *Sleep and wakefulness*. University of Chicago Press, Chicago, Illinois.
- Pagel JI, & Choukèr A, 2016. Effects of Isolation and Confinement on humans-Implications for manned space explorations. *Journal of Applied Physiology*, 120(12), 1449-1457.
- Siffre M, 1987. Rythmes Biologiques, sommeil et vigilance en confinement prolongée. *Proceedings of a Colloquium on "Space & Sea"*, Marseille, France, 24-27 November (ESA SP_280, March 1988).
- Siffre M, 1988. *Biological rhythms, sleep, and wakefulness in prolonged confinement*. NASA Technical Reports Server.
- Siffre M, 1990. Some problems of desynchronisation of sleep-wakefulness and circadian rhythms for long duration

spaceflights. *Proceedings of the Space & Sea Colloquium*, Paris, 24-26 September, ESA SP-321.

interferon production and hematological and immunological parameters. *Journal of interferon research*, **12**(2), 75-81.

Sonnenfeld G, Measel J, Loken MR, Degioanni J, Follini S, Galvagno A, & Montalbini, M, 1992. Effects of isolation on

Strapazzon G. 2013. Caves as an environment for astronaut training. *Wilderness & Environmental Medicine*

Table 1. Summary of isolation experiments conducted in caves – updated at January 2014. This table has been compiled with an Internet search using English, French, Italian and Spanish languages, and only contains information which could be retrieved from news and speleological bulletins available at the time. The table was compiled with the intention of identifying scientific research on humans conducted in caves environments

Year	From	To	Duration	Location
1938	04/06/1938	06/07/1938	32 days	Mammoth Cave, Kentucky
1942-1943	12/10/1942	April 1943	6 months	Verteba, Ukraine
1943-1944	05/05/1943	12/04/1944	344 days	Priest's Grotto, Ukraine
1943-1944	01/06/1943	28/07/1994	14 month	Sewers of Lvov, Poland
1953	?	?	14 days	Gaping Gill
1961	06/08/1961	07/09/1961	32 days - 756 hours	Grotta di Caudano
1962	13/04/1962	21/04/1962	7 days	Grotta di Bossea
1962	16/07/1962	17/09/1962	62 (58) days	Scarasson
1962	23/09/1962	26/11/1962	64 days	Katherine, Darwin Australia
1962	23/12/1962	30/12/1962	7 days	Grotte de Cavottes, Montrond le Chateau Besancon
1962-1964			4-8 days	Underground rivers: Saut, Reilly, Padillac, Vitarelle
1963	25/02/1963	23/05/1963	87 days	Yallingup (Nigilgi) caves, Australia
1963	31/05/1963	27/08/1963	88 days	Yallingup (Nigilgi) caves, Australia
1963	16/06/1963	29/09/1963	105 days	Stump Cross Cavern
1964			?	Gradeshnitsa, Bulgaria
1964			9 days	l'Aven Vigneron
1964	14/12/1964	12/03/1965	88 (83) days	l'Aven Vigneron
1964-1965	30/11/1964	05/04/1965	126 (120) days	l'Aven Ollivier
1965	12/04/1965	19/04/1965	7 (6) days	l'Aven Vigneron
1965	06/07/1965	27/07/1965	20 days	l'Aven Vigneron
1965	06/07/1965	27/07/1965	20 days	l'Aven Vigneron
1965	04/07/1965	25/07/1965	502 hours - 21 days	Alcoy Cave (Spain)
1966	27/03/1966	04/08/1966	127 (130) days	Gough Cave Boulder Chamber at Cheddar Caves
1966	01/06/1966	30/11/1966	181 (176) days	l'Aven Ollivier
1966			1 week	
1966			27 & 30 days	Semlehedskuyu cave, Buda hills, Budapest
1968	22/08/1968	15/01/1969	146 (128) days	l'Aven Ollivier
1969	06/02/1968	06/03/1968	28 (26) days	l'Aven Ollivier
1969	06/03/1969	26/03/1969	20 (5) days	l'Aven Ollivier
1969	24/06/1969	30/09/1970	463 days	Samr Cavern, Kopajkoshara, Yugoslavia
1970				Lepenitsa, Bulgaria
1971			30 days	Topchika Cave, Bulgaria
1972	13/02/1972	05/09/1972	205 days	Midnight Cave, Del Rio, Texas
1973				Pierre Saint Martin, France
1974			6 days	France
1977	March			Orlova Chucka, Russe
1977	17/09/1977	18/11/1977	62 days	Souhi Pech, Bulgaria
1979-1980	October 1979	February 1980	82 days	Snezhnaya "Snow" cave, Georgia
1984				Jean Bernard, France
1985	05/05/1985	08/06/1985	34 days ?	Grotta di Sant'Anna Vecchia, Calvana di Prato
1986-1988			~30 days	Sima de las Puertas de Illamina (BU56), Spain

Year	From	To	Duration	Location
?				Galata expedition Snezhnaya, Causcasus
1986	14/12/1986	12/07/1987	210 days	Frasassi (Grotta Grande del Vento)
1987	14/12/1987	31/01/1988	48 days	Grotta del fiume, Frasassi
1988			110 days	Gouffre du Valat-Nègre, France
1988			56 days	Ptichata Dupka, Balkan
1988	10/08/1988	29/11/1988	111 days	Gouffre du Valat Nègre, Millau
1989	13/01/1989	23/05/1989	130 days	Carlsbad, New Mexico
1991	21/11/1991	13/03/1992	113 days	Grotte de Cocaliere
1992	06/12/1992	05/12/1993	366 days	Grotta di Neurone, Pesaro. Underlab
1994	26/07/1994	21/04/1995	269 days	Underlab2, Frasassi
1996	05/04/1996	05/06/1996	61 days	Underlab, Grotta dei venti, Frasassi
1997	30/10/1997	16/04/1998	166 days	Underlab, Grotta dei venti, Frasassi
1999	30/11/1999	04/02/2000	75 days	Grotte de Clamouse
2006	14/10/2006	07/06/2007	235 days	Underlab, Grotta Fredda, Acquasanta Terme
2008			54 days	Grotta del Campanaccio, Santadi

Table 2. Number of articles screened, per category. The material retrieved was categorized in three categories: Peer Reviewed, Divulgative, Thesis, and according to the main topic covered, amongst the topics of interest to human related studies.

Categories	Papers	Thesis	
	Peer reviewed	Divulgative	
Atmospheric Science	22	2	0
Emergency Medicine	21	24	16
Human Physiology	11	12	0
Human Factor	0	0	0
Neuroscience	26	2	1
Psychological Aspects	1	3	0
Radiation	14	0	1
Tot.	95	43	18

Caves And Geotourism

Greg Brick, Ph.D.

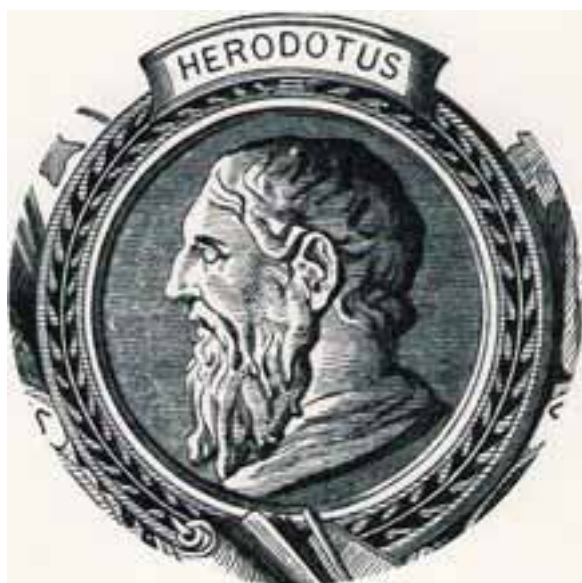
Affiliation: Minnesota Department of Natural Resources
500 Lafayette Road, St. Paul, Minnesota, 55155 USA

Abstract

Geotourism (*sensu lato*) is a new word for an old activity. While the bulk of the literature emphasizes recent decades, the Greek writer Herodotus (5th century BC) arguably became the world's first geotourist and perhaps the Father of Geotourism when, on a trip through Egypt, he described the accumulation of sediments in the Nile River delta. But this perspective only highlights the late arrival of caves in the context of geotourism (as distinguished from utilitarian visitation). Cave tourism developed in the late 18th and 19th centuries with the rise of the middle classes. Caves offer the purest form of geotourism: a journey through the Earth itself, involving close encounters with the enveloping rocks.

Keywords: geotourism, geoconservation, show caves

Geotourism (*sensu lato*) is a new word for an old activity, tourism with a geological emphasis. The core of geotourism is "geocuriosity" or curiosity about geological phenomena, whether at the casual, amateur, or professional level, beyond the level of merely aesthetic appreciation. Geological observations can be made by traveling persons who did not set out by design to observe them, but merely had an opportunity to do so in passing. Paid geological surveys are excluded by definition.



While the bulk of the literature (e.g., Hose 2008, 2011) emphasizes the geotourism of recent decades, which appears to be growing globally (Dowling 2010), its roots go back much further, as even these authors tacitly admit when they speak of the geotourism of the last three centuries. Indeed, the retrospective *Sensu Lato* pantheon features a different cast of characters. In the Ancient world, the Greek writer Herodotus (5th century BC) arguably became the world's first geotourist and perhaps the Father of Geotourism when, on a trip through Egypt, he described the accumulation of sediments in the Nile River delta. Another Greek geotourist was Pausanias (2nd century AD) who wrote a guidebook to Greece. Among the Romans, Pliny the Elder died while observing an eruption of Vesuvius—the first geotourist martyr.

The Medieval situation is murkier. While Shaw (1992) describes several explorers of the day, we must consider the overall attitude towards nature. For example, Matthew Paris in the mid-13th century drafted itineraries depicting the route from London to Jerusalem. He marginalized nature by using a series of parallel lines to indicate a boundary between the human world and nature (Gaudio 2000).

By Renaissance times, tourist interest had developed in caves such as the Grotto of Antiparos in the Mediterranean (Shaw 1992). But this perspective only highlights the late arrival of caves in the context of geotourism (as distinguished from utilitarian visitation).

Caves offer the purest form of geotourism: a journey through the Earth itself, involving close encounters with the enveloping rocks. A geoconservation message is implicit in the definition of geotourism, because visits by individuals or groups intent on partying or vandalism is not considered tourism by anyone's standards. Likewise, harvesting cave formations or minerals is a commercial activity, not tourism. That said, there is a certain irreducible amount of "wear and tear" that is involved with large numbers of humans visiting caves (e.g., Cope 2016) leaving open the question whether it is a "sustainable" activity in the long run.

It is here proposed that there are three strands of cave geotourism:

(1) Show caves and easily accessible wild caves for the casual visitor. According to Shaw (1992) cave tourism developed in the late 18th and 19th centuries with the rise of the middle classes. Hose (2008) and Cope (2016) emphasize the Peak District as the birthplace of geotourism in the U.K., paying especial attention to its caves, but Wookey Hole near Bristol, has a better claim as an early geotourism site in the U.K. (Shaw 1996). Many early cave visits are recorded in travel accounts (Stafford 1984).

(2) Dedicated travelers with a cave focus, taking Speleological Grand Tours. Shaw (1992) highlights four Europeans: Valvasor, Steinberg, Schmidl, and Martel. To this list I will add four Americans: Horace Carter Hovey, Luella Agnes Owen, Edwin Swift Balch, and Dr. William R. Halliday. But such geotourists are not confined to the West, as for example Xu Xiake in 17th century China (Hu 1991). This sort of geotourism is

more likely than other types to involve “geological innovation” or fundamental new insights (Rudwick 1996). Nor is this option confined to the wealthy tourist; for example, an article in the *Chicago Tribune* advocated a tour of India’s cave temples (Holt 1967).

(3) Organized events by cave exploring societies at the state or local level (e.g., NSS grottoes), national (e.g., NSS conventions), or international—our very own International Congress of Speleology.

References

Cope MA, 2016. Three centuries of open access to the caves in Stoney Middleton Dale Site of Special Scientific Interest, Derbyshire. IN TA Hose, ed., *Appreciating Physical Landscapes: Three Hundred Years of Geotourism*. Geological Society of London, Special Publication 417, 157-169.

Dowling RK, 2010. Geotourism’s global growth. *Geoheritage*, **3**, 1-13.

Gaudio M, 2000. Matthew Paris and the cartography of the margins. *Gesta*, **39**(1), 50-57.

Holt K, 1967. Journey to India’s famous cave temples. Tour goes from Aurangabad to Ellora, Ajanta. *Chicago Tribune*, July 9.

Hose TA, 2008. Towards a history of geotourism: Definitions, antecedents and the future. IN CV Burek and CD Prosser, eds. *The History of Geoconservation*. Geological Society of London, Special Publication 300, 37-60.

Hose TA, 2011. The English origins of geotourism (as a vehicle for geoconservation) and their relevance to current studies. *Acta Geographica Slovenica*, **51**(2), 343-360.

Hose TA, ed., 2016. *Appreciating Physical Landscapes: Three Hundred Years of Geotourism*. Geological Society of London, Special Publication 417.

Hu B, 1991. Xu Xiake, a Chinese traveller of the seventeenth century, and his contribution to karst studies. *Cave Science* **18**(3), 153-157.

Rudwick M, 1996. Geological travel and theoretical innovation: The role of ‘liminal’ experience. *Social Studies of Science* **26**(1), 143-159.

Shaw TR, 1992. *History of Cave Science: The Exploration and Study of Limestone Caves, to 1900*, 2nd Ed. New South Wales, Australia: Sydney Speleological Society.

Shaw TR, 1996. Why some caves become famous – Wookey Hole, England. *Caves and Karst Science*, **23**(1), 17-23.

Stafford BM, 1984. *Voyage into Substance: Art, Science, Nature, and the Illustrated Travel Account, 1760–1840*. Cambridge, MA: MIT Press.

(Abstract) **Cultural Karst-Landscape: A New Methodology of Social Science Research in Tropical Karst Regions**

Yayum Kumai

Affiliation: Himpunan Kegiatan Speleologi Indonesia (HIKESPI)

Abstract

The study of karst landscape is almost entirely covered by geoscience, such as geology, geography, hydrology and botany. In a karst region, especially tropical karst regions, a landscape also is an area of human settlements. The existence of mankind as one element in the ecology of karst region certainly needs attention. Thus the social sciences are useful as an approach to provide new insights in analyzing the karst areas inhabited by humans.

The position of social science here is directed to examine the relationship between human and natural elements. The role of social sciences are able to look at a study of this relationship and develop a new methodology to accommodate the complexities of karst community as a whole.

This presentation aims to explain a new methodology for social research in a tropical karst region in order to analyse the particular social dynamics of society in a tropical karst region, which is related to the uniqueness of karst geography and hydrology.

This essay contains two main aspects. Firstly, to formulate the correlation between the typology of tropical karsts and their components with anthro-socio aspects, and secondly, to introduce a methodology that can be applied in tropical karst regions.

Several approaches or methodologies for studying human relationships with nature already exist. One of them is the Ecological Anthropology, which uses the 'ecological method' to study the inter-relations between humans and their environment. Another is the Anthropology of Environmentalism that uses the 'ethnography method' to learn about environmentalism as a type of human action.

The purpose of this methodology is designed for use by all speleologists in tropical karst regions and to understand the complex interactions between the karst landscape and culture of the local community.

Modelling in Karst and Cave Environments

Small-scale modelling of arenitic caves in South American tepuis: Make your own tepui at home.

Roman Aubrecht^{1,2}, Tomáš Lánczos³, Ján Schlögl¹, Marek Audy⁴ and Petronela Filipčíková³

Affiliation: ¹ Department of Geology and Paleontology, Faculty of Natural Sciences, Comenius University, Ilkovičova 6, 842 15 Bratislava, Slovakia.

² Institute of Earth Sciences - Geophysical Division, Slovak Academy of Sciences, Dúbravská cesta 9, 845 28 Bratislava, Slovakia.

³ Department of Geochemistry, Faculty of Natural Sciences, Comenius University, Ilkovičova 6, 842 15 Bratislava, Slovakia.

⁴ Czech Speleological Society, Tyršova 332, CZ-679 06 Jedovnice, Czech Republic.
corresponding author - e-mail: aubrecht@fns.uniba.sk

Abstract

South American table mountains (tepuis) host the largest arenitic cave systems in the world. To explain speleogenesis in these insoluble rocks, two theories were introduced: a) arenization theory implying selective weathering of quartz cements and releasing of sand grains, b) selective lithification theory implying lithification by descending silica-bearing fluid flow. The latter presumes that the descending fluid flow becomes unstable on the interface between two layers with different porosity and splits to separate flow channels (“finger flow”). The arenites outside these channels remain unlithified. There is also a so-called “funnel-flow” which occurs at inclined layers. This works for cross-bedded arenites.

To verify the latter theory, small-scale modelling was performed, using sands and sodium-silicate solution. For experiments with contrasting grain-size, fine to medium sand fraction was used (0.08-0.5 mm), along with coarse (0.5-1.5 mm) fraction. For experiments with cross-bedded sediments, only the fine fraction has been used. The sands were layered and compacted in a transparent plexiglass boxes. Sodium-sili-

cate solution (so-called water glass) was left to drip for several hours to the top of the sediment.

Results of this small-scale modelling mimic the real diagenesis by descending silica-bearing fluids and match the real phenomena observed on the tepuis. The resulting lithified constructions in horizontally layered experiments with contrasting grain-size closely remind many geomorphological features observed on tepuis and inside their caves, e.g. “finger-flow” pillars, overhangs, imperfectly formed (aborted) pillars in forms of hummocks hanging from ceilings, locally also thicker central pillars that originated by merging of smaller fluid-flow channels. The models with cross-bedding display close similarity with triangular-shaped shelters and caves observed in aeolian sediments on Akopán Tepui.

The modelling showed that selective lithification theory can explain most of the geomorphological aspects related to the speleogenesis in tepuis, whereas the arenization theory can explain only particular problems.

Keywords:

1. Introduction

Huge cave systems were discovered in last two decades in the arenitic rocks (Matauí Formation – Mesoproterozoic) forming South American table mountains called tepuis. The largest systems are Ojos de Cristal (Roraima Sur) System discovered in 2002 (Šmída *et al.* 2003), Churí Tepuy System with the largest cave Cueva Charles Brewer discovered in 2004 (Šmída *et al.* 2010; for summary information about both systems see also Aubrecht *et al.* 2012) and Imawarí Yeuta System discovered in 2013 (Sauro *et al.* 2013b). Members of our team came with a new explanation of their genesis. It implies selective lithification of arenites by descending solutions enriched in silicic acid released during lateritization of overlying sediments rich in alumino-silicates. The down-penetrating solutions in sediments (e.g. sands and soils) locally split to separate flows (preferential flows) that are determined by various factors (for detailed information see: <http://soilandwater.bee.cornell.edu/research/pfweb/educators.htm>). In this case, the most important are the processes causing wetting front instability at the contact of fine-grained sand layer with underlying coarse-grained sand layer, where the wetting front splits to several channels forming so-called “finger-flow”. On the other hand, instability at the inclined layers forms so-called “funnel-flow”.

After lithification of beds with contrasting grain-size, “finger flow” pillars are created, standing between the lithified beds of finer-grained arenites. The remaining coarse-grained sediment between the pillars remains weakly lithified, or completely unlithified. Disruption of the rock massif and penetration of flowing water causes winnowing of the loose arenite and creates caves. Collapse of superposed winnowed horizons may lead to formation of volumetrically huge subterranean spaces (Aubrecht *et al.* 2008, 2011, 2012). Presence of “finger-flow” pillars is diagnostic for this type of speleogenesis (Aubrecht *et al.* 2013a).

Cross-bedded layers affected by “funnel-flow” display poorer diagenesis than other layers due to increased velocity of the fluid flow. Observations on the Akopán Tepui showed that the weaker lithification results in forming of triangular-shaped shelters and small caves.

To support the new theory, small-scale modelling of the arenitic caves by descending silica-bearing fluids was performed and discussed with competing arenization theory, which implies dissolution of recrystallized siliceous cement forming quartz overgrowths along the grain boundaries and subse-

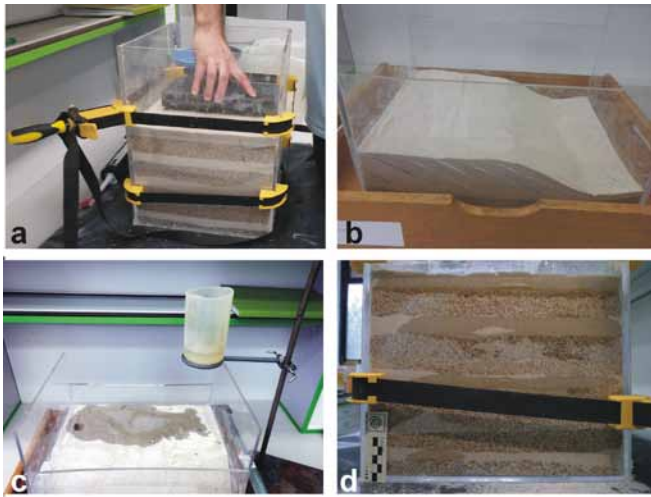


Figure 1. Photos documenting preparation and performance of the experiments. (a) Layered sand of various grain size sedimented and compacted in a plexiglass vessel. (b) Preparation of cross-bedded fine-grained sands. Cross-bedding is emphasized by thin kaolinite laminae (white). (c) Sodium silicate solution is dripping onto the cross-bedded sand. (d) Downward penetration of the wetting front in experiment using horizontally layered sands with contrasting grain-size. The wetting appeared in all three fine-grained layers, when it for the first time appeared as fingering on the vessel wall in the second coarse-grained layer. The wetting front in the first coarse-grained layer (its upper part) is till even and stable.

quent releasing and winnowing of sand grains (Martini 1979, 2002, 2004).

2. Material and methods

To verify the theory about selective lithification by descending silica-bearing fluids, experiments were performed, using layered sands with contrasting grain size and cross-bedded fine sands (Fig. 1). A commercially available sodium silicate (“water glass”) solution (concentration cca 36 %) was selected as a medium that best mimics lithifying silica-bearing fluids. After several experiments with firm vessels from transparent material, the best results were achieved with silicon-glued plexiglass boxes that were constructed directly in the lab.

For the experiments with contrasting grain-size sands, the vessels were filled with various layers of fine-grained sands (0.08-0.5 mm), along with coarse fraction (0.5-1.5 mm). The sands were layered and compacted (Fig. 1a) with the coarser fractions forming the thickest layers (5-10 cm). The fine-grained layers were thinner (2-3 cm). For experiments with cross-bedded sands, only fine-grained fraction was used (0.08-0.5 mm) mimicking wind-borne sand. The cross-bedded layer was formed between two horizontally-layered levels. The cross-bedding was increased by thin kaolinite intercalations each 1 cm (Fig. 1b). Sodium-silicate solution was left to drip for several hours to the top of the sediment and to soak inside (Fig. 1c).

The resulting lithified arenitic constructions were photodocumented and compared with field documentation and photos on the surface of the Churí and Akopán tepuis (parts of the Chimantá Massif) and Roraima Tepui, as well as in their cave systems (Churí Tepui Cave system and Ojos de Cristal Cave system).

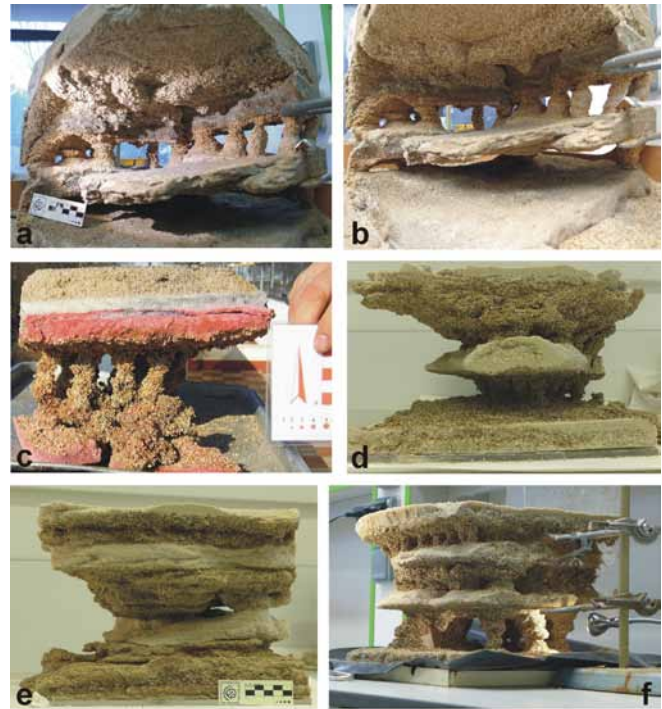


Figure 2. Lithified results of the modelling using layered sands with contrasting grain-size. (a-b) Most of “finger-flow” pillars developed in the central coarse-grained layer and less in the lower coarse-grained layer. The upper coarse-grained layer has been filled and lithified completely. Many of the pillars display uneven thickness and locally bulbous thickening in the lower part. (c) Earlier experiment performed in a firm plastic vessel. “Finger-flow” pillars were developed only in the central, 10cm thick coarse-grained layer. Bottom part and some pillars were destroyed during tumbling the material out of the box. (d) Due to rapid flooding, most of the pillars merged to one central pillar in this experiment. However, the original merging pillars are still discernible in the coarse-grained layers. Only one small pillar remained isolated in the lower layer (right of the lower part). (e) Most of the pillars again merged to one central pillar in this experiment, but a relict cavity with flat bottom and vaulted top still remains (middle right). (f) Thickest and largest pillars developed in the lower coarse-grained layer in this experiment. In this layer also an aborted pillar is visible (bottom center). Two upper layers were more filled by the lithifying liquid, but some small pillars are still visible, mainly at the margin of the upper coarse-grained layer. Number of pillars diminished downward but their size increased.

3. Results and interpretations

The final lithified product of the experiments using sands with contrasting grain-size in some cases displayed well-preserved isolated “finger-flow” pillars between well-lithified fine-grained layers (Fig. 2). In other cases, gradual soaking caused merging of some flow channels and forming of thicker pillars which sometimes merged to one central pillar (Fig. 2d-e), with the individual channels still observable at the pillar margin. But even in such cases, some cavities and isolated pillars were still preserved. The cavities have vaulted top and flat bottom (Fig. 2e) just like the caves, which Sauro et al. (2013a) presented as being typical for the horizontal caves in tepuis. Despite being created in small-scale modelling, all types of lithified products closely mimic the structures that were observed on the tepuis, or in their caves, e.g. cavities with flat bottoms and ceilings, supported by “finger-flow” pillars between them (Fig. 3a-c). The “finger-flow” pillars were mostly perpendicular to the layering; but slightly inclined pillars were common, too. Some pillars displayed bulbous

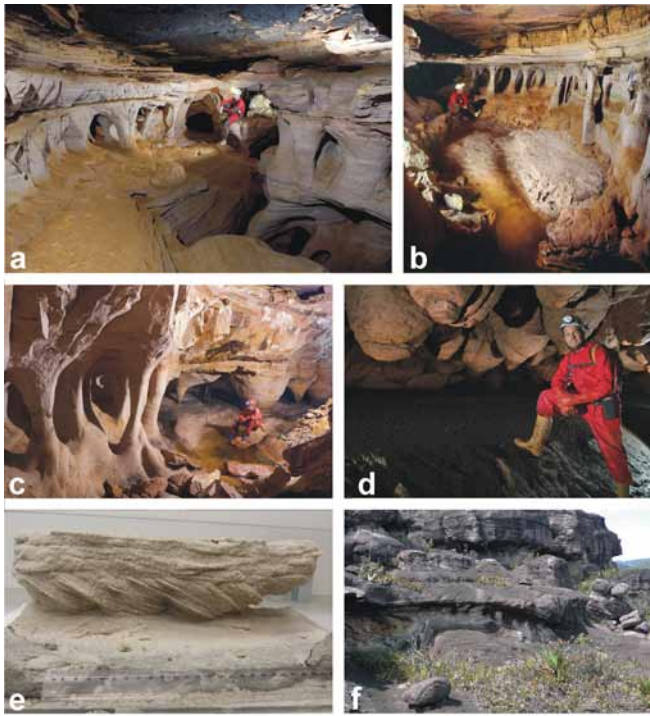


Figure 3. Field photos from caves in the Churí Tepui. (a) Superposed two levels with developed pillars. If origin of the pillars was predisposed by vertical cracks, existence of such superposition would be unlikely. Cueva de las Arañas. (b) Well-developed pillars in Cueva de las Arañas. Tops of some pillars show lithified merging “finger-flow” channels. The bed above the pillars would be again disrupted if they were predisposed by vertical cracks. (c) Well-preserved pillars in Cueva de las Arañas. (d) Aborted pillars (“tetas”) hanging below ceiling of Cueva Eladio (Sistema Brewer). (e) Lithified result of an experiment with cross-bedded sands. Note that the top and bottom layers are lithified evenly, whereas the cross-bedded layer between them displays poorer lithification and forms negative relief. (f) Field photo from Akopán tepui showing that the parallel-layered layers are hardly lithified, forming overhangs, whereas the cross-bedded layers form negative relief between them.

thickening (Fig. 2a-b) which is similar to some pillars in Imawarí Yeuta Cave in Auyán Tepui (Sauro et al. 2013b). Some pillars are imperfectly developed in their early stages, forming hummocks hanging from the ceiling (Fig. 2f), which closely mimic similar structures in the tepui caves called “tetas” (tits) by local cavers (Fig. 3d).

The resulting structures of experiments with cross-bedded sands display good lithification of horizontally layered sands and much poorer lithification of the cross-bedded sediment between them (Fig. 3e), showing triangular overhangs, which closely mimic the triangular shelters on the Akopán Tepui (Fig. 3f).

4. Discussion

The experiments showed that many geomorphological features observed on the surface of tepuis and in their caves can be created by small-scale modelling using descending diagenetic fluids. Not all aspects that are observable in the field can be reproduced in this scale. The coarse-grained layers were not thick enough to promote formation of perfectly shaped “finger-flow” pillars with widenings on both ends and smooth surface that might be modified by flowing water. However, the principal processes occurring in this system are obvious.

Against the selective lithification theory stands recently mainly the theory of arenization (Martini 1979, 2004). Our team already disputed several aspects on the pages of Geomorphology (Sauro et al. 2013a; Aubrecht et al. 2013a). However, the last paper concerning this matter of Sauro (2014) still supports the arenization theory, bringing new possible explanations about the origin of the pillars and the caves themselves. According to him, the pillars were pre-disposed tectonically by vertical cracks which limited them and the erosion removed the surrounding, more dissected rocks. In such case, however, it is difficult to explain common presence of undisturbed overlying and underlying beds, or local presence of interbeds that are supported by the pillars. On the other hand, these continuous, well-lithified beds are a typical product of selective descending fluid lithification, as evidenced by the experiments. The vertical cracks model also does not work in the cases of pillars that are still half-embedded in sandstone or sand.

If admitting validity of arenization theory, very complex models must be invented from case to case. On the other hand, the selective lithification model explains most of the aspects, which was proved also by small-scale 3-D modelling presented in this paper.

5. Conclusions

1. Large cave systems were discovered in arenites (quartzites and sandstones) forming the table mountains in northern part of South America.
2. To explain speleogenesis in these insoluble rocks, two theories were introduced: a) arenization theory implying selective weathering of quartz cements and releasing of sand grains, b) selective lithification theory implying lithification by descending silica-bearing fluid flow. The latter theory presumes that the descending fluid flow is unstable and locally splits to separate flow channels (so-called “finger flow”). The arenites outside these channels remain unlithified.
3. To verify the selective lithification theory, small-scale experiments were performed, involving layered sands with contrasting grain size and cross-bedded fine sands mimicking aeolian sediments. As the lithifying medium, sodium silicate (“water glass”) solution was left dripping on the sediment.
4. The resulting lithified constructions closely mimic many geomorphological features observed on tepuis and inside their caves, such as “finger-flow” pillars, overhangs, triangular shelters, aborted pillars in forms of hummocks hanging from ceilings. Locally also thicker central pillars that originated by merging of smaller fluid-flow channels were formed, with relic cavities with flat bottom and vaulted top. These are also typical for some tepui caves.
5. The modelling showed that selective lithification theory can explain most of the geomorphological aspects related to the speleogenesis in tepuis, whereas the arenization theory can explain only particular problems.

Acknowledgements

The authors acknowledge the financial support from the project APVV 14-0276.

References

- Aubrecht R, Lánczos T, Šmída B, Brewer-Carías Ch, Mayoral F, Schlögl J, Audy M, Vlček L, Kováčik L, Gregor M., 2008. Venezuelan sandstone caves: a new view on their genesis, hydrogeology and speleothems. *Geologica Croatica*, **61**(2-3), 345-362.
- Aubrecht R, Lánczos T, Gregor M, Schlögl J, Šmída B, Liščák P, Brewer-Carías Ch, Vlček L, 2011. Sandstone caves on Venezuelan tepuis: return to pseudokarst? *Geomorphology*, **132**(3-4), 351-365.
- Aubrecht R, Barrio-Amoros C, Breure A, Brewer-Carías Ch, Derka T, Fuentes-Ramos OA, Gregor M, Kodada J, Kováčik L, Lánczos T, Lee NM, Liščák P, Schlögl J, Šmída B, Vlček L, 2012. *Venezuelan tepuis – their caves and biota*. Acta Geologica Slovaca - Monograph, 1-168.
- Aubrecht R, Lánczos T, Gregor M, Schlögl J, Šmída B, Liščák P, Brewer-Carías Ch, Vlček L, 2013a. Reply to the Comment on “Sandstone caves on Venezuelan tepuis: Return to pseudokarst?”. *Geomorphology*, **197**(1), 197-203
- Aubrecht R, Lánczos T, Schlögl J, Vlček L, Šmída B, 2013b. Arenitic caves in Venezuelan tepuis: what do they say about tepuis themselves? In: M Filippi and P Bosák (Eds.). *Proceedings of the 16th International Congress of Speleology*, July 21-28, 2013. Brno, Czech Republic, Vol. **3**, pp. 221-226.
- Martini JEJ, 1979. Karst in Black Reef Quartzite near Kaapsehoop, Eastern Transvaal. *Annal of the South African Geological Survey*, **13**, 115-128.
- Martini JEJ, 2000. Dissolution of quartz and silicate minerals. In: AB Klimchouk, DC Ford, AN Palmer and W Dreybrodt (Eds.). *Speleogenesis, Evolution of Karst Aquifer*, January 2000 edition. NSA, Inc., Huntsville, Alabama, pp. 171-174.
- Martini JEJ, 2004. Silicate karst. In: J Gunn (Ed.). *Encyclopedia of caves and karst science*. Fitzroy Dearborn, London, pp. 1385-1393.
- Sauro F, 2014. Structural and lithological guidance in quartz-sandstone caves: evidences of the arenisation process. *Geomorphology*, **226**, 106-123.
- Sauro F, Piccini L, Mechcia M, De Waele J, 2013a. Comment on “Sandstone caves on Venezuelan tepuis: Return to pseudokarst?” by R. Aubrecht, T. Lánczos, M. Gregor, J. Schlögl, B. Smída, P. Liscák, Ch. Brewer-Carías, L. Vlcek, *Geomorphology* 132 (2011), 351-365. *Geomorphology*, **197**(1), 190-196.
- Sauro F, Vergara F, De Vivo A, De Waele J, Lira J, 2013b. In the House of Gods on Devil’s Mountain. Imawarí Yeuta Cave, Auyan Tepui, Canaima National Park, Venezuela. *NSS News*, September 2013, 7, 10-19.
- Šmída B, Audy M, Vlček L, 2003. Roraima 2003 expedition. Crystal Eyes Cave. *Bulletin of Slovak Speleological Society*, **34**(2 spec. vol.), 1-190 (in Slovak with English summary).
- Šmída B, Brewer-Carías Ch, Audy M, Mayoral F, Bakšić D, Vlček L, Stankovič J, 2010. Churi-Tepui Cave System: Inside the second largest quartzite cave in the world. *NSS News* **68**(7), 16-23.

Driving pressure of subterranean airflows: an analysis

Giovanni Badino

Affiliation: Dip. Fisica, Università di Torino, Ass. Geografica La Venta

Abstract

Airflow in caves are traditionally attributed to two basic physical models, the convection due to density differences between the external and internal atmospheres and the barometric movements due to changes of external atmospheric pressure. In fact, the experimental measurements that are now possible thanks to small sonic anemometers, are quantitatively not consistent with these models. A detailed analysis of the outside atmosphere phenomenology, up to second order effects, has shown the existence of two other processes able to create driving pressures, especially in high altitudes in caves, which have a comparable weight with the traditional processes. These two new processes are barometric circulations due to temperature variations and air circulations due to the external lapse rate. The first measurements seem to confirm the existence of these two processes.

Keywords: airflow in caves, convective airflow, lapse rate airflow, thermal barometric airflow

1. Introduction

The main causes of the cave airflows are usually considered to be changes in air pressure (barometric circulation) and the variations of the external temperature (convective circulation). Here it is shown that, in the details of convective circulation, are hidden two other causes: barometric changes induced by temperature variations at ground, and airflow due to anomalous lapse rates. The traditional treatments of the convective flow uses a hydrostatic approximation (constant air density, with various corrections): the driving pressure is then dependent on density differences between the internal and external columns of air. This term is related to differences in temperature and air humidity. It is common in meteorology to use the virtual temperature, which is the temperature of dry air having the same density as that considered. Normally it is higher than the real one by fractions of a degree or so. In this paper, it will be used in this convention.

It is expected that the convective currents are proportional to the difference between the external and the internal temperature $T_{\text{ext}} - T_{\text{int}}$, and so, when the outside temperature is very close to that of the cave, they cease. In fact, original measurements made with sonic anemometers and an external meteorological station outside do not match, if not in first approximation, the classical barometric plus convective model. The measurements showed that, in addition to the driving forces described above, there are other hidden terms.

2. Lapse rates

The main parameter here considered is the temperature change with altitude (lapse rate). A particle of air that moves vertically is subject to transformations for which can be more or less dense than the surrounding air, and then can be forced back, or to stay where it is (in equilibrium atmosphere), or forced to continue its rising. In air that is both dry and in equilibrium the lapse rate is $-9.7^\circ\text{C}/\text{km}$ ("dry adiabatic gradient"). In a humid atmosphere the lapse rate changes. When an air parcel rises and cools, a part of its water vapor condenses, releasing the evaporation, which then reduces cooling. In typical karst condition it becomes around $-4/-6^\circ\text{C}/\text{km}$. Another important lapse rate for the caves is that which

describes the heating of water in dissipative flow in a thermally insulated conduit, it applies $-2.34^\circ\text{C}/\text{km}$ [Badino, 2010].

In caves with great vertical development are mixed water and air flows and in fact typical gradients [Badino, 2010] of the great alpine caves are between -3 and $-4^\circ\text{C}/\text{km}$.

There are two non-trivial consequences: the two fluids are never in equilibrium, so that the system can never be at maximum entropy, and it follows that the air, on average, yields heat to the water. In fact, the water *subtracts* energy from caves, because it enters with a lower energy content than at exit.

On average, the atmosphere has a lapse rate of $-6.5^\circ\text{C}/\text{km}$ (International Standard Atmosphere). Reality is more complex, because air masses are not always in equilibrium: cold air can immobilize under a hotter mass, creating lapse rate inversion especially in winter. In other cases, the lapse rate is almost zero, or may vary considerably with the altitude.

Worldwide there are about 800 "sounding" stations that every day at 00 and 12 launch weather balloons that rise up to about 30 km altitude. The data sent to the ground are rapidly available to those for weather forecasts and can be found on the Internet (<http://weather.uwyo.edu/upperair/sounding.html>, accessed 09 May 2017).

These data show that in an alpine environment during summer the G_A lapse rate is between -9 and $-4^\circ\text{C}/\text{km}$, while in winter from -10 to over $+5^\circ\text{C}/\text{km}$.

3. The driving pressure

The calculation will be developed in this way;

- 1) To determine how the external pressure varies with altitude, with different lapse rates;
- 2) To determine how the pressure profile in the underground atmosphere;
- 3) To connect the two atmospheres by two extreme entrances;
- 4) To calculate the driving pressure at the entrances.

Definitions for all terms and units can be found in Table A.

The term G_A will be the external lapse rate, but now using the convention to eliminate the negative sign.

With this convention, the temperature with height z , is $T(z)=T_{A0} - G_A z$. It follows that the pressure varies as

$$\frac{dP}{P} = -\frac{M_{mol}g}{R(T_{A0} - G_A z)} dz$$

With solution:

$$P(z) = P_{A0} \left(1 - \frac{G_A z}{T_{A0}} \right)^s$$

There appears a dimensionless exponent s , which depends on the thermodynamic transformation performed by the air parcel when it moves vertically. That is

$$\begin{cases} s_{da} = \frac{M_{mol}g}{RG} = \frac{c_p}{R} = 3.5 \rightarrow \text{dry air} \\ s_{ISA} = s_{da} \left(\frac{G_{da}}{G_{ISA}} \right) = 3.5 \times \left(\frac{9.7}{6.5} \right) \approx 5.22 \rightarrow \text{in ISA} \\ s_c = s_{da} \left(\frac{G_{da}}{G_c} \right) = 3.5 \times \left(\frac{9.7}{3.5} \right) \approx 9.70 \rightarrow \text{incaves} \end{cases}$$

In the following it will be used the development:

$$(1-x)^n \approx 1 - nx + \frac{n(n-1)}{2} x^2$$

With $x \ll 1$, stopping to x or to x^2 for first and second order approximation. At first, the $P(z)$ becomes:

$$P(z) \approx P_{A0} \left(1 - s_A \frac{G_A z}{T_{A0}} \right)$$

In fact, this is the hydrostatic approximation (constant air density), with an error smaller than 1%, but it is easy to see that it is insufficient: the pressure differences that move even violent air currents (5 m/s) are of the order of 100 Pa, which is one-thousandth of the atmospheric pressure on the ground. So, it is necessary to go to the second approximation, but this first allows a qualitative analysis of the terms involved.

Figure 1 illustrates these parameters on a graph $P(z)$. The cave is encased in $h > z > h+H$.

Figure 2 shows the seasonal airflows with very large upper entrance (internal and external pressure are equal), and the low one instead acts as the bottleneck of the system flow [Badino, 1995].

In A there is a sudden drop in pressure at the lower entrance, causing an exiting airflow. The case C is winter and the B for an intermediate season, with no airflows.

The result is quite surprising because it appears that the convective circulation depends on the gradient of the curve $P(z)$ and not directly from the external and internal temperature differences.

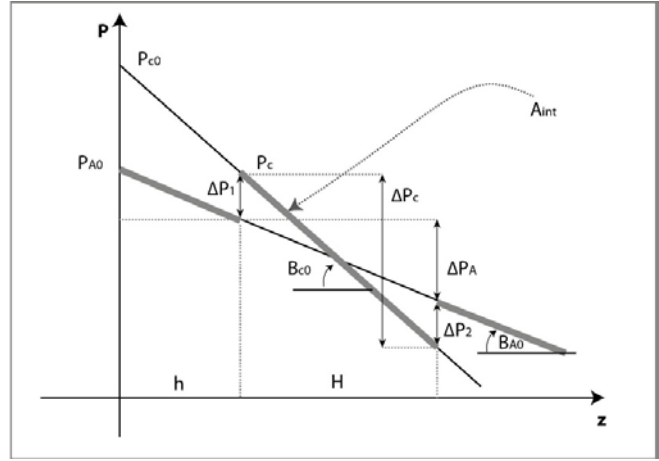


Figure 1. Internal and external atmospheres and parameters

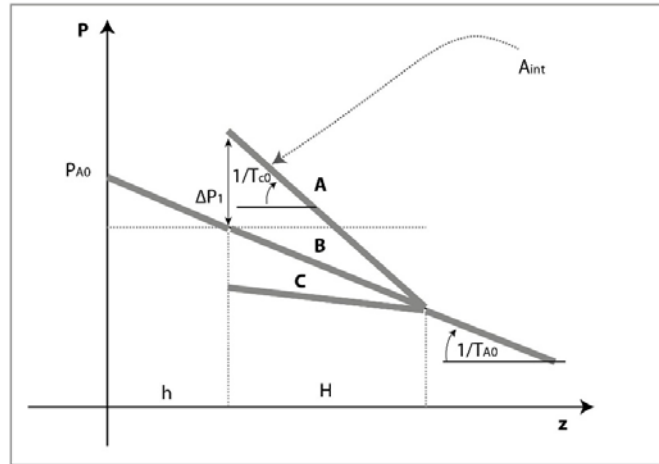


Figure 2. Airflow in different seasons

4. Second-order solutions: new driving pressures

After the previous qualitative analysis of the process, it possible to develop the calculation of the two atmospheres, external and internal.

Assuming that the regulating bottleneck is at the lower entrance, the exact solution is:

$$\Delta P_1 = P_{A0} \left(\frac{K_1 - K_2}{K_3} \right)$$

where:

$$\begin{cases} K_1 = \left(1 - \frac{G_c}{T_{c0}} h \right)^{s_c} \left(1 - \frac{G_A}{T_{A0}} (h+H) \right)^{s_A} \\ K_2 = \left(1 - \frac{G_A}{T_{A0}} z \right)^{s_A} \left(1 - \frac{G_c}{T_{c0}} (h+H) \right)^{s_c} \\ K_3 = \left(1 - \frac{G_c}{T_{c0}} (h+H) \right)^{s_c} \end{cases}$$

It is necessary to develop each term at the second-order. The calculation is very laborious, but it gives a simple form:

$$\Delta P_1 = \frac{\rho_{A0} g H}{T_{c0}} \left[(T_{A0} - T_{c0}) \left(1 - \frac{h}{L_{c0}} \right)^{s_A} + \frac{(H + 2h)}{2} (G_c - G_A) \right]$$

The first term in brackets is the classic, hydrostatic, approximation, but finally it has added a term that depends on the thermal gradient differences.

It is possible to call it “gradient convective circulation”.

In fact, if the cave has a significant volume, a temperature change at ground provokes a general variation of atmosphere volume. This, in turn, causes a pressure change in altitude, even with constant pressure P_{A0} . Such a temperature change causes barometric flows. In fact, by making a partial derivation of the function $P(z)$ gives, with constant pressure P_{A0} :

$$\frac{dP(z)}{dt} = P_{A0} s \frac{G_A z}{T_{A0}^2} \left(1 - \frac{G_A}{T_{A0}} z \right)^{s-1} \left(\frac{\partial T_{A0}}{\partial t} \right)$$

Then a change of the external temperature, corresponds necessarily to a phase of barometric air movement into the cave, although $dP_{A0}=0$, because the external atmosphere in front of the cave swells ($dT_{A0}>0$) or contracts ($dT_{A0}<0$) by sending air masses above or below the entrance. It is easy to show that this term has, for alpine caves, a weight comparable to that of the classical barometric changes.

This implies, for example, that in the morning the caves tend to blow, and to swallow air in the evening.

Table 1. This describes all symbols used and their units.

Symbol	Meaning	Dimensions
z	altitude	km
h	lower entrance altitude	km
H	cave vertical development	km
M_{mol}	air molar mass	g/mol
R	ideal gases constant	J/K
P_{A0}	external pressure at z=0	Pa
G_A	external lapse rate	K/km or °C/km
G_c	internal lapse rate	K/km
g	gravitational acceleration	m/s ²
P(z)	pressure at z	Pa
P_c	cave pressure at z=h	Pa
B_{A0}	external pressure gradient	Pa/km
B_{c0}	internal pressure gradient	Pa/km
T(z)	temperature at z	K or °C
T_{A0}	external temperature at z=0	K or °C
T_{c0}	cave temperature at z=0	K or °C
T_c	cave temperature at z=h	K or °C
s	polytropic index	adimensional
s_A	external polytropic index	adimensional
s_c	internal polytropic index	adimensional
ΔP_1	$P_{ext} - P_{int}$ at z=h (lower entrance)	Pa
ΔP_2	$P_{ext} - P_{int}$ at z=h+H (higher entrance)	Pa
ΔP_{ic}	total driving pressure	Pa

It is possible to call it “thermal barometric circulation”, pointing out that the usual barometric circulation is the air pressure measured at the cave entrance and not at z=0.

5. Convection neutral temperature

It is laborious but easy to develop the exact solution of $P(z)$ and obtain the T_{A0} temperature values at which the convection stops calling it X_{A0} . The solution is:

$$X_{A0} = G_A \left[h + \frac{H}{1 - \left(1 - \frac{G_c H}{T_{c0} - G_c h} \right)^{\frac{s_c}{s_A}}} \right]$$

Which gives, at the second-order:

$$X_A(h) = T_c + \frac{1}{2} (G_A - G_c) H$$

It has been shown above that summer lapse rates are usually between 9 e 4 °C/km:

$$T_c + 0.25H < X_A(h) < T_c + 1.25H$$

And during winter between 10 up to -5 °C/km:

$$T_c - 8.25H < X_A(h) < T_c + 1.75H$$

It shows that in the case of caves with large vertical development the temperature correction, especially winter and night, can be of several degrees centigrade. It is therefore not true that convective flows cease when $T_{\text{ext}} = T_{\text{int}}$.

6. Conclusions

The traditional description of convective circulations was seriously flawed from the physical point of view, but it seemed a reasonable approximation in comparison with the typical uncertainties involved in these problems.

A more accurate calculation has shown that the convective circulations are linked to pressure profiles of internal and

external atmospheres, with a key role played by lapse rates. It was also found that the variations of the outside temperature, causing a variation of the volume of the atmosphere, induce pressure variations that cause barometric circulations also with constant sea level pressure.

The experimental verification of this more complete model appears to be very difficult, but probably will allow understanding the airflow phenomenology of special caves such as those of Mars.

References

Badino G., 2010. Underground Meteorology, What's the weather underground?, *Acta Carsologica*, vol. **39/3**

Badino, G., 1995. "Fisica del Clima Sotterraneo", *Memorie IIS*, 7, II, pp. 137

A theoretical approach to the estimation of local Entropy production in caves

Giovanni Badino

Affiliation: Dip. Fisica, Università di Torino, Ass. Geografica La Venta

Abstract

The definition of the parameters to estimate the sensitivity of a cave, or some part, to external perturbation is not easy. It is used the concept of “cave energy”, but the constancy of the cave average temperature indicates that the average deposition of energy underground always equals zero. Here is theoretically introduced the concept of “local entropy production” in cave, deriving then the “Deconstructive Power”, a local “sensitivity” parameter that seems to be less ambiguous than those used until now.

Keywords: cave sensitivity, antropic impact, caves carrying capacity, caves energy, caves entropy production, maximum entropy

“You should call it entropy, for two reasons. In the first (...).

In the second place, and more important, nobody knows what entropy really is, so in a debate you will always have the advantage.”

J. von Neumann to C. Shannon, 1949

1. Introduction

The daily and seasonal temperature ranges, in the external environment, are heavily dependent on geographical location, which establishes the climatic type of a given area. Following, the focus will be on the average monthly temperature, assuming that it varies along the year, with a sinusoidal law:

$$T_{ext} = T_{ave} + T_A \sin(\omega t)$$

Where $\omega=2\pi/\tau$, T_{ave} is the local average temperature and τ is the period, which will be assume to equal to one year. The amplitude of the sine wave T_A is, therefore, half of the difference between the mean temperature of the warmest month and that of the coldest one.

The T_A amplitude depends on the climatic types, changing from 0.8 of Singapore to 18 of Ulan Bator. In Europe are around 6-8 °C [www.worldclimate.com].

The subterranean temperature range is always a small fraction of the external one; the local reduction factor depends on the thermal insulation, which depends on morphology, being subject to significant changes even a few meters range.

2. Inflowing energy

Cave systems are not isolated from the external environment because flows of water, air and heat conduction through the rock release thermal energy to the underground system.

The direct heat flow through the rock, either by pure conduction or by convection of interstitial water is, in general, very low and important only in the case of quite superficial systems, limited to scores of metres depths.

It should be distinguished [Badino, 2017] a more shallow region where the temperature varies with that of the inflowing fluids (Heterothermic Layer) and a deeper region in which the fluids have attained the equilibrium temperature (Neutral

Layer). The energy is primarily added or subtracted to caves by these fluid flows, which in general are not in equilibrium with the rock. It is useful to show some preliminary observation. The first, trivial, is that the cave internal energy depends on its average temperature, quite constant, which indicates that the sum of the energy flows into the system, averaged on long time scale, is zero.

$$\int_0^\infty \sum_j F_j(t, T_0) dt = 0$$

The average energy flow in almost all underground environments (including caves), have to equal zero. The observation seems paradoxical, given that a very useful parameter for assessing the cave sensitivity is its “energy level” [Heaton, 1986]. This point will be discussed in detail later on.

It is easy to make a simple “black blox” model, considering a cave with C_c heat capacity and temperature T_c . The inflowing energy comes from water and air, heat conduction through the rock, salts solution enthalpies of and possibly other characteristics of the cave, such as oxidation of organic materials, geothermal energy [Badino, 2005] and so on. Yet, the two main important terms are those of water and air. Being $F_a(t)$ and $F_w(t)$ the air and water flows (in kg/s) with respectively specific heat capacity C_a and C_w (in J/kg/K), and temperature $T_a(t)$ and $T_w(t)$.

The thermal energy deposited in C_c by a flow F_w at temperature T_w in a time Δt causes a change of the system temperature given by

$$\Delta T_c = \frac{F_w(t)}{C_c} [T_w(t) - T_c] \Delta t$$

The temperature of the incoming flow varies along the year. As shown above, the temperature system is constant T_c , which means that its value is such that the heat exchange between the outside and the cave on average is zero.

It is possible to estimate the relative weight of the flows of air and water, at least in a first approximation. The airflows in the typical Alpine caves are of the order 10 m³/s per square kilometre of karst (roughly 10 kg/s/km²), that is a thermal capacity flow of about 10⁴ J/s/K/km².

The typical water infiltration intensity is of the order of 1000 mm/a (30 kg/s/km²), which means a thermal capacity flow of 10⁵ J/s/K/km², an order of magnitude greater the airflow thermal capacity. Including in the estimation the presence of water vapour, which in many conditions can dominate the air enthalpy content, the water flow makes as the main term in the previous equation. It is possible to conclude that, at least in temperate climates, incoming water establishes the cave temperatures.

To conclude, it is easy to estimate that the power associated with the dissolution of the calcium carbonate is negligible. The energy required to dissolve it is -28.8 ± 0.3 kJ/mol (288 kJ/kg), then it results a required power of a fraction of watt.

3. The cave thermal capacity

Considering as “underground system” a rock body, its thermal capacity is simply its mass multiplied by the rock specific heat capacity. However, for a cave, an absence of rock, the problem is complex.

The energy content of external fluids is released or subtracted from the fluids (air and water) contained into the cave and from the rock surfaces exposed. Unfortunately, it is not possible defining uniquely this second, main term, since the rock depth involved in the thermal exchange is proportional to the square root of its duration.

In addition, the incoming fluids enter in thermal contact only with certain parts of the cave. Water flows along the lower parts of conduits, but also the airflows behave in a similar way. A rising air particle tends to cool (with a wet-adiabatic gradient) and then to flow like water in the lower parts of conduits, while when it descends its temperature increase thus tends to remain in contact with ceiling. These processes are mainly seasonal –as the global convective movements underground–, therefore create local thermal sedimentations, which are very common and easy to measure. They play an essential role in the cave ecology and in the underground glaciers formation, but heavily complicate “the cave thermal capacity” estimations.

Under these conditions, it is easy to solve [Badino, 2010] the Fourier equation for the driving, obtaining that the depth of the heat exchange in compact rock is twenty centimetres for the daily thermal exchanges, and few meters for annual exchanges.

This means that we can safely assume that for annual thermal disturbances of the cave thermal capacities is essentially that of the first few meters of rock surrounding it. This term is always much higher than the thermal capacity of the air and water in cave conduits; while these fluids can damp sudden fluctuations of temperature of the external inputs.

4. Internal energy and fluxes

The idea of “cave energy” can refer to its total energy U , in [J] or to its local density [Jm⁻³]. Or it may be considered the energy flow through the cave in the time unit, that is a power [W], which in turn can be considered in each subterranean region, thus in [Wm⁻³].

Given the stationarity of subterranean environmental conditions over time, the most important term is not its total energy content U , which remains constant, but the inflows and outflows, that is the power applied to the system from external environment.

The energy flows that infiltrate into the ground have roughly the outside temperatures, so it behaves like a sinusoidal wave around the value T_{ave} , both during the day and along the year.

Meteorological data most significant for the present discussion are the monthly average temperature, easily available [www.worldclimate.com]; the term T_A , amplitude of the sinusoidal wave, is equal to half of the total thermal excursion between the monthly average during hot and cold seasons.

To simplify calculations a square wave, and not a sinusoidal wave, will be used, assuming that the temperature oscillates between $(T_{ave} - T_A)$ during cold season and $(T_{ave} + T_A)$ during the hot season. In the numerical estimations, to maintain the energy flow in the individual periods equal to the sinusoidal case, it should be actually considered a square wave amplitude reduced by a factor $2/\pi \approx 0.64$.

This approach allows estimating, quantitatively, the power released to a cave or some underground region.

The thermal capacity of air is around 10³ J/kg/K, and then the average energy released during the hot season to a cave colder of ΔT by one kilogram of air is 10³ ΔT . In fact, an important energy released may be the latent heat of evaporation if the air-cooling causes condensation, but it is strongly variable and can be estimate as a correction.

It is then possible to estimate the typical power of an alpine cave. As seen above, typical fluid fluxes on a square kilometre are 10 kg/s of air and 30 kg/s of infiltrated water. Taking $T_A = 8$ °C, then an average temperature difference of 5 °C can be considered, including the square wave correction. It results that the power released by air is 50 kW/km² and by water around 600 kW. The air term is underestimated because it has been ignored the condensation term, nevertheless the water term dominates and the order of magnitude of power released to a similar cave results to be 0.1-1 MW/km².

It is interesting to consider the extreme case of Subterranean River of Sabang (Philippines). It is a cave some 33 km of length, essentially horizontal, with 25 km² of surface with an average fresh water flow of 1000 kg/s, seawater flow during tides of 800 kg/s, airflow around 100 m³/s and a rich biological activity.

The number of Salanganas (swallows) and bats can be estimated in some tenth of thousands, with an energy release (mainly outside, during hunting flights) is probably around some GJ/d, that is a negligible 10⁴ W on average.

The region is on the Intertropical Convergence Zone and its $T_A = 1.6$ (www.worldclimate.com). Its power is 100 kW in air, 8 MW for water; it is easy to show that the biological part is negligible.

The cave is one of the most powerful of the World; nevertheless, the power density per square kilometre is similar to the alpine caves.

The scenario changes in the case of very small caves, with entrances that do not permit significant convective airflows: it is the case, for example, of cave with prehistoric paintings. The water fluxes can be negligible and the energy flow is due to barometric airflow [Lewis, 1992]. Each time that the external pressure P_A changes, it appears an excess or a deficiency ΔV of cave air volume V_c given by

$$\Delta V = V_c \left(\frac{\Delta P}{P_A} \right)$$

The atmospheric pressure is obviously constant on a long period, but the total entering flux depends on the sum of atmospheric pressure decreases (i.e., half of the total variation sum)

$$\frac{1}{2} \sum_j \frac{|\Delta P_j|}{P_A} = 0.01 \text{ [d}^{-1}\text{]}$$

This means that in about 100 days, the external air completely replaces the internal air volume if the inflowing flow is uniformly mixed –in fact, a very strong hypothesis–.

The airflow intensity depends therefore on the cave volume, and have then to be studied in each case, but considering a typical volume of 10^4 m^3 , it results a flux of $100 \text{ m}^3/\text{d}$ and the power flow becomes some watts or less. Even with this trivially rough estimations, it becomes obvious that the entry of a person in a cave of this type, with its typical energy release of 100-200 W (neglecting water vapour, carbon dioxide and so on) has an impact far from zero. It is not surprising that painted caves are very small and usually have been found without significant entrances.

In conclusion, it is possible to state that the average maximum power released from the external environment to a cave system is around $0.1\text{-}1 \text{ MW}/\text{km}^2$, but can decrease to $1 \text{ kW}/\text{km}^2$ in the case of isolated caves and probably increase to scores of MW/km^2 for tropical *ponores*. Then, there is a factor 10^4 between the maximum and minimum power caves. For comparison, the Sun power deposition on Earth [Barry, 2010] has a maximum around $320 \text{ kW}/\text{m}^2$ in the regions of Sahara and a minimum of $50 \text{ kW}/\text{m}_2$ in the North Atlantic, a mere factor 6 between the two. The energetic variability of underground world is then by far larger than outside.

The entering fluids release these energies to the epidermal part of caves, but a similar –and more important– discussion may be done to the inner part, considering local fluid flows and local thermal disequilibria repeating the same calculations with corresponding terms.

At any rate, the total average energy flow on a long period have to be zero. Therefore, the previous calculations, concentrated on the average maximum energy depositions, have a doubtful physical meaning: do it correspond to a maximum impact of external environment onto the cave?

Does exist a more precise parameter to characterize the “environment sensitivity” to surrounding impact?

It is necessary to move to the Second Law of Thermodynamics.

5. An Entropy approach

The Entropy production is a key concept in ecological thermodynamics studies [Swanson, 1988], nevertheless its estimation for external system is extremely complex [Ozawa, 2004] and have received little quantitative verification [Meysman, 2010]. Caves are much simpler and it is possible to simplify the approach.

An ideal cave C_1 should be considered, with entering fluids as described above, but remaining unchanged, with constant temperature.

The thermal exchanges with outside, as outlined above, creates an Entropy variation of the system Universe+Cave. In particular, there is a release of thermal energy ΔQ_H from U at temperature $T+\Delta T$ to the cave at temperature T and an energy subtraction $-\Delta Q_L$ from U at temperature $T-\Delta T$ to the cave at T.

If the energy transfer would be reversibly done, for instance with an Ideal Carnot engine, the Entropy variation either of U and C_1 would be unchanged, because some work $L=\Delta Q_H-\Delta Q_L$ from U at temperature $T+\Delta T$ from U at temperature $T+\Delta T$ –given by Carnot cycle efficiency–.

In fact, no work is performed in this unchangeable cave, therefore $\Delta Q_H=\Delta Q_L$ (then ΔQ from here on), the process is irreversible and the Entropy increases by a factor L/T , that is

$$\Delta S_U = -\frac{\Delta Q}{T+\Delta T} + \frac{\Delta Q}{T-\Delta T} \approx 2\Delta Q \frac{\Delta T}{T^2}$$

The state of C_1 is unchanged then, being the Entropy a function of state, the cave entropy is constant, it has been the Universe entropy which has decreased during hot season (irreversible fluid cooling) and increased by a smaller factor during the cold season (irreversible fluid heating); the total increase is

$$\Delta S_U = 2\Delta Q \frac{\Delta T}{T^2}$$

The $2\Delta T$ is the total seasonal temperature range, ΔQ the amplitude of seasonal energy deposition and T the cave temperature, in kelvin. By the way, the Entropy increase is proportional to ΔQ , which shows that the approach to classify caves in terms of “average maximum energy absorbed” was reasonable when applying the Second Law of Thermodynamics.

Until now the discussion has involved an Ideal Cave C_1 , unchangeable –performing a closed thermodynamic cycle–, and moves to the Universe the entropic impact of inflowing fluids. This is unsatisfactory: real caves have small but not-zero temperature ranges, show large local non-homogeneities, their thermodynamics cycles are barely open and they might evolve –degrade?..–, exactly because are crossed by Universe fragments (air, water, cavers...), which all release energy.

6. Ideal and Real Caves

It is possible to consider a Real Cave C_R , with many different ($j=1, 2,..n$) local temperature ranges ΔT_{I_j} and energy deposition ΔQ_{I_j} . The described thermal exchange process U- C_1 can be divided in two steps:

1) An energy exchange between Universe and Cave R, $U-C_R$, the two in irreversible cycles;

2) An ideal energy exchange between C_R and C_I (which is in closed cycle, $dT=0, dS=0$), C_R-C_I .

In the first step, the Universe Entropy variation is smaller than in the ideal case $U-C_I$, and then the step 2 concludes the “fall” to the ideal situation.

This means that the second step allows comparing the difference between the real and the ideal cave or, in other words, that the entropy increase of Cave R measures its degradation in comparison with ideal situation. Finally, we can identify Cave R with the real cave and its Entropy increase as a measure of its degradation (or “evolution”?). The most precise term it should be “deconstruction”, to indicate irreversibility and, probably, local suppression of complex formation like speleothems, large crystals or, on Earth, macromolecules.

$$\Delta S_{Lj} = 2\Delta Q_{Lj} \frac{\Delta T_{Lj}}{T_{Lj}^2}$$

The various terms refer now to local parameters, then the equation gives the local Entropy increase for a ΔQ_{Lj} energy inflow. The index Lj for T can be omitted because the absolute temperature of caves is almost the same everywhere in the World, whereas the other terms are much more uncertain. The equation modified in terms of fluxes, using the inflowing power W_{Lj} becomes

$$\frac{\Delta S_{Lj}}{dt} = 2W_{Lj} \frac{\Delta T_{Lj}}{T_{Lj}^2}$$

The Entropy increase ΔS gives a measure of irreversibility of process, giving in this case the gap between the real and ideal conditions of a cave.

7. The Deconstructive Power

Another, more friendly, measure of irreversibility is the term $T\Delta S$, which has the meaning of “energy degraded by the irreversibility of process”, or “work lost due to the irreversibility” in [J], as previously seen.

Returning to fluxes and using the dQ_{Lj}/dt , that is the power flow to the cave region j , it is possible to pass from the local

deposited energy to the applied power ΔW_{Lj} ; writing the $T\Delta S$ flux in [W], it should be a measure of “irreversible energy released locally”, or “Deconstructive Power” D_w :

$$D_w = T \frac{\Delta S_{Lj}}{dt} = W_{Lj} \frac{2\Delta T_{Lj}}{T_{Lj}}$$

That is

$$[\text{dec. power}] = [\text{power}] \frac{[\text{temp. range}]}{[\text{temp.}]}$$

This parameter can be fundamental, but depends on the cave absolute temperature (almost everywhere in the range 270-300 K) and unfortunately on the local power fluxes (usually unknown) and local temperature range (seldom measured). So, its estimation has to be done in future, but it is well known for the experienced caver that speleothems, crystals and so on are usually associated with “more stable” cave parts, whilst along the water and air main streams are more uncommon.

It should be given a rough estimation from original data of the Rio Martino cave (Western Alps, Italy) a sub-horizontal resurgence 2.9 km long; the regional cavers association (AGSP) installed an internal meteorological station in 2004. Average water flow is around 60 kg/s, airflow around 2 kg/s. The temperature range near the station is around 1-2 °C. It is then possible to estimate in 3-500 kW the power flux involved into the cave. It results a D_w around 1.5 kW.

The graph shows the temperature variation due to the visit of a big group of cavers (with carbide lamps). The total energy released was 140 MJ during two hours, an average release of 20 kW. The ΔT_{Lj} was measured in 0.4 °C. The D_w is then 25 W, largely smaller than the previous. Is it possible to infer that the visit impact is negligible? These data are too rough and not sufficiently oriented to the local situation, but it is possible to presume that the approach is interesting.

To find a meaning of Deconstructive Power, it is possible to extend the approach outside. It is obvious that the external energy budget is completely different from the internal one, which have been estimated above with a dramatic simplification. Nevertheless, climatic data are easily accessible (www.worldclimate.com and [insolation from www.geocoops.com](http://www.geocoops.com))

Table 1. Environmental data and deconstructive power along North and South America.

	Lat	Tmed	2TA	Ins. [Wm ⁻²]	Dw		Lat	Tmed	2TA	Ins. [Wm ⁻²]	Dw
Sachs Harb	72	-14,2	36,1	100	14,0	Manaus	-3	26,6	1,5	175	0,9
Calgary	51	3,6	26,2	125	11,8	Recife	-8	25,5	2,9	200	1,9
Denver	39	10,1	23,7	200	16,7	Brasilia	-16	20,6	3,3	190	2,1
El Paso	32	17,3	21,9	250	18,9	Sao Paulo	-24	18,3	6,6	180	4,1
Torreón	25	22	13,1	250	11,1	Cordoba	-32	17,1	13,1	225	10,2
Mexico	20	16	5	220	3,8	Neuquen	-39	14,3	17,8	150	9,3
Managua	12	27,3	1	205	0,7	Rio Gallegos	-52	7,1	12	100	4,3
Bogota	5	13,9	0,9	200	0,6	Marambio	-64	-8,9	13	100	4,9

that is intriguing to see what happens considering the planet Earth as a cave.

Table A gives the external Deconstructive Power value estimated along the central parts of North and South America, including Arctic and Antarctic locations. As expected, the D_w reach a minimum in the most humid and equatorial climates (is the tropical rainforest the “Cave Earth” speleothem?..) and maximum in desert regions.

8. Conclusions

The D_w term (TΔS), estimated for local transformations underground, has many interesting characteristics:

- 1) It is proportional to the “energy released” by flowing fluids, then is consistent with more traditional approaches in cave sensitivity estimations;
- 2) It is always positive, both for water and air fluxes, which have different behaviours underground;
- 3) It includes the internal local temperature range, which is a fundamental parameter to estimate local thermal insulation;
- 4) It is proportional to the irreversibility of local thermal processes.

For these reasons, it seems useful to estimate this parameter D_w and verify its relation with the local “cave sensitivity”.

Above all, it will be interesting to measure it accurately both in different caves and in different regions of the same cave, to study what are the morphological differences corresponding to different “evolution powers”: presence of complex structures and so on.

Improving its definition, it can become an extremely useful parameter to estimate external environment sensitivity and ecology.

References

- Badino G., 2005. “Underground Drainage Systems and Geothermal Flux”. *Acta Carsologica*, **34/2**, 1, 277-316
- Badino G., 2010. “Underground Meteorology, What’s the Weather Underground?”. *Acta Carsologica*, vol. **39/3**
- Barry R. & Chorley R., 2010. *Atmosphere, Weather and Climate*. Routledge, 536 ppgg.
- Heaton T., 1986. A Tremendous Range in Energy Environments on Earth. *NSS News*, **301-4**
- Lewis, W., 1992. Atmospheric Pressure Changes and Cave Airflow. *NSS Bulletin*, 53
- Meysman F, Bruers S., 2010. Ecosystem Functioning and Maximum Entropy Production: a Quantitative Test of Hypotheses. *Philos. Trans. R. Soc. Lond. B Bio.l Sci.*; **365**(1545): 1405–1416.
- Ozawa, H., Ohmura A., Lorenz R., and Pujol T., 2003: The Second Law of Thermodynamics and the Global Climate System: a Review of the Maximum Entropy Production Principle. *Rev. Geophys.*, **41**, 1018
- Swenson R., 1988. Emergence and the Principle of Maximum Entropy Production. *Proceedings of the 32nd Annual Meeting of the International Society for General Systems Research*, **32**.

(Abstract) **Mapping Carbonate And Evaporite Brackish Aquifers, Texas, USA**

Andrea Croskrey

Affiliation: UT Grotto, USA

Abstract

Impacted by significant droughts, Texas has sought resilient water supplies. One option pursued is desalination of brackish groundwater. As of 2012, 34 municipal water supply plants had the combined brackish groundwater desalination design capacity to produce 277,000 cubic meters per day (m^3/day) of treated water.

Brackish groundwater is more saline than fresh water and less saline than seawater, with total dissolved solids ranging from 1,000 to 10,000 milligrams per liter (mg/L). In 2003, a statewide assessment estimated Texas aquifers contained 3,300 cubic kilometers (km^3) of brackish water. Karst aquifers account for approximately 530 km^3 of that volume.

The Brackish Resource Aquifer Characterization System is mapping brackish groundwater on a regional scale to understand the location, quantity, and quality of the resource. Since 2012, the team and contractors have completed 8 studies. Two of these, the Rustler and Blaine aquifers, are karst aquifers. For these studies, thousands of well locations and stratigraphic, lithologic, and water quality values were entered and managed in a database. Using GIS, the subsurface extent and depth of the aquifer is interpolated from outcrop lines and subsurface stratigraphic picks. This same process is used to model the storage space (porosity) in the aquifer. Usually there are few measured water quality samples for the brackish aquifers. Groundwater salinity is calculated from geophysical well logs with resistivity measurements using the correlation between total dissolved solids and electrical conductance. For areas without measured water quality, these calculated water quality values were used to map the extent of salinity ranges.

Karst aquifers require special consideration using this methodology. The presence of bicarbonate skews the correlation between total dissolved solids and specific conductance so corrections and special correlation values are applied. Additionally, secondary porosity development can change abruptly over a short distance. This makes it difficult to use interpolation methods designed to create gradational surfaces. In such cases, it could be more appropriate to use the Inverse Distance Weighted algorithm for interpolation instead of the Topo to Raster method. The regional study of the Blaine Aquifer supported the statewide estimate from 2003 that the aquifer contained 23-24 km^3 of brackish groundwater. The regional study of the Rustler Aquifer was able to identify and map the three water bearing units of the aquifer instead of assuming the entire Rustler Formation was water bearing. This resulted in reducing the brackish groundwater estimate from 45 km^3 to 23 km^3 for the Rustler Aquifer.

Chemical Analysis Of Underground Waters In Štefanová Cave (Central Slovakia) And Its Use For Finding Connections With Cave Slobody

Pavel Herich^{1,2}, David Havlíček³, Kateřina Havlíčková⁴

Affiliation: ¹ Slovak Speleological Society, Demänovská Valley Caving Club, Ploštín 91, 03101, Liptovský Mikuláš, Slovakia (herich@speleodd.sk)

² Slovak Caves Administration, Hodžova 11, 03101 Liptovský Mikuláš, Slovakia (herich@speleodd.sk)

³ Dept. of Inorg. Chem., Faculty of Science, Charles University, Albertov 6, 128 43 Praha 2, Czech Republic (havlicek@natur.cuni.cz)

⁴ Forestry and Game Management Research Institute, Strnady 136, 252 02 Jíloviště, Czech Republic (havlickova@vulhm.cz)

Demänovská valley and its caves are considered the most representative and many times in the worlds scientific literature mentioned example of contacting, allogeneic karst of monoclinical ridges uplands (Bella et al. 2014). Within the axis of the area are two biggest streams flowing from main ridge of the Low Tatras (Nízke Tatry) with the highest peak Chopok (2024 m a.s.l.). They concentrate water in parallel glacier valleys and continuing into carbonate area, where at the 15 km² area is created (during Quaternary period 300 m deep) the Canyon of Demänová, where they finally join. Several autochthonous streams here create side valleys with diverse degree of development. Carbonates consists of two geological units, Middle Triassic (Anis) limestones and dolomites of Fatrikum, where the most caves are created (black Gutenstein carbonates with rich crinoid layers under grey Ramsau dolomites), and simillarly built part of Hronikum.

About 300 caves have been registered in the Demänová valley, with a total amount of 70 kms of cave passages. The largest cave system of Slovak Republic – Demänová Cave System (DCS) reached 41,5 km of length with denivelation (vertical range) 196 m at the beginning of 2017, this is now at 87th place in the worlds longest caves list.

Serious and intensive speleological surveying and research work began in the early 20th century and lead eventually into a breakthrough discovery of famous Temple of Liberty in 1921 (For a few decades it was known as the Cave of Liberty). But even before that, caves in Demänová valley were known, as can be documented by archeological finds in caves. The first written item appeared in 1299. Until now, the exploration was mainly led by amateur speleologists, who had also participated in many research activities of some scientific organisations. In 1952 a new cave was discovered named Damänovská Cave of Peace, and in 1987 was connected into a single cave system with a total polygonal length of 20 km (plus another further 10 km is unsurveyed). Smaller discoveries followed until 2007, when a third, big discovery of Demänová caves had begun (Holík, Herich 2012). Štefanová cave now reaches 17 km and still continues. It has come close to DCS; only 55 m away through an unknown siphon passage that is a connection between two of the largest cave systems of Carpathian Mountains.

The descending vadose passages of Štefanová gradually collects waters from dozens of bigger and smaller rifts of the two allochthonous, intermittent rivers Demänovka and mainly the Zadná voda. Underground waters of Zadná voda cross pyramidal carbonatic peak called Stodôlka in west – east direction, perpendicular to the axis of valley, and three times

(20 – 40 m under surface creek bed of Demänovka) cross the second valley, where it gains some water from several rifts of Demänovka. There is one main collector, generally a 15 – 20 m wide continuing horizontal corridor with a planed ceiling but in one part it is 35 m wide, which continues to Jazerný dóm (Lake Hall). A 20 m deep sump which still continues and water reappears according to tracing experiments after two hours in DCS – Infernal Dome of Temple of Liberty (Pekelný dóm).

Accurate chemical analysis of underground waters can be useful tool for obtaining different information about studied cave system. If the samples are collected in approximate same time and during constant weather, when discharge does not change and the time needed for flowing water from one sampling place to another is (up to several hours), we can assume, that chemical composition is changed significantly only with the mixing of waters with different compositions from different origins. The results are more useful than results from classical tracing experiments and with less effort for cavers conducting the work in the caves.

Much more work, of course is performed in the laboratory.

The use of this method can be demonstrated on the simple example: Let's have two sources and one known spring. We would like to know, if both water sources are filling the same spring or not. If yes, the chemical composition of the spring must lie in all the indicators between the values from both sources. If we know the discharge of both sources, we can predict chemical composition of the water in the spring. If it does not fit, there must exist another unknown source of water. If we do not know the discharge of the sources, we can calculate the ratio from chemical analysis of the water in the spring.

We used this method twenty years ago when investigating Bohemia Cave in New Zealand, Mt. Owen, NW Nelson (Havlíček, Tásler 1999). But this New Zealand case was a much simpler situation. Due to very clean atmosphere (no acid rain) and all the waters originated only from carbonate rocks, it was sufficient to determine carbonate equilibria (total alkalinity) and contents of magnesium and calcium and (in some cases) iron and/or manganese. Therefore, we have supposed, that the same volume of analysis will be sufficient also for waters in Štefanová Cave. But after the evaluation it was clear, that in all the samples the “Quality Ions Balance“ was not OK, and there were some missing anions. The additional analysis of the same samples were done and we have determined significant amount of chlorides, sulfates and nitrates. The presence of nitrates and in some samples sulphates, can be due to acid rain, but the presence of chlorides is most prob-

ably caused by using sodium chloride for melting snow on the parking areas near buildings.

On the detailed map, presented on the poster, all the sampling places are marked. The size of the map do not allow us to present it in the proceedings. In Table 1 the sampling places, conductivities, temperatures, estimated water discharges and sampling times during one sampling day are presented. Table 2 represents the chemical analysis of the samples, which were done several months after collection. The iron and manganese content were mostly under the detection limit; the content of zinc was found around 0.01 mg/l in all the samples.

The conclusions following from the analysis are described in the poster, and the presumed connections are found and marked in the map. The discussion also deals with explanation of the chemical composition of the samples.

Table 1.

Sample No.	Sampling place	Conductivity [mS/cm]	Water temperature [°C]	Estimated discharge [l/s]	Sampling time
1.	Agate dome	234	4.7	?	11:57
2.	Behind the 2nd ladder	173	3.7	0.5	12:25
3.	Behind the narrow	170	3.7	0.5	12:35
4.	Under the cramps	297	5.6	2	12:55
6.	Beer fissure	222	6.1	10	15:20
7.	Beach narrow	124	4.2	3	15:40
8.	Under the Titan's dome	212	5.8	9	16:15
9.	Behind the 1st bivouac	162	2.9	0.5	16:35
11.	November room 2	209	5.3	3.5	17:45
12.	Streambed	209	5.7	20	18:25
13.	Inflow from the right	186	4.3	1	18:30
14.	Inflow from the left	169	5.2	0.1	18:35
15.	Inflow from the right	223	5.6	1	18:45
16.	Lake Hall	206	5.7	20	18:50
17.	Zadná voda (surface)	59	3.3	300	11:07
18.	Demänovka (surface)	127	3.9	50	11:18
19.	Behind the Chaos Room	229	5.9	3	12:51
20.	„Eldorado“ - waterfall	196	4.5	2	13:16
21.	„Eldorado“ - behind three shafts	194	4.8	2	13:40
22.	Dancing Rocks Dome	210	6.5	8	15:00
24.	Infernal Dome of Temple of Liberty	241	5.1	200	19:40
31.	November room - meander	164	3.5	2	18:00

References

Bella P, Haviarová D, Kováč L, Lalkovič M, Sabol M, Soják M, Struhár V, Višnovská Z, Zelinka J, 2014. Jaskyne Demänovskej doliny, Ramsarská lokalita stredohorského alogénneho krasu Západných Karpát. *Speleologia Slovaca* 4, 191

Havlíček D, Tásler R., 1999. Karst Water Chemistry in the System Bohemia Cave, Mt. Owen, New Zealand. *Book of abstracts, IVth International Meeting of Cavers in the Moravian Karst and IInd National Speleological Congress*, Jedovnice, pp. 7-10.

Holík L, Herich P., 2012. Jaskyňa Štefanová, objavy od roku 2009. *Spravodaj SSS*, 43(2), 13-24.

Table 2. Chemical analysis

Sample number	pH	T. Alk. mmol L ⁻¹	Ca ²⁺ mg L ⁻¹	K ⁺ mg L ⁻¹	Mg ²⁺ mg L ⁻¹	Na ⁺ mg L ⁻¹	Cl ⁻ mg L ⁻¹	N-NO ₃ ⁻ mg L ⁻¹	S-SO ₄ ²⁻ mg L ⁻¹	Sum		Ions Diff. % sC-sA	Quality Ions balance	Calculated corrected Conductivity µS cm ⁻¹ 25°C
										Anions µeq L ⁻¹	Cations µeq L ⁻¹			
1	7.05	1.306	30.00	0.55	9.46	1.52	1.38	0.996	15.65	2393	2355	-2	ok	244
2	7.01	1.191	20.60	0.72	6.37	4.78	9.38	1.314	3.28	1754	1778	1	ok	176
3	7.48	1.450	24.00	0.81	8.31	5.64	10.51	1.271	3.25	2039	2147	5	ok	205
4	7.57	2.986	52.20	0.24	9.20	0.75	1.43	1.127	2.24	3246	3400	5	ok	301
6	7.18	1.769	30.70	0.95	9.50	2.93	3.25	1.898	5.87	2363	2465	4	ok	233
7	7.26	1.018	17.10	0.61	5.04	2.54	1.93	1.208	2.61	1321	1394	5	ok	134
8	7.26	1.710	29.50	0.79	8.31	3.14	3.58	1.620	4.96	2236	2312	3	ok	219
9	7.34	1.101	19.70	0.82	6.11	4.68	8.02	1.243	3.32	1623	1710	5	ok	167
11	7.21	1.701	28.00	0.60	8.98	3.92	6.80	1.325	2.95	2172	2322	7	ok	215
12	7.21	1.738	30.70	0.80	8.47	3.24	3.82	1.599	4.57	2245	2390	6	ok	223
13	7.24	1.335	24.20	0.81	6.78	6.46	11.78	1.364	3.11	1958	2067	5	ok	199
14	6.99	1.301	24.40	0.69	5.85	4.32	7.34	1.346	3.00	1791	1904	6	ok	182
15	7.27	1.961	31.00	0.57	10.60	3.03	4.90	1.277	3.50	2408	2565	6	ok	235
16	7.32	1.682	29.80	0.74	8.24	2.96	3.97	1.577	4.52	2189	2312	5	ok	217
17	6.80	0.297	6.66	0.64	1.65	2.35	1.73	1.130	2.57	587	587	0	ok	64
18	6.89	0.742	13.10	0.80	5.44	3.65	6.16	1.200	3.34	1209	1280	6	ok	128
19	7.27	1.775	27.20	0.71	10.40	3.33	7.61	1.299	3.21	2282	2376	4	ok	223
20	7.26	1.368	25.80	0.68	6.21	4.84	8.38	1.381	3.22	1904	2026	6	ok	194
21	7.24	1.324	22.50	0.68	6.68	4.65	9.75	1.360	3.24	1898	1892	0	ok	188
22	7.25	1.506	26.10	0.93	8.76	2.10	1.90	2.061	6.35	2103	2138	2	ok	208
24	7.27	1.595	31.30	0.55	10.50	1.56	1.81	1.125	11.91	2469	2507	2	ok	247
31	7.24	1.400	24.10	0.82	6.65	4.27	6.87	1.175	3.60	1902	1956	3	ok	189

Geothermal Heat Flow in Caves: Modelling of Geothermal Heat Flow

Neville A. Michie, Ph.D.

Affiliation: Cave scientist, ACKMA, NSS #39726, 9 Patrick Street, Beacon Hill, NSW, Australia, 2100

Abstract

There is a flow of heat to the surface from the interior of the planet known as the geothermal flux. This flow is relatively uniform about the globe, and has a value in the order of 60 mW/m². Direct measurement of geothermal heat flow is quite difficult, involving bore drilling and logging on a considerable scale that would be inappropriate for cave studies. A site has been found where measurements of the thermodynamic parameters of cave air have been used, with the support of numerical modelling, to identify and quantify an active geothermal process in Carlsbad Caverns. The modelling is recursive, but converges rapidly to give robust solutions.

The phenomenon of geothermal flux concentration is shown. Modelling shows that Karst features interact with the geothermal flux to concentrate heat flow locally, and this interaction can control the climates in caves and the processes of speleogenesis. By using a scalar quantities approach, the several components of geothermal heat flow can be modelled and combined to give the heat flow pattern and quantitative estimates of partial and total heat transport. The modelling can be done on a PC using a spreadsheet application. The rules and methods are explained.

Examples are given of some simple cases of geothermal heat concentration and temperature distributions as well as the analysis of the chamber over Lake of the Clouds in Carlsbad Caverns, NM.

Keywords: Geothermal circulation, heat flow concentration, scalar model, Carlsbad Caverns, Carnot efficiency

1. Introduction

Geothermal heat flow in caves is quite important but is difficult to directly observe. Drilling and borehole logging is the industrial method of gathering geothermal data but it is quite unsuitable and far too costly to use in association with caves. The method that is useful is modelling. This can be an extremely complex, but for geothermal heat there is an available approach through using temperature. Where heat flow is a vector quantity, and its modelling is mathematically intricate, requiring three dimensional calculation, temperature is a scalar quantity, and the advantage of a scalar is that it can be used to calculate the state of a location as the superimposed contributions of many elements. This enables any point to be calculated from the model variables. This greatly simplifies calculation and the points can be in a chosen two dimensional plane. Much of this method has been gleaned from old texts discussing static electricity and magnetism, both of which follow the same inverse square laws.

It may be regarded as highly speculative to produce these models for caves without clear evidence of the phenomenon in caves, but now evidence from Carlsbad Caverns and Jewel Cave SD supports these models and provides validation (Michie 2017a; Michie 2017b).

2. Method

The process of modelling a geothermal heat flow in a cave is recursive. A tentative guess is made for an initial model to be calculated, and from the result a new guess is made until a fit, as good as is desired, is achieved, with the available field data. Although the approach is initially based on guesswork, the final solution is very robust and accurate.

There are some simplifying assumptions made in these models, but they are not critical as the model is not sensitive to them. Measurements of the thermal conductivity of limestone and marble vary from about 1 to 2 W/(m·K) Effectively

sampling of the material around a cave is virtually impossible, and the only difference between a high value and a low one is in the magnitude of the heat flow calculated, which is uncertain by that margin anyway. This statement may seem like condemnation of the whole modelling process, but the size of the heat flows being observed varies by many orders of magnitude.

Uniformity of the substrate is assumed, but this is acceptable in the absence of good data and the small effect it has on the outcome of the modelling.

Elements of the model:

1. In an infinite medium, a point source of heat will, when thermal equilibrium is reached, have a temperature field that falls off at an inverse square law with distance from the point source. A geometric factor of $1/(4\pi)$ applies because of the three dimensional heat flow. i.e. a 4π watts source in a medium conductivity = 1 produces a spherical isotherm of radius 1 metre with a temperature rise of 1 kelvin
2. A line source has a field that falls off as the log of the normal distance from the source. A long conduit or pipe can form a line source. Line sources/sinks are not discussed further here.
3. Temperature is a scalar quantity, and so the fields about two separate point sources can be linearly superimposed, that is at every point in the substrate the temperature change will be the sum of the effects from each source.
4. An overall vertical temperature gradient can be added to the model, its effect will be added as a contribution to the value of each point, its value will be proportional to the depth of the point from the surface which is at the Mean Annual Temperature (MAT).

5. A surface ground plane may be established by placing “mirror” points of opposite polarity and equal magnitude above the plane at a distance the same as the depth of the sources and sinks in ground. At the ground plane all heat flow is vertical, and continuous with virtual lines about the image points above the ground plane. The ground plane is assumed to be at the mean annual temperature of the site. The daily and annual temperature fluctuations are rapidly attenuated with depth, and their long term average is zero and so play no part in this steady state model. Surface transient temperature variation is calculable, and it may be relevant with surface climate change to build it into the model. The mathematics of transient temperature change on the surface of a half space are to be found in texts such as (Carslaw HS, Jaeger JC, 1947).

6. Within any closed contour of constant temperature (isotherm), the contents may be replaced by an infinitely conductive element at that temperature. In a void space filled with a fluid the thermal processes of radiation, upward convective heat transfer and coupled heat and mass transfer are so much more effective than heat conduction in the host rock that temperature differentials become negligible, and the space can be regarded as isothermal for water, or have a gradient of the adiabatic lapse rate for air.
7. Negative values of heat source behave in the same way as positive values, the quantities are scalar variables, so there are both heat sources and sinks.
8. The values of a grid of points can be quickly calculated in a spreadsheet and hand drawn isothermal contours can be interpolated. Each calculation of a potential is independent, that is it does not depend on the calculations for adjacent points, so errors do not accumulate.
9. Heat flow lines are locally normal (at right angles) to the isotherms.

Heat flow lines can be added to this modelling, but only with a considerable amount of computation. A program for a “crawler” to follow heat flow lines was used, it was quite slow, requiring huge numbers of iterations. It produced most informative maps; see Fig 4. Here heat flow lines were calculated in one metre increments, using two values on the isotherm at one metre spacing to establish the direction of a normal line one metre long. At the end of this line the procedure was repeated on a new isotherm, and two new points were established to make a normal heat flow line which was continued one more metre. The isotherms were established by an iterative procedure to quite high accuracy so that the cumulative error in the heat flow line would be acceptable. A list of coordinates of the heat flow line was used to draw the charts.

These heat flow lines are very informative, demonstrating the direction of heat flow but their relative position is arbitrary, depending on the first point chosen for each line. Values of heat flux for the model are made by using the source and sink magnitudes.

Figure 1 shows the components of an analysis of a buried source and sink in proximity to a surface plane which is at

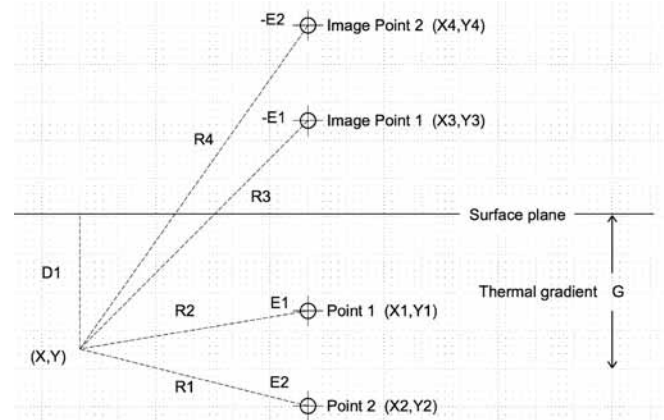


Figure 1. Scheme of variables in the model

the MAT and the parameters to compute the temperature at point (X,Y)

Point 2 is a point sink of heat E2 (a negative value), and Point 1 is point source of heat E1. The image points have powers that are the negative of Point 1 and Point 2. R1, R2, R3 and R4 are the distances from the point where the temperature is being calculated. The lengths of R1, R2, R3, R4 are calculated from the co-ordinates of the points. D1 is the depth of the point (X,Y), G is the temperature gradient from the surface before the sources and sinks were added, in kelvins /metre.

The temperature at the point (X,Y) is:

$$T = MAT + D1 \cdot G + E1 / (4 \cdot \pi) \cdot (R1)^2 + E2 / (4 \cdot \pi) \cdot (R2)^2 + E3 / (4 \cdot \pi) \cdot (R3)^2 + E4 / (4 \cdot \pi) \cdot (R4)^2$$

Do it yourself with a spreadsheet : If you make two axes on a spreadsheet as a column and row to give a grid of points, say 10 m intervals, you can make a generalised cell calculation, calculating the distances of the points from the cell position (Pythagoras) and applying the above formula, to get a matrix of temperature values. Print it out and draw isotherms by hand between the values to give a map of your model.

The sources and sinks do not need to be in the plane of the model, but the distances to the sources and sinks then have to be calculated in three dimensions.

A more detailed diagram requires a successive approximation program that finds the precise coordinates of a close-spaced series of points on the isotherms. The diagrams shown used Basic programs to calculate files of coordinates for each isotherm.

3. Results

Charts are shown, plotted from calculated coordinate pairs of values lying on a selected vertical plane though the ground.

The coordinates were found by a Basic program which increments the X axis in one metre steps when lines are inclined less than 45 degrees or increments the Y axis in one metre steps if the inclination is more that 45 degrees. A line of coordinates follows around a contour until it closes.

There is no reason for extreme accuracy in these calculations as each value of temperature is determined for those coordi-

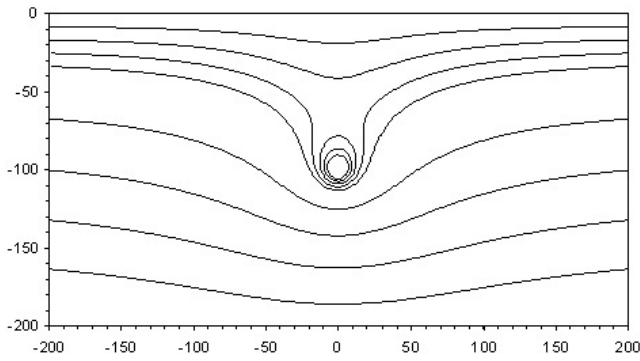


Figure 2. A buried heat sink

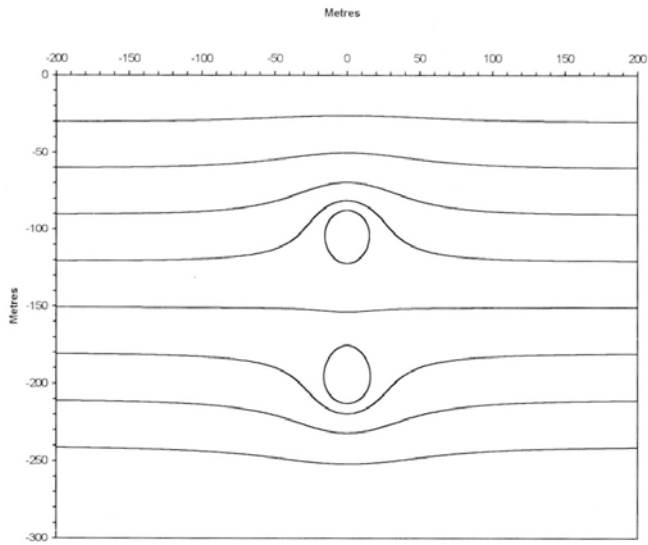


Figure 3. A buried source and sink

nates without dependence on the values from other coordinates.

Heat flow lines are a useful aid to visualising the capture of heat flow. There are, however, some limits to the use of these lines, as they start at arbitrary positions, so there are multiple possible lines, unlike isotherms that are unique. They are tedious to calculate, and can be inaccurate if approximation errors are allowed to accumulate. If sources and sinks are used that are not in the plane of the two dimensional model then the heat flow lines will have to be calculated in three dimensions.

Lines of heat flow are drawn starting at an arbitrary point. From the starting point, the value of the isotherm is found, then the slope of the isotherm is established between points plus and minus one metre from the starting point. A normal to that line is constructed for one metre to give a new point. A new isotherm is found for this point and the points either side on the isotherm are found to find the line normal to the isotherm at that point, and so on. Each point on the line of heat flow is determined with respect to the previous point. And so, unlike the temperature calculations, errors will accumulate, requiring the successive increment calculations to be made with very small error.

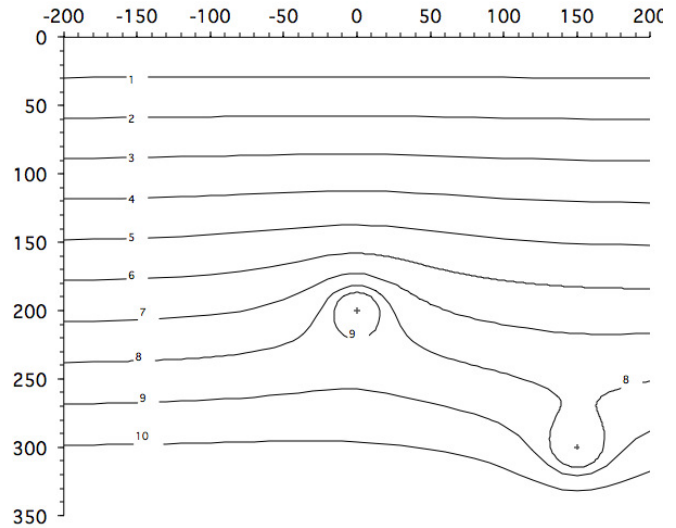


Figure 4. The analysis of the chamber over the Lake of the Clouds

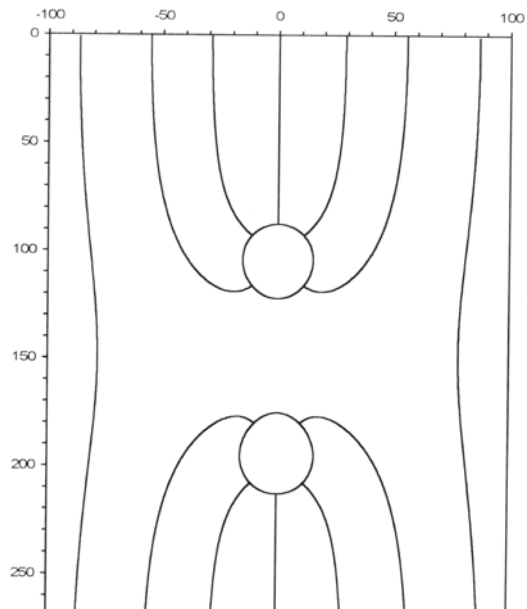


Figure 5. Heat flow lines for the case in figure 3

This computational procedure could take up to an hour on a PC to draw one heat flow line, so care should be taken to make the computations efficiently.

Figure 6 shows the Lake of the Clouds chamber as two points, a source and a sink, and a value of 500 watts was found to best fit the known measurements. The position of the chamber has been shaded, it covers an isothermal (with DALR gradient) region, which is quite close to the map of the cave.

Use of the model quickly demonstrates a process of heat concentration, where heat flow over a wide area is concentrated through the more conductive void spaces. This concentration of heat drives processes that can contribute to speleogenesis such as heat driven circulations (thermal gravity density flows A.K.A. "Natural Convection") and energy and material transport.

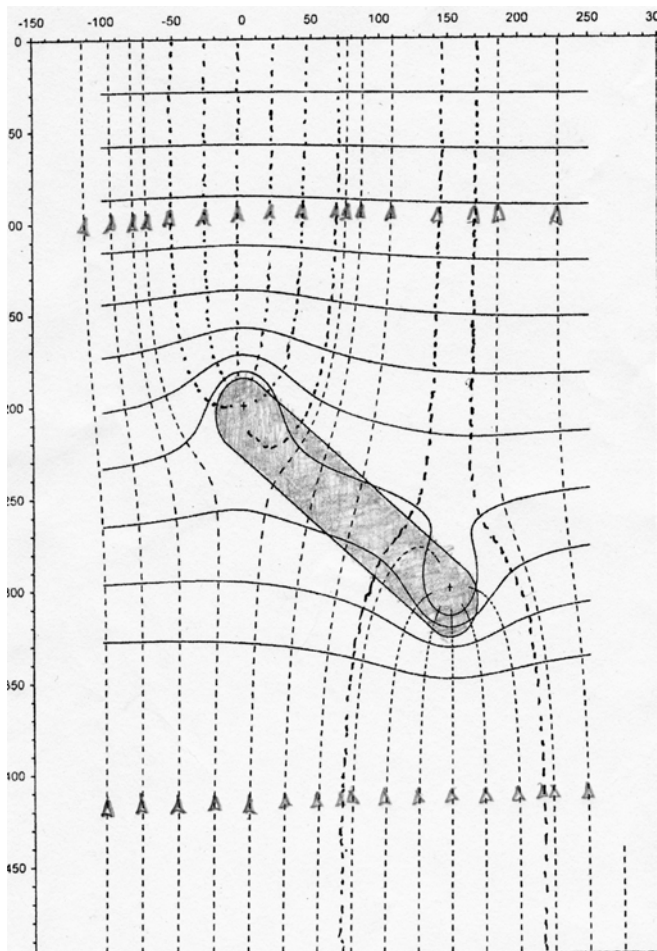


Figure 6. Isotherms and heat flow lines around the chamber over Lake of the Clouds

Combined with chemical excavation, the convective circulations can transport material from the deep cave to the surface and carry reactants from the surface to the depths of the cave.

4. Discussion

The method is quite rapid and shows the physical processes and their consequences. Changing the conductivity of the substrate only changes the required magnitude of the heat sources/sinks.

Other heat transfer mechanisms in a cave will compete with the geothermal heat flow, and near most cave entrances the

effects of the external weather will be much greater than the geothermal flow. Such effects as the chimney effect and the cold trap effect are much stronger, but are seasonal, so that over a period of a year the total heat transfer may tend to zero. Those effects will make observations of geothermal heat flow very difficult to observe. In deep cave situations, where annual changes are not detectable, the continued flow of energy will accumulate to a massive ever increasing value far greater than seasonal swings near the surface.

The thermal circulation is a heat engine, and the maximum available mechanical energy driving the circulation is able to be determined from the limiting efficiency of a Carnot cycle engine. In the Lake of the Clouds chamber case with an energy flow of about 500 watts and a temperature difference of less than a kelvin, the

$$\text{Carnot efficiency} = 1 - T_{\text{Low}} / T_{\text{high}}, \text{ (absolute temperatures)}$$

or 0.0033, so less than 1.7 watts of energy is available to circulate the fluid and overcome the drag of viscosity. To emphasise the effect of the time scale on this process, this drive amounts to 30 mega-joules per annum.

5. Conclusion

Geothermal heat flow can be seen to concentrate in cave structures to become capable of driving significant speleogenetic processes.

A model can be easily developed to find the magnitude of the heat sources and sinks which then provide the strengths of the heat flows in a cave. The use of temperature, being a scalar variable, facilitates the modelling.

References

- Carlsaw HS, Jaeger JC, 1947. *Conduction of Heat in Solids*. Oxford University Press, pp. 387.
- Michie NA, 2017a. Geothermal Heat flow in Caves: Heat Concentration and its Effects on Speleogenesis. This conference.
- Michie NA, 2017b. Geothermal Heat Flow in Caves: The Physics of the Geothermal Rims in Carlsbad Cavern. This conference.

Vadose Zone Hydrogeology In The Bossea Cave System (Southern Piedmont, Northern Italy)

Bartolomeo Vigna¹, Adriano Fiorucci¹, Alessia Nannoni², Jo De Waele²

Affiliation: ¹Department of Environment, Land and Infrastructure Engineering (DIATI), Politechnic University of Turin, Italy, bartolomeo.vigna@polito.it, adriano.fiorucci@polito.it

²Department of Biological, Geological and Environmental Sciences, Alma Mater Studiorum University of Bologna, Italy, alessia.nannoni2@unibo.it, jo.dewaele@unibo.it

Abstract

Bossea Cave is located in southern Piedmont (N Italy) and has a total development of more than 2 km. It is home of an underground scientific laboratory that monitors cave air, radon concentration, cave fauna, and subterranean waters. The cave hosts an important subterranean river that follows, at least in its initial portion, the tectonic contact between the underlying less permeable rocks (Permian volcanics) and the Mesozoic carbonates. This river receives water from several tributaries that have their recharge in the discontinuities of the overlying carbonate host rock (the vadose zone of the system). The thickness of this vadose zone is comprised between some tens of metres in the areas close to the cave entrance to more than 150 metres in its innermost parts. Many small water trickles and tributaries are monitored with multiparametric loggers (temperature, electric conductivity and water level). Several vadose waters are also sampled seasonally and analysed at the DIATI at Turin.

The most important of these tributaries, called “*polle*”, flow out of relatively open and karstified fractures close to the carbonate-volcanic contact and are monitored with loggers and a water level. These reach maximum flow rates during floods of less than 1 L/s. The other monitored spots are characterised by dripping sites, where water falls from the cave ceiling from tinier fractures often partially closed by carbonate speleothems. They have very low flow rates, often below 0.5 L/min. These are monitored using pluviometers placed below the dripping sites.

The great number of data acquired until present shows that the flow in the fracture network is strictly correlated to the main rainfall events, with fast and temporary increases in drip and flow rates. Both types of inflows show an impulsive response related to the recharge of the drainage network and the consequent transfer of hydraulic pressure in the entire vadose zone. The clear piston flow phenomena are characterised by temporary increases in both temperature and mineralization of the waters. Also the chemical analyses on waters sampled under different flow conditions do not show substantial differences of the concentration in several ions over time. The comparison between the chemical and physical parameters of the different waters, on the contrary, shows some differences, especially regarding temperature, electric conductivity, nitrates, calcium, magnesium and lanthanides. These discrepancies demonstrate the existence of complex flow paths and a heterogeneous network of fractures in the vadose zone with rock structure and permeability very different from zone to zone.

Keywords: Unsaturated zone, karst hydrogeology, dripwater, geochemistry, water flow

1. Study area

Bossea Cave is situated in southern Piedmont (N Italy), in the Ligurian Alps (Fig 1), and has a drainage area developed between 800 and 1700 m asl. The main recharge area is characterized by a karst surface generally covered with a thin blanket of colluvial deposits, and a series of loosing valleys with modest flowrates, varying according to the meteorological conditions. Infiltration waters feed an important underground river that can be followed underground for over 1 km of development in a show cave. These waters give rise to a set of springs close to the Corsaglia valley bottom (Banzato *et al.* 2011, Peano *et al.* 2011, Fiorucci *et al.* 2015, Fiorucci & Vigna 2015). The downstream part of the cave, the one encountered first by tourists, develops directly along the contact between the underlying low permeability basement rocks (Permian volcanics) and the carbonates (Triassic to Cretaceous dolostones and limestones) (Fig. 1b). This part is characterized by large rooms and impressive collapses. On the contrary, the innermost upstream part of the cave is composed of a vadose canyon that has carved along some major tectonic displacements. The cave has been explored up to two sumps connected by a network of phreatic conduits reaching a water depth of -70 m. The main underground stream receives a series of lat-

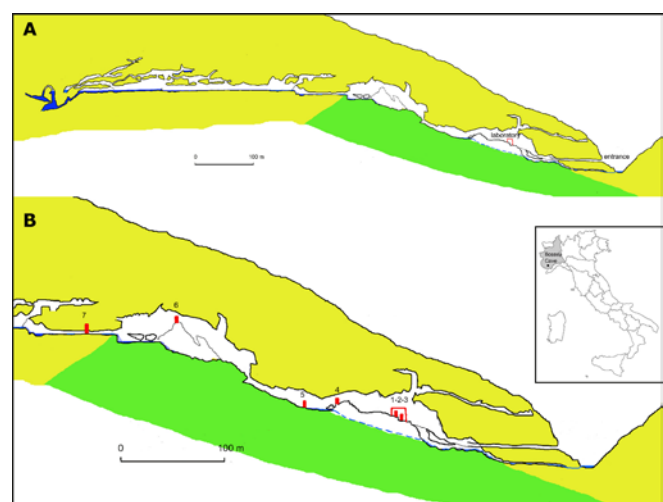


Figure 1. Location of Bossea Cave (in green the volcanic rocks, in yellow the carbonate rocks). A. Profile of the entire cave; B. Detail of the downstream part. The monitored stations are reported: 1 Polla Orso, 2 Sacrestia, 3 Cancelli Lab., 4 Milano, 5 Polletta, 6 Torre, 7 Polla delle Anatre



A



B

Figure 2. Monitoring equipment:
A. Rain gauges measuring drips in the cave;
B. Concrete weir for the measurement of flow rate of a small tributary

eral tributaries along its path. These tributaries, which are the main subject of this research, are related to the underground water flow occurring along the discontinuities in the rock lying above the cave (Vigna & Doleatto 2008). The thickness of this vadose zone ranges between 10 meters close to the artificial entrance to around 150 meters in the final parts of the cave (close to the sumps) (Fig 1a).

The surface morphology is characterized by relatively steep SE facing slopes, with bare rock outcrops, and a mostly thin soil cover. Landcover is mainly composed of broadleaf forest with laryx alternated with mountain meadows. The hydrodynamic and hydrochemical monitoring of these vadose inputs has allowed to collect important data for the definition of the water circulation in the unsaturated zone of this mountain karst.

2. The unsaturated zone

Several vadose water flows, generally characterized by a modest water flow, have been chosen in the cave to study the vadose zone hydrology. These points have been equipped with monitoring devices measuring electric conductivity (EC), temperature (T) and water level (P) in a continuous way (Fig 1). Seasonal sampling of these waters has also been carried out.

Chemical analyses on these waters have been performed in the labs of the Polytechnical University of Turin (DIATI).

The main inflows are representative of water flow in more or less karstified fractures, hosted in the carbonate rocks but often

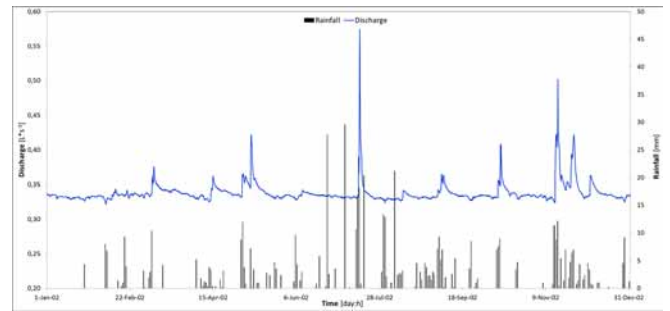


Figure 3. Flowrate at Polla delle Anatre and rainfall

close to the less permeable basement rocks. One of the most important monitoring points is the *Polla delle Anatre*, with a very constant flowrate that rises temporarily only during the main infiltration events. The other water points, known as *Polla dell'Orso*, *Polletta* and *Milano*, have very low flowrates but become important during main rain events, reaching flowrates of more than 0.5 L s^{-1} . Other measured points are dripping sites with very low flowrates, below 0.008 L s^{-1} , and drying out during long drought periods (*Sacrestia*, *Torre*, *Cancello Lab.*). For the monitoring of these sites different techniques have been used. Rain gauges have been placed under the drip-sites (Fig 2 A, B), while the bigger inflows have been equipped with v-shaped weirs, placing multiparametric loggers in the small pools created upstream of the weirs. All loggers have been set at 1 to 4 measurements per hour.

3. The hydrodynamic responses

The first hydrogeological monitoring equipment installed in Bossea Cave was that placed at the *Polla delle Anatre* in 1994, and in the following years the other points have been equipped progressively. All investigated springs are still functioning today (Fig 2). The large amount of acquired data, comprising very interesting periods such as after long drought, or before, during and immediately after floods, have allowed to understand the behavior and the structure of the water circulation in the unsaturated (vadose) zone of this karst aquifer. In periods characterized by no or extremely poor infiltration (winter months with temperatures below zero that do not allow the snow to melt, or summer periods with no rainfall) the flow rates of the water veins vary considerably from point to point. At the *Polla delle Anatre* the flow rate remains rather constant with a value of approximately 0.35 L s^{-1} , testifying a very stable base flow (Fig. 3). The other springs mostly remain active, with very low and constant flow rates of a couple of liters per hour. Only the *Polla dell'Orso* can have a zero flow rate for long periods, reactivating only after important rainfall.

The flow variation measured at the *Stillicidio dell'Orso* is the most anomalous one, characterized by a mean flow rate of 5 L h^{-1} , and important increases (up to 30 L h^{-1}) after intense rainfall. Following some flood events the flow rate has decreased to a mean and very constant value of less than 1 L h^{-1} . This change in behavior is not related to a seasonal variation, but must be due to a change in the underground circulation. The presence of fine sediments carried by these waters (and visible on the bottom of the containers used to monitor this springlet) demonstrates the transport of fines in its percolation paths, and these deposits might have been trapped in the recharge network.

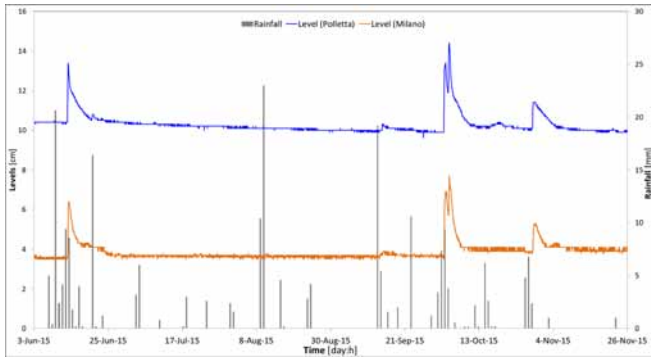


Figure 4. Water levels at monitoring point Milano and Polletta, and rainfall

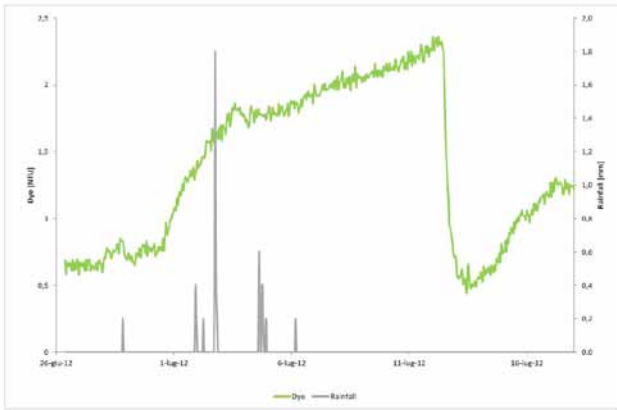


Figure 5. Tracer breakthrough curve at Milano monitoring point

The hydrogeological behavior of the unsaturated zone of the Bossea aquifer is best shown during the spring and autumn recharge periods. Studying the large dataset of hydrological data of the investigated springs it is easy to observe the difference in depletion curves between the monitored points. It is interesting to note that the increase in flow rate occurs in all the measured points in the same period. After heavy rainfall, after long drought periods, no evident increases in flow rate occur: a consistent part of the newly arriving rain-water is used to saturate the soil and the fracture network in the epikarst. During summertime the evapotranspiration subtracts an important amount of infiltration water, and also after heavy rain showers the flow rates in the monitored springs remain unaltered. Only once saturation is achieved in the different parts of the aquifer the infiltrating waters start to transmit their hydraulic pressure through the complex fracture network of the unsaturated zone. In all the monitored points in the unsaturated zone sudden increases in flow rate are observed, with peaks registered only a few hours after the maximum rainfall (Fig 4). Also the very slow drips in the cave respond in a very quick manner to the rain events.

A series of dye tests has also been carried out on the slope above the dripping points to study the water flow paths in the unsaturated zone. These tracer tests have normally been carried out during the natural recharge periods of the system. The tracers arrived at the dripping points after several days from their injection, and the breakthrough curves normally lasted for a considerable amount of time (Fig 5). These tracer experiments have shown the great difference between the flow

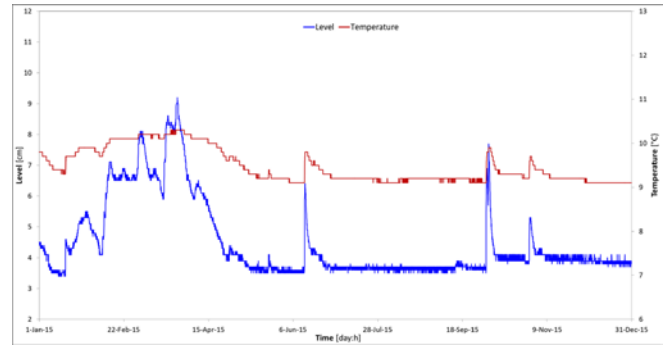


Figure 6. Milano monitoring point: water levels and temperature

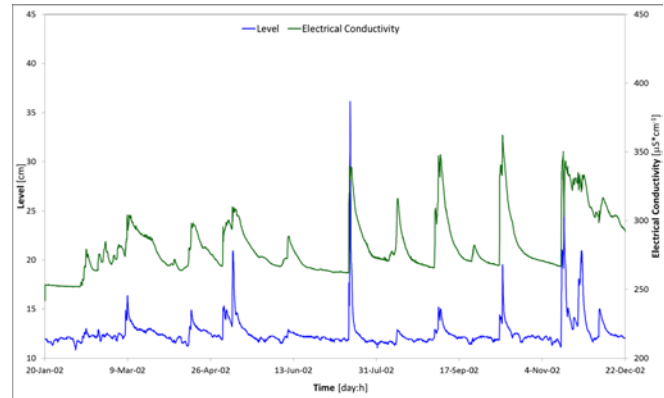


Figure 7. Polla delle Anatre: water level and electric conductivity

velocities measured in the cave (calculated between 5 and 20 md^{-1}) and the transmission of hydraulic pressure, which is extremely rapid when the fractured network is saturated.

4. The geochemical responses

The water temperature variations in time are very similar in all monitored points: during increases in flow rates also temperature rises reaching their highest annual values after important infiltration events. Also during springtime, when the main flow rate increases are related to melting of snow, and thus infiltrating waters have very low temperatures, the temperatures at the springs shows small increases instead, comprised between 0.5 and 0.8 °C (Fig 6).

The changes in electric conductivity (EC) measured at the springs after main rain events show a much more complicated, and yet not entirely explained, behavior respect to temperature. The *Polla delle Anatre* is characterized by evident increases in mineralization contemporaneous to the main flood events (Fig 7), while EC of the other monitored sites shows anomalous oscillations in the order of 20-40 μScm^{-1} .

The hydrochemical facies of the different springs are more or less constant in time (drought and flood) but are rather different among the monitored sites (Fig 8). *Milano* and *Polletta* are characterized by bicarbonate-calcic-magnesian facies, while the other sites are typically of the bicarbonate-calcic type. Among these last differences in the ratio $\text{Ca}^{2+}/\text{Mg}^{2+}$ are shown, varying between 4.11 (mean value at *Polla delle Anatre*) and 41.49 (mean value at *Sacrestia*). This wide variability in $\text{Ca}^{2+}/\text{Mg}^{2+}$ ratio is related to the different concentration in Mg^{2+} that is the only parameter, among the main elements, that changes between these different waters. The elements present with

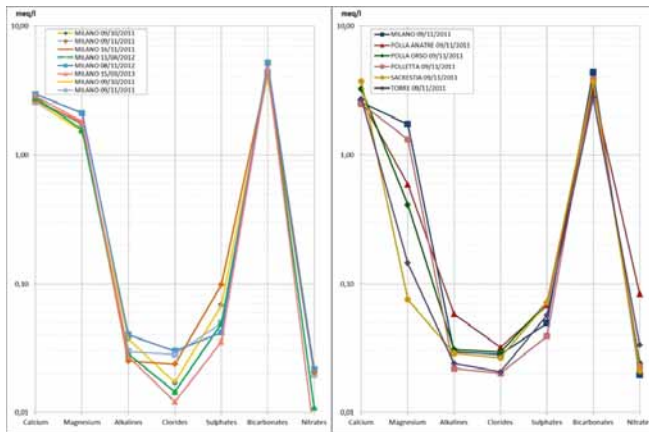


Figure 8. Schoeller diagrams: Left, different analyses at Milano; Right, Chemical composition of all the monitored waters on November 9, 2011.

concentrations below 0.1 meqL^{-1} (Na^+ , K^+ , Cl^- , and SO_4^{2-}) show the highest variations in time.

The *Polla delle Anatre* is characterized by concentration in alcali elements higher than that of chloride. This shows these waters derive from a fracture system mainly developed in the volcanic basement rocks.

The saturation indices of calcite and dolomite have been calculated using the ratio between the ionic activity product (the single ionic activity determined according to the Debye-Hückel equation) and the solubility product. The waters in almost all samples are supersaturated with respect to calcite, while they are sometimes undersaturated with respect to dolomite.

Taking into account all the samples a rather good correlation is evidenced between these two indices (r^2 of 0.7236). Considering every single monitoring point on its own these correlation coefficients are even greater than 96% (Fig 9), and angular coefficients of the single correlation lines are very similar to each other, ranging from a minimal value of 0.4393 (*Sacrestia*) to the highest of 0.5036 (*Polla delle Anatre*).

5. Conclusions

The overall analysis of the hydrodynamic and geochemical monitoring data in Bossea Cave has revealed the complexity of the unsaturated zone of this karst aquifer, characterized by many different independent and semi-independent hydrological circuits, mostly developed in a scarcely karstified fracture network.

Both the main arrivals and the small veneers and dripping points show an impulsive behavior, due to the transfer of a hydraulic pressure in the unsaturated zone of the aquifer. The hydrodynamic monitoring has evidenced a piston flow behavior, characterized by sharp and temporary temperature increases accompanied by rising electric conductivity of the arriving waters. The main infiltration events remobilize the resident waters in the fractured network, while the neoinfiltrating waters do not appear to arrive at the springs. Since every single monitoring point is recharged by an independent or semi-independent drainage network, the depletion

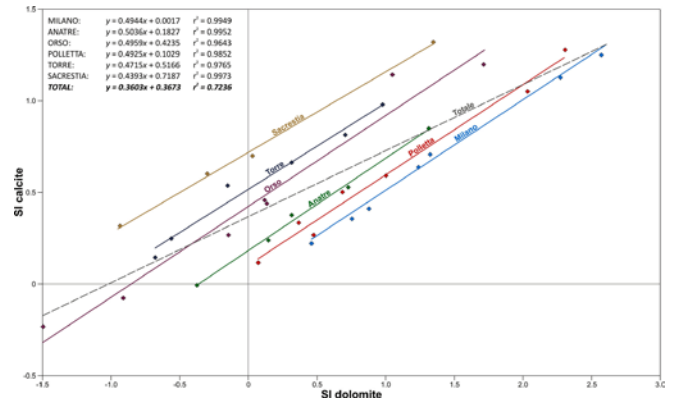


Figure 9. Saturation indices for calcite and dolomite of the different monitored waters.

curve of every single point is different from all the others. The chemical analysis of the waters, carried out only for the major elements, shows differences mainly in the ratio $\text{Ca}^{2+}/\text{Mg}^{2+}$ and, in some cases, in the ratio $(\text{Na}^+ + \text{K}^+)/\text{Cl}^-$. This last ratio, when it exceeds the value of 1, shows the waters to derive from a circulation network developed in the underlying volcanic rocks.

The calculated saturation indices show the waters to be always supersaturated with respect to calcite, and often also in dolomite, even after intense infiltration events. The correlation between these two saturation indices is very high when considering the single measuring points, but gets lower taking into consideration the whole dataset. This aspect seems to underline even more the complexity of the unsaturated zone of the Bossea aquifer, as shown also by the other geochemical parameters analyzed.

References

- Banzato C, Dallagiovanna G, Maino M, Peano G, Vigna B, 2011. Correlation between the geological setting and groundwater flow: the Bossea karst underground laboratory. *Geoitalia 2011*, Epitome 4, Torino, 19–23 Settembre 2011, p. 14.
- Fiorucci A, Moitre B, Vigna B, 2015. Hydrogeochemical study of Bossea karst system. *Proceedings of the international symposium in environmental safety and construction in karst areas*. Perm, Russia, 26–29 May 2015 pp. 290-294
- Fiorucci A, Vigna B, 2015. Hydrogeochemical study of some springs in the Ligurian and Maritime Alps (Piedmont, Italy). *Proceedings of the second Russian scientific Conference Water-Rock interaction: Geological evolution*. 06–11 September 2015, Vladivostok, Russky Island, FEFU Campus, Russia, pp. 229-233
- Peano G, Vigna B, Villavecchia E & Agnesod G, 2011. Radon exchange dynamics in a karst system investigated by radon continuous measurements in water: first results. *Radiation Protection Dosimetry*, 145(2), 173-177.
- Vigna B, Doleatto D, 2008. La circolazione idrica nella zona non satura di Bossea. *Ambiente carsico: I progressi degli studi in Italia sulla soglia del XXI secolo*. Bossea, 21–22 Maggio 2005, pp. 51-63.

Effects of photosynthesis and groundwater input on diel variations of electrical conductivity and calcite precipitation in Chaotian River, Guilin, China

Cheng Zhang^{1,2}, Jinliang Wang^{1,2}, Qiong Xiao^{1,2}

Affiliation: ¹Key Laboratory of Karst Dynamics, MLR/GZAR, Institute of Karst Geology, CAGS, Guilin 541004 China, e-mail: chzhang@karst.ac.cn

²International Research Center on Karst under the Auspices of UNESCO, Guilin 541004 China, e-mail: chzhang@karst.ac.cn

Jinliang Wang, email: jlwang@karst.ac.cn

Qiong Xiao, email: xiaoqiong@karst.ac.cn

Abstract

The short time scale research on diurnal or seasonal variations is valuable to the investigation of the relatively rapid biogeochemical processes in waters. Specific conductivity is frequently used to estimate the mixing ratio of different sources of water in hydrological studies. Taking Chaotian river, a tributary of Lijiang river, Guilin, China as an example, the diurnal fluctuation of specific conductivity and other chemical parameters were examined by conducting high resolution field monitoring and high frequency sampling. pH, DO, SpC, HCO_3^- and Ca^{2+} all showed diurnal variations, reflecting influence of photosynthesis and calcite precipitation. The Concentrations of Ca^{2+} and HCO_3^- at two monitoring sites showed a diel cycle of daytime decrease and nighttime increase, with an amplitude of 13-17 % and 18-25 % respectively during a 48-h period. The average Ca precipitation rate is estimated to be $0.8 \times 10^{-5} \text{ mmol L}^{-1} \text{ s}^{-1}$. The small rate could be related to the presence of inhibiting solute of dissolved organic carbon in water of Chaotian River. The nighttime increase in SpC could be explained by groundwater input from the upstream karst aquifer.

Keywords: specific conductivity; calcite precipitation; diel variation; aquatic vegetation; karst groundwater; Chaotian River

1. Introduction

With the development of high-resolution automatic online monitoring equipment and high-frequency automatic sampling techniques, more and more studies have been conducted on diel biogeochemical processes since the 1990s (Nimick *et al.*, 2011). The short time scale research on diurnal or seasonal variations is valuable to the investigation of the relatively rapid biogeochemical processes in waters (e.g. processes in stream flows). In addition, it also helps the assessment of watershed processes in upstream recharge areas. The existing studies (Dandurand *et al.* 1982, Spiro & Pentecost 1991, Guasch *et al.* 1998, Reichert 2001, Lorah & Herman 1988, Finlay 2003) on different orders of rivers show that biological processes (photosynthesis and respiration) and geochemical processes (bicarbonate equilibrium and calcite precipitation) are two main controlling factors for diurnal variations of water quality parameters such as pH, dissolved oxygen (DO), specific conductivity (SpC), and concentrations of Ca^{2+} and HCO_3^- in streams (Nimick *et al.*, 2005).

Tobias and Böhlke (2011) and Hayashi *et al.* (2012) monitored diurnal fluctuations of SpC in the rivers that have calcite-supersaturated water and support periphyton growth. Various aquatic plants and river beds have a strong influence on the chemistry of the large river. In general, SpC and Dissolved inorganic carbon (DIC) concentration are relatively higher in streams from carbonate-rich catchments than those from silicate-rich bedrock areas. Large diel variability in DIC concentrations and flux in first-order tributary has implications for the design of surface-water monitoring programs and interpretation of water quality records (Tobias and Böhlke, 2011).

SpC is closely correlated with the concentration of total dissolved ions, and is frequently used to estimate the mixing ratio of different sources of water in hydrological studies. The

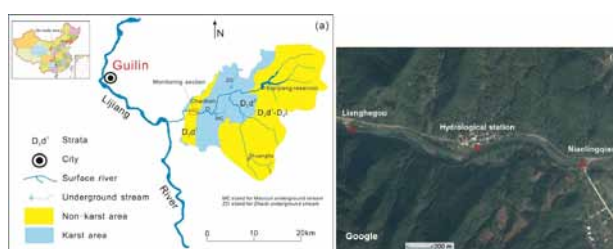


Figure 1. (a) Map of the Chaotian River watershed showing the extent of the karst aquifer. (b) Location of the monitoring sites and Chaotian hydrological station.

objectives of this study are to examine the diurnal fluctuations of SpC and other chemical parameters in a high-order river in southwest China karst region by conducting high resolution field monitoring and high frequency sampling, and understand the biological, chemical, and hydrological processes that cause these fluctuations.

2. Study sites

The study was conducted in the Chaotian River in southwest China, a tributary of the Lijiang River, Guilin, Guangxi Autonomous Region (Fig. 1a). There is a reservoir constructed in year 2005 upstream of the Chaotian River. The catchment area upstream of the long-term hydrological monitoring station in Chaotian is 476.34 km² and has an annual mean discharge of 11.13 m³ s⁻¹ during the year 1996 to 2005.

The annual average temperature of the study area is 18.8 °C and the annual average rainfall is 1,907 mm, with the wet season from April to August. Its drainage basin is mainly composed of Donggangling Formation (D₂d) of Devonian with sandstone-dominated (D₂d¹) headwaters in east part, and the lower reaches dominated by limestone (D₂d²). There are two subterranean streams developed in karst aquifer (Fig. 1a). The

outlets of these two streams are located at bank side of Chaotian River, approximately 300-500 m away from the riverbed. Ground water flows through a short-distance surface stream and enters the Chaotian River.

High-resolution data logger monitoring and water sampling was carried out at two sites: Nialingqiao (NLQ) with gravel riverbed and Lianghegou (LHG) with soil riverbed (Fig.1b).

To determine the variation of ion concentrations at different river reaches, water samples were collected at Chaotian hydrological station, groundwater outlets (Zhaidi and Maocun), Shuanghe (the confluence point of two branches), and the reservoir Si'anjiang on August 2, 2013. Water temperature of groundwater(20.8°C) is lower than that of reservoir(30.4°C) and river headwater(23.9°C), but is close to the average air temperature of Guilin city. Concentrations of calcium and bicarbonate, and SpC of groundwater with mean values of 69.0 mg L⁻¹, 216.5 mg L⁻¹, 360 μs cm⁻¹ respectively, are much higher than that of the river water, i.e. 5.83 mg L⁻¹, 24.4 mg L⁻¹, 61 μs cm⁻¹ respectively.

3. Materials and Methods

3.1. Field monitoring, sample collection and analytical methods

Detailed monitoring of chemical parameters and water sampling was conducted during a 96-h period in August 9–13, 2013, characterized by low daily mean flow of 2.91 m³s⁻¹, high daily mean temperature of 30.6–32.1 °C and clear sky conditions.

Two automatic sensors (YSI 6920) were installed at locations Nialingqiao (NLQ) and Lianghegou (LHG) respectively (Fig. 1b) to measure water temperature, pH, SpC, water level and DO at 5-min intervals with the accuracies of 0.1°C, 0.2, 1 μs cm⁻¹, 0.01 m, and 0.01 mg L⁻¹ respectively. The pH sensor was calibrated using the standard pH buffers for the expected measurement range before the installation. SpC sensor was calibrated using the 0.01-M KCl standard solution, and the data were recorded as values at 25 °C after temperature compensation. River water was sampled every 2 h at the same location using an auto-sampler (6700, Teledyne ISCO Inc.) and stored in high density plastic bottles until they were retrieved at the end of the sampling period and transferred to a refrigerated (4 °C) storage room. All sensors and the water-sample intake were located approximately 1 m from the shore at an approximate depth of 0.4 m. In line with the standards of GB/T8538-2008, the determination of hydrochemical compositions was performed in the Karst Geological Resources, Environmental Monitoring and Testing Center, Ministry of Land and Resources of China using an IRIS Intrepid II XSP plasma spectrometer.

3.2. Chemical data processing and equilibrium calculation

Water samples were analyzed within a few days of sample collection. Concentrations of Ca, Mg, Na, K, Cl and SO₄ were measured using IRIS Intrepid II XSP plasma spectrometer. From the field-measured pH and temperature, and concentration of major ions in the sample, CO₂ partial pressure (pCO₂), and calcite saturation index (SIC) were calculated using the

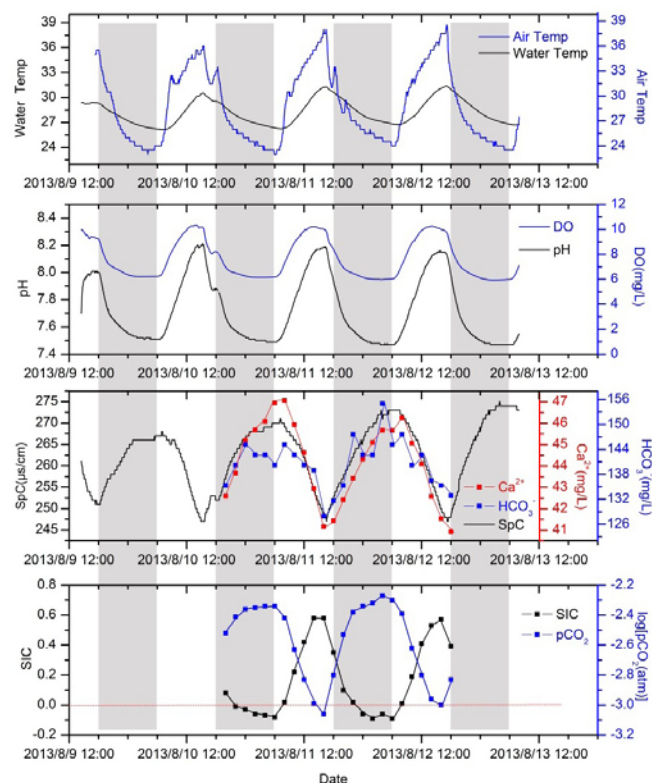


Figure 2. Detailed data at the Nialingqiao site, 9–13 August 2013

geochemical speciation program PHREEQC (Parkhurst and Appelo, 1999). The concentrations of Ca²⁺ and HCO₃⁻ were determined by in-situ titration and the ion concentrations of Mg²⁺, K⁺, Na⁺, Cl⁻ and SO₄²⁻ were the analytical data tested from the water samples in the laboratory.

4. Results

4.1. Diurnal fluctuations of chemical parameters

To examine the details of diurnal fluctuations, an intensive sampling campaign was conducted at the Nialingqiao site during a 48-h period (10–12 August 2013) (Fig.2a). Maximum air temperature was 38.0 °C at 16:30 on August 11 and 38.5 °C at 17:05 on August 12 (Fig. 2a). Maximum water temperature was 31.3 °C at 16:30 on August 11 and 31.4 °C at 17:05 on August 12, without lagging time behind air temperature. DO concentration started to increase immediately after sunrise at 6:30 each day (Fig. 2b) due to photosynthetic input of O₂ by periphyton. Maximum DO concentration was 10.21 mg L⁻¹ at 14:00 on August 11 and 10.27 mg L⁻¹ at 14:00 on August 12, which form a flat peak until 17:00, roughly coincided with the highest air temperatures. DO concentration decreased during nighttime due to degassing and respiration, reaching a stable value of 6.14 to 6.15 mg L⁻¹ (76.6% of saturation) during the night of August 10–11, and 6.00–6.01 mg L⁻¹ (75.6% of saturation) during the night of August 11–12 (Fig. 2b).

The Concentrations of Ca²⁺ and HCO₃⁻ at Nialingqiao and Lianghegou sites showed a diel cycle of daytime decrease and nighttime increase, with an amplitude of 13–17 % and 18–25 % respectively during the monitoring period. Specific conductivity (SpC) decreased during the daytime and increased during the nighttime (Fig. 2c). The minimum SpC was 247 μs cm⁻¹ at 16:30 on August 11, and 247 μs cm⁻¹ at 17:15 on August 12. Calcium concentrations and DIC had almost identical

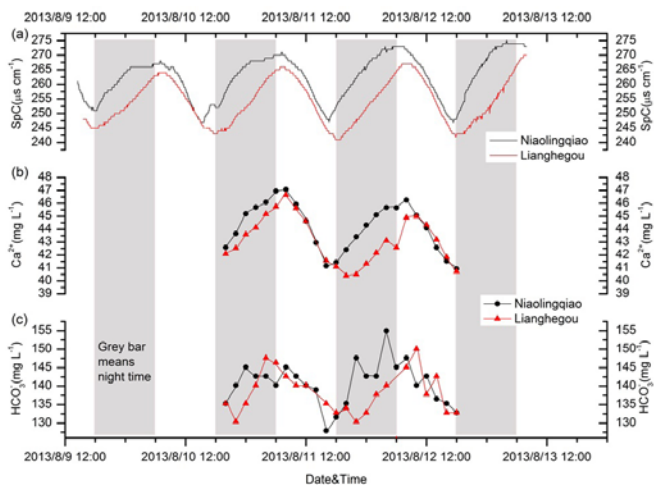


Figure 3. Comparison of the data measured at the Niaolingqiao (NLG) site and the Lianghegou (LHG) site in 9-13 August 2013

patterns to SpC (Fig. 2c). Of all the major ions analyzed, only Ca and DIC had distinct diurnal fluctuations. Therefore, the daytime decrease in SpC was caused by the decrease in Ca and DIC involving calcite precipitation.

Partial pressure of dissolved CO₂ (pCO₂) was calculated from the geochemical data using PHREEQC. The pCO₂ had a reverse trend of pH, decreasing during the daytime due to photosynthesis and increasing during the nighttime (Fig. 2d). Water in equilibrium with atmospheric CO₂ concentration (390 ppm by volume) should have a log[pCO₂] of -3.41. During the daytime, pCO₂ decreases with a minimum of -3.06, indicating consumption of CO₂, and all values of pCO₂ at the study site were clearly above the atmospheric equilibrium during the monitoring period. Nighttime maximum reached -2.27 in log scale, which was nearly fourteen times greater than the atmospheric equilibrium. The saturation index of calcite was positive during the daytime and negative during the nighttime in log scale, indicating that the river water was supersaturated in the day and unsaturated at night (Fig. 2d). Minimum value of saturation index at night was -0.09 in log scale, and maximum daytime value reached 0.58 in log scale.

4.2. Downstream propagation of chemical signals

At Lianghegou (LHG) located 1.65 km downstream of the Nialingqiao (NLQ) site (Fig. 1b), the data-logging sensors were also installed at LGH monitoring site with records of Water temperature, DO, pH, and SpC during our sampling event. During the monitoring period of 9-13 August 2013, the times of morning drop of SpC at NLQ site and LHG site were similar, but the afternoon peak were different (Fig. 3a). For example, on August 11, the morning drop at LHG site was only 15 min after the NLQ site, but the afternoon rise lag time was 125 min. The short time lag for the morning drop and long time lag for the afternoon rise between the two sites suggest that SpC and Calcium concentration at the LHG site is primarily controlled by local processes (especially caused by submerged aquatic vegetation) in the morning, and affected by the advection of SpC signals from upstream reaches in the afternoon. The pronounced lag time of the afternoon rise of SpC is supposed to be similar to the advection transit time between the two sites (Hayashi et al., 2012). Considering the short flow path between NLQ and LHG, this lag time is a bit longer than in normal, suggesting that the small dam con-

struction at LHG is the main cause that slowdown the flow rate.

5. Discussion

5.1. Calcite precipitation rate and processes

Water in the Chaotian River was supersaturated with respect to calcite (Fig. 2d) during the daytime and calcite precipitation occurred (Fig. 3b) indicating that photosynthesis provided a triggering mechanism for precipitation. This is consistent with findings from calcite-saturated rivers in other regions (Guasch et al., 1998; Spiro and Pentecost, 1991; Tobias and Böhlke, 2011). Laboratory experiment with calcite-coated gravels also proved that a high degree of supersaturation and the presence of abundant nucleation sites does not trigger precipitation (Hayashi et al., 2012), implying the presence of live periphyton is necessary for calcite precipitation.

The average precipitation rate estimated from the change in Ca concentration is 0.8×10^{-5} mmol L⁻¹ s⁻¹. This is slightly smaller than the precipitation rate (1.2×10^{-5} mmol L⁻¹ s⁻¹) reported by Hayashi (2012) for the saturation index ranging between 0.83 and 1.37. The low rate in this study could be related to the presence of inhibiting solute of dissolved organic carbon (DOC) (Lebrón and Suárez, 1998) in river water of southwest China subtropic region, because a substantial reduction of precipitation rate was observed in the presence of DOC at a concentration as low as 0.01 mmol C L⁻¹ as reported by Lebrón and Suárez (1998). The rate of nighttime increase in Ca is similar to that of daytime decrease.

It is likely that periphyton provided a mechanism that allows the water to overcome the kinetic barrier and precipitate calcite. One possibility is that periphyton is actively involved in the calcification of dissolved CO₂ and HCO₃ (Riding, 2000). Another possibility is that photosynthesis depletes CO₂ in the close proximity of photosynthetic cells, thereby creating a microenvironment having much lower pCO₂ and higher degree of calcite saturation than the bulk water (Hayashi 2012). This would allow calcite precipitation to overcome inhibiting mechanisms, indicating biogeochemical processes clearly play a central role in calcite precipitation at the Chaotian River. A similar mechanism was suggested by House et al. (1989) and Tobias and Böhlke (2011).

5.2. Nighttime increase in specific conductivity

The nighttime increase rapidly in SpC occurred after sunset (Fig. 2c), but the water still was supersaturated with respect to calcite (Fig. 2d) until 22:00. From that time the calcium saturation index decreased to the value below zero until early morning. Therefore, the increase cannot be explained simply by calcite dissolution. The most plausible explanation is addition of groundwater in karst aquifer that has higher Calcium and bicarbonate concentration and alkalinity than the river water both affected by calcite precipitation and recharged by sandstone area in upper reach. The upper reach of the Chaotian River is underlain by sandstone bedrock which is located in the east part of the watershed (Fig. 1a). The karst aquifer is located in the lower reach of the river implying that groundwater directly enters the Chaotian River first. It is estimated that roughly 80% of DIC at Chaotian Station is contributed by karst underground water on a year basis.

Two subterranean streams are located approximately 1-2 km upstream of NLQ monitoring site (Fig. 1a). The outlet is just several hundred meters away from the bank of Chaotian River. Karst groundwater flows through a short-distance tributary and drain it to the Chaotian River. Hayashi (2012) reported SpC decrease during the day is close related to radiation and the stop time of decreasing probably represents a condition in which the rate of ion removal by calcite precipitation is balanced by the rate of ion input by groundwater. pCO₂ increases and SIC decreases with the start of respiration after sunset and calcite precipitation completely stops, simultaneously SpC starts to increase rapidly due to groundwater input from the upstream karst aquifer.

SpC decrease at the LHG site during the day is consistent with the change at NLQ site, but the afternoon rise at the LHG site is delayed by 2 h compared to the NLQ site (Fig. 3a). The SpC rise observed at the LHG site at night is likely influenced more by the advection of the SpC signal from the NLQ site, because the river reach between NLQ and LHG is underlain totally by bedrock thus no extra groundwater input to the Chaotian River.

6. Conclusions

Results from high-resolution data logger monitoring and high frequency sampling indicated that the fluctuations of chemical parameters in Chaotian River are closely associated with biogeochemical processes. pH, DO, SpC, HCO₃⁻ and Ca²⁺ all showed diurnal variations, reflecting influence of photosynthesis and calcite precipitation. The SpC, concentrations of HCO₃⁻ and Ca²⁺ at Niaoling site showed a diel cycle of daytime decrease and nighttime increase, with an amplitude of 10%, 13 % and 17 % respectively.

The average Ca precipitation rate is estimated to be 0.8×10⁻⁵ mmol L⁻¹ s⁻¹. The small rate could be related to the presence of inhibiting solute of dissolved organic carbon in water of Chaotian River. The nighttime increase in SpC could be explained by groundwater input from the upstream karst aquifer.

Acknowledgement

This work was supported by the Special Fund of Chinese Academy of Geological Sciences (No. YYWF201639), fund from the Department of Science and Technology of Guangxi (16-380-13), the China Geological Survey Project (No. DD20160111) and IGCP 651. Special thanks are given to the anonymous reviewers whose constructive comments and suggestions have greatly improved this manuscript.

References

Dandurand J L, Gout R, Hoefs J, Menschel G, Schott J, Usdowski E, 1982. Kinetically controlled variations of major components and carbon and oxygen isotopes in a calcite-precipitating spring. *Chemical Geology*, **36**(3-4), 299-315.

Finlay J C, 2003. Controls of streamwater dissolved inorganic carbon dynamics in a forested watershed. *Biogeochemistry*, **62**(3), 231-252.

Guasch H, Armengol J, Martí E, Sabater S, 1998. Diurnal variation in dissolved oxygen and carbon dioxide in two low-order streams. *Water Research*, **32**(4), 1067-1074.

Hayashi M, Vogt T, Mächler L, Schirmer M, 2012. Diurnal fluctuations of electrical conductivity in a pre-alpine river: Effects of photosynthesis and groundwater exchange. *Journal of Hydrology*, **450-451**, 93-104.

House W A, Shelley N, Fox A M, 1989. Chemical modelling applications to experimental recirculating streams. *Hydrobiologia* **178**(2), 93-112.

Lebrón I, Suárez D L, 1998. Kinetics and mechanisms of precipitation of calcite as affected by pCO₂ and organic ligands at 25°C. *Geochim. Cosmochim. Acta* **62**(3), 405-416.

Lorah M M, Herman J S, 1988. The chemical evolution of a travertine-depositing stream: geochemical processes and mass transfer reactions. *Water Resources Research*, **24**(9), 1541-1552.

Nimick D A, Cleasby T E, McCleskey R B, 2005. Seasonality of diel cycles of dissolved trace-metal concentrations in a Rocky Mountain stream. *Environmental Geology*, **47**(5), 603-614.

Nimick D A, Gammons C H, Parker S R, 2011. Diel biogeochemical processes and their effect on the aqueous chemistry of streams: A review. *Chemical Geology*, **283**(1-2): 3-17.

Parkhurst D L, Appelo C A J, 1999. *User's guide to PHREEQC (Version 2) – A computer program for speciation, batch-reaction, one-dimensional transport, and inverse geochemical calculations: US Geological Survey Water-Resources Investigations Report (SuDoc I 19.42/4-99-4259)*, 1999, p. 310.

Reichert P, 2001. River water quality model no. 1 (RWQM1): case study II. Oxygen and nitrogen conversion processes in the River Glatt (Switzerland). *Water Science and Technology*, **43**(5), 51-60.

Riding R, 2000. Microbial carbonates: the geological record of calcified bacterialalgal mats and biofilms. *Sedimentology* **47** (Suppl. 1), 179-214.

Spiro B, Pentecost A, 1991. One day in the life of a stream—a diurnal inorganic carbon mass balance for a travertine-depositing stream (Waterfall Beck, Yorkshire). *Geomicrobiol J.* **9**(1), 1-11.

Tobias C, Böhlke J K, 2011. Biological and geochemical controls on diel dissolved inorganic carbon cycling in a low-order agricultural stream: Implications for reach scales and beyond. *Chemical Geology*, **283**(1-2), 18-30.

Speleological Research and Activities in Artificial Caves

A 100-km-Long subterranean Roman Aqueduct in northern Jordan?

Stephan Kempe¹ and Ahmad Al-Malabeh²

Affiliation: ¹Institute of Applied Geosciences, Technische Universität Darmstadt, Schnittspahnstr. 9, 64287 Darmstadt, Germany, kempe@geo.tu-darmstadt.de
²Hashemite University Zarka, Jordan, Malabite.ahmad@yahoo.com

Abstract

Northern Jordan hides one of the least-known marvels of the antique world: a system of subterranean aqueducts of Roman Imperial times, the Yarmouk-Decapolis Tunnel. The system may have been 106 km long, serving some of the Decapolis cities. The hypothesis of M. Döring (2008, 2016) states that it collected water in SW-Syria through channels (the Qanat Fir'aun) and conducted it through artificial tunnels, as far as Gadara (Umm Qays) above Lake Tiberias. It was constructed in Tertiary chalk which shows karstification so that a substantial section of the tunnels was plastered to make the walls water-tight.

At the Syrian border, at Al-Turrah, the tunnel begins at an altitude of 434.3 m a.s.l. (m above sea level). It supposedly ends at Gadara (Umm Qays) at 352.5 m a.s.l.. The tunnel length is 86 km, resulting in a slope 0.95‰. Many sections, however, had slopes of <0.2‰ (Döring 2016), much less than the 5‰, Roman architect Vitruvius recommended.

The tunnel was constructed by using multiple building shafts. In a 1 km-long section surveyed, these occur from 17 to 75 m apart, 37 m on average. Thus, teams could work up- and downslope simultaneously, economizing on construction time. Later, shafts were blocked, leaving few entrances today. Often the tunnel can only be followed by refuse piles of the building shafts, many of them lost by modern alterations.

Several reasons let us doubt that the tunnel existed as suggested. The first reason is its low slope which, in reality, is even lower than calculated above. This is because the tunnel not only needs to twist around side valleys but it is itself sinuous: in a km-long-section surveyed, sinuosities were 2.34, 1.34 and 1.46. At one place, the tunnel takes a loop of 40 m instead of going straight for 3 m. Thus, actual slope is much lower hampering the water flow over long distances in the first place. The second reason is that the slope in the measured section is 8.4 permille, i.e. much higher than could be tolerated. Even worse, the tunnel slants into the opposite direction. These findings were repeated in a second, albeit shorter section. Either these tunnels are not part of the main route or the tunnel served local and not long-distance purposes.

Keywords:

1. Introduction

In the area divided today among Jordan and Syria, a loose federation of about ten cities was called Decapolis (Fig. 1). After Pompejus conquered the area in 63 BC, these cities were part of the Roman Empire with Gadara (e.g., Hoffmann 2002) as its main town. When in 106 AD the Province Arabia was founded the cities were administered by the provinces Palestina Secunda, Arabia and Syria. The Pax Romana led to an increase in commerce with the Arabian Peninsula and Mesopotamia and led to substantial economic growth of the area, and an increasing population and its wealth. In turn the water demand increased. Gadara (Umm Qais), perched on a high ridge (Fig. 2) with view onto Lake Tiberias, was specifically in need of water. Cisterns and the spring at the foot of the mountain were not enough to supply the city with water for fountains, baths and gardens. The city therefore built a 23 km (or 30 km, according to Döring 2016) long aqueduct tunnel. It tapped the spring of Ain Turab to the east with a discharge of about 4 l/min (Döring 2016). To reach the city, a final valley was bridged. Even though locally always known in sections, the tunnel, its extent and function was explored only in the 1990's by German archeologists (e.g., Kerner 2002, 2004; Keilholz 2016).

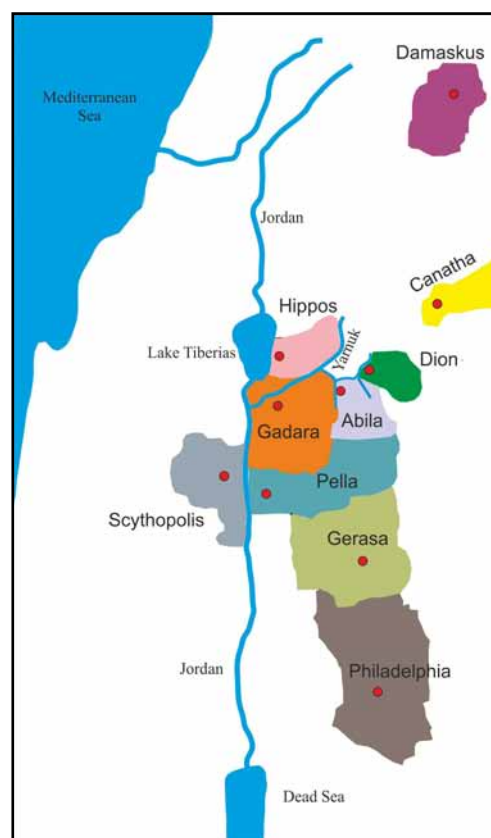


Figure 1. The area of the Decapolis (altered after Luz 2011)



Figure 2. Slant view of the antique city of Gadara, west of the present city of Umm Qais on a ridge. The red line depicts the aqueduct approaching the city from the East. In the background, Lake Tiberias, the Golan Heights and Mt. Hebron. Note pronounced erosion due to the lowering of the Dead Sea Rift. (Google Earth view from South, elevation 3x exaggerated).

Beyond this well-established tunnel system, many more traces of Roman underground engineering exist. Early travelers (see Döring 2016) already noted the existence of these aqueducts and speculated about their reach. Between 2004 and 2010, Mathias Döring, Hochschule Darmstadt, and his students studied the system of tunnels with the view of water engineers. As a result, Döring (2005, 2008, 2010) advanced the hypothesis that the Qanat Fir'aun collected water from productive springs in the Hauran (in Syria) in two branches of surface aqueducts feeding the collected discharge into a tunnel at Al-Turrah (Jordan). From there tunnels and a few bridges conveyed the water to Ain Turab, where it was fed into the existing tunnel to Gadara. A second tunnel above the old Ain Turab-tunnel was built but apparently not activated because of small mistakes in elevation-planning (Döring 2016). In 2016 Döring summarized his results including detailed maps of the studied tunnel sections and hydraulic conclusions in an inspiring book.

The area of Northern Jordan is discharging towards the Jordan-Dead Sea rift. Its lowering has caused the rivers to cut deep into the pre-existing plateau. The main river is the Yarmouk, flowing to the north of the Gadara ridge (Fig. 2). Most of its tributaries come from the south, the most imposing one is the Wadi Al-Shallalah (Fig. 3) around which the tunnel had to twist in order to keep altitude. The steep topography with the over 100 m deep gulches and canyons is also due to the low resistance of the rocks comprising the area: Tertiary chalk beds. The marls are relatively soft, intercalated with harder limestone layers and massive flint beds. On the one hand, the rock was relatively easily mined, but the weak rock also caused cave-ins and breakdown, so that the walls needed to be smoothed by plastering. The plastering was also necessary to keep the tunnels water-tight because of local karstification.

The Romans were masters in building aqueducts. One summarizing text book has survived the ages, Vitruvius' "De Architectura Libri Decem" (1st cent. AD). Vitruvius (8/6/1) states: "Water can be conducted in three ways, either in rivers, or by building channels or through pipes of lead or clay. If channels need to be build it should be constructed as firm as possible

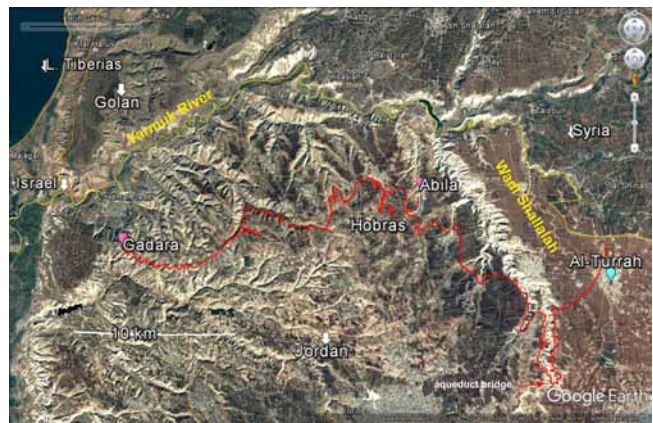


Figure 3. The possible course (red line) of the Decapolis Tunnel system according to Döring (2016). The Jordanian-Syrian border (yellow line) marks the course of the Yarmouk River. Southern tributaries have cut deep wadies, the most prominent is the Wadi Al-Shallalah to the east, around which the tunnel had to twist to keep its altitude. (Google Earth picture)

and the bed should slope no less than half a foot per 100 feet." i.e. 0.5% or 5‰. He further says (8/6/3): "If hills are situated between the city walls and the springs, then subterraneous tunnels need to be constructed to keep the advised slope. If the underground is composed of sandstone or rock then the tunnel can be built directly into it, but if it is composed of loose soil or gravel, then the sidewalls and an inverted arch need to be built to conduct the water within. The distance between the shafts of the tunnel section should be 120 feet", i.e. ca. 40 m. Excavating tunnels through closely spaced shafts is called qanat construction, a technique widely used in antique times to minimize horizontal transport of the mined rock to the surface and to enable many tunnel teams to work simultaneously.

2. Tunnel surveys

The surveys documented by Döring show that the tunnel is only accessible in small sections. For most of its tracing, the former building shafts had to be used. In some areas, the refuse piles of the building shafts are lost and the evidence of connecting certain sections is circumstantial. Nevertheless, an overall plausible picture emerged suggesting the tunnel system may have been 106 km long with only a few interruptions by aqueduct bridges (Döring 2016). Of this, an estimated 86 km (Döring 2016, p. 196) represent the direct connection to Gadara. It may in fact be the longest continuous antique water tunnel, surpassing even the better-known systems of Nimes, Lyon, Rome, Campi Flegrei, Carthage or Byzantium. Most convincing is that the sections seem to be at elevations sustaining a continuous dip towards Gadara. At Al-Turrah, the tunnel floor has an altitude of 434.3 and at Gadara of 352.5 m a.s.l., i.e. a difference of 81.8 m. The direct distance is 29 km, yielding a slope of 2.8‰. But because of the much longer length of 86 km the slope diminishes to 0.95‰. For comparison, the aqueducts providing Jerusalem have slopes of 2.8 to 0.9‰ (Mazar 2001).

In 2005 we began to explore certain sections of the tunnel system (Al-Malabeh 2005, 2007; Al-Malabeh and Kempe 2012, 2013, Al-Malabeh *et al.* 2008) aided by local informants. Two surveyed sections were long enough to yield additional and controversial data. Figure 4 shows section Hobras I East

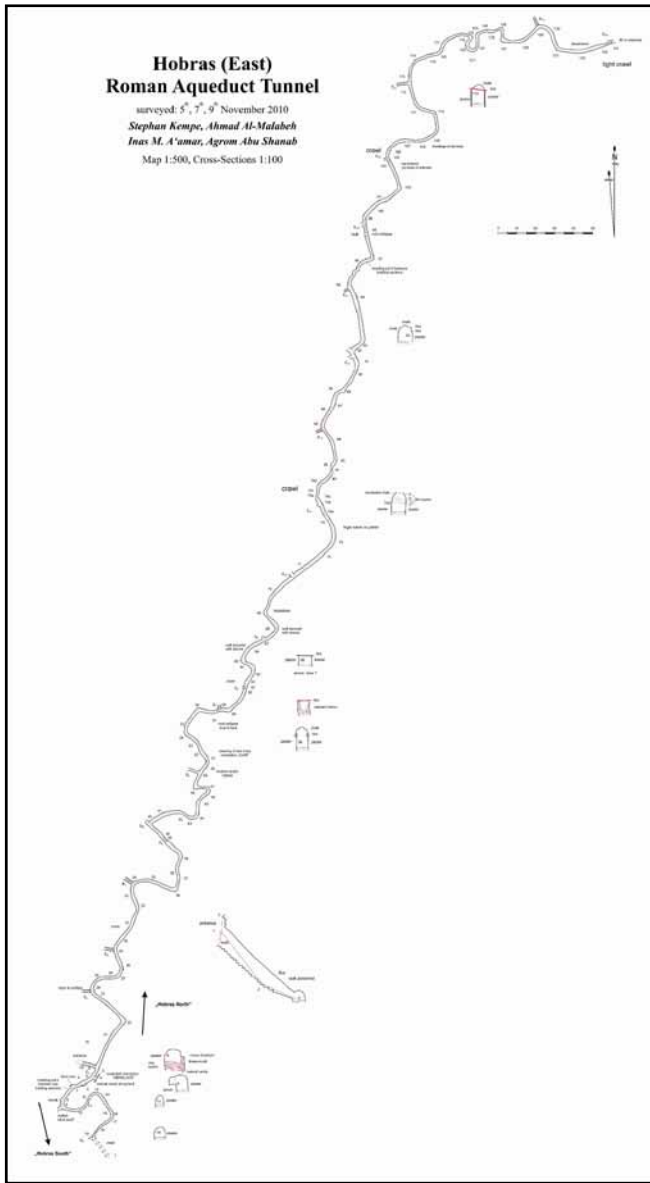


Figure 4. Map of ca. 1 km long section of Hobras I (East).

(see also Döring 2016, who reproduced this survey by permission on p. 134). Table 1 gives data on building shaft distances.

The average distance between the shafts is 37 m, close to the 40 m Vitruvius suggested. The ratio between the Real Distance and the Direct Distance gives a measure of passage sinuosity, i.e. 1.41. The reasons for such a high sinuosity is not entirely clear. A certain curving, however, is wanted: When two tunnels approach each other in parallel, then a



Figure 5. Panorama of hair-pin meander in the Hobras I (East) tunnel at St. 119, doubling passage length. Note plastered walls and notch in ceiling, the remains of the pilot tunnel.

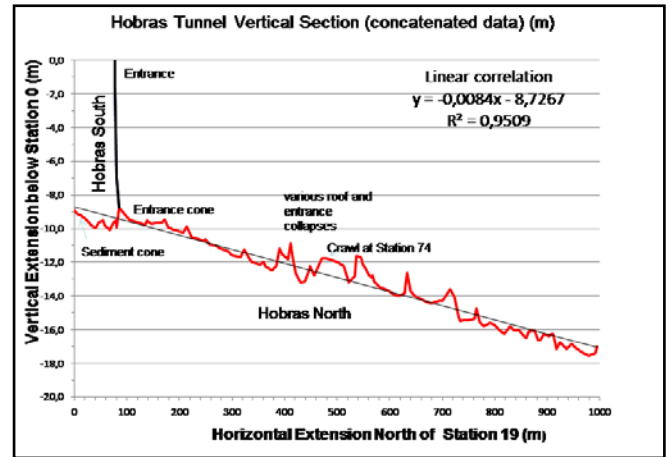


Figure 6. Vertical view of survey data of Hobras I (East). The linear regression equation shows a slope of 8.4 per mil towards the north. The local ups and downs are due to infill from collapsed shafts.

small mistake in direction could necessitate a sharp bend at the junction. If, however, the tunnels run at an angle of 20° to 30° towards each other they surely intersect at a high angle. Also, rock stability away from the valley should be better. However, this does not explain S-shaped or hair-pin curves.

The map reveals this high sinuosity: This is especially striking for Hobras South where the tunnel describes an S-curve, more than doubling the needed tunnel length. Similarly, at St. 119 a hair-pin curve of 115° occurs (Fig. 5). If the tunnel would have been continued straight, it would, after 3 m, have met the continuation at St. 123, saving 30 to 40 m of tunnel. Again, sinuosity can be calculated.

This is done for the three sections: Hobras South (St. 3-19), Hobras North N-directed (St. 3 to 117) and Hobras North E-directed (St. 117 to 134). The sinuosity thus calculated amounts to 2.34, 1.34 and 1.46, respectively. Thus, the total tunnel length is possibly significantly higher than estimated by Döring who used a factor of 1.1. If assuming that the sinuosity of Hobras-East is specifically high and that a typical sinuosity is 1.4, then the total tunnel length would be $(86 \text{ km}/1.1) \cdot 1.4 = 109.5 \text{ km}$ and the average slope would amount to 0.74‰. This does not prohibit water from flowing in the tunnel as a freely running stream. Some of the sections have a slope of only 0.2‰, specifically those between the Wadi Al-Shallah and Hobras.

This picture is, however, questioned when looking at the vertical section of the survey Hobras I (East) (Fig. 6). The tunnel is 10 m below the entrance (see cross-section of entrance on Fig. 4). The slope is not only 8.4‰, but also points northward.



Figure 7. Surveying across the collapse of a buildings shaft (to the left of caver). Note flint layer and notch in ceiling of pilot tunnel.

This precludes water flowing to Gadara. The survey was made by compass and Leica Laser DISTO that measures length and inclination at high precision. Nevertheless, it cannot be excluded that a systematic mistake was made by the instrument or by us, the surveyors. Also, we thought back-shots unnecessary since we assumed that the tunnel is directed to Gadara. Inclination was initially measured only to correct for the steeper shots up and down the sediment infills below the collapsed shafts (Fig. 7); the wrong direction of slope was only noticed after plotting the data. Two years later, we returned to Hobras and surveyed the tunnel on the western side of the valley (Hobras II, West). Döring (2016, p. 135) shows part of this tunnel. Our survey extended beyond that for 299 m from the entrance northward (Fig. 8). Two large S-bends increased the sinuosity 1.39 and again, the slope does not point to Gadara, but rises northward by 1.8 m, yielding a dip southward of 4 %.

3. Conclusions

The tunnels (Hobras I & II) on both sides of Wadi Traitab, north of Hobras not only have a higher sinuosity (ca. 1.4) but also a much higher dip than expected for the Decapolis Tunnel. They also dip into the wrong direction. Thus, they could have delivered water to Abila but not to Gadara (Figs.3, 9). Caution is, however, needed before rejecting the existence of the Gadara tunnel because cave survey techniques may not be adequate to the problem.

Table 1. Statistics of building shaft distances for 20 shafts of the Hobras I East section (survey 2010). SD = standard deviation, coef. var. = coefficient of variation, min = minimum, max = maximum.

N = 20	Direct Distance	Real Distance
Mean	36.9 m	52.1 m
SD	11.2 m	20.6 m
Coef. Var.	30.2%	39.6%
Min.	16.9 m	20.3 m
Max.	74.5 m	114.8 m

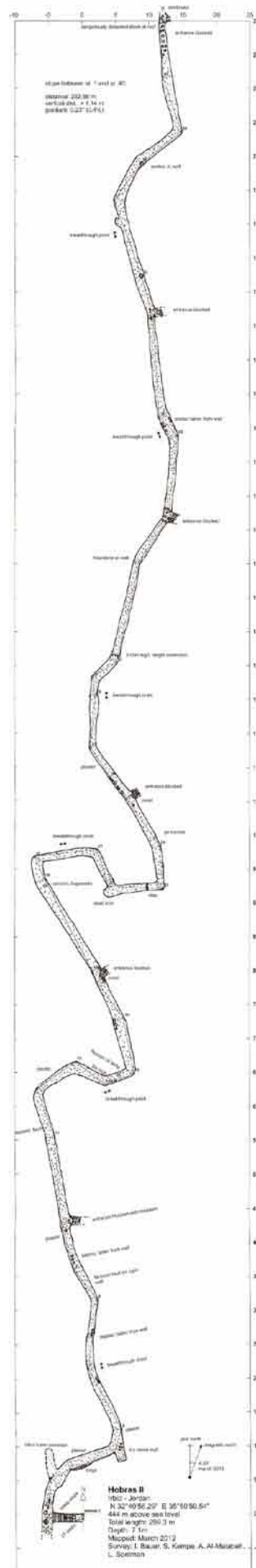


Figure 8. Map Hobras II (West).



Figure 9. View S into the valley of Hobras (village in background). Red: trace of the Gadara tunnel after Döring. Colored: Cave-Render traces of surveys of Hobras I East (left) and Hobras II West (right). Gadara is to the right (W) Abila to the left (E). (Google Earth picture, elevation 3x exaggerated).

References

- Al-Malabeh A, 2005. New discoveries supporting eco-tourism in Jordan. *1st Economic Jordanian Forum. Abstr. Book*, p. 6.
- Al-Malabeh A, 2007. Discovery of the Yarmouk-Decapolis Tunnel: The longest aqueduct in the antiquities. *2nd Economic Jordanian Forum. Abstr. Book*, p. 1.
- Al-Malabeh A, and Kempe S, 2012. Yarmouk-Decapolis Tunnel System: the most important underground discovery in Jordan of the last decade. *Abstr. Proceed. 15th Intern. Symp. on Vulcanospeleology*, Hashemite Univ. Zarka, Jordan, 15-22 March, 2012, p. 32.
- Al-Malabeh A, and Kempe S, 2013. The Roman Yarmouk-Decapolis Tunnel System, hypotheses and facts. *Abstr. World Archeological Congr.*, Dead Sea, Jordan, Jan. 2013.
- Al-Malabeh A, Kempe S, Rababeh S, 2008. Discovery of the longest water tunnel in the ancient periods: Decapolis Tunnel, North Jordan. *6th Conf. on Sci. & Techni.*, Rome, Abstr. Book, p. 9.
- Döring M, 2005. Römische Wasserversorgungstunnel im Norden Jordaniens, eine Voruntersuchung. *Zeitschrift des deutschen Palästina Vereins*, **121** (2205)2, 130-139.
- Döring M, 2008. Qanat Firaun, über 100 km langer Aquädukt in nordjordanischen Bergland. *Schriften der Deutschen Wasserhistorischen Gesellschaft* **1**, 189-204.
- Döring M, 2010. 106 km langer römischer Aquäduktunnel im jordanisch-syrischen Grenzgebiet. In: W Ließmann, M Bock, V Scholz and J Kugler (Eds.) *13. Intern. Bergbau- & Montanhistorik-Workshop St. Andreasberg, Tagungsband; Netzwerk Montanhistorik*, St. Andreasberg, 13-40.
- Döring M, 2016. Wasser für die Decapolis, römische Fernwasserleitung in Syrien und Jordanien. *Schriften d. Deut. Wasserhistorischen Gesellschaft* **12**, Siegburg, 292 pp.
- Keilholz P, 2016. Die innerstädtische Wasserversorgung von Gadara. In: M Döring (Ed), *Wasser für die Decapolis, römische Fernwasserleitung in Syrien und Jordanien. Schriften d. Deut. Wasserhistorischen Gesellschaft* **12**, Siegburg, pp. 257-292.
- Hoffmann A, 2002. Topographie und Stadtgeschichte von Gadara/Umm Qais. In: A Hoffmann, S Kerner (Eds). *Gadara – Gerasa und die Decapolis*, Verlag Philipp von Zabern, Mainz, pp. 98-124.
- Kerner S, 2002. Gadara – schwarz-weiße Stadt zwischen Adjlun und Golan. In: A. Hoffmann, S Kerner Eds), *Gadara – Gerasa und die Decapolis*, Verlag Philipp von Zabern, Mainz, pp. 189-211.
- Kerner S, 2004. The Water System in Gadara and other Decapolis Cities of Northern Jordan. In: HD Bienert, J Häser (Eds): *Men of Dikes and Canals*, *Orient Archäologie* **13**, 187-202.
- Luz M, 2011. http://olbigjimsplace.blogspot.de/2011_06_01_archive.html, accessed 2013.
- Mazar A, 2001. Untersuchungen über die Wasserleitungen nach Jerusalem. In: W Dierx, G Garbrecht, (Eds), *Wasser im Heiligen Land und archäologische Forschungen. Fontius-Ges. Supp. Bd. III*, pp. 165-194.
- Vitruvius, 2004. *De Architectura Libri Decem*. Matrix Verlag, Wiesbaden, 397 pp. (after translation into German by F. Reber, published in 1908).

Hypogea 2015 and 2017: a short, but very intense, history

Mario Parise¹, Roberto Bixio², Carla Galeazzi³, Ali Yamac⁴

Affiliation: ¹Department of Earth and Environmental Sciences, University “Aldo Moro”, Via Orabona 4, 70125 Bari, Italy, mario.parise@uniba.it; National Research Council, IRPI, Bari, Italy

²Centro Studi Sotteranei, Genova, Italy; roberto.bixio@gmail.com

³Egeria Centro Ricerche Sotteranee, Rome, Italy; carla.galeazzi3@alice.it

⁴OBRUK Cave Research Group, Istanbul, Turkey; ayamac@gmail.com

Abstract

In March 2015 at the National Research Council headquarters in Rome, Italy, the congress Hypogea 2015, an International Congress of Speleology in Artificial Cavities, was held. Organized by the Commission on Artificial Cavities of the International Union of Speleology (UIS) in co-operation with the local associations Egeria, ASSO and Roma Sotterranea, and under the auspices of UIS and the Italian Speleological Society (SSI), the congress was very successful. There were over 70 contributions from 11 countries that were organized in 8 different thematic sessions. As a result, a voluminous proceedings book of over 550 pages was printed and distributed at the congress, edited by Mario Parise, Carla Galeazzi, Roberto Bixio and Carlo Germani. The Italian experience left an indelible mark on the cavers interested in artificial cavities, and soon a proposal for organization of the congress in 2017 came from Turkey, in the remarkable landscape of Cappadocia. The work of preparation for the congress started soon after Hypogea 2015, and at the time of writing (December 2016) we are about to finalize the proceedings. These, once again, will be distributed as a nice volume that we hope will be another reference point for researches and activities in artificial cavities. In this contribution we summarize the activity so far completed, from the initial idea of Hypogea 2015, to the 2017 congress in Cappadocia. Aimed at moving further ahead, looking toward Hypogea 2019

Keywords: artificial cavities, UIs Commission, Hypogea

1. Introduction

Artificial cavities, that is the cavities excavated and realized by man during past epochs, are a long-time object of interest for a variety of scholars, which is not limited to cavers but also includes scientists and researchers (archaeologists, to historians, anthropologists, etc.), not used to the underground environment. Studying artificial cavities means opening a window on the history of the sites, since in many cases they have been the first place where human beings lived and performed their cults, or where they kept livestock, stored grains and other groceries. Actually, there are many different types of artificial cavities, and related sub-categories, as shown in the Typological Tree, the classification initially proposed by the Commission of Artificial Cavities of the Italian Speleological Society, and later approved also at international level by the corresponding Commission of the International Union of Speleology (UIS; Galeazzi, 2013; Parise et al., 2013).

This latter Commission since 2009 (year in which appointment of new president and members were carried out) have been particularly active, promoting a series of meetings, workshops and activities. For instance, it is worth to recall here the workshop organized in Turin (Italy) on May 18-20, 2012, dedicated to “*Classification of the typologies of artificial cavities in the world*”. The workshop consisted in 11 invited lectures covering several aspects of the classification of artificial cavities, plus additional 10 posters, and a final discussion devoted to establishing a general classification of artificial cavities. The workshop proceedings have been published in 2013 as a special issue of the journal *Opera Ipogea* (Parise, 2013).

In 2013, on the occasion of the 16th International Congress of Speleology at Brno (Czech Republic), the UIS Commission proposed a specific session, entitled “*Speleological Research and Activities in Artificial Underground*”, which was very successful, receiving 18 abstracts from 10 different countries worldwide.

Apart from these very successful activities, most of the work by the UIS Commission on Artificial Cavities was focused in the last years on the organization of a specific international congress. The chosen name was HYPOGEA, which well represents the underground world in which we are deeply interested. Two long years of preparation eventually allowed us to host the International Congress of Speleology in Artificial Cavities Hypogea 2015.

Organized by the UIS Commission on Artificial Cavities, in co-operation with the local associations Egeria, ASSO and Roma Sotterranea, and under the auspices of UIS and of the Italian Speleological Society, the congress was held in March 2015, at the National Research Council headquarters in Rome, Italy. Choice of the venue was straightforward: the city of Rome is worldwide famous for its extraordinary richness in history, with a huge number of testimonies present below the present city, in the forms of a great variety of artificial cavities, including the remains of the several km-long aqueducts built to supply with water the town (Judson and Kahane, 1963; Blackman, 1979; Hodge, 1992; Kolowski Ostrow, 2002). Further, during the last decades the general attention on artificial cavities in Italy has greatly increased, due to a number of

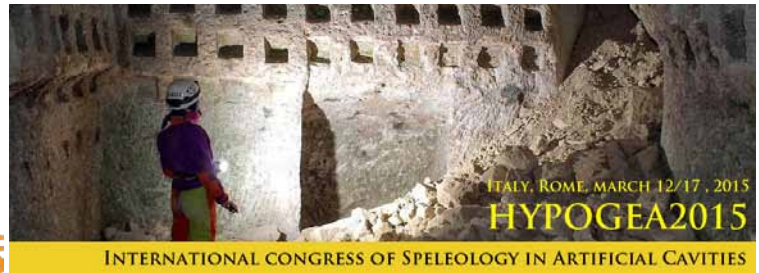
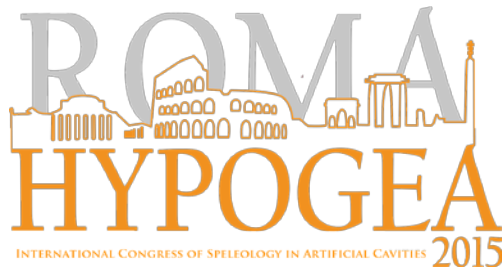


Figure 1. Logo and banner of the Hypogea 2015 Congress.



Figure 2. Hypogea 2015: shots taken during the sessions, held at the prestigious facility of the headquarters of the National Research Council of Italy in Rome, in the Marconi Hall. To the lower right corner, a moment of the “invasion” by the Roman gladiators.

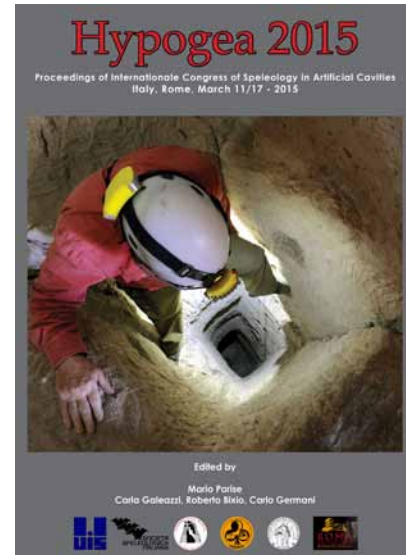


Figure 3. Cover page of the Hypogea 2015 proceedings.

problems linked to occurrence of sinkholes caused by ancient quarries and mines in several regions (Parise & Gunn, 2007; Parise, 2013, 2015; Parise & Vennari, 2013); thus, also from the standpoint of civil protection issues, the topic has become of wide interest.

Hypogea 2015 received over 70 contributions from 11 countries, that were organized in 8 different thematic sessions, covering the following issues:

- Hypogean civil dwellings;
- Hydraulic underground works;
- Mining works;
- Religious – Cult structures;
- Archaeological studies;
- New technologies for artificial cavities;
- Typologies, symbols, terms, and Cadastre of Artificial Cavities;
- Miscellaneous.

150 scholars from 15 countries attended the event. The official sessions were also enriched by accompanying events, such as a peaceful “invasion” of the congress hall by a group of Roman gladiators! It was an exhibition (Fig. 2) organized thanks to availability of an historical group, Gruppo Storico Romano, specialized in historical reconstruction and in the use of ancient clothes, outfits and weapons used during the Roman age.

A voluminous proceedings book of over 550 pages (Fig. 3), edited by Mario Parise, Carla Galeazzi, Roberto Bixio and Carlo Germani, was printed and distributed at the congress, containing the many interesting contributions presented (Parise et al., 2015).

Further, several field trips were organized, both during the days of the congress and as post-congress excursion (Fig. 4). In detail, the field trip in Rome gave the opportunity to “travel” during 23 centuries (from the 6th century B.C. to the 17th century A.D.), exploring arcaic water drains, mithraeums, ancient aqueducts, tuff mines, ancient roman houses, nimphaeus and inquisition cells. The post-congress excursions, on the other hand, covered sites as the Alban Hills and Narni. The Alban Hills, located a few kilometers south-east from Rome, in an area that was historically inhabited by Latin populations and by ancestors of the Romans, are extremely rich in underground sites, which include, among the others, the inlet of the Albano drain, some Nymphaeus, and the Catacomb of San Senatore at Albano. Narni, in Umbria region, is a town which preserves significant monuments of the Roman period, such as an imposing bridge built by Augustus and the long aqueduct named Formina. Destroyed during barbarian invasions, the town reached its maximum splendor in the Middle Ages, as shown by the urban characteristics and by several historical buildings. At Narni, the excursions were focused on the Formina Aqueduct and the underground of the St. Domenico Church, including the Inquisition cells. Overall, Hypogea 2015 was a great success, which definitely went beyond any positive expectation.



Figure 4. Images of some of the field trips organized for the Hypogea 2015 edition.

The Italian experience left an indelible mark on the cavers interested in artificial cavities, and soon a proposal for organization of the congress in 2017 came from Turkey, in the remarkable landscape of Cappadocia (Fig. 5). The work of preparation for the congress started soon after Hypogea 2015, by opening a dedicated website aimed at informing interested people, and at collecting the abstracts and full papers to be submitted to the congress (Fig. 6). At the time of writing (February 2017) we are about to finalize the proceedings. These, once again, will be distributed as a nice volume that we hope will be another reference point for researches and activities in artificial cavities.

As with Rome for the first edition of Hypogea, the choice of Cappadocia for the 2017 congress was dictated by the enormous relevance that this area of central Turkey has for the history of artificial cavities. Thousands of man-made caves, belonging to about all the categories in the artificial cavities classification, are distributed in this region, with some of the most famous worldwide underground settlements. Studied since several centuries as one of the most interesting sites for such features, Cappadocia never ceases to show new and unexpected sites of interest for the speleology in artificial cavities. Notwithstanding the difficult political situation, and the widespread attacks and problems in the last few years, we hope that the 2017 congress will be a good occasion to strengthen the relationships started in Rome. Aimed at moving further ahead, looking toward Hypogea 2019



Figure 5. The poster prepared to advertise the Hypogea 2017 Congress in Cappadocia.



Figure 6. The banner of the Hypogea 2017 Congress, at the website <http://hypogea2017.com>.

References

Blackman DR, 1979. The volume of water delivered by the four great aqueducts of Rome. *Papers of the British School at Rome*, **46**.

Galeazzi C, 2013. The typological tree of artificial cavities: a contribution by the Commission of the Italian Speleological Society. *Opera Ipogea*, **1**, 9–18.

Hodge AT, 1992. *Roman aqueducts and water supply*, London

Judson S, Kahane A, 1963. Underground drainage ways in southern Etruria and northern Latium. *Papers of the British School at Rome*, **31**, 74–99.

Koloski Ostrow AO (ed.), 2001. Water use and hydraulics in the Roman city. *Archaeological Institute of America, Colloquia and Conference Papers 3*, Kendall/Hunt Publication Co., 131 p..

Parise M (Ed.), 2013. Proceedings of the international workshop on speleology in artificial cavities “*Classification of the typologies of artificial cavities in the world*” (Torino/Italy – May 18-20, 2012). *Opera Ipogea*, 1/2013.

Parise M, 2013. Recognition of instability features in artificial cavities. In: Filippi M, Bosak P (Editors), *Proceedings 16th*

International Congress of Speleology, Brno, 21-28 July 2013, **2**, 224-229.

Parise M, 2015. A procedure for evaluating the susceptibility to natural and anthropogenic sinkholes. *Georisk*, **9**(4), 272-285, DOI:10.1080/17499518.2015.1045002.

Parise M, Gunn J, (Eds.), 2007. Natural and anthropogenic hazards in karst areas: Recognition, Analysis and Mitigation. *Geol. Soc. London, Special Publications*, **279**, 202.

Parise M, Vennari C, 2013. A chronological catalogue of sinkholes in Italy: the first step toward a real evaluation of the sinkhole hazard. In: Land L, Doctor DH, Stephenson B (Eds.), *Proc. 13th Multidisciplinary Conf. on Sinkholes and the Engineering and Environmental Impacts of Karst, Carlsbad (New Mexico, USA)*, 6-10 May 2013, National Cave and Karst Research Institute, 383-392.

Parise M, Galeazzi C, Bixio R, Dixon M, 2013. Classification of artificial cavities: a first contribution by the UIS Commission. In: Filippi M, Bosak P (Editors), *Proceedings 16th International Congress of Speleology, Brno*, 21-28 July 2013, **2**, 230-235.

Parise M, Galeazzi C, Bixio R, Germani C, (eds) 2015. *Proceedings of the International Congress in Artificial Cavities “Hypogea 2015”*. Rome, March 11-17, 2015, ISBN 978-88-89731-79-6, 543 pp.

Speleogenesis

Karst morphological processes and evolution of the limestone massif of Georgia from depositional, sedimentary, and structural investigations in Muradi Cave

Lasha Asanidze¹, Zaza Lezhava¹, Kukuri Tsikarishvili¹, Nino Chikhradze^{1,2}, Jason S. Polk³

Affiliation: ¹Department of Geomorphology, Vakhushti Bagrationi Institute of Geography, Ivane Javakhsishvili Tbilisi State University, Speleological Society of Georgia, Tamarashvili st. 6. 0177, Tbilisi, Georgia. asanidze.lasha@yahoo.com
²School of Natural Sciences and Engineering, Ilia State University, Cholokashvili Ave 3/5. 0162, Tbilisi, Georgia.
³Center for Human GeoEnvironmental Studies, Department of Geography and Geology, Western Kentucky University, Bowling Green, KY 42101, USA.

Abstract

The aim of this paper is to introduce the karst morphological processes and evolution of the limestone massif of the Caucasus region of Georgia from depositional, sedimentary, and structural investigations in Muradi Cave to the scientific and public community. In this work, we present a new study of the recently investigated Muradi Cave in the Racha limestone massif, which is located in the eastern part of the karst zone of western Georgia. Muradi Cave unique as the fact that it contains almost all types and subtypes of speleothems and sediments recorded nowadays in the caves of the Caucasus region, and the mineral aggregates found in Muradi Cave are rare for the caves of the Caucasus region. The lithological study of the terrigenous deposits allowed us to identify their sources, routes of transportation, and patterns of deposition. By taking into consideration the geological-geomorphological peculiarities and the results of the archeological materials of the region, it became possible to identify the age of the oldest deposits (Lower Pleistocene). Therefore, this investigation of an understudied area in Georgia, as well as the discovery of unique formations, provides new insights into the development of a large limestone massif in the region and the understanding of the region's speleological and geomorphological evolution.

Keywords: speleogenesis, limestone massif, Muradi Cave, speleothems, country of Georgia.

1. Introduction

The country of Georgia has a large extent of limestone massifs with well-developed karst features. The limestone massifs occupy more than 4,475 km², or 6.4%, of the entire territory of Georgia (Asanidze *et al.*, 2013a; Asanidze *et al.*, 2013b), and includes over 1,500 known caves (Asanidze *et al.*, 2017). One of these, Kruberka Cave is currently the deepest in the world (over 2,100 m in depth). Although it is the deepest known thus far, several other massifs in the region have the potential to also host extensive and deep cave systems (Tintilozov, 1976; Klimchouk, 2006, 2012; Klimchouk *et al.*, 2009). In addition to the potential for deep caves, the aforementioned limestone massifs of Georgia remain relatively understudied with regard to speleogenetic processes, including the presence of unique and interesting speleothem and mineralogical assemblages due to the possibility of geothermal and tectonic influences (Kipiani, 1974). It is important that the scientific exploration and research continue in the region in order to better understand the factors controlling speleogenesis and speleothem development, as well as to provide context for comparing to other similar complex karst regions throughout the world.

A local hunter discovered Muradi Cave some years ago, in the Racha limestone massif, and in November 2014, the Mountaineers and Travelers Club (led by Irakli Julakidze) discovered a narrow corridor when exploring the cave. After navigating the corridor, the club members found themselves in a previously unknown part of the cave. In 2015, complex scientific study supervised by the lead author was carried out in the cave by the speleological expedition of the Vakhushti Bagrationi Institute of Geography.

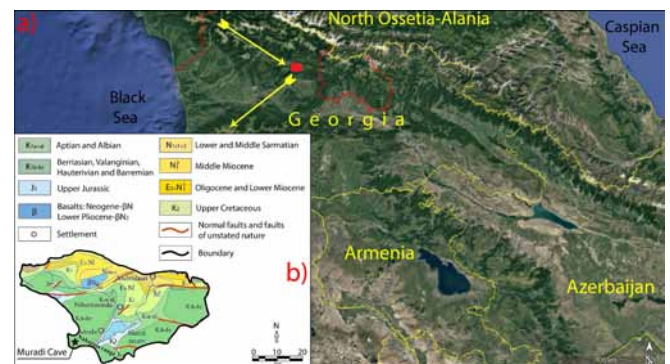


Figure 1. a). Study area, location of Muradi Cave in the Nakeralia range, b). Geological map of the Racha limestone massif (after Gudjabadze, 2003).

2. Study area

The Racha limestone massif is located in the eastern part of the karst zone of western Georgia (Asanidze *et al.*, 2017), where diverse surface and subsurface karst landforms are found; the total area of which exceeds 590 km² (Kipiani, 1974). Muradi Cave is located to the southwestern part of the Racha limestone massif, in to the Nakeralia range. The arch-like entrance of Muradi Cave (4 x 1 m) opens at the height of 1498 m above sea level (asl). The massif is a classic region throughout the Caucasus in terms of karst process development. The Bajocian porphyritic suite is the basis of the massif and the Cretaceous carbonate rocks participate in the structure of the complex (Rakviashvili, 1985). Rocks from almost every part of the Early and Late Cretaceous exist in the region (Fig. 1). The Muradi Cave is developed in the stratified limestones of Barremian age (Urgonian facies) with north-western (2900–3000/100–150) direction of the strata along the tectonic and bedding fractures.



Figure 2. Doline in the Nakerala range, 200 m away to the south from the entrance of Muradi Cave (photo by George Lominadze).

Nakerala range consists mainly of Cretaceous and Paleogene limestones, which has an important influence on the origin and development of the surface and underground karst features and on the water table and its fluctuation (Rakviashvili, 1985). The range has a monoclinic structure with its southern slope being steep and its northern slope slightly inclined. The direction of the dip is northeast and the strata are mostly limestones of the Barremian-Urgonian facies. The intensity of karst processes in such regions is considerable. The fault dislocations are a good basis for cave inception and groundwater infiltration. There is a rapid infiltration and inflow of surface water and there is almost no surface flow in the northern slope of the Nakerala range (Kipiani, 1974). The small surface streams are mostly associated with the rainy and snowmelt periods, during which the water flows out of the fissured limestones in the upper part of the hillocks and disappears into either ponors or the Muradi Cave entrance after a short distance.

A wide range of dolines is found in the Nakerala range. According to our observation, they range in size (bigger than 200 m in circumference and 20–30 m in depth), but mostly have large areas and significant depth, though it should be noted that the density of the dolines is heterogeneous. The doline density is approximately 40 per km² along the western slope, from where the humid air masses are flowing freely and precipitation easily reaches its annual maximum. Conical dolines are relatively widespread in the slope, which basically terminate in ponors draining into shafts and caves. Lakes are formed in some of the dolines (Fig. 2).

3. Methods

We used various methods to investigate Muradi Cave. The air temperature (°C) was measured in two different places of the cave by using the instrument Onset HOBO Pro V2 Data Logger. We also measured the water temperature in one section, where the small pool is developed (containing speleothems). The water temperature was measured by the instrument Enviro Safe pocket thermometer. We also used the XRD analysis method for determination of minerals in speleothems. By using a compass-clinometer and a laser dis-



Figure 3. 10-m vertical passage (chimney) between the lower and upper level in Muradi Cave (photo by Lasha Asanidze).

tance meter, the principal and individual passages of the cave were surveyed, and a 3D sketch was developed, using various computer software (Geographic Information Systems and Compass Survey Software).

4. Results and Discussion

Here, we present the results of this first study of the massif and Muradi Cave, including a morphometric cave analysis with a situational plan and 3D model of the cave and data from the geochemical and hydrological influences on its development. Collectively, this research was undertaken to provide the foundation for future research to determine the geologic and geomorphological influences on cave development and karst hydrology of the Racha limestone massif.

The survey of Muradi Cave revealed that it has one main passage and three short branches; however, the cave may have other undiscovered passages. This assumption is based on the intense air flow in the terminal section of the cave. The 171 meter long horizontal section of the lower cave level connects with the upper level through a 10 m vertical passage (Fig. 3).

By using a compass-clinometer and a laser distance meter, the principal and individual passages of the cave were surveyed, and a 3D sketch was developed, using various computer software (Fig. 4). It seems that this vertical passage (Chimney) was created by a waterfall entering from the surface. The cave's main passage and the adjacent corridors show traces of a previous stream as, clay-loam and sandy-loam sediments and breakdown are present on the floor, where as alluvium deposits were left on the walls. This section of Muradi Cave represents its lower level, and is characterized by strong air-flow, large breakdown deposits, but mostly lacks speleothems, except some that are desiccated or weathered.

Above the 10 m vertical chimney to the bottom of the dome is a second cave level, which is a sub-horizontal and tunnel-like section with several side passages. Located in the contact zone of the tectonic fractures and bedding planes, there is another passage (azimuth 25°) with an oval pool present at its terminus. The upper level, like the rest of Muradi Cave,

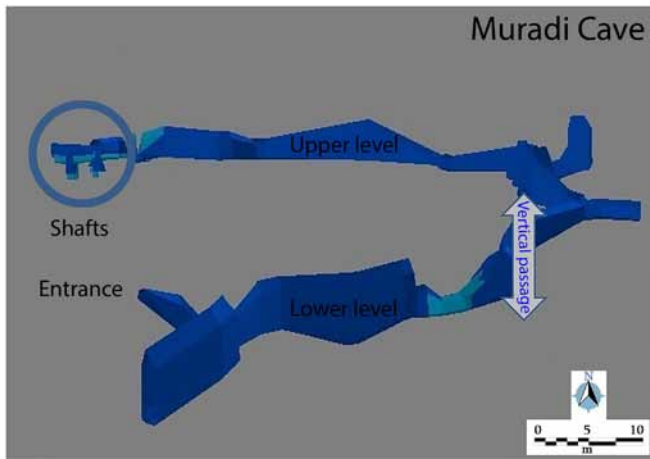


Figure 4. Compass-generated 3D model of Muradi Cave (by Lasha Asanidze). The total length of Muradi Cave is 660 m, average width 5 m, average height 8 m, floor's mean area is 3,500 m², and total volume is 29,000 m³. A narrow corridor descending westward at 60° from the entrance is filled with a great amount of breakdown.

lacks permanent streams; however, clear signs of the previous active influence of water is visible from passage morphology that includes vugs, rounded arches, and scallops from water moving at high velocity.

A tall canyon stretches for several tens of meters in the terminal section of the upper level of the cave has developed totally along a vertical fracture. On the floor, there are a series of pits with depths of 11, 42, 35, and 37 m respectively (Fig. 5).

Cold air movement is evident in the vertical section between the lower and upper passages, indicating the existence of some unknown galleries further beyond that point. In 2015, the air temperature measured in the two sections of the cave, one at the entrance and the second in the middle of the cave, near the speleothems formed in a pool. Near this pool, we also measured the water temperature, which was 7 °C on average (Fig. 5).

5. Cave morphology

It seems that one of the major areas with the active stream influence was the above-described terminal section of the cave. Later, tectonic stress and the resultant collapse of the entrance and a likely drop in the water table drastically changed the hydrological conditions of the cave, resulting in water draining from the Muradi Cave. As a result, the active flow of permanent and ephemeral streams into the cave ceased. It seems that a large ceiling collapse, formation of shafts in the floor, and the action of the infiltrating surface water depositing chemical (chemogenic) and silt deposits essentially changed the morphology of the cave.

At the sections where Muradi Cave is developed along bedding planes of the stratified limestones, the underground passages are characterized by clearly shaped linear and smoothed cross sections. Most of the upper level of the cave is of this type. In the zone of tectonic fractures influencing the cave's development, where the passages intersect with bedding planes, the cave morphology is more complex and domes are presented in the ceiling. The high and fractured arches (ceiling) of Muradi Cave are associated with vertical tectonic frac-

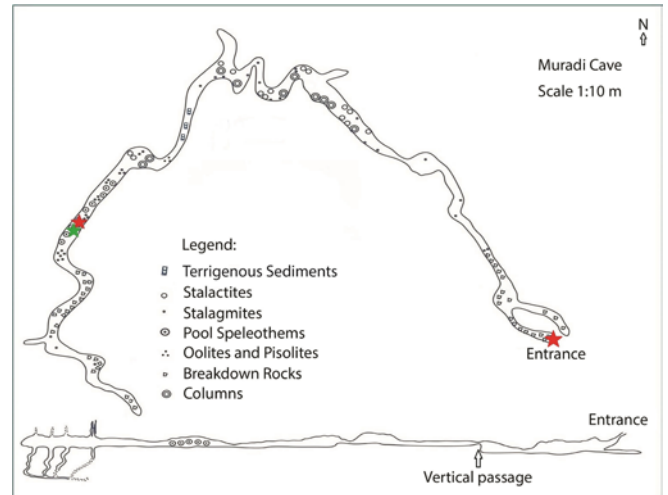


Figure 5. Schematic plan and cross-section of Muradi Cave (by Zaza Lezhava and Lasha Asanidze). The red asterisk indicates the places where the air temperature was measured; green asterisk indicates the place, where the water temperature was measured.

tures. This is particularly true near the entrance and in the terminal section of the cave.

While no permanent streams enter Muradi Cave, and there are no underground streams there is evidence of infiltration and condensate waters. The upper level of the cave has the bulk of the passages. It seems their formation was essentially influenced not so much by the lithological or structural conditions of the host bedrock, but the dynamics of the stream downcutting and dissolving the passage over long period of time. It is likely that the genesis of the meanders was much influenced by the turbulent flow of the rapidly moving currents resulting in the sculpting of the limestone bedrock and origination of meandering cave sections.

In Muradi Cave, which is in the zone of tectonic uplift in the Nakerala range, the incising streams dissolved the limestones more and more deeply and the meandering process developed accordingly as tectonic uplift occurred. In considering the location of the cave being in an intense uplift zone, the depth and regularity of the incision is clearly seen on the structural terrace levels in to the cave. Structural terraces that once were the underground river beds were developed at different heights due to the influence of vertical tectonic movements and incising streams. Now they are presented as fragmentary sections at various heights (1.2 – 1.5 m and 2.2 – 2.5 m) above the cave floor in the form of structural terraces. In Muradi Cave, the 10 m vertical passage from the upper to the lower level of the cave is important. This probably originated as a result of waterfalls from the vertical or very inclined sections of uplifted areas. Their dissolution intensified as they penetrated the bedrock, similar to the vertical domes found in Mammoth Cave and elsewhere in the world (Palmer, 2007).

5.1. Speleothems

The Muradi Cave is very rich in calcite speleothems. Almost all types of speleothems found mainly in the different section of the upper level have been found in other caves of Georgia to date. Stalactites, stalagmites, columns, shelfstones, oolites, pisolites, pool speleothems, and cave pearls, as well as special mineral aggregates including moonmilk and flowstone are



Figure 6. Calcite layers with alluvial sediment in Muradi Cave (photos by Lasha Asanidze).

found in the cave. Within the dry passages, most of these calcite formations are often desiccated or weathered.

In the relatively dry zones of the upper level of the cave, on the bottom and on the surfaces of some pools, there are accumulations of calcite rafts (3 x 5 cm or more, 1 – 1.5mm thick). The mechanisms of their formation are explained by Tintilozov (1963, 1976) as forming in dry periods when the small calcite crystals start to form in pools of water, and are retained as colloids as a result of surface tension. Later, when the cementing compounds are isolated from these colloid deposits, the lithified calcite plates are formed. As mentioned above, the isolation of the cementing crystals is particularly intense in the cave zones distinguished by very dry air, due to evaporation of the pooled water, which causes supersaturation with respect to calcite (Palmer, 2007; Perrin *et al.*, 2014). In some of these zones, the rafts merge to form large plates (1 x 2 m²). Particularly large and thick (20 – 25 mm) shelfstones formed from these conglomerated rafts are present in one of the wide corridor-like section of the second level of the cave.

These calcite speleothems found in Muradi Cave are very rare in the caves of the Caucasus and only found in Vakhushti Bagrationi's abyss (Abkhazeti, Georgia), and cover the surface of a basin dried out long ago (Tintilozov, 1976), and in Muradi Cave, this is the same situation. The terrigenous deposits found in the cave, which must have been present in the underground pool area before the water was present, are covered with a thick calcite layer. Consequently, the thorough laboratory study of the calcite crust found in Muradi Cave (chemical composition, spectral analysis, etc.) contains important information about the deposits' accumulation in the cave and general cave development, as well as providing some insight about the cave in the Upper Quaternary (Hill & Forti, 1997; White, 2007) (Fig. 6).

Mineralized calcite aggregates, including oolites, pisolites, shelfstone, some types of pool speleothems, and similar varieties are mostly found as thick layers (40 – 50 cm thick) in the underground pools (Fig. 7). Today, the ball-, egg-, truncated cone-like, cylindrical or shield-shaped minerals formed from

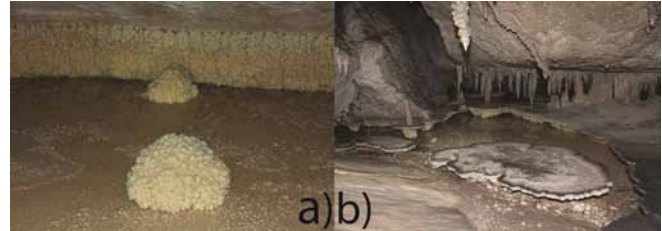


Figure 7. a) Pool calcite speleothems related to water table fluctuations. b) Shelfstone type of speleothems formed around the edges of the small pool surface (photos by Lasha Asanidze).



Figure 8. Beautiful spherical examples of pool speleothems. The smallest is 16cm and the largest is 180cm in circumference (photo by Lasha Asanidze).

water, supersaturated with calcite (Tintilozov, 1961, 1963, 1965, 1976).

Spherical formations formed by the calcite mineral aggregates are unique, and there is no known analog in caves in the Caucasus (Fig. 8). They are mostly subaqueous, lithified calcite balls of different sizes grown around stalactites at one level in shallow pool in Muradi Cave. They seem to have been formed at the same level in the water, perhaps as formations similar to phreatic overgrowth from supersaturated waters existing at higher water levels during times of tectonic change, flooding, or baselevel shifts (Merino *et al.*, 2014; Jacek, 2015).

The facts described above and our field observations allow us to state that there is no single specific condition of origination and development of the calcite balls. In addition, it seems that the conditions of their origin and development were created as a result of their combination and cementing, including a potential microbiological influence (Borsato *et al.*, 2000; Sallstedt *et al.*, 2014). X-ray diffraction (XRD) analysis confirmed these are 100% calcite. therefore, no secondary mineralization has occurred and these seem to have formed from the slow fluctuation of the water table, seeping supersaturated water, and drips from the stalactites on the surface of the water and dry floor of the pools during lower baselevel.

In our opinion, the major difference is observed in the scales and driving force, resulting in the ideally round, ball-like shapes, which warrant further study as possible records for the cave's development and hydrologic variability.

5.2. Cave sediments

In addition to the speleothem and calcite deposits, fluvial deposits (alluvium, detritus, sand, and silt) and lacustrine-mud deposits (clay and loamy-sand fractions) are also found in Muradi Cave. They are mainly found in the eroded pits and pools or have survived on the cave walls as individual fragments. Particularly worthwhile is the natural deposit of massive (up to 3 m) layers of terrigenous deposits identified at the bottom of one of the walls of a wide passage in the central part of the upper level of the cave. Fairly well-sorted alluvium is found in the upper layers of the sediment profile (with an average diameter of 5 – 6 cm) with large inclusions, as well as large stones with a diameter of 10 – 12 cm.

The petrographic composition of the individual layers in the section of the terrigenous deposits is somewhat similar, with minor differences and is mostly presented as follows: grey and light grey, very dense clays transient to silver (with a thickness of 10 – 15 cm); more or less well-sorted alluvium, with a clayey-loam as the infiller; dark brown clayey-loam with small inclusions of weathered detritus; orange clays; fine-grain clays with inclusions; untreated detritus of angular clastic limestones, which is a slightly weathered material and comprises 70–80% of the layer, with clay as infiller. In the lower part of the section, there are alternating layers of clayey-loam and weathered material with the interlayers comprised of clayey-loam and angular, untreated detritus.

Based on the visualization and evaluation of the terrigenous deposits, we note that the cave was subject to long periods of flooding. Almost all the strata of the cave deposits are deposited in turbulent or laminar waters evidenced by clear boundaries between the layers with respect of color and grain size. The limits of the layers deposited under laminar flow are almost horizontal or linear, while those of the layers formed in flowing water are non-linear. In addition, there are interlayers, streaks and pockets distinguished between the layers (Lezhava, 2015).

Muradi Cave has significant block talus and breakdown throughout, especially in the first level and terminal sections (with shafts) of the cave. They are linked to the areas of intercrossing of well-shaped, vertical tectonic fissures running in the ceiling of the cave with bedding planes. The cave seems to have been subject to much breakdown in the past, which can occur when water levels drop rapidly (Tintilozov, 1976; Lezhava, 2015). The volume of the collapsed limestone blocks is approximately 60,000 m³ while the size of individual blocks range from 15 to 30 m³. There are piles of both old and relatively new breakdown. Clear horizons of clay and dust are quite common on the old blocks, including coatings of thick calcite crusts, stalagmites, etc, but the new collapsed blocks, they are devoid of these.

6. Conclusions

The answers to some questions of morphology and evolution of Muradi Cave must be sought in determining and under-

standing the antiquity of the cave's development and how it fits within the context of the massif. The formation and development of Muradi Cave is closely associated with the formation of the Nakerala range in general (Tsagareli, 1964). The limestone relief of the Nakerala range follows the limestone relief of the southern slope of the Caucasus, together with the inception of the subsurface drainage network (dolines, shafts, etc.) before the Pleistocene glaciation and was subject to deep erosive jointing and collapse followed by a shift in baselevel. The origination and development of Muradi Cave ended before the Pleistocene age as shown by the Acheulean-age deposits and the cultural sediment layer found in the Tsona Cave (abs. altitude of 2,100 m) in the eastern part of the Racha limestone massif (Lubin, 1960), corresponding to the Lower Pleistocene. This is further supported by the remains of a cave bear (*Ursus spelaeus*) found in Tskhrajvari I cave (abs. altitude of 1435 m) located nearby in the Nakerala range, only 2.5 km away from Muradi Cave. The bears lived there no later than the Riss-Wurm Interglacial (Tsereteli, 1956), as the remains of the aforementioned cave bear in many caves of Crimea and Caucasus are found together and the remains date to be Acheulean age (Tsereteli, 1956).

It should be noted that no alluvium deposits from the paleoriver were found in the Nakerala Range until now. The alluvium of the paleoriver found in Muradi Cave holds important information to identify the evolution or paleogeographic context of caves. In this connection, we think it is necessary to continue studies in this field and in Muradi Cave to better understand this shift in climate and its effects on karst development in the region. The formation of Muradi Cave was probably over before the end of the Pleistocene period. The new orogenic movements in the Early Pleistocene intensified the fracturing of limestone strata and, therefore, the activity of karst forming processes. Further, the evolution of the river network and cave passages took place. The elevation of the southern slope of the Caucasus continued in the Middle Pleistocene. It continued to affect the movement of water underground and the development of caves. In terms of the absence of liquid water in the glacial periods, the karst processes and underground caves were preserved and, consequently, the karst processes were lessened or ceased. In contrast, the karst processes were intensely activated in the interglacial epochs with the contribution of more aggressive infiltrating waters. This process is more or less described in the cyclicity of sedimentation of the terrigenous deposits found in this study. Thus, during the next stage of the formation of Muradi Cave, the climate of the Pleistocene played an important role leading to the alternation of karst processes.

After the further tectonic uplift of the southern slope of the Caucasus, some of the streams in the cave incised deeper and constant currents started to flow in the vadose section of cave as they moved downward toward baselevel. A siphon lake developed in this section of the cave as shown by the morphological and geomorphological properties of the branching and thick clay layers on the bottom and walls of the cave. In the same period, the micro-fractures connecting the two levels of the cave must have connected and, as a result, the current was allowed to move freely and back flood into the first level. As a result, a deep (35–40 m²) shaft developed with a doline above it.

As the preliminary study of the terrigenous deposits found in the cave suggests, almost all horizons of the cave sediment deposits were deposited in alternating flowing or still water as clear boundaries between the horizons of different colors and grain sizes exist. The boundaries of the layers deposited in still water are almost horizontal and linear, while those deposited in flowing water are non-linear or wavy.

As a result of the tectonic activity, a large volume of breakdown is found on the floor of the cave with the block talus of both old and modern origins easily distinguished. There is a thick cover of clay or calcite crust over the old blocks, and stalagmites are also very common; the speleothems were destroyed in some areas of the cave. The cave seems to have been subject to another period of breakdown in the later Late Pleistocene. As a result, the cave was ultimately linked to the surface through a narrow entrance.

Acknowledgements

We would like to thank sincerely the Ivane Javakishvili Tbilisi State University and the Vakhushiti Bagrationi Institute of Geography for the financial support in the presented research. We also would like to thank the Shota Rustaveli National Science Foundation for the research funding within the Doctoral Programs Grant № DO/80/9-280/14 and the Fundamental Research Grant № FR/218/9-280/13. We are also grateful to George Gaprindashvili, Levan Tielidze, and Roman Kumladze for their help in the preparation of this manuscript.

References

Asanidze L., Tsikarishvili K., Bolashvili N., 2013a. Cave Tourism Potential in Georgia. *The 2nd International Symposium on Kaz Mountains (Mount Ida) and Edremit, proceedings & Abstracts*, p. 243–247.

Asanidze L., Tsikarishvili K., Bolashvili N., 2013b. Speleology of Georgia. *16th international congress of speleology*, at Czech Republic, Brno, volume 1, p. 29–32.

Asanidze L., Chikhradze N., Lezhava Z., Tsikarishvili K., Polk J., Chartolani G., 2017. Sedimentological Study of Caves in the Zemo Imereti Plateau, Georgia, Caucasus Region. *Open Journal of Geology*, 7, p. 465–477.

Asanidze L., Avkopashvili G., Tsikarishvili K., Lezhava Z., Chikhradze N., Avkopashvili M., Samkharadze Z., Chartolani Giorgi., 2017. Geoecological Monitoring of Karst Water in Georgia, Caucasus (Case Study of Racha Limestone Massif). *Open Journal of Geology*, 7, p. 822–829.

Borsato A., Frisia S., Jones B., & Van der borg K., 2000. Calcite Moonmilk: Crystal Morphology and Environment of Formation in Caves in the Italian Alps. *Journal of Sedimentary Research*, 70, p. 1179–1190.

Gudjabidze G.E., 2003. *Geological map of Georgia, Scale 1:500 000*. (Editor: Gamkrelidze et al). Georgian State Department of Geology and National Oil Company Saqnavtobi. Tbilisi, Georgia.

Hill C.A., & Forti P., 1997. *Cave Minerals of the world* (2nd ed.). National Speleological Society. Huntsville, USA.

Jacek S., 2015. Cave development in an uplifting fold-and-thrust belt: case study of the Tatra Mountains, Poland. *International Journal of Speleology*, 44(3), p. 341–359.

Kipiani Sh., 1974. *Karst of Georgia (attempt of geomorphological characterization)*. V-I, Publishing House metsniereba, (in Georgian), Tbilisi, p.13–20.

Klimchouk A.B., 2006. *The deepest cave in the world in the Arabika Massif and the evolution of the Black Sea*. Svet (Light), (in Russian), p. 33–36.

Klimchouk A.B., Samokhin G.V., Kasian Y.M., 2009. The deepest cave in the world in the Arabika Massif (Western Caucasus) and its hydrogeological and paleogeographic significance. *ICS Proceedings, 15th International Congress of Speleology*, p. 898–905.

Klimchouk A., 2012. Krubera (Voronja) Cave. *Encyclopedia of Caves*. Ukrainian Institute of Speleology and Karstology, Simferopol, Ukraine, p. 443–450.

Lezhava Z., 2015. *The Karst of Zemo Imereti plateau and its surrounding areas*. Publishing House Universali, (in Georgian). Tbilisi, Georgia.

Lezhava Z., Bolashvili N., Tsikarishvili K., Asanidze L., Chikhradze N., 2015. Hydrological and Hydrogeological Characteristics of the Platform Karst (Zemo Imereti Plateau, Georgia). *14th Multidisciplinary Conference on Sinkholes and the Engineering and Environmental Impacts of Karst*, At Rochester, Minnesota, USA, Volume: NCKRI Symposium 5; ISBN 978-0-9910009-5-1, p. 93–100.

Lubin V.P., 1960. Lower Paleolithic monuments of South Ossetia. *Materials and researches on the archeology of the USSR*, № 79. Paleolithic and Neolithic of the USSR, 4, Ed. USSR Academy of Sciences, (in Russian), p. 9–78.

Merino A., Gines J., Tuccimei P., Soligo M., & Fornos J., 2014. Speleothems in Cova des Pas de Vallgornera: their distribution and characteristics within an extensive coastal cave from the eogenetic karst of southern Mallorca (Western Mediterranean). *International Journal of Speleology*, 43(2), p.125–142.

Palmer A.N., 2007. *Cave geology*. Cave Books, Dayton, Ohio, 454 p.

Perrin C., Prestimonaco L., Servelle G., Tilhac R., Maury M., & Cabrol P., 2014. Aragonite – Calcite Speleothems; Identifying Original and Diagenetic Features. *Journal of Sedimentary Research*, 84, p. 245–269.

Rakviashvili K., 1985. On karst of the elevated Dzirula massif and Shaori tektonical block. *Caves of Georgia*. The collection, Issue 10. (in Russian), Tbilisi, p. 55–62.

Sallstedt T., Ivarsson M., Lundberg J., Sjöberg R., & Romani Juan R.V., 2014. Speleothem and biofilm formation in a granite/dolerite cave, Northern Sweden. *International Journal of Speleology*, 43(3), p. 305–313.

Tintilozov Z.K., 1976. Karst caves of Georgia (morphological analysis). (in Russian). Tbilisi, Georgia.

- Tintilozov Z.K., 1961. Rare stalactite shapes and concretions in the karstic caves of western Georgia. *Proceedings of the Vakhushti Bagrationi Institute of Geography*, Georgia Academy of Sciences (in Georgian). Tbilisi, p. 23–25.
- Tintilozov Z.K., 1963. Speleological observations into the karst caves of eastern Gumista Basin. *Speleological Collection: Caves and hollows of Georgia* (in Georgian). Vol. II, B. Tbilisi, p. 31-42.
- Tintilozov Z.K., 1965. Duripsh plateau short speleological essay. *Problems of Geography of Georgia*. (in Georgian). Tbilisi, p. 34–113.
- Tsagareli A.L., 1964. Quaternary tectonics of Georgia. Coll. Himalayan and Alpine orogeny, International geologists Congress. XXII session, *Reports of Sov. Geologists*, problem (II), (in Russian). Moscow, p. 42–56.
- Tsereteli D.V., 1956. Cemetery of cave bears in the vicinities of the Nakerala Pass (Tskhrajvari cave). *Ed. Az. SSR*, № 1. (in Russian), p. 59–64.
- White W.B., 2007. Cave sediments and paleoclimate. *Journal of Cave and Karst Studies*, **69**(1), p. 76–93.

A Third Kind Of Cave In The World: Anthropogenic

Greg Brick, Ph.D.

Affiliation: Minnesota Department of Natural Resources, 500 Lafayette Road, St. Paul, Minnesota, 55155 USA

Abstract

A popular classification divides caves into natural and artificial categories. However, pseudokarstic voids often develop adjacent to artificial excavations (e.g., sewers) in loosely-consolidated geologic formations. Neither natural nor artificial in origin, these “unintentional caves” are best classified as anthropogenic. While a challenge to dichotomous thinking, classic examples of anthropogenic caves will be given from the St. Peter Sandstone, a widespread cratonic sheet sand of the Midwestern United States.

Keywords: cave classification, anthropogenic caves, St. Peter Sandstone, pseudokarst

A popular classification divides caves into natural and artificial categories. However, pseudokarstic voids often develop adjacent to artificial excavations (e.g., sewers) in loosely-consolidated geologic formations. Neither natural nor artificial in origin, these “unintentional caves” are best classified as anthropogenic.

As preliminary, I would like to clarify the meaning of the term “natural cave.” Among the general public, I have found that unlined, artificial caves dug into bedrock will often be called “natural caves” by laypersons because the avowedly natural rock surface is visible. Whereas to most geologists, and here in this paper, natural refers to the space itself, not the walls.

Here are two classic examples of anthropogenic caves are exhibited by the St. Peter Sandstone, a widespread cratonic sheet sand of the Midwestern United States:

Schieks Cave, a maze cave in the St. Peter Sandstone underlying the city of Minneapolis, Minnesota, USA, has been attributed by Hogberg and Bayer (1967) to piping of the poorly cemented sandstone into the North Minneapolis Tunnel (Fig. 1). This tunnel is now the main sanitary sewer for the downtown area. The cave was discovered by tracing white sand carried by the sewer back to its source. A rusty well pipe reportedly found in the cave suggests that the cave initially was excavated by the hydraulic action of an artesian water well that flowed out of control. The time available to erode a void of this size, which underlies a city block, can be determined from the chronology. Construction of the tunnel began in 1889, while the earliest known record of the cave is a 1904 survey. In the sense that humans provided source and sink, the cave is not natural or artificial, but anthropogenic (Brick 2009).

The case of Chute’s Cave, also in Minneapolis, is more complex. A natural sandstone cave was discovered during construction of a tunnel by the St. Anthony Falls Water Power Company in 1866. The cave was enlarged artificially as shown by pick-marks on the walls. The cave was sealed off from the Phoenix Mill tunnel, a nearby water power tunnel, in 1874. Water leaked around the bulkhead, however, enlarging the cave to the extent that it caused Main Street to collapse, on 23 December 1880. The cave thus appears to have all three components: natural, artificial, and anthropogenic (Brick and Peterson 2004).

Camera Safari Explores ‘Lost World’ Under Loop

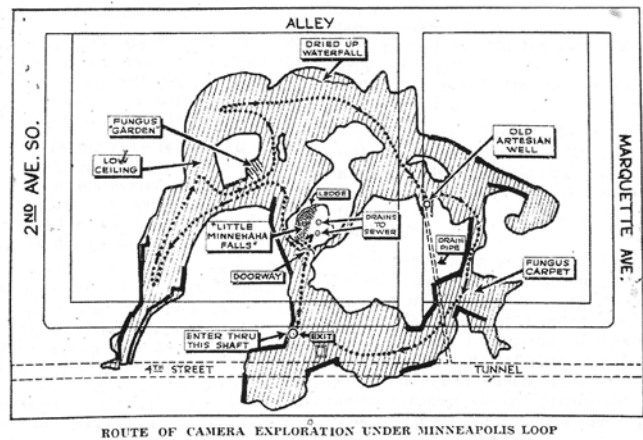


Figure 1. Schieks Cave, the largest anthropogenic cave in the St. Peter Sandstone under Minneapolis, Minnesota, USA. Located 23 meters below street level. The dotted line shows the photographer’s route through the cave. From Dornberg (1939).

References

- Brick G, 2009. *Subterranean Twin Cities*. Minneapolis, MN: University of Minnesota Press.
- Brick G, Petersen PA, 2004. Ten Cent Tour: The Story of Chute’s Cave. *Hennepin County History* 63(2): 4-25.
- Dornberg D, 1939. Camera safari explores ‘Lost World’ under Loop. *Minneapolis Journal*, April 16.
- Hogberg RK, Bayer TN, 1967. *Guide to the Caves of Minnesota*. Educational Series No. 4. Minneapolis, MN: Minnesota Geological Survey.

Evaluation of possible ongoing upwards condensation corrosion in Cueva del Pastor (Iberian Chain), Spain

Kelsey Budahn¹, Ira D. Sasowsky¹, Francisco Gutiérrez², Mario Gisbert³

Affiliation: ¹Dept. of Geosciences, University of Akron, Akron, OH, USA 44325-4101

²Dept. of Earth Sciences, University of Zaragoza, Calle Pedro Cerbuna 12, Zaragoza, Spain 50009

³Centro de Espeleología de Aragón, Calle Escultor Moreto 15, Zaragoza, Spain 50008

Abstract

Caves in the Iberian Chain of Spain are hypogene in origin, and many have undergone multiple significant episodes of (condensation?) corrosion. Cueva del Pastor (Shepherd's Cave) is a small cave near the northeastern margin of the range, in Cueva del Muerto Ridge, overlooking the Ebro River Basin. Having a total depth of 8 m and length of only 28 m, the cave is not significant by traditional measures, but has peculiar morphology and landscape position which suggest possible ongoing condensation corrosion in a non-thermal context. This may give insight in to similar processes in less optimal locations. The cave is developed in Jurassic, microcrystalline limestone of the Cuevas Labradas Formation, which dips gently eastward here. The entrance is a ~0.5 m circular opening, connected directly to a 4-m vertical shaft. The shaft is composed, in its upper parts, of a series of interconnected erosional spheroids ~1 m in diameter. The entrance is overhung on all sides, and is the breached top of the uppermost spheroid. The bulk of the cave at the base of the shaft has a floor of speleothem encrusted breakdown. At the northern end of the cave is a similar shaft (dome), which is not surface -connected, but has a thin roof and plant roots penetrating. Observations of intense moisture in this dome suggest ongoing condensation corrosion processes, and that the dome might eventually breach upwards to the surface. CO₂ content ranged from 400-600 ppm. We instrumented the dome with air and wall temperature sensors, along with humidity and pressure, logged on a 30-minute interval. The thin roof and proximity to a 70 m scarp allow potentially significant thermal and insolation effects which might intensify condensation processes. Average ceiling temperature fluctuates on a diurnal scale, and on a seasonal scale. From spring through winter the ceiling, floor, and rock wall temperatures fluctuate both seasonally and diurnally. However, the floor air and rock wall temperature are relatively stable compared to diurnal flux of the ceiling air. Much of the year, based on temperature alone, difference in air and wall temperature are great enough to be conducive to condensation formation on cave ceilings and walls. If upward growth is occurring, it is likely more rapid than top-down denudation of the bare rock surface above, meaning that "unroofing" occurs from below in this case.

Keywords: Spain, Iberian Range, Condensation Corrosion, Meteorology

1. Introduction

The development of dissolution caves is mainly considered to be driven by either epigene or hypogene groundwater flow (Palmer, 1991). However, in the past few decades the role of condensation corrosion as a possibly significant late-stage speleogenetic process has been recognized (Palmer, 2007) and been receiving more attention (Dublyansky & Dublyansky, 2000; Dreybrodt *et al.*, 2005; Sasowsky, 2014; Dublyansky & Spötl 2015). Condensation corrosion features are most commonly found in caves of hypogene origin, or where warm thermal waters promote condensation (e.g. Dublyansky & Spötl 2015). However, condensation corrosion can begin or continue to occur even closer to the land surface in an epigene setting. With the input of meteoric water and CO₂ gas driven dissolution of the bedrock, this takes place when warm air becomes trapped inside a cave causing a significant stratification of temperature and humidity (Palmer, 2007).

Condensation corrosion processes in caves have been evaluated in numerous settings (e.g. Hill, 1987; Jameson, 1991 & 1995; Dublyansky & Dublyansky, 1998), however the significance of this process on its own to control cave morphologies, and the microclimates that need to be in place to allow this, have yet to be fully explored. For additional background on condensation corrosion process refer to the above-mentioned references.

For the present study, we identified a unique small cave that appears to have both an active corrosion dome, and an inactive

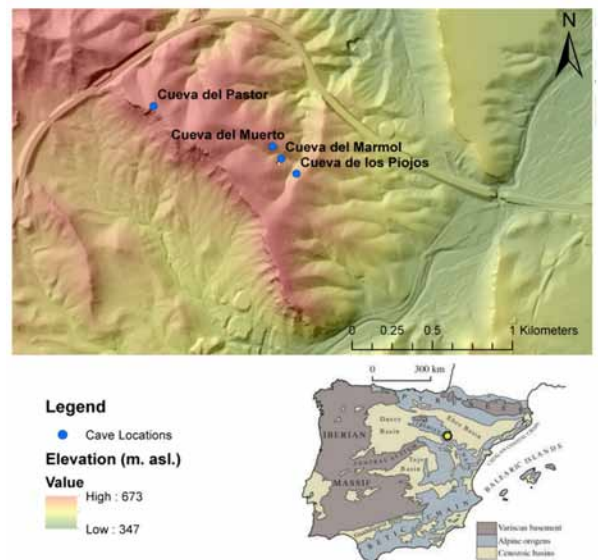


Figure 1. Location map and shaded DEM showing elevation for the study area. There are four caves on CMR, Cueva del Pastor is the furthest to the northwest. DEM data courtesy of Centro Nacional de Información Geográfica, 2015.

dome that has breached fully to the surface. We instrumented this cave to record high resolution, and high frequency, measurements of air and rock temperature, as well as air pressure and humidity. The goals were to confirm whether this shallow,

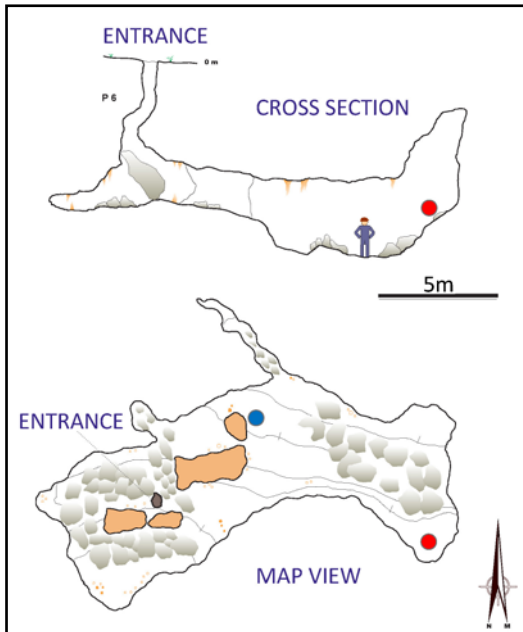


Figure 2. Cueva del Pastor cross section and map view (Gisbert and Pastor, 2015). The red dot indicates the micro-meteorological station location, and blue dot indicates the 2nd separate RH sensor location.

non-thermal system was undergoing active corrosion, and to elaborate the seasonal and other controls that might play a role in the process.

Understanding of condensation corrosion processes in non-thermal settings has the potential to illuminate an important speleogenetic mechanism, which may indeed be under-recognized due to other factors.

2. Study Site

Cueva del Muerto Ridge (CMR) is located on the southeastern edge of the Iberian Chain, and is underlain by north-eastward dipping Jurassic microcrystalline limestone of the Cuevas Labradas Formation (Gisbert & Pastor, 2009). Cueva del Pastor (CDP), which is the focus of this study, is on the northwestern edge of CMR, close to an 85 m escarpment (Figure 1). Small streams surround the ridge, however there is no evidence that CDP formed from flowing water; it is located high on the ridge and disconnected from current surface hydrologic networks/drainage. The crest of CMR is about 370 meters amsl. This locale is semi-arid, although the Ebro River Basin experiences between 200-300 mm/year of precipitation (Lopez-Moreno et al., 2011), CMR most likely sees precipitation totals on the lower end of those values.

This shallow cave has high potential for heat loss to, as well as from, the land surface. As shown on the cave profile (Figure 2) there are two domes in the cave. The western dome breaches the surface and is the entrance (Figure 3-A,B). The eastern dome does not breach the surface, though it comes close and has plant roots entering from its top (Figure 3-E,F). The eastern dome was the focus of the study. The entrance is circular (0.5 m, Figure 3-B) with a vertical shaft approximately 6 meters in depth from the surface to the cave floor (Figure 3-C,D), and an additional 2 m depth beyond this.

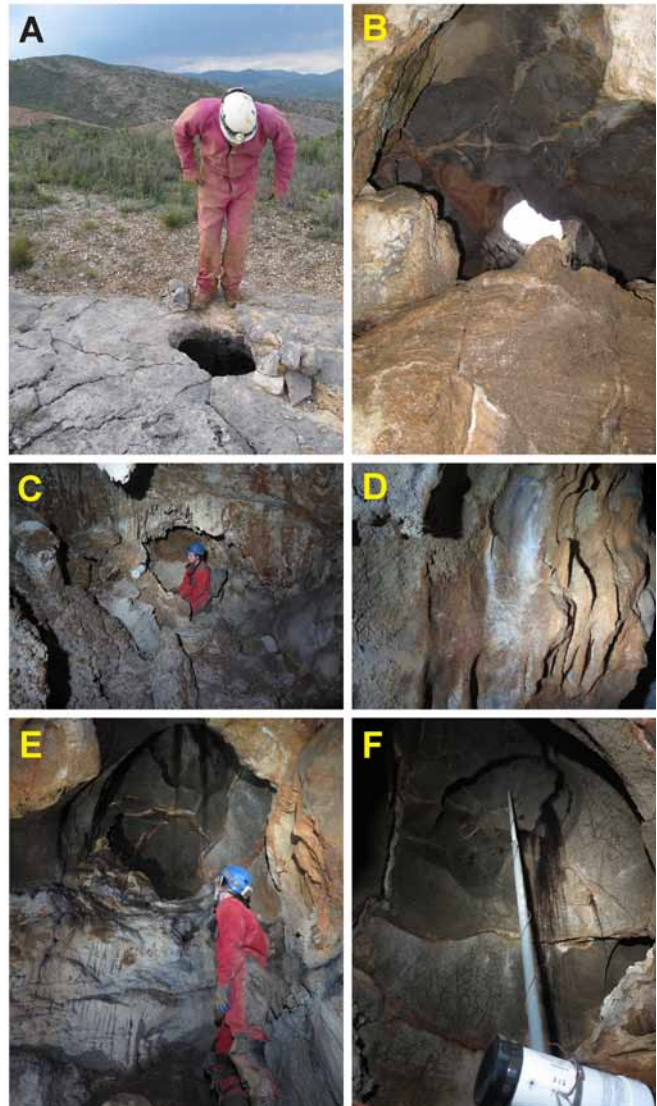


Figure 3. Photographs of Cueva del Pastor.

A) Entrance, view looking westward. The main Iberian Range is in the distance.

B) View upward to entrance from near bottom of entrance shaft. Note that the entrance hole is overhung on all sides by smoothly corroded bedrock, and shaft is a series of connected hemispherical voids.

C) Lowest point in cave. Model is sitting in a dry pool. Profuse coral-loid speleothems coat walls and breakdown at this level.

D) Secondary calcite crust (brown coating) formed by evaporation of thin films of condensed water at middle level. Height of view is circa 0.7 m.

E) Un-breached corrosion dome at East end of cave. Note plant roots entering through fractures, and condensation-related white flowstone.

F) Detail of monitoring installation. Large horizontal tubes contain logging devices. Slender vertical tube supports uppermost temperature sensor.

3. Methods

A custom built micro-meteorological station was installed in the eastern dome of CDP. It includes 3 temperature sensors (ceiling air, floor air, and rock wall), 1 pressure sensor, and 1 relative humidity sensor to measure the gradient from floor to ceiling. High resolution temperature instruments were selected to measure very small changes in temperature both spatially and over time. All instruments log at 30 minute intervals, and were in place from 23 March 2016 to 10 January 2017. The ceiling air sensor is raised into the eastern upward

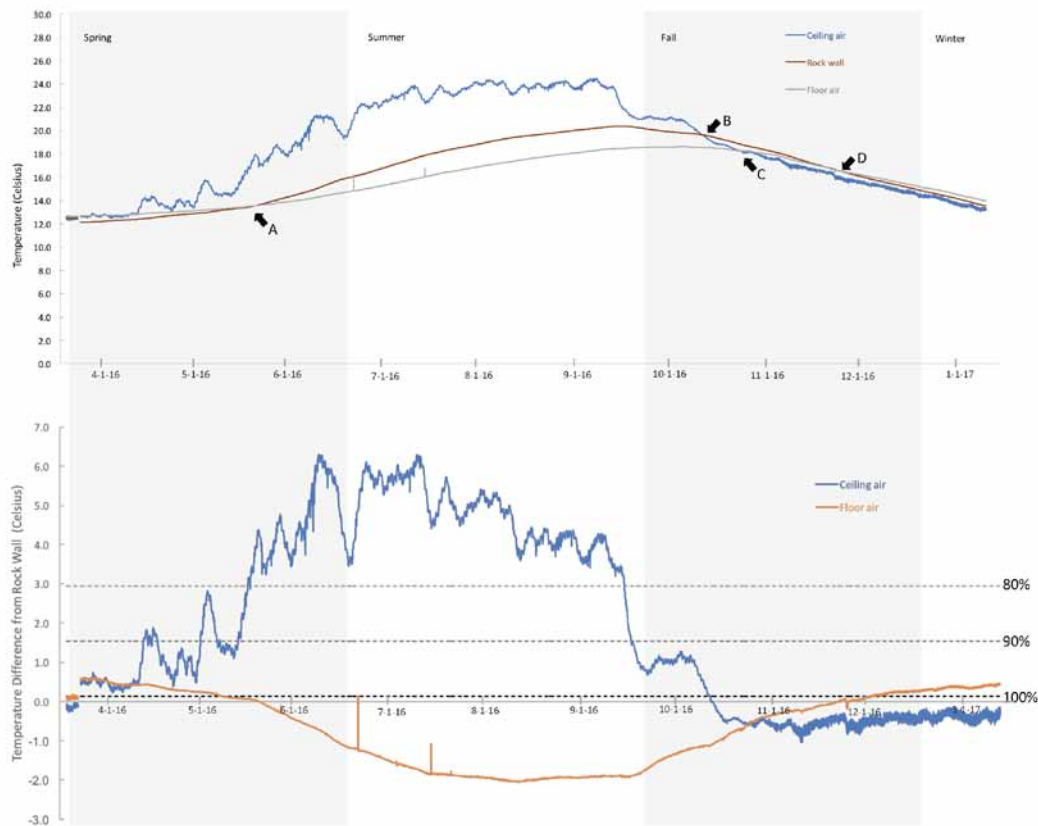


Figure 4. (A) shows ceiling air (blue) floor air (grey) and rock wall temperatures (brown) for the full period of record (23 March 2016 – 10 January 2017). The temperatures fluctuate seasonally, and ceiling air also fluctuate diurnally. Large spikes in the floor air temperature are due to cavers at the meteorological station. There are four instances throughout the year when the temperature inversions switch (i-iv) due to the dynamic changes in cave air and outside air temperature. (B) shows the difference in temperature between the ceiling air and floor air to rock wall temperature. The change in temperature between cave air and rock wall for most the year are great enough to produce condensation on the rock wall (Strahler, 1971). Due to the lack of reliable RH data from the station, theoretical RH threshold values were examined (80, 90, 100%) and when the differences are above the given RH threshold, conditions for condensation occur.

shaft at a height of approximately 3m from the logger box at the station. The floor air sensor is located near the floor of the station approximately 5 m below the ceiling sensor. The rock wall temperature sensor was placed into a hole that was drilled approximately 20 cm into the limestone cave wall and sealed with local clays. Temperature was measured using sensors designed in-house. They cover 0-30 °C temperature range with an accuracy of +/- 0.001 °C, and resolution of 0.017 °C. Relative humidity (RH) was measured using Honeywell HIH 4030/31 series RH sensors with 0-100% range, and +/- 3.5% accuracy.

Carbon dioxide (CO₂) was measured using a handheld Dräger pump and Dräger tubes (tube 100/a) with a range of 100 to 3000 ppm. The measurements were collected typically upon first arrival so that the influence of respiration CO₂ from cavers would not interfere with the background concentration. Temperature values at the time of measurement. In CDP two locations for CO₂ measurement were selected. One location was in the upper portion of the cave near the meteorological station, and the second was at the lower portion of the cave (Figure 2).

4. Results

The cave was visited numerous times over the past year. The eastern dome is frequently quite wet, and especially so after rain. This indicates that the fractured bedrock is permeable, and that meteoric water input is occurring at present.

In the beginning of the spring season the ceiling air and floor air are very similar and ceiling air fluctuates both above and below the floor air temperature (Figure 4A). Then in early spring the ceiling drastically warms and continues this warming trend with multiple small excursions downward. Ceiling air fluctuates on a diurnal scale, but the floor air and rock wall do not. The floor air and rock wall temperature also increase as the season progresses, but not as quickly or to as warm as the ceiling air. Initially the rock wall was colder than the floor air, but by late spring the rock wall temperature exceeds the floor air (Figure 4A-arrow i) by about 1 °C. All temperature measurements were on a consistent upward (warming) trend during spring.

In the summer, ceiling air is by far the warmest (Figure 4A). Still, it shows diurnal flux, and makes small excursions down-

ward on cool days. Throughout the entire summer season rock wall temperature is greater than floor air temperature by approximately 2 °C. All temperature measurements are on a consistent upward (warming) trend, but by the end of the summer have plateaued.

During Autumn (fall), after an abrupt drop in temperature at the end of summer, all temperature measurements begin a consistent downward trend (Figure 4A). In the beginning of the season ceiling air is the warmest, then rock wall temperature, and floor air is the coldest. Then, suddenly in early fall, the ceiling air drops below rock wall temperature, and then even below floor temperature (Figure 4A-arrow ii, iii), for a total inversion in the temperature stratification. By mid-fall the rock wall temperature has cooled enough that it is now very similar to floor air, and by mid-late fall the rock wall drops below the floor air temperature (Figure 4A arrow iv). At the end of the fall season floor air is the warmest, then rock wall temperature, and ceiling air is the coolest.

For the small amount of winter data that we have in the current record a few things can be said. The floor air is the warmest, then the rock wall temperature, and then the ceiling air is the coldest. All temperatures are on a consistent downward trend (Figure 4A).

In CDP, the RH values range from 40-75% during the spring season, then in May the values increase and remained steady between 87-97%. This may indicate a problem with the sensor.

Carbon dioxide concentrations were collected in March, July, and January. These values were near background atmospheric CO₂ concentrations during the spring and summer, and slightly elevated during the January measurement likely due to the exhalation of CO₂ from cavers that had been in the cave before taking the measurement. The values range from 400-600 ppm (n=5).

5. Discussion & Conclusions

Data from the current period of record indicates that there are many shifts in stratification seasonally. When at or near 100% relative humidity, a change in temperature of only 0.14 °C can result in a change of air under saturated to over saturated with respect to water vapor, and therefore, condensation will occur (Strahler 1971). Generally, for every 0.14 °C decrease in temperature, RH will increase 1%. Examination of theoretical RH values and differences in temperature from ceiling air to rock wall, and floor air to rock wall, indicate certain times of year that the stratification in temperature is favorable for condensation (Figure 4B). For a large portion of the year the conditions based on temperature alone are favorable for condensation formation.

During the spring (March-June) the difference in ceiling air temperature and the rock wall temperature is 2.297 °C. During the summer the difference in temperatures is even greater, 5.075 °C. During the fall season, the difference in temperature is 1.889 °C. These calculations were based on average seasonal temperatures for ceiling air and rock wall and suggest times when condensation could occur, although throughout the entire season these averages do not reflect all the individual temperature inversions (refer to Figure 4A). Warm moist air in contact with cooler bedrock is an ideal set-

ting for condensation water, films or droplets, to occur. In the early winter months, however, the average rock wall temperature is cooler than the cave air, thus not conducive to condensation, although relatively cool air from outside compared to relatively warm cave air may contribute to condensation near the breached entrance of the cave. Data collected during the winter span a very short duration, and more data are needed to make conclusive interpretations. Overall, throughout the spring, summer, and fall season of the current record, the difference in ceiling air temperature and the rock wall temperature exceeds the 0.14 °C change necessary to induce condensation at high humidity.

Figure 4B shows the relative temperatures of the bedrock wall and ceiling/floor air. From April through October (potentially of the period of record the wall temperature was less than the air temperature). This would provoke condensation at 100% RH, and is even possible for most of the summer if RH was as low as 80%. The graph also shows those occasions when temperature differences were great enough to provoke condensation at lower humidities.

CO₂ concentrations measured in the cave are in the range of open atmospheric values, as might be expected in a small cave that is open to surface air. Sparse vegetation with very thin soils overlay the cave, limiting other sources of CO₂. The minimum value recorded, 400 ppm (by volume) is equivalent to 4×10^{-4} atm partial pressure of CO₂. If dissolved into condensed water, the relatively low equilibrium concentration of about 50 mg/L of CaCO₃ may be achieved during neutralization (White, 1988, p. 131). This is significantly less than the values typically found in karst systems. Nevertheless, with the expected low saturation index, the water will be aggressive to the limestone bedrock, and capable of corrosion. If condensation is an ongoing process, then given enough time, significant bedrock removal may be effected.

Acknowledgements

Without the support from the Karst Waters Institute, Cave Conservancy Foundation, and National Speleological Society this project wouldn't have been possible. The collaboration with faculty and students from the University of Zaragoza Department of Earth Sciences, and the many members of the caving club Centro de Espeleología de Aragón has greatly enriched the quality of this research. Their input, and assistance both in the field and classroom was invaluable to our continued success. Tom Quick constructed the monitoring equipment, for which we are very grateful.

References

- Dreybrodt, W., Gabrovsek, F., and Perne, M., 2005, Condensation corrosion; a theoretical approach. *Acta Carsologica*, **34**, 317-347.
- Dublyansky, V.N., Dublyansky, Y. V., 1998, The problem of condensation in karst studies. *Journal of Cave and Karst Studies*, **60**, 3-17.
- Dublyansky, V.N., and Dublyansky, Y.V., 2000, The role of condensation in karst hydrogeology and speleogenesis, in: Klimchouk, A.B., Ford, D.C., Palmer, A.N., and Dreybrodt,

- W., 2000, *Speleogenesis evolution of karst aquifers*, National Speleological Society, Huntsville, AL, United States, 100-112.
- Dublyansky, Y.V., and Spötl, C., 2015, Condensation-corrosion speleogenesis above a carbonate-saturated aquifer; Devils Hole Ridge, Nevada. *Geomorphology*, **229**, 17-29, doi: 10.1016/j.geomorph.2014.03.019.
- Gisbert, M., and Pastor, M., 2009, *Cuevas y Simas de la Provincia de Zaragoza*, Centro de Espeleología de Aragón, 479 pp.
- Hill, C.A., 1987, Geology of Carlsbad Cavern and other caves in the Guadalupe Mountains, New Mexico and Texas. *Bulletin - New Mexico Bureau of Geology & Mineral Resources*, **117**, 150 p.
- James, E. W., Banner, J. L., Hardt, B., 2015, A global model for cave ventilation and seasonal bias in speleothem paleoclimate records. *Geochem. Geophys. Geosyst.*, **16**, 1044–1051, doi:10.1002/2014GC005658.
- Jameson, R.A., 1991, Features of condensation corrosion in caves of the Greenbrier karst, West Virginia. *NSS Bulletin*, **53**, 44.
- Jameson, R.A., 1995, Condensation, condensation corrosion & associated feature in Snedgars & Greenville Saltpeter Caves, in: Zokaites, C., Hansen, K.S., Vermeulen, S.E., ed., *Underground in the Appalachians: A guidebook for the 1995 convention of the National Speleological Society*, Huntsville, AL, National Speleological Society, 122-125.
- Lopez-Moreno, J.I., Vicente-Serrano, S.M., Moran-Tejeda, E., Zabalza, J., Lorenzo-Lacruz, J., Garcia-Ruiz, J.M., 2011, Impact of climate evolution and land use changes on water yield in the Ebro Basin. *Hydrology and Earth System Sciences*, **15**, 311-322, doi: 10.5194/hess-15-311-2011.
- Palmer, A.N., 1991, Origin and morphology of limestone caves. *Geological Society of America Bulletin*, **103**, 1-21.
- Palmer, A.N., 2007, *Cave Geology: Dayton, OH, USA*, Cave Books - Cave Research Foundation, 454 p.
- Sasowsky, I. D., 2014, Pondering the importance of subaerial corrosion as a speleogenetic agent, in: Klimchouk, I. Sasowsky, J. Mylroie, S.A. Engel, and A.S. Engel, Eds., 2014, *Hypogene Cave Morphologies*. Selected papers and abstracts of the symposium held February 2 through 7, 2014, San Salvador Island, Bahamas. Karst Waters Institute Special Publication 18, Karst Waters Institute, Leesburg, Virginia. 102.
- Strahler, A.N., 1971, *The earth sciences: United States*, Harper & Row: New York, NY, United States, 824 p.
- White, W. B., 1988, *Geomorphology and hydrology of karst terrains*, Oxford, Oxford University Press, 464 p.

Age And Speleogenesis Of Gypsum Caves In Emilia-Romagna (N Italy)

Andrea Columbu^{1,1}, Veronica Chiarini^{2,3}, Jo De Waele², Russell Drysdale^{1,3}, Jon Woodhead⁴, John Hellstrom⁴ and Paolo Forti²

Affiliation: ¹School of Geography, University of Melbourne (Australia), University of Melbourne, 221 Bouverie street, 3010, Melbourne, Australia acolumbu@student.unimelb.edu.au andrea.columbu2@unibo.it rnd@unimelb.edu.au
²Department of Biological, Geological and Environmental Sciences, University of Bologna, Via Zamboni 67, 40127 Bologna, Italy vero.ch88@hotmail.it jo.dewaele@unibo.it paolo.forti@unibo.it
³University of Savoie, Laboratoire EDYTEM, bd de la Mer Caspienne, Le Bourget du Lac cedex, F-73376, France
⁴School of Earth Sciences, University of Melbourne, Corner Swanston & Elgin streets, 3010, Melbourne, Australia jdwood@unimelb.edu.au j.hellstrom@unimelb.edu.au

Abstract

More than 600 caves have been surveyed in the Triassic and Messinian gypsum beds of the Northern Apennines (Emilia-Romagna region, N Italy). Despite the fact that these caves have been studied for a very long time, their age was inaccurately believed to be Late Glacial. In fact, the fast dissolution of gypsum and the regional uplift of the mountain chain lead to the belief that speleogenesis could have started only recently.

Dating of the infilling sediments can assess a minimum age of the cave passages. U-Th dating of carbonate speleothems sampled in these gypsum caves has been carried out in several karst areas in the region. The results show that caves started forming at least ~600 kyrs ago, and that caves were mainly carved during relatively cold climate stages, when rivers formed terraces at the surface and aggradation caused paragenesis in the stable and active cave levels. The carbonate speleothems, on the other hand, mainly formed during warm and wet intervals.

Keywords: U/Th dating; carbonate speleothems; evaporite karst; Middle Pleistocene; Paleoclimate

1. Introduction

Messinian gypsum outcropping in Emilia Romagna (North Italy) hosts more than 600 caves (De Waele *et al.* 2011). In this area, speleogenesis was inaccurately assigned to the Late Pleistocene-Holocene, with peaks during the late glacial (Demaria 2002; Forti 2003; Pasini 2012). Scarce radiometric ages (Forti and Chiesi 2001; Forti 2003), archeological (Miari 2007; Negrini 2007) and paleontological (Pasini 1969) findings sustained this idea. Speleogenesis in gypsum can occur up to hundred times faster than in carbonates (Klimchouk 2000); at the same time, the high solubility of gypsum makes the surface outcrops subjected to intense karst denudation, which can lead to the demolition of the underground cave systems. These are the main reasons why the age of the currently explorable caves, hence the inception of speleogenesis, has been underestimated. Establishing the age of a cave is not an easy task (Sasowsky 1998), especially in the cases where direct approaches, as dating speleogenetic byproducts (Polyak *et al.* 1998, 2016; Plan *et al.* 2012), are inapplicable. Thus, ages are most of the time estimated by dating cave infilling sediments (Audra *et al.* 2006), such as speleothems, fossils, artefacts, etc.. However, even with this methodology the age of speleogenesis could considerably be miscalculated, if dated materials are much younger than cave carving processes. Besides radiometric dating, cave evolutionary models should be sustained by geological, paleoclimatic and paleo-environmental considerations, in order to procure a truly reliable timing for karst processes.

We studied a dozen caves belonging to five different karst systems carved in the Emilia Romagna gypsum areas by dating,

using the U-Th method, twenty carbonate speleothems. Radiometric ages were then used to build a solid karst evolutionary model, in turn anchored to previously dated local geological events and the connection between climate cycles and speleogenesis (Columbu *et al.* 2015). This model, besides allowing to precisely estimate the age of speleogenesis in this portion of the Apennine chain, may also be applied to other gypsum karst areas having similar geological and climatic conditions.

2. Area of study, material and methods

Messinian gypsum in Emilia Romagna region belongs to the *Vena del Gesso* Formation (Vai and Martini 2001; Lugli *et al.* 2010), outcropping with well-recognisable cuesta-like morphologies. The formation is infrequently overlain by marine silt and clays (*Argille Azzurre* Fm. - Amorosi *et al.* 1998), littoral sandstones (*Sabbie Gialle* Fm. - Cyr and Granger 2008) and continental sediments (continental Quaternary - Amorosi *et al.* 2015). The explored caves and relative samples are (bracketed IDs refer to speleothems sampled in the quoted cave or in the area of the cave entrance – Fig. 1 for some examples): Abisso Mezzano (RT), 3 Anelli (3A), Abisso 50 (A50), Pozzo Pollini (PP), Grotta Oliver (GO) and Galleria Principale caves (RTy) in the Re Tiberio – Monte Tondo system; Spipola cave (SpD, Sp1, and SpS) in the Spipola-Acquafredda system; Peroni (P2 and P3) and Mornig (Mor2) caves in the Castelnuovo system; Rio Basino (RBT, RB1, and RB3) cave in the Rio Stella-Rio Basino system; Monte Mauro (MM2 and MM4) and Banditi (Ba1.1, Ba2.1 and BaBig) caves in the Monte Mauro system. All are epigenic caves, sub-horizontal in section; karst systems report stacked-like juxtaposition of these multi-level sub-horizontal passages. Their formation is



Figure 1. Calcite speleothems of the Emilia Romagna gypsum caves. A) The active flowstone forming on the riverbed of Rio Basino (photo Piero Lucci); B) A50 flowstone of Abisso 50, grown around 76 ka (MIS5a); C) The Banditi flowstone (a portion of BaBig) which grew during isotope stage MIS5e (photo Jo De Waele); D) One of the Monte Mauro flowstones (MM2) found in the forest, with the gypsum cave immediately dissolved but calcite flowstone preserved. This flowstone appears to have grown in two distinct periods somewhere between 240 and 320 kyrs ago (comprising both MIS9 and MIS7); E) Active flowstone in the Mornig cave (photo Francesco Grazioli).

linked to the lowering and stabilization of the local base level (i.e. rivers) (Columbu *et al.* 2015), considering that the rapid uplifting affecting the area triggers the incision of the Northern Apennines flank valleys. Speleothems are mostly calcite flowstones, and only three calcite stalagmites were sampled (BaBig, Mor2, SpS). Top and bottom of each speleothem was dated with the U-Th methodology; for the tallest speleothems, age constraints were improved by several internal dates. U-Th is the more widely used methodology for dating carbonate speleothems (Richards and Dorale 2003). Preparation of sub-samples for dating, mass spectrometer setting and statistical treatment of the final data strictly followed the protocols in force at the University of Melbourne – School of Earth Sciences, reported elsewhere in detail (Hellstrom 2003, 2006; Drysdale *et al.* 2009, 2012).

3. Results, discussion and final remarks

U-Th results are shown in Table 1; all speleothems grew during periods of relative warm and wet climate (Fig. 2) considering the last ~800 kyrs (Columbu *et al.* 2017). Conversely, sub-horizontal cave tunnels formed mostly during stages of relative cold and dry climates (Columbu *et al.* 2015). In fact, cave level altitudes correlate with strath river terraces that, in

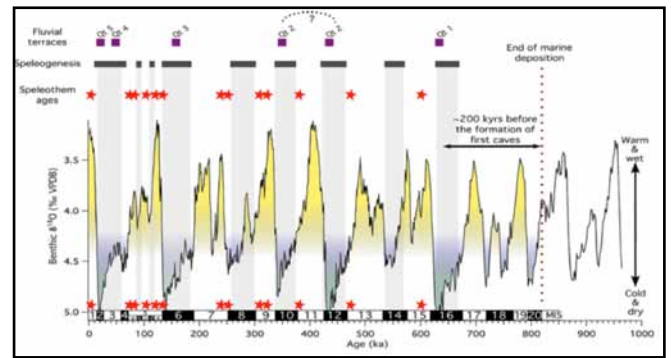


Figure 2. Speleogenetic processes over the last ~800 ka. Stars indicate the basal ages of the studied speleothems (except for the sample Ba2 at ~380 ka, which reported only the top age; Holocene ages are aggregated in a single star). The ages mainly fit with periods of warm and wet climate (yellow shading). The formation of the different cave levels (rectangles) is correlated with the cold-dry climate stage (gray shading) that occurred before the warm-wet period indicated by the age of the speleothems (see figure 3 and text), simultaneous with the deposition of most of the fluvial terrace sediments along the main river of the area (squares) (Cyr and Granger 2008; Picotti and Pazzaglia 2008; Wegmann and Pazzaglia 2009). The climatic curve (and MIS subdivision) refers to the $\delta^{18}O$ benthic stack of Liseicki and Raymo (2005). First caves were carved at least ~630 kyrs ago, 200 kyrs after the retreat of the Adriatic Sea.

the area of study, were all formed mostly during glaciation peaks (Cyr and Granger 2008; Picotti and Pazzaglia 2008; Wegmann and Pazzaglia 2009) (Fig. 3). An epigenic sub-horizontal cave tunnel is excavated parallel to the piezometric level at the same altitude as the base level (Fig. 3). During periods of climate deterioration, vegetation on the valley slopes is scarce, meaning that a high quantity of regolith is produced and available. Loose sediments are gravitationally conveyed toward the valley bottoms forming the terrace deposits. River terraces testify periods of stability in the paleo base level longer than 1,000 years (Wegmann and Pazzaglia 2009). This time-span is sufficiently long for the excavation of the epigenic sub-horizontal caves (Columbu *et al.* 2015), which operate as through-flow channels (Klimchouk 2000) transporting water from the sinking points (i.e. dolines or blind valleys) to the resurgences. During the following warm-wet period vegetation abounds, increasing the level of CO_2 in the soils. At the same time, cave carving proceeds slowly and tunnels previously formed are entrenched. These appear to be ideal environmental conditions for the formation of carbonate speleothems (Columbu *et al.* 2015) (Fig. 3). At the end of warm periods, the stability of base levels terminates and valleys, as well as fluvial terraces deposits, are incised. Gypsum karst systems react to the new hydrological situation by excavating deep and narrow vertical shafts, as the 30 m deep one visible in Monte Tondo (De Waele *et al.* 2013) (Fig. 3). Once base level gets stable at a new (lower) altitudinal position, another sub-horizontal cave passage is excavated, and the cyclical above-described speleogenetic process can start all over again.

Following the previous discussion, we used the U-Th speleothems' ages as temporal reference to establish the age of speleogenesis (Fig. 2). Cave formation is assigned to the first cold period before the warm stage that allowed the deposition of speleothems (Figs. 2 and 3). Major caves formed during marine isotopic stage (MIS) 14, 12, 10, 8, 6, 3, 2 and 1, but

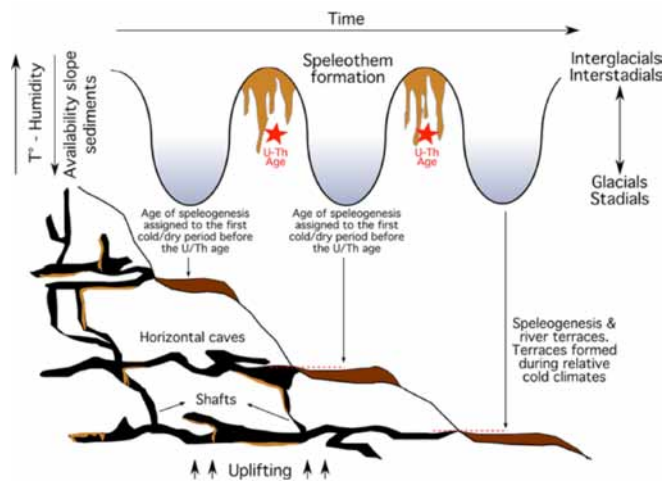


Figure 3. Schematic model of the formation of sub-horizontal cave levels and fluvial terraces in relation to cyclic climate changes. River terraces, formed during cold climates, record periods of stability in the paleo base level longer than 1,000 years (Wegmann and Pazzaglia 2009). Contemporaneously, sub-horizontal cave tunnels are carved at the same altitude. The oldest generation of speleothems in a certain cave level were deposited when the newly born cave reached a vadose status, during periods of relatively warm climates. The first cold period before the warm stage indicated by the speleothems is considered as the minimal age for the formation of the caves.

also during the glacial-like climate pulsations MIS5d and 5b (Fig. 2). The oldest speleothems in our collection provide a basal age of >580 ka (Ba1) and 468.00^{+130}_{-42} ka (MM4 flowstone). This suggests that caves already existed in the area at least since MIS15 (i.e. ~600 kyrs ago, testified by Ba1 age and the oldest possible MM4 age). Assigning the timing of speleogenesis to the coldest period just before MIS15 (MIS16), the excavation of the first caves likely occurred at least 630 kyrs ago. It could be argued that speleogenesis might have occurred even before, but speleothems representing that age were not sampled/analysed. Furthermore, geological and geomorphological considerations make this hypothesis unrealistic. In fact, the top age of the Sabbie Gialle Fm. (the terminal marine sequence covering the gypsum) is attested at 780-820 ka (= ~800 ka) (Falgueres 2003; Muttoni *et al.* 2011). Thus, the area was submerged at least until ~800 ka, a condition that made the formation of epigenic gypsum caves impossible. These epigenic caves could only have formed when the karstifiable aquifer was unconfined, meaning that the majority of sediments overlying the gypsum were removed before the inception of the first speleogenetic events. Moreover, these cave systems need a mature hydrological network at the surface able to efficiently convey water into the underground (i.e. formation of sinkholes, protovalleys, etc.). 200,000 years (i.e. from ~800 ka to ~630 ka) is considered a sufficient and reasonable timespan to permit the dismantling of most marine sediments covering the gypsum beds and for the creation of an efficient hydrological surface drainage network (Columbu *et al.* 2017).

With these new data, we sensibly reviewed the age of speleogenesis in the Northern Italian gypsum terrains, procuring solid geochronological and geomorphological evidences. In parallel, we established an evolutionary speleological model based on the cyclical dualism between speleothems being formed during relative wet and warm climate stages and main

sub-horizontal caves being carved during periods of relative dry and cold climate stages. This model may also be applied to other gypsum karst areas having similar geological and climatic conditions, which would be useful for refining the timing of other gypsum karst systems.

References

- Amorosi A, Caporale L, Cibin U, Colalongo M, Pasini G, Ricci Lucchi F, Severi P, Vaiani S, 1998. The Pleistocene littoral deposits (Imola Sands) of the northern Apennines foothills. *Giornale di Geologia*, **60**, 83-118.
- Amorosi A, Maselli V, Trincardi F, 2015. Onshore to offshore anatomy of a late Quaternary source-to-sink system (Po Plain-Adriatic Sea, Italy). *Earth-Science Reviews*, **153**, 212-237.
- Audra P, Bini A, Gabrovšek F, Häuselmann P, Hobléa F, Jeannin P-Y, Kunaver J, Monbaron M, Šušteršič F, Tognini P, 2006. Cave genesis in the Alps between the Miocene and today: a review. *Zeitschrift für Geomorphologie*, **50**(2), 153-176.
- Cheng H, Lawrence Edwards R, Shen CC, Polyak VJ, Asmerom Y, Woodhead J, Hellstrom J, Wang Y, Kong X, Spötl C, Wang X, Calvin Alexander E, 2013. Improvements in ^{230}Th dating, ^{230}Th and ^{234}U half-life values, and U-Th isotopic measurements by multi-collector inductively coupled plasma mass spectrometry. *Earth and Planetary Science Letters*, **371-372**, 82-91.
- Columbu A, Chiarini V, De Waele J, Drysdale RN, Woodhead J, Hellstrom J, Forti P, E, 2017. Late quaternary speleogenesis and landscape evolution in the northern Apennine evaporite areas. *Earth Surface Processes and Landforms*, in print.
- Columbu A, De Waele J, Forti P, Montagna P, Picotti V, Pons-Branche E, Hellstrom J, Bajo P, Drysdale RN, 2015. Gypsum caves as indicators of climate-driven river incision and aggradation in a rapidly uplifting region. *Geology*, **43**(6), 539-542.
- Cyr AJ, Granger DE, 2008. Dynamic equilibrium among erosion, river incision, and coastal uplift in the northern and central Apennines, Italy. *Geology*, **36**(2), 103-106.
- Demaria D, 2002. Emilia Romagna. In: G Madonia and P Forti (Eds.). *Le aree carsiche gessose d'Italia. Memorie dell'Istituto Italiano di Speleologia*, **2**(14), pp. 159-184.
- De Waele J, Forti P, Rossi A, 2011. Il carsismo nelle evaporiti dell'Emilia Romagna. In: P Lucci and A Rossi (Eds.). *Speleologia e geositi carsici in Emilia Romagna, Pitagora, Bologna*, pp. 25-59.
- De Waele J, Fabbri F, Forti P, Lucci P, Marabini S., 2013. Evoluzione speleogenetica del sistema carsico del Re Tiberio (Vena del Gesso Romagnola). In: M. Ercolani, P. Lucci, S. Piastra and B. Sansavini (Eds.). *I Gessi e la Cave i Monte Tondo. Studio multidisciplinare di un'area carsica nella Vena del Gesso Romagnola. Memorie dell'Istituto Italiano di Speleologia*, **2**(26), pp. 81-101.

Table 1. U-Th radiometric dating results. Mass of samples, ²³⁸U content, the uranium and thorium isotope activity ratios, and the corrected ages are provided. Uncertainties are expressed in 2σ notation. Ages are calculated using equation 1 of Hellstrom (2006) and the U and Th decay constants of Cheng et al, (2013). The raw ages were corrected using an initial ²³⁰Th/²³²Th activity ratio of 1.5±1.5.

Cave system	Cave	Sample ID	Mass (g)	²³⁸ U (ng/g)	(²³⁰ Th/ ²³⁸ U) _k ± 2σ	(²³⁴ U/ ²³⁸ U) _k ± 2σ	(²³² Th/ ²³⁸ U) _k ± 2σ	(²³⁰ Th/ ²³² Th) _k	Corrected Age (ka) ± 2σ
Monte Tondo - Re Tiberio	Abisso Mezzano	RT-A1 r	0.037	1483	0.6542 ± 0.0049	0.946 ± 0.004	0.000454 ± 0.000001	1440	130.58 ± 2.39
		RT-A1 bis	0.015	848	0.6541 ± 0.0043	0.945 ± 0.002	0.000657 ± 0.000006	995	131.10 ± 1.87
		RT-A1	0.106	1023	0.6558 ± 0.0012	0.945 ± 0.002	0.000848 ± 0.000007	774	131.74 ± 0.75
		RT 2015 1	0.020	1554	0.6490 ± 0.0035	0.944 ± 0.002	0.000402 ± 0.000003	1616	129.04 ± 1.53
		RT 2015 5	0.019	1656	0.6572 ± 0.0039	0.956 ± 0.002	0.000607 ± 0.000003	1082	128.67 ± 1.65
		RT-B1	0.009	934	0.6541 ± 0.0044	0.956 ± 0.003	0.000239 ± 0.000005	2733	127.57 ± 1.83
		RT 2015 7	0.019	1623	0.6510 ± 0.0028	0.957 ± 0.003	0.000730 ± 0.000004	892	125.77 ± 1.28
		RT-B I	0.010	1797	0.6479 ± 0.0052	0.952 ± 0.008	0.000125 ± 0.000001	5174	126.24 ± 3.20
		RT-B2	0.008	1068	0.6541 ± 0.0039	0.962 ± 0.003	0.000517 ± 0.000006	1266	125.87 ± 1.64
		RT-C1	0.010	1004	0.6562 ± 0.0046	0.965 ± 0.003	0.000599 ± 0.000007	1095	125.58 ± 1.85
		RT-CI	0.012	1748	0.6498 ± 0.0055	0.958 ± 0.002	0.000075 ± 0.000002	8677	125.35 ± 2.11
		RT-C m1	0.013	3127	0.6472 ± 0.0025	0.957 ± 0.002	0.000098 ± 0.000001	6606	124.95 ± 1.08
		RT-C m2	0.017	1619	0.6422 ± 0.0020	0.949 ± 0.002	0.000295 ± 0.000003	2176	125.14 ± 0.91
		RT-CII	0.012	1669	0.6389 ± 0.0053	0.951 ± 0.002	0.000250 ± 0.000003	2552	123.45 ± 2.02
		RT 2015 10	0.020	1696	0.6508 ± 0.0032	0.963 ± 0.002	0.000146 ± 0.000001	4448	124.36 ± 1.32
	RT-C2	0.015	972	0.6450 ± 0.0028	0.953 ± 0.002	0.000215 ± 0.000003	3004	125.17 ± 1.23	
	RT-DI	0.033	1764	0.6461 ± 0.0049	0.955 ± 0.001	0.000682 ± 0.000003	948	124.74 ± 1.85	
	RT-D III	0.050	1899	0.6484 ± 0.0048	0.961 ± 0.003	0.000684 ± 0.000003	948	123.94 ± 1.94	
	3 Anelli	3A	0.014	2970	0.5932 ± 0.0025	0.946 ± 0.002	0.002052 ± 0.000027	289	108.86 ± 0.98
		3A-2016-2	0.045	534	0.6016 ± 0.0024	0.960 ± 0.002	0.005345 ± 0.000025	113	107.69 ± 1.28
		3A-t	0.020	1157	0.6223 ± 0.0037	0.968 ± 0.003	0.038551 ± 0.000421	16	106.29 ± 7.23
	Abisso 50	A501	0.008	1681	0.5176 ± 0.0025	0.970 ± 0.002	0.033461 ± 0.000349	15	77.89 ± 6.06
		A502	0.011	1867	0.4843 ± 0.0024	0.965 ± 0.002	0.002576 ± 0.000037	188	76.10 ± 0.75
		A503	0.010	955	0.4829 ± 0.0024	0.975 ± 0.002	0.001806 ± 0.000019	267	74.69 ± 0.68
	Pozzo Pollini	D3	0.100	513	0.5378 ± 0.0021	0.973 ± 0.002	0.002398 ± 0.000013	224	87.80 ± 0.70
		PP	0.015	295	0.5207 ± 0.0045	0.976 ± 0.003	0.002766 ± 0.000019	188	83.14 ± 1.24
		PP1	0.009	795	0.5201 ± 0.0029	0.970 ± 0.002	0.018004 ± 0.000116	29	81.18 ± 3.23
		D2	0.100	652	0.4886 ± 0.0009	0.950 ± 0.001	0.008241 ± 0.000022	59	77.90 ± 1.40
		D4	0.100	670	0.4912 ± 0.0013	0.957 ± 0.001	0.008062 ± 0.000030	61	77.70 ± 1.40
	Grotta Oliver	PP2	0.017	1165	0.4859 ± 0.0028	0.968 ± 0.002	0.007278 ± 0.000078	67	75.21 ± 1.44
		GO1	0.012	1217	0.0921 ± 0.0009	0.949 ± 0.002	0.023011 ± 0.000284	4	7.10 ± 4.10
	Grotta Oliver	GO2	0.010	924	0.0962 ± 0.0007	0.943 ± 0.002	0.026957 ± 0.000186	4	6.96 ± 4.92
		GO-2016-2	0.044	1205	0.0670 ± 0.0004	0.939 ± 0.002	0.017181 ± 0.000321	4	5.03 ± 3.09
Galleria Principale	RTy 1	0.047	1511	0.0052 ± 0.0002	0.960 ± 0.001	0.000451 ± 0.000008	12	0.52 ± 0.08	
	RTy 2	0.045	1432	0.0035 ± 0.0002	0.960 ± 0.001	0.000613 ± 0.000014	6	0.29 ± 0.11	
	RTy 3	0.051	1548	0.0042 ± 0.0001	0.982 ± 0.002	0.002122 ± 0.000050	2	0.11 ± 0.36	
Spipola - Acquafredda	Spipola	Spd-2016-1	0.047	924	1.0480 ± 0.0042	1.126 ± 0.002	0.000147 ± 0.000002	7124	253.90 ± 4.41
		SpD-E	0.120	586	0.9303 ± 0.0097	1.026 ± 0.009	0.000416 ± 0.000004	2238	252.10 ± 14.77
		SpD-D	0.118	442	0.9061 ± 0.0104	1.009 ± 0.010	0.002357 ± 0.000026	384	246.63 ± 16.16
		SpD-C	0.049	1003	1.0197 ± 0.0064	1.112 ± 0.004	0.000020 ± 0.000001	50924	243.58 ± 6.52
		SpD-B	0.051	3052	1.0215 ± 0.0051	1.111 ± 0.004	0.000004 ± 0.000000	277192	245.55 ± 5.64
		SpD-A	0.050	1971	1.1318 ± 0.0055	1.207 ± 0.004	0.000465 ± 0.000009	2432	246.34 ± 5.31
		SpD b	0.063	429	0.9245 ± 0.0035	1.028 ± 0.002	0.000264 ± 0.000002	3506	243.53 ± 3.97
		Spd-2016-2	0.048	484	0.8964 ± 0.0035	1.007 ± 0.002	0.002002 ± 0.000039	448	239.34 ± 4.30
		Sp1-b	0.038	736	0.0170 ± 0.0004	1.029 ± 0.003	0.007400 ± 0.000186	2	0.63 ± 1.19
		Sp1-t	0.034	731	0.0071 ± 0.0002	1.024 ± 0.003	0.003287 ± 0.000071	2	0.23 ± 0.53
		Sp5-b	0.044	1012	0.0143 ± 0.0003	1.045 ± 0.002	0.001267 ± 0.000025	11	1.30 ± 0.20
Sp5-t	0.045	1062	0.0027 ± 0.0002	1.031 ± 0.002	0.000901 ± 0.000015	3	0.14 ± 0.14		
Castelnuovo	Peroni	P2-b	0.039	989	0.0818 ± 0.0007	0.984 ± 0.003	0.009378 ± 0.000174	9	7.89 ± 1.58
		P2-t	0.036	1120	0.0389 ± 0.0004	1.048 ± 0.003	0.000289 ± 0.000005	135	4.08 ± 0.06
		P3-B	0.035	1435	0.0479 ± 0.0009	1.014 ± 0.002	0.000412 ± 0.000011	116	5.22 ± 0.12
	P3-T	0.044	1368	0.0246 ± 0.0005	1.057 ± 0.002	0.000071 ± 0.000001	347	2.56 ± 0.05	
	Mornig	MOR2-b	0.020	1314	0.0424 ± 0.0006	0.880 ± 0.002	0.012795 ± 0.000034	3	2.99 ± 2.44
MOR2-t	0.021	2313	0.0218 ± 0.0003	0.857 ± 0.003	0.001254 ± 0.000005	17	2.57 ± 0.24		
Stella - Rio Basino	Rio Basino	RBT-b	0.049	1076	0.0588 ± 0.0005	0.893 ± 0.003	0.013927 ± 0.000202	4	4.84 ± 2.64
		RBT-t	0.052	1102	0.0432 ± 0.0005	0.887 ± 0.003	0.008033 ± 0.000094	5	3.95 ± 1.51
		RB3-b	0.050	511	0.0252 ± 0.0005	0.937 ± 0.003	0.004679 ± 0.000060	5	2.15 ± 0.83
		RB3-t	0.050	492	0.0089 ± 0.0004	0.950 ± 0.003	0.003228 ± 0.000060	3	0.47 ± 0.56
		RB1-b	0.034	569	0.0612 ± 0.0013	0.935 ± 0.002	0.011802 ± 0.000275	5	5.29 ± 2.11
RB1-t	0.042	494	0.0282 ± 0.0008	0.953 ± 0.002	0.010104 ± 0.000227	3	1.53 ± 1.77		
Monte Mauro	Monte Mauro	MM2-b	0.039	731	0.9225 ± 0.0042	0.981 ± 0.003	0.019454 ± 0.000541	47	316.17 ± 12.65
		MM2-t	0.034	1367	0.8783 ± 0.0031	0.990 ± 0.003	0.001359 ± 0.000028	646	239.98 ± 4.46
		MM4 b	0.021	556	0.9782 ± 0.0062	0.994 ± 0.003	0.001776 ± 0.000010	551	468.00 ±130/-42
	MM4 t	0.023	393	0.9375 ± 0.0060	0.995 ± 0.003	0.002130 ± 0.000009	440	313.44 ± 14.27	
	Banditi	BA 1.1	0.050	1071	0.9988 ± 0.0051	0.998 ± 0.004	0.111054 ± 0.000331	9	> 580 ± -
		BA 2.1	0.050	804	0.9569 ± 0.0045	0.991 ± 0.004	0.001508 ± 0.000023	635	378.00 ±29/-20
		BA_BIG_1	0.075	1837	0.6804 ± 0.0026	0.976 ± 0.004	0.000010 ± 0.000000	69553	131.29 ± 1.46
		BA_BIG_2	0.069	886	0.6776 ± 0.0030	0.987 ± 0.003	0.000011 ± 0.000001	62589	127.07 ± 1.40
BA_BIG_3		0.066	706	0.6563 ± 0.0029	0.990 ± 0.003	0.000039 ± 0.000001	16700	119.01 ± 1.26	
BA_BIG_4	0.070	870	0.6363 ± 0.0036	0.980 ± 0.003	0.000463 ± 0.000007	1277	113.36 ± 1.00		

- Drysdale RN, Hellstrom JC, Zanchetta G, Fallick AE, Sanchez Goni MF, Couchoud I, McDonald J, Maas R, Lohmann G, Isola I, 2009. Evidence for obliquity forcing of glacial Termination II. *Science*, 325(5947), 1527-1531.
- Drysdale RN, Bence TB, Hellstrom JC, Couchoud I, Greig A, Bajo P, Zanchetta G, Isola I, Spötl C, Banerjee I, Regattieri E, Woodhead JD, 2012. Precise microsampling of poorly laminated speleothems for U-series dating. *Quaternary Geochronology*, **14**, 38-47.
- Falgueres C, 2003. ESR dating and the human evolution: Contribution to the chronology of the earliest humans in Europe. *Quaternary Science Reviews*, **22**, 1345-1351.
- Forti P, Chiesi M, 2001. Idrogeologia, idrodinamica e meteorologia ipogea dei Gessi di Albinea, con particolare riguardo al Sistema carsico afferente alla Tana della Mussina di Borzano (ER-RE 2) (Albinea-Reggio Emilia). *Memorie dell'Istituto Italiano di Speleologia*, **2**(11), 115-139.
- Forti P, 2003. I sistemi carsici. In: A Biancotti and M Motta (Eds.). Risposta dei processi geomorfologici alle variazioni ambientali, Briganti, Genova, pp. 246-251.
- Hellstrom J, 2003. Rapid and accurate U/Th dating using parallel ion-counting multi-collector ICP-MS. *Journal of Analytical Atomic Spectrometry*, **18**, 1346-1351.
- Hellstrom J, 2006. U-Th dating of speleothems with high initial ^{230}Th using stratigraphical constraint. *Quaternary Geochronology*, **1**(4): 289-295.
- Klimchouk AB, 2000. Speleogenesis in non carbonate lithologies. In: AB Klimchouk, DC Ford, AN Palmer and W Dreybrodt (Eds.). *Speleogenesis, evolution of karst aquifers*. National Speleological Society, Huntsville, pp. 430-442.
- Lisiecki LE, Raymo ME, 2005. A Pliocene-Pleistocene stack of 57 globally distributed benthic $\delta^{18}\text{O}$ records. *Paleoceanography*, **20**(1), 1-17.
- Lugli S, Manzi V, Roveri M, Scheiber BC, 2010. The Primary Lower Gypsum in the Mediterranean: a new facies interpretation for the first stage of the Messinian salinity crisis. *Palaeogeography, Palaeoclimatology, Palaeoecology*, **297**(1), 83-99.
- Miari M, 2007. Ieneolitico. In: C Guarnieri (Eds.). *Archeologia dell'Apennino romagnolo: il territorio di Riolo Terme, Imola*, pp. 30-33.
- Muttoni G, Scardia G, Kent DV, Morsiani E, Tremolada F, Cremaschi M, Peretto C, 2011. First dated human occupation of Italy at ~0.85 Ma during the late Early Pleistocene climate transition. *Earth and Planetary Science Letters*, **307**(3-4), 241-252.
- Negrini C, 2007. Re Tiberio. In: C Guarnieri (Eds.). *Archeologia dell'Apennino romagnolo: il territorio di Riolo Terme, Imola*, pp. 51-52.
- Pasini G, 1969. Fauna a mammiferi del Pleistocene superiore in un paleoinghiottitoio carsico presso Monte Croara (Bologna). *Le Grotte d'Italia*, **4**(4), 1-46.
- Pasini G, 2012. Speleogenesis of the "Buco dei Vinchi" inactive swallow hole (Monte Croara karst sub-area, Bologna, Italy), an outstanding example of antigravitative erosion (or "paragenesis") in selenitic gypsum. An outline of the "post-antigravitative erosion". *Acta Carsologica*, **41**(1), 15-34.
- Picotti V, Pazzaglia FJ, 2008. A new active tectonic model for the construction of the Northern Apennines mountain front near Bologna (Italy). *Journal of Geophysical Research*, **113**, B08412.
- Plan L, Tschegg C, De Waele J, Spötl C, 2012. Corrosion morphology and cave wall alteration in an Alpine sulfuric acid cave (Kraushöhle, Austria). *Geomorphology*, **169**, 45-54.
- Polyak VJ, McIntosh WC, Güven N, Provencio P, 1998. Age and origin of Carlsbad Cavern and related caves from $^{40}\text{Ar}/^{39}\text{Ar}$ of Alunite. *Science*, **279**(5358), 1919-1922.
- Polyak VJ, Provencio P, Asmerom Y, 2016. U-Pb dating of speleogenetic dolomite: A new sulfuric acid speleogenesis chronometer. *International Journal of Speleology*, **45**(2), 103-109.
- Richards DA and Dorale JA, 2003. Uranium-series chronology and environmental applications of speleothems. *Reviews in Mineralogy and Geochemistry*, **52**(1), 407-460.
- Sasowsky ID, 1998. Determining the age of what is not there. *Science*, **279**(5358), 1874.
- Vai GB, Martini IP, 2001. *Anatomy of an orogen: the Apennines and adjacent Mediterranean*. Kluwer Academic Publishers, Dordrecht, Netherlands, pp. 631.
- Wegmann KW, Pazzaglia FJ, 2009. Late Quaternary fluvial terraces of the Romagna and Marche Apennines, Italy: climatic, lithologic, and tectonic controls on terrace genesis in an active orogen. *Quaternary Science Reviews*, **28**(1), 137-165.

Why We Should Thank A Proterozoic Meteorite For The Caves At Assynt, NW Scotland, UK

Trevor Faulkner

Affiliation: Limestone Research Group, GEES, University of Birmingham. Edgbaston, Birmingham, B15 2TT, UK.
Email: trevor@marblecaves.org.uk

Abstract

The carbonate rocks of the Durness Group at Assynt in Sutherland, NW Scotland, contain important bone caves and the three longest caves in Scotland. However, the shape of the containing, mainly linear, carbonate outcrop is intriguing, because it has an enigmatic bulge eastwards at the Assynt Culmination, which contains all these caves. Understanding the reason for the bulge has taken about 145 years, starting with the mapping of the complex local geology by Peach and Horne. They showed for the first time that thrusting could cause older rocks to over-ride and lie above younger rocks, as occurs along the Moine Thrust Zone in Assynt. However, it is only in the last eight years that detailed studies have revealed the probable reasons for the Assynt Culmination. Important clues concern the Moine movements, which probably had to traverse a deep depression in the basement rock beneath the town of Lairg, from the evidence of the Lairg Gravity Low, where the rock is less dense. Other clues concern the origin of the 1177 million-year-old Stac Fada deposits, which crop out along the Sutherland coast. Although initially thought to be of volcanic origin, they have since been re-interpreted as ejecta flow deposits from a meteorite impact. The remains of its crater are now buried beneath the Moine Supergroup and probably correspond to, and account for, the Lairg Gravity Low. Thus, there is a strong probability that alignments that include the Moine movement direction, the Assynt Culmination, and the Lairg Gravity Low arise from a large meteorite strike at 1177 Ma. This suggests that some of the Moine Supergroup descended into an enormous cratered depression in the basement rocks, which retarded the local Moine advance as it progressed towards the west, resulting in the bulge at Assynt. If the meteorite had not impacted, the Moine Thrust would likely have remained approximately linear and reached farther west than all the known caves at Assynt. In that case, the karst cave locations would have been covered by the Moine Supergroup succession and the caves could not have developed during the Quaternary. Thus, we probably have to thank a Proterozoic meteorite impact for the existence of all the caves at Assynt.

Keywords:

1. The Assynt enigma

The carbonate rocks of the Durness Group at Assynt in Sutherland, NW Scotland, UK, are important because they contain the archaeologically significant Creag nan Uamh Bone Caves and the three longest natural caves in Scotland: the Cnoc nam Uamh System, Allt nan Uamh Stream (ANUS) Cave and Uamh an Claonaite / Rana Hole. These caves are each over a mile long (Lawson, 1988, and later extensions). However, the shape of the containing Lower Ordovician / Cambrian outcrop (Figure 1) is intriguing. Primarily it comprises a rather narrow (1–3 km-wide) highly-faulted and imbricated, roughly linear, outcrop of mainly sedimentary Durness carbonates and quartzites of Early Cambrian age. These stretch 150 km from Durness in the north to Loch Kishorn in the south, along the foreland of the Moine Thrust Zone (or Belt: Butler, 2010, Fig. 2). The western edge of the outcrop abuts older Lewisian gneisses and the Torridonian Supergroup. The eastern edge commonly lies along the Moine Thrust. However, the outcrop expands to a width of 11 km at the Assynt Culmination (or Window), creating an enigmatic bulge eastwards for about 10 km from the lower Glencoul Thrust. There, the Ordovician / Cambrian rocks with various intrusions are exposed at the surface, rather than the Moine schists. Phemister (1960, pp. 23–24) suggested that this “great anomaly” arose because “during the thrust-movements, the block of Moine Schists opposite Assynt was compressed from the NNE and from the SSW and its westerly motion retarded relatively to the schists on the north and south”. Coward (1983) discussed the possibility of gravity-spreading structures and surge zones at Assynt. However, it now appears that a simpler

explanation for the bulge and an important speleological consequence follow from information provided by Amor *et al.* (2008), Leslie *et al.* (2010), Thigpen *et al.*, 2013, and Simms (2015).

2. Structural geology

Understanding the reason for the Assynt Culmination has taken about 145 years of diligent geological research. The extreme complexity of the local geology is illustrated in the 1-inch map of the Assynt District, which was published for the Geological Survey in 1923. This was based on the survey work of Peach and Horne (1884) and Peach *et al.* (1907), which started in 1871. Peach and Horne are commemorated with a statue at the Knockan Crag Visitor Centre (Figure 2), which is only 4 km from the Grampian Speleological Group caving hut at Elphin. These pioneering geologists showed that the older Moine schists lie above the younger sedimentary Durness carbonates along the western edge of the Moine Thrust, as can be seen at Knockan Crag (Figure 3). Westward tectonic movement caused the schists of the Neoproterozoic metasedimentary Moine Supergroup to over-ride the younger but topographically lower rocks during the later part of the Caledonian orogeny. Peach and Horne demonstrated convincingly that the deeper rocks are younger than the schists at the Moine Thrust Zone, which is counter-intuitive and was in opposition to the prevailing wisdom at the time. Later, Johnstone and Mykura (1989, p. 50 and pp. 54–55) reported that “The thrust sequence must be re-interpreted with the lower and younger thrusts transporting the older and higher thrusts to west-north-west in a piggy-back fashion. The Sole Thrust

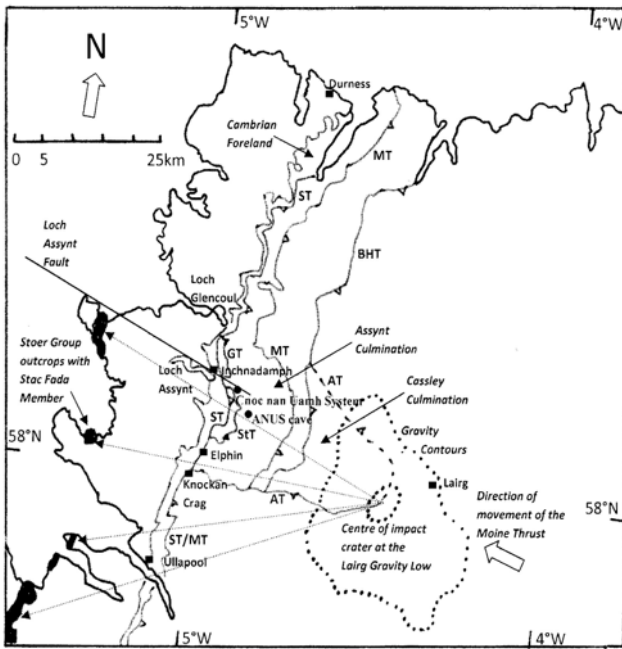


Figure 1. Simplified structural geology and ejecta deposits in Sutherland, NW Scotland, UK. ST Sole Thrust; GT Glencoul Thrust; StT Stronchrubie Thrust; MT Moine Thrust; BHT Ben Hope Thrust; AT Achness Thrust. Dotted arrows show the proposed directions of flow from the impact crater. Other information from the references cited in text.

is then the latest structure and in many areas the Moine Thrust is the earliest”, which “is difficult to date” but “may be of Precambrian age. Major thrust movement along the Moine Thrust Zone appears to have terminated before 420 Ma (Mid-Silurian).” The Moine Thrust and the Sole Thrust were estimated to have displacements of 70 and 25 km (Coward, 1983). Metamorphic grade and temperature also increased eastwards and upwards, from the foreland to the hinterland (Thigpen *et al.*, 2013).

3. Recent studies

Dating by Goodenough *et al.* (2011) has shown that the earliest ductile movement on the Moine Thrust occurred after 447.9 ± 2.9 Ma. The latest ductile movement along the lower thrusts was complete by 429 ± 0.5 Ma. Structural research following Peach and Horne (1884) has exposed a stark contrast in tectonic behaviours north and south of Assynt, as reviewed by Butler (2010). Revision of the Assynt District geological map has also identified two types of thrust systems, north and south of Inchnadamph, where the Sole Thrust is faulted sinistrally by the Loch Assynt Fault (Krabbendam and Leslie, 2010; Figure 1). North of the central Traligill river, the Sole Thrust merges with the Glencoul Thrust near Loch Glencoul and then runs roughly parallel to the Moine Thrust. To the south, it runs below many other thinner thrust slices, the next lowest thrust being the Stronchrubie Thrust, and merges with the Moine Thrust at Knockan Crag. Metamorphic temperatures also show a pronounced increase of 200°C as the edge of the Moine Thrust sheet is traced southwards towards Assynt (Thigpen *et al.*, 2013), indicating partial melting at a greater depth. The latest understanding of the complex geology and tectonic evolution of the Scottish Caledonides, summarised



Figure 2. Statue of Ben Peach and John Horne

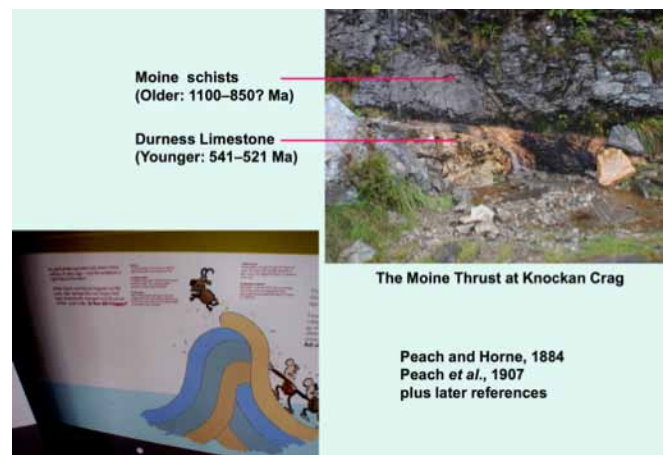


Figure 3. The Moine Thrust at Knockan Crag at the Knockan Crag Visitor Centre

by Dewey *et al.* (2015), does not consider the reasons for the Assynt Culmination.

Rather than the Plemister (1960) compressional concept, Leslie *et al.* (2010) provided evidence that the bulge at Assynt arose from the Cambro-Silurian Moine movements that had to traverse a depression within the Lewisian Complex basement rocks around the town of Lairg. They modelled this depression as being c. 3 km deep. This created the ductile “Cassley Culmination”, between a parallel bulge in the Ben Hope Thrust and the higher Achness Thrust, which extends westwards from Lairg towards the lower brittle-ductile Assynt Culmination. The evidence for the basement depression is provided by the Lairg Gravity Low (Figure 1). This is a prominent feature of the onshore gravity field in northern Scotland, which Leslie *et al.* (2010) illustrated as being centred about 30 km SE of the Moine Thrust. Remarkably, the direction from this centre to the middle of the eastward bend around the Assynt Culmination corresponds to the ESE to WNW direction of carry of the Moine Supergroup itself (Peach and Horne, 1884). But why should there be a basement depression and the gravity low at Lairg?

Another local enigma concerns the origin of the Stac Fada Member, within the Bay of Stoer Formation of the Mesopro-

terozoic Stoer Group, which lies west of the Moine Thrust Zone and the Durness carbonates. This Member crops out in at least 13 places along 50 km of the Sutherland coast, with variable thicknesses that reach a maximum of 22.4 m at the outcrop west of Elphin (Amor *et al.*, 2008). It is composed of a polymict clastic-matrix breccia with cogenetic melt particles. The matrix grains are broadly consistent with derivation from the Lewisian gneiss basement and associated dykes or from Stoer Group sediments (Simms, 2015), so that the Member was initially thought to be of volcanic origin. However, Amor *et al.* (2008) re-interpreted it as comprising an ejecta ‘blanket’ created by a dense, turbulent, water vapour-borne ground-hugging flow with air-fall components from a crater produced by a meteorite. Evidence for high pressure shock metamorphism, diagnostic of a meteorite strike, is provided by the presence of shocked quartz and biotite and by the addition of meteoritic material, including enriched Cr, Ir and Ni. The Member was well-preserved by rapid freezing and rapid burial and is among the oldest of the rocks formerly referred to as the “Torridonian”, which Parnell *et al.* (2011) dated at 1177±5 Ma. Amor *et al.* (2008) suggested that the impact was likely in an area lying west of the current coastline.

Disputing the direction of the ejecta flow, Simms (2015) has recently proposed that a 2.5 km diameter meteorite, travelling at 19 km per second, created a crater well to the east of the current coast that was initially 25 km across and 8 km deep. Importantly he suggested that the remains of such a crater, with a final diameter of 40–50 km and a depth reduced by collapse and local isostatic rebound, is now buried beneath the Moine Supergroup rocks and corresponds to, and accounts for, the Lairg Gravity Low. Such an impact at Lairg would explain the likely radial flow directions of the ejecta to their present exposures (where not eroded away or still covered by younger rocks of the Stoer and Torridon groups), 50–65 km to the west (Figure 1; Simms, 2015, Fig. 14), which reduce in thickness with distance from Lairg. At this time, the whole area lay on the southeastern side of the Rodinia super-continent, adjacent to the present NE America and Greenland. This was over 700 Ma prior to the opening of the Iapetus Ocean

and its closing during the Caledonian Orogeny. Thus, from this evidence, it seems that the basement depression assumed by Leslie *et al.* (2010) to be associated with the Lairg Gravity Low was caused by a meteorite impact.

Following the latest revelations by Amor *et al.* (2008), Leslie *et al.* (2010), Thigpen *et al.*, 2013, and Simms (2015), concerning the nature of the structural geology at Assynt, the Lairg Gravity Low and the Stac Fada meteorite, the scenario illustrated in Figure 1 is unlikely to be a coincidence. Indeed, there is a strong probability that the alignment with the direction of Moine movements of the middle of the Assynt Culmination (with its different thrust sequences north and south of the central Loch Assynt Fault and the increased paleotemperature of the Moine Thrust base there), the Cassley Culmination, and the Lairg Gravity Low arises from a large meteorite strike at 1177 Ma. These observations led Faulkner (2016a) to build on the argument by Leslie *et al.* (2010). He deduced that from 448–429 Ma, during the Caledonian metamorphism, some of the Moine Supergroup rocks descended into the enormous remnant buried bowl-shaped cratered depression in the Lewisian basement that had been created by a meteorite strike 729 Ma before. Although the depression depth might have been reduced by later sediment infill, this downward diversion locally retarded the westward advance of the Moine rocks, so that the adjacent Achness, Ben Hope and Moine thrust edges could not keep pace with the edges of the same thrusts to the north and south, resulting in the culminations at Cassley and Assynt and the bend in the Ben Hope Thrust. It can be surmised that the original volume of the ‘missing’ Moine schists at Assynt (prior to erosion following the Caledonide movement) roughly equals the remaining volume of the collapsed crater subsequent to deposition, prior to the thrusting. Simms (2016) commented that an additional mechanism could have been the creation of extensive radial and / or concentric fractures caused by the impact, which also influenced the later local Moine movement. Table 1 provides a simplified timescale for events at Assynt, from the cited references.

Table 1. Simplified timescale at Assynt

Eon /Period	Age or range (Ma)	Event		
Quaternary	0	Glacial erosion and main speleogenesis		
	2.58			
		Denudation		
Silurian	429	Moine thrusting and Caledonian metamorphism		
Ordovician	448			
Cambrian	509	Marine deposition of Durness Group carbonates		
	541			
Proterozoic	750	Terrestrial deposition of Torridonian Group sandstones	Marine deposition of Moine Supergroup and later Grenville and Morarian metamorphism	
	c. 1000			
	c. 1000	Deposition of Stoer Group		
	1177	Meteorite strike and Stac Fada ejecta deposit		
	c. 1200	Deposition of Stoer Group		
	c. 1200	Lewisian metamorphism, cooling, uplift and erosion		
Archean	2900			

4. Conclusions

If the meteorite had not impacted, it is reasonable to assume that what is now left of the eroded leading edge of the Moine Thrust would have remained approximately linear and reached at least as far west as the Glencoul and Stronchrubie Thrusts, in line with some of its present limits north and south of Assynt. However, all the known caves at Assynt lie east of these thrusts (where they exist). Hence, in that case, their locations would have all been covered by the Moine Supergroup and these karst caves could not have developed by dissolution and stream erosion within the Quaternary. Thus, the Bone Caves, the three mile-long caves and the other caves in the Durness Limestone at Assynt probably owe their existence to the impact of a meteorite in Proterozoic times.

Acknowledgements

Mike Simms is thanked for presenting his paper at the University of Birmingham, UK, on 30 November 2015, for subsequent correspondence, and for explaining the formation of the meteorite crater at Lairg in a Channel 4 TV programme *Walking Through Time*, which was broadcast in the UK on 24 September 2016. This paper expands on the previous letter (Faulkner, 2016a) and a later article (Faulkner, 2016b). David Lowe is thanked for improving the geological terminology in an earlier draft.

References

- Amor, K., Hesselbo, S.P., Porcelli, D., Thackrey, S., Parnell, J., 2008. A Precambrian proximal ejecta blanket from Scotland. *Geology*, **36**, 303–306.
- Butler, R.W.H. 2010. The role of thrust tectonic models in understanding structural evolution in NW Scotland. *Geological Society, London, Special Publications*, **335**, 293–320.
- Coward, M.P. 1983. The thrust and shear zones of the Moine thrust zone and the NW Scottish Caledonides. *Journal of the Geological Society*, **140**, 795–811.
- Dewey, J.F., Dalziel, I.W.D., Reavy, R.J. and Strachan, R.A. 2015. The Neoproterozoic to Mid-Devonian evolution of Scotland: a review and unresolved issues. *Scottish Journal of Geology*, **51**, 5–30.
- Faulkner, T. 2016a. Comment on: Simms, M.J., The Stac Fada impact ejecta deposit and the Lairg Gravity Low: evidence for a buried Precambrian impact crater in Scotland? [*Proc. Geol. Assoc.*, **126**(6), 742–761 (2015)] and the consequence for the formation of caves within the Durness Limestone outcrops at Assynt, Sutherland. *Proceedings of the Geologists' Association*, **127**(1), 107–108.
- Faulkner, T. 2016b. Why we should thank a meteorite for the caves at Assynt. *Grampian Speleological Group Bulletin* 5th Series **2**(1), 13–15.
- Geological Survey. 1923. Assynt District. 1:63360.
- Goodenough, K.M., Millar, I., Strachan, R.A., Krabbendam, M and Evans, J.A. 2011. Timing of regional deformation and development of the Moine Thrust Zone in the Scottish Caledonides: constraints from the U–Pb geochronology of alkaline intrusions. *Journal of the Geological Society*, **168**, 99–114.
- Johnstone, G.S. and Mykura, W. 1989. *British Regional Geology: The Northern Highlands of Scotland*. Fourth Edition. HMSO. 219 pp.
- Krabbendam, M. and Leslie, A.G. 2010. Lateral variations and linkages in thrust geometry: the Traligill Transverse Zone, Assynt Culmination, Moine Thrust Belt, NW Scotland. *Geological Society, London, Special Publications*, **335**, 335–357.
- Lawson, T.J. 1988. *Caves of Assynt*. Grampian Speleological Group. 90 pp.
- Leslie, A.G., Krabbendam, M., Kimbell, G.S. and Strachan, R.A. 2010. Regional-scale lateral variation and linkage in ductile thrust architecture: the Oykel Transverse Zone, and mullions, in the Moine Nappe, NW Scotland. *Geological Society, London, Special Publications*, **335**, 359–381.
- Parnell, J., Mark, D., Fallick, A.E., Boyce, A. and Thackrey, S. 2011. The age of the Mesoproterozoic Stoer Group sedimentary and impact deposits, NW Scotland. *Journal of the Geological Society*, **168**, 349–358.
- Peach, B.N. and Horne, J. 1884. Report on the geology of the North-West of Sutherland. *Nature*, **31**(785), 31–35.
- Peach, B.N., Horne, J., Gunn, W., Clough, C.T., Hinkman, L.W. and Teall, J.J.H. 1907. *The geological structure of the North-West Highlands of Scotland*. Memoir of the Geological Survey of Great Britain. HMSO. Edinburgh.
- Phemister, J. 1960. *British Regional Geology. Scotland: The Northern Highlands*. Third Edition. HMSO. Edinburgh. 104 pp.
- Simms, M.J. 2015. The Stac Fada impact ejecta deposit and the Lairg Gravity Low: evidence for a buried Precambrian impact crater in Scotland? *Proceedings of the Geologists' Association*, **126**(6), 742–761.
- Simms, M.J. 2016. Reply to comment by Trevor Faulkner on “The Stac Fada impact ejecta deposit and the Lairg Gravity Low: evidence for a buried Precambrian impact crater in Scotland? [*Proc. Geol. Assoc.*, **126**(6), 742–761 (2015)] and the consequence for the formation of caves within the Durness Limestone outcrops at Assynt, Sutherland”. *Proceedings of the Geologists' Association*, **127**(1), 109.
- Thigpen, J.R., Law, R.D., Loehn, C.L., Strachan, R.A., Tracy, R.J., Lloyd, G.E., Roth, B.L. and Brown, S.J. 2013. Thermal structure and tectonic evolution of the Scandian orogenic wedge, Scottish Caledonides: integrating geothermometry, deformation temperature and conceptual kinematic-thermal models. *Journal of Metamorphic Geology*, **31**, 813–842.

Are There Any Pre-Quaternary Caves In Scandinavia?

Trevor Faulkner

*Affiliation: Limestone Research Group, GEES, University of Birmingham, Edgbaston, Birmingham, B15 2TT, UK.
trevor@marblecaves.org.uk*

Abstract

Many dissolutional caves are known in Norway and Sweden, mainly formed in stripe karst Caledonide marble outcrops that have negligible primary porosity. Speleogenesis was commonly initiated by tectonic inception, mainly in fractures caused by isostatic rebound during one or more Quaternary deglaciations, followed by dissolution in aggressive water during deglacial speleogenesis and sporadically by later interglacial speleogenesis. Dissolutional caves in other limestones, fracture and talus caves, and many sea caves, also occur in both countries. It is an interesting question about whether any cave passages, of any type, and in any lithology, could have survived to the present if they had formed before the major glaciations started at the beginning of the Quaternary period, 2.58 Ma BP. This paper examines these possibilities and draws the conclusion that the survival of any non-hypogenic cave passages formed before the Mid-Pleistocene Revolution would be exceptional.

Keywords: Scandinavia, Caledonides, Pre-Quaternary, marble, fracture, talus

1. Introduction

There are over 2600 known dissolutional caves formed in Caledonide metamorphic limestones (marbles) of Cambro-Silurian age in both Norway (David St.Pierre, pers. comm., 2016) and Sweden (Hans Beskow, pers. comm., 2016). Figure 1 shows a simplified structural geology and convenient geographical partition for Scandinavia and marks the eastern limit of the Caledonide thrusts onto the older basement rocks. Over 1100 of these caves are in 'northern Scandinavia', north of Mo-i Rana; >1200 are in 'central Scandinavia', between Mo-i-Rana and Gäddede (Faulkner, 2005a and later reports); and >200 are in 'southern Scandinavia'. Nearly 50 karst caves in sedimentary limestones and basement marbles also occur in southern Sweden. Norway has >600 non-karst caves, including sea caves at various heights above the present sea level, some being huge (St. Pierre and St. Pierre, 1980; Sjöberg, 1988; Faulkner, 2005b). Sweden has >2300 non-karst caves, of which >300 are sea caves, >800 are tectonic fracture caves and >1200 are tectonic talus caves, formed in various lithologies. This paper examines the interesting question about whether any cave passages, of any type, and in any lithology, could have survived to the present, if they had formed before the c. 50 Quaternary glaciations of the last 2.58 million years.

2. Evolution of the Scandinavian landscape

Scandinavia is part of the Caledonian–Appalachian fold and thrust belt, an ancient mountain chain formed by the Caledonian Orogeny during the plate tectonic opening and closing of the Iapetus Ocean. The closure produced four major allochthons as metamorphic and igneous rocks were thrust south-eastwards over the older Baltic Shield basement. They include >850 outcrops of stripe karst marble just in central Scandinavia, in the steeply-foliated amphibolite-grade Uppermost Allochthon (mainly in Norway) and in the Køli Nappes of the Upper Allochthon in both countries (Faulkner, 2005a). Over 120 small marble outcrops in the lower Seve Nappes of the Upper Allochthon in Sweden contain no known caves. The slightly-dipping Middle and Lower Allochthons of low metamorphic grade occur along the whole length of the Scandes. Narrow outcrops also occur near Oslofjord (not shown on Figure 1) that contain several significant caves. Various

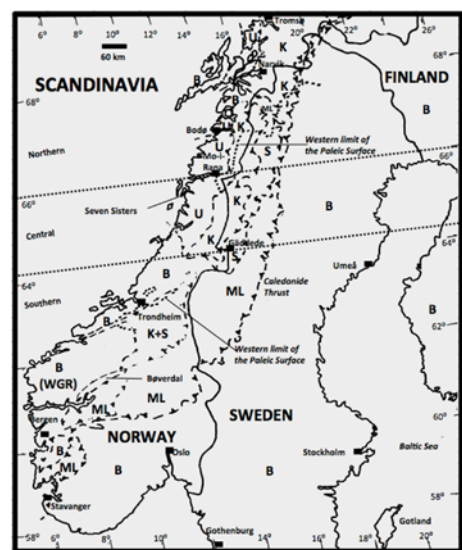


Figure 1. Simplified structural geology of Scandinavia, from various sources, also showing the western limit of the paleic surface, according to Rudberg (1997). U Uppermost Allochthon; K Køli Nappes and S Seve Nappes, both in the Upper Allochthon; ML Middle and Lower Allochthons; WGR Western Gneiss Region; B Pre-Cambrian basement; the 1:2,000,000 geology map provided by Ramberg et al. (2008) puts Bøverdalen and the Dumdalen side valley in the Lower Allochthon.



Figure 2. Horn summits above glacially-smoothed bedrock at the Seven Sisters.

authors have estimated that the original Caledonides reached altitudes up to 10 km, but most of these thrust sheets have since been eroded away.

The Caledonian Orogeny was followed by increased crustal rigidity and a peneplanation during the Carboniferous (Peulvast, 1985). A later uplifted Scandinavian Marginal Bulge was probably driven by the rifting associated with the opening of the Atlantic Ocean. The approximate present Scandinavian coastline was established by the start of the Mesozoic. However, the Late Cretaceous global marine transgression likely led to a reversal, reducing any exposed land in mid-Norway to one of low relief (Riis, 1996). A Palaeogene uplift of 600 m at the coast rose to 1200 m inland. Plio-Pleistocene times had further coastal and maximum net uplifts of c. 600 m and 800 m. From the evidence of its wide strandflat and dated karst materials, there has been no significant (non-isostatic) uplift in mid-Norway in the last 0.5 Ma. Riis (1992) noted that deposits dated to 300 ka BP in caves situated more than 1000 m below local mountain summits show that there was a considerable relief in Norway earlier in the Quaternary.

3. Quaternary glacial erosion

The whole of Scandinavia was covered by major icesheets during the Quaternary. Clark *et al.* (1999) argued that early glaciations on thick, deeply weathered, Tertiary soft beds allowed fast flows of relatively thin (~2 km) icesheets in 41 ka glacial cycles. However, after sufficient glacial erosion of the regolith, exposure of crystalline bedrocks in core areas caused northern icesheets formed after the Mid-Pleistocene Revolution (MPR) at c. 1 Ma BP to thicken to ≥ 3 km in 100 ka glacial cycles. Plio-Pleistocene erosion removed some 500–700 m of bedrock (Riis, 1996). Dowdeswell *et al.* (2010) showed that an average of 524 m of bedrock in north central Norway was eroded in the last 2.7 Ma, of which 230 m occurred in the final 600 ka (an average of 38 m per glacial cycle), showing greatest erosion later in the Quaternary. Erosion was fastest beneath large valley glaciers with several tributaries. The greatest glacial sculpting formed the most ‘peaky’ mountains and ‘horn’ summits along the coast, such as the Seven Sisters (Figure 2). The long lengths and the depths of the fjords demonstrate the erosive powers of the ice streams during many glaciations. At the same time, cold-based glacial erosion can be negligible in high areas with low relief. The entrenchment of U-shaped valleys by glaciation has been estimated by various methods (Faulkner, 2010, Table 1). Thus, glacial valleys in the mountains of Scandinavia can deepen by 15–108 m during each 100 ka glacial cycle, partly dependent on rock type and valley orientation, with 40 m being used as typical herein. The rate of retreat of each glacial valley shoulder is assumed to equal the rate of valley deepening.

4. The (non) relevance of the paleic surface

The response to the Pleistocene glacial fluctuations was ten times more pronounced on the steeper, western, side of the mountains, which all lie within the Caledonide thrusts, than on the gently-sloping lee side (Rudberg, 1997). Thus, the influence on the glacially-scoured high Swedish plateaux was much less marked, as the mean erosion across the whole of Scandinavia from all glaciations was only 16 m, according to Peulvast (1985). The *paleic surface* is one that is “not too much

changed by glacial erosion” (Rudberg, 1997, p. 185). This can occur at high plateaux and ridges, if the Quaternary icesheets remained cold-based there most of the time, preserving a relict landscape. In Sweden, the paleic surface appears almost everywhere, and the glacial impact is pronounced only along major valley floors (Stuevold and Eldholm, 1996). Rudberg (1997) produced somewhat subjective maps of his assumed pre-Quaternary paleic surfaces. These show in the Norwegian county of Nordland and near Trondheim that the only ‘paleic’ surfaces that might survive in the Scandinavian Caledonides are commonly located in the higher and eastern parts, mainly east of the Uppermost Allochthon and near the international border (Figure 1).

For any cave passage formed before the Quaternary to survive, it formed farther from its contemporary surface than the amount of subsequent erosion. This includes any passages originally longer than the amount of horizontal retreat, for caves emerging at cliffs and steep valley sides. Any caves below an uneroded paleic surface would therefore be candidates for being formed before the Quaternary. However, the literature cited by Goodfellow *et al.* (2008) shows that all the studied relict Scandinavian landscapes lie east of the Caledonide marble outcrops. Additionally, Steer *et al.* (2012) concluded that there was a Plio-Pleistocene glacial origin for the high-elevation low-relief surfaces in western Scandinavia, from estimates of off-shore sediments that cannot be derived just from the erosion of the glacial valleys and fjords. This places doubt on the concept of the ‘paleic surface’ in Norway and the border area, as supported by the general absence of heavily weathered summits, rock pinnacles and autochthonous blockfields (Sollid and Sørbel, 1979) and by the presence of glacially smoothed bedrock in many Norwegian karst cave areas. This evidence suggests that the Scandinavian Caledonides have been covered by thick fast-flowing erosive warm-based icesheets. Thus, there is probably no effective paleic surface for any marble outcrops there, and cave ages can be considered from other principles.

5. Survival of the Scandinavian Caledonide karst caves

The speleogenesis of the caves formed in the central Scandinavian Caledonide marble outcrops is discussed in a companion paper by Faulkner and White (2017). The caves commonly developed top-down and middle-outwards (TDMO: Faulkner, 2008), with lower interglacial hydraulic pathways commonly formed after each glaciation. They were involved in a race to develop along deeper fractures during each deglaciation and interglacial, before being removed by subsequent glaciations and by interglacial weathering, which operate top-down and extremities-inwards (Faulkner, 2010). Some palaeocaves possibly developed prior to the Quaternary glaciations, which then removed them. Caves therefore share some features of life-forms: they are born, grow and then die.

To consider the effects of erosional removal, Faulkner (2007; 2010) defined a subsurface cave distance (SSCD) as the orthogonal distance from the surface to the centre of a cave passage. In central Scandinavia, the SSCD is always less than one eighth of the depth of the local glacial valley and / or fjord base below adjacent summits. This provides a probable constraint on the opening of tectonic inception fractures during

deglacial isostasy and implies that there were few deep 'open' fractures there before the Quaternary glaciations. Exceptionally, Ytterlihullet has a depth of 180 m and an SSCD of 93 m, eight other caves in central Scandinavia have an SSCD of c. 50 m and the rest remain even closer to the surface. From a typical erosion rate of 40 m per glacial cycle, this strongly suggests that all existing passages would be removed by only a few more Quaternary glaciations and that most developed during and following the final, Weichselian, deglaciation. Only c. 25 'multi-cycle' caves were identified. Faulkner (2013a) proposed a methodology to relate passage ages to glacial cycles. He concluded that the oldest surviving passages in this area are in Toerfjellhola, which formed at the Elsterian deglaciation at the end of MIS12, at c. 427 ka BP.

There are several Caledonide marble caves in southern Scandinavia with lengths >100 m. Because they tend to have single tier morphology, with active vadose streams and an SSCD commonly <10 m, they are likely to have developed during the Weichselian deglaciation and the Holocene. However, the survey section of Øvre Elvegrotta in Bøverdalen (Figure 1; SSCD = 30 m: Lauritzen, 1980, Fig. 2) suggests four phases of development, with progressive upstream captures of its powerful stream. These might have all occurred during and following the Weichselian deglaciation, but without further study, it is at least possible that they partly represent the remaining passages below a palaeo cave system that has since been eroded away. In that case, the upper passages could have survived several glacial cycles. There are also several shorter caves in the area near Oslo. They have formed in a low angle karst in the Lower Allochthon that abuts a large granitic pluton, which caused further alteration of the marble by contact metamorphism (Ramberg *et al.*, 2008). Commonly phreatic in morphology and close to the surface, these caves are unlikely to survive another glaciation and probably formed during Weichselian deglaciation.

6. Northern Scandinavia

Uniquely among all the other Caledonide terranes, there are many longer, deeper, larger, more complex and therefore probably older, multi-cycle caves in northern Norway, supported by speleothem ages up to 600 ka BP (Lauritzen, 1991). Reduced high-altitude glacial erosion, away from the central 'saddle' area that focussed E-W ice streaming in central Scandinavia, possibly allowed older high-level passages to survive longer there. At least seven of the caves have SSCD/Relief ratios >0.125 (Table 1). Faulkner (2008) suggested that these deeper systems might exploit deeper and older, possibly open, inception fractures caused by long-range plate tectonics associated with the widening of the Atlantic Ocean, which could date back to the Mesozoic. Fractures in some low metamorphic grade, low-angle, karst outcrops might also act like inception horizons and reach greater depths.

In northern Norway the SSCD varies up to 400 m, much greater than in any other Caledonide area. However, four factors need to be considered. Firstly, for deep cave passages to enlarge by dissolution, active hydraulic pathways need to exist within the marble outcrop. These would probably rely on the creation of deep valleys or fjords by glaciation. Secondly, at a bedrock removal rate up to 40 m per glacial cycle, the lowest (active) level in the Scandinavian cave with the largest SSCD, Tjoarvekrajgge, could be removed by another ten glaciations, making it unlikely that its older higher levels or those in most other caves existed before the MPR. Thirdly, studies of the sectional surveys of these caves rarely indicate as many as ten levels of cave development. Indeed, Tjoarvekrajgge appears to have four levels (Finnesand *et al.*, 2007). Fourthly is the relatively small size of most cave passages, which limits the time of phreatic dissolution. One of the oldest of all the non-arctic Caledonide marble caves might be Rågge Javre Raige, which complies with the TDMO model and just complies with the one-eighth relationship. From its section survey (Lauritzen *et al.*, 1991), it has about ten development levels, so that its remaining upper passages may have survived for ~1 Ma as the

Table 1. Some deeper caves in Northern Scandinavia

Cave	Vertical Range m	SSCD ^a m	Local Relief m	Ratio SSCD/Relief	Notes and References
Plurdal Cave System	131	131	600	0.2	In valley floor, to base of Steinugleflåget sump. Davidsen <i>et al.</i> (2014).
Greftkjelen / Greftsprekka System	315	200	500	0.4	8 levels, with high-level relict vadose passages in complexly folded karst. Holbye (1983).
Svarthammarhola	157	c. 80	600	0.13	Relief to fjord base. Passage size: Max width = 60m. Max height above boulders = 25m. Westlund (2008).
Okshola / Kristihola	260	c. 200	500	0.4	Streamway beneath a hill. Palaeo spring 120m above rising. Heap (1970). Skoglund and Lauritzen (2010).
Reinvikgrotta	250	160	600	0.25	In Bonådal. Relief to base of Leirfjord. Husdal and Olsen (2014).
Tjoarvekrajgge	497	400	c. 1000	0.4	In dipping marble in Bonådal. 4 levels. Relief to base of Leirfjord. Finnesand <i>et al.</i> (2007).
Rågge Javre Raige	580	177	1460	0.12	About 10 levels. Relief to base of Hellemo fjord. Lauritzen <i>et al.</i> (1991).
Vaderieppigrottan	150	120	800	0.15	On Norwegian side of Vadvedalen. Forsberg (2014).

^aSSCD: SubSurface Cave Distance. Some figures are estimates. These caves are all in Norway.

adjacent fjord deepened and widened. Greftkjelen, which is formed in complexly folded karst, has an SSCD of 200 m and does not follow the TDMO model, having large high-level vadose passages. It appears to have eight levels (Holbye, 1983), but its oldest stalagmite date is only c. 190 ka BP (Holbye and Lauritzen, 1983).

The above analysis may be compared with previous judgements about the geological timescales for individual cave developments, mainly in northern Scandinavia, where many relict phreatic caves 'hang' high on valley sides. The earlier suggested timescales included all possibilities of postglacial, proglacial, subglacial, late-glacial, interglacial and preglacial speleogenesis. These ideas were proposed when only four major Pleistocene glaciations were known, dating from about a million years ago. It is considered here that subglacial enlargement by dissolution was unlikely near glacial maxima, when the Scandinavian ice sheet extended over 100 km from the present coast. Any warm-based subglacial water flow over the marble would commonly have been slow and therefore nearly saturated with calcite and non-aggressive in glacial timescales. Any faster flow along subglacial waterways would be restricted to valley bottoms, would not affect higher caves, and is regarded here as a deglacial process.

Haugane and Grønlie (1988) postulated a Miocene age for the relict phreatic Hammernesgrotta, based on Tertiary uplift and the time to erode the early valley down to the cave level. However, their dismissal of a high limestone dissolution rate in fast-flowing meltwater (e.g. Faulkner, 2013b) ignored contemporary knowledge of dissolution kinetics. Lauritzen (1990) concluded that the 4 m-diameter passages formed in a short interval between 1.1 and 0.32 million years ago, using a faster dissolution rate. Nevertheless, these passages could have formed in 2000 years at a wall-retreat rate of 1 mm per annum during the later deglaciations of the Quaternary.

Lauritzen (1990) also considered other possible pre-Quaternary cave ages. Based on his model, he concluded that Stordalsgrotta and Salthölene could be older than 1.6 Ma, despite their diameters being only 5 m and 3 m, and that the large through-cave Solvikhulen and the huge Svarthammarhola, which are only 2.3 km apart, could be older than 2.57 Ma. Solvikhulen lies at 150 m a.s.l. This is similar to the deglacial marine limit (DML) in this area, from a Younger Dryas uplift map (Sorensen *et al.*, 1987). The cave tapers horizontally from an entrance width of 50 m and vertically from an entrance height of 30 m (Olsen and Danilova, 2015). This morphology is common for caves formed or modified by the sea (Faulkner, 2005b), and thus Solvikhulen, although now 50 km inland from the main coastline, has likely been enlarged by marine action. Svarthammarhola has large entrances at c. 205 m and c. 250 m a.s.l., and increases in size internally to 60 m wide by 25 m high, above large boulders (Westlund, 2008). Its oldest dated speleothem is of late MIS7 age (Lauritzen *et al.*, 2005). Svarthammarhola would have been above the sea during Weichselian deglaciation, it does not have a tapering morphology, and it contains phreatic tubes and vadose entrenchments. However, both it and Solvikhulen were possibly and probably below sea level during earlier deglaciations and during the onsets of the later glaciations and during some Weichselian interstadials, as discussed generally by Faulkner (2005b) and below. Thus, both caves were probably enlarged

by various marine processes when greatly depressed isostatically (as Faulkner, 2005b, suggested for the entrance to the nearby Okshola / Kristihola system). They appear to have rather small SSCDs, and might not survive another glaciation. Thus, rather than being candidates for pre-Quaternary genesis, they probably formed over the last few glacial cycles.

Isacsson (1999) proposed that Korallgrottan in central Sweden was primarily formed by flows from a much larger Pre-Quaternary catchment area. However, Faulkner (2011) deduced that it was inundated beneath a deglacial ice-dammed lake for over 900 years in the early Holocene. This would have enlarged its existing passages, which could themselves have been initiated during earlier deglaciations. Because its SSCD is only c. 50 m, this cave has probably survived for only a few glacial cycles. Skoglund and Lauritzen (2010) estimated that high-level relict vadose passages in the complex upper maze in Okshola / Kristihola (which has a large SSCD of 200 m) fed a palaeo spring that is 120 m above the present resurgence and deduced an origination prior to the MPR. Their argument is based on the negligible present catchment area and an assumed much later capture downstream after enhanced glacial incision following the MPR. However, that incision could have occurred in three glacial cycles.

7. Caves in the Baltic Shield and sedimentary limestones

There are c. 30 reported small caves formed in basement marbles in Sweden, with lengths ≤ 230 m and depths ≤ 8 m. They all lie beneath the less-eroded paleic surface, but because they commonly carry at least a seasonally-active stream at shallow depth, it is likely that most developed in the Holocene. Several caves in southern Sweden have formed in sedimentary porous Cretaceous limestones. Two have lengths ≥ 200 m, with depths of 4 m and 12 m, and a maze-like relict morphology, perhaps suggestive of a hypogenic origin. Glacial erosion might have been small here: the age of these caves is unknown. Lummelundagrottan, on the Baltic island of Gotland (Figure 1), has a phreatic morphology, with diameters up to 5 m and several sumps c. 20 m below the surface of an extensive outcrop of indurated sedimentary Silurian limestone. Gotland lay beneath a large icestream flowing south during glacial maxima, and thus experienced significant glacial erosion and large earthquakes during isostatic rebound (Mörner, 2003). During deglaciation, the area was flooded by the Baltic Ice Lake, the brackish Yoldia Sea, and the freshwater Ancylus Lake, all of whose aggressive waters could have enlarged inception fractures into phreatic passages. Hence, Lummelundagrottan probably formed from the early Holocene. Basset (1985, pp. 287 and 289) and Lauritzen (1988) discussed evidence of palaeokarst in surviving sedimentary limestones in northern and southern Norway that might date back to the Silurian or earlier periods.

8. Tectonic caves

There are >2000 tectonic fracture and talus caves in Sweden and many in Norway, where Ljøtehølet has a depth of 55m (Schroeder, 1980). The longest tectonic cave is Bodagrottorna in Sweden, which comprises a field of large talus blocks above fractures that reach a depth of 11 m (Mörner, 2003). The cave formed by the 'blowing up' of a hill top roche moutonnée by a

large deglacial earthquake c. 9700 years BP. It is surmised that most tectonic caves in Scandinavia were formed by seismic or aseismic movements during deglacial uplift (Faulkner, 2006). Because of the weakened nature of the bedrock, it is likely that traces of such caves would be bulldozed away by another glaciation, even under cold-based ice, so that the present tectonic caves probably all formed in the early Holocene.

9. Sea caves

Sjöberg (1988) discussed 33 of the large Norwegian littoral caves that were formed by wave-abrasion. They face the Atlantic Ocean, in steep cliffs above the wide strandflat. The largest is Halvikshulen, which has an entrance that is 250 m wide and 80 m high and extends to a length of 340 m. In common with many of these caves, it is well above present sea level, with a level floor at 117 m a.s.l. The through cave Torghatten has western and eastern entrance floors at 109 m and 138 m a.s.l. and a length of 160 m (Møller and Fredriksen, 2008). The oldest deposits in Skjonghelleren, with a floor at 30–45 m a.s.l., were dated to 80 ± 9 ka BP (Larsen and Mangerud, 1989). Many of these caves lie above the DML, and therefore predate the Holocene, and some formed in marble with marine-enlarged entrances into pre-existing passages. The extremely tall entrances of the larger high-level caves provide evidence of formation by upward stoping during one or more glacial onsets or interstadials, when a rapid build up of ice caused isostatic depression and a rising local sea level (Faulkner, 2005b). The width of the strandflat below the longest sea caves is ≥ 25 km. If it formed primarily during the Quaternary, the rate of retreat of the sea cliffs was ≥ 1000 m/100 ka. A length of 1000 m far exceeds the length of any sea cave, suggesting development within the Weichselian. However, these caves would have previously been longer, before being shortened by later glaciation. There are also many elevated 'tunnel caves' formed along tectonic fissures up to 200 m a.s.l. by the previous rolling of stones by wave action at the 'High Coast' of Sweden (Sjöberg, 1981). Glacial isostatic depression was very high here, and Sjöberg (1981) related the age of each cave to its altitude during Holocene uplift and the existences of the Ancylus Lake and the early Baltic Sea.

10. Conclusions

Many cave passages, especially deeper ones in northern Scandinavia that might have formed along Atlantic ridge-push tectonic fractures, have certainly survived several glacial cycles following their formation. A few of these might have survived ten glacial cycles, with ages up to about one million years, i.e. from the time of the Mid-Pleistocene Revolution. These likely represent the oldest existing cave passages in Scandinavia, apart from the possibility of hypogenic systems surviving in exposed sedimentary limestones, which could be of any age following diagenesis. Consequently, the continuing existence of Tertiary passages in unexplored caves that predate the formation of their local glacial valleys would be exceptional. The great majority of the caves in central and southern Scandinavia probably originated during Weichselian deglaciation, with some active, mainly vadose, passages plus all the mainly-vadose caves, being entrenched only during the Holocene. The huge sea caves along the Norwegian coast are too short to have survived a complete glaciation, and were probably formed during high sea levels early in the Weich-

selian or during its interstadials. All the tectonic fracture and talus caves likely formed during rapid uplift near the start of the Holocene. Because fractures and caves themselves reduce the resistance of bedrock or talus to glacial erosion, there is a tendency for shallow caves, in any lithology, to be removed by the glaciation that follows their formation. Thus, the sites of many present caves may indicate the sites of 'palaeocaves in the sky' that previously existed above and / or beyond them, and to some of which they might have previously connected.

References

- Basset MG, 1985. Silurian stratigraphy and facies development in Scandinavia, in: Gee DG, Sturt BA (Eds). *The Caledonide Orogen – Scandinavia and Related Areas*. John Wiley, 283–292.
- Clark PU, Alley RB, Pollard D, 1999. Northern hemisphere ice-sheet influences on global climate change. *Science*, **286**, 1104–1111.
- Dauidsen K, Finnesand T, Grundstrøm S, 2014. Uthenting av de to omkunnede grottedykkerne fra Steinugleflåget i Plurdaalen. *Norsk Grotteblad*, **62**, 29–41.
- Dowdeswell JA, Ottesen D, Rise L, 2010. Rate of sediment delivery from the Fennoscandian Ice Sheet through an ice age. *Geology*, **38**(1), 3–6.
- Faulkner TL, 2005a. *Cave inception and development in Caledonide metacarbonate rocks*. PhD Thesis. University of Huddersfield.
- Faulkner T, 2005b. Modification of cave entrances in Norway by marine action. *Proceedings of the fourteenth International Speleological Congress*, Athens. Paper O-69, 259–263.
- Faulkner T, 2006. Tectonic inception in Caledonide marbles. *Acta Carsologica*, **35**(1), 7–21.
- Faulkner T, 2007. The one-eighth relationship that constrains deglacial seismicity and cave development in Caledonide marbles. *Acta Carsologica*, **36**(2), 195–202.
- Faulkner T, 2008. The top-down, middle-outwards model of cave development in Caledonide marbles. *Cave and Karst Science*, **34**(1), 3–16.
- Faulkner T, 2010. An external model of speleogenesis during Quaternary glacial cycles in the marbles of central Scandinavia. *Cave and Karst Science*, **37**(3), 79–92.
- Faulkner T, 2011. Ice-dammed lakes in the central Swedish Mountains. *Grottan*, **46**(1), 16–25.
- Faulkner T, 2013a. A methodology to estimate the age of caves in northern latitudes, using Toerfjellhola in Norway as an example. *Sixteenth International Speleological Congress Proceedings*, **3**, 342–348.
- Faulkner T, 2013b. Speleogenesis and scallop formation and demise under hydraulic control and other recharge regimes. *Cave and Karst Science*, **40**(3), 113–132.
- Faulkner T, White S, 2017. Cave development in two highly-contrasting epigenic limestone lithologies. This volume.

- Finnesand T and 5 authors, 2007. Tjoarvekrajgge 1993–2007. *Norsk Grotteblad*, **49**, 28–68.
- Forsberg A, 2014. Vadveriehppidalen: Vadvevaggens siste grottejomfruelige utpost (eller?). *Norsk Grotteblad*, **62**, 17–23.
- Goodfellow BW, Stroeven AP, Hättestrand C, Kleman J, Jansson KN, 2008. Deciphering a non-glacial glacial landscape mosaic in the northern Swedish mountains. *Geomorphology*, **93**, 213–232.
- Haugane E, Grønlie A, 1988. Tertiary Caves in Nordland, Norway. *Cave Science*, **15**(3), 93–97.
- Heap D, 1970. Report of the British speleological expedition to Arctic Norway, 1969. *Kendal Caving Club Journal*, **5**, Section 2, 39pp.
- Holbye U, 1983. Grottenes utvikling, Greftmarmoren and Stamlederfaser i grottene ved Greftvatnet. *Norsk Grotteblad*, **11**, 14–34.
- Holbye U, Lauritzen S-E, 1983. Stalagmittdateringer fra Greftkjelen. *Norsk Grotteblad*, **11**, 34–35.
- Husdal T, Olsen JH, 2014. Reinvikgrotta. *Norsk Grotteblad*, **63**, 8–15.
- Isacsson G, 1999. Korallgrottan - ett nyckelhål till historien. *Jämtlands Grottförening Årsskrift*, 1999, **9–11**, 18.
- Larsen E, Mangerud J, 1989. Marine caves: on-off signals for glaciations. *Quaternary International*, **3/4**, 13–19.
- Lauritzen S-E, 1980. Speleologisk arbeid i Syd-Norge 1973–1980. *Norsk Grotteblad*, **2**(6), 22–26.
- Lauritzen S-E, 1988. Paleokarst in Norway. *Cave Science*, **15**(3), 129–131.
- Lauritzen S-E, 1990. Tertiary Caves in Norway: a Matter of Relief and Size. *Cave Science*, **17**(1), 31–37.
- Lauritzen S-E, 1991. Uranium series dating of speleothems. A glacial chronology for Nordland, Norway for the last 600 Ka. *Striae*, **34**, 127–132.
- Lauritzen S-E, Kyselak J, Løvlie R, 1991. A new survey of Råggejavri-Raigi and the Hellemofjord karst, Norway. *Cave Science*, **18**(3), 131–137.
- Lauritzen S-E and 4 authors, 2005. The Svarthamar cave research project, Fauske, north Norway. *Proceedings of the 14th International Congress of Speleology, Athens*, Volume 2, Paper P12, 4pp.
- Møller JJ, Fredriksen PT, 2008. Hullet gjennom Torghatten. *Norsk Grotteblad*, **51**, 26–28.
- Mörner N-A, 2003. *Paleoseismicity in Sweden: a novel paradigm*, 320 pp.
- Olsen HO, Danilova L, 2015. Storhellarhola. *Norsk Grotteblad*, **64**, 4–5.
- Peulvast J-P, 1985. Post-orogenic morphotectonic evolution of the Scandinavian Caledonides during the Mesozoic and Cenozoic, in Gee DG, Sturt BA (Eds.). *The Caledonide Orogen – Scandinavia and Related Areas*, John Wiley, 979–998.
- Ramberg IB, Bryhni I, Nøttvedt A, Rangnes K, 2008. *The Making of a Land: Geology of Norway*. Norsk Geologisk Forening, 624 pp.
- Riis F, 1992. Dating and measurement of erosion, uplift, and subsidence in Norway and the Norwegian shelf in Glacial Periods. *Norsk Geologisk Tidsskrift*, **72**(3), 325–331.
- Riis F, 1996. Quantification of Cenozoic vertical movements of Scandinavia by correlation of morphological surfaces with offshore data. *Global and Planetary Change*, **12**(1–4), 331–357.
- Rudberg S, 1997. Glacial and interglacial erosion in Scandinavian mountains in a W–E comparison including an approach to a quantitative calculation. *Zeitschrift für Geomorphologie*, **41**(2), 183–204.
- Schroeder I, 1980. Tektoniske Grotter. *Norsk Grotteblad*, **2**(6), 7–9.
- Sjöberg R, 1981. Tunnel Caves in Swedish Archean Rocks. *Cave Science*, **8**(3), 159–167.
- Sjöberg R, 1988. Coastal Caves Indicating Preglacial Morphology in Norway. *Cave Science*, **15**(3), 99–103.
- Skoglund RØ, Lauritzen S-E, 2010. Morphology and speleogenesis of Okshola, Fauske, northern Norway: example of a multi-stage network cave in a glacial landscape. *Norsk Geologisk Tidsskrift*, **90**, 123–139.
- Sollid JL, Sørbel L, 1979. Deglaciation of western central Norway. *Boreas*, **8**, 233–239.
- St.Pierre S, St.Pierre D, 1980. Caves of Velfjord, south Nordland, Norway, with particular reference to Sirijordgrotten. *Transactions of the British Cave Research Association*, **7**(2), 70–82.
- Steer P, Huisman RS, Valla PG, Gac S, Herman F, 2012. Bimodal Plio-Quaternary glacial erosion of fjords and low-relief surfaces in Scandinavia. *Nature Geoscience*, **5**, 635–639.
- Stuevold LM, Eldholm L, 1996. Cenozoic uplift of Fennoscandia inferred from a study of the mid-Norwegian margin. *Global and Planetary Change*, **12**(1–4), 359–386.
- Sørensen R, Bakkelid S, Torp B, 1987. *Land Uplift, 1:5000000 Nasjonalatlas for Norge*, Statens kartverk.
- Westlund A, 2008. Svarthammarhola. *Norsk Grotteblad*, **50**, 46–47.

(Abstract) **Speleogenesis In Two Highly Contrasting Epigenic Limestone Lithologies**

Trevor Faulkner¹ And Susan White²

Affiliation: ¹ Limestone Research Group, GEES, University of Birmingham. Edgbaston, Birmingham, B15 2TT, UK.

Email: trevor@marblecaves.org.uk

² Environmental Geoscience, Latrobe University, Bundoora, Victoria, Australia.

Email: s.white@latrobe.edu.au

Abstract

The characteristics of caves in two highly-contrasting epigenic karst environments are described and compared. These are the dendritic caves formed in Cambro–Silurian marbles of the Helgeland Nappe Complex in north central Norway that have negligible primary porosity but which have been subjected to many Quaternary glacial processes, and the caves formed in the porous dune eogenetic limestones of the western Otway Basin, southeastern Australia, of predominantly mid- Pleistocene age. Following inception, caves in both environments followed the principles established by the Palmer-Dreybrodt model of the physics and chemistry of calcite dissolution. The marble caves formed quickly in fast-flowing aggressive water under fast first-order dissolution kinetics and mechanical erosion. The caves in dune limestones formed **relatively** quickly, but in slow-moving saturated waters, where slow high-order kinetics would be expected along a single conduit. Mixing corrosion was probably important, driving dissolution into first-order kinetics earlier than otherwise, explaining the young ages. This suggests that there is a need to quantify dissolution rates and speleogenetic timescales applicable to various conditions of mixing corrosion in flank-margin conditions, building on previous modelling work.

1. Introduction

Caves form by dissolution in nearly all limestone lithologies. It is interesting therefore to compare the types of caves formed in two epigenic karst environments, with no evidence of hypogene speleogenesis (Klimchouk, 2007), which may be regarded as rather extreme examples from several different viewpoints. The telogenetic metalimestones of the Helgeland Nappe Complex (HNC) in the Uppermost Allochthon of north central Norway at c. 65°N were metamorphosed to a high grade, amphibolite marble, facies during the Cambro–Silurian Caledonian Orogeny. The negligible primary porosity of the marble likely restricted karstic speleogenesis until the Quaternary glacial cycles produced significant tectonic inception fractures. These could be enlarged by aggressive dissolution at high flow rates during deglaciation and subsequent interglacials, to create 626 explored caves with a total passage length of 47km. The syngenetic karst of the western Otway Basin in southeastern Australia at 34°S is formed in eogenetic strandline dune deposits of predominantly mid-Pleistocene age, with high porosity and high permeability. Some hundreds of caves, many of them short but with others of over 3 km in total passage length, have formed there in slow-moving, nearly saturated, water, probably as a result of increased aggressivity arising from either meteoric infiltration, causing mixing corrosion or along the halocline on a flank margin setting. These two contrasting environments have guided the distinctive morphologies and the comparable timescales for speleogenesis by calcite dissolution of caves that at least share a common epigenic heritage.

Carbonate hostrock weathering by sea salt precipitation in El Orón-Arco Cave (Cartagena, SE Spain)

Fernando Gázquez¹, José-María Calaforra², Fernando Rull³, Jesús Medina³, Andrés Ros⁴, José Luis Llamusí⁴ and Juan Sánchez⁴

Affiliation: ¹Department of Earth Sciences, University of Cambridge, Downing Street, Cambridge, CB2 3EQ, United Kingdom. f.gazquez@ual.es

²Departamento de Biología y Geología y CAES Cambio Global, Universidad de Almería, Carretera de Sacramento s.n, La Cañada de San Urbano, Almería, 04120, España. jmcalaforra@ual.es

³Departamento de Física de la Materia Condensada, Cristalografía y Mineralogía. Universidad de Valladolid. Paseo de Belén, 7, 47011, Valladolid, España

⁴Centro de Estudios Ambientales y del Mar. CENM-naturaleza, Alcántara, 5, Cartagena, Murcia, 30394, España. cenm@cenm.es

Abstract

El Orón Cave, also known as Arco Cave (Cabo Tiñoso, Cartagena), was discovered in 1980 and has been explored by speleologists over the past decade. This cavity has turned into a tourist attraction for the Murcia Region (SE, Spain) because of its striking speleothems and unique morphologies, which considerably differ from other cavities in this region. The main cave passages run along a fracture parallel to the shoreline and are developed in limestones and dolostones of the Alpujarride complex of the Cabo Tiñoso Formation. This fault is closely related to the cave formation and the morphology of the Cabo Tiñoso cliff itself. No clear evidence of phreatic dissolution or signs of subterranean runoff are found in this cave, while two brackish-water lakes at sea-level are the only visible waterbodies at present. The carbonate bedrock shows clear evidence of chemical and mechanical weathering of soluble salts (halite and gypsum) due to seawater seepage and their subsequent precipitation due to evaporation in the cave. This mechanism has produced detachment of rock fragments and mechanical spalling, leading to massive chambers and in-situ accumulations of detrital deposits. The cave also hosts a wide variety of rare speleothems, including monocrystalline gypsum stalactites (chandeliers) with halite apexes and hollow gypsum hemispheres (blisters) associated with carbonate eccentrics. Seawater seepages through the carbonate bedrock and evaporation within the cave created most of these speleothems. Such unique features make El Orón-Arco Cave quite distinctive amongst the caves in Spain.

Keywords: coastal caves, gypsum, halite, speleothems, salt weathering.

1. Introduction

The mechanisms involved in the formation of caves are generally linked to dissolution of carbonate hostrock by waters subsaturated in calcium carbonate (Audra and Palmer, 2015). This karstification process creates voids in the rock and, in subsequent stages, can produce breakdown and collapse of cave ceilings, eventually leading to the formation of large chambers and passages. Regarding coastal caves, the corrosion of the carbonate hostrock is controlled by the mixing of fresh water and seawater that generates solutions subsaturated in calcite and, thus, with a great capability to dissolve limestone (Myroie and Myroie, 2007). Recently, Ginés and Ginés (2007) claimed that the detachment and breakdown of blocks is a remarkable agent for the genesis and evolution of caves in coastal areas.

In addition to coastal caves formed by this mechanism of classic karstification, the genetic processes in others are related to the geomorphological evolution of the shoreline, in many cases the result of erosion that causes landslides and fracturing of the geology (Moore, 1954). The caves that develop in fractures are generally called flank margin caves, and display distinctive features compared to caves formed by dissolution. For example, these cavities normally lack features generated by subterranean water course or phreatic conduits, such as scallops, smoothed surfaces or cupolas. In the current paper, we examine the geomorphology and speleological features of El Orón-Arco Cave in the Cabo Tiñoso (Cartagena, Murcia). This coastal cave shows distinctive geomorphological char-

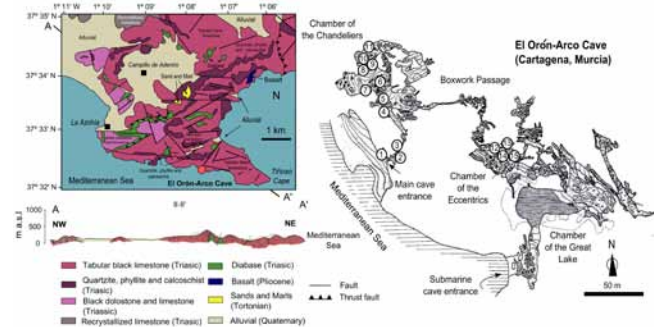


Figure 1. Geological setting of Cabo Tiñoso (after Gordillo et al., 1972) and topography of El Orón-Arco Cave (produced by Llamusí, Inglés and Ros, 1984-1998). Sampling sites are indicated.

acteristics and rare speleothems that lead us to study its mineralogy in detail to be able to shed light on their genetic mechanisms.

2. Geological Setting

El Orón-Arco Cave is located in the southern flank of Cabo Tiñoso (Scabby Cape) in Cartagena, Murcia Region, SE Spain. The part of the cave so far surveyed is the result of the connection of El Arco Cave, surveyed in the 1980s (Llamusí et al., 1990) and El Orón Cave (Puch, 1998). The subterranean network extends over 1500 m and has two entrances. One of them is a submarine access to the Arco Cave, also known as

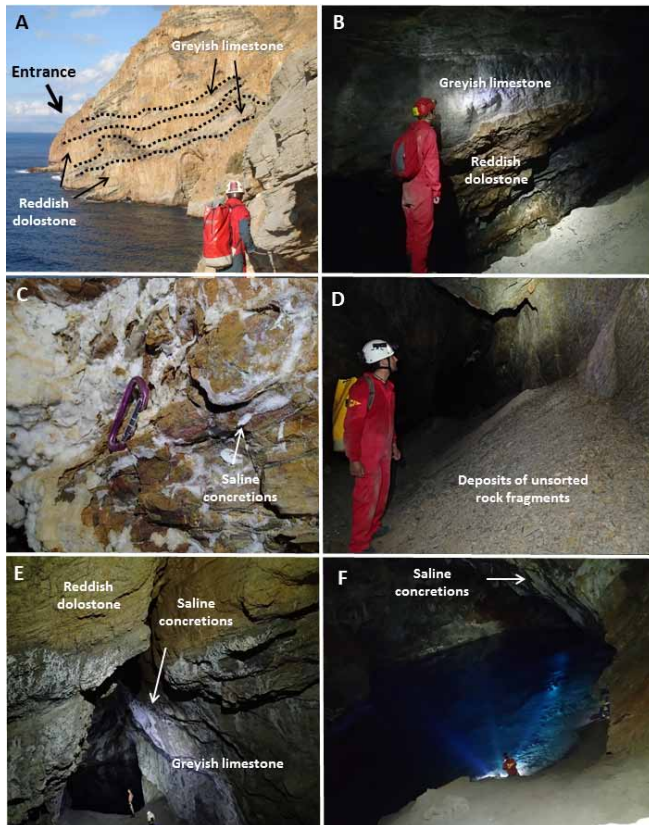


Figure 2. A. Interbedded highly foliated greyish limestones and reddish dolostone in which El Orón-Arco Cave is hosted; B. Contact between the limestones and the dolostone inside the cave; C. Saline concretions on the cave walls; D. Piles of unsorted rock fragments on the cave walls; E. Altered limestone and saline concretions; F. Saline concretions on the walls of the Chamber of the Great Lake.

Cave of the Lake because it hosts a 1200 m² brackish lake. The subaerial entrance is 200 m to the northwest of the submarine access, in the cliff of Cabo Tiñoso, lying at 10 m. a.s.l. (Fig. 1). The cave is developed along a fracture running W to E and parallel to the shoreline, in the slightly metamorphosed Triassic limestone and dolostone of the Alpujarride Formation of Cabo Tiñoso (García-Tortosa *et al.*, 2000). A series of greyish limestones and interbedded reddish dolostones outcrop both in the cave (Fig. 2A) and outside (Fig. 2B).

3. Methods

3.1. Reconnaissance of geomorphological features and sampling of speleothems

We performed a detailed photographic study of the geomorphological and speleothemic features of El Orón-Arco Cave (Figs. 2 and 3). In addition, we collected 15 mineral samples for mineralogical analysis. Saline concretions on the cave walls and appearing in foliation planes of the host rock (Orón-01; Orón-02, Fig. 3A; Orón-03, Fig. 3B; Orón-04, Fig. 3D; Orón-05, Fig. 3C; Orón-06, Fig. 3G) were sampled in different sectors of the cave (see Fig. 1 for sampling site locations). We took samples of the foliated greyish and reddish materials that comprise the cave hostrock (Orón-07 and Orón-08). A sample of yellowish unconsolidated, sandy material (Orón-09) was taken from a fracture following the foliation of the greyish host rock.

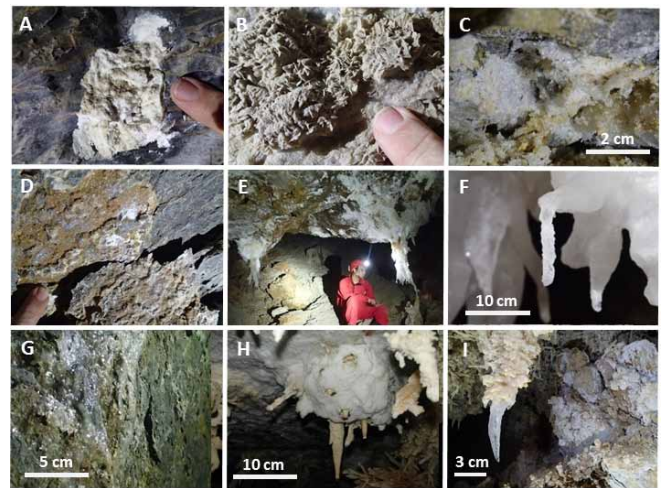


Figure 3. Speleothems in El Orón-Arco Cave: A. Concretions of gypsum on the carbonate hostrock; B. Aggregate of gypsum crystals covered by sandy materials; C. Saline concretions (gypsum + halite) in planes of the hostrock; D. Sugar-textured calcite infillings in planes of the hostrock; E. Gypsum "chandeliers"; F. Details of the apex of a "chandelier"; G. Saline coating on the cave walls; H. Hollow gypsum hemispheres ("blisters") perforated by carbonate eccentrics; I. Gypsum single crystals hanging from the tip of a carbonate dripstone.

In the Chamber of the Chandeliers, a sample of the whitish microcrystalline crust that occurs all over the ceiling in this location was collected (Orón-10; Fig. 3E). Another sample comprised fragments of a c. 1 m long transparent crystal that hung from the cave ceiling, reassembling a "chandelier" (Orón-11; Fig. 3E). In places, the apex of these crystals show a c. 10 cm long and 1 cm wide hollow cylinder, resembling a soda straw, made of a transparent microcrystalline mineral (Orón-12; Fig. 3F). In the Chamber of the Eccentrics, we took a fragment of a hollow hemisphere c. 10 cm in diameter from the cave ceiling (Orón-13; Fig. 3I), which was perforated by carbonate speleothems (Orón-14; Fig. 3I). Lastly, a transparent single crystal detached from the tip of a stalactite, similar to that in Fig. 3J, was collected (Orón-15).

4. Results And Discussion

Evidence for carbonate host-rock weathering by sea salts precipitation

El Orón-Arco Cave shows no signs of dissolution processes – either phreatic or vadose – that could support an origin linked to conventional karstification mechanisms. Indeed, the cave lacks both the typical morphologies related to water flow and any signs of subaqueous carbonate dissolution, including scallops, smoothed surfaces or cupolas. In contrast, the cavity displays clear evidence for chemical/mechanical weathering processes, which are behind the formation of its passages and chambers.

The most striking vestiges of such mechanisms are probably the deposits of unsorted carbonate hostrock fragments (<1 mm to tens of centimetres), which rest against the walls of the passages into the Chamber of the Chandeliers and in the entrance of the Boxwork Passage (Fig. 2D). The appearance of these passages reassembles that of a mine gallery riddled with mine debris; however, this cave has not been subject to mining activity and all its geomorphological features are orig-

inal. The cave walls and ceilings are made of easily detachable rock that crack and eventually fall naturally to the cave floor and accumulate as piles of unsorted detritus. This mechanism is currently active and was observed during our visits to the cave. Indeed, the accumulation of rock debris in the smaller passages (e.g. the access to the Boxwork Passage) represents a serious challenge to accessing the cave: these galleries are prone to obstruction and frequently need to be unblocked by speleologists.

The cave host rock is made of greyish limestone and reddish dolostone, the latter containing small amounts of iron oxides (Table 1). In the planes of the carbonate beds, whitish and yellowish saline concretions and efflorescences are observed projecting out into the cave (Figs. 2 and 3). The mineralogical analyses (XRD and Raman spectroscopy) of these materials reveal the presence of minerals typically derived from evaporated seawater, including halite, gypsum and occasionally calcite (Table 1). We suggest that capillary uplift and infiltration of seawater through the carbonate formation of Cabo Tiñoso, and subsequent evaporation of the solution in the cave produces the crystallization of evaporites in planes and pores of the host rock.

The crystallization pressure of salts causes fracturing and disaggregation of the original carbonate materials. Besides, the motion of the faults in the Cabo Tiñoso may have favoured the enlargement of the cave voids and the ejection of the disaggregated materials. To the best of our knowledge, this mechanism has not been described in other caves to date; however, similar processes of capillary uplift of saline waters and crystallization of salts are broadly known to be responsible for the decay of building materials and limestone sculptures (e.g. Gázquez et al., 2015)

4.1. Genesis of singular gypsum/halite speleothems

Infiltration and capillary uplift of seawater and subsequent evaporation in the cave is also responsible for the formation of singular speleothems in El Orón-Arco Cave. Evaporation of infiltrated seawater is favoured by the relatively high air

temperature in the cave (c. 19°C during our visit) and likely low relative humidity (not measured). The crystallization of halite in the form of crusts and soda-straws strongly suggest the presence of relatively dry conditions, so halite dissolves in an atmosphere where relative humidity is above ~75% (Wexler and Hasegawa, 1954). In some of these speleothem formations – for example in the gypsum chandeliers of the Chamber of the chandeliers – a typical mineral series of seawater evaporation can be observed, starting with microcrystalline gypsum and selenite gypsum (Fig. 3E), and finishing with halite in the form of a soda-straw in the tip of the selenite crystals (Fig. 3F). These gypsum chandeliers are similar to those described in Lechuguilla Cave, New Mexico, EEUU (Davis, 2000); however, in El Orón-Arco the origin of SO_4^{2-} and Ca^{2+} is likely seawater.

El Orón-Arco Cave also hosts gypsum “blisters” speleothems on the ceiling of the Chamber of the Eccentrics. These speleothems comprise hollow gypsum hemispheres that, in places, are perforated by aragonite stalactites and eccentrics (Fig. 3H). Similar blister speleothems have been described in Cupp-Coutunn Cave (Turkmenistan), where their formation seems to be related to oxidation of pyrite (FeS_2). Again, in El Orón-Arco Cave the infiltration and evaporation of seawater is proposed as the main source of SO_4^{2-} and Ca^{2+} for the crystallization of gypsum. How these speleothems form is not yet clear, and their genetic mechanism will be the subject of future investigation.

5. Conclusions

The formation mechanisms of El Orón-Arco Cave have been linked to the motion of a fault that runs parallel to the cliff of the Cabo Tiñoso, and to salt weathering of the carbonate host rock by infiltration and capillary uplift of seawater that subsequently evaporates within the cave, leading to precipitation of evaporite minerals (gypsum and halite) in pores and planes of the carbonate. The crystallization pressure of salts produces cracking of the hostrock at different scales. The detached rock fragments accumulate in piles that rest against the cave walls. The same process of seawater infiltration is responsible for the

Table 1. Mineralogy of the speleothems and hostrock of El Orón-Arco Cave.

Sample	Description	Mineralogy
Orón -01	Saline concretions in planes of the host rock	Halite, Gypsum
Orón -02	Whitish coatings on the cave wall	Gypsum
Orón -03	Aggregate of planar crystals	Gypsum
Orón -04	Sugar-textured infillings in planes of the host rock	Halite
Orón -05	Saline concretions in planes of the host rock	Halite, Gypsum
Orón -06	Transparent coatings on the cave wall	Gypsum
Orón -07	Greyish carbonate host rock	Calcite
Orón -08	Reddish carbonate host rock	Dolomite, Goethite
Orón -09	Yellowish sand in planes of the host rock	Halite, Gypsum, Quartz
Orón -10	Microcrystalline coatings on the ceiling over a chandelier	Gypsum
Orón -11	Chandelier	Halite, Gypsum
Orón -12	Transparent “soda-straw” from the tip of a chandelier	Halite
Orón -13	Hollow hemisphere (“blisters”)	Gypsum
Orón -14	Eccentric from inside a gypsum blister	Aragonite
Orón -15	Single crystal from the tip of a carbonate stalactite	Gypsum

precipitation of gypsum and halite in speleothems of uncommon morphology, including gypsum chandeliers, halite soda-straws and gypsum blisters.

Future studies will address the corroboration the proposed model of cave formation using geochemical data. This will include analysis of stable isotopes of gypsum, and investigations of the assembly of secondary minerals and the original carbonate hostrock at microscale. In addition, genetic models for the formation of the gypsum chandeliers and the blisters of El Orón-Arco Cave will be developed.

Acknowledgements

The authors are grateful to all the speleologists that collaborated in the survey in El Orón-Arco Cave. This research was supported by the Federación de Espeleología de la Región de Murcia, RODCLE®, and funds from the Water Resources and Environmental Geology Research Group (University of Almería), the Andalusian Global Change Observaory Center CAESCG)r and the Department of Physics of Condensed Matter at University of Valladolid (Spain).

References

Audra Ph, Palmer A, 2015. Research frontiers in speleogenesis. Dominant processes, hydrogeological conditions and resulting cave patterns. *Acta Carsologica*, **44**(3), 315-348.

Davis DG, 2000. Extraordinary features of Lechuguilla Cave, Guadalupe Mountains. *Journal of Cave and Karst Studies*, **62**, 147-157.

García-Tortosa FJ, López-Garrido A, Sanz de Galdeano C, 2000. Las unidades de Cabo Tiñoso y Peñas Blancas:

Revisión y caracterización estratigráfica de las unidades alpujárrides del sector entre Mazarrón y Cartagena (Murcia, España). *Estudios Geológicos*, **56**, 31-40.

Gázquez F, Rull F, Medina J, Sanz-Arranz A, Sanz C, 2015. Linking groundwater pollution to the decay of 15th-century sculptures in Burgos Cathedral (northern Spain). *Environmental Science and Pollution Research*, **22**, 15677-15689.

Ginés A., Ginés. J, 2007. Eogenetic karst, glacioeustatic cave pools and anchialine environments on Mallorca Island: a discussion of coastal speleogenesis. *International Journal of Speleology*, **36**, 57-67.

Gordillo A, Espinosa J, Martín JM, Pérez A, 1972. *Mapa Geológico Cartagena*. 1:50.000. IGME.

Llamusi JL, Ingles S, Ros A, Rodríguez A, Pérez C, 1990. Cavidades Submarinas del Cabo Tiñoso (Cartagena). *Revista Caliza*, **1**, 24.

Moore D.G, 1954. Origin and development of sea caves. *National Speleological Society Bulletin*, **16**, 71-76.

Mylroie JR, Mylroie JE, 2007. Development of the carbonate island karst model. *Journal of Cave and Karst Studies*, **69**(1), 59-75.

Puch C, 1998. *Grandes Cuevas y simas de España*, Barcelona pg. 781-782.

Wexler A, Hasegawa S, 1954. Relative humidity-temperature relationships of some saturated salt solutions in the temperature range 0 °C to 50 °C. *Journal of Research of the Natural Bureau Standards*, **53**, 19, RP 2512.

Cave Sediments In Škocjanske Jame And Unroofed Caves Above Them, SW Slovenia

Nadja Zupan Hajna¹, Andrej Mihevc¹, Petr Pruner^{2,1}, & Pavel Bosák^{2,1}

Affiliation:

¹Karst Research Institute ZRC SAZU, Titov trg 2, 6230 Postojna, Slovenia

²Institute of Geology AS CR, v. v. i., Rozvojová 269, 165 00 Praha 6, Czech Republic

Abstract

Škocjanske jame (the Škocjan Caves, UNESCO World Heritage and RAMSAR) are situated in the area known as the Divaški kras (Divača Karst), the SE part of Kras Plateau (also known as the Classical Karst). The area is extremely rich in surface karst forms, caves and especially in unroofed caves, which were defined from this area for the first time. Clastic fill of unroofed caves and still existing caves consist mainly of weathering products of Eocene flysch rocks and carbonates eroded from the Reka River catchment area. The biggest caves in the area are Škocjanske jame and Kačna jama where underground flow of Reka River may be found. River sinks into Škocjanske jame and water flows about 250 m below the surface toward Kačna jama, then to Labodnica cave (Abisso di Trebiciano) in Italy and finally to Timavo springs N of Trieste. Fluvial deposits and collapse rocks in caves as Škocjanske jame, Divaška jama and Trhlovca were studied by Gospodarič, who correlated them with Pleistocene climate changes but not older than 400 ka. Fluvial sediments on the karst surface originally linked to surface water flows, predecessor of the Reka River, were lately identified as cave deposits. Fluvial sediments and speleothems from the Škocjanske jame, caves and unroofed caves on the surface were sampled. The mineral composition of all studied sediments both in unroofed caves and caves of the region is very similar. In almost all samples relatively equal mineral composition prevailed, indicating the main source from flysch rocks which were differentially weathered. The samples contained quartz, clay minerals and the minerals microcline, plagioclase, muscovite and heavy minerals (tourmaline, rutile) which are typical of Eocene flysch rocks in the Reka River catchment area. The process of flysch transport into the caves continues for few million years, but the intensity varied over time. Large areas of cave sediments on Divača Karst having their origin in flysch rocks shows that in some period flysch rocks weathered intensively and the sediments were transported to the then existing caves. The erosion of flysch rocks was probably accelerated in the colder climate and due to increased rainfall or/and due to tectonic uplifting of the landscape. Mineralogical, sedimentological and paleomagnetic analysis of clastic sediments from various caves of the Divača Karst confirmed their provenance, depositional style and age. The results indicate that the origin and sedimentation environments in the caves did not change for at least 5 Ma.

Keywords: mineral composition, cave sediments, unroofed caves, Classical Karst, SW Slovenia

1. Introduction

Divaški kras (Divača Karst), SW Slovenia is SE part of Kras carbonate plateau (Fig 1) spread out above Trieste Bay in “Dinaric” direction, NW-SE. The plateau consists of Cretaceous and Tertiary limestones and dolomites and is surrounded by Eocene flysch sediments (Jurkovšek et al. 1996). This flysch represents the last marine sedimentation in the area (Zupan Hajna et al. 2010).

At Škocjanske Jame the river sinks and flows underground for about 35 km to the Timavo springs N of Trieste; on its way it is reached in 8 caves (Fig 2). Smaller tributaries and the Reka flow over Eocene flysch rocks before disappearing underground and they are loaded by weathered remains of them. Quartz pebbles and sands were found on the karst surface and they were in the past associated to fluvial transport of weathered remains of flysch rocks over karst in so-called pre-karstic phase (e.g. Radinja 1986).

The karst morphology of Divaški kras (Fig. 3) is exceptional; on an area of 32 km² there are the sinks of the river Reka, 15 large collapse dolines and hundreds of dolines which represent about 12 % of the area (Mihevc 2001). Numerous caves are known, the biggest among them are Škocjanske jame, Kačna jama, Divaška jama and Trhlovca. On the surface, at elevations 400–450 m a.s.l., there are numerous unroofed caves, proved by allogenic cave sediments and massive flowstone. The first recognized unroofed cave was 350 m long cave near Povir village (Mihevc and Zupan Hajna 1996; Mihevc et al. 1998) which was filled by fluvial sediments and speleothems. The largest, 1.8 km long, is known in Lipove doline

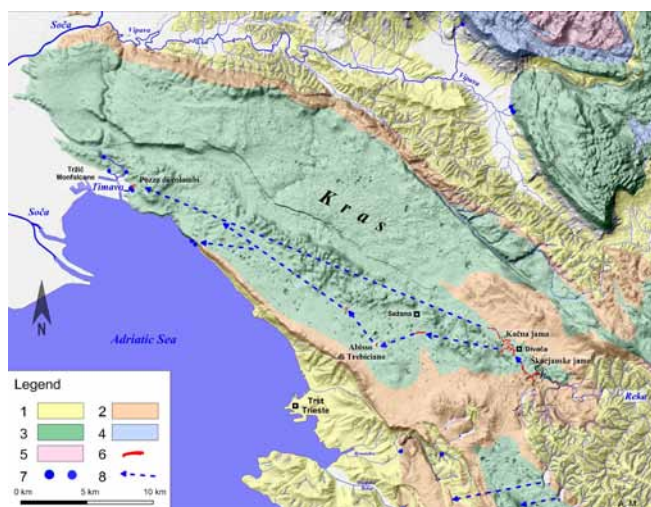


Figure 1. Kras Plateau with geology and underground water flow directions from Reka ponor to the springs. Legend: 1 - Eocene Flysch; 2 - Paleogene limestones; 3 - Cretaceous limestone and dolomite; 4 - Jurassic limestone and dolomite; 5 - Triassic limestone and dolomite; 6 - caves with water flow; 7 - springs; 8 - direction of water flow.

above Škocjanske jame; also long one is present at Radvanj collapse doline and one at Risnik Industrial Zone (Risnik IZ). The actual underground river bed in Škocjanske jame is 230 m below those unroofed caves. Morphological analysis of several unroofed caves on the Divaški kras (Mihevc 2001) and paleomagnetic dating of sedimentary fills (Zupan Hajna et al. 2008, 2010), have indicated cave origin and an age of a few million years.

in one sample relatively high amount of goethite, and traces of plagioclase (Zupan Hajna 1998). The sediments are older than 1.77 Ma, and may be also about 5.23 Ma old (Bosak *et al.* 1998; Zupan Hajna *et al.* 2008, 2010).

Close to the ponor of Reka to Škocjanske Jame at Naklo (slope of Sušica valley), at an elevation of 385 m a.s.l., there were sediments of a completely filled cave. These sediments were mainly flysch sandstone pebbles and sand. The sand consisted of quartz, calcite, muscovite/illite group of minerals, montmorillonite, microcline and traces of plagioclase.

Sediments from unroofed caves (Fig. 3) have very similar mineral composition (Fig. 4). From Lipove doline unroofed cave yellow/brown soil consists of quartz, muscovite/illite group of minerals, plagioclase, chlorite, vermiculite and amphibole. Amphibole does not occur in flysch, but indicates an eolian origin (e.g. from some volcanic eruption, desert sand or even loess). In Risnik IZ sandy clay and sand consisting mainly of quartz, calcite, muscovite/illite group of minerals, kaolinite, chlorite and microcline with traces of plagioclase. In the roofless cave at Povir, very similar sediments were found to other caves in the area. Very similar sediments were found in other caves in the area, but there were present also traces of tourmaline and rutile which indicate a slightly different origin than in the Reka catchment area.

4. Conclusions

Nevertheless only detailed mineralogical and paleomagnetic analysis of unroofed cave fill confirm that their nature, origin and their age is older than was initially expected (for summary see Zupan Hajna *et al.* 2008, 2010 and Knez *et al.* 2016). Studied paleomagnetic properties of the sediments in the caves Divaška jama, Trhlovca and in Divača profile (Bosak *et al.* 1998, 2000; Zupan Hajna *et al.* 2008), gave results that the age of the sediments is most probably up to 5 Ma.

Clastic fills of unroofed caves and still existing caves of Divaški kras consist mainly of weathering products of Eocene flysch rocks eroded from the Reka River catchment. In all cases, relatively equal mineral compositions prevailed, indicating the main source is the flysch sediments which were weathered to different degrees. Mineral composition of Eocene flysch sandstones of Brkini mountain SE of Divača, which is the catchment area of the Reka, varies more in quantity of individual minerals as by the presence of different minerals. On Divaški kras fluvial sediments from unroofed caves are also an important source of superficial soils.

The process of flysch transport into the caves of Divaški kras continues from about 5 Ma ago till now, but the intensity has varied over time.

Acknowledgements

The research was supported by the research Program Karst research No. P6-0119 financed by Slovenian Research Agency and Plan of the Institutional Financing of the Institute of Geology AS CR, v. v. i. No. RVO67985831.

References

- Bosák P, Pruner P, Zupan Hajna N, 1998. Paleomagnetic research of cave sediments in SW Slovenia. *Acta Carsologica*, **28**, 151-179.
- Bosák P, Pruner P, Mihevc A, Zupan Hajna N, 2000. Magnetostratigraphy and unconformities in cave sediments: case study from the Classical Karst, SW Slovenia. *Geologos*, **5**, 13-30.
- Gospodarič R, 1984. Cave sediments and speleogenesis of Škocjan Caves. *Acta Carsologica*, **12**, 27-48.
- Gospodarič R, 1985. On the speleogenesis of Divaška Jama and Trhlovca cave. *Acta Carsologica*, **13**, 5-36.
- Jurkovšek B, Toman M, Ogorelec B, Šribar L, Drobne K, Poljak M, Šribar L, 1996. *Geological map of the southern part of the Trieste – Komen plateau 1-50.000. Cretaceous and Paleogene carbonate rocks*. Inštitut za geologijo, geotehniko in geofiziko, Ljubljana.
- Kranjc A, 1989. Recent fluvial cave sediments, their origin and role in speleogenesis. *Opera 4. razreda*, SAZU, ZRC, Karst Research Institute, Ljubljana.
- Knez M, Slabe T (Eds.), Gabrovšek F, Kogovšek J, Kranjc A, Mihevc A, Mulec J, Otoničar B, Perne M, Petrič M, Pipan T, Prelovšek M, Ravbar N, Šebela S, Zupan Hajna N, Bosák P, Pruner P, Liu H, 2016. *Cave Exploration in Slovenia. Discovering Over 350 New Caves During Motorway Construction on Classical Karst*. Springer International Publishing, Switzerland.
- Mihevc A, 2001. *Speleogeneza Divaškega krasa*. Zbirka ZRC, **27**, Ljubljana.
- Mihevc A, Slabe T, Šebela S, 1998. Denuded caves – an inherited element in the karst morphology; the case from Kras. *Acta Carsologica*, **27**, 167-174.
- Mihevc A, Zupan Hajna N, 1996. Clastic sediments from dolines and caves found during the construction of the motorway near Divača, on the classical Karst. *Acta carsologica*, **25**, 169-191.
- Radinja D, 1986. The Karst in the light of fossilized fluvial deposition. *Acta Carsologica*, **14-15**, 101-108.
- Zupan Hajna N, 1995. A comparison of the mechanical cave sediments from the caves the Škocjanske jame, the Labodnica, the Prevala II and the Mejame. *Annales for Istrian and Mediterranean Studies*, **7**, 117-120.
- Zupan Hajna N, 1998. Mineral composition of clastic sediments in some dolines along the new motorway Divača-Kozina. *Acta Carsologica*, **27**, 277-296.
- Zupan Hajna N, Mihevc A, Pruner P, Bosák P, 2008. Palaeomagnetism and Magnetostratigraphy of Karst Sediments in Slovenia. *Carsologica*, **8**, ZRC Publishing, Ljubljana.
- Zupan Hajna N, Mihevc A, Pruner P, Bosák P, 2010. Palaeomagnetic research on karst sediments in Slovenia. *International Journal of Speleology*, **39**(2), 47-60.

Abstract

The general conceptual model of speleogenesis in the vadose zone infers an epikarstic zone followed by a vertical vadose zone, which is characterized by meandering canyons and shafts. In this vertical zone, the model foresees that water transits in a more or less straight line down to either the water table or an impervious layer. The detailed study of Réseau Stéphane (Siebenhengste area, Switzerland) reveals that the vertical zone is not necessarily a mere straight transfer zone, but that waters may divide, unite, and create completely different pathways in its speleogenetic evolution, resulting in intricate complex patterns of cave. This is not a new concept. Réseau Stéphane, however, is a well-suited case study for such behaviour and is thus presented here.

Keywords: Speleogenesis, vadose, Switzerland, flow capture.



Figure 1. Schematic sketch of general flowpaths in the vadose zone: waters generally coalesce and descend shafts (from Jeannin 1996, modified).

1. Introduction

Speleogenesis in the vadose zone is rarely discussed in literature. The general concept of speleogenesis gives an epikarst zone at the top, a (sub)vertical vadose transfer zone, and either a vadose drawdown of the waters along the dip of an impervious level, or a development of tubular caves along the (epi)phreatic water level (Palmer 1991, Häuselmann *et al.* 2003, Ford & Williams 2007).

Commonly, the vadose transfer zone, which is the main subject of this presentation, is regarded as the place where the water flow is rapid, within meandering canyons or shafts, and where different rivers show a tendency to coalesce and form a dendritic pattern, until one large cave stream results (Audra & Palmer 2013, Jeannin 1996), this is illustrated in Figure 1. However, this concept is not always valid, and instead of joining other rivers, a given river can find other pathways in geo-

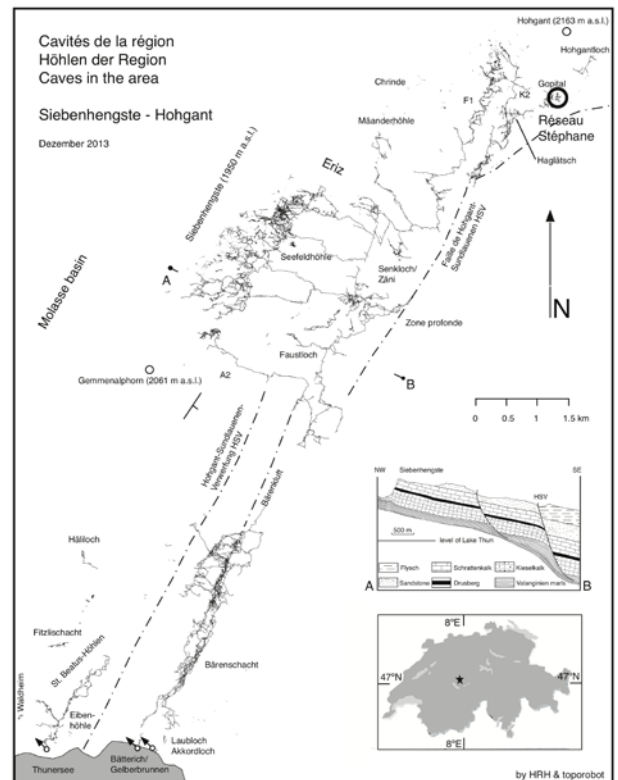


Figure 2. Overview of the Siebenhengste-Hohgant area and location of Réseau Stéphane. A map of Switzerland and a geological cross-section is inserted.

logic time. This is understandable in low-dip subhorizontal meandering canyons, where fractures can enlarge sufficiently to capture waters and divert its pathway. It is, however, much less understandable in sub vertical vadose shafts. The Réseau Stéphane (Gopital, Hohgant, Switzerland) is a good case study of such behaviour.

2. Geographical and geological setting

Réseau Stéphane is an essentially vertical vadose cave that intersects, at one point, an older phreatic conduit. The cave is 1640 m long and 207 m deep. It is within the catchment area of the well-known Siebenhengste-Hohgant cave system, but on its NE side: in the small Gopital valley that is south of Hohgant mountain (Fig. 2), at an altitude of 1846 m a.s.l. Climate is temperate humid; average annual temperature is

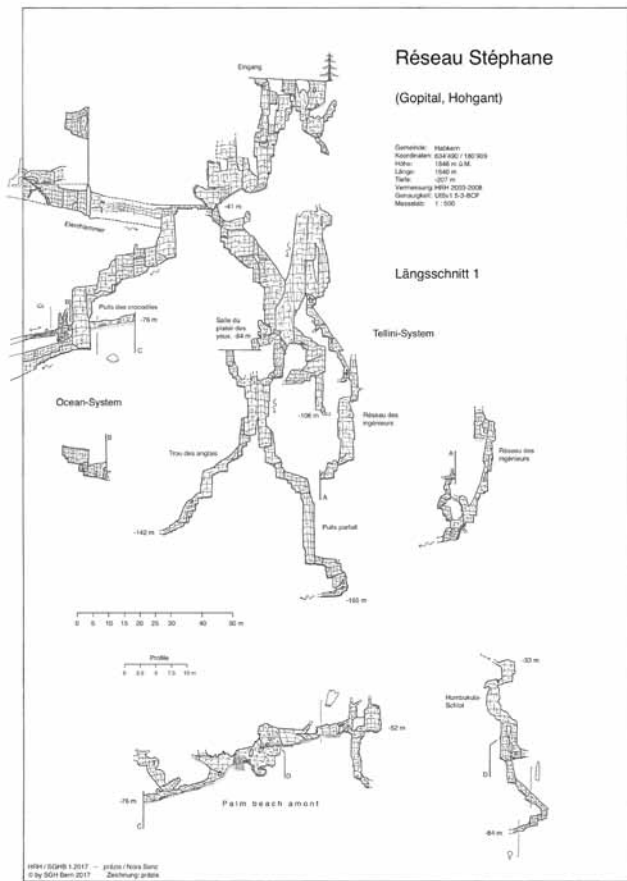
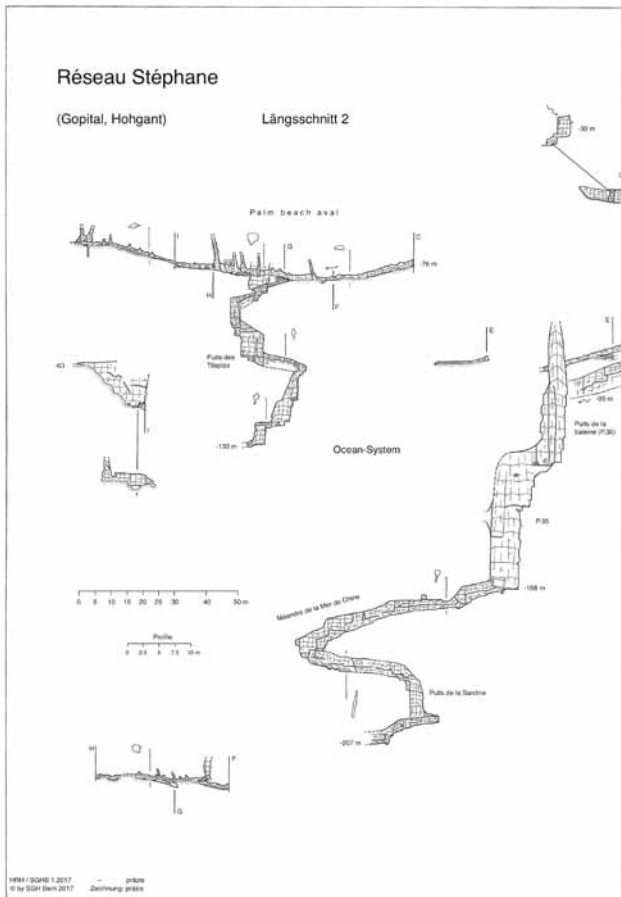


Figure 3. Developed longitudinal section, part 2.

Figure 4. Developed longitudinal section, part 1.

around 2 °C, and precipitation is 1600-1800 mm/year, much of which falls as snow in winter time.

The geology is rather simple: The whole cave is developed in Cretaceous Urgonian limestone, which has a thickness of about 200 m. At its base, the cave just meets the underlying impervious Drusberg marl also of Cretaceous age. Several small fractures condition speleogenesis in a minor way.

3. Structure of the cave

The cave was found in the 70s by the Belgian caving club CARSS, who then explored the cave (not without digging through many obstacles) and made a first map, which was later published (Delvaux & Dodge, 1982). In the context of a revision of the whole caving area, the cave was remapped between 2003 and 2008 by the HRH (Caver’s association of the Hohgant region) that comprises all clubs working in the Siebenhengste-Hohgant region. The longitudinal section is presented in Figs. 3-4 in extension, since only good-quality mapping permitted the insights into water flow and speleogenesis that are presented here. For space reasons, the plan view is omitted.

The vertical entrance of the cave leads to a narrow meandering canyon. Digging in the breakdown leads to the “Tellini system”, where a succession of shafts and narrow meandering canyons leads down to -165 m. If the initial meandering canyon is followed upstream (made passable by dynamite) towards the “Ocean system”, a shaft is reached, where a permanent trickle of water is found. Across the shaft, the upstream part of the canyon (“Eierchlemmer”) opens, but the passage

is very selective and only for slim cavers. Below the shaft, a meandering canyon leads to a next drop, named “Crocodile shaft”. This shaft intersects a phreatic conduit of passable dimensions. Its upward path is called “Palm beach” and presents several branching passages of both phreatic and vadose origin. Its downward path leads to the “Whale shaft (Puits de la baleine)” and the following narrow meandering canyon.

4. Observations of river flow

The small river discussed here has its origin in the meandering canyon “Eierchlemmer”. An attentive reading of the cave map reveals that this canyon originally continued towards the shaft zone of the Tellini system, where it combines with the meandering canyon coming from the entrance. The waters then descended the smaller shafts down to the area “Pleasure for the eyes (Plaisir des yeux)”. From there, the water first took the rightmost canyon-shaft. Regressive erosion in the shaft led, in a later stage, to the meandering canyon to the left. The later regressive erosion, more headward, formed the zone towards the “Perfect shaft (Puits parfait)”. This stage did not last long, another headward capture led to the leftmost meandering canyon. The ultimate headward capture of the “Eierchlemmer” river led to the first shaft leading to the “Ocean system” and the “Crocodile shaft”. The waters continued (and still continue) their way at its base in another meandering canyon that eventually gets too narrow. Figure 5 reveals the flowpaths in a schematic sketch. In white the presently used passage is seen, the older passages are progressively darkened. It is easy to see on the plan view that flow direction

Hypogene? Caves Modified By Meteoric Flows - Geomorphology Of Cliefden Caves And The Belubula River Valley

Ian Household¹ and Armstrong Osborne²

Affiliation: ¹Postgraduate student, School of Geosciences, University of Sydney

²Sydney School of Education and Social Work, University of Sydney

Abstract

Speleogens, sub-aqueous speleothems, cave sediments and surface landform evolution at the Cliefden karst were examined to test the hypothesis that many karst systems in Australia's eastern highlands were originally developed through hypogene processes. Whilst geochemical analysis of speleothems provided only equivocal support for early stage hypogene solution, passage morphology suggests either hypogene or ascending low-energy meteoric flow may have been important controls. It proved difficult to separate hypogene from meteoric passages using morphology alone, given equifinality of forms derived from both low energy rising meteoric and hypogene systems. Later epiphreatic modification was much easier to recognise. Surveying of erosion surfaces, terraces, epi-phreatic passages and cave sediments provided a much clearer picture of relationships between later stage speleogenesis and surface landform evolution. Covering a vertical relief of 200 metres, the Cliefden karst area contains the most complete suite of erosion surfaces, terraces and genetically associated cave levels/sediments in Australia's eastern highlands.

Keywords:

1. The Cliefden Karst system

The Cliefden karst system is found midway between Blayney and Canowindra, on the "Boonderoo" and "Angullong" properties in the Western Incised Zone of New South Wales. It has developed adjacent to the mid-Miocene Mt Canobolas shield volcano in the highly contorted Upper Ordovician Cliefden Caves Limestone Subgroup. This comprises extensive deposits of pure lime mudstones (the Belubula Limestone) between various thinly bedded and at times less pure carbonate units - the younger Vandon Limestone and underlying Fossil Hill Limestone (Webby and Packham 1982) (Fig.1).

The carbonates were exposed following post-mid Miocene incision of the 200 m deep Belubula River valley, providing human access to cave passages developed under predominantly phreatic and epi-phreatic conditions. Rare evidence of vadose development may be discerned in some areas.

Major caves have developed in lower, more massive units of the Belubula Limestone, where linear passages have formed along strike. Maze-like systems are more common in the thinly bedded upper units of the Belubula Limestone and adjoining Fossil Hill/Vandon Formations. Sulfidic interbeds and joint-controlled, sulfide-rich veins are common in the thinly bedded strata.

The Cliefden Warm Spring, rare in NSW karst systems, suggests the possibility of long-term hypogene development of phreatic caves - many passage shapes correspond with what have been described as characteristic hypogene morphologies elsewhere. As these features may also have developed through low energy, ascending meteoric flows, geochemical analysis of cave deposits, karst waters and assessment of the evolution of the karst aquifer were undertaken to test this hypothesis.

2. Landscape evolution

Evolution of the karst aquifer was related to the area's geomorphic history, as changes in recharge, hydraulic head and discharge characteristics have reacted to developing surface landforms. The Belubula River valley is a Cainozoic feature, initiated as a response to the mid Cretaceous uplift

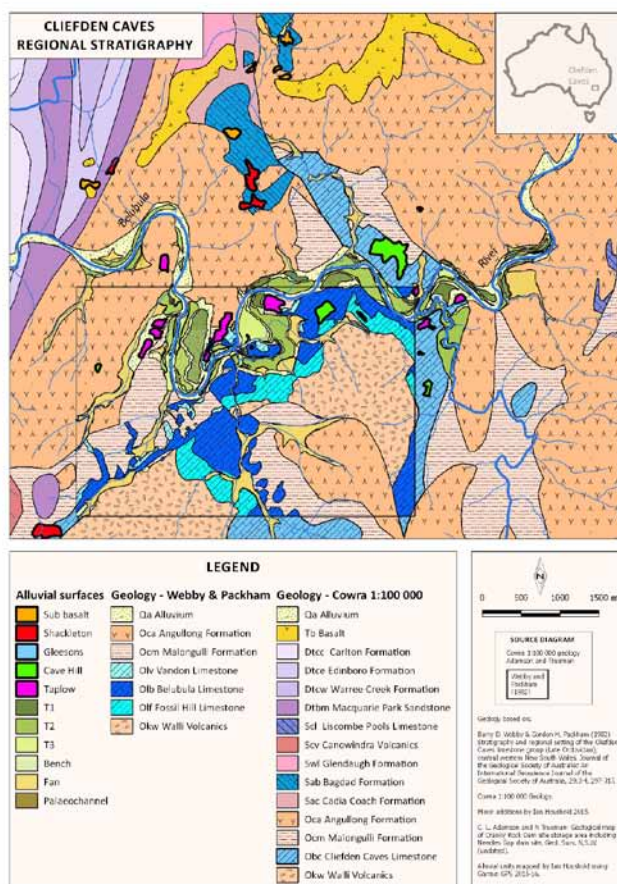


Figure 1. Regional stratigraphy, Cainozoic erosion surfaces and alluvial deposits, Cliefden karst area.

Source: Base map - Cowra 1:100 000 digital geology, Webby and Packham (1982).

of the Eastern Highlands. A second phase of regional uplift occurred along with doming around Mt Canobolas. A third uplift phase, associated with post-Miocene neotectonic compression, may also have affected the area.

Two landscape-scale erosion surfaces are found in the upper and mid reaches of the Belubula catchment, at approximately 950 m and 650 m above sea-level (the 'upper' and 'lower' surfaces). Both surfaces have been distinctly domed around Mt Canobolas.

Near Bathurst, lava field type basalt flows on fluvial gravels covering the upper surface are dated to 18-21 Ma (Wellman and McDougall 1974, Gibson 2007), providing a minimum age for planation.

Flood basalt related to the earliest phases of the Mt Canobolas eruptions (~12.8 Ma – Gibson 2007) cover both surfaces, flowing down valleys dissecting the pre-existing escarpment. Following planation of the upper surface, the Cliefden Caves Limestone was buried beneath up to 400 m of overlying Ordovician sediments and volcanoclastics. At the lower surface stage, overlying units were reduced to a maximum thickness of 200 metres. During both of these stages any direct meteoric contribution to subsurface flows would have been minimal given the depth, hydraulic characteristics of the rock and low hydraulic gradients. Any truly hypogene cave development would have occurred during, or prior to these times, independent of descending flows. The most likely source of hypogene acid would have been CO₂ generated by volcanism.

Incision of the lower surface commenced after the Mt Canobolas eruptions. Downcutting would have been relatively rapid, associated with retreat of a major knickpoint generated by volcanic doming and/or isostatic rebound (Bishop and Brown 1992). During this period an increasing proportion of meteoric groundwater would have invaded the karst, along with increasing hydraulic gradients and greater influence of the piezometric surface on groundwater flows.

Immediately west of the karst a thrust faulted, synclinal strike ridge composed of competent Devonian sandstones and conglomerates is traversed by the river at Needles Gap. This ridge has been a significant local control on valley deepening throughout the Cainozoic, influencing the rate of incision of the river in the vicinity of the karst and promoting development of an upstream alluviated karst basin.

The karst basin contains an unusually complete record of Late Miocene - Holocene incision and aggradation. 12-12.8 Ma basalt flow remnants are found on the plateau edge at "Angulong", immediately north of Cliefden Caves, covering extensive finely rounded quartz gravel deposits. In places these deposits have been silicified to thicknesses of 1-2 metres. The underlying bedrock contact has been termed the 'Sub-basalt Surface' for this project.

Below this, gravels of mixed lithologies and associated silcretes are found on a planed surface at approximately 570 m ASL on the ridge north of Needles Gap and further upstream (the 'Shackleton Surface'). During the latest phases of the Mt Canobolas eruptions (~11.7 Ma - Gibson 2007), more viscous trachyte lavas were emplaced on the earlier basalts and parts of this surface, allowing incision and planation of the Sub-basalt Surface to be dated.

Episodic retreat of the Belubula River knickpoint, interspersed by climatically controlled aggradational phases, occurred from the mid Miocene to present. Increasing relative dryness, and more extreme climatic fluctuations between glacial and interglacial periods in the Quaternary led to cyclic erosion/planation of bedrock straths in interglacials, and deposition of



Figure 2. The "Cave Hill" surface, T1 and T2 terraces, all planed bedrock straths covered with 2-3 metres of alluvium. Showing section line in Fig. 3.

alluvial covers during glacials. Four erosional strath terraces, capped by a few metres of mixed lithology gravels, sands and clays are found at approximately 75m ("Cave Hill" surface), 25 m ("Taplow" surface) 12 m (T1 terrace) and 8 m (T2 terrace) above the river bed (Fig. 2). The T3 terrace forms the active floodplain, approximately 4 metres above the river.

Correlating dispersed pockets of the lower terrace deposits was not straightforward, as using elevation alone to differentiate alluvial units was unreliable. For this reason, materials from the 5 lowest terraces were sampled for fine-fraction grain-size analysis, magnetic susceptibility and colour. Mineralogy was determined using X-ray diffraction. Statistical analysis of all lines of evidence provided the most likely correlation of terraces, presented in Fig. 1.

3. Cave systems

Whilst over 100 caves have been mapped at Cliefden, morphology is best expressed in five major systems: Main Cave, Murder/Childrens/Boonderoo, Taplow Maze/Island Cave, Gable/Swansong Cave, and Tetanus Cave. Of these, only Main Cave has developed entirely in the Belubula Limestone; the others have formed in a combination of the Belubula Limestone and overlying, thinly bedded Vandon Limestone or in the case of Tetanus Cave, the underlying Fossil Hill Limestone.

Lithology and hydrogeological relationships have controlled cave morphologies. Initial development was a series of structurally controlled, three dimensional phreatic mazes, superimposed by sub-horizontal epi-phreatic development which linked mazes into more linear features. The majority of caves were drained without significant vadose modification, although in restricted areas vertically stacked solution notches suggest both episodic vadose incision or paragenetic roof solution, related to incision and aggradation phases in the valley. The massive nature of Belubula Limestone has accentuated epi-phreatic forms in lower levels as more widely spaced joints and beds tended to constrain flows to fewer conduits. Upper levels in thinly bedded limestone have retained their maze-like character.

Currently no caves contain actively flowing vadose streams, with all subsurface intersections of the water table restricted to pools of outcropping groundwater. No attempts have been made to trace this water, or of the two obviously active inflow systems in the area - Davys Creek and Gleesons Creek. Whilst it is presumed that Davys Creek water resurges at the head of a major tufa-depositing spring (Carthew and Drysdale 2003) the most likely underground course of Gleesons Creek water is to the Belubula River or the Warm Spring at the downstream margin of the karst. All cave passages below river level

are flooded, with groundwater levels fluctuating seasonally over 2-3 metres in response to river stage. This suggests the current regional piezometric surface is controlled by the river level, and that the river is not significantly gaining or losing through the karst area.

The highest of the geomorphically significant caves is Tetanus Cave, a single, large phreatic room, with minor surrounding pressure tubes, located at the elevation of the Cave Hill surface, approximately 75 metres above the river in thinly bedded, sulfide rich Fossil Hill Limestone. It provides evidence for the oldest level of phreatic development at Cliefden, along with potential for studying the effects of sulfuric acid on cave development.

Childrens Cave is the highest of the Murder/Boonderoo/Childrens system, and the second-highest epiphreatic cave at Cliefden, with significant horizontal development at approximately 25 metres above the river. Both Murder and Boonderoo Caves contain epiphreatic levels stepping down to river level. All three caves are oriented approximately north-south along the strike, with passages short-circuiting the meander loop of the Belubula River as it incised Large Flat.

The remaining caves all contain distinct levels of epiphreatic modification over 15 vertical metres, with Main Cave containing many sub-horizontally planed ceilings at multiple levels. Collapse into epiphreatically de-stabilised chambers has opened a large rockfall chamber high in the hill, although still below the level of the "Cave Hill" erosion surface.

The Gable-Swansong system retains much of its original phreatic morphology, with many large cupolas and domes pocketing the ceilings of the main chambers. These are common in massive units of the Belubula Limestone, whilst intricate three-dimensional mazes have developed in overlying thinly bedded units. Paragenetic passages (with associated fine clastic fills) are common in the maze section. Only at the very lowest levels are horizontal solution notches common, often containing finely laminated sediments.

Taplow Maze/Island Cave is a complex, three-dimensional system developed predominantly in the Vandon Limestone, where the highest phreatic passages have been truncated by planation of the "Taplow" Surface, approximately 25 metres above the river. Two large north-south trending passages traverse the underlying Belubula Limestone and contain relict stacked horizontal solution notches potentially indicating vadose entrenchment. It is likely that Taplow Maze originally connected to Island Cave through the now eroded neck of the meander cutoff at Large Flat.

All caves contain widespread deposits of mainly fine laminated silts and clays. Almost no fluvial gravels have entered the system, other than as reworked gravitational deposits derived from overlying surface terraces. Many of these deposits show evidence of multiple, overlapping phases of deposition and re-solution/re-excavation.

4. Initial hypogene cave development?

High resolution "Zebedee" point cloud surveys of the major caves by CSIRO, Orange Speleological Society and Sydney University Speleological Society (Zlot 2015) provide excellent representations of passage morphologies for geomorphological analysis (Fig. 3). Surveys support visual interpretation of early phreatic development, and highlight well developed

cupolas indicating solution in upwelling flows. These features are common in many southeast Australian caves, suggesting to Osborne (2010) that many may have originally developed through hypogene solution, or at least as *per ascensum* passages resulting from either thermal convection or artesian pressure.

As the Cliefden area contains a permanently flowing warm spring, nearby Neogene volcanism and caves with speleogens similar to demonstrably hypogene passages elsewhere (eg Klimchouk 2009), it was chosen to test Osborne's hypothesis of widespread early hypogene karstification in eastern Australia. Whilst carbonic acid is the most likely solvent for both hypogene and meteoric speleogenesis at Cliefden, the presence of sulfidic interbeds and veins in thinly bedded limestone units may also have provided a minor source of sulfuric acid following oxidation as piezometric levels fell.

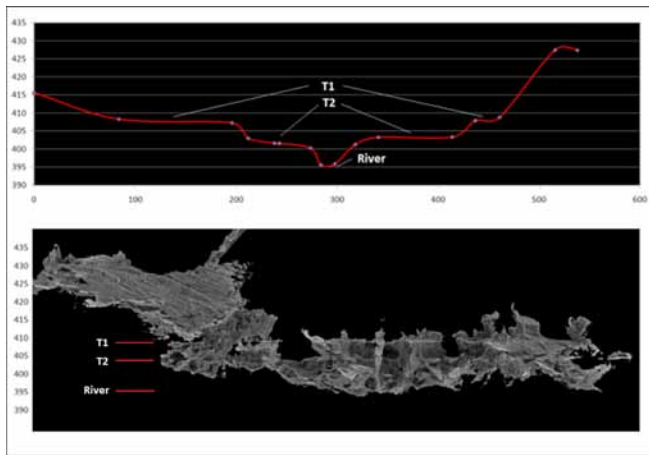
Sub-aqueous speleothems, including passage linings, dog-tooth spar and mamillaries (both calcite and gypsum) were sampled and their mineralogy assessed using X-ray diffraction. Water samples from springs, cave pools and local wells were also sampled. Calcite and water samples were analysed for oxygen and carbon isotopes and results compared with results from dated, Quaternary aged Cliefden stalagmites and associated dripwater, previously analysed by McDonald (2005). Although some samples indicated water sources which may have been slightly warmer than present, O isotope ratios were essentially similar to McDonald's calcite and dripwater signatures. C isotopes indicate a surficial source for carbonic acid. C and O isotope data do not therefore support the hypothesis that either deeply sourced or significantly warmer water sources were involved in the initial excavation of cave passages.

Whilst speleothem geochemistry does not obviously support a hypogene origin for early cave development, it is possible that sub-aqueous material associated with original solution may have been chemically or mechanically weathered from passage walls during subsequent high water levels - many of today's remnants are very fragile, and obviously represent only a small proportion of what was originally present. So, at Cliefden the question of meteoric vs hypogene development of the early stages of speleogenesis now rests on interpretation of passage morphology rather than geochemistry.

At present no definitive atlas of hypogene vs meteoric phreatic speleogens is available, particularly for unconfined, steeply bedded carbonates such as those in Australia's Eastern Highlands. Many of the speleogens at Cliefden including cupolas, half-tubes, cusps, bellholes, pits, juts, blades, projecting corners and pseudonotches, known to be produced by hypogene processes elsewhere, may also have been developed through pressurised meteoric speleogenesis, including ascending flows in low-energy phreatic loops, (*sensu* Stage 1, Ford and Ewers 1978). Unfortunately, for the more common speleogens both processes lead to equifinality of form - an issue not restricted to eastern Australia (Audra and Palmer 2015).

5. Cave - surface landform relationships

Whilst a hypogene origin for the Cliefden karst is equivocal, the role of slow, pressurised, nothephratic flows (*sensu* Jennings 1985) in early speleogenesis (regardless of water or acid sources) is supported by both morphology and geochemistry. Point cloud surveys and passage observations also demon-



Point cloud survey of Main Cave showing horizontally planed ceilings, aligned with DGPS survey of terrace surfaces (section shown in Plate 1). Epi-phreatic modification of an older, structurally controlled phreatic maze. Data source: Zlot (2015).

strate the influence of epiphreatic development in later stage speleogenesis, suggesting strong relationships between surface landform evolution, migration of the piezometric surface and epiphreatic modification of older systems.

To analyse these relationships, cave sections were compared with differential GPS surveys of terrace treads and bedrock straths and compositions of cave/terrace sediments were compared using XRD. Long sections of terraces were produced, along with valley cross sections at each of the major cave systems, and cave levels were combined (Fig. 3).

These comparisons suggest strong genetic relationships between major epi-phreatic cave levels, the current river controlled piezometric surface and the T1, T2, T3 and “Taplow” surfaces. Tetanus Cave is found at the level of the “Cave Hill” surface, however a local knickpoint in Davys Creek, between this cave and the Belubula River, makes a genetic correlation less certain.

6. Discussion

Whilst early stage hypogene development of the Cliefden karst remains equivocal, this project has demonstrated a significant genetic relationship between the evolution of the surface landscape and later epi-phreatic stages of cave development. Accurate surface levelling with DGPS and use of Disto X and “Zebedee” point cloud cave surveys have provided a basis to accurately represent surface and underground morphologies, and comparison of surface and cave sediments using X-ray diffraction supports a strong correlation between surface and cave sediment units at similar levels. No dating has been undertaken yet, however the potential for U/Th, U/Pb analysis of key speleothems, K/Ar dating of volcanics, and palaeomagnetic analysis of fine cave sediments and silcretes are likely to provide a detailed timeframe for development of the surface and underground landscape post the 12 Ma eruption of Mt Canobolas. This may add significant detail to our understanding of the late Cainozoic evolution of the eastern highlands.

Acknowledgements

We acknowledge the valuable contribution of members of the Orange Speleological Society, particularly Bruce Howlett, Denis Marsh, Glen Griffith and Ian Curtis for field assistance

and Sydney University Speleological Society members Phil Maynard, Mike Lake and Kevin Moore for access to cave survey data and assistance with interpretation of point cloud data.

References

- Audra P. and Palmer A. N. 2015. Research frontiers in speleogenesis. Dominant processes, hydrogeological conditions and resulting cave patterns. *Acta Carsologica* **44**:3, 315–348.
- Bishop P. and Brown R. 1992. Denudational isostatic rebound of intraplate highlands: The Lachlan River Valley, Australia. *Earth Surface Processes and Landforms* **17**: 345–360.
- Carthew K.D. & Drysdale R. N. 2003. Late Holocene fluvial change in a tufa-depositing stream: Davys Creek, New South Wales, Australia. *Australian Geographer*, **34**:1, 123–139.
- Ford D.C. and Ewers, R.O. 1978. The development of limestone cave systems in the dimensions of length and depth, *Canadian Journal of Earth Science* **15**(11); 1783–1798.
- Gibson D. 2007. Potassium-Argon Ages of Late Mesozoic and Cainozoic Igneous Rocks of Eastern Australia. *CRC LEME Open File Report* 193.
- Jennings J.N. 1985. *Karst Geomorphology*. Basil Blackwell, Oxford.
- Klimchouk A. 2009. Morphogenesis of hypogenic caves. *Geomorphology* **106** (2009) 100–117.
- McDonald J. 2005. *Climate controls on trace element variability in cave drip waters and calcite: a modern study from two karst systems in SE Australia* [unpublished PhD thesis]. The University of Newcastle.
- Osborne R.A.L. 2009. Hypogene caves in deformed (fold belt) strata: observations from eastern Australia and central Europe. In: *Hypogene speleogenesis and karst hydrogeology of artesian basins*. Ukrainian Institute of Speleology and Karstology, Special Paper 1, 2009.
- Osborne R.A.L. 2010. Rethinking eastern Australian caves. From: Bishop, P. & Pillans, B. (eds) *Australian Landscapes*. Geological Society, London, Special Publications, 346, 289–308.
- Webby B.D. and Packham G.H. 1982. Stratigraphy and regional setting of the Cliefden Caves limestone group (Late Ordovician), central-western New South Wales. *Journal of the Geological Society of Australia* **29**:3–4, 297–317.
- Wellman P. and McDougall, I. 1974. Potassium-argon ages on the Cainozoic volcanic rocks of New South Wales. *Journal of the Geological Society of Australia*, **21**:3, 247–272.
- Zlot R. 2015. Cliefden Caves: Zebedee 3D data collection v1. CSIRO data collection <http://doi.org/10.4225/08/554C628401D73>

(Abstract) **The oldest meteoric caves in Norway?
The Reingardslia Cave Documentation project.**

Stein-Erik Lauritzen, Rannveig Øvrevik Skoglund, Marie Heggstad, Hege Kilhavn, Severin Lølkes,
Einar Taule Øyehaug, Ida Marie Gabrielsen, Alexander Gulbrandsøy Stadheim, Sverre Aksnes

Affiliation: University of Bergen, Norway

Abstract

The marble cave system of Reingardslia in Rana, North Norway is one of the longest known, and largest of the region. They were first documented by Gunnar Horn in the 1930'ies. One of the caves, Larshullet, was later known as the deepest cave in northern Europe, as documented by Railton and Corbel in 1951. This discovery actually triggered the later attention from 299-Luauritzen foreign caves through the 1950- 1970 period. In 1960, the caves were protected by law and have since been gated as a nature reserve. In 2015, a three- year project was commenced for re-mapping and documenting the state and scientific values in the cave system. During this work, we have connected and expanded most of the caves into an integrated system of 9 km length. Six MsC works are running on paleoflow, sediments, mineralogy and fracture tectonics. Previous U- series and isotopic studies on speleothems have revealed the caves as the oldest dated in Scandinavia. These results will be discussed towards a new speleogenetic model of the system.

(Abstract) **Pre-Quaternary, hypogenetic caves in south Norway**

Stein-Erik Lauritzen, Sven Dahlgren

Affiliation: University of Bergen, Norway

Abstract

he Dalen-Kjørholt limestone mines at Porsgrunn, South Norway, is exploiting upper Ordovician (encrinitic) limestone for cement production. Up through the years, numerous large vugs with calcite crystals have been intersected through the mining, making the site famous among mineral collectors. The crusts consist of several generations of macro-crystalline calcite of various habitus, with minor amounts of marcasite, palygorskite and occasional quartz. Some of them may be stalactitic, but certainly helictitic. We have undertaken a detailed study of these vugs and surveyed them by speleological techniques. Several cores were drilled through the mineral lining and into wallrock in order to study isotopes, chemistry and chronology at the interface. We have demonstrated that many of the vugs are not simple fissures, but display rounded and multi-stage cross-sections, with a sharp interface between cave wall and mineral crust. This clearly indicate a substantial corrosional history after tectonic fracturing, but prior to mineralization. They are mine-caves. Preliminary U- series dating attempts reveal secular equilibrium in the U/U system (> 1.5 myr); further progress is only available through Pb/U techniques and in progress. The vugs are therefore to be regarded as a system of hypogenetic caves of unknown, but certainly pre-Quaternary origin.

Analysis of scallops in Gomantong Caves, by GIS processing of 3D terrestrial laser scanner data

Joyce Lundberg¹, William Carroll¹, Warren Roberts², Donald A McFarlane², Manfred Buchroithner³, and Guy van Rentergem⁴

Affiliation: ¹Carleton University, Ottawa, Canada
²The Claremont Colleges, California, USA
³Technische Universität, Dresden, Germany
⁴Koningin Astridstraat, Deinze, Belgium

Abstract

Gomantong Caves, occupying much of the isolated karst tower of Gomantong Hill, Sabah, Borneo, are relict phreatic caves (now famous for their huge populations of bats and swiftlets), with no evidence of any vadose phase. Here we explore the speleogenesis by analysing the phreatic scallop remnants to determine former flow direction and thus hydraulic gradient. Data, at centimeter-scale resolution, were acquired from 3D terrestrial laser scanning using a FARO3D TLS. Eight populations of scallops were studied. Scan data were extracted using SCENE LT software, and imported into ArcGIS. For each surface (3-4 m² in area), digital elevation models were produced of hill-shade and of slope. Cross sections highlighted the scallop asymmetry and thus direction of water flow.

The cave is largely made up of dip tubes tilting downwards from the entrances at an angle of ~22° and opening into large central passages. Surfaces in Simud Hitam (Black Cave) are strongly modified such that the original scallops are often destroyed. Scallops in Simud Puteh (White Cave) are generally well preserved. Analysis of the scallops indicates that water flow in these phreatic passages had been upwards in the dip tubes and outwards towards the entrances. This implies a rising water source from depth, and a distant recharge source.

Keywords:

1. Introduction

Gomantong Hill (5.51° N, 118.06° E) is an isolated limestone outcrop on the flood plain of the Kinabatangan River, ~30 km south of Sandakan, NW Borneo, that encompasses a sizeable cave system (McFarlane, 2013). Gomantong Caves include the lower level Simud Hitam (or Black Cave, with the tourist boardwalk) and the upper level, less accessible, Simud Puteh (or White Cave) (Figure 1a). The caves are famous for their bird's nest harvesting and the huge population of bats. They are developed in the ~300 m-thick outcrop of Gomantong Limestones, of upper Oligocene to lower Miocene age, made up of isolated inliers of mainly reefal limestone, lying unconformably on, or interfingering with, sandstones and shale turbidites. Landscape development and speleogenesis is presumed to have occurred in the last couple of million years since Late Pliocene tectonism tilted and folded the beds. Gomantong Hill is a synclinal feature, with dips of ~5-25° and in the region of the cave the dip is 20-30° to the NW (Wilford, 1964).

The cave is developed along bedding planes and steeply inclined joints, but in places shows substantial modification that often disguises the original shape. The bedding plane passages are typical phreatic dip tubes, elliptical in cross section with scalloped walls and ceilings, the dip at ~20°, but variable. The joint passages are high with very complex arch-shaped cross sections. Evidence for the former phreatic origin is now often hard to detect, many of the surfaces having been significantly altered by post-speleogenetic modification (Lundberg *et al.*, 2012). The caves are now fully drained, with only one minor in-cave stream, and appear to have been drained rapidly, no vadose stage being apparent.

In an attempt to elucidate the original speleogenesis and hydrology, we mapped and measured the remnants of phreatic scalloping on the cave walls and ceilings using 3D terrestrial laser scanning. Several of the scalloped surfaces can be seen clearly in the cave. However, many are far too high to reach by conventional caving techniques and many cannot be seen under normal lighting conditions – hence the unique advantage of 3D scanning data: information can be acquired that otherwise would be unattainable. In addition, we exploit the extraordinary density of data to make measurements that in the field may be very time-consuming and considerably less accurate. Taking further advantage of modern technology, we married the 3D point-cloud data with GIS techniques to produce maps of slope for each site. Scallop asymmetry allows the reconstruction of former flow directions and scallop dimensions allow calculation of former flow velocity (Curl, 1974). Together with passage dimensions from the point-cloud data, we can then produce estimates of former hydraulic gradients and discharges.

2. Methods

Three-dimensional laser scan data were collected during two field sessions, in August 2012 and 2014, using a FARO Focus3D instrument (details in McFarlane *et al.*, 2013). Visualization of the point cloud data was done with Faro SCENE LT software.

Areas of potential interest were identified in the field and from the point cloud data. Two types of scallops are apparent in the cave, the more common being scallops from former fluvial current activity (the features of interest here), and the less common being air scallops from ongoing condensation corrosion by diurnally-exchanging currents of humid air. The

ated by amalgamation of several formerly distinct phreatic tubes (Lundberg and McFarlane, 2012), has few clear passages and scallops could be measured in only two areas.

Some parts of the cave yielded no paleo-flow data because they had no detectable scallops or scallops so severely modified as to preclude measurement. Surfaces have been modified by a variety of processes, most related to biogenic activity and associated condensation corrosion, and, in the large chambers, by roof collapse.

Our results show that all passages studied show paleo-flow rising in the tube, uphill against the direction of dip, and all generally towards the east (Figure 1b). Flow has shifted towards the north in the lowest-level outlet, the main entrance to Simud Hitam, Black Cave.

Examples of passage cross sections are shown in Figure 3. Flow velocity, calculated from Sauter means of scallop lengths ($n = 25-50$), and discharge, calculated from passage cross sectional areas and velocity, are shown in Table 1.

4. Discussion

Terrestrial laser scanning is increasingly being employed in technically-difficult and complex caves (e.g., Buchroithner and Gaisecker, 2009). Terrestrial laser scanning at Goman-tong has now imaged virtually all of Simud Hitam and Simud Puteh. The size of the point-cloud dataset creates significant software processing challenges but these can be addressed by point sub-sampling, and by breaking the data set into sections for separate processing in ArcMap software.

The results of this analysis of scallop asymmetry show a pattern of flow, for all sites with measurable scallops, that rises from depth, flowing upwards and generally eastwards, in the direction of the modern coastline. Many classic phreatic caves show looped sequences of dip tubes and lift tubes (e.g., Ford and Williams, 2007, p. 225). None of the passages in Goman-tong shows descending flow. The implication is that recharge occurred from a distant source, most likely in the highlands surrounding the basin of the Kinabatang River, resulting in rising waters in Gomantong, closer to sea level. Most of the geology of the region is non-karstic, so flow would probably have followed simple Darcian laws. The rising tubes suggest

Table 1. Velocity and discharge data.

Passage Name	Cross sectional area (m ²)	Velocity (m/s)	Discharge (m ³ /s)
Bapa Tinobatang	40.1	0.021	0.80
Simud Puteh upper level	21.1	0.029	0.62
Simud Puteh main entrance	98.6	0.048	4.82
Kudong	54.8	0.032	1.75
Ulun Ulun	49.4	0.013	0.57
Lobing Payau	81.3	0.027	2.09
Simud Hitam main entrance	245.7	0.037	9.16

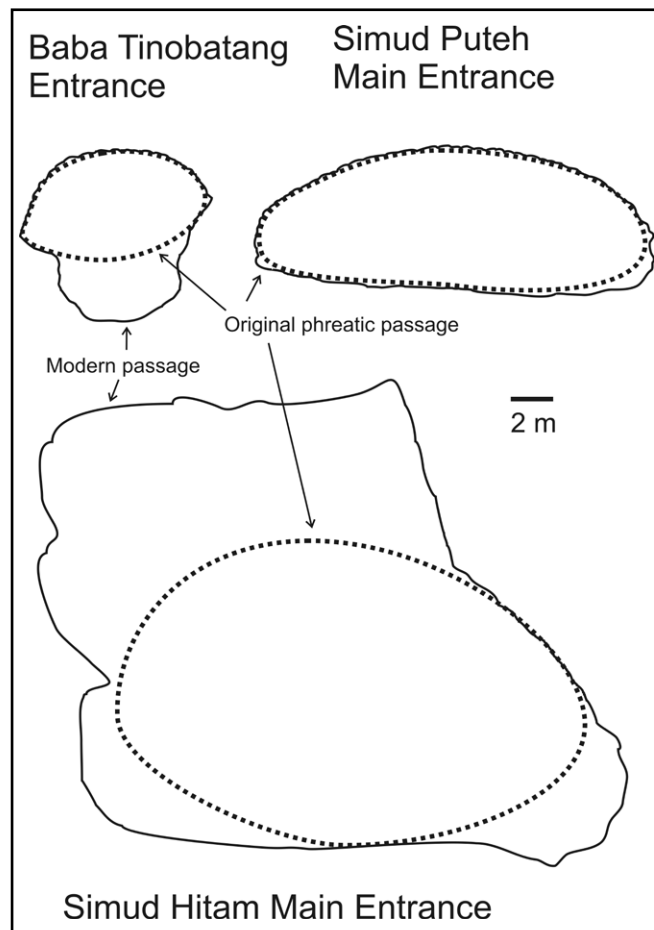


Figure 3. Examples of passage cross sections. The modern cross section is shown as a solid line. The reconstructed former phreatic surface is shown as a dotted line. The upper-level cave passages are largely unmodified.

that artesian flow may have been important, the non-limestones rocks and perhaps fault zones acting as aquitards. As base level was lowered, the outlets shifted, finally emerging from the main entrance to Simud Hitam.

Acknowledgements

Many thanks to: FARO International, Singapore, who kindly provided the FAROFocus3D TLS instrument and shipping to Sabah; Dr. Charles Leh Moi Ung (Sarawak Museum); Datuk Sam Mannan, Director, Sabah Forestry Department. Field work was funded in part by a grant from the National Geographic Society.

References

- Curl, R.L., 1974 - Deducing flow velocity in cave conduits from scallops. *Natl. Speleol. Soc. Bull.* **36**, 1-5.
- Buchroithner M.F. & Gaisecker T., 2009 - Terrestrial Laser Scanning for the Visualization of a Complex Dome in an Extreme Alpine Cave System. In: *Photogrammetrie-Fernerkundung-Geoinformation (PFG)*, 2009, **4**, 329 - 339.
- Ford, D.C. & Williams, P. 2007 - *Karst Hydrology and Geomorphology*. Wiley. pp. 562.
- Lundberg J., & McFarlane D.A., 2012 - Post-speleogenetic biogenic modification of Gomantong Caves, Sabah, Borneo. *Geomorphology* **157/158**, 153-168.

McFarlane, D.A. 2013 – The hollow hill of Gomantong.
Descent, **230**, February/March 2013, 35-36.

McFarlane D.A., Buchroithner M., Lundberg J., Petters C.,
Roberts W., & Van Rentergen G., 2013 – Integrated three-
dimensional laser scanning and autonomous drone surface-
photogrammetry at Gomantong caves, Sabah, Malaysia.
Proceedings of the 16th International Congress of Speleology,
Brno. **2**, 317-319.

Wilford, G.E., 1964 – *The Geology of Sarawak and Sabah
Caves*. Bulletin 6, Geological Survey, Borneo Region, Malay-
sia. Brunei, Kuching.

Woodward, E. & Sasowsky, I.D., 2009 – A spreadsheet pro-
gram (ScallopEx) to calculate paleovelocities from cave wall
scallops. *Acta Carsologica* **38**(2), 303-305.

Flank Margin Caves In Telogenetic Limestones In Italy

Arriolabengoa Martin¹, D'Angeli Ilenia Maria², De Waele Jo², Parise Mario³, Ruggieri Rosario⁴, Sanna Laura⁵, Madonia Giuliana⁶, Vattano Marco⁶

Affiliation: ¹Department of Mineralogy and Petrology, Faculty of Science and Technology, University of the Basque Country (UPV/EHU), Leioa, Spain, martin.arriolabengoa@ehu.eus

²Department of Biological, Geological and Environmental Sciences, University of Bologna, Italy, ilenia.dangeli@alice.it; jo.dewaele@unibo.it

³Department of Earth and Environmental Sciences, University "Aldo Moro" of Bari, Italy (ex CNR-IRPI Bari, Italy), E-mail: mario.parise@uniba.it

⁴Centro Ibleo di Ricerche Speleo-Idrogeologiche, Ragusa, Italy, info@cirs-ragusa.org

⁵Institute for Biometeorology, CNR, Sassari, Italy, speleokikers@tiscali.it

⁶Department of Earth and Sea Sciences, University of Palermo, Via Archirafi 22, 90123 Palermo, Italy, giuliana.madonia@unipa.it; marco.vattano@unipa.it

Abstract

Almost 20% of Italy is characterized by the outcropping of carbonate massifs ranging in age from Cambrian to Quaternary. Coastal karst is present in many Italian regions: from North-East to South and West: the Gulf of Trieste, the Conero (South of Ancona, Marche), the Adriatic coast of Apulia including Gargano, Murge and Salento, Maratea in Basilicata, Cilento in Campania, Circeo and Gaeta in Latium, Argentario and Giannutri Island in Tuscany, the southernmost part of the Ligurian Alps, Palermo Mts., San Vito Lo Capo, Syracuse coast and Marettimo Island in Sicily, and, especially, in Sardinia, which has carbonate rocks touching the sea along the coast of Balai near Porto Torres, Capo Caccia-Punta Giglio (Alghero), Sinis and Buggerru along the western littoral, Capo Teulada and Capo Sant'Elia at Cagliari, Capo Figari, Tavolara Island and the Gulf of Orosei along the eastern mountainside.

Recent researches have revealed several coastal cave systems that have a clear origin by mixing corrosion, in which the aggressive solution derives from the mixing between saline and fresh water at the watertable interface (the so-called flank margin caves). Glacioeustasy and tectonic movements can control the position of sea level with respect to coastal carbonate outcrops. For this reason these coastal caves represent useful records of sea-level stillstands. These caves are normally organized in sub-horizontal levels, and are characterized by the lack of high flow velocity markers (scallop) and alluvial sediments. Instead, they show rounded cave passage morphologies, often with horizontal wall notches, a characteristic swiss-cheese or sponge morphology, and passages that narrow going away from the coastline (due to the decreasing of sea water influence and mixing-corrosion effect). This paper describes some flank margin cave systems found in Apulia, Sicily, and Sardinia. In particular, five cave systems are illustrated: Sant'Angelo caves (Apulia), Pellegrino and Rumena caves (Sicily), and Giuanniccu Mene cave and Fico cave (Sardinia), explaining their relationship with past sea levels and local uplift rate.

Keywords: salt-fresh water mixing, coastal karst, cave geomorphology, coastal uplift, speleogenesis

1. Introduction

Despite the fact that Italy has a very long coastline, being bathed on its northwestern, western, southern and eastern borders by the Ligurian, Tyrrhenian, Ionian, and Adriatic seas respectively, carbonate rocks crop out only locally along its rocky shoreline. Most of these coastal karst areas are composed of Mesozoic rocks, limestones and dolostones of Triassic, Jurassic and Cretaceous age, but also Miocene or Cambrian limestones occur locally. All these lithologies are mostly well diagenised, so-called telogenetic limestones (Chocquette and Pray 1970), with a poor primary porosity and its permeability mainly caused by structural elements (bedding planes and fractures).

Coastal caves in these carbonate rocks are mainly derived by marine abrasion and erosion processes, and sometimes are related to freshwater outflows from the continental catchment areas. Extensive underwater cave systems are especially known from Sardinia (Gulf of Orosei, De Waele 2004). These caves are characterized by clear morphological indicators of fast running waters, such as scallops and fluvial sediments, and only in their most proximal areas to the sea they can have clues of mixing dissolution. The main morphologies are

largely dominated by fluvial karst erosion, with only a minor imprint of dissolutional features.

Smaller caves, often with isolated chambers, or a sponge-work pattern, are known from Apulia (Onorato *et al.* 2003; Belmonte *et al.* 2009), from Syracuse (Guido *et al.* 2013), and from Capo Palinuro in Campania (Antonoli *et al.* 2004). Many of these caves were formed when sea level was lower than today, but their speleogenetic history has never been studied.

Whereas coastal mixing processes have been described since a long time (e.g. Cigna *et al.* 1963; Plummer 1975; Back *et al.* 1986; Smart *et al.* 1988), the model for cave development in a typical coastal mixing zone was published only in 1990 (Myroie and Carew 1990). These coastal mixing caves (flank margin caves) are characterized by the lack of fluvial sediments and scallops, rounded and smoothed cave wall morphologies, dissolutional notches, locally swiss-cheese morphologies (spongework), and typical plan form with interconnected passages and rooms at intersections more or less parallel to the coastline and passages tapering out going inland, away from the mixing zone. This model was first developed in young eogenetic limestone settings, such as those of the Bahamas



Figure 1. Location of the studied caves: 1. Rumena and Fantasma Caves, San Vito Lo Capo area; 2. Pellegrino Cave, Plemmirio, Syracuse; 3. Fico Cave, Gulf of Orosei; 4. Giuanniccu Mene Cave, Quirra area; 5. Sant'Angelo Cave, Ostuni.

and other carbonate islands in the Caribbean and the Pacific, but also explained cave genesis in coastal areas with hard well-dissolved limestones (e.g. Mylroie *et al.* 2008).

In the past few years several flank margin caves have also been found in coastal areas at different altitudes above sea level in Italy (Ruggieri and De Waele 2014; D'Angeli *et al.* 2015). These caves have often an importance in sea level change studies, being precise markers of past highstands (Mylroie and Carew 1988; Florea *et al.* 2007). These uplifted flank margin caves are located in the San Vito Lo Capo peninsula (Ruggieri and De Waele 2014) and in the Plemmirio Marine Protected area south of Syracuse, both located in Sicily, in the Gulf of Orosei (Central-East Sardinia) (D'Angeli *et al.* 2015), in the area of Quirra (Southeast Sardinia), and in the area of Ostuni (Apulia) (Fig. 1). Plan views of the caves are given in Fig. 3.

2. San Vito Lo Capo (Sicily)

Several caves have clear morphologies of mixing-corrosion in the salt-freshwater boundary, not only close to the coasts, but also at a certain distance inland on ancient coastal limestone cliffs. Although some of these caves are hosted in the Pleistocene eogenetic carbonates of old marine terraces, most are mixing-corrosion caves in massive Triassic to Lower Cretaceous limestones. The best examples are Rumena, Scurati, and Fantasma caves, but other twenty cavities have been classified as flank margin caves in this area (Ruggieri, 2015). Their position at different altitudes (10-20 m, 60-75 m and 95-110 m asl) indicates variable sea level highstands during which these caves were carved. The exceptional discovery of fossil corals on the walls of Rumena cave at 95 m asl, and their dating



Figure 2. Typical salt-fresh water mixing dissolutional morphologies. A. The dissolutional notch at 70 m asl in Fantasma Cave (Sicily) (photo Rosario Ruggieri); B. Notch and smooth morphologies in the Pellegrino Cave (Syracuse, Sicily) (photo Marco Vattano); C. Wavy roof and notch in the 22 m asl level of Fico Cave, Sardinia (photo Ilenia M. D'Angeli); D. Cupola carved in the Devonian marbles of the Giuanniccu Mene Cave (Sardinia) (photo Laura Sanna); E. The rounded morphologies and notches in the lower Sant'Angelo cave passages, Ostuni (Apulia) (photo Mario Parise).

using Sr isotopes (see Ruggieri, 2015) has allowed this highstand to be estimated at MIS29 or MIS31 (ca. 1 Ma), while the Fantasma cave and its mixing-corrosion notch (Fig. 2A), together with the Scurati caves at 70 m asl would be related to MIS19 (ca. 790-761 ka). These evidences suggest an average coastal uplift rate of around 0.9 mm/ka for this area of Sicily, and also demonstrate that not all sea level highstands are recorded in the geological record, being erased during successive highstands (Ruggieri and De Waele, 2014).

3. Plemmirio Marine Protected area (Sicily)

Miocene carbonate rocks form coastal cliffs up to 50 meters high in the Maddalena peninsula, southeastern Sicily. These fossiliferous biocalcarenes and calcirudites of the Monti Climiti Formation (Serravallian-Burdigalian) create a horst structure bounded by NNW-SSE trending normal faults (Grasso and Lentini 1982). The area is characterized by a series of marine terraces located at altitudes centered at 10, 20, 40 and 48 m asl, and two submerged terraces at 10 and 32 m bsl (Di Grande and Raimondo 1982; Guido *et al.* 2013). One of the most extensive karst systems in the area is Pellegrino Cave, over 2 km long, characterized by a branching network of anastomotic passages with typical rounded wall sculpturing (Fig. 2B) more or less parallel to the ancient coastal cliff and the actual coastline. This cave is believed to have formed during MIS 5e (Marziano and Chilardi 2002).

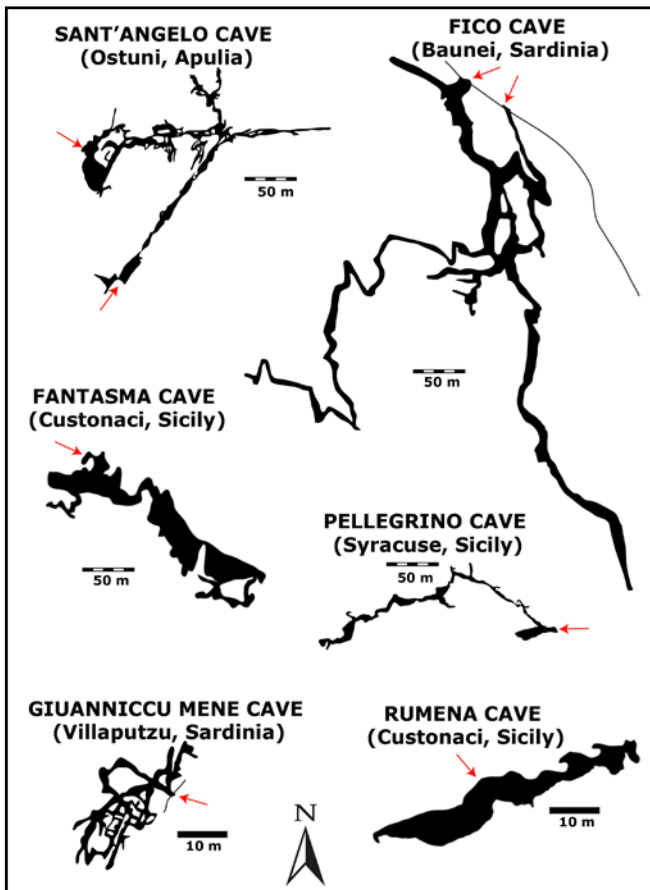


Figure 3. Plan views of the flank margin caves described in the text. Red arrows indicate cave entrances. Note scale for caves is the same for the four bigger ones (above) and the two smaller ones (below).

4. Gulf of Orosei (Sardinia)

This area is one of the most extensive and impressive limestone coasts of Italy, stretching North-South for 37 km from Cala Gonone to Santa Maria Navarrese with vertical carbonate cliffs reaching 700 meters in height (De Waele 2004). This coastal karst is renowned for its very long cave systems, but also extensive underwater cave systems (De Waele *et al.* 2009). Until recently these compact Jurassic limestones were believed to host only epigenic cave systems, shaped by dominant fluvial processes and, only in the areas closest to the coast, by some minor coastal mixing processes. A detailed observation of the morphologies in the Fico Cave, instead, has shown this cave to be mostly formed by salt-fresh water mixing-corrosion processes along major structural discontinuities. In fact, it mostly develops parallel to the coastline, along fractures, lacks the typical scallops and fluvial sediments (except for one smaller but active underwater branch), and has some typical morphologies of mixing dissolution (rounded walls and ceiling, dissolutional notches) (Fig. 2C). The altitude of the cave levels and notches above present sea level indicate the cave to have formed over the last 1 Ma during several sea level highstands, the main level, now at 14 m asl, started to be carved during MIS9 but it developed mainly in the Tyrrhenian age (MIS5e). The higher levels (22, 40, 50 and 63 m asl) in older interglacials, while the now active submerged level at -10 m below sea level probably formed during MIS7. This cave, the only flank margin type of cave preserved in this coastal stretch, sheds new light on the presumed stability of Sardinia's coastlines since Eemian (MIS5e) (D'Angeli *et al.* 2015).

5. Giuanniccu Mene Cave (Quirra, Sardinia)

In the municipality of Villaputzu (Southeast Sardinia), some Middle-Upper Devonian marbles crop out in the isolated Quirra Castle hill at about 1 km from the coastline (Corradini *et al.* 1998; Cabboi *et al.* 2005). This karst relief is bordered to the west and to the south by the Quirra river which flows into the Tyrrhenian Sea crossing a lowland at 8 m asl. These marble outcrops host several small caves, the most important of which (Giuanniccu Mene Cave) reaches 135 meters of development (Bartolo *et al.* 1986). This cave opens at 8 m asl at the southern foot of the hill, on the left bank of the Quirra River, and is occasionally flooded during flash floods. Its labyrinth of small passages is characterized by smooth wall morphologies, a series of extremely well developed cupolas (Fig. 2D), lack of scallops and presence of only small quantities of stream pebbles. These features indicate that this cave was most probably carved by salt-fresh water mixing-corrosion during the Tyrrhenian (MIS5e) highstand, when this part of the floodplain was part of the coastline.

6. Ostuni (Apulia)

The Murge plateau in its southeastern part is dissected by an important fault that is morphologically expressed, striking NW-SE between the villages of Fasano and Ostuni. In this area the Upper Cretaceous Altamura limestones are overlain by the fossiliferous Ostuni limestones of Upper Campanian-Maastrichtian age and form a stepwise morphology of a set of terraces lowering to the Adriatic coast (Delle Rose and Parise 2003; Parise 2011). The Sant'Angelo cave system opens at the foot of one of these carbonate cliffs, probably a fault scarp modified by coastal erosion, at about 150 m asl. This 1.5 km long cave is characterized by a NW-SE striking main passage, developed along a fault-line, and a set of anastomosing wide and low passages with the typical mixing-corrosion morphologies (rounded walls, swiss-cheese morphologies) (Fig. 2E) and lacking scallops or stream sediments. Its elevation above sea level suggests its age to be Lower Pleistocene, and dating of this karst void might help in understanding local uplift rates and timing of these (and lower lying) marine erosion surfaces.

7. Conclusions

Although Italy has several coastal caves, most were described to have formed by marine erosion (wave action) along lithological or structural weaknesses, or by the carving of underground streams fed by the large coastal karst catchment areas and flowing out to the sea through cave passages. The effect of salt-fresh water mixing in the dissolution of these diagenized (telogenetic) carbonate rocks was believed to be important only in the parts of the caves nearest to the sea. The observation of clear signs of coastal mixing-corrosion, such as rounded wall morphologies, in-cave notches, anastomosing passages, and the lack of stream or marine sediments and scallops on the wall in some coastal caves has demonstrated them to be of the flank margin type. This kind of caves is now known from areas very close to the present coastline (e.g. Fico Cave), but also at slightly higher altitudes (e.g. Pellegrino Cave, Giuanniccu Mene Cave), or even rather far from the present coastline and at much higher altitudes (e.g. Sant'Angelo Cave, Rumena Cave, Fantasma Cave). These caves are good past sea level indicators, often better preserved than any other marker at the surface (e.g. tidal notches, marine abrasion platform,

raised beach sediments), and their age determination can help in getting new clues on Pleistocene sea level changes and/or coastal uplift along the western Mediterranean coast.

References

- Antonoli F, Bard E, Potter EK, Silenzi S, Improta S, 2004. 215-ka History of sea-level oscillations from marine and continental layers in Argentarola Cave speleothems (Italy). *Global and Planetary Change*, **43**(1), 57-78.
- Back W, Hanshaw BB, Herman JS, Van Driel JN, 1986. Differential dissolution of a Pleistocene reef in the ground-water mixing zone of coastal Yucatan, Mexico. *Geology*, **14**, 137-140.
- Bartolo G, Lecis A, Puccu S, 1986. Il Monte del Castello di Quirra e le sue grotte. *Guido Bartolo editore*, Cagliari, 91 p. (Italian)
- Belmonte G, Ingrosso G, Poto M, Quarta G, D'Elia M, Onorato R, Calcagnile L, 2009. Biogenic stalactites in submarine caves at the Cape of Otranto (SE Italy): dating and hypothesis on their formation. *Marine Ecology*, **30**(3), 376-382.
- Cabboi N, De Waele J, Ulzega A, 2005. Geomorfositi nel salto di Quirra. *Rendiconti del Seminario della Facoltà di Scienze dell'Università di Cagliari*, **75**(1-2), 173-194.
- Choquette PW, Pray LC, 1970. Geologic nomenclature and classification of porosity in sedimentary carbonates. *AAPG bulletin*, **54**(2), 207-250.
- Cigna AA, Cigna LR, Vido LL, 1963. Quelques considérations sur l'effet-sel dans la solubilité des calcaires. *Annales de Spéléologie*, **18**(2), 185-191.
- Corradini C, Ferretti A, Serpagli E, 1998. The Silurian and Devonian sequences in SE Sardinia. Sardinia Field-Trip Guide book, *Giornale di Geologia* (special issue), **60**, 71-74.
- D'Angeli IM, Sanna L, Calzoni C, De Waele J, 2015. Uplifted flank margin caves in telogenetic limestones in the Gulf of Orosei (Central-East Sardinia—Italy) and their palaeogeographic significance. *Geomorphology*, **231**, 202-211.
- Delle Rose M, Parise M, 2003. Le grotte di Ostuni in relazione alla locale serie stratigrafica. *Puglia Grotte, bulletin Gruppo Puglia Grotte, Castellana-Grotte*, 53-62.
- De Waele J, 2004. Geomorphologic evolution of coastal karst: the Gulf of Orosei (Central-East of Sardinia, Italy). *Acta Carsologica*, **33**, 37-54.
- De Waele J, Schafheutle M, Waelde T, 2009. Speleogenesis of extensive underwater caves along the Gulf of Orosei (Central-East Sardinia, Italy). In: WB White (Ed.), *Proceedings of the 15th International Congress of Speleology*, Kerrville (USA), **1**, pp. 469-476.
- Di Grande A, Raimondo W, 1982. Linee di costa Plio-Pleistoceniche e schema litostratigrafico del Quaternario siracusano. *Geologica Romana*, **21**, 279-309.
- Florea LJ, Vacher HL, Donahue B, Naar D, 2007. Quaternary cave levels in peninsular Florida. *Quaternary Science Reviews*, **26**(9-10), 1344-1361.
- Grasso M, Lentini F, 1982. Sedimentary and tectonic evolution of the eastern Hyblean Plateau (southeast Sicily) during Late Cretaceous to Quaternary times. *Palaeogeography, Palaeoclimatology, Palaeoecology*, **39**, 261-280.
- Guido A, Heindel K, Birgel D, Rosso A, Mastandrea A, Sanfilippo R, Russ F, Peckmann, J, 2013. Pendant bioconstructions cemented by microbial carbonate in submerged marine caves (Holocene, SE Sicily). *Palaeogeography, Palaeoclimatology, Palaeoecology*, **388**, 166-180.
- Marzano C, Chilardi S, 2002. Contribution to knowledge of the Pleistocene mammal-bearing deposits of the territory of Siracusa (southeastern Sicily). *9th ICAZ Conference, Durham, in T O'Connor (Ed.), Biosphere to Lithosphere*, pp. 94-109.
- Myroie JE, Carew JJ, 1988. Solution conduits as indicators of late Quaternary sea level position. *Quaternary Science Reviews*, **7**(1), 55-64.
- Myroie JE, Carew JL, 1990. The flank margin model for dissolution cave development in carbonate platforms. *Earth Surface Processes and Landforms*, **15**, 413-424.
- Myroie JE, Myroie JR, Nelson CS, 2008. Flank margin cave development in telogenetic limestones of New Zealand. *Acta Carsologica*, **37**(1), 15-40.
- Onorato R, Forti P, Belmonte G, Poto M, Costantini A, 2003. La grotta sottomarina lu Lampiùne: novità esplorative e prime indagini ecologiche. *Thalassia Salentina*, **26**, 55-64.
- Parise M, 2011. Surface and subsurface karst geomorphology in the Murge (Apulia, Southern Italy). *Acta Carsologica*, **40**(1), 79-93.
- Plummer LN, 1975. Mixing of sea water with calcium carbonate ground water. In: EHT Whitten (Ed.), *Quantitative Studies in the Geologic Sciences*, Geological Society of America Memoir, **142**, pp. 219-236.
- Ruggieri R, 2015. *Speleological and speleogenetic aspects of the Monti di Capo San Vito (Sicily): influence of morpho-tectonic evolution*. Ph.D. thesis, University of Nova Gorica, Springer edition, 267 p.
- Ruggieri R, De Waele J, 2014. Lower-to middle Pleistocene flank margin caves at Custonaci (Trapani, NW Sicily) and their relation with past sea levels. *Acta Carsologica*, **43**(1), 11-22.
- Smart PL, Dawans JM, Whitaker FF, 1988. Carbonate dissolution in a modern mixing zone. *Nature*, **335**, 811-813.

Geothermal heat flow in caves: Heat Concentration and its Effects on Speleogenesis.

Neville A Michie Ph.D.

Affiliation: Cave Scientist. ACKMA, NSS #39726, 9 Patrick Street, Beacon Hill, NSW, Australia, 2100.

Abstract

A geothermal heat driven convective circulation has been discovered in the chamber over the Lake of the Clouds, Carlsbad, NM. The observations required measurements of a high degree of precision, depending on the MicroPsychrometer, an aneroid altimeter and an appropriate method of data reduction.

A model of heat flow was calculated showing a process of concentrating geothermal heat flow from a wide area. This circulation is in an air-filled cave and it must follow that a similar circulation existed when the cave was water filled. Speleogenesis would have been assisted if not completely driven by this geothermal energy capture which drives circulation and transport of reactants across chemical gradients to aid chemical excavation.

This process is related to other caves and other cave observations at Lechuguilla Cave and Carlsbad Caverns, New Mexico; Jewel Cave, South Dakota; Gough's Cave, Cheddar, U.K. The circulations are part of the mechanisms for formation and transport of manganese dioxide, the evolution and mobility of radon in caves. They cause the interaction between speleogenesis and glaciation which controls cave structure.

Keywords: Geothermal heat concentration, MicroPsychrometer, speleogenesis, radon, manganese dioxide, glaciation

1. Introduction

The small flux of heat to the surface of the Earth known as the Geothermal Heat Flux, has a magnitude on land of about 0.06 W/m^2 . In limestone areas it produces a temperature gradient of about $1 \text{ }^\circ\text{C}$ per 30 metres depth. Measurement of the magnitude and effects of the geothermal flux are normally only available with bore drilling and sampling, so generally only sparse data are available and then only in areas of economic interest.

Measurement of geothermal effects in caves is usually overwhelmed by the cyclic nature and short term effects of surface climate, so it is only in deep caves that geothermal effects become dominant, and conditions become sufficiently constant for measurements to be meaningful.

This does not mean that geothermal flux has no effect in parts of caves that are more influenced by the surface, as geothermal heat flow is continuous and its effects accumulate, while surface conditions cycle with the seasons and weather, and their net effect can be quite small.

An example of geothermal heat flow was discovered in the air column over the Lake of the Clouds in Carlsbad Caverns (Michie 2017b).

2. Method

On an initial visit to the cavern above the Lake of the Clouds, exploratory measurements were made of the barometric pressure, air temperature and humidity. The instruments used were a Thommen 6000m aneroid altimeter and the MicroPsychrometer, a specially developed instrument for precision measurement of air conditions in caves, based on the design of the WMO reference Psychrometer (Wylie and Lalas 1981). The MicroPsychrometer resolves, and is accurate to, 0.01°C and measures a wet-bulb depression temperature to 0.01°C , (about 0.1 % RH), while sampling about a cubic meter of air. The instrument has a large LED readout and so can be read without the observer entering the zone where a human body

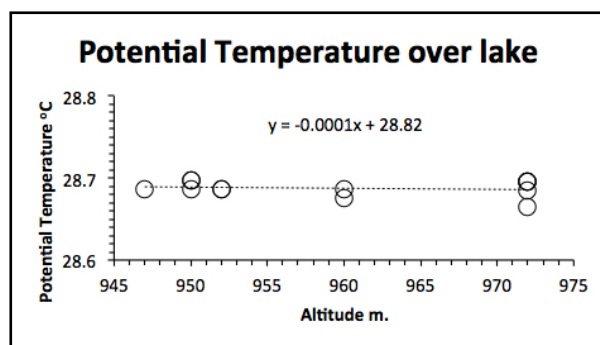


Figure 1.

would thermally contaminate the measurements. The measurements were used to calculate the thermodynamic properties of the air; temperature, relative humidity, dew-point temperature, mixing ratio, enthalpy and most significantly potential temperature, according to the methods in (Wylie and Lalas 1981) and (ASHRAE 1989).

At Jewel Cave, SD, observations were made of the crystal lined tunnels and general air movements and their response to barometric pressure variations (Michie 1998a).

At Gough's Cave, Cheddar, UK, an extensive study of air movements and airborne radon daughter concentrations was made to locate the source of the radon (Michie 1998b).

3. Results

The measurements from the chamber over Lake of the Clouds showed a lapse rate which was very close to the dry adiabatic lapse rate, (DALR), see Figure 1, and this could not be explained until, several years later, potential temperature, see Figure 2, was added to the parameters that were calculated. Then the extraordinary uniformity was observed in the potential temperature which was quite constant. Only a thermal convective circulation, and only geothermal heat flow, could be responsible for this situation so finally direct observation of geothermal heat flow in caves had been made.

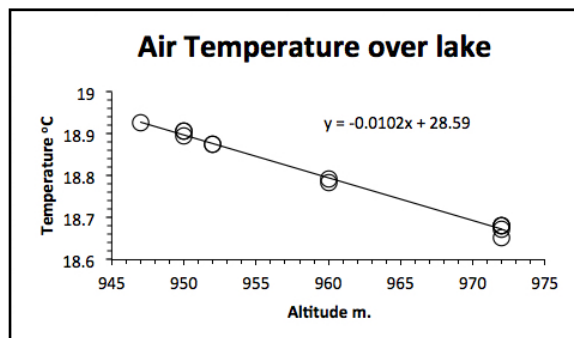


Figure 2.

Thermal modelling was used to analyze the process in the cave (Michie2017a).

Jewel Cave observations: Although there are large passages these did not seem to connect to the surface to be part of the surface drainage system. Nor were they part of an underground river system. Where they started and where they finished was a mystery. These tunnels have scattered deep deposits of manganese dioxide on the floors and the walls were lined with calcite crystals.

Gough's Cave observations: the measurement and analysis of the air circulation and radon daughter measurements showed that the radon was evolving from the flowing underground water, and so the radon was being transported in the flow of water from an unknown source.

4. Discussion

The geothermal temperature gradient of about 30 degrees per km is much more than the adiabatic lapse rate of both water (0.1 K/km) and air (10 K/km) so that fluid filled cavities in karst rock are thermally unstable. At the size range of pores in rocks this has little effect. The contents of larger cavities are effectively isothermal, because free convection and cavity radiation are greatly more efficient at upwards heat transport than thermal conduction in the surrounding limestone. These voids in the limestone offer an easier path for heat flow to the surface so that adjacent heat flow is attracted to flow through the cavities.

Modelling (Michie 2017a), shows that this process of geothermal heat capture increases the local heat flux in caves by orders of magnitude. See Figure 3.

As the cavities become larger the degree of heat capture increases by about the square of the cavity height.

The thermal convective circulation over Lake of the Clouds transports heat and water from the lake to the walls and roof of the chamber. A value of 500 watts was found for the amount of heat captured by the chamber. Further discussion of the air circulation is found in (Michie 2017a, b).

The presence of the thermal circulation in this chamber which is air-filled leads to the conclusion that when the chamber was being formed and was filled with water a similar amount of geothermal heat would have been captured and would have driven a convective circulation in the water.

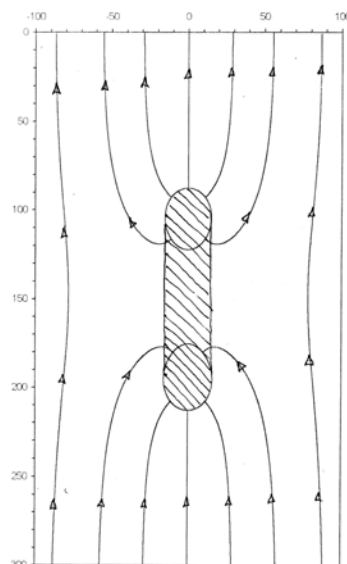


Figure 3. Model of heat flow in a 100m. high chamber in a cave.

To deduce the effects of this circulation we now consider the observations of Jewel Cave. This cave has considerable vertical extent and so when water filled it would have captured enough geothermal heat to drive large convective circulations. Water from the upper levels was circulated through the vertical extent of the cave and through the lower levels.

From the time of deposition on a sea bed, limestone has been in a eutrophic state with organic material absorbing all oxygen and reducing minerals. This situation has left a gradient of oxygen demand which increases with depth. When geothermal circulation develops oxygen from the surface is transported across this gradient. Reduced minerals such as manganese sulphide are oxidized to soluble sulphates while sulphuric acid is formed. The solution of the minerals and corrosion by the sulphuric acid and carbon dioxide from oxidizing organic deposits excavates the limestone and extends the geothermal circulation while the soluble minerals are carried up and away to mix with the with the surface groundwater. Bacteria, stygofauna and fungi, supported by the oxygen and organic material, transpire carbon dioxide and add to the corrosion of the limestone. The deposits of manganese dioxide found in Jewel Cave are remnants of this process and were deposited in a secondary process when the dissolved manganese sulphate absorbed more oxygen near the surface and deposited colloidal manganese dioxide. Many other minerals may have been involved in similar reactions but have not left such a permanent trace.

The velocity of water circulations may be quite low, water is very efficient at transporting heat.

The passages would not then have flow inertia effects like scallops, but surfaces would be sculpted by boundary layer effects which would selectively dissolve prominences.

The unusual calcite crystals lining tunnels in Jewel Cave the tunnels may be a consequence of a common ion effect with the sulphate ions, and CO₂ introduced by the groundwater.

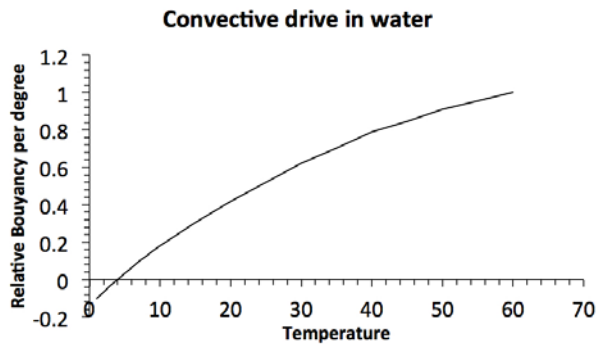


Figure 4. Density of water

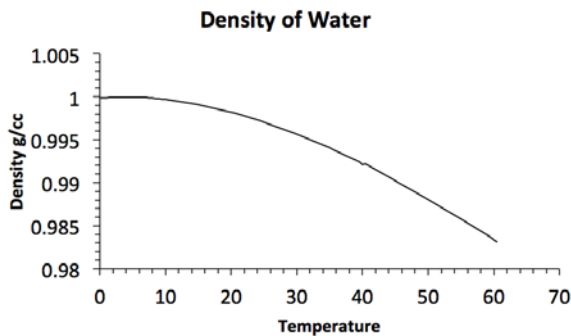


Figure 5. Rate of change of density with temperature.

More evidence that supports the geothermal circulation excavation model is the way Jewel Cave avoids the surface. The tunnels in the cave rise and fall parallel to the surface topography but generally do not connect. The excavation of this cave would have taken place during an ice-age with a surface of permanent ice and possible permafrost. It is a characteristic of water that its density has a maximum at about 4 °C, (Figure 4) and the factor of buoyancy per degree (Figure 5) that drives a convective circulation would have become negative at low temperatures. This sets the conditions for a thermal circulation being unable to continue within hundreds of meters of the surface.

The glaciation negated the thermal circulations above a depth in the rock where significant thermal drive could occur. With a temperature gradient of one degree per 30 metres, this would be about 240 metres deep before the temperature would be above 8 °C.

The mechanism of sulphide oxidation and transport may be applicable to the occurrence of radon in caves. It long was a puzzle how radon from low concentrations of Uranium in rocks could reach the surface in the 5 day window when the isotope was in gaseous form. Diffusion of single atoms in crystalline material is extremely slow. However, parent species like uranium may be in a reduced form of a sulphide in the rock and would be subject to oxidation, solution and removal in the geothermal excavation process, and then would be transported to the surface where increased oxygen concentrations could precipitate the Uranium as an oxide onto the surface of calcite crystals. From this surface it could release the radon gas atom into the surrounding air or water. The investigation of radon in Gough's Cave, Cheddar, UK, located the highest

concentrations over the flowing water of the underground river (Michie 1998b).

Lechuguilla Cave with its extensive gypsum deposits and many deep chambers must host geothermal air circulations now and was probably formed by geothermal excavations when water filled.

The geothermal convection processes in caves are also important to the stygofauna in ground water and Karst systems as food sources and oxygen for respiration will depend on the continuation of the circulations. A real threat to these conditions is the exploitation of geothermal heat by wells designed to cool the rock to "mine" geothermal energy.

5. Conclusion

The (small flux of heat to the surface known as the) Geothermal Heat Flux can become a significant factor in cave climate and in speleogenesis.

Observations to verify this were elusive, until a combination of improved instrumentation and a better parameter for analysis were used on data from above the Lake of the Clouds at Carlsbad Caverns.

The air circulation it is shown is driven by geothermal heat energy. It follows that when the cave was water filled, a similar circulation would have existed, and been part of the process that excavated the cave.

Modelling, using temperature as a parameter, was critical to the identification of this process, and provided verification and quantification of the process in the Lake of the Clouds chamber. The confirmation of the modelled predictions allows this model to be applied to other caves to explain observed phenomena.

Jewel Cave SD shows evidence of geothermal convection of water and chemical excavation, with the geothermal drive interacting with glaciation.

Lechuguilla Cave has vast excavated chambers which will show geothermal air circulations.

At Gough's Cave, Cheddar, UK the release of radon fits a pattern of geothermal chemical excavation and deposition of uranium oxide on the surface of calcite where it is then available for the rapid release of radon gas into the flowing cave water.

Geothermal energy exploitation poses great threats to groundwater species that rely on geothermal circulations.

References

- ASHRAE, 1989 Psychrometrics In: RA Parsons (Ed.) *ASHRAE Fundamentals*, Chapter 6, American Society of Heating, Refrigeration and Air Conditioning Engineers, Inc. Atlanta pp 6.1-6.10.
- Michie NA, 1998a. Field notes – Jewel Cave S.D. March, 1998 Climate survey hosted by Mike Wiles. Unpublished.

Michie NA, 1998b. Field notes – Gough's Cave, Cheddar, UK, July 1998, a project with John Gunn's Limestone Group, Huddersfield University. Unpublished.

Michie NA, 1999. Field notes – Carlsbad 30th October 1999, Routine measurement and data were gathered on a familiarization trip with Stan Alison. Unpublished.

Michie NA, 2017a. Geothermal Heat Flow in Caves: Modelling of Geothermal Heat Flow. This Conference.

Michie NA, 2017b. Geothermal Heat Flow in Caves: The Physics of the Geothermal Rims in Carlsbad Cavern. This conference.

Wylie RG, Lalas T, 1981. *The WMO Reference Psychrometer*. CSIRO, Australia, Sydney. pp. 58.

A Chronology of Karstification In Puerto Rico Using Cosmogenic Dating Of Cave Sediments

Thomas E. Miller¹, Gilles Brocard², Jane K. Willenbring³

Affiliation: ¹Department of Geology, University of Puerto Rico, Mayagüez Campus, HC1 Box 3555, Las Marias, PR 00670

²School of Geosciences, University of Sydney, Camperdown Campus, 2006 NSW, Australia

³Scripps Institution of Oceanography, University of California San Diego, Vaughan Hall 210, 8675 Discovery Way, La Jolla, CA 92093 USA

Abstract

The geomorphic history of cave development in Río Camuy and Río Tanamá agrees with cosmogenic dating of sediments in these two large cave systems. Local surveys of caves have shown that the present neighboring rivers of the Camuy and Tanamá were once united by large cave conduits down which the ancestral Camuy flowed east along the structural strike to the Tanamá. This combined flow [about $6 \text{ m}^3 \text{ s}^{-1}$] allowed the Tanamá River to maintain surface flow while down-cutting northward in a deep canyon, following the dip of the limestone to the Atlantic Ocean. Thick sediments in two large caves (close to sea level at the Tanamá outlets) were analyzed using *in-situ*-produced ^{10}Be and ^{26}Al in river-borne quartz, and provided burial dates of 4.6 and 4.7 My (Million years old), a minimum age to begin karstification. Fossils found in young upper-Pliocene aged carbonates suggest an upper age for uplift of Puerto Rico of 5.5- 6 My. The cave conduit that had channeled the Camuy discharge to the Tanamá was active until about 4.5 My, after which it was abandoned when the Camuy River developed its own route north following the dip. Over the following million years - to 3.6 My, new groups of conduits formed and were subsequently abandoned along upper reaches of the Camuy River; the currently active lower galleries of the Camuy Caves have developed since then. Deprived of the Camuy discharge, the Tanamá was also subsequently pirated underground through nine caves.

Keywords: cosmogenic dating, caves, karst, Puerto Rico

1. Introduction

Cave conduit formation and sequential abandonment influence the evolution of the surrounding drainage surfaces and the regional topography. The differential decay of the radioactive cosmonuclides ^{10}Be and ^{26}Al is now frequently used with other methods [e.g. speleothem U-Th, paleo-magnetic fields], or alone, to date the burial of sediments in caves, broadening the accuracy of boundary ages for cave formation (Stock *et al.* 2005). Cosmogenic burial dating is typically best suited for dating sediments where depositional age ranges between a few hundreds of thousands of years to 6 My. Cave sediments experience less weathering and reworking than their surface equivalents stored in river terraces, and are also protected from erosion over much longer periods. Spatial correlations between deposits in cave systems and surface features are also aided by the preservation of geometrical and cross-cutting relationships between sequentially-abandoned cave conduit straths. With accurate cosmogenic dating, other useful geologic properties can also be extracted such as rates of denudation, and resistance of different rocks to erosion, as was determined in the recent study by Brocard *et al.* (2016) using caves in Puerto Rico. From this same set of cave data we chose two well surveyed cave systems in Puerto Rico exceeding 20 km in extent to test the degree of agreement between cave sediment burial dating and the timing of significant cave development previously-determined from the geomorphic relationships between conduits, and between conduits and surface valleys. This study represents the first cosmogenic dating of karst conduits in Puerto Rico and the Caribbean.

Deposition of reefal carbonates over the recently emerged Puerto Rico landmass ended in the Early Pliocene time with the deposition of the 5.6 My Quebradillas Limestone. Sedimentation ended due to rapid 4-5° northward tilting of the Puerto Rico-Virgin island tectonic block (van Gestel *et al.*,

1999; ten Brink, 2005), which forced its crowning reef platform to sink 4.5 km into the Puerto Rico Trench, while the southern ledge of the platform emerged. Removal of these Miocene carbonates by shoreline and continental erosion exposed the underlying Tertiary shales and the Jurassic-Paleogene volcanic basement. Erosion has since restricted the E-W outcropping of the carbonate belt to a maximum 25 km N-S width along the northern coast, which rises inland with an average topographic slope of 2° up to an elevation of about 400-500 m.

The northern homoclinal 4° dip of its beds produces a series of landward-facing cuestas. Intense karstification since emergence has produced a dramatic epikarst, and the rivers that initially flowed across the emerged carbonates were soon diverted into it (Monroe, 1976; Moussa, 1987).

We have studied the timing of sinking and integration of two of the most extensive cave systems of Puerto Rico: those of Río Camuy and of Río Tanamá. Although both streams have similar elevations, discharges, catchment areas, and climate, their geomorphology and cavernous development are quite different due to distinct geology and chronology of development. Both cave systems, however, have been valuable in their ability to provide information concerning the age of karstification of the Camuy Karst Block, and the uplift of Puerto Rico and its erosional history (Miller, 2009). Both streams initiated side by side over the volcanoclastic rocks of the Central Cordillera before flowing north, towards the Atlantic Ocean, across the Oligo-Miocene sedimentary cover. They first encountered the Oligocene San Sebastian Shales and then the Miocene Lares Limestone, into which they sank within two 2 km after contact. The subterranean Río Camuy has produced more than 20 km of surveyed cave passages grouped into conspicuous levels (straths) of galleries that exhibit lateral and vertical offsets. Río Camuy meanders underground over a surface straight

distance of 11 km before reappearing at a series of baseflow and wet season resurgences hosted within the chalky Cibao Formation. Río Tanamá flows within a deep gorge through Tertiary limestones and across exhumed hills of Cretaceous volcanoclastic rocks before joining Río Grande de Arecibo, 16 km farther downstream in a straight line. The river successively passes beneath three travertine bridges and six bedrock caves of variable length, which altogether have a cumulative length of about two kilometers (Miller, 2004; 2010).

2. Cosmogenic Dating And Methods

Terrestrial cosmogenic ^{10}Be and ^{26}Al are produced in the O and Si atoms in quartz crystals in the uppermost few meters beneath the Earth's surface by high energy cosmic rays. Cosmogenic production during subsequent downslope transport, fluvial transport, and transitory storage in floodplains is generally regarded as minimal compared to the initial exhumation in mountainous settings. Once buried in a cave, the grains are shielded from further production and the original $^{26}\text{Al}/^{10}\text{Be}$ ratio of ~ 7 then decreases predictably with time due to faster decay of ^{26}Al compared to ^{10}Be (half-lives of 0.71 and 1.4 My, respectively). The concentration of these isotopes in buried quartz grains can thus be used to retrieve the minimal burial age of the sediments (Lal, 1991; Granger and Muzikar, 2001).

We sampled former sandy and gravelly underground deposits to insure proximity to the former river channels, and minimize the uncertainties typically associated with overbank deposits that may have been deposited in abandoned galleries during exceptional floods or following lower-conduit choking long after gallery abandonment. We therefore assume that the range of deposits only slightly postdate cave formation, and immediately predate cave abandonment and river rerouting towards lower elevation conduits. Quartz grains were extracted from the sandy matrix of sandy-gravelly alluvium and from igneous gravel of diorite, quartz diorite and granodiorite from outcropping plutonic bodies located in the headwaters. Quartz isolation, purification, and dissolution; ion exchange extraction; and precipitation of beryllium were performed at the University of Pennsylvania Cosmogenic Isotope Laboratory (PennCIL) following an adaptation of the technique of Kohl and Nishiizumi (1992). Inductively coupled plasma optical emission spectroscopy (ICP-OEEOS) measurements indicated elevated total Al concentration in quartz after etching, higher in the standard fraction (0.25–0.5 mm) than in the 0.5–1.0 mm and 1–2 mm fractions, which were used to gain dating precision. Selected fractions had Al concentration ranging from 25 to 90 ppm that did not require ^{27}Al carrier addition. About 220 μg of ^9Be carrier (Scharlau BE03450100 carrier batch 2Q2P—14 October 2010) with a measured $^{10}\text{Be}/^9\text{Be}$ ratio of $1.5 \cdot 10^{15}$ was added to each sample during quartz dissolution. Ti and Fe were precipitated at pH 13 and removed prior to the ion exchange chromatography separation of Be and Al. Be and Al hydroxides were precipitated at pH 8–9, oxidized to BeO and Al_2O_3 over an open butane-propane flame and mixed with Nb and Ag, respectively. $^{10}\text{Be}/^9\text{Be}$ and $^{26}\text{Al}/^{27}\text{Al}$ ratios were measured by accelerator mass spectrometry (AMS) at PRIME Laboratory, Purdue University. Results were normalized to standard 07KNSTD for ^{10}Be and 319500KNSTD for ^{26}Al (Nishiizumi *et al.*, 2007, Balco *et al.*, 2008) with an assumed $^{10}\text{Be}/^9\text{Be}$ ratio of $2.79 \cdot 10^{11}$

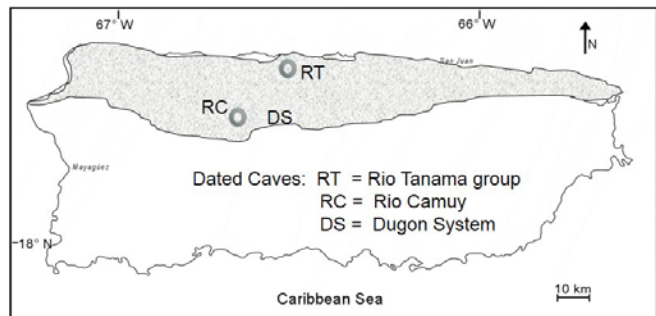


Figure 1. Puerto Rico and location of the sample sites. The shaded arrow is the karst area bordering the Atlantic Coast and rising inland; these Tertiary rocks comprise 90% of the Island's karst.

(Balco, 2009). $^{10}\text{Be}/^9\text{Be}$ and $^{26}\text{Al}/^{27}\text{Al}$ ratios of the procedural blanks were 2.8 ± 0.8 – $3.4 \pm 0.7 \cdot 10^{15}$ and $2 \pm 6 \cdot 10^{15}$, respectively. Reported 1 sigma uncertainties (Table 1) encompass uncertainties on Purdue accelerator mass spectrometry measurement, uncertainties on the primary standard, an estimated 2% uncertainty on the Be concentration of the carrier solution, and uncertainties on the procedural blanks. The production ratio of $^{26}\text{Al}/^{10}\text{Be}$ and the decay constants are those used in the CHRONUS online calculator (Balco *et al.*, 2008) version 2.2.1 (Balco, 2009).

3. Collection

The framework of the Río Tanamá and Río Camuy caves is well known, and most of the significant conduits were surveyed decades ago. However, a noteworthy finding of the recent decade was the Dugón System, a dissected series of three large, previously-connected cave conduits lying at higher elevation (which are therefore older) than the oldest known Camuy cave headwater fragments. Their elevation declines from west to east, indicating a flow gradient directly towards the Tanamá catchment. We therefore surmise that these caves once routed water from the Río Camuy watershed to the Río Tanamá along a generally-strike-oriented path (Miller, 2009, 2010). They augmented the discharge of Río Tanamá to $6 \text{ m}^3\text{s}^{-1}$, allowing that river to armor its bed with clastic sediment and maintain a surface flow probably all the way to Río Grande de Arecibo, following the structural dip and the trend of a large surface lineation. Each of these segments, namely the ancient Tanamá, the Dugón System, and the recent Camuy, contains dateable sediments that record important events of their evolution (Fig. 1).

We sampled two large, filled, ancient cave conduits near the mouth of Río Tanamá [Group RT]. They are exposed in the walls of crosscutting younger conduits and preserve 10 to 15 m-thick deposits of sand and rounded stream gravel and cobbles. One of these is crosscut by Cueva Sorbetos, which is accessed through a cliff wall above the Río Tanamá (at 90 m asl), while the other is exposed in Cueva Jaguar just above the post-glacial coastal filling of the Río Grande de Arecibo valley (20 m asl), and interpreted as a likely former outlet of the Tanamá to that river. These passages may continue farther downstream below current sea level, onshore below the coastal plain, and/or offshore, as caves or alluviated river valleys, due to post-emergence tilting of the carbonates (Meyerohoff, 1927). Thick (>10 m) accumulations of river sediments farther upstream in one of the caves of the Dugón System

[DS] record the approximate time of separation and diversion of the Camuy River to its present northward course.

The uppermost Camuy passages [RC] postdate the abandonment of the Dugón conduits and are organized in several segmented sections on both sides of the present Río Camuy above the ponor that marks the current entrance to its subterranean course. Presumably, other passages used to exist farther upstream and have been eroded away by incision and enlargement of the Río Camuy gorge. The RC fossil conduits all head north down the structural dip and are younger, or contemporary to the Dugón conduits; several contain clastic sediments of high elevation and great age.

Results And Discussion

We sampled eight deposits in six caves for $^{10}\text{Be}/^{26}\text{Al}$ dating (Fig. 1). Three geomorphic events of known relative age are expected to closely agree with ages provided by these measurements (Table 1), namely: 1, the initiation of the karst cave systems, which most closely follows the emergence of the carbonate platform, and therefore most closely follows the deposition of the Quebradillas Limestone (post-5.6 My), 2, the diversion of the Camuy River from its combined flow of Ríos Camuy and Tanamá, and the abandonment of the Dugón System, and 3, the development of the younger, modern set of vertically-tiered Camuy cave conduit straths.

$^{26}\text{Al}/^{10}\text{Be}$ burial ages (Table 1) are in broad agreement with the relative time scale of known geomorphic events, although some measurements carry large uncertainties. These uncertainties result from the fact that the measured quartz grains have a naturally elevated ^{27}Al content, and that the caves are quite old enough to result in a decay of ^{26}Al so great that it brings the $^{26}\text{Al}/^{27}\text{Al}$ ratio close to the threshold of detection. First, the absolute ages of the ancient, united lower Tanamá conduits (Cuevas Sorbetos and Jaguar), are, at 4.6 My, 4.7 My, and 4.4 My, consistently younger than the age of emergence of the carbonate platform (after 5.6 My). Second, these ages are, as expected, at or older than that of the pre-piracy Dugón System (4.5 My). Third, the ages of the post-piracy conduits of

the Camuy System are the same, at 4.5 My for Cueva Oscura (the highest of these caves), or less (3.6 and 4.0 My) for the nearby, lower elevation Cueva Ensueño, and finally 4.0 My for the extensive Cueva Humo level which is about 40 m above the modern underground water course of Río Camuy.

A likely history for the major conduits draining the Camuy Karst Block is therefore uplift beginning about 5.5 My ago, and commencement of epikarst erosion shortly thereafter. Within a few hundreds of thousands of years, rivers had established allogenic catchments on non-soluble rocks, flowing down-dip to the Atlantic Ocean. The largest rivers were able to maintain surface courses by cutting canyons entrenched 200 m or more into the uplifting limestone, while smaller streams that did not meet the minimum flow threshold ($6 \text{ m}^3 \text{ s}^{-1}$) to armor their beds were diverted underground.

The combined eastward-flowing Río Camuy and northward-flowing Río Tanamá were thus able to maintain surface flow across the karst platform, perhaps for several hundreds of thousands of years, cutting a deep, narrow canyon. Once the Camuy River split off to flow north approximately 4.5 My ago, both the Tanamá and Camuy rivers became unable to maintain surface discharge. The Tanamá then cut half a dozen caves down to a new base level, leaving eroded stream-cut notches on top of all the new bedrock cave bridges.

The Camuy's path to the Atlantic today is more direct and efficient than was its shorter and lower gradient underground to the Tanamá, however its redirection may have been the ultimate result of the large combined stream incising deeply enough to encounter and exhume older volcanoclastic rocks. That these rocks (at least in this area) are more resistant to erosion than limestone is shown by the abandonment of a large valley of the Tanamá stream incised into one of these exhumed hills, and its subsequent down-cutting > 40 m alongside the contact of the limestone and the volcanoclastics, forming a large cave. The difficulty and delay in increasing the gradient would have made the Río Camuy's route north increasingly attractive, to the point of diversion.

Table 1. ^{10}Be and ^{26}Al Concentrations and Burial Age of Quartz in the Caves

Cave ^a	Grain Size (ϕ)	East (deg) ^b	North (deg) ^b	Elev (m)	[^{10}Be] 10^4 at g^{-1}	[^{26}Al] 10^4 at g^{-1}	$^{26}\text{Al}/^{10}\text{Be}$	Burial Age (My)
Lower Tanamá Group								
SOR	4–2	-66.72	18.40	90	3.91 ± 0.30	2.86 ± 0.28	0.73 ± 0.09	4.6 ± 0.6
JAG	-3–4	-66.69	18.39	20	3.82 ± 0.19	2.52 ± 5.6	0.7 ± 0.2	4.7 ± 1.0
	4–2				4.43 ± 0.38	3.56 ± 0.37	0.80 ± 0.11	4.4 ± 0.6
Cueva Larga (Dugón System)								
LAR ^c	1–0	-66.81	18.32	330	3.40 ± 0.21	2.50 ± 0.32	0.74 ± 0.10	4.5 ± 0.6
HUM	-3–4	-66.83	18.31	290	5.89 ± 0.22	5.57 ± 2.68	0.9 ± 0.5	4.0 ± 2.0
ENS	0–1	-66.8	18.32	310	6.46 ± 0.45	7.76 ± 0.54	1.20 ± 0.12	3.6 ± 0.4
	4–2				7.44 ± 0.40	6.96 ± 0.47	0.94 ± 0.08	$4.0 \pm .4$
OSC	1–0	-66.82	18.32	340	5.45 ± 0.29	4.11 ± 0.36	0.75 ± 0.08	4.5 ± 0.5

^aCave Names: JAG = Jaguar, SOR = Sorbetos, LAR = Larga, HUM = Humo, ENS = Ensueño, OSC = Oscura

^bLocation of cave entrances (purposely imprecise for the sake of cave preservation).

^cThe Larga deposit was sampled along the descending conduit about 30 m below the highest entrance. Analyzed sediment grain size fraction given in phi scale with particle diameter $D = D^0 2^{-\phi}$ with $D^0 = 1 \text{ mm}$.

The rest of the Camuy caverns' history is that of successive northward development, with vertical abandonment of lower-gradient passages and galleries, occurring over the next million years (3.6 My). More sampling of large burial deposits, and locating new sites, is needed to expose the details of each level's development.

4. Conclusions

The results of the $^{26}\text{Al}/^{10}\text{Be}$ dating process (Table 1) are in broad agreement with the relative time scale of known geomorphic events:

1. The times of cave sediment burial in Cuevas Sorbetos and Jaguar (4.4 My, 4.6 My, 4.7 My) are more recent than those of the Pliocene Quebradillas Fm. (5-6 My), *yet*
2. Older than that of pre-piracy Dugón System (4.5 My).
3. For post-piracy conduits of the Camuy System, the dates are the same 4.5 My for Cueva Oscura (the highest of these caves), but are 3.6 and 4 My for the nearby but lower elevation Cueva Ensueño, and finally 4 My for the extensive Cueva Humo strath which is about 40 m above the modern underground flow of the Río Camuy.

The study shows that information can be obtained from cosmogenic dating of cave-buried sediments in terms of absolute dates that can be used to apply temporal limits to important geologic events.

Future work can be broadened to aid in determining rates of denudation, aggradation, uplift, etc. by distinguishing between the several straths within the Río Camuy caves. Other cave data from elsewhere on the island can also be added to that of local speleothem data to combine their regional stories with that of the Camuy Karst Block.

Numerous surface stream terraces and straths of the karst areas also need to be examined to see how they relate to the cavern data. Abundant instances of catchment piracy exist in the volcanoclastic areas that can probably explain some of the migration history of the subterranean straths. Finally, the hundred-vertical meters of offshore karst presently drowned and alluviated by sea level rise can to some extent be understood by analyzing the cosmogenic data associated with the mobile knickpoints and stream gradients common in the mountains of Puerto Rico.

Acknowledgments

Marcie Occhi, Virginia Department of Mines, Minerals, and Energy, Charlottesville, Virginia.

This work was supported in part by the NSF-funded Luquillo Critical Zone Observatory (LCZO; EAR-1331841) and NSF grant 1349261.

References

Balco G, 2009. ^{26}Al - ^{10}Be exposure age/erosion rate calculators: Update from v. 2.1 to v. 2.2, CRONUS Online Calculator. Available at <http://hess.ess.washington.edu>.

Balco GJ, Stone O, Lifton N A, and Dunai TJ, 2008. A complete and easily accessible means of calculating surface exposure ages or erosion rates from ^{10}Be and ^{26}Al measurements, *Geochron.*, **3**, 174–195.

Brocard, GY, Willenbring JK, Miller TE, and Scatena FN, 2016. Relict landscape resistance to dissection by upstream migrating knickpoints, *J. Geophys. Res. Earth Surf.*, **121**, doi:10.1002/2015JF003678.

Granger DE, and Muzikar PF, 2001. Dating sediment burial with *in situ*-produced cosmogenic nuclides: Theory, techniques, and limitations, *Earth Planet. Sci. Lett.*, **188**, 269–281.

Kohl, CP, and Nishiizumi K, 1992. Chemical isolation of quartz for measurement of in-situ-produced cosmogenic nuclides, *Geochem. Cosmochim. Acta*, **56**, 3583–3587.

Lal D, 1991. Cosmic ray labeling of erosion surfaces: In situ nuclide production rates and erosion models, *Earth Planet. Sci. Lett.*, **104**, 424–439, doi:10.1016/0012-821X(91)90220-C.

Meyerhoff HA, 1927. Tertiary physiographic development of Porto Rico and the Virgin Islands, *Bull. Geol. Soc. Am.*, **38**, 557-576.

Miller TE, 2004. Surface and subterranean drainage piracy, reorganization, and knickpoints of the Río Tanamá and Río Camuy, Puerto Rico. *Geological Society of America Annual Meeting, Abstract with Programs* **36**(5):11.

Miller TE, 2009. Puerto Rico caves and karst. In: AN Palmer and MV Palmer (Eds). *Caves and Karst of the U.S.A.* National Speleological Society, Alabama, U.S.A., p. 332-337, 339-343.

Miller TE, 2010. Stream Pirates of the Caribbean: Tanamá and Camuy Rivers in the Northern Karst of Puerto Rico. *Espeleovista Puerto Rico*, Federación Espeleológica de Puerto Rico. Núm. 2, 2010, pp. 8-13. 9 Figures. http://www.cuevaspr.org/revista_espeleologica/espeleovista_puerto_rico_num_2.pdf (access 25 Jan 2017)

Monroe WH, 1976. *The karst landforms of Puerto Rico*, US Geological Survey Prof. Paper 899, pp. 69.

Moussa MT, Seiglie GA, Meyerhoff AA, and Taner I, 1987. The Quebradillas Limestone (Miocene-Pliocene), northern Puerto Rico, and tectonics of the northeastern Caribbean margin. *Geological Society of America Bulletin*, **99**(3), 427.

Nishiizumi K, Imamura M, Caffee MW, Southon JR, Finkel RC, and McAninch J, 2007. Absolute calibration of ^{10}Be AMS standards, *Nucl. Instrum. Meth. Phys. Res. Sect. B: Beam Interactions with Materials and Atoms*, **258**, 403–413.

Stock GM, Granger DE, Sasowsky ID, Anderson, RC, Finkel RC, 2005. Comparison of U–Th, paleomagnetism, and cosmogenic burial methods for dating caves: Implications for landscape evolution studies. *Earth and Planetary Science Letters*, **236** (2005), 388–403.

ten Brink US, 2005. Vertical motions of the Puerto Rico Trench and Puerto Rico and their cause, *J. Geophys. Res.*, **110**, B06404, doi:10.1029/2004JB003459.

van Gestel, J-P, Mann P, Grindlay NR, and Dolan JF, 1999. Three-phase tectonic evolution of the northern margin of Puerto Rico as inferred from an integration of seismic reflection, well, and outcrop data, *Marine Geol.*, **161**, 257–286.

Tracing the origin of cave sands: State of the art in the Moravian Karst

Jiří Robert Otava

Affiliation: Czech Geological Survey, Leitnerova 22, CZ-658 69 Brno, Czech Republic; jiri.otava@geology.cz

Abstract

The analyses of translucent heavy minerals in cave sands has brought good results in provenance studies due to distinct composition of assemblages. In the case of Moravian Karst, Czech Republic, there are several specific “end members” controlled by surrounding rock complexes. **Granitoids** and respectively Devonian clastics at the western vicinity of Moravian karst limestone strip are rich in **amphibole, epidote and zircons**. The **Northerly complex of lower Carboniferous flysch deposits** (Culmian facies turbidites) has brought a mixture of **epidotes and garnets**. The **Eastern neighbourhood flysch deposits** has also been a source of **garnets**. **Cretaceous paleokarst** deposits have most important typomorphic minerals **staurolite and kyanite**. **Miocene Otnangian sands** are almost always rich in **staurolite**. Finally, the **Pleistocene loesses** have a typical **amphibole-garnet mixture**. That is why the comparison and evaluation of translucent heavy mineral assemblages of allochthonous sands should serve in the caves of Moravian karst (and thus off course in many karst caves of the world) as a key to their source and/or their origin. Final task is to understand better the history of karst, or more often of the paleokarst processes.

Keywords: cave sands, provenance, heavy minerals, paleokarst.

1. Introduction, geological background

Moravian Karst is a S-N trending limestone strip between Brno City in the south and Sloup Village in the north, some 1-4 km wide and about 25 km long. It is surrounded with wide variety of non- karstic rocks (Fig. 1). Limestones form generally a morphological depression and the surface drainage pattern in the northern, eastern, and western vicinity continues from non-karstic rocks deep below the limestone surface. Provenance studies done on ancient cave sands are actually an analogue to recent water tracing tests. The “tracers” of the past are the translucent heavy minerals transported into the cave corridors and rooms from various sources during the geological and paleokarst history.

Provenance studies are an important tool for understanding the directions of movement of allochthonous cave deposits in the past in any karst area. Gravel (psaphitic) sediments reflect directly the source and pebble analysis is a relatively simple and direct method for provenance determination. In the absence of gravel deposits, the finer fraction sediments can be investigated. The information about source involved in sandy (psammitic) cave sediments is usually more complicated and “macroscopically” hidden. Hundreds of analyses of heavy mineral assemblages both from source rocks and from cave sands were done in Moravian karst and its surrounds over the last decades. Step by step many specific mineral assemblages and sources were defined and proved. Thus a good background for recent provenance studies was prepared. Recently almost any assemblage analyzed from the cave sands in Moravian Karst can be attributed to one or more sources.

2. Heavy mineral assemblages

2.1. Methods

Several hundred cave sands were sampled together with rocks of all geological formations surrounding the Moravian Karst. Samples of solid rocks were disaggregated by a hydraulic crusher. All samples of crushed rocks and cave sand were wet sieved to retention 0.25 – 0.6 mm size fraction. Forty grams of each sample were used for separation in tetrabromethane ($C_2H_2B_4$, $d=2,96 \text{ g/cm}^{-3}$). Between 150 and 800 grains of

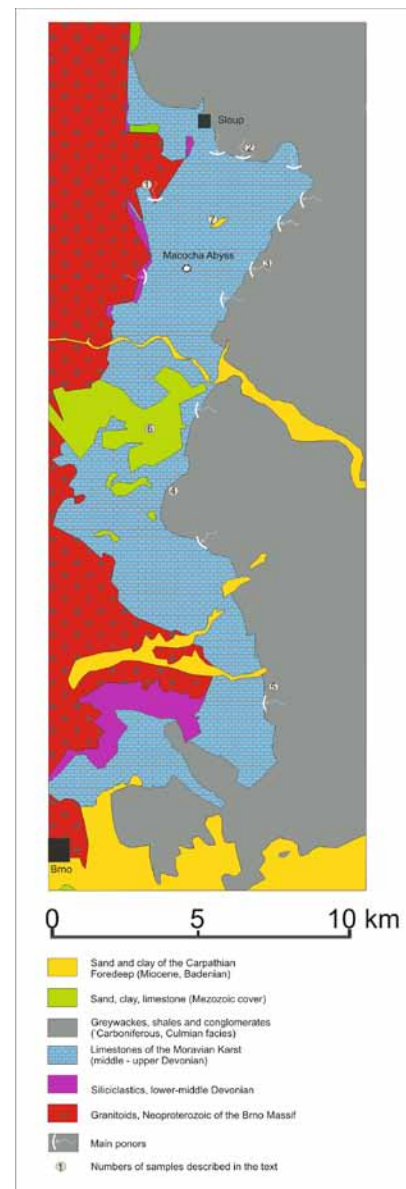


Figure 1. Simplified geological map of the Moravian Karst with main ponors and localities of heavy mineral samples.

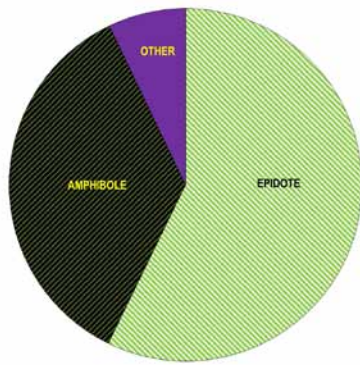


Figure 2. Translucent heavy mineral assemblage derived directly from Devonian clastics and granitoids of the Brno Massif, locality 1 on fig. 1, Suchdolský ponor, Dóm Juniůrů.

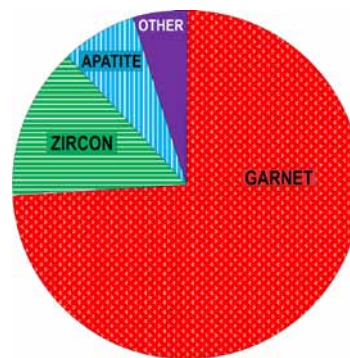


Figure 4. Translucent heavy mineral assemblage of the Culmian greywacke at NE, locality 3 on fig. 1, Krasovský potok Valley.

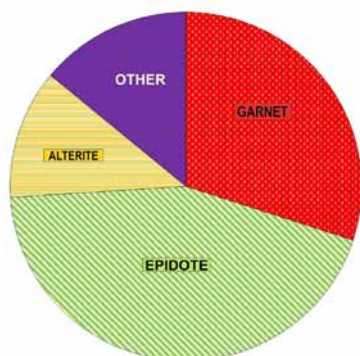


Figure 3. Translucent heavy mineral assemblage of the northern Culmian greywacke, locality 2 on fig. 1, Helišova skála.

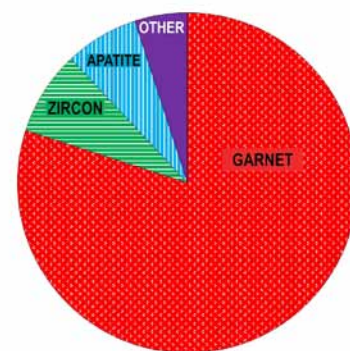


Figure 5. Translucent heavy mineral assemblage of the Culmian greywacke easterly from the Moravian Karst, locality 4 on fig. 1, Habrůvka Village.

translucent heavy minerals were counted per sample. The heavy fraction was analyzed on glass slides in a 5 cm² rectangular pool of the immersion liquid using a polarizing microscope. All samples were prepared in the laboratories of the Czech Geological Survey.

3. Interpretation and discussion of heavy mineral results

All potential source rocks of cave sands were evaluated systematically. They are arranged generally from the oldest, to the youngest and a selection of the most typical assemblages are shown in pie diagrams (Fig. 2-8) and located on Fig. 1. Finally ternary plots showing the possibilities of the source differentiation (Fig. 9 and 10) are presented. The most valuable activity for collecting samples was basic geological mapping in the northern part of Moravian Karst (Baldík et al. 2017) and in the central part of the area (Otava et al. 2013).

3.1. Western source

The main heavy minerals derived from the Neoproterozoic Brno Massif granitoids are predominantly **epidote** and **amphibole**, locally **sphe**ne with **minor zircon**s. The sands derived directly from granitoids (locality 1 in Fig. 1) were analyzed as an example of such assemblage (Fig. 2).

3.2. Northern source

Greywackes of the Culmian facies (Protivanov Formation, Mississippian, Carboniferous) cropping out northerly from

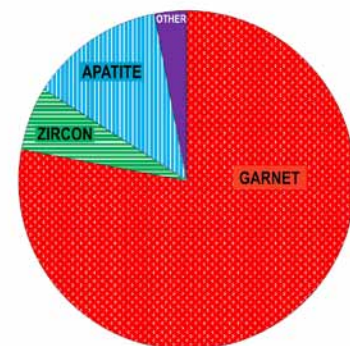


Figure 6. Translucent heavy mineral assemblage of the Culmian greywacke SE from the Moravian Karst, locality 5 on fig. 1, Hádek near Ochoz

the carbonates of the Moravian Karst have mainly epidotic assemblages with significant amount of garnet, alterites (altered Ti minerals), locally with sphene and zircon (Fig 3).

3.3. Eastern sources

There is a large area and mass of younger Culmian siliciclastics of Mississippian age supplying the caves of the Moravian Karst from E and NE. The translucent heavy mineral assemblages of the lower Carboniferous sediments are mostly garnetic, and the finer greywackes have higher amounts (around 10%) of apatitic and zircon (Figs. 4, 5, 6).

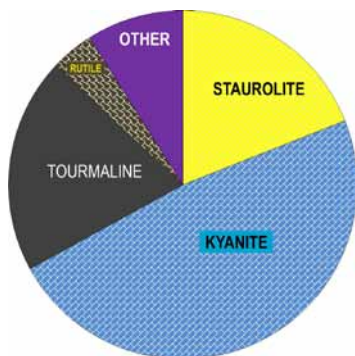


Figure 7. Translucent heavy mineral assemblage of the Cretaceous sands, locality 6 on fig. 1, Rudice-Seč.

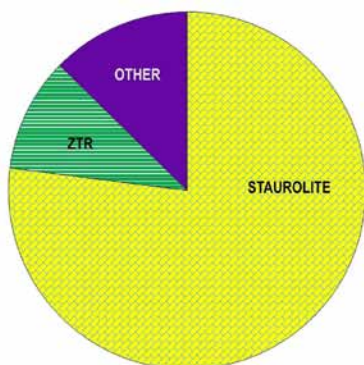


Figure 8. Translucent heavy mineral assemblage of the terrestrial Miocene, locality 7 on fig. 1, Ostrov, borehole OM3. ZTR means ultra-stable minerals zircon + tourmaline + rutile.

3.4. Mezozoic, Cretaceous source

There is an important and distinct source of cave sands coming from Cretaceous products of kaolinic weathering. The sands themselves fill depressions in the Devonian limestones and were locally redeposited into fluvial cave sands. Typomorphic minerals of the assemblage are kyanite, staurolite, with smaller amounts of andalusite and sillimanite and from the ultra-stable suite rutile and tourmaline (Otava, Morávek 2013) (Fig. 7).

3.5. Cenozoic, Miocene source

Cenozoic sediments are present in Moravian Karst as remnants of mostly clayey fill of the pre- Miocene karst canyons (marine Tortonian of the Carpathian Foredeep) and as some denudation relics of older (Ottangian) terrestrial sands and gravels. The terrestrial relics were often redeposited especially in the caves at higher positions above the recent surface and underground drainage system (Bajer et al. 2013). The translucent heavy fraction of such sands are typically show a larger share of staurolite (fig.8).

4. Examples of provenance studies of the cave sands:

It is of course not too complicated to recognize the provenance of fluvial cave sands deposited close to entrance of any ponor of the Moravian Karst, no matter if it is at the eastern, northern or western margin of limestones. The method of translucent heavy fraction analyses as shown on Fig. 9

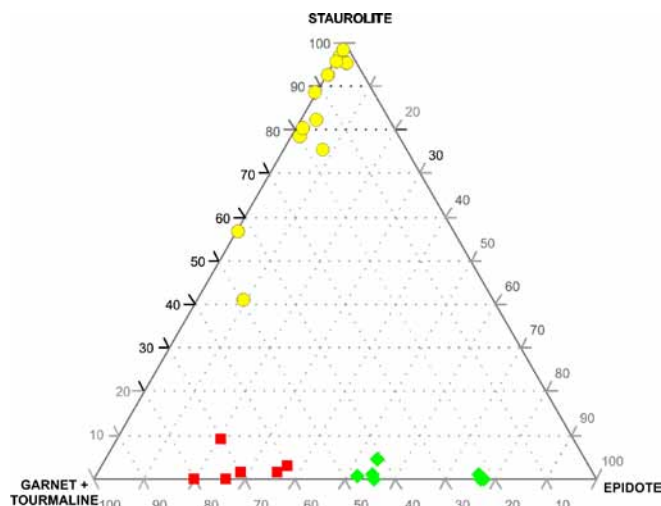


Figure 9. Distinguishing of source of cave sands in the northern part of the Moravian Karst

- terrestrial Miocene source;
- eastern Culmian source;
- ◆ western and northern sources.

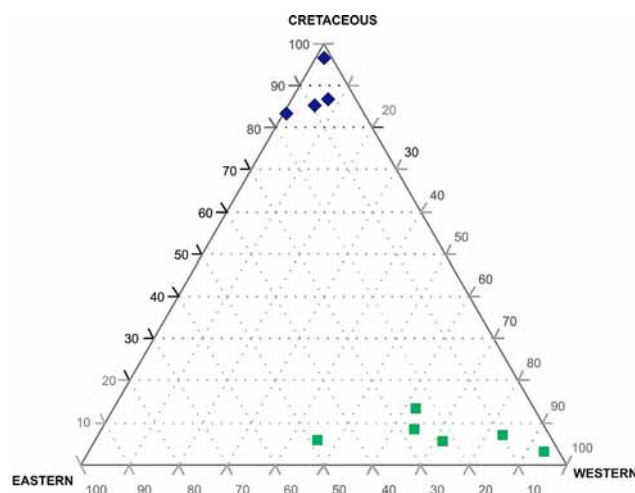


Figure 10. Cave sands of the Macocha Abyss and its closest vicinity are divided in two groups with different provenance: The first one ◆ comes from Cretaceous paleokarst fill (staurolite, kyanite, tourmaline, rutile), while the second one ■ comes mainly from western vicinity of Moravian Karst (epidote, amphibole) with various admixture of the eastern source (garnets).

is very useful in cases of cave sands in central parts of the limestone massif and especially in caves of unclear origin and landscape position.

5. Conclusions

This method of translucent heavy mineral analyses has been used to trace the provenance of cave sands in the Moravian karst. Several examples distinguishing the source of sands in enigmatic positions are presented. The first one shows differences between cave sands coming from W and N, i.e. from granitoids and the old Culmian area, from the E (younger Culmian) and from terrestrial Miocene sediments (Fig.9). The other example is from cave sands in the closed vicinity of the Macocha Abyss. The result shows mixing of a prevailing western source with minor shares of the eastern source and another clearly different source, the products of Cretaceous paleokarst fill (Fig. 10).



Figure 11. Cretaceous kaolinic quartz sands in a palokarst depression, locality 6 on fig. 1, Rudice-Seč

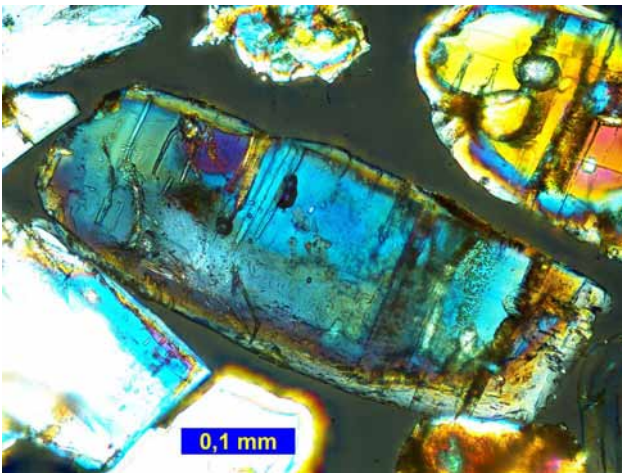


Figure 12. Kyanite – one of the most characteristic heavy mineral of the Cretaceous paleokarst fill. Photo in crossed polars.

6. References:

Bajer, A., Otava, J., Vít, J., Lisá, L. (2013): Finding of Miocene relic in Pod hradem Cave, Moravian Karst. *Zprávy vlastivědného muzea v Olomouci*, 305. s. 120–126. ISSN 1212-1134. Olomouc.

Baldík, V., Buriánek, D., Čáp, P., Franců, J., Fůrychová, P., Gilíková, H., Janderková, J., Kašperáková, D., Kolečka, V., Krejčí, V., Kryštofová, E., Müller, P., Novotný, R., Otava, J., Pecina, V., Rez, J., Sedláček, J., Sedláčková, I., Skácelová, Z., Večeřa, J., Vít, J. (2017): *Geological map 1:25, 000, Ostrov u Macochy, 24 – 233 with explanatory booklet*. Czech Geological Survey, Prague and Brno.

Otava, J., Balák, I., Baldík, V., Bubík, M., Buriánek, D., Čáp, P., Černý, J., Franců, J., Fůrychová, P., Gilíková, H., Havlín, A., Hladil, J., Janderková, J., Kociánová, L., Kolečka, V., Konečný, F., Kryštofová, E., Kumpan, T., Melichar, R., Müller, P., Paleček, M., Pecina, V., Pecka, T., Sedláček, J., Sedláčková, I., Šrámek, J., Tomanová Petrová, P., Večeřa, J., Vít, J. (2013): *Geological map 1:25, 000, Jedovnice, 24 – 411 with explanatory booklet*. Czech Geological Survey, Prague and Brno.

Otava, J., Morávek, R. (2013): *Excursion Guide B3CZ, A3CZ The Most Interesting Karstological Phenomena of Moravia*. 16th International Congress of Speleology, July 21-28. Brno. Excursion Guide B3CZ, A3CZ. 32 s., – Czech Speleological Society, Praha, Czech Republic. Praha. ISBN 970-80-905493-3-3.

(Abstract) **Interpretation of Regional Geomorphic Events from Dissolution Caves**

Arthur N Palmer

Affiliation: State University of New York

Abstract

The various tiers (“levels”) in epigenic solution caves are related to the evolution of the surrounding landscapes. Mammoth Cave (USA), with its many successive levels, provides an exceptionally clear example, because its passages have been dated by analysis of cosmogenic radionuclides in quartz gravels. Its evolutionary history mirrors that of the Mississippi River and its eastern tributaries, which involved complex diversions by continental glaciers.

Several changes in erosional base level are recorded in the cave. Two show a great contrast in style. The levels are not stratigraphically controlled, as they are discordant to the strata. One was gradational, stepping downward to the next major level in a sequence of several tubular conduits, indicating a lengthy and gradual drop in regional base level. Another at a lower elevation was abrupt, with canyons or shafts extending uninterrupted from one level of tubes to the next level 15 m lower, suggesting a sudden local base-level drop. It was initiated by rapid deepening of the Ohio River 100 km to the north, triggered by diversion of a huge catchment area into its headwaters by a glacial advance. This drop was translated to the cave area via the local Green River by waterfalls eroding headward past the cave. These two events represent major developmental stages in the Mississippi-Ohio system. Sediment dating indicates ages of approximately 1.5 and 1.0 Ma (million years ago), and the difference in diversion style clarifies the nature of the surface events.

This otherwise peaceful cave also contains evidence for catastrophic floods, such as transport of sandstone boulders up to a meter in diameter in piles up to 5 m high. They are accompanied by centimeter-scale scallops on nearly all limestone surfaces, which show high velocities and local reversals of direction from much-slower flow before and after. Prolonged or repeated flooding at about 1 Ma is indicated, possibly caused by failure of natural dams related to periglacial activity south of recognized glacial maxima. In addition, the highest levels of Mammoth Cave, and others in the region, contain sediment fill up to 23 m thick. They correlate with an extensive erosional-depositional surface that extends throughout much of the east-central USA and indicate a major climatic or isostatic event of ca. 2.5 Ma. Similar techniques can be applied to many epigenic caves.

(Abstract) **Variation between lithology, carbonate versus sandstone, as an erosional control on a fluviokarst system**

Eric Wade Peterson¹, Toby J Dogwiler², Andrew Francis¹

Affiliation: ¹Illinois State University
²Missouri State University

Abstract

Fluviokarst systems, a combination of surface and internal (subsurface) drainage, are common in areas where there is contact between carbonate and non-carbonate rocks. Lithological differences between the rock types are believed to control erosional resistance that serve as a key component in the development of fluviokarst. Carbonates are susceptible to both physical and chemical weathering, while non-carbonate rocks, specifically siliciclastic rocks, are weathered by physical processes due to low solubility. This work examines the role of lithology in the development of a fluviokarst system where siliciclastic rocks overlie limestones. Using the stream profile for a river in a topographic steady-state, stream power can be calculated with the equation: $\frac{dz}{dx} = \frac{U}{K} \left(\frac{A}{A_0} \right)^m \left(\frac{z}{z_0} \right)^n$, where z is elevation, x is horizontal distance, U is the rate of uplift, K is the erodibility coefficient, A is drainage area, and m and n are exponents related to hydrologic conditions. An integral method transforms the equation such that elevation, instead of slope, is the dependent variable and the spatial integral of drainage area is the independent variable. The integral method scales erosion with drainage area, allowing for the comparison of the steepness index (U/K) along the main stem to those along the tributaries and for the analysis of equilibrium within a single stream or for an entire watershed. Using the integral method, the control of lithology on the development of a fluviokarst system in eastern Kentucky was examined. The Horn Hollow system in Carter Caves State Resort Park has developed in limestone overlain by a sandstone caprock; we examine whether the system is in equilibrium and if lithology has a role in the state of equilibrium. Results indicate that the sandstone stream segments are in greater equilibrium than the limestone segments. Disequilibrium can be caused by a number of factors including uplift, changes in base level, climate, and variation in lithology. As the only dissimilarity among the controlling factors in our study area is lithology, we interpret that to be the cause of disequilibrium in the Horn Hollow. With a mean of 0.03, the steepness index of the limestone segments is statistically higher than the mean steepness index (0.01) of the sandstone segments ($t(51) = -10.10$, $p < 0.01$). Because the U of the rock units is the same, the K of the sandstone must be higher than the limestone, suggesting the sandstone is eroding at a faster rate and/or the limestone is more resistant.

(Abstract) **Exploring The Mechanisms And Consequences Of Cave Roof Collapses Using
The National Corvette Museum Sinkhole Case Study**

Jason S Polk, Leslie North, Pat Kambesis, Brian Ham, Ric Federico

*Affiliation: Center for Human GeoEnvironmental Studies,
Department of Geography and Geology, Western Kentucky University*

Abstract

In recent years, the prevalence of sinkhole (doline) activity around the globe, such as cover collapses, cave collapses, subsidence, urban sinkholes, and other related processes and mechanisms that cause landscape failure in karst area, gained increasing attention. Many areas are now also considering changes to building codes, policies, and insurance regulations that address sinkhole threats. In 2014, a major collapse of a cave roof occurred at the National Corvette Museum (NCM) in Bowling Green, Kentucky, USA and received international media attention. Over a two-year period, investigation of the sinkhole included multiple lines of study, including geophysical, cave survey, drilling, and hydrogeologic techniques, to determine the cause, extent, and best remediation course for the sinkhole. The geophysical study was confirmed by cave survey results and remediation involved a micropile-supported concrete floor to prevent future risk in case of additional collapse. Breakdown is abundant in the cave in which the sinkhole formed and the progression of the roof failure likely occurred over a long span of time, eventually giving way due to a variety of conditions, including speleogenetic and climatic factors that came together recently to influence the collapse. Subsequently, an examination of sinkholes in the area produced more than a dozen examples of major cave collapse sinkhole entrances in varying landuse settings; thus, indicating cave roof collapses may be more common than previously realized and the speleogenetic mechanisms influencing the timing, occurrence, and proclivity of these types of sinkholes may be improved in determining future areas of risk. Beam length of limestone beds and location of breakout domes in relation to the surface should be considered when evaluating known cave passages for possible risk of future collapse, particularly in developed areas. Following remediation of the NCM sinkhole in 2016, an educational exhibit was opened to improve public understanding of karst and sinkhole formation processes, including a focus on cave roof collapses. Since then, cave collapses and development issues are still occurring and the lack of understanding and regulation promulgate further likelihood of these in the future. Additional emphasis on this type of sinkhole risk and related surface failures should be included when discussing the potential loss of property and reduce the risk of sinkhole impacts. Outcomes of the National Corvette Museum sinkhole study and outreach efforts provide a model for future methods by which scientists and the public may improve sinkhole prevention and reduce risk factors.

Contenda cave genesis (Estremenho karst massif , Portugal)

Rodrigues, P.^{1,2,3}, Robalo, P.^{1,2,4}, Amendoeira, V.^{1,5}

Affiliation: ¹Grupo de Espeleologia e Montanhismo, Rua Maria Veleda, nº 6 - 7º Esq, Alfofo, 2650-186, Amadora. paulor2005@yahoo.com gem@gesmo.org

²Núcleo dos Amigos das Lapas Grutas e Algarves. nalga.espeleo@gmail.com

³Comissão Científica da Federação Portuguesa de Espeleologia, Estrada Calhariz de Benfica, 187, 1500-124 Lisboa.

⁴Comissão de cadastro da Federação Portuguesa de Espeleologia, Estrada Calhariz de Benfica, 187, 1500-124 Lisboa.

⁵Direção da Federação Portuguesa de Espeleologia, , Estrada Calhariz de Benfica, 187, 1500-124 Lisboa.

Abstract

Contenda Cave is located near Mira de Aire, on the northern border of Minde's polje, in Estremenho karst massif, central Portugal. The Estremenho karst massif is the largest karst area in Portugal. From 2007 to 2015 several works were conducted in the cave. The cave is 1792 m length and 97 m deep (+17 m, highest part and -80 m, deepest part). Contenda Cave acts as an episodic spring along with several springs also located on the northern border of Minde's polje. Minde's polje altitude is around 200 m ASL. The cave presents a curvilinear branchwork pattern. It is developed along two levels of galleries. A upper level of galleries initially develops towards southwest and then turns north. This gallery's average altitude is about 200 m ASL, the same altitude as the cave entrance. The lower level gallery is 70 to 80 m deep, at an altitude of about 130 – 120 m ASL, and develops roughly to north-northwest. The lower galleries gently dive into the phreatic zone. The phreatic zone is explored by cave diving, in search for a connection to the close-by Moinhos Velhos's cave, the second largest cave of Portugal. The two gallery levels are connected by pits or steep diving galleries. At high-water, groundwater rises from the phreatic zone, reaching the upper level and the cave entrance. Then the entrance acts as spring supplying water to a temporary waterline, which together with water from other springs, in some years, floods the polje. The 70 – 80 m height difference between the two cave levels corresponds to the active vadose zone thickness. The cave is epigenic, developed in the phreatic zone, however nowadays most of the cave's known extension is in the semi active zone. The cave location, at the border of Minde's polje is due to a permeability difference between middle and upper Jurassic limestones, which contact through a fault close to the cave entrance. The cave development is strongly controlled by layer's strike and dip (N40W to N50W/20S) in some areas and in others by subvertical fractures, with direction ranging from N10W to E-W.

Keywords: Contenda, Estremenho karst massif, topographical survey, geology survey, cave dive

1. Introduction

Contenda Cave is located near Mira de Aire, in the south border of the São Mamede plateau, Portugal. This plateau is a geomorphologic unit of Estremenho karst massif (Fig. 1), the largest karst massif of Portugal, defined by Fernandes Martins (1949). The cave entrance is located on the northern border of Minde's polje (Fig. 2); along with several springs are located. Contenda is one of those springs, an episodic spring, according to Bögli's (1980) classification. Contenda Cave is partially filled with water during most of the year, enabling fieldwork, on most of the cave, for a period of 8–9 months every year.

The cave is located close to Moinhos Velhos's Cave, the second largest cave of Portugal, according to the published topographies. The connection between Moinhos Velhos and Contenda, was proved using dye tracing in 1986 (Almeida *et al.*, 1995).

2. Speleometry

The known extension of the cave was surveyed. The cave is 1792 m length and 97 m deep (+17 m, highest part and -80 m, deepest part). The depth measurements are given relative to the cave entrance.

3. Cave description

The cave topography is presented on figure 3. The cave presents a curvilinear branchwork pattern, according to Palmer's (2003) classification. It has two entrances, one is a small shaft,

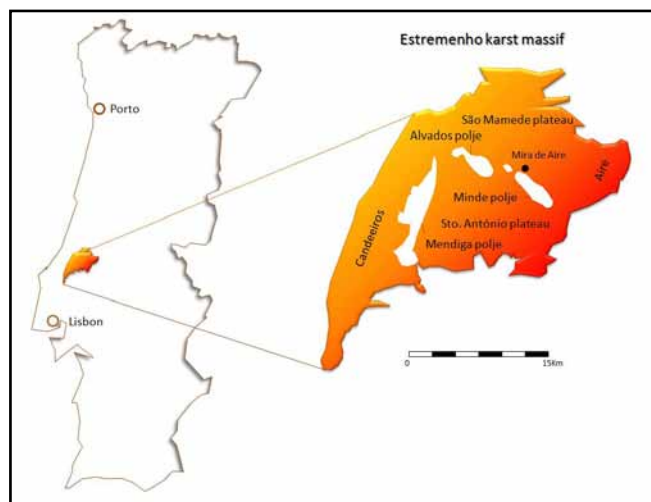


Figure 1. Location of Estremenho karst massif and massif sketch

nowadays obstructed, and the other is a temporary spring. It is developed along two levels of galleries. A upper level of galleries initially develops towards southwest and then turns north. This gallery average altitude is about 200 m, the same altitude as the cave entrance. The lower level galleries are 70 to 80 m deep, at an altitude of about 130 – 120m, and develop roughly to north-northwest. The lower level has two levels of galleries, an upper one, named SPE66 (70 m deep, 130 m of altitude) and a lower one, (80 m deep and 120 m of altitude), where a water stream can be found, because of this the gallery



Figure 2. Contenda's Cave map (plotted in red) over a satellite photo. At west of Contenda (plotted in yellow) is a scheme of Moinhos Velhos Cave. The scheme is roughly based on Crispim, 2014. Both caves are connected as proved by dye tracing, although the physical connection is not yet been made. Gruta da Pena is another outflow spring of Moinhos Velhos cave as is Contenda's Cave.

is named River gallery. The lower galleries gently dive into the phreatic zone. The two gallery levels are connected by two sets of pits, about 60 m deep, and a steep diving gallery (the Affluent gallery). At high-water, groundwater rises from the phreatic zone, reaching the upper level and the cave entrance.

The phreatic zone has been explored by cave diving. The terminal zone of SPE66 by Rui Pinheiro (2008 and 2009), and the River gallery by António Mendes (2011 and 2013). A later exploration in a particularly dry year (2015) allowed dry access to the usually flooded terminal zone of SPE66 gallery. The SPE66 gallery continuous horizontally roughly to north and then east, after a crossable sump it ends on yet another flooded pit. The water stream of the River gallery continues both to northwest and southeast. The diver explored and mapped some tenths of meters on both ends of the river, with some variations on depth inferior to 10 m. The river continues. Contenda Cave is approximately at 40 – 50 m (on a straight line) from the Moinhos Velhos-Pena cave.

4. Geological and hydrogeological setting

The cave develops, in Bathonian (Dogger) limestone (Fig. 4), belonging to the "Calcários Mícritos da Serra de Aire" Formation, mainly composed of micritic limestone. As can be established from the geological map the cave is developed on a flank of a regional fold. This flank has a monocline with an attitude roughly NW-SE/20S.

The cave entrance is close by to the northern border of Minde's polje. The polje is about 4 km long by 2 km wide and its bottom has an average altitude of 200 m (Almeida *et al.* 1995). The polje's North and South borders are defined by faults. The polje is a depressed block between faults.

Several temporary springs, all of them associated with important caves (Almeida *et al.*, 1995) are located on the poljes NW and NE limit. In the rainy season the springs outflow join on a waterline that runs over the polje until it reaches some ponors. Periodically, the ponors are insufficient to drain the polje and it forms a temporary lake.

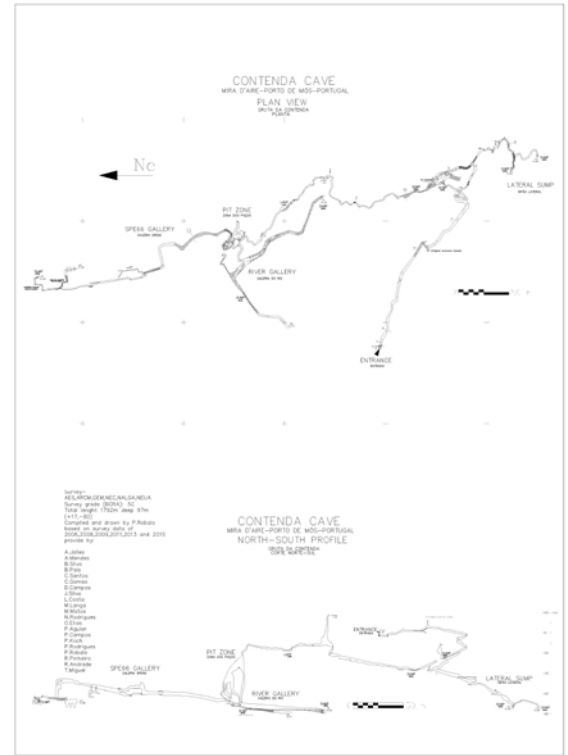


Figure 3. Topography of Contenda Cave.



Figure 4. Contenda Cave map plotted on a geological map (sheet 27-A-Vila Nova de Ourém), greyish blue - formation of "Calcários micríticos of Serra de Aire" (Batoniano, Dogger), pale blue- formation of Camadas de Cabaços e Montejunto (Oxfordian to Kimmredigian, Malm), pale brown - Holocenic sediments, black solid lines - faults. The red dots at South are ponors.

All caves, whose entrances are located near the northern border of Minde's polje are near a fault (with a NW-SE direction), that borders the north of the polje. Apparently this fault produces a barrier effect, allowing the lateral contact between Dogger Limestone with a large karstification potential, and the Malm Limestone with lower permeability. This fault probably acts as a barrier to water flow in the perpendicular direction of the fault but also as a preferential line of water flow, parallel to the fault. Crispim (1995) points out the importance of this fault, enabling contact among rocks of very different permeability and also stating that the spring zones area are located along the contacts between the rocks of different permeability.

5. Structural control

The cave has several kinds of structural controls. The upper gallery seems to be controlled mostly by the bedding planes,

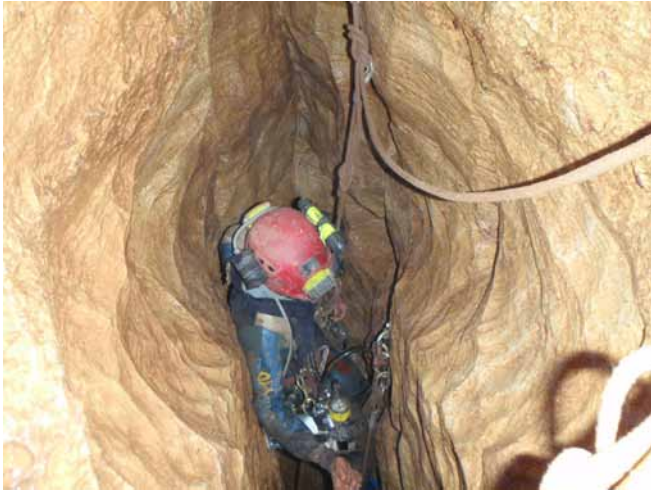


Figure 5. Structural control of SPE66 gallery by a fracture, plan view



Figure 7. The River gallery



Figure 6. Structural control of SPE66 gallery by a fracture, side view



Figure 8. The River gallery

in some areas by the bedding strike and in other areas by the dip of the bedding. The bedding planes measurements, conducted inside the cave reported values of N40W to N50W/20S for the strike and dip of the beds. This value is in agreement with the value above mentioned for the layers attitude of the area. Several fractures cross the main gallery and also have some influence in the gallery development. The area where the main and the affluent gallery meet, a fracture with an attitude of N50W /vertical controls the development of both galleries. Fractures with an attitude roughly N30E/vertical also control other parts of the main gallery.

The affluent gallery development is controlled mostly by the layers dip and in some areas by several fractures. The fractures have the following attitude N40W to N50W/vertical, N10W/vertical, and E-W/vertical. The pit development is mainly controlled by fractures with an orientation ranging from N50W to N60W. The SPE66 gallery is structurally controlled mostly by a family of fractures of attitude roughly N10W/80E, although some small portions of the gallery are controlled by

fractures of another family of attitude N60E to N80E/Vert. The areas controlled by this last family of fractures connect the areas controlled by the fractures of the N-10W/80E family. The River gallery development is controlled by the layers strike in some sections and in others by the layers dip.

6. Karstic zonation and water circulation

The entire surveyed non-flooded cave galleries can be considered as being in the high-water zone of the vadose zone as defined by Bögli (1980). The Ramsar report (2005) refers a 100 m water level fluctuation on Minde's polje area, this thickness can be considered the high-water vadose zone. Also according to Crispim (1987), in the close by Moinhos Velhos Cave, the zone of temporary oscillation of the phreatic level has a maximum 80 m thickness. As Contenda Cave is considered a Moinhos Velhos outflow spring, one can consider the entire Contenda Cave depth is representative of the local vadose high-water zone thickness, and indeed the cave depth (counting from the cave entrance) is around 80 m, this value is quite close to the one mentioned on Moinhos Velhos Cave.

Considering the cave morphology, the water circulation above described, and the fact that Contenda Cave seems to be a episodic spring, one may consider that groundwater circulation is probably limited, for most of the year, to the "River

gallery” (where there is usually groundwater circulation even in the summer), to the lower parts of SPE66 gallery, and to unknown gallery to where the affluent gallery connects.

An estimate of the water flow velocity, when the galleries were formed, was obtained based on the length of flutes observed along the cave walls. The calculation was performed using the Curl formula (Bögli, 1980; after Curl, 1966). The velocity of water flow, which carved the scallops is in the order of the few tenths of meters per hour. These values are on the same order than the ones referred by Almeida *et al.* (1995) for a dye tracing test between Moinhos Velhos and Contenda, revealing an average velocity of 16 m/h for a travel distance of 800 m up to Contenda Cave.

7. Genesis

The cave galleries are epigenic and of phreatic origin. The cave has abundant scallops, cupolas, sumps, and reacts quickly to recharge, with water level rising, at most, in few days after strong rainfall. Based on the scallops and sediments the water should flow from the deepest part of the cave (SPE66 gallery, river gallery and affluent gallery) to the main gallery where it flows until reaching the cave entrance. As explained above, most of the cave is the high water vadose zone, and is probably dry most of the year. This allows some vadose circulation, in limited parts of the cave, with water coming probably from some rainfall infiltration.

8. Conclusions

Contenda Cave is a epigenic cave of phreatic origin, which entrance acts as a episodic spring who opens on the northern border of Minde's polje. This border is defined by a fault (with a NW-SE direction), that puts in contact highly karsifiable limestone (at North of the fault) with lower karsifiable limestone (at South of the fault). This fault must probably acts as a barrier to water flow in the perpendicular direction of the fault but also as a preferential line of water flow, parallel to the fault. The cave develops, north of Minde's polje, mostly to northwest on direction of the close by Moinhos Velhos's cave, from which it is 40 – 50 m in a straight line. Contenda Cave is an outflow spring of Moinhos Velhos's cave. The velocity of water flow, which carved the scallops, in the cave walls was in the order of the few tenths of meters per hour. This value is quite close to the nowadays water circulation velocity, obtained by dye tracing. The cave development is strongly controlled by layer's strike and dip (N40W to N50W/20S) in some areas and in others by subvertical fractures, with direction ranging from N10W to E-W.

Acknowledgements

This work was only possible due to the support of the following cavers, by alphabetical order: A. Leal A. Jalles, A. Barros, A. Calambra, A. Mendes, A. Monteiro, A. Reis A. Santos, B. Domingues, B. Monteiro, B. Pais, C. Gomes, C. Pereira, C. Santos, D. Campos, D. Fialho, F. Videira, F. Lucas, F. Silva, H. Ferreira, H. Frade, I. Granjo, I. Palygiewicz J. P. Janela, J. P. Lopes J. Pinheiro, J. Silva, L. Costa, L. Meira, L. Sobral, M. Costa, M. Matos, M. Pereira, M. Jalles, M. Borges, M. Lopes, M. Matias, M. Messias, N. Rodrigues, O. Elias, P. Silva, P. Alexandre, P. Almeida, P. Campos, P. Aguiar, P. Pinto, P. S. Koch, R. Lopes, R. Andrade, R. Francisco, R. Pinheiro, R. Agap-

ito, S. Lopes, S. Lopes, S. Barbosa, S. M. Santos, T. Regala, Ti. Matias T. Miguel U. Lopes, V. Lourenço. and V. Toucinho.

The work has been conducted by members of the following speleological associations, by alphabetic order: AES, AESDA, ARCM, CEAE-LPN, GEM, GEMA, NEC, NEL, NEUA, NEC, SAGA e SpeleoKlub Warszawski.

References

- Almeida C., Silva M.L. & Crispim J.A., 1995. National report for Portugal, Cost Action 65 “Hydrogeological aspects of groundwater protection on karstic areas”, Final report, Directorate of Science, Research and development, p. 211-220.
- Bögli A., 1980. *Karst Hydrology and Physical Speleology*, Springer-Verlag, Berlin Heidelberg New York.
- Crispim J.A., 1987. Evolução da Hidrologia Subterrânea na Gruta de Moinhos Velhos (Mira de Aire), Departamento de Geologia da Faculdade de Ciências de Lisboa, Sociedade Portuguesa de Espeleologia, ALGAR, Lisboa, *Bol. Soc. Port. Espeleologia*, 1, 3-8.
- Crispim J.A., 1995. *Dinâmica Cársica e Implicações Ambientais nas Depressões de Alvalade e Minde*. Tese de Doutoramento em Geologia, especialidade de Geologia do Ambiente. Departamento de Geologia. Faculdade de Ciências, Universidade de Lisboa.
- Manupella G., Telles Antunes M., Costa Almeida C.A., Azerêdo A.C., Barbosa B., Cardoso J.L., Crispim J.A., Duarte L.V., Henriques M.H., Martins L.T., Ramalho M.M., Santos V.F., Terrinha. P., 2000. *Carta Geológica de Portugal – Vila Nova de Ourém, Folha 27-A*, scale 1:50000, e nota explicativa, Instituto Geológico e Mineiro, Lisboa.
- Martins A.F., 1949. Maciço Calcário Estremenho. *Contribuição para um estudo de geografia física*. Oficinas da impressão de Coimbra.
- Palmer A.N., 2003. Speleogenesis in Carbonate rocks. 43-60 pp. In: *Evolution of karst: from prekarst to cessation*. Postojna-Ljubljana ZCR.
- Rodrigues P. & Robalo P., 2008. *Gruta da Contenda*. Available online: <http://nalga.wordpress.com/gruta-da-contenda-17m-73m>
- Parque Natural das Serras de Aire e Candeeiros, 2005. *Information Sheet on Ramsar Wetlands (RIS)*. Available online: http://sites.wetlands.org/reports/ris/3PT016_RISen06.pdf
- Crispim J.A., Constantino R., Duarte J., 2014. *Espeleomergulho nas Grutas de Mira de Aire: importância para o conhecimento da rede espeleológica, a captação de água subterrânea e a divulgação das grutas turísticas*. CuevaTur 2014/ Iberoamérica Subterrânea.

The Origin Of Jewel Cave And Its Relationship To Landscape-Scale Processes – Part 1

Michael E. Wiles

Affiliation: Jewel Cave National Monument, 11149 U.S. Highway 16, Custer, SD 57730
Mike_Wiles@nps.gov

Abstract

With over 186 miles (300 km) of mapped passages, Jewel Cave is the third longest cave in the world. This paper documents the intimate relationships between the cave and the geologic structure, contacts, and topography, as they exist today. These relationships do not support a paleokarst, hypogenic, or epigenetic origin. Instead, a new model describes cave development as the result of local groundwater moving through a confined sandstone layer.

Hell Canyon is in the bottom of a south-plunging syncline. A cross-section illustrates how the cave passages assume the shape of an elongate lens, located just below the Pahasapa/Minnelusa contact. The lower boundary is a maximum of 250 (75 m) feet below the contact, but thins at each end, where the permeable, basal Minnelusa sandstone is exposed. These exposures occur in the Pass Creek drainage, Teepee Canyon, Lithograph Canyon, and Hell Canyon.

The apparent recharge areas were in Pass Creek and Teepee Canyon, and the discharge was in Lithograph Canyon and Hell Canyon. Groundwater initially moved through a shallow confined aquifer comprised of the basal Minnelusa sandstone, which was initially confined by the underlying Pahasapa Limestone and an overlying Minnelusa limestone. Although Laramide fractures provided secondary porosity, they weren't necessarily continuous enough to provide landscape-scale permeability. As water from the sandstone circulated into the discontinuous fractures of the Pahasapa, dissolutional enlargement integrated them to form the system of interconnected cave passages known today. This is summarized with diagrams illustrating a four-step process.

Keywords:

1. Discussion

Most carbonate caves form in two or three stages: 1) fracturing, 2) phreatic dissolution, and sometimes 3) vadose enlargement. Vadose activity only occurs after the cave drains and begins to pirate surface streams – something that didn't occur in the Black Hills area. Moreover, significant dissolution depends on the existence of a natural mass transfer system to move dissolved mass from one location to another. It requires: 1) a solute (limestone), 2) a continuous initial flow path, 3) an energy gradient (elevation difference between recharge and discharge areas), 4) a transport medium (groundwater), and 5) a solvent (acidic solution).

Figure 1 shows that nearly all cave passages in the southern Black Hills lie beneath a Minnelusa cap (Wiles, Ohms, & Pflitsch, 2009), so it's obvious that the Minnelusa once played a role in forming the passages. There are no large caves (or remnants of large cave systems) in the uncapped portions of limestone, and none are longer than 500 feet (150 m). Therefore, large cave systems could not have formed until after the Minnelusa cap eroded back to its present configuration. Consequently, evidence of the five requirements should be visible within today's geomorphological setting.

Jewel Cave consistently stays in the upper 250 feet (75 m) of the Pahasapa Limestone, the *solute*, which is locally 430 feet (130 m) thick. Its passages are large and mazy beneath the hillsides, but diminish in size and complexity where they approach the surface drainages.

Additionally, a cross-section of the solutionally enlarged fractures shows a lens that thins out as it approaches the surface drainage at each end (Figure 2). Throughout the Black Hills,

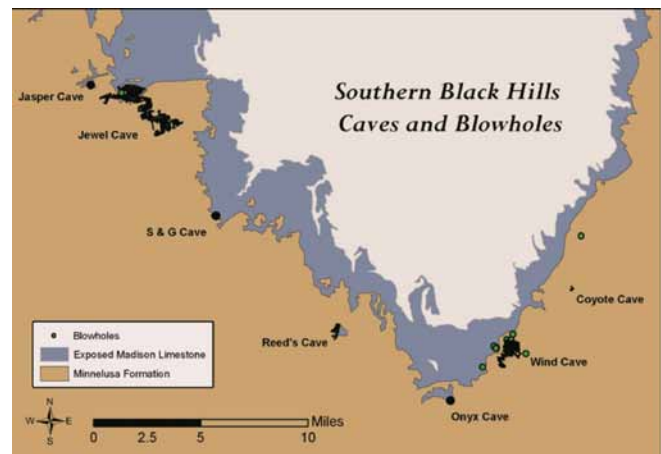


Figure 1. Caves and the Minnelusa cap

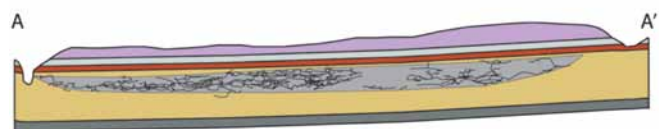


Figure 2. Lens shape of solutionally enlarged fractures. Cross-section base on Figure 3.

it is common for cave passages to diminish in complexity and rise up where they approach surface drainages.

The pattern of cave passages also shows a strong correlation with the geological structure, as it exists today. Hell Canyon is aligned with the axis of a south-plunging syncline (Figure 3), and the cave itself wraps around a curved strike, dipping into

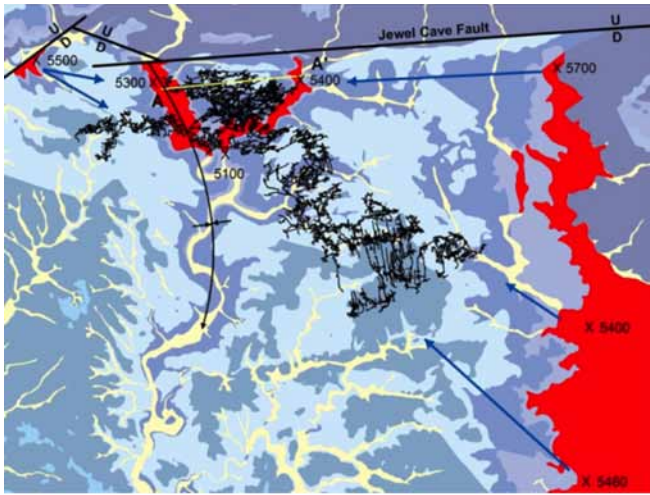


Figure 3. Sandstone outcrops in red. Geology from Fagnan (2009)

the syncline. Because of these strong correlations, it appears that the processes shaping the modern topography were also responsible for forming the cave at the same time.

The stratigraphy (Table 1) would have placed limits on the flow of the paleohydrologic system. The Englewood Limestone lies immediately beneath the Pahasapa, but its lowest 15 feet is actually impermeable red shale, which even today prevents the rising of water from the underlying Deadwood Sandstone, below. A 40-foot (12 m) subunit of Minnelusa sandstone (subunit 1) rests on top of the Pahasapa Limestone, followed by a 50-foot (15 m) subunit of Minnelusa limestone with interbedded clastics (subunit 2) and up to 30 feet (9 m) of impermeable red shale (base of subunit 3), which precludes the direct infiltration of meteoric water from above. However, the subunit 1 sandstone is quite permeable (Wiles, 1992), and capable of moving water laterally from a distant recharge area. It provides the *initial flow path*. Figure 3 shows the sandstone outcropping at Pass Creek and Teepee Canyon (right edge and upper left). These are the proposed recharge areas. The proposed discharge areas 200-300 feet (60-90 m) lower, at Lithograph and Hell Canyons (near A and A', respectively). This provides the *energy gradient*.

Based on literature, the basal sandstone is assumed to have a permeability of about 10%, and would have served as a confined aquifer, moving water (the *transport medium*) from the

Table 1. Description of stratigraphy

Unit		Description	Thickness	
			Feet	m
Minnelusa	3	basal shale, sandstones, limestone cap	120	37
	2	thin-bedded, cherty limestone	50	15
	1	basal medium-to-coarse grained sandstone	40	12
Pahasapa		limestone, crossbedded dolomitic sandstone in lower half	430	130
Englewood		limestone, red shale in lower half	30	9
Deadwood		sandstone and dolomite, 10 feet (3 m) of sandstone at top	190	58

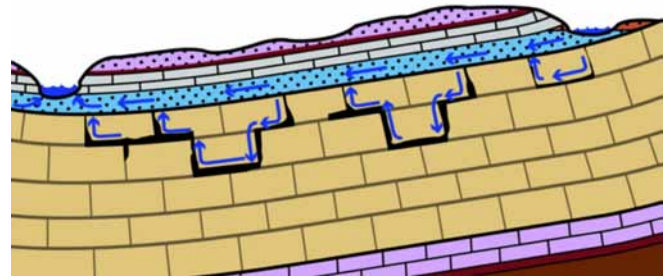


Figure 4. Stage 1

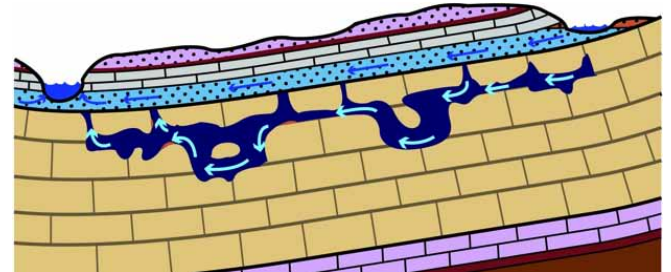


Figure 5. Stage 2

higher to lower streams, and supplying water to the developing cave system along the way.

The *solvent* is assumed to be a carbonic acid solution, with CO₂ being derived from soils along the banks of the losing streams. Because of the confined nature of the sandstone aquifer, it couldn't lose CO₂ through degassing. In other words, it would maintain full aggressiveness over the entire distance from recharge to discharge (Palmer, 2012). In fact, the effective permeability of sandstone is 3-6 times greater than the present cave-sized permeability in the limestone, so dilution of the acidity in the sandstone (caused by the depleted water returning from the limestone) would have been minimal. Following is a proposed sequence of events:

Stage 1 - Because the sandstone is much more permeable than the initial state of either limestone (above or below), the water would first flow almost exclusively through the sandstone. However, it could circulate down into the discontinuous fractures in the Pahasapa Limestone, and back up into the sandstone, as long as it emerged at a point of lower energy gradient. (See figure 4.)

Stage 2 - The discontinuous nature of the fractures would result in isolated cells of dissolution, which would begin to coalesce as the nascent cave passages were enlarged. The basal Minnelusa sandstone would sometimes collapse into the still-developing cave passages. (See figure 5.) This model anticipates the fill entering contemporaneously with cave development, rather than 300 million years earlier, so the fill is best described as *neofill*, rather than *paleofill*.

Stage 3 - Once Hell Canyon (and Lithograph Canyon) had cut all the way through the sandstone aquifer, the sandstone would drain and stop functioning as a confined aquifer, and the water remaining in the Pahasapa would be essentially stagnant. Unenlarged fractures may have slowly drained water from the cave. Once air entered the aquifer, the water would begin to degas. This would cause cave water to become supersaturated, and precipitate the ubiquitous calcite spar on cave surfaces. (See figure 6.)

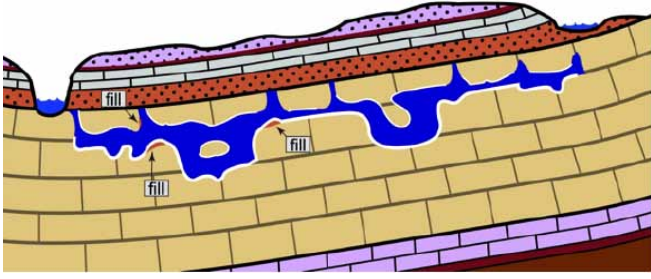


Figure 6. Stage 3

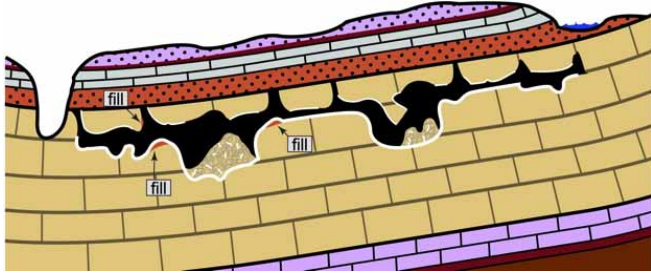


Figure 7. Stage 4

Stage 4 - As the water drained, buoyancy was removed, and many of the larger rooms collapsed into piles of breakdown. (See figure 7.) With further draining, air connections became more integrated, and barometric air flow became more prominent.

Although these observations don't provide an exact method for dating the speleogenesis of the cave, they *do* narrow the possibilities. The deposition of calcite spar essentially marked the end of cave development. A single U/Pb date at the top of the spar indicates an age of around 15 ma (Polyak, 2015). Since the CaCO_3 equilibrium is controlled by dissolved CO_2 , once the CO_2 was removed, the precipitation would have become irreversible, and the spar would have precipitated relatively quickly. Conceptually, at a rate of only 1 mm/year, an 8-inch (20 cm) layer of spar could be deposited in only 200

years. Because of calcite's relationship with CO_2 , it is doubtful that the deposition could have occurred over an extended period of time, such as millions of years.

In conclusion, this model is geomorphically compatible with present day surface and cave features. It explains the development of cave passages with 1) no direct recharge from meteoric water, 2) no recharge from below, and 3) no paleokarst origins. The cave could have finished forming as recently as 15 million years ago. Part 2 of this paper will address how *quickly* this process might have occurred.

Acknowledgements

I'd like to express my appreciation to Dwight Deal, for jump-starting the exploration at Jewel Cave, and for doing the first comprehensive geological study. Herb and Jan Conn first introduced me to the cave itself, and helped fan my interest from spark to fire. It's always been good to spend time with Art and Peg Palmer, and benefit from their insights and personal support. And there would be nothing to study, except for the tens of thousands of hours donated by hundreds of volunteer cave explorers, past and present.

References

- Fagnan, B.A., 2009, *Geologic Map of the Jewel Cave Quadrangle, South Dakota: 7.5 Minute Series Geological Quadrangle Map 9*, South Dakota Geological Survey.
- Palmer, A. N., 2012, Personal communication.
- Polyak, V.J., 2015, Personal communication.
- Wiles, M. E., 1992. *Infiltration [of groundwater] at Wind and Jewel Caves, Black Hills, South Dakota*: Master's thesis, South Dakota School of Mines and Technology.
- Wiles, M. E., Ohms, R. E., and Pflitsch, A., 2009, *Cave Airflow Studies and the Potential Extent of the Jewel Cave System: 15th International Congress of Speleology Proceedings*.

The Origin Of Jewel Cave And Its Relationship To Landscape-Scale Processes – Part 2

Michael E. Wiles

Affiliation: Jewel Cave National Monument, 11149 U.S. Highway 16, Custer, SD 57730
Mike_Wiles@nps.gov

Abstract

With over 186 miles (300 km) of mapped passages, Jewel Cave is the third longest cave in the world. Previous work has demonstrated an intimate relationship between the cave and the geologic structure, contacts, and topography as they exist today.

A rough estimate of hydrologic properties shows that, under optimal abiotic conditions, there would have been sufficient flow to remove the entire volume of cave in as little as 1.1 million years. However, the carbon dioxide required for dissolution could have been produced by the interaction of microbes and the organic carbon of shale layers within the confined aquifer, which could have even accelerated the rate of dissolution.

The distribution of ellipsoidal quartzite clasts – scattered across 1,500 square miles (3,885 km²) of the western and southern flanks of the Black Hills – cross-cuts sedimentary rocks from the Mississippian Pahasapa Limestone through the Cretaceous Lakota Formation. Additionally, cobbles of an Inyan Kara pebble conglomerate have been transported three miles from west to east, across three major north-south drainages. These provide a timing element for a Hills-wide event that can be correlated with the cave, because of a quartzite clast emplaced within the cave before the deposition of the calcite spar. A single U-Pb date places the spar at 14.7Ma, the presumed end of dissolutional flow.

These observations continue to define a framework consistent with geologically recent cave development. Once the hydrologic parameters of a crucial sandstone unit have been determined, there will be sufficient information to begin computer modeling, to provide valuable insight on how all the observations fit together. More work is needed to determine the source, transport method, and timing of the quartzite clasts. Finally, it is a near certainty that Jewel Cave did not form under completely abiotic conditions. More work is needed to determine the role of biospeleological processes.

Keywords:

1. Discussion

Part 1 of this paper assumed that cave dissolution ended with the precipitation of calcite spar, around 14.7 Ma. This paper considers the minimum amount of time required for the entire dissolutional process to accomplish its work. This can be approximated by estimating the maximum flow rate through a control volume and then multiplying by a reasonable solubility ratio for calcite.

Calculations are based on the trapezoidal control area in Figure 1, which outlines passages on the east side of Hell Canyon; it is assumed that the same processes occurred simultaneously on the west side of the canyon. There are approximately 150 miles of known passages in the control area, but it will be assumed that an additional 300 miles of undiscovered passages exist in the blank portions. It is further assumed that these are “average-sized passages” – about one million cubic feet per mile (17,300 m³/km). So around 450 million cubic feet (12.7 million m³) must be removed by dissolution.

Figure 2 depicts a control volume – an idealized geometry for the sandstone unit supposed to take on the initial flow of the system.

Volumetric flow is given by $Q=KAh/L$, where $K=T/d$. The actual transmissivity (T) is currently unknown, but similar to that measured for the Deadwood Sandstone (Wiles, 1992). Therefore:

$T = 510$ gal/day-ft²; $A = 316,800$ ft²; $L = 21,120$ ft (average);
 $h = 350$ ft (average); and $d = 40$ ft. Solving for the volumetric flow rate, $Q = 3.2 \times 10^6$ ft³/yr (0.9×10^6 m³ yr).

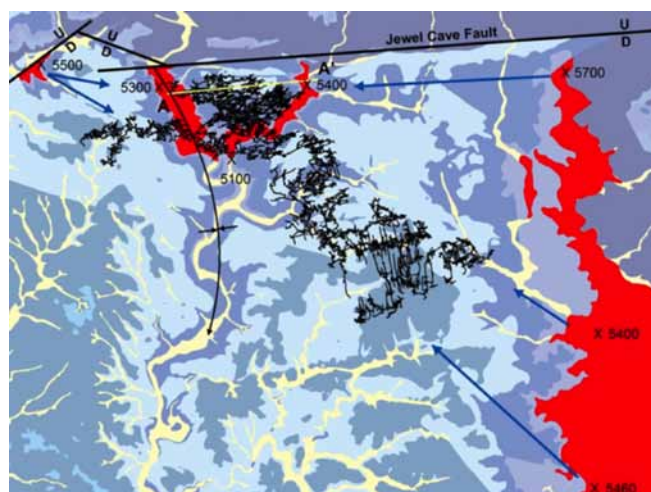


Figure 1. Trapezoidal control area

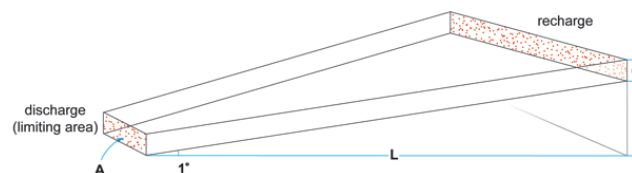


Figure 2. Idealized control volume of sandstone

For comparison, Q is about 10 ft³/s (0.3 m³/s), or only 1% of the average flow of Rapid Creek, elsewhere in the Black Hills

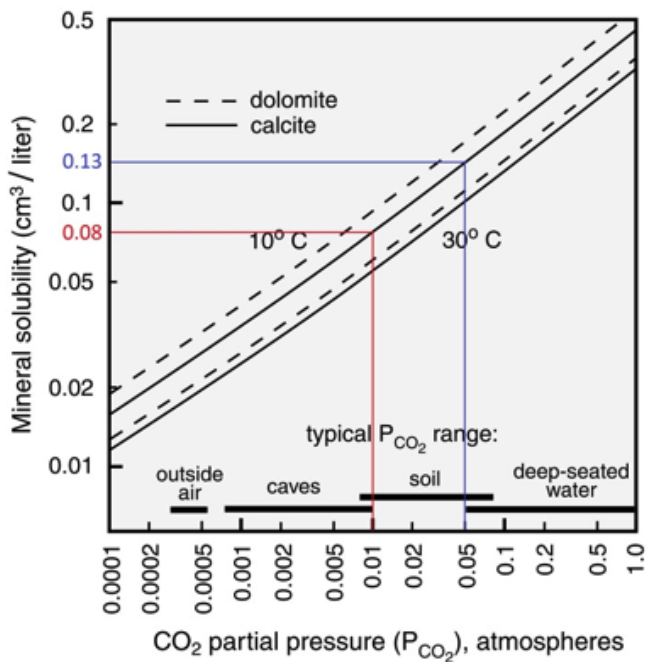


Figure 3. Solubility curve (from Palmer, 2007)

of South Dakota. It doesn't require more than could be reasonably supplied by stream sizes common to the area.

Assuming an optimum partial pressure of CO₂ in soil, and a temperature of 10°C, the mineral solubility ratio (*r*) would be 0.13 cm³/l, or 0.13 x 10⁻³ (see Figure 3). So, the amount of limestone removed annually would be *Q* · *r*, or (3.2 x 10⁶ ft³/yr) · (0.13 x 10⁻³); or *Q* · *r* = 0.00042 x 10⁶ ft³/yr. Therefore *Q* = (450 x 10⁶ ft³) / (0.00042 x 10⁶ ft³/yr) = 1.1 x 10⁶ years.

The model currently assumes that CO₂ is derived from soils along stream banks at the recharge areas. However, a thickness-compensatory red shale at the top of the sandstone presents another possibility. Besides helping confine the aquifer, the shale could provide a source of "free" carbon that could be metabolized by microbes in the water. Fresh CO₂ would be an obvious byproduct that might have been available in virtually unlimited supply. This had the potential to accelerate the dissolution rate by orders of magnitude (Barton, 2015 and Boston, 2016). The actual role and effects of microbes are still speculative, but after a century of abiotic assumptions, it is certainly time to consider the potentially game-changing roles microbiota might play in geochemical processes.

Another clue to the timing of events is the presence of ellipsoidal orthoquartzite clasts. Some are agatized, but the vast majority appears to be composed of quartz sandstone, cemented with silica. To date, three clasts have been found inside Jewel Cave. One is coated with calcite spar, and was therefore emplaced prior to precipitation of the calcite (Figure 4).

None are found near known entrances, and all are separated from the surface by hundreds of feet of non-cave-bearing rock. Many more are scattered across the surface near the Pahasapa/Minnelusa contact. For many decades, local geologists assumed they were concretions, formed at the base of the Minnelusa Formation. However, since 2009, the author has mapped over 10,000 clasts distributed over 1,500 square miles (Figure 5).



Figure 4. Quartzite clast inside Jewel Cave

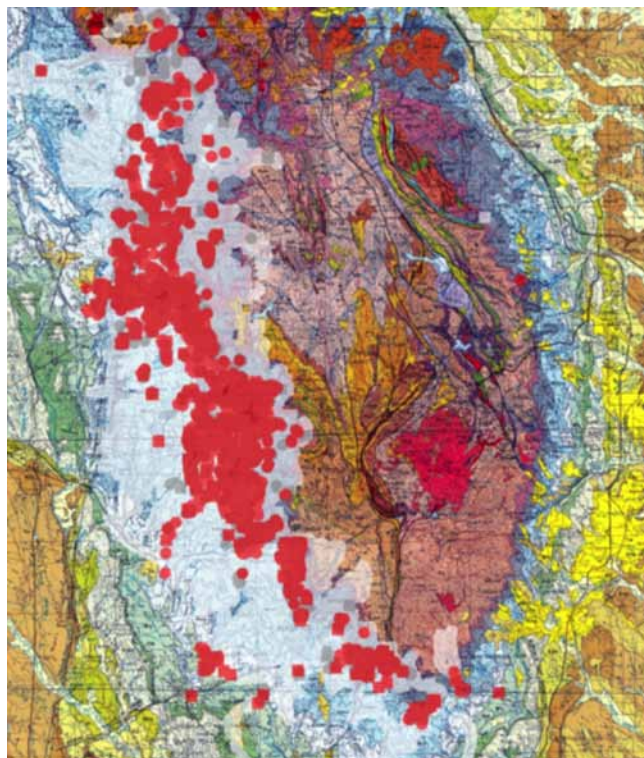


Figure 5. Location of quartzite clasts, in red

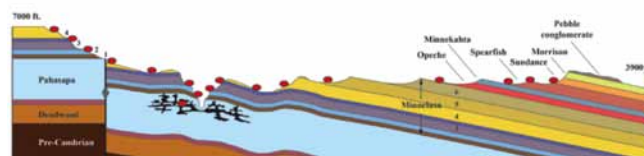


Figure 6. Distribution of quartzite clasts relative to Jewel Cave

They lie on top of strata ranging from the Mississippian Pahasapa limestone to the Cretaceous Lakota Sandstone, at elevations ranging from 3,900 to 7,000 feet, (Figure 6). Because the distribution of clasts cross-cuts the erosional landscape, it is apparent that the clasts were placed after the erosion; about the time landscape features were reaching their present configuration, but before the large drainages were fully incised.



Figure 7.



Figure 8. Rounded cobble of Inyan Kara pebble conglomerate

Recently, several clasts have been found in known vertical fault planes, and surrounded by red shale from the downthrown block (Figure 7). This implies that they were deposited on the surface before the faulting occurred. Therefore, it is conceivable that a few clasts descended into large fractures *before* cave passages were formed, and that the fractures were subsequently sealed by in-filling red shale. If so, later dissolution could have formed a passage around the clast (and adjacent fill), and then precipitated calcite spar before the draining of the cave – resulting in a configuration similar to Figure 4.

Although this may seem like a paleofill scenario, where infiltrating waters are directed along the path of ancient “paleo-filled” passages, that’s not really the case. These were fractures, not preexisting passages; and the cave clearly conforms to today’s topography, structure, and stratigraphy – none of which existed in pre-Pennsylvanian time. In fact, after deposition, the Pahasapa was flat lying when the Pennsylvanian sea encroached. There had been no uplift, no structure, no hills and valleys, and no overlying rock layers. Therefore, these observations represent distinctly younger events, by at least 300 million years.

Surprisingly, no local source has been found for the quartzite clasts, so it is worth considering that they might have been transported from the west, perhaps the Bighorns or Laramie Peak. As unlikely as this might sound, this study found rounded cobbles of an Inyan Kara pebble conglomerate (Figure 8), located over three miles east of their origin, the crest of Elk Mountain ridge. To arrive at their new location, they had cross perpendicular to three major north-south drainages, most likely prior the main incisions of the canyons.

While these have a known local source, they clearly support the possibility of eastward travel across drainages by a presently unknown mechanism.

In conclusion, the evidences suggests that quartzite clasts of unknown origin were deposited on an erosional surface around the time the landscape was reaching modern configuration, but before the final incision of major canyons. Later incision occurred in response to an uplift that also created large fractures which some of the clasts fell into, and were sealed by shale collapsing in after them. A sandstone aquifer carried the initial flow from recharge to discharge areas, distributing water to fractures in the limestone. The confined nature of the aquifer prevented CO₂ from degassing; maximizing the effectiveness of dissolution. The amount of flow was controlled by the hydrologic properties of aquifer. At reasonable, estimated flow rates, this model could remove the entire volume of Jewel Cave in 1.1 million years, freeing any quartzite clasts, and then coating at least one of them with calcite spar, prior to the final draining. The presence of microbial life might have supplemented the amount of CO₂ in the water, and could have significantly enhanced the dissolution rate.

Details about the interaction of cave development with landscape events remain uncertain, but the origin of Jewel Cave cannot be adequately explained without taking all these observations into account.

Acknowledgements

This work would not have been accomplished without much dialogue with Art and Peg Palmer for over 30 years. Former SDSMT geology professors, Perry Rahn and Alvis Lisenbee, have a wealth of knowledge; they’re always willing to listen patiently, and then encourage me with additional relevant ideas to pursue. Kyle Hazelwood is a SDSMT PhD geology student with enthusiasm, a keen eye for field work, and a healthy ability to think outside the box; it has been a pleasure to discuss our often differing observations, and discover the common connections between them.

References

- Palmer, A. N., 2007, *Cave Geology*, Cave Books, Dayton Ohio.
- Barton, H. A., 2015, Personal communication.
- Boston, P. J., 2016, Personal communication.
- Wiles, M. E., 1992, *Infiltration [of groundwater] at Wind and Jewel Caves, Black Hills, South Dakota*: Master’s thesis, South Dakota School of Mines and Technology.

Shi Wenqiang^{1,2}, Erin Lynch¹, Zhang Yuanhai¹

¹*Institute of Karst Geology, Chinese Academy of Geological Sciences / Key Laboratory of Karst Dynamics, MLR&GZAR, Guilin, Guangxi 541004, China*

²*School of Earth Sciences, China University of Geosciences, Wuhan, Hubei 430074, China*

The Jingxi City is located in the southwest of Guangxi Zhuang Autonomous Region in southern China (Fig.1). The area of the city is 3322 km² with more than 80 percents is covered by carbonate rocks.



Figure 2 The peak clusters landform

There are many typical peak clusters and numerous karst caves which are developed on the pure limestone, dolomitic limestone and biological limestone from Middle Devonian to Late Carboniferous (Fig.2).

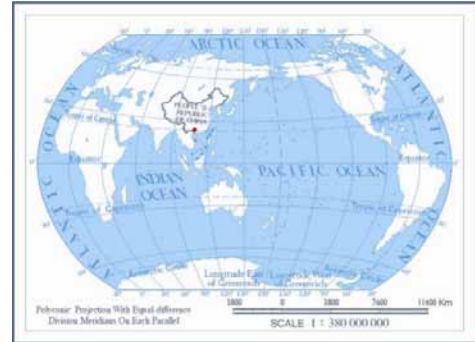


Figure 1 The location of the study area

Due to situate in the transition zone between the Yunnan-Guizhou Plateau to Guangxi Basin, the Jingxi region is characterized by obvious step landform. In each step region there are different subarea features of karst caves. For example, in the northwest area of high altitude the vertical shaped caves develop. The middle part with foot caves and the southeast area of low altitude with the peculiar underground streams, light through caves and tiankeng. They have a very close connection and can reflect the regional hydrogeological evolution process jointly (Fig.3).

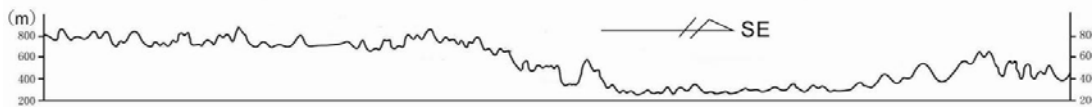


Figure 3 The obvious step landform from northwest to northeast in the study area

The form and scales of caves in Jingxi area is distinctly controlled by topography, lithology and geological structure. At the same time, they have the special layered features because of the neotectonic uplift effect which could have compares well with global famous Himalayan tectonic movement. So the cave here is nice repository for Quaternary geological environment research of southern China, and East Asia.



Figure 4 The waterfall of 268m depression



Figure 5 The rare lip-shaped stalactite

Within a short distance the river and subterranean stream appear alternately. The rare lip-shaped stalactite in the cave is very ornamental and has become a karst geological heritage feature (Fig 5). Early in 2003, the professional Chinese and Foreign covers conducted cave exploration here, and now more and more cavers arrive here and want to explore the magic karst land (Fig 6).

In southeast Jingxi there is significant difference in uplift rate of up to 300m resulting in an obvious knick point. Under these circumstances both the river and underground conduit water incise a lot and form large-scale waterfall (Fig 4).

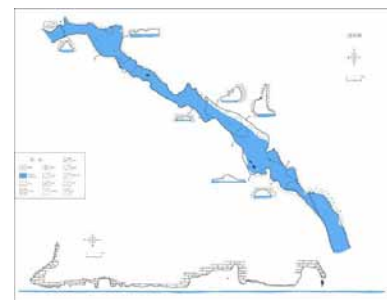


Figure 6 The cave figure of a water cave in study area

Speleothem Research

An Hypothesis On The Evolution Of Complex Flowstones

Giovanni Badino¹, José Maria Calaforra², Jo De Waele³ & Paolo Forti³

Affiliation: ¹La Venta Esplorazioni Geografiche & Department of General Physics, , University of Torino, Italy, badino@to.infn.it
²La Venta Esplorazioni Geografiche & Department of Biology and Geology, CAES Global Change, University of Almeria, Spain, jmcalaforra@ual.es
³La Venta Esplorazioni Geografiche & Department of Biological, Geological and Environmental Sciences, Italy, jo.dewaele@unibo.it, paolo.forti@unibo.it

Abstract

During a speleological expedition to the Puerto Princesa Underground River (Palawan, Philippines) a drapery characterized by several close-to-horizontal ribs has been noticed. Its study allowed to present an hypothesis on the evolutionary mechanism leading to its development which may fit also for other complex speleothems, like the stepped flowstones, which are very common all around the world. These flowstones present several close-to-horizontal steps, widening's and narrowing's along their growth axis, often giving rise to “organ-pipe” structures and pseudo-stalactites, the genesis of which cannot be justified by means of the general theory explaining the growth of normal speleothems, which is based on a steady flow of the feeding water.

Keywords: Complex flowstones; speleothems; genetic model.

1. Introduction

The morphological characteristics of speleothems are mainly controlled by the type of water flow feeding them (Hill & Forti, 1997). This characteristic has allowed to create theoretical models defining the shape of some of the most common speleothems such as stalagmites (Franke, 1975; Curl, 1973; Dreybrodt, 1999; Kaufmann, 2003; Romanov *et al.*, 2008), stalactites (Curl, 1972, Kaufmann, 2003; Short *et al.*, 2005), and rimstone dams (Wooding, 1991). These models are mainly based on the in time evolution of supersaturation during the flow of the feeding water over the speleothem.

Detailed geochemical (stable isotope) studies and petrography on speleothems often can allow to reveal the processes that caused the feeding water to precipitate carbonate (mainly calcite and aragonite), and thus the evolution of waters in underground environments due to a variety of processes active in these environments (i.e. differential CO₂ and/or H₂O loss from a water film, differential aerosol deposition, deposition in subaqueous environments) (Caddeo *et al.*, 2015). Recent studies also focused on the effect of the steady flow hydrodynamics in developing “crenulations” (ripple-like structures characterized by a wavelength close to 1 cm) over stalactites, stalagmites and flowstones (Camporeale & Ridolfi, 2012; Vesipa *et al.*, 2015).

In this case the variation of the supersaturation was induced by variation in the thickness of the water film and/or the development of micro-bubbles of gas within the water, inducing enhanced diffusion of CO₂ to the cave atmosphere.

All these models are based on the assumption of stationary homogeneous flow conditions, but most of the real speleothems evidence complex morphological patterns, which cannot be explained in such boundary conditions.

The most common of these forms are typical in large flowstones, stalagmites and columns, which exhibit a series of “steps” along their surface with the close-to-vertical area in between steps characterized by indented surfaces resembling “organ pipes” or by upside-down conical flat surfaces (Fig. 1).

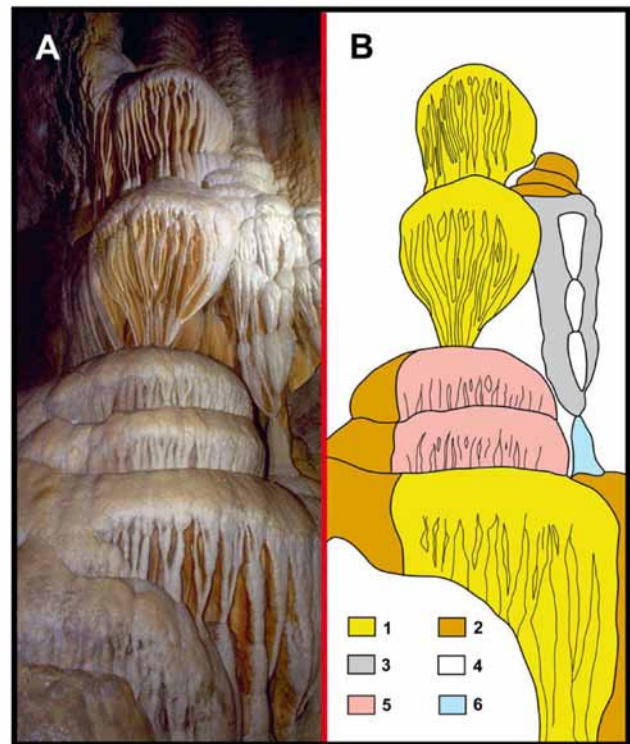


Figure 1. A: Re Tiberio cave (Emilia Romagna, Italy): a big complex flowstone, evolution of which was totally independent from the underlying shape of the rock surface. B: graphic restitution of its principal characteristics: 1: “octopus”; 2: big steps; 3: upside-down conical drapery; 4: sequence of upside-down cones; 5: “organ pipes”; 6: stalagmite. (Photo by Carlo Azzali).

These intervals can even be indented by draperies (commonly called “organ pipes” or “octopus”) and can also allow the evolution of pseudo-stalactites and corresponding stalagmites below.

Even though the “octopus” and/or “frozen waterfall” flowstones (as they are normally referred to in the English speaking world) are very common, the commonly accepted genetic mechanism of flowstones (Hill & Forti, 1997) explains only

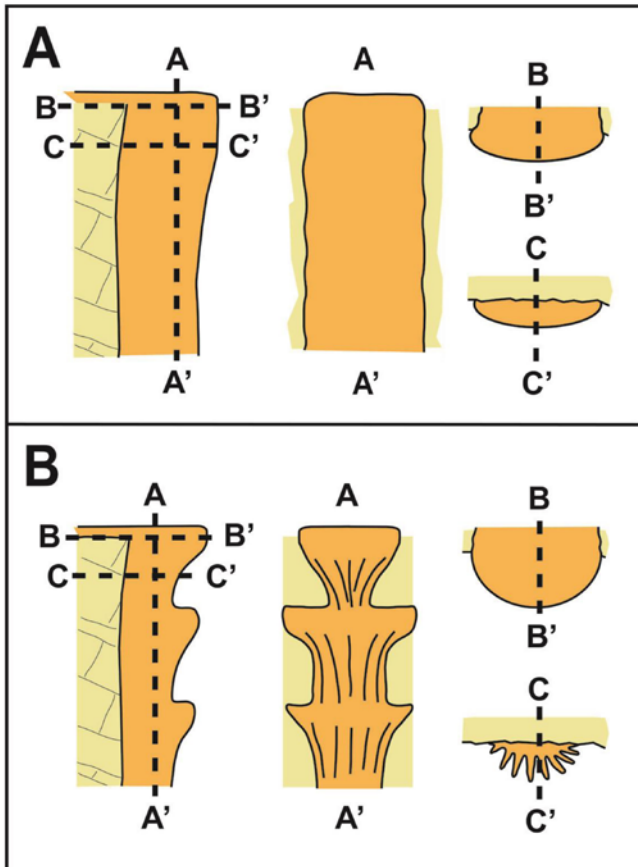


Figure 2. A: structure of a “normal” flowstone developing on a subvertical cave wall; B: superimposed “octopus” structure.

the development of rather flat close-to-vertical surfaces as a consequence of the deposition from a water film flowing simultaneously over the entire speleothem surface (Fig. 2A).

Moreover such mechanism is unable to justify the presence of steps, beside those directly inherited from discontinuities of the rock substratum, and has even more problems justifying the indented surfaces (Fig. 2B).

In fact, until now the evolution of the flowstones has been regarded as the simple consequence of the steady flow of a more or less supersaturated water layer, which consequently causes a rather homogeneous deposition over the whole speleothem. If the feeding on top of the speleothem is constant, the flow along its close-to-vertical surface will result homogeneous, thus the speleothem growth is expected to consist (and practically it is in many occurrences) of superimposed calcite layers, the thickness of which must, at least theoretically, progressively decrease from the top to the bottom of the speleothem, following the progressive lowering of the initial supersaturation induced by the CaCO_3 deposition.

2. A new genetic hypothesis

The way to explain the genesis and the development of the complex speleothems was given by the study of a recently found peculiar drapery. In fact, inside the Puerto Princesa Underground River (Palawan, Philippines) a “ribbed drapery” has been discovered, the evolution of which has been controlled by the peculiar regimen of its feeding water flow (Badino *et al.* 2016). In fact it has been evidenced that the

sub-horizontal ribs along the drapery sides developed due the sudden local increase in supersaturation induced by the transition from laminar steady flow to subcritical, or critical, flow during the short and rare rainstorms. Moreover the peculiar Palawan climate allowed also to state that evaporation has a very scarce, if any, influence on the development of the ribs.

The morphology of the “ribbed drapery” is obviously more simple than those sometimes present in the complex speleothems: in fact the ribbed drapery may be regarded as a bi-dimensional structure while the other speleothems are fully tridimensional.

As for the ribbed drapery of Palawan, a sudden supersaturation increase always occurring in the same place is necessary to justify the presence of the sudden variation in the flowstone steepness, and its evolution into the stepped form. The supersaturation must occur just at the beginning of the close-to-horizontal section of each step.

As in the case of Palawan, evaporation cannot play a relevant role, being unlikely that it will constantly affect only a few selected places, being inactive on all the other parts of the speleothem. Therefore the only mechanism allowing the evolution of the steps of the complex speleothems can only be the variation of the feeding water flow.

Flow velocity will, in fact induce, in some given areas, the transition from sub-critical to critical velocity (or even from laminar to turbulent flow) with consequent local variation of the thickness of the water film, up to its splitting-up, and the evolution of micro-bubbles inside the water. As explained above, all these processes induce a stationary supersaturation which causes the development of a flat surface. For this reason all stepped flowstones, if they are independent from the geometry of the substratum, must be characterized by high flow periods followed by periods of low or even null flow.

The distance between subsequent steps may be very different. This happens because in the flowstones the enhanced supersaturation may be induced not only by the increase of flow rate but also by the presence discontinuities in the substrate (Fig. 3).

In any case the development of the horizontal part is induced by turbulence, the increase of which is controlled by the flow regimen, which is directly proportional to turbulence. Therefore the development of the steps mainly occurs during the water pulses, being scarce or even null in the dry periods.

Once the genesis of the steps is defined, the fact that the dimension of their close-to-horizontal upper part may greatly vary must be explained. The step dimension not only varies among different flowstones but also from step to step within the same speleothem.

The close-to-horizontal development of a single step is controlled by the time lapse in which the turbulence-induced supersaturation is maintained in spite of the progressive deposition of CaCO_3 .

This time, in turn, depends on two different factors: 1) the initial supersaturation degree, which is controlled by the amount of turbulence, and 2) the velocity of the feeding water, which allows a longer effect along the close-to-horizontal path.

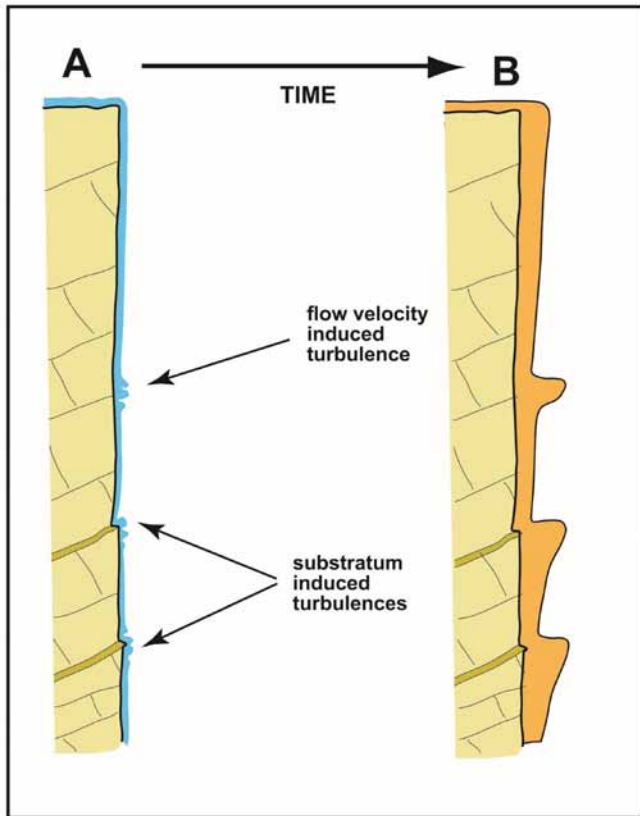


Figure 3. A: turbulence may be induced both by increase in the flow velocity or the presence of discontinuities in the substratum; B: it is impossible to distinguish steps developed by one or the other of these mechanisms on a simple morphological basis.

In the case of the Palawan drapery the amount of the feeding water was necessarily constant over each rib and therefore the only conditioning factor was the initial supersaturation. For this reason most of the ribs have a similar size, with significant variations only induced by the coalescence of two or more subsequent ribs (Badino *et al.* 2016).

In the case of flowstones, the amount of feeding water, and consequently the flow velocity, may be very different from step to step: this because the complex shape of the speleothem allows for an easy local diversion and/or merging of the original feeding water. If the starting supersaturation for each step is kept roughly constant, which is reasonable (the feeding water is generally homogeneous), their close-to-horizontal length will be controlled only by the flow rate, because the deposition will always last roughly the same time, but the distance covered by the water will increase with velocity (Fig. 4).

Anyway this is not completely true because the larger steps will increase their elevation more than the smaller ones.

This occurs because the longer close-to-horizontal path will cause a slightly higher reduction in the water flow velocity with consequent increase of the thickness of the deposited calcite layers.

The high variability of the water flow over the different sections of a complex flowstone makes it extremely difficult to exactly define the mechanisms by which other forms beside the just discussed ones develop. Anyway, on the basis of the diversion and merging of the feeding water it is possible to justify the existence of inclined surfaces linking an upper step to a lower one: in fact the inclined surfaces develop as a

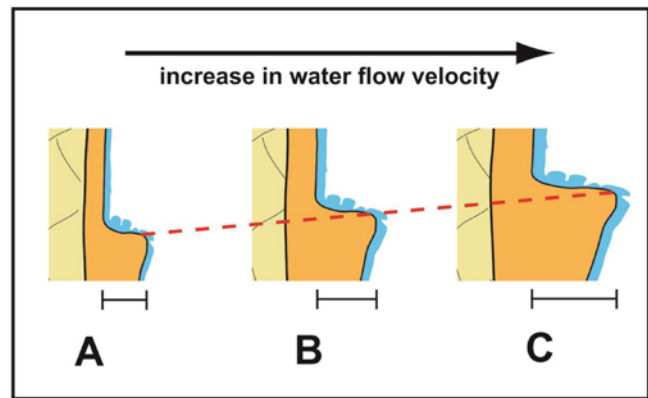


Figure 4. The dimension of the close-to-horizontal upper part of the step is directly proportional to the flow rate and the larger steps increase their elevation more rapidly than the smaller ones.

consequence of the very different flow rate characterizing the two steps, which consequently have a different vertical growth velocity.

The evolution of the flowstone just below a close-to-horizontal step may result even more different: it may be close-to-vertical or progressively more indented, and may exhibit rather flat surfaces or more or less indented ones and finally may progressively reduce its size assuming a shape of a reverse cone, eventually becoming a true drapery (pseudo-stalactite) which, finally, sometimes allows the evolution on the lower step of a small stalagmite.

The evolution of all these different forms is ruled by the flow regimen in that specific flowstone area and of its variation in time. In reality the controlling factor is just the water flowing after the water pulse, because the supersaturation created during these pulses is almost completely consumed for the close-to-horizontal expansion of the steps.

At the end of a feeding period, if the still flowing water is enough to maintain a homogeneous layer over the whole close-to-vertical area, the resulting speleothem surface will be more or less smooth and flat, and its projection will be inversely proportional to the flow velocity (Fig. 5A).

This happens because the residual supersaturation will be exhausted over a short distance and consequently the growing layers will become thinner downwards.

But if the water flow after the pulse is scarce, the water layer becomes unable to cover the whole surface below the step and the surficial tension downstream will progressively reduce the area interested by active flow, giving, once again, rise to flat and smooth surfaces but more or less resembling an upside-down triangle or cone. This kind of evolution may also be induced if the available water downstream is progressively reduced by evaporation.

The indentation of the sub-vertical lower part of the step is inversely proportional to the flow rate.

If after the pulse, the water flow becomes heterogeneous, some places below the step will be characterized by a higher flow (rills), and therefore they will develop faster with respect to the others with scarce or no flow at all. In other words, the

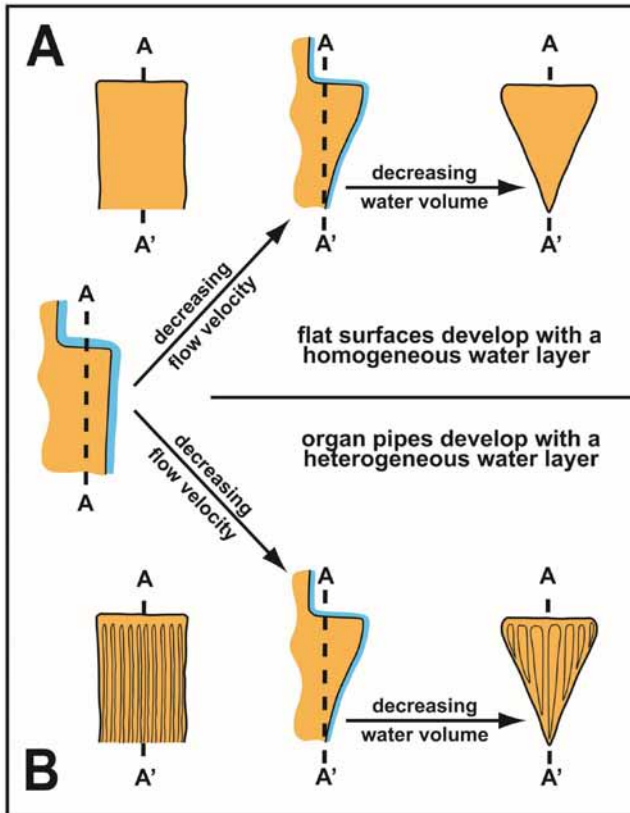


Figure 5. Evolution of the lower part of a step. At the end of the water pulse flat surfaces develop if the speleothem remains completely covered by water, otherwise indented structures (organ pipes) develop.

heterogeneous flow gives rise to privileged flow paths, which will induce the evolution of an “organ pipe” structure, becoming progressively more spaced, thinner and with deeper divides if the heterogeneity of the flow is greater (Fig. 5B).

Normally the “organ pipe” flowstones are still close-to-vertical or scarcely protruding, because the feeding flow is fast enough to ensure a constant deposition from the top to the bottom of the “pipes”. Finally, when the feeding water after the pulse is scarce and slow, thus allowing a fast downstream decrease of the deposited CaCO_3 , the protruding of the structure becomes progressively higher, while the few active rills decrease and coalesce downstream, the whole structure becomes similar to an elongated reverted cone with only a few deep indentations: in this case octopus-like forms develop. During the pulses, the octopus shape enhances the possibility of dripping from the edge of some of its “tentacles”. This process will induce the evolution of small pseudo-stalactites (secondary draperies) over the “tentacles”, while the falling drips from their tips will possibly cause the development of a true stalagmite over the flat close-to-horizontal surface of the underlying step (Fig. 6A). Eventually, if this process remains active for enough time, the pseudo-stalactite joins the stalagmite to form a true column.

Anyway the evolution of pseudo-stalactitic draperies will be induced also by another mechanism, which activates only if the flow changes dramatically from high flow to dry periods. If this happens, in the periods of highest flow the amount of water reaching the step cannot remain totally adherent to the speleothem, mainly at the transition between the upper close-to-horizontal part and the octopus below. In this manner the

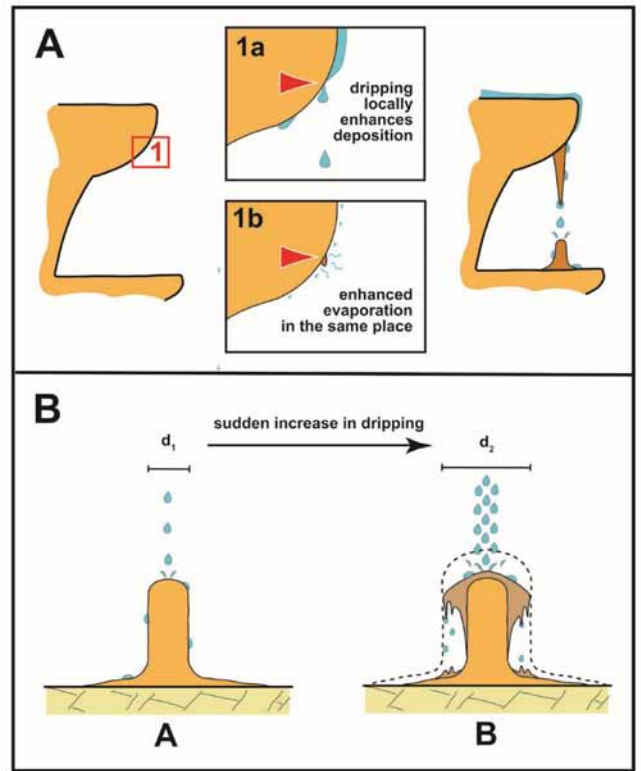


Figure 6. There are two mechanisms causing the evolution of pseudo-stalactites from an “octopus” structure and the consequent possible growth of a stalagmite. A: during high flow periods a stationary dripping forms in a place where enhanced deposition becomes active due to a localized increase in supersaturation (1a), exactly in the same places enhanced evaporation occurs during the low flow to dry periods (1b). B: a sudden increase in the water flowing during the pulses will cause an evolution similar to the well-known one of the stalagmites: A- the shape of a stalagmite in equilibrium with the feeding water; B- the stalagmite shape induced by a recent sudden increase in feeding water (the dotted line shows the new and not yet achieved equilibrium diameter)

same conditions are achieved which rule the development of a stalagmite that undergoes a great sudden increase of feeding water (Fig. 6B). In fact it is renowned that in steady dripping conditions, the stalagmite diameter is directly proportional to the amount of the feeding water (Franke, 1965), lowering when it decreases and becoming larger if it increases.

But when the increase is very high, before reaching the equilibrium diameter, the top of the stalagmite will expand rapidly with respect to its lower part thus transforming itself into a kind of “mushroom”.

The excess of feeding water, dripping from the edge of the “mushroom cap” causes the development of pseudo-stalactite draperies and possibly of stalagmites below them (Fig. 6B).

It is easy to distinguish the stalagmites developing below a flowstone step thanks to this mechanisms: in fact they will correspond to small pseudo-stalactites not necessarily related to pre-existing octopus tentacles.

In conclusion it has been demonstrated that the complex flowstones evolve only when the amount of the feeding water dramatically changes in time. Their close-to-horizontal surfaces develop mostly during high flow periods, while the

forms characterizing the close-to-vertical parts below are controlled by the water regimen during the low flow periods.

3. Final remarks

The study of the Puerto Princesa Underground River ribbed drapery (a simple bi-dimensional structure) suggested that its evolution was totally controlled by the feeding flow regimen during the short but strong rainstorms which characterize this island's climate (Badino *et al.* 2016).

This study allowed also to give a first genetic explanation for other more complex (tridimensional), extremely common but poorly understood speleothems: the stepped flowstones. The transition from subcritical to critical flow velocity and/or the variation in the water layer thickness are the parameters ruling the development of the steps.

Anyway it has to be stressed that if the definition of the evolution of the ribbed drapery may be considered fully exhaustive, the same cannot be said for the stepped flowstones. In fact, at the moment it was only possible to define the main mechanisms allowing the evolution of their general forms, while an explanation for their second order characteristics is still lacking. Further detailed petrographic and geochemical studies might allow to unravel their genesis in more detail.

References

Badino G., 2013. *Cave climate*. In: De Vivo A. & Piccini L. (Eds.), *The River of Swallows- A brief guide to the environmental features of the Puerto Princesa Underground River, Philippines*, Tintoretto, 76-78

Badino G., Calaforra J.M., Forti P., Garofalo P., Sanna L., 2011. The present day genesis and evolution of cave minerals inside the Ojo de la Reina cave (Naica Mine, Mexico) *International Journal of Speleology*, **40**(2), 125-131.

Badino G., Calaforra J.M., De Waele J., Forti P., 2016. *The ribbed drapery of the Puerto Princesa Underground River (Palawan, Philippines)* submitted to International Journal of Speleology

Brennen C.E., 1995. *Cavitation and Bubble dynamics*. Oxford University Press, 268 p. <http://caltechbook.library.caltech.edu/archive/00000001/00/bubble.htm7/8/2003>

Caddeo G.A., Railsback L.B., De Waele J. & Frau F., 2015. Stable isotope data as constraints on models for the origin of coralloid and massive speleothems: The interplay of substrate, water supply, degassing, and evaporation. *Sedimentary Geology*, **318**, 130-141.

Camporeale C., Ridolfi L., 2012, Hydrodynamic-driven stability analysis of morphological patterns on stalactites and implications for cave paleoflow reconstruction. *Physical Review Letters*, **108**, 238501 (doi:10.1103/PhysRevLett.94.018501)

Chanson H., 2009, Current Knowledge In Hydraulic Jumps And Related Phenomena. A Survey of Experimental Results. *European Journal of Mechanics B/Fluids*, **28**(2), 191-210.

Chanson H., 2012. Momentum Considerations in Hydraulic Jumps and Bores. *Journal of Irrigation and Drainage Engineering*, **138**(4), 382-385.

Coombes M.A., La Marca E.C., Naylor L.A., Piccini L., De Waele J., Sauro F., 2015. The influence of light attenuation on the biogeomorphology of a marine karst cave: A case study of Puerto Princesa Underground River, Palawan, the Philippines. *Geomorphology*, **229**, 125-133.

Curl R.L., 1972. Minimum diameter of stalactites. *National Speleological Society Bulletin*, **34**(4), 129-136.

Curl R.L., 1973. Minimum diameter of stalagmites *National Speleological Society Bulletin* **35**(1), p.1-9

Dreybrodt W., 1999. Chemical kinetics, speleothem growth and climate. *Boreas*, **28**(3), 347-356.

Eggers J., 1997. Nonlinear dynamics and breakup of free-surface flows. *Reviews of Modern Physics*, **69**(3), 865-929.

Franke H.W., 1965. The theory behind stalagmite shapes. *Studies in Speleology* **1**(2-3), 89-95.

Hill C. & Forti P., 1997. *Cave minerals of the World*. National Speleological Society, Huntsville, USA, 463 p.

Kaufmann G., 2003. Stalagmite growth and palaeo-climate: the numerical perspective. *Earth and Planetary Science Letters*, **214**, 251-266.

Piccini L. & Iandelli N., 2011. Tectonic uplift, sea level changes and Plio-Pleistocene evolution of a coastal karst system: the Mount Saint Paul (Palawan, Philippines). *Earth Surface Processes and Landforms*, **36**(5), 594-609.

Romanov D., Kaufmann G. & Dreybrodt W., 2008. Modeling stalagmite growth by first principles of chemistry and physics of calcite precipitation. *Geochimica et Cosmochimica Acta*, **72**(2), 423-437.

Short M.B., Baygents J.C. & Goldstein R., 2005. Stalactite growth as a free-boundary problem. *Physics of Fluids*, **17**, 083101.

Short M.B., Baygents J.C., Warren Beck J., Stone S. A., Toomey III R.S. & Goldstein R.E., 2005. Stalactite growth as a free-boundary problem: a geometric law and its platonic ideal *Physical Review Letters*, **94**, 018501.

Vesipa R., Camporeale C. & Ridolfi L., 2015. Thin-film-induced morphological instabilities over calcite surfaces. *Proceedings Royal Publishing Society A*, **471**(2176), 20150031. <http://dx.doi.org/10.1098/rspa.2015.0031>

Wooding R., 1991. Growth of natural dams by deposition from steady supersaturated shallow flow. *Journal of Geophysical Research Solid Earth*, **96**(B1), 667-682.

Multiproxy Analysis Of Holocene Stalagmites From Bosnia And Herzegovina

Chiarini V.^{1,2*}, Couchoud I.^{2,4}, Drysdale R.^{2,3}, Bajo P.⁴, Milanolo S.^{5,6}, Hellstrom J.⁴, Frisia S.⁷, De Waele J.¹

Affiliation: ¹ Department of Biological, Geological and Environmental Sciences (BIGEA), University of Bologna, Italy. veronica.chiarini3@gmail.com; jo.dewaele@unibo.it

² Laboratoire EDYTEM, UMR CNRS 5204, Université de Savoie, Chambéry, France. isabelle.couchoud@univ-smb.fr

³ School of Geography, University of Melbourne, 221 Bouverie St, Carlton VIC 3053, Australia.

⁴ School of Earth Science, University of Melbourne, Australia. rnd@unimelb.edu.au; petrabajo@gmail.com; j.hellstrom@unimelb.edu.au

⁵ Hydro Engineering Institute Sarajevo – HEIS, Stjepana Tomića 1, 7100 Sarajevo, Bosnia and Herzegovina. simone.milanolo@heis.ba

⁶ Centre for Karst and Speleology – CKS, Sarajevo, Bosnia and Herzegovina

⁷ Earth Sciences, SELS, The University of Newcastle, NSW Australia. silvia.frisia@newcastle.edu.au

Abstract

The Mediterranean area is a hotspot for present day and future climate change. The understanding of past climate dynamics in this area is of great importance to gain insight in the pattern of regional climate variability in response to hemispheric and global climate changes. In the central Mediterranean, contrasting climate responses have been observed during the last 12 ka with drier/wetter conditions in the northern/southern regions lasting until about 6-5 ka, followed by a trend toward the opposite conditions. Carbonate mineral stalagmites are continental archives able to provide simultaneous information about past climate and environmental changes. With the aim to get a deeper understanding of Holocene climate dynamics in the Balkan Peninsula, five stalagmites were collected from two Bosnian caves (Govještica and Mračna Pećina; Prača Valley) in the frame of a PhD project involving the Universities of Bologna (Italy) and Savoie Mont Blanc (France) with the collaboration of the University of Melbourne (Australia). Here we present the multiproxy methodological approach adopted for the study of these samples and some anticipations of the major findings.

Keywords: trace elements, stable isotopes, calcite petrography, palaeoclimate, palaeo-environment

1. Study Area

Mračna Pećina (also known as Banja Stijena) and Govještica caves are both located on the left side of the canyon of the river Prača (43°46'20.8" N; 18°53'14.5" E and 43°46'26.2" N; 18°53'18.9"E), about 40 km East from Sarajevo (Bosnia and Herzegovina; Fig. 1) (Milanolo *et al.* 2013). Both caves develop at the foot of the Romanija plateau that reaches the highest elevation of 1500 m a.s.l. in its western portion, while the central and southern portions overlying the caves reach an elevation comprised between 800 and 1000 m a.s.l. The Mračna Pećina cave network develops in Triassic massive limestone and is characterised by a W-E orientation, coherent with a major thrust line. Govještica cave is a resurgence located few hundred metres downstream the Mračna Pećina cave at the elevation of 580 m a.s.l. It develops in the same hostrock and has a major NW/SE orientation.

2. Materials And Methods

Four (BS8, BS9, BS14 and BS15; Fig. 2) out of the five studied stalagmites were found already broken near to the main chamber of Mračna Pećina cave (between 50 and 100 m from the artificial entrance), whereas one sample (G5; Fig.2) was found in the "Sala delle Ossa" (Hall of Bones) in Govještica cave (Fig. 1).

Stalagmites BS14 and BS15 are characterised by a flat and regular lamination and by a squat shape (respectively 9 and 10 cm). BS8, BS9 and G5 present a candle shape and are, respectively, 14.5, 14 and 37 cm tall. While BS9, BS14 and

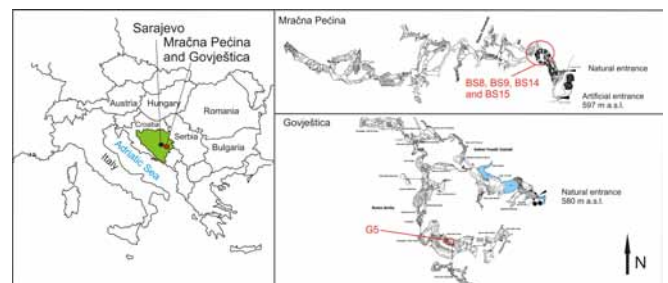


Figure 1. Left: Map of Bosnia and Herzegovina, and location of the capital city, Sarajevo, Mračna Pećina and Govještica cave. Right: Mračna Pećina and Govještica cave maps. The red circles indicate the area where the stalagmites were collected

BS15 are formed by a yellowish calcite, B8 and G5 display cleaner and lighter calcite crystals.

Preliminary dating was performed with the U/Th method at the University of Melbourne (School of Earth Science):

- G5 stalagmite grew during the last glacial period (from ~ 73.0 until ~ 12.5 ka) and the early part of the Holocene (from ~9 ka until ~6 ka). Only the stalagmite portion covering the Holocene period has been considered for this study.
- Stalagmite BS8 covers almost entirely the Holocene from ~ 11.0 ka until ~0.7 ka. However, major growth interruptions occur between ~8.9 and ~7.9 ka, ~7.5 and 5.0 ka and ~ 3.9 and 2.5ka.

- Stalagmites BS9, BS14 and BS15 grew during the later half of the Holocene (from ~ 5 to ~1 ka for BS9, from ~6 to ~2 ka for BS14 and from ~4 to ~1 ka for BS15).

Samples for $\delta^{13}\text{C}$ and $\delta^{18}\text{O}$ analyses were drilled at a 1 mm increment. All carbonate isotope samples were analysed at the School of Geography, University of Melbourne.

Trace element concentrations have been analysed by laser-ablation ICP-MS, continuously along the vertical growth axis of stalagmite BS15 at the School of Earth Sciences (University of Melbourne) (Woodhead *et al.* 2007; Drysdale *et al.* 2012). Correlation coefficients have been calculated between trace elements and between the trace element and stable isotope values.

Petrography was studied on thin sections prepared for stalagmites BS8, BS9, BS14 and BS15 and calcite textures were described and recognised. Since it was not possible to observe petrographic changes along the growth axis of stalagmites BS8 and BS9, a high resolution petrographic examination was performed only for stalagmites BS14 and BS15. In these stalagmites, textures have been classified every millimetre corresponding to the stable isotope profiles along the growth axis, on the basis of the deduced intracrystalline microporosity and the observed inter-crystalline porosity. The classification proposed in Frisia (2015) was considered a starting point and was modified and adapted to this specific case (for further details see Chiarini *et al.* 2017).

3. Results And Discussion

3.1. Stable isotope variations

BS8, BS9, BS14 and BS15 stalagmites present $\delta^{18}\text{O}$ ratios dispersed in the same range of values; stalagmite G5 displays slightly lighter $\delta^{18}\text{O}$ ratios. All $\delta^{18}\text{O}$ profiles present high variability without remarkable long-term trends.

$\delta^{13}\text{C}$ values present bigger differences among the analysed samples, with lower average values characterising stalagmites BS9, BS15 and the younger portion of stalagmite BS8. The latter presents markedly higher $\delta^{13}\text{C}$ values before ~ 7 ka followed by lower values during late Holocene. A weak trend toward slightly higher $\delta^{13}\text{C}$ values is recognisable in BS15 and BS9 during the last 4 ka. BS14 does not present any trend, but displays large fluctuations of $\delta^{13}\text{C}$. G5 presents a trend toward lower values from ~ 10 ka until ~ 8 ka followed by a weak trend toward relatively higher values.

3.2. Trace elements in stalagmite BS15 coupled with stable isotope variations

Among divalent cations (Sr, Ba, and Mg), the results show a strong covariation between Sr and Ba, and an antiphase trend between Mg and both Sr and Ba. The trivalent cation Y, the metals Cu and Zn, and the electronegative element P are linked by positive correlations, resulting in common trends. These elements are characterised by strong adsorption behaviour in soils, compared to the solution preference of the divalent cations like Sr and Mg (Borsato *et al.* 2007 and references therein). Trace element variation in the precipitated calcite is related to several factors that can

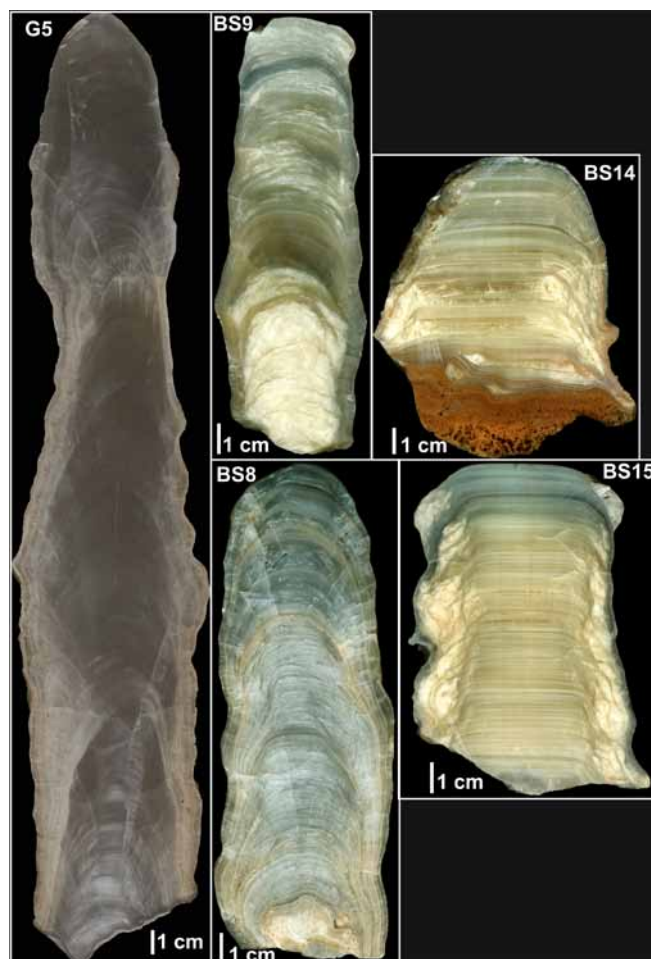


Figure 2. Polished sections of the studied stalagmites. G5 comes from Govještica cave; BS8, BS9, BS14 and BS15 come from Mračna Pečina cave.

more or less be directly linked to environmental and/or climate changes. The presence of a strong negative correlation between Sr and Mg ($r = -0.62$; Fig. 3) suggests their variation to be related to groundwater residence time: drier conditions, which induce longer residence times, are thought to be responsible for selective leaching of Mg from soil or host rock (i.e. higher Mg in dripwater) and slower growth rate leading to decreased Sr concentration in the precipitated calcite (e.g. Fairchild *et al.* 2000; Huang and Fairchild 2001). Given the strong positive correlation between $\delta^{13}\text{C}$ and

Mg concentration ($r = 0.72$; Fig. 3), $\delta^{13}\text{C}$ ratios can be considered as a hydrological proxy. Drier periods are indeed associated with slower drip rate causing longer residence time, and calcite deposition under thinner

Films of fluids. These conditions are thought to be responsible for $\delta^{13}\text{C}$ increases (Affek and Zaarur 2014)

3.3. Petrography and its contribution to palaeo-environmental signal interpretation

Stalagmite BS8 shows alternation of compact and open columnar calcite (Frisia *et al.* 2015 and references therein). Higher porosity is associated with higher growth rate and markedly higher $\delta^{13}\text{C}$ ratios from the bottom until 52 mm from the top (i.e. early Holocene until ~ 7.5 ka). This could suggest a strong cave ventilation possibly related to a

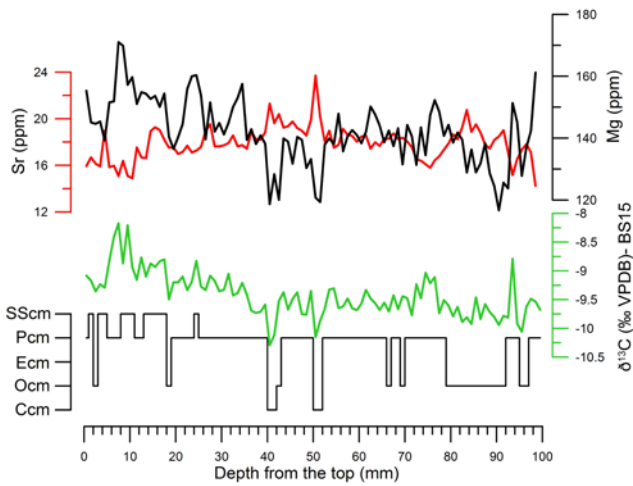


Figure 3. Trace elements (Sr and Mg: average calculated for each millimetre corresponding to the stable isotope profile), $\delta^{13}\text{C}$, and petrography variations in stalagmite BS15.

stronger temperature seasonality during this period, compared to the Late Holocene, characterised instead by compact columnar calcite associated with higher $\delta^{13}\text{C}$ ratios (Deininger *et al.* 2012).

Stalagmite BS9, which grew during the Late Holocene, is formed by columnar microcrystalline calcite, which alternates with dendritic calcite, suggesting its formation under irregular drip rate (high seasonality) and strong supply of foreign particles (Frisia *et al.* 2015).

The columnar microcrystalline calcite also characterises the Late Holocene BS14 and BS15 stalagmites that also present dendritic texture in their flanks. At the lamina scale different columnar microcrystalline calcite subtypes have been identified and classified into: compact columnar microcrystalline calcite (**Ccm**), open columnar microcrystalline calcite (**Ocm**), elongated columnar microcrystalline calcite (**Ecm**), porous columnar microcrystalline calcite (**Pcm**) and *stricto sensu* columnar microcrystalline calcite (**SScm**) (Chiarini *et al.* 2017). The cross-comparison of the classified textures with both stable isotope and trace element composition showed the presence of a link between geochemical parameters and calcite fabrics, suggesting the presence of a common factor triggering both geochemical and textural changes. In particular, progressively higher $\delta^{13}\text{C}$ and Mg concentration are found from **Ccm** to **SScm** and **D** suggesting that calcite precipitation occurred under increased hydrological stress (Fig. 4). This approach has thus allowed using calcite fabrics to extract fragments of palaeoenvironmental information.

More specifically, groups of laminae showing a **Ccm** fabric present the lowest $\delta^{13}\text{C}$ ratio and the highest Sr content. These are also bounded by wavy and brownish surfaces suggesting the occurrence of strong infiltration events causing a massive flushing of organic matter after a relatively dry period (i.e. Mediterranean-like climate). **Ocm** fabric, characterised by an increased porosity, suggests the presence of slightly drier conditions if compared to **Ccm** conditions of deposition. **Ecm** fabric only appears in the younger portion of BS14 and is associated with a generally

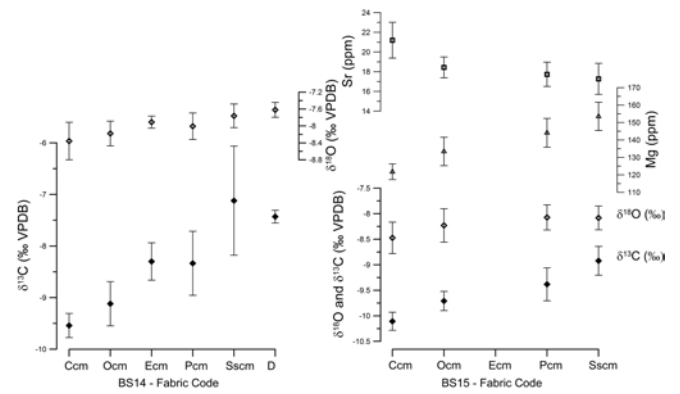


Figure 4. Isotope-fabric plots for BS14 and BS15 stalagmites and trace element-fabric plot for stalagmite BS15. For each fabric type, average $\delta^{13}\text{C}$ and $\delta^{18}\text{O}$ (for BS14 and BS15) and average Sr and Mg content (for BS15) values are plotted with their standard deviation.

drier climate. **Pcm** fabric deposited under dry conditions and slow drip rates, as shown by $\delta^{13}\text{C}$ higher than **Ecm** and lower Sr content. Finally, the **SScm** fabric and the **dendritic** fabric mainly occur, respectively, in the upper 18 mm of stalagmite BS15 and in the upper 3 mm of stalagmite BS14. **SScm** is associated with higher $\delta^{13}\text{C}$ values but $\delta^{18}\text{O}$ values are comparable to those of **Pcm**. In this stalagmite portion, brown laminae are faint or absent, suggesting a lack of significant flushing events and/or low vegetation activity. The presence of **dendritic calcite** at the top of BS14, associated with isotopic values comparable to the **SScm** in the same stalagmite, would also indicate generally drier conditions (Chiarini *et al.* 2017).

4. Conclusions

Stalagmites sampled in two caves in Bosnia and Herzegovina have been studied. A multiproxy approach involving cross-comparison of geochemical and petrographic data has been adopted for 4 out of the 5 considered stalagmites. A petrography micrologging method has been applied, allowing for the extraction of palaeoenvironmental information. This method enabled the interpretation of climate-related signals recorded in stalagmites with stable isotope profiles showing a noisy signal and lacking of clear trends. Comparison of stable isotopes, micropetrography and trace elements has allowed identifying hydrological changes as the main forcing parameter in stalagmites BS14 and BS15, showing the presence of a long-term trend towards slightly drier conditions during the Late Holocene for the studied region. Conversely, petrographic observations performed at lower resolution in stalagmites BS8 allowed for the identification of strong seasonality during the first millennia of the current interglacial period.

Acknowledgements

We are grateful to the “Gruppo Speleologico Bolognese/Unione Speleologica Bolognese” for the technical help during sampling campaigns in Bosnia, to the “Federazione Speleologica dell’Emilia Romagna” and the “Gruppo Speleologico Faentino” for funding provided. A special thanks to Emilie Chalmin (Université Savoie Mont-Blanc, France) and Diego Ercole Angelucci (University of Trento, Italy) for the support provided during microscopic observations

and Fausto Desalvo (Department of Mathematics, University of Bologna, Italy) for the help provided in the statistical analyses.

References

- Affek H, Zaarur S, 2014. Kinetic isotope effect in CO₂ degassing: insight from clumped and oxygen isotopes in laboratory precipitation experiments. *Geochimica et Cosmochimica Acta*, **142**, 319-330.
- Borsato A, Frisia S, Fairchild IJ, Somogyi A, Susini J, 2007. Trace element distribution in annual stalagmite laminae mapped by micrometer-resolution X-ray fluorescence: implications for incorporation of environmentally significant species. *Geochimica et Cosmochimica Acta*, **71**, 1494-1512.
- Chiarini V, Couchoud I, Drysdale R, Bajo P, Milanolo S, Frisia S, Greig A, Hellstrom J, De Waele J, 2017. Petrographical and geochemical changes in Bosnian stalagmites and their palaeo-environmental significance. *International Journal of Speleology*, **46** (1), 23-39.
- Deininger M, Fohlmeister J, Scholz D, Mangini A, 2012. Isotope disequilibrium effects: The influence of evaporation and ventilation effects on the carbon and oxygen isotope composition of speleothems – A model approach. *Geochimica et Cosmochimica Acta*, **96**, 57-79.
- Drysdale R, Paul BT, Hellstrom JC, Couchoud I, Greig A, Bajo P, Zanchetta G, Isola I, Spötl C, Baneschi I, Regattieri E, Woodhead JD, 2012. Precise microsampling of poorly laminated speleothems for U-series dating. *Quaternary Geochronology*, **14**, 38-47.
- Fairchild IJ, Borsato A, Tooth AF, Frisia S, Hawkesworth CJ, Huang Y-M, McDermott F, Spiro B, 2000. Controls on trace element (Sr-Mg) compositions of carbonate cave waters: implications for speleothem climatic records. *Chemical Geology*, **166**, 255-269.
- Frisia S, 2015. Microstratigraphic logging of calcite fabrics in speleothems as tool for palaeoclimate studies. *International Journal of Speleology*, **44** (1), 1-16.
- Hellstrom J, 2006. U-Th dating of speleothems with high initial ²³⁰Th using stratigraphical constraint. *Quaternary Geochronology*, **1**, 289-295.
- Hendy CH, 1971. The isotopic geochemistry of speleothems - I. The calculation of the effects of different modes of formation on the isotopic composition of speleothems and their applicability as palaeoclimatic indicators. *Geochimica et Cosmochimica Acta*, **35**, 801-824.
- Huang Y., Fairchild I.J., 2001. Partitioning of Sr²⁺ and Mg²⁺ into calcite under karst-analogue experimental conditions. *Geochimica et Cosmochimica Acta*, **65**, 47-62.
- Milanolo S, Preti N, Cella G, 2013. Govještica Cave – Prača Canyon, BIH. *Naš Krš Sarajevo*, **23**, 43.
- Woodhead JD, Hellstrom J, Hergt JM, Greig A, Maas R, 2007. Isotopic and elemental imaging of geological materials by laser ablation inductively coupled plasma-mass spectrometry. *Geostandards and Geoanalytical Research*, **31** (4), 331-343.

Comparison Of South Asian And Tropical Australian Stalagmites Reveals Expansion And Contraction Of The Indo-Pacific Tropical Rain Belt Over The Last 3000 Years

Rhawn F. Denniston^{1*}, Caroline C. Ummenhofer², Alan D. Wanamaker, Jr.³, Matthew S. Lachniet⁴, Gabriele Villarini⁵, Yemane Asmerom⁶, Victor J. Polyak⁶, John Cugley⁷, David Woods⁸, William F. Humphreys⁹

Affiliation: ^{1*}Presenting and Corresponding Author: Department of Geology, Cornell College, Mount Vernon, IA 52314 USA; rdenniston@cornellcollege.edu
² Department of Physical Oceanography, Woods Hole Oceanographic Institution, Woods Hole, MA 02543 USA
³ Department of Geological and Atmospheric Sciences, Iowa State University, Ames, IA 50011 USA
⁴ Department of Geoscience, University of Nevada Las Vegas, Las Vegas, NV 89154 USA
⁵ IHR-Hydroscience and Engineering, University of Iowa, Iowa City, IA 52240 USA
⁶ Department of Earth and Planetary Sciences, University of New Mexico, Albuquerque, NM 87131 USA
⁷ Australian Speleological Federation, Perth, Western Australia, Australia
⁸ Department of Environment and Conservation, Broome, Western Australia, Australia
⁹ Western Australian Museum, 49 Kew Street, Welshpool, WA 6106, Australia

Abstract

The Hadley Circulation involves the atmospheric exchange between the tropics and subtropics, with warm, moisture-laden air rising near the equator, flowing poleward to approx. 30° latitude, descending, and finally returning to the tropics. Rainfall is concentrated in the areas of the ascending limb while the descending limb produces zones of high pressure and aridity. Modeling experiments and satellite observations have suggested recent changes in the strength and positioning of the Hadley Circulation in response to a warming climate, with implications for rainfall across much of Australia.

The intertropical convergence zone (ITCZ) represents the rising (wet) arm of the Hadley Circulation and migrates annually between a global average of 9°N–2°S, following summer heating of the continents. The asymmetry between the hemispheres is a response, in part, to the greater landmass in the Northern Hemisphere (continents warm more than oceans). The movement of the ITCZ across the equator defines the tropical rain belt (TRB), a region of enormous terrestrial and marine biodiversity and home to 40% of people on Earth. The TRB is dynamic and responds to changes in climate. Geologic and biologic records have shown that in some regions (e.g., South America) the TRB shifted south as a coherent system during periods of Northern Hemisphere cooling such as the Little Ice Age (AD 1400–1850). Southward displacement of the TRB would have reduced rainfall at the previous TRB northern margin as the ITCZ would not have penetrated as far north as it had during previous boreal summers. At the previous TRB southern margin, rainfall would be increased as the ITCZ moved even further south than normal. However, a small number of studies have suggested that instead of moving latitudinally as a coherent system, the TRB expanded and contracted, with in-phase changes in rainfall between the hemispheres (i.e., drier in both hemispheres during cool periods/wetter during warm periods).

We attempted to better understand past dynamics of the Indo-Pacific TRB by developing a precisely-dated, oxygen isotopic stalagmite record of monsoon rainfall from the central Australian tropics (the southern margin of the regional TRB) spanning the last 3000 years. When compared to stalagmite records of monsoon rainfall from southern China (the northern TRB margin), in-phase rainfall changes are apparent, suggesting the Indo-Pacific TRB expanded and contracted numerous times over multi-decadal to centennial scales. State-of-the-art climate model simulations of the last millennium suggest linkages to changes in the structure of the Hadley Circulation.

Keywords: stalagmite, monsoon, oxygen isotope, tropical rain belt, Australia

1. Introduction

The TRB marks the region of the tropics traversed by the ITCZ and is characterized by intense seasonal rainfall (Figure 1). The mean location of the planetary ITCZ has varied over recent millennia in response to changes in the temperature gradient between the hemispheres. For example, millennial-scale cold periods that punctuated the last glacial period led to a southward shift in the TRB, resulting in wetter conditions in the Southern Hemisphere (SH) and drier conditions in the Northern Hemisphere (NH) (Wang *et al.*, 2001; Wang *et al.*, 2004; Partin *et al.*, 2007; Griffiths *et al.*, 2009; Ayliffe *et al.*, 2013; Denniston *et al.*, 2013a). The position of the TRB has continued to shift southward slowly during the

Holocene (since 11,500 years ago) in response to changes in Earth's orbital precession that has moved NH summer toward aphelion (Haug *et al.*, 2001). At the same time, short-term shifts have occurred as the high northern latitude cooled and ice cover expanded at times such as the Little Ice Age (AD 1400–1850) (Broccoli *et al.*, 2006; Chiang and Friedman, 2012). While several studies have identified anti-phasing of monsoon rainfall between the hemispheres for the Holocene (i.e., drier in the NH/wetter in the SH) (Bird *et al.*, 2011), a small number of studies in Africa (Collins *et al.*, 2011) and the Indo-Pacific (Konecky *et al.*, 2013; Yan *et al.*, 2015) have suggested that the TRB expanded and contracted, producing

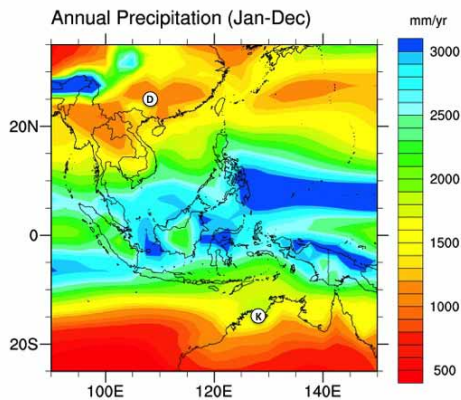


Figure 1. Annual rainfall for the period AD 1900-2005, based on the multi-ensemble mean for the ALL forcings scenario in the Last Millennium Ensemble. Circles denote locations of Dongge cave (D) and KNI-51 (K).

symmetrical interhemispheric changes in rainfall (i.e., drier or wetter in both the NH and SH).

Stalagmites are widely used paleomonsoon proxies because they offer high temporal resolution, can be dated precisely using uranium-thorium (U-Th) techniques, and are sensitive to changes in monsoon activity through amount effects on oxygen isotopes in precipitation (Dansgaard, 1964). The majority of stalagmite-based monsoon reconstructions have been developed from caves in the NH tropics, and as a result, the evolution of SH monsoons remain less well understood. This is particularly true for the southern margin of the Indo-Australian Summer Monsoon (IASM) across the Australian tropics. This study reports oxygen isotopic analyses and precise U-Th dating of stalagmites from cave KNI-51 (15.3°S, 128.6°E), located in the eastern Kimberley (Denniston *et al.*, 2016). The KNI-51 record reflects monsoon activity across the southern margin of the Indo-Pacific TRB and is integrated here with stalagmite records from the northern TRB margin in China to examine regional TRB dynamics during the last 3000 years. In order to better evaluate these findings, cutting-edge paleoclimate models of the last millennium are examined to constrain the origins of TRB behaviour.

2. Points of Comparison from the Northern Margin of the Indo-Pacific TRB

Three stalagmite records of past monsoon variability from the northern margin of the regional TRB were compared with the KNI-51 time series. The caves are located in China and together form a roughly north-south transect through the East Asian Summer Monsoon (EASM) regime (Figure 1): Wanxiang cave (33.3°N, 105.0°E) (Zhang *et al.*, 2008); Heshang cave (30.5°N, 110.4°E) (Hu *et al.*, 2008); and Dongge cave (25.3°N, 108.1°E) (Wang *et al.*, 2005). Of these, Dongge cave is particularly well situated to capture subtle modern variations in modern ITCZ activity (and thus in TRB width). KNI-51 lies within the IASM, and the Chinese cave sites are located within the EASM, both of which are integrated within the larger Austral-Asian monsoon system.

This study focuses on nine stalagmites composed of fast-growing (≤ 2 mm/year) aragonite, ideal for high-resolution records. Isotopic analyses were performed at a scale that achieved ~4

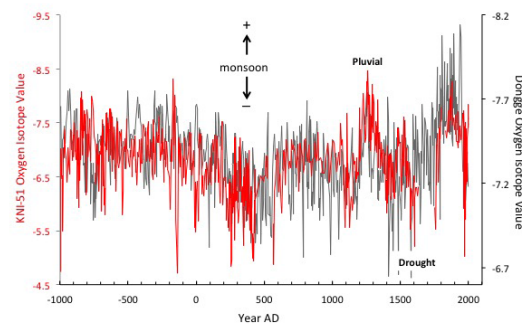


Figure 2. Comparison of stalagmite oxygen isotopic records of monsoon variability over the past 3000 years from Dongge cave (dark grey; Wang *et al.*, 2005) and KNI-51 (red; Denniston *et al.*, 2016). Intervals identified as “drought” and “pluvial” were examined in detail using the Last Millennium Ensemble climate model simulations (see Figure 3).

years between measurements, consistent with the Chinese cave records. KNI-51 stalagmites were precisely dated, with two standard deviation errors typically ranging from ± 1 –30 years (Denniston *et al.*, 2013b; Denniston *et al.*, 2015) This KNI-51 time series spans the majority of the last 3000 years, with the longest gap from AD 1640–1750. In most cases, oxygen isotopic compositions of KNI-51 stalagmites are similar in terms of isotopic value and temporal trend with samples of similar age. This result suggests that the stalagmites may be reliably interpreted as a record of past monsoon activity.

3. TRB Dynamics over the Last 3000 Years

The manner in which Australian monsoon rainfall, as reconstructed from KNI-51 stalagmites, has changed over the past 3000 years is remarkably similar to variations in the EASM recorded by stalagmites in China. Multi-decadal to centennial-scale periods of increased monsoon rainfall (lower oxygen isotopic ratios) at KNI-51 coincide with periods of increased rainfall in China (Figure 2). As a north or south shift in the TRB would have resulted in anti-phasing of rainfall between the hemispheres, the observation that past monsoon variability in Australia and China was synchronous and of the same sign is best explained by expansion and contraction of the Indo-Pacific TRB. Both sites feature sharp reductions in monsoon rainfall during the three ice-rafted debris (Bond) events which are associated with reductions in the Atlantic Meridional Overturning Circulation (Wang *et al.*, 2005) as well as drought periods identified in Vietnamese tree rings (Buckley *et al.*, 2010) and a Chinese stalagmite (Zhang *et al.*, 2008), and which have been tied to the collapse of the “hydraulic city” of Angkor, the capital of Khmer Empire in Cambodia and the Chinese Yuan dynasty (the Khmer Drought is dated to AD 1340–1430 (Buckley *et al.*, 2010) and AD 1370–1460 at KNI-51). The correlation coefficient, r , between the KNI-51 record and stalagmite DA from Dongge cave (Wang *et al.*, 2005) is 0.45 using a 251-year loess filter and 0.37 using a 101-year loess filter.

4. Climate Model Analysis of TRB Behaviour

To examine the origins of TRB dynamics, we compared the KNI-51 and Dongge DA records from the last millennium with output from the Last Millennium Ensemble (LME)

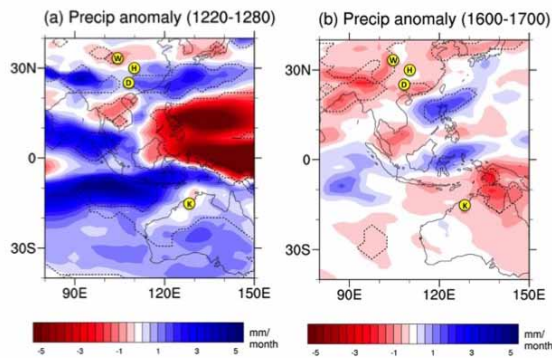


Figure 3. Last Millennium Ensemble analysis of precipitation anomalies associated with (a) pluvial and (b) drought periods identified in both the KNI-51 and Dongge cave stalagmite records. Anomalies during the drought and pluvial periods are relative to the analysis period 850-1850 AD and are based on the multi-ensemble mean in the ALL forcing scenario using 13 ensemble members. Interhemispheric symmetry in rainfall at the margins of the tropical rain belt in southern China and northern Australia, along with an opposite response in the core of the tropical rain belt, is tied to expansion (a) and contraction (b) of the Hadley circulation.

(Otto-Bliesner *et al.*, 2016), a high-resolution suite of climate model simulations conducted by the National Center for Atmospheric Research with the Community Earth System Model. A series of monthly global gridded variables from this state-of-the-art model participating in the Coupled Model Intercomparison Project, phase 5 (CMIP5) were analyzed (Taylor *et al.*, 2012). Model ensemble members span AD 850-1850 and are sensitive to changes in solar intensity, volcanic emissions, greenhouse gases, aerosols, land use conditions, and orbital parameters, together and individually.

The model largely captures the mean climatology of NH and SH summer monsoon precipitation, though the austral monsoon precipitation extends too far into the interior of the Australian continent, a problem common to current-generation climate models (Sherwood and Maher, 2015) (Figure 1). In addition, the simulated precipitation over northern Australia (spanning 14°-16°S, 125°-130°E) in an area surrounding the cave site is consistent with the stalagmite monsoon reconstruction at KNI-51 over the last millennium.

To assess TRB dynamics in more detail, we focused on the most prominent multi-decadal pluvial period (AD 1220-1280) and drought period (AD 1600-1700) of the last 1000 years (Figure 2). During the pluvial, the LME simulations reflect wetter conditions across southern China and across northern Australia; substantial decreases in rainfall mark the central and eastern core of the TRB (Figure 3a), consistent with an expansion of the regional TRB via a more poleward positioning of the ITCZ.

For the drought period, the model shows modest reductions in rainfall across the Australian tropics and southern China as well as weakly enhanced rainfall through much of the TRB core (Figure 3b). This result is generally consistent with our stalagmite analysis as well as regional proxy-based studies for the LIA (Yan *et al.*, 2015). Why the model more accurately captures rainfall variability during the pluvial than the drought is unclear but may be linked to the model's anomalously deep penetration of monsoon rainfall into the Australian interior

that limits its sensitivity to changes in meridional circulation in the area of KNI-51 during TRB contractions.

The LME also allows examination of hydroclimatic changes to individual forcings. When the model is forced solely by volcanic emissions, the resulting spatial distribution of reduced monsoon rainfall during the drought period is remarkably consistent with the stalagmite data. A second driver of particular relevance is solar irradiance because the three Holocene stalagmite records from Dongge cave, as well as the Wanxiang cave record (Zhang *et al.*, 2008), have been demonstrated to record solar variability (Wang *et al.*, 2005; Duan *et al.*, 2014). However, spectral characteristics suggestive of solar variability are weak or absent in the KNI-51 monsoon reconstruction.

5. Conclusions

The TRB has expanded and contracted at multi-decadal to centennial time scales across the Indo-Pacific over the last 3000 years. This finding sharpens attention on the response of tropical rainfall to anthropogenic forcing in coming decades.

Acknowledgements

Funded by the US National Science Foundation P2C2 program (to R.D. and C.U.), the Center for Global and Regional Environmental Research and Cornell College (to R.D.), and the Penzance and John P. Chase Memorial Endowed Funds at Woods Hole Oceanographic Institute (to C.U.). Global Precipitation Climatology Center data set by the German Weather Service accessed via <http://gpcc.dwd.de>; CESM1(CAM5) Last Millennium Ensemble Community Project and super-computing resources provided by NSF/CISL/Yellowstone. Special thanks to the owners and leaseholders of Carlton Hill Station, the Bunuba People of Windjana, the Western Australia Bureau of Parks and Wildlife, and Donna Cavlovic, Kym Cugley, Steve Stevets, as well as Michael Barthelmes, Daniel Cleary, and James Garrett.

References

- Ayliffe L, Gagan M, Zhao J-X, Drysdale R, Hellstrom J, Hantoro W, Griffiths M, Scott-Gagan H, St Pierre E, Cowley J, and Suwargadi B 2013. Rapid interhemispheric climate links via the Australasian monsoon during the last deglaciation. *Nature Communications* 4, 1-6.
- Bird B, Abbott, M, Vuille, M, Rodbell, D, Stansell, N, Rosenmeier, M 2011. A 2,300-year-long annually resolved record of the South American summer monsoon from the Peruvian Andes. *Proceedings of the National Academy of Sciences USA*, 108, 8583-8588.
- Broccoli J, Dahl K, Stouffer R 2006. Response of the ITCZ to Northern Hemisphere cooling. *Geophysical Research Letters* 33, L01702.
- Buckley B, Anchukaitis K, Penny D, Fletcher R, Cook E, Sano M, Nam L, Wichienkeo A, Minh T, Hong T 2010. Climate as a Contributing Factor in the Demise of Angkor, Cambodia. *Proceedings of the National Academy of Science USA* 107, 6748-6752.
- Collins J, Schefub E, Heslop D, Multiza S, Prange M, Zabel M, Tjallingii R, Dokken T, Huang E, Mackensen A, Schulz M,

- Tian J, Zarriess M, Wefer G 2010. Interhemispheric symmetry of the tropical African rainbelt over the past 23,000 years. *Nature Geoscience* **4**, 42-45.
- Chiang J, Friedman A 2012. Extratropical Cooling, Inter-hemispheric Thermal Gradients, and Tropical Climate Change. *Annual Reviews in Earth and Planetary Science*, **40**, 383-412.
- Dansgaard W 1964. Stable isotopes in precipitation. *Tellus* **16**, 436-468.
- Denniston R, Wyrwoll K-H, Asmerom Y, Polyak V, Humphreys W, Cugley J, Woods D, Peota J, Greaves E 2013 North Atlantic Forcing of Millennial-Scale Australian Monsoon Variability during the Late Glacial. *Quaternary Science Reviews* **72**, 159-168.
- Denniston R, Wyrwoll K-H, Polyak V, Brown J, Asmerom Y, Wanamaker A, LaPointe Z, Ellerbroek R, Barthelmes M, Cleary D, Cugley J, Woods D, Humphreys W 2013. A Stalagmite Record of Holocene Indonesian-Australian Summer Monsoon Variability from the Australian Tropics. *Quaternary Science Reviews* **78**, 155-168.
- Denniston R, Ummenhofer C, Wanamaker A, Lachniet M, Villarini G, Asmerom Y, Polyak V, Passaro K, Cugley J, Woods D, Humphreys W 2016. Expansion and contraction of the Indo-Pacific tropical rain belt over the last three millennia. *Scientific Reports* **6**, 34485.
- Duan F, Wang Y, Shen C-C, Wang Y, Cheng H, Wu C-C, Hu H-M, Kona X, Liu D, Zhao K, 2014. Evidence for solar cycles in a late Holocene speleothem record from Dongge Cave, China. *Scientific Reports* **4**, doi: 10.1038/srep05159.
- Griffiths M, Drysdale R, Gagan M, Zhao J, Ayliffe L, Hellstrom J, Hantoro W, Frisia S, Feng Y, Cartwright I, St. Pierre E, Fischer M, Suwargadi B 2009. Increasing Australian-Indonesian monsoon rainfall linked to early Holocene sea-level rise. *Nature Geoscience* **2**, 636-639.
- Haug G, Hughen K, Sigman D, Peterson L, Rohl U 2001. Southward migration of the Intertropical Convergence Zone through the Holocene. *Science* **293**, 1304-1308.
- Hu C, Henderson G, Huang J, Xie S, Sun Y, Johnson K 2008. Quantification of Holocene Asian monsoon rainfall from spatially separated cave records. *Earth and Planetary Science Letters* **266**, 221-232.
- Maher P, Sherwood S 2015. Skill in simulating Australian precipitation at the tropical edge. *Journal of Climate* doi: 10.1175/JCLI-D-15-0548.1.
- Otto-Bliesner B, Brady E, Fasullo J, Jahm A, Landrum L, Stevenson S, Rosenbloom N, Mai A, Strand G 2016. Climate Variability and Change since 850 C.E.: An Ensemble Approach with the Community Earth System Model (CESM), *Bulletin of the American Meteorological Society* doi:10.1175/BAMS-D-14-00233.1.
- Partin J, Cobb K, Adkins J, Clark B, Fernandez D 2007. Millennial-scale trends in west Pacific warm pool hydrology since the Last Glacial Maximum. *Nature* **449**, 452-455.
- Taylor K, Stouffer R, Meehl G 2012. An overview of CMIP5 and the experiment design. *Bulletin of the American Meteorological Society* **93**, 485-498.
- Wang Y, Cheng H, Edwards R, An Z, Wu J, Shen C-C, Dorale J, 2001. A high-resolution absolute-dated late Pleistocene monsoon record from Hulu Cave, China. *Science* **294**, 2345-2348.
- Wang X, Auler A, Edwards R, Cheng H, Cristalli P, Smart P, Richards D, Shen C-C 2004. Wet periods in Northeastern Brazil over the past 210-kyr linked to distant climate anomalies. *Nature* **432**, 740-743.
- Wang Y, Cheng H, Edwards R, He Y, Kong X, An Z, Wu J, Kelly M, Dykoski C, Li X 2005. The Holocene Asian monsoon: links to solar changes and North Atlantic climate. *Science* **308**, 854-857.
- Yan H, Wei W, Soon W, An Z, Zhou W, Liu Z, Wang Y, Carter R, 2015. Dynamics of the intertropical convergence zone over the western Pacific during the Little Ice Age. *Nature Geoscience* **8**, 315-320.
- Zhang P, Cheng H, Edwards R, Chen F, Wang Y, Yang X, Liu J, Tan M, Wang X, Liu J, An C, Dai, Z Zhou, J Zhang, D Jia, J Jin, L Johnson K 2008. A test of climate, sun, and culture relationships from an 1810-year Chinese cave record. *Science* **322**, 940-942.

(Abstract) **Periods of speleothem growth in northern Eurasian caves: a preliminary overview**

Yuri V. Dublyansky¹, Christoph Spötl¹, Denis Scholz², Gina E. Moseley¹, Lawrence R. Edwards³

Affiliation: ¹Institute of Geology, Innsbruck University, Innrain 52, 6020 Innsbruck, Austria

²Denis Scholz, Speleothem Research Group, University of Mainz

³Department of Earth Sciences, University of Minnesota, Minneapolis, USA

Abstract

Northern Eurasia is a vast continental area with a very low density of paleoclimate records. The occurrence of speleothem growth, and the lack thereof, provide important constraints on the chronology and relative change of climate over large geographical areas and hundreds of thousands of years.

Here we report periods of growth determined by U-Th dating of 43 stalagmites and 15 flowstone samples collected in 17 caves in Crimea (3 caves), southern Ural (5 caves), central Ural (2 caves), northern Ural (2 caves), Altai Mountains (2 caves), and eastern Sayan Mountains (3 caves). These areas are located along a 4,200 km-long longitudinal band (between 44.5°N in Crimea and 55.7°N in eastern Sayan). In the Ural Mountains, a separate transect stretches ca. 900 km in north-south direction (53°N to 60.7°N). In each area, samples were collected from several caves, located between a few and tens of kilometers apart. These data can, therefore, be interpreted in terms of regional paleoclimate rather than local cave conditions.

Speleothems on the Crimean Peninsula grew during Marine Isotope Stages (MIS) 5e, 4, 3 and the Holocene; in the southern Ural during MIS 11, 10, 8, 7, 6, 5, 4, 3, 2 and the entire Holocene; in the central Ural during MIS 7, 5e and the Holocene (starting at 9.9 ka); in the northern Ural during post-MIS15, 7 and 5e; in the Altai Mountains during MIS 11, 4, 3 and the Holocene; in eastern Sayan during pre-MIS 11, 9, 8(?), 7, 5e, and the Holocene (starting at 9 ka). The reported record likely over-represents the younger growth periods.

This data base is work in progress, but provides some interesting insights already. For example, speleothem growth in Crimea seems to have been quite common during MIS 4 and 3, whereas stalagmites of Holocene age are rare. Speleothem growth occurred much more frequently in the southern compared to the northern Ural. The most recent generation of speleothems started to form during Termination I (ca. 14.5 ka) in the southern Ural, and in the Preboreal (ca. 9.9 ka) in the central Ural, while no Holocene stalagmites were found in northern Ural caves.

(Abstract) **Stalagmite isotopic record from Mallorca (Western Mediterranean) over the last 120 ka: paleoclimatic implications**

Oana-Alexandra Dumitru¹, Bogdan P Onac¹, Victor J Polyak², Jonathan G Wynn¹, Yemane Asmerom²,
Joan J Fornós³

Affiliation: ¹School of Geosciences, University of South Florida

²Earth & Planetary Sciences, University of New Mexico Albuquerque, New Mexico 87131

³Unibersitat de les Illes Balears, Palma, Spain.

Abstract

With global climate change, the Western Mediterranean is projected to become warmer and drier, thus, likely to generate major societal and economical impacts. In the light of this, a thorough understanding of climate forcing and responses triggered by past global events is essential. Here we present a detailed, accurately dated isotopic record spanning the past 121 kyr from a stalagmite (CAM) collected in Campanet Cave (Mallorca Island). The growth history combined with the isotopic record, mineralogical and petrographical analyses, provides evidence of climatic changes in the Western Mediterranean.

A high-resolution chronology was obtained based on 25 U-series dates, all of which are in stratigraphic order. The dates reveal that CAM begun its growth $\sim 121 \pm 0.6$ ka and, except for one major hiatus (67 to 53 ka), it grew continuously until present. $\delta^{18}\text{O}$ values range from -6.2 to -0.6‰ , whereas $\delta^{13}\text{C}$ vary between -10.4 and 0.5‰ . The speleothem formed in isotopic equilibrium with seepage waters as suggested by four Hendy tests and if comparing $\delta^{18}\text{O}$ of modern drip water with newly precipitated calcite soda straws. However, $\delta^2\text{H}$ values in fluid-inclusion from this stalagmite along with a strong correlation between $\delta^{18}\text{O}$ and $\delta^{13}\text{C}$, indicate that kinetic fractionation have dominated during at least few parts of its growth (e.g., MIS 5c).

Considering the modern hydroclimatic setting in Mallorca, we argue that during the intervals of poor correlation between $\delta^{18}\text{O}$ and $\delta^{13}\text{C}$, the variability of $\delta^{18}\text{O}$ in CAM is likely related to changes in amount and source of precipitation. During periods when $\delta^{18}\text{O}$ and $\delta^{13}\text{C}$ covary, we interpreted the carbon isotopic profile assuming that high $\delta^{13}\text{C}$ would most likely reflect low biogenic CO_2 productivity in soil, thus a dry climate.

Based on this, the major climatic events identified by the $\delta^{18}\text{O}$ and $\delta^{13}\text{C}$ time series are: MIS 5e termination, C24, and C23 cold events, prolonged aridity during MIS 5c, dry-to-wet shift at MIS 5c/5b boundary, and moist climate at the beginning of MIS 5a. The growth cessation of CAM is tentatively associated with Heinrich event H6, which brought much colder conditions and sparsely vegetated landscape. The low growth rates and monotonous C and O isotopic profiles across MIS 3-1, suggest relatively stable climatic conditions with effective precipitations that remained slightly above the growth/cessation threshold.

Geochronology Of Jinfo Cave, The Oldest Cave In China

Huang Bao-Jian, Zhang Jing, Zhai Xiu-Min, Luo Shu-Wen, Shi Wen-Qiang

Affiliation: Institute of Karst Geology, CAGS/Key Laboratory of Karst Dynamics, MLR&GZAR, Guilin, Guangxi 541004, China

Abstract

Several dating methods were applied to the geochronology of Jinfo Cave to reconstruct the ground surface processes. Using cosmogenic nuclides $^{26}\text{Al}/^{10}\text{Be}$, the burial age of quartz sands of calcite-cemented pebble in a branch passage was found to be $5.7\pm 1.6/-0.9$ Ma, indicating the cave was formed during the Pliocene. A U-Pb age from the base of a stalagmite which grew on a slope of an enormous breakdown pile, is 1.56 ± 0.10 Ma, revealing the massive collapse occurred before the mid-Pleistocene. ESR ages of the upper parts of stream-transported fine clastic sediments with the extant thickness of 20~60 meters, correspond to three key depositional periods from the late Early Pleistocene to the early Middle Pleistocene. These correspond to MIS 15e, 17 and 21. U-series dating of speleothems demonstrate the five main chemical precipitation periods correspond to MIS 53, 7a, 5, 4 and 1.

Keywords: $^{26}\text{Al}/^{10}\text{Be}$ dates, U-Pb dates, U-series dating, ESR dating, OSL dating, Jinfo cave, Jinfoshan karst, South China

1. Introduction

Jinfo Cave is the longest and the most complicated infilled branchwork cave in the cave system located at ~2000m a.s.l. on the Jinfoshan Karst. This is one of the areas of South China Karst on the World Heritage List. Many Chinese scholars have thought the caves are some of the oldest caves in China. Zhang Ren *et al* (1998) sampled 5 pieces of stalagmites in Gufo Cave near Jinfo Cave and dated them using U-series dating. Three of them were found to be over 0.35 Ma (the limit of this dating method in the lab). They inferred that the high-altitude cave systems in the Jinfoshan mountains had a long history and formed in the early of Quaternary. This work filled the gap of cave formation time but failed to offer an accurate formative age of caves in this area. The current work was undertaken as part of the preparation prior to applying for inscription on the UNESCO World Heritage List.

2. Outline Of Jinfoshan Karst

Jinfoshan Mountain is located at Nanchuan Prefecture south-east of Chongqing City, in the transitional zone between the Yunnan Plateau and the Sichuan Basin. This is also the transitional area between Step II and Step III of the Chinese stepped topography. As the northernmost end and highest part of Daloushan Range, Jinfoshan Mountain has been isolated from the main Yunnan-Guizhou Plateau by the erosion of the surrounding valleys. It resembles a detached elongated island surrounded by massive cliffs. Its summit attains 2238.2 m elevation asl, in contrast to the surrounding valleys, with elevations at about 700 m asl. As a World Heritage site, the Jinfoshan karst covers only the upper part of Jinfoshan Mountain, at an elevation ranging from approximately 1200 to 2238 m asl. The Jinfoshan karst and its buffer zone contain two precipitous cliffs standing 150 to 500 m high, with an enclosed margin perimeter 50 and 65 km, long respectively. The two precipitous cliffs divide the core zone covering 6,744 ha and its buffer zone of 10,675 ha.

Jinfoshan karst developed in the Lower Permian limestones (327~453m thick), confined between the overlying Upper Permian coal measures (165~207m thick) and the underlying Silurian shale and siltstone clastics (798~1284m thick) which constitute the buffer zone. The sandwich-like lithology structure confines the development of the karst. The karst is dominated by ancient-originated underground river cave systems dismembered by the retreat of cliff, and by a series of exokarst

features including stone forest (shilin), residual hills, uvala, doline, and karst spring topography.

Jinfoshan karst has over 25km of large trunk cave passage (~60m wide), typical of that developed in humid tropical karst areas. The size of passages is indicative of formation by large allogenic rivers but no trace of their former course remains and the trunk passages are entirely relict. All of the principal passages are relict underground river conduits that are oriented along or close to the strike of the gently dipping rocks, a very common relationship in solution caves created by meteoric water. They are largely at elevations above 2000m and although short sections of relict caves are known at similar altitudes in China and elsewhere (for example in the Pamir Mountains, Uzbekistan) these are thought to be the highest extensive horizontal caves on earth.

Several caves have entrances in the cliff faces and have clearly been truncated by retreat of the cliff face. Remnants of older phreatic tubes are present in the roof of several sections of trunk passage, but the passage enlargement was largely under vadose conditions. However, there is no vadose trenching in the passage floors indicating that the upstream water supply was removed before the downstream end was truncated.

3. Jinfo Cave And Its Sediments

Jinfo cave, with unfinished survey length of over 12.8 km, comprises a wide passage (trunk passage, 20~60m wide) tubes (medium size branch passages, 4~10m wide), canyons (narrow-high branch passages of network maze, 0.5~1m wide) and vadose shafts (dome-pits), as well as related sediment sequences including fluvial clastic sediments, collapse bedrock piles and secondary chemical deposits.

3.1. Fluvial clastic sediments

The trunk passages contain extensive allogenic sediment deposits that are thought to largely date to the phase when the cave was active rather than being later fill deposits. These are:

- Cemented sediment: a conglomerate to a very coarse sandstone cemented by calcite, consisting of round or sub-round pebbles, gravel, coarse sand grains and few quartz crystals. These are ideal material for cosmogenic nuclides $^{26}\text{Al}/^{10}\text{Be}$ burial age dating. These are only found at the branch section near the junction of trunk passage and branch passage.

- Loose sediment: the principal fluvial clastic sediments ubiquitously distributing on the cave floor. Using a super-high-density resistivity method, it was found to be 25~60m thick, and consists of fine-grain layers (fine-grain sand, silt and silty clay) and coarse layers (sub-round pebble, gravel and coarse sand). The sand layers are ideal materials for ESR dating.

Besides this sediment, a loose sediment fan consisting of angular gravels and sands was deposited over the loose sediments mentioned above, These are the latest fluvial clastic sediments which were flushed into the cave by floods from the surface. It is suitable material for OSL dating.

3.2. Collapse piles

Several large breakdown piles have been found on the floor of trunk passage of Jinfo cave. Consisting of angular blocks of bedrock (with a few broken speleothems), the biggest pile is over 500m long, 15~60m wide and over 10m high, making up a step-like breakdown pile. Some stalagmites are growing on top of the pile. These formed from failure of the roof bedrock.

3.3. Secondary chemical deposits

Secondary chemical deposits in Jinfo Cave include speleothems which are deposited on the surface of the fine-grain clastic sediments. Most are gypsum, epsomite and saltpetre. However due to the small aggregate thickness of carbonate rock and the effect of aggressive seepage water flow from coal measures above, few speleothems developed. However stalagmites and flowstones are ideal dating materials for U-series or U-Pb dating techniques.

4. Dating Results And Conclusion

As most of the upper part of fluvial clastic sediments being mined for nitrate-rich materials and because of the constraints from sampling thick sediments, it is difficult to select the ideal

age-dating techniques to establish the formative and development times of the cave. Stalagmites, the cemented pebbles, the upper part of fluvial clastic sediments and diluvium to date were sampled for dating and, some preliminary results have been acquired (Table.1).

According to the characteristics of the cave and sediments, some conclusion have been drew as follows:

1. The cemented pebble layer sedimented at 5.7(+1.6-0.9) Ma, is the oldest sediments in Jinfo cave. This demonstrates that Jinfo Cave formed before 5.7(+1.6 -0.9) Ma and Jinfo Cave is thought to be the oldest cave in China and even in Asia which has dating data supported.
2. The oldest stalagmite was deposited at 1.56±0.10Ma which is growing on top of the biggest breakdown bedrock pile. It is the oldest stalagmite in China and perhaps in Asia and indicates that the massive breakdown of roof occurred before 1.56±0.10Ma.
3. From about 0.6×0.8Ma, every the interval of 0.1Ma, the massive sedimentation occurred once, which correspond to MIS15e,17,21, a great deal of clastic material was deposited.
4. There exist multi-phase speleothem deposition. The principal deposition stages are 1.56, 0.2, 0.1, 0.09, and 0.06 Ma and currently, which correspond respectively to MIS53, 7a, 5, 4, and 1 stages.
5. At about 0.09Ma, a massive flood flushed into the cave through the dolines and formed the diluvium fans covering the former clastic sediments in some sections of the cave and may have blocked the passage.
6. The evolution of Jinfo Cave, other high-altitude cave systems and geomorphic processes can be inferred from a combination of the dating results and the characteristics of karst features (another paper is being prepared).

Table 1. Preliminary dating results of Jinfo Cave

Sediment	Dating method	Age/Ma	Analyzing organization
Cemented pebble	²⁶ Al/ ¹⁰ Be	Burial age 5.7±1.6 -0.9	Purdue University
Stalagmite	U-Pb isochron age	1.56 ± 0.10	Melbourne University
Medium-fine grain sand	ESR	0.81±0.12	Qingdao Institute of Marine Geology
Silty clay	ESR	0.72±0.11	Qingdao Institute of Marine Geology
Silty clay	ESR	0.71±0.11	Qingdao Institute of Marine Geology
Silt	ESR	0.60±0.09	Qingdao Institute of Marine Geology
Gravelly sandy clay	OSL	>0.09	Nanjing University
Stalagmite	U-Th	>0.38	Institute of karst geology
Stalagmite	U-Th	>0.38	Institute of karst geology
Stalagmite	U-Th	>0.38	Institute of karst geology
Stalagmite	U-Th	>0.38	Institute of karst geology
Stalagmite	U-Th	>0.38	Institute of karst geology
Stalagmite	U-Th	0.097+0.0095-0.0089	Institute of karst geology
Stalagmite	U-Th	0.090+0.0068-0.0065	Institute of karst geology

Geothermal Heat Flow in Caves: The Physics of the Geothermal Rims in Carlsbad Cavern.

Neville A. Michie, Ph.D.

Affiliation: Cave scientist. ACKMA. NSS, # 39726.
9 Patrick Street, Beacon Hill, NSW, Australia, 2100

Abstract

Observations show that a geothermal heat induced air circulation exists in the chamber over the Lake of the Clouds in Carlsbad Caverns, N.M. USA. A stalagmite with attached rims is at the top of this chamber and a model of the physical process that forms them is described.

The rims are formed by a simple solution and deposition process by condensation water, and their thickness is controlled by a self limiting process controlled by their geometry. They are very dependent on the properties of the geothermal air circulation.

The properties of the geothermal air circulation are discussed here.

The model of the process is likely to apply to many other rims in deep caves.

Keywords: Geothermal convection, psychrometrics, model, rim.

1. Introduction

At the top of the Lake of the Clouds chamber there is a stalagmite with a protruding appendage. The appendage is a rim (Hill and Forti 1997), and it seems to be similar to other rims reported from other deep caves. The rim appears to consist of a porous mass of fine calcite crystals one side of which has a glazed appearance like wax melted by a stream of hot air. The rim has a more or less uniform thickness and an irregular outline. The location of this rim is significant, as it lies between the thermal circulation of air above the Lake of the Clouds (Michie 2017a) and an area which is more connected to the lateral passage connecting to the main cave, and which has a slightly lower temperature. The rim is subject to a slow continuous flow of heat and moisture from the geothermal circulation. The air in the cave in this region is nearly saturated. Air flow is so slow that it is imperceptible and temperature differences are quite small.

The explanation of the phenomenon of rim formation lies in the small gradients of temperature and humidity and the slow air movement maintained by the geothermal heat flow, all of which are stable over very long periods of time.

2. Method

Air temperature and humidity (wet bulb temperature depressions) with associated barometric pressures were measured with the MicroPsychrometer (Michie 2017a) and a Thommen 6000m altimeter, at five sites in the chamber over the Lake of the Clouds, in Carlsbad Cavern. Only the upper half of the chamber was accessible, but the measurements made provided adequate information to prove the existence of the circulation. Although the measurements were not repeated over time, subsequent research has established that conditions would be extremely stable and unlikely to change in any time scale that would be available to contemporary observers. (e.g. human lifetime)

The data from the measurements was used to calculate the psychrometric parameters of potential temperature, relative humidity, dew point temperature, mixing ratio, temperature of adiabatic saturation and enthalpy. These calculations used the methods in (Wylie and Lalas 1981) and (ASHRAE 1989). Modelling of the geothermal heat flow through the cave (Michie 2017b) supported the measurement of heat and mass flow.

3. Results

The measurements of the air mass above the Lake of the Clouds showed a constant potential temperature, (Figure 1). (Potential temperature is the temperature that a parcel of air would have if instantaneously compressed to the standard pressure of 1013.25 hectopascals. It is used mainly in the study of the stability of air masses).

The rate at which the air temperature fell with increasing altitude in the chamber was very close to the dry adiabatic lapse rate, (DALR), about 10 K/km., (Figure 1). This is very significant because in other thermal convection processes, (e.g. thunderstorms), rising air cools at the Moist Adiabatic Lapse Rate, (MALR) which at this temperature is only about 3 K/km.

The heat content (Enthalpy), Figure 3, and moisture content (Mixing Ratio), Figure 4, fell with increasing altitude, showing that heat and moisture from the lake was being transported to the walls and roof of the upper part of the chamber. Relative humidity was below 100%, (Figure 5).

4. Discussion

The conforming of this flow to a fixed potential temperature and DALR is extraordinary and must be taken as a characteristic of low energy thermal convection flows in air. In this circulation air rises, carrying heat and moisture, but it is always mixing with the descending return air to make a column of air

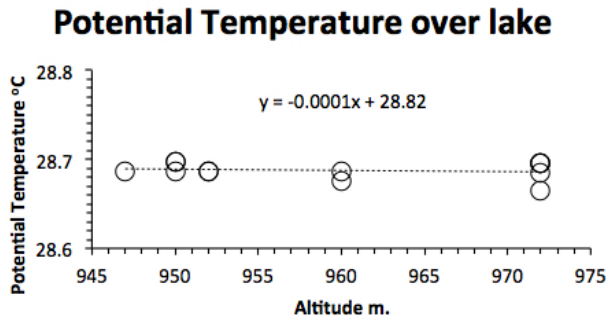


Figure 1.

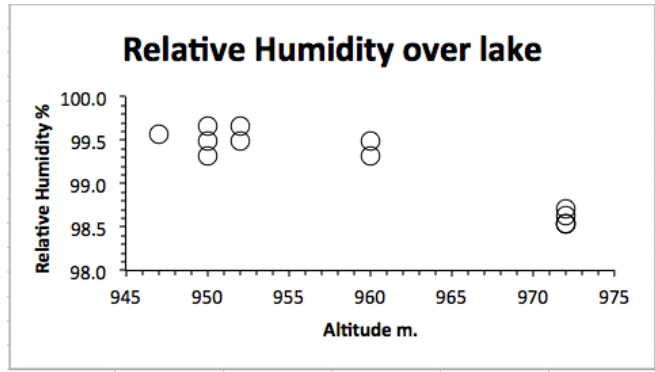


Figure 5.

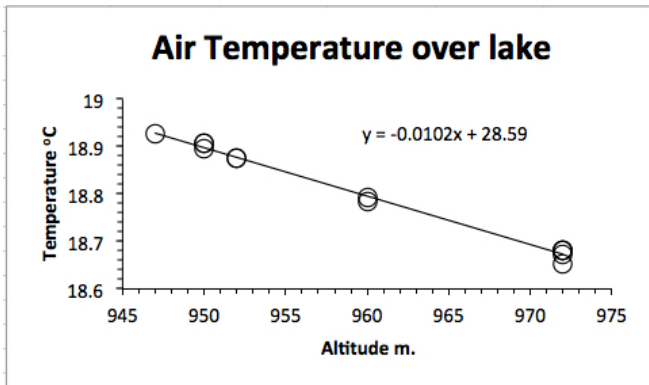


Figure 2.

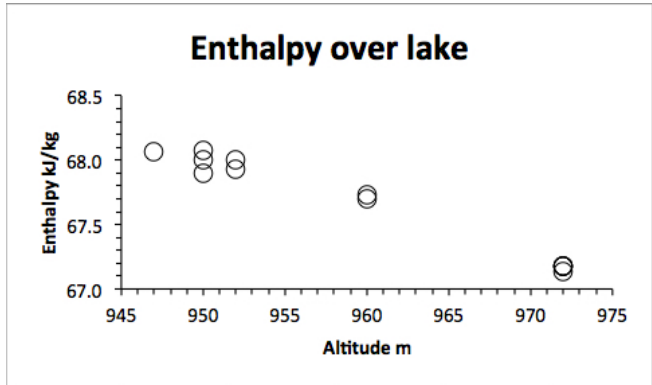


Figure 3.

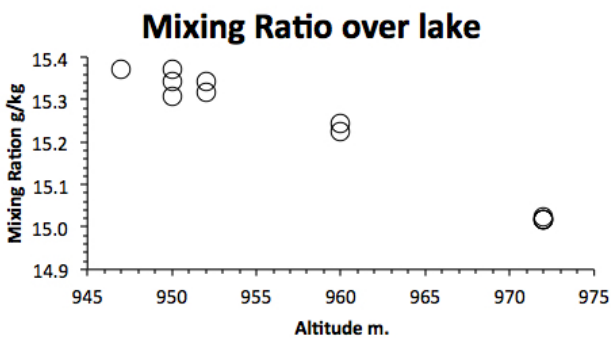


Figure 4.

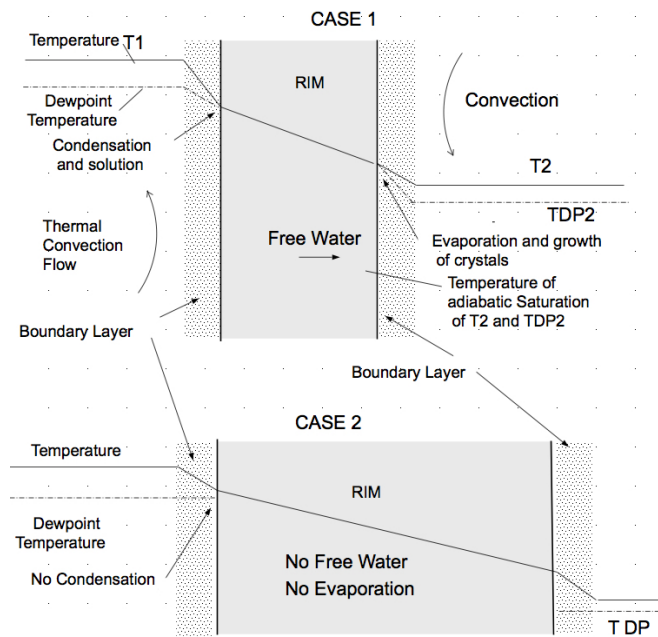


Figure 6. The two cases of thin and thick rims

with composite properties. It appears that the circulation can only proceed within the constraints of the DALR and constant potential temperature. The very low velocity of air movement results in a chaotic motion controlled by the buoyancy and heat and mass exchange. It is important to note that the air physically moves from lake to roof before returning, carrying moisture and heat energy. Trace gasses such as carbon dioxide and radon would also be moved

The formation of the rim can be analysed as a one dimensional model. (Figure 6).

In Case 1, the warm humid air from the geothermal circulation T1, measured at 18.39 °C, heats the rim and elevates its temperature. The moist air condenses water onto the front of the rim, which is below the dew-point temperature of the incident air. The rim conducts the sensible heat from the circulation and the latent heat of condensation to the back of the rim where the heat, both sensible and latent is lost to the cooler air, T2, measured at 18.20 °C, by convection and evaporation.

Calcite dissolved on the front of the rim, and together with calcite in water from the body of the stalagmite crystallises on the rear face of the rim to extend the rim. In Case 2 the

rim has grown thicker, and has more thermal resistance. The heating on the front face has lifted the temperature of the face above the dewpoint of the geothermal flow. Therefore condensation ceases, and the quantity of heat conducted to the rear face has been decreased because of the thicker insulation of the rim. The cooling by convection on the rear face is insufficient to cool the front face below the dew-point temperature of the geothermal circulation. Evaporation ceases as there is no free water, and growth ceases.

The rim can only grow while it is thin, and the only direction for growth is sideways. Thus thin rims grow while the cooling on the rear face is sufficient to cause condensation on the front face, a self-limiting process.

The thermal circulation also transports water and heat to the roof and walls, the water drains down the porous walls into any lake at the bottom of the chamber, with dissolved calcite from the walls. As this water evaporates again it will cause the excess calcite to crystallise leaving crystals in the lake. This process is quite slow, but over thousands of years significant crystal growth can occur.

5. Conclusion

The chamber contains an active geothermal circulation transporting heat and moisture in the cave. The heat flow drives processes including the construction of rims.

Rims are speleothems in deep caves, and grow through geothermal heat transport through the thickness of the rim. They form at the junction of a thermal convective circulation and a zone of lower temperature. Their growth will be slow, because they rely on simple solution by condensation water rather than the process of dissolution of carbon dioxide that is a component of the mechanism forming so many other speleothems. Their thickness is limited by the temperature and humidity gradients that build them.

References

- ASHRAE, 1989 Psychrometrics In: RA Parsons (Ed.) *ASHRAE Fundamentals*, Chapter 6, American Society of Heating, Refrigeration and Air Conditioning Engineers, Inc. Atlanta pp 6.1 -6.10
- Hill, C. Forti, P. *Cave Minerals of the World*. 1997. National Speleological Society, Huntsville, USA. pp 463, Page 91-92.
- Michie NA, 2017a. *Geothermal Heat Flow in Caves: Heat Concentration and its Effects on Speleogenesis*. This conference.
- Michie NA 2017b. *Geothermal Heat Flow in Caves: Modelling of Geothermal Heat Flow*. This conference.
- Wyie RG, Lalas T. 1981. *The WMO Reference Psychrometer*. CSIRO, Sydney, Australia. pp 58.

The genesis of hollow stalagmites in caves of the Khammouane karst, Laos

Claude Mouret

Affiliation: Freelance geologist, Km1 La Tamanie, 87 380 Magnac-Bourg, France claude.mouret.geospel@orange.fr

Keywords:

Large numbers of hollow stalagmites in caves of Khammouane were discovered by the author in 2002. Their genesis was not obvious to understand. Therefore, morphological, topographical, geological and climatological information was gathered from several caves. The following conclusions were reached from analysis of the data.

Hollow stalagmites are mainly encountered in the higher parts of fossil sloping caves or on top of lateral slopes in large passages. They usually lie above a cave-fill floor but are present occasionally on top of big boulders weighing several tons. The cave fill often displays calcite layers interbedded with clay and silt.

Usually, no stalactite is associated with a stalagmite and the latter is located vertically below sharp lows of the cave roof.

We interpret formation of hollow stalagmites in the large majority of cases as follows:

1. Condensation water drips from the ceiling and gradually dissolves calcite layers on the floor, so that a through hole is made.
2. When pressure conditions are favourable, air circulation within the cave brings uprising wet air.
3. This wet air creates a mineral deposit around the hole, which may be enhanced by biological activity.
4. The rim deposit gradually rises in elevation, which can be up to 1.75 m, as observed.

However, some exceptions exist. Hollow stalagmites on boulders in subhorizontal fossil passages cannot be explained by the previous process. In this case, wet air due to condensation water dripping has to be enough to support microbial activity able to enhance peripheral carbonate deposition. These favourable settings are not numerous.

Overall, hollow stalagmites are related to favourable settings, where a combination of chemical and biological carbonate precipitation occurs, though in various proportions. Condensation water is associated with the process, as an initiating cause.

Around 200 hollow stalagmites were discovered in 2002 by the author in Tham Phiseua, a cave in the karst of Khammouane. A first review was published (Mouret, 2005) followed by interpreted X-Ray analyses (Mouret and Lapointe, 2009). Because the genesis of the stalagmites was not as evident the author decided to observe their habitat in several caves in Khammouane. Results of observations and a number of conclusions are presented here.



Figure 1. Photos 1 to 9. Shapes of hollow stalagmites: straight, curved, with bowls, branching, open on top in various ways, partly eroded.



Figure 2. Photos 10 to 21. Hollow stalagmites. Bar for scale: 5 cm.

Columns from left to right:

Tham Lô 2; Tham Lô 2; Tham Koun Don K2; Tham Phiseua PH2.

Centre: vertical part, top: horizontal cross-section or top, Bottom: cross-section. White line on Tham Lô section (column 2) is the internal contour of upper section.

1. Description of hollow stalagmites

Hollow stalagmites show a variety of shapes and proportions. However they present the permanent following features (Figs 1 & 2):

- They are taller than large, except when they are young,
- The tallest one observed is 1.75 m high,
- Their height/ width ratio is highly variable, from tall and slim to low and massive.
- Their shape varies from regular to bumpy,
- Their outer aspect is often irregular, both in diameter and in rugosity,
- They are usually open at the top, though there are exceptions,
- They show one or more internal longitudinal axial holes,

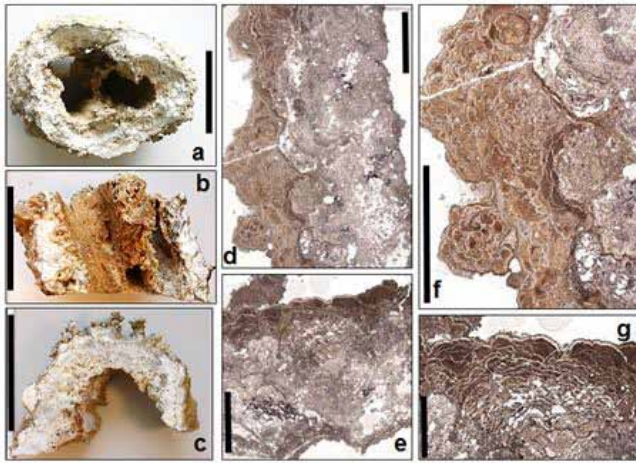


Figure 3. Photos 22 to 28. Stalagmite from Tham Koun Dôn, K3, with two holes. (views d, e, f, g are thin sections in natural light, NL). Scale bar is 5 cm for a, b, c; 1 cm for d, e, f; 0.5 cm for g.
 a: top section;
 b: long section;
 c: bottom cross-section;
 d: thin section, vertical;
 e: thin section, horizontal;
 f and g: close up views of d and e.

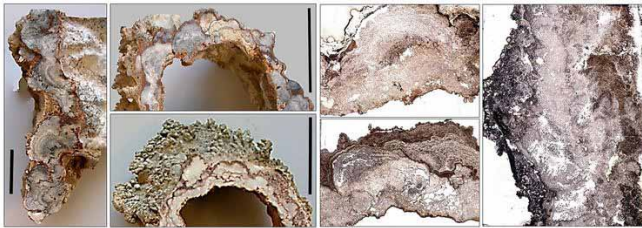


Figure 4. Photos 29 to 31. Tham Lô, 2. Vertical section (left) and horizontal cross-section of hollow stalagmite from Tham Lô. Bar is 5 cm. Photos 32 to 34. Tham Phiseua, PH1, thin sections (NL): Z (top left) and Ph30 (below) horizontal cross-sections; right: vertical section (Ph1). Each thin section is 2 x 3.5 cm.

- They may show branching and obliquity, under certain conditions.

The detailed shape is variable, with an outer aspect from relatively smooth to rugged or thorny. The central hole has a variable diameter and the wall/ hole thickness ratio may vary significantly. Some stalagmites do not show axial hole (any-more?), but they can be located, in the cave, between stalagmites with hole and aligned with them. Other stalagmites do show a branching hole, with a part not vertical at all.



Figure 5. Photos 35, 36 and 37. Groups of stalagmites with no associated stalactite (Tham Phiseua, 35, 36). Stalagmites on cave floor and on rock bridge, no stalactite (Tham Koun Dôn, 37).

2. Internal composition and fabric

Hollow stalagmites show a rather variable mineral composition (Table 1) with a dominant mix of calcite and aragonite. Gypsum may be present in high proportions, in a limited number of samples. Dolomite, siderite and quartz are sometimes present in low proportions (Mouret and Lapointe, 2009).

Hollow stalagmites show different compositions between caves. This needs to be investigated with more detail, as well as the variability in a single stalagmite.

The internal fabric does not show parallel laminae. Instead, there is a succession of nodule-like structures, which may or may not coalesce. Their base, either flat or squeezed between other nodules, is always located on the inner side of the stalagmite. Layers of nodules may be seen resting on more regular, amalgamated, internal layers (Photos 27 to 32).

3. Habitat

Hollow stalagmites very rarely show associate stalactites (Photos 35, 36). They lie preferably on high elevation passages in sloping caves (the higher the more numerous in Tham Phiseua (Fig 6) and in Tham Koun Don). However, shorter hollow stalagmites can be found on nearly flat passages covered with thin flowstones.

Hollow stalagmites are often encountered on cave fill which drape the sloping passage at the top of which they are located. However, they can also be, although much less often, on isolated rocks or rock bridges (Photo 34). Serial observations have shown that they are almost systematically present below the sharp lows of the cave roof, underneath their lowest point. In some places, they are located not far from rims.

4. Origin of hollow stalagmites

Our observations and especially our conclusions from our field work show that hollow stalagmites are associated with

Table 1. Range of mineralogical compositions of hollow stalagmites in three caves (punctual samples).

%	Number of Samples	Calcite	Aragonite	Gypsum	Dolomite	Siderite/ Quartz
Tham Phiseua	10	Av: 42; STD: 20. (17-77)	Av: 49; STD 22 (21-77)	(57-68 in 2 samples)	(3-5 in 2 samples)	S:1 in 1 sample
Tham Koun Don	5	Av 34; STD 27 (4-68)	Av 66 (large variation)	0	0	Q: 1 in 1 sample
Tham Lô	3	97-99	0	0	0	Q: 1-3

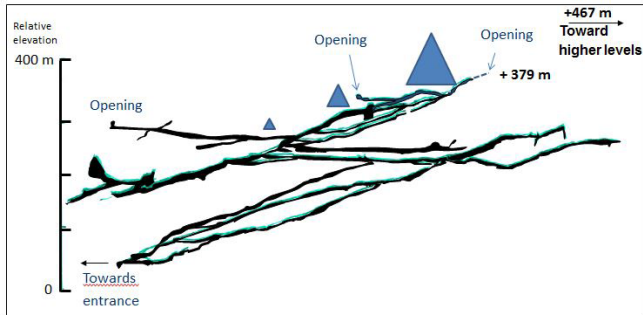


Figure 6. Semi-developed long section of Tham Phiseua (latest explorations not shown). Sloping parts of the cave follow the structural dip. Blue triangles are larger where hollow stalagmites are more numerous.

unusual cave climate, air circulation and also, often, to fluid circulation within cave fill.

Water condensation at the cave roof does occur under certain weather conditions. We observed it a number of times but it is ephemeral. For instance, the cave roof may look dry, but sand on the cave floor below its low points is wet, showing that aerial conditions have already re-evaporated water droplets, whereas porous sand has “kept the record”.

The location of hollow stalagmites below low points of cave roofs, especially in upper parts of sloping passages near cave openings is due to condensation. The stalagmites are systematically located below low points of the passage roof and follow a line passing through these low points. Occasionally they follow fractures. Water dripping has to be present where there is no fracture (most cases) to carry it. The bare surface of the roof shows no mineral deposition on it, and instead, there is corrosion. Rounded shapes are consistent with this. Aggressive condensation water progressively creates a hole in the cave floor and this hole may gradually pierce through floor sediments, including flowstone.

Variation of dripping water chemistry may occur, as weather conditions vary throughout time, and therefore may include some carbonate content, from time to time. Some deposition on the cave floor, due to splashing, may occur when deposition starts, but it ceases when the deposit height does not allow it anymore or when the central hole is deep already.

The fabric of stalagmites shows a growth by centrifugal deposition of nodule-like features and vertical aggradation. Though this is not completely proven at this stage, microbiological action is likely in the deposition of the stalagmites. Otherwise, it is difficult to explain deposition on the edge and on the top, but not in the axial hole where corrosion occurs, instead. Microbiological action is especially probable in stalagmites which are located on stone boulders or rock bridges (Fig 5. Photo 37).

Where the cave floor is made up of calcite flowstones, which may be interbedded with other mineralogical deposits, siliclastic sediments or even carbonate debris, the hole from the stalagmite may pierce through the flowstones which act as covers above porous sediments. In some cases, it may also reach late channels between the cave fill and the rock underneath (Fig. 6. Photos 38 to 41). In this case, enhancement of

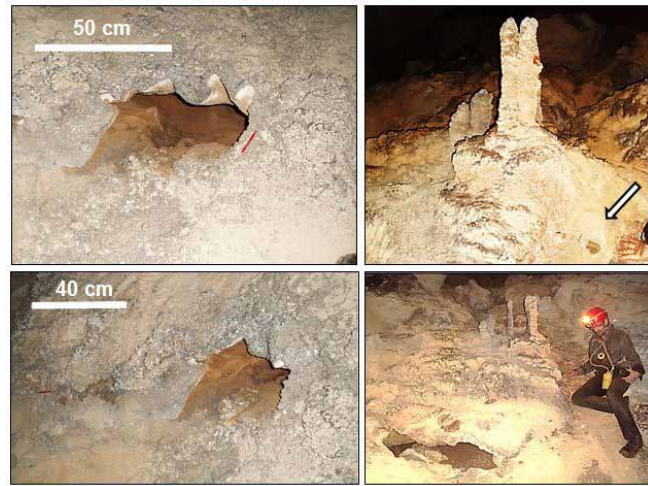


Figure 7. Photos 38 to 41. Tham Koun Don. Top left: upper opening of a space between sediments and cave floor, seen from above (top slope is at the bottom of the view). Below: lower opening of a space below sediments, carrying air and sometimes water. Top right: twin stalagmites on top of a flowstone, associated with lateral vents (one in front of the arrow). Below: same place seen from further away. At the bottom left of the view, there is the large outlet of a narrow way with air and water below the flowstone.



Figure 8. Photos 42 to 47. From hollow stalagmites to rims, a selection of shapes.

air circulation through the hole occurs and it may also change to some extent the dynamics of stalagmite growth.

The air from the hole is wet and may facilitate life in, and immediately around, the stalagmite when it flows upward through it. Life may be facilitated and stalagmite growth may show some change. For instance, this is probably the way how oblique branches may form on pre-existing stalagmites.

5. Hollow stalagmites and rims

The most typical hollow stalagmites are high (up to 1.75 m) and slim, but there is a wide range of shape and proportions from stalagmites to rims. Despite rims being often located on plain rock (but not always, as some rest on boulder piles or on sediments) and hollow stalagmites mostly on sediments, both kinds of speleothems display a bottom hole, a peripheral wall and no stalactite above, they all form as a result of wet air circulation (with probable occasional condensates) in the passage substratum or wall. One could associate the larger diameter of rim holes to the fact that bearing rock is poorly porous and the smaller diameters of stalagmite holes to the fact that



Figure 9. Photo 48. Twin stalagmites and two associated tubes below (arrows): one upward and one downward.

fluid circulation is less focused towards the vent, because of the sediments are overall more porous, but this needs further investigation.

Some hollow stalagmites are positioned on rock, where there is no hole passing through the rock and in this case, we have to consider a model without enhancement by air circulation and probably the action of life.

6. Conclusion

Hollow stalagmites are certainly a very attractive record of cave fossil passages functioning, as they mix unusual mor-

phology, a variety of settings, mineralogical variations, cave weather, seasonal variations and life. However, to what extent the different factors are involved remains a question to be answered quantitatively, which needs much more complex instrumentation and long term recording. So is the need to study modalities of internal stalagmite evolution, such as hole plugging or enlarging, or even diagenetic evolution.

Acknowledgements

Warm thanks are addressed to the many tens of cavers who came in the caves of Khammouane with the author and especially to Jean-François Vacquié and Jacques Rolin. Many thanks also to Philippe Lapointe and TOTAL who supported the study.

References

- Mouret C, 2005. CD-ROM [available on paper in 2008]. Main 2001 to early 2005 results on the karst of Khammouane, central Laos: long caves, sloping caves, hollow stalagmites and others. *UIS, 14th Internat. Congr. Speleo.*, Athens, Kalamos, Proc., Vol. 2, Paper O143, p. 411-415.
- Mouret C, 2010. CM- Réflexions sur le creusement vertical ascendant dans les karsts, basés sur plusieurs exemples choisis au Laos et en France. *Spéléo-Club de Paris, Proc. 19th Rencontre d'Octobre*, 10-11 oct. 2009, Saint-Laurent-en-Royans, p. 126-138.
- Mouret C, 2011. Les réseaux obliques du karst du Khammouane. Une introduction. *Spéléo-Club de Paris, Proc. 20th Rencontre d'Octobre*, Labastide-Murat, 2010, p. 74-82.
- Mouret C, Lapointe Ph, 2009. Mineralogy of chemical deposits in hypogenic Phiseua Cave, Khammouane, Central Laos. USA, Texas, Kerrville, *15th International Congress of Speleology, Proc.*, Vol. 1, p. 312-317.

Symmetrical Helictites and Geopetal forms from South Eastern Australian Caves

Jill Rowling

Affiliation: Co-Chair, Program Committee Speleo2017
Sydney University Speleological Society, Australia

Abstract

Symmetry and vertical orientation are not features normally associated with helictites, however some helictite forms from caves in eastern Australia exhibit these features. Tantanoola show cave in South Australia contains excellent examples of upward-growing helictites, both as heligmities and an upward-growing vermiform type, apparently sprouting from the sides of columns. They appear to develop normally outwards from the columns, but then bend at 90 degrees and continue vertically for some distance. The bend may be similar to a 'cave turnip'. A smaller but similar shaped upward-growing form is found in the Star Chamber of Wollondilly show cave, Wombeyan Caves, New South Wales (NSW). A quadrant-shaped symmetrical speleothem with optically discontinuous segments occurs in several caves including Orient show cave, Jenolan Caves, NSW. A novel related form in Orient Cave appears as a symmetrical pair of "hands" and may possibly be twinned. Self-symmetric (fractal) helictites occur in The World of Mud, Mammoth Cave, Jenolan Caves, and in Sigma Cave, Wombeyan. Rod-shaped helictites occur at Jenolan and Wombeyan. A broken rod-shaped fringed helictite in Sigma Cave was compared with one at Ribbon Cave, Jenolan. A simpler form of rod without branches has a symmetrical cross section. The geopetal orientation of the fringe suggests influence from dripping water at the tips. Ribbon helictites at Jubilee Cave, Jenolan are also symmetrical, having an L shape (one canal, twofold symmetry) or a T shape (2 canals, twofold symmetry).

Further work is needed to determine growth mechanisms.

Keywords:

1. Introduction

The simplest form of helictite is the long tapered cylinder, with a fine central capillary which transports water from the cave wall to the growing tip. Moore and Sullivan (1997), and Hill and Forti (1997) note that in general a helictite tip comprises three twinned calcite crystals and the structure develops in random directions depending on which of the planes between crystals happens to open when hydrostatic pressure increases (i.e. during wet periods). Gravity generally does not play a part, except in occasional cases where there is enough water seeping out of the tip to allow a drip to develop. Rowling (1997) described a ribbon form of helictite with a planar or flag-like structure. A heligmite is a helictite which develop vertically from a substrate. They may be branched, but are typically vermiform as shown in Fig 1. They are probably the most simple geopetal (gravitationally-influenced) helictite form.

2. Methods

This poster / paper is a discussion of helictites based on in-cave photography using a variety of film and digital cameras over several years of cave visits. More detailed work was done on ribbon helictites by Rowling (1997).

2.1. Upward-curving (geopetal) helictites

Tantanoola show cave is near Mount Gambier, South Australia. It is developed in dolomite / dolostone, part of the Gambier Limestone. The cave comprises a single chamber, well decorated with stalactites, stalagmites, straws, columns, heligmities and L-shaped geopetal helictites. The latter are a vermiform type, and develop from the sides of columns and rock ledges. They appear to develop normally outwards from their substrate, but then bend and continue mainly upwards. They are typically 10 to 50 cm long but one or two appear



Figure 1. Large broken heligmite in Tantanoola Cave, South Australia showing central canal.

to have developed over a metre (Fig 2). A smaller geopetal form is found in the Star Chamber of Wollondilly show cave, Wombeyan Caves, New South Wales (NSW), and could be influenced by air movement. Several vermiform helictites grow upwards very close to the wall (Fig 3).

2.2. Rod- and Saw- shaped helictites

Rod-shaped helictites and ones with a sawtooth lower edge occur at Jenolan and Wombeyan caves. These can get quite large, for example one in Ribbon Cave, Jenolan, is around 500 mm long and about 20 mm thick. The two types, rod-shaped or saw-shaped appear to depend on whether the helictite grows upward or downward. The angle made between the helictite and its substrate is typically 90 degrees, although



Figure 2. Large geopetal L-shaped helictites on a stalactite at Tantanoola Cave.



Figure 3. Small geopetal helictites in Star Chamber, Wollondilly Cave.

the substrate can be a hanging wall which makes the helictite appear to droop downwards. Where the rod helictite grows upward, it stays remarkably even in diameter (Fig 4). The simplest form of rod helictite is unbranched and has a symmetrical cross section with 4, 5 or 6 apparent sides. In cases where it grows downward, the lower edge appears to lengthen and a remarkably regular fringe of small stalactites develops, suggesting that the helictite can get quite wet (Fig 5). A broken 'saw' helictite in Sigma Cave, Wombeyan, was sketched in-situ, and later compared with those seen at Ribbon Cave, Jenolan. The Sigma Cave helictite had a central canal which branched regularly to the fringe tips, and an apparent vertical twin plane. The saw area was covered with fine crystals resembling aragonite, with random orientation. The geopetal orientation of the fringe suggests influence from dripping water at the tips.

Interesting small ice structures were photographed by the author in Dobsinska Ice cave in Slovakia. They resemble a saw helictite with only one 'wing' or 'blade' (Fig 6).



Figure 4. Rod helictite from Ribbon Cave, Jenolan.



Figure 5. Several forms of rod and saw helictites from Orient Cave, Jenolan.



Figure 6. Ice helictites? In Dobsinska Ice Cave, Slovakia.

2.3. Butterfly shapes, quadrants and hand shaped speleothems

Butterfly and quadrant-shaped speleothems occur in several caves including Wyanbene Cave (NSW) and Orient Cave. Shining a laser pointer at one of the hand-shaped speleothems revealed optically discontinuous segments, suggesting radial growth from several capillary tubes (canals) and possibly capillary planes (Figs 7, 8). The butterfly shape is similar to those described from the Caverns of Sonora, U.S.A. (Hill and Forti, 1997). The hand-shaped form is particularly novel and



Figure 7. Butterfly, quadrant and hand shaped speleothems, Orient Cave.



Figure 9. Horn-shaped fractal helictite from Sigma Cave.



Figure 8. Boxy quadrant speleothems in Orient Cave.

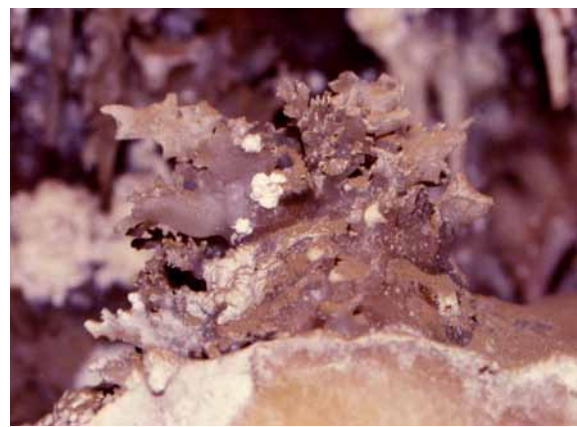


Figure 10. Group of fractal helictites from Sigma Cave, Wombeyan Caves.

in Orient Cave occur as a pair. In Commonwealth Pit, Orient Cave, a similar form occurs in a group of saw and rod-shaped helictites, and appears to be a saw helictite in which the fringe of stalactites has become more significant to the speleothem's growth compared with the rod section.

2.4. Fractal helictites

Self-symmetric (fractal) helictites occur in The World of Mud, Mammoth Cave, Jenolan Caves, and in Sigma Cave (Figs 9, 10). The overall shape of the Sigma fractal helictite can be seen repeated on a smaller scale when viewing the structure under the microscope and resembles a Sierpinski fractal pattern. The base of the helictite comprises three separate calcite crystals, possibly sharing a twin plane. Twinning appears to be a feature of horn shaped protuberances. The main horn is twinned axially. Its tip has a 90 degree chamfer made up from two 45 degree chamfers on each of the twinned tips. Like a ribbon helictite (Rowling, 1997), upper edges appear spiky and etched whereas lower edges appear smooth. Under the microscope the surface has fields of aligned spiky scales like miniature sharks' teeth.



Figure 11. Fractal helictites, possibly aragonite, The World of Mud, Mammoth Cave, Jenolan.

In the World of Mud, fractal helictites occur in the ceiling of an area with aragonite speleothems, dark and light coatings and plenty of mud (Fig 11).

2.5. Ribbon Helictites

Ribbon helictites at Jubilee Cave, Jenolan are symmetrical, having an L shape (one central canal) or a T shape (2 central canals) (Fig 12). They were reported to the 12th ICS (Rowling, 1997). Like heligmites, they develop normally from the substrate but then the central canal turns 90 degrees and forms a



Figure 12. Ribbon helicite. View of broken ribbon through microscope showing central canal.

flattened ribbon of calcite. The crystallites forming a ribbon helicite resemble lublinitite variety of calcite. Ovals on the surface are thought to be precursors of rod shaped helicites as they have a similar cross-section (Fig 13).

3. Discussion

3.1. Upward-growing geopetal helicites

As distinct from heligmmites, these L-shaped helicites grow outward from a vertical surface then curve 90 degrees and continue upwards. It has been suggested (Andy Spate, pers. comm.) that there is a hollow at the lower 90 degree bend which may contain hydromagnesite. If so, this part of the helicite may be similar to a 'cave turnip' (Hill and Forti 1997).

Possibly magnesium minerals from the dolostone bedrock may be transported in solution and then deposited as hydromagnesite near the tip of a developing vermiform helicite. A "cave turnip" may form near the tip, engulfed by calcite. It is conjectured that hydromagnesite, if present, would tend to stay near the bottom of the 'turnip'. The top of the 'turnip' may stay open as a pore, and a conventional vermiform heligmite continues to develop but with hydromagnesite in the central canal. If by chance the helicite starts to grow more horizontally during a growth period, hydromagnesite blocks the lower part of the pore (forming another "turnip") and leaving only the upper surface free for growth.

At Tantanoola Cave, some upward-curving helicites resemble calcite covered tree roots. Tree roots occur near the cave entrance, and it is tantalising to think that plants may influence the structure so consistently. Plants near the cave include a shrub-like mallee eucalyptus, which is well-known for having long roots.

3.2. Rod- and Saw- shaped helicites

The main apparent difference between rod and saw shaped helicites is the angle made with the substrate, typically a wall. Possibly an excess of water due to the geometry is allowing the

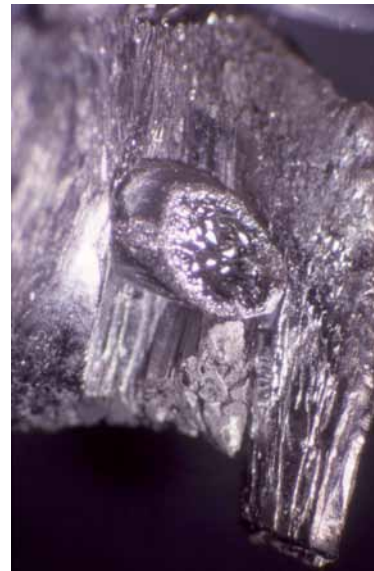


Figure 13. Ribbon helicite. Part of a metal coated helicite sample showing Oval feature.

central canal of saw helicites to expand along a vertical twin plane, letting more water through during wet periods.

Ice helicites (Fig 6) are presumably formed on ice which is melting underneath the surface, possibly by a wet ice surface developing a thin skin of ice due to the air being colder at times than the main body of ice. These ephemeral structures appear to have a capillary but it is not known whether the structure is twinned. The icicle at the end would be from water seeping from the capillary, and the flag shape appears to be from surface water seeping at times along the outside like a cave shawl.

Lava dribblets may be similarly formed, but at a higher temperature and density extreme. On other worlds with lower gravity, they may form structures more like the ice helicites.

3.3. Butterfly shapes, quadrants and hand-shaped speleothems

Possibly very wet saw helicites can form into the quadrants and clear 'hand' shapes seen in Orient Cave, but to achieve a butterfly shape one would expect twinning to occur early in the helicite's development. Some quadrant- and hand-shaped speleothems appear to be recrystallised, or could be developed as a series of twinned segments. If needle-form calcite is involved in the development of these speleothems, as has been noted by Rowling for ribbon helicites, then it is possible that water is being guided along radial needles, initially held apart by biogenic films.

3.4. Fractal helicites

Chemical influence, possibly magnesium or manganese, may be responsible for the self-symmetry as the repeat pattern seems to be at a very small scale. Twinning on three planes is common for helicites but the unit cell in this case is slightly different to "normal" calcite, allowing the structure to repeat at a smaller scale.

3.5. Ribbon helictites

Ribbon helictites have tiny ovals which resemble the start of rod-shaped helictites. Rowling (1997) observed that the ovals appear to be twinned near the helictite's central canal and have a fibrous core with a smooth crystalline outer section, and another apparent twin plane along the length of the short tube. If ribbon helictites can have L or T shapes (1 or 2 central canals) can they be precursors to the quadrant shapes?

4. Further work

Further work is needed to determine growth mechanisms. In the case of geopetal helictites, examples need to be properly examined to determine if there is a strong influence from Mg and the helictites' orientation. The relationship between initial angle and crystal orientation for saw and rod helictites needs further work, as does the extension of these forms to quadrants, butterflies and the paired 'hand' forms. The influence of needle form calcite should be considered, as different organisms often influence calcite growth. It should be possible to examine helictites' structures for microorganisms. Comparing the rod forms to the ovals on ribbon helictites could be further examined. Perhaps the orientation is determined early on, with fibrous calcite (lublinite) conducting more water and thus orienting the helictite (geopetal form).

5. Conclusions

Identifying common growth patterns is the first part of understanding how helictites develop particular forms. Similar forms suggest similar influences on the helictite's growth. Geopetal helictites are interesting because they are a capillary

structure in which gravity has more influence compared with other helictites. Fractal and symmetrical helictites are also interesting, not only because of their beauty in the show caves but also suggests novel ways that calcium carbonate can be deposited.

Acknowledgements

Many thanks to the managers of Tantanoola Cave for allowing photography during guided tours. The Wombeyan Caves photos were taken during field work by the author when studying cave aragonite. Observations at Wombeyan and Jenolan were only made possible by the kind understanding of staff and managers at Jenolan Caves and Wombeyan Caves, NSW, who permitted access to the show caves for the purpose of studying the speleothems between 1992 and 1994. All photos and sketches are by the author. The Sigma Cave sample was taken during permitted field work in 2002 during the author's work on cave aragonites of NSW.

References

- Hill, C. and Forti, P. (1997), *Cave Minerals of the World*, 2nd edn, National Speleological Society, USA.
- Moore, G. and Sullivan, N. (1997), *Speleology: Caves and the Environment*, 3rd edn, Cave Books, USA.
- Rowling, J. (1997). Ribbon Helictites from Jenolan Caves, NSW Australia. In: *Proceedings of the 12th International Congress of Speleology, Vol 1 Symposium 7: Physical Speleology*, p263-266. Swiss Speleological Society, La Chaux-de-fonds, Switzerland.

(Abstract) **Symmetrical Helictites and Geopetal forms from South Eastern Australian Caves**

Jill Rowling

Affiliation: Co-Chair, Program Committee Speleo2017, member of Sydney University Speleological Society, Australia

Abstract

Symmetry and vertical orientation are not features normally associated with helictites, however some helictite forms from caves in eastern Australia exhibit these features. Tantanoola show cave in South Australia contains excellent examples of upward-growing helictites, both as heligmites and an upward-growing vermiform type, apparently sprouting from the sides of columns. They appear to develop normally outwards from the columns, but then bend at 90 degrees and continue vertically for some distance. The bend may be similar to a 'cave turnip'. A smaller but similar shaped upward-growing form is found in the Star Chamber of Wollondilly show cave, Wombeyan Caves, New South Wales (NSW). A quadrant-shaped symmetrical speleothem with optically discontinuous segments occurs in several caves including Orient show cave, Jenolan Caves, NSW. A novel related form in Orient Cave appears as a symmetrical pair of "hands" and may possibly be twinned. Self-symmetric (fractal) helictites occur in The World of Mud, Mammoth Cave, Jenolan Caves, and in Sigma Cave, Wombeyan. Rod-shaped helictites occur at Jenolan and Wombeyan. A broken rod-shaped fringed helictite in Sigma Cave was compared with one at Ribbon Cave, Jenolan. A simpler form of rod without branches has a symmetrical cross section. The geopetal orientation of the fringe suggests influence from dripping water at the tips. Ribbon helictites at Jubilee Cave, Jenolan are also symmetrical, having an L shape (one canal, twofold symmetry) or a T shape (2 canals, twofold symmetry).

Further work is needed to determine growth mechanisms.

3D Photogrammetry Of Speleothems With The Astronauts Of The European Space Agency “Caves” Training Course

Tommaso Santagata⁽¹⁾, Jo De Waele^(1,2), Francesco Sauro^(1,2), Loredana Bessone⁽³⁾

Affiliation: ¹ La Venta Esplorazioni Geografiche, Via Priamo Tron 35/F - 31100, Treviso (Italy), www.laventa.it
tommaso.santagata@laventa.it

² Department of Biological, Geological and Environmental Sciences, University of Bologna, Via Zamboni 67, 40127 Bologna, Italy jo.dewaele@unibo.it cescosauro@gmail.com

³ Directorate of Human Space Flight and Operations, European Space Agency, Linder Höhe, 51147 Köln, Germany, loredana.bessone@esa.int

Abstract

The CAVES training course (Cooperative Adventure for Valuing and Exercising human behaviour and performance Skills) managed by the European Space Agency (ESA), since 2011 involves international crews of astronauts preparing them to work and perform scientific activities under real exploration conditions in a cave environment. During the 2016 training course in Sardinia (Italy), photogrammetry has been used in order to teach astronauts the use of 3D mapping techniques as a resource that could be used also on the surface of other planets. Several speleothems of Sa Grutta and Tiscali caves have been mapped with photogrammetric techniques. The 3D models realised were subsequently analysed to obtain information on size, volume, shape and morphology of the detected surfaces. This article is focused on the methods used and results obtained from the analysis of the 3D models.

Keywords: Cave photography; 3D modelling; morphometry; geomorphology; documentation

1. Introduction

In the last six years, several caves of the Supramonte area (Sardinia, Italy) have been studied and observed carefully thanks to the scientific activities realized as part of the CAVES training course organized by the European Space Agency (ESA). The main objective of this course is to prepare international crews of astronauts to work safely and as a multicultural team in a difficult environment such as a cave, performing scientific tasks that includes taking geological and microbiological samples in water and sediments, mapping the cave, taking photographs, monitoring air flows and other physical parameters such as carbon dioxide, radon levels, temperature and humidity in the cave atmosphere (Bessone *et al.* 2013).

A part of the 2016 CAVES training course was dedicated to giving astronauts an introduction about 3D mapping technologies and instruments that can be used in harsh conditions, focusing the activities in the cave on 3D photogrammetric techniques. Photogrammetry allows acquiring metric data through the acquisition and analysis of series of frames that can be obtained using standard digital cameras. This technique has been widely used in the documentation of rock art caves (e.g. Lerma *et al.* 2010; Sadier *et al.* 2012; Robert *et al.* 2016). In recent years we have seen a remarkable development of these methods, cameras and software for digital photogrammetric survey, and today we are able to make a three-dimensional reconstruction of small or in some cases even large areas.

Several others techniques and instruments such as laser scanners or image-based sensors can be used in most situations (e.g. Fabbri *et al.* 2017), but these tools are costly and difficult to use in dark, muddy and wet conditions, while photogrammetry allows to easily reconstruct 3D models even in caves.

The 3D models realized by the astronauts were analysed to store information on size, volume, shape and morphology of

the surveyed areas. These exercises have shown the astronauts that it is possible to reconstruct 3D models and use photogrammetric techniques to study geometric relationships of natural rock surfaces without any physical contact, just with one camera in few minutes of operational work.

2. Methods

Digital photographs were taken with a Nikon Coolpix AW110 from a couple of meters distance from the chosen objects. Targets were placed nearby to allow post-processing of the photographs.

Astronauts have performed digital close range photography of four different morphologic features (Fig. 1): a karren field, and underwater finger-like speleothems, spherical cemented sediments (so-called “dolls”), a three meters high and two meters wide stalagmite. The work was carried out by a team of 3 astronauts, one handling the camera, and two illuminating the scene with their Scurion© lights.

This geomatic technique allows acquiring metric data through the acquisition and analysis of photographs made with high overlap. By correcting images from lens- and perspective distortions, digital photogrammetry allows extracting accurate measurements from photographs. It is also possible to create 3D meshes and point cloud models using dedicated free software.

With the addition of measurable reference points (markers) it is possible to obtain scaled 3D models with high precisions (millimetres) depending on distance from the object, its dimension and camera resolution.

The different photographic datasets acquired by the astronauts during the six days in Sa Grutta cave were subsequently selected and processed using the software Reality Capture. The data have allowed obtaining three-dimensional models in the form of point clouds from which triangulated mesh

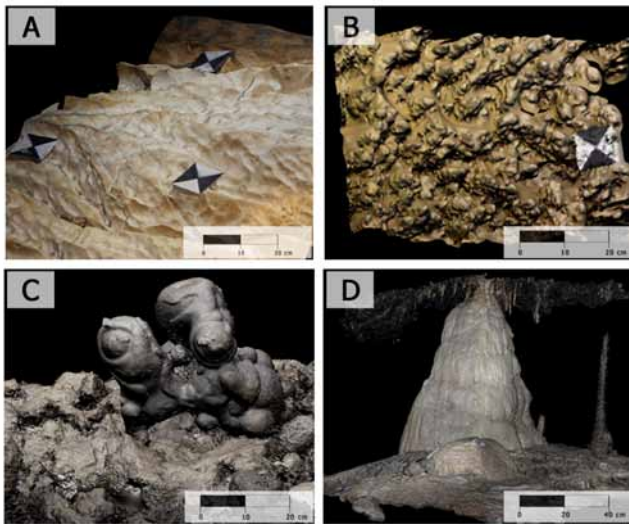


Figure 1. 3D models of the four studied objects: A) Underground karren, Chaos; B) Finger-like subaqueous speleothems, Chaos; C) Interstitial limestone formations (“dolls”), close to Bajkal Lake; D) Monviso stalagmite.

models were derived and morphological analysis were performed.

Using the software 3DReshaper, through specific tools it was possible to reconstruct the best surface through spheres and calculate the volume of small parts of the detected surfaces in order to obtain statistical records. Three-dimensional polylines and contour lines have been extracted with the aim to produce sections of the detected speleothems.

3. Results and potential applications

The first surveyed area is a peculiar karren field in the area of Chaos. The surveyed surface is about 3 m² and the overall photographic work was performed in less than 15 minutes. Photogrammetry showed a great potential as a simple tool to perform morphometric studies on the karren field. Karren channels are 7 to 18 cm width with depth between 2 to 14 cm. It is possible to extract contour lines, aspect and slope maps, which could be used for geomorphologic studies.

The second area consists in a field of finger-like speleothems growing in a dry pool in the same area. Here the surveyed area is more than 4 m². Also in this case the quantitative metric information can be easily used for morphometric studies: fingers have a mean height of 5 cm with a diameter ranging from 4 mm to 8 cm. Statistic analysis can be performed extracting metric data from each finger.

Another interesting morphological feature are the so-called “dolls”, which are cemented sediment eroded in forms of spheres. Thanks to the photogrammetric model it was possible to estimate the diameter variability of the agglomerate spheres between 1 to 12 cm, with a volume between 4.2 to 28 cm³ (Fig. 2).

The last case was the Monviso stalagmite, a huge speleothem that has required several photographs for the photogrammetric model. The surveyed area is 9 m², with the stalagmite being 1.7 m high. It has been possible to elaborate several horizontal sections of the stalagmite, in order to calculate the total volume (1.6 m³). Thus photogrammetry is clearly an important tool also for speleothem researches.

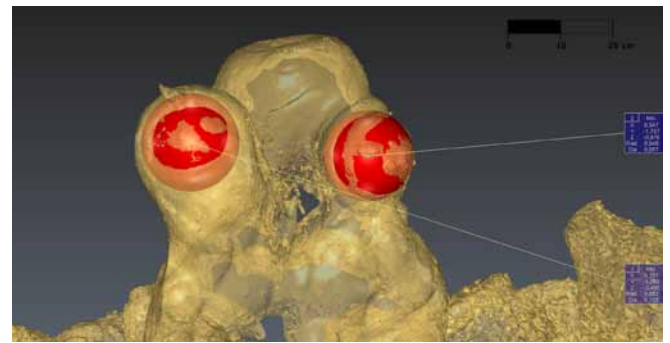


Figure 2. Volume calculation of the different sediment spheres constituting the doll feature by sphere fitting models.

4. Conclusions

The studies carried out during CAVES 2016 have shown these photographic field techniques to be easily applied after a short training to the astronauts. The results of the 3D photogrammetry have improved after each session, and the 3D model created of the object studied last (Monviso) was much better than the earlier ones, showing that field practice is necessary to get better results. These techniques will surely be very helpful in the exploration of remote places, including Mars or the Moon, where 3D photography will be able to carry home a detailed view of the morphologies encountered. The following data elaboration then gives the necessary information to the scientists at home for detailed morphometric analysis of the landforms and objects documented by the explorers. Caves, being devoid of vegetation and natural light sources, are ideal places to train astronauts for taking pictures using artificial light sources.

References

- Bessone L, Beblo-Vranesevic K, Cossu QA, De Waele J, Leuko S, Marcia P, Rettberg P, Sanna L, Sauro F, Taiti S, 2013. Esa Caves: training astronauts for SPACE exploration. In: M Filippi & P Bosak (Eds.), *Proceedings of the 16th International Congress of Speleology*, Brno 19-27 July 2013, Volume 1, pp. 321-327.
- Fabrizi S, Sauro F, Santagata T, Rossi G, De Waele J, 2017. High-resolution 3-D mapping using terrestrial laser scanning as a tool for geomorphological and speleogenetical studies in caves: An example from the Lessini mountains (North Italy). *Geomorphology*, **280**, 16-29.
- Jerma JL, Navarro S, Cabrelles M, Villaverde V, 2010. Terrestrial laser scanning and close range photogrammetry for 3D archaeological documentation: the Upper Palaeolithic Cave of Parpalló as a case study. *Journal of Archaeological Science*, **37**(3), 499-507.
- Robert E, Petrognani S, Lesvignes E, 2016. Applications of digital photography in the study of Paleolithic cave art. *Journal of Archaeological Science: Reports*, **10**, 847-858.
- Sadier B, Delannoy J-J, Benedetti L, Bourlès D, Jaillet S, Geneste J-M, Lebatard A-H, Arnold M, 2012. Further constraints on the Chauvet cave artwork elaboration. *Proceedings of the National Academy of Sciences USA*, **109**(21), 8002-8006.

Multilevel karst system evolution in relationship to palaeoclimate and palaeogeography: hints from a 500 ky speleothem record from the Piani Eterni Karst System, Belluno Dolomites, Italy

Francesco Sauro^{1,2}, Andrea Columbu^{2,3}, Joyce Lundberg⁴, Jo De Waele²

Affiliation: ¹ Gruppo Speleologico Padovano CAI, Progetto Piani Eterni

² Dipartimento di Scienze Biologiche, Geologiche e Ambientali, Università di Bologna, Istituto Italiano di Speleologia, Via Zamboni 67 – 40126 Bologna (Italia); e-mail: cescosauro@gmail.com; jo.dewaele@unibo.it

³ School of Geography, University of Melbourne, VIC, 3010, Australia; e-mail: acolumbu@student.unimelb.edu.au

⁴ Department of Geography and Environmental Studies, Carleton University, Ottawa, K1S 5B6, Canada; e-mail: joycelundberg@carleton.ca

Abstract

Piani Eterni is the deepest and longest multilevel karst system of the Dolomites. The geometric distribution and stratigraphic-structural guidance of palaeo-epiphreatic levels have been studied in detail in recent times, but there are still several open questions regarding the palaeoclimatic and palaeogeographic factors that have controlled its evolution through time.

Over the last three years, several stalagmites were sampled and dated with the U-Th method. Speleothems have been collected at different altitudes, from palaeo-epiphreatic conduits without vadose entrenchments. The research focused on speleothems that have registered different flooding events, testified by silty and sandy layers. These events could have happened only when the conduits were still very close to the epiphreatic zone and the speleothems formed immediately after the formation and draining of the epiphreatic conduits. The temporal record of the speleothems and their vertical distribution in the cave, compared to the presence of fluvial terraces and glacial deposits in the nearby Mis Valley, are shown to be in agreement with the uplift rate of the region. U-Th and stable isotope analyses (oxygen and carbon) show that speleothems were mostly deposited during climatically unstable periods following the MIS11, MIS9, MIS7 and MIS5 interglacial peaks.

This is a novel example of study based on the palaeoclimate significance and growth history of speleothems in relation to the formation of the hosting conduits and epiphreatic oscillations, bringing new insights on the evolution of multilevel karst systems.

Keywords:

1. Introduction

Speleothems from the Alps are demonstrably valuable tools for palaeoclimate and palaeo-environmental reconstructions (Boch *et al.* 2011), with numerous examples from caves in the northern sector: i.e., Austria (Spötl *et al.* 2006; Holzkamper *et al.* 2005; Meyer *et al.* 2009; Moseley *et al.* 2015), Germany (Niggeman *et al.* 2003), and Switzerland (Luetscher *et al.* 2015). Only a few studies considered the southern side (Frisia *et al.* 2000, 2005; Huang *et al.* 2001; Chiarini *et al.* 2017), mostly in Italian territories. Therefore, we try to reconcile this gap by extensive exploration (Sauro *et al.* 2013), and related sampling campaign, of the Piani Eterni karst system, carved in the Southern limb of the Italian Alps (Dolomiti Bellunesi National Park). Piani Eterni is the deepest (> 1000 m) and longest (> 40 km) karst system of the Dolomites, characterised by a multi-level assemblage of interconnected tunnels of three main morphological types: palaeo-epiphreatic, draw-down and vadose conduits.

For the present study, speleothems, mostly stalagmites, were sampled at different altitudes (from 1650 to 860 m a.s.l.) in palaeo-epiphreatic passages with no evident signs of vadose entrenchment. The speleothems demonstrated an excellent propensity to be dated using the U-Th method, yielding accurate geochronological control on the minimal age of palaeo-epiphreatic tunnels in which they grew. Moreover, the speleothem calcite layers are intercalated with sand and silt laminae, testifying to the occurrence of cyclical cave flooding. Multiple U-Th ages were determined along the speleo-

thems growth axis, constraining the timing of such floods. In addition, speleothems were analysed for oxygen ($\delta^{18}\text{O}$) and carbon ($\delta^{13}\text{C}$) stable isotopes, which can procure important clues about climate (e.g., rainfall and temperature) and environment (e.g., vegetation above the cave and karst hydrogeological flow) at the time of calcite deposition (McDermott 2004; Fairchild *et al.* 2006).

In summary, we have examined the morphology and vertical distribution of cave tunnels, the presence of fluvial terraces and glacial deposits at the surface, speleothem ages and their growth history, and the occurrence of cave flooding, aiming to: 1) constrain the timing of cave formation and oscillation of the palaeoepiphreatic level; 2) reconstruct the speleogenetic dynamics in relation to palaeoclimatic variations; 3) understand the most favourable environmental phases for the deposition of speleothems; 4) build a background for the creation of the first palaeoclimate record of the area. In addition, this work aims to better understand the timing and geomorphic events related to a major fluvial capture of the nearby Mis Valley, a hypothesis already proposed by previous authors.

2. Area of study, materials and methods

The Piani Eterni karst system lies in the Erera-Brendol plateau (Fig.1), carved into limestone (upper levels, ~1900-1500 m a.s.l.), dolomitised limestone (middle levels, ~1500-1300 m a.s.l.), and dolomite (lower levels, 1500-900 m a.s.l.) belonging respectively to the *Calcarei Grigi* and *Dolomia Principale* formations. Part of the middle levels is also excavated into

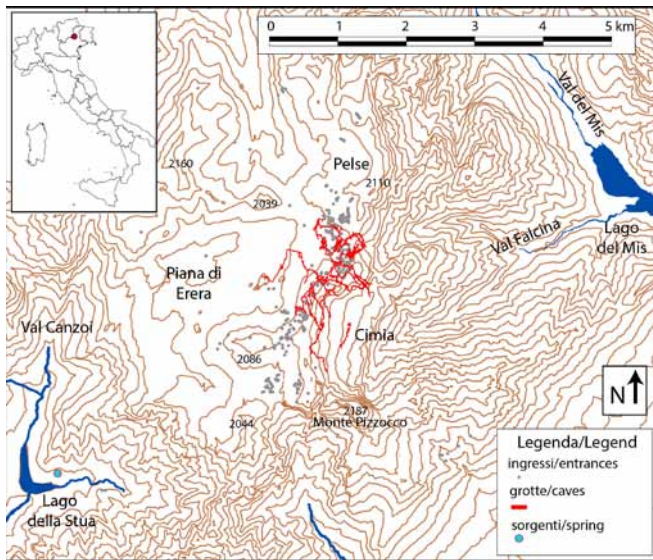


Figure 1. Location of the Piani Eterni plateau and cave system (red lines) in between the Mis Valley to the east and Canzoi Valley to the west.

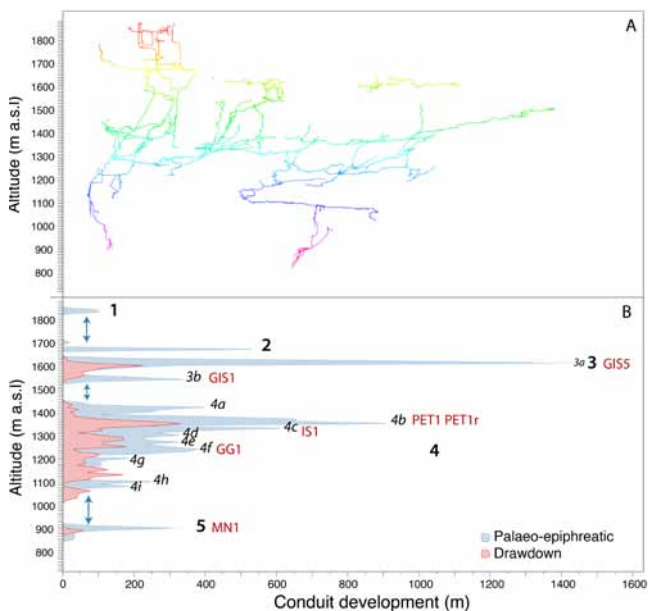


Figure 2. Distribution of cave conduits and sampled speleothems: A) Projected section of the cave systems, the colour palette follows the altitude of the different sectors; B) Cumulative distribution of palaeo-epiphreatic conduits (numbers in black indicate the main palaeo-epiphreatic levels and sublevels) and drawdown conduits along the system and altitude location of the sampled speleothems. Vertical double blue arrows on the left indicate altitudinal ranges where only vadose passages have been documented, probably corresponding to abrupt carving phases of the nearby Mis Valley.

a bituminous dolomitic unit that has not yet been officially named (Riva *et al.* 2008). Numerous and interconnected caves constitute the karst system, comprising deep shafts accessible from the glacial-karst hollow located at the top of the massif, and one cave (Grotta Isabella) accessible from the eastern flank of the plateau (Salogni, 2007). Abisso Bluette and O6 caves, recently discovered around Cimbia area, could also be connected to Grotta Isabella. Sauro *et al.* (2013) demonstrated that the formation of the system was driven by the interaction between the palaeo-piezometric level and tectonic and stratigraphic inception surfaces. In particular, the intersec-

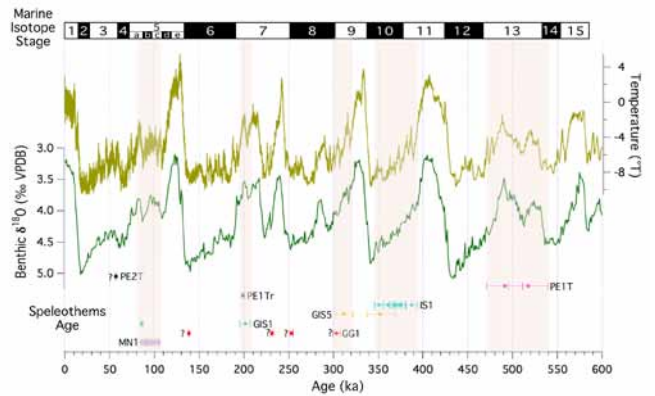


Figure 3. Speleothem ages vs. palaeoclimate variations. From top to bottom: marine isotopic stages alternation (black and white rectangles); Temperature curve (Epica Community members, 2006) and LR04 $\delta^{18}\text{O}$ benthic stack palaeoclimatic curve (Lisiecki and Raymo 2005); Speleothem ages and associated errors (capped horizontal lines). Speleothem life-span mostly coincides with warm and wet stages (orange bars), considering the correlation with the benthic $\delta^{18}\text{O}$ -curve. Correlation is not attempted for speleothems with hiatuses and reporting only few ages (PE2T, GG1, GIS5); these samples are marked with question marks and will need more detailed dating in the future.

tion between the bituminous strata and the Cimbia fold-axis, coupled with palaeo base level stillstands, created extensive epiphreatic levels at well-recognisable altitudes (Fig.2).

All the palaeo-epiphreatic levels were represented in the speleothems collected. Four complete stalagmites (MN1, GG1, IS1, GIS5), one incomplete stalagmite (PET1), and one flowstone section (GIS5) were sampled. Hand specimen and petrographic observations proved that these speleothems are formed by layers of columnar calcite (in accordance with Frisia 2015), and, in most of them (MN1, GG1, IS1, PET1), alternating with sandy and silty detrital material related to flooding events.

For U-Th dating, 10 to 100 mg slices were hand-drilled along the stalagmite growth axis, and analysed at Carleton University (Canada) and the University of Melbourne (Australia). Preparation of sub-samples, mass spectrometry and statistical treatment of the final data followed the protocols detailed in Lundberg *et al.* 2014 in Carleton University and Drysdale *et al.* (2009, 2012) in Melbourne University. $\delta^{18}\text{O}$ and $\delta^{13}\text{C}$ data were obtained following Drysdale *et al.* (2009) (analyses at Melbourne University).

3. Results

All samples have high uranium content (up to 5.4 $\mu\text{g/g}$), probably due to the presence of the uranium-rich bituminous unit, an important parameter for obtaining precise U-Th ages. From the lower to the upper cave levels, U-Th analyses returned the following results (Fig. 3):

- MN1 (880 m a.s.l., level 5, 20 dates, with silty layer) grew between 106 and 84 ka during MIS 5;
- GG1 (1250 m a.s.l., level 4f, 4 dates, with silt layers) started to grow at 303 ka during MIS 9 and then continued with various hiatuses until 138 ka.

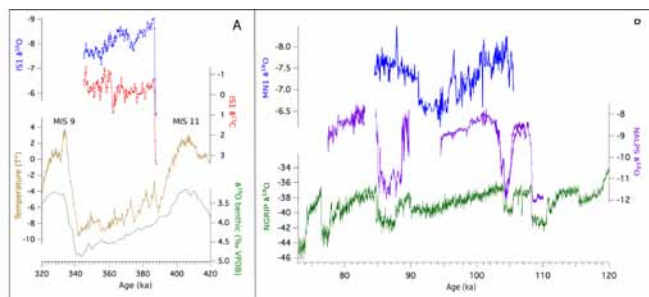


Figure 4. $\delta^{18}\text{O}$ and $\delta^{13}\text{C}$, obtained for IS1 (A) and MN1 (B) reveal interesting oscillations similar to those proposed by marine (Lisiecki and Raymo 2005), ice-sheet (NGRIP project members 2004; EPICA community members 2006) palaeoclimate records, and NALPS Speleothems (Boch *et al.* 2011).

- IS1 (1340 m a.s.l., level 4c, 10 dates, with silt layers) grew between 380 and 340 ka during MIS 11;
- PE1T (1380 m a.s.l., level 4b, two dates, with silt layers) grew between 517 (top) and 491 ka (bottom) during MIS 13. This collapsed stalagmite has a small regrowth stalagmite on the base PE1Tr that has been dated to 198 ka.
- GIS1a and GIS1b (1570 m a.s.l., level 3b, no silt layers) is a flowstone composed of two main layers with a hiatus in between, where the base of GIS1a was dated to 201 ka and the base of GIS1b was dated to 86 ka.
- GIS5 (1620 m a.s.l., level 3a, no silt layers) grew between 352 to 311 ka.

$\delta^{18}\text{O}$ and $\delta^{13}\text{C}$, obtained for IS1 and MN1 and GG1, reveal interesting oscillations similar to those proposed by marine (Lisiecki and Raymo 2005) and ice-sheet (NGRIP project members 2004; EPICA community members 2006) palaeoclimate records (Fig. 4).

4. Discussion and final remarks

U-Th results show that most of the stalagmites were preferentially deposited after the peak of the three last interglacial stages before the Holocene: MN1 and GIS1b after marine isotopic stage (MIS) 5e, GIS1a and PE1Tr after MIS7, GIS5 between MIS10 and MIS9, IS1 after MIS11. These periods are characterised by “transitional” climate between full interglacial (i.e., on average, warm and humid) and full glacial (i.e., cold and dry, with glaciers at high altitudes and latitudes). For example, the period just after MIS5e saw the establishment of large-scale, abrupt millennial-scale warm-cold oscillations, known as Dansgaard-Oeschger events or Greenland stadials-interstadials succession (Dansgaard *et al.* 1993; NGRIP project members 2004). The few dates on sample GG1 do not help with this story since they show only that it started to grow after the peak of MIS9 and continued, with several undetermined hiatuses, up to MIS6. The oldest speleothem, PET1, grew during, rather than after the peak of, the interglacial MIS13. However, MIS13 never reached optimal climatic conditions (i.e., in terms of temperatures, precipitation and sea levels) comparable with the other interglacials, and shows many climate fluctuations during the interglacial. Thus, we preliminarily infer that the deposition of speleothems at Piani Eterni study area was prevalent during periods of climate instability, further testified by the presence of detrital layers

(indicating cyclical floods). In IS1, six main flooding events have been identified in a timespan of 9,000 years (~368-377 ka). The above-mentioned correlation between speleothem $\delta^{18}\text{O}$ and $\delta^{13}\text{C}$ and other multi-proxy climate archives gives us confidence about the sensitiveness of these speleothems to the climate at the surface (Fig. 4). The regional vs. local significance of IS1 and MN1 $\delta^{18}\text{O}$ and $\delta^{13}\text{C}$ will be investigated in detail in the near future.

In addition to palaeoclimate, those speleothems that have recorded flood events (MN1, GG1, IS1, and PET1) could provide insights on the speleogenetic evolution of the area in relationship with the incision of the nearby Mis Valley. In the study area, epiphreatic levels represent periods of relative stability of the water table at intersection with inception horizons (Sauro *et al.* 2013). Determining the exact timing of void formation is extremely hard (Sasowsky 1988) if direct dating strategies (e.g., alunite dating in sulphuric acid caves, Polyak *et al.* 1998) are inapplicable. Speleothems might have been deposited thousands or hundreds of thousands of years after cave carving. Nonetheless, flooding in epiphreatic levels (with no vadose morphologies) recorded by stalagmites directly testifies that conduits were still close to the epiphreatic zone and that speleothems were deposited a short time after their excavation and draining, when the oscillations of the water table were still able to reach these conduits during exceptional flood events. Thus we can consider the maximum age of these speleothems as approximating the moment when the epiphreatic levels were definitely abandoned by the water table oscillations.

Recognisable fluvial and glacial terraces in the nearby Mis Valley are located at the same altitude as the studied epiphreatic tunnels, highlighting that the reaction of surface and underground drainage to palaeo base level entrenchment was probably synchronous (Pambianco 2015). The presence or lack of drawdown conduits connecting the different palaeo-epiphreatic levels suggest that the entrenchment was either progressive or abrupt, depending on which of the main agents of valley deepening dominated, between uplift, glacial carving or accelerated erosion processes such as in the case of fluvial capture. Based on these concepts, the study of these relationships between speleothem dates and the architecture of the cave levels has allowed us to identify a probable fluvial capture of the Mis Valley toward the south after MIS5 (Pambianco 2015; Fig. 3).

In conclusion, the configuration of Piani Eterni karst system and its relation with geomorphological elements at the surface, coupled with the geochemical analyses of speleothems that grew over the last ~500,000 years, offered the opportunity to study this portion of Dolomites from a multidisciplinary point of view: speleogenesis, landscape evolution and palaeoclimate variations. From a speleogenetic perspective, the advancement of this work will increase the knowledge of base level-driven evolution of high altitude multilevel karst systems, which could be exploited in other regions having similar geological and climatic conditions.

References

Boch R, Cheng H, Spötl C, Edwards RL, Wang X, Häuselmann Ph, 2011. NALPS: a precisely dated European

- climate record 120–60 ka. *Climate of the past*, **7**(4), 1247–1259.
- Chiarini V, Couchoud I, Drysdale R, Bajo P, Milanolo S, Frisia S, Greig A, Hellstrom J, De Waele J., 2017. Petrographical and geochemical changes in Bosnian stalagmites and their palaeoenvironmental significance. *International Journal of Speleology*, **46**(1), 33–49.
- Dansgaard W, Johnsen SJ, Clausen HB, Dahl-Jensen D, Gundestrup NS, Hammer CU, Hvalberg CS, Steffensen JP, Sveinbjornsdottir AE, Jouzel J, Bond G, 1993. Evidence for general instability of past climate from a 250-kyr ice-core record. *Nature*, **364**, 218–220.
- Drysdale RN, Hellstrom JC, Zanchetta G, Fallick AE, Sanchez Goni MF, Couchoud I, McDonald J, Maas R, Lohmann G, Isola I, 2009. Evidence for obliquity forcing of glacial Termination II. *Science*, **325**(5947), 1527–1531.
- Drysdale RN, Bence TB, Hellstrom JC, Couchoud I, Greig A, Bajo P, Zanchetta G, Isola I, Spötl C, Banerjee I, Regattieri E, Woodhead JD, 2012. Precise microsampling of poorly laminated speleothems for U-series dating. *Quaternary Geochronology*, **14**, 38–47.
- EPICA community members, 2006. One-to-one coupling of glacial climate variability in Greenland and Antarctica. *Nature*, **444**(7116), 195–198.
- Fairchild IJ, Smith CL, Baker A, Fuller L, Spötl C, Mathey D, McDermott F, 2006. Modification and preservation of environmental signals in speleothems. *Earth-Science Reviews*, **75** (1–4), 105–153.
- Frisia S, Borsato A, Fairchild IJ, McDermott F, 2000. Calcite Fabrics, Growth Mechanisms, and Environments of Formation in Speleothems from the Italian Alps and Southwestern Ireland. *Journal of Sedimentary Research*, **70**(5), 1183–1196.
- Frisia S, Borsato A, Spötl C, Villa IM, Cucchi F, 2005. Climate variability in the SE Alps of Italy over the past 17000 years reconstructed from a stalagmite record. *Boreas*, **34**(4), 445–455.
- Frisia S, 2015. Microstratigraphic logging of calcite fabrics in speleothems as tool for palaeoclimate studies: *International Journal of Speleology*, **44**(1), 1–16.
- Holzammer S, Spötl C, Mangini A, 2005. High-precision constraints on timing of Alpine warm periods during the middle to late Pleistocene using speleothem growth periods. *Earth and Planetary Science Letters*, **236**(3–4), 751–764.
- Huang Y, Fairchild IJ., Borsato A, Frisia S, Cassidy NJ, McDermott F, Hawkesworth CJ, 2001. Seasonal variations in Sr, Mg and P in modern speleothems (Grotta di Ernesto, Italy). *Chemical Geology*, **175**(3–4), 429–448.
- Lisiecki LE, Raymo ME, 2005. A pliocene–pleistocene stack of 57 globally distributed benthic $\delta^{18}O$ records. *Paleoceanography*, **20**(1), 1–17.
- Luetscher M, Boch R, Sodemann H, Spötl C, Cheng H, Edwards RL, Frisia S, Hof F, Muller, W, 2015. North Atlantic storm track changes during the Last Glacial Maximum recorded by Alpine speleothems. *Nature Communications*, **6**, 6344.
- Lundberg J, Musil R, Sabol M, 2014. Sedimentary history of Za Háčovnou Cave (Moravia, Czech Republic): A unique Middle Pleistocene palaeontological site. *Quaternary International*, **339–340**, 11–24.
- McDermott F, 2004. Palaeo-climate reconstruction from stable isotope variations in speleothems: a review. *Quaternary Science Reviews*, **23** (7–8), 901–918.
- Meyer MC, Cliff RA, Spötl C, Knipping M, Mangini A, 2009. Chronology and paleoenvironment of Marine Isotope Stage 3 from two high-elevation speleothems, Austrian Alps. *Quaternary Science Reviews*, **28**(15–16), 1374–1391.
- Moseley GE., Spötl C, Cheng H, Boch R, Min A, Edwards RL, 2015. Termination-II interstadial/stadial climate change recorded in two stalagmites from the north European Alps: *Quaternary Science Reviews*, **127**, 229–239.
- Niggemann S, Mangini A, Richter DK, Wurth G, 2003. A paleoclimate record of the last 17,600 years in stalagmites from the B7 cave, Sauerland, Germany. *Quaternary Science Reviews*, **22**(5–7), 555–567.
- NGRIP, North Greenland Ice Core Project Members. 2004. High-resolution record of Northern Hemisphere climate extending into the last interglacial period. *Nature*, **431**(7005), 147–151.
- Pambianco C, 2015. *Analisi della correlazione tra i livelli paleo-freatici del sistema carsico dei Piani Eterni e i Terrazzi dell'adiacente Val del Mis* (Parco nazionale delle Dolomiti Bellunesi). Bachelor Thesis, University of Bologna.
- Polyak VJ, McIntosh WC, Güven N, Provencio P, 1998. Age and Origin of Carlsbad Cavern and Related Caves from $^{40}Ar/^{39}Ar$ of Alunite. *Science*, **279**(5358), 1919–1922.
- Riva A, Perissinotto M, D'alberto L, Zoppello C, 2008. Geology of the Piani Eterni Karst Complex. *Rendiconti online Società Geologica Italiana*, **4**, 71–74.
- Salogni M, 2007. PE10, Piani Eterni. *Speleologia Veneta*, **15**, 35–50.
- Sasowsky ID, 1998. Determining the age of what is not there. *Science*, **279**(5358), 1874.
- Sauro F, Zampieri D, Filipponi M, 2013. Development of a deep karst system within a transpressional structure of the Dolomites in north-east Italy. *Geomorphology*, **184**, 51–63.
- Spötl C, Mangini A, Richards DA, 2006. Chronology and paleoenvironment of Marine Isotope Stage 3 from two high-elevation speleothems, Austrian Alps. *Quaternary Science Review*, **25**(9–10), 1127–1136.

Recent developments in speleothem research

Jon D. Woodhead^{1*}, John Hellstrom¹, J.M. Kale Sniderman¹, Russell N. Drysdale^{2,3}

Affiliation: ¹School of Earth Sciences, University of Melbourne, Parkville, Victoria, 3010, Australia.

²School of Geography, University of Melbourne, Parkville, VIC 3010, Australia.

³Environnements, Dynamiques et Territoires de la Montagne, UMR CNRS, Université de Savoie-Mont Blanc, 73376 Le Bourget du Lac, France.

Abstract

Speleothems preserve a versatile and robust archive of information concerning the physical, environmental and climatic conditions prevalent at their time of formation. Depending on the sample and on the analytical technologies used, this information may represent timescales from years to millions of years before the present day. This contribution describes three recent innovations in the scientific study of speleothems at the University of Melbourne.

Keywords: Speleothem, U-Pb geochronology, palynology, low-impact sampling

1. U-Pb dating

For the past four decades the utility of speleothems in a scientific context has relied upon radiometric dating using the U-series ('U-Th') chronometer which employs short-lived radionuclides in the ²³⁸U decay chain. While this methodology forms the mainstay of most speleothem studies, unfortunately it is limited in its application to the past ~700,000 years, meaning that many older materials remain impervious to study. Karst phenomena have however, almost certainly been present on the Earth throughout most of the Phanerozoic, with recognisably 'modern' processes established coincident with the rise of vascular plants in the Silurian. It is likely, therefore, that our intense interest in late Quaternary speleothems may only begin to scratch the surface of their utility.

Recent development of the U-Pb chronometer for speleothems now allows us to constrain the timing of their growth well beyond the limits of the U-Th method — in fact back many hundreds of millions of years in age (e.g. Woodhead et al., 2010). A landmark paper by Richards et al. (1998) first demonstrated that speleothems could be studied using U-Pb dating, but in the intervening years this potential remained relatively little exploited. Over the past decade the University of Melbourne laboratory has been working to further develop the speleothem U-Pb chronometer to the point where the methodology is now considered both robust and routine. As with U-Th dating, the primary prerequisite to successful dating lies in the requirement for clean samples with low 'common Pb' content (i.e. with very low clay/dust content); sample pre-screening of some form (e.g. by LA- ICP-MS) is thus highly recommended. Low-level clean-room protocols and U-Pb isotope dilution experience are also a necessity. Corrections for initial disequilibrium in the ²³⁸U-²⁰⁶Pb decay chain can form a significant source of uncertainty (up to ~100ka) for samples just a few million years in age but their relative significance diminishes for older materials.

Application of this new methodology is transforming our understanding of landscape evolution and allows us to tap into a greatly extended range of climate records. Furthermore, dating of speleothems associated with a variety of faunas is providing invaluable age constraints on the evolution of hominins (e.g. Pickering et al., 2011) and many other faunal lineages such as the Oligocene-Miocene World Heritage fossil

mammal deposits of Riversleigh, Queensland (Woodhead et al., 2016).

We are currently using the U-Pb chronometer to (1) develop high-resolution speleothem chronologies of glacial terminations to 'anchor' ice-core and sediment proxy records, (2) develop probability density distributions of speleothem growth as proxies for effective precipitation throughout the Neogene, (3) provide age constraints in studies of hominin evolution and vertebrate palaeontology, (4) constrain rates of karst evolution and speleogenesis, and (5), in combination with speleothem palynology (see below), to monitor changing landscapes and ecosystems across space and time.

2. Speleothem palynology

Various attempts have been made in the past to extract fossil pollen trapped in growing speleothems (e.g. Bastin, 1978) but these have often been confounded by the typically very low pollen counts encountered, and the resulting potential for contamination by abundant modern pollens which are ubiquitous in the environment. Using clean-room protocols we have now developed methodologies to reliably extract fossil pollen from speleothems at concentrations as low as a few grains per gram. Pollen spectra recovered in this way can be complemented by robust radiometric dating using U-Th and U-Pb methods and thus form a unique archive of past environmental change. Using this approach it is possible to generate environmental reconstructions across much of the Neogene where formation of Australia's widespread, deeply weathered regolith has actually destroyed many of the more traditional organic climate proxies.

As an example, we extracted fossil pollens from Nullarbor speleothems (Sniderman et al., 2016), dated using U-Pb methods, to document variations in regional precipitation over the last 6 million years, spanning Australia's descent into aridity. This analysis (see Figure 1) indicates that, in the latest Miocene and earliest Pliocene before ca. 5 Ma, mean annual precipitation (MAP) in the Nullarbor region was ca. 480 mm i.e., slightly wetter than today. However, soon after 5 Ma, MAP rose rapidly (within ca. 100 ka, or within ≤350 ka, at the 95% confidence level) and was maintained for ca. 1.5 My at levels two to four times higher than today.

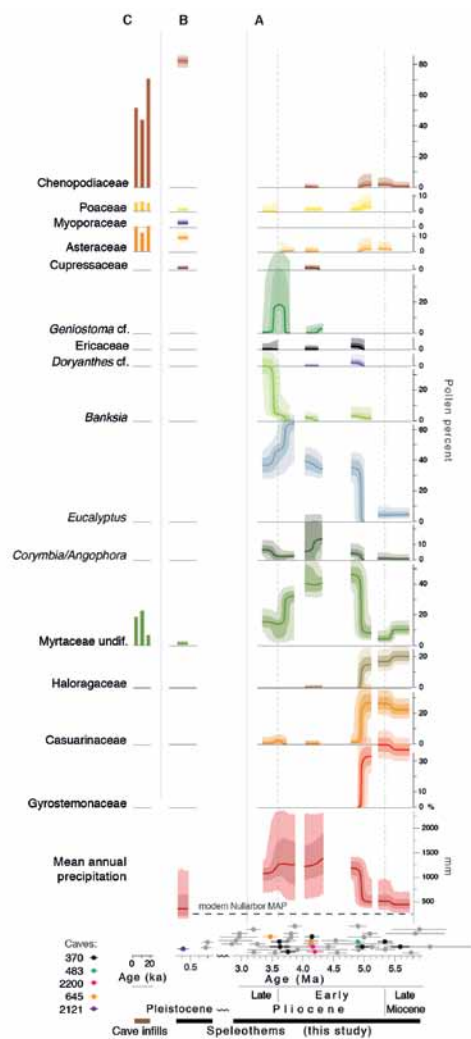


Figure 1. Late Miocene, Pliocene, and Middle Pleistocene vegetation change in semiarid southern Australia reproduced from Sniderman et al. (2016). Monte Carlo simulations of the late Miocene–Pliocene (A) and Middle Pleistocene (B) U–Pb–dated Nullarbor speleothem pollen record, accounting for Gaussian uncertainties in speleothem ages and in pollen percentage counts, and of the Nullarbor mean annual precipitation reconstruction derived from the pollen assemblages. The chenopod-dominated Middle Pleistocene assemblage is very similar to the composition of Late Pleistocene and Holocene pollen records (C) from Nullarbor cave/doline infills, confirming that the speleothem pollen assemblages register the surrounding vegetation in comparable ways to conventional fossil pollen records. U/Pb ages $\pm 2\sigma$ errors are shown for 13 polleniferous samples (color-coded by cave), against the backdrop of other Nullarbor speleothems investigated for pollen (gray).

3. Low impact sampling

Typically, speleothem sampling for palaeoclimate studies involves the use of intact stalagmites, with obvious implications for cave management and conservation. With new developments in geochronology allowing relatively rapid acquisition of data, it is now possible to consider entirely new strategies that have far lower impact. Rather than collecting single, large stalagmites, many hundreds of far smaller (just a few gram) fragments, the products of damage by earthquake, rock-fall, flooding or human activity (essentially speleothem ‘rubble’) can be collected and dated. The distribution of ages recorded provides information on the timing of past periods of relatively fast speleothem growth, corresponding to changes in effective precipitation over time, in addition to

providing important constraints on the timescales of cave development. Selected samples can then be subjected to further analysis for palaeotemperature determination or pollen extraction. Although this method is subject to potential sampling and preservation biases, preliminary experiments suggest that it can provide valuable insights into palaeoclimatic and geomorphological history. Examples will be presented at the conference.

4. Opportunities for community engagement.

Many of the new developments above provide opportunities for greater cooperation between speleothem scientists and other groups. For example, one of the primary limitations to the utility of the U–Pb method for dating speleothems is in fact not a technical issue at all – rather it is the difficulty in locating old samples to date! Over the past few decades, speleothem scientists have become accustomed to considering samples beyond the range of the U–Th chronometer as ‘undatable’. Many of these materials are then simply forgotten or, even worse, discarded. We are constantly looking for older materials to study and this is an area where other scientists (e.g. geomorphologists), cave managers and caving groups can all provide valuable advice or suggestions as to where they believe the oldest materials may be found.

Similarly, with the case of rubble sampling, it is not actually necessary for geochronologists to be present at all during sampling, which can easily be performed in a low-impact way by caving groups or cave managers wherever required and with appropriate permits in place. We could therefore envisage a system whereby multiple groups could simultaneously collect materials suitable for dating (after appropriate instruction) – in this way speleothem scientists gain valuable samples for their climate studies (and from far more diverse locations than they might visit individually) while the field samplers (caving groups or cave managers) gain valuable radiometric age data with which to interpret cave development in a particular region, cave, or cave section of interest. This approach places the sampling itself into the hands of the groups with the greatest experience, and simultaneously provides data for scientific research while fostering a better understanding of the timescales of cave development.

5. Conclusions

The next decade will be an exciting time for speleothem research. The development of new technologies and low impact sampling protocols will provide opportunities for reconstructing past climates and environments in far greater detail, while also transforming our understanding of karst processes and landscape evolution. Please visit <http://www.speleothemscience.org> to monitor further developments.

Acknowledgements

Our speleothem research programs would not be possible without advice and assistance from individual cavers, caving groups, cave managers, and National Parks staff. Especial thanks to Michael Archer, Steve Bourne, Dale Carnin, Paul Devine, Rolan Eberhard, Sue Hand, Lindsay Hatcher, Danny Mitton, Gavin Prideaux, John Prince, Liz Reed, Susan and Nicholas White, and many others who have contributed their time and expertise in numerous locations both near and far.

References

- Bastin, B., 1978. L'analyse pollinique des stalagmites: Une nouvelle possibilité d'approche des fluctuations climatiques du Quaternaire, *Annales de la Société Géologique de Belgique*, **101**, 13-19.
- Pickering, R., Dirks, P.H.G.M., Jinnah, Z., de Ruiter, D.J., Churchill, S.E., Herrires, A.I.R., Woodhead, J.D., Hellstrom, J.C. and Berger, L.R., 2011. *Australopithecus sediba* at 1.977 Ma and implications for the origins of Genus Homo. *Science* **333**, 1421-1423
- Richards, D.A., Bottrell, S.H., Cliff, R.A., Strohle, K., and Rowe, P.J., 1998. U-Pb dating of a speleothem of Quaternary age: *Geochimica et Cosmochimica Acta*, **62**, 3683-3688.
- Sniderman, J.M.K., Woodhead, J.D., Hellstrom, J., Jordan, G.J., Drysdale, R.N., Tyler, J.J., Porch, N., 2016. Pliocene reversal of late Neogene aridification. *Proceedings of the National Academy of Sciences* **113**, 1999-2004.
- Woodhead, J., Reisz, R., Fox, D., Drysdale, R., Hellstrom, J., Maas, R., Cheng, H & Edwards, R.L., 2010. Speleothem climate records from deep time? Exploring the potential with an example from the Permian. *Geology*, **38**, 455-458.
- Woodhead, J., Hand, S., Archer, M., Graham, I., Sniderman, K., Arena, D.A., Black, K., Godthelp, H., Creaser, P., Price, E., 2016. Developing a radiometrically-dated chronologic sequence for Neogene biotic change in Australia, from the Riversleigh World Heritage Area of Queensland. *Gondwana Research* **29**, 153-167.

Sustainable Development of Karst

Support for sustainable eco-tourism in Puerto Princesa Underground River (Palawan, Philippines) – Project 2016-2017

Antonio De Vivo¹, Paolo Forti², Leonardo Piccini³

Affiliation: ¹La Venta Esplorazioni Geografiche, Via Priamo Tron, Treviso, Italy.
tonodevivo@gmail.com

²La Venta Esplorazioni Geografiche & Italian Institute of Speleology, via Zamboni 67, 40125 Bologna, Italy.
paolo.forti@unibo.it

³La Venta Esplorazioni Geografiche & Department of Earth Science – Università di Firenze, Italy. leonardo.piccini@unifi.it

Abstract

The Puerto Princesa Underground River (PPUR) is one of the largest subterranean estuaries of the world, where tides propagate over 5 km inside the cave. The PPUR, consisting of over 30 km of giant galleries, hosts an extremely complex ecosystem based on the huge colonies of bats and swiftlets. Its natural uniqueness was recognized as World Heritage by UNESCO on 1999, while the first part of its navigable branch was transformed into a show cave some 20 years earlier. A peculiarity of this cave is that, even though it is visited by more than 300000 people/year, no fixed structures have been established inside it, which therefore should be still considered as a totally pristine cave. In the last few years, tourist pressure has been growing exponentially and first evidences of ecological problems, mainly related to the diurnal resting of bats, have been noticed during the most crowded days. Therefore the Local Government together with the Natural Park Direction decided to investigate how to manage the increasing tourism and limiting the impact on the natural environment of the PPUR and its surrounding areas.

The possibility to develop a research project dedicated to this goal was recently given by the Philippines-Italy Debt for Development Swap Program. The project was prepared by Tagbalay Foundation of Puerto Princesa (Palawan) and La Venta Esplorazioni Geografiche Association (Italy). It was accepted and granted at the end of 2015. The first field activities started in November 2016 and they are for 1 year. The main targets of the project are: 1- defining the “carrying capacity” of PPUR by completing the exploration and the multidisciplinary studies started over 25 years ago; 2- upgrading the awareness of the Local and National authorities, stakeholders and citizens on the importance and fragility of the PPUR ecosystem; 3- searching for alternative and/or additional caves to divert a part of the incoming tourists; 4- suggesting new side activities (merchandizing, open air activities etc.) to improve the economy of local inhabitants without increasing the anthropic pressure on PPUR.

Keywords: Underground estuary, cave ecosystem, show cave, Palawan

1. Introduction

The outflow portal of the Puerto Princesa Underground River (PPUR) has always been known to local people, and the first explorers were people living in the area, probably pushed to enter the cave searching for drinkable water and swallows' nests. PPUR (at that time known as Mt. St Paul Underground river) was declared National Park in 1971, but only a small part of the cave was known, no map was available and no one imagined what unique and amazing scientific discoveries were hidden inside. The first documented speleological exploration was made by Australian cavers in 1980 and 1981 (Hayllar, 1980, 1981). In 1989 to 1991 the first research project took place, coordinated by the Italian Speleological Society, which led to the discovery of new large side branches (Piccini & Rossi, 1994). This exploration made this cave one of the most important of the Far East and gave the start to a new series of expeditions which have been led by La Venta Esplorazioni Geografiche Association for the last 20 years (Piccini *et al.*, 2007; De Vivo *et al.*, 2009; De Vivo & Piccini 2013, De Vivo & Forti, 2014). During these expeditions, studies on hydrodynamics and hydrochemistry (Forti *et al.*, 1993; Forti, 2014), on speleothems and cave minerals (Billi *et al.* 2013; Badino *et al.* 2017), on cave meteorology (Badino 2010), on paleontology (Forti *et al.*, 2011) and finally on its ecosystem (Messana, 1994; Sbordonì, 2007) were undertaken.

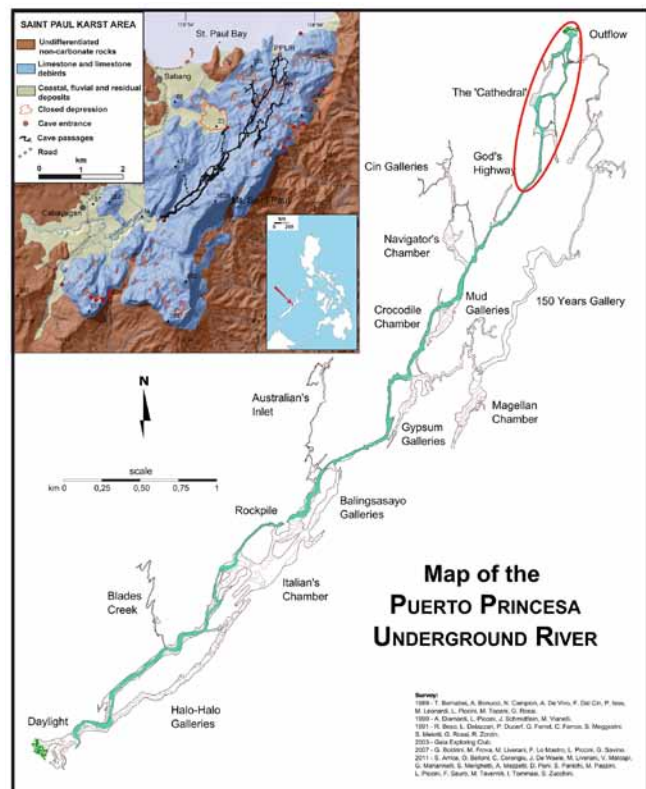


Figure 1. Index map, geological sketch and present day development of the PPUR (modified after De Vivo *et al.*, 2013): the red circle marks the sector open to the tourism.

Currently the PPUR is one of the largest subterranean estuaries of the world, where tides propagate up to 5 km upstream inside the cave. Over 30 km of giant galleries host an extremely complex ecosystem based on the huge colonies of bats and swiftlets. Over the past 20 years, many changes have occurred transforming this once virtually unknown cavity into what it is today: a fully-accredited UNESCO World Heritage Site (1999), a highly protected National Geological Monument (2003), an ASEAN Heritage Site (2005) (Restificar *et al.*, 2006) and, more recently, one of the New Seven Wonders of Nature (2012). But the most relevant thing is that the first 2 km of the PPUR (Fig. 1) has been transformed into the most visited show cave of the Philippines and one of the most visited of the whole far East Asia, with some 300000 visitors/year.

A peculiarity of this cave is that, even though visited by more than 300000 people/year, no fixed structures at all (fixed lights, artificial trails, etc.) have been built inside it, and therefore it can be still considered a totally pristine cave. Anyway in the last years, tourist pressure over the cave has been growing exponentially and first evidences of ecologic problems, mainly related to the diurnal rest of bats, have been recently noticed during the most crowded days. Therefore the Local Government together with the Natural Park Direction decided to investigate how to manage the increasing tourism and limiting the impact on the natural environment of the PPUR.

2. Project objectives

At the end of 2015 the Tagbalay Foundation (Philippines) and the La Venta Association (Italy) elaborated a research project intitled “*Support for Sustainable Eco-Tourism in the Puerto Princesa Underground River Area*”, which obtained a grant from the Philippines-Italy Debt for Development Swap Program. The project had the main objective to improve the surveys and the studies on PPUR, with special regard to ensure the safeguard of its ecosystem without negative effects on the tourism activities in Palawan.

It is worth mentioning here that, at least for Italy, it is the first time for a speleological association to be officially inserted as “principal partner” in an international co-operation project.

In the final document the project’s targets are listed as:

1. Ensure the continuous preservation of PPT and its surrounding areas, through: A) Evaluation of the Puerto Princesa Underground River and its ecosystem’s response to possible high-impact tourism in order to scientifically define its “limits” in terms of tourists/day, tourists/month and tourists/year; B) Confirmation and verification of previous scientific findings within the Underground River system, particularly with regard to the discoveries of rare minerals, flora and fauna that can be recorded and for which ample protection will be required for sustainability considerations; C) Allow for continuous monitoring of the cave’s environmental status particularly the energy levels, the ecological balance, flow of the river and other matters of scientific concern; D) Collaborate with local scientists in the research and documentation, to ensure full turnover of knowledge to Filipinos and to develop a group who will have a stake in the preservation of the river.

2. Create a group of “trainers” knowledgeable on the science of caving, as an additional means of passing on technology to all current and future cave personnel, tour guides, etc. Support the socio-economic development of the communities surrounding the PPUR area and thereby prevent ongoing environmentally harmful practices resulting from lack of income, through: A) Search for and development of new caves and tributaries within the area of the Puerto Princesa Underground River to augment current tourist package in the PPUR area and help local personnel better manage and maintain the sustainable development of ecotourism in the area, in anticipation of increased tourism activity in the future. This shall be done with the intention of sustaining the environmental condition while helping create more local employment and livelihood opportunities to assist in poverty alleviation; B) Training and orientation of the local population in order to improve their capacity to satisfy visitors and maintain the pristine features of the Puerto Princesa Underground River and other karst systems / caves within the protected area. C) Preparation of training and teaching tools and materials for improving and extending the tourist offer beyond the Puerto Princesa Underground River’s surroundings, eventually covering Puerto Princesa city as a whole. Printed and audio-visual materials can then be used for marketing/promotional effort, which is what happened for PPUR, where La Venta findings played a key role in establishing its uniqueness and generating interest from tourists worldwide.

3. Description of the project and scheduled activities

The Project is based on two field expeditions, one on November-December 2016 and the second in April-May 2017. The first field activities started in November 2016. The expedition was attended by 16 researchers and cavers who spent three weeks in Palawan.

In the first expedition a large part of time was devoted to scientific research, in particular to investigate the cave climate and fauna, both fundamental to define the carrying capacity for the show cave activities.

In order to obtain detailed data on the cave climate, several automatic devices have been placed in the different branches of the karst system (Fig. 2), with the aim to monitor the air temperature values every 15 minutes. Hopefully, these sensors will run for one year, or even more, thus allowing us to define in detail the PPUR microclimate, a fundamental knowledge not only for the detailed definition of the cave meteorology, but also to fully understand the energetic transfers among the ecosystems existing in the different part of the cave. Other automatic devices have been placed along the seven kilometers of the underground river (Fig. 2) in order to obtain detailed information on the hydro-dynamic and hydro-physic parameters of the karst system, which are deeply influenced by tides and by the heavy rainstorms that characterize the climate of Palawan.

From the ecological point of view, the cave presents three distinct ecosystems (Messana, 1994; Sbordonni, 2007), each characterized by the different nature (presence of fresh, brackish and saline sea water) and the abundance (or scarcity) of

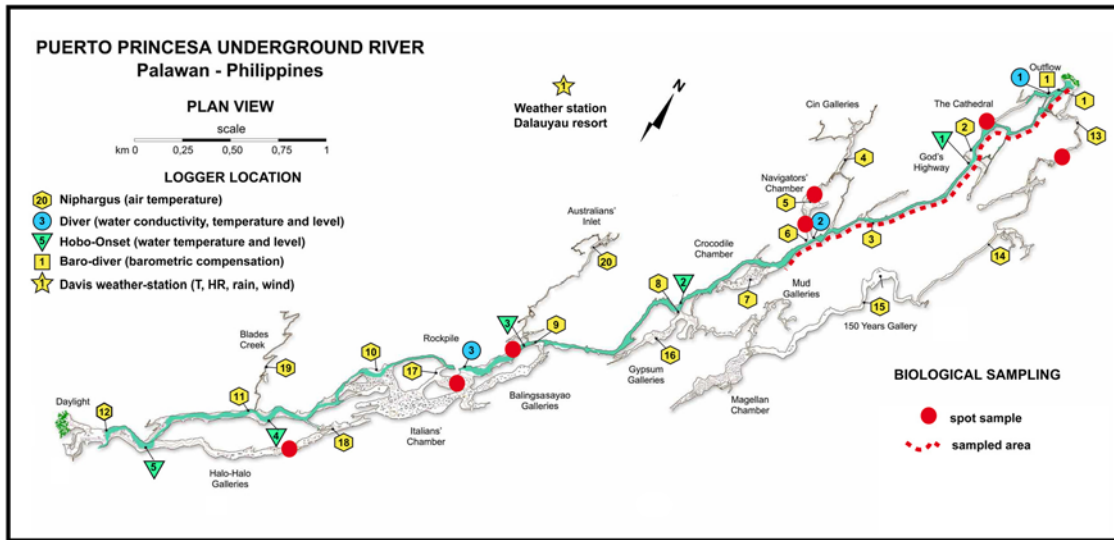


Figure 2. Datalogger and biological sampling location within PPUR

trophic resources: these features make the PPUR system an extraordinary natural laboratory to study the evolutionary processes and the ecology of the hypogean environments.

Up to now no systematic biological study has been performed on PPUR, but this gap will be hopefully filled within this project. During the first expedition biological observation and sampling were performed mainly along the underground river (Fig. 2). But in the next field season the furthest region of the cave will be investigated. The first results confirm the extraordinary ecological significance of this cave, and, even if the study of the sampled specimens are still to be completed. Several new species of living organisms have been already found (Paolo Agnelli & Stefano Vanni, unpublished data).

The effective carrying capacity of the tourist branch of PPUR will be defined only at the end of the monitoring period on the basis of the collected data. The huge energy naturally flowing inside the cave (over 10 to 20 million of watts, Giovanni Badino unprinted data), together with the strict rules imposed on the visitors by the Park, suggest that the actual tourist number is probably compatible with the cave ecologic equilibrium.

Actually the main hazard for the PPUR ecosystem comes from agriculture practices in its recharge areas, where the use of pesticides is rapidly increasing, thus endangering the survival of the huge bat and swiftlet colonies, which are the base of the trophic chain within PPUR.

Beside biology and climate, other scientific aspects such as karst morphology, hydrodynamics, cave mineralogy and speleogenesis have been considered in the project, even if they already were object of systematic studies in the past (De Vivo *et al.* 2013). In particular some core drilling of speleothems are planned in order to obtain calcite samples suitable for U/Th ages, which will chronologically define the main evolutionary steps of this complex karst system over the last 600.000 years and perhaps even more.

In the paleontological field the interest has been focused on the 3D high precision scan of the sirenian remains observed during the 2011 expedition (Hayllar, 1980; Forti *et al.*, 2011)

and of a fossilized dolphin recently discovered in a small cave in the SW sector of St. Paul karst area. The relative abundance of fossil remains, which are well exposed by the differential erosion in the walls of PPUR and other caves of the same area, encourage us to insert into the project a systematic search and documentation of these remains in order to promote their safeguard and preservation.

Another fundamental point faced before and during the first project expedition was that related to capacity building. La Venta prepared the didactic materials for a specific 3 day course devoted to the Park rangers and staff. People attending the course were also guided into the cave, where all the teachers explained the most interesting features occurring in the tourist sector in order to improve the quality of the talks eventually given to visitors.

An important target of the project is the involvement of local scientists and stakeholders in research and eco-sustainable, tourism related activities. This co-operation will become fundamental in the near future because more and more local people are starting up field commercial activities (opening of new show caves, adventure trekking in the karst area, etc.), which need to be correctly developed to avoid the risk of irreparable damage to the karst and to the cave environments of the Park. In this regard the recently occurred (2015) foundation of the first caving club of Palawan (La Karst of Puerto Princesa) is important, because it ensures the regular presence on site of a well-trained and ecologically minded association, which should be in strict contact with the Park Administration.

Currently, no specific PPUR related merchandizing (cave guides, fliers, postcards, posters, DVD etc.) are available at all in Sabang (the village from which the cave tour starts) and/or in Puerto Princesa (the Palawan capital town). It is well known that such type of business may represent up to 30% of the total income of a show cave and therefore La Venta emphasized to the Park Administrators and other stakeholders to start planning such trade, offering its knowledge and documentation acquired during the 20 years of research (De Vivo & Piccini, 2013).



Figure 3. PPUR, along the underground river: panoramic view of the shooting the *One Planet* documentary close to the sirenian fossil (Photo by Patrizio Rubcich)

Cave exploration is an important point of the project too. During the 2016 expedition four new branches have been discovered and documented: the whole mapped length is about 1 kilometer. Several other promising points have been noticed and they will become object of exploration and surveying in the 2017 expedition.

Thanks to the instruments made available by Leica geosystem, the 3D mapping of the PPUR system started. The scanning will go on during the next expedition in order to obtain not only fundamental documents for the study of the main karst morphologies and speleothems, but also to create in a near future a “virtual tour” of the PPUR, in particular of those areas which will never be interested by tourist paths. In 2016 much time was spent to support the shooting of a new scientific-naturalistic documentary by the French *One Planet* (Fig. 3), which will be presented in the 2017.

Finally an agreement was reached in between the Park Administration and Tagbalay Foundation of Puerto Princesa and La Venta to develop an internet site dedicated to PPUR: La Venta will contribute to this project by making disposable all its material, collected in the past 25 years of exploration and documentation of the PPUR.

4. Final remarks

This short outlook on the main activities performed during the first expedition of the project. The next expedition will be in April-May 2017 and will last 4 weeks and the number of participants will be slightly higher than that of the first one. This because the job to be done is noticeably larger and we need to be sure that all the targets of the project will be fully achieved. In particular in the second expedition the biological systematic study of the PPUR will be expanded to achieve a satisfactory overall knowledge of the different ecosystems present in PPUR. But, from the speleological point of view, the most important activity will be the search for new cave entrances on the virtually unexplored top of the Mt St Paul, which was reached only once during the 2011 expedition and where some active sinkholes exist. The aim of this exploration is to search for an upper entrance to the PPUR, which will thus become by far the deepest cave of Philippines (potentially reaching a depth close to 1000 m) and one of deepest of the Far East Asia. At the end of the Project, all the results of the

exploration and research undertaken within this astonishing cave over the last 25 years will be reported in a printed book edited by La Venta Association. In conclusion, this project wishes to present a challenge in maintaining the PPUR and its karst area as a worldwide renowned tourist attraction and, in the same time, an example of a well-managed protection area: this goal can be achieved only through a careful and detailed scientific study and documentation.

Acknowledgements

The Authors thanks the Municipality of Puerto Princesa and the PAMB for the support given during the expeditions to the PPUR

References

- Badino G., 2010. Underground Meteorology, What's the weather underground? *Acta Carsologica*, **39**(3), 427-448.
- Badino G., Calaforra J.M., Forti P., 2017. Genesis and evolution of a ribbed drapery of the Puerto Princesa Underground River (Palawan, Philippines). *International Journal of Speleology*, in press.
- Billi S., Forti P., Galli E., Rossi A., 2013. Robertsite: un nuovo fosfato di grotta scoperto nella Tagusan Cave (Palawan – Filippine). *Congresso Nazionale di Speleologia*, Trieste 2011, 306-311.
- Coombes M.A., La Marca E.C., Naylor L.A., Piccini L., De Waele J., Sauro F., 2015. The influence of light attenuation on the biogeomorphology of a marine karst cave: A case study of Puerto Princesa Underground River, Palawan, the Philippines. *Geomorphology*, **229**, 125-133.
- De Vivo A., Forti P. (Eds.), 2014. *Puerto Princesa Underground River (Palawan Philippines): geological sketch, plan view, projected section and main points of interest (1991-2011)*. Map, supplement to Kur 21.
- De Vivo A., Piccini L. (Eds.), 2013. *The River of Swallows, La Venta*, 87 p.
- De Vivo A, Piccini L, Mecchia M., 2009. Recent explorations in the St. Paul karst (Palawan, Philippines). *Proceedings XV International Congress of Speleology*, Kerville, Texas (USA), v. 3, 1786-1792.
- De Vivo A., Piccini L., Forti P., Badino G., 2013. Some scientific features of the Puerto Princesa Underground River, one of the new 7 wonders of nature. *Proceedings XVI International Congress of Speleology*, Brno, v. 3, 35-41.
- Forti P. (Ed.), 2014, *Puerto Princesa Underground River (Palawan, Pilippines): Bathimetric, Hydrochemical, Hydrodynamical, and climatological data (1990-2011)*. Map, supplement to Kur 21.
- Forti P., Piccini L., Rossi G., Zorzin R. 1993. Note preliminari sull'idrodinamica del sistema carsico di St. Paul (Palawan, Filippine). *Proceedings European Conference on Speleology*, H el ecine (Belgium), 1992, *Bulletin Soci et  G eographique de Li ege*, **29**, 37-44.

- Forti P., Russo N., Lo Mastro F., 2011. Laventino, il sirenide di Palawan – Laventino, Palawan's siren. *Kur*, **17**, 14-15.
- Hayllar T., 1980. A description of the St. Paul Cave, Palawan, Philippines. *The Journal of the Sydney Speleological Society*, **24**(7), 153-158.
- Hayllar T., 1981. Caving on Palawan. *The Journal of the Sydney Speleological Society*, **25**(12), 215-231.
- Messana G., 1994. Biologia. In Piccini L., Rossi G., (Ed.) Le esplorazioni speleologiche italiane nell'Isola di Palawan. *Speleologia*, **31**, 57-60.
- Piccini L., Iandelli N., 2011. Tectonic uplift, sea level changes and Plio-Pleistocene evolution of a costal karst system: the Mount Saint Paul. *Earth Surface Processes and Landforms*, **36** (1), 594-609.
- Piccini L., Mecchia M., Bonucci A, Lo Mastro F., 2007. Recent speleological explorations in the St. Paul Karst. Technical Notes. *Kur*, **9**.
- Piccini L., Rossi G., 1994. Le esplorazioni speleologiche italiane nell'Isola di Palawan. *Speleologia*, **31**, 5-61.
- Restificar S., Day M., Urich P., 2006. Protection of karst in the Philippines. *Acta Carsologica*, **35**, 121-130.
- Sbordoni V., 2007 Life in caves. *Kur*, **9**, 14-15.

Karst Underground Protection, Education And Rise Of Public Awareness; Examples From Slovenia

Nadja Zupan Hajna

Affiliation: Karst Research Institute ZRC SAZU, Titov trg 2, 6230 Postojna, Slovenia

Abstract

The characteristics of the karst underground make it an extremely sensitive and vulnerable system that is highly susceptible to influences from the surface. Water from the surface percolates rapidly underground, where it flows through open conduits. The rate of self-cleaning is thus dependent on the rate of flow and the type of pollution, but in general is extremely low or non-existent in karst areas. Negative impacts are therefore able to spread rapidly into the underground, where they affect caves and conditions in them, altering the habitats of underground organisms, and also have an effect on water, which they can pollute to such an extent that it is no longer drinkable. Water and pollutants can enter the underground in several ways, in dispersed form through bare or covered karst surface with precipitation; and in concentrated form through ponors. Once underground, they move freely through open karst conduits, where the rate of self-cleaning is very low or non-existent. Caves are extremely sensitive to human influences. In isolated locations damage is lasting and is only slowly eliminated or overgrown, especially where there is no washing away by running water. A broken stalactite which has been growing for a thousand years or more means the destruction of information about past speleogenetic and climatic events. Even a small change in the cave environment can cause a great change on habitat. Caves are affected by everything that happens on the surface above the cave and within its area of influence. People represent a serious threat to nature through their way of life and frequently ill-considered interventions in the environment.

With the purpose to raise awareness of the importance of the karst and to protect the karst underground, i.e. caves, waters and fauna various projects were conducted in recent years in Slovenia (e.g. KUP – Karst Underground Protection, ŽIVO! – Life and water!). Many activities were also undertaken to different audiences to ensure the special environmental and natural features of the karst areas were recognised through promotion of their importance. The biggest achievement was the education of children in schools and raising the awareness of the local and regional administrations and population of all age groups about the environmental and biological value of the karst area and importance of drinking water deriving from karst springs.

Keywords: karst underground, protection, education, public awareness, Slovenia

1. Introduction

Karst is vulnerable due to a thin cover layer of the soil, rapid water infiltration, rapid groundwater drainage and the potential spread of contamination in different directions, as well as long-term retention of harmful substances (Petrič 2010; Prelovšek and Zupan Hajna 2011; Zupan Hajna *et al.* 2015). Assessment of the vulnerability of karst waters indicates the ability level of the karst environment to neutralize potential contamination (self-cleaning and regeneration); the assessment is based on geological and hydrological properties of karst underground.

Population and compact settlements pose a major risk for pollution of the underground caves and of drinking water in karst areas, mainly due to the inflow of large quantities of municipal sewage, and large amounts of various kinds of waste (Prelovšek and Zupan Hajna 2011). The threat of mass tourism in karst areas and unregulated show caves is just as significant as careless caving.

In unpopulated areas, the karst remains clean and undamaged. With the settlement of karst surfaces, people start interfering with it and changing it, whereby the natural balance in the environment is disturbed, the water gets polluted, biodiversity affected, geological heritage and information are destroyed, as do various surface karst formations and caves. The most common karst pollutants are municipal and domestic waste water, landfill leachates, roads runoff, inappropriate farming practices and the like.

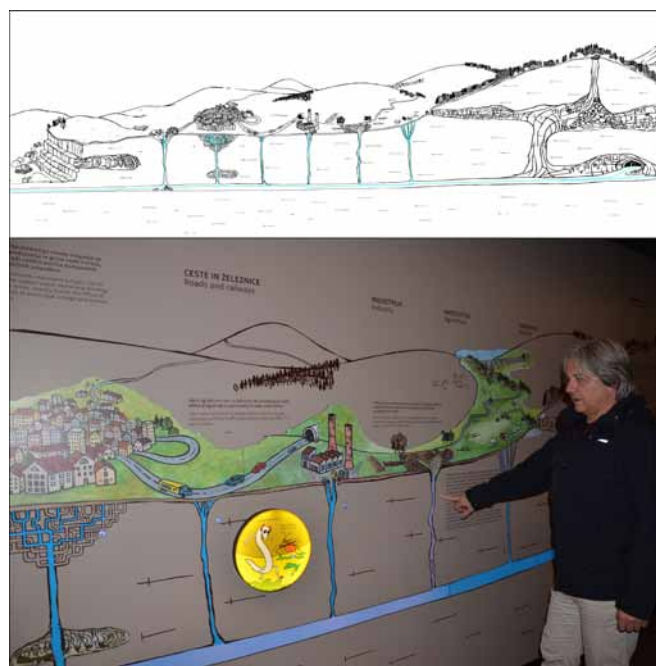


Figure 1. Drawing of karst underground and pollutants (upper); and photo from its implementation (lower); prepared by Zupan Hajna in 2015 for the exhibition at Postojna Cave with the aim of raising awareness of the cave visitors (EXPO Postojna Cave Karst; <http://www.postojnska-jama.eu/>; photo J. Hajna).

Despite a number of new waste management technologies, a large part of garbage ends up in landfill. Landfills pose a significant threat to the environment due to high concentrations

of harmful substances that are easily washed into the underground. Tourism is also a very significant cause of destruction of the karst natural environment, specific formations and caves, mainly due to construction of roads and hiking trails, infrastructure, the setting up of information centres and tourist complexes, golf courses, waste disposal and discharge of sewage.

2. Caves

People have been using and exploiting caves for various purposes since the dawn of their existence. Only recently, however, have people become aware of the fact that caves are also an important part of natural heritage. Due to their specific characteristics (e.g. relatively constant humidity and temperature, fauna) caves are extremely sensitive to various external influences and visits. In isolated places it takes a long time to repair or the damage is even permanent.

Easily accessible caves are the most vulnerable ones. Unsupervised visits of non-speleologists to caves often result in caves being devastated, because people are not aware of the consequences caused by their actions, while moving around caves (breaking speleothems, leaving behind garbage, writing on walls and speleothems). Combined with careless behaviour unregulated cave tourism brings about various negative effects, such as acts of vandalism (speleothem breakage), waste and sewage, which disproportionately increase the intake of substances and energy (light) in an otherwise poor environment and as well as the introduction of decaying materials such as wood, iron. In order to minimize these changes and damage, it is necessary to observe the laws of individual countries, the guidelines of the International Union of Speleology (UIS) and the International Show Caves Association (ISCA), and to educate new speleologists/cavers on the level of national organisations, societies and clubs.

All caves in Slovenia are state property and are protected by law (Cave Protection Act, OG RS, No. 2/2004). The Act regulates protection and use of underground caves, protection regimes, protection measures and other rules of conduct. Caves have the status of subterranean geomorphological natural assets of national importance. Despite the ban, numerous caves are many times unfortunately damaged and sometimes used as landfill sites. Waste in caves is not visible on the surface: "out of sight, out of mind". To prevent such behaviour, it is necessary to actively protect caves and ensure their prudent and controlled use. And most of all, it is important to inform and raise public awareness about the importance of caves and their preservation.

Education of various target groups, from the youngest children in kindergartens and schools to adult population, life planners, legislators, and especially potential visitors, is important due to the exceptional geological, geomorphological and archaeological content inside caves, their vulnerability, the specific nature of their environment and habitats.

3. Karst Waters

A typical karst characteristic is that the water drainage mostly underground. Short sections of the water flow through the underground can be observed in some of the caves, however, for the most part flow cannot be seen. In the karst, water from



Figure 2. Rubbish in the cave within the water protection zone of Rižana spring (SW Slovenia) was cleaned within the KUP Project in 2011; estimated amount of waste was 16 m³ (photo J. Hajna).

different recharge areas is often combined. Given the characteristics of water drainage (e.g. Petrič 2010) in karst areas and the recharge mode (diffused recharge from the karst surface and spot-focused recharge through sinking rivers), different recharge and drainage zones are set up in the karst. Water in the karst mainly flows through large and small channels with high water flow speeds (even up to 100 m/h), whereas in porous aquifers, the speed is lower (up to 10 m/day). Therefore, the residence time of water in the karst underground is mostly very short, from a few hours up to a few days. Karst areas are characterized by large karst springs with a large catchment area (from tens to hundreds of km²).

Water from karst springs is important for the water supply; drinking water from karst aquifers supplies $\frac{1}{4}$ of the world and $\frac{1}{2}$ of Slovenia's population (Zupan Hajna *et al.* 2015). The quality of the water from a spring depends on hydrological conditions and pollutants in the spring catchment area. The existing problems in relation to pollution and protection of karst groundwater will not be solved merely through legal regulations. Cooperation is needed between experts, regulators and operators for the sake of prudent land use planning and protection of karst waters. However, it is also necessary to change people's attitude to nature and natural resources through education about the characteristics of the karst.

4. Examples of good practice

The best way to get to know and understand the karst is the study of its surface, caves, waters and ecological characteristics; this has been the aim of the Karst Research Institute ZRC SAZU in Postojna (Slovenia) since 1947. With a view of protecting and raising awareness of the importance of surface phenomena, caves, water and biodiversity in the karst areas Institute performs various activities on different levels as monitoring of tourist caves (e.g. Gabrovšek *et al.* 2014; Ravbar and Šebela 2015), monitoring of cave fauna (e.g. Culver and Pipan 2014), water tracing tests (e.g. Petrič 2010), publications (e.g. Prelovšek and Zupan Hajna 2011; Zupan Hajna *et al.* 2015), exhibitions and educational trails for diverse clients (e.g. museums, caves, municipalities) and implements various projects funded by the EU, Slovene Government, Agencies, etc. (<http://izrk.zrc-sazu.si/>).

Among several others, there were two big projects of IPA Operational Programme Slovenia-Croatia 2007-2013 which are presented here; KUP – Karst Underground Protection (2009-2011) and ŽIVO! Life – Water! (2014-2015).

Partners on KUP Project were Istrian Region (Croatia), Karst Research Institute ZRC SAZU (Slovenia), Natura Histrica (Croatia) with collaborators from Croatian Biospeleological Society, Učka Nature Park, Notranjski Museum Postojna and Speleological Association of Slovenia. Objectives of the project were:

- raising awareness of the importance of karst in the local (life) and trans-national (professional) level
- protection of karst underground (caves, water, fauna)
- SLO-HR Cooperation in local and regional level

The KUP had the intention to connect and gather all institutions, and other interested parties able and willing to contribute to the improvement and protection of the environment and to the promotion of speleology through various activities:

- The renovation of the abandoned school building in the Croatian village Vodice, near the Slovenian border and converted it into a research centre as a “Speleo House”.
- Biospeleological research was implemented through an international team who studied 12 selected speleological targets in the project area (6 in Slovenia and 6 in Croatia). Evaluation studies were made in all researched caves, in addition to publications.
- Cleaning of 12 caves (6 in Croatia and 6 in Slovenia) with the objective of reduce the strain and pollution of underground waters and preserve natural water sources and the corresponding aesthetic, tourist and recreational value of the caves was performed by caving clubs from both sides of the state border.
- Organization of 6 Workshops for local population and interested public in Croatia and 2 International Karstological Schools were organised in Postojna: 18th IKS “Dinaric Karst” in 2010 with the purpose to present characteristics of Dinaric karst and its comparison with the other karst regions; and 19th IKS “Karst Underground Protection” with the purpose to emphasise the importance of underground protection including caves, water and fauna. Among two Excursion Guides and Programs also two books on topics were published (Mihevc *et al.* 2010, Prelovšek and Zupan Hajna 2011).

Partners on ŽIVO! Project were Istrian Region (Croatia), Karst Research Institute ZRC SAZU (Slovenia), Natura Histrica (Croatia), University of Rijeka, Faculty of Construction (Croatia) and National Laboratory for Health, Environment and Food (Slovenia).

Objectives of the project were:

- ensuring scientific research base for the conservation of karst aquifers and water resources, networking of regional institutions for the protection of the environment, reducing environmental risks through monitoring systems



Figure 3. Undamaged caves, clear water and undisturbed fauna should be the goal of all visitors and inhabitants of karst and caves (photo J. Hajna).

- contribution to improving the quality of life through reducing ecological risks and adequate management of water resources, and connect the environmental sector with the tourism sector
- equipping of “Speleo House” and dissemination of knowledge on karst aquifers to general public (kindergartens, primary schools, professional and interested public)

Implementation was done through various activities:

- Joint Slovenian and Croatian studies on the geology, geomorphology and hydrogeology.
- Study on the joint management of water resources in the project area with the aim to collect results, design a base for more effective protection of water resources, and consequently, to improve their quality; with publishing of manual instructions for water managers in the region in Slovene and Croatian language (Biondić *et al.* 2015).
- Organization and implementation of Workshops on karst and caves for children in kindergartens and schools to educate children from the childhood and also to instruct their teachers.
- Publication of monograph “Life and water on karst” (Zupan Hajna *et al.* 2015) for the interested public (researchers, students, cavers)
- An educational – documentary movie “Life and water on karst” (2015) was produced with an emphasis on the protection of groundwater and the importance of karst springs as a high-quality supply of drinking water for the interested public (pupils, students, cavers); look for details in the paper Zupan Hajna *et al.* in this Proceedings (17 ICS, 2017)

5. Conclusions

The important objectives of the all projects and activities were education and obtaining attention from different population groups on karst, surface forms, underground water flow, caves, fauna and importance of their protection. Objectives were achieved with the results of scientific research as well

as educational activities at various levels of society. The main purpose and the ultimate goal of all the activities, is to leave the pristine underground, caves, water and fauna, to our children.

Acknowledgments

The studies and promotion and protection of karst were supported by the Institute research Program "Karst research" No. P6-0119 financed by Slovenian Research Agency, Interreg and other projects; e.g. two projects were financed by EU and SVLR (Slovenian Government office for Local Self-Government and Regional Policy) of IPA Operational Programme Slovenia-Croatia 2007-2013: Karst Underground Protection (2009-2011) and Life – Water! (2014-2015).

References

Biondić R, Brun C, Crnko T, Diković S, Kogovšek J, Koželj A, Mihevc A, Otoničar B, Pernić P, Petrič M, Pipan T, Pretnar G, Radišić M, Ravbar N, Rubinić J, Ružić I, Zupan Hajna N, 2015. Study. *Characteristics of water resources in transboundary area of northern Istria* (in Slovene), Karst Research Institute ZRC SAZU, Postojna, Rijeka, Koper.

Culver DC, Pipan T, 2014. *Shallow subterranean habitats: ecology, evolution, and conservation*. Oxford University Press, XXII, Oxford.

Gabrovšek F, Grašič B, Božnar M, Mlakar P, Udén M, Davies E, 2014. Karst show caves – how DTN technology as used

in space assists automatic environmental monitoring and tourist protection – experiment in Postojna Cave. *Natural hazards and earth system sciences*, **14**(2), 443-457.

Mihevc A, Prelovšek M, Zupan Hajna N. (Eds), 2010. *Introduction to the Dinaric Karst*. Karst Research Institute ZRC SAZU, Postojna.

Petrič M, 2010. Characterization, exploitation and protection of the Malenščica karst spring, Slovenia: case study. In: Krešič N, Stevanović Z (Eds). *Groundwater hydrology of springs: engineering, theory, management and sustainability*. Burlington, Butterworth-Heinemann, 428-441.

Prelovšek M, Zupan Hajna N (Eds), 2011. *Pressures and protection of the underground karst: cases from Slovenia and Croatia*. Karst Research Institute ZRC SAZU, Postojna.

Ravbar N, Šebela S, 2015. The effectiveness of protection policies and legislative framework with special regard to karst landscapes: Insights from Slovenia. *Environmental science and policy*, **51**, 106-116.

Zupan Hajna N, Ravbar N, Rubinić J, Petrič M (Eds), 2015. *Life and water on karst: monitoring of transboundary water resources of Northern Istria*. ZRC Publishing, Ljubljana.

EXPO Postojna Cave Karst. <http://www.postojnska-jama.eu/en/come-and-visit-us/expo-postojna-cave-karst/> (access 23 Jan 2017)

Educational Film ŽIVO! (“LIFE!”) – Life And Water In The Karst Region

Nadja Zupan Hajna, Metka Petrič, Nataša Ravbar

Affiliation: Karst Research Institute ZRC SAZU, Titov trg 2, 6230 Postojna, Slovenia

Abstract

The educational/documentary film was created as part of the transboundary project ŽIVO! – “LIFE” – life and water in the karst region that has been financed by the European IPA Programme of Transboundary Cooperation between Slovenia and Croatia in years 2014–2015. The film was made by the Karst Research Institute ZRC SAZU and Digital Studio. The aim of the project was the protection of nature and environment with the emphasis on karst waters. Therefore the film presents the karst and karst hydrogeology of Northern Istria, and highlights in particular the vulnerability of the karst to various human activities. The main focus of attention is on karst water sources and their protection. The aim of this film was to spread the knowledge of scientific findings about karst, caves and the water sources in the border region of Slovenia and Croatia. There is usually no water on the karst surface because it infiltrates through fissures in the rocks and then flows deep into the underground. Because there is no thick soil cover the karst surface is rocky and unsuitable for cultivation. Consequently, the karst was never densely populated, and the people who persevered there lived modestly and worked hard to survive. The karst is also the landscape which extends over almost half of Slovenia and Croatia and also along states border. The area has numerous significant karst springs which are of vital importance for the water supply of the region. The recharge areas of karst springs are very vulnerable due to their complex structure, and this poses complicated challenges for their protection. 1000 DVD copies have been made in 3 languages: Slovenian, Croatian and English. So far the film has been shown on the Slovene national television, and in many student programs at the universities of Brazil, Canada, China, Estonia, Slovenia and elsewhere.

Keywords: karst, caves, transboundary aquifer, movie, SLO/CRO project

1. Introduction

The karst region covers almost half of Slovenia and Croatia's surface: Slovenia 43% or 8,700 km² (Gams 2003), Croatia 46% or 26,000 km² (Matas 2009). Most of it is a part of the so-called Dinaric Karst which stretches from Slovenia to Albania. In the two countries, karst springs provide drinking water to almost half of the inhabitants.

In Slovenia in 2016 over 11,000 caves were registered in Cave Register (Speleological Association of Slovenia, 2016), 92 caves longer than 1000 m and 60 caves deeper than 300 m. The deepest is cave Čehi 2 (depth 1505 m) and the longest Cave System Migovec (length 28,496 m). In Croatia over 900 caves were known in 2016 with 66 caves longer than 1000 m and 55 caves deeper than 250 m (Hrvatski speleološki poslužitelj, 2016). The deepest is Cave system Lukina jama – Trojama (depth 1431 m) and the longest Cave System Kita Gačešina – Draženova Puhaljka (length 32,227 m)

The ŽIVO! Project area (Zupan Hajna *et al.* 2015), called Northern Istria, stretches across the states border of Slovenia and Croatia (Fig. 1), and is characterized by well-developed karst surface morphology and complex underground water flow. Due to its characteristics, karst is bare and difficult to live in. The reasons for this are the rocky landscape, lack of surface waters, sparse soil as well as dissected and difficult terrain.

The project area features alternating karst and non-karst terrain, i.e. very permeable limestone and dolomite and very poorly permeable flysch. The tectonically deformed and thrust rock bed forms the base for varied relief as well as the fragmented surface features and the manner of water flow. At the contact of the flysch and limestone there are therefore typical morphological forms of contact karst (Mihevc 1997), such as blind valleys, ponors where surface water flows into the subsurface, and on the other hand large karst springs drain the karst aquifer.

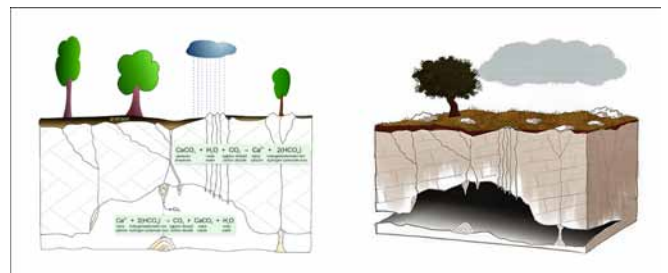


Figure 1. Karst and non-karst areas of the Northern Istria with hydrogeology and underground water connections; Slovenia/Croatia states border (from Zupan Hajna *et al.* 2015)

Three of them have been used to supply about 300000 inhabitants with drinking water: Rižana, Sv. Ivan and Bulaž. Their catchments are very complex comprising karst and non-karst areas. The springs are recharged by autogenic recharge and by sinking rivers. The underground water flow has been investigated by many tracer tests (Biondić *et al.* 2015). Drainage areas of the observed springs often overlap and flow paths cross each other.

One of the tasks of the ŽIVO! project was to improve the existing model of managing water sources and protecting their quality in the Northern Istria and to raise public and local authorities' awareness on karst characteristics and particularities.

2. Film content

Film is educational-documentary and focuses on the protection of underground water and the importance of karst springs for high-quality supply of the population with drinking water. The film was primarily made for the use in the educational system (primary and secondary schools, high schools

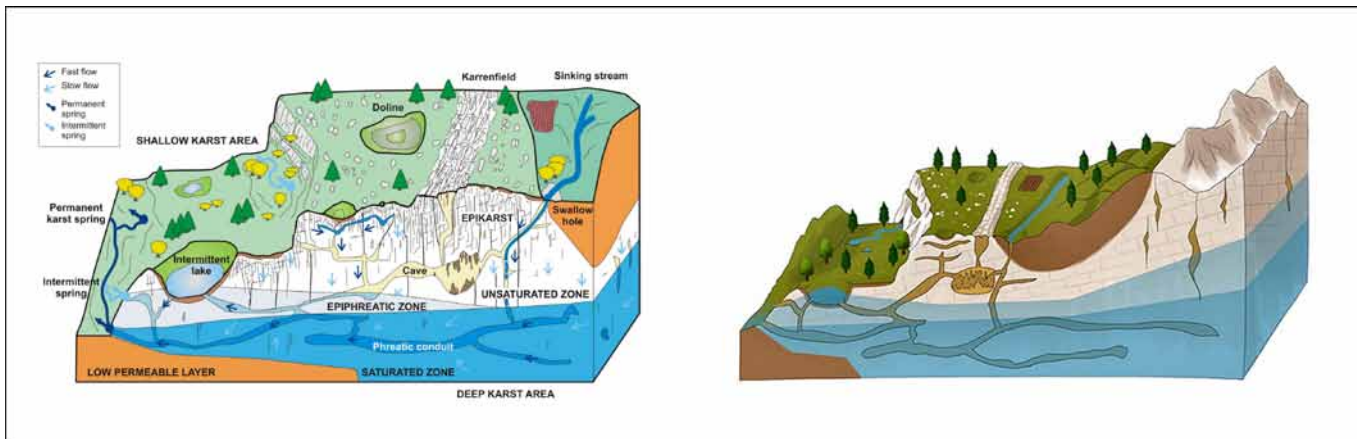


Figure 2. Sketch of limestone dissolution and prepared model for movie animation (after Zupan Hajna 2015)

and university programs), as well as for the presentation of the importance of the sustainable use and protection of karst waters to the general public.

With the content of the film we wanted to explain karst formation, forms, carbonate rocks – water interaction, properties of karst aquifers, man and karst interaction, water resources and their endangerment and the importance of scientific research and karst protection.

Here are presented some highlights from the movie and sketches, which were used as a base for animations.

2.1. The importance of karst

The natural wonders of the karst are truly a sight to behold. The Postojna Cave is probably one of the most renowned karst caves in the world and undeniably the main Slovene tourist attraction known to millions of people worldwide. The Cerknica polje and lake are among the most eminent karst poljes in the world, and the intermittent lake is home to various birds and thus an ornithologist's paradise. The Škocjan Caves (Slovenia) and Plitvice Lakes (Croatia) are even included on the UNESCO list of world heritage sites due to their uniqueness.

But usually the karst surface is rocky, not pretty and perhaps unsuitable for cultivation. Karst areas generally have no surface streams or thick soil. All precipitation quickly sinks beneath the surface, and even rivers disappear through ponors (sinkholes) into the karst, where their waters flow deep underground. For this reason karst areas have never been densely populated and the people who have persevered here have eked out a meagre existence and worked hard to survive.

2.2. Rocks and water

The occurrence of karst relies on carbonate rocks and precipitation, which is enriched with carbon dioxide from the atmosphere and infiltrates through the soil (Ford and Williams 2007). It forms weak carbonic acid which dissolves carbonate rocks. The infiltration of precipitation is very fast due to the thin soil cover and high permeability. Precipitation enters the underground by diffusing through the fissures in the rocky surface (Fig. 2).

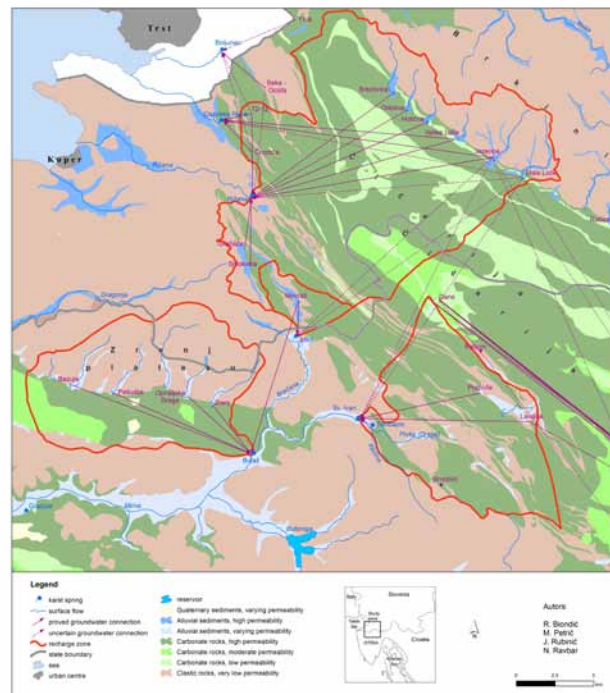


Figure 3. A sketch showing peculiar karst geomorphology and hydrogeology has been used for the movie animation (modified after Ravbar & Sebelja 2015)

Watercourses which collect water in non-karst areas also sink in the karst underground through open channels and caves. The rivers which flow into karst from non-karstic rocks form, on the contact, morphological shapes such as blind valleys and ponor caves - characteristics of the landscape and that kind of karst is also named “contact karst”. Rivers which disappear through ponors flow deep into the underground. In some places, water flows can be reached through caves which are open to the surface. The waters of sinking streams in Podgrajsko podolje (Slovenia) flow underground towards the Rižana spring (Slovenia) or/and to the Bulaž and Sv. Ivan springs (Croatia).

2.3. Aquifers

The areas of carbonate rocks which contain water and allow the water to pass are called karst aquifers. The water there appears in void spaces of different shapes and sizes. The pores

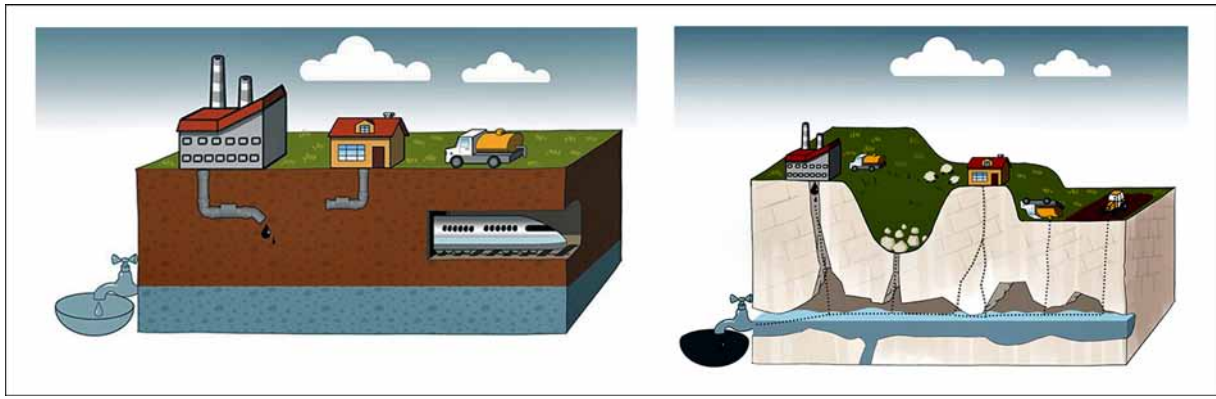


Figure 4. Prepared sketch of non-karst (left) and karst (right) underground and characteristics of water flow for the movie animation (after Ravbar & Šebela 2015)

between the rock grains, fissures and karst channels form favourable conditions for the generally fast flow of water underground. There are several parts of aquifers based on the characteristics of water flow and water storage (unsaturated or vadose zone, epiphreatic zone, saturated or phreatic zone).

The great diversity in the flow and the storing of underground water is typical for karst. The flow velocity in karst is much higher in comparison to the non-karst aquifers and reaches hundreds of m/h. Based on hydrological conditions, the velocity and direction of the underground flow changes often and can cause that certain parts of the aquifer recharge one or the other spring. The underground water of an aquifer discharges through numerous karst springs. These springs are of vital importance to a great number of inhabitants, since they are the most important source of their drinking water (Petrič 2010).

In karst border area between Slovenia and Croatia, surface and especially subterranean hydrographic networks have evolved. The Rižana, Sv. Ivan and Bulaž springs are transboundary water sources of exceptional importance for supplying drinking water to Slovenia's coastal region of Primorje and the Istrian region. They are fed from a complex aquifer structure which is recharged both through direct infiltration of precipitation and also through sinking streams, which enter into the highly permeable conduits of the karst aquifers. This binary structure renders them extremely vulnerable to various sources of contamination. Their effective protection requires a good knowledge of the processes of water flow and the transport of substances in the system of precipitation – karst aquifer – springs, both in terms of quantity and quality of karst water.

2.4. Man on karst

The presence of man on karst is strongly connected to the natural resources there. The karst surface is rocky, very diverse and unsuitable for cultivation due to its thin soil cover.

In the past, settlement was closely linked to water resources such as sinkhole ponds, active caves and karst springs. If there were no springs, they used precipitation collectors. Over time, larger urban settlements developed alongside traffic routes, which now, due to their growth, pose a threat to the karst landscape and even more to the water in the underground karst.

2.5. Water resources and their risk to contamination

Every karst spring has a recharge area. This is a karst and non-karst area from where surface and underground waters flow towards the spring. The borders of waterflow towards different springs and into different river basins are known as watersheds. A unique characteristic of karst is that water from a certain area flows towards different springs, thus their recharge areas may overlap. Tap water in the southwestern part of Slovenia, in Istria and in northern Kvarner, most likely comes from one of the big karst springs. Two of the biggest karst springs are the Rižana spring and the Sv. Ivan spring near Buzet.

Karst aquifers are highly vulnerable to the consequences of pollution due to their unique characteristics. As water moves through the underground, it can carry with it pollutants from the surface. In non-karst aquifers, the potential pollution spreads differently than in the karst ones. In a non-karst aquifer, the diffuse pollution slowly penetrates through the pores between the grains, which enable the decomposition of some pollutants before they reach the water source.

For karst, the extremely rapid infiltration of fluids into the underground is typical. The decomposition and retention of pollutants are low due to the thin soil layer and scarce vegetation. Due to this, they can reach the spring in high concentrations. Remoteness from the water spring does not necessarily mean greater safety against pollution.

Since pollution remediation in the karst region is only effective, if at all possible, in exceptional cases, it is especially important to understand the process of water flow and pollutant transport through a karst aquifer.

2.6. Scientific research & water protection

Due to the diverse structure of karst aquifers, the classic hydrogeological methods are insufficient for thorough research. The basic research method in numerous studies is monitoring the physical and chemical parameters of spring water. First, scientists conduct a field study in which they sample spring water or water in accessible water caves in carefully chosen intervals according to hydrological conditions. The analyses are then carried out in laboratories.

A precondition for proper protection requires being well acquainted with karst water characteristics. The scheme for

protection and pollution prevention must be based on prior scientific findings and legally summed up by the Decree on the water protection area. According to the vulnerability of the area, the recharge area of the spring is divided into water protection zones with different degrees of protection. Within these the permitted, limited and prohibited activities are determined.

3. Conclusions

The most protected are the most vulnerable karst areas where pollution could have catastrophic consequences (Prelovšek & Zupan Hajna 2011). Considerable research has confirmed that underground karst water does not consider political borders and flows independently. The protection of cross-border aquifers is and will be efficient only when activities are coordinated on both sides of the border. Intergovernmental cooperation between Slovenia and Croatia is significant for the lives of the inhabitants on both sides of the border. Cooperation in the research of cross-border aquifers and the determination of protection measures is necessary. Intergovernmental cooperation in raising the awareness of karst and the karst water resources is also very important.

People are a part of the constant water cycle and at the same time guardians of this exceptional natural resource. It is of vital importance that we realize that we can destroy it or preserve it for many generations to come.

The film has been presented at various events as conferences, meetings, multimedia competitions, in student programs at the universities of Slovenia and abroad and in the schools. In June 2016 it was broadcasted on Slovenian national television. It has gained a lot of positive reviews and we can assume that its purpose has been achieved.

Acknowledgments

The production was financed by EU and SVLR (Slovenian Government office for Local Self-Government and Regional Policy) of IPA Operational Programme Slovenia-Croatia 2007-2013: project ŽIVO! – Life – Water! (2014-2015). Film was shot on both sides of the border with the participation of all project partners, local residents and managers of water resources in the project area!

References

- Ford DC, Williams P, 2007. *Karst Hydrogeology and Geomorphology*. Wiley, Chichester.
- Gams I, 2003. *Kras v Sloveniji v prostoru in času*. ZRC Publishing, Ljubljana.
- Matas M, 2009. *Krš Hrvatske: geografski pregled i značenje*. Geografsko društvo, Zagreb – Split.
- Mihevc A, 1997. Kras morphology. In: A Kranjc (Ed), *Kras: Slovene Classical Karst*. ZRC Publishing, Ljubljana.
- Petrič M, 2010. Characterization, exploitation and protection of the Malenščica karst spring, Slovenia: case study. In: N Krešič and Z Stevanović (Eds). *Groundwater hydrology of springs: engineering, theory, management and sustainability*. Burlington, Butterworth-Heinemann, 428-441.
- Prelovšek M, Zupan Hajna N (Eds.), 2011. *Pressures and protection of the underground karst: cases from Slovenia and Croatia*. Karst Research Institute ZRC SAZU, Postojna.
- Ravbar N, Šebela S, 2015. The effectiveness of protection policies and legislative framework with special regard to karst landscapes: Insights from Slovenia. *Environmental science and policy*, **51**, 106-116.
- Zupan Hajna N, 2015: What is karst? In: N Zupan Hajna et al. (Eds). *Life and water on Karst: monitoring of transboundary water resources of Northern Istria*. ZRC Publishing, Ljubljana, 6-14.
- Zupan Hajna N, Ravbar N, Rubinić J, Petrič M (Eds), 2015. *Life and water on karst: monitoring of transboundary water resources of Northern Istria*. ZRC Publishing, Ljubljana.
- Speleological Association of Slovenia, 2016. *The longest and deepest caves in Slovenia*. <http://www.jamarska-zveza.si> (access 13 Jan 2017)
- Hrvatski speleološki poslužitelj, 2016. *Croatian caves deeper than 250 m, longer than 1000 m*. <http://speleologija.hr/spilje> (access 13 Jan 2017)

(Abstract) **Evaluating Human-Environmental Impacts to the Karst Landscape of Phong Nha-Ke Bang National Park, Vietnam using a modified Karst Disturbance Index Methodology: Implications for Sustainable Tourism**

Leslie North¹, Jason Polk¹, Nguyet Vu Thi Minh², Tuan Tong Phuc², Vo Van Tri²

Affiliation: ¹ Center for Human GeoEnvironmental Studies (CHNGES)
Department of Geography and Geology Western Kentucky University
² Vietnamese att.. TBA

Abstract

Karst environments are complex, interconnected landscapes vulnerable to anthropogenic impacts. The Karst Disturbance Index (KDI) is one method of evaluating the anthropogenic disturbances in a karst landscape using various data. The original KDI, proposed by van Beynen and Townsend (2005), consists of 30 environmental indicators contained within five categories: geomorphology, hydrology, atmosphere, biota, and cultural. This research utilized both the original method of applying the KDI, as well as a modified method, which evaluates known disturbances rather than potential indicators of disturbance, to calculate a disturbance score for Phong Nha-Ke Bang National Park, Vietnam. Geographic Information Systems were also used to calculate disturbance scores for multiple locations throughout the park, as opposed to a single score for the entire region. Based on collected data, karst disturbance scores range from 0.11 to 0.40 within the park core and buffer zones. Similar to findings of other KDI applications, a significant lack of data was noted with regard to cave and groundwater biota throughout the study area. Tourism was found to be a significant contributor to karst disturbance in the Park, with the likelihood of increased degradation high as tourism continues to rise throughout the region. This research is intended to advise future sustainable development activities, particularly those related to tourism in the region, as well as advance techniques for evaluating and managing karst environments.

The Geoheritage Significance Of Cliefden Caves, NSW, Australia

Armstrong Osborne

Affiliation: Sydney School of Education and Social Work, A35, The University of Sydney, NSW 2006.
Vice President, Save Cliefden Caves Association armstrong.osborne@sydney.edu.au

Abstract

Cliefden Caves is arguably the most significant karst area in Eastern Australia that is not in public ownership in a conservation area. Cliefden Caves is also an internationally significant Ordovician stratigraphic and palaeontological site, has a well documented set of tufa dams and has one of the only three warm springs in New South Wales (NSW) that rise from bedrock, rather than from an artesian basin. The caves are now under threat from flooding due to proposals to construct a dam on the Belubula River downstream of the caves. While the original proposal to build a dam that would flood the caves, the fossil sites and the warm spring appears to have been abandoned, the construction of a dam at the site presently proposed is likely to flood the warm spring and at least partially flood the caves.

With more than one hundred recorded caves, Cliefden Caves is one of the most cavernous karsts in Eastern Australia. The caves at Cliefden have a network pattern guided by geological structure. While they are located close to the Belubula River there is little evidence that streams or the river have ever flowed through the caves. The caves show evidence of solution by rising groundwater, possibly related to the adjacent warm spring. One of the most significant caves at Cliefden is Taplow Maze Cave with a network of passages 3 km long. This cave has a complex arrangement of morpho-structural zones and the bedrock of the cave is folded into a plunging syncline. Studies are underway to investigate the cave morphology and its relationship to geological structure and lithology.

Cliefden Caves contain an abundance and great diversity of speleothems, most in very good condition, including, rare blue stalactites and shawls, known from only one other locality in NSW, very rare polyhedral, monocrystalline stalactites and columns, and significant deposits of helictites. Work is continuing to investigate and document the geoheritage of the caves. Emphasis is currently being given to the isotopic ratios of crystalline deposits in the caves, and to the relationships between morphology, structure and lithology in Taplow Maze Cave. It is expected that new information will be available to present orally at the Congress.

Keywords: Cliefden, Cave, Geoheritage, Australia, Dam

1. Background

Cliefden Caves are located in the valley of the Belubula River, a tributary of the Murray-Darling System that drains inland Eastern Australia. European knowledge of the caves dates back to the 1830s when cave entrances were recorded on cadastral maps. In 1908 the NSW Government Superintendent of Caves inspected the caves and recommended that the government should resume the land because the caves were "well worth preserving" (Trickett, 1909). This did not occur so the caves remain on private land and are considered to be the most significant karst area in Eastern Australia that is not in public ownership. Scientific interest in the fossils in the limestone at Cliefden Caves dates from the 1890s and continues today.

There have been proposals to dam the Belubula River and flood both the fossil sites and the caves in the 1930s, 1940s, 1960s and 1970s. These were abandoned largely on geotechnical grounds (Harper, 1931, Kenny, 1941, Adamson & Truman, 1962, Boyd, 1970). The present threat to the caves arose in 2014 when the dam proposal re-emerged as "a solution to the lack of water storage, and addressing job losses in our region" (J. Cobb, MP Media Release, 21/1/2014).

2. Elements Of Surface Geoheritage Significance

2.1. Ordovician Fossil Sites

Palaeontological research commenced at Cliefden in the 1890s and is continuing today. The Ordovician marine fossils

and the palaeoenvironment at Cliefden Caves is recognised as being internationally significant. Key features of the fossil sites include the world's oldest known in situ brachiopod shell beds, the world's oldest known rugose corals and one of the most diverse deep-water sponge faunas ever recorded. Two of the sites, Fossil Hill and Trilobite Hill, have long been recognised as significant with at least 62 scientific papers published in international journals, documenting 191 genera and 263 species of fossils from these and other sites in the vicinity of Cliefden Caves. Of the fossils found at Cliefden, 45 genera and 101 species are unique to the area threatened by flooding from some of the proposed dams.

2.2. Warm Spring

Warm springs rising from Palaeozoic rock (as opposed to artesian springs rising from the Australian Basin) are rare in NSW with only three documented, all in karst areas. These are the Cliefden Warm Spring, the warm spring at Wee Jasper and the warm spring at Yarrangobilly Caves. There has been little study of warm springs in NSW apart from the description of the Cliefden warm spring by Trickett (1909). The water rising from the spring has a temperature of 29 degrees C, ten degrees higher than the cave temperature of 19 degrees C.

2.3. Tufa Dams

Active tufa dams are uncommon in NSW creeks and have received little study. The tufa dams in Davy's Creek at Cliefden Caves are the most studied in NSW. Drysdale *et al.* (2003) showed that deposition at the tufa dams was dependant on

weather conditions, making tufa dams a likely source of information about past climatic conditions. Carthew and Drysdale (2010) demonstrated that it was possible to use information from the tufa deposits to construct a history of stream development in Davy's Creek.

2.4. Surface Karst Forms

There has been no formal study of the surface karst at Cliefden however informal observations show that well-developed karren fields, dominated by rillenkarrren are developed on outcrops of the massive limestone. Towards the southern end of the limestone, blocky outcrops locally known as "graveyard" karst occur. As with other Eastern Australian karsts dolines are uncommon. One unroofed cave has been identified at Cliefden but has yet to be investigated.

3. Elements Of Underground Geoheritage Significance

3.1. The Pattern of Cave Development

While caves in most karsts in Eastern Australia have a north-south orientation following the Tasmanic structural grain (Osborne 2017a), at Cliefden, however, there is a variety of cave orientations. Transmission Cave, developed in limestone dipping steeply to the northeast, has a NW-SE orientation. Cliefden Main Cave, developed in gently dipping limestone, striking E-W near the nose of an anticline, has a SW-NE orientation with many elements trending NNW-SSE. The Murder-Boonderoo Cave System is developed in steeply dipping limestone striking to NNE-SSW. Gable-Swansong Cave is developed along the axis of an anticline and Taplow Maze Cave is developed in a northerly plunging syncline.

Cave development at Cliefden shows strong structural and lithological guidance. Osborne (1978) investigated the structural and lithological guidance of Main Cave, Transmission Cave and the Murder-Boonderoo Cave System, but this work has not been undertaken for any other caves.

Osborne and Branagan (1988) described Cliefden Caves as "structurally controlled nothephreatic networks" using the term nothephreatic in the sense of Jennings (1977) meaning solution by relatively slow-moving water below the watertable.

Osborne (2001) used Transmission Cave as an example of a Hall and Narrows cited Swansong Cave as an example of a cupola-dominated cave.

The production of high-resolution cave maps by members of the Sydney University Speleological Society, particularly Phil Maynard is assisting in extending this work to Taplow Maze Cave and other caves. As well as solution cavities there are late-stage breakdown chambers in Cliefden Caves; the largest is the 40m by 50m Main Chamber in Main Cave.

3.2. Maze Caves

There is significant scientific discussion concerning the origin of maze caves and oil companies are funding research on maze caves in southern Europe and South America as these caves are seen as physical models for oil reservoirs in karst rocks.

Most maze caves, including the longest cave in Australia, the 120 km+ long Bullita Cave in northeastern Western Australia, have formed in beds of soluble rocks in sedimentary basins and have a rectilinear pattern of development. Maze caves in Eastern Australia, like Taplow Maze Cave, however do not occur in sedimentary basins, but are developed in Orogens (zones with folded rocks).

Of the two largest caves at Cliefden, Main Cave has maze-like features, while Taplow Maze Cave is a maze cave *sensu stricto*. While 1970s mapping showed that Main Cave had some maze-like features, new mapping shows that Main Cave has an underlying maze structure, overprinted by later solutional and breakdown events.

Taplow Maze Cave is a complex multilevel maze with development along two axes, but other Eastern Australian maze caves formed in folded rock, such as Dip Cave at Wee Jasper, NSW, Main Cave at Mt Etna, Qld and the longest maze cave in Eastern Australia, the 10 km Queenslander Cave at Chillagoe, Qld are developed along a single principal axis, without significant lateral development.

While the structures of most maze caves can be divided into a small number of morpho-structural domains (the 120km Toca da boa vista Cave in Brazil has 4 domains), the 3km Taplow Maze Cave has 6 morpho-structural domains making it one of the most complex known maze caves. Taplow Maze Cave has a number of other unusual features; "Y" junctions, when most maze caves have "T" junctions and cross-junctions. Taplow Maze Cave also has offset cross-junctions and parallel tubes which the author has only previously observed in the Caverns of Sonora in Texas. The floor and side feeders, diagnostic features of caves formed by water rising from below, compare favourably with those in the giant gypsum maze caves of the Ukraine.

Taplow Maze Cave is unusual in another way, as much of the northern part of the cave is developed in thinly bedded relatively impure limestone, while almost all other large caves in Eastern Australia, including Cliefden Main Cave, are developed in massive high-purity limestone. Taplow Maze Cave would appear to contain the largest volume of cave formed in thinly bedded limestone in Eastern Australia.

While the investigation of Taplow Maze Cave is incomplete, what is currently known of the cave makes it significant at a National level, and it is potentially significant at an International level.

3.3. Speleogens

Cliefden Caves contain a range of speleogens including pendants, spongework, cupolas, vertical and horizontal blades, bridges, cusps, pockets and zones with elaborate solution forms, all indicating solution by slow moving or convecting water.

3.4. Conventional Speleothems

Cliefden Caves contain a diversity and abundance of speleothems in good condition and with a high degree of integrity. Making reliable comparisons with other sites is difficult, however the helictite masses are particularly abundant and well developed at Cliefden and compare favourably with other

Eastern Australian examples of helictite masses such as those in The Temple of Baal at Jenolan, NSW.

3.5. Blue Aragonite Speleothems

Blue aragonite stalactites and shawls are rare and only known from two localities in Australia (Cliefden and Wombeyan) with Cliefden having the most examples. Blue speleothems are rare at an International level. Hill and Forti (1997) mention only one locality in France and the author is aware of only two other localities, one in Thailand and another in Greece, making the Cliefden deposits significant at an International level.

While there has been some study of the cause of the blue colour of the speleothems and their mineralogy and chemistry was investigated by Osborne (1978) and Turner (2002), their isotopic composition and the substrate on which they formed has not been previously investigated. This investigation is now taking place. Blue aragonite speleothems are highly regarded internationally by mineral collectors. One gated cave at Cliefden has been broken into in the past and part of a blue stalactite was stolen, making the blue speleothems both rare and threatened.

3.6. Subaqueous Calcite Crystal Deposits

Deposits of spar, clouds, raft breccia and unconsolidated calcite rafts are abundant at Cliefden. Isotopic studies are underway to determine the likely depositional temperature and carbon source for these deposits.

3.7. Polyhedral Speleothems

Polyhedral speleothems are very rare and Cliefden is the only known locality in Australia. The author has only found one French paper describing them (Andrieux, 1962). Polyhedral speleothems do not appear to be described in any of the standard texts on cave minerals or cave geology. Samples in the Australian Museum collection are being studied in collaboration with Ross Pogson, but some work, micro-sampling and measuring of orientation, will be needed in the field as the provenance of the museum specimens is not certain. The polyhedral speleothems are significant at an International level.

3.8. Overgrown Speleothems

Overgrown speleothems are also unusually abundant at Cliefden. Samples in the Australian Museum collection are also being studied. As with the polyhedral speleothems some work, micro-sampling and measuring of orientation, will be needed in the field. Isotopic analysis will be used to compare the overgrowth with the original substrate to determine the nature of the water that formed the overgrowth.

3.9. Sulfate Deposits

There is a great deal of gypsum in the caves; the largest quantity occurs as wall coatings in the upper parts of Taplow Maze Cave. Isotopic and chemical studies are underway to determine the source of the sulfur and likely paragenesis of these deposits and thus their geoheritage significance.

3.10. Cave Sediments

There are at least five types of clastic sediment in the caves. These include red earth with bone fragments, laminated clays, unconsolidated angular chert fragments in a clay matrix and less common, clay with rounded pebbles.

Much of the sediment is found below flowstone and calcite raft false floors, suggesting that there have been phases of sediment filling and emptying in the past. The mineral composition of sediments is being investigated using X-ray diffraction. It is intended to attempt palaeomagnetic dating of the sediment sequences in the near future.

Using samples from caves in the Island (a hill at Cliefden), Osborne (1978, 2000) described a process where percolating water removed matrix from cave sediments, replacing it with sparry calcite cement. Osborne (2007) found evidence for a similar process in palaeokarst deposits in Okno Cave, Slovakia. New work in Murder Cave at Cliefden has revealed an extreme form of this process where what appears to the naked eye to be metres-thick sequences of bedded sediment turn out to be composed almost entirely of crystalline calcite, with tiny bone fragments as the only original material remaining.

3.11. Palaeokarst Deposits

Before the current threat to the caves, palaeokarst deposits were not known to occur at Cliefden Caves. Recent work has shown the presence of deposits that behave like palaeokarst in Swansong Cave and Gable Cave. These include a bridge formed in partly lithified sediment, and partly lithified sediment forming cave walls. Osborne (2017b) described these as “features on the boundary of palaeokarst”. There are also unconfirmed reports of palaeokarst deposits in the lower sections of Taplow Maze Cave. More work is needed on palaeokarst at Cliefden.

3.12. Vertebrate Fossils

There has been little study of the vertebrate fossils in the caves. Bone fragments likely to be of Pleistocene age have been observed in red silt deposits in a number of caves, but are yet to be systematically studied. There is also a report of a ghost bat fossil being excavated from Cliefden Caves in the 1960s (Molnar *et al.* 2007).

3.13. Cave Minerals

In addition to sulfates and carbonates, the caves contain bat-related phosphatic deposits and manganese deposits. These are now being investigated using X-ray diffraction.

4. Conclusions

The geoheritage significance of the Ordovician fossils, strata and palaeo-environmental evidence at Cliefden Caves are shown to be significant at a State level by their inclusion in the Geological Heritage of NSW (Percival, 1979, 1985) and at a National level by their inclusion in Australia's Fossil Heritage: a catalogue of important Australian fossil Sites (Australian Heritage Council, 2012), which describes the fossil localities at Cliefden as being the “best exposures of Late Ordovician island marine invertebrate fossil assemblages in Australia”.

The large number of endemic fossil species found at these sites (45 genera and 101 species unique to the area) and with more

than 62 papers published in international journals, Cliefden Caves is a site of International significance for Ordovician fossils, strata and palaeoenvironment.

Warm springs that rise from bedrock are rare in NSW, so the Cliefden warm spring is significant at a State level. The tufa dams at Cliefden, the best-studied examples of tufa dams in NSW, are also significant at a State level.

From what is currently known, the caves at Cliefden are significant at a State level or National level. Some elements of the cave geoheritage such as the blue aragonite speleothems and polyhedral speleothems are significant at an International level. Taplow Maze Cave is significant at a National level as the largest cave in impure limestone in Eastern Australia. It is likely that continuing study of Taplow Maze Cave will result in some of its other characteristics being recognised as significant at a National or International level.

A great deal of work is required if our knowledge of the caves is to become as sophisticated as the current knowledge of the Ordovician marine fossils and their palaeoenvironment at Cliefden Caves.

Acknowledgements

The author would like to thank the Dunhill and Crossing families for access to their caves, members of the Orange Speleological Society and the Sydney University Speleological Society for their assistance in the caves, his research student Ian Houshold and the authors' student assistants Harrison Burkitt and Oxana Repina for their help and for asking difficult questions, and his wife, Penney for her patience and assistance with proofing and polishing the text.

Financial support for analysis and lab work was received from a contract research project funded by the Save Cliefden Caves Association, grants from the Australian Speleological Federation Karst Conservation Fund and donations from generous members of the public.

References

Adamson CL, Trueman NA, 1962. Geology of the Cranky Rock and Needles proposed dam storage areas, *New South Wales Geological Survey Reports*, **11**.

Australian Heritage Council, 2012. *Australia's fossil heritage: a catalogue of important Australian fossil sites*. CSIRO Publishing, Collingwood.

Andrieux C, 1962. Etude cristollographique des édifices stalactitiques. *Bulletin of the French Society of Mineralogy and Crystallography*, **85**, 67-76.

Boyd GL, 1970. *A comparative study of three proposed dam sites, Central Western NSW*. The University of New South Wales, Kensington, BSc (Applied Geology) Honours thesis unpubl.

Carthew KD, Drysdale RN, 2010. Late Holocene fluvial change in a tufa depositing stream: Davys Creek, New South Wales, Australia. *Australian Geographer*, **34**(1), 123-139.

Drysdale R, Lucas S, Carthew K, 2003. The influence of diurnal temperatures on the hydrochemistry of a tufa-depositing stream. *Hydrological Processes*, **17**, 3421-3441.

Harper LF, 1931. *Examination of suggested dam site, Belubula River*, NSW Mines Department Papers Ms.31/18921, unpubl.

Hill C, Forti P, 1997. *Cave minerals of the world, second edition*. National Speleological Society, Huntsville, AB, USA.

Jennings JN, 1977. Caves around Canberra. In: Spate AP, Brush J, Coggan M. (Eds.). *Proceedings of 11th Biennial ASF Conference*. Australian Speleological Federation, Broadway, NSW, 79-95.

Kenny EJ, 1941. *Dam sites on the Belubula River*, NSW Mines Department Papers Ms. 41/1609, unpubl.

Molnar ME, Hall LS, Mahoney JH, 2007. New fossil localities for *Macroderma* Miller, 1906, (*Chiroptera: Megadermatidae*) in New South Wales and its past and present distribution in Australia, *Australian Mammalogy*, **7**(2), 63-73.

Osborne RAL, 1978. Structure, sediments and speleogenesis at Cliefden Caves, New South Wales. *Helictite*, **16**(1), 3-31.

Osborne RAL, 2000. Petrography of lithified cave sediments. Geological Society of Australia, *Abstracts 59, 15th Australian Geological Convention*, Sydney, July 2000, 373.

Osborne RAL, 2001. Halls and narrows: Network caves in dipping limestone, examples from eastern Australia. *Cave and Karst Science*, **28**(1), 3-14.

Osborne RAL, 2007. Intensely lithified palaeokarst deposits in Okno Cave, Demänovská Valley, (Slovakia). *Geologica Carpathica*, **58**(6), 565-578.

Osborne RAL, 2017a. Hypogene caves of the Tasmanic karsts of eastern mainland Australia. In: AB Klimchouk, Arthur Palmer, Philippe Audra, Jo DeWaele, Augusto Auler, (Eds.). *Selected Hypogene Karst Regions and Caves of the World*, Springer.

Osborne RAL, 2017b. Palaeokarst deposits in caves: examples from Eastern Australia and Central Europe, *Acta Carsologica*, in press.

Osborne RAL, Branagan DF, 1988. Karst Landscapes in New South Wales. *Earth Science Reviews*, **25**(1988), 467-480.

Percival IG, 1979. *The geological heritage of New South Wales*. A report prepared for the Australian Heritage Commission and the Planning and Environment of New South Wales, 63-70.

Percival IG, 1985. Cliefden Caves – Belubula river valley. *The geological heritage of New South Wales*, Volume 1, National Parks and Wildlife Service, Sydney, 21-23.

Trickett O, 1909. Report of the Cliefden Caves, Warm Spring and Fossil Hill, Belubula River. *Annual Report of the Department of Mines*, NSW, 1908, 172.

Turner K, 2002. Chromophores producing blue speleothems at Cliefden, NSW. *Helictite*, **38**(1), 3-6.

(Abstract) **Index of the sustainable use of karst environments**

Philip van Beynen

Affiliation: School of Geosciences, University of South Florida, Tampa, Florida, USA

Abstract

With growing populations and ever increasing pressure on resources, the need to live sustainably with our environment is more important than ever. When considering such anthropogenic pressure, karst landscapes are as vulnerable, if not more so, than any other environment. Such vulnerability arises from the rapid transit times of percolating water, the poor filtering ability of the carbonate bedrock, and the highly specialized biota of the subterranean karst. The Karst Sustainability Index (KSI) was created as a standardized metric of sustainable development practices in karst settings. The KSI uses predetermined targets to ascertain the overall sustainability of a karst region. Indicators are designed to incorporate common measures of sustainability for the three domains of social, environmental, and economic resource use. Benchmarking the current state of karst environments allows the comparison of sustainability practices temporally and spatially to highlight areas where remedial policies or actions are needed. This is the first index to incorporate the emerging field of environmental sustainability with karst landscape assessment. To test the applicability of the KSI, a study was undertaken in the Tampa Bay Metropolitan Area which encompasses four counties that are entirely karst. The TBMA was found to be progressing towards the sustainable management of karst resources and the KSI provided a robust measure of the degree to which a karst region is moving towards a sustainable future.

(Abstract) **Sanitation And Right To Health: An Analysis Of Urban Solid Waste Disposal In The Karst Of Minas Gerais, Brazil**

Isabela Dalle Varela¹, Luiz Eduardo Panisset Travassos²

Affiliation: ¹Professor of Constitutional Studies at Newton Paiva University Center and Promove College. Doctorate Student at the Graduate Program in Geography - PUC Minas, Brazil. Scholarship provided by CAPES. dallevara@gmail.com

²Doctor in Karstology. Researcher and professor at the Graduate Program in Geography - PUC Minas, Brazil. luizepanisset@gmail.com

Abstract

The State of Minas Gerais, Brazil, has approximately 580,000 sq. Km. From this total, around 29,000 sq. Km are made of carbonate rocks. With a total of 853 municipalities and some serious environmental problems, the biggest one is the final waste disposal, particularly in cities that are identified as mid-sized ones. Such cities in Brazil are those considered to have many of the urban equipment found in big metropolis, but not with the proper care regarding the environment. Thus, many of them face intense unplanned economic growth, undergoing significant environmental and social changes. Since 2000, many legal instruments were published to discipline the waste disposal, although reality is far from ideal. Therefore, this work is intended to demonstrate how karst waters might be extremely polluted due to leachate's percolation from improper waste disposal sites. In Brazil, it was established three categories to designate landfills. From the most environmentally incorrect sites for waste disposal to the better suitable for these activities it is possible to identify waste dumps (*lixões*), controlled landfills (*aterros controlados*) and sanitary landfills (*aterros sanitários*). In each Brazilian State, around 80% of their municipalities have less than 20,000 inhabitants and no sufficient financial resources required to construct a sanitary landfill. Unfortunately, many mid-sized cities with more than 150,000 inhabitants are in karst areas developed in Proterozoic carbonates of the Bambuí Group that favours the development of karst. The research showed that in 2001, 600 municipalities did not have the minimal requirements for an adequate waste disposal. According to the Solid Waste Disposal Panorama of Minas Gerais from 2014, 54.08% of urban population was covered by treatment systems or final waste disposal strategies in 232 municipalities. In 2015, governmental agencies stated that an increase of 3.63% was recorded representing 57.71% of population covered (9,647,120 inhabitants) in a total of 296 municipalities. At first glance, one can think that a lot of improvement was made, but if the focus is directed to karst areas, one can identify 167 municipalities that are developed in karst areas (covered or bared). From these municipalities, 34 have mid-sized cities and from these, 19 are over karst and 4 near it. Primary results show that the right to health and sanitation may be compromised due to lack of studies regarding the importance of karst in maintaining environmental quality, and how these mid-sized cities should develop over this fragile geosystem.

Keywords: Sanitation; Waste Disposal; Karst; Mid-sized cities; Minas Gerais; Brazil

Other Topics

(Abstract) **Finspac Through the Ages**

Alkantana, Cahyo

Affiliation: President of Federation of Indonesian Speleological Activities

Abstract

The Federation of Indonesia Speleological Activities (FINSPAC) was established on May 22nd, 1983 at Cilacap Regency, Central Java. A year later, on 1984, FINSPAC officially joined Union Internationale de Speleologie as the 45th member and since then, became the only recognized scientifically-professional institution in speleology by Indonesian Scientific Institution (Lembaga Ilmu Pengetahuan Indonesia (LIPI)

Indonesia as an archipelago, contains vast and massive limestones which exhibit extravagant karst features such as conical hills (Gunung Sewu), tower (Maros), or pinnacle (Sangkulirang Mangkalihat). Karst in Indonesia contains significance values which are comprised by scientific values, economical, and even socio-cultural values. The limestone of Indonesia extended in 154,000 km² area and distributed in all across the island. However, all of those karst areas are facing serious threats from cement and extractive industry. FINSPAC's visions and missions are to facilitate, guide, increasing quality, and also coordinate all speleology activities in Indonesia. It is done by developing the understanding and awareness of importance and significance values from caves and the surrounding environment.

Sustainable Tourism Industry is one of the FINSPAC's struggling to fight against cement or extractive industry which threatened karst environment. FINSPAC is considering it was more effective to fight extractive industry through tourism industry rather than doing seminar and demonstration. Tourism is considered to be more powerful because from it FINSPAC is able to empower people and gives more benefits. People around karst will be more productive while gain more income rather than they sold their land to Mining Corporation.

More than 60 Basic and Advance Caving Courses had been done by FINSPAC since 1983 with more than 2850 participants (and still going on) had graduated and scattered broadly across Indonesia. FINSPAC produce Indonesian future leaders which had knowledges, empathy, and participating on karst's conservation.

Recently, FINSPAC's alumni hold many strategic position on government e.g. at Tourism Ministry and hold strong motivation to maintain and conserve karst region. Recently, since 2015, FINSPAC was also provider of the Cave Guide Course, Ecotourism, and Speleotourism Management for the karst guide. From the Cave Guide Course, FINSPAC had yielded 400 cave guides who graduate from the course and still goes on. FINSPAC is also issued the guide certification from National Profession Certification Board to form professional cave guide who protect cave and its environment.

A Verbal Dispute Between A Bat And A Partridge: A Satiric Allegorical Poem From The Medieval Period

Konstantina Aretaki

Affiliation: Hellenic Speleological Society (Department of Western Crete) National Library of Greece

Abstract

In manuscript, no 701, held in the National Library of Greece, among other texts, there is a text in poetic form under the name "Tale of a bird-tracker about the Birds", consisting of 500 verses. All the birds are invited to an official dinner-party by the Eagle, who celebrates the wedding of his son, at which a verbal conflict between 15 pairs of birds takes place. One of these pairs is the bat and the partridge. The poem probably dates at late 13th or early 14th c. AD and the specific manuscript from the beginning of the 16th c. Until today, six other manuscripts have been found in libraries around the globe (Vienna, Constantinople, St Petersburg, Escorial-Spain etc.) containing variations of the same poem. In a sarcastic manner, all the birds mock each other giving a very accurate description of their characteristics and their behavior as it was conceived by the people of the 14th c. AD. Through these words, we can assume the beliefs held by the people during that era, as regards to the bats. The manuscript also contains drawings of the birds (among them the bat). It is an allegorical text with a didactic and ethical aim.

Keywords: bat, manuscript, Byzantium, poem, folklore, tales

1. Animal and bird tales

"Poulologos" is a "curious" medieval narrative poem about birds, in the demotic Greek language. It belongs to the allegorical satirical stories under the title "Ai peri ta zoa istoriai" (Stories about animals), including stories about terrestrial animals (Tale of the Quadrupeds), air animals (Poulologos) and sea animals (Opsarologos) to which are attributed human features including advantages and defects (Camariano 1939). From Aesop's Fables, the mythical story-teller of ancient Greece, to the "Romans de Renard" (Novels about the Fox) from the Middle Ages and the French story-teller Jean de La Fontaine (1621–1695), the literary production for animals was always rich. They were circulated widely, as folk tales, and they were possibly transmitted orally (Krumbacher 1891).

These stories about animals were very popular during the last Byzantine (13th–15th) and post-Byzantine centuries (16th–17th). They were created mainly to entertain the Byzantine people, though reading or listening, to play an educational role, because "they teach young people for the various kinds of animals and their characteristics" and additionally to give a moral meaning, because "they teach that God protects and shields the weak from the illusory promises of evil and blood-thirsty persons", such as indicated in the first lines of "Quadrupeds" (Eideneier 2016). Furthermore, many scholars state that these poems use the allegorical animal stories for social and political satire. These gatherings of animals ("Quadrupeds") and birds ("Poulologos") or the trials of vegetables ("Porikologos") and fishes ("Opsarologos"), which end in epic quarrels, are the settings for the satire. The caustic humor, indiscretion and juxtaposition, and the folkloric information or information about the real habits of the animals, through praise and reproach of the wrangling animals, it is not just they are present but they are fascinating. Some scholars note that they parody and satirize the Byzantine etiquette and ritual, and the ecclesiastical issues of the same period and that they are a clear allusion to the political life of the Byzantines emperors.

In this article, I analyze one of these narratives, in which the main characters are the birds, the "Poulologos" (a dialogue of

birds, a bird-parliament) (Kazhdan 1995). It is a poem of 668 (or fewer lyrics, depending on the variant or gaps that exist in the manuscripts) by an anonymous writer. It belongs to the Zoological Literature of the Byzantine period which contains many allusions to contemporary life and events. From one point of view, it can be seen as a popularized scientific manual of ornithology of the period with an educational and didactic character. From the other hand, the satirical and allegorical purpose is obvious emerging through the constant mixing of animal and human characteristics, as well as the mocking words of the birds. Moreover, it can be regarded as a reproach against the privileged classes and the aristocracy, the nefarious advisers, but also towards the Emperor himself, who, instead of being pleased by the false flattery of a few corrupt courtiers, should try to acquire and retain the respect, the appreciation and the love of his people. Such ideas are genuinely innovative and disruptive to the prevailing political and social situations of the time in which the poem was written, as well as being intertemporal, and very common to all eras (Plemmenos 2000, Veis 1906 a,b, Tsavari 1987).

It is a text with great popularity and diffusion in relation to the other animal stories, as it is evidence of the comparatively rich manuscriptal tradition, comprising the seven manuscript codices of the Byzantine and post-Byzantine period containing different variations, that have survived until today and are scattered in various libraries worldwide. None of these variations is the original work. The recorded modifications on these seven manuscripts could have derived either from the transmission of the text by word of mouth or by the intervention of the copiers (usually monks), who copied the text in subsequent periods, which resulted in more or less significant changes to the original, by adding, removing or modifying some parts (especially the end of the story, as we will see below).

It is very difficult to draw conclusions about the author, the date, the place of writing, the language, even the exact text of the poem. It was written presumably in Constantinople in the late 13th or early 14th century (between 1274 and 1331) according to the indirect information throughout the texts themselves, while it continued to be copied until the 17th cen-



Figure 1.

tury. These later versions could be written in other provinces of the Byzantine Empire.

The hypothesis of “Poulologos” is similar to the storyline of the text about the land animals (Quadrupeds). The King Eagle invites all the birds to a wedding reception in order to celebrate the marriage of his son. The birds eat and drink in abundance, but at the end, entrained by the historically existing contrasts and animosities between them, the feast ends in a large brawl, where birds bicker, argue and quarrel among themselves, listing each one his own virtues and the vices of the opponent by using “dirty” language (that produces lot of laughs). Poulologos is a true folk manual for ornithology, because it describes with admirable precision the characteristics and habits of the 28 birds, which are presented conversing in 14 consecutive pairs. In the seven manuscripts appear at least 45 birds. The characteristics of each bird are given through imaginary stories, traditions and legends which reflect perceptions about these birds that come from antiquity and survive to the present day (Apostolidis 1896).

This text was first presented to the public after the publication of the Vienna manuscript by Guilielmus Wagner in 1874 (Wagner 1874), and thereafter it continues to employ the scholars with descriptions, annotations or critical editions of all the existing variants (Papadopoulos–Keramefs 1884, Blass 1888, Codera 1891, Wunch, 1897, Veis 1906a, b, Zoras 1956, Krawczynski 1960, Tsavari 1987, Eideneier 2016 *et al.*).

2. Codex Atheniensis 701

In September 2016, I started working in the Department of Manuscripts at the National Library of Greece. Among the 5276 manuscripts of the collection I tracked down the codex “Atheniensis 701” that contains mainly religious texts and hymns and other historical and philosophical texts, but also one variant of Poulologos, entitled “The tale of the bird-tracker about the birds”. It is surprising the mix of so many different types of texts in the same codex, which indicates the specificity of the personality of the manuscript owner. This manuscript was probably copied in the 16th century, by a monk named Meletios, as mentioned in the scribe note. The codex consists of 257 leaves (or 261 including the “side-leaves”), it is written on paper, it has a leather wooden lining and its dimensions are 15 X 10 cm (Sakkelion 1892, Veis 1906a, Tsavari 1987).

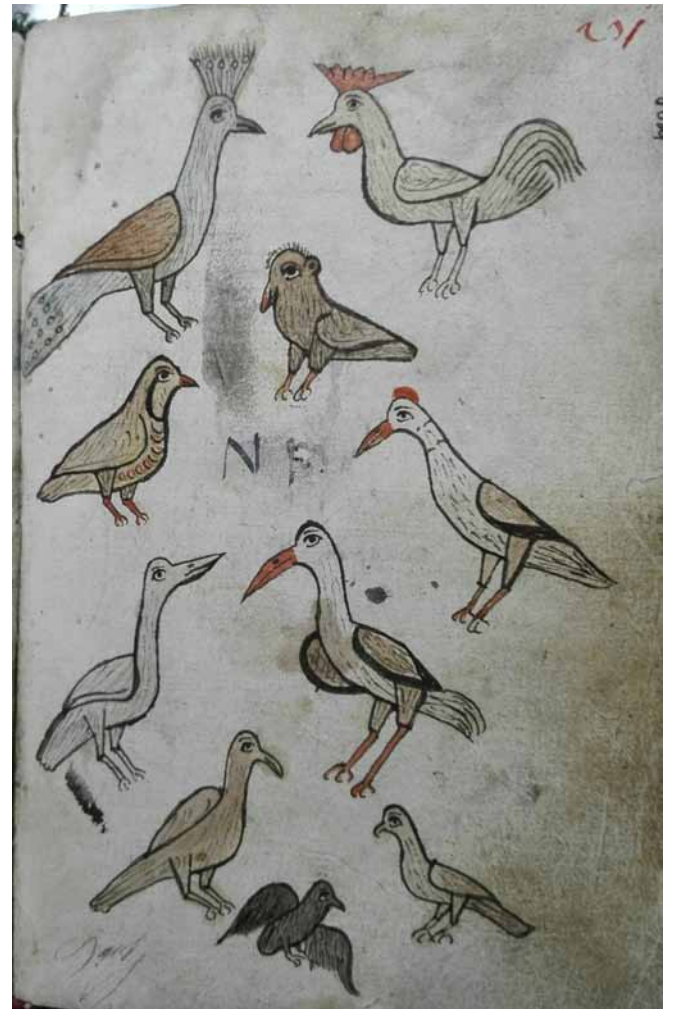


Figure 2.

The poem of “Poulologos” is comprised of 19 sheets (from 216 verso with a full page picture of a two-headed eagle to 234 recto) that includes 500 verses. The text is decorated with 12 images of the pairs of the disputant birds (24 birds) between the dialogues, as well as two pictures of the two-headed eagle and pictures of 14 birds gathered together. Most of the images are doodles, a fact that does not help to identify the birds they represent. But the Copier writes above each picture the name of the related bird (Apostolidis 1896, Tsavari 1987). In most of the seven manuscripts there are empty spaces between the dialogues of the birds probably destined to be have been drawn later with the images of the birds. While the first part in the different versions of the manuscripts is almost the same, with only minor differences, the end shows significant differences in the variations, with two opposite solutions. According to the five of the seven manuscripts, when the bird’s dispute culminates and there is a risk of a general conflict, the King Eagle intervenes, threatening the wranglers that he will proceed with tough sanctions. So, the birds are forced to stop, the serenity is restored and they dissolve in peace and love. But the version of the manuscript of the Athenian codex (and one more), ends with a dramatic struggle of life and death, whence, as in nature, the birds of prey come out winners. The small birds, entrained by the words of the lark, argue that the rulers should earn the respect of the people with their love and not by force. As a result, they rebel and dethrone the king eagle and they put the lark on his throne. When the eagle

learns, what has happened, he sends the largest birds of prey (also his advisers) to attack the small birds, which in panic flee and seek refuge, wherever they can.

3. The bat and the partridge

One of the disputing pairs is the bat and the partridge (*perdix graeca*). Their dialogue begins with the portrayal of the pair (Figure 1) and occupies 53 verses. The bat is depicted again, with all the other birds together (Figure 2). The bat is classified differently at the seven manuscripts. In the oldest manuscripts, it is called “mouse”, while in the Athenian codex of the 16th century and another which it dates from the 17th century, it is called “bat”. The bat “attacks” first the partridge. She says that the partridge is living immorally and that she is the cause of bloodshed. More specifically, the bat accuses her of being a “prostitute” apparently shown by her short and fancy dress and because she squawks to call her lovers. Moreover, she says she is bloody, as shown by the red legs and the red beak. The partridge strikes back mocking the bat for her humble profession and adds that the bellows burned the only outfit she had. On the categories of the bat the partridge answers that she is not immoral, her legs are not bloody, but she wears expensive socks in purple color (the color of the Byzantine Emperor’s clothes). She speaks with pride of her red lips and beautifully colored eyes and says that she is not dressed as a prostitute, but as a lady. Concerning the accusation of shouting to her lovers she mentions that she chirps in the dawn to the amusement of the others. She is also a doleful mother, who protects her chicks from the peregrine falcon (who has already killed 12 of her 20 children).

It is striking that the creator of this poem of the 13th-14th century, while he is well aware of the physiology of the other birds, he considers the bat to be a bird. The ambivalent nature of this animal is already mentioned in the Aesop’s tales of Ancient Greece. According to the Aesopian legend, when the bat was once caught by a cat, the bat begged her not to eat her, because she was not a bird, which by nature the cat hunts, but a mouse. And when she was again caught by another cat, which was hostile to the mice, the bat begged her not to eat her, because she was not a mouse, but a bird.

The bat’s physique gave rise to the following Greek folkloric tradition: At first the bat was a beautiful and proud mouse. It walked into a church and grabbed a piece of holy bread and ate it. Then God decided to punish the greedy mouse for its bad behavior, so he gave it wings to fly, but he took from it the daylight and left it at the night. A variation of that tradition is the following: The bat was first a mouse. One day she entered a church and she found a piece of holy bread which had fallen on the floor and not only did she not eat it but she lifted it from the ground with care and kept it as a talisman. God was so pleased with her reverent action that he gave it wings to lift the holy bread higher to the heaven.

In our text “Poulologos” there is an unknown etiological myth, which explains why the bat has a black back and a white belly: the bat was working on a blacksmith’s forge and while she was working the bellows, the dirty smoke blackened the back of her dress and melted the front part of it. Because the bat had no other dress to wear on Holy Saturday, she patched the burned dress with a piece of white linen cloth (Tsavari 1987).

From the above story, we will try to assume which are the common species of bats to the area where the poem was formed, where they usually had been seen by the local people or the poet giving them the idea to create this story. The most common species of bats in the eastern Mediterranean and Greece which dwell in caves and buildings are the *Rhinolophus ferrumequinum*, *Rhinolophus hipposideros*, *Pipistrellus pipistrellus*, and *Pipistrellus kuhli* which have gray fur and black wings. This physical appearance may have given the poet the idea to create the story of the black and white dress. There is also a species of bat in Greece with a clear white belly and a darker back such as *Rhinolophus blasii*, *Myotis blythii*, *Myotis myotis*, *Hypsugo savii*, *Myotis emarginatus* and *Miniopterus schreibersii*. But most probably, the black and white perception comes from the contradiction of the colors of the dark black wings of the bats and the lighter gray colored fur of their body (Dietz *et al.*, 2014).

4. Bats in the mythology and the folk tales of the world

There are many myths, folk tales and legends about bats all over the world reflecting the perception and the common knowledge of people. Because of their dual nature (they are mammals, yet can fly), or because of their nocturnal habits and their ability to navigate in the dark, they have long been associated with deities, supernatural forces and the mystery. Dwelling in dark caves, which in many cultures it is considered to be the gateway to the land of the deads, they were associated with darkness and death. But, in the mythologies of differing cultures bats can symbolize both good and evil, life and death. From ancient Greeks to the indigenous peoples of the Americas and the Far East, from antiquity until nowadays we find several stories about bats.

Aristotle (384–322 BC), the ancient Greek philosopher named the bats “Chiropter” because they fly with their hands and he writes: “*For as the eyes of bats are to the blaze of day, so is the reason in our soul to the things which are by nature most evident of all*” (Crystalwind 2017). The Greek storyteller Aesop (7th c. B.C.) using animals as main characters of his stories, created three tales about bats. In those tales, bats were portrayed as cunning, intelligent and unfair creatures. It was presented by Aesop as the embodiment of opportunism. The dual nature of this animal is emphasized. In each of the three Aesop’s fables, it is presented as an animal that doesn’t hesitate to take advantage of its dual nature depending on the situation (Cach & Dec 2017). The bat always chooses the more beneficial option for itself. For example, in the Greek mythology, there is the myth of the Minyades, the daughters of king Minyas, Alcithoe, Leucippe and Arsippe. When all the other women were reveling and raging over the mountains in Bacchic joy to worship the god Dionysus, these sisters alone remained at home, devoting themselves to their usual occupations. Dionysus, furious because of their disobedience made them lose their sanity. Zeus felt pity for them and sent Hermes to transform them into bats (Wikipedia 2017a).

In ancient Babylonia, the Ivory Coast, Uganda and Zimbabwe bats are considered physical manifestations of the spirits of the dead who come to visit their relatives. But in Madagascar and Ghana, the flying foxes are assumed to be the souls of criminals, sorcerers and the unburied dead. In Tanzania, a winged

bat known as Popobawa, is believed to be a shapeshifting evil spirit that assaults and sodomises its victims. In the mythology of the East Nigerians there is a story about a bat and a bush rat. The bat tricks the bush rat into bathing in a pot of hot water so he can cook him. When he is to be arrested, he flies away and hides, so only at night when it is dark he dares to venture out (Wikipedia 2017b).

The Mayans often used bats in their stories and findings from this civilization include many carvings of the bat figure. They are often part of their paintings and drawings on vessels and other materials. They are shown as symbols of death or trickery and the underworld. In Mayan mythology, Camazotz was a deity associated with bats and human sacrifice. He was the God of the Caves and is described as having the body of a human with the head and wings of a bat. In the Popol Vuh book of the Post Classic Kiche kingdom in Guatemala's western highlands, Camazotz resided in the Bat-house located in the Underworld, a labyrinth of caves through which huge bats flew. While legends differ, he was responsible for the seventh test of initiation undertaken by the Mayan Hero Twins, Hunahpu and Xbalanque, during their trials in the underworld of Xibalba. Other stories in this culture show the bat to once be a very conceited bird itself. It was then punished and all those pretty features fell off. Out of shame and embarrassment the bat began moving about only at night, in the shadows, so that it would not be detected by other creatures (Miller & Taube 1993, Boot 2009).

However, not all legends surrounding bats are negative. In a myth from Polynesia, Leutogi, a princess of the Samoan Islands, was sent to the neighboring island of Tonga to become the second wife of the king. One day she found, rescued and nourished a baby bat. The bats did not forget her act of kindness. When she was sentenced to death by fire accused as a witch, thousands of bats filled the sky and urinated on the pyre, extinguishing the flames and saving Princess Leutogi. The Tongans then exiled Leutogi to a barren and deserted island, expecting her to soon starve to death. Leutogi, however, survived there for many years thanks to the bats, who kept her constant company, and who brought her plenty of fresh fruit and nuts for food every day. In time, Princess Leutogi became a goddess and protector of the bats, and was worshiped by her native Samoans. In China, many legends associate bats with good fortune, longevity and happiness and a group of five bats represents the five causes of happiness: wealth, health, long life, virtue and a natural death. In Chinese, the name of the bat contains the same sound as the word for happiness (fu). The ancient Chinese had also noted that their presence protected their people from the diffusion of malaria (as they eat the mosquitoes). The bat is similarly lucky in Poland, geographical Macedonia and among the Kwakiutl (North American Indians on the Pacific Northwest Coast) and Arabs. For some ancient Mayans, they symbolized Transformation and Rebirth (BatWords 2017b, Wikipedia 2017b).

In medieval Europe, bats have long been associated with witchcraft, black magic and darkness. In France, in 1332, Lady Jacaume of Bayonne was burned as a witch because swarms of bats had been seen around her home. It was commonly thought that witches used the blood of bats as an ingredient to boost the powers of their magical brews and potions. People in rural Scotland and northern England suspected bats of being

messengers between witches and the devil. During the Middle Age, residents of western Europe and England believed that bats spread disease¹. Also in Europe, in the Tyrol regions of Austria, it was believed that if a man wore the left eye of a bat, he may become invisible, and in areas of central Germany, if he wore the heart of a bat bound to his arm with red thread, he would always be lucky at cards (Crystalwind 2017).

The legends of vampires and Dracula around Transylvania have been tales passed down the generations. Such folklore is believed to have started as a means of keeping people from being out alone at night in the dark. Abraham Stoker (1847–1912) was an Irish author, who wrote the Gothic novel *Dracula* in 1897 which combined mysterious bats with a shape-shifting vampire. In Shakespeare's *Macbeth*, written around 1603–1605, the Weird Sisters (three witches) incorporate the fur of a bat in their hellbroth. In the *Tempest* (Act I, Scene 2) he had Caliban place a curse on his master Prospero, which included the line: "All the charms of Sycorax, toads, beetles, bats, light on you". The association of the fear of the night with this animal was treated as a literary challenge by Kenneth Opiel, who created a best-selling series of novels, beginning with *Silverwing* (1997), which feature bats as the central hero. But not all the bat fictional characters of the night are associated with villains. There are also heroes, such as Batman, who is considered the opposite version of the feared Dracula. The list of folklore concerning bats is endless. They have been the story line for books, comics, movies even from the early period of cinema (Bela Lugosi as Dracula in a film of 1931) and animated television series (the British Count Duckula was very famous in the late 80's). Bats appear even in video-games like *Sonic the Hedgehog* in which one of the characters is Rouge the Bat. Bats are also associated with Samhain and Halloween, with an abundance of decorative bats. The number of traditions still goes on... It is obvious that this fictional trait in modern culture, in movies and on TV, continues to give the bat the evil and sinister reputation today (BatWords 2017a, Wikipedia 2017b).

Based on the above review of selected myths, legends and fables from around the world, it can be said that quite an unambiguous pattern is being established. The bat is an animal condemned to live in the twilight zone. In most myths, it symbolizes the darkness, the underworld, the death, the evil and the supernatural, and as such it is appealing to the contemporary popular culture. But it is also treated as a symbol of duality and duplicity in ancient cultures, which can be interpreted as a sign of intelligence and wisdom, however it can also be evidence of the treacherous and double-faced nature of the bat. To others, bats can bring good luck and long life. There is no other animal with such contradictory qualities.

¹ This is most likely because of the bat's similarity to the rat which was usually blamed for the spread of the plague.

Acknowledgements

I was informed about the bat species commonly found in Greece from Panagiotis Georgiakakis, a specialist for the bats from the Natural History Museum of Crete.

References

- Apostolidis N. Ch., 1896. Επιστημονικός καθορισμός των εν Πουλολογω αναφερόμενων πτηνών. *Επετηρίς Παρανασσού*, pp. 110-137 (in greek).
- BatWords (2017a). *Bats in popular culture*: <http://www.batworlds.com/bats-in-popular-culture/> (last access 12-05-2017)
- BatWords (2017b). *Bats in mythology*: <http://www.batworlds.com/bats-in-mythology/> (last access 12-05-2017)
- Blass. F., 1888. Die griechischen und lateinischen Handschriften in alten Serail zu Constantinopel. *Hermes XXIII* (Berlin).
- Boot E., 2009. "The Bat Sign in Maya Hieroglyphic Writing: Some Notes and Suggestions, Based on Examples on Late Classic Ceramics". http://www.mayavase.com/boot_bat.pdf
- Camariano A., 1939. Poricologos si Opsarologos grelesc. Extras din "Cercetari Literare" III, Bucuresti, pp. 33-140.
- Cach M. & Dec C. (2017). *The Symbolism of a Bat. Bat in the Cultures of the World*: <http://www.gothamwdeszczu.com.pl/en/2014/12/12/the-symbolism-of-a-bat-bat-in-the-cultures-of-the-world/> (last access 12-05-2017)
- Codera F., 1891. Catalogues de la Bibliotheque de Constantinople. *Bulletin de Real Academia la Historia XIII* (4-6).
- Crystalwind (2017). *Bats-myths, folklore and fact*: <http://www.crystalwind.ca/mystical-magical/legends-fables-and-folklore/folklore/bats-myths-folklore-and-facts> (last access 12-05-2017)
- Dietz, C., D. Nill & O. von Helversen, 2014. "Handbuch der Fledermäuse Europas und Nordwestafrikas". Biologie, Kennzeichen, Gefährdung. Kosmos verlag, Stuttgart.
- Eideneier H., 2016. *Διήγησις των Τετραπόδων Ζώων και Πουλολόγος*, University of Crete editions, Heraklion (in greek).
- Kazhdan A. P., 1995. "The Oxford Dictionary of Byzantium", Oxford University Press, Oxonii.
- Krawczynski S., 1960. *O Poulologos: Kritische Textausgabe mit Übersetzung sowie sprachlichen und sachlichen Erläuterungen*, Akademie-Verlag.
- Krumbacher K., 1891. *Geschichte der Byzantinischen Literatur von Justinian bis zum Ende des Ostroemischen Reiches*. Beck, Munchen.
- Miller M., Taube K., 1993. *An Illustrated Dictionary of the Gods and Symbols of Ancient Mexico and the Maya*. Thames & Hudson, London.
- Papadopoulos-Keramefs A., 1884. *Μαυρογορδάτιος Βιβλιοθήκη*. Voutiras, Constantinople (in greek).
- Plemmenos G., 2000. *Πολιτικά debates και σάτυρα στο Βυζάντιο*. Vima (5 June 2000) (in greek).
- Sakkelion A. and I., 1892. Κατάλογος των Χειρογράφων της Εθνικής Βιβλιοθήκης της Ελλάδος. Athens (in greek).
- Tsavari I., 1987. *Ο Πουλολόγος*. Cultural Centre of the National Bank of Greece, Athens (in greek).
- Veis N.A., 1906a. "Ο Πουλολόγος του κώντικα 701 της Εθνικής Βιβλιοθήκης της Αθήνας", Part I. Noumas 209, pp. 4-7 (in greek).
- Veis N. A., 1906b. "Ο Πουλολόγος του κώντικα 701 της Εθνικής Βιβλιοθήκης της Αθήνας", Part V. Noumas 216, pp. 2-4 (in greek).
- Wagner G., 1874. *Carmina Graeca Medii Aevi*. Aedibus B.G. Teubneri, Leipzig.
- Wunch R., 1897. Zur Escorial – Handschrift Ψ- IV – 22. *Byzantinische Zeitschrift VI*, pp.158- 163.
- Zoras G.Th., 1956. "Ο Πουλλολόγος" (κατά νέαν παραλλαγήν). University of Athens, Athens (in greek).
- Wikipedia (2017a). Minyades: <https://en.wikipedia.org/wiki/Minyades> (last access 12-05-2017)
- Wikipedia (2017b). Bats – Mythology: <https://en.wikipedia.org/wiki/Bat#Mythology> (last access 12-05-2017)

Linked Data, the Semantic Web, and the Karst Information Portal

Jason Boczar¹, George Veni²

Affiliation: ¹The University of South Florida Libraries, Digital Scholarship and Publishing Librarian
4202 E. Fowler Ave, LIB 122 Tampa, FL 33620-5400 jboczar@usf.edu

²National Cave and Karst Research Institute, 400-1 Cascades Avenue, Carlsbad, New Mexico 88220 USA
gveni@nckri.org

Abstract

The Karst Information Portal (KIP) launched in 2007 with the expressed mission to provide multidisciplinary cave and karst information on a global scale. With its recent migration to the SobekCM digital platform at the University of South Florida libraries, KIP exemplifies an open access repository aimed to promote varied karst study works that are freely available to anyone in the world. KIP makes the unprecedented growth of available information accessible, searchable and organized through the semantic web or similar standards which enable proper organization and dissemination of information. Behind the facade of the portal's public access point are data linking standards that enable describing complex data structures. These standards are the backbone of digital collections and assists in making them interoperable. By using the METS and MODS standards, KIP is able to deliver important karst-related information. These standards enable interoperability for KIP with any other systems and provides easy ways to disseminate information. semantic web standards also provide ways for KIP administrators to find information to easily add to the portal, keeping it relevant and up to date. As of January 2017, KIP has 3,695 searchable items available for open use.

Keywords: Karst information portal

1. Background

A crucial goal of scholarly research is its quick and widespread dissemination. One way that research is made available is via Open Access which, as described by Peter Suber (2015), is "digital, online, free of charge, and free of most copyright and licensing restrictions." By eliminating barriers to access, such as strict copyright and monetary barriers, Open Access research is able to move more fluidly across the World Wide Web. The Karst Information Portal (KIP) makes research available freely and openly:

"The Karst Information Portal (KIP) is a growing international community seeking to create an open system for karst-related information. The goal is a web-based worldwide information network, easily accessible to scientists, researchers, and other stakeholders as a means to inform research, to enhance collaboration, and to address policy decisions in karst environments." (Suber, 2015)

In addition to creating an open environment for karst research, KIP creates a repository of articles related to karst that are not freely available. By including a record of these articles KIP can position itself as a bibliography of karst information with either full-text or hyperlinks to full-text.

By using current technologies such as digital libraries and utilizing semantic web or similar standards, the KIP administrators are able to keep records organized. This helps users and it helps administrators. Users find quality research and articles about karst. The objects in KIP, whether they are books, book chapters, articles, white papers, etc., are provided for anybody who is searching KIP for karst and cave-related information. Administrators use the technologies in KIP as important interfaces with other information search systems (i.e. Google crawlers). These technologies also help with migrating the data into future platforms.

2. The Semantic Web

The World Wide Web is a connection of elements and objects. The objects are the actual pieces that make up the general content of the internet (i.e. audio, video, images, text documents). The elements are defined as what connects the objects. Traditionally, the web has been a connection of documents and these documents were designed for humans to read (Shadbolt, 2006). HTML documents connected together with hyperlinks produce the interconnectedness that is expected of web browsing. The web of documents creates a system where, when a user searches for something in a search engine, it is up to the user to interpret the meaning of a search term (Képéklian, 2015).

The semantic web aims to help alleviate a problem of linking between documents. Tim Berners-Lee (2006), who coined the term, states that the "semantic web isn't just about putting data on the web. It is about making links, so that a person or machine can explore the web of data. With linked data, when you have some of it, you can find other, related, data." The semantic web is designed as a system that will evolve "a Web that consisted largely of documents for humans to read to one that included data and information for computers to manipulate." (Shadbolt, 2006) This has important implications for administrators of KIP as well as the findability of information in search engines.

KIP more closely aligns as a digital library than a standard webpage. The semantic web does function with digital libraries but the relationship is slightly different. Giorgio Poletti (2006) lays out the similarities well: "At a first glance, information technology and cultural assets seem worlds separated by large gaps. On the contrary it has been shown how similar the two worlds are and how their aims are convergent and their problems are comparable. The growing attention towards such themes has much greater value as it shows the need of structuring knowledge and not just to diffuse it with new materials." If the goal of the semantic web is to take the human

part of the World Wide Web and enable it to be machine readable then the connection to digital libraries becomes clear. Librarians have been contextualizing information to enable machine-readable metadata for decades.

3. KIP And The Semantic Web

Berners-Lee, Hendler, and Lassila (2001) envisioned that the “semantic web will bring structure to the meaningful content of Web pages, creating an environment where software agents roaming from page to page can readily carry out sophisticated tasks for users.” KIP occupies a small space on the Web. Nevertheless, by utilizing the ideas and practices of the semantic web, KIP is able to connect and make karst research available. Berners-Lee *et al.* (2001) also state that, “[f]or the semantic web to function, computers must have access to structured collections of information and sets of inference rules that they can use to conduct automated reasoning.” The semantic web seeks to use machine-readable metadata in order to communicate between computers. KIP accomplishes this in a few different ways.

3.1. Universal Resource Identifiers

KIP presents and provides full-text articles when possible. KIP is thus a centralized location for open access, free-to-read and share texts about karst. However, because of copyright restrictions, there is a lot of research that cannot be placed in KIP for full-text access. That does not prevent KIP from being a central repository for those points of research. By using specific URIs (Universal Resource Identifiers), mostly DOI (digital object identifier) links, KIP is able to link directly to relevant KIP articles or other forms of research.

DOIs are a piece of the semantic web. The DOI Handbook states that “Because the DOI system is designed for network awareness and interoperability, it is easy to build a wide variety of modern applications using DOIs. For example, the DOI system is used in internal processes in multiple industries, for publishing and reporting across corporate and national boundaries, and in the emerging field of semantic web applications.” (International DOI Foundation, 2015) As Shadbolt, Berners-Lee, and Hall (2006) state, “associating a URI with a resource means that anyone can link to it, refer to it, or retrieve a representation of it.” KIP utilizes many different elements and parts in order to adhere to semantic web standards.

3.2. METS and MODS

At its core, Metadata Encoding and Transmission Standard (METS) and Metadata Object and Description Schema (MODS) are XML (Extensible Markup Language) formats that preserve the bibliographic information of collections on the internet. Created by and used for digital libraries, cultural heritage, and museums, these formats give digital libraries a way to utilize XML, a key component of the semantic web, in order to provide descriptive data for different types of metadata.

“METS provides an open, standardized XML encoding format for storing the descriptive, administrative, structural and behavioral metadata needed to manage complex digital objects.” More precisely, METS “...was designed to address several fairly specific needs of the digital library community.

It needed to provide a framework for descriptive, administrative and structural metadata. It also needed to provide some flexibility for local practice with respect to descriptive and administrative metadata, while promoting standardization where possible. It had to provide mechanisms for encoding structural metadata for time-based media, in addition to support for text and still image materials.” (McDonough, 2006) A key piece of METS is that it is an open, standardized XML. The XML format is essential for the semantic web because of its flexibility and interoperability.

MODS provides a way to describe objects by using a rich, XML format. Developed as a sort of compromise between MARC 21 and Dublin Core, “MODS is intended to complement other metadata formats and to provide an alternative between a simple metadata format with a minimum of fields and little or no substructure such as Dublin Core and a very detailed format with many data elements having various structural complexities such as MARC 21.” (Guenther, 2003) MODS is able to “represent constituent parts and express their interrelationships, for example, it allows the description of journal articles and the definition of their relationship to the journal’s description.” (Bountouri, 2009) MODS is important for digital libraries because it takes into consideration two of the most popular metadata schemas, MARC 21 and Dublin Core, and attempts to make it compatible and flexible for digital objects.

3.3. Interoperability

A key feature of the web and in particular the semantic web is interoperability. Interoperability provides a way for different systems to read and work with other systems. Libraries focus on interoperability in order to maintain and adhere to the standards of preservation. By using METS and MODS, KIP is able to adequately work within the necessary parameters of interoperability. Adhering to standards set forth for digital libraries, other users and systems are able to gather information from KIP.

A key consideration for any database or repository is future migrations. Technological changes are an inevitable part of the future and addressing those concerns from the beginning helps with the process. One of four different areas described by Dulock and Cronin (2009) regarding preservation of metadata includes “providing technical metadata necessary for format migration and future access.” Having open standards that provide as much information as possible from the onset gives the easiest chance that platform migrations in the future go smoothly. METS and MODS provide these open standards by using XML because of its ability to exchange data (Broeder, 2011).

3.4. KIP and RDF

Those knowledgeable with the semantic web will by now notice that Resource Description Framework (RDF) is glaringly absent in this discussion. The platform that KIP resides on, SobekCM, does not use RDF but instead uses MODS and METS. MODS and METS are ways for digital libraries, as a distinct type of website, to operate. By using these two XML-based metadata standards, digital libraries provide ways for other machine interfaces to handle the information of the objects in the library. Basing these metadata standards on pre-

vious standards that have already been in place by librarians for decades, i.e. MARC 21, they provide a way of bridging the gap between a strict description of an object and a semantic approach that uses XML and offers interoperability. While RDF is used for many semantic web applications it's not used in SobekCM because MODS and METS offers a customized experience specific to digital libraries.

4. Conclusion

Despite not using one of the key components of the semantic web, RDF, this paper addresses the many different ways that KIP uses common ideas from the semantic web. The work done to instill the principles of the semantic web, the “enabling machines to *comprehend* semantic documents and data, not human speech and writing” (Berners-Lee, 2001), and helps create a database and repository of KIP related information. This body of knowledge is organized in a way that enables migration to new systems and increased discoverability via MODS and METS machine-readable code.

As of January 2017, KIP has 3,695 searchable items available for open use. More items are added frequently. KIP is accessed at www.karstportal.org, and welcomes contributions of new items. Items will only be posted following clear permission from the author or publisher.

References

Berners-Lee T, *et al.*, 2001. The Semantic Web. *Scientific American*, **284**(5), 34-43.

Berners-Lee T, 2006. Linked Data. W3C, <https://www.w3.org/DesignIssues/LinkedData.html> (access 7 Dec 2016)

Bountour L, Gergatsoulis M, 2009. Interoperability Between Archival and Bibliographic Metadata: An EAD to MODS Crosswalk. *Journal of Library Metadata*, **9**(1-2), 98-133.

Broeder D, *et al.*, 2011. A pragmatic approach to XML interoperability – the Component Metadata Infrastructure (CMDI). *Final Proc. Balisage: The Markup Conference*. Montréal, Canada.

Dulock M, Cronin C, 2009. Providing Metadata for Compound Digital Objects: Strategic Planning for an Institution's First Use of METS, MODS, and MIX. *Journal of Library Metadata*, **9**(3-4), 289-304.

Guenther R, McCallum S, 2003. New Metadata Standards for Digital Resources: MODS and METS. *Bulletin of the American Society for Information Science and Technology*, **29**(2), 12-15.

International DOI Foundation, 2015. *DOI Handbook: Introduction*. doi.org, https://www.doi.org/doi_handbook/1_Introduction.html (access 2 Jan 2017)

Karst Information Portal Brochure, http://digital.lib.usf.edu/design/aggregations/karst/uploads/KIP_Brochure_2015-02-25.pdf (access 25 Jan 2017)

Képéklian G, *et al.*, 2015. From the Web of Documents to the Linked Data. In: E Zimányi and RD Kutsche (Eds). *Business Intelligence*. Springer International Publishing, pp. 60-87.

McDonough P, 2006. METS: standardized encoding for digital library objects. *International Journal on Digital Libraries*, **6**(2), 148-158.

Music Library Association-Bibliographic Control Committee, 2008. Final Report. http://c.ymcdn.com/sites/www.musiclibraryassoc.org/resource/resmgr/BCC_Working_Groups/BCC2008MSWG1.pdf (access 20 Jan 2017)

Poletti G, 2006. Semantic Web and Digital Libraries. In: A Cartelli (Ed.). *Teaching in the Knowledge Society: New Skills and Instruments for Teachers*. Information Science Publishing, Hershey, pp. 271-285.

Shadbolt N, *et al.*, 2006. *The Semantic Web – The Semantic Web Revisited*. IEEE Intelligent Systems, **21**(3), 96.

Suber P, 2015. *Open Access Overview – Focusing on open access to peer-review research articles and their preprints*. <http://legacy.earlham.edu/~peters/fos/overview.htm> (access 25 Jan 2017)

(Abstract) **The PSS and the 16th year of the annual Philippine National Cave Congress.**

Eric Bontuyan

Affiliation: Philippine Speleological Society

Abstract

This a photo presentation of the Philippine Speleological Society, it's 16 years as an organization, the partnership with the Philippine government and the challenges in the Philippine political scene. Also in the presentation is the annual national Congress in different parts of the country, showcasing some of the local as well as cultural cave practices in each location, Philippine cave laws and the process and involvement of the PSS in the formulation and implementation of these laws.

Caving Activities As A Support For The Analysis Of Natural And Anthropogenic Disasters

Mario Parise^{1,2}

Affiliation: ¹Department of Earth and Environmental Sciences, University "Aldo Moro", Via Orabona 4, 70125 Bari, Italy, mario.parise@uniba.it
²National Research Council, IRPI, Bari, Italy

Abstract

Geological hazards (or geo-hazards) pose a serious threat to the built-up environment, and are the cause of severe damage and economic losses to society, especially when involving the underground setting. The final phase of evolution of instability processes may be very rapid, if not catastrophic, often resulting in casualties. In karst, the main geo-hazard is represented by sinkholes, involving both natural caves and man-made cavities. Studies on sinkholes, which necessarily have to include underground surveys, are typically performed by scientist-cavers, or by cavers acting in support of the scientists. The role of cavers is crucial, since they are able to evaluate the situations of danger existing underground, and to reach sites where non-cavers are not able to go. This allows cavers to collect a fundamental documentation of what is happening underground, which must be taken into account by authorities and people in charge of land management and planning.

Starting from several case studies and experiences in southern Italy, this contribution intends to highlight the role of cavers as support for the analysis of natural and anthropogenic disasters; the goal is also to stimulate discussions about role, duties and responsibilities of caving associations when dealing with civil protection issues.

Keywords: geological hazards, speleology, civil protection, hazards

1. Introduction

Geological hazards (or geo-hazards, as often indicated in the scientific literature) pose serious threat to the built-up environment, and are at the origin of severe damage and economic losses to society. Forecasting the occurrence of geological hazards is not an easy matter, and in many fields such an issue is still the subject of research and discussions (Guzzetti, 2016), since no methodology seems to be able to accurately predict when a hazard will occur. Especially when involving the underground setting, the final phase of evolution of instability processes may be very rapid, if not catastrophic; this often results in casualties, and economic losses to society, together with a series of never ending discussions and polemics about the possibility (or the impossibility) of forecasting the hazard.

In karst, the main geo-hazard is represented by sinkholes due to the presence of natural caves (Parise & Gunn, 2007; Parise, 2008, 2015b; De Waele *et al.*, 2011; Gutierrez *et al.*, 2014). Apart from those linked to natural karst caves, sinkholes may also occur in those urban settings where in the past man excavated in different epochs and for a number of purposes a variety of artificial cavities. Studies on sinkholes, which necessarily have to include underground surveys and observations, are typically performed by scientist-cavers, or by cavers acting in support of the scientists. The role of cavers is crucial, since they are able to evaluate the situations of danger existing underground, and to reach sites where non-cavers are not able to go. This allows cavers to collect a fundamental documentation of what is happening underground, which must be taken into account by authorities and people in charge of land management and planning.

The interaction between the anthropogenic structures at the surface (buildings, infrastructures, communication routes, etc.) and the underground is a very delicate issue (Formicola *et al.*, 2010), with a high number of variables involved. Where



Figure 1. Cavers involved in topographic survey of a natural sinkhole (photos a and b), and while entering sinkholes related to collapses within ancient underground quarries of calcarenite rock masses (photos c and d).

possible direct data from underground should always be pursued, while also taking into account the safety of the operators.

In this contribution, starting from case studies and experiences in southern Italy, the role of cavers as support for the analysis of natural and anthropogenic disasters is pointed out. It is also intended to stimulate discussions about the role, duties and responsibilities of caving associations, when dealing with civil protection issues.

2. Geological hazards linked to the underground

Different types of geological hazards may affect different localities, to varying degrees which depend upon the intensity of the hazard and the exposition of the anthropogenic elements at risk. From earthquakes to volcanic eruptions, from landslides to floods, each type derives from the local geological and structural setting and history. While knowledge of “where” a geological hazard (i.e., susceptibility) might happen is quite well developed in many situations, understanding of “when” it will happen (i.e., hazard) is still poorly understood (for definition, see Varnes, 1984).

In this framework, the geological hazards linked to the underground environment are even more difficult to be dealt with. The underground is typically hidden, so that all the processes acting there typically show their effects, only during the final generally catastrophic, phase of their evolution (Delle Rose *et al.*, 2004; Canakci, 2007; Hermosilla, 2012). Long-time processes may be acting underground, causing degradation in the rock mass, through intense weathering (Fookes & Hawkins, 1988; Zupan Hajna, 2003; Andriani & Walsh, 2006; Ghabezloo & Pouya, 2006; Calcaterra & Parise, 2010, and references therein), all of this will only be clear at the time of the hazard occurring.

The underground environment is visited only by a very few people, who frequent it occasionally. Nevertheless, the problems posed by instability processes developing and occurring underground, cannot be disregarded, since they are often the cause of losses and casualties to the society. This is true both in relation to natural karst caves, but also for those of anthropogenic origin (many different typologies of artificial cavities are included in the classification by the UIS Commission on Artificial Cavities; see Galeazzi, 2013, and Parise *et al.*, 2013a). Due to their distribution, typically below or in the proximity of built-up areas, the second category (artificial cavities) is by far the cause of most problems, at least in a country with a long history such as Italy (Fiore & Parise, 2012; Parise & Vennari, 2013).

In Apulia, south-eastern Italy, research carried out in the last decades demonstrated that the large majority of sinkholes were related to ancient underground quarries (Pepe *et al.*, 2013; Parise & Vennari, 2017), created to extract the calcarenite rocks for construction purposes, as also happened in other Italian regions (Ferrero *et al.*, 2010). The reasons why quarries were excavated underground was likely due to the need to preserve the ground surface for agricultural practices, and also due to the presence of rock layers with the best physical properties occurring at a certain depth, rather than outcropping at the surface (Parise, 2010, 2012). With time, however, once the working activity was stopped, and the quarries had been abandoned, memory of the location of the underground voids was lost, while urban expansion often moved toward the sites originally utilized for quarry extractions. Therefore, buildings and communication routes began to be built just above very complex networks of underground cavities, with consequent problems for public safety.

Due to an increasing number of events which occurred since the 1990s, several actions were started by the Basin Authority of Apulia (the body in charge of managing the land, with specific regard to geo-hydrological hazards). The establishment

of a new building code required detailed geological studies in areas determined to be at risk in order to verify and mitigate any hazardous situations (Caggiano *et al.*, 2007; Barnaba *et al.*, 2010).

3. The role of cavers

Cavers are, by definition, people who explore and visit the underground. Their capability to move in underground environments in safety, together with the great experience acquired in continuous activity of explorations in difficult environments, make them a very precious resource for ascertaining what is happening underground, and if problems are likely have to be registered at the surface. Notwithstanding this experience, and the official role cavers have in many rescue operations (i.e., saving human lives after earthquakes, recovering people from mountains and impervious conditions, etc.), their role is not always fully appreciated. In several cases the local authorities, or the people in charge of management of the emergency phase, decide not to involve cavers, or to assign them a secondary role.

When dealing with the underground, cavers must necessarily be fully involved. First, the goal must be to understand the real development of the natural cave, or of the artificial cavity, at the origin of the problem: where it extends, what are its morphometric features (length, width, height), and how it is correlated with the above buildings and infrastructures. All of this requires a detailed topographic survey (Fig. 1), which typically cannot be completed underground with the classical topographic technique used at the surface. When passages are very narrow or limited, and the progression made difficult by breakdown processes, the presence of water, or of different types of wastes, the speleological approach must be followed. In the last decades, cavers have greatly progressed in the precision and reliability of their topographic surveys, so that nowadays they are able to produce very detailed maps, linked to surveillance points outside of the cave, and therefore able to be properly geo-referenced (Martimucci & Parise, 2012).

It is worth mentioning the sequence of events that were registered at Gallipoli (southern Apulia) on March 29, 2007, when a sinkhole opened in Via Firenze, due to collapse of the roof of a wide calcarenite quarry, located at a few meters from the surface (Delle Rose, 2007; Parise, 2012). Notwithstanding the recommendations by cavers and sinkhole experts, the local authority decided to fill the sinkhole with rubble materials, without carrying out a detailed survey with the goal to understand the real development of the cavity, and to check the likely interactions with the buildings above. As a consequence of the heavy weight of the trucks used for carrying the infilling materials, the sinkhole enlarged (luckily, with no consequence for the driver), reaching the corner of a 4-storey building, and threatening its stability. Only at that stage, was it eventually decided to proceed with a different approach, through specific investigations by cavers.

The cavers' work, however, does not stop with the topographic survey. Observation of the main features produced by the instability (Parise, 2013, 2015a), both in terms of those already occurred, and those with the potential to occur is fundamental to allow geologists and engineers to fully comprehend what is happening, and what sectors of the cave would be more prone to future instability (Liu *et al.*, 2000; Swedzicki,



Figure 2. Mapping the instability features observed underground: in this case, continuous crack within a pillar, after occurrence of a sinkhole.



Figure 3. Data collection in the underground environment: above, measuring the attitude of joints (first two pictures) and producing the topographic survey of the cave (picture to the right); below, using the Schmidt hammer (left) and performing the Barton test (right) for the geo-mechanical characterization of the carbonate rock mass.

2001; Hutchinson *et al.*, 2002; Waltham & Swift, 2004). Further, these pieces of information are necessary to properly reconstruct the geological and geotechnical models, aimed at developing 2D and 3D analyses of the study site (Hatzor *et al.*, 2002; Waltham & Lu, 2007; Parise & Lollino, 2011), while also eventually designing the necessary interventions and stabilization works. To this aim, sketches, photographs and videos produced by caver teams are of crucial importance (Fig 2).

For instance, the long sinkhole history at Altamura (central Apulia), where tens of sinkholes have opened in the last decades due to underground quarries (Pepe *et al.*, 2013), the activity by cavers was of great importance to document the different phases of infilling the voids. This was a necessary stage to ensure the stability of the area, and to facilitate its full reclamation, since future expansion of the town was planned.

Cavers are familiar with breakdown materials, falls and collapses (White & White, 1969; Klimchouk & Andrejchuk, 2002; White, 2005; Iovine *et al.*, 2010). In many caves, they walk and move over these materials, which have covered the real pavement of the cave system with meters-high piles of rocks. In several cases, exploration of the cave system has proceeded thanks to narrow passages within breakdown materials. These experiences, as well as the ability to identify the most dangerous sites, are of great importance when cavers are involved in underground surveys in areas affected by sink-

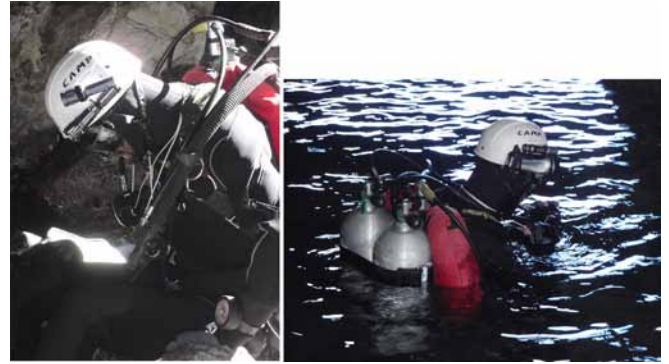


Figure 4. Cave scuba diver preparing for the survey in a coastal cave.

holes, and allow cavers to collect the necessary information in order to fully understand the mechanisms acting on the walls and the roof of the cavity (Kowalski, 1991; Tharp, 1995; Diederichs & Kaiser, 1999; Andrejchuk & Klimchouk, 2002; Parise & Lollino, 2011).

When properly trained, or if accompanied by geologists, cavers may also directly take measurements and data (Fig 3), including strata and fault attitude, stratigraphic observations, geo-mechanical properties of rock masses by means of tools such as the Schmidt hammer (for measurement of the in situ compressive strength) or the Barton profilometer (for estimating the joint roughness for peak shear strength). For such measurements, the best option is to have a caver geologist in the team.

Further, when dealing with flooded caves, the investigation is even more complicated, and requires expert cave dives to be performed (Fig 4). This has been object of several experiences in Apulia, both along coastal areas, in order to investigate marine and karst caves, as at Polignano a Mare on the Adriatic coast (Parise *et al.*, 2013b), and inland, to explore flooded caves linked to the development of sinkholes at the surface, as in the case of Torre Castiglione near Porto Cesareo on the Jonian coastline (Bruno *et al.*, 2008; Basso *et al.*, 2013; Margiotta *et al.*, 2013, in preparation).

4. Conclusions

Italy has a very long history of civilization and ancient settlements, which is at the origin of the large number of artificial cavities in the country. These, combined with the diffuse karst areas, and the thousands of related natural caves, determines a high vulnerability to sinkholes for many sectors of the Italian territory. Management of these geological hazards cannot be pursued without taking into the due consideration the role played by cavers, and the remarkable contribution they might add to investigate and solve the problems. In southern Italy, and in particular in the Apulia region on many occasions over the last two decades the actions by cavers have been fundamental for the correct approach to investigate and understand sinkhole problems. Nowadays this is well acknowledged also by the main institutions, including the Civil Protection Service of Apulia Region and the Basin Authority of Apulia.

References

- Andrejchuk V, Klimchouk A, 2002. Mechanisms of karst breakdown formation in the gypsum karst of the Fore-Ural regions, Russia (from observations in the Kungurskaja Cave). *Int. J. Speleol.*, **31**(1/4), 89–114.
- Andriani GF, Walsh N, 2006. Physical properties and textural parameters of calcarenitic rocks: qualitative and quantitative evaluations. *Eng. Geol.*, **67**, 5–15.
- Barnaba F, Caggiano T, Castorani A, Delle Rose M, Di Santo AR, Dragone V, Fiore A, Limoni PP, Parise M, Santaloia F, 2010. Sprofondamenti connessi a cavità antropiche nella regione Puglia. *Proc. 2nd Int. Workshop "I sinkholes. Gli sprofondamenti catastrofici nell'ambiente naturale ed in quello antropizzato"*, Rome, 3-4 December 2009, 653-672.
- Bruno E, Calcaterra D, Parise M, 2008. Development and morphometry of sinkholes in coastal plains of Apulia, southern Italy. Preliminary sinkhole susceptibility assessment. *Engineering Geology*, **99**, 198-209.
- Basso A, Bruno E, Parise M, Pepe M, 2013. Morphometric analysis of sinkholes in a karst coastal area of southern Apulia (Italy). *Environmental Earth Sciences*, **70**(6), 2545-2559.
- Caggiano T, Di Santo AR, Fiore A, Palumbo N, 2007. Attività dell'Autorità di Bacino della Puglia per l'individuazione, il censimento e la pianificazione degli interventi per la messa in sicurezza dei territori a rischio sprofondamento per la presenza di cavità sotterranee. *Geologi & Territorio*, 4-2006/1-2007, 32-34.
- Calcaterra D, Parise M (Eds.), 2010. Weathering as a predisposing factor to slope movements. *Geol. Soc. London, Eng. Geol. Sp. Publ.* **23**, 233.
- Canakci H, 2007. Collapse of caves at shallow depth in Gaziantep city center, Turkey: a case study. *Eng. Geol.*, **53**, 915–922.
- Delle Rose M, 2007. La voragine di Gallipoli e le attività di protezione civile dell'IRPI-CNR. *Geologi & Territorio*, 4/2006-1/2007, 3-12.
- Delle Rose M, Federico A, Parise M, 2004. Sinkhole genesis and evolution in Apulia, and their interrelations with the anthropogenic environment. *Natural Hazards and Earth System Sciences*, **4**, 747–755.
- De Waele J, Gutierrez F, Parise M, Plan L, 2011. Geomorphology and natural hazards in karst areas: a review. *Geomorphology*, **134**(1–2), 1–8.
- Diederichs MS, Kaiser PK, 1999. Tensile strength and abutment relaxation as failure control mechanisms in underground excavations. *Int. J. Rock Mech. Min. Sci.*, **36**, 69–96.
- Ferrero AM, Segalini A, Giani GP, 2010. Stability analysis of historic underground quarries. *Comput. Geotech.*, **37**, 476–486.
- Fiore A, Parise M, 2012. Sprofondamenti connessi a cavità di origine antropica in Puglia. *Geologia dell'Ambiente*, **2**, 41-45.
- Fookes PG, Hawkins AB, 1988. Limestone weathering: its engineering significance and a proposed classification scheme. *Quart. J. Eng. Geol.*, **21**, 7–31.
- Formicola W, Gueguen E, Martimucci V, Parise M, Ragone G (2010). Caves below quarries and quarries above caves: problems, hazard and research. A case study from southern Italy. *Geol. Soc. Am. Abstr. with Program*, **42**(5).
- Galeazzi C, 2013. The typological tree of artificial cavities: a contribution by the Commission of the Italian Speleological Society. *Opera Ipogea*, **1**, 9–18.
- Ghabezloo S, Pouya A, 2006. Numerical modeling of the effect of weathering on the progressive failure of underground limestone mines. In: Van Cotthem A, Charlier R, Thimus JF and Tshibangu JP (Eds). *Eurock 2006 – Multiphysics coupling and long term behavior in rock mechanics*. Taylor and Francis, London, 233–240.
- Gutierrez F, Parise M, De Waele J, Jourde H, 2014. A review on natural and human-induced geohazards and impacts in karst. *Earth Science Reviews*, **138**, 61-88, doi: 10.1016/j.earscirev.2014.08.002.
- Guzzetti F, 2016. Forecasting natural hazards, performance of scientists, ethics, and the need for transparency. *Toxicological & Environmental Chemistry*, **98**(9), 1043-1059.
- Hatzor YH, Talesncik M, Tsesarsky M, 2002. Continuous and discontinuous stability analysis of the bell-shaped caverns at Bet Guvrin, Israel. *Int. J. Rock Mech. Min. Sci.*, **39**, 867–886.
- Hermosilla RG, 2012. The Guatemala City sinkhole collapses. *Carbonates and Evaporites*, **27**(2), 103–107.
- Hutchinson DJ, Phillips C, Cascante G, 2002. Risk considerations for crown pillar stability assessment for mine closure planning. *Geotech. Geol. Eng.*, **20**, 41–63.
- Iovine G, Parise M, Trocino A, 2010. Breakdown mechanisms in gypsum caves of southern Italy, and the related effects at the surface. *Zeitschrift fur Geomorphologie*, **54** (suppl. 2), 153–178.
- Klimchouk A, Andrejchuk V, 2002. Karst breakdown mechanisms from observation in the gypsum caves of the Western Ukraine: implications for subsidence hazard assessment. *Int. J. Speleol.*, **31**(1/4), 55–88.
- Kowalski WC, 1991. Engineering geological aspects of different types of karst corrosion and fracture generation in karst masses. *Bull. Int. Ass. Eng. Geologists*, **44**, 35–46.
- Liu D, Wang S, Li L, 2000. Investigation of fracture behavior during rock mass failure. *Int. J. Rock Mech. Min. Sci.*, **37**, 489–497.
- Margiotta S, Negri S, Pagliara A, Parise M, Quarta TAM, 2013. Combining geological and geophysical surveys with cave explorations for the assessment of the sinkhole susceptibility in coastal areas. *Geophysical Research Abstracts*, **15**, 8185.

- Martimucci V, Parise M, 2012. Cave surveys, the representation of underground karst landforms, and their possible use and misuse. *20th International Karstological School "Karst forms and processes"*, Postojna, 18-21 June 2012, Guide Book & Abstracts, 69-70.
- Parise M, 2008. Rock failures in karst. In: Cheng Z, Zhang J, Li Z, Wu F and Ho K (Eds). *Landslides and Engineered Slopes. Proc. 10th Int. Symp. on Landslides*, Xi'an (China), June 30– July 4, 1, 275–280.
- Parise M, 2010. The impacts of quarrying in the Apulian karst. In: Carrasco F, La Moreaux JW, Duran Valsero JJ and Andreo B (Eds). *Advances in research in karst media*. Springer, 441–447.
- Parise M, 2012. A present risk from past activities: sinkhole occurrence above underground quarries. *Carbonates and Evaporites*, 27(2), 109–118.
- Parise M, 2013. Recognition of instability features in artificial cavities. In: Filippi M, Bosak P (Editors), *Proceedings 16th International Congress of Speleology*, Brno, 21-28 July 2013, 2, 224-229.
- Parise M, 2015a. A procedure for evaluating the susceptibility to natural and anthropogenic sinkholes. *Georisk*, 9(4), 272-285, DOI:10.1080/17499518.2015.1045002.
- Parise M, 2015b. Karst geo-hazards: causal factors and management issues. *Acta Carsologica*, 44(3), 401-414.
- Parise M, Lollino P, 2011. A preliminary analysis of failure mechanisms in karst and man-made underground caves in Southern Italy. *Geomorphology*, 134(1-2), 132–143.
- Parise M, Gunn J, (Eds), 2007. *Natural and anthropogenic hazards in karst areas: Recognition, Analysis and Mitigation*. Geol. Soc. London, Special Publications, 279, 202.
- Parise M, Vennari C, 2013. A chronological catalogue of sinkholes in Italy: the first step toward a real evaluation of the sinkhole hazard. In: Land L, Doctor DH, Stephenson B (Eds), *Proc. 13th Multidisciplinary Conf. on Sinkholes and the Engineering and Environmental Impacts of Karst*, Carlsbad (New Mexico, USA), 6-10 May 2013, National Cave and Karst Research Institute, 383-392.
- Parise M, Vennari C, 2017. Distribution and features of natural and anthropogenic sinkholes in Apulia. In: Renard P, Bertrand C (Eds), *Advances in the hydrogeology of karst and carbonate reservoirs*. EuroKarst 2016, Neuchatel. Springer, ISBN 978-3-319-45464-1, 27-34.
- Parise M, Galeazzi C, Bixio R, Dixon M, 2013a. Classification of artificial cavities: a first contribution by the UIS Commission. In: Filippi M, Bosak P (Editors), *Proceedings 16th International Congress of Speleology*, Brno, 21-28 July 2013, 2, 230-235.
- Parise M, De Pasquale P, Martimucci V, Meuli V, Pentimone N, Pepe P, 2013b. Grotta della Rondinella a Polignano a Mare: un progetto di ricerca della Federazione Speleologica Pugliese. In: Cucchi F, Guidi P (Eds.), *Proc. XXI National Congress of Speleology*, Trieste, 2-5 June 2011, 437-448.
- Pepe P, Pentimone N, Garziano G, Martimucci V, Parise M, 2013. Lessons learned from occurrence of sinkholes related to man-made cavities in a town of southern Italy. In: Land L, Doctor DH, Stephenson B (Eds.), *Proc. 13th Multidisciplinary Conf. on Sinkholes and the Engineering and Environmental Impacts of Karst*, Carlsbad (New Mexico, USA), 6-10 May 2013, Natl. Cave and Karst Research Inst., 393-401.
- Swedzicki T, 2001. Geotechnical precursors to large-scale ground collapse in mines. *Int. J. Rock Mech. Min. Sci.*, 38, 957–965.
- Tharp TM, 1995. Mechanics of upward propagation of cover collapse sinkholes. *Eng. Geol.*, 52, 23–33.
- Varnes DJ, 1984. *Landslide hazard zonation: a review of principles and practice*. Unesco Press, Paris.
- Waltham T, Lu Z, 2007. Natural and anthropogenic rock collapse over open caves. In: Parise M and Gunn J (Eds.). *Natural and anthropogenic hazards in karst areas: recognition, analysis and mitigation*. Geol. Soc. London, sp. Publ. 279, 13–21.
- Waltham AC, Swift GM, 2004. Bearing capacity of rock over mined cavities in Nottingham. *Eng. Geol.*, 75, 15–31.
- White EL, 2005. Breakdown. In: Culver DC and White WB (Eds.). *Encyclopedia of caves*. Elsevier, Amsterdam, 56–60.
- White EL, White WB, 1969. Processes of cavern breakdown. *Bull. Natl. Speleol. Soc.*, 31 (4), 83–96.
- Zupan Hajna N, 2003. Incomplete solution: weathering of cave walls and the production, transport and deposition of carbonate fines. *Carsologica*, Postojna-Ljubljana, 167.

(Abstract) **Managing WNS-related Increases in Bat-Human Contacts at Mammoth Cave National Park, KY, USA**

Rickard Stanley Toomey

Affiliation: Toomey National Park Service (US), Mammoth Cave National Park; Cave Research Foundation

Abstract

Since early in the White-nose Syndrome (WNS) response in North America, people have discussed the possibility that altered bat behaviour caused by this disease would lead to increased contact between bats and human (with potential increases in rabies prophylaxis). In the winters of 2013-14, 2014-15, and 2015-16, Mammoth Cave National Park experienced marked increases in bat-human contacts that can be attributed to altered bat behaviour. In 2014 twelve people came in contact with a bat; eleven of these occurred between January and April, and most resulted from a bat flying into a person on a cave tour. In 2015 the pattern was similar, with seven bat-human contacts between January and April. In 2016 two bat-human contacts occurred between January and April. Over the three years most of these contacts occurred inside Mammoth Cave, but four occurred on the surface. Previous to these years, recorded bat contacts averaged fewer than one per year. The fact that the majority of contacts are during the winter, while the majority of visitation is in the summer supports the conclusion that the increased contacts relate to WNS.

The increased bat-human contacts caused the park to request assistance from a National Park Service (US) Disease Outbreak Investigation Team comprised of state and federal wildlife health and public health personnel as well as park staff. In response to the contacts, in consultation with the team, the park took several actions. These included 1) improving information for visitors about bats behaving unusually, 2) developing standardized procedures for bat-human contacts, 3) coordinating response to contacts with state and federal public health officials, 4) implementing increased monitoring of bats on tour routes and in developed areas, 5) deploying kits to allow employees to safely respond to downed bats, and 6) increasing the number and range of park personnel with rabies pre-exposure vaccinations.

Can the UIS also become a sports body and why should it?

Arjan van Waardenburg

Affiliation: Speleo Nederland

1. Introduction

The UIS functions mainly as an organization of scientist. However, the great majority of its affiliated members are sportive or recreational cavers. With sport comes competition. Both recreational and sportive caving are greatly neglected by the UIS.

And now the UIS itself is confronted with upcoming competing organisations. Only one of them can become the internationally recognised body for sportive caving. The UIS has no ambition to become that body, but our competition has. Simply because it opens up the way to funding your activities. Once this new internationally recognised body has come into being, the sportive or recreational cavers will drain away from the UIS to that new body. Not only because it is where the money will be, but also because their specific interests come first, not last as in the UIS. That new body, in turn, will have no interest in science. So in the long run, the bond between scientists and cavers will be lost. Two completely different cultures will develop and it will be much harder for the scientist to team up with cavers to execute his research (see also "Restructuring the UIS").

2. Changes needed

Being the internationally recognised body for sportive caving equals being affiliated with SportAccord. To become a member of SportAccord, the UIS must fulfil a list of requirements. There are two ways accomplish this. The easy way is to amalgamate with our competition. They will provide the manpower to take the necessary steps. Unfortunately, the UIS board has blocked this path by alienating the people in question. Perhaps for good reasons, but surely a short-sighted policy. And faithful to the adagium "if you cannot join them, beat them" they are now going there own, separate way.

So we are left to our own resources. At this point in time (2017) the UIS is still at an advantage, we represent 55 countries on all continents. But this will not last for long. For a sports organization it is relatively easy to find funding and sponsors. So if you are a sports official, you can make a living on it. If you are an official of an emerging sport, there is a career waiting for you. So, now the Russians have proven that a sports caving organization is economical feasible, others will follow. And the bigger the sport, the more money can be made. So its natural tendency is not only to grow locally, but also to cooperate internationally. Ten years from now, or perhaps twenty, they will gain SportAccord membership.

Unless we beat them to it. Only one organization per sport can be a SportAccord member.

3. Steps to be taken

Unfortunately, we are overtaken by developments within SportAccord. They are revising their application procedures. So the list I prepared is now obsolete, but nevertheless I can make an educated guess of what will be needed:

There will be a definition of sport. The definition is likely to include competition (although CMAS (scuba diving), UIAA (mountaineering) and ILS (life saving) are members.

The definition may require physical exercise (although FIDE (chess) and WBF (bridge) are members). If so, we will be restricted to disciplines as 100m SRT, obstacle courses, etc. If not, we can also include disciplines like map making. We can also invent new disciplines e.g. pitch rigging, with points for efficiency, speed, safety, etc.

For each discipline we will need to organise national and international competitions and make a rulebook.

Only worldwide organizations are allowed. There will be a requirement like "at least 40 affiliated national organisations on at least 4 continents".

We will have to comply with standards for sports in general, like having a disciplinary committee or doping controls.

All in all there is some work to do. But it does not need to be the board (of mainly scientists) that have to take on the brunt of the work. Let us set up a sports section or committee and we have a reservoir of 30.000+ cavers to man it. Surely we can find some that are enthusiastic and competent.

4. On finances

The current situation is that the UIS board's policy to block national organizations form serious funding. Two examples France is eligible for € 7.000,- in grants if only caving would be a non-Olympic sport. The Netherlands are eligible for €9.500,- in grants if only the UIS would be a member of SportAccord.

The reason the board gives for blocking a SportAccord membership is that the UIS cannot afford the SportAccord membership fee, 4000,- CHF. Even after a sponsor was found to bridge the first two years of membership, an additional condition was raised: the sponsorship had to be made permanent.

It is easy to see this is bad judgement: there simply is a profit to be made here. The first two years are for free. For the next few there could be an arrangement with France and the Netherlands to pay the dues. In the longer term this is unfair, so a financial restructuring of the UIS will be necessary (see "Restructuring the UIS")

The above course of events illustrates a mayor defect in the UIS organisation. It is not that the board actively wants to damage recreational caving. The problem is that ivory towers have only small windows. The board misses out on social developments. When the UIS was founded, people where inclined to follow authorities without criticism. Cavers followed professors. Today an alumnus no longer has authority. The organisation of the UIS should develop to reflect that fact. If the UIS cannot accommodate the developing needs of cavers, they will start their own organisations, apart from the

UIS. And de fruitful cooperation between the two strains of speleologist will greatly decrease, to the detriment of science.

5. Conclusion

It is worthwhile to become a SportAccord member. It will bring facilities to the sporting caver that are, as yet, only wanted by a few, but will be wanted by many in the future. As it takes time to get organised, it pays to prepare for that future. So develop the UIS to become "SportAccord ready". Once there, it is simply economical to also become a member.

Restructuring the UIS

Arjan van Waardenburg

Affiliation: Speleo Nederland

1. Introduction

In speleology the scientist is dependent on the explorer. The explorer, in turn is dependent on the caver. The first dependency is not uncommon, e.g. the archeologist cannot execute an excavation without employing a large number of volunteers and the biologist will never know about the numbers and diffusion of birds without the bird watching community. The second dependency is unique in science; there is not other branch of science that depends on a sport for acquiring a mayor part of its knowledge.

Generally speaking, there are two careers in speleology. The scientist starts out as geologist, environmentalist, etc. who gets an interest in caves. He is formally educated in his field and makes a living from it. Many of them are not well versed in exploration technique and even if they are, they are still very dependent on amateurs to form a team.

On the other end of the spectrum, there is the caver. He starts caving for various reasons: e.g. recruitment by friends or clubs, sigh of adventure or even trill seeking. To him, caving is foremost a sport. Most of them remain at that level, but a limited percentage progresses to a semi scientific level, e.g. exploration and map making. A few even become scientists.

An example to illustrate this is Carlsbad Caverns NP. Some caves in the park are reserved for scientific use only. Scientists can get access, cavers cannot. As a result, those caves remain largely unmapped, unexplored, and thus un-researched. While having the same potential as (not reserved) Lechuquilla, the number of publications is limited to say the least. One could arguably state that those caves that are reserved for scientific use only, are, in fact, lost to science.

The conclusion must be that speleological research will be seriously hampered if the link with the sportive caver is lost. (And the reverse is thru as well: if you are ignorant of geology or hydrology, you will not find much new cave.)

And the beginning of just that rift between science and sport caving is now evident for some years.

Sport has some advantages above science. Everybody understands the basic concepts of sport in general: physical exercise, good for your health, competition, being the best and being a sport hero. Science on the other hand, is often perceived as incomprehensible by definition and therefore boring. So when an entrepreneur wants to advertise his product, he will look for a sport, not a science. The caver is the new Marlboro man.

From an administrative point of view, sport promotes a more healthy population. Subsidization of sport, therefore, can be a means to reduce the cost of public health. The return on investment for a speleological research project is far less obvious to most politicians.

In short, there is much more money in sport than in science.

When the UIS was founded, there was not so much distinction between amateurs and professionals. Since then, the professionals have professionalized and the amateurs have attracted a large number of recreational cavers. Nowadays, the majority of UIS associated individuals caves just for the sport of it. The UIS, in its organization as well as in its politics, reflects a situation that no longer exists.

2. Ideas to adapt the organization.

The current situation is "one country, one vote". So e.g. Luxembourg is just as influential as the USA. This does not seem right. Let us go for "one man, one vote". Every country can still have one delegate, but when it comes to voting, that delegate can cast as many votes as there are associated cavers / speleologists in his country. The consequence will be that every country will have to set up a national organization that keeps track of a list of members, so as to establish the numbers of votes that country can cast. And that list must be made available to the UIS to check.

The problem with democracy is in the dictatorship of the majority. The scientists will be vastly outnumbered by the recreational cavers. So the scientific interest needs some form of guaranteed protection. This can be achieved by dividing the UIS in two statutory sections, science and caving. Each section decides its own internal business, any proposal concerning both sections, needs a majority vote from both sections. To prevent the cavers from taking over the science section we need to set some criterion to qualify for scientific membership, say, at least three scientific publications in the last five years. Other criteria are also possible: being alumni or scientific employee in speleology or a related field.

3. On national organizations

This new structure implies national organizations, as opposed to the current situation, where any individual can become a delegate, and it is left to him if and how he consults the people he represents. As such, it is a step to a more professionally organized UIS. Ideally, every country is represented by a single, national body, structured similar to what is proposed here for the UIS. There are two reasons to deviate from that situation: over-organization and under-organization.

In current situation, an over-organized country, with two (or more) competing national organizations, cannot be represented. Two anecdotes: Remember the conference in Athens? The host country, Greece could not decide on a single delegate. Remember Brno? Argentina send two delegates and it was the single, personal decision of one of them that Argentina could be represented at all. Both where shameful situations and need to be rectified.

The proposed set up offers an elegant solution for these situations: each delegate can cast as many votes as the number of individuals he can show to represent.

On the other end of the spectrum there are a number of countries where speleologists and/or cavers are few and far between. Setting up and maintaining a full fledged organization would be too heavy a burden for them. The UIS must respect that. There will always be speleological emerging countries and they must not be hampered by requirements they cannot (yet) fulfill. Also, there will be cultural differences that must be respected too. The UIS can promote organization by setting guidelines, or even subsidize some actions to organize a country.

So the idea is to promote organization, unification and professionalization, but not to require it.

4. On finances.

The current state of affairs is that the UIS is greatly underfunded. Although the basic membership fee is € 300,-, many countries pay only € 50,- and as there are only some 55 member states, it is easy to see there cannot be sufficient funding to run a serious organization.

There is another way to go about funding: “one man, one dollar” can be the guiding principle. A conservative guess of 30.000 cavers worldwide brings a multiplication of the budget. However, for national organizations of the poorer countries, this still may be too much of a burden. So it makes sense that the annual fee for each country should not only be directly proportional to the number of affiliated members, but also to the relative living standards of the member countries. A simple and widely accepted way to compare living standards is to use its GDP at PPP per capita. GDP is the gross domestic product or value of all final goods and services produced within a nation in a given year. A country's GDP at PPP (purchasing power parity) is the sum value of all goods and services produced in the country valued at prices prevailing in a single reference country and its currency. The CIA World Factbook published these numbers for all nations and is updated on a weekly basis.

So the annual fee for each country can be calculated as follows: First, set a budget. Then, for each member country, calculate the product of its GDP at PPP per capita and the number of affiliated members. Add the products of all countries. Divide the budget by this sum, then, for each country, multiply the outcome with the product above.

Yes, the individual caver now has to pay for the UIS. But it will be about the price of a penlight. If you cannot afford to buy an extra penlight a year, can you be a caver at all?

5. Conclusion

Currently sportive and recreational caving is a subordinate activity within the UIS, while they are the main source of its funding. This is unfair and leading to a rift between sportsmen and scientists, to the detriment of both. Reorganizing the UIS along the above outlines can remedy this.

6. How to proceed

If the assembly chooses to reorganize the UIS, it is impractical to request the board to devise complete new statutes for approval on the next congress. As the devil is the detail, too many delegates will find something “unacceptable”. And again we will have lost four years. What we need to do is to set up a small committee that will work out a general outline, send it to all delegates for comments and alternative proposals, diffuse those to all delegates, and give them a deciding vote over conflicting proposals. Then the committee will work out the new version in more detail and initiate a new round of discussion and voting. In, say, four rounds we will have a new statute that is in all parts the most widely carried solution. And ready for approval on the next congress.

Is in cave competition really unacceptable?

Arjan van Waardenburg

Affiliation: Speleo Nederland

1. Introduction

In recent years we see an increase in the use of caves for sportive purposes. People want to pitch themselves against the cave, like a climber against the rock face. Or, they want to prove they are the best caver by setting a record time for going to the bottom and back. It stands to reason that setting speed records conflicts with conservation: there is no time to carefully avoid touching vulnerable items in the cave.

The UIS has responded, first by tightening the code of ethics, then by denying the culprits access to UIS activities. It did not work. They now run their own organization and carry on as before. I would say this was to be expected in advance. So the short term material consequences of this policy are non-existent. However, morally we have won the battle: the UIS can claim to be the champion of cave conservation. But the price is high: we have created an alienated, hostile, competing organization.

2. An alternative policy

What if we would have accepted in cave competition? Would it not have been possible to give some direction to their activities? Lead them to caves that are less vulnerable or already worn out?

Belgium has a system that maintains a (short) list of wild caves that are deemed fit for guided trips for the general public. Only caves that are relatively safe, invulnerable and invaluable appear on that list. A similar policy could have been applied to in cave competition. We lose the high moral ground, but, in the long run, we will save more caves.

We are a bit incongruous about cave conservation. We lose caves on a daily basis to some form of commercial exploitation. And the UIS rarely takes any action against it; if any action is taken, it is almost always done by local cavers. (Note: those are the sportsmen, not the scientists.) UIS also supports large scale events, e.g. Eurospeleo 2016. More than a 1000 trips were made, a great success, according to some board members. Even if each and every participant just tiptoed around, the total impact must be considerable. As conservation purists, how can you justify that? The UIS is hardly the Greenpeace of the caves.

A more mathematical approach is to calculate how many caves we lose to various forms of exploitation. How many are lost to mining, quarrying, flooding by dams, conversion to habitations or show caves, etc. etc.? And how many can we expect to lose to in cave competition? We should at least have some good estimates about these numbers. As they do not exist (to my knowledge) how can we justify that it is only in cave competition that we condemn?

3. Conclusion

Why not strive to a relation with the in cave competitors similar to the relation with ISCA? Converting a cave to a show cave does a lot of damage to the cave, from blasting speleothems to lampenflora. However, cooperation in a positive atmosphere has given them the tools and strengthens their motivation to minimize impact. The UIS should try the same path with in cave competition.

Author Index Volume 2

- Nadia , Aamoum, 2
Angel A, Acosta-Colón, 107
Sverre, Aksnes, 285
Mahmoud Ahmed, Al Shanti, 3, 4, 184
Ahmad, Al-Malabeh , 232
Cahyo, Alkantana, 385
V., Amendoeira, 310
Bernard, Angeli, 70
Konstanina, Aretaki, 386
Martin, Arriolabengoa, 291
Lasha, Asanidze , 242
Yemane, Asmerom , 331, 336
Roman, Aubrecht , 202
Marek, Audy , 202
Giovanni, Badino , 206, 322
P., Bajo, 210,327
Silvia P., Barredo Codesal , 20
Ingo, Bauer, 118
Daniel, Ben-Tov , 13
Loredana, Bessone , 194, 352
Roberto, Bixio , 237
Lee Anne , Bledsoe, 5
Jason, Boczar , 261
Terry, Bolger , 156
Corrado, Bongiorno , 138
Eric, Bontuyan, 394
Pavel , Bosak, 34, 275
Anton, Brancelj , 66
Greg, Brick , 198, 249
Gilles, Brocard , 299
Manfred, Buchroithner , 141, 145, 148, 287
Kelsey, Budahn , 250
Shannon, Burnett, 9
Vladimir , Buslov, 13
José Maria, Calaforra , 271, 322
Marco, Camorani, 87, 137
William , Carroll, 287
Miha, Čekada , 108
Weihai, Cheng, 48
Veronica, Chiarini , 255, 327
Nino, Chikhradze , 242
Emily B.J. , Coffey, 194
Andrea, Columbu , 255, 354
I., Couchoud, 327
Leandro Cosme Oliveira, Couto , 12
Andrea, Croskrey, 215
John, Cugley , 331
Ilenia Maria, D'Angeli , 291
Sven, Dahlgren, 286
Jianling, Dai , 57
Luca, Dal Molin, 87
Isabela, Dalle Varela , 382
R.S. , Dbar, 61
Ada, De Matteo, 137
Antonio, De Vivo , 362
Jo, De Waele , 223, 255, 322, 327, 352, 354
Umberto, Del Vecchio, 137
Rhawn F., Denniston , 331
Joel, Despaigne, 50
Toby J., Dogwiler , 308
Russell N. , Drysdale, 255, 327, 358
Yuri V., Dublyansky , 335
Oana-Alexandra, Dumitru , 336
John, Dunkley , 156
Lawrence R., Edwards, 335
Ya.A., Ekba, 61
István, Eszterhás , 157
Trevor, Faulkner, 260, 270
Ric, Federico, 264, 309
Daniela, Festi , 87
Petronela, Filipčíková , 202
Adriano, Fiorucci , 210
Joan J., Fornós, 336
Paolo, Forti , 255, 322, 362
Andrew, Francis , 308
S., Frisia , 327
Amos, Frumkin, 13, 17
Ida Marie, Gabrielsen, 285
Carla, Galeazzi , 237
Yongli, Gao , 57
Davor, Garašić , 26, 30
Mladen, Garašić , 26, 30
Fernando, Gázquez , 271
Alena, Gessert, 39
Mario, Gisbert , 250
Gaetano, Giudice , 138
Melisa, Glock Galli , 20
Mateusz, Golicz, 112
Petra, Gostinčar , 108
E.A., Grabenko, 61
Chris, Groves , 5, 93
Stefan, Gumhold , 141
Francisco, Gutiérrez , 250
Steve, Gutting , 131
Arief Abdurrahman, Hakim , 38
Brian , Ham, 309
Sidiq, Harjanta , 37
Eko, Haryono , 37, 38
Philipp, Häuselmann, 278
David, Havlíček , 216
Kateřina, Havlíčková , 216
Marie, Heggstad, 285
John, Hellstrom , 117, 255, 327, 358
Kenneth, Henn , 56
Pavel, Herich, 21
Zdenko , Hochmuth, 39
Ivan, Horáček, 66
Ian, Household , 281
Bao-Jian , Huang, 337
Hans-Peter, Hubrich , 44
William F., Humphreys, 331
Han, Hyung-chul, 191
Xiaozhen, Jiang , 57
Zhongcheng, Jiang , 48
Ki, Jin-Seok, 191
Farouk, Kadded, 87
O.I. , Kadebskaya, 61
Patrician N., Kambesis, 49, 50, 309
Stephan, Kempe , 44, 118, 186, 232
Christhild, Ketz-Kempe , 186

Hege, Kilhavn, 285
 T.M., Kuderina, 61
 Mladen, Kuhta, 51
 Yayum, Kumai, 200
 Woo, Kyung-Sik, 191
 Mohammad Ainul, Labib, 38
 Matthew S., Lachniet, 331
 Borivoj, Ladišić, 108
 Mike, Lake, 123
 Tomáš, Lánczos, 202
 Boaz, Langford, 13, 17
 Stein-Erik, Lauritzen, 90, 285, 286
 Marta, Lazzaroni, 138
 Szabolcs, Leél-Össy, 56
 Mingtang, Lei, 57
 Zaza, Lezhava, 242
 Sorin, Lisker, 17
 José Luis, Llamusi, 271
 Heros Augusto Santos, Lobo, 380
 Severin, Lølkes, 285
 Joyce, Lundberg, 141, 145, 148, 287, 354
 Shu-Wen, Luo, 335
 Weiquan, Luo, 57
 Erin, Lynch, 320
 Kim, Lyoun, 191
 Giuliana, Madonia, 291
 Daniel E., Martínez, 20
 B.R., Mavlyudov, 161
 Donald, McFarlane, 141, 145, 148, 287
 Jesús, Medina, 171
 Douglas M., Medville, 166
 Neville A., Michie, 219, 295, 339
 Andrej, Mihevc, 34, 66, 275
 S, Milanolo, 327
 Thomas E., Miller, 299
 Joseph N., Mitchell, 127, 131
 Evelyn J., Mitchell, 127
 Patrícia Monteiro, Montenegro, 380
 Gina E., Moseley, 335
 Claude, Mouret, 70, 170, 171, 172, 178, 342
 Joan, Mylroie, 74
 John, Mylroie, 74
 Fadi Henri, Nader, 78
 Alessia, Nannoni, 214
 Ana Claudia, Neri, 380
 Vu Thi Minh, Nguyet, 375
 Leslie, North, 309, 375
 Klaus, Oegg, 87
 Bogdan P, Onac, 336
 Armstrong, Osborne, 381, 376
 Jiří Robert, Otava, 303
 Einar Taule, Øyehaug, 285
 Stefanie Linzmaier, Palma, 380
 Arthur N, Palmer, 307
 Mario, Parise, 237, 291, 395
 Eric Wade, Peterson, 308
 Metka, Petrič, 371
 Leonardo, Piccini, 137, 362
 Jason S., Polk, 242, 309, 375
 Victor J., Polyak, 331, 336
 Gheorghe M., Ponta, 79
 Petr, Pruner, 34, 275
 Nataša, Ravbar, 371
 Andres, Ris, 271
 P., Robalo, 310
 Warren, Roberts, 287
 P., Rodrigues, 310
 Jacques, Rolin, 70
 Alessio, Romeo, 87, 136, 138
 Andrés, Ros, 271
 Jackie, Rowe, 5
 Jill, Rowling, 123, 346, 351
 Rosario, Ruggieri, 83, 291
 Fernando, Rull, 271
 Luis Enrique, Sánchez, 380
 Juan, Sánchez, 271,
 Laura, Sanna, 291
 Tommaso, Santagata, 87, 136, 137, 138, 252
 Muhamad Haviz Damar, Sasongko, 37, 38
 Ira D., Sasowsky, 250
 Francesco, Sauro, 87, 137, 138, 182, 352, 354
 Nico, Schertler, 141
 Ján, Schlögl, 202
 Denis, Scholz, 335
 Juswono Budi, Setiawan, 37
 Wenqiang, Shi, 320, 337
 Harry, Shick, 186
 Heather, Siebert, 144
 Rannveig Øvrevik, Skoglund, 90, 285
 Daytyn, Smbat, 83
 J.M. Kale, Sniderman, 358
 Giuseppe, Spitaleri, 138
 Christoph, Spötl, 335
 Alexander Gulbrandsøy, Stadheim, 285
 Giacomo, Strapazzon, 194
 George, Szentes, 157
 I.V., Tokarev, 61
 Rickard Stanley, Toomey, 400
 Luiz Eduardo Panisset, Travassos, 12, 382
 Mónica, Trezza, 20
 Kukuri, Tsikarishvili, 242
 Tong Phuc, Tuan, 374
 Autumn, Turner, 93
 Adranik, Ugujyan, 83
 Caroline C., Ummenhofer, 331
 Victor, Ursu, 79
 Eliyahu, Valdman, 13
 Philip, van Beynen, 381
 Guy, van Rentergem, 141, 145, 148, 287
 Vo, Van Tri, 375
 Arjan, van Waardenburg, 401, 403, 405
 Marco, Vattano, 138, 291
 George, Veni, 151, 391
 Bartolomeo, Vigna, 214
 Gabriele, Villarini, 331
 Richard Roo, Walters, 154
 Alan D., Wanamaker Jr, 331
 Jinliang, Wang, 227
 John, Webb, 9, 102
 Elizabeth L., White, 98
 William B., White, 98
 Susan, White, 9, 102, 270
 Michael E., Wiles, 314, 317
 Jane K., Willenbring, 299

Jon, Woodhead , 255, 358
David, Woods, 331
Robert A.L., Wray , 182
Jonathan G., Wynn, 330
Qiong, Xiao , 227
Shemesh, Yaaran, 13
Ali, Yamac , 237
Mukhammad Awaludin, Zaenuri, 37
Xiu-Min, Zhai, 337
Yuanhai, Zhang, 48, 105, 320
Jing, Zhang , 337
Cheng, Zhang , 227
Lucrezia, Zuccarelli , 194
Ghufran, Zulqisthi , 38
Nadja, Zupan Hajna , 34, 275, 367, 371

